IFMBE Proceedings

Olaf Dössel • Wolfgang C. Schlegel

Volume 25/III

World Congress on Medical Physics and Biomedical Engineering 7–12 September, 2009 Munich, Germany

Radiation Protection and Dosimetry,
Biological Effects of Radiation

Springer

IFMBE Proceedings Volume 25/III

Series Editor: R. Magjarevic

11th International
Congress of the IUPESM

MEDICAL PHYSICS AND BIOMEDICAL ENGINEERING

WORLD CONGRESS 2009

For the benefit
of the Patient.

Sept 7–12, 2009
Munich, Germany

IUPESM
IOMP IFMBE

International Organization for Medical Physics
IOMP

The International Federation for Medical and Biological Engineering, IFMBE, is a federation of national and transnational organizations representing internationally the interests of medical and biological engineering and sciences. The IFMBE is a non-profit organization fostering the creation, dissemination and application of medical and biological engineering knowledge and the management of technology for improved health and quality of life. Its activities include participation in the formulation of public policy and the dissemination of information through publications and forums. Within the field of medical, clinical, and biological engineering, IFMBE's aims are to encourage research and the application of knowledge, and to disseminate information and promote collaboration. The objectives of the IFMBE are scientific, technological, literary, and educational.

The IFMBE is a WHO accredited NGO covering the full range of biomedical and clinical engineering, healthcare, healthcare technology and management. It is representing through its 58 member societies some 120.000 professionals involved in the various issues of improved health and health care delivery.

Previous Editions:

IFMBE Proceedings WC 2009, "World Congress on Medical Physics and Biomedical Engineering",
Vol. 25, 2009, Munich, Germany, CD

IFMBE Proceedings SBEC 2009, "25th Southern Biomedical Engineering Conference 2009",
Vol. 24, 2009, Miami, FL, USA, CD

IFMBE Proceedings ICBME 2008, "13th International Conference on Biomedical Engineering"
Vol. 23, 2008, Singapore, CD

IFMBE Proceedings ECIFMBE 2008 "4th European Conference of the International Federation for Medical and Biological Engineering", Vol. 22, 2008, Antwerp, Belgium, CD

IFMBE Proceedings BIOMED 2008 "4th Kuala Lumpur International Conference on Biomedical Engineering",
Vol. 21, 2008, Kuala Lumpur, Malaysia, CD

IFMBE Proceedings NBC 2008 "14th Nordic-Baltic Conference on Biomedical Engineering and Medical Physics",
Vol. 20, 2008, Riga, Latvia, CD

IFMBE Proceedings APCMBE 2008 "7th Asian-Pacific Conference on Medical and Biological Engineering",
Vol. 19, 2008, Beijing, China, CD

IFMBE Proceedings CLAIB 2007 "IV Latin American Congress on Biomedical Engineering 2007, Bioengineering Solution for Latin America Health", Vol. 18, 2007, Margarita Island, Venezuela, CD

IFMBE Proceedings ICEBI 2007 "13th International Conference on Electrical Bioimpedance and the 8th Conference on Electrical Impedance Tomography", Vol. 17, 2007, Graz, Austria, CD

IFMBE Proceedings MEDICON 2007 "11th Mediterranean Conference on Medical and Biological Engineering and Computing 2007", Vol. 16, 2007, Ljubljana, Slovenia, CD

IFMBE Proceedings BIOMED 2006 "Kuala Lumpur International Conference on Biomedical Engineering",
Vol. 15, 2004, Kuala Lumpur, Malaysia, CD

IFMBE Proceedings WC 2006 "World Congress on Medical Physics and Biomedical Engineering",
Vol. 14, 2006, Seoul, Korea, DVD

IFMBE Proceedings BSN 2007 "4th International Workshop on Wearable and Implantable Body Sensor Networks",
Vol. 13, 2006, Aachen, Germany

IFMBE Proceedings ICBMEC 2005 "The 12th International Conference on Biomedical Engineering",
Vol. 12, 2005, Singapore, CD

IFMBE Proceedings EMBEC'05 "3rd European Medical & Biological Engineering Conference, IFMBE European Conference on Biomedical Engineering", Vol. 11, 2005, Prague, Czech Republic, CD

IFMBE Proceedings ICCE 2005 "The 7th International Conference on Cellular Engineering",
Vol. 10, 2005, Seoul, Korea, CD

IFMBE Proceedings NBC 2005 "13th Nordic Baltic Conference on Biomedical Engineering and Medical Physics",
Vol. 9, 2005, Umeå, Sweden

IFMBE Proceedings Vol. 25/III
Olaf Dössel · Wolfgang C. Schlegel (Eds.)

World Congress on Medical Physics and Biomedical Engineering 7–12 September, 2009 Munich, Germany

Radiation Protection and Dosimetry, Biological Effects of Radiation

Springer

Editors

Prof. Dr. Olaf Dössel
Univ. Karlsruhe
Inst. Biomedizinische Technik
Kaiserstr. 12
76128 Karlsruhe
Germany
E-mail: olaf.doessel@ibt.uni-karlsruhe.de

Prof. Dr. Wolfgang C. Schlegel
Deutsche Krebsforschungszentrum (DKFZ)
Abt. Medizinische Physik in der
Strahlentherapie
Im Neuenheimer Feld 280
69120 Heidelberg
Germany
E-mail: w.schlegel@dkfz-heidelberg.de

ISSN 1680-0737
ISBN 978-3-642-03901-0 e-ISBN 978-3-642-03902-7

Also available as set Vol. I–XIII ISBN 978-3-642-03897-6

DOI 10.1007/978-3-642-03902-7

Library of Congress Control Number: 2009934297

The IFMBE Proceedings is an Offical Publication of the International Federation for Medical and Biological Engineering (IFMBE)

Typesetting: Data supplied by the authors
Production & Cover design: Scientific Publishing Services Pvt. Ltd., Chennai, India.

Printed on acid-free paper

9 8 7 6 5 4 3 2 1

springer.com

Preface

Present Your Research to the World!

The World Congress 2009 on Medical Physics and Biomedical Engineering – the triennial scientific meeting of the IUPESM - is the world's leading forum for presenting the results of current scientific work in health-related physics and technologies to an international audience. With more than 2,800 presentations it will be the biggest conference in the fields of Medical Physics and Biomedical Engineering in 2009!

Medical physics, biomedical engineering and bioengineering have been driving forces of innovation and progress in medicine and healthcare over the past two decades. As new key technologies arise with significant potential to open new options in diagnostics and therapeutics, it is a multidisciplinary task to evaluate their benefit for medicine and healthcare with respect to the quality of performance and therapeutic output.

Covering key aspects such as information and communication technologies, micro- and nanosystems, optics and biotechnology, the congress will serve as an inter- and multidisciplinary platform that brings together people from basic research, R&D, industry and medical application to discuss these issues.

As a major event for science, medicine and technology the congress provides a comprehensive overview and in–depth, first-hand information on new developments, advanced technologies and current and future applications.

With this Final Program we would like to give you an overview of the dimension of the congress and invite you to join us in Munich!

Olaf Dössel
Congress President

Wolfgang C. Schlegel
Congress President

Preface

Welcome to World Congress 2009!

Since the first World Congress on Medical Physics and Biomedical Engineering convened in 1982, medically and biologically oriented engineers and physicists from all continents have gathered every three years to discuss how physics and engineering can advance medicine, health and health care and to assess the clinical, scientific, technical and professional progress in their fields. In the tradition and the mission of our professions, which are the only ones involved in the whole loop of health and health care from basic research to the development, assessment, production, management and application of medical technologies, the theme of WC 2009 is "For the Benefit of the Patient". Thus, in addition to scientific aspects, the Congress will focus on all aspects of safe and efficient health technology in both industrialized and developing countries, including economic issues, the perspectives that advanced technologies and innovations in medicine and healthcare offer for the patients and the development of societies, the progress of MBE and MP, including health policy and educational issues as well as the need for the regulation and classification as health professionals of those biomedical/clinical engineers and medical physicists who are working in the health care systems.

The World Congress as the most important meeting of our professions, bringing together physicists, engineers and physicians from all over the world, including the delegates of the 138 constituent organizations of the IUPESM representing some 140,000 individual members, is the best place to discuss these issues, thereby contributing to the advancement of the physical and engineering sciences, our professions and thus to global health.

It gives me great pleasure to welcome you to this important event. I wish you a rewarding and enjoyable congress and a most pleasant time in Munich, the ‘metropolis with heart’ that has so much to offer.

Joachim H. Nagel
President of the IUPESM

Preface

Let's talk!
Is our level of communication between Medical Physics, Biomedical Engineering, Clinical Engineering, Medical Informatics, Tissue Engineering, etc. and Medicine good enough? We would like to answer: yes, we are quite good, but not good enough! There is a lot of room for improvement. Let' start right on the spot - on the World Congress on Medical Physics and Biomedical Engineering 2009. And please remember: communication is 50% talking and 50% listening.

Let's work together!
Do we have a perfect level of collaboration in our field? OK, we are quite good, but we can do better. Just to give an example: there should be no funded project in Medical Physics or Biomedical Engineering where there is no medical partner. And vice versa: medical doctors should join their forces with physicists and engineers if they are aiming at improvements on medical devices or healthcare systems. Let's start right here in Munich, September 2009, with innovative projects and innovative ways of cooperation.

Let's get to know each other!
It's known for more than thousand years: people who know each other personally and from face to face can talk with better mutual understanding, collaborate with less friction losses, are much more successful ..... and have much more fun. Plenty of chances to make new friends and to refresh old relations on World Congress on Medical Physics and Biomedical Engineering 2009!

And here are the numbers:
More than 3000 scientists working in the field of Medical Physics and Biomedical Engineering meet in September 2009 in Munich. They come from more than 100 nations. They submitted about 2800 contributions. 10 plenary talks and 46 keynote lectures bring us to the top level of science in our field. 75 companies show their latest achievements in the industrial exhibition. It's definitely the largest market place of ideas and innovations in Medical Physics and Biomedical Engineering of the year 2009.

August 2009 Olaf Dössel

Table of Contents

Is The MOSFET Dosimeter Feasible at Diagnostic X-Ray Energies for Interventional Radiology?

K. Chida[1], Y. Inaba[2], I. Yanagawa[2], H. Saito[1], T. Ishibashi[1] and M. Zuguchi[1]

[1] Department of Radiological Technology, Tohoku University Graduate School of Health Sciences, Sendai, Japan
[2] Department of Radiology, Tohoku University Hospital, Sendai, Japan

Abstract— **To reduce the risk of skin injury during interventional radiology (IVR) procedures, it has been suggested that physicians track patients' dose. However, the patient's skin dose is very rarely monitored because of the lack of a feasible method for use in IVR. The metal oxide semiconductor field effect transistor (MOSFET) dosimeter is designed to measure patient exposure dose during radiotherapy applications at megavoltage photon energies. Our purpose in this preliminary study was to evaluate the feasibility of using a MOSFET dosimeter to measure patients' skin dose during exposure to diagnostic X-ray energies used in IVR.**

Dose measurements were performed using the OneDose™ dosimetry system (OneDose). This small system uses a dosimeter based on MOSFET technology. OneDose measurements were compared with measurements obtained using a calibrated thimble-type 6-mL ion chamber. The energy dependence of the OneDose system was measured at 60-120 kV (tube voltage) on diagnostic X-ray equipment. The dependence of the OneDose sensor on the X-ray beam angle in air was measured. Variation in the sensitivity of the OneDose sensor was evaluated.

The OneDose dosimetry system showed high sensitivity, and the responses were roughly uniform from 60 to 120kV, and its response was nearly angle-independent. There was little variation in the sensitivity of multiple OneDose sensors. The OneDose is almost invisible on X-ray images at diagnostic energies.

Although the OneDose system does not provide real-time dose monitoring, it will be feasible for use at diagnostic X-ray energies for measuring patients' exposure dose during IVR.

Keywords— **interventional radiology, skin dose, radiation injury, metal oxide semiconductor field effect transistor (MOSFET), dose measurement**

I. Introduction

As protection from radiation is important in interventional radiology (IVR), the radiation dose should be measured [1,2]. Metal oxide semiconductor field effect transistor (MOSFET) dosimeters are widely used to measure exposure dose in radiation therapy, which uses high X-ray energies [3]. The purpose of this preliminary study was to evaluate the feasibility of using MOSFET dosimeters to measure patients' skin dose during exposure to diagnostic X-ray energies used in IVR.

II. Methods

A. MOSFET dosimeter

Dose measurements were performed using the OneDose™ dosimetry system (OneDose, Sicel Technologies, Inc. USA). This small system uses a dosimeter based on MOSFET technology, and consists primarily of a sensor and a reader. It is battery powered and no cables connect the dosimeter sensor to the reader during irradiation. OneDose systems are generally pre-calibrated for Co-60. The OneDose system is designed as an easy-to-use dose measurement tool. Before the start of irradiation, the sensor is inserted into the reader and initialized. After irradiation, the sensor is re-inserted into the reader and the dose information is read out.

B. Fundamental measurement

The energy dependence of the OneDose system was measured at 60, 70, 80, 90, 100, 110, and 120 kV (tube voltage) on diagnostic X-ray equipment using a high-frequency inverter generator (UD-150, Shimadzu, Japan).

OneDose measurements (air-KERMA) were compared with measurements obtained using a calibrated (reference: traceable from the national standard exposure dose) thimble-type 6-mL ion chamber (Model No. 9015, Radcal, USA). Irradiation was performed in air, under the same conditions, using the OneDose sensor and the reference ion chamber. Differences in the average ± SD value based on four measurements at each tube voltage were evaluated.

We also evaluated the correction factors (Fcs) for the OneDose system. The Fc was calculated as follows:

Fc = reference ion chamber measurement / OneDose measurement.

The dependence of the OneDose sensor on the X-ray beam angle in air was measured at 0, 45, 90, and 180 degrees along the short and long axes of the sensor. Under the same X-ray irradiation conditions (80 kV), the angle dependence was evaluated using the 0° measurement as the reference value. The average ± SD values obtained from

O. Dössel and W.C. Schlegel (Eds.): WC 2009, IFMBE Proceedings 25/III, pp. 1–2, 2009.
www.springerlink.com

four measurements at each angle were evaluated. Variation in the sensitivity of the OneDose sensor was evaluated by using 10 sensors under the same X-ray irradiation conditions (80 kV).

III. Results

The OneDose dosimetry system showed high sensitivity, and the responses were roughly uniform from 60 to 120 kV. Consequently, in the range of diagnostic X-ray energies, the average Fcs of the OneDose was approximately 0.28.

Figures 1 and 2 show the angle dependence of the OneDose sensor along the long and short axes. There was very little change in the response of the sensor with change in the beam angle.

The coefficient of variation in the sensitivity of the 10 OneDose sensors was approximately 2.6%. The maximum sensitivity was 1.075-fold the minimum value.

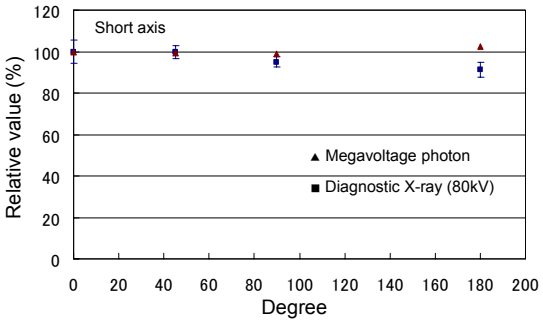

Fig. 1 Angle dependence of short axis of OneDose sencor. (Relative value as reference in 0 degree measurements.)

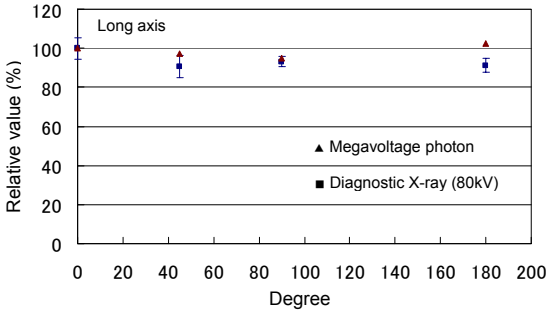

Fig. 2 Angle dependence of long axis of OneDose sencor. (Relative value as reference in 0 degree measurements.)

IV. Discussion

The OneDose MOSFET dosimeter is designed to measure a patient's exposure dose during radiotherapy applications using megavoltage photon energies. However, the performance of the OneDose system in exposure to diagnostic X-ray energies has not been investigated.

The response of the OneDose system was almost constant at diagnostic X-ray energies, although the sensitivity was higher than at megavoltage photon energies. Therefore, the OneDose system can be used at diagnostic X-ray energies after Fc correction.

At megavoltage photon energies, the response of the OneDose sensor is almost independent of the angle. We found that the angle dependence was minimal at diagnostic X-ray energies.

V. Conclusion

At diagnostic X-ray energies, the Fcs for the OneDose MOSFET detector system was approximately 0.28 and its response was nearly angle-independent. There was little variation in the sensitivity of multiple OneDose sensors. The OneDose is almost invisible on X-ray images at diagnostic energies. Furthermore, the OneDose is easy to handle. Therefore, it is feasible for use at diagnostic X-ray energies for measuring patients' exposure dose during IVR.

Acknowledgment

We acknowledge Mr. Yoshiaki Morishima, and Mr. Hiroo Chiba, Tohoku Employees' Pension Welfare Hospital, Sendai, Japan, for their invaluable assistance.

References

1. International Commission on Radiological Protection. ICRP publication 85: (2001) avoidance of radiation injuries from medical interventional procedures. Ann ICRP 30/2: Publication 85.
2. Chida K, Kagaya Y, Saito H et al (2007) Total entrance skin dose: An effective indicator of the maximum radiation dose to a patient's skin during percutaneous coronary intervention. Am J Roentgenol 189: W224-227.
3. Marcie S, Charpiot E, et al (2005) In vivo measurements with MOSFET detectors in oropharynx and nasopharynx intensity-modulated radiation therapy. Int J Radiat Oncol Biol Phys 61:1603–6.

Author: Koichi Chida, PhD
Institute: Tohoku University Graduate School of Health Sciences
Street: 2-1, Seiryo, Aoba
City: Sendai, 980-8575
Country: Japan
Email: chida@mail.tains.tohoku.ac.jp

Doses to patients from photo-neutrons emitted in a medical linear accelerator

M.K. Saeed[1], O. Moustafa[1], O.A. Yasin[2], C. Tuniz[3] and F.I. Habbani[4]

[1]Radiation & Isotope Center, Khartoum, P.O. Box 846, Sudan
[2]Faculty of Science & Technology, Alneelain University, Khartoum, P.O. Box 12702, Sudan
[3]ICTP, Strada Costiera 11, 1-34014 Trieste, Italy
[4]Faculty of Science, University of Khartoum, Khartoum, P.O. Box 321, Sudan

Abstract— **Study of doses to patients from emitted photo-neutrons in a medical linear accelerator (Varian 2100C) was carried out. Dose calculation was performed using Monte Carlo Geant4 code. The model was used to calculate the neutron fluence, as a function of the neutron energy inside the treatment room to estimate the effective dose to patients. The ambient dose equivalent versus field size for patients is reported in this study. The ambient dose equivalent using 1 x 1 cm^2 field size, at isocenter and x-ray modes of 20, 18, 15 and 10 MV, was found to be 1.85, 1.79, 0.61, and 0.06 $mSv.Gy^{-1}$, respectively. The mean energies of emitted photo-neutrons were 0.48, 0.44, 0.40, and 0.16 MeV at x-ray modes, of 20, 18, 15, and 10 MV, respectively.**

Keywords— **Monte Carlo Geant4 simulation; photo-neutrons; ambient dose equivalent**

I. Introduction

In a radiation treatment facility using a linear accelerator the emitted photo-neutrons can constitute hazard to healthy tissue for patients undergoing radiotherapy.

Several studies [1-3] have been devoted to the study of the photo-neutron dose (or dose equivalent) compared to the photon dose for patients. Some investigators have identified the typical radionuclides produced in the treatment room by the activation of the air [4-6].

The goal of the present study was to estimate the effective doses at the isocenter from photo-neutrons produced in a medical linear accelerators. Measurements of such doses from neutrons are difficult to perform with the standard nuclear instrumentation, due to the high fluence rate of photons with respect to neutrons and the pulsed radiation field. Therefore a computer code allowing a suitable simulation of the entire process of the photo-neutron production and transport across the accelerator head represents a useful tool to evaluate the undesired neutron leakage dose to the patient. The Monte Carlo code Geant4 has been used to achieve the goal of this study.

II. Materials and methods

In this work the Monte Carlo code Geant4 was used to simulate the photo-neutron production in the linear accelerator Varian Clinac 2100C, equipped with the multileaf collimation system (MLC), installed at the Maggiore Hospital (Trieste, Italy).

The point of interest in the treatment room of Clinac 2100C in the present calculations was selected at the machine isocenter. Fig. 1 shows a geometrical model simulated with Geant4 for the linac head components, including the target, flattening filter, secondary collimator jaws, and MLC. To model the energy degradation of the photo-neutrons travelling inside a treatment room, a typical model of a treatment room in the hospital was simulated. The room has dimensions of 7 x 7 x 5 m^3, surrounded by concrete walls and is filled with dry air.

The Monte Carlo code Geant4 requires the specification of the physical processes included for the simulations. The following typical processes were included: Rayleigh and Compton scattering, pair production, the photoelectric effect for the x-rays, for electrons and positrons ionization, Bremsstrahlung and e^+- e^- annihilation, as well as multiple scattering and photo-nuclear reactions. All particles, both photons and electrons, are tracked to the end of their path, while the cut-off range for the production of secondary particles was set at 0.1 mm, according to the dimension of the detector geometries employed.

Table 1 shows the calculated electron pencil beam kinetic energy incident on the target and x-ray modes used in the present simulation. 1.25 x 10^{15} electrons incident on the target was found necessary to deliver an absorbed dose of 100 cGy under the following conditions: (1) source-surface distance (SSD): 100 cm; (2) field size: 10 x 10 cm^2 at the isocenter.

The ambient dose-equivalent from photo-neutron contamination arising from a Clinac 2100C was calculated using the Monte Carlo Geant4 code as a function of the radiation field size. The number of initial histories was 3000

O. Dössel and W.C. Schlegel (Eds.): WC 2009, IFMBE Proceedings 25/III, pp. 3–6, 2009.
www.springerlink.com

million for the 40 x 40 cm^2, 2500 million for the 10 x 10 cm^2 and 1000 million for the 1 x 1 cm^2 field size. The ambient dose-equivalent was calculated using the fluence to ambient dose-equivalent conversion coefficients presented by ICRP Publication 74 [7].

Table 1 Calculated electron beam kinetic energy for different x-ray modes from tungsten target with thickness of 0.5 cm.

X-ray mode (MV)	Electron beam kinetic energy (MeV)
20	22.3
18	18.8
15	15.9
10	10.3

Extensive validation of Geant4 calculations was performed by the code developers [8]. For the validation of the code in this work a calculated x-ray percentage depth dose (PDD) and a measured PDD was compared. The dimensions of the water phantom used in the dose calculations were 50 x 50 x 40 cm^3. The depth doses were calculated by the Monte Carlo Geant4 code for depths from 0 to 20 cm using the absorbed energy in the central axis. The measurements were performed using Cylindrical Type Chamber (CC13) and computerized water phantom (Blue Water Phantom). The chamber has a leakage current less than 4 x 10^{-15}A. The Blue phantom has motors capable to scan in three dimensions and has dimensions of 48 x 48 x 48 cm^3. The accuracy of the position was ± 0.5 mm along the axis. The phantom tank was placed on a trolley for the convenient movement of the assembly. A computer controlled the movement of the CC13 Chamber using OmniPro-Accept system [9]. The difference between measurement and calculation was determined using:

$$\text{Difference}(\%) = \frac{\text{Calculation} - \text{Measurement}}{\text{Measurement}} \text{x} 100$$

The percentage depth dose for 10 MV photons calculated by the code and measured with the CC13 chamber is shown in Fig. 2. The field size was 10 x 10 cm^2 and the SSD was 100 cm. The maximum difference between the measured PDD and the corresponding calculations was 2%, while the difference in the descending part of the curves was less than 1%.

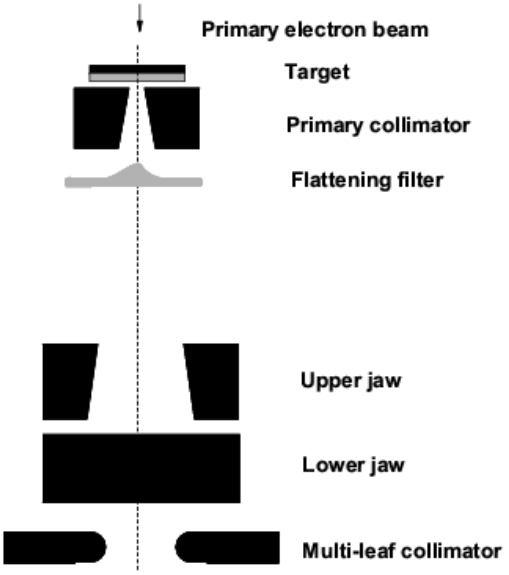

Fig. 1 Geometrical model of Clinac 2100C simulated with Geant4.

III. RESULTS AND DISCUSSION

Neutron history files were generated, for the detector geometry used, which contained the parameters of number, position, direction, energy and track length for the neutrons generated from photo-interactions. The neutron histories at the point of interest were analyzed by OriginPro Version 7.5 SR0 software.

The results of neutron yields at the components of the head (target, flattening filter, primary collimator and jaws) with 1 x 1 cm^2 field size are shown in Fig. 3. The results of neutron yields are in good agreement with previously published data [10]. It was found that the maximum neutron yield was produced at the target and flattening filter, with increase of neutron yield with x-ray mode. Fig. 4 shows the average energy of the photo-neutrons at the isocenter, calculated as a function of the x-ray modes.

The neutron fluence was estimated at SSD of 100 cm as the neutron number divided by area of the detector. The ambient dose equivalent using 1 x 1 cm^2 field size, at isocenter and x-ray modes of 20, 18, 15 and 10 MV, was found to be 1.85, 1.79, 0.61, and 0.06 $mSv.Gy^{-1}$, respectively. The mean energies of neutrons were found to be 0.48, 0.44, 0.40, and 0.16 MeV at x-ray modes of 20, 18, 15, and 10 MV, respectively.

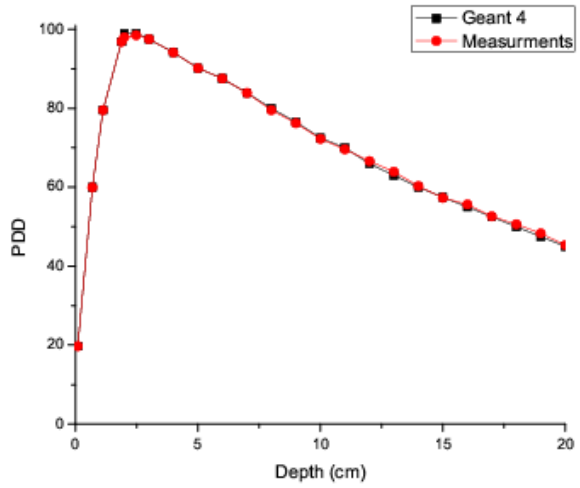

Fig. 2 Comparison of percentage depth dose of 10 MV photon beam of Clinac 2100C calculated by Geant4 code versus measurements. (SSD = 100 cm and 10 x 10 cm2 field size).

Fig. 5 shows the ambient dose equivalent and fluence of neutrons per unit area per Gy against the radiation field size at the isocenter plane. It is evident that as the size of the radiation beam increases, so does the photo-neutron fluence, with the difference between the smallest and the largest field size being in the order of 23.5 %. It is clear that the photo-neutron production at other linac head components above the movable collimators contribute to the dose increment at the isocenter. Thus, as the field size increases, more and more photo-neutrons are able to reach the isocenter.

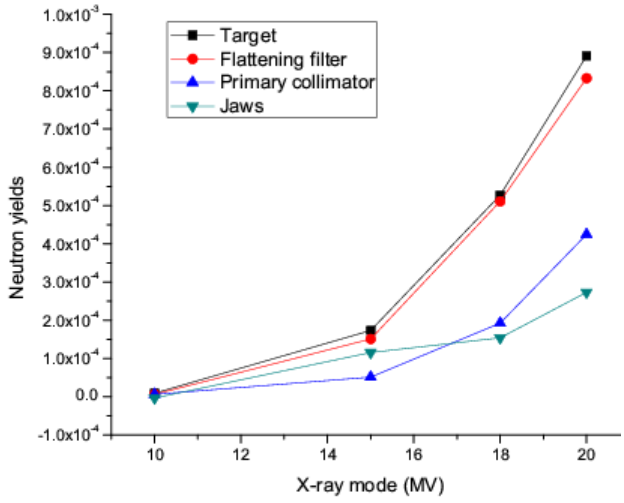

Fig. 3 Geant4-calculated neutron yields in the Varian Clinac 2100C head

(1 x 1 cm2 field size).

Comparison with measurements values using a Bonner sphere system based on passive gold activation detectors published for a Varian Clinac 2100C [11-13] shows a good agreement for x-ray mode of 18 MV and 15 MV respectively for 10 x 10 cm^2 and 40 x 40 cm^2field sizes.

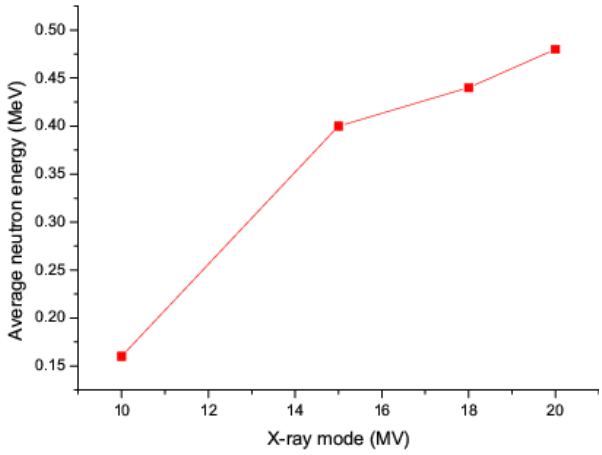

Fig. 4

Fig. 4 Average energy of the leakage neutrons around the Varian Clinac 2100C head (minimum field size), calculated with the Geant4 code.

IV. CONCLUSION

The results indicate that the neutron dose equivalent from photo-neutrons to patients in a typical linac treatment facility should not be neglected. The whole body neutron dose does represent a real secondary cancer induction threat. Neutron field evaluation is therefore necessary to optimize the treatment. The photo-neutron contamination arising from a medical lineal accelerator has been calculated in head components and as a function of the radiation field size. The derived data have been used to estimate the ambient dose equivalent from photo-neutrons to patients receiving radiation treatment by a linear accelerator. The present method, using Monte Carlo simulation, proved to be a reliable tool in the study of doses to patients from emitted photo-neutrons in a medical linear accelerator.

ACKNOWLEDGMENT

The authors would like to appreciate the co-operation and help provided by Prof. Gianrossano Giannini of University

of Trieste. The corresponding author would like to thank Dr. Francesco Longo and Riccardo Bevilacqua for assistance, for their prompt replies and suggestions in using Geant4 code. The corresponding author wishes to thank Prof. Nadia Binggeli and express his gratitude for the support given by International Center for Theoretical Physics through the Sandwich Ph.D. Programme, (Trieste, Italy).

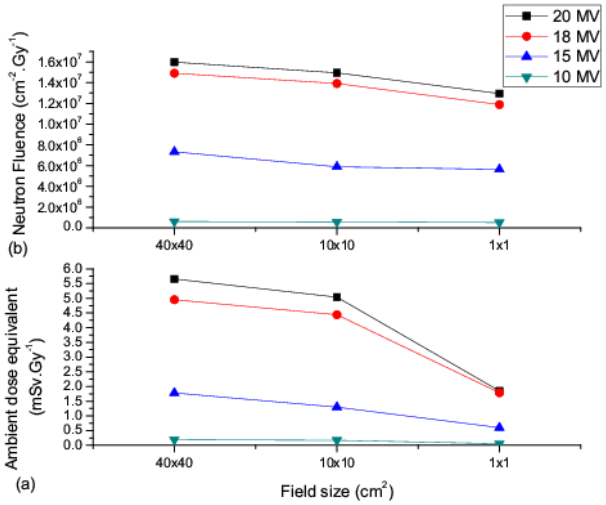

Fig. 5 (a) Ambient dose equivalent (mSv/Gy) and (b) the neutron fluence Φ (cm-2.Gy-1) against the radiation field size at the isocenter plane calculated with the Geant4 code.

References

1. NCRP Report No. 79. (1984) Neutron contamination from medical accelerators. National Council on Radiation Protection and Measurements, Washington, DC
2. Garnica-Garza H. M. (2005) Characteristics of the photo-neutron contamination present in a high-energy radiotherapy treatment room. Phys. Med. Biol. 50:531-539
3. McGinley P. H. and Landry J. C. (1989) Neutron contamination of x-ray beams produced by the Varian Clinac 1800. Phys. Med. Biol. 34:777-783
4. McGinley P. H. and White T. A. Jr. (1983) Air activation produced by high-energy medical accelerators. Med. Phys. 10:796-800
5. McGinley P. H., Wright B. A. and Meding C. J. (1984) Dose to radiotherapy technologist from air activation. Med. Phys. 11:855-858
6. McGinley P. H. (2002) Shielding techniques for radiation oncology facilities. expanded 2nd ed., Medical Physics Publishing, Madison, WI
7. International Commission on Radiological Protection. Conversion coefficients for use in radiological protection against external radiation. ICRP Publication 74, (1996) Annals of the ICRP, 26 (Pergamon Press)
8. GEANT4. A simulation toolkit. GEANT4 Collaboration, August (2002) SLAC-PUB- 9350
9. OmniPro-Accept Ver. 6.1 Manual, at www.scanditronixwellhofer.com
10. Mao X. S., Kase K. R, Liu J. C., Nelson W. R., Kleck J. H. and Johnson S. (1997) Neutron sources in the Varian Clinac 2100C/2300C medical accelerator calculated by the EGS4 code. Health Phys. 72 (4)
11. Thomas D. J., Hawkes N. P., Jones P. Kolkowski and Roberts N. J. (2007) Characterization and utilization of a Bonner sphere set based on gold activation foils. Radiat. Prot. Dosim. 126:229-233
12. Thomas D. J., Bardell A. G. and Macauly E. M. (2002) Characterization of a gold foil-basid Bonner sphere set and measurements of neutron spectra at a medical accelerator. Nucl. Intr. Meths. Phys. Res. A 476:31-35
13. Fernández F., Domingo C., Amgarou K., Castelo J., Bouassoule T., Garcia M. J. and Luguera E. (2007) Neutrons measurements in A Varian 2100C Linac facility using a Bonner sphere system based on passive gold activation detectors. Radiat. Prot. Dosim. 126:361-365

Correlation between Radiation sensitivity and body weight

S. F. Akber[1] and T. S. Kehwar[2]

[1]Department of radiation Oncology, Case Western Reserve University, Cleveland, Oho 44106
[2]Division of Medical Physics, Department of Radiation Oncology, University of Pittsburgh Cancer Institute, Pittsburgh, PA 15232

Abstract – **The main aim of the paper is to establish a correlation between body weight of different species and their mean lethal dose (LD_{50}). Analysis of LD_{50} with body weight of different species following whole body irradiation yields a good correlation. Results indicate that as the body weight increases, LD_{50} decreases, which follows the relation** $LD_{50} = k_1 \log_e(W) + C_1$**, where k_1 and C_1 are constants, respectively.**
Keyworlds **– LD50, Body weight, TD50**

I. Introduction

Radiation sensitivity is generally determined by the cell-survival curve. In the case of the whole organ, there are mainly two kinds of cell. One is the functional cells that perform organ / tissue specific functions and other is the proliferate cells that divide and replace dead functional cell that have completed their life span. In these groups of cells, they perform various functions and may have different mechanism. Therefore, the radiation sensitivity derived from cell-survival curves becomes frivolous, because it does not represent the whole organ. No comprehensive data are available at the cellular level or on the whole organ concerning the effects of radiation on dividing cells within the organ. Another important factor is the kinetics of the cell population as a whole, of which the cells are an integral part of the organs. These factors within the organs are not fully understood, and hence radiation sensitivity of normal human organs along with total body irradiation, is still debated with pro and con arguments.

II. Materials and methods

We abstracted two set of LD_{50} data of species from the literature. The LD_{50} values along with their body weight were obtained from Hall and Giaccia [1]. Oxygen consumption rate of the species were taken from Schmidt-Nielsen [2]. In the second set of data LD_{50} values were obtained from Bond [3]. Bond [3] did not provide body weight of any species we, therefore, used body weight of oxygen consumption given by Schmidt-Nielsen [2].

III. Results and discussion

Several investigators have tried to quantify the radiation sensitivity of human organs based on the outcome of clinical radiation treatment. The radiation sensitivity of human organs is defined in terms of radiation tolerance dose (TD_{50}), mean lethal dose (D_o) for an individual organ where LD_{50} (mean lethal dose) is assigned for whole body radiation sensitivity. However, the TD_{50}, D_o, and LD_{50} are neither well-defined nor reasonably well known concepts. The general assumption is that the degree of injury that is considered to have been either tolerated or lethal is often on the time after irradiation. Different investigators have, therefore, arrived at different absolute values of $TD_{50,}$ D_o, and LD_{50}. Hence, there is considerable disagreement as to its actual value. Furthermore, no tissue parameter has so far been assigned as a common factor, which may influence radiation sensitivity. Akber [4] has shown that TD_{50} compiled by Emami, et al. [5] against organ weight yield a correlation coefficient of 0.62. Similarly, using D_o of Cohen [6] values against organ weight in six human organs yield a correlation coefficient of 0.94.[7] It appears from these studies that as the organ weight increases by assembling many cells of different functions, TD_{50} and D_o decreases.

Hall et al. [1] and Bond [2] LD_{50} values for several mammals as well as their body Weights were assessed.

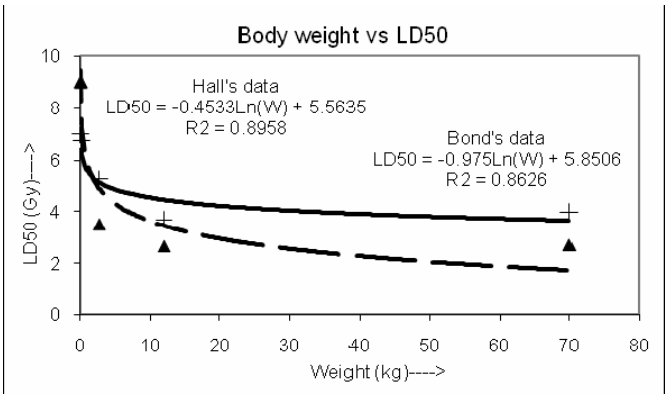

Fig. 1 Correlation between total body irradiation dose (LD50) and body weight in mammals.

Fig. 1 shows the LD_{50} points of these data sets and corresponding best fit regression lines obtained by fitting these data, using the method of least square fit, into the equation (1)

$$LD_{50} = k_1 \log_e(W) + C_1 \quad (1)$$

Where k_1 and C_1 are the constants and W is the body weight in kilogram. The best fit regression lines give the values of k_1 = - 0.4533 and C_1 = 5.5635 for Hall's [1] and k_1 = - 0.975 and C_1 = 5.8506 for Bond's (3) data sets. It is interesting to observe in Fig. 1 that the LD_{50} decreases as the logarithmic of body weight increases yielding correlation coefficients of

O. Dössel and W.C. Schlegel (Eds.): WC 2009, IFMBE Proceedings 25/III, pp. 7–8, 2009.
www.springerlink.com

0.8958 and 0.8626 for Hall et al's [1] and Bond's [3] data sets respectively.

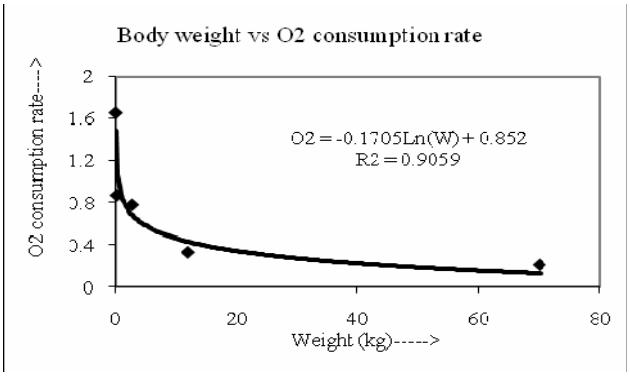

Fig. 2. Correlation between oxygen consumption rate and body weight in mammals.

The best fit regression line obtained by fitting oxygen consumption rate data of Schmidt-Nielsen [2] versus average body weight of the species shown in Fig. 2. It is seen that the O_2 consumption rate (liter $O_2kg^{-1}h^{-1}$) decreases as logarithmic body weight increases. The equation used for the best fit is

$$O_2 = k_2 \log_e(W) + C_2 \quad (2)$$

From the best fit regression line the values of k_2 and C_2 were found -0.1705 and 0.852, respectively, with a correlation coefficient of 0.9059.

Similar equation, as used in Figs 1 and 2, was used to fit O_2 consumption data of Schmidt-Nielsen [2] with Hall's [1] and Bond's [3] LD_{50} data. The equation may be written as

$$O_2 = k_3 \log_e(LD_{50}) + C_3 \quad (3)$$

The best fit regression lines of these data sets are shown in Fig. 3.

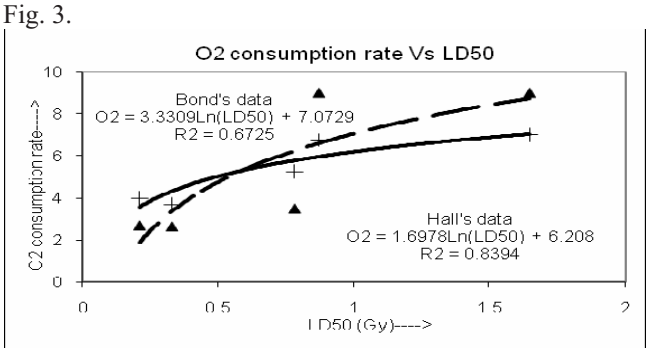

Fig. 3. Correlation between oxygen consumption rate and total body irradiation dose (LD50).

The values of k_3 and C_3 were found 1.6978 and 6.208 for Hall's [1] data, and 3.3309 and 7.0729 for Bond's [3] data with respective correlation coefficients of 0.8394 and 0.6725.

It is seen in Fig. 3 that as the O_2 consumption rate increases per gram of tissue. LD_{50} increases as well.

From Fig. 2 and equation (2) it is clear that the O_2 consumption rate (liter $O_2kg^{-1}h^{-1}$) is related to the body weight. While Fig. 3 and equation (3) reveal that the O_2 consumption rate is related to the LD_{50}, therefore LD_{50} is related to the body weight, which is shown in Fig 1 and equation (1).

It appears that as the body weight/organ increases in size and weight, having cells of different function, specific O_2 consumption rate per gram of tissue decreases, and hence becomes more sensitive to radiation. Why this is so? In small mammals, blood releases O_2 more readily because of its lower affinity for O_2. For example, unloading pressure of O_2 for human blood is 28 mm Hg and about 45mm Hg for mouse blood. These differences are indeed directly related to the metabolic characteristics of mammals [2]. Furthermore, Max Ruben studied the metabolic rate of dogs of various sizes. He observed that smaller dogs had a higher metabolic rate per unit body weight compared to the larger dogs [2]. It is therefore, one might conclude that higher metabolic rates, which are indicative of higher oxygen consumption rates per gram of tissue, be responsible for yielding higher LD_{50} in smaller species. It is, therefore, very important that in planning total body irradiation (TBI), body weight may be taken in consideration for determining the optimal dose.

References

1. Hall, E. and Giaccia AJ. (2006) Radiobiology for the Radiologists. p.122. Lippicott Williams and Wilkinks. NY.
2. Schmidt - Nielsen K. (1990) Animal Physiology. 4th edn. Cambridge, UK: Cambridge University Press. pp. 195.
3. Bond VP. (1969) Comparative Cellular and Species Radiosensitivity. P.9, Bond VP, and Sagahara T, Eds., Igaku Shoin, Tokyo.
4. Akber, S.F. (2000) Correlation of Radiation Tolerance Dose of Normal Human Organs with Organ Weight. Blood and Water Content. Am J Clin Oncology 23: 360-364.
5. Emami, Lyman J., Brown A., Coia L., Goitein, M., et al.(1991) Tolerance of normal tissue to therapeutic irradiation. Intl J Radiat Oncology Biol Phys 21: 109-122.
6. Cohen, L. (1983) Biophysical Models in Radiation Oncology. CRC publication. pp. 30.
7. Akber SF, *Kehwar TS*. Correlation between Mean Lethal Dose and Organ Weight. Journal of Radiotherapy in Practice 8(3), 2009.

Simulation of Human Eye for Ophthalmic Brachytherapy Dosimetry Using MCNP-4C Code

S. Asadi[1,*], S. Farhad Masoudi[1], and M. Shahriari[2]

[1] Department of Physics, K.N. Toosi University of Technology, P.O. Box 15875-4416, Tehran, Iran
[2] Department of Radiation Application, Shahid Beheshti University, Tehran, Iran

Abstract— **This paper proposes study through which human eye with tumour (choroidal melanoma) has been simulated through with MCNP-4C code. The simulation is done by using a three dimensional method in the most general manner possible (taking in to consideration different parts of the eye like: Lens, cornea, retina, choroid, sclera, anterior chamber, optic nerve and tumour). That is to say that all the said parts have been simulated in a manner that the final result could be the complete and exact simulation of the eye globe. Dose distribution in some parts of the eye has been determined and the central axis depth-dose curves for one ^{125}I seed in the central slot of Modulay or pure gold plaque has been calculated and comparison has been made afterwards to those calculated by Thomson et al. the results have shown good agreement. Besides, mean absorbed dose values due to both Iodine source (16mm, 12mm) were obtain for each one of the different structures which compose the eye model and can give relevant information in eventual clinical analyses.**

Keywords— **MCNP-4C, brachytherapy, eye plaque, COMS, Choroidal Melanoma**

I. Introduction

Brachytherapy using ophthalmic plaques is a term used to describe the short distance treatment of cancer with radiation from small encapsulated radionuclide sources. This way has shown to be a good alternative to enucleation for the treatment at eye tumour [1 - 2]. Nowadays making use of artificial radioactive element like (^{137}Cs, ^{192}Ir, ^{198}Au and ^{125}I) is rapidly on the increase. These radioactive materials with different shapes and structures have been the object of clinical studies with a focus towards providing minimum irradiation to healthy tissues while delivery maximum doses to the tumour [3]. In this work, Mont Carlo code MCNP-4C using ^{125}I seeds and COMS-style Plaque are used to study dosimetry in some parts of eye. Though there are many different plaque models available, the COMS Protocol required the use of plaques of standardized design, consisting of a dome-shaped gold alloy (Modulay) backing with a silicon polymer carrier holds brachytherapy seeds in their positions.[4]

II. Materials and Metods

With regard to complexity of man's eye in terms of it's geometrical aspect and it's structure, complete simulation of the eye in three dimensional manner (simulation of all parts of the eye (i.e., Cornea, Retina, Choroid, Sclera, Lens, Anterior Chamber, Optic nerve, and bulk of the eye comprising Vitreous body)) and also exact determination different components of the said parts, there is the need for full information about eye globe geometry and composition. Simulation of all the above mentioned components has been done by MCNP-4C code, precisely and completely in a three dimensional manner that complete detailed information about this issue will be noticed subsequently in further paper.

A. The eye anatomy

The adult human eye averages 24mm in diameter and the normal anteroposterior diameter varies between 21 and 26 mm, so Eye globe has been defined as a spherical shell of diameter 24.6 mm [5-6].This anatomy is composed of three layers enclosing the eye body, namely Retina (inner), Choroid (middle), and Sclera (outer) as shown in Figure1. These layer's diameters have no fixed dimension all over them, both Sclera and Choroid are 1 mm thick on average. The complete information about eye geometry which have been used for simulating eye globe have been taken from some medical reference [5-8]. Interface among different shapes with specific characteristics has been used in order to define eye globe geometry for MCNP_4C code. These characteristic have been determined in a manner that the dimensions of main parts of the eye could be in conformity with medical data.

O. Dössel and W.C. Schlegel (Eds.): WC 2009, IFMBE Proceedings 25/III, pp. 9–12, 2009.
www.springerlink.com

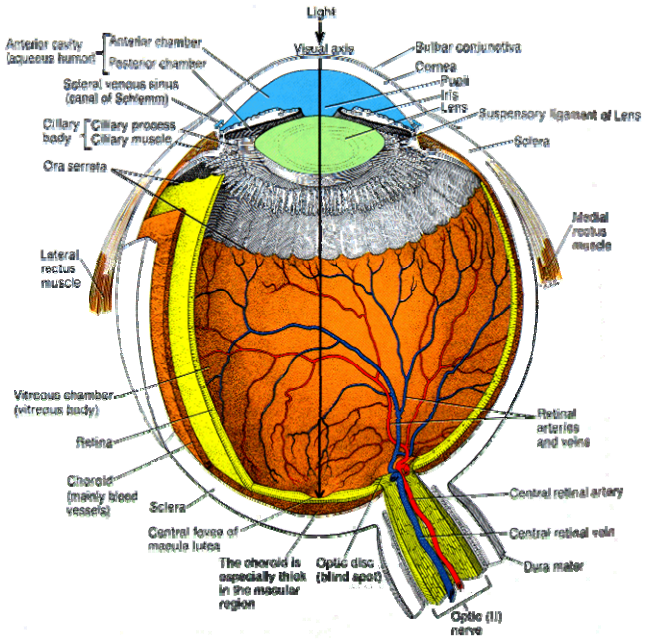

Fig. 1 Human eye diagram[9]

Lens, for instance, is the common volume between eye globe and an ellipsoid component is described by the following equations:

$$6.25(x)^2 + 4.94(y)^2 + 16(z-0.73)^2 \le 1 \quad (1)$$

$$(x)^2 + (y)^2 + (z)^2 \le 1.23^2 \quad (2)$$

The lens composition and density are from ICRU Report 46[10], and are quoted in Table 1.

Table 1. Composition and densities of lens

Tissue/ Material	Percent by weight elemental composition							
	H	C	N	O	Na	P	S	Cl
	9.6	19.5	5.7	64.6	0.1	0.1	0.3	0.1

Density=1.07(gr/cm^3)

B. The eye tumours

Head and neck, prostate, breast and lung cancers and eye tumours too could be reported to as diseases as nowadays are treated by brachytherapy[11-12]. Eye tumours are generally secondary tumours which develop as a result of spread of cancers existing in other parts of the body. However retinoblastoma and melanoma are two kinds of main tumours which develop inside the eye globe and grow there. Choroidal melanoma is the most common intraocular cancer for adults. Tumour volume assume different sizes and shapes, eye of patients with tumours from 2.5 to 10 mm in height and a basal diameter of 16 mm or less are treated with a radioactive plaque if randomized to radiation.[13-14] For this study, Y=0.5 cm on the plaque's central axis (i.e. 0.5 cm from interior surface of the sclera in) is taken as the tumour apex. The tumour has been assumed to be on the equator temporal to the eye ball.

C. Ophthalmic applicators

The GE Healthcare/oncura model 6711 for 125 I are focus of this study. COMS standard eye plaques with diameters 12, 16, and 20mm are modeled. Plaques are constructed of the gold alloy Modulay with a density of 15.8 g/cm^3 is less dense than pure gold (19.3 g/cm3). The seed carrier insert is made of silastic which has a density of 1.12 g/cm^3. [14-20]

III. Result and Discussion

In most simulation, the eye plaque is modeled at the center of a 30×30×30 cm^3 water phantom of mass density 0.998 g/cm^3. In this work, simulations in which the eye plaques are modeled in the water phantom are also performed. The effect of the plaque backing alone is studied by performing simulations with one ^{125}I seed in the central slot of 12 and 20 mm plaques with silastic insert replaced with water and backing constructed of pure gold. Figure 2 shows the central axis depth-dose curves for one ^{125}I seed in the said qualification. Doses have been obtained by scoring the energy deposited in an array of 0.5×0.5×0.5 mm^3 voxels, with the first voxel centered on Y=-0.5 mm on the plaque's central axis (i.e. 0.5mm from posterior surface of the sclera) and extending out to the opposite side of the eye from the plaque and tumour. The doses for the various configurations are quoted relative to the doses for the same seed in water (no plaque present, in order to connect with TG-43 type calculations). The values show good agreement with the results provided by Thomson et al[7].

Table 2 shows the average dose in some parts of the eye globe with consideration of 16mm and 12mm plaques. With regard to the definition of plaque near the tumour area, the higher dosage received by tumour compared to that received by lens, is justifiable.

Figure 3 shows the central axis depth-dose curves for fully loaded 16 and 12 mm plaques. Interseed attenuation as an effect of considering multiple plaques, has been shown

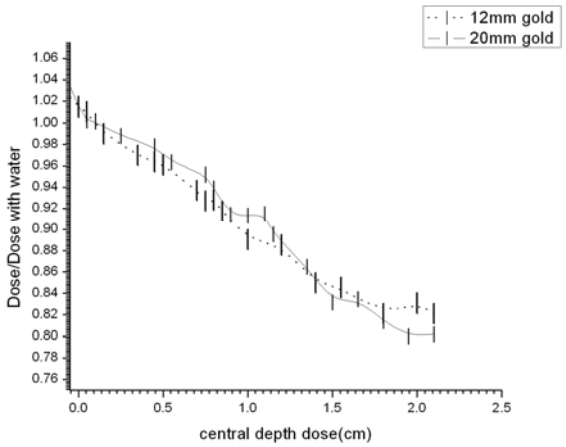

Fig. 2 Ratio of the doses along the plaque's central axes for a single seed at the center of a 12 or 20 mm plaque with a gold backing and water insert to the doses with water (no plaque) ^{125}I

Table 2. Average doses in the eye components due to 16 mm plaque

Eye component	Average dose (Gy $Bq^{-1}s^{-1}$)	
	12mm	16mm
Optic nerve	1.606E-15	1.851E-15
Optic nerve wall	4.633E-16	5.154E-16
Lens	7.376E-15	7.88E-15
Tumour	12.593E-14	12.60E-14
Vitreous body	2.432E-13	2.434E-13
Retina	6.395E-16	6.572E-16
Choroid	9.609E-15	9.995E-16
Sclera	2.935E-14	3.090E-14
Anterior chamber	3.759E-15	4.087E-15
Cornea	1.998E-15	2.270E-15

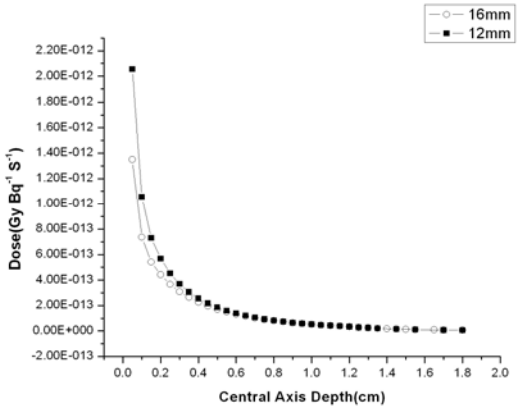

Fig. 3 Central Depth dose curves for 12 and 16mm plaques

in this figure. The comparison has been made afterwards to those calculated by H. Yoryaz et al[13]. this comparison has been made with 20mm plaque. The result have shown good agreement .

IV. Conclusion

By defining eye geometry in a three dimensional manner with the MCNP_4C code and by defining standard sources, the rate of dosage received by different parts of the eye has been examined. With regard to the fact that the final results are in conformity to the results reported by different authorities, this way can be used as the way that mentioned about for remedying different types of tumours with various characteristic.

Refrences

1. Manimaran S (June 2007). "*Radiobiological equivalent of low/high dose rate brachytherapy and evaluation of tumor and normal responses to the dose*". Radiate Med **25** (5): 229–35.
2. Ernest Rand Simpson, MD,FRCS(C) *"Uveal Melanoma Approaches to Management ",* Evidence-based Eye Care, By peter J. Keretes, Thomas Mark Johnson , chapter 13
3. Collaborative Ocular Melanoma Study Group, COMS Manual of Procedures, Ch 13:brachytherapy,physical clinical aspects COMS manual of procedures PB95-179693 (National Technical Information Service, Springfield, VA, 1995)
4. Collaborative Ocular Melanoma Study Group, COMS Manual of Procedures, Ch 12: Radiation therapy, COMS manual of procedures PB95-179693 (National Technical Information Service, Springfield, VA, 1995)
5. "*Adlers Physiology of the Eye"*:Clinical application/ Edited by William M.Hart,Jr , Washington University School of Medicine
6. *"Fundamentals and Principles of Ophthalmology",* Basic and Clinical Science Course, American Academy of Ophthalmology(section 2) (1998-1999)
7. R. M. Thomson, R. E. P. Taylor."*Mont calro dosimetry for ^{125}I and ^{103}Pd eye plaque brachytherapy"* Ottawa Carleton Institude of Physics, Carleton University Campus, 5530-5543,(2008)
8. A.Peratta. "*3D Low frequenvy electromagnetic modeling of the human eye with boundary elements*" Engineering Analysis with Boundary Elements 32 ,726-735 (2008)
9. The Gale Group, *www.scienceclarified.com/Ex-Ga/Eye.html*
10. ICRU, Photon, Electron, Photon and Neutron Interaction Data for Body Tissues,ICRU Report 46, ICRU, Washington D.C., 1986
11. Mazeron JJ, Noël G, Simon JM, Racadot S, Jauffret E (February 2003). "*[Brachytherapy in head and neck cancers]*(in French). *Cancer Radiother* **7** (1): 62–72. PMID 12648718.
12. Merrick GS, Butler WM, Wallner KE, Galbreath RW, Adamovich E (2005). "*Monotherapeutic brachytherapy for clinically organ-confined prostate cancer*". *W V Med J* **101**
13. Helio Yoriyaz, Andrea Sanchez. *"A new human eye model for ophthalmic brachytherapy dosimetry"* Radiation Protection Dosimetry ,316-319,(2005)

14. Sou-Tung Chiu-Tsao, Ph.D. "*Episcleral eye plaques for treatment of intra-ocular Malignancies and benign diseases"* Beth Israel Medical Center & St. Luke's – Roosevelt Hospital Center New York, NY. ABS?AAPM Summer School, Seattle, July 21, 2005
15. J. H. KIM, M.D., Ph. D., and B. HILARIS, M.D. *"Iodine 125 source in interstitial tumour therapy"* J. H. KIM, M.D., Ph.D., and B. HILARIS, M.D. New Yourk. Clinical and Biological Considerations
16. The collaborative Ocular Melanoma Study Group (COMS). "*The COMS Randomiized Trial of Iodine 125 Brachytherapy for Choroidal Melanoma".* COMS report No. 17, Arch. Ophthalmol. 951-965,(2001)
17. Iikka Puusaari, Jorma Heikkonen, and Tero Kivela. "*Effect of radiation Dose on Ocular Complications after Iodine Brachytherapy for Large Uveal Melanoma".* Investigative Ophthalmology & Visual Science. Vol. 45, No. 10 ,3425-3434 (2004)
18. *"Source and their application in brachytherapy"* ICRU , Report 72, Oxford University Press,21-27(2004)
19. J. H. Kim, M.D., PH.D., and B. Hilaris, M.D. "*Iodine 125 Source In Interatitial Tumor Therapy"*clinical and Biological considerations.New York , Vol 123, No 1 , 163-169
20. R. E. P. Taylor and D. W. O. Rogers. "*Amersham OncoSeed, 6711".* The CLRP TG-43 Parameter Database for brachytherapy , Carleton University
21. H. H. Ertl. L. E. Feinendeqen. H. J. Heiniger. *"Iodine-125, a Tracer in Cell Biology: Physical Properties and Biological Aspects."* PHYS. MED. BIOL., Institude of medicine , jermany, 447-456, (1970)

*Author: Somaye Asadi
Institute: K.N. Toosi University of Technology, P.O. Box 15875-4416
Street: Shariati
City: Tehran
Country: Iran
Email: s_asadi@sina.kntu.ac.ir

Radioprotective Effects of Hesperidin against Genotoxicity Induced by Gamma Irradiation in Human Lymphocytes

Seyed Jalal Hosseinimehr[1,2,*], Aziz Mahmoudzadeh[3], Amirhossein Ahmadi[1], Soheila Mohamadifar[3], and Shahram Akhlaghpoor[3,4]

[1]Department of Medicinal Chemistry, Faculty of Pharmacy, Mazandaran University of Medical Sciences, Sari, Iran
[2] Pharmaceutical Research Center, Mazandaran University of Medical Sciences, Sari, Iran
[3]Novin Medical Radiation Institute, Tehran, Iran
[4]Department of Radiology, Faculty of Medicine, Tehran University of Medical Sciences, Tehran, Iran.

[*]Address for correspondence: Tel.& Fax: +98-151-3261244; E-mail: sjhosseinim@yahoo.com, sjhosseinim@mazums.ac.ir

Abstract—**The radioprotective effect of hesperidin against genotoxicity induced by gamma irradiation has been investigated in vivo/ in vitro in cultured blood lymphocytes from human volunteers. Peripheral blood samples were collected from human volunteers at 0 (10min before), and at 1, 2 and 3 h after a single oral ingestion of 250 mg hesperidin. At each time point, the whole blood was exposed in vitro to 150 cGy of cobalt-60 gamma irradiation, and then the lymphocytes were cultured with mitogenic stimulation to determine the micronuclei in cytokinesis blocked binucleated cell.**

For each volunteer, the results showed a significant increase in the incidence of micronuclei after exposed to gamma irradiation as compared to control samples. The lymphocytes in the blood samples collected at 1 h after hesperidin ingestion and exposed in vitro to gamma rays exhibited a significant decrease in the incidence of micronuclei, as compared with similarly irradiated lymphocytes from the blood sample collected at 0 h. The maximum protection and decrease in frequency of micronuclei was observed at 1 h after ingestion of hesperidin with 33%.

This data have important application for the protection of human lymphocyte from the genetic damage and side effects induced by gamma irradiation in patients undergoing radiotherapy

Key words: Hesperidin, Radioprotective, Micronucleus, human,

O. Dössel and W.C. Schlegel (Eds.): WC 2009, IFMBE Proceedings 25/III, p. 13, 2009.
www.springerlink.com

Iranian doctor's knowledge about received dose by patients in diagnostic radiology

[1]Karim Ghazikhanlou Sani

1- Karim Ghazikhanlou Sani, Master of sciences in Medical physics, Faculty member of Hamadan University of Medical Sciences, Department of radiology, Hamadan University of Medical Sciences, Hamadan, Iran. Email: ghazi@umsha.ac.ir

ABSTRACT: The purpose of this study is to investigate the level of doctor's knowledge about radiation doses received by patients in radiological examinations. A questionnaire was compiled and the most commonly requested radiological investigations were listed. Participants were asked to identify the average dose of radiation received by patients when they underwent a posterior-anterior hand x-ray. Most of doctors could not correctly estimate the amount of radiation dose received by patients in a routine radiography of hand and was not aware of annually maximum permissible dose to general Pubic. Some of doctors did not know that sonography and MRI have no radiation dose.

KEY WORDS: doctor's knowledge, radiation, dose, radiological procedures.

INTRODUCTION:

The average radiation dose annually received by general public is 2.5msv, and 15% of them are related to medical exposures [1, 2]. The use of radiation in the medical practice has evolved since its beginning and 30% to 50% of medical decisions are affected by radiologic examinations [3]. However, the hazards of Ionizing radiation are irrefutable. According to recently studies in United Kingdom was estimated that 100-250 death per year occurred because of harmful effects of medical radiation exposures [1, 4]. Awareness of doctors about hazards of radiation is the main factor for decreasing the patients' dose in medical practices [2, 4].

First step in radiation protection can by applied in ordering the Radiologic investigations [3, 4]. Increasing the doctor's knowledge about radiation dose received by patients in different diagnostic Imaging and hazards of radiation led to optimizing the radiologic examination prescriptions [3, 4]. If doctors be aware of radiation dose received by patients in different radiological investigations, they avoid ordering of unnecessary examinations and also could be prescribe counter part examinations with low or without radiation risk [3-5].

Increasing the doctor's knowledge of radiation hazards is a part of radiation protection programs [5]. Instruction the doctors and radiographers besides special regarding to radiation dose delivered in different Imaging modalities seems to be necessary. For correct estimation of patients received dose in different radiologic examinations can be referred to the results of radiation doses surveyed by NRPB in 1980's [6, 7]. In this study doctor's knowledge about radiation dose received by patients undergoing commonly requested radiological examinations and their awareness of radiobiology have been evaluated.

METHODS AND MATHERIALS:

This cross- sectional questionnaire based study was conducted between October 2007 and April 2008. For Implementation of the study, first, a list of commonly requested radiological investigations was conducted. After literature review, correct values of radiation dose received by patients in different investigations were obtained from average values mentioned in these studies [1, 2, 4, 6, 8-15]. Also, UNSCER 2000 published details of radiation doses of radiological examinations in different countries, but there was not advanced data about Iran [16]. We compared the correct values by doses presented in this report, too. Different studies show variations in estimated received dose by patients; therefore, we accepted a deviation of 20% above and below the correct value.

The prepared Questionnaire consisted of 5 main categories. The questionnaire form are presented in table1.

RESULTS:

The results of this study indicate that only 58.3% of doctors (49 GPs, 21 SPs) know the units of radiation absorb dose measurement units. Only 10 (20.4%) GPs could correctly estimate the amount of radiation dose received by patients in a routine

O. Dössel and W.C. Schlegel (Eds.): WC 2009, IFMBE Proceedings 25/III, pp. 14–17, 2009.
www.springerlink.com

Table1: The questionnaire form

	Questions	Correct answer
1	What are the absorb dose measurements units?	Rad, Gy, Sv, Rem
2	How much is the mean radiation received dose by patients in a routine radiography of hand (hand-PA)?	0.02 mSv
3	How much is the annually maximum permissible radiation dose of general public?	1 mSv
4	What is the most sensitive organ to radiation?	Genital organs
5	If we suppose the radiation dose received by patients in a routine radiography of hand (Hand-PA) as unit, what's your estimation of below mentioned radiological examinations proportional to routine radiography of hand?	

	Radiological investigation	Equivalent No of hand x rays
A	Chest-PA	1-10
B	Skull-AP	2
C	Thoracic-AP	20
D	Lumbar-AP	35
E	Abdomen (K.U.B)	35
F	Lumbar-Lat	100
G	Lumbosacral-Lat	175
H	CT of skull	100
J	CT of chest	400
K	CT of abdomen	500
L	Ultrasound of abdomen	0
M	Ultrasound of kidneys	0
N	MRI of abdomen	0
O	MRI of head	0
P	Barium-swallow	125
Q	Barium-follow	75
R	Intravenous urography (I.V.U)	150
S	Barium-enema	350
T	Mammography	70
W	Cerebral Angiography	370
U	Abdominal Angiography	1000
V	Isotope scan of Kidneys (DMSA)	140
X	Thyroid Isotope scan	50

radiography of hand, but none of SPs correctly answered. 17.8% of GPs (15 form 84), and 25% of SPs (9 from 36) was aware of annually maximum permissible dose to general Pubic.

The correct choice about the most sensitive organ to radiation was 81% and 92% by GPs and SPs, respectively.

Results of estimation the received dose by patients in commonly requested radiological examinations proportional to the dose Delivered in a routine radiography of hand, have been shown in Table 1. The percentages of correct, under and over estimate have been shown in this table, as well. 10.7% (9) of GPs did not know that sonography have no radiation dose, but all of the SPs correctly answered this question. Similar question about MRI examination showed that 13% of GPs did not aware of lake of radiation dose in this Imaging modality, although all of the SPs correctly answered.

Table 1: Percentage of doctor's estimations about received dose by patients in commonly requested radiological examinations proportional to the dose delivered in a routine radiography of hand.

Type of examination \ Percentage of estimations		Percentage of general physicians estimations			Percentage of specialists physicians estimations		
		Under estimate	Correct estimate	Over estimate	Under estimate	Correct estimate	Over estimate
Plain radiography	Chest- PA	0%	6.0%	94.0%	0%	8.0%	92.0%
	Skull-AP	0%	15.5%	84.5%	0%	25.0%	75.0%
	Thoracic-AP	58.4%	28.6%	13.0%	50.0%	33.3%	16.7%
	Lumbar-AP	65.5%	27.4%	7.1%	33.4%	33.3%	33.3%
	KUB	70.2%	23.8%	6.0%	75.3%	16.7%	8.0%
	Lumbar-Lat	0%	13.1%	0%	92.0%	8.0%	0%
	Lumbosacral-Lat	83.2%	14.3%	2.5%	92.0%	8.0%	0%
	Barium swallow	47.0%	19.0%	7%	50.0%	16.7%	33.3%
	Barium follow	77.4%	14.3%	8.3%	53.3%	16.7%	30.0%
	I.V.P	76.3%	16.7%	7%	53.3%	16.7%	30.0%
	Barium enema	68.9%	13.1%	0%	92.0%	8.0%	0%
CT Scan	CT-Skull	71.5%	25.0%	3.5%	58.7%	33.3%	8.0%
	CT-Chest	82.1%	25.5%	2.4%	66.7%	33.3%	0%
	CT-Abdomen	79.8%	20.2%	0%	58.7%	33.3%	8.0%
Mammography	Mammography	97.0%	3.0%	0%	87.0%	17.0%	0%
Angiography	Cerebral	78.5%	19.0%	2.5%	66.6%	16.7%	16.7%
	Abdominal	94.0%	6.0%	0%	75.0%	25.0%	0%
Isotope Scan	Kidneys	79.9%	13.1%	7%	83.3%	16.7%	0%
	Thyroid	82.3%	10.7%	7%	61.1%	25.0%	13.9%

DISCUSSION:

Adequate training to doctors is requested to reduce the patients' radiation dose [2, 4]. Implementation of radiation protection courses and education of practical issues, as radiation dose received by patients and radiation safety, during the medical education programs could be an effective method for reducing the patient's dose in medical exposures [3, 4].

The results of the current study demonstrated that awareness of doctor's in the field of radiation dose delivered by Different Imaging modalities is not appropriate. Whereas correct estimation of patients' dose by doctors in the field of plain radiography, CT scan, Contrast media radiography, Mammography and angiography was not appropriate. Most of doctors underestimated the dose Delivered in above mentioned radiological examinations. But Doctor's knowledge about sensitive organs to radiation and low radiation risk examination was Ideal.

To the best of our knowledge there was not the same study in Iran, but similar studies were carried out in other countries. Comparing the results of this study with other similar investigations is shown in Table 2. It must be mentioned that the other similar studies use routine chest x-ray (chest-PA) as the assessment criteria of the dose delivering in other examinations. But because of more variation in the dose delivered in Chest x-ray radiography in the recent studies results, we choose the dose in a hand x-ray as an assessment criterion. Therefore, the differences in some parts may be because of this reason.

Also, it most be noted that most o doctors (about 40 SPs and 70 GPs) didn't admit to participate in this study and didn't read the questionnaire. They claimed that have no awareness about that or have no time for reply.

Table 2: Comparing the results of this study with other similar investigations.

		Awareness about lake of radiation dose in MRI	Awareness about lake of radiation dose in ultrasound	Correct estimation of patients received dose			
				Abdominal radiography	Barium meal	Angiographic examinations	Abdominal CT
Siralkar et al. 2003 in UK [4]		92%	95%	1.5%	5%	-	6%
Arslanoglu et al. 2006 in Turkey [8]		72.6%	96%	0%	1.7%	2.4%	8.2%
Current study	General physicians	88.1%	89.3%	23.8%	14.3%	12.5%	20.2%
	Specialist physicians	100%	100%	16.7%	16.7%	20.8%	33.3%

AKNOWLEDGEMENT:

This study was supported by grants from research deputy of Hamadan University of Medical Sciences (Iran).

REFERENCES:

1- AD Quinn, CG Taylor, T Sabharwal, T Sikdar. Radiation protection awareness in non-radiologists. The British Journal of Radiology 1997; 70:102–106.

2- N Rahman, S Dhakam, A Shafqut, S Qadir, FA Tipoo. Knowledge and practice of radiation safety among invasive cardiologists. JPMA 2008; 58:119-122.

3- M tavakoli, F seilanian Toosi, S Saadatjou. Knowledge of medical students on hazards of ionizing radiation. Journal of medical education spring 2003; 3(1): 3-6.

4- S Shiralkar, A Rennie, M Snow, RB Galland, M H Lewis, K Gower-Thomas. Doctors' knowledge of radiation exposure: questionnaire study. BMJ 2003; 327:371-2.

5- M Victoria Marx. The Radiation Dose in Interventional Radiology Study: Knowledge Brings Responsibility. J Vasc Interv Radiol 2003; 14:947–951.

6- BF Wall, D Hart. Revised radiation doses for typical X-ray examinations. BJR 1997; 70: 437-439.

7- J George, JP Eatouch, PJ Mountford, CJ Koller, J Oxtoby, G Frain. Patient dose optimization in plain radiography based on standard exposure factors. The British Journal of Radiology 2004; 77: 858–863.

8- A Arslanoĺu, S Bilgin, Z Kubal, MN Ceyhan, MN ilhan, I Maral . Doctors' and intern doctors' knowledge about patients' ionizing radiation exposure doses during common radiological examinations. Diagn Interv Radiol 2007; 13:53-55

9- Andrew C Downie. Sarah J Gorse. Doctors' knowledge of exposure to ionizing radiation (letters). BMJ 2003; 327: 1166-1167.

10- BJ Mcparland. A study of patient radiation doses in interventional radiological procedures. BJR1998; 71:175-185.

11- T Smith, I Gordon, JP Kelly. Comparison of radiation dose from intravenous urography and 99TCm DMSA Scintigraphy in children. BJR 1998; 71: 314-319.

12- SP Waddington, AL Mckenzie. Assessment of effective dose from concomitant exposures required in verification of the target volume in radiotherapy. The British Journal of Radiology 2004; 77: 557–561.

13- WR Arthur, J Dhawan, MS Norell, AJ Hunter, AL Clark. Does cardiologist- or radiographer-operated fluoroscopy and image acquisition influence optimization of patient radiation

exposure during routine coronary angiography? The British Journal of Radiology 2002; 75: 748–753.
14- P Dawson. Patient dose in multislice CT: why is it increasing and does it matter? The British Journal of Radiology 2004; 77: S10–S13.
15- Michal Rassin PhD, RN, , Pnina Granat MA, RN, Miri Berger MA, RN and Dina Silner. Attitude and Knowledge of Physicians and Nurses About Ionizing Radiation. Journal of Radiology Nursing 2005; 24(2): 26-30 (Abstract).
16- United Nations Scientific Committee on the Effects of Atomic Radiation. www.unscear.Org/ reports/ 2000_1. Annex D: Medical radiation exposures.

Corresponding author:
Karim Ghazi-khanlou Sani, Department of Radiology technology, Faculty of Para-medicine, Hamadan University of Medical Sciences, Hamadan, Iran.
Telephone: +98 811 8282801
Fax: +98 811 8281442
E-mail: ghazi@umsha.ac.ir

Biological Effect of Single, Very Large Dose Fractions as Used in Intraoperative Radiotherapy (IORT)

C. Herskind, L. Ma, Q. Liu, and F. Wenz

Department of Radiation Oncology, University Medical Center Mannheim, University of Heidelberg. Mannheim, Germany

Abstract— **Intraoperative radiotherapy differs from conventional fractionated radiotherapy by giving a large dose in a single fraction. Various studies suggest that biological effects of dose fractions larger than 5-10 Gy may be different from those induced by conventional fraction sizes. Here, we classify the clinical dose response for different patterns of tumor cells left after surgery. Isoeffective doses of single fractions estimated from fractionated radiotherapy by using the linear-quadratic formalism are consistent with clinical experience from tumor control after radiosurgery. Using a model cell line in vitro, we show that the DNA repair response induced by 6-18 Gy differs from that after 0-2 Gy suggesting saturation of the repair machinery. Possible influences of the tumor microenvironment that may contribute to making very large dose fractions more effective than predicted from clonogenic cell inactivation alone are reviewed.**

Keywords— **Intraoperative radiotherapy, radiobiology, linear-quadratic model, DNA repair, dose reponse**

I. Introduction

Intraoperative radiotherapy (IORT) differs from conventional radiotherapy in several aspects regarding fractionation (single, high dose versus multiple fractions of 1.8-2 Gy/day), total dose (15-25 Gy versus 50-70 Gy) and total treatment time (completion *during* the surgical session versus duration of 5-7 weeks, frequently starting 4-5 weeks after surgery to avoid interfering with wound healing). Furthermore, some treatment modalities involve protracted irradiation with low-energy photons differing in radiation quality (*1; 2*). These differences will impact on the biological effectiveness of IORT in terms of cellular responses such as DNA repair, cell death, recovery, and proliferation after surgery and/or irradiation.

At the moment, estimates of biological effect are based mainly on experimental in vitro and in vivo data obtained with single doses or fraction sizes in the range, 1-10 Gy. Extrapolation of such data usually relies on the linear-quadratic (L-Q) formalism which has not been validated at higher doses. Clinical data on radiosurgery, however, show dose-dependent local control of small solid tumours by single doses of highly localized radiation in the range 15-25 Gy (*3-5*) and it has been suggested that the biological effects in this dose range may be different from effects observed at lower doses (*6*). In the present work we classify clinical dose-response relationships relevant to IORT with single high doses, and test the linearity or non-linearity of the dose-response of DNA repair foci in the low (0-2 Gy) and high (6-18 Gy) dose range.

II. Materials and Methods

Clinical dose response was approximated by logistic functions. Isoeffective doses for single large fractions were calculated by extrapolation of the linear-quadratic (L-Q) formalism to a single fraction:

$$BED = nd\left[1 + d/(\alpha/\beta)\right] = D_s\left[1 + D_s/(\alpha/\beta)\right] \quad (1)$$

Here BED is the biologically effective dose, n is the number of fractions and d the fraction size for fractionated radiotherapy. Equation (1) was solved with respect to the single-fraction IORT dose, D_s, with α/β being the ratio of the linear and quadratic coefficients of the L-Q model.

Chinese hamster V79 cells were cultured in RPMI1640 medium supplemented with 10% fetal bovine serum und incubated at 37 °C under 5% CO_2. The cells were irradiated with 10 MeV electrons from a radiotherapy machine (Siemens) using 20 mm water-equivalent build-up, fixed with methanol 30 or 240 minutes after irradiation and stained with a monoclonal antibody (Millipore) specific for phosphorylated histone γH2AX. After staining with a FITC-conjugated second antibody, the number of γH2AX positive foci was counted in at least 50 cells per condition and the mean number per cell was calculated.

III. Results

Dose-response curves of tumor control probability (TCP) as function of dose usually show a sigmoid curve shape for solid tumours treated with conventional, fractionated radiotherapy (Figure 1). In other cases, such as early breast cancer, radiotherapy is given to the tumour bed after excision of the solid tumor. For this tumor, conventional external

O. Dössel and W.C. Schlegel (Eds.): WC 2009, IFMBE Proceedings 25/III, pp. 18–21, 2009.
www.springerlink.com

radiotherapy with 25 x 2 Gy typically reduces the risk of recurrence from 30% to 10% implying that 70% of the patients are free of recurrence-forming foci (*1*). An additional boost of 16 Gy to the tumour bed further reduces the risk approximately two-fold (*7*). In this case, the dose-response curve is unlikely to be sigmoid and TCP probably shows an increase even after low doses because some patients will have recurrence-forming tumor foci with very few cells (*1*). An intermediate situation may be envisaged where resection of a tumor is incomplete with a few mm^3 of tumour tissue containing 10^5-10^6 cells left in 50% of the cases. This is expected to produce an intermediate sigmoid dose-response curve as shown in figure 1.

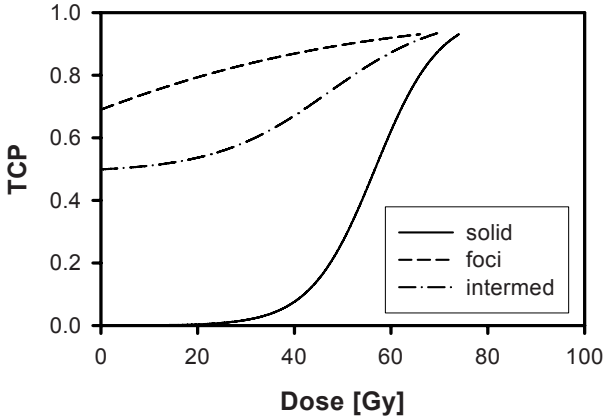

Figure 1. Classification of clinical dose-response curves for tumor control probability (TCP) after conventional, fractionated radiotherapy. Solid tumors show a sigmoid dose-response curve while sporadic tumor cell foci after removal of the primary tumor show a continuously increasing curve. A dose-response curve intermediate between the two is expected after incomplete tumor resection leaving a small amount of residual tumor tissue in 50% of the patients.

For treatment of tumors with IORT, the L-Q model may be used as a first approximation to estimate isoeffective doses of single fractions. Assuming a standard treatment for a solid tumor with 30 fractions of 2 Gy per fraction, the L-Q model with α/β = 10 Gy would predict an isoeffective single dose of 22.3 Gy. This dose is consistent with doses used to control small tumors in different sites with radiosurgery (see Introduction). For tumor-bed irradiation with 25 x 2 Gy after breast-conserving surgery, the L-Q model would predict an isoeffective single dose of 20 Gy. Recent data on hypo-fractionation indicate that α/β for local recurrence of breast tumors may be as low as 4 Gy (*8*), which would yield an isoeffective single dose of 15.4 Gy.

In order to compare the cellular radiation response in the dose ranges used for daily fractionation and IORT, we measured induction and repair of DNA repair foci at 0-2 Gy and 6-18 Gy. Figure 2a shows a linear induction of γH2AX foci 30 minutes after irradiation which was reduced in a linear fashion at 240 minutes indicating that DNA repair was proportional to dose in this range. By contrast, only a moderate, further increase in the number of γH2AX foci occurred in the range 6-18 Gy, indicating saturation of the repair system (Figure 2b). In this dose range, the decrease in the number of foci at 240 minutes owing to repair was constant independent of dose, supporting the hypothesis that the repair system was unable to adapt to the increased amount of damage in a dynamic fashion. Thus γH2AX foci showed non-linearity with dose consistent with saturation of the DNA repair system.

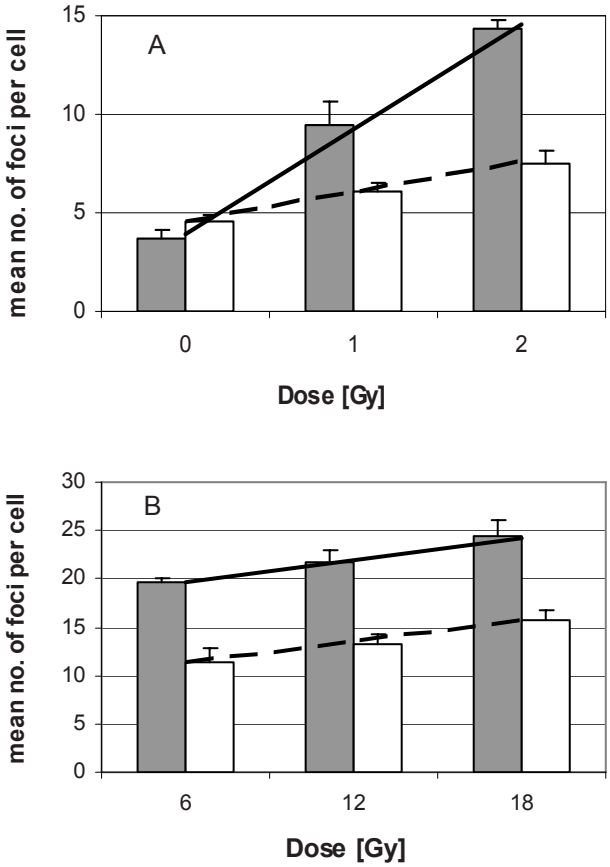

Figure 2. Dose-response for induction and attenuation of γH2AX repair foci in V79 cells. Closed bars represent induction at 30 minutes post-irradiation, open bars represent foci remaining at 240 minutes post-irradiation. Induction of foci proportional to dose was observed in the dose range 0-2 Gy. Repair after 240 minutes was proportional to the amount of damage (A). Non-linear induction of foci with constant amount of repair, independent of dose, was observed in the dose range 6-18 Gy (B).

IV. Discussion

IORT is gaining importance as clinical data in novel indications, e.g. breast cancer, become available. A number of new modalities including mobile linear accelerators and low-energy x-ray machines have been developed. In most cases, IORT is applied to eradicate residual tumour cells after excision of the tumor bulk. Hence the required dose will generally be lower than for sterilisation of solid tumors. For tumor-bed irradiation of sporadic tumour cell foci after breast conserving surgery, even small doses may contribute to reducing the risk of local recurrence since part of the patients are likely to have foci containing very few cells (*1*).

The isoeffective doses calculated from fractionated radiotherapy schedules using the L-Q model are consistent with doses used in radiosurgery to control tumours in various sites (*3-5*). This may appear surprising since the use of the L-Q model for calculating isoeffective doses for single-dose IORT is controversially debated. Thus the L-Q formalism for fractionation has not been validated for fraction sizes larger than 6-8 Gy. Furthermore, some analyses suggest that the L-Q model may overestimate cell killing at high doses (*9*). However, the 'true' shape of in vitro cell survival curves at high doses is extremely difficult to establish because of the requirement to detect single clonogenic cells on a large background of inactivated cells at surviving fractions below 10^{-3} to 10^{-4}. In fact, even details of the experimental design, the composition of the culture medium, and the way cells are handled, may influence the results. In addition, while it is frequently assumed that the α/β ratio determined from fractionation studies is equivalent to the values obtained from in vitro cell survival curves, the equivalence has not been unequivocally proven. For example, it may not hold true for late normal-tissue reaction which is influenced by other factors than clonogenic cell inactivation, such as cytokines (*10*).

Various pieces of evidence suggest that the efficacy of high single doses may be greater than expected from clonogenic cell inactivation alone. Thus clinical and experimental studies on radiosurgery indicate that vascular damage in the stroma may be important (*6*). High doses of radiation may induce apoptosis in microvascular endothelial cells of certain normal tissues, mediated by radiation-induced release of the second messenger, ceramide (*11; 12*). Furthermore, high-dose irradiation may stimulate immunogenic signals (*10; 13-15*) and influence the microenvironment in other ways. Belletti et al. (*16*) recently demonstrated that in vitro stimulation of tumor cell proliferation, migration and invasion by wound fluid isolated from unirradiated breast cancer patients was inhibited in wound fluid from patients who had received IORT according to the TARGIT protocol using low-energy x rays (Intrabeam®, Zeiss Surgical GmbH, Oberkochen, Germany). Thus, if the microenvironment mediates effects of IORT beyond the direct clonogenic tumor cell inactivation this might partly compensate deviations from the L-Q model at high doses. This would argue in favour of using the L-Q formalism as an approximation, for estimating clinical effects of very large dose fractions.

In addition to these clinical effects, the cellular response to radiation may also be different at high compared with low doses. The data on γH2AX foci presented here demonstrate sub-linearity at higher doses, supporting the hypothesis that DNA repair is saturated as the dose increases. Although this may not necessarily translate directly into radiosensitivity measured by the colony formation assay, it emphasizes that biological effects of very large dose-fractions may have a different quality from those induced by conventional fraction sizes. For example, accumulation of damage might result in suboptimal processing of the lesions. One may speculate whether cellular recovery processes such as repair of sublethal damage (SLD), and perhaps also potentially lethal damage (PLD) repair, might be related to the limited capacity of the DNA repair machinery.

The clinical as well as the cellular effects of high doses may help explain the greater than expected efficacy of IORT as a boost in breast cancer (*17; 18*) and of stereotactic body radiation therapy (SBRT) of various tumours (*19*). Finally, the short overall treatment time of IORT eliminates repopulation of residual tumour cells in the time between surgery and the start of conventional external radiotherapy, and during the 5-6 weeks course of fractionated radiotherapy. Thus several biological effects support exploring IORT as an alternative to conventional radiotherapy within controlled clinical studies. However, more experimental studies are needed to obtain quantitative data for high-dose irradiation, and long-term clinical monitoring is mandatory to assess outcome and toxicity of IORT.

V. Conclusions

IORT for residual tumour cells will in general require lower doses than local control of solid tumours. In some cases, the shape of the dose-response curve may show an increase in local control even by low doses. Estimates of isoeffective doses for single fractions using the L-Q formalism are consistent with clinical experience of tumor control after radiosurgery. Saturation of DNA repair processes may lead to increased severity of cellular damage at high doses. Furthermore, clinical effects involving the microenvironment may render large dose fractions more effective than

predicted from clonogenic cell inactivation alone. Further biological studies of high-dose radiotherapy with very few fractions are recommended.

Acknowledgment

This work was supported in part by Zeiss Surgical GmbH, Oberkochen, Germany.

References

1. C. Herskind, J. Griebel, U. Kraus-Tiefenbacher, et al. (2008), Sphere of equivalence--a novel target volume concept for intraoperative radiotherapy using low-energy X rays. *Int. J. Radiat. Oncol. Biol. Phys.* 72, 1575-1581.
2. C. Herskind, V. Steil, U. Kraus-Tiefenbacher, et al. (2005), Radiobiological aspects of intraoperative radiotherapy (IORT) with isotropic low-energy X rays for early-stage breast cancer. *Radiat Res* 163, 208-215.
3. P. C. Gerszten, S. A. Burton, W. C. Welch, et al. (2005), Single-fraction radiosurgery for the treatment of spinal breast metastases. *Cancer* 104, 2244-2254.
4. H. Hof, M. Muenter, D. Oetzel, et al. (2007), Stereotactic single-dose radiotherapy (radiosurgery) of early stage nonsmall-cell lung cancer (NSCLC). *Cancer* 110, 148-155.
5. J. Lutterbach, D. Cyron, K. Henne, et al. (2003), Radiosurgery followed by planned observation in patients with one to three brain metastases. *Neurosurgery* 52, 1066-1073; discussion 1073-1064.
6. J. C. Flickinger, D. Kondziolka and L. D. Lunsford (2003), Radiobiological analysis of tissue responses following radiosurgery. *Technol Cancer Res Treat* 2, 87-92.
7. H. Bartelink, J. C. Horiot, P. M. Poortmans, et al. (2007), Impact of a higher radiation dose on local control and survival in breast-conserving therapy of early breast cancer: 10-year results of the randomized boost versus no boost EORTC 22881-10882 trial. *J Clin Oncol* 25, 3259-3265.
8. J. R. Owen, A. Ashton, J. M. Bliss, et al. (2006), Effect of radiotherapy fraction size on tumour control in patients with early-stage breast cancer after local tumour excision: long-term results of a randomised trial. *Lancet Oncol* 7, 467-471.
9. M. Guerrero and X. A. Li (2004), Extending the linear-quadratic model for large fraction doses pertinent to stereotactic radiotherapy. *Phys Med Biol* 49, 4825-4835.
10. C. Herskind, M. Bamberg and H. P. Rodemann (1998), The role of cytokines in the development of normal-tissue reactions after radiotherapy. *Strahlenther Onkol* 174 Suppl 3, 12-15.
11. H. J. Ch'ang, J. G. Maj, F. Paris, et al. (2005), ATM regulates target switching to escalating doses of radiation in the intestines. *Nat. Med.* 11, 484-490.
12. A. Haimovitz-Friedman, R. N. Kolesnick and Z. Fuks (1997), Ceramide signaling in apoptosis. *Br. Med. Bull.* 53, 539-553.
13. C. Herskind, K. Fleckenstein, J. Lohr, et al. (2004), [Antitumoral action of interferons and interleukins in combination with radiotherapy. Part I: immunologic basis]. *Strahlenther Onkol* 180, 187-193.
14. F. Lohr, C. Herskind, J. Lohr, et al. (2003). *Modification of Radiation Response. Cytokines, Growth Factors, and Other Biological Signals: Medical Radiology. Diagnostic Imaging and Radiation Oncology*. C. Nieder, L. Milas & K. K. Ang (eds). Springer-Verlag: Berlin, Heidelberg, New York, pp 205-226.
15. A. A. Lugade, E. W. Sorensen, S. A. Gerber, et al. (2008), Radiation-induced IFN-gamma production within the tumor microenvironment influences antitumor immunity. *J. Immunol.* 180, 3132-3139.
16. B. Belletti, J. S. Vaidya, S. D'Andrea, et al. (2008), Targeted intraoperative radiotherapy impairs the stimulation of breast cancer cell proliferation and invasion caused by surgical wounding. *Clin. Cancer Res.* 14, 1325-1332.
17. R. Reitsamer, F. Sedlmayer, M. Kopp, et al. (2006), The Salzburg concept of intraoperative radiotherapy for breast cancer: results and considerations. *Int. J. Cancer* 118, 2882-2887.
18. J. S. Vaidya, M. Baum, J. S. Tobias, et al. (2006), Targeted intraoperative radiotherapy (TARGIT) yields very low recurrence rates when given as a boost. *Int. J. Radiat. Oncol. Biol. Phys.* 66, 1335-1338.
19. R. D. Timmerman, B. D. Kavanagh, L. C. Cho, et al. (2007), Stereotactic body radiation therapy in multiple organ sites. *J Clin Oncol* 25, 947-952.

Author: Carsten Herskind, Ph.D.
Institute: Dept. of Radiation Oncology, University Medical Center Mannheim
Street: Theodor-Kutzer-Ufer 1-3
City: D-68167 Mannheim
Country: Germany
Email: carsten.herskind@medma.uni-heidelberg.de

Molecular Mechanisms of Radiation-Induced Second Cancers

C. Herskind and F. Wenz

Department of Radiation Oncology, University Medical Center Mannheim, University of Heidelberg. Mannheim, Germany

Abstract— **Second primary cancers are a rare but relevant late effect of radiotherapy. However few studies have looked into the molecular mechanisms. In this work, basic mechanisms of carcinogenesis, DNA repair and radiation-induced genetic changes are reviewed. Ionizing radiation does not induce changes in specific genes but can inactivate tumor suppressor genes and, more rarely, activate oncogenes in a stochastic fashion. Radiation-induced genomic instability is likely to play a major role, too. A single mechanism is unlikely to explain all second cancers.**

Keywords— **Radiotherapy, carcinogenesis, second primary cancers, DNA repair, genomic instability.**

I. Introduction

With increasing numbers of long-term survivors after cancer therapy, second primary cancer is becoming a relevant late adverse effect of radio- and/or chemotherapy. Although advances in dose delivery have led to smaller treatment volumes, intensity-modulated radiation therapy involves larger total body doses and distribution of dose to larger volumes of normal tissue (1). Radiation does not induce specific types of cancers but increases the frequency of cancer types which also occur spontaneously. Indeed, radiation is a relatively inefficient carcinogen compared with certain chemicals (2). Since no specific marker for therapy-induced cancer is available, second cancers are identified by their increased incidence in patients treated with radiotherapy for primary cancer compared with control patients treated without radiotherapy (1).

Few studies have been made into the molecular mechanisms of second cancers after radiotherapy (3). On the other hand, considerable knowledge of the cellular and molecular response to radiation, and of the molecular genetics of cancer, has been gathered in the past few decades. The purpose of this work was to present an overview of the major molecular mechanisms relevant for induction of second cancers after radiotherapy.

II. Materials and Methods

A number of operational models of carcinogenesis exist based on various types of spontaneous cancers. Molecular concepts that may fit such models are reviewed. Different types of repair of radiation-induced DNA damage are presented and compared with repair of damage induced by other carcinogens. The cellular radiation response detecting DNA damage and regulating DNA repair, genomic stability and elimination of damaged cells by apoptosis is reviewed. Finally, examples are presented how changes in gene expression and regulation of cellular processes may lead to a malignant phenotype and development of second cancer.

III. Results

Basic concepts

Various operational models have been developed to explain the stochastic element and the long latency of carcinogenesis (4). Most of these models involve one, two or more stages and some form of clonal expansion of cells. Some models associate such stages with steps of *initiation* conferring a growth advantage, *promotion* where clonal expansion takes place and *conversion* in which the pre-malignant cell becomes malignant, and which leads to a macroscopic tumour after a certain *lag time*.

Cancer cells are frequently assumed to arise from normal stem cells (5), however they must escape apoptosis or replicative senescence acting as tumor suppressor mechanisms (6-8). Molecular biology studies have identified a number of *oncogenes* and *tumour suppressor genes* that may be responsible for the different steps of carcinogenesis. Generally, oncogenes stimulate proliferation while tumour suppressor genes prevent inappropriate proliferation. If a person has inherited a mutant allele of a tumour suppressor gene from one parent, the cells will be heterozygote for that gene but the other allele is usually sufficient for normal function. However, if the other allele is mutated or lost later, the tumour suppressor function is lost. This is an example of *loss of heterozygosity (LOH)* indicative of genomic instability and mutations involved in malignant transformation. *Genomic instability* is a common feature of cancer cells that may increase the probability of these steps occurring. Genomic instability includes chromosome instability (CIN) associated with breakage and fusion of chromosomes, and microsatellite instability (MIN), i.e. changes in simple sequence repeats (SSR) of microsatellite DNA.

O. Dössel and W.C. Schlegel (Eds.): WC 2009, IFMBE Proceedings 25/III, pp. 22–25, 2009.
www.springerlink.com

DNA repair

Radiation induces a broad spectrum of damage in DNA, including base damage, apurinic sites, single-strand breaks (ssb), double-strand breaks (dsb), DNA-DNA and DNA-protein cross-links, and multiply damaged sites. Although induction is rather unspecific, the types of damage differ from those induced by UV irradiation or alkylating agents. In particular, dsb are induced by few other agents than ionizing radiation.

Normal cells are highly efficient in repairing most types of DNA damage. Different types of base damage induced by UV irradiation or cytotoxic agents are repaired by special forms of base repair showing little overlap with repair of damage induced by ionizing radiation (9). Thus methyl groups induced by alkylating agents are removed by O6-Methylguanine-DNA Methyltransferase (MGMT). UV photoproducts are repaired by photolyases or by nucleotide excision repair, a complex mechanism involving up to 30 different proteins. Other forms of incorrect base pairing are repaired by mismatch repair (MMR).

The broad spectrum of radiation-induced base damage is repaired mainly by base excision repair (BER) of which two major variants exist (10). 'Short-patch' BER replaces only a single nucleotide while 'long-patch' BER replaces 2-13 nucleotides. Short-patch BER repairs a major part of radiation-induced base damage and is essentially error free (9).

DNA single-strand breaks are repaired mainly by short-patch BER (11) while two major pathways exist for dsb repair (9, 12). Nonhomologous end joining (NHEJ) joins DNA ends with minimal homology and operates in all cell cycle phases. Normally, this is done with a low error rate but a variant backup pathway is more error prone leading to increased rate of mutation (13). The other major pathway, homologous recombination (HR), is essentially error free. It requires a second intact copy of the gene and thus operates in the G2 phase of the cell cycle after DNA has been replicated.

Although most DNA damage is correctly repaired, misrepair may lead to cell death or mutation. Unrepaired dsb are considered lethal to the cell. Misrepair of dsb may result in chomosome aberrations, many of which are lethal while others, in particular chromosome translocations, may be stably transmitted to daughter cells. Misrepair can also result in non-lethal deletions in coding sequences. If deletion changes the reading frame this frequently results in premature termination of transcription and C-terminal truncation of the polypeptide product. Furthermore, errors in repair of base damage or single-strand breaks produce point mutations. Thus incorporation of an incorrect nucleotide may change the genetic code of an exon.

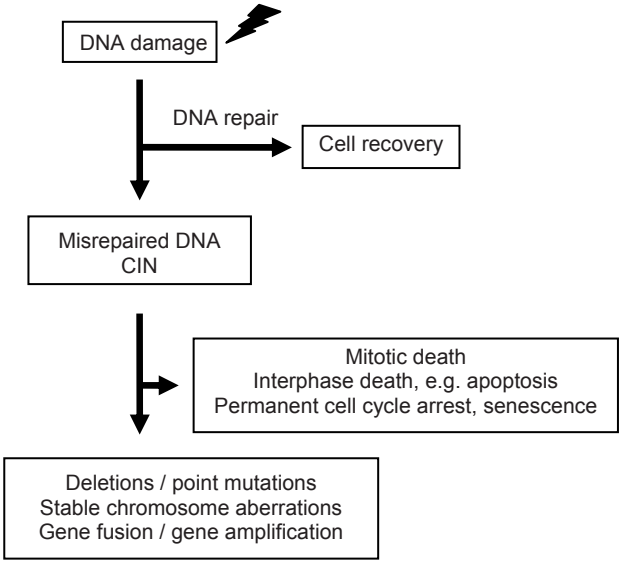

Figure 1. Cellular outcomes of radiation-induced DNA damage after repair and misrepair in normal cells.

The cellular response to radiation is regulated by a complex molecular network involving gene products associated with sensitivity to ionizing radiation and/or increased risk of cancer (14). Dsb are detected by the MRN complex consisting of Mre11, Rad50 and Nibrin, the product of the Nijmegen Breakage Syndrome gene, NBS1 (15). The ATM kinase (the product of the Ataxia Telangiectasia Mutated gene) plays a central role in orchestrating the dsb response, and phosphorylates a number of downstream elements including the tumour suppressor TP53, NBS1, and the breast cancer associated gene 1 (BRCA1) (14, 16). A number of these genes, e.g. NBS1, ATM, BRCA1, and TP53, are also involved in maintaining chromosomal stability thus providing a link between dsb repair and CIN (17, 18). MIN, on the other hand, is associated with an increase in the mutation rate at the nucleotide level caused by a defect in the MMR system and appears to be mutually exclusive with CIN (19).

Types of genes involved in carcinogenesis

Mutations and changes in gene expression can contribute to carcinogenesis at different levels. Thus constant stimulation of proliferation by growth factors or cytokines, such as the epidermal growth factor (EGF) may be caused by activation, gene amplification or autocrine loops. Membrane receptors for such factors, so-called receptor tyrosine kinases (RTK), can be mutated in such a way that permanent signaling occurs in the absence of the ligand as in the case of certain deletions within the EGF receptor (20). Mutation of effector molecules involved in signalling from

RTKs, such as the G-protein RAS, may similarly result in constant activation of signaling in the absence of ligands. However, signaling pathways may also be turned on by inactivation of a negative regulator such as APC in the Wnt/β-catenin pathway in some colorectal cancers. In other cases, activation of an oncogene results from fusion with an unrelated gene leading to inappropriate signaling. A prototype example is chronic myeloid leukemia (CML) with the Philadelphia chromosome in which the ABL oncogene is fused with the BCR gene.

Mutation in genes involved in cell cycle control play an important role in carcinogenesis. A prominent example is inactivation of the retinoblastoma (RB) tumor suppressor gene which inhibits DNA replication. Children predisposed to hereditary retinoblastoma carry a germline mutation in one RB allele, and LOH due to somatic inactivation of the intact allele is a decisive step in malignant transformation. Another tumor suppressor acting on the cell cycle is the cdk inhibitor p16(Ink4a) which is essential for the senescence checkpoint together with TP53 (21). p16(Ink4a) inhibits a cyclin-dependent kinase (cdk) required for cell cycle progression, mediating permanent cell cycle arrest via pRB. Thus cancer cells must overcome the senescence checkpoint that prevents unlimited cell division of progenitor cells. Furthermore, activation of telomerase, a specialized enzyme for extending the teleomeres that stabilize the ends of the chromosomes, is important for immortalization (22).

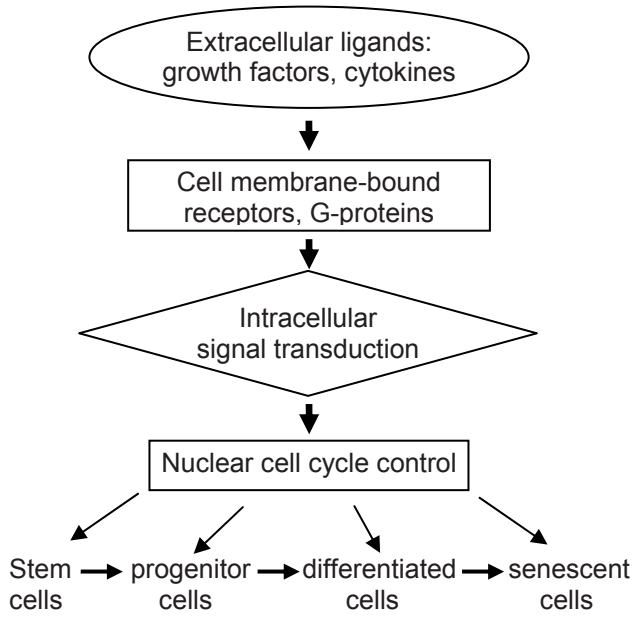

Figure 2. Different levels of proliferation control in a cell lineage of renewing normal tissue. Development of cancer requires loss of homeostasis, involving stimulation of growth signals and loss of anti-growth control.

The different levels of proliferation control are shown schematically in figure 2.

IV. Discussion

Because of the stochastic nature of damage induction by ionizing radiation, mutation of a specific gene is an inefficient process. Furthermore most mutations inactivate the function of a gene product whereas activating mutations are rarer. Therefore, the probability that a particular oncogene is activated by ionizing radiation is low and is mainly associated with gene fusion such as BCR-ABL in the Philadelphia chromosome found in CML. In some cases, deletion of short nucleotide sequences may result in constitutive activation of a signalling component, such as in the case of deletions within EGFR. In general, however, deletions usu ally lead to loss of function. Although one might expect inactivation of tumor suppressor genes to play a major role in second cancers after radiotherapy, the probability is reduced because both alleles must be inactivated unless heterozygosity already exists.

Since oncogenes and tumor repressor genes constitute only a small fraction of the human genome, the probability of mutating a set of different genes cooperating to produce malignancy is relatively low. Therefore, radiation-induced genomic instability may play a major role for the development of malignant changes (23). Notably, genomic instability can be induced in bystander cells receiving little or no irradiation (2). However, it is not known whether genetic instability is a primary event or whether it arises during progression.

In order for genetic instability to be propagated, cells must be tolerant to misrepair and genomic changes, and thus be able to suppress apoptosis or permanent cell cycle arrest induced by the DNA damage and replicative senescence check points. Furthermore, proliferation is necessary for expression and clonal expansion of mutations involved in malignant transformation. This probably explains the long latency period before clinical appearance. The increased relative risk for radiation-induced cancer in young persons may be understood from the inverse relationship between cell proliferation and increasing age. On the other hand, changes in the microenvironment of normal tissue with increasing age may promote tumor formation in older persons (6, 21)

One may speculate whether cancer patients have an increased risk of developing second cancers after radiotherapy. However, a study on the risk of mammography in patients patient with early-onset familial breast cancer, carrying a mutation in BRCA1 or BRCA2, concluded that a highly increased risk of radiation-induced cancer was

unlikely (24). Presumably, this is related to the low probability of radiation-induced inactivation of the second allele.

A wide spectrum of genetic changes is found in different cancers, and genetic variation may be found even within a single tumor. Thus many different combinations of genetic changes may lead to a malignant phenotype, and genomic instability is a frequent feature. Therefore, it is unlikely that a particular sequence of oncogene activation and inactivation of tumor suppressor genes exists which is common to all cancers and must occur for tumor development. Given the stochastic nature of radiation-induced damage it is possible that no single mathematical model will apply to all different types of second malignancies. In fact, one- and two-step models may not apply to most therapy-induced solid tumours (25). The higher relative risk of sarcomas compared with carcinomas, together with their in-field appearance, strongly suggests that different mechanisms of induction may be operating (26).

V. Conclusions

Ionizing radiation is an unspecific carcinogen producing a spectrum of DNA damage different from damage induced other agents, e.g. chemotherapy or UV radiation. Misrepair of DNA dsb results in deletions, chromosome aberrations and genomic instability. Although most gene mutations inactivate the gene product, e.g. a tumor suppressor, some result in permanent stimulation of a growth signaling pathway. In more rare cases, an oncogene can become activated by fusion with an unrelated gene in a stable chromosome translocation. Many different combinations of genetic changes involving stimulation of proliferation, inactivation of different tumor suppressor mechanisms, and genomic instability, can lead to malignant transformation. Therefore, mathematical models developed with a particular tumor system in mind should be carefully validated for the tumor in question before being applied to second cancers.

References

1. Hall EJ. Intensity-modulated radiation therapy, protons, and the risk of second cancers. *Int J Radiat Oncol Biol Phys* 2006;65:1-7.
2. Little JB. Radiation carcinogenesis. *Carcinogenesis* 2000;21:397-404.
3. Travis LB, Rabkin CS, Brown LM*, et al.* Cancer survivorship--genetic susceptibility and second primary cancers: research strategies and recommendations. *J Natl Cancer Inst* 2006;98:15-25.
4. Little MP, Heidenreich WF, Moolgavkar SH*, et al.* Systems biological and mechanistic modelling of radiation-induced cancer. *Radiat Environ Biophys* 2008;47:39-47.
5. Beachy PA, Karhadkar SS, Berman DM. Tissue repair and stem cell renewal in carcinogenesis. *Nature* 2004;432:324-331.
6. Campisi J. Cellular senescence as a tumor-suppressor mechanism. *Trends Cell Biol* 2001;11:S27-31.
7. Collado M, Blasco MA, Serrano M. Cellular senescence in cancer and aging. *Cell* 2007;130:223-233.
8. Hanahan D, Weinberg RA. The hallmarks of cancer. *Cell* 2000;100:57-70.
9. Christmann M, Tomicic MT, Roos WP*, et al.* Mechanisms of human DNA repair: an update. *Toxicology* 2003;193:3-34.
10. Almeida KH, Sobol RW. A unified view of base excision repair: lesion-dependent protein complexes regulated by post-translational modification. *DNA Repair (Amst)* 2007;6:695-711.
11. Caldecott KW. Single-strand break repair and genetic disease. *Nat Rev Genet* 2008;9:619-631.
12. O'Driscoll M, Jeggo PA. The role of double-strand break repair - insights from human genetics. *Nat Rev Genet* 2006;7:45-54.
13. Wang M, Wu W, Rosidi B*, et al.* PARP-1 and Ku compete for repair of DNA double strand breaks by distinct NHEJ pathways. *Nucleic Acids Res* 2006;34:6170-6182.
14. Kastan MB, Bartek J. Cell-cycle checkpoints and cancer. *Nature* 2004;432:316-323.
15. van den Bosch M, Bree RT, Lowndes NF. The MRN complex: coordinating and mediating the response to broken chromosomes. *EMBO Rep* 2003;4:844-849.
16. Deng CX. BRCA1: cell cycle checkpoint, genetic instability, DNA damage response and cancer evolution. *Nucleic Acids Res* 2006;34:1416-1426.
17. Morales JC, Franco S, Murphy MM*, et al.* 53BP1 and p53 synergize to suppress genomic instability and lymphomagenesis. *Proc Natl Acad Sci U S A* 2006;103:3310-3315.
18. Motoyama N, Naka K. DNA damage tumor suppressor genes and genomic instability. *Curr Opin Genet Dev* 2004;14:11-16.
19. Rajagopalan H, Lengauer C. Aneuploidy and cancer. *Nature* 2004;432:338-341.
20. Riely GJ, Politi KA, Miller VA*, et al.* Update on epidermal growth factor receptor mutations in non-small cell lung cancer. *Clin Cancer Res* 2006;12:7232-7241.
21. Campisi J. Senescent cells, tumor suppression, and organismal aging: good citizens, bad neighbors. *Cell* 2005;120:513-522.
22. Wright WE, Shay JW. Telomere biology in aging and cancer. *J Am Geriatr Soc* 2005;53:S292-294.
23. Sigurdson AJ, Jones IM. Second cancers after radiotherapy: any evidence for radiation-induced genomic instability? *Oncogene* 2003;22:7018-7027.
24. Goldfrank D, Chuai S, Bernstein JL*, et al.* Effect of mammography on breast cancer risk in women with mutations in BRCA1 or BRCA2. *Cancer Epidemiol Biomarkers Prev* 2006;15:2311-2313.
25. Allan JM, Travis LB. Mechanisms of therapy-related carcinogenesis. *Nat Rev Cancer* 2005;5:943-955.
26. Brenner DJ, Curtis RE, Hall EJ*, et al.* Second malignancies in prostate carcinoma patients after radiotherapy compared with surgery. *Cancer* 2000;88:398-406.

Author: Carsten Herskind, Ph.D.
Institute: Dept. of Radiation Oncology, University Medical Center Mannheim
Street: Theodor-Kutzer-Ufer 1-3
City: D-68167 Mannheim
Country: Germany
Email: carsten.herskind@medma.uni-heidelberg.de

Diagnostic Reference Levels in Computer Tomography at IPOCFG, EPE

A.R. Roda[1], M.C. Lopes[1], and A.M. Fausto[2]

[1] Medical Physics Department of the IPOCFG, EPE, Coimbra, Portugal
[2] Physics Department of the University of Aveiro, Aveiro, Portugal

Abstract— **In this work we estimated the doses related to the Computer Tomography (CT) for the most frequent clinical examination protocols at the Radiology Department of the Oncology Institute of Coimbra. The dose evaluation methodology followed the European Guidelines. We determined Diagnostic Reference Levels (DRL) in terms of one slice, (Volume) Weighted Computed Tomography Dose Index - ($CTDI_{vol}$) $CTDI_w$, and in terms of complete exam, Dose Length Product – DLP for 3 CT scanners: Siemens Somaton Plus 4, GE HiSpeed LX/i and Siemens Somaton Sensation Open. The results were compared with the European Reference Levels EUR 16262 and with MSCT Bongartz (2004). A sample of 225 adult patients, both male and female, of standard size was selected, with a minimum of 10 patients for each clinical protocol and CT scanner. Local DRL's were assigned as the average of the results for the 3 CT scanners. In general, DRL results are below the European reference levels for all protocols except thoracic, lumbar and sacrum spine. Additionally, effective doses were determined with the ImPACT's CT dosimetry spreadsheet and were compared with those published in ICRP 102. To give more accessible information to the patient and physician, we converted the effective doses in terms of background equivalent radiation time (BERT) using the World average annual dose of 2.4 mSv/year.**

Keywords— **Computer Tomography, Weighed Computer Tomography Dose Index, Dose Length Product, Diagnostic Reference Levels, Effective Dose.**

I. Introduction

Recent EC Radiation Protection Report Data [1] estimates that Computer Tomography (CT) is a radiological modality responsible for 30% to 50% of the collective doses due to medical exposure, although it represents only about 4% of the radiological diagnostic practices. Diagnostic Reference Levels (DRL) are dose constraint levels for medical exposures, concerning the optimization of radiological medical practices. The aim of this concept is to favor the minimization of the patient radiation doses without compromising the quality of diagnostic information.

European DRL's were empirically established in the 1999 European Guidelines on Quality Criteria for Computed Tomography [2] and reviewed in 2004 [3]. They are based on the 3rd quartile (75 percentile) value of the doses distribution for a representative sample of radiological installations. According to the Portuguese Legislation [4], licensees shall be responsible for the establishment of recommendations concerning the optimization of patient radiation doses assuring that medical exposures are in agreement with the European Diagnostic Reference [2]. Furthermore, licensees are responsible for assuring that patient radiation doses are available to the physician who prescribes the examination. In this work we estimate the local DRL's for the CT examination protocols in IPOCFG, EPE, where about 11 260 CT exams are performed annually.

II. Material and Methods

Dose evaluation methodology follows the European Guidelines [2,3]. The study involved a sample of 225 adult patients, both male and female, with an average value of: age (58±14(1σ) years), height (163±10(1σ) cm) and weight (70±11(1σ) kg). A minimum of 10 patients were selected for each CT scanner and each of the following clinical protocols: brain-general, face-sinuses, neck, chest-mediastinum or survey, abdomen-liver and spleen, pelvis-general, cervical spine, lumbar spine, thoracic spine and sacrum vertebra. The evaluated protocols concern 3 CT scanners: Siemens Somaton Plus 4 (P4), GE HiSpeed LX/I (GE) an Siemens Somaton Sensation Open (OPEN). Local DRL's were established, in terms of one slice, (Volume) Weighted Computed Tomography Dose Index - $CTDI_w$ ($CTDI_{vol}$), and in terms of the complete exam, Dose Length Product – DLP, according with Nagel 2000 definition [5], where $CTDI_{vol}$ is the $CTDI_w$ divided by the pitch.

For radiation output measurements we used the RADCAL 9095 electrometer and a 100 mm pencil shaped ionization chamber, model 10×9-3CT, calibrated in air kerma.

$CTDI_{100,air}$ was measured with the ionization chamber in air, at the CT isocenter, perpendicular to axial plane, using a proper support for keeping distance from the CT table. The measurements were performed at reference conditions, meaning sequential mode with the following acquisition parameters: tube voltage (120 kV), tube current (100 mA for GE and OPEN, 110 mA for P4), rotation time (1 second), slice thickness (h=10mm), pitch (p=1), and Scan Field of View (SFOV=250mm). A set of in air measurements were performed to obtain $CTDI_{100,air}$ dependence with the

O. Dössel and W.C. Schlegel (Eds.): WC 2009, IFMBE Proceedings 25/III, pp. 26–29, 2009.
www.springerlink.com

acquisition parameters. The variation of the individual parameters was used to determine the corresponding correction factors.

$CTDI_w$ was determined for different tube voltage combinations, by measuring $CTDI_{100,c}$ e $CTDI_{100,p}$ and using the expression:

$$CTDI_w = \frac{1}{3} CTDI_{100,c} + \frac{2}{3} CTDI_{100,p} \quad [mGy] \qquad (1)$$

where $CTDI_{100,c}$ and $CTDI_{100,,p}$ measurements were performed with the ionization chamber placed respectively at the center and periphery of the 16 cm and 32 cm diameter circular CT dose evaluation phantoms.

Phantom factors for head (H) and body (B), $P_{H/B}$ for different tube voltage combinations were determined using the mathematical expression:

$$CTDI_{w,H/B} = CTDI_{100,air} \cdot P_{H/B} \quad [mGy] \qquad (2)$$

$CTDI_w$ for a particular CT examination series, $CTDI_w(kV,mA,s,h)$, was determined by multiplying the reference $CTDI_{100,air}$, $CTDI_{100,air}(kV_0,mA_0,s_0,h_0)$, by each acquisition parameter correction factor, F_i (i=kV,...,h) and correspondent phantom factor, $P_{H/B}(kV)$.

DLP for the total examination was evaluated using $CTDI_w$ determined for each individual sequence and summing all the sequences involved in each protocol examination according with European recommendations [3].

Average $CTDI_w$ and DLP results for each CT scanner and each protocol were compared with EUR 16262 reference levels published in 1999. For all the protocols where only one CT scanner was involved, these results were established as the IPOCFG, EPE local DRL. For each of the other protocols the local DRL was obtained as the average value of the results for the 3 CT scanners. Since there were no relevant changes in the interpretation of the results for the protocols that involved the 3 CT scanners, we compared the local DRL with only the more recent European DRL published in Bongartz 2004 [3].

Average effective doses for each protocol were calculated with CTDosimetry spreadsheet of the ImPACT[6][7] using 2006 version that provides simultaneously $CTDI_w$, $CTDI_{vol}$ and DLP of each sequence, for a large set of scanners models.

In order to present the dose information in a friendly way to the physician and the patient we used Cameron approach [8], expressing the effective dose of each radiological exam in terms of BERT (Background Equivalent Radiation Time), based on the world average annual dose for natural exposure of 2.4 mSv/yr recommended by the UNSCEAR [9]. For further discussion, we compared the results with the effective doses from ICRP Publication 102 [10].

III. Results and Discussion

Table 1 presents the average acquisition parameters for all CT scanners in each clinical protocol.

Table 1 Sample average acquisition parameters for each clinical protocol (h is the slice thickness and L is the length of the acquisition).

Protocol	kV	mAs	h(mm)	L(cm)	Pitch
Cerebrum	132	236	7.3	7.4	1.0
Skull Base	132	237	2.8	7.6	1.0
Face - Sinuses	120	61	2.3	12.1	0..55
Neck	123	169	3.1	18.5	1..3
Chest	126	141	5.3	26.9	1.4
Abdomen	126	159	5.7	22.4	1.4
Pelvis	125	153	5.3	19.0	1.4
Cervical Spine	123	200	1.8	17.2	0..9
Lumbar Spine	140	250	3.4	20.0	0..9
Thoracic Spine	140	250	3.2	25.3	0..9
Sacro Spine	140	250	3.0	15.0	0..9

All acquisitions used tube voltages in the range 120 to 140 kV, applied mAs of 120 to 200 mAs in the single slice CT, GE and P4, and in the range 60 to 320 mAs for Multislice CT, OPEN. Slice thickness varied in the range 2.5 to 8 mm and pitch ranged from 0.55 to 2.0.

Figures 1 and 2 present respectively, the average $CTDI_w$ and DLP results obtained for each protocols in the 3 CT scanners and compares them with the DRL's of the EUR 16262 [2]. For cervical and sacrum spine we used the reference value for vertebral and paravertebral structures, and for thoracic and lumbar spine we used the reference values for routine abdomen.

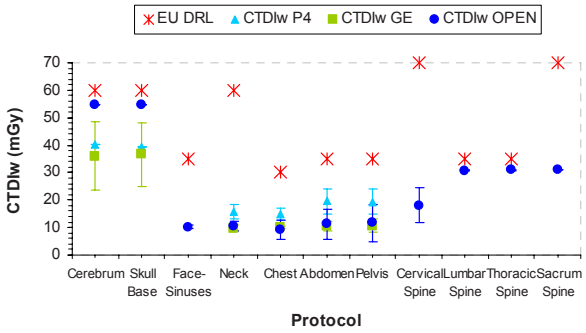

Fig. 1 Comparison of the average $CTDI_w$, with the EUR 16262 DRL for each CT. The bars represent standard deviation for each sample.

For all CT scanners the average $CTDI_w$ ($\pm 1\sigma$) values are below the European DRL for all protocols. For face-sinuses, neck and cervical spine, the results are considerably lower and, for lumbar and thoracic spine the results are of the same order of magnitude of the routine abdomen reference level.

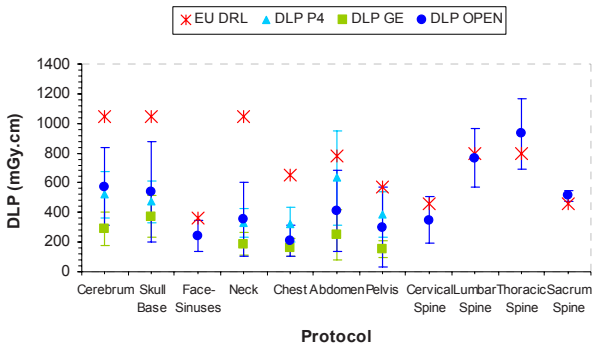

Fig. 2 Comparison of the average DLP, with the EUR 16262 DRL, for each CT. The bars represent standard deviation for each patient sample.

Considering the average DLP, thoracic and sacrum spine results are above and all other protocols are below the European DRL. For face and sinuses, cervical and lumbar spine the results are of the same order of magnitude of the European DRL. Observing standard deviations for DLP we see that some individual results overcome the European DRL in all spine protocols and in the abdomen protocol, for CT P4. In the cerebrum, skull base, neck, chest, abdomen, and pelvis protocols, the complete exam frequently involved different series of acquisitions: one without contrast and in cases like abdomen, 2 or 3 more series, with contrast. This fact explained the DLP results for abdomen protocol in CT P4.

In general, average DLP results for Multi-slice CT (OPEN) were higher and more scattered. Although the technological evolution tendency is to reduce doses with the optimization of practices, faster CT models, facilitate the increasing of the acquisitions length, leading to higher DLP results.

The $CTDI_w$ and DLP results obtained for neck protocol are very low compared to European DRL suggesting further investigation concerning the quality of the images.

Figure 3 shows the results for local DRL in terms of $CTDI_{vol}$ and compares them with the reference values proposed by Bongartz 2004 [3]. For sacrum spine we used the reference value of lumbar and thoracic vertebra-trauma.

Local DRL in terms of $CTDI_{vol}$ for cerebrum, skull base, face and sinuses, neck, chest, abdomen, pelvis and cervical spine are all below the revised European values. These results also apply to the 1999 reference levels.

We know that reference levels revised in 2004 tend to be lower than those published in 1999, but another important change cannot be ignored. The change from $CTDI_w$ to $CTDI_{vol}$ in the revised European reference levels of 2004, gave new importance to the pitch factor. That change, clearly influenced face and sinuses protocol results. With a pitch factor of 0.55 for face and sinuses protocol, the local DRL result considerably increased being now of the same order of magnitude of 2004 DRL. Also, in the case of spine protocols the reviewed DRL's are completely different from the previous value. Even if we choose as reference the value for abdomen (15 mGy), a pitch factor of 0.9 instead of 1.4 would suggest a reference $CTDI_{vol}$ for spine of 23 mGy instead of 15 mGy. This might explain why local DRL for lumbar, thoracic and sacrum spine, largely exceed the 2004 but not the 1999 reference levels.

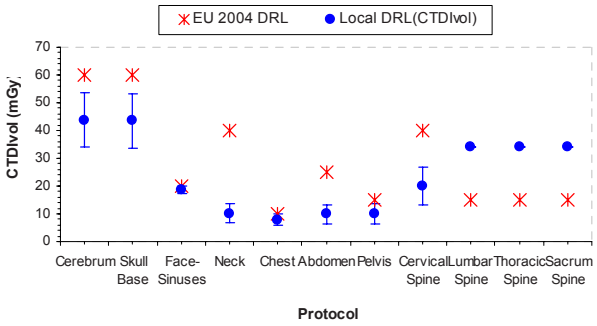

Fig. 3 Local DRL in terms of $CTDI_{vol}$ and comparison with Bongartz 2004 for each protocol. The bars represent the standard deviation for each protocol sample.

Results for spine protocols led to an investigation of the acquisition parameters selected for the protocols. An image quality evaluation is in progress to find if it is possible to change the protocols in order to comply with 2004 DRL.

Table 2 Local DRL in terms of DLP and comparison with Bongartz 2004 European survey results.

Protocol	DLP (mGy.cm)	EU DLP	
		Average	Percentile 75
Cerebrum + Skull Base	937 ± 249	781	945
Face and Sinuses	243 ± 105	210	279
Neck	292 ± 102	-	-
Chest	230 ± 81	350	421
Abdomen	430 ± 193	788	989
Pelvis	280 ± 117	577	688
Cervical Spine	350 ± 154	-	-
Lumbar Spine	767 ± 197	-	-
Thoracic Spine	932 ± 237	-	-
Sacrum Spine	514 ± 36	-	-

Table 2 shows the results for local DRL's in terms of DLP and compares them with the average and 75 percentile results of Bongartz 2004 European survey, when available. It should be noted that DRL in terms of DLP are not defined in the document. Therefore we have followed prior

approaches of choosing the 3rd quartile of the distribution as the relevant reference level using multi-slice values for face and sinuses.

Comparing cerebrum and skull base total DLP with cranium-acute stroke protocol from Bongartz, we are within the 3rd quartile of the DLP European survey, which is also true for face and sinuses chest, abdomen and pelvis. The decrease in reference levels since 1999 more significant in chest protocol did not change our results.

For the other protocols we lack revised European reference values for comparison. Nevertheless thoracic and sacrum spine protocols already exceeded the DLP reference level from 1999, and the $CTDI_{vol}$ values were higher. Also spine exam prescriptions do not generally specify the length to scan, leading to scans of the whole spine instead of a selected region. If the tendency is to progressively lower the reference levels, we can state that our local DRL for spine protocols will certainly exceed the European values.

The average effective doses for each protocol and BERT conversion are expressed in Table 3, along with effective doses from ICRP Publication 102 [10] for comparison. As we expected, effective doses for spine exams are considerably high.

Table 3 Average Effective Doses and BERT conversion for each protocol, and effective doses from ICRP 102 (Brix et al) [10] for comparison.

Protocol	E (mSv)	BERT	$E_{ICRP102}$ (mSv)
Cerebrum + Skull Base	2.4	12 months	2.8
Face and Sinuses	0.6	3 months	0.8
Neck	2.5	13 months	2.0
Chest	4.5	23 months	5.7 - 6.2
Abdomen	8.0	40 months	7.2 - 8.8
Pelvis	6.9	34 months	8.7 - 11.5
Cervical Spine	3.3	17 months	2.9
Lumbar Spine	14.7	6 years	8.1
Thoracic Spine	18.4	8 years	-
Sacrum Spine	13.6	6 years	-

IV. Conclusions

The IPOCFG, EPE local DRL's are in agreement with the revised European DRL's for all the protocols, except lumbar, thoracic and sacrum spine. For these CT exams, both scan parameters and volume of acquisition need further investigation. Nevertheless, it is possible that our local DRL will remain above the 3rd quartile of the European surveys, since we are an Oncology Hospital and deal with very specific radiological imaging prescriptions. It seems important to fill in the gap and establish specific European reference levels for metastases evaluation spine protocols that are lacking in Bongartz 2004 publication and also in EUR 16262.

Acknowledgment

The authors acknowledge and thank the medical and technician staff of the Radiology Department of the Oncology Institute of Coimbra for providing valuable input to the study.

References

1. European Commission Radiation Protection Nº154. European Guidance on Estimating Population Doses from Medical X-Ray Procedures, 2008
2. European Commission, Office for Official publications of the European Communities, Quality Criteria for Computed Tomography, EUR 16262, Luxembourg, 1999
3. Bongartz el al (2004) European Guidelines for Multi-slice Computer Tomography, Funded by European Commission, March 2004, Contract number FIGM-CT2000-20078-CT-TIP
4. Decree-law nrº 180/2002 of 8 of August, Diário da República, I Série A nº 182, pp 5707-5743, 2002
5. Nagel H D, (2000), Radiation Exposure in Computed Tomography: Fundamentals, Influencing parameters, Dose Assessment, Optimization, Scanner Data, Terminology, COCIR – European Coordination Committee of the Radiological and Electromagnetical Industries, 2nd edition, December, 2000
6. Jones D G, Shrimpton P C, Normalized organ Doses for X-ray Computed Tomography Calculated using Monte Carlo Techniques, Software Report NRPB-SR250 publication, 1993, http://www.impactscan.or
7. Jones D G, Shrimpton P C, Survey of CT practice in the UK Part 3: Normalized organ Doses for X-ray Computed Tomography Calculated using Monte Carlo Techniques, NRPB-R250 publication, December 1991
8. Cameron J R (1999), A radiation Unit for the Public, Physics and Society News 20:2, 1991
9. United Nations Scientific Committee on the Effects of Atomic Radiation, Sources and Effects of Ionizing Radiation, Volume I, SOURCES UNSCEAR 2000, Report to the General Assembly with Scientific Annexes, United Nations sales publication, 2002
10. International Commission on Radiological Protection, Managing Patient Dose in Multi-Detector Computed Tomography (MDCT), Annals of ICRP publication 102, March 2007.

Address of the corresponding author:

Author: Ana Rafael Roda
Institute: Portuguese Oncology Institute Francisco Gentil of Coimbra
Street: Av. Bissaya Barreto, nº 98
City: 3000-075 Coimbra
Country: Portugal
Email: a.roda@ipocoimbra.min-saude.pt

Estimation of External Natural Background Gamma Rays Doses to the Population of Caspian Coastal Provinces in North of Iran

A. Shabestani Monfared

Department of Medical Physics, Babol University of Medical Sciences, Babol, Iran

Abstract—**The effect of natural background radiation on health is still challenging. However, it is cleared that it depends on dose received by population. The estimation of external natural background gamma rays doses to the population of Caspian coastal provinces in north of Iran was the main goal of study. Gamma rays was measured using calibrated radiation survey meter in random 51 urban and rural health centers to estimate the exposure to population (Total population = 6888118 persons) in residential areas of Gilan, Mazandaran and Golestan (Total area 59240 Km^2) as Caspian coastal provinces in north of Iran. Results showed that the average dose rate in the area under study is about 60.37±14.88 nSv/h or 0.53 mSv/yr (Range 30 to 90 nSv/h or 0.26 to 0.79 mSv/yr). The data from Ramsar is excluded from the estimation because of a very high natural background radiation found in that area (Max. 240 mSv/yr). No significant difference was found between the doses of the provinces (P=0.237). The external natural background gamma rays doses to the population of Caspian coastal provinces in north of Iran was found to be nearly equal to the average value in the world (0.5 mSv/yr). Further national studies are suggested.**

Keywords— **Background radiation, Gamma rays, Caspian sea, Iran**

I. Introduction

Large populations all over the world continue to be exposed to natural background radiation [1]. It can be noted that the biological effects of relatively high doses of radiation have been known a little after the discovery of X–ray and radioactivity. The best scientific evidence of human radiation effects initially came from epidemiologic studies of atomic bomb survivors in Hiroshima and Nagasaki. However, the effect of the natural background radiation at low and very low doses on human health is still the matter under discussion [2]. Therefore the first step for determining health effects of radiation is measuring dose. The natural background radiation dose/dose rate is investigated by many researchers in various parts of the world and a wide range of results are reported [3, 4, 5]. The estimation of external natural background gamma rays doses to the population of Caspian coastal provinces in north of Iran was the main goal of study.

II. Materials and Methods

Environmental terrestrial gamma radiation dose rates were measured using a Geiger survey meter (Graetz X5CPlus – Germany) calibrated by Iranian Atomic Energy Organization (IAEO) in random 51 urban and rural health centers to estimate the exposure to population (Total population = 6888118 persons and total area 59240 Km^2) in residential areas of Gilan (Population = 2658902 persons, Area 14711 Km^2), Mazandaran (Population = 2602008 persons, Area 24091 Km^2) and Golestan (Population = 1627208 persons, Area 20438 Km^2) as Caspian coastal provinces in north of Iran. We used local health centers as dosimetry places because of 98.9% coverage of population for health services. Data were analyzed using ANOVA in SPSS-16 software. Figure 1 shows the total area under study.

Fig. 1 The total area under study

O. Dössel and W.C. Schlegel (Eds.): WC 2009, IFMBE Proceedings 25/III, pp. 30–32, 2009.
www.springerlink.com

III. RESULTS

Table 1 shows the results of the study for Gilan Province.

Area Name	Province	Dose Rate (nSv/hr)
Somesara/Hendkhale/Markaz	Gilan	69
Somesara/Hendkhale/Khane		49
Somesara/Laksar		44
Somesara/Nargestan		55
Somesara/Chamsaghal		56
Somesara/Sookhiande		72
Amlash/Girgooraber/Markaz		60
Amlash/Girgooraber/Khane		73
Amlash/Kashkoor		78
Shaft/Choobar		70
Shaft/Bijarsar		65
Shaft/Mobarakabad		50
Astara/Sayadlarcheran		55
Astara/Gilde		57
Astane/Sakookalaye		40
Astane/Lashkam		87
Astane/Sookhtehkooh		90
Mean ± SD		62.94 ± 14.31

Table 2 shows the results of the study for Golestan Province

Area Name	Province	Dose Rate (nSv/hr)
Kordkooy/Alang	Golestan	56
Kordkooy/Chardeh		55
Ramian/Sadabad		62
Ramian/Arazgol		61
Gonbad/Gavaznitape		67
Gonbad/Sarli		62
Kalaleh/Malaysheykh		80
Kalale/Ginglik		70
Kalaleh/Soofisheykhdaz		75
Mean ± SD		65.33 ± 8.43

Table 3 shows the results of the study for Mazandaran Province

Area Name	Province	Dose Rate (nSv/hr)
Mahmoodabad/Azadmon	Mazandaran	56
Mahmoodabad/bonde		55
Amol/Amol		62
Amol/Noori		61
Amol/Tajan jar/olia		67
Amol/Tajanjar/sofla		62
Amol/ Tajanjar/ansari		80
Tonkabon/Sharifabad		70
Tonkabon/Lashtoo		75
Tonkabon/Darvishsara		50
Sari/Khoramabad		65
Sari/Shahableylam		45
Sari/Zavarmahale		60
Savadkooh/Zirab		61
Savadkooh/Zirabbala		52
Savadkooh/Madan		50
Galoogah		62
Galoogah/Lamrask		30
Galoogah/Tirtaj		30
Galoogah/Sarajmahale		75
Galoogah/Ghalepayan		30
Chaloos/Marzanabad		68
Chaloos/Toolir		30
Chaloos/Pardangoon		40
Chaloos/Shahrestan		84
Mean ± SD		56.84 ± 16.56

Results showed that the average dose rate in the total area under study is about 60.37±14.88 nSv/h or 0.53 mSv/yr (Range 30 to 90 nSv/h or 0.26 to 0.79 mSv/yr). The data from Ramsar is excluded from the estimation because of a very high natural background radiation found in that area (Max. 240 mSv/yr) [6,7]. No significant difference was found between the doses of the provinces (P=0.237).

IV. Discussion

Results show that the Mean dose rate in the area under study is 60.37 nSv/h or 0.53 mSv/yr. The average radiation dose rate in some parts of Nigeria is reported by Ajayi et al as 60 nGy/h which is equal with the results of the present study [3]. Harb et al in Egypt and Lu & Zhang in China have reported the natural background radiation level about 10 times lower than the similar value in the present study [8, 9]. The terrestrial gamma radiation dose rate in north-west areas and Punjab province of Pakistan (0.34 and 0.28 mSv/y respectively) which were investigated by Rahman et al and Fatima et al in 2008 (10, 4) are about one-half of the mean dose rate of the present study. Also El-Taher et al from Egypt [11], Osmanlioglu et al from Turkey [5] and Oyedele from Namibia [12] have measured the dose rate from environmental radioactivity about 45 nGy/h, 0.06 and 0.07 mSv/y respectively which are much lower than the 0.53 mSv/y in the present study especially in two latter cases. Zunic et al have measured the level of natural radiation exposure to the population of rural population of Yugoslavia as high as 430 nGy/ h [13] which is much higher than the measured values in the present study.

V. Conclusions

The external natural background gamma rays doses to the population of Caspian coastal provinces in north of Iran was found to be nearly equal to the average value in the world (0.5 mSv/yr). It seems that the values of terrestrial gamma radiation dose rate vary over different soil types and for different underlying geological characteristics present in the various study areas. Further national studies are suggested.

Acknowledgment

We would like to thank Mr. Nasrollahpoor Shirvani and their colleagues for providing dosimetry data.

References

1. Karam PA, Leslie SA. (1999) Calculations of background beta – gamma radiation dose through geologic Time. Health Phys. 77: 662-667.
2. UNSCEAR. Sources and effects of ionizing radiation.. United Nations scientific committee on the effects of atomic radiation (UNSCEAR),New York, 2000.
3. Ajayi OS, Ibikunle SB, Ojo TJ.(2008). An assessment of natural radioactivity of soils and its external radiological impact in southwestern Nigeria. Health Phys. 94(6):558-66
4. Fatima I, Zaidi JH, Arif M, Daud M, Ahmad SA, Tahir SN. (2008) Measurement of natural radioactivity and dose rate assessment of terrestrial gamma radiation in the soil of southern Punjab, Pakistan.Radiat Prot Dosimetry. 128(2):206-12.
5. Osmanlioglu AE, Kam E, Bozkurt A. (2007) Assessment of background radioactivity level for Gaziantep region of southeastern Turkey.Radiat Prot Dosimetry . 124(4):407-10.
6. Ghiassi-nejad M, Mortazavi SMJ, Cameron JR, Niroomand Rad A,Karam PA. Very high background radiation areas of Ramsar , Iran. Preliminary Biological studies. Health Physics, 82(1) , 87-93 , 2002 .
7. Sohrabi M, Recent radiological studies of high level natural radiation areas of Ramsar. ICHLNR , 3-7 , 1990 .
8. Harb s. Natural Radioactivity and External Gamma Radiation Exposure at the Coastal Red Sea in Egypt. Radiat Prot Dosimetry. 2008 130(3):376-84.
9. Lu X, Zhang X. Measurment of Natural Radioactivity in Beach Sands From Rizhao Bathing Beach,China.Radiat Prot Dosimetry. 2008 130(3):385-8.
10. Rahman S, Matiullah , Mujahid SA, Hussain S. Assessment of the radiological hazards due to naturally occurring radionuclides in soil samples collected from the north western areas of Pakistan. Radiat Prot Dosimetry. 2008;128(2):191-7.
11. El-Taher A, Uosif MA, Orabi AA. Natural radioactivity levels and radiation hazard indices in granite from Aswan to Wadi El-Allaqi southeastern desert, Egypt. Radiat Prot Dosimetry. 2007;124(2):148-54.
12. Oyedele JA. Assessment of the natural radioactivity in the soils of Windhoek city, Namibia, Southern Africa. Radiat Prot Dosimetry. 2006;121(3):337-40.
13. Zunic ZS, McLaughlin JP, Walsh C, Birovljev A, Simopoulos SE, Jakupi B, Gordanic V, Demajo M, Trotti F, Falk R, Vanmarcke H, Paridaens J, Fujimoto K. Integrated natural radiation exposure studies in stable Yugoslav rural communities. Sci Total Environ. 2001 May 14;272(1-3):253-9.

Author: Dr. Ali Shabestani Monfared
Institute: Babol University of Medical Physics
Street: Ganjafrooz
City: Babol
Country: Iran
Email: monfared_ali@yahoo.com

Patient dosimetry and image quality in conventional diagnostic radiology: a practical optimization experience from a Serbian hospital

O. Ciraj-Bjelac, D. Arandjic, D. Kosutic, M. Kovacevic

Vinca Institute of Nuclear Science, Radiation and Environmental Protection Department, Belgrade, Serbia

Abstract— **The optimization of image quality vs. patient dose is an important task in medical imaging. Maximal validity of optimization has to be based on clinical images. Simultaneous measurement of patient dose levels and image quality assessment is used to investigate possibilities for dose reduction and maintain image quality. The survey was conducted in a general hospital performing more than 60000 images annually and representing typical Serbian practice. For five most frequent diagnostic projections patient exposure was measured using kerma area product meter. Image quality was assessed by experienced radiologists using "European Guidelines on Quality Criteria for Diagnostic radiographic Images". Following examination types were included into the survey: chest PA, chest LAT, pelvis AP, lumbar spine AP, lumbar spine LAT and pelvis. Comparing actual radiographic technique with recommended technique in European Guidelines, modification of practice was proposed and implemented and image quality was re-assessed. At least 10 adult patients were followed for each projection, before and after corrective actions. Large dose saving without compromising diagnostic information were found for some examination types, showing that this simple method is very efficient dose reduction tool in conventional diagnostic radiology. Also, need for staff training and difficulties related to practical implementation of optimization methods in Serbia were discussed.**

Keywords— **diagnostic radiology, patient dose, image quality, optimization**

I. Introduction

The optimization of image quality vs. patient dose is an important task in medical imaging [1,2]. The effective use of ionizing radiation in diagnostic radiology involves the interplay of three factors: image quality, radiographic technique and patient dose [3, 4]. Maximal validity of optimization has to be based on clinical images [5].

II. Materials and methods

Simultaneous measurement of patient dose levels and image quality assessment is used to investigate possibilities for dose reduction and maintain image quality.

The survey was conducted in a local hospital performing more than 60 000 images annually and representing typical Serbian practice.

Three most frequent diagnostic procedures (five projections) were included into the study. Initially, skull radiography PA and LAT was part of the study as well, but the number of patients was not enough to make any valid conclusions with the specified timeframe.

Preliminary, image quality was assessed by experienced radiologists using "European Guidelines on Quality Criteria for Diagnostic radiographic Images" [5]. Following examination types were included into the survey: chest PA, chest LAT, pelvis, lumbar spine AP and lumbar spine LAT based on their frequency.

Comparing actual radiographic technique with recommended technique in European Guidelines [5], modification of practice was proposed and implemented. Then image quality was re-assessed in the subsequent study. At least 10 adult patients were followed for each projection, before and after corrective actions.

Radiography examinations were performed using two relatively new imaging systems. Innomed x- ray system was used exclusively for chest radiography; while Philips unit was used for other examination types. The later was equipped with Automatic Exposure Control (AEC) setting. The basic features on x-ray units used for this study are shown in the Table 1.

Table 1 Characteristics of radiography units enrolled in the study

Manufacturer and model	Philips Duodiagnost	Innomed TOP X HF
Generator	High frequency	High frequency
Installation date	2002	2002
Radiographic device	Grid table	Grid table/vertical stand with grid
Nominal focal spot	0.6mm/1.2mm	0.6mm/1.2mm
Anti-scatter grid	r=12; 36/cm	r=10; 40/cm
Screen film nominal class	400	400
Screen type	CEA G 400	CEA G 400
Film type	Kodak MXG	Kodak MXG
AEC	yes	no
Radiation output (80 kVp, 100cm)	62 μGy/mAs	88 μGy/mAs
HVL (80 kVp)	3.3 mm Al	2.6 mm Al
Total filtration	3.7 mm Al	2.1 mm Al

Quality Control test were performed on both units prior the study. Both units met stated criteria [6]. The exception was low filtration in the unit used for chest radiography.

O. Dössel and W.C. Schlegel (Eds.): WC 2009, IFMBE Proceedings 25/III, pp. 33–36, 2009.
www.springerlink.com

For the purpose of patient dose assessment kerma are product was measured for each patient. Using these results and data on field size and geometry Entrance surface air kerma was calculated accordingly [7], for the purpose of comparison with Diagnostic Reference Levels [5]. Dose surveys were performed before and after corrective measures, alongside with image quality assessment.

Image quality was assessed by two experienced radiologist using well known European Quality Criteria [5]. Following examination types were enrolled: chest PA and LAT, pelvis and lumbar spine AP and LAT. Skull radiography was eventually omitted for before mentioned reasons. Each criterion for particular examination as given in European guidelines was assessed with yes or now, i.e. fulfilled or not.

General image quality assessment included optical density, contrast, sharpness and beam limitation [5]. These were assessed visually by radiologists, using yes or now for each. Then, the assessment results were summed for each film. Finally, each film was assigned with a mark from 1 to 4 with respect to its acceptability (1=fully acceptable, 2=probably acceptable, 3=only acceptable in limited clinical conditions and 4=unacceptable).

After preliminary image quality assessment staff was instructed to change their working habits where appropriate. In practice, this means that exposure factors were changed and tube filtration was increased. As a base, recommended radiographic techniques from European guidelines were used. It is worth mentioning, that operators were not willing to change their working habits willingly.

III. Results

Table 2 presents results on radiography technique, patient dose measurements and image quality assessment for preliminary and subsequent study. Also, the percentage of images which had all criteria fulfilled is shown in the Table 2.

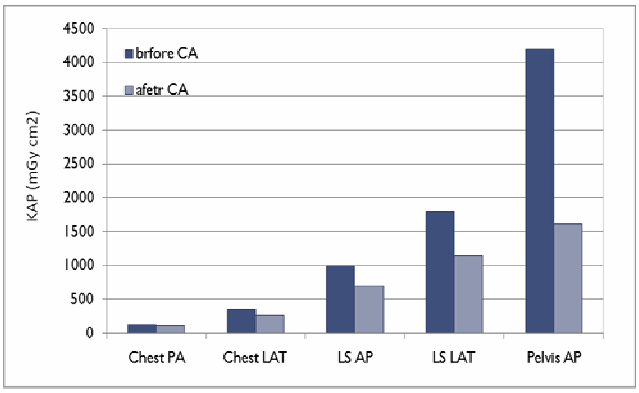

Fig. 1 Results of patient dose measurements before and after implementation of corrective actions (CA)

Figure 1 presents patient dose values before and after implementation of corrective actions. A decrease in dose values up to 60% can be observed. Figure 2 presents data on general film assessment for preliminary and subsequent study, respectively.

Table 2 Typical radiography technique, patient dose and image quality before and after introduction of corrective measures

Procedure	N	U (kVp)	Q (mAs)	FFD (cm)	KAP (mGy·cm^2)	ESD (mGy)	No of criteria	All criteria fulfilled (%)	General film acceptability (%) 1	2	3	4
Before corrective action												
Chest PA	38	66±1	5±1	150	125±8	0.16	10	24	40	40	20	0
Chest LAT	10	85±3	8±0	150	356±48	0.46	10	30	50	30	20	0
LS AP	19	90±2	15±9	100	1000±500	3.1	7	79	84	16	0	0
LS LAT	19	133±2	15±5	100	1800±700	5.6	9	74	68	16	10	6
Pelvis AP	10	64±7	96±55	100	4200±2100	6.6	7	80	80	20	0	0
After corrective action												
Chest PA	27	70±3	5±1	150	116±11	0.15	10	34	40	48	12	0
Chest LAT	10	86±3	8±0	150	259±37	0.34	10	50	50	30	20	0
LS AP	17	90±0	10±7	100	700±360	2.2	7	88	88	6	6	0
LS LAT	17	133±2	9±4	100	1140±520	3.6	9	88	94	0	4	0
Pelvis AP	11	80±4	18±8	100	1610±640	2.5	7	91	80	20	0	0

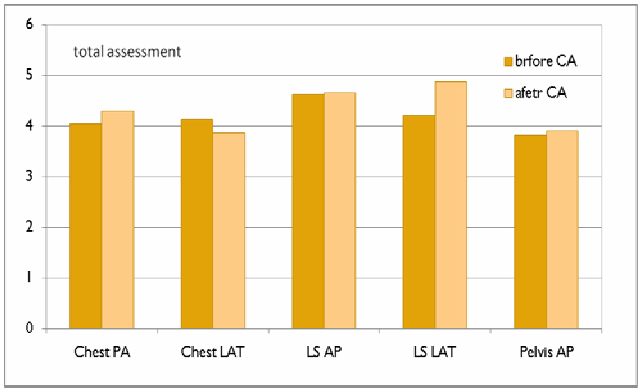

Fig. 2 Results of general image quality assessment before and after implementation of corrective actions (CA)

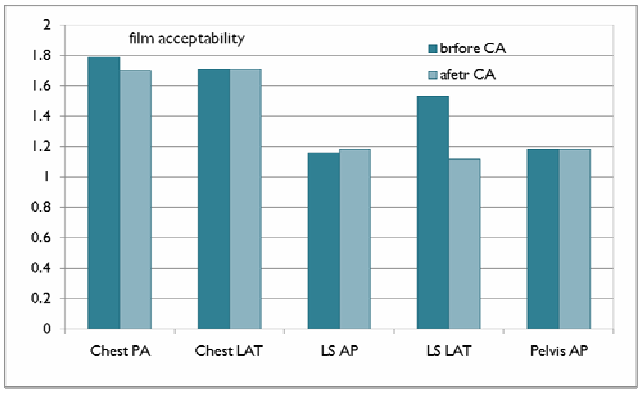

Fig. 3 Results on the film acceptability assessment before and after corrective actions before and after implementation of corrective actions (CA)

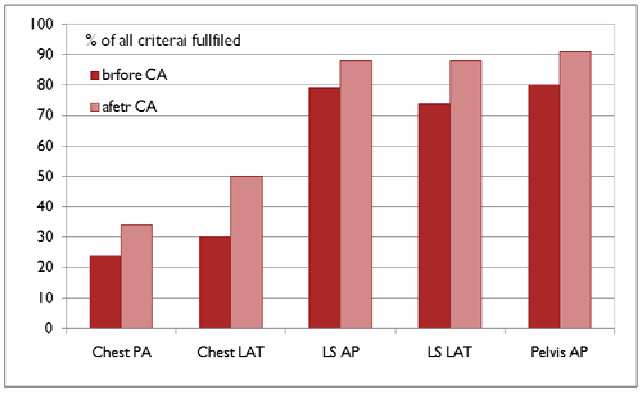

Fig. 4 Fulfillment of image quality criteria before and after corrective actions before and after implementation of corrective actions (CA)

Results on the film acceptability assessment, before and after corrective actions, are presented in Figure 3, while Figure 4 presents the degree of compliance with diagnostic requirements according to European quality criteria, again before and after corrective actions. Apparently, there is a considerable degree of overall compliance of resulting scope for both preliminary and subsequent study. It should be noted that both radiologist were close in assessments of image quality and film acceptability.

IV. Conclusions

Similarly to finding from previous studies [2-4,8-9], preferences of softer images were used to justify application of low kVp values, particularly in chest radiography. Staff was not even aware that it is possible to use hard-beam technique. There was also a degree on non-compliance for a few specific criteria. An outstanding example, in the case of Chest PA radiography, is criteria on "visualization " of the spine thought the hart shadow". By using high kVp values, this particular criterion was not fulfilled. However, it appears that it is not critical for overall image quality assessment. It should be noted that equipment for QC of viewing boxes was not available during the survey.

Also, it is worth mentioning that for the participating staff it was the first to be involved in project of this kind, particularly to perform image quality assessment. In spite of their enthusiasm, it was not possible to carry on without permanent presence of a medical physicist on site. This is not the case in Serbian practice, since hospitals do not have medical physic departments focused on diagnostic radiology and medical physics service in this filed is provided by external technical services on annual basis.

Large dose saving without compromising diagnostic information were found for some examination types, showing that this simple method is very efficient dose reduction tool in conventional diagnostic radiology.

The usefulness of European quality criteria was demonstrated.

References

1. Muhogora W, Rehani M, Ciraj Bjelac O, et al. (2008) Patient doses in radiographic examinations in 12 countries in Asia, Africa and Eastern Europe - Initial results from IAEA projects. Am J Roent. 190: 1453-1461
2. Ciraj O, Markovic S, Kosutic D (2005) First results on patient dose measurements from conventional diagnostic radiology procedures in Serbia and Montenegro. Rad Prot Dosim 113:330-335
3. Ciraj Bjelac O, Loncar M, Kosutic D, Kovacevic M, et al. (2007) Patient Doses and Image Quality in Chest Radiography: the Influence of Different Beam Qualities, Nuclear Technology and Radiation Protection 22: 48-52
4. W. E. Muhogora and A. M. Nyanda (2001) Experiences with the European guidelines on quality criteria for radiographic images in Tanzania. Journal of Applied Clinical Medical Physics 4:219-226

5. European Commission. European guidelines on quality criteria for diagnostic radiographic images, EUR 16260 ISBN92-827-7284-5, Brussels 1996
6. Institution of Physics and Engineering in Medicine. Recommended standards for the routine performance testing of diagnostic x-ray imaging systems. IPEM Report No. 91, York, UK, 2005.
7. Mooney R, Thomas P (1998) Dose reduction in a pediatric X-ray department following optimization of radiographic technique. Br J Radiol 71: 852-860
8. Behrman R, Yasuda G (1998) Effective dose in diagnostic radiology as a function of x-ray beam filtration for a constant exit dose and constant film density Med Phys 25: 780-790.
9. Peet D, Ramsdale M (2000) Objective image quality measurement and the EC quality criteria for lumbar spine radiographs. Rad Prot Dosim 90: 169-172

Author: Olivera Ciraj-Bjelac
Institute: Vinca Institute of Nuclear Sciences
Street: M. P. Alasa 12-14, Vinca
City: Belgrade
Country: Serbia
Email: ociraj@vinca.rs

The Effect of Spatially Nonuniform Electromagnetic Field and Antitumor Drug on Growth of Maglinant Tumor

V.E. Orel, N.A. Nikolov, A.V. Romanov, I.I. Dzyatkovskaya, Yu.I. Mel'nik

National Cancer Institute / Medical Physics & Bioengineering Laboratory, Kyiv, Ukraine

Abstract— **The effect of spatially nonuniform electromagnetic field on transformation of radio waves and thermal descriptions in phantoms and malignant tumour during electromagnetic irradiation was investigated. It is shown that the structure of heat formation on the surface of phantoms depends on the degree of nonuniformity of electromagnetic field (EF) and it is similar to computed EF distribution. Output descriptions of magnetic component after EF transformation in a phantom more depended on phantom' size and spatial heterogeneity than electric component. The treatment of experimental animals was carried out with DOXO in the dose 1.5 mg/kg. The animal tumors were exposed by EF with the frequency 40 MHz inside using two types of loop elliptic applicators. First type of applicator with straight profile (ASP) had small asymmetry of electric component a_E = – 0.03 a.u., magnetic component a_H = 0.16 a.u. and specific adsorption rate (SAR) = 8.8 W/kg. Second type with the circular arc in profile (ACAP) had increased asymmetry of EF a_E = 0.89 a.u., a_H = 0.48 a.u. and SAR = 1.6 W/kg. The temperature inside tumor was nonlinearly increased up to 39.1°C during 15 min electromagnetic irradiation (EI) by ASP and up to 37.9°C with the use of ACAP. Animals were housed in 4 groups: 1 – control (no treatment); 2 – DOXO-administration; 3 – DOXO-administration + EI by ASP; 4 – DOXO-administration + EI by ACAP. The maximal inhomogeneity in thermograms' structure of tumor surface visualized after EI by EF with increased asymmetry. Since 14th day after tumor transplantation the tumor volumes for animals from 4 group was statistically significant decreased in comparison with the animals of 1, 2 and 3 groups on 88%, 79% and 82% ($p < 0.05$) accordingly in average. At the same time, the complete resorption on 20th day after tumor transplantation for 40% animals from 4 group were observed.**

Keywords— **spatially nonuniform electromagnetic field, doxorubicin-resistant Guerin's carcinoma, doxorubicin, moderate hyperthermia.**

I. Introduction

One of the branches in hyperthermia for treatment of malignant tumor known as inductothermia is based on the use of magnetic and electric components of electromagnetic field (EF) in the radiofrequency spectrum for the localization and the concentration of heat during anticancer neoadjuvant therapy or activation of susceptor material implanted in the tumor [1]**.** The magnetic component of EF causes heating in tumor tissues through induced eddy currents. Spatialy nonuniform EF can cause different changes in protein synthesis of cells. [2]. Spatially nonuniform pattern of EF and temperature can be described mathematically by nonlinear (chaos) theory including fractal structure, autocorrelation factor and asymmetry of EF distribution [3]. In paper [4], it was suggested to produce the spatially nonuniform pattern with eddy current orthogonal to the magnetic force lines during treatment of a tumor by regionally-focused hyperthermia. Really, it is possible to suppose that nonuniform electromagnetic field will activate a non-equilibrium thermodynamical process in a tumor and increase antitumor activity of drug. However, it was not studied yet. This paper examines the effect of spatially nonuniform electromagnetic field on antitumor activity of doxorubicin (DOXO) during the treatment of animals with DOXO-resistant Guerin's carcinoma.

II. Materials and methods

Electromagnetic irradiation: We used the first prototype of the device for medical treatment called "Magnetotherm" (Radmir, Ukraine) [5]. The basic elements of apparatus are the power module, device of control and management, high-frequency generator, devices of defence and management, co-ordinate device and inductive applicator for electromagnetic irradiation (EI). The frequency of EI was 40 MHz with an initial power of 60 W. The animal tumors irradiated locally by an inductive coaxial applicator that had differed by the geometry and asymmetry of EF. In the first case (Fig. 1a), the applicator took the form of an ellipse on a horizontal plane with the semi-axes 1.5×2.5 cm. The profile was a straight-line segment (ASP). In the second case (Fig. 1b), the profile of the same applicator with increased asymmetry of EF had been an arc of the circle (ACAP) with the radius 2.3 cm.

EF distribution was computed according to [6]. EF isolines for 10×10 cm irradiated region are presented in Fig. 2. An asymmetry of electromagnetic components (*a*) and specific adsorption rate (*SAR*) of EI were calculated according to [7, 8].

O. Dössel and W.C. Schlegel (Eds.): WC 2009, IFMBE Proceedings 25/III, pp. 37–40, 2009.
www.springerlink.com

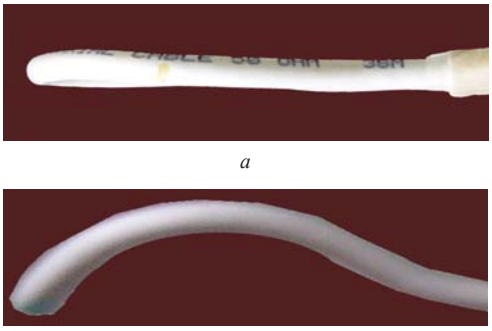

a

b

Fig. 1. Appearance of inductive applicator: *a* – loop with the profile of straight-line segment; *b* – loop with the profile of an arc of the circle

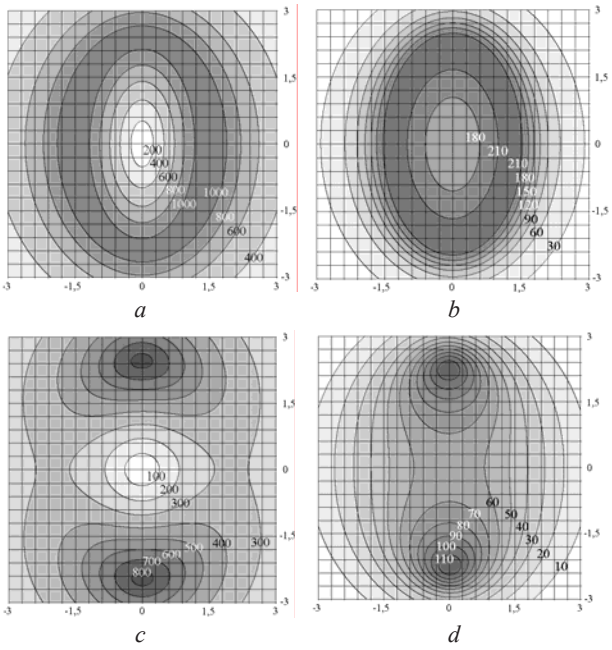

a *b*

c *d*

Fig. 2. The isolines of EF. The applicator with straight-line segment in profile: *a* – electrical component with a_E = 0.1 a.u.; *b* – magnetic component with a_H = 0.64 a.u. *SAR*=8.8W/kg. The applicator with an arc of the circle in profile: *c* – electrical component with a_E =0.16 a.u.; *d* – magnetic component with a_H = 1.42 a.u. *SAR*=1.6W/kg. Distance to the plane of applicator was 0.5 cm; the values on isolines indicated the tension of the electrical field in V/m and the magnetic field in A/m; the distance on the axis of abscissas and ordinates is indicated in cm

The greater asymmetry a_E =0.16 a.u and a_H = 1.42 a.u. was obtained for the applicator with the profile in the form of an arc of the circle.

Temperature studies. As mentioned above, hyperthermia can extend the thermal treatment by drug efficiency through non-equilibrium heating in the tumor. Therefore, we used asymmetric EF to activate the non-equilibrium thermodynamical process in the tumor. The nonlinear dynamics of temperature changes in the center of the tumor under EI measured by the fiber-optic thermometer TM-4 (Radmir, Ukraine). The inhomogeneity of digital thermograms' structure was estimated by the Shannon entropy equation meant for a statistical measure of the disorder (non-equilibrium of thermodynamical process) of a system [7].

Change of the temperature inside phantoms after EI calculated according to equation

$$\Delta T = T_{30} - T_0, \quad (1)$$

where T_0 = 37 °C – initial temperature of the phantom before EI, T_{30} – temperature on 30 min after beginning of EI.

Phantom studies: EF transformation in tumor tissues was simulated by two tissue equivalent phantoms: geterogeneity rubber foam phantom treated by NaCl 0.9% solution and control homohenety NaCl 0.9% solution phantom coated by polyethylene. Electric (E) and magnetic (H) components estimated by measuring elements which was connected to the amplifier, analog-to-digital converter and personal computer (DMPB-1, Ukraine). The change of electric (ΔE) and magnetic (ΔH) component under the influence of phantoms was calculated:

$$\Delta E = E - E_0, \quad (2)$$

$$\Delta H = H - H_0, \quad (3)$$

where E and H is electric and magnetic field intensity under phantom, E_0 and H_0 is electric and magnetic field intensity in the air, respectively.

Tumor transplantation: DOXO-resistant Guerin's carcinoma was acquired according to [9]. Thirty sequential subcutaneous transplantations of Guerin carcinoma cells ($3 \cdot 10^6$ per animal) received from DOXO-treated rats. The transplantation of DOXO-resistant Guerin's carcinoma was performed subcutaneously by standard method.

Treatment of animals: Animals were housed in 4 groups: 1 – control (no treatment); 2 – DOXO-administration; 3 – DOXO-administration + EI by ASP; 4 – DOXO-administration + EI by ACAP. The treatment of experimental animals was carried out with DOXO (Pharmacia & Upjohn) in the dose 1.5mg/kg. Animals were treated five times by DOXO and EI since the eighth day after the tumor transplantation. Treatments were performed two days each for ten days.

Statistical analysis: Statistical processing of numerical results was carried out using Statistica 6.0 (© StatSoft, Inc. 1984–2001) computer program with parametric Student's *t*-test.

III. Results and discussion

Phantom studies: The transformation of EF and thermal patterns in phantoms was investigated during EI by spatially nonuniform EF. It is shown in Fig. 3 that the structure of heat formation on the surface of phantoms depends on the degree of EF nonuniformity and it is similar to computed in Fig. 2 EF distribution . Relative increase of magnetic field strength $\Delta H/H_0$ in phantoms after EI by ACAP was in 3.5 times greater than by ASP on the average (Table 1). Relative increase of temperature $\Delta T/T_0$ in phantoms was smaller in 5.4 times after EI by ACAP compared to ASP on the average. In rubber foam phantom the ratio $\Delta T/T_0$ increased in 8.6 times after EI by ACAP compared to NaCl 0.9% solution phantom. It testifies stronger transformation of nonuniform EF for heterogenous structure of rubber foam phantom than for homogeneous structure of NaCl 0.9% solution phantom.

Thermal studies of tumor: Analyzing obtained in Fig. 4 results, it is necessary to notice that after fifteen and thirty minutes of EI by ASP temperature in the center of tumor nonlinearly increased to 38.4°C and 40°C, accordingly. That was rather higher, than after EI by ACAP where temperature was to 37.9 and 39.1°C, accordingly. Thermal patterns on tumor surface after EI are presented in Fig. 5. Computer analysis of thermal patterns shows that maximal inhomogeneity (entropy) was on the tumor's surface and display panel under EI with increased asymmetry by ACAP. The structure of heat formation on the surface of DOXO-resistant Guerin's carcinoma depends on the degree of EMF nonuniform.

The changes of tumor volume: As it is shown in Fig. 6, the growth kinetics of tumor volumes on 10 and 12th day after tumor transplantation was identical. Since 14th day after transplantation tumor volumes for animals from 4 group was statistically significant decreased in comparison with the animals of 1, 2 and 3 groups on 88%, 79% and 82 % ($p < 0.05$) accordingly in average. At the same time the complete resorption on 20th day after tumor transplantation for 40% animals from 4 groups were observed. The recurrent tumor growth hadn't been detected for 4 months after the treatment. The results of these experiments were retested 4 months later.

According to the presented data, it is possible to suppose that recorded effects of growth inhibition for DOXO-resistant Guerin's carcinoma after treatment by DOXO and electromagnetic local irradiation by spatially nonuniform EF at non-equilibrium heating may be connected with the initiation of nonlinear process of membrane depolarization [8].

Table 1. The ratios $\Delta E/E_0$, $\Delta H/H_0$ and $\Delta T/T_0$ for phantoms

Phantom	Applicator	$\Delta E/E_0$, %	$\Delta H/H_0$, %	$\Delta T/T_0$, %
NaCl 0.9% solution	ASP	47 ± 3	8.0 ± 1.0	0.20 ± 0.02
NaCl 0.9% solution	ACAP	19 ± 3*	20.0 ± 3.1*	0.10 ± 0.01
Foam rubber	ASP	49 ± 6	7.0 ± 0.5	6.2 ± 1.0
Foam rubber	ACAP	28 ± 4*	31.0 ± 3.5*	0.7 ± 0.2*

* $p < 0.05$ compared to similar parameter of ASP

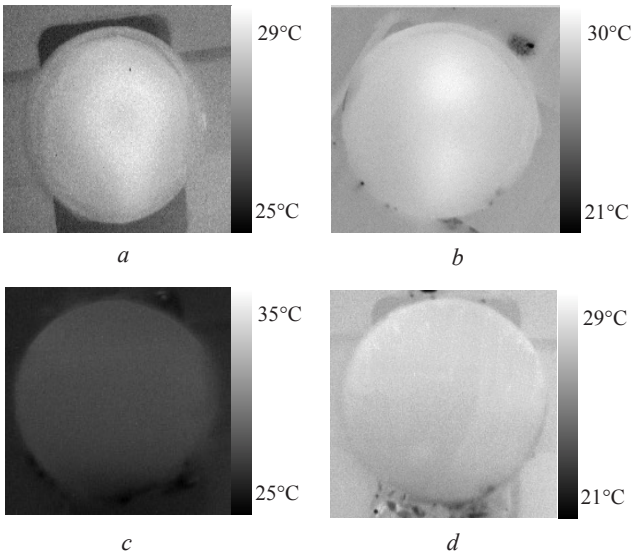

Fig. 3. Thermal pattern on phantom surface after electromagnetic irradiation by ASP of foam rubber (*a*), ACAP of foam rubber (*b*), ASP of NaCl 0.9% solution (*c*), ACAP of NaCl 0.9% solution (*d*)

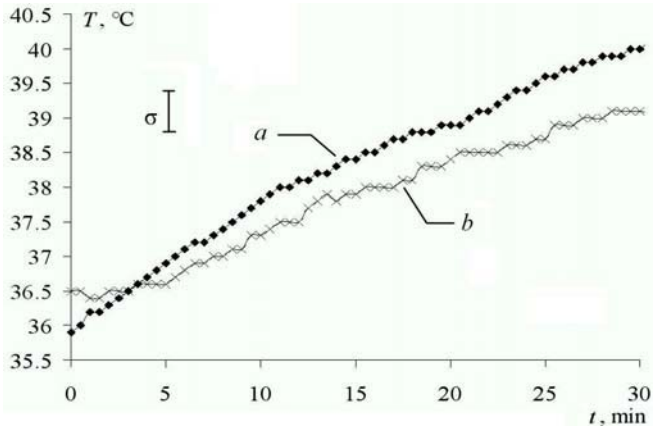

Fig. 4. The temperature changes after transplantation on 15 day in the center of tumor during EI by ASP (*a*) and ACAP (*b*).

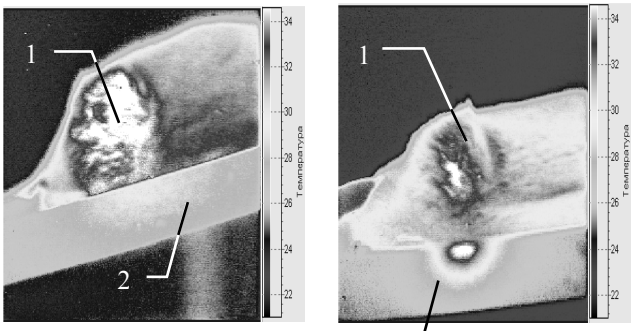

a *b*

Fig. 5. Thermal patterns and entropy (*S*) on tumor surface (1) and display panel (2) after EI by ASP (*a*) and ACAP (*b*)

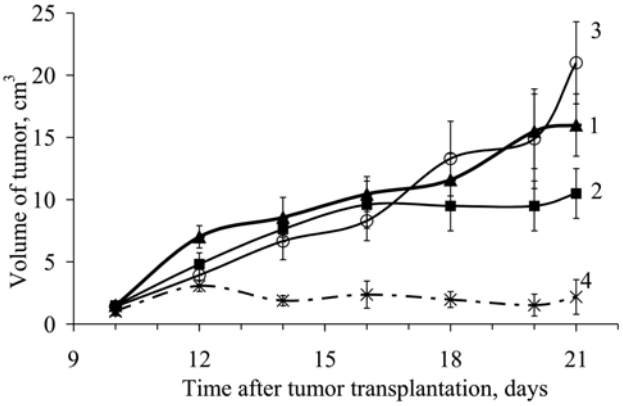

Fig. 6. DOXO and EI-induced changes in the growth kinetics of DOXO-resistant Guerin's carcinoma: 1 – without DOXO and EI (control); 2 – DOXO; 3 – DOXO + EI by ASP; 4 – DOXO + EI by ACAP

Conclusions

The aforementioned effects of tumor growth inhibition for DOXO-resistant Guerin's carcinoma after treatment by DOXO and electromagnetic local irradiation with spatially nonuniform EF activate non-equilibrium thermodynamical process in tumor at physiological temperatures that may find pragmatic applications in clinical practice.

References

1. Ivkov R, De Nardo S, Daum W et al (2005) Application of high amplitude alternating magnetic fields for heat induction of nanoparticles localized in cancer. Cli Can Res 11: 7093–7103
2. Goodman R, Henderson A (1988) Exposure of salivary gland cells to low-frequency electromagnetic fields alters polypeptide synthesis. Proc Natl Acad Sci USA 11: 3928–3932
3. Orel V, Kozarenko T, Galachin K et al (2007) Nonlinear Analysis of Digital Images and Doppler Measurements for Trophoblastic Tumor. Non Dyn, Psyh, and Life Sci 11: 309–331
4. Boddie A Jr, Frazer J, Yamanashi W (1987) RF electromagnetic field generation apparatus for regionally-focused hyperthermia. United States Patent N4674481 on 23.06.1987.
5. Nikolov N, Orel V, Smolanka I et al (2008) Apparatus for Short-Wave Inductothermy "Magnetotherm". NBC Proc. 2008, A Katushev, Yu Dekhtyar, J Spigulis (eds), Springer-Verlag, Berlin, Heidelberg, pp 294–298
6. International Series of Monographs in Electrical Engineering. Computer Techniques for Electromagnetics (1973) Edited by R. Mittra. Pergamon Press, Oxford – New York – Toronto – Sydney – Braunschweig
7. Moseley H (1988) Non-ionizing radiation. Medical physics handbooks. Adam Hilger, Bristol & Philadelphia.
8. Korn G, Korn T (1968) Mathematical handbook for scientists and engineers. MacGraw-Hill Book Company, New York
9. Solyanik GI, Todor IN, Kulik GI, Chekhun VF. (1999)Selective mechanism of the emergence of Guerin`s carcinoma resistance to doxorubicin. Experimental oncology 21: 264–268

Author: Valeriy E. Orel
Institute: National Cancer Institute
Street: 33/43, Lomonosova
City: Kyiv
Country: Ukraine
Email: v-orel@i.com.ua

Prevention of Overexposure by Means of Active Protective Reactions and Magnitude of Temporary Blinding from Visible Laser Radiation

H.-D. Reidenbach[1]

[1] Cologne University of Applied Sciences, Institute of Applied Optics and Electronics,
Research Laboratory on Medical Technology and Non-Ionizing Radiation,
Betzdorfer Str 2, D-50679 Koeln, Germany

Abstract— **It has been shown in a field trial with 205 subjects who got an instruction, that active protective reactions could protect up to 80 % of the exposed volunteers against laser radiation during a period of 1.4 seconds. This is a considerable improvement compared with the unreliable blink reflex, which works only in every 5th case.**

Therefore adequate instruction to perform active protective reactions, i. e. moving the head or closing the eyes, might be a valuable contribution to prevent any potentially hazardous laser radiation and increases the safety against laser radiation arising from wrong labeled class 2 laser products and true class 3R lasers emitting in the visible spectrum.

Temporary blinding as the result of a dazzling light in the visual field arising from class-1 and class-2 lasers at wavelength of 632.8 nm and 532 nm has been investigated.

It was found that already at output powers below 30 µW of a He-Ne-laser the subjects reported intense glare effects and felt uncomfortable due to the high brightness. The durations of afterimages took up to 300 s and have been measured as a function of the angle between the line of sight and the laser beam direction for exposure durations up to 10 s. A dose relationship has been found which determines the afterimage duration. The inability to read due to the disturbance produced by afterimages lasts for about 20 s even if the exposure is not more than 0.25 s from a laser with about 0.8 mW.

Keywords— **Active protective reactions; laser; class 2; afterimage; temporary blinding.**

I. Introduction

The most effective approach toward laser safety was the introduction of an appropriate laser classification system according to the degree of potential optical radiation hazard.

The accessible emission limit (AEL) for class 2 is derived by multiplying the maximum permissible exposure (MPE) for 0.25 s with the area of a 7-mm aperture, which is equivalent to the pupil diameter of the dark adapted eye [1].

In the case of low power lasers the safety philosophy is based on natural aversion responses including the blink reflex since many years.

On the other hand it was found in a total of 2,020 volunteers that the blink reflex occurred in not more than 16.7 % of all cases if an irradiation is performed with a class-2 laser product. In addition it has been shown with 829 volunteers that aversion responses in terms of head movements and eye closure occur only in 5.9 % [2]. Therefore the possibility of an overexposure exists due to the lack of natural aversion responses.

For workers it is claimed for example in the European Directive 2006/25/EC that they shall not be exposed above the exposure limit values [3].

While minimum health and safety requirements regarding the exposure of workers to risks arising from laser radiation can be stated in such a directive, the general public might be adequately protected if products with potentially hazardous optical emission are either not allowed on the market or sufficient safety instructions are given in the accompanying user information.

Due to the fact that not only deterministic effects like thermal damage to the retina are important in order to work in a safe manner with bright light sources like laser emitting in the visible spectrum, indirect effects arising from temporary blinding should be regarded in a risk assessment. Since indirect effects have not been included in most safety analysis up to now and there was not enough information available, investigations have been performed in order to improve the current knowledge.

II. Methods and material

A. Active protective reactions

Laser belonging to class 2 according to IEC 60825-1 [4] are based on the safety philosophy that aversion responses prevent that the maximum permissible exposure values are exceeded. Although it has been convincingly shown that these natural behavior does not really exist in any case [5], the proposal to reduce the currently allowed output power from 1 mW to 0.6 mW or 0.7 mW, which would be equivalent to an upper limit in compliance with the guidelines of the International Commission on Non-Ionising Radiation Protection (ICNIRP) [6, 7] for exposure durations of 2 s or 1 s, respectively, was not seriously agreed.

O. Dössel and W.C. Schlegel (Eds.): WC 2009, IFMBE Proceedings 25/III, pp. 41–44, 2009.
www.springerlink.com

Due to the fact that a great many of class-2 laser are used without problems and that there are but a few reports concerning minor eye damage the standardization commissions did not change the previous classification.

In order to find another solution a comparative study has been performed where part of the subjects became informed of the intended test procedure and a control group was uninformed. In addition the informed subjects have been instructed and asked to perform active protective reactions in the case of an unexpected laser beam in order to estimate the reaction times and frequencies of the various physiological behavioral patterns. Simultaneously the subjects were asked to carry out a special visual task on a monitor which was part of an especially developed eye-tracking system [8]. In detail, the subjects had to "catch" the reflection from their own eye and to "guide" this to a stationary cross on a monitor screen and at the time of coincidence of both spots a laser beam was released for a predetermined time duration, namely 0.25 s or 1 s. The respective laser output power was chosen to be 80 % of the allowed limit value in order to comply with feasible measurement uncertainties.

A total of 205 subjects got an instruction, whereas 316 have been uninformed. The investigations have been done in field trials at two different locations.

B. Temporary blinding

The fact that dazzle, flash-blindness and afterimages may be caused by bright visible optical radiation is well-known, but functional relationships are not yet available up to now.

For this purpose a helium-neon laser (632.8 nm), and a frequency-doubled Nd:Yttrium Vanadate laser (532 nm) have been applied as a dazzling light source.

Two set-ups were used in order to perform the investigations. In one case a helium-neon laser was mounted on a movable assembly where the respective beam position and direction could be adjusted on a semicircle between -40 degrees nasally and +60 degrees temporally. In detail the measurement of the afterimage duration has been done for exposure durations of 1 s, 5 s, and 10 s at power settings of 5 μW, 10 μW, 20 μW, and 30 μW.

The measurement stop criterion was taken as the point in time when the afterimage disappeared and could not be retrieved not even by squinting.

The time consuming trials have been done with a total of 10 volunteers in the laboratory.

In a second set-up an alignment situation was designed where the subject was placed in a chin rest and fixated a point through which a laser beam from either a He-Ne- (632.8 nm) or solid-state laser (532 nm) could be released during a preset exposure duration. This arrangement assured that the fovea was being hit definitely. Immediately after the exposure the subject turned his/her head to an especially developed reading test on a monitor for the determination of temporary blinding from laser irradiation. The respective time needed to gain the previous acuity – determined as reading capability – was registered. In this context it is important to assert that an afterimage was still present but no longer obstructed the test words.

A total of 19 persons have been tested in this manner.

III. Results

A. Active protective reactions

In contrast to the results obtained with 316 uninformed subjects, where only about 7 % showed a blink reflex, we have found in field trials with 205 instructed persons, that active protective reactions, i. e. immediately closing the eyes and/or moving the head, are able to protect up to 34.4 % within 240 ms, up to 74.4 % within a second [9] and 80 % after 1.4 s against laser radiation.

Active lid closure started already at 120 ms and showed a saturation after about 400 ms (Fig. 1, black triangle). This shows that a lid closure due to an instruction can be nearly as quick as a blink reflex, but happens more often.

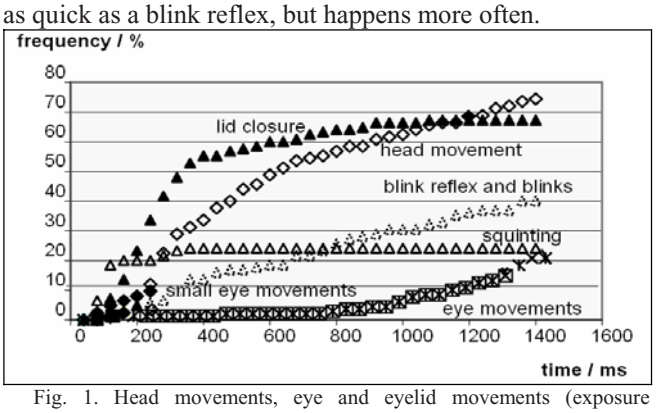

Fig. 1. Head movements, eye and eyelid movements (exposure duration: 250 ms; laser power: 0,8 mW, 125 subjects). Determination of active protective reactions was extended up to 1.4 s.

The results achieved in one part of this study on active protective reactions taken with 125 test persons have shown that squinting, which is regarded as a blink reflex below threshold, is the quickest reaction followed by the blink reflex (Fig. 1, open triangles), but limited to about 23 %. The exposure duration was 250 ms and the laser power 0.8 mW. Eye blinks and the blink reflex have been added in Fig. 1 since in both cases a reopening of the upper lid takes place within about 300 ms whereas in a voluntary lid closure the eyes stay closed over a much longer time duration due to the deliberate action. This clearly favors active lid closure as a protective means.

Small eye movements occur only during the very early time of the stimulation (Fig. 1, black diamonds) whereas distinct eye movements are elicited much later.

Figure 2 shows a comparison between normal aversion responses including the blink reflex and active protective reactions as a result of different irradiations (0.8 mW and 250 ms or 0.55 mW and 1 s). Natural physiological protection, i. e. aversion responses including the blink reflex, has been found with a frequency of about 12 % within 250 ms and increases to about 26 % after 1.4 s. On the contrary active protective reactions increase relatively rapid to about 35 % within 250 ms and slowly reach saturation. A maximum protection of about 80 % was achieved (Fig. 2).

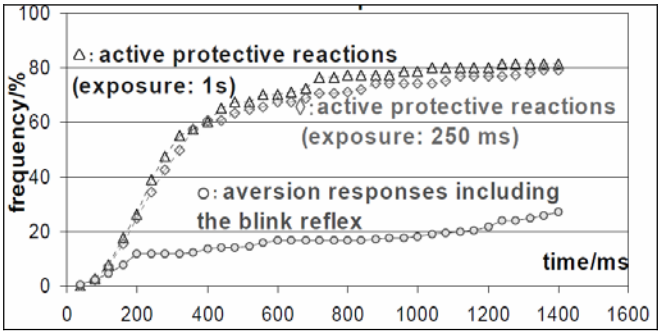

Fig. 2. Comparison between normal aversion responses including the blink reflex and active protective reactions for different exposure situations (0.8 mW, 250 ms or 0.55 mW, 1 s)

The comparison of both situations clearly shows the improvement achieved with active protective reactions.

B. Temporary blinding

The investigations with a laser beam which irradiated the retina at various locations have shown a strong dependence on the angle between the line of sight and the beam direction. Afterimage durations up to 300 seconds were found if the fovea of the human retina is irradiated from a class-1 laser beam, whereas much lower values are valid in the parafoveal region and in the periphery [10].

In addition a dose-relationship has been found between the duration of an afterimage and the applied optical energy in the investigated time interval between 0.5 s and 10 s.

Because of the psychological glare as a result of the laser irradiation more detailed investigations have been made only with an exposure located 5° temporal to the fovea. The results are shown in Fig. 3. Since the afterimage lasts about a factor of 2 longer in the fovea the maximum afterimage duration can be derived from the applied optical energy $P \cdot t_{exp}$ according to the following relationship (eq. 1):

$$\frac{t_{afterimage,fv}}{s} \approx 50.6 \cdot \ln\left(\frac{P \cdot t_{exp}}{\mu J}\right) - 13.4 \qquad (1)$$

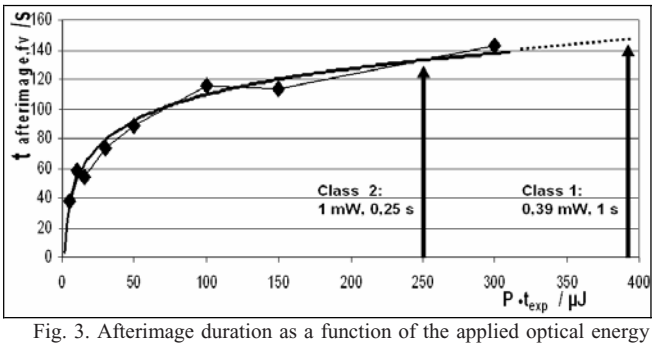

Fig. 3. Afterimage duration as a function of the applied optical energy (irradiation 5° temporal to the fovea, diamonds: measurement mean values)

In the tests with subjects performing a procedure like an alignment it has been found that a green laser beam produces longer durations of disturbance compared with a red one as far as the reading capability is concerned. The delay times measured have been between 13 s and 19 s for 532 nm and between 4s and 14 s, with one exception at 22 s, for 632.8 nm, if the exposure duration was 0.25 s and the power limited to a maximum of 0.783 mW. The respective numbers were between 22 s and 35 s for a green laser beam (cf. Fig. 4) and between 2.5 s and 19 s for the red laser beam if the exposure duration was 0.5 s and the power cap at 0.66 mW.

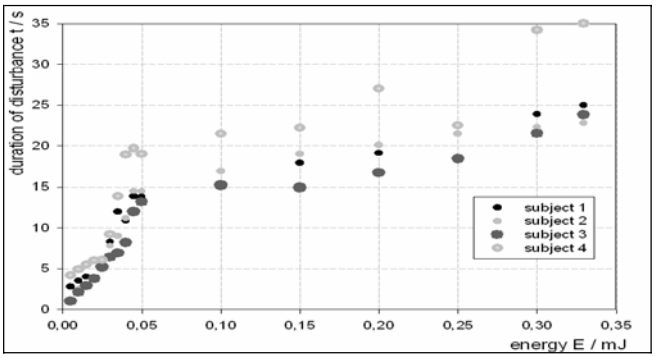

Fig. 4. Duration of disturbance as a function of the applied optical energy (laser wavelength: 532 nm, exposure duration: 0.5 s, 4 subjects)

A comparison of figs. 3 and 4 shows that about 10 % of the total afterimage duration can be expected as disturbance time in order to perform visual tasks unrestricted after an irradiation with a laser beam in the above given power and exposure duration range.

IV. Discussionn

Since the eyes are not in danger as far as accidental and short-term exposure is regarded, laser products of class 2 may be applied without any additional protective measures if it is ensured that neither a deliberate intrabeam viewing of

more than 0,25 s nor a repeated intrabeam viewing into a specular reflected laser beam could happen.

There was a strong belief in aversion responses and especially in the blink reflex as a reliable physiological reaction if a bright light is viewed. A laser source certainly represents a very bright light.

Compliance with the exposure limit values will ensure that workers exposed to laser radiation are protected against all known adverse health effects, since the limits on exposure to optical radiation are based directly on established health effects and biological considerations.

There are currently very few, if any, reported eye injuries due to lasers especially belonging to class 2 and it has not been convincingly shown that a true class 2 laser is capable of producing serious eye damage at all.

As far as the MPE values are concerned an exposure duration of 0.5 s instead of 0.25 s is equivalent to exceeding the MPE by about 22 % and a duration of 1 s means that the MPE is exceeded by 44 %. But on the other if the output power is exceeded by a factor of 2, e. g. 2 mW instead of 1 mW, than an intrabeam viewing of only 0.5 s or 1.0 s would correspond to a 32-fold or 64-fold overexposure, respectively. This should be prevented if possible.

Normally people can adapt to changing luminous conditions and perform well regardless of the illumination level, but glare might impair visual functions strongly and with a lasting effect, due to the fact that the adaptation system is overridden and an afterimage is formed.

The situation where the pupil of a stabilized head was aligned to the beam satisfies worst case accommodation, but nonetheless disturbance of visual functions can result in distracting and even dangerous situations. Its value might be depicted from Fig. 3, where two not unusual situations of a class-2 and class-1 laser illustrate the interference from temporary blinding even after relatively short irradiations.

V. Conclusions

Our findings do not state that class 2 laser are no longer safe, but that users of such lasers should be instructed to perform active protective reactions, i. e. close the eyes actively and avert the head in the case of intrabeam viewing as soon as possible. To exceed the MPE is not necessarily dangerous, but active protective reactions can prevent a violation of the MPE values and thus fulfill regulatory issues and simultaneously can be regarded as “prudent precaution”, describing a situation, in which laser safety could be increased without restricting the normal use disproportionately.

In addition the knowledge of some quantitative relationships between laser exposure with a certain value and the expected disturbance of visual functions should improve the handling of low power laser products.

Acknowledgment

The research has been funded by the Federal Institute for Occupational Safety and Health (BAuA) in Germany.

References

1. Reidenbach H-D (2007) Laser Safety. In: Handbook of Lasers and Optics (ed. Träger, F). Springer. New York, chap. 21
2. Reidenbach H-D, Dollinger K, Hofmann J (2005) Results from two research projects concerning aversion responses including the blink reflex. SPIE Proc. B5688, Ophthalmic Technologies XV, Manns F, Söderberg P G, Ho A, Stuck B E, Belkin M (eds.), pp 429-439
3. Directive 2006/25/EC of the European Parliament and the European Council of 5 April 2006 on the minimum health and safety requirements regarding the exposure of workers to risks arising from physical agents (artificial optical radiation) (19th individual Directive within the meaning of Article 16(1) of Directive 89/391/EEC), OJ L 114, 27.4.2006, p.38
4. International Electrotechnical Commission, IEC 60825-1: 2007-03 (2nd edition), Safety of laser products - Part 1: Equipment classification and requirements (former edition: IEC 60825-1: 1993 + A1:1997 + A2:2001, Safety of laser products – Part 1: Equipment classification, requirements and user’s guide.)
5. Reidenbach H-D (2006) Results of Investigations on the Blink Reflex as a Protective Means against Laser and LED Radiation: A Description Based on Fundamental Psychophysical Laws. Proceedings Second European IRPA Congress on Radiation Protection, (15– 19 May 2006, Paris, IRPA 2006), TA-68, pp 1-12
6. ICNIRP (1996) Guidelines on Limits of Exposure to Laser Radiation of Wavelengths between 180 nm and 1000 µm. Health Physics 71:804 – 819
7. ICNIRP (2000) Revision of guidelines on limits for laser radiation of wavelengths between 400 nm and 1,400 nm. Health Physics 79:431 – 440
8. Reidenbach H-D (2005) Aversion responses including the Blink reflex: Psychophysical behaviour and active protection reactions as an additional safety concept for the application of low power lasers in the visible spectrum. ILSC 2005, Conf. Proc., 67 – 76
9. Reidenbach H-D, Hofmann J, Dollinger K (2006) Active Physiological Protective Reactions should be used as a Prudent Precaution Safety Means in the Application of Low-Power Laser Radiation. Proceedings World Congress on Medical Physics and Biomedical Engineering 2006, (August 27 – September 1, COEX Seoul, Korea; IFMBE). Vol. 14, pp 2569-2572
10. Reidenbach H-D (2007) Local Susceptibility of the Retina, Formation and Duration of Afterimages in the Case of Class 1 Laser Products and Disability Glare Arising from HB-LEDs. ILSC 2007, Conference Proceedings pp 102 – 111

Address of corresponding author:
Author: Hans-Dieter Reidenbach, Prof. Dr.
Institute: Cologne University of Applied Sciences,
Res Dept Medical Technology and Non-Ionizing Radiation
Street: Betzdorfer Str 2
City: Koeln, D-50679
Country: Germany
Email: hans.reidenbach@fh-koeln.de

Dose Distribution in Pediatric CT Abdominal Examination: Phantom Study

R. Gotanda[1, 2], T. Katsuda[3], T. Gotanda[1], A. Tabuchi[1], H. Yatake[1] and Y. Takeda[1]

[1] Graduate School of Health Sciences, Okayama University, Okayama, Japan
[2] Departments of Radiological Sciences, Ibaraki Prefectural University of health Sciences, Ibaraki, Japan
[3] School of Medical Engineering, Faculty of Health Care Sciences, Himeji Dokkyo University, Hyogo, Japan

Abstract— **To keep radiation doses during computed tomography (CT) examinations as low as reasonably achievable, performing a detailed dose measurement is important. A flexible acrylic sheet roll CT dosimetry phantom (SRCT-P) with radiochromic film (RF) was developed to estimate in detail the dose distribution during pediatric CT examination. The SRCT-Ps were elliptically-shaped by rolling up flexible acrylic sheets (1.1 g/cm^3). The dose distributions in the SRCT-P (body thickness and width: 6-8 cm [neonates], 10-12 cm [infants], and 14-16 cm [three-year-old children]) were evaluated. RFs were positioned from the center to the surface along the long- and short-axis directions in each SRCT-P. The scanning parameters of the single detector CT were 120 kV, 250 mA, 1.0 sec/rot, a slice thickness of 5 mm, and a 1.0 beam pitch. When the mean center dose at 10-12 cm on the SRCT-P was taken as 100%, the mean center doses at 6-8 or 14-16 cm were 145 or 43%, respectively, and the mean surface doses for 0, 90, and 180 degrees at 6-8, 10-12, and 14-16 cm of the SRCT-P were as follows: 158%, 159%, and 140%; 132%, 125%, and 116%; and 164%, 128%, and 131%, respectively. The center dose was increased with a decrease in the phantom size. The surface doses were decreased with decreasing phantom sizes of 14-16 to 10-12 cm; however, surface doses were increased with decreasing phantom sizes of 10-12 to 6-8 cm. The detail dose distribution of a CT examination can be measured separately by using a SRCT-P with a RF.**

Keywords— **radiochromic film, computed tomography, phantom, radiation dosimetry**

I. Introduction

The radiation risks from computed tomography (CT) have been recently reported in many studies [1, 2]. Caution should be exercised in the pediatric setting because children have more rapidly dividing cells than adults and a longer life expectancy [1]. To keep radiation doses during CT examination as low as reasonably achievable [1, 3], it is important that the CT scanning parameters are adjusted appropriately for each individual's weight and size, and thus the accurate and high-resolution dose measurement and identification of the maximum dose position are required.

Radiochromic films (RFs) have been developed for measurement of the absorbed dose of low energy photons [4] and are used to measure CT dose profiles [5].

RFs are self-developing and radiation-sensitive. The amount of darkening is proportional to the absorbed dose. The RFs are very easy to handle due to insensitivity to interior room light and resistance to water. To measure the CT dose profiles, the RFs are placed on an empty paper box or placed in the prove holes in the CT dose phantom [5].

The CT dose phantom has been designed to measure the CT dose index (CTDI) [6, 7], the CDTI variations (CTDIw and CTDIvol), and the dose-length product (DLP) [7] using a pencil-type ionization chamber. There are two types of CT dose phantoms (a body phantom [32 cm] and a head phantom [16 cm]) [6]. The phantom shapes are circular cylinders of polymethyl-methacrylate (1.19 ± 0.01 g/cm^3) [6]. Each phantom has 5 probe holes (the inside diameter is 1.31 cm) to insert a pencil-type ionization chamber. The phantom diameter, shape, and dose measurement position in the phantom are limited. In addition, the evaluation of the absorbed dose in a local area and the detailed dose distribution in a phantom are difficult.

As a preliminary, a sheet roll CT dosimetry phantom (SRCT-P) is made from a 100% vinyl chloride sheet [8]. The SRCT-P is made by rolling up the sheet. Thus, the developed SRCT-P is flexible in terms of the determination of the phantom size and shape, and the depth of the measurement position in the phantom is arbitrarily decided by inserting RFs between the sheets. Additionally, the identification of the maximum dose position in the SRCT-P, evaluations of the absorbed dose in a local area, and the detailed dose distribution in the phantom are facilitated. However, the specific gravity (1.3 g/cm^3) is greater than that of the CT dose phantom (1.19 ± 0.01 g/cm^3) used for defining the Food and Drug Administration (FDA).

In this study, the sheet materials were changed to flexible acrylic sheets (1.1 g/cm^3); additionally, the SRCT-Ps were elliptically-shaped for accurate measurement of the CT dose in clinical practice. The absorbed doses and the dose distributions in the SRCT-P (body thickness and width: 6-8 cm [neonates], 10-12 cm [infants], and 14-16 cm [three-year-old children]) were evaluated.

O. Dössel and W.C. Schlegel (Eds.): WC 2009, IFMBE Proceedings 25/III, pp. 45–48, 2009.
www.springerlink.com

II. Materials and methods

A. The flexible acrylic sheet roll CT dosimetry phantom (SRCT-P)

The CT dosimetry phantom was elliptically-shaped by rolling up the flexible acrylic sheet (specific gravity, approximately 1.1 g/cm^3; SANVIC, Inc., Tokyo, Japan). The thicknesses of the sheets were 0.5 mm, and the width of the sheets was 17 cm each. The phantom center core is shown in Fig. 1.

The phantom sizes were arbitrarily set by controlling the length of the sheet. The measurement position of the absorbed dose was also decided arbitrarily. The depth of the measurement position was made at 0.5 mm intervals by inserting RFs between the sheets.

GAFCHROMIC EBT film (EBT−film, Lot No. 47277-03I; International Specialty Products [ISP], Wayne, NJ, USA) was used as a dosimeter. The measuring dose range of the EBT-film was designed to be 1-800 cGy. EBT-film is a transmitted-type film, and an economical flatbed scanner can be used for the measurement of film density [4].

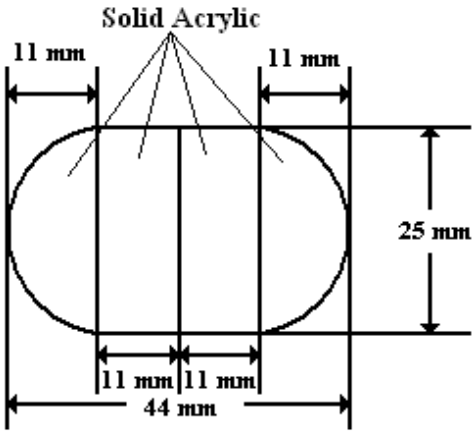

Fig. 1. The central core of the SRCT-P.

B. CT dose dosimetry

A schematic arrangement of the exposure method for CT dose dosimetry is shown in Fig. 2. The SRCT-P was held on the CT bed for measurement of the CT dose in clinical practice. The center of each SRCT-P was always located at the isocenter of the gantry. The SRCT-P sizes were set at 6-8, 10-12, and 14-16 cm to measure the relationships among the phantom sizes, the absorbed doses, and the depth of dose distributions along the short and long axes direction in the phantom. The EBT-films were cut to a width of 20 mm and a length of 70 mm. The EBT-films were positioned from center-to-surface along the long and short axes direction at each SRCT-P. The arrangement of films is shown in Fig. 2. The scanning parameters of the single detector CT (Asteion; Toshiba, Tochigi, Japan) were 120 kV, 250 mA, 1.0 sec/rot, a beam pitch of 1.0, and a 95 mm exposure range.

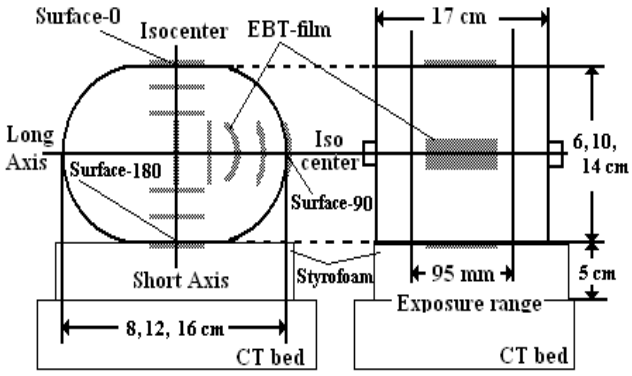

Fig. 2. Schematic arrangement of the CT dose dosimetry.

C. Analysis of the EBT-film

For image data acquisition, EBT-films were scanned before and after exposure using a flat bed scanner (Epson ES-2200; Seiko Epson Co., Nagano, Japan) in RGB (48 bit) mode, 150 dpi, with the protection film of a liquid crystal (LCD-150; Sanwa Supply Inc., Okayama, Japan). The EBT-films were placed on the scanner bed in the same orientation (active components coating the direction of the film parallel to the short dimension of the scanner bed). To remove any increase in density error due to time differences, films were scanned at a constant time (12 hours) from post-exposure [4].

Image data of the EBT-films were changed into the red mode and 16-bit gray scale with Adobe Photoshop 6.0 (Adobe Systems Incorporated, San Jose, CA, USA), and were analyzed with Image J 1.36 (National Institutes of Health [NIH], Bethesda, MD, USA).

In the image date before and after exposure, a region of interest (ROI) for analysis was determined at the same position on each film, and the pixel values of the ROI were measured.

To adjust the color shading in the clear polyester layer of the EBT-film and to evaluate the practical density increase of each film, the pixel values of the ROIs on the pre-exposure films were subtracted from the pixel values of the ROIs on the 12 hour post-exposure films. The pixel values after this subtraction were defined as the net pixel value (NPV).

D. CT dose dosimetry

For measurement of the mean dose, the size of the ROI (50 pixels x 350 pixels) was set at the center of each film. The NPV of each film was analyzed and the dose distributions at each phantom size were calculated using the calibration curve (Fig. 3). The mean absorbed dose and the mean depth dose distribution among different phantom sizes were analyzed using spreadsheet software (Excel 2003; Microsoft Co., Redmond, WA, USA).

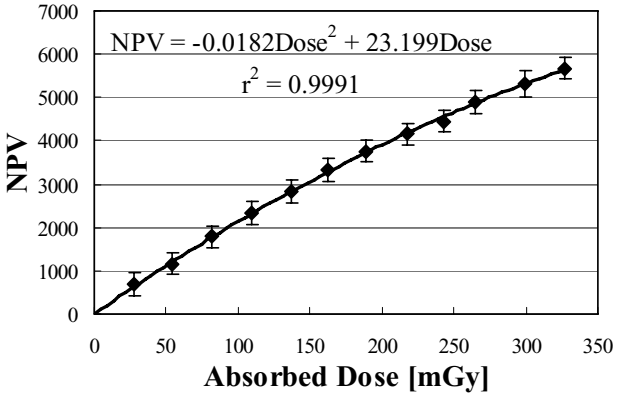

Fig. 3. Calibration curve for EBT-film.

III. Results

A. CT dose dosimetry

The mean depth dose distributions along the long- or short-axis directions are shown in Figs. 4 or 5, respectively. The maximum dose area was the surface at each SRCT-P. At 6-8 cm on the SRCT-P, homogeneous distribution was shown. At 10-12 and 14-16 cm on the SRCT-Ps, the absorbed doses in the phantom, except a center and surface, were almost the same value. In all of the SRCT-Ps, the absorbed doses of the bed side (depth < 0) were lower than the opposite side (depth > 0) along the short-axis direction (Fig. 5).

The ratios of the center and surface doses are shown in Fig. 6. When the mean center dose at 10-12 cm on the SRCT-P was taken as 100%, the mean center doses at 6-8 or 14-16 cm were 145% or 43%, respectively, and the mean surface doses for 0, 90, and 180 degrees at 6-8, 10-12, and 14-16 cm on the SRCT-P were as follows: 158%, 159%, and 140%; 132%, 125%, and 116%; and 164%, 128%, and 131%, respectively. The center dose was increased with a decrease in the phantom size. The surface doses were decreased with decreasing phantom size (14-16 cm to 10-12 cm); however, the surface doses were increased with decreasing phantom size (10-12 cm to 6-8 cm). Additionally, the surface doses for 180 degrees at each SRCT-P were lower than the other surface doses.

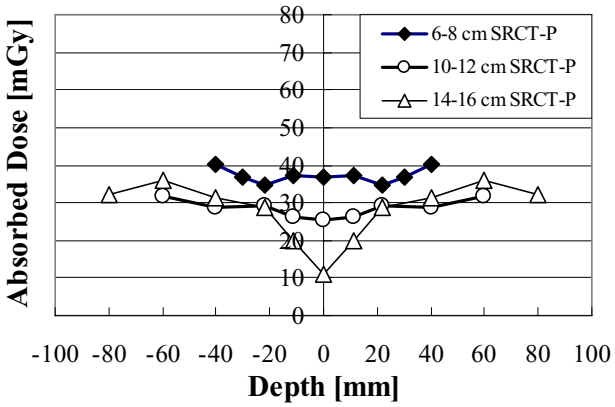

Fig. 4. The mean depth dose distribution along the long-axis.

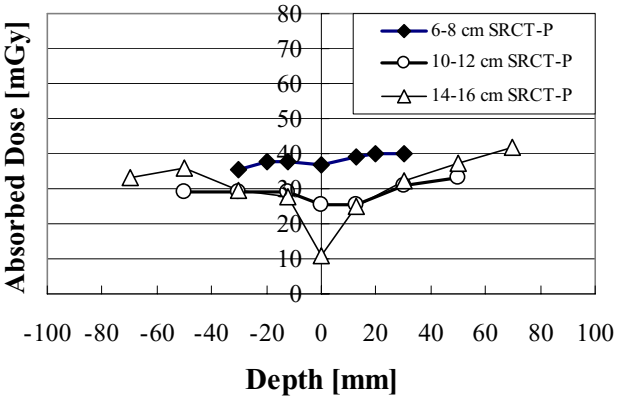

Fig. 5. The mean depth dose distribution along the short-axis.

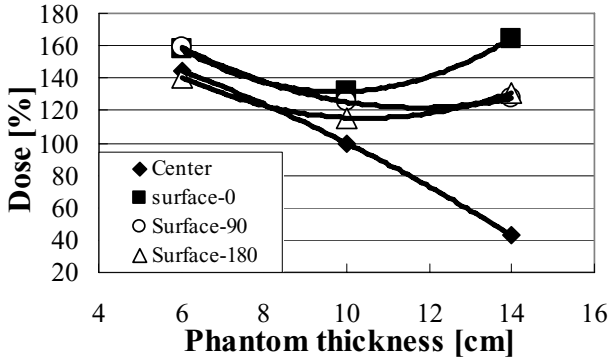

Fig. 6. The ratio of the center and surface dose.

IV. Discussion

A. The shape of the SRCT-P

The current CT dose phantoms are limited in shape, size, and dose measurement position. The developed SRCT-P is flexible in terms of the determination of the phantom shape, size, and dose measurement position. The SRCT-P shape can assume any form because the SRCT-P shape is determined by the central core. In this study, the SRCT-P shape was elliptical. Also, the sizes of the SRCT-P were appropriately set at 6-8 cm, 10-12 cm, and 14-16 cm due to control of the sheet length. Furthermore, the dose measurement positions were determined at all positions in the SRCT-P with 360 degrees and at 0.5 mm depth intervals by inserting the RFs between the sheets. This indicated that the evaluation of the absorbed dose in a local area and the detailed dose distribution in a phantom is possible by using the SRCT-P with a RF. It is considered that the acrylic flexible SRCT-P is suitable for the absorbed dose measurement in the CT examination.

B. CT dose dosimetry

In this study, the SRCT-P sizes were set at 6-8 cm for neonates, 10-12 cm for infants, and 14-16 cm like for three-year-old children. The maximum dose area in neonates was at the surface; however, the dose distribution was almost homogeneous in the phantom. In infants and three-year-old children, the maximum dose areas were at the surface; however, the surface doses of infants were lower than in three-year-children at the same CT parameter. Additionally, the absorbed doses in the phantom, except the center and surface, were almost the same value. This result indicated that the dose distribution became complex with patient size and CT dose measurement with an elliptically-shaped phantom was important to obtain an accurate dose evaluation in the pediatric abdominal CT.

In all of the SRCT-Ps, the surface doses for 180 degrees were lower than other surface doses; additionally, the absorbed doses of the bedside (depth < 0) were lower than the opposite side (depth > 0) along the short-axis direction. This result indicated that the attenuation with the CT bed influenced the dose distribution.

It is important that the CT scanning parameters are adjusted appropriately for each individual's weight and size and for the region being scanned [1, 3]. On any parameter, the accurate and high-resolution dose measurement and identification of the high dose areas are possible using SRCT-Ps with RFs. In particular, the SRCT-P is flexible in terms of the phantom shape, size, and dose measurement position. Therefore, the SRCT-P combined with RF dosimetry is suitable for the measurement of the absorbed dose from CT examination.

V. Conclusion

The results indicated that the dose distribution in pediatric abdominal CT becomes complex with patient size. In the current study, accurate dose measurement and maximum dose areas were identified. To keep radiation doses during CT examination as low as reasonably achievable, it is important that the CT scanning parameters be adjusted appropriately for each individual's size and weight under an identification of the high dose area. The dose measurement by SRCT-P with RF will become one of the evaluation methods for adjusting parameters.

Acknowledgment

We would like to sincerely thank Kawagoe Tohru of INABATA & CO., LTD. (Tokyo, Japan) and Motohisa Masuda of SANVIC, Inc. (Tokyo, Japan) for providing flexible acrylic sheets.

References

1. FDA Public Health Notification. Reducing Radiation Risk from Computed Tomography for Pediatric and Small Adult Patients. (2001) at http://www.fda.gov/cdrh/safety/110201-ct.html
2. Brenner D, Elliston C, Hall E et al (2001) Estimated risks of radiation-induced fatal cancer from pediatric CT. AJR Am J Roentgenol. 176: 289-296
3. Siegel MJ, Schmidt B, Bradley D et al (2004) Radiation Dose and Image Quality in Pediatric CT: Effect of Technical Factors and Phantom Size and Shape. Radiology. 233:515-522
4. International Specialty Products web site. at http://www.ispcorp.com/products/dosimetry/content/gafchromic/index.html
5. Gorny KR, Leitzen SL, Bruesewittz MR et al (2005) The calibration of experimental self-developing Gafchromic HXR film for the measurement of radiation dose in computed tomography. Med. Phys. 32:1010-1016
6. Title 21. Food and Drugs Subchapter J. Radiological Health Part 1020; Performance Standards for Ionizing Radiation Emitting Products, Sec. 1020.33. Computed tomography [CT] equipment. at http://www.accessdata.fda.gov/scripts/cdrh/cfdocs/search/search.cfm?db=CFR&ID=1020.33
7. McNitt-Gray MF (2002) AAPM/RSNA Physics Tutorial for Residents: Topics in CT. Radio.Graphics. 22:1541-1553
8. Gotanda R, Katsuda T, Gotanda T et al (2007) Computed tomography phantom for radiochromic film dosimetry. Australas Phys Eng Sci Med. 30:194-199

- Corresponding Author: Rumi Gotanda
- Institute: Ibaraki Prefectural University of health Sciences
- Street: 4669-2 Ami, Ami-machi
- City: Inashiki-gun, Ibaraki-ken
- Country: Japan
- Email: gotanda@ipu.ac.jp

Ionization Effects Produced by Neutron Interaction Products in BNCT Field

S. Mohammadi

Physics Department, Payame Noor University, Mashad 91735, IRAN

Abstract- **The Ionization effects of charged particles produced in neutron interactions for Boron Neutron Capture Therapy are considered here using SRIM Monte Carlo Code. The estimated values of these effects in a Plexiglas acrylic phantom are shown to agree well with the available experimental values in high Boron concentration areas. As expected, the ionization effects from lithium and alpha particles are significant. In the low Boron areas, proton ionization makes an important contribution and its effect on healthy tissue should not be ignored.**

Keywords: **BNCT; Ionization effects; Lithium; Alpha; Protons; Healthy tissue**

I. INTRODUCTION

In Boron Neutron Capture Therapy (BNCT), a tumor is irradiated by thermal neutrons [1]. Boron atoms are introduced to the tumor and gather in the cancer cells. Higher thermal neutrons interaction cross-section of Boron causes strong impressive ionization damage to the tumor. Boron -10 thermal neutron capture results in the following nuclear reactions :

$$\begin{aligned} n + {}^{10}B &\longrightarrow {}^{7}Li + {}^{4}He\ (\%6.3) \quad Q = 2790\ keV \\ &\longrightarrow {}^{7}Li^{*} + {}^{4}He\ (\%93.7) \quad Q = 2310\ keV \\ &\quad \downarrow {}^{7}Li + \gamma \qquad (1) \end{aligned}$$

The produced lithium and alpha particles have a high Linear Energy Transfer (LET); they deposit their energy within ranges of 4.1 and 7.7 μm respectively, which are comparable to a typical cell dimension. The energy deposition depends strongly on spatial deposition of the B-10 nuclei and in concentrations in the tumor [2]. In addition to the absorbed dose due to B-10 neutron capture, many other dose components are present. Protons are recoil products from the interaction of both fast and epithermal neutrons with hydrogen nuclei in $n + p \rightarrow n' + p'$ interaction. Carbon recoil products come from the interaction ^{12}C (n, n)^{12}C.

In addition to the above interaction, neutrons have another interactive mode with atomic nuclei in matter. The interaction of epithermal neutrons with matter in the BNCT field can result in protons, carbon and oxygen ions as products. The charged particles produced move in matter and ionized it, deposit their energy and eventually have remarkable destructive effects. In this research, the ionization effects of all particles produced in a Plexiglas acrylic phantom are investigated. The unwanted ionization effects are compared with the ionization effects caused by Lithium ions and alpha particles are considered to be basic ionizing particles in BNCT.

We study charged particle tracks in matter by using The Stopping and Range of Ions in Matter (SRIM) code [3]. The precision of a Monte Carlo approach for computing charge particle trajectories in matter depends mainly on the precision of the calculation of the stopping power properties of the matter. A direct calculation of charge particle stopping powers in matter is practically possible by using the transport of ions in matter and by using SRIM computer code. It is proved that the SRIM Monte Carlo modeling could adequately predict the dose to tissue in BNCT treatment.

II. MATERIAL AND METHOD

To simulate a neutron field and charged particle trajectories, we use a Plexiglas acrylic phantom ($C_4H_6O_2$, ρ = 1.17 g cm^{-3}) in considering BNCT and simulate charge particle tracks by Monte Carlo computing using the SRIM computer code. This phantom is used to be able to compare the obtained Monte Carlo calculations with available experimental values. Epithermal neutrons have different modes of interaction with tissue being considered here. Elastic scattering can take place upon interaction with hydrogen, carbon and oxygen nuclei. Elastic scattering cross-sections for these interactions are shown in figure 1[4]. To be able to evaluate the effect of charged particles produced from neutron interactions, the initial energies of particles are needed. Recoiled protons in the elastic scattering of epithermal neutrons by a hydrogen nucleus have the same energy as the incident nucleus; they move in matter and ionize it. These calculations are done by using SRIM computer code. Recoiled carbon ions in ^{12}C (n, n)^{12}C

O. Dössel and W.C. Schlegel (Eds.): WC 2009, IFMBE Proceedings 25/III, pp. 49–52, 2009.
www.springerlink.com

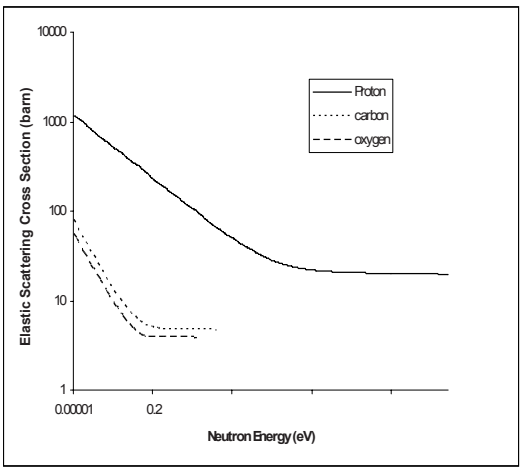

Fig 1. Elastic scattering cross-section variation

and oxygen ions in ^{16}O (n, n)^{16}O elastic interactions have average initial energies of 2.84 keV and 2.215 keV, respectively. Furthermore, the thermal neutrons capture by B-10, results in alpha particles and lithium ions with 1470 and 840 keV initial energies, respectively. Several useful statistical quantities can be defined to estimate the statistical accuracy of the results obtained by SRIM code. Straggling range (σ), Skewness (γ) and Kurtosis (β) are defined as [5]:

$$\sigma = \langle (\Delta)^2 \rangle^{1/2} \quad (2)$$
$$\gamma = \langle \Delta x^3 \rangle / \langle \Delta x^2 \rangle^{3/2} \quad (3)$$
$$\beta = \langle \Delta x^4 \rangle / \langle \Delta x^2 \rangle^2 \quad (4)$$

In this way, straggling range is the square root of the variance, which itself is the second moment distribution of the range. The skewness tells whether the peak is skewed towards the surface (negative values) or away from the surface (positive values). Negative skewness indicates that the most probable depth (the peak position) is greater than the mean depth, and positive values indicate the reverse. Kurtosis indicates the extent of the distribution tails, with a value of 3.0 indicating a Gaussian distribution. Since both the shallow and deep tails contribute, no simple rule indicates what a deviation from 3.0 means for the ion distribution. In general, values from 0 to 3 indicate abbreviated tails, and values above 3 indicate broad tails[5].

III. RESULTS AND DISCUSSION

In using Plexiglas phantom, the energy loss versus depth due to ionization by alpha particles and lithium ions produced by the capture of thermal neutrons in Boron-10 are shown in figure 2. The effects of recoiled particles in this ionization process can be neglected; they are not much in evidence in the figure. The same curves for carbon and oxygen ions are shown in figures 3 and 4 respectively. The effects of recoiled particles in these ionization interactions are comparable to those of the direct ionization effects by carbon and oxygen ions. Furthermore, the energy loss versus depth in Plexiglas due to ionization for protons and recoils are shown in figure 5. It can be seen that ionization effects due to the recoiled particles can be neglected.

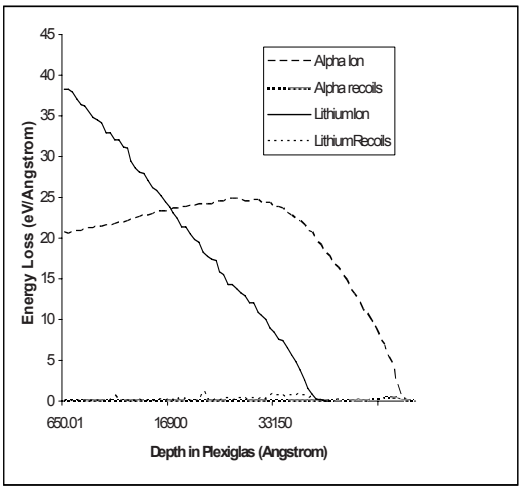

Fig 2. Lithium ions and Alpha particle energy loss

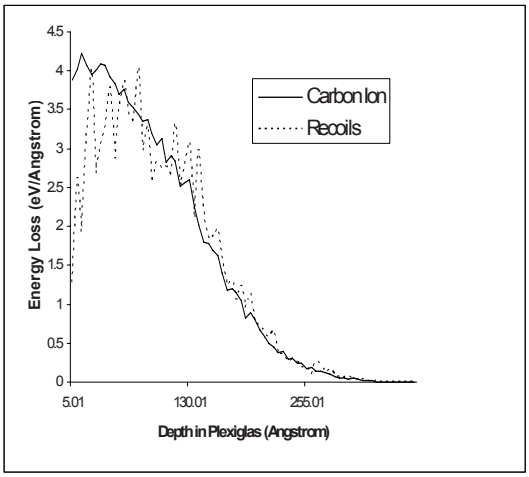

Fig 3. Carbon ions and recoils energy loss

The calculated ion ranges for the various ions are shown in figure 6. It can be seen that the alpha particles produced from thermal neutron capture by boron have the largest ion range (from generation to stop location), in comparison to the other particles produced. SRIM results for the calculated ion initial energy, energy loss and defined statistical quantities for various ions are

shown in table 1.
Each alpha particle produced can ionize the matter in a sphere concentrated on the

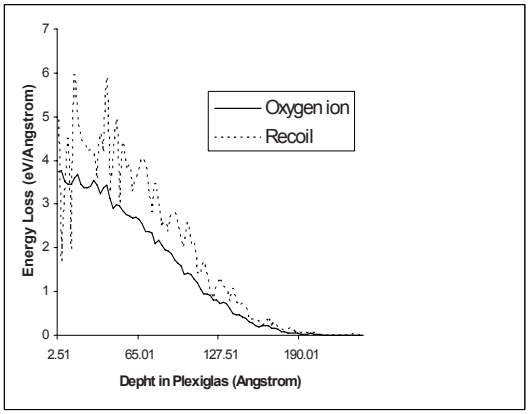

Fig 4. Oxygen ions and recoils energy loss

generation location with a radius equal to 7.120 μm. From its initial energy (1470 keV), it can deposit about 98.6% (1450 keV) for ionizing media. Furthermore, it is obvious from table 1 that oxygen ions have the least range in Plexiglas relative to other particles. Every oxygen ion from its initial energy (2.21 keV) deposits 0.332 keV, namely 13.57 per cent, for direct ionization and 0.426 keV (18 per cent) for indirect secondary ionization. Ionization energy is saved in a sphere of radius 0.011 μm centered on the generation location. The remaining ion energy is spent for increasing thermal vibrations of atoms in media. In order to be able to compare the straggling range for ions, we define parameter η as [3]:

$$\eta = \frac{\sigma}{x} = \frac{\left\langle (\Delta x)^2 \right\rangle^{1/2}}{x} \qquad (5)$$

where η is a criterion for uncertainty concerning the frontier of sphere.

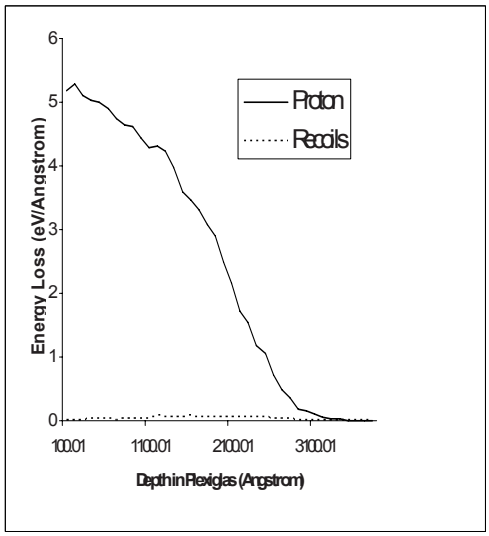

Fig 5. Proton and recoils energy loss

It can be seen from table 1 that the oxygen and carbon ions have the least range of straggling and lithium ions and alpha particles from Boron neutron capture have the largest straggling. But, the defined η indicates that uncertainty for lithium ions and alpha particles is small and for other ions becomes larger.

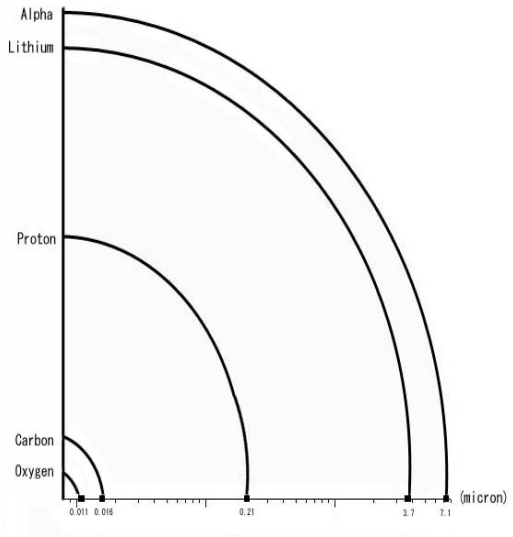

Fig 6. Comparing radius of spheres

The skewness values for alpha particles, protons and lithium ions are negative, indicating that their peak is skewed towards the surface. Carbon and oxygen ions have positive skewness indicating peak is away from the surface. Therefore, carbon and oxygen ions with high probability will stop before reaching their mean stopping location, while alpha particles, protons and lithium ions will more likely stop after their mean stopping location.

Kurtosis values for carbon and oxygen ions are in the range from 0 to 3 and therefore have abbreviated tails; alpha particles, protons and lithium ions have a kurtosis value above 3 and therefore have broad tails. Kurtosis values for oxygen, carbon and protons indicate a distribution similar to a Gaussian shape. An experimental evaluation of the beam quality of the clinical BNCT neutron field at Kyoto university reactor, based on a microdosimetric technique was studied by Endo, et al [6]. It was shown that the estimated relative contributions of the neutron dose on proton, alpha particles and carbon ions are 0.9, 0.07 and 0.03, respectively. In this evaluation, the effects of oxygen and lithium ions were not considered. In the mentioned experimental evaluation, a Tissue Equivalent Proportional Counter (TEPC) and a

Carbon Walled Proportional Counter (CWPC) were used for measurements and the results obtained compared. The TEPC and CWPC were filed by methane-based tissue equivalent and CO_2 gases respectively, at a certain pressure [6]. As CWPC does not contain hydrogen neither in the wall nor in filling gas, the recoiled carbons from elastic scattering produced in tissue can be simulated. In order to be able to compare experimental results to our calculated values using SRIM code, the per cent of ionization effects by protons, carbon ions and alpha particles are calculated and given in table 2. It can be seen that there is a good agreement for protons, but the relative contribution to neutron dose from alpha particles and carbon ions in SRIM calculation are equal. It is also obvious that ionization effects due to the other particles are insignificant when compared with the effects due to lithium ions and alpha particles. Because of the low concentrations of boron in matter as compared with oxygen, hydrogen and carbon, clearly the probability of alpha or lithium productions is very small in comparison to protons and recoiled oxygen and carbon atoms. But, in fact the ionization from these particles can have serious effects and damages in the amount of dose absorbed. For example, in a typical experiment, if the boron concentration is considered to be 2000 *ppm* [2], and we assume the probability of interaction is proportional to particle concentration and neutron interaction cross section in 10 keV[4], the calculated per cent of ionization effects of these particles is shown in table 3. It can be seen that the ionization effects depend strongly on protons and so the dose amount needs to be kept low. Furthermore, the ionization effects due to carbon and oxygen ions are not ignorable. In BNCT, we can control the boron concentration dose in the tumor relative to healthy tissue, but we should not ignore the effect of protons on health tissues.

Table 1. SRIM results for energy and statistical quantities

	Proton	C-12	O-16	He	Li-7
Ion Initial Energy (keV)	10	2.84	2.21	1470	840
Energy Loss in Range (keV)	9.172	0.566	0.322	1451	803.3
Recoil Energy Loss (keV)	0.001	0.529	0.426	0.003	0.014
Struggle (μm)	0.050	0.006	0.004	0.164	0.203
Skewness	-0.55	0.10	012	-2.69	-3.01
Kurtosis	4.06	2.61	2.59	25.76	30.66

Table 2. Per cent of ionization effects due to carbon, proton and alpha

	Carbon	Proton	Alpha
This Work	0.055	0.89	0.055
Reference (8)	0.03	0.9	0.07

Table 3. Per cent of ionization effects due all particles

Carbon	Proton	Oxygen	Lithium	Alpha
11.17	51.31	4.14	11.89	21.49

IV. CONCLUSIONS

For protons, carbon ions, alpha particles, lithium and oxygen ions produced in BNCT, their range and other important statistical parameters were calculated using the SRIM Monte Carlo code. The ionization effects due to these particles were estimated in a Plexiglas acrylic phantom and compared with the available experimental values, showing a good agreement. It is also shown that ionization effects due to the recoiled charged particles compared to the effects due to lithium ions and alpha particles are insignificant. Having considered the Boron concentration and relevant neutron beam cross sections, it is sown that the ionization effect of protons on the healthy tissues is more than the other by-products and should not be ignored. Finally, it is proved that the used SRIM Monte Carlo modeling is adequate to predict the dose to tissue in BNCT treatments.

REFERENCES

1. Daniel C Medina1, Xin Li, and Charles S Springer Jr, (2005) Pharmaco-thermodynamics of deuterium-induced oedema in living rat brain via 1H2O MRI: implications for boron neutron capture therapy of malignant brain, tumours, Phys. Med. Biol. 50.

2. Kenichi Tanaka, Tooru Kobayashi, Gerard Bengua, Yoshinobu Nakagawa, Satoru Endo and Masaharu Hoshi, (2005) Characteristics of boron-dose enhancer dependent on dose protocol and 10B concentration for BNCT using near-threshold $^{7}Li(p,n)^{7}Be$ direct neutrons, Phys. Med. Biol. 50.

3. Ziegler J. F., Biersack J. P., (2003) the Stopping and Range of Ions in Matter, SRIM-2003.26.

4. Neutron Cross Section Lab., available in http://www.nea.fr/janis

5. Ziegler J. F.,(2003) The Stopping and Range of Ions in Matter, Instruction Manual, version 96.xx.

6. S. Endo, Y. Onizuka, M. Ishikawa, M. Takada, Y. Sakurai, T. Kobayashi, K. Tanaka, M. Hoshi and K. Shizuma, (2004) Microdosimetry of neutron field for boron neutron capture therapy at Kyoto university reactor, Radiation Protection Dosimetry, 110.

Author: S. Mohammadi
Department: Physics
Institute: Payame Noor University
City: Mashad
Country: Iran
E-mail: Mohammadi@pnu.ac.ir

Criteria for Acceptability for Radiological, Nuclear Medicine and Radiotherapy Equipment – Part 4: Nuclear Medicine Equipment

S. Christofides[1], L. Malone[2], S. Mattsson[3] and P. Horton[4]

[1] Nicosia General Hospital, Medical Physics Department, Nicosia, Cyprus
[2] Formerly of Medical Physics and Clinical Engineering Department, Beaumont Hospital, Dublin, Ireland
[3] Department of Radiation Physics, Lund University, Malmö University Hospital, Sweden
[4] Quality Assurance Reference Centre, Wallsend, Newcastle upon Tyne, UK

Abstract— **In 2007, the European Commission commissioned a group of Experts to undertake the revision of Report RP91 on "Criteria for Acceptability of Radiological (including Radiotherapy) and Nuclear Medicine Installations", which will be published soon. This paper presents the revised criteria for Nuclear Medicine Equipment.**

Keywords— **Acceptability Criteria, Suspension Levels, Nuclear Medicine, Performance parameters**

I. Introduction

This paper is a part of the revision of Report RP91 on "Criteria for Acceptability of Radiological (including Radiotherapy) and Nuclear Medicine Installations" [1]. It deals with Nuclear Medicine equipment only.

The safe, efficient and efficacious practice of nuclear medicine involves the integration of a number of processes. The quality of each process will have an impact on the overall quality of the clinical procedure and the benefit to the patient. It is important, therefore, that each process be conducted within the framework of a quality assurance programme that, if followed, can be shown to achieve the desired objectives with the desired accuracy.

The levels of activity in radiopharmaceuticals to be administered clinically are governed primarily by the need to balance the effectiveness and the safety of the medical procedure by choosing the minimum absorbed dose delivered to the patient to achieve the required objective i.e diagnostic image quality or therapeutic outcome. To realize this goal, it is important to keep in mind that a nuclear medicine procedure consists of several components, all of which must be controlled in order to have an optimal outcome.

Although the quality assurance of radiopharmaceuticals is an important process [2], it is not an objective of this paper. However, the performance testing of the equipment needed to carry out the quality assurance of radiopharmaceuticals is, both for therapeutic and diagnostic procedures. Devices are included for the determination of administered dose and radiochemical purity such as activity measurement instruments (dose calibrator), gamma counter, thin layer chromatography scanner and high performance liquid chromatography radioactivity detector.

More specifically the objective is to specify acceptable performance tolerance levels (suspension levels) for the equipment used in Nuclear Medicine procedures, both for gamma camera and positron emission based procedures. *In-vitro* Nuclear Medicine diagnostic equipment and instruments are not covered since these do not contribute to the patient exposure.

Some Positron Emission Tomography Installations also have in-house production of the radiopharmaceuticals they use (e.g. FDG labelled with F^{18}), utilising either self-shielded cyclotrons or cyclotrons placed in a specially designed bunkers. This activity is regarded as a radiopharmaceutical manufacturing activity and therefore is outside the scope of this report.

The instruments needed for therapeutic procedures and intra-operative probes are also covered, since these are used directly on the patient to trace the radiotracer administered to the patient.

When equipment no longer meets the required performance tolerance levels (suspension levels), it should be withdrawn from use, may be disposed of, and replaced (Article 8 (3) of Directive 97/43/Euratom) [3]. Alternatively, following a documented risk assessment involving the Medical Physics Expert (MPE) and the Physician, the equipment may be considered for use in less demanding tasks for which a lower specification of performance is acceptable. The operator must be advised of these circumstances.

The performance parameters, with their stated suspension levels are intended to assist in the decision making process regarding the need for maintenance or removal from use of the equipment concerned.

II. Methodology

The methodology used in this work is described in the paper introducing this project [4]

O. Dössel and W.C. Schlegel (Eds.): WC 2009, IFMBE Proceedings 25/III, pp. 53–55, 2009.
www.springerlink.com

III. RESULTS

This section of the revised RP91 report considers equipment used for:

1 Nuclear medicine therapeutic procedures
2 Radiopharmacy quality assurance programme
3 Gamma camera based diagnostic procedures
4 Positron emission based diagnostic procedures
5 Hybrid diagnostic systems
6 Intra-operative probes

Each part is comprised of a brief introduction and a list of relevant equipment. For each piece of equipment, a brief introduction and a table with the applicable performance parameters and their suspension levels is given. To illustrate this, the material developed for Intra-Operative Probes is reproduced.

Intra-Operative Probes

Radiotracer techniques using intra-operative gamma probes are procedures that surgeons can use to localise more easily small tumours or lymph nodes to be removed in a surgical procedure. Use of intra-operative probes decreases operating time, decreases patient morbidity and improves staging accuracy. All of these can lead to improved treatment, improved quality of life and higher long-term survival rates [5].

The most common type of intra-operative probe is the non-imaging gamma probe. Other types such as imaging intra-operative probes and beta probes are less well established or are still under development and therefore their performance parameters are less rigorously defined at present. Furthermore a wide range of gamma probe systems is commercially available with different detector materials, detector sizes and collimator abilities. Various methods of evaluating such equipment have been proposed [6, 7]. For these reasons suspension levels do not exist to cover all the types of intra-operative probes.

For the most common application, that of the detection of the Sentinel Lymph Node (SLN), minimum requirements of a gamma probe system has been recommended [8, 9]. These were derived mainly from comparison studies of commercially available probe systems and are presented in Table 1. It is recommended that the user of a particular probe system establish a quality assurance system for the particular probe system in use and establish suspension levels taking into account the manufacturer's recommendations.

Table 1: Suspension Levels for a SLN intra-operative gamma probe system.

Physical Parameter	*Suspension Levels*	*References*	*Type* [1]
Radial Sensitivity (far field)	FWHM > 40°	Wengenmair H. http://www.sln-kompetenzzentrum.de/gammaprobes.pdf	C
		NEMA-NU3: 2004 (section 3.9)	
Spatial Resolution	FWHM >15mm for lymph nodes in head, neck and supraclavicular region	Wengenmair H. http://www.sln-kompetenzzentrum.de/gammaprobes.pdf	C
	FWHM > 20mm for lymph nodes in extremities, axilla and groin	NEMA-NU3: 2004 (section 3.5)	C
Sensitivity	< 5.5 cps/kBq	Wengenmair H. http://www.sln-kompetenzzentrum.de/gammaprobes.pdf	C
		NEMA-NU3: 2004 (section 3.1 – 3.4)	
Shielding	> 0,1 of minimum system sensitivity	Wengenmair H. http://www.sln-kompetenzzentrum.de/gammaprobes.pdf	C

In a similar fashion the suspension levels are given for the rest of the equipment used in the list given above.

IV. CONCLUSIONS

Throughout this project it was evident that there are few publications that give hard values for suspension levels, especially for new and evolving technologies in Nuclear Medicine. Due to this fact, it was necessary to quote an acceptable tolerance levels for each parameter which is related to the value used for acceptance testing or commissioning of the equipment and on values quoted by the manufacturer.

It was also evident that case studies describing the suspension of equipment based on the performance parameters falling outside defined tolerance levels or hard parameter values were not available in the published literature. It is recommended that such case studies should be published for future use in defining more definite suspension levels.

[1] For the definition of "Type", see reference [4].

Since technology is evolving continuously and new equipment regularly comes on the market, it is necessary for the regular review and updating of the suspension levels recommended in this project takes place.

Acknowledgment

The authors of this paper would like to express their sincere thanks to al those who reviewed the Nuclear Medicine Equipment section of this project for their valuable and constructive comments.

This project is carried out under a contract with the European Union Commission, Directorate General for Energy and Transport (DG TREN), with contract no. TREN/07/NUCL/S07.70464.

References

1. RP91Criteria for acceptability of radiological (including radiotherapy) and nuclear medicine installations, 1997.
2. IAEA Technical Report Series No. 454, "Quality Assurance for Radioactivity Measurements in Nuclear Medicine, STI/DOC/010/454, IAEA, Vienna, 2006
3. Council Directive 97/43/Euratom of 30 June 1997 on health protection of individuals against the dangers of ionising radiation in relation to medical exposure, and repealing Directive 84/466/Euratom, OJ L180, 9.7.1997, p. 22-27
4. Criteria for acceptability for radiological, Nuclear medicine and Radiotherapy Equipment - Part 1: Introduction and Methodology, These proceedings.
5. Halkar R. K. and Aarsvold J. N. "Intraoperative probes", Journal of Nuclear Medicine Technology, Vol. 27, No. 3, September 1999, pp. 188-192.
6. NEMA NU3-2004, "Performance Measurements and Quality Control Guidelines for Non-Imaging Intra-operative Gamma Probes", NEMA, 2004.
7. IEC TR 61948-1:2001, "Nuclear medicine instrumentation – Routine tests – Part 1: Radiation counting systems"
8. Wengenmair H., Kopp J., "Gamma Probes for Sentinel Lymph Node Localization: Quality Criteria, Minimal Requirements and Quality of Commercially Available Systems", http://www.sln-kompetenzzentrum.de/gammaprobes.pdf
9. Yu S. K., et al., "Intraoperative Gamma Probe for Sentinel Node Localisation: Evaluation Study", J Hong Kong College of Radiologists, 2005;8:40-48.

Author: S. Christofides
Institute: Medical Physics Department, Nicosia General Hospital
Street: 215 Old Nicosia Limassol Road
City: Nicosia 2029
Country: Cyprus
Email: cstelios@cytanet,com,cy

Criteria for Acceptability for Radiological, Nuclear Medicine and Radiotherapy Equipment – Part 3: Radiotherapy Equipment

P Horton[1], I-L Lamm[2], W Lehmann[3], and S Lillicrap[4]

[1] Quality Assurance Reference Centre, Wallsend, Newcastle, UK
[2] Lund University Hospital, Lund, Sweden
[3] University Hospital of Saarland, Homburg, Germany
[4] University of Bath, Bath, UK

Abstract— **In 2007, the European Commission has commissioned a group of Experts to undertake the revision of Report RP91 on "Criteria for Acceptability of Radiological (including Radiotherapy) and Nuclear Medicine Installations", which will be published soon. This paper presents the revised criteria for Radiotherapy Equipment.**

Keywords— **Acceptability Criteria, Suspension Levels, Radiotherapy, Performance parameters**

I. Introduction

This paper is a part of the revision of Report RP91 on "Criteria for Acceptability of Radiological (including Radiotherapy) and Nuclear Medicine Installations" [1] and it deals with Radiotherapy Equipment only.

The safe, efficient and efficacious practice of radiotherapy involves the integration of a number of processes. The quality of each process will have an impact on the overall quality of the treatment and the benefit to the patient. It is important, therefore, that each process be conducted within the framework of a quality assurance programme that, if followed, can be shown to achieve the desired objectives with the desired accuracy. More specifically the objective is to specify acceptable performance tolerance levels (suspension levels) for the equipment used in radiotherapy.

When equipment no longer meets the acceptable performance tolerance levels (suspension levels), it should be withdrawn from use (Article 8(3) of Directive 97/43/Euratom) [2]. Following a documented risk assessment by the Medical Physics Expert (MPE) and the practitioner, the suspended equipment may be considered for use in more limited circumstances or be replaced. The documented risk assessment must include a rationale for and the extent of any continued use. The operators must be advised in writing of these circumstances.

II. Methodology

The methodology used in this work is described in the paper introducing this project [3]

III. Results

This section of the revised RP91 report considers the following radiotherapy equipment:

1 Linear accelerators
2 Simulators
3 CT Simulators
4 Cobalt-60 Units
5 Kilovoltage Units
6 Brachtherapy
7 Treatment Planning Systems
8 Dosimetry Equipment
9 Radiotherapy Networks

Each part is comprised of a brief introduction and a list of performance characteristics with their tolerance/suspension levels. Specific reference is not made to safety issues, but these need to be checked at acceptance, and after maintenance and upgrades.

The performance tolerances/suspension levels quoted in this section have been taken from recognised international and national standards in the first instance, supplemented by guidance from national and international professional bodies. These include International Electrotechnical Commission (IEC), International Atomic Energy Agency (IAEA), European Society for Therapeutic Radiology and Oncology (ESTRO), American Association of Physicists in Medicine (AAPM), Canadian Association of Provincial Cancer Agencies (CAPCA) and the Institute of Physics and Engineering in Medicine (IPEM).

.

O. Dössel and W.C. Schlegel (Eds.): WC 2009, IFMBE Proceedings 25/III, pp. 56–57, 2009.
www.springerlink.com

Acknowledgment

The authors of this paper would like to express their sincere thanks to all those who reviewed the Radiotherapy Equipment section of this project for their valuable and constructive comments.

This project is carried out under a contract with the European Union Commission, Directorate General for Energy and Transport (DG TREN), with contract no. TREN/07/NUCL/S07.70464.

The authors gratefully acknowledge the permission of the following bodies to quote their standards and test methods: The International Electrotechnical Commission (IEC), International Atomic Energy Agency (IAEA), European Society for Therapeutic Radiology and Oncology (ESTRO), American Association of Physicists in Medicine (AAPM), Canadian Association of Provincial Cancer Agencies (CAPCA) and the Institute of Physics and Engineering in Medicine (IPEM).

References

1. RP91Criteria for acceptability of radiological (including radiotherapy) and nuclear medicine installations. European Commission, 1997.
2. Council Directive 97/43/Euratom of 30 June 1997 on health protection of individuals against the dangers of ionising radiation in relation to medical exposure, and repealing Directive 84/466/Euratom, OJ L180, 9.7.1997, p. 22-27
3. Criteria for Acceptability for Radiological, Nuclear Medicine and Radiotherapy Equipment – Part1: Introduction and Methodology (in preparation), 2009

Author: P. Horton
Institute: QA Reference Centre
Street: Silverlink Business Park
City: Wallsend NE28 9ND
Country: UK
Email: patrick.horton10@btinternet.com

Half-Value Layer Measurement for Effective Energy, Using Radiochromic Film and Step-Shaped Aluminum Filter

T. Gotanda[1, 2], T. Katsuda[3], R. Gotanda[1, 4], A. Tabuchi[1],
T. Kuwano[1], K. Yamamoto[1], H. Yatake[1], K. Kashiyama[1] and Y. Takeda[1]

[1] Graduate School of Health Sciences, Okayama University, 5-1 Shikata Cho, 2-Chome, Okayama 700-8558, Japan
[2] Department of Radiology, Oishi Hospital, 1-7-15 Kawaguchi Cho, Fukuyama City, Hiroshima 720-0822, Japan
[3] Health Care Sciences, Himeji Dokkyo University, 7-2-1 Kamioono, Himeji City, Hyogo 670-8524, Japan
[4] Department of Radiological Sciences, School of Health Sciences, Ibaraki Prefectural University of Health Sciences, Ibaraki 300-0394, Japan

Abstract— **The effective energy of diagnostic X-rays is important for quality assurance and quality control purposes. However, the half-value layer (HVL), which is necessary to evaluate the effective energy, has not been ascertained because of the high cost of the ionization chamber (IC) required and because the measurements are time-consuming and complicated. To solve these problems, a method using radiochromic film (RCF) and step-shaped aluminum (SSAl) filters has been developed. Gafchromic EBT (GAF-EBT), which has a weak energy dependence, was used as the RCF. The X-ray tube voltage for HVL was measured as 120 kV. The SSAl filter area, the full exposure area, and the non-exposure area were set on the GAF-EBT so as to obtain correct data. The density ratio of the SSAl filter area was calculated using the densities of the full exposure area and the non-exposure area. The GAF-EBT was scanned using a flat-bed scanner before and after exposure. To remove the image acquisition error of the flat-bed scanner, the scanning image of the GAF-EBT before exposure was subtracted from it after exposure. The HVL was evaluated using the density attenuation ratio of the GAF-EBT. Then, the effective energies obtained using the GAF-EBT and the IC were compared. The HVL and the effective energy with X-ray tube voltage of 120 kV using the GAF-EBT were 4.56 mm and 41.0 keV, respectively. The difference ratio of the effective energy between the GAF-EBT and IC methods was 5.9%. The effective energy can be measured using GAF-EBT easily and with high precision. The measurement time using GAF-EBT is extremely short compared with the IC method. Moreover, the effective energy can be measured inexpensively using the GAF-EBT.**

Keywords— **half-value layer, effective energy, radiochromic film, Gafchromic EBT**

I. Introduction

The effective energy of an X-ray beam is one of the standard quality assurance (QA) and quality control (QC) tests for various radiological systems. In the radiation-quality management of complex X-ray generators, the half-value layer (HVL), which is used to calculate the effective energy, is important. In general, HVLs are measured by means of an ionization-chamber (IC) dosimeter, and this is referred to as the standard method. However, the HVL is not monitored constantly. The reasons for this are the high cost of the IC, which also needs regular calibration, and the fact that not all institutions have an IC. In addition, it is a time-consuming process owing to the number of measurement points.

Recently developed radiochromic films (RCFs) can easily be used to measure absorbed doses, because they do not need development processing and they indicate a density change that depends on the absorbed dose [1, 2]. In addition, RCFs are cost-effective in comparison with an IC dosimeter [3]. Therefore, an HVL measurement method using RCF was performed, instead of the standard method. Gafchromic EBT (GAF-EBT: International Specialty Products, Wayne, NJ) was used as the RCF, because it has a weaker energy dependency than all other RCFs [3-6]. It is not necessary for the film density to be converted into absorbed dose, because the calibration curve of the absorbed dose versus film density is a straight line in the low dose range for HVL measurements of X-rays in the diagnostic range [3]. Therefore, the HVL can be evaluated using only the ratio of the density distribution of the RCF. One of the main characteristics of RCF that sets it apart from the IC dosimeter is that it can be used to measure two-dimensional dose distributions, as well as serving as a general X-ray film. On the basis of this characteristic, the HVL may be evaluated easily and simply using the density distribution and a step-shaped aluminum (SSAl) filter. The purpose of this study is to address four issues associated with the standard method, namely the high cost and need for regular calibration of the IC dosimeter and the complex and time-consuming nature of the measurements, and to evaluate the use of the GAF-EBT in determining the effective energy simply and at any time or place.

II. Materials and Methods

A. Gafchromic EBT

The GAF-EBT is rectangular shape measuring 20.32 cm x 25.4 cm; the thickness is 234 μm [3] and it is clear blue in color. When the active component is exposed to radiation, it

O. Dössel and W.C. Schlegel (Eds.): WC 2009, IFMBE Proceedings 25/III, pp. 58–61, 2009.
www.springerlink.com

changes to a dark-blue color. The energy dependence of the response of the GAF-EBT is minimal (within 10%) over the 50 kVp to 10 MVp X-ray range [3, 6]. GAF-EBT is suitable for HVL measurement of X-rays in the diagnostic range because of the very weak energy dependence of the dose response. Disadvantages are that more than 2 h is necessary to stabilize the film density post exposure [7], and measurement density is affected by humidity when a flat-bed scanner is used [3]. Additionally, there are non-uniformity errors caused by the coating of the GAF-EBT film. These errors parallel (down-web) and vertical (cross-web) to the direction of the coating are 0.5% and 1.0%, respectively [3]. The GAF-EBT was kept at room temperature, 20-25°C, in a shading bag. It should be noted that the GAF-EBT is inexpensive in comparison with an IC.

B. Step-shaped aluminum filter

An SSAl filter of more than 99.8% purity has been designed (Fig. 1). The SSAl filter is rectangular in shape, with dimensions of 20 mm x 100 mm, and its thickness increases from 1 mm to 25 mm (the specific thicknesses of the steps are 1, 2, 3, 5, 7.5, 10, 12.5, 15, 20, and 25 mm).

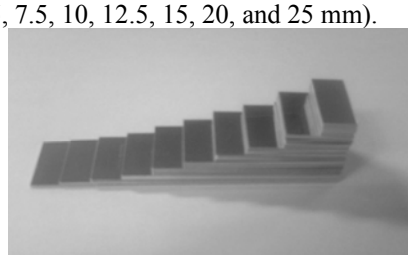

Fig. 1 Design of the SSAl filter

C. HVL measurement of the GAF-EBT

HVL measurements were performed by setting the exposure parameters of the X-ray generator (DRX-2924HD, Toshiba Medical, Tochigi, Japan) to 120 kV, 250 mA, 4.0 s (0.4 s x 10). The anode□cathode direction of the X-ray tube was set perpendicular to the long axis of the GAF-EBT (down-web direction) to avoid any X-ray heel effect.

The GAF-EBT of approximate dimensions 20 cm x 25 cm was used. The GAF-EBT was measured in the down-web direction to minimize the non-uniformity error. The thickness of the aluminum was varied in the long axis direction of the GAF-EBT. The exposed GAF-EBT is shown in Fig. 2.

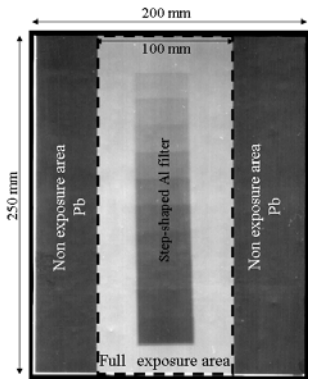

Fig. 2 Scanned image of the GAF-EBT after exposure

A central 100-mm band of the GAF-EBT was set as the exposure area, and lead masking plates (thickness 2 mm) were placed on either side of the exposure area to create non-exposure areas. The SSAl filter was placed in the center of the exposure area. The full exposure area, non-exposure area, and SSAl filter area were set in the GAF-EBT. The full exposure area was used to compensate for a non-uniformity error caused by the active layer of the GAF-EBT, while the non-exposure area was used to compensate for a non-uniformity error caused by the protection layer.

The experimental set-up of the exposure method for measuring the HVL is shown in Fig. 3. The SSAl filter was placed on an empty paper box. The distance from the X-ray focus to the SSAl filter was set at 500 mm to reduce the influence of diagonally incident X-rays. The distance from the SSAl filter to the GAF-EBT was also set at 500 mm to reduce the influence of scattered radiation from the SSAl filter. To avoid backscattered radiation from the floor, the distance between the floor and the GAF-EBT was set at over 500 mm.

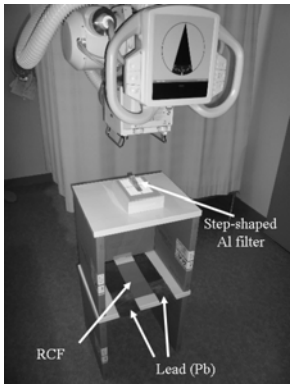

Fig. 3 Arrangement of the exposure method for HVL measurement

The GAF-EBT was scanned using a flat-bed scanner (EPSON ES-2200, Seiko Epson Co., Nagano, Japan) in

RGB (48 bit) mode, 100 dpi, with the protection of a film of liquid crystal (LCD-150, Sanwa Supply Inc., Okayama, Japan) to remove of the Moire artifact. The GAF-EBT was scanned by setting of transmission type [3]. To remove an error caused by the image acquisition of the flat-bed scanner, the GAF-EBT was scanned before and after exposure.

The image data of the GAF-EBT were divided into R, G, and B modes (each 16 bit), and the R mode was used. It was converted to a gray scale and inverted to black and white, and was analyzed using Image J version 1.40g image analysis software (National Institutes of Health, MD, USA). In this study, the HVL for X-ray tube voltages of 120 kV was measured using 1-15 mm thicknesses of the SSAl filter.

The region of interest (ROI) included the following sequence: a non-exposure area, a full exposure area, the SSAl filter area, a full exposure area, and a non-exposure area. In terms of density, an exposure area and a non-exposure area were set at 100% and 0%, respectively, and the density ratio of the SSAl filter area could then be calculated. To minimize the non-uniformity error in the down-web direction, these processes were performed for all thicknesses of the SSAl filter. The attenuation curve for HVL measurement was obtained using the density ratio of each SSAl filter thickness. The HVL was then calculated using the attenuation curve. In addition, the effective energy was calculated on the basis of the HVL. The conversion from the HVL to the effective energy was calculated using the recent data of Seltzer and Hubbell at the National Institute of Standards and Technology [8].

D. Comparison with the standard method using the IC

HVL measurement using an IC dosimeter was performed for comparison with the method using the SSAl and GAF-EBT. The exposure parameters were 120 kV, 200 mA, 0.05 s. The thicknesses of the Al filter were 1, 2, 3, 4, 5, 7.5, 10, 12.5, and 15 mm. A normal geometric arrangement of the exposure method for measuring the HVL was adopted to minimize the influence of scattered radiation (similar to Fig. 3). Exposure and dosimetry measurements were performed three times for each Al thickness, and averaged dose values were used. The HVL and the effective energy were then calculated. The results of the method using GAF-EBT were compared with those of the standard method in order to evaluate its applicability.

III. Results

Figure 4 shows density profile curves before and after exposure on the ROI in the cross-web direction. The subtraction of the scanning image before exposure and after exposure provided a flat density profile curve without a non-uniformity error of the GAF-EBT.

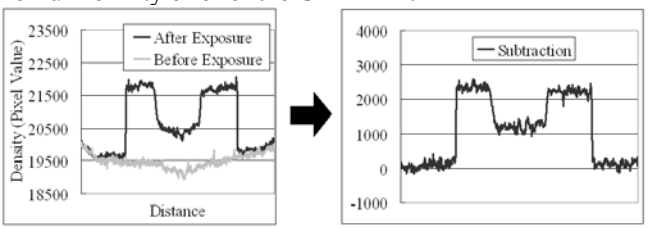

Fig. 4 Density profile curves before and after exposure, and after subtraction

Figure 5 shows the attenuation curves at 120 kV obtained by means of the GAF-EBT method, and by the standard method with an IC dosimeter. The HVLs and effective energy using the GAF-EBT and IC were 4.03 mm and 4.56 mm, and 38.7 keV and 41.0 keV, respectively. The determination coefficients for the attenuation curves for both the method using the GAF-EBT and the standard method were more than 0.99. The difference ratio of the HVL for the GAF-EBT and IC methods was 13.2%. In addition, the difference ratio of the effective energy was 5.9%.

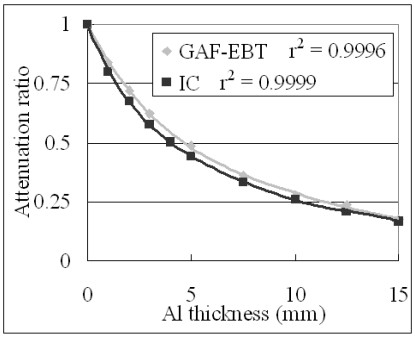

Fig. 5 Attenuation curves at 120 kV using the GAF-EBT, and the standard method using an IC dosimeter

IV. Discussion

A. Non-uniformity error of the GAF-EBT

The GAF-EBT is capable of two-dimensional measurements in the same way as a film dosimeter. So it was possible to evaluate the HVL by this method using the SSAl filter. However, the measurements were subject to a non-uniformity error in various areas of the GAF-EBT sheet. The density profile curve of the sheet before exposure tended to be high at both sides, and low in the center (Fig. 4). The curve after exposure was affected by this error. To remove this error, the scanning image of the GAF-EBT before exposure was subtracted from that after exposure.

Therefore, a flat curve without a non-uniformity error was produced. Additionally, in the case of the GAF-EBT, compensation based on the data for the exposure area, the non-exposure area, and the SSAl filter area was applied at all thicknesses of the SSAl filter to take into account the non-uniformity error in the down-web direction. Therefore, any non-uniformity errors of the active layer and the protective layer were removed. Measurement results of high precision using the GAF-EBT were provided. It is considered that the HVL measurement was made easier by improvement and development of the analysis method.

B. Advantage of the GAF-EBT

The measurement time with the GAF-EBT was extremely short compared with the IC method, because fewer X-ray shots were needed. In order to provide equal precision, X-ray shots were necessary 24 times in the IC and 10 times in the GAF-EBT. It is suggested that the method using the SSAl and the GAF-EBT could reduce the load on X-ray tubes. In addition, the repeat setup of a geometric arrangement for each aluminum thickness did not have to perform. Therefore it is considered that the method using GAF-EBT and SSAl offers a facile means of determining the HVL.

Moreover, it is considered that the effective energy can be measured inexpensively using the GAF-EBT in comparison with the IC.

C. Applicability for the effective energy measurement

The difference ratio of the effective energy using the IC dosimeter and the GAF-EBT was 5.9%. The method using the GAF-EBT can be used to measure the effective energy with errors within several percent. It is considered that effective energy measurement is possible, because the influence of the energy dependence of the GAF-EBT is small in the HVL measurement. Consequently, it is suggested that the method using the GAF-EBT may be of practical use for QA and QC in all institutions. In addition, it is considered that the method using the GAF-EBT will offer highly precise HVL measurement by further improving the analysis method in future.

V. Conclusions

The method using the GAF-EBT as RCF described herein has two advantages in HVL measurement for the evaluation of effective energy. Firstly, an IC dosimeter is not needed. The effective energy can be measured inexpensively without an IC dosimeter within an error range of less than 10% using only GAF-EBT. In addition, the HVL could be evaluated repeatedly because, unlike an IC dosimeter, the GAF-EBT could be used without regular calibration. Secondly, the HVL measurement time is greatly reduced. Using the GAF-EBT and the SSAl, measurements can be made in a very short time compared to the standard method using an IC dosimeter. In the light of these findings, it is considered that the GAF-EBT method offers a facile means of determining effective energy for QA and QC at any place or time, without the need for an IC dosimeter.

Acknowledgment

The authors would like to thank Dr. Michihiko Oishi for providing the various equipment used in these investigations.

References

1. Butson MJ, Yu PKN, Cheung T et al. (2003) Radiochromic film for medical radiation dosimetry. Mater. Sci. Eng. R Rep, 41:61-120.
2. Cheung T, Butson MJ, and Yu PKN. (2005) Reflection spectrometry analysis of irradiated GAFCHROMIC XR type R radiochromic films. Appl. Radiat. Isot., 63(1):127-129.
3. International Specialty Products website. Available at: www.ispcorp.com
4. Dini SA, Koona RA, Ashburn JR et al. (2005) Dosimetric evaluation of GAFCHROMIC XR type T and XR type R films. Am. Coll. Med. Phys. 6(1):114–134.
5. Butson MJ, Cheung T, and Yu PKN. (2005) XR type-R radiochromic film X-ray energy response. Phys. Med. Biol., 50(15):195–199.
6. Butson MJ, Cheung T, and Yu PKN. (2006) Weak energy dependence of EBT GAFCHROMIC film dose response in the 50 kVp10 MVp X-ray range. Appl. Radiat. Isot., 64(1):60-62.
7. Cheung T, Butson MJ, and Yu PKN. (2005) Post-irradiation colouration of GAFCHROMIC EBT radiochromic film. Phys. Med. Biol., 50:281-285.
8. Seltzer SM and Hubbell JH. (1995) Table and graphs of photon mass attenuation coefficients and mass energy-absorption coefficients for photon energies 1 keV to 20 MeV for elements Z=1 to 92 and some dosimetric materials, National Institute of Standards and Technology.

Author: Tatsuhiro Gotanda
Institute: Okayama University
Street: 5-1 Shikata Cho, 2-Chome
City: Okayama 700-8558
Country: Japan
Email: tat151826@yahoo.co.jp

Influence on Erythropoiesis and Blood Catalase Activity Low Intensity Electromagnetic Millimeter Radiation

Ts. I. Adamyan[1], E. S. Gevorgyan[1],H.H.Hovhanisyan[1], S. M. Minasyan[1], V. P. Kalantaryan[2] and A. A. Hakhoumian[2]

[1]Department of Human and Animal Physiology, Yerevan State University,Yerevan, Armenia
[2]Department of Microwave Radiophysics, Yerevan State University,Yerevan, Armenia

Abstract- **The present study was undertaken to investigate changes of the blood catalase activity and regeneration processes in the circulatory system of rabbits under conditions of bone-marrow deficiency and long-term exposure to low-power extremely high frequency electromagnetic radiation (EHF EMR) at frequency of 50.3 GHz. As it is known, this frequency is resonant for the vibrations of water hexagonal structures[1]. During both whole-body and head area exposure to EHF EMR the animals were placed in front of the center of the conical antenna, at distance of 500 mm and 150 mm from the radiating end of the antenna (far field zone). The spatial peak incident power density (IPD) was measured to be as 0,05 mW/cm^2 and spatial peak specific absorption rate (SAR) at the skin surface was calculated to be as 2 W/kg.The results of our experiments show that repeated exposures can cause erythrogenetic activity, prolonged retyculocyte crisis, hemoglobin and erytrocyte content growth, as well as faster retyculocyte maturation. The obtained data demonstrate that living organisms react to low-intensity monochromatic radiation mobilizing their internal resources. Namely, regenerative processes are intensified and compensation mechanisms gain broader capacities. Deficiency of bone marrow in the result of its removal does not significantly affect the erythrogenesis. Irradiation on the rabbits head area increases catalase activity in peripheral blood, maximum of which was registered 20-fold and on the 10-th day after 25-fold influences.The character of changes of the catalase activity does not depend on the changes of total number of erythrocytes.**

The observed activation of catalase probably, promotes the enhancement of the power antioxidant system of the organism.

Keywords-**Extremely high frequency electromagnetic radiation, low-intensity millimeter waves, erythrogenesis, bone-marrow deficiency,blood catalase,erythrocytes.**

I.Introduction

According to literature facts, the millimeter-wave therapy increases the level of immune resistance, influences different stages of pathogenesis, changes enrymatic reaction activity and growth rate, destroys microorganisms [2,3].It has shown that millimeter waves have strong effect on the process and bioelectric activity of neurochemical functions of the brain. Penetrating into the organism this radiation is transformed into information-carrying signals performing guidance and adaptation control or rehabilitation processes in the organism. Different physical factors,affect the organism, in the same way as electromagnetic waves, provoking changes in the functioning of different organs/systems. Erythron plays an essential role in development of such processes, as it actively contributes to the maintenance of functional state of the organism.

This investigation has the aim to study the characteristics of regenerative processes in the circulatory system and blood catalase activity change under the effect of non–thermal(low intensity) and non-ionizing coherent electromagnetic radiation millimeter range.

II.Methods

Experiments were carried out on rabbits of the same weight, age and sex. The animals underwent 30-day exposure with G4-141 coherent electromagnetic waves generator (Russian made) with frequency of 50.3 GHz, in correspondence with resonance frequency of vibrations of hexagonal structures of water [1]. A whole-body exposure of rubbits to Extremely High Frequency Electromagnetic Radiation (EHF EMR) was conducted in the far-field zone of conical antenna at a distance of 500 mm from the radiating end of the antenna. Incident power density (IPD) value in the plane of exposed object was of 0,05 mW/sm^2 . To calculate the SAR, we used dielectric parameters of the skin $\varepsilon' = 14$, $\varepsilon'' = 18$ and skin density $\rho = 1.15$ g/cm^3 [2]. Specific absorption rate on the surface of skin of animals back was calculated by the formula [3]

$$SAR = \frac{\sigma\xi(1-R)P_0}{n\rho} \qquad (1)$$

O. Dössel and W.C. Schlegel (Eds.): WC 2009, IFMBE Proceedings 25/III, pp. 62–65, 2009.
www.springerlink.com

where $\sigma = \varepsilon_0 \varepsilon'' \omega = 50.4$ S/m is the electric conductivity of skin at the frequency of 50,3GHz, $\varepsilon_0 = 8.85 \cdot 10^{-12}$ F/m is the vacuum dielectric constant, ω is the circular frequency, ξ = 377 Ω is the vacuum wave impedance, P_0 is the incident power density, R=0.5 is the reflection coefficient, n = 4.2 is the refractive index of the skin.

Calculated value for the SAR is received about 2W/kg. Animals of the control group were sham-exposed by placing the rubbits into the exposure zone when the generator was turned on but the output power was attenuated to zero. Duration of the exposure and sham-exposure was 60 minutes.

Normally, 24 hours after the bone marrow extraction and on the 5th, 10th, 15th, 20th, 25th, 30th days and 2 weeks after the exposure the following features of erythropoesis were analyzed: the quantity and colorimetric characteristics of erythrocytes, reticulocytes, hemoglobin, maturation rate of reticulocytes, the cellular content of the bone marrow.In order to assess the functional alternations of erythroid branch, the bone marrow index of erythronormoblasts protoplasm maturation has been revealed.

In catalase activity change experiments the animals were exposed under a single, 5-, 10-, 20-,25- and 30-fold radiation. In case of a single radiation the studies were carried out before the radiation effect and on the 5-th, 30-th, 90-th minutes after it. Have been calculated the catalasen umber Cn, represented as quantity (in milliliter) of decomposition hydrogen peroxide - H_2O_2 in 30 minutes, the absolute number of erythrocytes in blood periphery, catalase index Ci – the ratio of Cn to the numbers of erythrocytes in 1 mm^3 of blood (in millions). In multiple radiation the studies of the mentioned characteristic values were carried out before the radiation effect and after it on the 5-th minute

III. Results and discussion

Hypochrome changes of erythrocyte and hemoglobin amounts were observed without irradiation during 24 hours after the bone marrow withdrawal. As compared to the starting point, the amount of erythrocytes had fallen by 13.5%, hemoglobin by 21.33% (Fig 1). Thus the color index changed to value 0. 68. The latter was accompanied by increase in relative and absolute quantities of reticulocytes , as well as their maturation rate (Fig.2). On the 5th day of irradiation, normochrome decrease of erythrocytes and hemoglobin content was observed. Reticulocytosis and high level of their maturation rate were the same in the mentioned period. In the phase of marrow extraction, the amount of myelocaryocites and erythroid branch cells was low. The myelocaryocites level is 95300 ± 3115 and erythroid branch cells 38.0 ± 1.2 in normally. On the 5th day of irradiation they were respectively 68000 ± 2045 ($p < 0{,}001$) and $27{,}0 \pm 0{,}678$ ($p < 0{,}001$). However, the marrow index of erythronormoblasts protoplasm maturation remained unchanged (0. 6). On the 10th day of the experiment, moderate increase of erythrocytes and hemoglobin amount has been observed (5% and 9% correspondingly). On mentioned time the increase of cells, not containing hemoglobin proerythroblasts and erythroblasts was seen in marrow, which confirms the acceleration of proliferative processes. On the 15th day the growth of erythrocyte and hemoglobin quantities continued. The quantity of reticulocytes and their maturation rate were high. On the 20th day of studies the erythrocyte and hemoglobin quantities were within the limits of physiological vibration 94.48%, 94.28%. As compared to the 15th day, the absolute and relative amounts of reticulocytes had decreased, but still were on the high level compared to the starting point. The observed variations in the peripheral red-blood indices are likely to be related with intensification of marrow proliferative and maturatoin processes. This fact is confirmed by high activity of erythroid cells in the extracted marrow domain and the growth of hemoglobin-containing normoblasts quantity.

During 25 to 30 days after exposure the quantities of erythrocytes and hemoglobin have not undergone any essential changes compared to the 20th day . The absolute and relative amounts of reticulocytes on the 30th day varied within the limits of starting point. In 2 weeks after stopping the irradiation, all parameters of erythropoiesis have returned to the initial values. It should be noted that the marrow index of cytoplasm maturation of erythronormoblasts have not changed during the whole investigation period.

Catalase activity change investigations have shown that on the 5-th minute after single low intensity EMR influence Cn and Ci have an increase and absolute number of erythrocytes in peripheral blood decreased .A gradual decrease of the Cn level up to the norm was registered during the following 30, 60, and 90 minutes. Analogical changes were registered for the Ci characteristic values, but for the all mentioned periods of time it was on the relatively higher level. The catalase activity and the absolute number of erythrocytes were not changed synchronously. The carried out investigations on blood catalase have shown that on the 5-th minute after single low intensity EMR influence Cn and Ci have an increase and absolute number of erythrocytes in peripheral blood decreased .A gradual decrease of the Cn level up to the norm was registered during the following 30, 60, and 90 minutes. Analogical

changes were registered for the Ci characteristic values, but for the all mentioned periods of time it was on the relatively higher level. The catalase activity and the absolute number of erythrocytes were not changed synchronously. After 5-fold radiation effect the character and value of the changes of Cn, Ci and the total erythrocyte number were analogical to the changes compared to a single radiation effect. After 10- and 20- fold radiation effect an increase of the catalyze activity was observed (Fig.3).

IV. Conclusions

The results obtained show that, after removal of the marrow, repeated application of millimeter electromagnetic radiation activates the erythropoiesis, enhances the long-lasting reticulocyte maturation process, increases the erythrocytes and hemoglobin content. Stability of erythrocytes and hemoglobin quantities during 20 to 30 days after extraction and irradiation of marrow, strong intensification of reticulocyte maturation process, as well as the acceleration of proliferative branch erythroids and maturation processes allow us to conclude that multiple exposure of living organism to coherent electromagnetic millimeter radiation mobilizes its preservation power. The latter tends to enhance the regenerative processes and broaden the capacities of compensational mechanisms, as a result of which the removal of marrow does not seriously affect erythropoiesis. Our obtained results agree on the literature, according to which in case of combined action of millimeter range electromagnetic radiation and anti-tumor preparations the impairment of hemopoietic system decreases significantly and stimulates the proliferative activity of stem cells of marrow, as compared with isolated effect of the mentioned drugs.

The data obtained prove that in single, 5-, 10-, 20-fold and on the 10-th day after 25-, 30-fold radiation effect of 60-minute-duration of EM radiation on the rabbits' head the increase of catalase activity in peripheral blood was observed, maximum of which was registered in 20-fold and on the 10-th day after 25-fold influence (Fig.3). The character of changes of the catalase activity do not depend on the changes of total number of erythrocytes. The observed in our experiments activation of the peroxisomatic catalase enzyme , probably, promotes the enhancement of the power antioxidant system of the organism.

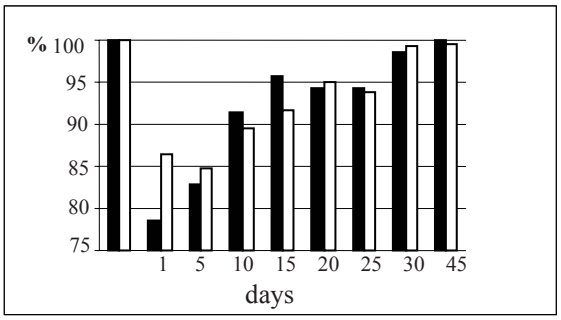

Figure 1: The change by percent amount of erythrocytes in 1 ml blood (white) and amount of hemoglobin (gram/%)(black) under influence of electromagnetic radiation (EMR)

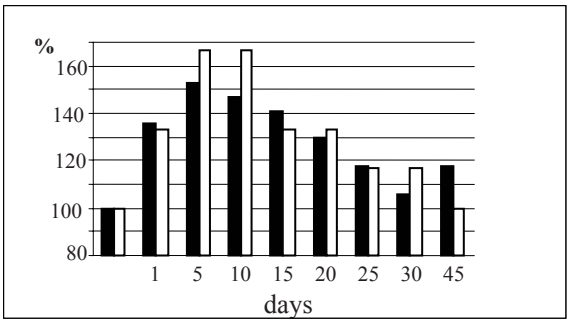

Figure 2: The change by percent relative amount of retuculocytes ($^{0}/_{00}$) (black) and the rapidity of retuculocytes ripening in an hour (white) under influence of electromagnetic radiation (EMR)

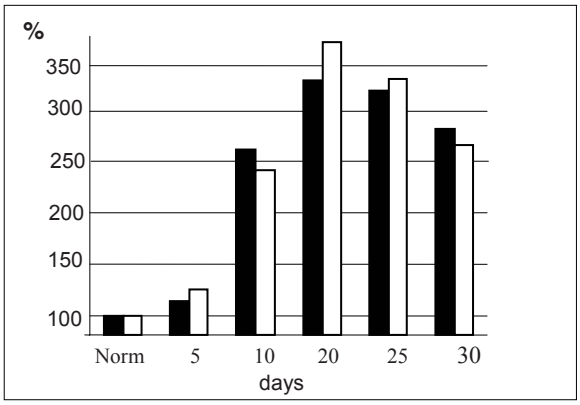

Figure 3: The change by percent catalase number Cn (black) and catalase index Ci (white) in the blood under influence of electromagnetic radiation (EMR)

References

1. Petrosyan V, Sinitsin N, Elkin V, Devyatkov N, Gulyaev Yu, Betski O at al. (2001) The role of resonance molecular-wave processes in the environment and their application for control over and correction of states of ecological systems.Biomed Radioelectron 5-6:62-129
2. Gapeev A, Chemeris N (2000) Model approach to the analyses of effects of modulated electromagnetic radiation on animal cells. Biophysics 45: 299-312
3. Gapeev A, Mikhailik E, Chemeris N (2008) Anti-inflammatory effects of low-intensity extremely high-frequency electromagnetic radiation: Frequency and power dependence.Bioelectromagnetics 29: 197-206

Vitaly Kalantaryan
Yerevan State University
A.Manoogian str.1
Yerevan
Armenia
vkalantaryan@yandex.ru

Quality Assurance in Digital Volume Tomography

F.H. Schöfer and C. Hoeschen

Institute of Radiation Protection, Helmholtz Zentrum München - German Research Center for Environmental Health
Munich, Germany

Abstract— **Digital Volume Tomography is a method of rising value in dentistry as well as in oral and maxillofacial surgery. The different systems commercially available offer a variety of characteristics due to their different construction and the different reconstruction algorithms in use. Especially the missing possibilities to export raw data linearly and the fact that there is no common output scale like the Hounsfield scale in computed tomography make it difficult to evaluate images of test phantoms in a unified way. We present measurements of resolution, homogeneity, contrast to noise ratio and modulation transfer function from datasets built from a test phantom by different commercial systems. The results are connected to dose measurements and the comparability of results from different systems is discussed as well as the possibility of statements about differences in their efficiency.**

Keywords—**DVT, Phantom, MTF, Contrast to Noise Ratio**

I. Introduction

In dentistry as well as in oral and maxillofacial surgery Digital Volume Tomography (DVT) is a method of rising importance. In other reports the method is compared to different dental modalities in respect to diagnostic value [1, 2]. Here we aim for the measurement of the physical properties of image generation at different commercially available DVT systems.

A special emphasis lies on the suitability of the different parameters for a regular ascertainment of the quality of systems in clinical use.

In computed tomography the Hounsfield scale is defined to describe radiographic density of the specimen under examination. Its direct connection to the linear attenuation coefficients of the materials examined makes the resulting datasets directly comparable. In contrast the DVT systems available today do not work on a common output scale. All systems offer possibilities for the export of datasets but the datasets exported by different systems have is no common scale connecting the exported data grey scales. In addition they rely on individual scanning geometries and reconstruction algorithms. This makes the comparison of raw data difficult. Raw data export is also not regularly implemented in the systems.

The aim of this study is to evaluate different values measurable in exported datasets after unknown image generation and processing. The results are examined concerning their suitability as measures of system quality and performance and for the detection of malfunctions.

In chapter II. Material And Methods the techniques used are described as well as how the different parameters under evaluation are obtained. In chapter III. Results the resulting data is presented. In chapter IV. Conclusions and Discussion the value of the results for quality assurance of DVT systems in clinical use is summarized and discussed.

II. Material and Methods

A. Material

Phantom: Datasets were generated from imaging a phantom at different commercial DVT systems. For our examinations we used a commercially available phantom (cf. Fig. 1).

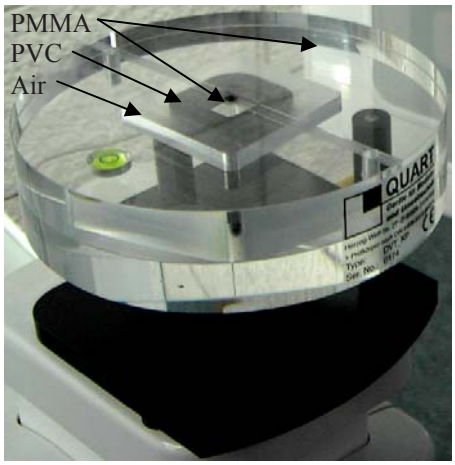

Fig. 1 Phantom:
PMMA cylinder containing an inset of PVC around PMMA in air.

The phantom is to simulate the maxillofacial and the mandibular region of a patients head. Based on the head phantom for dose measurements in computed tomography systems it is a cylinder made of PMMA of 16cm diameter. In addition to the PMMA representing radiographic properties close to soft tissue it contains an inset ring of PVC representing bone and air around it (cf. Fig. 2).

O. Dössel and W.C. Schlegel (Eds.): WC 2009, IFMBE Proceedings 25/III, pp. 66–69, 2009.
www.springerlink.com

The phantom contains a bubble level and markings in order to help to place it concentric and aligned horizontally with the reconstructed volume.

Software: The datasets were exported by the different DVT systems' software. The evaluation was performed by software provided with the phantom. It leads to a quantitative description of system properties like large scale homogeneity, statistical noise, the scale values derived from PMMA and PVC radiation interaction, the Nyquist frequency and the modulation transfer function.

B. Methods

The datasets of the different systems are loaded into a separate computer program, first a section through homogeneous PMMA and second a section through a layer composed of PMMA, PVC and air. The grayscale is reduced to 255 levels for all images. The software version used provides fully automated selection of regions of interest.

Contrast: As a main property of a system imaging soft tissue and bone the difference between the average grey values of the equivalent plastic materials PMMA and PVC define the basic contrast. The corresponding regions of interest are manually chosen in the middle of one side of the 1cm wide PVC ring and in the center of the surrounded 2*2cm² square of PMMA (cf. Fig. 2).

Noise: In order to obtain measures for the noise fluctuation of the pixel values the standard deviation of regions of interest placed manually in PMMA and PVC is calculated (cf. Fig. 2).

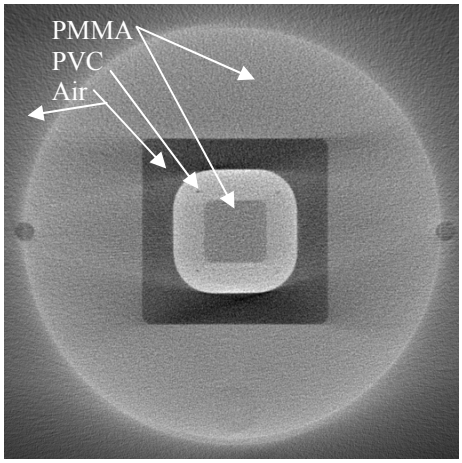

Fig. 2 Section of the phantom imaged to obtain noise, contrast and MTF

Homogeneity: In order to obtain a measure for the large scale homogeneity of the datasets sections through the PMMA are evaluated. The image slice dataset is automatically sectioned into 49 regions each a seventh part of length and width of the image. Five regions of interest are chosen: one in the center and the second neighbors to all four sides horizontally and vertically (cf. Fig. 3). The pixel values of the regions of interest are averaged and differences of all pairs are calculated. The homogeneity measure is the maximal result divided by with the contrast (see above) of the system under examination.

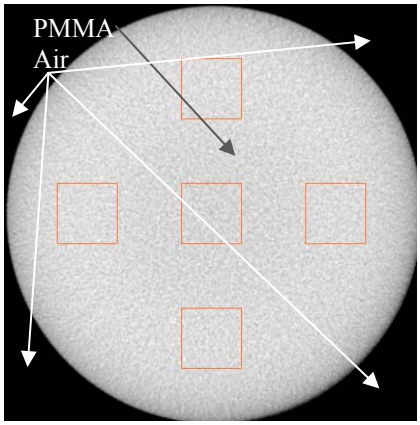

Fig. 3 Section through a homogeneous PMMA layer of the phantom and regions of interest used to examine the large scale homogeneity.

Nyquist Frequency: The Nyquist Frequency is derived directly from the resolution of the dataset sectioning the PVC ring of 1cm width. A region imaging the PVC and the neighboring PMMA and air was chosen manually from a corresponding section of the dataset (cf. Fig. 4).

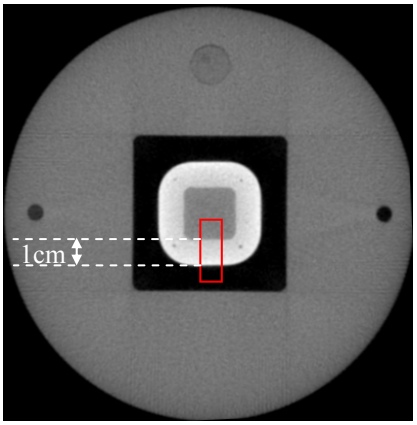

Fig. 4 Section of the phantom and the region used to obtain the Nyquist frequency (red frame)

Modulation Transfer Function: The modulation transfer function is obtained in a horizontal section at the edge between PVC and air. The corresponding region of the image is chosen manually. The change of the pixel values across the edge is recorded averaging pixel lines parallel to the edge. The result is differentiated and analyzing the row of difference values moving away from the maximum at the edge they are set to zero when the first one gets below zero.

It turned out useful in order to reduce artifacts from data processing differences to make the values symmetric around the maximum. This is achieved by averaging pairs of values neighboring the maximum symmetrically. The result is Fourier transformed, normalized and the scale transformed to the spatial frequency up to the Nyquist frequency.

Dose: Measurements of the entrance dose were performed at the detector without the phantom in the radiation cone. The geometry of the systems was investigated in order to allow the calculation of dose values in the imaged volume.

III. Results

The contrast between the gray values connected to PMMA and PVC and the noise level were determined as basic properties of the sectional image datasets. Putting them into relation leads to the contrast to noise ratio. The known linear connection of this value to the applied dose was reproduced (cf. Fig. 5).

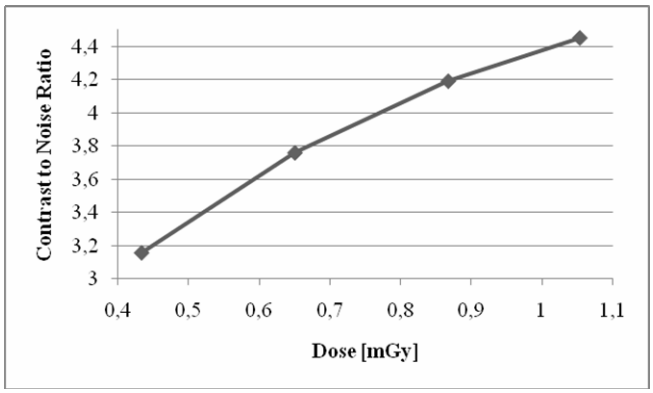

Fig. 5 Contrast to noise ratio vs. Entrance Dose

The determination of contrast to noise ratios was stable with repeated measurements. In one system the values could be compared after the creation of two datasets, one with double spatial resolution and the double of the dose: the contrast to noise ratio was reduced by a factor of 2 accordingly.

The examination of large scale homogeneity shows that PMMA is reproduced to one gray scale value within 10% of the contrast between PMMA and PVC. One system showed deviations up to 15% compared to the contrast.

Measured MTF curves showed a similar course for systems of similar values for contrast to noise ratio and spatial resolution (cf. e.g. 2 and 3b in Fig 6). Doubling the spatial resolution and the dose leads to a higher MTF curve (cf. e.g. 3a in Fig 6) and to half the contrast to noise ratio. The system with the lowest contrast to noise ratio has the highest values of modulation transfer (cf. e.g. 1 in Fig 6).

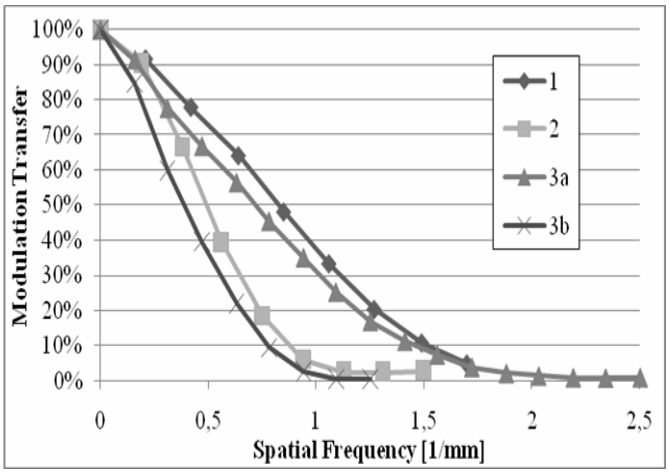

Fig. 6 MTF curves of three DVT systems (one run twice in high and low resolution)

Taking a second dataset from a DVT system that used a comparatively high entrance dose after adding additional filtering (0.2mm Cu) did not change any of our values apart from the dose measurement.

IV. Conclusions and Discussion

Unknown image processing does change the results for the quality properties checked by imaging the phantom. Nevertheless it is highly improbable that hardware or software malfunctions remain unseen when checking the whole set regularly. The results were stable when repeated. Checking the whole set of values and comparing them to a first measurement will secure the continuous function of a DVT system and show clearly that everything is in order.

The reconstructed data sets' resolution is not directly dependent on the detector resolution of the system. Comparing different values of the spatial resolution of different systems has to take the contrast to noise ratio and the dose applied to the volume under investigation into account. As the scanning geometries of the systems available have not been

made to become comparable the dose values have to be interpreted carefully.

When comparing different systems it should be kept in mind that the values can be traded against each other. E.g. the evaluation suggests that the MTF can be improved by accepting a lower contrast to noise ratio. For a ranking of the devices on a scale of dose efficiency the expectable image information per dose has to be found. The results presented here suggest building this scale by a connection of contrast to noise ratio, spatial resolution, MTF and Dose.

On the other hand the whole sets of values collected at different systems show differences in quality parameters traded against each other.

The introduction of additional filtering at one of the systems without any influence on the quality measures examined here is a good example of how quality assuring measurements lead to an optimization of the relation between image quality and dose in the application of DVT systems.

ACKNOWLEDGMENTS

We thank members of the task force DVT of the German Standardization organization DIN who helped collecting the datasets at different clinically used DVT systems and Dr. H. Schöfer for fruitful discussion. We thank Quart GmbH Zorneding, Germany for providing equipment especially the phantom and the evaluation software.

REFERENCES

1. Guerrero M E, Jacobs R, Loubele M, Schutyser F, Suetens P and Steenberghe D v. (2006) State-of-the-art on cone beam CT imaging for preoperative planning of implant placement. Clinical Oral Investigations 10:1-7
2. M. Cohnen, J. Kemper, O. Möbes, J. Pawelzik and U. Mödder (2002) Radiation dose in dental radiology. European Radiology 12:634-637

Author: F.H. Schöfer
Institute: Institute of Radiation Protection,
Helmholtz Zentrum München
German Research Center for Environmental Health
Street: Ingolstaedter Landstrasse 1
City: Neuherberg
Country: Germany
Email: felix.schoefer@helmholtz-muenchen.de

DICOM DOSE: CAPTURE AND REPORTING

S. Balter[1], H. Blendinger[2]

[1]Radiology and Medicine, Columbia University Medical Center, New York City, USA
[2]Siemens Healthcare, Forchheim, Germany

Abstract— **An increasing fraction of imaging equipment is capable of measuring its own X-ray output. Quality management processes in diagnostic and interventional radiology require access to patient exposure data. DICOM now provides tools for communicating dosimetric and related data in a comprehensive manner. A first-generation structured report (RDSR), optimized for fluoroscopically guided procedures, was released as part of the 2007 DICOM Standard. Similar structures for mammography and computed tomography are in the 2008 Standard. The RDSR is a DICOM object that is created and managed separately from the creation and storage of images. Even if images are discarded (e.g. fluoroscopy, rejected radiographs), the RDSR will record all of the radiation used during a procedure.**

All of the data in a RDSR is in public fields, each identified by a DICOM tag or unique concept name. The RDSR always contains patient and examination data, total dose data for the entire procedure. For interventional procedures, the RDSR also contains technical, geometric, and dosimetric data for each individual irradiation. RDSRs are designed to be distributed on a network and captured by free-standing dose-management ACTORS as well as by RIS and PACS. The IHE Radiation Exposure Monitoring (REM) Profile gives additional guidance and supplies use cases for RDSR handling. In addition RDSRs can also be stored within an imaging system and manually downloaded.

This paper will focus on interventional systems including examples of dose modeling for individual patients. Many additional uses for the RDSR are foreseen. These include monitoring the use of radiation during conventional procedures (e.g. chest radiography) as part of a facility quality management program; and the development of reference levels.

Keywords— **DICOM, IHE REM, Quality Program, Dose Documentation, Interventional Fluoroscopy**

I. Introduction

This manuscript is the next in a series of reports documenting the development of DICOM dose reporting [1, 2].

The collection of clinical radiation dose information is of considerable value for reasons that include; image quality assurance, estimating the radiation load on the population attributable to medical imaging [3], optimizing dose utilization at individual facilities, and monitoring dose delivered to individual patients.

The dosimetric quantities used for diagnostic imaging are the subject of the ICRP Report 74 [4]. This manuscript uses and extends the concepts given in ICRP-74.

Modern X-ray generators are equipped with several dose reporting tools [5]. These can include; simple displays of the technical factors, Kerma Area Product (P_{KA}) meters, dose at a reference point meters ($K_{a,r}$), and perhaps reconstructions of skin dose distributions on the surface of a patient. In the clinic, parts of the available information might be; displayed until manually copied, printed as a dose report, or included in the header of a DICOM image. DICOM headers provide an incomplete picture of patient dose simply because no header is stored unless an image is stored.

II. Measures of patient dose

Traditional 'dose' tracking is simply counting the number and size of the sheets of film used to complete an examination. This provided a reasonable control mechanism since acceptable films could only be produced within a relatively narrow detector-dose range. A facility could estimate patient dose from this information plus knowledge of imaging geometry and an output calibration of the relevant generator.

Digital images are often stored in DICOM format. Image headers provide tags that support the tradition of recording technical factors. These fields can only be completed by systems that integrate X-ray production and image detection into a unified whole. Assuming that all of the images are saved, dose reconstruction from such systems is of similar complexity to that of conventional film-based systems. Fluoroscopic dose data or the dose data associated with rejected images is seldom saved in conventional DICOM exam headers.

A. Number of exposures and fluoroscopic time.

Many clinicians regard fluoroscopy time as a synonym for dose. Fluoro-time is reported as "dose" in at least one major MIS. There is a general increase of patient dose with fluoroscopic time However; it is a poor metric for an individual patient. Its validity further declines when there is a radiographic component of the procedure.

O. Dössel and W.C. Schlegel (Eds.): WC 2009, IFMBE Proceedings 25/III, pp. 70–73, 2009.
www.springerlink.com

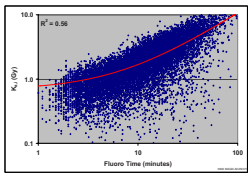

Figure 1. Relationship between fluoroscopic time and Ka,r for a series of 11,000 procedures performed in a cardiac catheterization laboratory. Greater variability can be observed in a general interventional radiology laboratory.

Figure 1 illustrates variability observed in a very large series of diagnostic and interventional procedures performed in the cardiac catheterization laboratory of a major institution[1]. Even though the R^2 of 0.56 implies some predictability, there is an order-of-magnitude variability of $K_{a,r}$ for most fluoroscopic times. This is due to differences in patient size, projection angles, and the amount of cine used for these procedures.

B. Kerma Area Product (P_{KA})

Instrumentation for the determination of Kerma Air Product (P_{KA}) has been available for decades. This instrumentation is more commonly found on equipment installed within the European Union. P_{KA} measurements meet the dose recording requirements in the EURATOM Directive.

P_{KA} measurements form the basis for much of the European work in developing reference levels for diagnostic imaging procedures. An excessive mean P_{KA} for a particular examination may indicate too much dose delivered to the patient's skin, too large an X-ray field, or a combination of these two factors. Thus tracking P_{KA} provides useful tools for both an institution's conformance with reference levels and local quality management practices.

Literature exists modeling the relationship between the P_{KA} delivered by specific examinations and the Effective Dose (E) delivered by those examinations [6, 7]. These reported conversion factors will differ depending on the technical details of the procedure and the organ weighting factors used for the calculations [8-10].

Documenting the total KAP delivered to patients by an imaging department serves several important purposes. Even though the KAP required to produce an archived digital image is often available in the image header, the total KAP associated with the procedure is less often available because of the loss of information associated with non-archived images and with fluoroscopy.

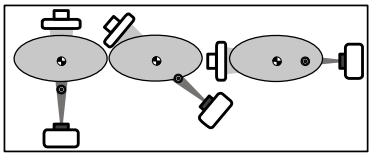

Figure 2 Motion of the reference point relative to the patient's skin as the fluoro. gantry rotates.

[1] Collection and publication of this data was approved by the Hospital's Institutional Review Board (Ethics Board).

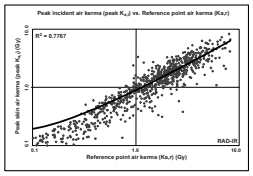

Figure 3. The relationship between $K_{a,r}$ and PSD for a subset of 800 procedures included in the RAD-IR project [11].

C. Accumulated dose at the IEC Reference Point ($K_{a,r}$)

Patients undergoing interventional procedures are at risk for deterministic skin injuries. The IEC introduced the interventional reference point and the associated dose meter as an estimator for skin dose [12]. The FDA has required such instrumentation on all fluoroscopes manufactured after June 15 2006 and sold in the USA. The accumulated air kerma (measured without scatter) is designated $K_{a,r}$. For an isocentric fluoroscope, the reference point is located on the beam's central ray and 15 cm from the isocenter toward the X-ray tube.

The location of the reference point approximates the location of the patient's skin. The reference point moves relative to the patient as the X-ray system moves. (Figure 2).

$K_{a,r}$ is an estimator of actual peak skin dose. It is possible to improve the estimate by appropriately correcting for distance between the reference point and the patient's skin, beam motion during a procedure, and backscatter. The interventional RDSR provides sufficient information to make these calculations.

The relationship between peak skin dose (PSD, maximum incident air Kerma on any portion of the patient's skin) and $K_{a,r}$ was studied in the RAD-IR project (9). In this project, PSD was estimated using CareGraph (Siemens Healthcare, Malvern PA) dose modeling software. The results are shown in Figure 3. It was concluded that $K_{a,r}$ provides a clinically useful operational surrogate for PSD.

III. DICOM DOSE PROJECT

A. DICOM overview

There is a great deal of useful data recorded in DICOM headers [13]. Much of this is contained in public TAG-VALUE pairs (i.e. the TAG is specified in the DICOM dictionary). However important data may also be stored in manufacturer specific private fields. The stored fields, their units of measure, and the apportionment of stored data between public and private fields can vary by manufacturer, equipment model, and software release.

DICOM headers typically only report the factors associated with the accompanying image or image series. Therefore dose information is likely to be lost if the images are

never stored (e.g. fluoroscopy) or discarded instead of being sent to the archive (e.g. retakes).

The need for an improved dose reporting system was first seen in documenting fluoroscopically guided interventions. Here fluoroscopy typically delivers around half the total KAP or IEC dose. The range of fluoroscopic contributions to individual procedures can be from zero to 100%.

B. DICOM Standard: Supplement 94

This extends the DICOM standard by with tags needed to report dose and dose related factors in public fields. (One of the goals of the DICOM-DOSE project is to eliminate private dose fields.) Supplement 94 is limited to projection radiography and fluoroscopy.

The Radiation Dose Structured Report (RDSR) was introduced as a new DICOM object. The RDSR provides a place to accumulate all of the dose information associated with a study irrespective of the storage of any or all of the images produced by that study.

ACTORS also introduced as the tool needed to manage and archive RDSRs. This ACTOR accepts RDSRs and stores them in a compatible archive. ACTORS may be produced to archive RSDRs in a PACS archive, a medical informatics system, or in a stand-alone system.

Streaming transfers have been proposed. These would provide a data stream for real-time dose modeling and reconstructions. Inputs from the medical physics community are needed to clarify the need for this service and to define its extent.

C. IEC Publicly Available Specification 61910-1

PAS 61910-1 (Radiation dose documentation – Part I: Equipment for radiography and radioscopy) defines two conformance levels that manufacturers can use to claim an appropriate degree of compliance with this document. Level 1 is intended for systems used only for general radiography and fluoroscopy where the risk of reaching deterministic dose levels is negligible. Level 2 is intended for interventional systems.

The PAS defines the fields required in a RDSR at each conformance level. Thus essential data will be available in a standard format. This will facilitate dose documentation, and dose comparison.

A RDSR contains its own header block and a set of data corresponding to each irradiation event. The latter is defined as a single actuation of the exposure switch (e.g. single radiograph, fluoroscopic series, DSA run).

The header contains the usual demographic and system identifiers along with summary dose data. Since the object of the RSDR is to report dose data, it also contains fields designating the accuracy of the dose measurements, and the organization responsible for validating this claim.

An irradiation event contains details of the geometric, technical, and dosimetric factors associated with that irradiation. Provisions have been made to assure congruence between the irradiation event data and the data stored in the header of the associated images.

In principle, the set of irradiation events is complete enough to estimate the distribution of dose within the patient. However, work is needed to better define the location and orientation of the X-ray beam in patient space.

Streaming of irradiation events to an ACTOR during a procedure is expected to provide the basis for real-time dose maps. The design and engineering of clinically useful dose-distribution displays without unnecessarily distracting the operator is expected to be an interesting area for research.

D. The IHE Radiation Exposure Monitoring Profile

With the introduction of DICOM RDSR, the fundamentals for an IHE profile exist (www.ihe.net). The definition of such a profile will help manufacturers and implementers to clearly understand to which technical level solutions have to extend for interoperability of RDSR implementations. The IHE Radiation Exposure Monitoring (REM) Profile is now available and draft implementations will be tested in 1st quarter of 2009.

The REM profile defines roles and transactions to be fulfilled to allow a complete workflow from X-Ray systems generating reports, to long-term storage in PACS and specific processing of reports including forwarding to dose registers. So the traditional roles *Acquisition Modality* and *Image Manager/Archive* are used to define the basic interchange of DICOM Dose SR from X-Ray system to PACS. The new roles of Dose *Information Consumer* and *Dose Information Reporter* denote systems that receive or actively retrieve Dose SR to combine and process the contained information. The *Dose Information Reporter* is seen with extended features to communicate Dose SR information with an external regional/national *Dose Register*, which is the 3rd new role introduced within REM profile. The potential of this approach is multifaceted, the guidance of medical physicist community will influence if new dedicated system will preferably be used for dose information processing or the existing RIS systems extend their partially existing features to a full Dose QA option.

IV. Dosimetry note

The values reported by DICOM-DOSE are only as accurate as the accuracy of the measurements made by the imag-

ing equipment. The FDA and IEC both require an accuracy of ± 35% for $K_{a,r}$. IEC also requires ± 35% for P_{KA}. The IAEA Code of Practice for Diagnostic Radiology [14] estimates an uncertainty of less than 10% when calibrating a clinical beam using a traceable dose meter. DICOM-DOSE expects clinical dose-reporting instruments to be periodically checked against standard instruments. Note that there is no requirement to recalibrate the clinical dose-meter. The RDSR has fields intended to record the correction information.

V. Example

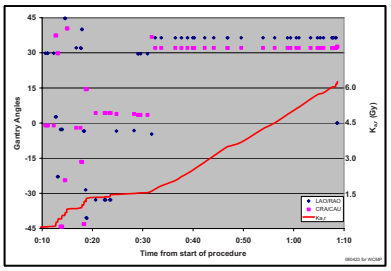

Figure 4 Simulated DICOM-DOSE Outputs for an actual interventional procedure. Please see the text for further information.

Implementations of DICOM-DOSE are planned for release in 2009. This section presents an example of how DICOM-DOSE might be used. This documents an actual major interventional coronary procedure. The following was used for a post-procedure discussion with the operator regarding the possibility of radiation skin injury.

The reported total $K_{a,r}$ for this procedure was 6269 mGy. The correction factor for the fluoroscope was 0.97. The backscatter factor is approximately 40%. If the beam did not move, and the reference point was exactly on the patient's skin, the PSD would be 8.5 Gy. Such a dose indicates the possibility of a significant injury.

The log for this procedure documents 186 irradiation events in 70 minutes. Figure 4 shows the X-ray beam angles for each irradiation as well as the accumulation of $K_{a,r}$ over the procedure. The key interval is 35 minutes at 36° LAO / 32° CAU. $K_{a,r}$ for this region was 4583 mGy with an estimated PSD of 6.2 Gy. The patient developed an erythema on her right shoulder resulting in skin discoloration three months later. The discoloration faded within six months of the procedure. This patient is still followed by the lab.

VI. Conclusion

Many dosimetric measures can be obtained from modern imaging equipment. The deployment of DICOM-DOSE is expected to facilitate dose collection and management on an institutional [15], national, and world-wide basis

VII. References

1. Balter, S., *Patient Dose Reporting in Digital Imaging*, in *World Congress of Medical Physics and Biomedical Engineering*. 2006: Seoul, Korea.
2. Balter, S., *Capturing patient doses from fluoroscopically based diagnostic and interventional systems.* Health Phys, 2008. **95**(5): p. 535-40.
3. Suleiman, O.H., S.H. Stern, and D.C. Spelic, *Patient dosimetry activities in the United States: the nationwide evaluation of X-ray trends (NEXT) and tissue dose handbooks.* Appl Radiat Isot, 1999. **50**(1): p. 247-59.
4. ICRU, *Report 74: Patient Dosimetry for X-Rays Used in Medical Imaging*. JICRU, 2005. **5**(2).
5. Balter, S., *Methods for measuring fluoroscopic skin dose.* Pediatr Radiol, 2006. **36 Suppl 14**: p. 136-40.
6. Bor, D., et al., *Comparison of effective doses obtained from dose-area product and air kerma measurements in interventional radiology.* Br J Radiol, 2004. **77**(916): p. 315-22.
7. Yakoumakis, E., et al., *Differences in effective dose estimation from dose-area product and entrance surface dose measurements in intravenous urography.* Br J Radiol, 2001. **74**(884): p. 727-34.
8. Smans, K., et al., *A study of the correlation between dose area product and effective dose in vascular radiology.* Radiat Prot Dosimetry, 2008. **130**(3): p. 300-8.
9. Bogaert, E., K. Bacher, and H. Thierens, *A large-scale multicentre study in Belgium of dose area product values and effective doses in interventional cardiology using contemporary X-ray equipment.* Radiat Prot Dosimetry, 2008. **128**(3): p. 312-23.
10. Stratakis, J., et al., *Radiation dose and risk from fluoroscopically guided percutaneous transhepatic biliary procedures.* J Vasc Interv Radiol, 2006. **17**(1): p. 77-84.
11. Miller, D.L., et al., *Radiation doses in interventional radiology procedures: the RAD-IR study: part II: skin dose.* J Vasc Interv Radiol, 2003. **14**(8): p. 977-90.
12. IEC, *IEC 60601. (2000). Medical electrical equipment - Part 2-43: Particular requirements for the safety of X-ray equipment for interventional procedures*. 2000: Geneva.
13. Vano, E., et al., *On the use of DICOM cine header information for optimisation: results from the 2002 European DIMOND cardiology survey.* Radiat Prot Dosimetry, 2005. **117**(1-3): p. 162-5.
14. IAEA, *Dosimetry in diagnostic radiology: An international code of practice* in *TECHNICAL REPORTS SERIES*. 2007, International Atomic Energy Agency.
15. Miller, D.L., et al., *Quality improvement guidelines for recording patient radiation dose in the medical record.* J Vasc Interv Radiol, 2004. **15**(5): p. 423-9.

Author: Stephen Balter, Ph.D.
Institute: Columbia University Medical Center
City: New York, New York
Country: United States
Email: sb2455@columbia.edu

CT Quality Assurance Protocol and its validation in various Ministry of Health Hospitals in Oman.

Arun Kumar.L.S., Rashid Al-Hajri and Sultan Al-Busaidy.
Medical Physics and Radiation Protection Service,
DGEA, Ministry of Health, PO Box 393,
Muscat-100, Sultanate of Oman.

Abstract-**Computed Tomography(CT) is extensively adopted in diagnostic imaging world over due to various advantages over other imaging techniques. This eventually resulted in higher population doses. Oman is also not an exception to this. In 2007, there is a fifteen percentage increase in CT examinations in Ministry of Health hospitals alone than the previous year. To obtain good quality CT scans with optimal patient dose, a comprehensive radiation acceptance and quality assurance programme has to be in place for CT scanners. Here in this study validation of such a programme employed in Ministry of Health, Oman for CT scanners in various Ministry of Health hospitals is discussed. Though a large number of parameters were analysed for the study, we include a few from them – Computer Tomography Dose Index (CTDI), Scatter radiation levels, CT numbers, Noise, Slice thickness from four different vendors.**

Introduction: Computed Tomography (CT) is one of the important imaging modality in diagnostic radiology and this has revolutionized diagnostic imaging since its discovery during early 70's. The use of CT is increasing steadily since then. In US currently more than 62 million CT scans were performed per annum. In Oman, this number corresponds to 27,761 CT examinations for the year 2007 which shows a fifteen percentage increase from the previous year. The number of CT scanners per million population is 26 in the US and 64 in Japan. In Oman, this is about 8 per million. As the number of CT scanners are increasing will eventually result in the increase of associated radiation doses and the consequent risk of cancer in adults and particularly in children. In Oman, as of now there is no nationally approved legislation for radiation acceptance and quality assurance protocol for the new and existing CT scanners. We, therefore follow the International Atomic Energy Agency approved acceptance and testing protocol for the acceptance of CT scanners. Here, we discuss a protocol adopted for Oman for the comprehensive radiation acceptance and quality assurance testing of CT scanners installed in ministry of health hospitals, before handing over for routine patient care work. The radiation parameters measured include scatter radiation levels, Computed Tomography Dose Index (CTDI), Dose Length Product (DLP) and image parameters such as noise, CT numbers, Slice thickness, resolution, alignment, bed movement etc. The above cited parameters were analysed for all the CT scanners installed in various Ministry of Health hospitals during 2006-08 period from different vendors. However, we will include a few of the above parameters in this study. The objective of the current study is to make sure that all CT scanners units attached for clinical use meets WHO/IAEA standards as the Sultanate does not have currently a national protocol for acceptance of CT scanners.

Materials and Methods: Among the parameters - CTDI, Noise, CT numbers and Slice thickness are included in this work. Scatter radiation levels were measured using body phantom and Victoreen NERO 8000 unit by connecting externally a 400 cc scatter chamber. Exposure mode of the NERO 8000 is used for the scatter measurements by applying the stored calibration factor of the chamber and by employing the temperature - pressure correction for the air. Exposure or rate measurements can be performed according to the need.

CTDI was estimated using 100 mm pencil CT chamber which is coupled to a Victoreen 8000 NERO unit externally along with PMMA head and body phantoms. The exposure is measured using the user entered beam width in mm and the CT probe calibration factor.

For the measurement of CTDI, ionization chamber which is supported by the phantom, is placed on the couch top. The head and body phantoms are orientated such that one of the peripheral dose measurement holes corresponds to the position of the maximum air kerma at a depth of 10 mm below the phantom surface. The four dose measuring holes equally spaced around the periphery are used for measurement along with the central one in both phantoms. Three readings of each hole position of the pencil chamber were taken after correcting them for the temperature and pressure of air and finally averaged.

The measured dose values at a depth of 10 mm below the phantom surface will not be uniform because of the presence of the patient couch and the effect of any over scan. The dose maximum is identified by using a series of measurements done with different orientations of the phantom. In some situations, the scan start angle may vary from scan to scan, making the position of dose maximum difficult to locate. In such situation, the method of the IPEM protocol was adopted. It may be possible to operate the machine in 'engineer' mode to control the start angle of the scan. If this is not possible, a series of measurements taken for one peripheral hole can be used to determine the range of values. If the position of the maximum varies from scan to scan, a practical approach for routine measurements is to use the fluoroscopy mode and to make the measurements for three complete axial rotations of the scanner. At least one set

O. Dössel and W.C. Schlegel (Eds.): WC 2009, IFMBE Proceedings 25/III, pp. 74–77, 2009.
www.springerlink.com

of measurements for CTDI was obtained with three sets of readings in each phantom hole to determine reproducibility and to establish whether there is any variation due to over scan. Thereafter, single readings in each phantom hole were used. Measured data and exposure parameters were recorded in an excel sheet for easy analysis.

From the CTDI readings corresponding to peripheral and central locations of the pencil chamber, weighted CTDI (CTDIw) was estimated. From the weighted CTDI and tube loading (mAs), normalized weighted CTDI was estimated.

Image noise, slice thickness and CT number were analysed/ measured with AAPM CT performance phantom (manufactured by Victoreen) by using water phantom section, slice thickness insert and CT number insert respectively. In addition to the above, image noise was measured by using another simple CT water phantom.

Image noise was measured for an ROI of 500 mmsq at the centre and four other locations on the edge - two symmetrically opposite horizontal and vertical points each for 500 mAs and 50 mAs respectively

The measurement of Slice thickness was performed for various irradiated slice thicknesses. The slice thickness was not found to be uniform as this is varying from vendor to vendor.

CT number estimation was done for an ROI of 500 mmsq. over different materials of the CT number insert. Also, for CT numbers, an additional set of measurements were performed by using an in house developed CT number insert.

Results and Discussion: All new CT scanners installed for the period 2006-08 were included in this analysis. The measured normalized weighted CTDI values for head and body phantoms are given in Table I & II respectively. As the CT scanners are from four different vendors, uniform selection of slice thickness could not be effected for nCTDI w and other measurements. The slice thickness for which measurements could not be made are marked as 'xx'. Similarly, the measurements corresponding to slice thickness 2.5mm, 1.25m and 0.625 mm of Scanner in Hospital B are clubbed together with 3mm, 1.5 mm and 0.75 mm respectively for tabulation and analysis with '*' mark. In general, it can be stated that nCTDIw values vary as expected.

The CT number insert in the performance phantom had five different materials- Polyethylene, polystyrene, nylon, polycarbonate and acrylic with CT numbers -92, -24, 92, 102 and 120 respectively. Water and air were located within the performance phantom. The in-house developed CT number insert had polyethylene, polystyrene, Teflon, Perspex and polycarbonate with CT numbers -68.42, -986.5, 973.68, 131.58 and 105.26 respectively.

The measured CT numbers for various CT scanners using Performance Phantom insert is shown in Table III. The measured values are reasonably in good agreement with the expected values.

The image noise was analysed by measuring the mean CT number of the ROI and standard deviation. The values are given in Table IV. As a thumb rule, if the image is reconstructed with standard algorithm and by using small FOV, the mean of the centre ROI should be ± 3. The mean of the central ROI of all the CT scanners are falling within this value. Also, the uniformity difference between central ROI and average of the peripheral ROI's should be ± 3. This value also hold good for all except one CT scanner.

Table I : Normalised Weighted Computed Tomography Dose Index (nCTDIw) for Head Phantom

Slice thickness	nCTDIw (Head)				
	Hospital				
	A	B	C	D	E
10	xx	0.207	0.164	0.176	0.159
9	0.615	xx	xx	xx	0.448
6	0.374	xx	xx	xx	0.683
5	xx	0.104	0.183	0.225	0.391
4.5	1.238	xx	xx	xx	0.414
3/2.5*	1.244	0.052*	0.188	0.196	0.570
1.5/ 1.25*	1.489	0.026*	xx	xx	1.596
0.75 / 0.63*	2.114	0.013*	xx	xx	3.212

The measured slice thickness variations among various CT scanners is shown in Table V. The measured slice thickness values were more or less in fair agreement with the set values of 5 mm and above. For values below 5mm, there is large variation from the set values as expected. The percentage deviation of the measured values increase as slice thickness value decrease as expected.

Table II : Normalised Weighted Computed Tomography Dose Index (nCTDIw) for Body Phantom.

Slice thickness (mm)	nCTDIw (Body)				
	Hospital A	Hospital B	Hospital C	Hospital D	Hospital E
10	xx	0.079	0.076	0.106	0.578
9	0.323	xx	xx	xx	0.148
6	0.677	xx	xx	xx	0.216
5	xx	0.039	0.086	0.112	0.123
4.5	0.652	xx	xx	xx	0.261
3/2.5*	0.646	0.019*	0.085	0.127	0.392
1.5/ 1.25*	0.809	0.009*	xx	xx	0.811
0.75/0.63*	1.095	0.004*	xx	xx	1.054

Table III : Measured values of CT numbers.

Material	Density (ρ) g/cc	CT Numbers					
		Expected	Hospital A	Hospital B	Hospital C	Hospital D	Hospital E
Air	0.001293	-1000	-1024	-989.6	-978.11	-1020	-983.9
Water	1	0	1	0.51	1.35	5.9	-2.3
Polyethylene	0.95	-92	-79.6	-72.37	-97.4	-96.17	-74.4
Polystyrene	1.05	-24	-24	-27.11	-28.93	-25.9	-28.1
Nylon	1.1	92	77	103.85	98.16	96.5	105.6
Polycarbonate	1.2	102	120	102.44	97.58	100.51	104.5
Acrylic	1.19	120	125	128.37	129.12	138.8	130.3

Table IV : Noise Analysis

ROI	Noise										
	mAs	Hospital A		Hospital B		Hospital C		Hospital D		Hospital E	
		CT#	SD	CT#	SD	CT#	SD	CT#	SD	CT#	SD
Centre	500	1.8	2.1	0.92	3.21	2.23	2.4	1.19	0.056	0.5	17.4
Top		0.6	2	0.93	2.37	1.79	2.16	1.27	0.055	-3	13.1
Bottom		2.2	1.9	0.68	2.47	2.44	2.32	0.66	0.02	-2.2	13.3
Left		2.3	2	1.01	2.58	1.84	2.18	1.4	0.05	-2.7	13.1
Right		1.4	1.8	0.96	2.52	2.41	2.24	1.6	0.06	-2.9	12.4
Centre	50	0.9	6	0.35	10.26	1.85	5.06	2.92	0.07	-0.1	5.1
Top		0.9	5.5	0.15	7.85	1.29	4.48	0.95	0.01	-1.8	3.8
Bottom		1.6	5.5	0.34	8.02	2.01	4.64	4.5	0.052	-0.4	3.6
Left		2.1	5	0.43	8.23	1.39	4.63	1.09	0.013	-1.2	3.4
Right		1.2	5.3	0.43	7.65	2.06	4.49	2.38	0.026	-1.1	3.5

Table V : Measurement of Slice thickness

Slice thickness (mm)	Slice thickness Measured (mm)				
	Hospital				
	A	B	C	D	E
12	12.7	xx	xx	xx	12.4
10	xx	xx	12	13	xx
6	7.7	xx	xx	xx	7.4
5	xx	7	7	8	xx
3/2.5*	5.6	5*	4	5.5	4.8
1.5/ 1.25*	xx	3*	3.0	xx	xx

Conclusion: The extensive use of CT results in remarkable increase in population dose than plain film radiography. This is particularly important as the awareness of carcinogenic potential of low doses of x-ray radiation is increasing significantly. Hence wherever possible steps may be taken to reduce the radiation exposure to the population from CT examinations by limiting the number of examinations prescribed, by switching to other non-radiation modalities such as MRI, US for the same patient and finally, by reducing the dose to the individual patient during CT scanning. In this study we have tried to achieve the last option of dose reduction in Oman by validating a comprehensive QA protocol for CT scanners in Ministry of Health hospitals. Results shown that CT scanner units operating at optimal parameters deliver decreased radiation exposure to patients. Also, the dose to patients will be significantly affected if the radiation parameters are not set properly. Thus a well performed QA programme in accepting CT scanners will yield good quality scans and this in turn delivers an optimal dose to the patients undergoing CT investigations there by reducing the population dose as a whole.

Precise Mapping of Skin Dose to Avoid Further Radiation-induced Epilation

M. Hayakawa[1], T. Moritake[2], F. Kataoka[1], T. Takigawa[1], Y. Koguchi[3], Y. Miyamoto[3] and Y. Matsumaru[1]

[1] Department of Endovascular Neurosurgery, Toranomon Hospital, Tokyo, Japan
[2] RadGenomics Research Group, National Institute of Radiological Sciences, Chiba, Japan
[3] Oarai Research Center, Chiyoda Technol Corporation, Ibaraki, Japan

Abstract— **Although several cases of radiation-induced skin injury (RSI) have been reported in association with neurointerventional procedures, in most cases the absorbed doses to these regions are not measured directly; therefore, we built the first direct measurement system that enables the ideal dosimetry for entrance skin dose (ESD) during neurointerventional procedures to be easily determined. This system was then applied to a patient who underwent long and repetitive procedures to establish the efficacy of precise mapping of ESDs using a number of radiophotoluminescent glass dosimeters (RPLDs) with the aim of avoiding RSI. A previously healthy 55-year-old man underwent two transvenous embolizations for dural arteriovenous fistula in the right cavernous sinus, with an interval of 2 months. To measure ESDs throughout the procedures, the patient wore a fitted dosimetry cap made of a thin stretchable material that closely covers the head and neck and contains 60 RPLD chips with sufficient radiolucency for fluoroscopy. After the first procedure, temporal epilation occurred in the occipital region. Precise mapping of ESDs revealed that this region was exposed to 5.4 Gy, the maximum dose for this procedure. In the first procedure, the X-ray tube was generally positioned straight for an optimal posterior–anterior view; however, in the second procedure we intermittently used the second-best position to prevent further RSI. In this position, the maximum ESD was 1.1 Gy in the right posterior-temporal region and the epilation site was exposed to ≤0.8 Gy. Thus, the patient did not develop any further epilation and was completely free from RSI by 3 months after the second procedure. We conclude that direct dosimetry using multiple RPLDs can accurately reveal the maximum ESD and that precise information regarding ESD can prevent further RSIs from subsequent procedures.**

Keywords— **Neurointervenitonal procedure, Protection, Radiation-induced skin injury, Entrance skin dose, Radiophotoluminescent glass dosimeter**

I. Introduction

Radiation-induced skin injuries (RSIs) such as epilation or ulceration have been reported more frequently in recent years because of the increasing number of interventional radiological procedures, which are less invasive than open surgery [1].

Although several cases of temporary epilation were reported as RSI following neurointerventional procedures [2–11], an ideal dosimetry technique for calculating the patient's entrance skin dose (ESD) has yet to be established, meaning that the ESD at the region of RSI cannot be determined correctly. Clinicians have paid little attention to RSIs or to establishing a method for avoiding RSIs.

In this context, we built the first direct measurement system for calculating ESD using multiple radiophotoluminescent glass dosimeters (RPLDs) set on the surface of the patient's head and neck. To establish the efficacy of precise mapping of ESDs to avoid RSIs, the system was then applied to a patient who underwent long and repetitive procedures.

II. Materials and Methods

A. Dosimetry Technique

The ESDs of the patient, which include tissue backscatter, were measured using small RPLD chips (Chiyoda Technol, Tokyo, Japan) as previously reported [2, 12]. The glass chips are 8 mm square and 1 mm thick, with sufficient radiolucency for fluoroscopy. A cap to cover the head and neck was made of thin stretchable polyester and equipped with 60 RPLD chips. The chips were placed at suitable positions with high reproducibility. At each point, one RPLD chip was applied. After obtaining informed consent, the patient was measured for ESDs wearing the fitted dosimetry cap (Fig. 1) throughout the procedures.

B. Angiogram Technique

We used a single-plane X-ray device for all interventional procedures. The total procedure time, total fluoroscopic time, dose-area product (DAP), and most commonly used tube position are recorded in Table 1. Fluoroscopy was performed in pulse mode with a rate of 15 pulses per second. DSA was performed at 3 frames per second. The field size was almost always selected at 14 cm for both fluoroscopy and DSA image acquisitions.

O. Dössel and W.C. Schlegel (Eds.): WC 2009, IFMBE Proceedings 25/III, pp. 78–81, 2009.
www.springerlink.com

Fig. 1 Photographs of the fitted dosimeter cap equipped with RPLDs

Table 1 Angiographic parameters during transvenous embolization for CSdAVF

Parameter	First TVE	Second TVE
Total procedure time (min)	220	160
Total fluoroscopic time (min)	79.1	74.6
DAP (Gy × cm^2)	292.2	297.3
Tube position for AP view	Straight	LAO
Tilt angle	no	7 degrees caudal
Rotation angle	no	48 degrees to the left

Note: CSdAVF = cavernous sinus dural arteriovenous fistula; TVE = transvenous embolization; DAP = dose–area product; AP = anteroposterior; LAO = left anterior oblique.

III. Results

A. Case Illustration

A previously healthy 55-year-old man noticed right retro-orbital throbbing pain on September 2006. After 2 months, he gradually developed double vision due to right abducens nerve palsy; magnetic resonance angiography performed on April 2007 demonstrated a right cavernous sinus dural arteriovenous fistula (CSdAVF).

Under general anesthesia, transvenous embolization (TVE) for the CSdAVF was performed in June 2007. Platinum coils were delivered via the right internal jugular vein to occlude the fistulae at the anteromedial aspect of the right CS. Although residual fistulae at the lateral aspect were obvious, the procedure was stopped because the maximum dose of contrast medium had been reached.

The patient was discharged without any neurological improvement or complication; however, a square-shaped area of hair loss developed in the occipital region approximately 2 weeks after the first therapeutic interventional procedure (Fig. 2).

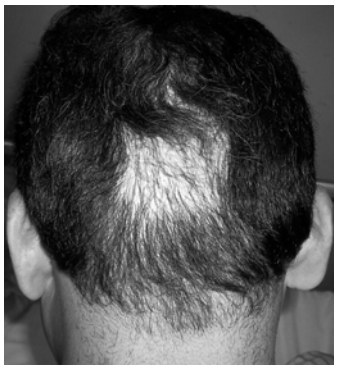

Fig. 2 Photograph of the patient's head showing the square-shaped area of hair loss in the occipital region that occurred approximately 2 weeks after the first transvenous embolization.

After a 2-month interval, the second TVE was performed for the residual fistulae on August 2007. Although the optimal X-ray tube position for the anteroposterior view was straight, to prevent further radiation skin injury, we intermittently used the second-best position (7-degree caudal tilt with 48-degree rotation to the left side) and its periphery (Table 1).

The residual fistulae were almost completely obliterated by the platinum coils without any further development of skin injury. Spontaneous hair regrowth occurred 3 months after the second procedure.

B. ESDs to Patient

The distribution of ESDs for the first procedure is shown in Fig. 3A. Although the maximum ESD was 5.4 Gy at the occipital area (point 28 in Fig. 3A), the adjoining areas (points 15, 16, 27, 29, 37, and 38) recorded doses less than 1.2 Gy. These measurements matched the regional epilation on the patient's head. We considered that the regional epilation was caused by the high accumulated dose delivered to the small region because the position of the X-ray tube had remained almost unchanged throughout the procedure (Table 1).

In the second procedure, we observed a marked reduction in maximum ESD to 1.1 Gy in the right posterior-temporal region (point 26, Fig. 3B) even though the values for DAP and total fluoroscopic time were almost the same as those for the first TVE procedure (Table 1). In addition, the ESD at point 28, which showed maximum ESD in the first TVE, was less than 0.8 Gy. Accordingly, the accumulated dose over the two procedures showed a more uniform distribution than that for the first procedure.

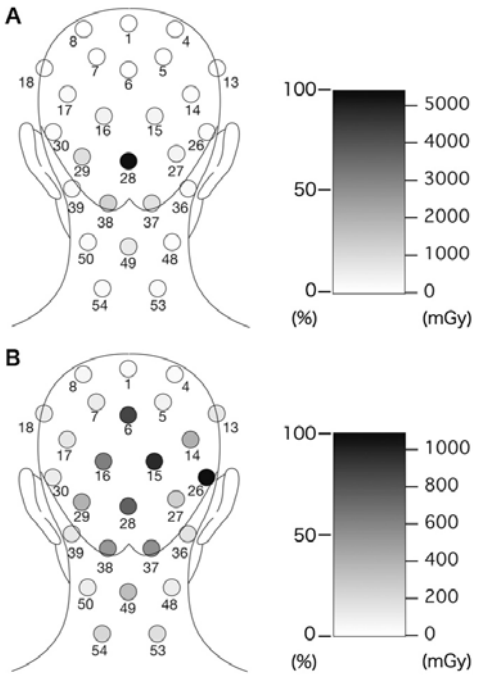

Fig. 3 Distribution of absolute entrance skin dose for our patient. The relative (percentage) dose distribution to the maximum entrance skin dose is also shown by the gray scale. A: After the first transvenous embolization, showing maximum ESD of 5.4 Gy at the occipital area (point 28). B: After the second transvenous embolization, showing ESD of 0.8 Gy at point 28.

IV. Discussion

RSI is a well-acknowledged deterministic effect that occurs as a consequence of interventional procedures using fluoroscopy. Temporary epilation is an RSI, having an estimated threshold dose of 3 Gy. Therefore, the International Commission on Radiological Protection (ICRP) recommends recording the maximum ESD and its location if the dose exceeds 1 Gy (for procedures that may be repeated) or 3 Gy (for any procedure) in interventional procedures [13]. In addition, the United States Food and Drug Administration (FDA) recommends that the absorbed skin dose should be recorded in the patient's medical record [14]; however, an ideal dosimetry procedure or ESD recording system for interventional procedures has yet to be established.

In the present study, we measured the patient's ESDs in a single-step operation using a fitted dosimetry cap equipped with 60 RPLD chips. The results of RPLDs are not available for several days; however, the chips are easily fitted to or detached from the surface of the patient's head and neck using this cap without hindering medical activities. In addition, the chips are easily set on suitable positions with high reproducibility.

Regarding our second interventional procedure, it was not always necessary to view the lesions from the same angle as that in the first procedure, except as a final check. Therefore, we were free to choose the second-best angle for exposure, obtaining fine-dose mapping before the second procedure; this consequently prevented further epilation.

V. Conclusions

We developed a direct dosimetry method using multiple RPLDs that were used in a case study to accurately estimate the maximum ESD for first and second radiological procedures (5.4 and 1.1 Gy, respectively). We also showed that information regarding ESD distribution from an initial procedure could assist the physician to prevent further RSIs in subsequent procedures if alternative tube positioning is intermittently adopted.

References

1. Koenig TR, Mettler FA, Wagner LK (2001) Skin injuries from fluoroscopy guided procedures: part 2, review of 73 cases and recommendations for minimizing dose delivered to patient. AJR 177:13-20
2. Moritake T, Matsumaru Y, Takigawa T et al. (2008) Dose measurement on both patients and operators during neurointerventional procedures using photoluminescence glass dosimeters. Am J Neuroradiol 29:1910-1917
3. Huda W, Peters KR (1994) Radiation induced temporary epilation after neuroradiologically guided embolization procedure. Radiology 193:642-644
4. Kuwayama N, Takaku A, Endo S et al. (1994) Radiation exposure in endovascular surgery of the head and neck. Am J Neuroradiol 15:1801-1808
5. Antonella T, Bianca Maria P, Giorgio A (1999) Temporary hair loss simulating alopecia areata after endovascular surgery of cerebral arteriovenous malformations: a report of 3 cases. Arch Delmatol 135:1555-1556
6. Mooney RB, McKinstry CS, Kamel HAM (2000) Absorbed dose and deterministic effects to patients from interventional neuroradiology. Br J Radiol 73:745-751
7. Wen CS, Lin SM, Chen Y et al. (2003) Radiation-induced temporary alopecia after embolization of cerebral arteriovenous malformations. Clin Neurol Neurosurg 105:215-217
8. Nannapaneni R, Behari S, Mandelow D et al. (2007) Temporary alopecia after subarachnoid haemorrhage. J Clin Neurosci 14:157-161

9. Thorat JD, Hwang PY (2007) Peculiar geometric alopecia and trigeminal nerve dysfunction in a patient after Guglielmi detachable coil embolization of a ruptured aneurysm. J Stroke Cerebrovasc Dis 16:40-42
10. Suzuki S, Furui S, Matsumaru Y et al. (2008) Patient skin dose during neuroembolization by multiple-point measurement using a radiosensitive indicator. Am J Neuroradiol 29:1076-1081
11. O'Dea TJ, Geise RA, Ritenour ER (1999) The potential for radiation-induced skin damage in interventional neuroradiological procedures: a review of 522 cases using automated dosimetry. Med Phys 26:2027-2033
12. Nishizawa T, Moritake T, Matsumaru Y et al. (2003) Dose measurement for patients and physicians using a glass dosimeter during endovascular treatment for brain disease. Radiat Prot Dosimetry 107:247-252
13. International Commission on Radiological Protection (2000) Avoidance of radiation injuries from medical intervention procedures. ICRP publication 85. Ann ICRP 30:7-67
14. Food and Drug Administration (1994) Public Health Advisory: avoidance of serious x-ray-induced skin injuries to patients during fluoroscopically-guided procedures. Rockville, MD: Center for Devices and Radiological Health

Address of the corresponding author:

Author: Takashi Moritake
Institute: National Institute of Radiological Sciences
Street: 4-9-1, Anagawa, Inage-ku
City: Chiba
Country: Japan
Email: moritake@nirs.go.jp

The comparative analysis of various methods of CT effective doses estimation

S.A. Kruchinin, M.I. Zelikman

Research and Practical Centre of Medical Radiology, Moscow, Russia

Abstract — **Comparative analysis of spiral CT effective dose evaluation (thorax exams) on the basis of two estimation methods and techniques: with use of anthropomorphic body phantom and thermoluminescent detectors or using results of CT dose index (*CTDI*) measurements is presented. It is shown that estimates based on anthropometrical body phantom approximately 1,5 – 1,7 times exceed those received on the basis of *CTDI* measurements for multislice computer tomography without dependence on CT type.Effective dose estimates for single-slice CT are practically equal for both methods discussing.**

Keywords — **Spiral multislice CT, effective dose.**

I. Introduction

By data from the literature, the share of CT exams in total amount of different diagnostic imaging methods makes an order of 6 % [1]. Contribution of this modality to the integrated effective dose exceeds 40 % - that is the maximum indicator in comparison with other methods. And every year this figure becomes more and more. For example, number of CT exams has made 60 million in the USA in 2005 (that is 20 times more than in 1980) and already about 4 million exams is spent in pediatrics. In 2006 the average one year effective dose on the USA citizen reached 3,2 mZv, i.e. has increased more than 6 times for 20 years [2]. It is necessary to notice that approximately 50 % of all CT exams done in the USA are cardiovascular exams.

As for Russia, the data concerning integrated effective dose produced by CT are very poor. But it is obvious that at appreciable annual growth of number of similar exams in hospitals all around the country (and in Moscow particularly) the tendency of effective dose increasing will repeat experience of the leading countries (for example the USA).

The aim of the present work is to provide the comparative analysis of CT effective dose evaluation (thorax exams) on the basis of two estimation methods and techniques: with use of special anthropomorphic body phantom and thermoluminescent detectors or using results of CT dose index (*CTDI*) measurements.

II. Materials and methods

As a test object in our experiments the anthropomorphic body phantom ATOM (company-manufacturer CIRS) was used. This phantom is formed by separate elements with thickness 25 mm. Every element contains cylindrical deepenings (5 mm in diameter) intended for thermoluminescent detectors (simultaneously 35 detectors have been used). After placing all the detectors phantom ATOM was located on CT patient table and the topogram and thorax scannings were carried out. To provide more exact evaluations (to be sure that the detectors sensitivity threshold has been reliably exceeded) some scannings (6 -9 for each CT type) with the same set of parameters were carried out.

An average value of the absorbed and equivalent dose was measured for each body by results of these exams and then the effective dose was estimated under the formula:

$$E = \sum_M W_M \cdot H_M, \tag{1}$$

where: H_M – equivalent dose in body or fabric with number M, and W_M – the weighing factor for body or fabric. A unit of an effective dose measure – is Sievert (Sv).

The second method of CT effective dose estimation for thorax exams is based on computer tomography dose index (*CTDI*) measurement. *CTDI* represents the integrated dose along the z-axis from single axial scan (one rotation of x-ray source). This method is more simple in practical use with comparison with the previous one.

The computer tomography dose index is measured in the cylindrical Acrylic (PMMA) test object (32 cm diameter – "body" of the adult person equivalent). This test object has 5 cylindrical holes (one in the center and 4 peripheral at 1 cm from the age) in which the integrated dose is measured. For these measurements the Unfors Mult-O-Meter 601 was used. This device allows to register the value of dose integrated on the all extent of "pencil" ionization chamber's sensitive area (100 mm).

For an effective dose estimation on the basis of *CTDI* for helical (spiral) multislice computer tomographs a concept of "pitch" has been offered in literature where pitch was defined as follows:

$$pitch = \frac{I}{T}, \tag{2}$$

O. Dössel and W.C. Schlegel (Eds.): WC 2009, IFMBE Proceedings 25/III, pp. 82–84, 2009.
www.springerlink.com

where: I – spiral step, mm; T – slice thickness, mm. For spiral tomographs also a volume CT dose index ($CTDI_{vol}$) is used. $CTDI_{vol}$ is defined as product of weighed $CTDI$ ($CTDI_w$) and quantity of x-ray source rotations necessary for passing the length equal to a slice thickness:

$$CTDI_{vol} = CTDI_w \cdot n = CTDI_w \cdot \frac{1}{pitch}. \quad (3)$$

As a unit of $CTDI_{vol}$ measure commonly mGy is used. Further a product of $CTDI_{vol}$ and scanning length L is calculated:

$$DLP = CTDI_{vol} \cdot L = CTDI_w \cdot \frac{1}{pitch} \cdot L, \quad (4)$$

CT effective dose E is evaluated by using dose index for an investigated body part $eDLP$ [mSv / (mGy·cm)]:

$$E = eDLP \cdot DLP. \quad (5)$$

For comparison of CT effective dose evaluations on the basis of dose index estimations there were used not only measured values of $CTDI$ but also DLP values displayed on the CT monitor in process of ATOM phantom exams (they were calculated in the tomograph with use of calibration data for set parameters of scanning).

Tests were carried out on the following types of CT:

- Aquilion 64 (Toshiba Medical Systems);
- Aquilion 16 (Toshiba Medical Systems);
- Light Speed VCT (GE Medical Systems);
- Somatom AR.STAR (Siemens Medical Systems).

III. Results and discussion

Tests for various types of CT were carried out with setting of following spiral scanning parameters.

Aquilion 64: tube potential U_a = 120 kV; tube current I_a = 200 mA; time of one tube rotation t_{rot} = 0,5 s (total time of scanning t_{scan} = 7,13 s); range of table moving R = 320 mm; slice thickness T = 0,5 mm; number of slices N = 64 (scanning area $T \cdot N$ = 32 mm); $pitch$ = 0,7.

Aquilion 16: U_a = 120 kV; I_a = 100 mA; t_{rot} = 1,0 s (t_{scan} = 21,32 s); R = 320 mm; T = 1,0 mm; N = 16 ($T \cdot N$ = 16 mm); $pitch$ = 0,938.

Light Speed VCT: U_a = 120 kV; I_a = 200 mA; t_{rot} = 0,6 s (t_{scan} = 5,6 s); R = 320 mm; T = 0,625 mm; N = 64 ($T \cdot N$ = 40 mm); $pitch$ = 0,86.

Somatom AR.STAR: U_a = 110 kV; I_a = 105 mA; t_{rot} = 1,5 s (t_{scan} = 51 s); R = 320 mm; T = 10 mm; N = 1 ($T \cdot N$ = 10 mm); $pitch$ = 1,0.

Results of effective dose estimations received by using of various methods and techniques for four CT types were tabulated (see Table 1). For effective dose estimations on a basis of $CTDI$ the dose index $eDLP$ = 0,017 mSv/(mGy·cm) was applied (breast of the adult person) [3].

Table 1 CT effective dose estimates (various methods and techniques)

CT type	CT effective dose estimation by using ATOM phantom, mSv	CT effective dose estimation on basis of *CTDI* measurements, mSv	CT effective dose estimation on basis of *DLP* displayed on CT monitor, mSv
Aquilion 64	14,8	8,5	9,8
Aquilion 16	10,7	6,9	6,6
Light Speed VCT	9,3	6,4	6,2
Somatom AR.STAR	7,8	7,7	-

The data presented in Table 1 testifies that distinction in estimates of CT effective dose on the basis of measured DLP values and DLP values displayed on CT monitor and calculated in the device with use of calibration data (as it was written these values were fixed in process of ATOM phantom scanning) practically does not exceed 15 % for all types of computer tomographs (absence of the data in the last row of the last column is defined by that DLP value does not exist on the monitor of Somatom AR.STAR). For multislice spiral CT the effective dose values received by use of ATOM phantom approximately 1,5 - 1,7 times exceed estimates based on $CTDI$ method. For single-slice device Somatom AR.STAR effective dose estimate based on $CTDI$ method is practically equal to that received by use of body phantom ATOM and thermoluminescent detectors.

The divergence of values for multislice spiral CT (1,5 – 1,7 times), in our opinion, can be explained by the following. Dose indexes for various body parts presented in special literature have been calculated with use of mathematical simulation (Monte-Carlo method) in which a set of parameters corresponds to spiral but a single-slice scanning. The discussed results will be co-ordinated with the data from reference sources in which possibility of estimation divergence in a range of 2 times for multislice spiral CT (various estimation methods and techniques) is underlined [4].

Also it is interesting to compare spiral CT effective doses for devices of similar design but with different number of detectors lines (number of simultaneously registered slices). Taking into account that scanning parameters settings at experiments carrying out differed it is offered to compare the effective dose values divided by tube current and scanning time product (мАс), a range of table moving in mm and number of x-ray source rotations necessary for

Table 2 Normalized effective dose values

CT type	Normalized effective dose (by using ATOM phantom), mSv/(mAs·mm)	Normalized effective dose (on basis of *CTDI* measurements), mSv/(mAs·mm)
Aquilion 64	0,1	0,060
Aquilion 16	0,1	0,065

passing the length equal to a slice thickness (return pitch), i.e. parameters linearly influencing on a dose level – normalized effective dose values. For comparison we will consider computer tomographs Aquilion 64 and Aquilion 16, results of calculations are presented in Table 2.

The data presented in Table 2 shows that normalized effective dose estimates received by use of ATOM phantom for both CT models practically do not differ that testifies a high accuracy of the experiments carried out in the given way. Normalized effective dose values by using ATOM phantom exceed those achieved on the basis of *CTDI* measurements 1,5 – 1,7 times that will very well be co-ordinated with the results presented in Table 1. Also it is important to notice that distinction in effective dose estimates carried out by using various methods and techniques decreases with reduction of number of simultaneously registered slices in spiral CT. This result confirms our assumption that dose indexes for body parts were calculated for parameters setting corresponding with single-slice scanning.

IV. Conclusions

1. The carried out analysis of spiral multislice CT effective dose estimations by using various methods and techniques has shown that estimates received using an anthropometrical body phantom and thermoluminescent dosimeters approximately 1,5 – 1,7 times exceed those received on the basis of *CTDI* (without dependence on CT type).
2. This divergence which increases with number of simultaneously registered slices (with other things being equal) can be explained that presented in reference sources dose indexes for body parts have been calculated with use of mathematical models (Monte-Carlo method) in which a set of parameters corresponds to the single-slice scanning.
3. Work on specification of dose index values for various body parts with reference to spiral multislice CT is to be done.

References

1. United Nations. Sources and Effects of Ionizing Radiation, 2000 Report to the General Assembly, Scientific Committee on the Effects of Atomic Radiation (UNSCEAR), UN, New York (2000).
2. American College of Radiology. White Paper on Radiation Dose in Medicine, 2007; 4; p.p.272-284.
3. European Commission's Study Group. European Guidelines on Quality Criteria for Computed Tomography, EUR 16262 EN, European Communities, Luxembourg (1999).
4. American College of Radiology. Computed Tomography (CT) Accreditation Program. Phantom Testing Instructions. Accessed February 18, 2007.

Author: Kruchinin Sergey Alexandrovich
Institute: Research and Practical Centre of Medical Radiology
Street: Srednyaya Kalitnikovskaya, 28/1
City: Moscow
Country: Russia
Email: s.kruchinin@rpcmr.org.ru

Criteria for Acceptability for Radiological, Nuclear Medicine and Radiotherapy Equipment – Part 1: Introduction and Methodology

K. Faulkner[1] J. Malone[2], S. Christofides[3], S. Lillicrap[4]

[1] Quality Assurance Reference Centre, Wallsend, Newcastle, UK
[2]Trinity College, Dublin, Ireland
[3] Nicosia General Hospital, Medical Physics Department, Nicosia, Cyprus
[4] University of Bath, Bath, UK

Abstract— **In 2007, the European Commission has commissioned a group of Experts to undertake the revision of Report RP91 on "Criteria for Acceptability of Radiological (including Radiotherapy) and Nuclear Medicine Installations", which will be published soon. This paper introduces the project and presents the methodology adopted to revise the acceptability criteria.**

Keywords— **Acceptability Criteria, Remedial Levels, Suspension Levels, Performance parameters, Ionising Radiation**

I. Introduction

The Euratom Treaty governs the work of the European Commission in the field of Radiation Protection and the Council Directives made under it. The most prominent is the Basic Safety Standards Directive (BSS) on the protection of exposed workers and the public (96/29/Euratom)[1]. In 1997 the Council issued a complementary Directive to the BSS on the Protection of persons undergoing medical exposures (97/43/Euratom) [2]. Both Directives require the establishment by Member States of criteria of acceptability of radiological (including radiotherapy) and nuclear medicine installations.

Experience showed that drawing up such criteria, especially as regards the technical parameters of equipment, sometimes created difficulties. Member States requested guidance in these criteria.

In response, the European Commission published the first edition of Report RP91 on "Criteria for Acceptability of Radiological (including Radiotherapy) and Nuclear Medicine Installations" in 1997 [3]. This was an initial attempt to specify minimum standards of performance in a single document. It defined a level of performance at which remedial action was required. The document specified a series of parameters that characterised equipment performance and acceptable levels of performance. In its time it has proved to be a useful document that was applied in Member States to various degrees up to and including incorporation into National Legislation.

Since its publication, a series of weaknesses have emerged over time that its acceptability criteria inevitably required revision to reflect developments in equipment, the improvements in testing methodologies and improvement in the accuracy of measurement methods. This has an impact on acceptability criteria as it enables tolerances to be revised. Knowledge and practices have also evolved since its publication.

In 2007, the European Commission has commissioned a group of Experts to undertake the revision of RP91, which will be published soon. This group of experts is drawn from Europe and North America and has inputs from manufacturers and standards organisations through the International Electrotechnical Commission.

This paper presents the methodology adopted to revise the acceptability criteria.

II. Methodology

A. Purpose

The revised publication is intended to:

1. Update existing acceptability criteria.
2. Update and extend acceptability criteria to new types of installations. In diagnostic radiology, the range and scope of the systems available has been greatly extended (e.g. computed radiography, digital radiography, digital fluoroscopy, multi-slice (CT) and Dual energy absorptiometry (DXA)). In nuclear medicine there are PET systems and hybrid scanners. In radiotherapy, there are linear accelerators with multi-leaf collimators capable of intensity modulated radiotherapy (IMRT).
3. Identify an updated and more explicit range of techniques employed to assess criteria of acceptability,
4. Provide criteria that have a reasonable opportunity of being accepted, and that are achievable throughout the member states.
5. Deal, where practical, with the implications for screening techniques, paediatrics, high dose techniques and other special issues noted in the 1997 Directive.

O. Dössel and W.C. Schlegel (Eds.): WC 2009, IFMBE Proceedings 25/III, pp. 85–88, 2009.
www.springerlink.com

6. Promote approaches based on an understanding of and that attempt to achieve consistency with those employed by the MDD [4], industry, standards organizations and professional bodies
7. Make practical suggestions on implementation and verification

B. Methods

To achieve this, the development and review process has involved a wide range of individuals and organizations, including experts from relevant professions, professional bodies, industry, standards organizations and relevant international organizations. It was easier to achieve the last objective with radiotherapy than with diagnostic radiology. This is because of a long tradition of close working relationships between the medical physics and international standards communities which has facilitated the development and adoption of common standards in radiotherapy. An attempt has been made, with the cooperation of IEC, to import this approach to the deliberations on diagnostic radiology and to extend it, where it already exists, in nuclear medicine.

The intent has been to define parameters essential to the assessment of the performance of radiological medical installations and set up tolerances within which the technical quality and equipment safety standards of medical procedures are ensured. The methods for performance assessment recommended generally rely on non-invasive measurements open to the end user. The guidance will benefit the holder of radiological installations, bodies responsible for technical surveillance, and authorities charged with verifying compliance of installations with regulations on grounds of technical safety. However, it is important to bear in mind that this publication follows the precedent established in RP 91, is limited to the equipment and does not address wider issues such as those associated with, for example, the requirements for buildings and installations, or Information Technology (IT) systems such as Picture Archiving and Communication Systems (PACS) and/or Radiological Information Systems (RIS).

C. Definitions

A critical reading of the directive, RP 91, and the professional literature reveals some shift or "creep" in the meaning of the terms remedial and suspension level since they came into widespread use in the mid 1990s. In the interest of clarity, these have been redefined in a way that is consistent with both their usage in the directive and their current usage, as follows:

Suspension Levels: A level of performance that requires the immediate removal of the equipment from use.

Following a documented risk assessment involving the MPE and the practitioner, the suspended equipment may be considered for use in limited circumstances. The holder and operators must be advised in writing of the suspension and/or limitations in use.

A suspension level not being met requires that the equipment is taken out of service immediately. Not meeting this level makes the equipment unsafe, or performance so poor, that it would be unacceptable to society. The level is based on minimum standards of safety and performance that would be acceptable in the EU and represents the expert judgement of the working group and reviews based on the knowledge of what is acceptable amost their peers and informed by social, legal and political circumstances that prevail in the EU.

D. Criteria

It was not possible to devise a single acceptable approach to proposing values or levels for the criteria selected. Instead a number of approaches, with varying degrees of authority and consensus attached to them, have been adopted and grouped under headings A to D as follows:

Type A Criterion

This type of criterion is based on a formal national/international regulation or an international standard.

A reasonable case can sometimes be made for using a manufacturer's specification as a criterion of acceptability. For example, with all CE marked equipment which meets specification will either meet or exceed the essential safety standards with which the equipment complies. Thus, testing to the manufacturer's specification could be taken as a means of ensuring the criteria of acceptability are met or exceeded in the area they address.

At a less demanding level a case can be made that compliance with the relevant IEC, CENELEC or national standards might be taken as compliance with criteria that the industry has deemed to be essential for safety. In practice, this approach may be limited in value as the tests required may not be within the competence of end users or service engineers in the field. Thus different agreed approaches to verification will be required. Development in this area is essential to the harmonization referred to above. In particular agreed methodology is essential in any system of equipment testing. Standards organizations provide a useful role

model in this regard, which this publication has tried to emulate.[1]

Type B Criterion

This type of criterion is based on formal recommendations of scientific, medical or professional bodies.

Where industrial standards are not available or are out of date, advice is often available from professional bodies, notably the Institute of Physics and Engineering in Medicine (IPEM) and the American Association of Physicists in Medicine (AAPM), NEMA, BIR, ENMS, ACR, etc. More detailed advice on testing individual systems is available from the AAPM, earlier IPEM publications and a wide range of material published by many professional bodies and public service organizations (Nucl Med, RT, IMPACT, etc etc). Much of the material is peer reviewed and has been a valuable source where suitable standards are not available.

Type C Criterion

This type of criterion is based on material published in well established scientific, medical or professional journals

Where neither standards nor material issued by professional bodies are available the published scientific literature has been consulted and a recommendation from the drafting group has been proposed and submitted to expert review by referees. Where this process led to a consensus, the value has been adopted and is recommended.

Type D Criterion

The Type D situation arises where it has not been possible to make a recommendation. In this situation the approach based on the following is recommend:

This leaves a small residue of areas in which it has not been possible to make recommendations for a variety of reasons. For example, where the technology involved is evolving rapidly, listing a value could be counterproductive. It could become out of date very rapidly or it could act as an inhibitor of development. In such situations we feel the criterion of acceptability should be determined by the institution holding the equipment based on the advice of the Medical Physics Expert or Radiation Protection Adviser as appropriate.

The criteria of acceptability proposed are identified as belonging to one or other of these categories. In addition at least one reference to the primary source for the value and the method recommended is provided. Some expansion on the approach and the rationale for the choice is provided, where deemed necessary in an Appendix. Test methods are only fully described if they cannot be referred to in high quality accessible reference.

III. RESULTS

The outcome of the work of this project is the establishment of suspension levels for:

1. Radiology Equipment
2. Nuclear Medicine Equipment, and
3. Radiotherapy Equipment.

These are discussed in the individual papers addressing each Equipment type [5, 6 and 7].

IV. CONCLUSIONS

In reviewing suspension levels across three areas of use of radiological equipment, it was clear that suspension levels were most advanced for radiotherapy as a result of long term collaboration between medical physicists and industry. In diagnostic radiology however there are few published studies in the suspension of equipment from use, this is particularly relevant for CT Scanners.

ACKNOWLEDGMENT

The authors would like to thank all the reviewers for their helpful comments.

This project has been undertaken via a contract with the European Union Commission, Directorate General for the Environment and Transport (DGTREN) under contract number TREN/07/NUCL/S07.7064

[1] When equipment standards are developed so that their recommendations can be addressed to and accepted by both "manufacturers and users", the question of establishing criteria of acceptability becomes much simplified. Highly developed initiatives in this regard have been undertaken in radiotherapy (see IEC 60976 and IEC 60977). These "provide guidance to manufacturers on the needs of Radiotherapists in respect of the performance of medical electron accelerators and they provide guidance to users wishing to check the manufacturer's declared performance characteristics, to carry out acceptance tests and to check periodically the performance throughout the life of the equipment". This approach has much to offer to other areas.

References

1. Council Directive 96/29/Euratom of 13 May 1996 laying down basic safety standards for the protection of the health of workers and the general public against the dangers arising from ionising radiation, OJ L 159, 29.6.1996 p. 1-114
2. Council Directive 97/43/Euratom of 30 June 1997 on health protection of individuals against the dangers of ionising radiation in relation to medical exposure, and repealing Directive 84/466/Euratom, OJ L180, 9.7.1997, p. 22-27
3. RP91Criteria for acceptability of radiological (including radiotherapy) and nuclear medicine installations, 1997.
4. Council Directive 93/42/EEC of 14 June 1993 concerning medical devices, OJ L169, 12.7.1993, p. 1–43
5. Criteria for acceptability for Radiological, Nuclear Medicine and Radiotherapy Equipment – Part 2: Radiology Equyipment, These Proceedings.
6. Criteria for acceptability for Radiological, Nuclear Medicine and Radiotherapy Equipment – Part 3: Radiotherapy Equyipment These Proceedings.
7. Criteria for acceptability for Radiological, Nuclear Medicine and Radiotherapy Equipment – Part 4: Nuclear Medicine Equyipment These Proceedings.

Author: K. Faulkner
Quality Assurance Reference Centre
Street: Unit 9, Kingfisher Way, Silverlink Business Park
City: Wallsend NE28 9ND
Country: UK
Email: Keith.faulkner@nhs.net

Radiation Exposure to Critical Organs in Orthopantomography

M.T. Bahreyni Toossi[1], F. Akbari[1], Sh. Bayani[1], A. Jafari[1] and M. Malakzadeh[1]

[1] Medical Physics Research Center, Faculty of Medicine, Mashhad University of Medical Sciences, Mashhad- Iran

Abstract— **nowadays, radiography seems a necessary procedure in diagnosis and treatment of patients with dental problems. According to the ALARA Principle, dentists must take radiographs of sufficient quality at the lowest possible radiation dose to the patients. The assessment of patient dose on panoramic radiography is difficult because of dynamic nature of the imaging process and the narrow width of the x-ray beam. The present work describes an experiment undertaken using thermoluminescence dosemeters to obtain the absorbed dose in organs and sensitive tissues in head and neck region during panoramic radiography, based on patient measurement. The overall mean ESD on thyroid, right and left lens of eyes, parotid glands (right and left) and occipital region in orthopantomography were 38, negligible, negligible, 367, 319, 262μGy, respectively. The results show that there are differences between patient doses examined by different OPG systems.**

Keywords— **orthopantomography, OPG, ESD, panoramic radiography, thermoluminescence dosemeters.**

I. Introduction

Since the discovery of x-rays in 1895, x-rays have been widely used as the most important and reliable scientific tool for effective proper diagnosis of diseases as well as assessing the results of a given treatment to patients. More than a third or half of all crucial medical decisions are dependent on x-ray diagnosis and early diagnosis of some disease depends completely upon x-ay examination. The fact that diagnostic procedures are responsible for maximum population dose arising from man-made sources, cannot be ignored. UNSCEAR (2000) reports that the contribution of the radiation dose due to all diagnostic procedures is 80-90% of the total dose due to man-made radiation sources [1]. According to UNSCEAR 2000 Report, dental radiography is one of the most frequent types of radiological procedures performed [2].

In UK alone, a national survey during the period 1997 to 1998 estimated that over 19 million intraoral radiographs were undertaken each year. Data concerning 1991-1996 show that in countries belonging in healthcare level 1, 365 intraoral examinations were performed, on average, per 1000 population [3]. The number of images obtained using OPG technique has increased from 800000 in 1979 to 1200000 in 1982 in Italy, with a 10-15% increases expected for 1983[4]. Although the exposure associated with dental radiography is relatively low, any radiological procedure should be justified and optimized in order to keep the radiation risk as low as reasonably achievable [2].

Panoramic dental tomography is a successful technique, used by several professionals, such as radiologist, odontologist and maxillofacial surgeons, for the diagnosis of dental diseases. The equipments used for these procedures are characterized by the fact that the tube and the cassette holder are mobile, so they rotate from one side of the patient's head around his back to the other side. During this motion the film cassette moves in a synchronic way producing a two-dimensional image of the entire curved jaw with orthogonal projections of the teeth. The x-ray beam is very narrow horizontally and it reaches the collimator passing through the vertical slit of the cassette holder. One of the many advantages reported for panoramic radiography is reduction of the radiation dose as a result of the use of a fluorescent intensifying screen or film combinations and machine technology. Some reports suggested that the panoramic dose was one tenth of that received from a complete mouth survey and compared favorably with a single periapical radiograph [5]. Although the radiation risk is generally low, dental radiographs mean an increased risk for induction of parotid tumers or thyroid cancer [6].

Several methods have been proposed for assessing patient dose in panoramic dental radiography. In previous studies doses measured in phantoms or following hybrid procedures using patients and phantoms [5, 6, 7, 8]. In particular, measurements performed on patients are scarce [9].

Generally, the entrance skin doses in different projections are measured, and the best way to measure them is by using a thermoluminescence dosemeter (TLD). The TLDs are quite small, easy to put on the patient nor impair diagnostic information. Ionization chambers are not recommended owing to the exposure measurements are affected by partial volume effects and lack of charg-particle equilibrium (due to the movement and narrowness of the beam). By that reasons, measurements of the exposure are not accurate [7]. TLD-100 (LiF:Mg,Ti) is the most commonly used thermoluminescent material for patient dosimetry (Burke and Sutton 1997). The minimum detectable dose (MDD) for TLD-100 is believed to be 50-100 μGy [8].

O. Dössel and W.C. Schlegel (Eds.): WC 2009, IFMBE Proceedings 25/III, pp. 89–92, 2009.
www.springerlink.com

The concept of diagnostic reference levels (DRL) has assumed an important place in recent years in the management of radiation doses delivered to a patient in diagnostic and interventional radiology. The concept has been introduced in to European Union legislation and recommended by ICRP and IAEA. ICRP (1996) has recommended that diagnostic reference levels be established for common types of diagnostic examinations and broad types of equipment [1]. In Iran, as many other developing countries, there is no guideline for medical exposures. The main purpose of this study is an attempt for the first time to evaluate DRL for OPG examination in the greater Khorasan province.

II. Material and method

To measure the absorbed dose, LiF:Mg,Ti thermoluminescence dosemeter (TLD-100) were used. The TLDs were annealed at 400°c for 1 hour followed by a treatment at 75°c for 18 hour in an air oven. Afterwards, the TLDs were cooled down to room temperature. Each single TLD has to be calibrated individually in order to indicate the absorbed dose in microgray. The calibration was performed for diagnostic x-ray energy (70 kVp). All TLD-100 belonged to one batch and they were characterized individually. TLD chips were placed inside plastic sachets and were used in pairs to reduce uncertainties in measurements. The sachets were placed on thyroid gland and eye lids. Two additional TLD chips were used to determine the background radiation. After 24h irradiated TLDs were read in a manual TLD Reader (Harshaw TLD reader model 3500). The reading out was performed with WinREMS software. The more energy a TLD is absorbing during the procedure, the more photons would emit during heating. Perior to every measurement, the TLDs were annealed.

In this study 6 orthopantomography systems in 6 centers were studied. A sample of at least 15 patients per x-ray unit was chosen. The patients mean age and weight were 35 years and 69 kg. A total of 1000 TLD were read in this study. Mean value of the two calculated ESDs was taken as measured dose at the point of interest.

III. Results

Table 1, 2 summerize the results obtained for pantomographic units in use in Mashhad. Table 1 shows technical Parameters of the OPG systems used in this work, while values of mean ESDs, the highest and the lowest doses are given in Table 2.

Table 1 Technical Parameters of the OPG equipment

Center	kV rang	mA range	Time (s)
A	66-70	6-8	18
B*	64-66	4-5	18
C*	64-68	12-14	16
D	64-66	5-6	18
E	60-68	4-8	18
F	68-72	6-9	16

* B and C are equipped by CR systems

Table 2 mean skin dose measurements (μGy)

Organ	Mean ESD	Highest dose	Lowest dose
Lefteye	Negligible	-	-
Righteye	Negligible	-	-
Thyroid	38	47	21
Left parotid	319	358	296
Right parotid	367	432	330
Occipital	262	300	208

IV. Discussion

Radiation doses to sensitive head and neck organs have been investigated in many studies. Different panoramic machines and different radiographic techniques are practiced. The reason for such studies is the existence of sensitive organs such as bone marrow, thyroid gland, salivary glands, brain and eye lenses close to radiation field.

Nearly 85% of the cumulative parotid dose from diagnostic radiography is caused by dental X-ray examination [6]. Exposure to ionizing radiation will increase the risk of thyroid cancer, and 10% of people with thyroid cancer will die. A significant reduction (15%-30%) of absorbed dose to the thyroid gland was obtained using smaller field size in panoramic radiography [10].

According to Table 2, there are differences in absorbed doses of the same organ for different units. It might be due to the different parameters used by the individual dentists or due to differences in the units themselves, tube-film distance, beam directions, or scanning motion. The lowest doses belonged to center B. In this center, conventional film processing had been replaced by computed radiography. Digital imaging has several advantages such as speed, image manipulation, quality, archiving, access to patient records and the absence of chemicals. Due to these advantages lower mAs is used and a reduction in radiation is expected.

An interesting point which can be seen when comparing different centers is that center C is equipped by CR system

Table 3 result of organ doses and comparison with other authors

Organ doses (μG)	This work (2009)	Kaeppler et al [6]	Gonzalez et al [9]	Melgar et al [7]	Bartalota et al [4]
eyes	Negligible	18	-	7	1-14
Thyroid	38	62	-	63	13-37
parotid	343	1181	-	-	90-314
Occipital	267	-	530	348	-

but no reduction in dose was observed, even in some cases the highest received dose belonged to this center. This may be due to incorrect use of CR and the implementation of high mAs.

Our analysis of comparison of absorbed dose in different unit show the fact that different dentists have their own preferred contrast for the film to be diagnostically acceptable. Images made with lower tube voltage often has better contrast which is more diagnostically favorable for most of dentists. However, lower voltage must also be accompanied by longer exposure time to get enough radiation onto the image receptor that in turn increases the patient exposure. According to our results, new generation of orthopantomography systems deliver lesser doses. These units use a microprocessor control system and are designed to improve image quality by providing a patient positioning, light beam alignment system, an adjustable improved-image-geometry focal through and a smaller focal spot.

Fig. 1 shows a diagram of beam vertical collimation. Light-shaded area covered by primary beam.

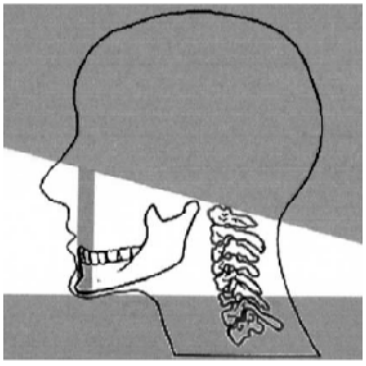

Fig. 1 diagram of beam vertical collimation

Note that eye and thyroid are outside the area of primary exposure.

According to this study, absorbed dose was highest in the region of the parotid glands, which were always along two lateral axes of rotation. Dose received by the thyroid gland, mainly due to scattered radiation, is comparably less than the dose received by the parotid glands. On the other hands, the thyroid gland is one of the most radiosensitive organs and dose imparted in the thyroid gland should be minimized whenever possible. Dosimeters placed on the eyes received no measurable dose. The mean dose measured in the occipital region is one of the highest entrance surface doses to be measured along the x-ray beam trajectory since orthopantomography either increases the selected kilovoltage when scanning this area or reduce the scanning speed to avoid a shadow produced by the cervical spine.

V. Conclusions

Orthopantomography is a useful diagnostic tool in dentistry and is of considerable value in orthodontics and oral surgery. These benefits considerably outweigh any associated radiological hazard. Nevertheless, in line with the recommendations of the ICRP, all exposures should be kept as low as reasonably achievable (ALARA principle) [4].

Present Legislation requires all dentists taking radiographs to ensure that the dose to the patient is as low as reasonably practicable in order to achieve the required diagnostic purpose.

Several studies have been performed to estimate organ doses, arising from different location of dosimeters and different kinds of panoramic machines yielded different results. In Table 3 some of these results are presented.

Our results show that in some cases dose values are lower than those proposed in other papers. Multiple causes can produce these variations: irradiation geometry, image equipments and type of technique applied, positioning and accuracy of TLD measurements, positioning of patients, etc. therefore we can't compare these results.

GONZALEZ et al. reported that maximum dose in OPG is received in occipital region and measured DRL in Madrid for that region [9]. But in the present study, we measured the highest dose in parotid and therefore the establishment of DRL for OPG in parotid glands is recommended.

Many factors influenced the dose required to produce a good quality image. These factors can include tube voltage, exposure time, film speed, film processing and viewing facilities. With knowledge of these factors, there must be potential for significant dose reduction for dentists currently operating at the upper end of the dose range.

As in Iran there is no national DRLs for orthopantomography, it's not clear whether in case of the OPG systems used in this study, reducing the radiation dose to a level that still provides a diagnostically acceptable image quality is necessary. We hope that results of this study can be used in establishing a national DRL.

Acknowledgment

The authors are thankfull to the office of vice president for research affairs of Mashad University of Medical sciences for financing this research work.

References

1. Arun Chougule. (2005) Reference Doses in Radiological Imaging. Pol J Med Phys Eng 11(2):115-126
2. Looe H K, Pfaffenberger A, Chofor N et al. (2006) Radiation Exposure to children in intraoral dental radiology. Radiation Protection Dosimetry 121(4):461-465 DOI 10.1093/rpd/nc1071
3. Hatziioannou K, Psarouli E, Papanastassiou E et al. (2005) Quality Control And Diagnostic Reference Levels in Intraoral Dental Radiographic Facilities. Dentomaxillofacial Radiology 34:304–307
4. Bartolotta M, Calenda E, Calicchia A et al. (1983) Dental Orthopantomography: Survey of Patient Dose. Radiology 146: 821-823
5. Danforth A, Clark E. (2000) Effective dose from radiation absorbed during a panoramic examination with a new generation machine. Oral and Maxillofacial rRadiology 89(2):236-240
6. Kaeppler G, Buchgeister M, Reinert S. (2007) Influence of the rotation center in panoramic radiography. Radiation Protection Dosimetry 1-6 DOI 10.1093/rpd/ncm319
7. Melgaer J, Martin C, Montes C et al. Radiation Doses in Dental Panoramic Tomography
8. Mortazavi SMJ, Ghiassi-Nejad M, Bakhshi M et al. (2004) Entrance Surface Dose Measurement on the Thyroid Gland in Orthopantomography: The Need for Optimization. Iran. J. Radiat. Res 2(1):1-7
9. GONZALEZ L, VANO E, FERNANDEZ R. (2001) Reference Doses in Dental Radiodiagnostic Facilities. BJR 74:153–156
10. Talaeipour A, Sakhdari S, Sahba S. (2006) comparison Between Absorbed Doses in Target Organs in Panoramic Radiography, Using Singkle Emulsion And Double Emulsion Films. Acta Medical Iranica 45(3):171–175

Author: M. T. Bahreyni Toossi
Institute: Medical Physics Research Center, Faculty of Medicine, Mashhad University of Medical Sciences
Street: Vakil abad
City: Mashhad
Country: Iran
Email: mbahreyni@yahoo.co.uk, bahreynimt@mums.ac.ir

First Report of Radiation Dose to Pediatric Patients Arising From Diagnostic Chest and Abdomen Examination

M. Malekzadeh[1], M.T. Bahreyni Toossi[1], Sh. Bayani Rodi[1], M.T. Shakeri[2] and F. Akbari[1]

[1] Medical Physics Research Center, Faculty of Medicine, Mashhad University of Medical Sciences, Mashhad- Iran
[2] Department of Community of Medicine and Public Health, Mashhad University of Medical Sciences, Mashhad- Iran

Abstract— **A survey of the entrance surface doses in the routine radiography of children in Mashhad has been carried out in five departments, using thermoluminescence dosimeter. Chest and abdomen were covered in this study. Data were collected for 344 pediatric patients. Findings revealed that some of these were high doses due to a lack of standardization in procedure, resulting in use of low tube voltages and high currents for examination and usage of grid for all patients are higher than the recommended reference values of CEC and NRPB.**

Keywords— **Pediatric, Diagnostic Radiation, Entrance Surface Dose, Thermoluminescence Dosimeter**

I. Introduction

The optimization of radiological procedures requires special attention to pediatric patients, since the risk factors of arising from ionizing radiation are greater for children than adults. The International Commission on Radiological Protection dose not recommend application of dose limits for patients but points out the importance of application of reference levels as a tool in the process of optimization of protection in medical exposure [1]. European states within the CEC are required to establish and use diagnostic reference levels (DRLs) in x-ray examinations[2]. So far no DRL has been established for pediatric radiological examinations in Iran. However, the risk of lethal cancer from radiation exposure of children is expected to be 2-4 times higher than for adults per dose unit the reason for this difference is not fully clear, but greater cell proliferation rate and longer life expectancy for children both result in a higher risk of developing late effects [3]. Diagnostic radiology plays an important role in the assessment and treatment of neonates requiring intensive care. Moreover, the small sizes of newborn infants brings all organs within or closer to the useful beam, resulting in a higher exposures to effective dose conversion factor per radiograph than may be the case for adult [4]. It is therefore important to ensure that radiation doses from radiographic examinations carried out in neonatal units are kept to a minimum whilst maintaining the quality of radiographic images.

The aim of this study was to measure the ESD values for the most frequent radiographic examinations carried out in a radiology department and to compare them with available international and European DRLs [5]. The present study is the first attempt to evaluate pediatric patient doses in Iran.

It will provide guidance on where efforts on dose reduction will need to be directed to fulfill the requirements of the optimization process and serve as a reference for future work, as well as provide information for comparison with patients of the some category in other countries.

II. Materials and methods

All examinations monitored in this work were carried out in five radiology wards: located at a general, pediatric, Maternit hospitals and a private clinic. The study group included patients who were referred to the radiology departments of 5 randomly selected departments in Mashhad.

Initially, questionnaires were distributed to radiographers and patients. They were asked to provide information related to patients such as: age, sex, weight, height and radiographic parameters i.e: peak tube voltage (kVp), exposure setting (mAs), focus to film distance (FFD), film size and grid usage. The following quality control tests were performed on individual X-ray machines: timer accuracy, kVp accuracy, mA Linearity, mA reciprocity and reproducibility of exposure. For this purpose, an UNFORS Mult-O-Meter model 303 was employed ,also quality control were performed on mobile X-ray machine which are used for radiography in neonatal intensive care unites.

The ESD was used to assess radiation dose to the patient for following selected examination: chest (PA/AP) and abdomen (AP).The sample was divided in two groups :(0-1 years old and 3-7 years old). We chose these group due to (0-1 years old group is the most radiosensitive groups in population and mid-range child (5 years old) with radiosensitivity between that of infants and teenagers [6].

In order to assess patient dose arising from diagnostic radiology, guidelines established by the UK National Radiological Protection Board (NRPB) [7]. Advocate estimation of ESD by thermoluminescence (TL) dosimetry. Therefore, in this work, TL dosimetry was adopted to measure ESDs. TL dosimetry materials such as lithium fluoride or lithium borate are very sensitive to radiation, small in diameter,

O. Dössel and W.C. Schlegel (Eds.): WC 2009, IFMBE Proceedings 25/III, pp. 93–95, 2009.
www.springerlink.com

nearly tissue equivalent and consequently are practically invisible on most radiographs. This means that their use does not interfere with the clinical diagnosis. TLD calibration is provided by irradiation of a group of TLDs, by diagnostic X-rays (80 kV, total filtration of 3.0 mmAl), to a known dose (mGy range) measured by a 6 cm ion chamber and Radcal monitor (model 9015) [8]. The ESD was measured directly by LiF: Mg. Ti, thermoluminesent dosimeters, type TLD-100 for each patient, two TLDs were placed inside a plastic sachets attached to skin surface at the point of intersection with the central beam axis. Mean value of the two calculated ESDs was taken as measured dose at the point of interest. To anneal TLD-100 LiF chips, they were heated at 400°C for 1 h, cooled down slowly to ambient temperature and then reheated at 75°C, for 18 h. These chips were latter read by Harshaw 3500 TLD Reader.

Microsoft excel was employed for data manipulation and ESD calculation. Data analysis was performed using the SPSS version 13 software.

III. Results

A total number of ESD measurements were carried out for 344 patients referred to five randomly selected departments of Mashhad. In all five departments included in this study chest and abdomen X-rays were performed for ≤1 year and (3-7) years groups, except for Maternity hospital.

ESD measurements arising from two common X-ray examinations performed on pediatric examinations of two age groups are summarized in table 1. For examinations and age categories where the sample size was very small (≤7) corresponding figures are showed in italics.

Table 1 Summary of ESD measurements for some routine X-ray examinations performed in five randomly selected hospitals of Mashhad

Department	Age group	Sample size (chest)	Sample size (abdomen)	Tube potential (kVp) chest	Tube potential (kVp) abdomen	Mean ESD (μGy) chest	Mean ESD (μGy) abdomen
A	≤1y	18	12	46-57 *[-,64]	46-57 *[-,64]	65.99	68.61
A	3-7y	22	12	48-74 *[-,78.6]	50-66 *[-,71]	98.42	128.50
Mobile (NICU)A	newborn	14	10	40-41	41-42	46.92	48.30
B	≤1y	15	8	44-47	46-49	76.59	105.02
Mobile (NICU)B	newborn	17	9	42-49	43-44	65.19	95.57
B	3-7y	11	*7*	47-62	55-62	107.65	*117.50*
C	≤1y	36	*4*	50-60	50-62	74.79	*78.01*
C	3-7y	32	13	55-67	50-70	95.23	224.32
D	newborn	19	*7*	50-60 *[-,50]	50-60 *[-,50]	191.85	*197.30*
Mobile (NICU) D	newborn	20	8	60-65	60-65	34.57	32.40
E	≤1y	15	10	60-66	57-63	195.84	242.76
E	3-7y	*7*	18	66-70	66-73	*134.47*	345.43

-NICU=Neonatal Intensive Care Unit

-* kVp measured with Mult-O-Meter (≤ 50 kVp not measurable)

-Results from small sample sizes are given in *italics*.

IV. Discussion

This survey showed that the most common pediatric X-ray examination is chest X-ray. For the age group of (≤1y), entrance surface dose for examination varied from 34.57 μGy to 195.84 μGy for chest examination and from 32.40 μGy to 242.76 μGy for abdomen. For the age group (3-7y), ESD was between 95.23 μGy and 134.47 μGy for chest examination and between 117.50 μGy and 345.43 μGy for abdomen. The large variation in ESD values indicates that reducing patient doses can be done by changes in parameters (kVp, mAs), without loss of image quality also these variations are influenced by patient's body size**.**

It is evident from table 1 that all departments were using low kVp, between 40 and 78.6 for chest PA examination while the EC recommendations is (60-65 kVp for neonatal,70-80 kVp for children up to 5 years and 100-120 kVp for older children)[2]. Cases were observed in C department where low kVp and FFD as low as 75cm were used. Consequently, higher ESDs were encountered in that department. The use of optimum FFD is considered very important, since there is a direct relationship between shorter FFD, higher patients dose and decreased geometric sharpness [2]. In C department, Computed Radiography (CR) in addition to screen/film systems was used. In our study, we didn't observe any reduction in dose due to application of CR (94.46 μGy for CR versus 68.72 μGy screen/film systems). It should be noted that this result has been obtained by comparing chest x-rays of two groups of 15 children below one year. Perhaps it would be better if we could increase our sample size (number of children), also in another study it

was observed that the application of CR systems gave rise to a slightly higher dose, 70 μGy for CR versus 50 μGy for screen/film systems [9]. Low kVp setting in E department, and application of grid for all patients were the causes of higher ESDs.

The lowest mean ESDs were obtained for both examinations performed by a mobile system, in D department, this is due to higher kVp setting, which is in accordance with EC recommended values of (60-65 kVp for neonatal) while at the room high mAs and low kVp setting in conjunction with the use of grid for all neonatal examination performed these caused higher ESDs, also the relevant machine failed kVp accuracy tests carried out by unforce Mult-O-Meter. Table 2 is presenting summaries of DRLs values reported by NRPB, the EC and mean ESDs accomplished in this study.

Table 2 summery of DRLs suggested dy NRPB, EC and Mean ESD values obtained in this study.

Examination	Age category	Mean ESD(μGy) this study	DRL(μGy) NRPB2000[10]	DRL (μGy) EC [2]
CHEST	newborn	84.63	50	80
CHEST	≤1y	105.04	50	
CHEST	3-7y	108.94	70	100
ABDOMEN	≤1y	108.49	400	
ABDOMEN	3-7y	203.94	500	1000

Average ESD obtained for some age groups, in abdomen examination do not exceed DRLs previously reported by other researchers (table 1 & 2), but for chest examination, we observed mean ESDs were greater than the DRLs. These can be attributed to lower tube potential setting used in the centers in this study, furthermore, antiscatter grid were used, which can caused abrupt increase of ESD observed in the related centers.

V. Conclussions

The unusual high doses observed in some departments, emerged from the use of low kVp and the application of grid in all examinations.

The vast majority of published reports on patient's dose from X-ray examinations reveal large difference between different X-ray departments. The large differences are indicating that optimization was generally ignored.

The outcome of this work shows that the examination technique in pediatric radiology is not yet optimized and the non optimized procedures contributed to considerable variations in radiation dose of children. Quantitative methods for the assessment of patient doses should be implemented in all radiology departments. However, the risk versus benefit of each radiograph is important and must be considered carefully, especially as radiation effects are cumulative.

The establishment of national reference doses to this group of patients could be an important attitude to show a special concern with their protection. Pediatric radiologists, equipment manufacturers, and our professional societies need to work together so that we can estimate and record patient dose and develop accreditation standards. A balance is needed between diagnosis and radiation exposure to protect children.

Acknowledgment

The authors are grateful to the office of vice president for research in Mashhad University of Medical Sciences for research affairs. We would like to acknowledge the co-operation of all staff of radiology departments participating in this study.

References

1. Larissa Oliveira, Fillipe Machado, Simone Kodlulovich Dias et al. (2008). Radiation Dose to Pediatric patients undergoing Chest X-ray procedures in Rio de Janeiro, Brazil. IRPA 12. 12th International Congress of the International Radiation Protection Association Argentina (20080.
2. Commission of the European communities European guidelines on quality criteria for diagnostic radiographic images in paediatrics. EUR 16261 EN (Luxembourg: office for official publications of the European communities)(1996).
3. H B L Pettersson, K Falth-Magnusson, J Petrsoliden et al. (2005). Radiation risk and cost-benefit analysis of a paediatric radiology procedure: results from a national study. British journal of radiology 78, 34-38.
4. C I Armpilia, BSc (Hons), MSc, I A J Fife, BSc(Hons), MSc and P L Croasdale (2002). Radiation dose quantities and risk in neonates in a special care baby unit .The British Journal of Radiology, 75, 590–595.
5. Konstantinos A, Gogos Emmanuel N, Yakoumakis Ioannis A, et al. (2003). Radiation dose considerations in common paediatric X-ray examinations Pediatr Radiol 33: 236–240.
6. Karen E, Thomas.June E. parnell-parmle, Salwa Haidar. et al. (2006). Assessment of radiation dose awareness among pediatricians. Pediatr Radiol 36:823_832.
7. NRPB IPSM COR. National protocol for patient dose measurements in diagnostic radiology. Chilton: NRPB (1992).
8. Hart, D., Miller, M.C. and Wall, B. F. Doses to patients from medical X-ray examinations in the UK-2000 Review. Chilton, U.K. NRPB-W14 (2002).
9. Walter Huda. Assessment of the problem: pediatric doses in screen-film and digital radiography Pediatr Radiol (2004) 34(Suppl 3): S173–S182
10. Hart D, Wall BF, Schrimpton PC, Bungay DR, Dance DR. Reference doses and patient size in paediatric radiology. NRPB R-318.Chilton: HMSO 2000.

Author: M.T. Bahreyni Toossi
Institute: Medical Physics Research Center, Faculty of Medicine, Mashhad University of Medical Sciences
Street: Vakil abad
City: Mashhad Country: Iran
Email: mbahreyni@yahoo.co.uk, bahreynimt@mums.ac.ir

Dental treatment with fluoride at various stages of tumor therapeutic irradiation

W. Fränzel[1] and R. Gerlach[2]

[1] Department of Physics, Martin Luther University Halle, 06099 Halle, Germany
[2] Clinic of Radiation Therapy, Martin Luther University Halle, 06097 Halle, Germany

Radiation caries is stated after tumor therapeutic irradiation of the head-neck area. An expression of this is the disintegration up to a complete tooth loss. Different kinds of therapy aim to stop this disintegration. In this study, 3 different methods of tooth conservation using fluorides have been examined on their effect on the mechanical properties of the teeth. In the first method the remineralization took place after the cumulative dose of 60 Gy had been applied, in the second one, the remineralization took place before each dose und in the third one during the irradiation.

tooth, radiation, nanoindentation, hardness, elastic modulus

I. Introduction

Malignant tumors in the head-neck area are treated by irradiation therapy [1]. Despite a carefully planned irradiation it is inevitable, that healthy neighbouring tissue, i.e. bones, mucosa, teeth and even the salivary gland, is damaged by the irradiation. For the teeth, this means that shortly after the first applied irradiation doses (2 Gy) defects on the tooth substance are identified [2]. The reason for this dental damage, the so-called radiation caries [3], is primarily the structural change of the tissue caused by irradiation. The mechanical properties are significantly deteriorated; fissures and an increasing roughness of the surfaces are observed [4]. The additional change of the oral environment enhances the radiogenic caused tooth destruction due to the changed composition of saliva and the reduction of salivary flow favoring plaque, demineralization and increased carious microorganisms [2, 5] and enhances the radiogenic caused tooth destruction. The mechanical properties however change only marginally [6].

Preventive normal oral hygiene will be more intense if it is combined with regular fluoridation of teeth, because a lower caries increase was observed [2]. In addition, the use of solutions containing calcium and phosphate complementary to fluoride application is recommended [7] to apply remineralizing substances such as calcium and phosphate.

Another approach suggested by Thiel [8] is the daily application of high-concentrated fluoride via gel carriers before beginning the radiation therapy.

The aim of this study is to compare how the hardness and elasticity are affected by various preventive measures - remineralization after irradiation, before every radiation fraction, and during irradiation.

II. Material and methods

We used 30 freshly extracted retained third molars, which had been stored in physiological solution (0.9% NaCl) at 6°C.

After cutting the teeth in half using a diamond-coated band saw under continuous water cooling (Exakt - Trennschleifsystem Makro, Exakt Apparatebau, Norderstedt, Germany) the pulps were removed. The separation planes of the halves were ground with successively decreasing grain size (1200, 2400, 4000; Exakt-Mikroschleifsystem, Exakt Apparatebau, Norderstedt, Germany) under continuous water cooling and finally polished (λtech, England) with a hard synthetic tissue (MD-Dur, Struers), ethylenglycol suspension and diamond spray (grain size 1 and 0,25 µm, DP-Spray P, Struers) as an abrasive. This procedure ensured optimal surface flatness. On each tooth half a 2 x 2 mm^2 region of interest (ROI) was marked in enamel and dentine, whereas the ROI at the second half is adverse at the same place. As consequence we had four groups of teeth – a reference or control group and three test groups.

After the mechanical characterization of all groups, the first test group was fractionally irradiated. The irradiation was performed with a linear accelerator (MXE-2, Siemens AG, Germany), overall 30 times (6 MV, 2 Gy/day, 5 days/week). Thus the teeth were irradiated with 60 Gy, nearly in accordance with the clinical situation. During irradiation the teeth were fixed on plastic plates (Technovit 4071VCL) and enclosed with physiological solution for a homogeneous dose distribution [3].

A group of 10 samples was treated after irradiation (60 Gy) according to the clinical practice with flouride preparation (elmex gelee®, GABA GmbH, Lörrach, Germany) over 12 days. During the application and thereafter, the teeth were stored in a neutral calcium phosphate solution at 37°C to support the remineralization with phosphate ions. After the completion of the remineralization treatment, the mechanical properties were measured again.

A second group was remineralized with elemex gelee®, and a 15 hours lasting storage in the neutral calcium phosphate solution at 37°C before each irradiation. After each dose the mechanical properties were measured aswell.

The third group was remineralized during the irradiation. The teeth were coated immediately before irradiation with

O. Dössel and W.C. Schlegel (Eds.): WC 2009, IFMBE Proceedings 25/III, pp. 96–98, 2009.
www.springerlink.com

elemex gelee® and together with the calcium phosphate solution irradiated at each dose. After each irradiation the teeth were stored as mentioned above. Then the mechanical properties were measured.

The measurement of hardness and elastic modulus in dentin and enamel was performed with a NanointenderII® (MTS-Systems, Knoxville, TN, USA) using a Berkovich-indenter in "load control mode" with a constant force rate at room temperature (app. 21°C). The loading was carried out up to the maximum load of 1mN. 12 intends were created in each marked area and evaluated accordingly to Oliver und Pharr [9].

III. Results

Figure 1 for the hardness and fig. 2 for the elastic modulus show that the irradiation decreases the mechanical parameters of the teeth tissues lasting. After an irradiation of 60 Gy, the values are clearly decreased for the hardness and elastic modulus: the hardness about 95% for enamel and about 75% for dentine, the elastic modulus about 93% for enamel and 75% for dentine.

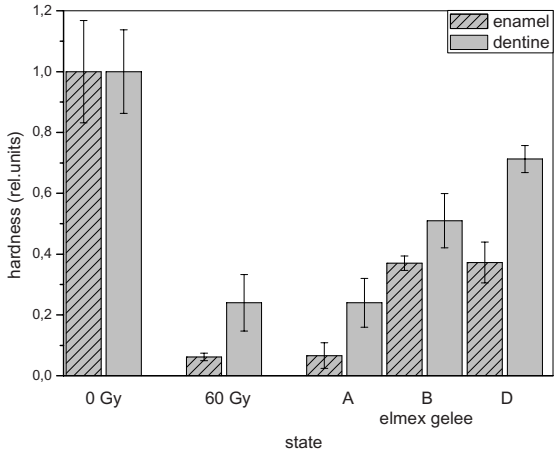

Fig. 1 Hardness of enamel and dentine in relative units in dependent of the state: 60 Gy is after complete irradiation, A means remineralization after irradiation, B is before irradiation, and D during irradiation.

A remineralization after the irradiation will not enhance the hardness in enamel and dentine (A in Fig. 1). Only the elastic parameter of enamel has slightly increased to about 35% of the initial value.

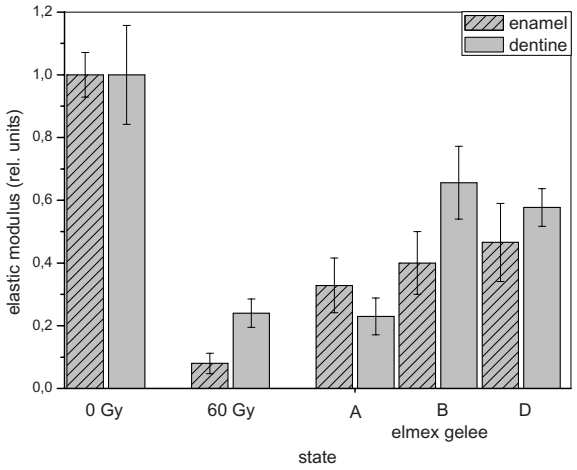

Fig. 2 Elastic modulus of enamel and dentine in relative units in dependent of the state: 60 Gy is after complete irradiation, A means remineralization after irradiation, B is before irradiation, and D during irradiation.

A remineralization after the irradiation will not enhance the hardness in enamel and dentine (A in Fig. 1). Only the elastic parameter of enamel has slightly increased to about 35% of the initial value.

If the teeth are intensively remineralized before each radiation dose, the decrease of the hardness is about 50% of the initial value in dentin and in enamel about 62% (B in Fig. 1). The elastic modulus decreases in dentine about 35% and in enamel about 60% of the initial values.

At the remineralization procedure during irradiation (D in Fig. 1), the gained hardness in enamel is as high as in the remineralization before irradiation method. In dentine we measured about 70% after irradiation. The elastic modulus is about 47% in enamel and about 58% in dentine.

IV. Conclusions

Tumor therapeutic irradiation destroys the dental tissue firstly. The hardness and elasticity are strongly decreased. A remineralization after the irradiation therapy with fluorid elmex gelee® is not sufficient enough to improve the mechanical properties of the dental tissue. It does not lead to a noticeable re-hardening. Only the elastic parameter of enamel seems to have an enhancement.

A more succesful way of remineralization is an intensive therapy before or during each radiation dose. The remineralization in such a manner diminished the reduction of hardness and elasticity in comparision with the reminera-

lization after a complete radiation therapy with a cumulative dose of 60 Gy.

References

1. Folwaczny M, Hickel R (2001) Aspekte der zahnärztlichen Betreuung immunsupprimierter Patienten. Dtsch Zahnärztl Z 56: 285-297
2. Klapproth J (2003) Der Einfluss tumortherapeutischer Bestrahlungen auf das De- und Remineralisationsverhalten von humanem Dentin – eine in-vitro-Studie. Dissertation. University Halle
3. Grötz KA, Duschner H, Kutzner J, Thelen M, Wagner W (1997) Neue Erkenntnisse zur Ätiologie der sogenannten Strahlenkaries. Strahlenther Onkol 173: 668-676
4. Ding J (2004) Untersuchung der mechanischen Eigenschaften von tumortherapeutisch bestrahltem humanen Zahngewebe (Dentin/ Schmelz). Master Thesis. University Halle
5. Cooper JS, Fu K, Marks J, Silverman S (1995) Late effects of radiation therapy in the head and neck region. Int J Radiation Oncology Biol Phys 31: 1141-1164
6. Fränzel W, Gerlach R, Hein H-J, Schaller H-G (2001) Effect of tumor therapeutic irradiation on the mechanical properties of teeth tissue. Z Med Phys 16: 148-154
7. Beetz I, Rößler R, Kielbassa AM (1999) Kariesprophylaxe während und nach einer Strahlentherapie. Prophylaxe Impuls 3: 156-163
8. Thiel HJ (1989) Radiation caries. Radibiol Radither (Berl) 30**: 1**93-211
9. Oliver WC, Pharr GM (1992) An improved technique for determining hardness and elastic modulus using load and displacement sensing indentation experiments. J Mater Res 7: 1564-1582

Author: Dr. Wolfgang Fränzel
Institute: Martin Luther University, Department of Physics
Street: Friedemann-Bach-Platz 6
City: 06108 Halle/Saale
Country: Germany
Email: wolfgang.fraenzel@physik.uni-halle.de

Electron absorbed fractions in skeletal soft tissues based on red bone marrow segmentation at runtime in μCT images of human trabecular bone

R. Kramer[1], H. J. Khoury[1], J. W. Vieira[2, 3], K. Robson-Brown[4] and D. Fuelle[5]

[1] Departamento de Energia Nuclear, Universidade Federal de Pernambuco, Avenida Prof. Luiz Freire, 1000, CEP 50740-540, Recife, Brazil
[2] Centro Federal de Educação Tecnológica de Pernambuco, Recife, PE, Brazil
[3] Escola Politécnica, UPE, Recife, PE, Brazil
[4] Department of Archaeology and Anthropology, University of Bristol, Bristol, UK
[5] Infineon Technologies AG, Neubiberg, Germany

Abstract— **Skeletal dosimetry determines equivalent dose or absorbed fractions in the red bone marrow (RBM) and the osteogenic cells on bone surfaces (BSC). Following a method used earlier for the BSC, RBM and yellow bone marrow (YBM) have been segmented in the marrow cavities of μCT images of human spongiosa at runtime, i.e. during the execution of the Monte Carlo calculation, which avoids the necessity to segment RBM and YBM externally in μCT images for many different cellularities and to store the data. Using this internal RBM/YBM segmentation, this study presents electron absorbed fractions for the RBM and the BSC as a function of the voxel resolution and also compares the results with data from other investigations.**

Keywords— **Skeletal dosimetry, Monte Carlo methods, human phantoms, absorbed fractions, red bone marrow**

I. Introduction

Skeletal dosimetry is concerned with the assessment of equivalent dose to the haemopoietic stem cells of the marrow, called active or 'red bone marrow' (RBM) and to the osteogenic cells on the endosteal bone surfaces, called endosteum or 'bone surface cells' (BSC). Pioneered by the group of W. Bolch [1] at the University of Florida, USA, the application of μCT images of human bone, segmented into marrow and bone, was also introduced into the project on skeletal dosimetry at the University of Pernambuco [2,3]. However, μCT images of human bone segmented into cortical bone, trabecular bone and marrow, do not automatically provide for a spatial definition of RBM and BSC volumes, i.e. that these soft tissues have to be defined by additional segmentation within the spongiosa, which represents the trabecular bone structure filled with skeletal soft tissues.

RBM shares the space of the trabecular marrow cavities with adipocytes, called inactive or 'yellow bone marrow' (YBM), which usually are not considered to be a radiosensitive target tissue. Depending on the bone site, RBM and YBM occupy different volumes inside the marrow cavity. For the reference adult [4], for example, RBM volume fractions, also called 'cellularity factors' (CFs), are 0.7, 0.6, 0.48, 0.38 and 0.25 for the spine, the ribcage, the pelvis, the skull/mandible and the long bones, respectively. In the adult skeleton, only the upper parts of the upper arm and leg bones contain RBM, while the BSC cover all trabecular bone surfaces, cortical bone surfaces next to spongiosa and cortical medullary bone surfaces. Currently, the surface layer of the BSC is considered to be 10 μm thick. It is likely that this thickness will be raised to 50 μm in the future [5]. Equivalent dose to the BSC has recently been calculated by Monte Carlo (MC) methods based on the segmentation of the endosteum at runtime, while RBM equivalent doses were still determined as equivalent dose to the marrow weighted by the corresponding bone-specific cellularity factor [3]. This study will introduce the segmentation of RBM and YBM in μCT images of spongiosa at runtime and will present absorbed fractions of energy for the RBM and the BSC as a function of the voxel resolution when electron emitting radionuclides are concentrated in the RBM.

II. Materials and Methods

With respect to the methods used in this study, earlier papers have already extensively described the 1.2mm cubic voxel-based adult human phantoms MAX06 and FAX06, the processing of the μCT images, the concept of the 8 SP cluster method, which transports radiation particles through these images using the EGSnrc MC code. "8 SP" stands for: 8 micro matrices systematically and periodically applied to

O. Dössel and W.C. Schlegel (Eds.): WC 2009, IFMBE Proceedings 25/III, pp. 99–102, 2009.
www.springerlink.com

spongiosa voxels of the human skeleton [2, 3]. Therefore, this section will focus on the new developments, i.e. the acquisition and processing of a lumbar vertebra bone sample and the segmentation of RBM and YBM in the marrow cavities.

A first lumbar vertebra (L1) was scanned with a microCT scanner Skyscan 1172 (Skyscan Corporation, 2630 Aartselaar, Belgium) with 80 kV (100 μA) at 30 μm and 60 μm resolution at the Imaging Laboratory for Anthropology of the University of Bristol, UK. The skeleton, a donation to medical science, came from an anatomical teaching collection. The subject was a female adult of 30 years, height of 1.49 m and unknown weight. The 30 μm scan resulted in 1068 images with 1984 x 1984 pixels each, while the 60 μm scan produced 534 images with 992 x 992 pixels each. The segmentation procedure followed the published protocol [2, 3]. After the removal of noise with a median filter (kernel size 3x3x3), the images were segmented into trabecular bone and marrow using the histogram-based threshold function of the SCION Imaging Software [6]. Finally, two 2.4mm cubes, each of them consisting of 2x2x2=8 1.2mm micro matrices were extracted from the spongiosa of the two segemented images. The trabecular bone volume fractions (TBVFs) were found to be 8.26% and 8.32% for the 30 μm and the 60 μm resolutions, respectively.

A micro matrix is a 3-dimensional (3D) array consisting of numbers "1" for the marrow cavity and numbers "2" for trabecular bone. Until now, the MC code read the cluster with the 8 micro matrices, then it segmented the 10 μm BSC layer in marrow voxels neighbouring trabecular bone voxels and calculated the corresponding BSC volume. During radiation transport, energy deposited was directly scored in the segmented BSC volume. The remaining cavity volume was considered to represent bone marrow and the RBM volume was not segmented but calculated as the marrow volume multiplied by the bone-specific CF factor. Correspondingly, during radiation transport, energy deposited was scored in the marrow volume and multiplication by the CF factor yielded the contribution for the RBM.

Examining biopsy slides of bone marrow, Bolch et al found that trabecular YBM appears preferably in groups of three adipocytes, each of which is approximately a spherical cell with a mean diameter of ~ 57 μm [7]. When RBM and YBM have to be segmented based on a given CF factor, the first approach one usually would think of is to do this in the cavity volume of the micro matrices. However, different bones have different CF factors and in nuclear medical applications it is common practice to calculate energy absorbed fractions for a whole range of cellularities [7]. Consequently, one would have to segment the micro matrices many times and store them for the corresponding application. In order to be more flexible with respect to the targeted cellularity, it was decided to segment RBM and YBM at runtime, similar to the concept of the BSC segmentation. After reading the 8 micro matrices, the MC code selects randomly a marrow micro voxel within the 3D array stored in the EGSnrc setup. Then two neighbouring marrow voxels are also randomly selected to form a group of three adipocytes. Using the micro matrices with 60 μm resolution has the advantage to be able to simulate the 57 μm spherical adipocytes quite closely. This random process is repeated until the targeted (1-CF) fraction of YBM is attained and a corresponding number of "1" marrow voxels has been classified as "3" YBM voxels. The remaining "1" voxels are now considered to represent RBM voxels. Then, the MC code segments the BSC layer in RBM and YBM voxels neighbouring trabecular bone voxels, calculates the corresponding volumes for all skeletal tissues, transports the particles through the micro matrices in the phantoms spongiosa voxels and scores the energy deposited in all segmented skeletal tissues separately. A recent paper suggested that RBM can more frequently be found close to the trabecular bone surface compared to the central parts of the marrow cavity [8]. However, this study assumes that the RBM and the YBM are uniformly distributed throughout the marrow cavity. If final quantitative data on the spatial RBM distribution become available, the segmentation algorithm can readily be changed.

Apart from the RBM and BSC being the two target tissues, the following skeletal tissues are usually considered as relevant source regions for bone-seeking radionuclides: trabecular bone volume (TBVOL), trabecular bone surface (TBSUR), marrow volume (MAVOL) and red marrow volume (RMVOL). The older method based on the unsegmented marrow (MA) can be used for all source regions, except for the red marrow volume. The new method based on RBM/YBM segmentation (3Y) can be applied to all the mentioned source regions.

III. RESULTS

Absorbed fractions in the RBM and the BSC of the lumbar spine/sacrum of the MAX06 phantom have been calculated based on the micro matrices scanned at 30 μm and 60 μm for electrons isotropically emitted from all four source regions with initial energies between 10 keV and 4 MeV for the MA method and for the 3Y method. The statistical errors were less than 0.3% for electrons emitted in MAVOL

and RMVOL for all initial energies, while for the source regions TBVOL and TBSUR the statistical errors were less than 1% for all energies, except below 30 keV, where the statistical errors were smaller than 4%. The thickness of the BSC layer was 10 μm and the cellularity factor was 0.7, i.e. the marrow volume consisted of 70% RBM and 30% YBM. Tissue compositions were those mentioned before [2, 3]. First results are presented here for the 3Y method when the RBM is the source region.

Figure 1 presents AFs for the RBM and the BSC in the lumbar spine of the MAX06 phantom calculated using the 3Y segmentation method based on 30 and 60 μm voxel resolution for electrons uniformly distributed in the RMVOL.

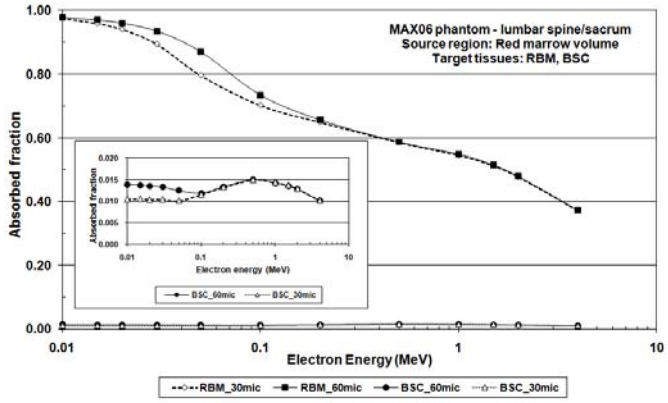

Figure 1. RBM and BSC AFs for 30 and 60 μm voxel resolution when RMVOL is the source region.

Starting with the RBM AF based on 60 μm resolution, one finds that at 10 keV 97.9% of the emitted electron energy is absorbed by the RBM itself, while 1.4%, 0.66% and 0.04% are deposited in the BSC, in the YBM and in trabecular bone, respectively. At 10 keV, the CSDA range of electrons in soft tissue is about 2.5 μm i.e. that emitted in a 60 μm RBM voxel, electrons have a high probability to deposit most of their energy in the start voxel. The electron range increases with increasing kinetic energy, which causes a decrease of the RBM AF. Now, the emitted energy is increasingly absorbed by other skeletal tissues, especially by the YBM, but for higher energies also by trabecular and cortical bone. At 4 MeV, the RBM AF is 0.373, i.e. only about one third of its initial value seen at 10 keV.

Compared to the RBM AF, the BSC AF is so small that the linear scale of figure 1 does not allow for a reasonable presentation. Therefore, a close-up figure has been inserted into figure 1, which shows that the BSC AF for 60 μm resolution varies between 0.01 and 0.015 over the whole range of energies.

Using the micro matrices based on 30 μm voxel resolution leads to a decrease of the RBM AF of 0.3% at 10 keV and of 9.3% at 50 keV. Above 500 keV the differences between the 30 μm and the 60 μm RBM AFs remain below 0.3%. For the energy deposition by a 10 keV electron with a CSDA range of 2.5 mm in soft tissue it does not make a lot of difference if this electron is emitted in a 30 μm or in a 60 μm RBM voxel: In both cases there exists a high probability that the 10 keV electron deposits most of its energy in the start voxel. With increasing energy however, electrons with greater ranges would leave 30 μm RBM voxels earlier to deposit a part of their energy in neighboring skeletal tissues than a 60 μm RBM voxel, because the latter has a 8 times larger volume. Consequently, the 30 μm RBM AF decreases faster with increasing energy. At 500 keV, the CSDA range in soft tissue is about 1770 μm, which is 60 and 30 times greater than the linear dimensions of the 30 μm and the 60 μm RBM voxel, respectively. Therefore, for emitted electron energies above 500 keV and the voxel resolutions investigated here, the RBM AFs become independent of the voxel resolution.

For the BSC AFs, the close-up figure shows a different situation. The greatest difference between the two AFs occurs with 32.4% at 10 keV. For increasing emitted electron energy one finds 22.8%, 2.6% and 0.8% for 50, 100 and 200 keV, respectively. The 10 μm BSC layer is a segmented part of RBM and YBM voxels neighboring trabecular bone voxels. For 60 μm resolution, a 60x60x10 μm^3 BSC volume is located next to a 60x60x50 μm^3 RBM volume, while for 30 μm resolution a 30x30x10 μm^3 BSC volume has only a 30x30x50 μm^3 RBM volume next to it, i.e. that for 60 μm resolution the BSC layer receives energy depositions from electrons coming from a neighboring volume which is 10 times larger than that for 30 μm voxel resolution. Obviously, because of the electron range the voxel resolution effect on the BSC AF is greatest for small energies and becomes smaller as the electron energy increases.

Bolch et al [7] segmented RBM and YBM in the μCT images of two femoral heads and calculated RBM AFs when the RBM is the source region. The cubic voxel size of the μCT images was 88 μm and the average TBVF of the two samples was 37%. The results have been published for various cellularities also in tables, which facilitates a comparison with other data.

From an earlier study [3], μCT images of a femoral neck with a TBVF of 15.6% and scanned at 26 mm resolution

were used for a comparison between the RBM AFs of this study and that of Bolch et al`s investigation for 50% cellularity. The RBM AFs from the two studies are shown by the two solid lines in figure 2. The two RBM AFs show some basic agreement, however, some differences need to be explained.

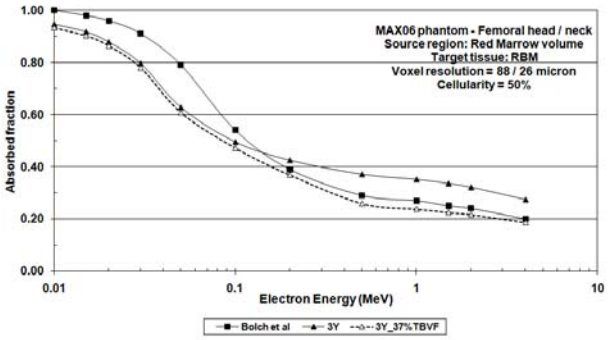

Figure 2. Comparison of RBM AFs from two different studies

For low electron energies, the RBM AF calculated using the 8 SP cluster method starts at 10 keV with a value of 0.946, decreases to 0.627 at 50 keV and reaches 0.273 at 4 MeV. The RBM AF determined by Bolch et al starts at 10 keV with a value of 1.0, decreases to 0.79 at 50 keV and reaches 0.2 at 4 MeV. As for the differences at low electron energies, one has to take the voxel resolution into account. With a cubic voxel size of 88 µm, Bolch et al`s RBM voxels are almost 40 times larger than the 26 µm cubic RBM voxels used in this study, which leads to significantly more energy deposition in the 88 µm RBM voxels for the reasons already discussed above.

At energies above 100 keV, one has to take the TBVF into account. Bolch et al`s bone samples contained 37% of trabecular bone, while the femoral neck used in this study had a TBVF of 15.6%. When the TBVF increases, the RBM AF decreases, because more electrons are absorbed by thicker trabeculae when they travel from one marrow cavity to the next. In order to prove this assumption, the TBVF of the µCT images of the femoral neck was increased to 37% by an algorithm already used in earlier studies [2,3]. The dashed line in figure 2 shows, as expected, that increasing the TBVF from 15.6 to 37% has little effect on the RBM AF for electron energies up to 100 keV, but has a significant decreasing effect for higher energies, which brings the two RBM AFs closer together.

IV. CONCLUSIONS

This study presented a new method for the segmentation of RBM and YBM at runtime of MC calculations. Application of the method to µCT images of a lumbar vertebra scanned at two different voxel resolutions showed that when the RBM is the source region, the RBM and the BSC electron AFs depend on the voxel resolution for low electron energies. Comparison with data from another investigation showed agreement, taking into account the effects of the voxel resolution and the TBVFs.

ACKNOWLEDGMENT

The authors would like to thank the Conselho Nacional de Desenvolvimento Científico e Tecnológico (CNPq) and the Fundação de Amparo à Ciência do Estado de Pernambuco (FACEPE) for financial support.

REFERENCES

1. Shah A P, Bolch W E, Rajon D A, Patton P W and Jokisch D W (2005) A Paired-Image Radiation Transport Model for Skeletal Dosimetry *J Nucl Med* **46**, No.2, 344-353
2. Kramer R, Khoury H J, Vieira J W and Kawrakow I (2006) Skeletal dosimetry in the MAX06 and the FAX06 phantoms for external exposure to photons based on vertebral 3D-microCT images *Phys.Med.Biol.* **51** 6265-6289
3. Kramer R, Khoury H J, Vieira J W and Kawrakow I (2007) Skeletal dosimetry for external exposure to photons based on µCT images of spongiosa from different bpne sites *Phys.Med.Biol* **52** 6697-6716
4. ICRP International Commission on Radiological Protection (1995) Basic Anatomical and Physiological Data for use in Radiological Protection: The Skeleton. *ICRP Publication 70* (Oxford: Pergamon)
5. Bolch W E, Shah A P, Watchman C J, Jokisch D W, Patton P W, Rajon D A, Zankl M, Petoussi-Henss N and Eckerman K F (2007) Skeletal Absorbed Fractions for Electrons in the Adult Male: Considerations of a Revised 50-mm Definition of the Bone Endosteum *Rad.Prot.Dos.* **127** 169-173
6. SCION Image for WINDOWS (2000) Scion Corporation, www.scioncorp.com
7. Bolch W E, Patton P W, Rajon D A, Shah A P, Jokisch D W and Inglis B A (2002) Considerations of Marrow Cellularity in the 3-Dimensional Dosimetric Models of the Trabecular Skeleton *J Nucl Med* **43**, No.1, 97- 108
8. Watchman C J, Bourke V A, Lyon J R, Knowlton A E, Butler S L, Grier D D, Wingard J R, Braylan R C and Bolch W E (2007) Spatial Distribution of Blood Vessels and $CD34^+$ Hematopoietic Stem and Progenitor Cells Within the Marrow Cavities of Human Cancellous Bone *J Nucl Med* **48**: 645-654

Author: Richard Kramer
Institute: Instituto de Energia Nuclear, Federal University of Pernambuco
Street: Avenida Prof. Luiz Freire, 1000
City: Recife
Country Brazil:
Email: rkramer@uol.com.br

Patient Dose Reduction in some Routine Radiographic Examination in Iran

M.R.Deevband[1], M.J.KeykhaFarzaneh [2], M.R. Kardan [1,3], H.R. Khosravi[1,3], F.Faghihi[2] and R.Faghihi[2]

[1] National Radiation Protection Department, Tehran, Iran
[2] Shiraz University, Shiraz, Iran
[3] Nuclear sciences and technology research institute, Tehran, Iran

Abstract— **The purpose of this study was to survey image quality and the entrance surface air kerma for patients in radiographic examinations and to perform comparisons with diagnostic reference levels. In this study, image quality and patient radiation doses were surveyed in 50 hospitals from different proviences in Iran. The rate of unsatisfactory images and image quality grade were noted, and causes for poor image quality were investigated. The entrance surface doses for adult patients were determined in terms of the entrance surface air kerma on the basis of X-ray tube output measurements and X-ray exposure parameters. Comparison of dose levels with diagnostic reference levels was performed. The image quality improved up to 10 percentage points in different hospitals after implementation of a quality control (QC) program. Patient doses varied by a factor of up to 22, although the majority of doses were below diagnostic reference levels. The mean entrance surface air kerma values in mGy before QC were 0.48 (chest, posterior-anterior), 3.4 (lumbar spine, anterior-posterior(AP)), 8.81 (lumbar spine, lateral), 3.56 (abdomen, AP), 2.79 (pelvis, AP), 2.27 (skull, AP) and 1.5 (skull , lateral) and after QC were 0.37 (chest, AP), 3.13 (lumbar spine,AP), 7.56 (lumbar spine, lateral), 3.34 (abdomen, AP), 2.71 (pelvis, AP), 2.1 (skull, AP) and 1.43 (skull , lateral) . Patient doses were found to be similar to doses in developed countries and patient dose reductions ranging from 3% to 23% were achieved. Comparison with other surveys indicates that patient dose levels in these hospitals are not higher than those in developed countries.**

Keywords— **Diagnostic radiology, Entrance skin air kerma, patient radiation doses, Image quality.**

I. Introduction

In 2000, the report of the United Nations Scientific Committee on the Effects of Atomic Radiation (UNSCEAR) indicated that the frequency of radiographic examinations over the preceding 5 years had roughly doubled and in some countries even tripled [1]. There are two concerns from the radiation protection point of view. The first concern is poor image quality produced in radiographic examinations. It is increasingly recognized that there is a tremendous amount of waste of resources, particularly in developing countries, because images of poor quality have been reported in earlier studies to be as much as 15-40% of all images[2]. Poor-quality images result in unnecessary radiation exposure to patients through repeated radiographic examinations, loss of diagnostic information, and increased social costs in addition to the economic costs of health care. The second concern is the significant variation in dose levels to patients of similar size undergoing the same type of radiographic examination. In 1982, ICRP stated that the dose to patients from a given type of examination may vary between hospitals by a factor of 2 to 10[3].

II. Materials and methods

The project was implemented in two phases from December 2007 to December 2008, each phase covering the assessment of both image quality and patient dose .The work in phase 1 involved assessment of the baseline data by scoring image quality and identification of the causes for poor image quality for a 1-month period. Along with image quality assessment, dose assessment for at least 10 adult patients per selected radiographic projection was also performed. Before beginning phase 2 of the survey, quality control (QC) tests were performed to identify equipment malfunctions and to apply appropriate corrective actions based on image quality assessment and equipment performance. Finally, in phase 2, reassessment of the image quality and patient doses for the same types of examination as in phase 1 was performed for another 1 month.

A. Image Quality Assessment

Image quality assessment in the selected 1-month period was performed in both phases as described in the previous section and involved all radiographic examinations. The CEC quality criteria for diagnostic radiographic images [4] were supplied to the participating centers for use by experienced radiologists in image quality assessment. The use of quality criteria in this survey was mainly intended to reduce inters observer variability by guiding radiologists on how to grade the quality of radiographic images. The quality criteria were expected to be in the minds of radiologists and were not used for image grading on any

O. Dössel and W.C. Schlegel (Eds.): WC 2009, IFMBE Proceedings 25/III, pp. 103–105, 2009.
www.springerlink.com

specific criterion basis. Instead, each radiographic image was graded as A, B, or C[4,5].Grade an images were those clearly accepted by reporting radiologists without any remark or reservation. Grade B included all images that were accepted with some remarks or reservations. Grade C images were those that should be rejected. In addition to this analysis, the participating centers were requested to document the main causes for B- or C-graded images, such as overexposure or under exposure, artifacts, field-size misplacement, processing problems, or any other problems[3-5].

B. *Patient Dose Assessment*

The patient dose assessment was also done in two phases as it was for image quality assessment. It involved the most common seven radiographic projections: chest, PA; lumbar spine, AP; lumbar spine, lateral; abdomen, PA; pelvis, AP; skull, PA and; skull, lateral; The quantity used was the entrance surface air kerma, which is the quantity currently recommended for patient dose assessment and for comparing patient dose levels with diagnostic reference levels in general radiography[6].

For X-ray tube output measurements, the appropriate dosimeter (DIADOS E from PTW manufacture) was connected to an electrometer and placed on a low scattering material (cardboard) on a patient support setup in the vertical position. The dosimeter was positioned in the central beam axis at a preferable X-ray tube focal spot-detector distance of 50 cm. The radiation field size at focal spot-detector distance was set to just cover the dosimeter to avoid the possible influence of scatter radiation to the dosimeter. The typical field size was 10 x 10 cm, and the tube potential was set at 40 kVp and any mAs value (depending on convenient tube load conditions). A radiographic exposure was made and the dosimeter reading recorded. This step was repeated once more at the same kVp and mAs settings and the average dosimeter reading determined. The X-ray tube output was determined as the ratio of average dosimeter reading (in air kerma) to the tube current-time product used for tube voltages 40-110 kVp in steps of 10 kVp. The values of the X-ray tube output per mAs were plotted against the tube potential and the resulting curve was fitted using a power function.The incident air kerma for each adult patient undergoing a particular radiographic examination was determined by the product of the X-ray tube output value and the actual mAs used in the radiographic examination. The entrance surface air kerma value was then calculated by multiplying incident air kerma to the patient's surface by the appropriate backscatter factor (BSF), which depends on the tube potential, total filtration, and radiation field size[6].

III. Results

The image quality improved up to 10 percentage points in different hospitals after implementation of a quality control (QC) program. Patient doses varied by a factor of up to 22, although the majority of doses were below diagnostic reference levels. The mean entrance surface air kerma values in mGy before QC were 0.48 (chest, posterior-anterior), 3.4 (lumbar spine, anterior-posterior(AP)), 8.81 (lumbar spine, lateral), 3.56 (abdomen, AP), 2.79 (pelvis, AP), 2.27 (skull, AP) and 1.5 (skull , lateral) and after QC were 0.37 (chest, AP), 3.13 (lumbar spine,AP), 7.56 (lumbar spine, lateral), 3.34 (abdomen, AP), 2.71 (pelvis, AP), 2.1 (skull, AP) and 1.43 (skull , lateral) . Patient doses were found to be similar to doses in developed countries and patient dose reductions ranging from 3% to 23% were achieved.

The survey of image quality and patient dose levels in representative centers in Iran has been presented in figure 1. The application of diagnostic reference levels has been shown to have the potential for dose reductions without adversely affecting the image quality.

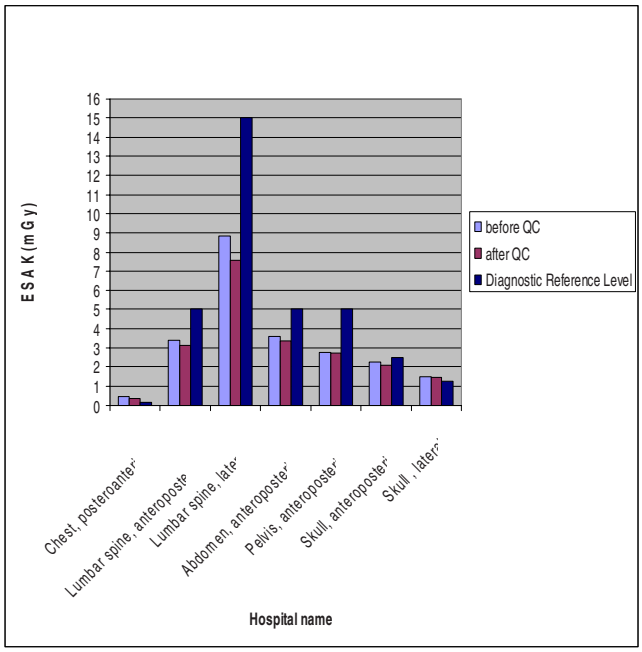

Fig. 1 Entrance Surface Air Kerma in all examinations and projection

IV. Discussion and conclusion

The additional advantage of dose reduction can be an increased X-ray tube life, although there are limited data to support this assumption [7]. The experience from this study should form a basis to strengthen QA programs where they exist and establish such programs where they do not yet exist. Such QA programs are necessary to ensure that appropriate radiation exposure is delivered to the image receptor to produce an image quality that is adequate for the diagnostic task. The potential for increased awareness of such a need for optimization is one of the positive impacts of this study in reducing unnecessary patient doses without compromising the image quality.

References

1. United Nations Scientific Committee on the Effects of Atomic Radiation. *Sources and effects of ionizing radiation: report to the General Assembly; annex D, medical radiation exposures.* New York, NY: United Nations, 2000.
2. Rehani MM. *Diagnostic imaging: quality assurance.* New Delhi, India. Jaypee Brothers Medical Publishers, 1995: 14-23, 43.
3. International Commission on Radiological Protection (ICRP). *Protection of the patient in diagnostic radiology.* ICRP publication 34. Oxford, United Kingdom: Pergamon Press, 1982.
4. European Commission. *European guidelines on quality criteria for diagnostic radiographic images.* Publication EUR 16260 EN. Brussels, Belgium: European Commission, 1996.
5. Rehani MM, Arun Kumar LS, Berry M. Quality assurance in diagnostic radiology. *Ind J Radiol* 1992;2 : 259-263.
6. International Commission for Radiation Units and Measurements (ICRU). Patient dosimetry for x-rays used in medical imaging. *J ICRU* 2005; 5: IV -VI.
7. Gray JE, Archer BR, Butler PF, et al. Reference values for diagnostic radiology: application and impact. *Radiology* 2005; 235: 354-358.

Author: M.R.Deevband
Institute: National Radiation Protection Department
Street: North of Kargar
City: Tehran
Country: IRAN
Email: mdeevband@aeoi.org.ir

A study of maternal and foetal doses arising from V/Q and CTPA scanning during pregnancy

K.L.Fleckney[1], L.A.Hunt[1], and P.I.Ignotus[2]

[1] Department of Medical Physics, Kent Oncology Centre, Maidstone, UK
[2] Department of Radiology, Kent and Sussex Hospital, Tunbridge Wells, UK

Abstract – **This work explores the variation in foetal and maternal dose resulting from two different imaging techniques to diagnose pulmonary embolism during pregnancy. Current published literature was used in conjunction with our centre's protocols to estimate a foetal dose, and a maternal whole body dose, and breast dose following both CT pulmonary angiography (CTPA) and a nuclear medicine perfusion scan. These doses were used to calculate risk factors of cancer induction in both the foetus and the mother and to explore the risk of breast cancer induction in the latter following breast irradiation. It was found that both techniques have their advantages; however foetal dose during the 3rd trimester for both were the same order of magnitude, while maternal breast doses were two orders of magnitude higher for CTPA than perfusion scanning.**

Keywords – **foetal, maternal, effective dose, breast, CTPA.**

I. Introduction

Many pregnant patients in Kent undergo a diagnostic imaging procedure for the diagnosis of pulmonary embolism (PE) annually. UK national guidance [1] published in 2007 by the Royal College of Radiologists (RCR) states that the use of CT pulmonary angiography (CTPA) is the investigation of choice in patients with a high clinical suspicion of pulmonary embolus. These guidelines do not contain specific information about the management of suspected PE in pregnant patients. The use of CTPA is actually recommended over that of a nuclear medicine ventilation perfusion (V/Q) scan, due to increased accuracy in patients with pre-existing pulmonary disease. However, in pregnant patients, due to the lower incidence of pulmonary disease in this age group, the use of a V/Q scan can provide an alternative method of diagnosing PE. Recommendations by The Prospective Investigation of Pulmonary Embolism Diagnosis [2] state that 69% of their investigators recommend a V/Q scan for diagnosis of PE in pregnant patients.

In the UK, all patients undergoing X-ray examinations require the procedure to be justified [3]. This justification should include the benefit and detriment to the patient as a result of the examination proceeding.

The use of ionising radiation in pregnancy, although with risks, can be justified given that the presence of a PE is the leading cause of maternal death. It is generally considered that the risk of maternal mortality due to PE is greatest during the third trimester; however there is evidence to suggest there is an equal likelihood of thrombosis occurring throughout each stage of pregnancy [4].

Much literature exists discussing foetal risks following in-utero irradiation. ICRP Publication 90 [5] states that the embryo and foetus are highly radiosensitive during the entire term of prenatal development. The nature and severity of these induced biological effects depend on the gestational age of the developing foetus at the time of the exposure. The foetal doses expected for both CTPA and V/Q scans, are generally thought to be several orders of magnitude below that considered to induce malformations or mental retardation.

The current protocol for a V/Q scan in our Centre involves the administration of 80MBq of ^{99m}Tc-DTPA aerosol followed by 100MBq of ^{99m}Tc-MAA intravenously, which is in line with guidelines published by the BNMS [6]. Due to the risks of ionising radiation to the developing foetus it has been proposed that a half-dose perfusion only scan is performed in pregnant patients with no ventilation performed as a rule.

II. Aims of this work

This work aims to use current published literature to assess both the maternal radiation dose and foetal absorbed radiation dose. The published doses will be corrected to allow for differences in protocol between our Centre and those used in the published studies. The determination of dose will allow resulting risks to be calculated for each method of diagnosis. In the case of the maternal dose, both the whole body effective and breast doses will be considered. Where possible, dose and therefore risk data for the foetus is presented dependent upon foetal gestational age.

III. Method

A. Determining Dose from V/Q scan

The current Admission of Radioactive Substances Advisory Committee (ARSAC) guidance [7] was used to estimate the maternal effective dose from both the ventilation, and full and half-dose perfusion scanning. This guidance presents uterine doses which could not be used to accurately determine the foetal dose as they do not consider the cross-placental transfer of radioactive medicinal products to the foetus.

O. Dössel and W.C. Schlegel (Eds.): WC 2009, IFMBE Proceedings 25/III, pp. 106–109, 2009.
www.springerlink.com

Instead, ICRP Publication 84 [8] was used to estimate foetal dose. It adopts typical uterine and foetal doses for common radiopharmaceuticals per unit of activity, including ^{99m}Tc-MAA and DTPA, calculated by Russell et al [9]. Critically they present data dependant upon foetal developmental age.

ICRP Publication 80 [10] was used to calculate the maternal breast dose. The published data does not consider the impact of hormonal changes during pregnancy affecting radiopharmaceutical uptake, and this will not be considered further as part of this study.

Both current, full-dose, and proposed, half-dose, perfusion protocols were considered during dose calculations to both the mother and foetus.

B. Determining Dose from CTPA

A study by Winer-Muram et al [11], considers the foetal radiation dose in patients undergoing helical CT for diagnosis of PE. They present theoretical dose data calculated using Monte Carlo techniques at 120kV, which can be corrected for factors such as different milliampere second values and scan pitch. They show that as the pregnancy progresses the foetal dose increases.

The study presented mean foetal absorbed dose, and maximum foetal absorbed dose which was defined, for cranial-caudal progression, as being a point in the uppermost 1cm of the foetus, or the portion closest to the scanned volume. The mean foetal doses were used from this work and applied to local scan parameters in our Centre. The maximum absorbed dose to the foetus was also calculated, but will not be used for any risk analysis as only a relatively small part of the foetus receives this dose.

The data used in this work was obtained from one CT scanner in the Centre, a Sensation 64 (Siemens Medical Solutions, Erlangen, Germany).

The current scan protocol used is described in Table 1. The mAs is automatically modulated by the scanner to ensure optimum image quality, and therefore varies between patients.

Table 1 – CTPA Scan Parameters

Parameter	Current Protocol
kV	120
Rotation time	0.5s
Detector Collimation	0.6 mm
Slice Thickness	0.75 mm
Pitch	0.75mm

Examination data for 72 female CTPA patients, aged between 15 and 45, was obtained via the radiology information system. To minimise statistical errors, all female CTPA patients were considered, rather than only taking the small number of pregnant patients who underwent CTPA. To verify the data, the Dose-Length Products (DLPs) were checked for a selection of patients using the information stored on the picture archive and communication system (PACs) along side the images.

Effective mAs values, averaged automatically by the system over the whole scan length, for each patient were noted and used to determine the average mAs values delivered for a typical CTPA scan. The maximum effective mAs value from the patient group was noted and used to determine maximum foetal doses. $CTDI_{vol}$ values were also noted and averaged for the patient group.

The ImPACT CT Dose calculator [12] was used to estimate the maternal absorbed dose to the breasts and whole-body effective dose, based on the current scan protocol. The scan length was adjusted to give similar DLPs and $CTDI_{vol}$ to the average values of those in the patient group. Effective dose and breast dose were calculated for maximum, minimum and mean DLPs for the whole group. It was noted that patients with remarkably high DLP figures were particularly large patients and this may result in an error in estimating the breast and effective doses in these cases. ImPACT CT dose takes an average female patient as 60Kg.

In 2007 the ICRP Publication 103 [13] recommended new tissue weighting factors for the calculation of effective dose. Critically, to this study, the weighting factor for breast sensitivity to radiation for the effective dose has increased from 0.05 to 0.12. Therefore it was felt important to manually update the ImPACT CT Dose package to consider the new recommendations for all organs.

Minimal literature [14] exists to show an increased risk of breast cancer following breast irradiation around the time of pregnancy. However, the study group was small, involved therapy energies in the MV range, and there was limited patient follow up. Further work to verify this link, in particular for the diagnostic range of energies, would be beneficial.

IV. Results

A. Foetal Dose

From all CTPA examinations a mean mAs of 119 was determined, with all mAs values in patient group falling in the range 47.2 – 349. A pitch of 0.75 was used for all scans. The mean of the data presented by Winer-Muram et al [11] for each trimester was adjusted for the scan parameters in the patient group and is displayed along with V/Q scan data in table 2. Both mean and maximum absorbed foetal doses were determined for CTPA.

B. Maternal Dose

From all CTPA examination data in the patient group, the mean DLP value was 273mGycm, with all DLP values in patient group falling within the range 156-478mGycm. Effective dose and absorbed breast dose values obtained from the ImPACT software for the mean, minimum and maximum DLPs in the patient group are shown in table 3.

Table 2 – Absorbed Foetal Doses

Examination		Absorbed Foetal Dose (mGy) 1st Trimester	2nd Trimester	3rd Trimester
CTPA	Mean[i]	0.016	0.042	0.115
	Maximum[ii]	0.032	0.140	0.726
^{99m}Tc DTPA	80MBq	0.344	0.184	0.240
^{99m}Tc MAA	50MBq[iii]	0.200	0.250	0.200
	100MBq	0.400	0.500	0.400

[i] Averaged at all points over the foetus.
[ii] Point dose at uppermost 1cm of foetus, or portion closest to scan volume.
[iii] Representing half nominal administered activity.

Table 3 – Maternal Doses

Examination		Effective Dose (mSv)	Absorbed Breast Dose (mGy)
CTPA[iv]		5.7 (3.6 – 25)	12 (8 – 52)
^{99m}Tc DTPA	80MBq	0.560	0.152
^{99m}Tc MAA	50MBq[v]	0.550	0.250
	100MBq	1.100	0.500

[iv] bracketed values show dose range based on min and max DLPs.
[v] representing half nominal administered activity.

C. Risk Analysis

Foetal risks from ionising radiation were taken from a joint report by the National Radiological Protection Board (NRPB), The College of Radiographers and the RCR in 1998 [15]. All foetal doses determined during this study were considerably lower than the limit for deterministic effects outlined in the NRPB report. The number of excess cancer cases (leukaemias and solid tumours) up to the age of 15 years following irradiation in utero should be taken as 1 in 17,000 per mGy, in addition to natural incidence which will be taken from this report as 1 in 650. This risk factor was used to determine foetal risk of developing childhood cancer for both CTPA and V/Q scans during pregnancy, as shown in table 4.

Maternal risks were considered as a two-fold problem; the risk of developing any malignancy, and the specific risk of breast cancer induction following irradiation of the breasts. ICRP Publication 103 gives risk factors for non-site specific cancer induction after exposure to radiation at a low dose rate (5.5×10^{-2} Sv^{-1}). Natural incidence of cancer has been estimated on the UK Government's National Statistics website [16] as 1 in 3.

A report produced for the NHS in 2003 [17] assessed the risk-benefit processes involved in the UK's national breast screening programme. It lists the risk factors of developing radiation-induced breast cancer for a range of ages at exposure. Between the ages of 20 – 40 the risk is fairly constant peaking at 18 in 1 million per mGy. At the age of 15 this risk rises sharply to 43 in 1 million per mGy. The risk factors used to provide further justification of a clinical protocol in the management of pregnant patients will only be taken from the 20 – 40 year old age group. All of these risk factors should be considered in conjunction with the natural occurrence. UK National statistics state that a women's natural chance of contracting breast cancer in their lifetime is 1 in 9 [16].

Maternal risk factors, as a result of the doses previously stated, are shown in table 5.

Table 4 – Foetal Risk Factors

Examination		Foetal Risk (all given as incidence in 1 million) 1st Trimester	2nd Trimester	3rd Trimester	Natural Incidence of Childhood Cancer (to age 15)
CTPA		0.9	2.5	6.8	1 in 650 *(equivalent to 1538 in 1 million)*
^{99m}Tc DTPA	80MBq	20.2	10.8	5.9	
^{99m}Tc MAA	50MBq	11.8	14.7	11.8	
	100MBq	23.5	29.4	23.5	

Table 5 – Maternal Risk Factors

Examination		Whole Body Cancer Induction (risk in 1 million)	Natural Incidence of Cancer	Breast Cancer Induction (risk in 1 million)	Natural Incidence of Breast Cancer
CTPA		314	1 in 3 *(equivalent to 333,333 in 1 million)*	216	1 in 9 *(equivalent to 111,111 in 1 million)*
^{99m}Tc DTPA	80MBq	31		2.7	
^{99m}Tc MAA	50MBq	31		4.5	
	100MBq	61		9.0	

V. Discussion

For maternal risk, the results indicate a large difference in dose, and therefore risk, between the two imaging techniques. The current half-dose perfusion scan protocol for pregnant patients represents a 10-fold decrease in maternal effective dose and a 48 times lower

breast dose compared to CTPA. The risk, therefore, will also decrease in line with dose. No literature could be sought to quantify the increased uptake of MAA given hormonal changes in the breast. Therefore, the risk factors presented here may be a significant underestimate and should be used with this in mind.

As pregnancy progresses, ratio of risk for the foetus from half-dose perfusion scanning, compared to CTPA decreases as shown in table 6. Consideration should be made for the larger patients, where the mAs used during CTPA is significantly greater than 119. For the case of our maximum mAs (349), half dose perfusion may yield a significantly lower foetal dose than CTPA. Consideration should also be made as to whether the half-dose perfusion technique is as reliable in large patients, due to increased attenuation by the patient.

Table 6 – Ratio of foetal risk: CTPA vs half dose perfusion

1st Trimester	2nd Trimester	3rd Trimester
1 : 13	1 : 6	1 : 2

Although the risks of cancer induction to the foetus during half-dose perfusion scanning are double that of CTPA in the last trimester, the risks for both of these techniques compared to natural incidence of cancer induction are still considerably small (2 orders of magnitude).

Furthermore it is logical to assume that, due to the method of breakdown of MAA within the body, encouraging the pregnant patient to drink extra fluids and to empty their bladder regularly will help to reduce foetal dose attributable to the activity in adjacent bladder, if perfusion scanning takes place.

A study by Kennedy et al [18] showed that the use of a lead apron on the maternal abdomen to shield the foetus, during CTPA, can significantly reduce the foetal dose by up to 40%.

VI. Conclusions

For third trimester pregnancies, foetal risks from CTPA are just over half that from half-dose perfusion scanning, but both are low when compared to natural incidence of child hood cancer.

Maternal risks from CTPA, are an order of magnitude higher compared to half-dose perfusion, with breast doses being 2 orders of magnitude higher. It is felt that the breast risk may even be greater due to possible increased radio-sensitivity of the breasts during pregnancy. It is understood that the amount of diagnostic information yielded in CTPA far outweighs that of a perfusion scan.

Consideration should be made, in each individual case, whether the amount of information needed, or likely to be gained, justifies the higher dose to the mother.

As a result of this study, protocols have been changed in our centre to recommend that best practice would be that all pregnant patients undergo half-dose perfusion scanning if at all practical.

References

1. The Royal College of Radiologists. Making the best use of clinical radiology services: referral guidelines. London: The Royal College of Radiologists, 2007.
2. Diagnostic Pathways in Acute Pulmonary Embolism: Recommendations of the PIOPED II Investigators. Radiology 2007::242:15–21.
3. IR(ME)R Ionising Radiation (Medical Exposure) Regulation 2000 (SI 2000 No 1059) London, HMSO.
4. Toglia MR, Weg JG. Venous thromboembolism during pregnancy. N Engl J Med 1996; 335:108-114.
5. ICRP (2003). Biological Effects of Prenatal Irradiation (Embryo and Fetus). ICRP Publication 90. Ann. ICRP 33(3).
6. British Nuclear Medicine Society. Ventilation / Perfusion Imaging for Pulmonary Embolic Disease Guideline. BNMS at http://www.bnms.org.uk.
7. Admission of Radioactive Substances Advisory Committee. Notes for Guidance on the Clinical Administration of Radiopharmaceuticals and Use of Sealed Radioactive Sources. Chilton, UK. Health Protection Agency, Radiation Protection Division. March 2006.
8. ICRP (2000). Pregnancy and medical radiation. ICRP Publication 84. Ann. ICRP 30(1).
9. Russell JR, Stabin MG, Sparks RB, Watson E. Radiation absorbed dose to the embryo/fetus from radiopharmaceuticals. Health Phys. 73(5):756-769; 1997.
10. ICRP (1998). Radiation dose to patients from radiopharmaceuticals: (Addendum 2 to ICRP Publication 53). ICRP Publication 80. Ann. 28 (3).
11. Winer-Muram HT, Boone JM, Brown HL, Jennings SG, Mabie WC, Lombardo GT. Pulmonary Embolism in Pregnant Patients: Fetal Radiation Dose with Helical CT. Radiology 2002;224:487-492.
12. ImPACT CT Patient Dosimetry Calculator, Version 0.99x, St. Georges Hospital, London, UK.
13. ICRP (2007). ICRP Publication 103: The 2007 Recommendations of the International Commission on Radiological Protection. Ann. ICRP 2007;37:
14. Chen J, Lee RJ, Tsodikov A, Smith L, Gaffney D. Does Radiotherapy around the time of pregnancy for Hodgkin's disease modify the risk of breast cancer? Int, J. Radiation Oncology Biol. Phys 2004;5:1474-1479.
15. NRPB CoR RCR. Diagnostic Medical Exposures: Advice on Exposure to Ionising Radiation during Pregnancy. Chilton, NRPB (1998).
16. UK Office of National Statistics at http://www.statistics.gov.uk
17. NHSBSP. Review of radiation risk in breast screening. NHSBSP Publication 54, Sheffield, (2003).
18. Kennedy EV, Iball GR, Brettle DS. Investigation into the effects of lead shielding for foetal dose reduction in CT pulmonary angiography. Br J Radiol 2007;80:631-638

Katy L Fleckney
Kent Oncology Centre
Hermitage Lane
Maidstone,
UK
katy.baker@nhs.net

Study and Analysis of Radiation Level at Different Hospitals in Nepal.

Kanchan P. Adhikari[1], L.N. Jha[2], Pedro Galan Montenegro[3]

[1]Medical Physicist & Radiation Safety Officer, NAMS, Bir Hospital, Kathmandu, Nepal
[2]Prof. & Head, Central Department of Physics, Tribhuvan University, Kathmandu, Nepal
[3]University of Malaga and Head of Medical Physics Department, Hospital Regional Carlos Haya, Malaga, Spain

Abstract - **In Nepal, diagnostic use of radiation has been practiced for a long time. We have no radiation regulatory board, which controls the radiation protection activities. This study was done to develop radiation safety culture to benefit Nepalese People, to create awareness on radiation, to make the radiation workers aware on possible radiation health hazard and to know their view on radiation protection, to make inventory of availability of equipment of the surveying hospitals and to initiate steps towards establishment of Nepalese code of radiological Practice. The following activities were carried out to assess the status of radiation protection at different radiological centers, questionnaire for radiation workers, radiation dose level measurement and made an inventory of availability of radiation producing equipment of surveyed hospitals. The dose level were measured by Roentgen Gamma Ray Dosimeter (RGD27091) and FAGFH40F1. To calculate equivalent dose level *H* (mSv/week) we measure dose rate level in each area D (mSv/min) in an exposition at higher kV, mA_m and min_m**

$$H\left(\frac{mSv}{week}\right) = D\left(\frac{mSv}{\min}\right) \cdot \frac{1}{I_m(mA_m)} \cdot Workload\left(\frac{mA.\min}{week}\right)$$

Altogether 15 Hospitals were monitored, and 86 radiation workers entertained the questionnaire. Some radiation workers are not qualified and do not have knowledge on radiation but doing X-ray procedure. Most of the general X-ray and CT working areas are safe but some need more protection, in the patient entering door and control console area. In Fluoroscopy some exceeds the dose limit noted by International Commission on Radiological Protection (ICRP). None of the surveyed hospitals have Personnel monitoring system. Most of the radiation workers are aware of radiation hazard and wanted TLD for personnel monitoring, radiation regulatory board and radiation act. The interesting thing we found during our survey is that some unqualified personnel are exposing the patients.

Keywords - **Dose Limit, Workload, Radiation Protection, Personnel monitoring.**

I. Introduction

The science of Radiological Protection aims to provide an appropriate standard to preserve the health of the people from the harmful biological effects of ionizing radiation without unduly compromising with the beneficial practices. Medical imaging with ionizing radiation and Radiotherapy have evolved steadily over the last century, interspersed several significant breakthroughs.

Radiological Services in Nepal have a long history. The diagnostic use of ionizing radiation first started in 1923. Since then tremendous development has taken place in the field of radiology and radiotherapy. In 1988, Bir Hospital started the first CT in Nepal and first Nuclear Medicine in Nepal. In 1991, Bir hospital has also started the first Radiotherapy unit with Tele Cobalt machine. Right now, we have facilities providing radiological services all over the country. Latest radiological equipments are being imported. Newer modalities are being introduced in major hospitals and diagnostic facilities. Small X-ray set-ups are also being established on a day-by-day basis. This quantitative increment may have a positive impact on the health service system of the country; however, the quality of service being delivered cannot be overlooked, especially if the subject relates to radiation.

At present there are four Tele-Cobalt machines, three Linear Accelerators, three Simulators, two High Dose Rate (HDR) Brachytherapy, one Orthovoltage therapy machine, one Gamma Camera (SPECT), four Magnetic Resonance Imaging (MRI) machine, more than twenty Computed Tomography machine and about more than 800 X-ray machines in the country. There are about 300 qualified professionals (Radiologists, Radiation Oncologists, Medical Physicists/Radiation Safety Officers, Radiographers/Technologists, Radiation Therapists/Radiation Therapy Technologists, Nuclear medicine Physicians, Nuclear Medicine Technologists.) are working in the field of diagnostic radiology, radiotherapy, nuclear medicine.

With all the above-mentioned background the field of Radiology, Radiotherapy and Nuclear Medicine has become much diversified in Nepal. We all know that

O. Dössel and W.C. Schlegel (Eds.): WC 2009, IFMBE Proceedings 25/III, pp. 110–113, 2009.
www.springerlink.com

ionizing radiation can be harmful to human health so these radiations should be used very carefully. Whenever radiation is used the advantage and benefit should always be greater than risk and harm from it. Radiation has both beneficial and harmful effects. The use of ionizing radiation in medical field for diagnostic and therapeutic purposes is the benefit. Keeping the scientific fact of effects of radiation in mind, ICRP has been suggesting recommendations and guidelines pertinent to radiation protection. Other countries and their regulatory boards follow these recommendations. According to ICRP, radiological practice and dose limits to be followed. The aim should be to make aware the radiation worker from the harmful effects of radiation and keep them within the dose limit noted by ICRP. All international boards including International Labor Organization, United Nations Scientific Committee on Effects of Atomic Radiation (UNSCEAR) and World Health Organization (WHO) International Atomic Energy Agency (IAEA) accept these limits. But the scenario in Nepal is quite different.

In Nepal, there are no specific rules or regulation as well as any monitoring system for workers regarding radiation. Consequently over 95% of medical radiation workers have never been monitored for their radiation exposure. In Nepal, only some hospitals are monitoring its radiation workers. Since the prevailing scientific opinion is that radiation is dangerous at any level, and the effect of radiation is cumulative over time, it is therefore imperative that all radiation workers be monitored and known the potential risk level and their job. Under this requirement, virtually all radiation workers (radiologists, radiographers, radio-technologists and medical physicists) need to be regularly monitored for radiation exposure and to take appropriate measure to make certain that those who are exposed to radiation should not get radiation dose above the dose limit.

Though the history of radiation practice is long, we still don't have a legislative body or any sort of radiation act to set standards of radiation protection and radiological activities. Besides, there are no official records of the exact number of the radiological facilities in operation. The number and types of X-ray units; the number of radiation workers and their qualifications; the radiation safety measures and the working conditions of workplace are still unknown. No governmental organizations or private organizations have been keeping these statistics. Beside a couple of therapeutic centers, no radiation workers or facilities are being monitored for their radiation exposure and effects. The use of substandard X-ray units with erratic output, repeat exposures due to incompetence of radiation workers, a paucity of skilled and qualified radiation workers, lack of standard working conditions all have contributed in the diminution of the quality of diagnostic service being delivered. All these factors, consequently, have resulted in unnecessary radiation dose to the general public and the occupational workers themselves as well, so as quality assurance of practice. .

Nepal is resided by people of diverse class with different knowledge and social standard. Unsurprisingly, we have people from distant places who think that X-rays would treat their ailments. However, we do have so-called high class, well educated people from cities who insist to accompany their patients to the X-ray examination room. Moreover, even the health professionals exhibit their poor knowledge of radiation while some are over-conscious about radiation. They are worried that they would develop cancer if they were exposed for more than three times a year. These facts merely imply that the knowledge of the general public and even the health professionals regarding radiation protection is poor.

II. Objectives of the Study

In Nepal, diagnostic use of ionizing radiation has been practiced for a long time. We have no radiation regulatory board, which controls the radiation protection activities.

1. To develop radiation safety culture to benefit Nepalese People.
2. To create awareness on radiation used in medical field.
3. To make the radiation workers aware on possible radiation health hazard and to know their view on radiation protection.
4. To make inventory of availability of equipment of the surveying hospitals.
5. To initiate steps towards establishment of Nepalese code of Radiological Practice.

III. Materials and Methods of the Survey

The following activities were carried out to assess the status of radiation protection at different radiological centers.

1. Questionnaire for Radiation Workers
2. Radiation Dose Level Measurement
3. Made an inventory of availability of radiation emanating equipment of surveyed hospitals.

Questionnaire for radiation workers consists of one to twenty-five questions seeking information regarding professional responsibility, protection training, personnel dose monitoring, institutional and self-motivation towards radiation safety, etc. In addition, this questionnaire also intends to acquire the information about knowledge on radiation protection from the concerned radiation personnel involved in his/her work.

To find out the level of radiation at the radiological facilities Roentgen Gamma Ray Dosimeter (RGD 27091) and FAG FH40F1 were used. All the instruments have digital display of readings and calibrated.

To measure the radiation level, six specific locations were selected and identified by the capital letters A-F that stand as follows:

For General X-Ray

A: At Control Console, B: Outside the X-ray room (door closed)/Corridor, C: patient's waiting room, D: Dark room, E: Behind the wall where X-ray tube is often directed, F: Leakage radiation (at 1 m from X-ray tube)

For CT

A: At control console, B: At door near the control console, C: Outside the patient entering door, D: Patients' waiting room, E: Floor above the CT machine

The equivalent dose rates in air at different locations at the specified reference points (A, B, C, D & E) were measured. For the purpose of dose rate measurement at different locations, a scattering medium was used. Measurement behind the chest stand wall was done without a patient or a phantom.

A. Radiation Level Calculation

First of all, to calculate the radiation level in different areas, we have to consider the different characteristic parameters of radiation like Kilo-Volt (kV), mille-ampere (mA) & Time (s).

The parameter taken to evaluate radiation level is about: KV- 100 or 120 (we evaluate the radiation level in worst condition of irradiation, high energy of irradiation), time (t) is about 2 s (death time of survey meter is longer than 0.1 s), Intensity (I) is 50 mA. All the readings are taken with irradiation of scattering medium.

We calculate the radiation level is through the workload (mA.min/week).

The current workload in each unit could be calculated as

$$\sum_i \left(mA \;.\min\right)_i \cdot N_i$$

N_i examination number of kind i and (mA.min) used techniques for examination kind i

In this research, to evaluate the radiation level in different areas the following standard is used to find out the workload as published in DIN 6812.

Then in each area:

$$H\left(\frac{mSv}{week}\right) = D\left(\frac{mSv}{\min}\right) \cdot \frac{1}{I_m(mA_m)} \cdot Workload\left(\frac{mA.\min}{week}\right)$$

The operational dose limits for H are as follows:

For radiation workers: 0.4 mSv/week

For public: 0.02 mSv/week

The exposure to measure $\dot{D}$ must be used the higher kV, long time (t) to avoid death time of the survey meter or detector.

IV. ANALYSIS OF QUESTIONNARE

Altogether 86 radiation workers including Radiologist, Radiographer, Dark Room Assistant, Radio-technician, Radiation Oncologist, MD Resident, Radiation Safety Officer/Medical Physicist, Radiography students entertained the questionnaire representing the different hospitals.

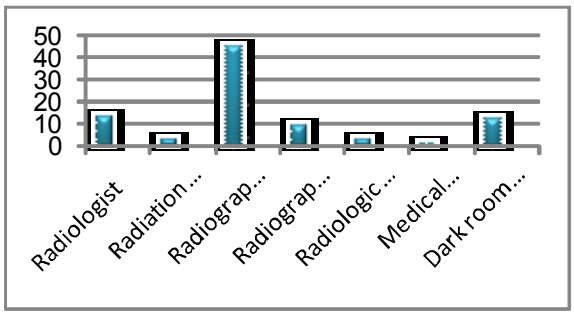

Fig 1: Distribution of Radiation Workers entertaining questionnaires

The distribution of workers by their age, the radiation personnel were maximum numbers in the age group of 20-30. The distribution of personnel by their job duration, the maximum number is between 15-20 years. The total is different because students do not have job duration. In the question about awareness of exposure rate and dose limit, most of the radiation workers are aware on exposure rate but most of them do not have any idea about dose limit. In the question about type of film processor, most of the hospitals are using manual film processor and two hospitals are using auto processor. Almost all the radiation workers are not received any kind of training in radiation protection. Some are mentioned that they had studied about radiation protection during their study. All the radiation workers who filled the questionnaire agree

on radiation safety and protection training. Most of the radiation workers placed radiation as their higher priority. Government owned hospitals (Ministry of Health & Population) are providing radiation hazard allowance and other hospitals are not providing radiation hazard allowance. None of the surveyed institution has personnel dose radiation monitoring system. The responses about the probability to be harmed due to ionizing radiation in the given situations are shown below.

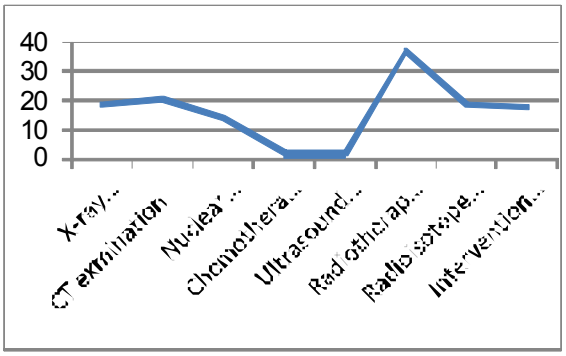

Fig 2: Probability to be harmed due to ionizing radiation in the given situations

The responses in the question about radiation risk for patient in different clinical cases are shown below.

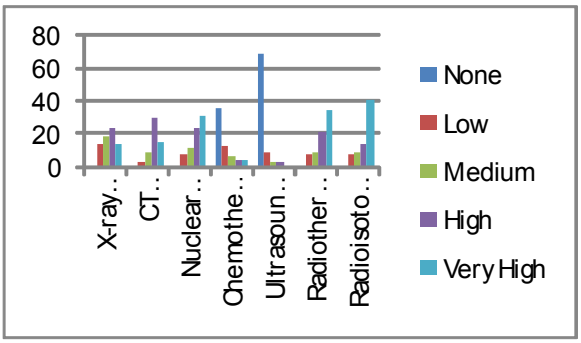

Fig 3: Radiation risk for patient in different clinical cases.

During the survey we found that most of the young and fresh graduate radiation workers and students are aware on radiation protection.

IV. Conclusion

Altogether fifteen Hospitals were monitored. Most of the general X-ray and CT working areas are safe but some need more protection, in the patient entering door and control console area and have to maintain their X-ray room (window, door). In Fluoroscopy some exceeds the dose limit noted by International Commission on Radiological Protection (ICRP). None of the surveyed hospitals have Personnel monitoring system. Altogether 86 Radiation workers filled the questionnaire. There are no personnel monitoring system in all the surveyed centers. Almost all radiation workers want TLD for personnel monitoring and Radiation Act. Most of the radiation workers are aware of radiation hazard and aware on radiation protection. We found some radiation workers are unqualified and have not knowledge on radiation protection. Some workers are over-conscious about radiation.

References

1. Annals of ICRP, ICRP Publication 92.
2. Safety Series No. 115, IAEA, Vienna 1996.
3. NCRP Report 49. Structural Shielding Design and Evaluation for Medical Use of X-Ray and Gamma Rays of Energies up to 10 MeV. 1976
4. NCRP Report 147. Structural Shielding Design for Medical Use of X-Ray Imaging Facilities. 2004
5. DIN 6812. Medical X-Ray equipment up to 300 kV. Rules of construction for structural radiation protection, New Publication 2006.09.
6. Kanchan P. Adhikart et al. (2007) RADIOPROTECTION N54 VOL XIV 2007, Spain. Radiation Survey at Different Public & Private Hospitals in Kathmandu Valley and Different Parts of Nepal, pp 34
7. American Association of Physicists in medicine at http:// www.aapm.com
8. IAEA at http:// www.iaea.org

Author address:

Author: Kanchan P. Adhikari
Institute: NAMS, Bir Hospital
Street: Mahabuddha
City: Kathmandu
Country: Nepal
Email: kanchanadhikari@hotmail.com

Radiation protection in cardiac catheterization laboratories: Non-shielded parts of the body contribute significantly to the effective dose of the operator

H. von Boetticher[1], J. Lachmund[2] and W. Hoffmann[3]

[1]Klinikum Links der Weser, Department of Radiology and Academy of Radiation Protection, Bremen, Germany

[2]ATLAS Elektronik GmbH, Department MLO, Bremen, Germany

[3]Ernst-Moritz-Arndt University Greifswald, Institute for Community Medicine, Greifswald, Germany

Abstract- **Radiation exposure dosimetry was performed with thermoluminescence dosimeters using one Alderson Phantom in the patient position and a second one in the typical position of the operator. Various types of protective clothing as well as fixed shields were considered in the calculations. The effective dose E was determined on the basis of the recommendations of the publications 60 and 103 of the International Commission on Radiological Protection. - The doses of the unshielded organs (brain, thyroid, parts of the active bone marrow and additionally – according to the ICRP 103 approach - salivary glands, extrathoracic region and oral mucosa) contribute significantly to the effective dose of the staff. Therefore an additional shielding of these organs reduces the effective dose more than an increase of the lead equivalency of the existing apron. Relative to the exposure without lead protection, the use of only a lead apron of 0.35 mm with an additional thyroid collar reduces E to 9.7 % (ICRP 103). Using a supplementary side shield and both a side and face shield E decreases to 7.0 % and 2.6 % respectively. We recommend face shields and thyroid protection collars as a necessary part of anti-X-ray protection for cardiac catherization laboratories.**

Keywords- **Coronary angiography, radiation exposure, radiation protection devices, thyroid protection collar, effective dose**

I. Introduction

There is a great variability in radiation protection devices for the personnel in cardiology: Lead curtains or lead acrylic glass shields are not generally used in all catheterization laboratories. The individual doses can vary considerably depending on lead equivalency and design of X-ray protection garments. The actual effect of the different protection devices is difficult to assess. In radiation protection the effective dose provides a quantitative measure for the probability of stochastic effects. Therefore in this study the quality of radiation protection devices is evaluated based on the extent to which the effective dose of a staff member is reduced.

II. Materials and Methods

Radiation exposure dosimetry for the personnel was carried out in a cardiac catherization laboratory equipped with a single plane cineangiography unit (Integris, Philips Medical Systems). To determine effective dose values for different X-ray equipment, measurements of scattered radiation were performed using a male Alderson Phantom in patient position and a female Alderson Phantom in typical position of the operator. Various types of personal radiation protection garment as well as fixed shields were later considered mathematically in the calculations. For dosimetry, thermoluminescence dosimeters (LiF-100 H; Thermo Eberline Trading / Harshaw) were placed in the operator phantom at multiple organ-specific locations. For each recording, al least 90 dose measurements were conducted according to a standardized protocol [1]. The effective doses were calculated on the basis of ICRP 60 [2] and ICRP 103 [3].

The effect of lead apron on the effective dose in the Alderson Phantom measured without radiation protection was derived using published data on the amount of scattered radiation passing through lead [4]. Values for a typical average tube voltage of 87.5 kV (0,35 mm lead: 6.04 %; 0.5 mm lead: 3.30 %) were estimated by interpolation. The values refer to the ambient dose equivalent H*(10) which is an approximation to the effective dose. The effect of lead side shielding was derived from the dose reduction factors previously published by von Boetticher et al. [1]. For the head, thorax and abdominal organs, the factor 3.96 and for the pelvis the factor 10.3 was used.

III. Results

Effective doses for the operator are provided in Tab. 1, assuming use of protective garment with 0.35 and 0.5 mm lead equivalent, respectively. All values assume additional use of a thyroid protection collar with 0.5 mm Pb. Without thyroid protection the effective dose increases by a factor of

O. Dössel and W.C. Schlegel (Eds.): WC 2009, IFMBE Proceedings 25/III, pp. 114–115, 2009.
www.springerlink.com

1.8-2.6 (ICRP 60) [5] and 1.5-1.9 (ICRP 103) respectively. Separate values were calculated considering no shielding, shielding of only the lower part of the body, and of the lower and the upper part, respectively. Effective doses are relative to the respective values of a person without protective garment and no installed shielding.

An increase in lead equivalent of the protective apron from 0.35 to 0.5 reduces the transmission by a factor of 1.83. The effective dose, however, decreases only by a factor of 1.29 (ICRP 103). Hence the impact of a more efficient apron on the effective dose is only marginal. A combination of an apron with 0.35 mm lead with a permanent lower protection reduces the effective dose by a factor of only 1.39, whereas a combination of this apron with a permanent upper and lower protection reduces the effective dose considerably by a factor of 3.7 (Tab. 1).

Table 1 Relative effective dose of the operator during cardiographic examination considering different protective clothing (with use of a thyroid protection collar) and protection systems. The values are normalized to the dose value without protective garment and no installed shielding.

	Relative effective doses (ICRP 60)	Relative effective doses (ICRP 103)
lead apron 0.35 mm Pb	6.6 %	9.7 %
lead apron 0.50 mm Pb	4.4 %	7.5 %
lead apron 0.35 mm Pb + permanent lower protection	3.5 %	7.0 %
lead apron 0.50 mm Pb + permanent lower protection	3.3 %	6.8 %
lead apron 0.35 mm Pb + permanent upper and lower protection	1.8 %	2.6 %
lead apron 0.50 mm Pb + permanent upper and lower protection	1.2 %	2.0 %

IV. Discussion

Shielding factors for protective garment can readily be misinterpreted: the attenuation factor of protective garment should not be confused with a reduction of the effective dose due to the garment. Particularly, it is not possible to extend a reduction of the transmission by a factor of almost 2 to a similar reduction in effective dose.

These systematic differences are a consequence of the major contribution of organs not covered by the protective apron to the effective dose. Only a reduction of the exposure to these organs can considerably reduce the effective dose. On the other hand a further reduction of the exposure to organs already shielded has only a limited effect, e.g. the additional use of only a permanent lower protection. According to ICRP 60 the unprotected organs in the head and neck region which are relevant to the calculation of the effective dose are the thyroid and a part of the red bone marrow. ICRP 103 adds the salivary glands, the extrathoracic region and the oral mucosa to this list [6]. Therefore ICRP 103 would cause noticeably higher effective doses for personnel standing next to the examination table.

V. Conclusions

Since radiation protection aims to minimize the effective dose, the implementation of ICRP 103 will increase the relevance of the organs in the head and neck region, which are not protected by conventional radiation-protective clothing. Particular attention should be paid to improve radiation protection of this part of the body (e.g. overhead suspension shielding and thyroid protection collars).

References

1. von Boetticher H, Meenen C, Lachmund J, Hoffmann W, Engel HJ (2003) Radiation exposure to personnel in cardiac catheterization laboratories. Z Med Phys 13:251-256 (in German)
2. International Commission on Radiological Protection (1991) Recommendations of the International Commission on Radiological Protection, Publication 60, Pergamon Press, Oxford, New York, Frankfurt
3. International Commission on Radiological Protection (2007) 2007 Recommendations of the International Commission on Radiological Protection, Publication 103, Pergamon Press, Oxford, New York, Frankfurt
4. Deutsches Institut für Normung (German Institute of Standardization) (2002 / corrigienda 2004). Medical X-ray equipment up to 300 kV, Radiation protection rules for installation. DIN 6812. Berlin: Beuth (in German)
5. von Boetticher H, Lachmund J, Hoffmann W, Lange HW (2008) Optimizing radiation protection of the operator during cardiac catheterization by minimizing the effective dose. IRPA 12: 12th International Congress of the International Radiation Protection Association, Buenos Aires, Argentinien, 19-24 October 2008, TS III.3.3-231
6. von Boetticher H, Lachmund J, Looe HK, Hoffmann W, Poppe B (2008) Recommendations of the ICRP change basis for estimation of the effective dose: What is the impact on radiation dose assessment of patient and personnel? Fortschr Roentgenstr 180:391-395

Dr. H. von Boetticher, Klinikum Links der Weser, Senator-Wessling-Str. 1, D-28277 Bremen, Germany; heiner.boetticher@klinikum-bremen-ldw.de

Calculation of Normalized Organ Doses for Pediatric Patients Undergoing CT Examinations on Four Types of CT Scanner

J.T.M. Jansen and P.C. Shrimpton

CRCE / Radiation Protection Division, HPA, Chilton, Didcot, United Kingdom

Abstract— **Patient doses due to Computed Tomography (CT) are becoming increasingly important in diagnostic radiology, with there being particular concern about examinations on children owing to their increased radiosensitivity. We have computed organ doses normalized to $CTDI_{air}$ using the University of Florida (UF) voxelized pediatric phantoms in relation to the General Electric 9800, Philips LX, Siemens DRH and Siemens Sensation 16 CT scanners. For a whole body examination, the normalized effective dose E_{103} (as a convenient summary of organ doses) increases by 30% when the age decreases from 14 years to 9 months. This trend is consistent with published results from our previous study based on pediatric and adult mathematical phantoms. Further calculations of normalized effective doses for adult mathematical phantoms also show good agreement with that study under similar conditions of modeling, although updated dose coefficients differ from the previously published data by +35% ± 2%, +16% ± 8% and -6% ± 5%, for examinations of the head & neck, chest, and abdomen & pelvis, respectively. These differences are due to changes in both the definition of effective dose (E_{60} to E_{103}) and the adult MIRD-like phantom (from NRPB18+ to HPA18+) to incorporate the new risk and remainder organs.**

Keywords— **Computed tomography, dosimetry, pediatric, conversion coefficients.**

I. Introduction

Computed Tomography (CT) examinations are becoming increasingly important in diagnostic radiology, in view of their rising numbers and relatively high doses. Since radiation risks in general decline with increasing age at exposure, there is particular concern about examinations on children. Unfortunately, the availability of pediatric organ dose conversion coefficients for contemporary CT scanners has been quite limited. Accordingly, we have computed normalized organ doses for some pediatric voxel anthropomorphic phantoms and 4 types of CT scanner. In this paper, these dose data are summarized for convenience in terms of the effective dose. However, it should be recognized that the International Commission on Radiological Protection (ICRP) has only defined this quantity for radiological protection purposes in relation to a Reference Person on the basis of tissue weighting factors for humans averaged over both sexes and all ages [1], and not necessarily for children of specific sex.

II. Material and Methods

The small Personal Computer (PC) Cluster used at the Health Protection Agency (HPA) and the methods applied for the simulation of CT examinations are described elsewhere [2]. MCNPX version 2.6.0 [3] was used as the radiation transport code to compute the organ doses for the anthropomorphic phantoms and the Computed Tomography Dose Index free-in-air expressed in air ($CTDI_{air}$), where both are normalized per starting photon. Normalized organ doses, derived as each organ dose divided by the CTDI free-in-air, have been calculated for scans of consecutive 1 cm thick transverse slices along each of the anthropomorphic phantoms, except for the Siemens Sensation 16 where the slice thickness was 1.2 cm. Each single slice calculation involved 100 million starting photons and the statistical uncertainty in the calculated effective dose was less than 1%, for slices with an appreciable effective dose value.

The five pediatric voxel phantoms were developed by the University of Florida [4] [5] and represent a 9 month male, 4 year female, 8 year female, 11 year male and 14 year male, and are named UFV02 to UFV06, respectively. The following modifications were made. For the calculation of the red bone marrow dose, the adult Oak Ridge National Laboratory (ORNL) fluence to dose function [6] was substituted by the age dependent dose enhancement factors of King and Spiers [7], relating to ages 1.7 (for UFV02), 9 (for UFV03 to UFV06) and 44 years (adult). Red bone marrow composition was according to the International Commission on Radiation Units and Measurements (ICRU) Report 44 [8] and the mass energy absorption coefficients due to Seltzer [9]. The active marrow distribution for the various bones was based on Cristy [10] for ages 0, 1 (UFV02), 5 (UFV03), 10 (UFV04 and UFV05), 15 (UFV06), 25 and 40 years. In addition, the ORNL fluence to bone surface dose [6] was changed to the average dose to the bone mixture, although this is probably an overestimation of the bone surface or endosteal dose. For the purposes of comparison, calculations were also carried out for adult Medical Internal Radiation Dose (MIRD) like phantoms developed by the National Radiological Protection Board (NRPB), now HPA, as NRPB18+ [11] and (updated for ICRP Publication 103 [1]) HPA18+ [2].

O. Dössel and W.C. Schlegel (Eds.): WC 2009, IFMBE Proceedings 25/III, pp. 116–119, 2009.
www.springerlink.com

All ICRP Publication 103 [1] risk and remainder organs are segmented in the pediatric phantoms apart from the lymph nodes, oral mucosa and male breast, for which the surrogate organs adipose tissue, larynx and pharynx, and thymus are used, respectively. Effective doses according to both ICRP Publication 60 (E_{60}) [12] and Publication 103 (E_{103}) [1] have been calculated from the normalized organ doses. When deriving values of E_{60}, the remainder rule was applied [12], the remainder dose involved a mass weighted calculation [13] and the colon dose [14] was calculated as the mass weighted upper and lower large intestine (with the upper large intestine being removed from the remainder organs). Three old CT scanners have been simulated, namely the General Electric 9800, Philips LX and Siemens DRH, operated at tube voltages of 120, 120 and 125 kV, respectively. As a contemporary scanner, the Siemens Sensation 16 has been simulated, operated with tube voltages of 80, 100, 120 and 140 kV in both head and body mode.

III. Results and Discussion

In Fig 1, the normalized effective dose, E_{103}, is shown against the z-axis position from -20 cm to the top of the head for the various pediatric phantoms for a Siemens Sensation 16 scanner operated at 120 kV, in body mode. The bottom of the trunk is at position 0 cm. Differences in size between the various phantoms is shown by the increasing positions on the axis for the top of the head.

The variation in the normalized effective dose with position along the phantom is more than one order of magnitude. The three highest peaks in the effective dose curves for the various phantoms are due to the high contributions from the following organs: breast (always the highest peak), stomach, gonads (ovaries and testes) and thyroid. In general, the normalized effective dose conversion coefficients decrease with increasing age and size of the pediatric phantoms.

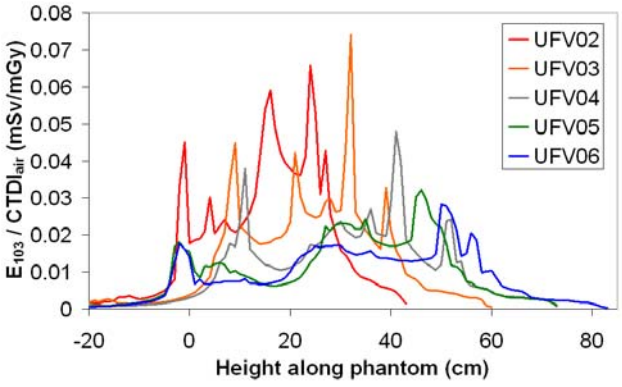

Fig. 1 Normalized effective dose E_{103} for the Siemens Sensation 16 with a nominal slice (beam) thickness of 1.2 cm.

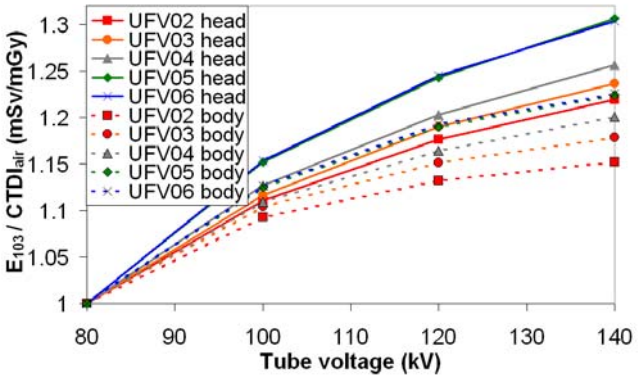

Fig. 2 Increase in normalized effective dose with tube voltage for the Siemens Sensation 16 scanner.

In Fig 2, the relative increase in the normalized effective dose, E_{103}, is shown as a function of the applied tube voltage (80, 100, 120 and 140 kV) for the body and head filtration modes of the Siemens Sensation 16 scanner and the various pediatric phantoms, UFV02 to UFV06.

The normalized effective dose increases with increasing tube voltages due to the beam hardening effect. The increase in conversion coefficient becomes less with increasing tube voltage, as shown by the convex curvature. The increase in normalized effective dose for a fixed tube voltage (100, 120 or 140 kV) increases with the age or physique (length, width or depth) of the phantom, with as an exception the UFV05 and UFV06 phantoms and scanner operation at 140 kV in head mode, where the points are very close. The increase in normalized effective dose is always less for the body mode compared with the head mode of scanner operation. This is due to the thicker filtration in body mode in comparison with the head mode, leading to a harder beam.

In Fig 3, the ratio of the effective dose, E_{103} versus E_{60}, is shown along the height of the various pediatric phantoms for the Siemens Sensation 16 scanner operated at 120 kV in body mode.

For all phantoms, the lowest effective dose ratio, E_{103}/E_{60}, occurs at the position of the gonads due to the reduction in the gonads weighting factor from 0.20 to 0.08. Sex differences are apparent in the position of this lowest ratio: at the testes (UFV02, UFV05 and UFV06) or the ovaries (UFV03 and UFV04). The highest ratio occurs for the male phantoms at the position of the thymus, used as a surrogate for the breast, since the weighting factor for the breast has increased from 0 to 0.12 as the risk organ has

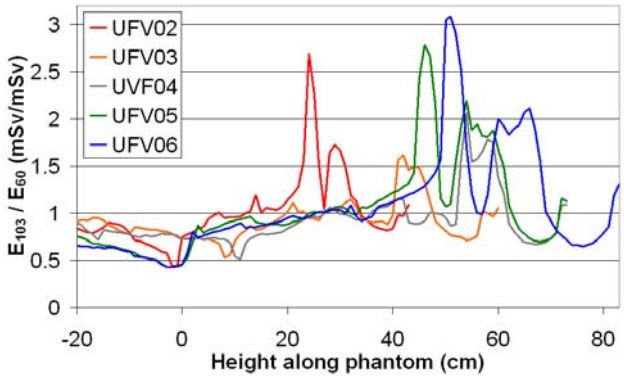

Fig. 3 Ratio of the effective doses E_{103} and E_{60} along the height of the phantoms for the Siemens Sensation 16 scanner operated at 120 kV in body mode.

changed from female breast [12] to breast [1]. For the female phantoms, the breast weighting factor has moderately increased from 0.10 to 0.12. For all phantoms the ratio is reduced at the brain location due to the reduction in weighting factor from 0.025 (remainder rule applied) to 0.01. For the region just inferior to the brain, the ratio is high due to the new risk organs of salivary glands, extra thoracic region and oral mucosa, with a total tissue weighting factor of 0.028. This trend is partly offset by the reduction in the thyroid tissue weighting factor from 0.05 to 0.04.

In Fig 4, the age dependences of the effective doses E_{103} and E_{60} for whole body exposure are shown for the Siemens Sensation 16 scanner operated at 120 kV in body mode.

Both normalized effective doses decrease with increasing age, with E_{60} being between 1 to 2% above E_{103} for all ages. The increase in normalized effective dose from 14 years to 9 months is about 31% for both effective doses. The range

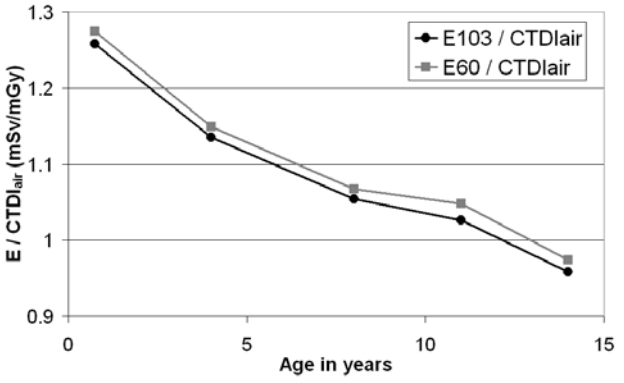

Fig. 4 Age dependence of the normalized effective doses for the Siemens Sensation 16 scanner operated at 120 kV in body mode.

given by Khursheed et al. [11] is an increase in normalized effective dose (E_{60}) between 25% and 100%, for the trunk region and an increase by about 85%, for the head & neck region; these data relate to a change in age from 15 years to 1 year and the General Electric 9800, Philips LX and Siemens DRH scanners.

In Table 1, the present calculations of normalized effective dose E_{60} and E_{103} for adult mathematical phantoms are compared with data given by Khursheed et al. [11] for their examination categories of head & neck, chest, and abdomen & pelvis.

The agreement between the data of Khursheed et al. [11] and the present calculations of E_{60} using the similar NRPB18+ phantom is good and well within 10%, the level of rounding in their paper, for all the examinations. Normalized values of effective dose E_{60} for the updated HPA18+ phantom are somewhat increased compared with those for NRPB18+: by 19% ± 5%, 0% ± 3% and 3% ± 2%, for scans of the head & neck, chest, and abdomen & pelvis, respectively, for all scanners in Table 1 combined. The increase observed for the head & neck region is due to the

Table 1 Normalized effective doses, E_{60} and E_{103}, for the General Electric (GE) 9800, Philips LX and Siemens Sensation 16 in body and head modes operated at 120 kV and the Siemens DRH operated at 125 kV, for three examinations and two adult phantoms. The scan lengths are 25, 27, and 43 cm for the head & neck, chest, and abdomen & pelvis examinations, respectively.

Examinations	Scanner model	Khursheed et al. [11]	NRPB18+	HPA18+	
		$E_{60}/CTDI_{air}$ (μSv / mGy)			$E_{103}/CTDI_{air}$ (μSv / mGy)
Head & neck	GE 9800	44	41	52	61
	Philips LX	57	54	63	76
	Siemens DRH	61	59	67	82
	Sensation 16 body	-	63	73	89
	Sensation 16 head	-	59	69	83
Chest	GE 9800	100	104	102	112
	Philips LX	170	170	167	189
	Siemens DRH	200	204	213	250
	Sensation 16 body	-	188	185	207
	Sensation 16 head	-	174	170	191
Abdomen & pelvis	GE 9800	170	173	181	168
	Philips LX	300	285	297	268
	Siemens DRH	350	351	365	330
	Sensation 16 body	-	326	329	306
	Sensation 16 head	-	297	300	279

changes in the phantom to accommodate the extrathoracic regions, salivary glands and oral mucosa surrogates, and the restyled head and brain, as described by Bouchet et al. [15]. Changing the definition from E_{60} to E_{103} increases the value of normalized effective dose for the head & neck, chest, and abdomen & pelvis examinations by 20% ± 2%, 13 ± 3% and -8% ± 2%, respectively. The present values of E_{103} derived for the HPA18+ phantom are increased relative to normalized effective doses E_{60} published by Khursheed et al. [11] for a range of scanners by 35% ± 3%, 16% ± 8% and -6% ± 5% for examinations of the head & neck, chest and abdomen & pelvis, respectively.

IV. Conclusions

The normalized effective dose, $E_{103}/CTDI_{air}$, varies widely with height along the anthropomorphic voxel phantoms and in general increases with decreasing age and size. Dose coefficients for the Siemens Sensation 16 scanner vary with the tube voltage and filtration as expected, due to the beam hardening effect. Differences between normalized effective doses, E_{60} and E_{103}, can be explained by changes in the tissue weighting factors. For scans of the whole body, the normalized effective dose increases by 31% when the age decreases from 14 years to 9 months. Absolute values of effective dose for CT examinations on children will, of course, depend on the particular exposure settings used.

Normalized effective doses (E_{60}) calculated for examinations of the head & neck, chest, and abdomen & pelvis using the NRPB18+ adult MIRD-like mathematical phantom show good agreement with previous data published by Khursheed et al. [11]. However, normalized effective doses E_{103} calculated using the updated HPA18+ phantom differ from these published data on average by +35% for the head & neck examination, +16% for the chest examination and -6% for the abdomen & pelvis examination, in relation to the General Electric 9800, Philips LX and Siemens DRH scanners.

Acknowledgment

The authors wish to thank Prof W.E. Bolch of the University of Florida for making their pediatric phantoms available to us.

References

1. International Commission on Radiological Protection (2007). The 2007 recommendations of the ICRP. ICRP Publication 103. Ann ICRP, 37:2-4
2. Jansen JTM, Shrimpton PC, and Zankl M (2009). Development of PC based Monte Carlo simulations for the calculation of scanner-specific normalized organ doses from CT. In "International Conference on Mathematics, Computational Methods & Reactor Physics", Saratoga Spring (NY) May 3-7, 2009. American Nuclear Society, LaGrange Park, IL
3. Pelowitz DB (2005). MCNPX User's manual, version 2.6.0. Los Alamos National Laboratory, Los Alamos, NM
4. Lee C, Lee C, Bolch WE (2006). Age-dependant organ and effective dose coefficients for external photons: a comparison of stylized and voxel-based paediatric phantoms. Phys. Med. Biol. 51:4663-4688
5. Lee C, Lee C, Williams JL, Bolch WE (2006). Whole-body voxel phantoms of paediatric patients - UF series B. Phys. Med. Biol. 51:4649-4661
6. Cristy M and Eckerman KF (1987). Specific absorbed fractions of energy at various ages from internal photon sources. I Methods ORNL/TM-8381/V1, Oak Ridge National Laboratory, Oak Ridge, TN
7. King SD and Spiers FW (1985). Photoelectron enhancement of the absorbed dose from X rays to human bone marrow: experimental and theoretical studies. Br J Radiol, 58:345–356
8. International Commission on Radiation Units and Measurements (1989). Tissue Substitutes in Radiation Dosimetry and Measurement. ICRU Report 44, Bethesda, MA
9. Seltzer SM (1993). Calculation of photon mass energy-transfer and mass energy-absorption coefficients. Radiat Res, 136:147–170
10. Cristy M (1981). Active bone marrow distribution as a function of age in humans. Phys Med Biol, 26:389–400
11. Khursheed A, Hillier MC, Shrimpton PC and Wall BF (2002). Influence of patient age on normalized effective doses calculated for CT examinations. Br J Radiol 75:819-830
12. International Commission on Radiological Protection (1991). 1990 Recommendations of the ICRP. ICRP Publication 60. Ann ICRP, 21: 1-3
13. International Commission on Radiological Protection (1991). Annual limits on intake of radionuclides by workers based on the 1990 recommendations. ICRP Publication 61. Ann ICRP, 21: 4
14. International Commission on Radiological Protection (1995). Age-dependent doses to members of the public from intake of radionuclides: Part 3 Ingestion dose coefficients. ICRP Publication 69. Ann ICRP, 25: 1
15. Bouchet LG, Bolch WE, Weber DA, Atkins HL and Poston JW Sr (1999). MIRD pamphlet No. 15: Radionuclides S values in a revised dosimetric model of the adult head and brain. J Nucl Med 40:62S-101S

Authors: Jan T. M. Jansen & Paul C. Shrimpton

Author: Jan T. M. Jansen
Institute: Health Protection Agency
Division: Radiation Protection Division
City: Chilton, Didcot, Oxfordshire, OX11 0RQ
Country: United Kingdom
Email: jan.jansen@hpa.org.uk

Preview of a series of adult human phantoms for radiation protection dosimetry

R. Kramer[1], H. J. Khoury[1], V. F. Cassola[1], V. J. de Melo Lima[2]

[1] Departamento de Energia Nuclear, Universidade Federal de Pernambuco, Avenida Prof. Luiz Freire, 1000, CEP 50740-540, Recife, Brazil
[2] Departamento de Anatomia, Universidade Federal de Pernambuco, Recife, Brazil

Abstract— **In the area of radiation protection in radiology and nuclear medicine it is common practice to use adult human phantoms to simulate average humans for the assessment of organ and tissue absorbed doses. However, most patients do not have body heights and/or body weights of the average human, which can lead to significant errors for organ and tissue absorbed doses to be determined for a specific patient. In a special phantom development project at the Departamento de Energia Nuclear of the Universidade Federal of Pernambuco, 32 adult human phantoms, 16 for each sex, will be designed to cover a certain range of body heights and body weights, to be used in organ and tissue absorbed dose assessment tools, like in the recently released software CALDose_X. This study reports mainly on the first step of this project, namely the improvement of the existing adult phantoms MAX06 and FAX06 to become the starting points for the development of the new phantom series.**

Keywords— **Human phantoms, organ absorbed doses, polygon mesh surface, patient risk, CALDose_X**

I. Introduction

Using the MAX06 and the FAX06 human phantoms [1], a software, called CALDose_X, was recently made available to the public (www.grupodoin.com), which calculates organ and tissue absorbed doses, as well as radiation risks for examinations commonly performed in X-ray diagnosis [2]. The MAX06 and FAX06 phantoms are based on ICRP89 [3], i.e. that they correspond with respect to body height, body weight and all segmented organ and tissue masses to a 35-year old average Caucasian adult male and female, respectively.

All over the world, adult patients submitted to examinations in radiology and nuclear medicine deviate often significantly from the physical properties of the ICRP89 reference person: Patients are slimmer or fatter, smaller or taller and younger or older than a person simulated by the MAX06 or the FAX06 phantoms. The anatomical variations influence the organ and tissue absorbed doses received by the patient and consequently his or her radiation risks, with the fat distribution being the most influential anatomical parameter with respect to organ or tissue absorbed doses, followed by the variations of body height and by the effects due to the adult aging process.

In order to make CALDose_X more patient-specific, a phantom development project based on the MAX06 and the FAX06 phantoms was initiated at the Departamento de Energia Nuclear of the Universidade Federal de Pernambuco in Recife/Brazil, which has as objective to provide a series of 32 human adult phantoms, 16 for each sex, as a function of the body weight and the body height, thereby focusing on the two most important anatomical parameters influencing organ and tissue absorbed doses and omitting the adult age-related effects for the time being.

Consequently, the task ahead is to change especially the fat distribution and the body height of the MAX06 and the FAX06 phantoms. Although being a better true to nature representation of the human body compared to the earlier mathematical phantoms, voxel phantoms still have their limitations, especially representing complicated structures, like the walled and twisted small intestine, or when major anatomical changes, like to the whole body fat distribution, have to be made, which turned out to be either impossible or at least a very laborious process.

Software tools, developed in the area of computer graphics, have increasingly been used in the area of human phantom development recently [4, 5, 6, 7]. Some of these tools, freely available on the internet, will be used for the development of the new series of adult human phantoms. This study is a preview of this project, because it reports mainly on the first step of the process, which is a revision of the existing MAX06 and FAX06 phantoms, because at the time of their release in 2006, complicated walled organs, like the gastrointestinal (GI) tract, could not be modeled correctly just by voxel manipulation and also the position of some

O. Dössel and W.C. Schlegel (Eds.): WC 2009, IFMBE Proceedings 25/III, pp. 120–123, 2009.
www.springerlink.com

organs had to be corrected in order to better account for a person with upright posture. This process led to the revised average adult phantoms, called MAX_AA and FAX_AA, which are improved versions of the MAX06 and the FAX06 phantoms and represent the starting point for the development of derived adult phantoms with different body weights and/or body heights. AA stands for Average-Average, i.e. this is a phantom with average height and average weight. A version with average height, but with more weight would be denoted Average-Fat (AF). A preliminary version of the female average fat phantom, FAX_AF, will be shown below together with the AA-type versions.

II. MATERIALS AND METHODS

Compared to the existing phantoms, the MAX_AA and the FAX_AA models represent improved versions especially with respect to the modeling of the GI tract, the repositioning of organs like the urinary bladder, uterus and prostate and the appearance of the body surface. The process described below is based on the polygon mesh surface method, but other options, like NURBS (non-uniform rational B-spline) surfaces, can be used for this purpose as well [6].

Conversion from voxel to polygon mesh surface

In order to re-model existing complicated organs of a voxel phantom, one first has to convert the voxel-based object into a polygon mesh surface (PMS) representation. This can be achieved with ImageJ 3D Viewer, a plug-in for the ImageJ software (http://rsweb.nih.go/ij/), developed by Schmid [8]. This free, open source software, written in Java language, works on all major operational platforms, like WINDOWS, Linux and MAC. Organs, like the small intestine and the colon, both walled and twisted objects, which are difficult to model on a voxel basis, were extracted together with the stomach from the MAX06 and the FAX06 phantoms and their surfaces were saved separately as WaveFront files, preserving always reference points from the first and the last slice of the organ in order to facilitate later the re-fitting of the organ into the phantom.

Re-modeling organs

The PMSs of the extracted organs were imported into the BLENDER software, also a free, open source software (www.blender.org), which can be used with all major operating systems. An object based on polygon meshes, called ICOSPHERE, was added to the graphic environment of the BLENDER software, which allows for the fitting of ICOSPHERE to the volume of an imported voxel structure, like in case of the stomach of the MAX06 phantom shown in figure 1.

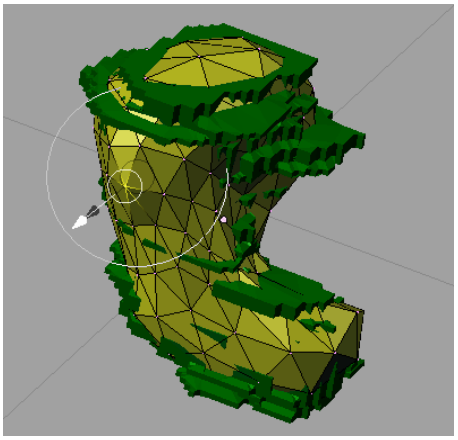

Figure 1. Adjusting ICOSPHERE to the volume of the stomach extracted from the MAX06 phantom

For the modeling of the intestines, Bezier curves have been used to define first the direction of a curve, as shown in figure 2a for the case of the colon, and later the surface surrounding that curve applying the BLENDER tool “bevOb”, displayed in figure 2b.

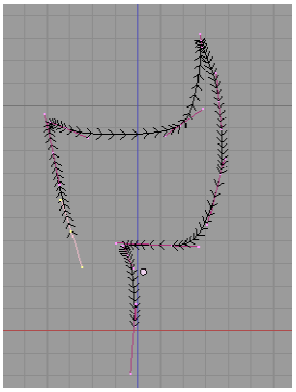

Figure 2a

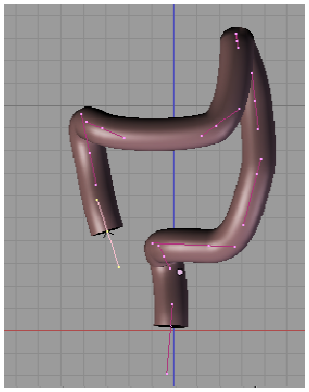

Figure 2b

Application of Bezier curves for the modeling of the colon

Re-voxelization and re-fitting into the phantom

After having been re-modeled with BLENDER 3D, the -based organ volumes were exported as VRML 2.0 files to the BINOX software [9, 10], which converts 3D models into 3D voxel matrices. Finally, by applying ImageJ, the remodeled and re-voxelized organs were re-fitted into the volume, where the organ had been extracted at the beginning of the whole re-modeling process.

Re-modeling the surfaces of the phantoms

In order to improve the appearance of the phantoms, freely available adult male and female 3D body surfaces were downloaded from the internet [11, 12] and fitted to the surfaces of the MAX06 and the FAX06 phantoms.

III. RESULTS

Figure 3 presents the GI tract (stomach, small intestine and colon) as voxel representation in the MAX06 phantom on the left, the newly designed polygon mesh surface-based GI tract in the center and the re-voxelized GI tract on the right, which shows that when polygon mesh surface-based objects are voxelized, surfaces lose their smoothness. However, compared to the original GI tract on the left, the new voxel GI Tract still represents a significant improvement.

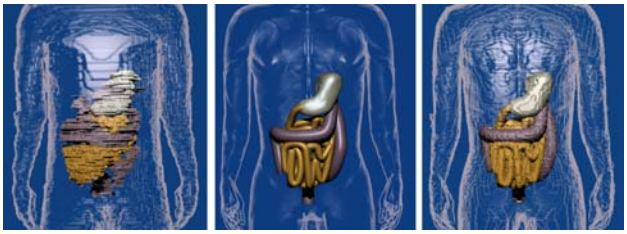

Figure 3. GI tract of the MAX_AA phantom in the original voxel representation (left), designed with PMSs (center) and re-voxelized and re-fitted into the phantom (right)

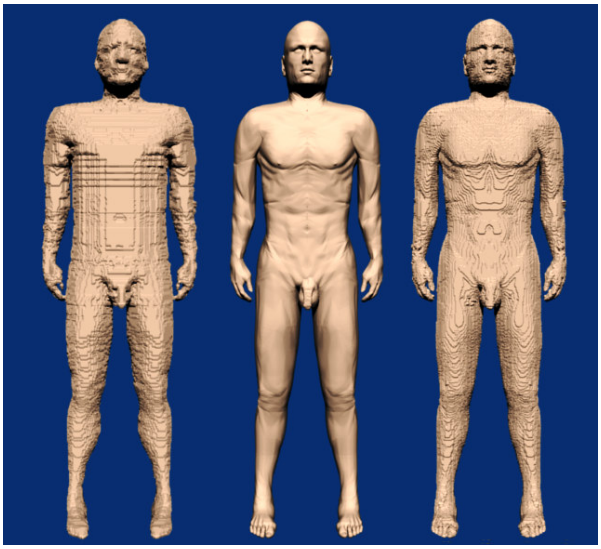

Figure 4. MAX06 voxel (left), MAX_AA PMS (center) and MAX_AA voxel (right)

Figures 4 and 5 show the MA06 and the FAX06 phantoms, respectively, on the left, the polygon mesh-based versions AA in the center and the new voxel versions AA on the right, demonstrating the improvement of the body surface.

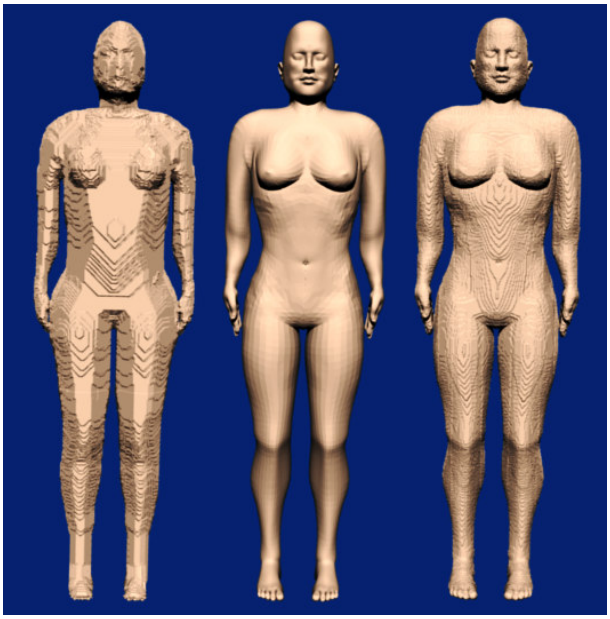

Figure 5. FAX06 voxel (left), FAX_AA PMS (center) and FAX_AA voxel (right)

Phantoms with different body heights and different body weights will be derived from the new average phantoms MAX_AA and FAX_AA. Figure 6 displays a first preliminary version of an adult female with average height, but with more weight, the version FAX_AF (Average-Fat).

IV. CONCLUSIONS

To make organ and tissue absorbed dose estimates more patient-specific has become an important task in radiation protection in radiology and nuclear medicine. The anatomical variations of human bodies among patients, especially the mass of fat and its distribution as subcutaneous and visceral fat throughout the body, can have a strong influence on the results of organ and tissue absorbed dose assessments. Consequently, it is necessary to develop human phantoms which take these anatomical variations into account. This study reported on the first step of a project, which will develop a series of adult human phantoms as a function of body weight and body height. Improved ver-

sions of the MAX06 and the FAX06 phantoms have been developed based on PMSs, called MAX_AA and FAX_AA, which will serve as platform for the derivation of additional 15 phantoms per sex with different body weights and body heights. One of the first applications of the new phantom series will be its introduction into the CALDose_X software.

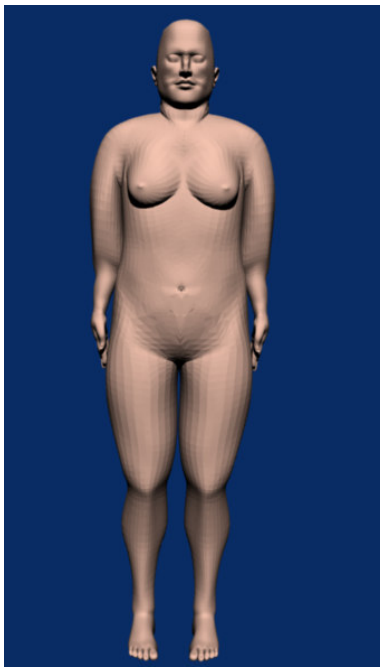

Figure 6. FAX_AF mesh-based phantom

ACKNOWLEDGMENT

The authors would like to thank the Conselho Nacional de Desenvolvimento Científico e Tecnológico (CNPq) and the Fundação de Amparo à Ciência do Estado de Pernambuco (FACEPE) for financial support.

REFERENCES

1. Kramer R, Khoury H J, Vieira J W and Lima V J M (2006) MAX06 and FAX06: Update of two adult human phantoms for radiation protection dosimetry *Phys. Med. Biol.* **51** 3331-3346
2. Kramer R, Khoury H J and Vieira J W (2008) CALDose_X a software tool for the assessment of organ and tissue doses, effective dose and cancer risk in diagnostic radiology, *Phys. Med. Biol.* **53** 6437-6459
3. ICRP International Commission on Radiological Protection (2002) Basic Anatomical and Physiological Data for Use in Radiological Protection: Reference Values *ICRP Publication 89* Ann. ICRP 32 (3-4) Elsevier Science Ltd., Oxford.
4. Lee C, Lodwick D, Hasenauer D, Williams J L, Lee C and Bolch W E (2007) Hybrid computational phantoms of the male and female newborn patient: NURBS-based whole body models, *Phys. Med. Biol.***52** 3309-3333
5. Xu X G, Taranenko V, Zhang J and Shi C (2007) A boundary-representation method designing whole-body radiation dosimetry models: pregnant females at the ends of three egstational periods – RPI-P3, -P6 and –P9, *Phys. Med. Biol.* **52** 7023-7044
6. Lee C, Lee C, Lodwick D and Bolch W E(2007) NURBS-based 3-D anthropomorphic computational phantoms for radiation dosimetry applications, *Rad. Prot. Dos.* **127** 227-232
7. Jeong J H, Cho S, Lee C, Cho K W and Kim C H (2008) Development of deformable computational model for Korean adult male based on polygon and NURBS surfaces, 11th International Conference on Radiation Shielding, April 13-18, 2008, Callaway Gardens, Pine Mountain, Georgia, USA
8. Schmid, B (2007) ImageJ 3D Viewer. Virtual Insect Brain Project, http://132.187.25.13/home/?category=Download&page=Viewer3D
9. Min, P Binvox:3D mesh voxelizer, http://www.google.com/search?q=binvox, Last accessed January 2009.
10. Nooruddin F and Turk G (2003) Simplification and repair of polygonal models using volumetric techniques. IEEE Trans. Vis. Comput. Graphics **9** 191–205
11. Artist-3d, http://artist-3d.com/, Last accessed January 2009
12. The Official Blender repository, http://e2-productions.com/repository/, Last accessed January 2009

Author: Richard Kramer
Institute: Instituto de Energia Nuclear,
Federal University of Pernambuco
Street: Avenida Prof. Luiz Freire, 1000
City: Recife
Country: Brazil
Email: rkramer@uol.com.br

Optical enhancement of DNA-base radio-resistivity

Ramin M. Abolfath, Lech Papiez, Strahinja Stojadinovic, and Timothy Solberg

Department of Radiation Oncology, University of Texas, Southwestern Medical Center, Dallas, TX 75390

Abstract— **We propose a mechanism which uses the simultaneous application of circularly polarized light and an external magnetic field to control the polarization of the free radicals and create S=1 electron-hole spin excitations (excitons) on nucleotide-base. We deploy an ab-initio molecular dynamics model to calculate the characteristic parameters of the light needed for optical transitions. The effect of spin-injection on the formation of a free energy barrier in diffusion controlled chemical reaction pathways leads to the control of radiation-induced base damage. The proposed method allows us to manipulate and partially suppress the damage induced by ionizing radiation.**

Keywords— **radiation protector, DNA damage**

I. Introduction

Ionizing radiation is both hazardous and beneficial to living organisms, and is extensively used for cancer treatment in radiation therapy [1]. A major problem in the application of ionizing radiation to cancer treatment is the protection of normal cells and tissues against unavoidable exposure to radiation during radiation treatment. It is now well understood that the ionization or excitation of the DNA molecules, either directly or indirectly, can lead to DNA single or double strand breaks. As a result, mis-repaired DNA molecules can lead to specific genetic aberrations and/or mutations which could cause carcinogenesis in normal cells or lead to fatal damage in normal or cancer cells [2,3]. Low linear-energy-transfer (LET) ionizing radiation creates approximately 1,000 single strand breaks (SSBs) and 40 double strand breaks (DSBs) per gray (1Gy=1J/Kg) in typical mammalian cells [4,5,6,7]. The level of DNA molecular base damage is between 2,500 and 25,000 per Gy in a cell, which is about 2.5 to 25 times the yield of sugar-phosphate induced damage in the DNA backbone [4,7]. In indirect mechanisms, the water molecules surrounding the DNA molecule which compose 80% of a cell, may be excited by ionizing radiation in form of free radicals, e.g., a charged neutral hydroxyl (OH). The motion of OH-radicals which are randomly produced throughout the cell is governed by diffusion processes. Massive DNA damage can result from a large number of DNA dehydrogenations caused by free radicals. For example, a free radical can diffuse to reach a DNA molecule and remove a hydrogen ion from it to form a water molecule. Detailed studies at the molecular level are necessary to better understand, and potentially modify, radiation-induced DNA damage.

II. Methods

In this work, we apply the Pauli exclusion principle [8,9,10] which prevents two electrons with parallel spin form occupying a single spatial orbital, to propose a mechanism that magnetically shields the DNA molecule and allows manipulation of the diffusion of hydroxyl radicals and the OH-DNA relative motion.

A free radical carries an odd number of electrons with an unpaired spin in the outermost open shell that makes free radicals highly reactive. The electronic ground state of DNA-molecule is S=0 spin-singlet (in the absence of an external magnetic field). The OH-radical, which contains nine electrons, carries a dipole magnetic moment. In a random interaction of ionizing radiation with a biological system, the initial direction of OH-radical magnetic moment immediately after its generation is random. However, by applying a weak external magnetic field (B_{ext}) (which defines the quantization axis) and using a circularly polarized light field parallel to the direction of the light propagation, a molecular transition corresponding to $\Delta J = \pm 1$ can be induced by means of optical pumping [11] of the OH-radicals [12]. Here J denotes the total angular momentum of diatomic OH-radical [13]. In a similar fashion, by applying a second circularly polarized light field one may excite an electron-hole pair (exciton) in the DNA molecule. Because the circularly polarized light carries angular momentum ± 1, the exciton has a particular spin polarization. Here the spin of exciton is $S = 1$ with polarization along the light propagation direction (because of angular momentum selection rules). Figure 1 schematically shows the generation of the optically pumped exciton by circularly polarized light. The injection of photo-electrons with the spin out of equilibrium may lead to a dramatic effect in the collective dynamical behavior of DNA molecules and the interaction with OH-radicals. For example the OH-DNA repulsive magnetic force provides a potential barrier which blocks the diffusion pathway (see Fig. 1(b)) of OH-radicals toward the DNA molecules. This is expected to hinder the DNA dehydrogenation and consequently increase the cell radio-

O. Dössel and W.C. Schlegel (Eds.): WC 2009, IFMBE Proceedings 25/III, pp. 124–127, 2009.
www.springerlink.com

resistivity. To verify this hypothesis, an *ab-initio* Car-Parrinello molecular dynamical model (CPMD) [14,15] is deployed, in which the potential energy of the system can be calculated on-the-fly, as needed for the conformations of the dynamical trajectory, to simulate the chemical reaction pathways. For illustration of the method we consider a system of interest consisting of a DNA nucleotide base, (e.g., guanine) in the presence of the OH-radical. We assume that a photon with circular polarization interacting with guanine can induce an optical transition in the form of an $S=1$ exciton. Here we investigate the effect of an exciton produced in this way on the guanine-dehydrogenation pathway, assuming that another photon generated through interactions with ionizing radiation creates a free radical in the vicinity of guanine. We adopt computational parameters and variables needed for the CPMD calculation of the dynamical trajectory of the gas phase nucleotide bases in the presence of OH-radicals [16], where the consistency of CPMD results for guanine with other quantum chemistry approaches has been investigated.

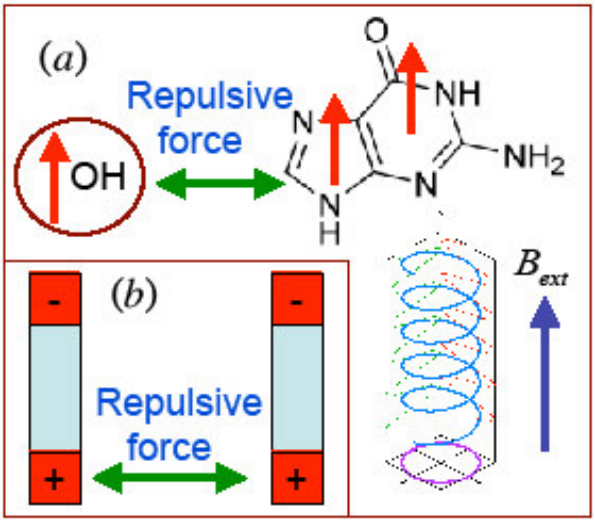

Figure 1: Schematically shown in (a) the injection of photo-generated electrons in DNA-nucleotides with spin polarization (shown by arrows) along the direction of circularly polarized light and external magnetic field. The net magnetic force between two parallel magnetic moments localized in OH and DNA-nucleotide is repulsive. This is similar to two separated magnetic moments which interact like Heisenberg antiferromagnetic exchange coupling (b).

III. RESULTS

We identify the dehydrogenation of the nucleotide bases as a function of their spin multiplicity. The ground and excited states of the nucleotide correspond to spin singlet $S=0$, and spin triplet $S=1$ states. The latter can be realized through the application of circularly polarized light as discussed above (see Fig. 1). The CPMD micro-canonical dynamics (constant energy ensemble) were performed after wave-function optimization following dynamical equilibration at $T=300K$ and re-quenching of the wave-function. Our CPMD studies consist of two classes of spin-restricted calculations, as the total spin along the quantum axis is subjected to the constraints $S_z=1/2$, and $3/2$, corresponding to doublet and quartet spin configurations. In both calculations the initial distance between OH-radical and nucleotide is considered to be about 2 A. We selectively choose an initial coordinate for OH-radical in the neighborhood of the nucleotide where the Hydrogen transfer shows a reactive path in normal state of DNA (the doublet spin configuration in the absence of circularly polarized light and magnetic field). The initial and final states of the molecules are shown in Figures 2-4. The final configurations of the molecules have been obtained after 0.6 ps where the rearrangement of the atomic coordinates have been deduced from a dynamical trajectory calculated by CPMD. According to our results, a rapid dehydrogenation of the nucleotides takes place for a system with $S_z=1/2$ (total spin-doublet) as shown in Figure 3. This process leads to the formation of a water molecule. In contrast, as shown in Figure 4, in the quartet spin configuration the repulsive exchange interaction, analogous to Heisenberg antiferromagnetic coupling which originates from the Pauli exclusion principle, blocks the exchange of hydrogen and hence the chemical reaction. To systematically check the convergence of the results, we increased the size of the molecule by adding sugar-phosphate rings to guanine and found this to have no influence on the spin-blocking effect. To estimate the energy needed for the polarization of the nucleotide in the absence of OH-radicals, we calculated the energy of the ground and excited states of the gas-phase nucleotide in spin singlet and triplet multiplicities. For guanine we calculated the spin singlet-spin triplet energy gap

$$\Delta_0 \equiv E_{Triplet} - E_{Singlet} \approx 2.68eV$$

This provides an estimate for the frequency of the circularly polarized light, which is within the range of the visible spectrum of the electromagnetic waves, $\lambda = 463nm$ (light blue). To determine the stored magnetic energy due to the optical injection of spin, we calculated the energy of the gas-phase nucleotide in the presence of one OH-free radical with spin doublet and quartet multiplicities. For the molecules shown in Figure 2, we find the energy gap

$$\Delta_0 \equiv E_{Quartet} - E_{Doublet} \approx 3.54eV$$

Here the excessive magnetic energy which originated from spin-spin repulsive interactions (which resemble the antiferromagnetic exchange interaction in the Heisenberg model) can be deduced to be $\Delta_1 - \Delta_0 \approx 0.86eV$. This

energy can be interpreted as the excessive energy barrier due to the alignment of the spins in the DNA molecule and OH, and is the source of the magnetic repulsive force which makes the diffusion of OH toward DNA molecules less likely. After photon absorption, the nucleotide is spin polarized along the direction determined by the polarization state and the propagation direction of the circularly polarized light. The polarized state of the nucleotide then decays quantum mechanically to its unpolarized ground state either by spontaneous photon emission (electron-hole recombination) or through photon-electron spin decoherence. For instance, spin-orbit coupling governs the decay mechanism in the non-rediative process. Using Fermi's golden rule to calculate the life-time of the triplet state we find $\tau = \Gamma_{T\to S}^{-1} \approx 100\,ps$. The spin-triplet life time of nucleotide τ turns out to be significantly larger than the dehydrogenation time scale. However, electronic relaxed excitonic states with empirical lifetime of several 100 ps have been reported recently [17]. It is therefore possible to increase the radio-resistivity of the DNA molecule within this time scale through optically pumped spin polarization. It is important to compare τ with other time-scales in the process. The initial ionization takes place in approximately 1 fs (10^{-15} second). The primary free radicals produced by ejection of electrons have a life time of nearly 100 ps, and the reported OH-radical life-time is approximately 1 ns [3]. With a moderate intensity laser pump (see below) it is possible to increase significantly the resistance of DNA molecules against irradiation.

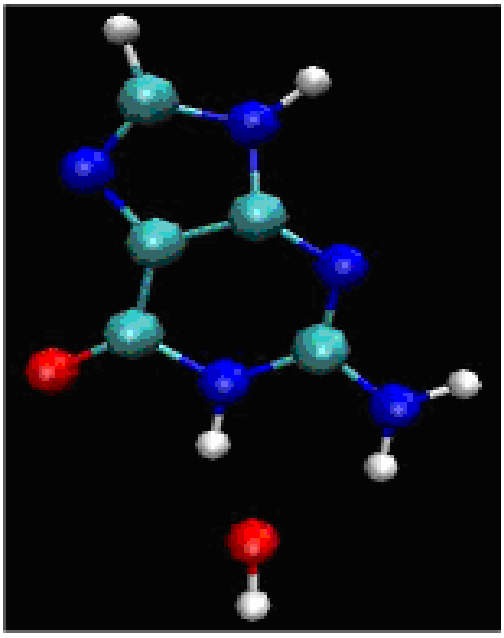

Figure 2: Initial state of Guanine molecule in the presence of irradiated induced OH-free radical.

In order to estimate the technical requirements for the described approach above, one could assume that an aqueous solution of DNA will be irradiated with a dose of 1Gy (1J/Kg). It is known [18] that 100eV of absorbed photon/electron energy produce about 6 OH radicals. Therefore 1Gy of radiation produces approximately 4 x 10^{13} OH radicals in 0.1 cm^3 of water. If the number of injected excitons can be exceeded by at least ten times, through the application of a laser pump with moderate intensity, it is possible to increase significantly the resistance of DNA molecules against irradiation.

As an example, at a dose rate of 1.4 Gy/min a laser pump power of $P = 10 N_{OH} \dfrac{\hbar\omega_0}{\tau_{irr}} \approx 12\times 10^{-6}$ watt would be required, which is well within technically achievable limits.

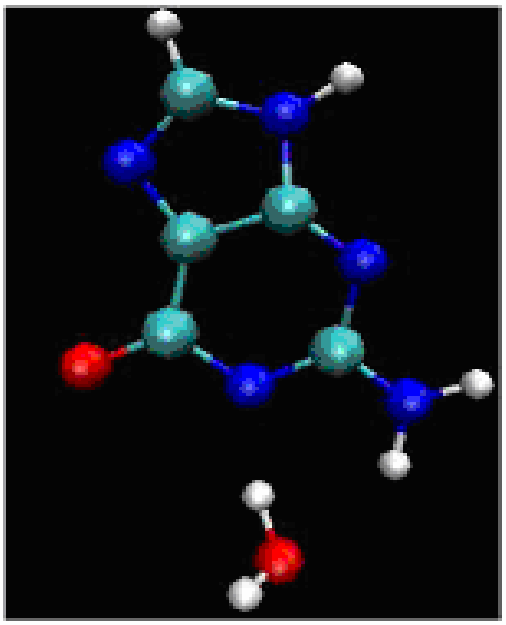

Figure 3: The state of de-hydrogenated Guanine by OH free radical at t = 0.6 ps. The polarization state of the system is spin doublet $(S = 1/2)$.

IV. CONCLUSION

In conclusion, we have theoretically explored a mechanism which involves the injection of spin polarized excitons in DNA molecules to control and manipulate the radiosensitivity of cells by using a circularly polarized light field and external magnetic field. The mechanism proposed here is based on the selection rules applicable to optical transitions between energy levels of the DNA-molecules and

optical pumping of the OH-radicals, and we have employed a microscopic *ab-initio* molecular dynamics model to computationally study the dehydrogenation mechanism at the molecular level. The results of this study may be used as a guideline to develop new techniques for radiation therapy and radiation protection purposes.

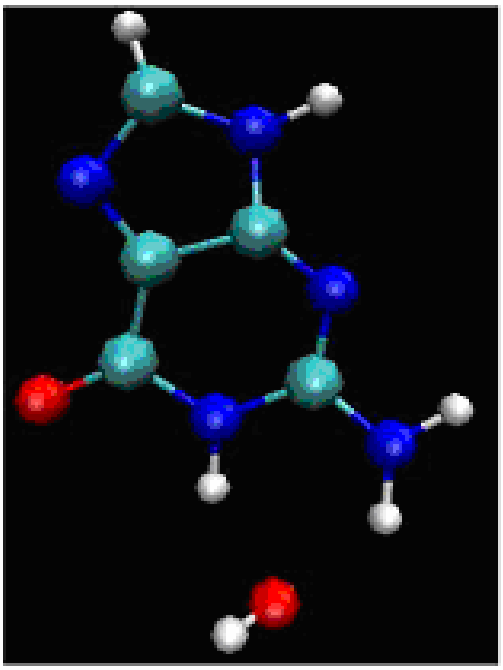

Figure 4: The state of radio-resistive Guanine at. t = 0.6 ps. The polarization state of the system is spin quartet $(S = 3/2)$ induced by circularly polarized light in the presence of weak magnetic field. Due to injected polarized photo-electrons localized in Guanine, the dehydrogenated Guanine does not form.

V. REFERENCES

[1] Faiz M. Khan, The Physics of Radiation Therapy, (Williams Wilkins, Baltimore, 1994).
[2] L. G. Burdelya, et al. Science 320, 226-230 (2008).
[3] Eric J. Hall, Radiobiology for the Radiologist, (Lippincott Williams & Wilkins, Baltimore, Fifth Edition, 2000).

[4] J.F. Ward, Prog. Nucleic Acid Res. Mol. Biol. 35, 95 (1988); Radiat. Res. 142, 362 (1995); Errata, Radiat. Res. 143, 355 (1995).
[5] D. T. Goodhead, Int. J. Radiat. Biol. 65, 7 (1994).
[6] H. Nikjoo, et al., Int. J. Radiat. Bio. 71, 467 (1997).
[7] V. A. Semenenko, and R. D. Stewart, Radiat. Res. 161, 451 (2004).
[8] L. D. Landau, and E. M. Lifshitz, Quantum Mechanics: Non-Relativistic Theory (Pergamon, Oxford, 2003).
[9] K. Ono et al., Science 297, 1313 (2002).
[10] S. Koshihara et al., Phys. Rev. Lett. 78, 4617 (1997); I. Zutic, et al., Rev. Mod. Phys. 76, 323 (2004).
[11] Thad G. Walker and William Happer, Rev. Mod. Phys. 69, 629 (1997); William Happer, Rev. Mod. Phys. 44, 169 (1972).
[12] G.H. Dieke, and H. M. Crosswhite, J. Quant. Spectrosc. Radiat. Transf. 2, 97 (1962); Sebastiaan Y. van de Meerakker et al., Phys. Rev. Lett. 95, 013003 (2005).
[13] G. Herzberg, The Spectra and Structures of Simple Free Radicals, (Dover Publications Inc. New York, 1971).
[14] R. Car, and M. Parrinello, Phys. Rev. Lett. 55, 2471 (1985).
[15] J. Hutter et al., CPMD code, version 3.13, MPI fuer Festkoerperforschung, Stuttgart IBM Zurich Research Laboratory, 1990-2008.
[16] C. J. Mundy et al., J. Phys. Chem. A. 106, 10063 (2002); Y. Wu et al., J. Phys. Chem. A. 108, 2922 (2004).
[17] I. Buchvarov et al., Proc. Natl. Acad. Sci. 104, 4794 (2007); Q. Wang, and T. Fiebig in Charge Migration in DNA, Ed. T. Chakraborty (Springer-Verlag, Berlin, 2007).
[18] Yamaguchi Hiroshi et al., J. Radiat. Res. 46, 333 (2005).

Corresponding Author: Ramin Abolfath
Institute: University of Texas, Southwestern Medical Center
Street: 5801 Forest Park Rd.
City: Dallas, TX 75390
Country: USA
Email:Mohammad.Abolfath@UTSouthwestern.edu

Radiology workload analysis – role and relevance in radiation protection in diagnostic radiology

P Charnock[1], C Baker[2], S Baily[2], J Fazakerley[1], R Jones[1], BM Moores[1], R Wilde[1]

[1] Integrated Radiological Services Limited, Liverpool, England

[2] University Hospital Aintree, Liverpool, England

Abstract— **It has been demonstrated that data entered by radiographers into Radiology Information Systems (RIS) can be used as dose audit data, removing the necessity for radiographer to separately collect data for patient dose audit purposes. Access to RIS data also provides the potential for much more analysis. The data entry process itself can be audited, and is now routinely performed at a small number of hospital sites in the North-West region of the UK. An analysis of the number of examinations performed by a single tube is possible together with the generation of dose audit data. This information is useful for departmental managers to investigate why certain rooms are being used more than others or for certain types of examinations. The work a tube does can be compared with life expectancy enabling better planning within the tube life cycle. In addition, the RIS contains extra information concerning the operator. Once again, the departmental manager can use this analysis to look at operator work patterns and scheduling. This will assist any investigations in the case of accidental exposure of staff.**

This paper begins by introducing the term 'tubeload' and then gives examples of analyses that have been performed using data from a large hospital over a three-month period. Results are shown detailing the initial types of analyses that have been performed on single rooms, single operators and the site overall. The results are then discussed with emphasis on what further analyses could be performed and how this information could be used as a basis for decision making in radiation protection.

Keywords— **Tubeload, RIS, dose audit, radiology workload**

I. Introduction

It is known and accepted that a quality assurance (QA) program and dose audits are an essential part of both radiation protection and equipment performance [1-3]. Between 1992 and 2002 an application has been designed and built for the purposes of entering not only patient dose data, but also QA data [4-7]. It is called the Quality Assurance Dose Data System (QADDS) and was built using visual basic and a Microsoft Access 2 database. However, Access 2 became dated and unsupported so it was decided to re-engineer the application as a web based application on a Java platform.

Around the same time, RIS was being introduced to hospital departments. These systems would link the patient's details through referral to the exposure and allow the operator to record details of the exposure. The advent of digital radiography meant that images could also be stored along with details from the rest of the imaging chain [8-10].

With a RIS in place, however, radiographers were now being asked to record exposure details separately to that which is already been entered on to the RIS when performing a patient dose audit. With the upgraded structure and design of the application, investigations were made into whether the information entered into RIS could be imported directly into it, reducing the need for radiographers to record the same data twice and also enabling continuous patient dose audit. This proved successful [11-14] and is the current system in place for a number of hospitals [15] in order to help them fulfill their dose audit requirements [1, 16-17].

The report sent to hospitals also includes an audit of quality of the data that has been entered into the RIS on site. It was noted that there were omissions of data or wrong data types entered into fields of the RIS, which would cause errors if placed in a data type specific field within a database. However, a hospital departmental manager requested this information for audit purposes [18], which lead to the discussion of what other information and analyses could be taken from this data. There is much more information held within the RIS other than the kV and mAs for each examination, and, with this information in a large multi-site database, much more powerful analyses can be performed. It is possible to describe each room in terms of the number of examinations performed, and also the tubeload, which is defined as the kV multiplied by the mAs, given in Joules [19]. In addition, the operators who perform each examination are recorded in RIS. It is possible to show the number of examinations performed and which rooms each operator uses. Each operator can be analyzed by workload, which could be used as indication of occupational risk.

O. Dössel and W.C. Schlegel (Eds.): WC 2009, IFMBE Proceedings 25/III, pp. 128–131, 2009.
www.springerlink.com

II. Methodology

A. Current process of dose audit

Full details of the process for uploading the data into QADDS are being also submitted for publication, however a brief summary is reproduced here.

- The RIS manager will run a query which will return data on all examinations performed, within specified parameters, such as timescale, & rooms, as a comma separated variable (CSV) file, a standard Microsoft Excel (XLS) file or an extensible markup language file (XML)
- The file is sent to a central repository by an automated file transfer protocol (FTP)
- The file is checked for errors in the data (blank fields, extremes of data)
- The error free data is placed in the database and a report is produced showing a breakdown of how much data was auditable (*see definitions*)
- The database is interrogated using an off-the-shelf statistical package to produce two reports. The first being a patient dose audit report and the second detailing tubeload per room (*see definitions*) and operator workload

All of the above steps can be automated.

B. Definitions

Previous work has defined data supplied for dose audit purposes as either 'auditable' or 'un-auditable' [11, 15]. Patient entrance surface dose (ESD) is calculated using exposure factors [23]. If any of the data required for this calculation is missing, and no assumptions can be made regarding the missing data, it is assumed to be un-auditable.

Preliminary analyses showed that simply stating how many examinations had been performed by an individual tube was not indicative of how much work had been performed by the tube. For example, a tube that performs 50 low exposure examinations, such as extremity, may do less work than, say, 10 high exposure examinations, such as lumbar spine. To be able to prove this, an indication of how much work the tube does is required. The term '*tubeload*' is used by manufacturers [19, 20], and tubeload per examination is also used here.

C. The data

The data for this study was received from a large hospital and consists of 58815 records from the period 1st May 2008 to 31st July 2008. 10 rooms (6 main and 4 A&E) were chosen for the purposes of this study (35857 records). 12 operators were also chosen at random from a total of 129 for the further analysis.

III. Results

The results can be split into a number of sections:

A summary table with the number of examinations distinguished by room is shown in table 1 and a summary graph showing the distribution of tubeload is shown in Fig. 1. Extra information about how much of the data is auditable/un-auditable, broken down by month can also be included on request of the departmental manager

Each room is then analyzed individually in terms of number of examinations by type (Fig. 2), tubeload by examination type and operators that have performed examinations in each room

Each operator is then analyzed in terms of the distribution of the rooms they have worked in and examinations performed, again by frequency and tubeload.

The RIS data can be analyzed further in a number of different ways, but space precludes its inclusion here.

Table 1 Summary Table

Room Name	Number of Records	% Auditable
Room 1	16825	92.1
Room 2	4630	94.5
Room 3	2773	87.6
Room 4	2497	88.1
Room 5	264	1.5
Room 6	582	40.4
Room 7	375	16.5
Room 8	3919	94.6
Room 9	2639	96.9
Room 10	1353	95.9

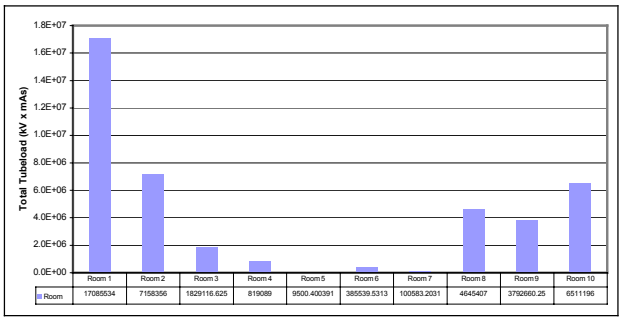

Fig. 1 Graph of tubeload for selected rooms

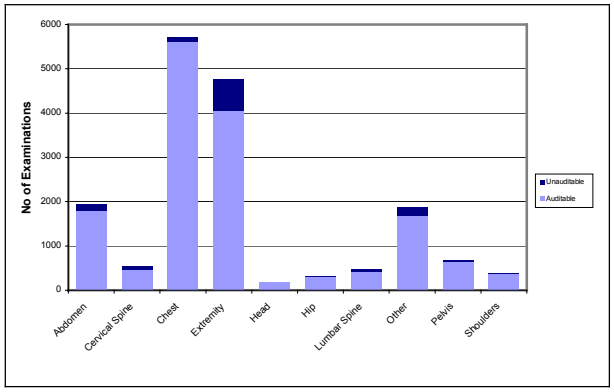

Fig. 2 Number of examinations by type performed in Room 2

IV. DISCUSSION

A. Room Use

It has been noted that for Rooms 1-7, the tubeload relates closely to the number of examinations. On inspection of Rooms 8-10, it is noted that Room 10 performed 1353 examinations when compared with Room 8, which did almost three times more with 3919 (table 1). However the tubeload for Room 10 is about 30% higher than Room 8 (fig. 1). Even taking the number of examinations into account (table 2), Room 10 has a higher tubeload per examination by almost 2.5 than the nearest. Room 10 is generally used for higher dose examinations such as abdomen. The expected lifetime of all of these tubes is given as 7 years, however, this information could provide reasoning for more frequent QA given the harder working tubes such as Room 10 or Room 1 for sheer numbers may be more likely to require replacement sooner. This is being investigated by correlation with tube replacement frequencies from the department to give a more accurate indication that a high tubeload or tubeload per examination has been the cause of a replacement. In addition, tubeload per examination can be compared with the manufacturers recommendations for maximum tubeload. If the tube is working at a high percentage of the maximum, investigations can begin into how to lower the tubeload.

This information also provides evidence for better risk prevention. Any incident of staff exposure in Room 10 will have more of a consequence than a staff exposure in Room 8.

Table 2 Tubeload per examination for each room

Room Name	Tubeload per examination (J)
Room 1	1015.485
Room 2	1546.481
Room 3	659.616
Room 4	328.029
Room 5	35.986
Room 6	662.439
Room 7	268.222
Room 8	1185.335
Room 9	1437.358
Room 10	4812.414

B. Examination Types performed

Approximately every five years, the National Radiation Protection Board (NRPB), now merged with the Health Protection Agency (HPA) [21] release a document detailing the doses for a selected number of examinations [17]. The aim of their report is to set national reference doses for the most commonly used examinations to ensure compliance with the IR(ME)R recommendation of using diagnostic reference levels (DRLs). The latest review [22] states that 23,000 ESD records, collected with thermoluminescent devices (TLDs), and 57,000 dose area product (DAP) data records were collected for common plain film examinations from 316 hospitals in the UK over 5 years. In the present study over 58,000 records were collected on a single hospital site over a three-month period with minimum time and effort. In addition, approximately 20% of data supplied to the HPA was rejected due to missing information. Less than 15% of this study was classified as unauditable, however, this 15% contributes information that is of use to the hospital. The methodology proposed in this paper would seem to be eminently suited to large-scale dose audits with minimum time and effort

C. Operator work patterns

The first finding of the study was to show where data was missing from the RIS system. It was noticed that one particular operator was consistently leaving fields blank in the RIS. In order to ensure adherence to the standards for clinical audit [1, 18, 21], staff should be following procedures created by the hospital radiation protection committee (RPC). This process requires audit, which this study has shown can be provided.

This study also shows which operators have been working in high tubeload rooms more often than others. It is noted that one operator (operator 2) performed 266 exami-

nations in Room 10 whereas the next most frequent user of this room did 138. This raises the question of whether the high tubeload is because one operator uses higher exposure factors than necessary. There is also the increased risk of a significant staff exposure to this particular operator. The departmental manager may wish to train other staff to perform the procedures that are predominately performed in Room 10, whilst at the same time, operator 2 may be rescheduled to work in rooms with lower tubeload.

To show this information to a departmental manager can be achieved for a sample of 10 operators, however this study comprised of 129 operators. Future studies will establish a method for simplifying the presentation of this information for all operators with departmental managers being given opportunity to select staff for more detailed analyses.

V. CONCLUSIONS

It can be shown that analysis of RIS data in terms of radiology workload can be useful for x-ray departments in a number of areas. The data management techniques will also be employed in routine QA programs as required by IR(ME)R 2000 in the UK. Whilst this is being rolled out to hospitals in the north west of the UK, further analyses are also being undertaken to improve this fledgling service

ACKNOWLEDGMENT

The author wishes to thank the University Hospital, Aintree for their involvement, interest and patience and colleagues at Integrated Radiological Services Ltd for their input and providing resource for this work.

REFERENCES

1. The Ionizing Radiation (Medical Exposure) Regulations 2000, SI 2000 No 1059. London: HMSO 2000.
2. The Ionizing Radiation Regulations 1999, SI1999 No 3232. London: HMSO 1999
3. Recommended Standards for the Routine Performance Testing of Diagnostic X-Ray Imaging Systems, 2005: IPEM Report 91
4. Cole PR et al, Computer applications in radiation protection. Radiat. Protect. Dosim., 1995: 57(1-4): 203-206
5. Ward M et al, Central dose data management and analysis in IT driven radiation protection strategies. Radiat. Protect. Dosim., 2005: 114(1-3): 135-142
6. Garrard R. Design and development of a quality assurance management system in mammography. M.Sc. Thesis in PC interfacing and software application, University of Central Lancashire, UK (1993)
7. Kerom G. Development of a database application for use in mammography quality control. M.Sc. Thesis in PC interfacing and software application, University of Central Lancashire, UK (1994)
8. The Royal College of Radiologists, Radiology Information Systems. London: The Royal College of Radiologists. Available from http://www.rcr.ac.uk [Accessed 11/02/2009]
9. Pilling J. Installing PACS in a large acute hospital. Br. J. Healthc. Comput. Inform. Manag., 2002: 19(7): 35-37
10. Charnock P. Effects of monitor specification on soft-copy reporting in mammography. M.Sc. Thesis in Medical Physics, University of Manchester, UK (2007)
11. Wilde R et al. (2008) Automating patient dose audit and clinical audit using RIS data. IPEM Proceedings or the 14th Annual Scientific Meeting, Bath, UK, pp63-64
12. Ward et al, Medical physics expert led audit and research opportunities presented by hospital information systems. IPEM Proceedings of the 13th Annual Scientific Meeting, Cardiff, UK, pp61-62
13. Valentin J, Managing Patient Dose in Digital Radiology (ICRP Pub. 93). Annals of the ICRP, 2004: 34 (1): 1-73
14. Warren-Forward H et al, An assessment of exposure indices in computed radiography for the posterior-anterior chest and the lumbar lateral spine. Br. J. Radiol., 2007: 80: 26-31
15. Fazakerley J et al. The development of a 'gold standard' patient dose audit data set. IPEM Proceedings of the 14th Annual Scientific Meeting, Bath, UK, pp61
16. Guidance on the Establishment and Use of Diagnostic Reference Levels for Medical X-Ray Examinations, 2004: IPEM Report 88
17. Hart D, Hillier MC and Wall BF. Dose to Patients from Radiographic and Fluoroscopic X-ray Imaging Procedures in the UK – 2005 Review. Health Protection Agency, HPA-RPD-0292005, 2007. ISBN 9780859516006
18. Department of Health. A strategy for NHS information quality assurance. 2004, Available from: http://www.dh.gov.uk/en/Publicationsandstatistics/Publications/PublicationsPolicyAndGuidance/DH_4125508 [Accessed 11/02/2009]
19. Farr RF, Allisy-Roberts PJ, Physics for Medical Imaging, Elsevier Health Sciences, 1996 ISBN: 9780702017704
20. McClelland IR. X-Ray Equipment Maintenance and Repairs Workbook for Radiographers and Radiological Technologists. World Health Organization, 2004, ISBN 9241591633
21. Department of Health. Guidance on the establishment and use of diagnostic reference levels (DRLs). 2007, Available from http://www.dh.gov.uk/en/publicationsandstatistics/publications/publicationspolicyandguidance/DH_4007957 [Accessed 11/02/2009]
22. Hart D et al. National reference doses for common radiographic, fluoroscopic and dental x-ray examinations in the UK. Br. J. Radiol., 2009: 82: 1-12
23. George J et al. Patient Dose Optimization in Plain Radiography Based on Standard Exposure Factors. Br. J. Radiol., 2004: 77: 858-863

Corresponding Author:

Author: P Charnock
Institute: Integrated Radiological Services Limited
Street: Unit 188 Century Buildings, Tower Street
City: Brunswick Business Park, Liverpool
Country: England
Email: paulcharnock@irs-limited.com

Use of active personal dosemeters in interventional radiology: a systematic study in laboratory conditions.

I. Clairand[1], J-M. Bordy[2], J. Daures[2], J. Debroas[1], M. Denozière[2], L. Donadille[1], M. Ginjaume[3], C. Itié[1], C. Koukorava[4], A-L. Lebacq[5], P. Martin[6], L. Struelens[5], M. Sans Mercé[7], M. Tosic[7], F. Vanhavere[5].

[1] Institut de Radioprotection et de Sûreté Nucléaire (IRSN), France
[2] CEA-LIST Laboratoire National Henri Becquerel (CEA LNHB), France
[3] Institute of Energy Technology, Universitat Politècnica de Catalunya (UPC), Spain
[4] Greek Atomic Energy Commission (GAEC), Greece
[5] Belgian Nuclear Research Centre (SCK•CEN), Belgium
[6] MGP Intruments (MGPi), France
[7] University Hospital Center Vaudois (UPC), Switzerland

Abstract—**The optimization of the use of active personal dosemeters (APDs) in interventional radiology is performed by one of the work packages of the ORAMED project (2008-2011), which is a Collaborative Project supported by the European Commission within its 7th Framework Program. Interventional radiology procedures can be very complex and they can lead to relatively high doses to medical staff who stand close to the primary radiation field and are mostly exposed to radiation scattered by the patient. For the adequate dosimetry of these scattered photons, APDs must be able to respond to low-energy [10-100 keV] and pulsed radiation with relatively high instantaneous dose rates. Very few devices can detect low energy radiation fields and none of them are specially designed for working in pulsed radiation fields. The work presented in this paper is aimed at 1) studying the radiation field characteristics encountered in interventional radiology 2) making a selection of APDs deemed suitable for application in interventional radiology 3) defining, by measurements under laboratory conditions, the dose, the energy, the dose rate and the angular response of the selected APDs.**

Keywords— **ORAMED, active personal dosemeters, interventional radiology, pulsed radiation**

I. Introduction

The optimization of the uses of active personal dosemeters (APDs) in interventional radiology is performed by one of the work packages of the ORAMED project, which is a Collaborative Project (2008-2011) supported by the European Commission within its 7th Framework Program.

APDs are used for the monitoring of occupational doses in many applications of ionizing radiation. In interventional radiology, the possibility to assess the dose in real time is particularly interesting since operators can receive relatively high doses while standing close to the primary radiation field and being exposed to radiation scattered by the patient. A lack of appropriate equipment is identified in the field of APDs for typical fields in interventional radiology. Very few devices can detect low energy fields (10-100 keV), and none of them are especially designed for working in pulsed radiation fields. This problem was clearly highlighted during two international intercomparisons: one performed in the framework of the CONRAD project, a coordination action supported by the European Commission within its 6th Framework Program [1,2] and a previous one organized by EURADOS and IAEA [3].

The work presented in this paper consisted in 1) studying the real radiation field characteristics encountered in interventional radiology in terms of energy, angular distribution, dose rate and pulse characteristics 2) making a selection of APDs deemed suitable for application in interventional radiology according to the previous results of the CONRAD and IAEA-EURADOS groups 3) defining, by measurements under laboratory conditions, the dose, the energy, the dose rate and the angular response of some selected APDs.

The typical fields/parameters encountered in interventional radiology were gathered through questionnaires sent to hospitals, literature and quality control outputs. Calculations of dose rate at specific points of interest and typical scattered spectra were performed as well.

Then, an evaluation of the behavior of six commercial APD models deemed suitable for application in interventional radiology was performed through tests in laboratory conditions with continuous X-ray beams.

This study is the first step of the characterization of these APDs. Some additional tests under laboratory conditions as well as in hospitals with pulsed X-ray beams are planned to complete this work.

O. Dössel and W.C. Schlegel (Eds.): WC 2009, IFMBE Proceedings 25/III, pp. 132–135, 2009.
www.springerlink.com

II. Material and Methods

A. Typical fields encountered in interventional radiology

A questionnaire was sent to several European countries to find out which were the main type of interventional operations performed and with which technical conditions (type of devices used, kilo-Voltage, filtration of the tube, number of frames, etc.). This information was compared and completed by analyzing the output of several quality control studies performed in typical interventional radiology departments. During these quality controls, the X-ray systems were tested at both typical and extreme situations in fluoroscopy and acquisition mode, in order to obtain the range of dose rate values possibly encountered

In addition, the dose rate in the scattered beam at the level of the operator for tube position 0° and 90 ° was calculated with MCNPX [4] and the scattered spectra at the operator position were calculated using the Monte Carlo codes MCNPX [4] and Penelope [5] for tube high voltages equal to 50, 70, 90, 120 kV and for different filtrations: 4.5 mmAl with and without additional Cu filtration [0 - 0.1 - 0.3 - 0.6 - 0.9 mmCu].

B. Selection of APDs

The selection of APD models was based, on the one hand, on the results from two international intercomparisons: one performed in the framework of the CONRAD project, a coordination action supported by the European Commission within its 6th Framework Program [1,2] and a previous one organized by EURADOS and IAEA [3], and, on the other hand, on the available usage data from different European countries. A pre-requisite for consideration was that each unit should respond to photon energies down to 20 keV. Six APDs were selected for the study (Figure 1): DMC 2000XB (MGPI), EPD Mk2.3 (Siemens), EDMIII (Dosilab), PM1621A (Polimaster), DIS-100 (Rados) and EDD30 (Unfors).

Fig 1. Active personal dosemeters tested for this study

C. Tests under laboratory conditions

The tests were made in calibration laboratories of the Institute of Radiological Protection and Nuclear Safety (IRSN) in Fontenay-aux-Roses (France) and of the Belgian Nuclear Research Center (SCK•CEN) in Mol (Belgium). These two laboratories are accredited according to the ISO standard 17025 [6]. Several beam qualities described in ISO standard 4037-3 [7] were applied: N-15, N-20, N-25, N-30, N-40, N-60, N-80, N-100, N-120, S-Cs and S-Co.

III. Results

A. Typical fields encountered in interventional radiology

The compilation of data (Table 1) gathered from the questionnaires and from quality control measurements gives an overview of typical fields encountered in interventional radiology whatever the considered procedure. The dose rate obtained by quality control measurements in the direct field at the level of the table ranges from 2 to 360 Gy.h^{-1}. The dose rate in the scattered beam at the level of the operator for tube position 0° and 90° was found ranging from 5.e-3 to around 10 Gy.h^{-1}. In addition, calculations showed that the influence of the filtration of the scattered spectra is very small. The energy of the scattered spectra is ranging from 20 to 100 keV (Figures 2 and 3).

Table 1 Typical fields characteristics in interventional radiology

Parameter	Range
High peak voltage	50-120 kV
Intensity	5-1000 mA
Inherent filtration	4.5 mmAl
Additional filtration	0.1 – 0.9 mmCu
Pulse duration	1 - 20 ms (typically 10-20 ms)
Pulse frequency	1 – 30 pulse.s^{-1}
Dose rate in the direct beam (table)	2 to 360 Gy.h^{-1}
Dose rate in the scattered beam (operator)	5e-3 to 10 Gy.h^{-1}

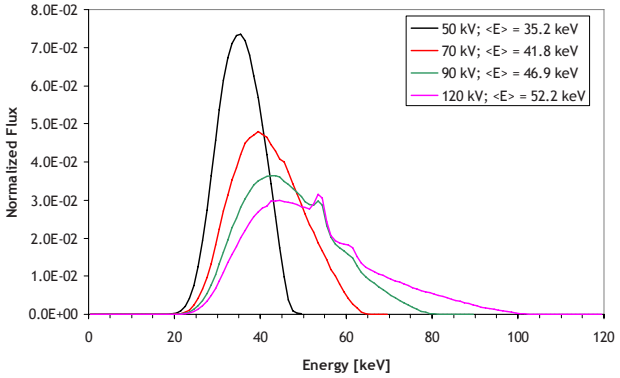

Fig. 2. Scattered spectra calculated with MCNPX considering a filtration of 4.5 mmAl + 0 mmCu

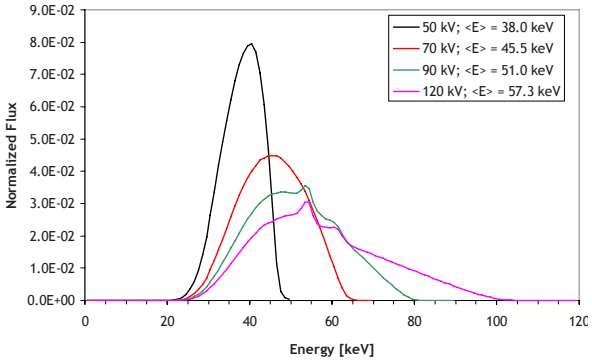

Fig 3. Scattered spectra calculated with MCNPX considering a filtration of 4.5 mmAl + 0.9 mmCu

B. Response of APDs

The dose response (Figure 4) of tested APDs is linear in the dose ranges indicated by each manufacturer in the technical notice. The DIS-100 was not tested for technical reasons mentioned hereafter.

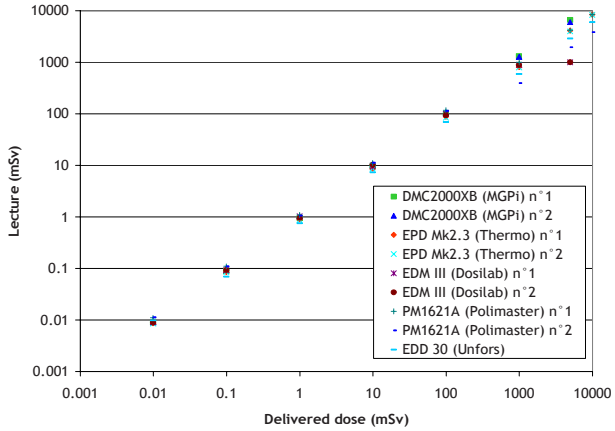

Fig 4. Dose response of APDs

The dose rate response of APDs is presented in figure 5. Most APDs can stand high dose rates until 10 $Sv.h^{-1}$, except PM 1621A and EDD 30 which cannot stand 1 $Sv.h^{-1}$. A problem was observed for one of the two PM 1621A for which the response is diverging rapidly from 1 Sv/h. The DIS-100 was not tested because it was noticed that it does not stand integrated doses above 4 Sv.

The response due to photon radiation energy for tested APDs is presented in figure 6. The response due to photon radiation energy is within the interval 0.71 – 1.67 as it is required in ISO 61526 standard [8] from ^{137}Cs energy down to 24 keV for all APDs except EDD 30.

The angular response due to photon radiation energy is within the interval 0.71 – 1.67 [8] from ^{137}Cs energy down to 24 keV for all APDs except for DIS-100 for which some points are slightly outside the interval at 24 keV.

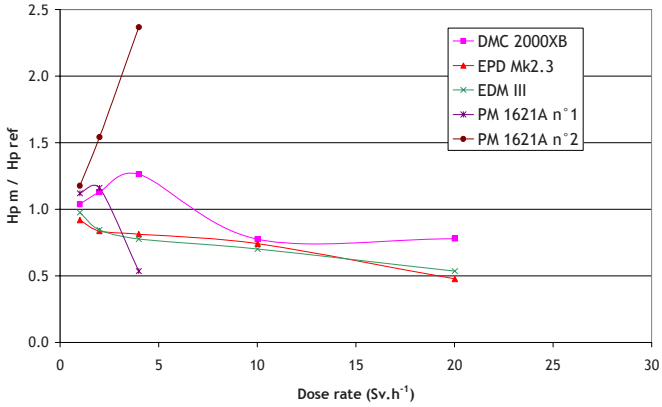

Fig 5. Dose rate response of APDs

IV. Conclusions

The response of the tested APDs fulfils the ISO 61526 standard requirements. Most of them present a satisfactory response at low energies from 24 keV, which is sufficient for interventional radiology. Most APDs can stand high dose rates up to 10 $Sv.h^{-1}$, except PM 1621A and EDD 30 which saturate for dose rates above 1 $Sv.h^{-1}$. In addition, DIS-100 saturates for integrated doses above 4 Sv.

This study is the first step of characterization of these dosemeters. Some additional tests are in progress under laboratory conditions with pulsed beams in CEA-LNHB in France and are planned in real conditions in hospitals.

Acknowledgment

The research leading to these results has received funding from the European Community's Seventh Framework Programme ([FP7/2008-2011] under grant agreement n° [211361].

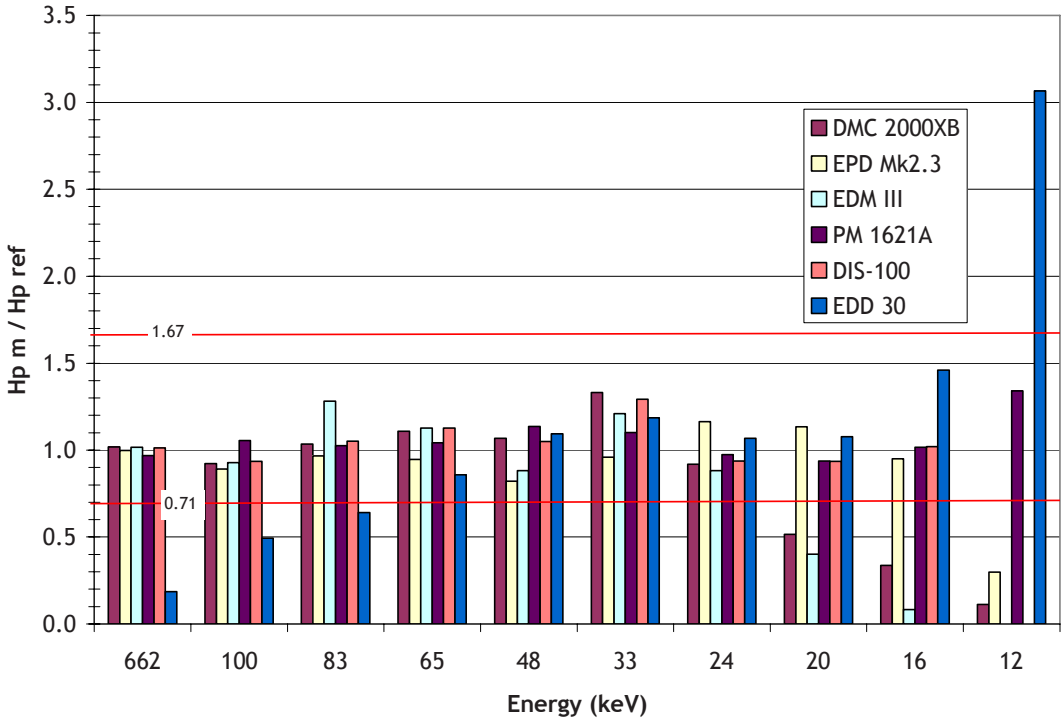

Fig 6. Energy response of APDs

References

1. Clairand I, Struelens L, Bordy J-M, Daures J, Debroas J, Denozieres M, Donadille L, Gouriou J, Itie C, Vaz P and d'Errico F. (2008) Intercomparison of active personal dosemeters in interventional radiology. Radiat. Prot. Dosim. 129 (1-3), pp. 340-345
2. Bordy J-M, Daures J, Clairand I, Denozière M, Donadille L, d'Errico F, Gouriou J, Itié C and Struelens L. (2008) Evaluation of active personal dosemeters for interventional radiology. Radiat. Prot. Dosim. 131 (1), pp. 87-92
3. International Atomic Energy Agency. (2007) Intercomparison of personal dose equivalent measurements by active personal dosimeters. Final Report of a joint IAEA EURADOS Project. IAEA Report IAEA-TECDOC-1564 (Vienna: IAEA)
4. MCNPX, 2005. Pelowitz, D.B. (ed.). MCNPX User's manual, version 2.5.0. Los Alamos National Laboratory. Report LA-CP-05-0369
5. Salvat, F. (2006) PENELOPE 2006: A code system for Monte Carlo simulation of electron and photon transport, Workshop Proceedings Barcelona, Spain, 4-7 July 2006, OECD 2006 NEA No. 6222, Nuclear Energy Agency Organisation for Economic Co-operation and Development
6. International Organization for Standardization. General Requirements for the Competence and Calibration of Testing Laboratories ISO 17025 (Geneva ISO) (1999)
7. International Organization for Standardization. X and gamma reference radiation for calibrating dosemeters and doserate meters and for determining their response as a function of photon energy - Part 3: calibration of area and personal dosemeters and the measurement of their response as a function of energy and angle of incidence. ISO 4037 (Geneva: ISO) (1999).
8. International Electrotechnical Commission. Radiation protection instrumentation. measurement of personal dose equivalent Hp(10) and Hp(0.07) for x, gamma, neutron and beta radiation: Direct reading personal dose equivalent and/or dose equivalent rate dosemeters (1998) IEC 61526 Geneva: IEC

Author: Isabelle Clairand
Institute: Institute of Radiological Protection and Nuclear Safety (IRSN)
Street: DRPH/SDE/LDRI BP 17
City: Fontenay-aux-Roses
Country: France
Email: isabelle.clairand@irsn.fr

Diagnostic Reference Levels in Cardiology and Interventional Radiology

Ph. R. Trueb[1], A. Aroua[2], A. Stuessi[1], E. Samara[2], R. Treier[1], F. R. Verdun[2], F. Bochud[2] and W. Zeller[1]

[1]Radiation Protection Division, Federal Office of Public Health, Berne, Switzerland
[2]University Institute of Applied Radiation Physics, CHUV/University of Lausanne, Lausanne, Switzerland

Abstract—**The purpose of this paper is to present a strategy to define diagnostic reference levels DRL for fluoroscopic, dose-intensive examinations in cardiology and interventional radiology. This work is part of the project of the Federal Office of Public Health of Switzerland to translate the guidelines of the ICRP and the EU into action. After the 2002 survey in all University Hospitals in Switzerland this work will present the results of the 2006-2007 survey performed in small and medium sized hospitals. The data of the small and medium sized hospitals are analyzed to establish DRL. They are corrected to patient size and analyzed in respect to the difficulty of the examination, the experience of the operator and the type of image detection system. The results of the study will be compared to those of the former study in the University Hospitals.**

Keywords— **Diagnostic Reference Level DRL, Cardiology, Interventional Radiology**

I. Introduction

X-ray examinations involving fluoroscopy, particularly those of the digestive system, angiography and interventional examinations contribute significantly to the total collective dose due to medical exposure even if their frequency is relatively low. A survey on the exposure of the Swiss population by X-ray imaging indicated that this contribution amounts up to 29% [1]. Moreover, these types of examinations, which deliver effective doses to the patient of the order of few mSv to few tens of mSv, can lead to extremely high entrance surface doses, up to a few Gy, leading to a significant risk of deterministic effects.

Several international bodies address seriously the issue of radiation protection of the patient and the radiologist for dose-intensive examinations. The International Commission on Radiological Protection (ICRP) dedicated one of its publications to the means and methods to set up in order to prevent the lesions that may be induced by interventional radiology [2]. Similarly, the European Directive 97/43 Euratom states in its article 9 that "Member States shall ensure that appropriate radiological equipment, practical techniques and ancillary equipment are used for the medical exposure […] involving high doses to the patient, such as interventional radiology, computed tomography or radiotherapy." [3]

In Switzerland the Federal Office of Public Health set up in early 2000 with the collaboration of the University Institute of Applied Radiation Physics a working group on the optimization of radiation protection in the case of dose-intensive X-ray examinations (Optimierung des Strahlenschutzes bei dosisintensiven Untersuchungen in der Radiologie – OSUR). Several medical associations concerned by the issue were invited to take part in this working group: general practitioners, radiologists, cardiologists, radiographers, medical physicists. One of the main issues addressed by the working group relates to diagnostic reference levels (DRLs), whose definition, establishment and implementation have become in recent years of central importance in the management of radiation doses delivered to the patient in diagnostic and interventional radiology. In fact, several international, regional and national bodies showed an increasing interest for this subject [3-6], a great number of papers were dedicated to DRLs and several scientific meetings and journals included DRLs in their priority topics [7].

The International Commission on Radiological Protection (ICRP) introduced the term "DRL" for the first time in 1996 [8], specifying that it is advisory, set by professional bodies, apply to dose to patients or intake of pharmaceutical, and call for local review if consistently exceeded.

The ICRP compiled in 2001 different sets of DRLs proposed at the international level [4]. The data presented in the ICRP report covers fifteen radiographic views for adult patients, and for pediatrics in a few cases, three fluoroscopy examinations, ten CT examinations, mammography and five dental examinations.

In 2002 a survey was organized by the OSUR group with aim to study the patient exposure due to dose intensive applications of fluoroscopy in Switzerland [9]. This survey was performed in the university hospitals of Switzerland to study the clinical practice of 8 fluoroscopic examinations and to collect dose values to determine the corresponding DRL.

O. Dössel and W.C. Schlegel (Eds.): WC 2009, IFMBE Proceedings 25/III, pp. 136–139, 2009.
www.springerlink.com

Even if it is difficult to deal with DRLs in the case of complex X-ray examinations, their use is important for such dose-intensive examinations since it provides guidance for proper dose management.

II. Material and Method

A. Participating Centers and chosen examinations

In the beginning, 84 hospitals were asked to participate in the survey and give a list of the examinations in cardiology, interventional radiology and fluoroscopy of the digestive system, which they perform frequently. 65 hospitals (77%) answered the questionnaire and were willing to participate.

From this list of 65 hospitals 32 were chosen to be in the survey due to following considerations: existence of dose-area-product meter (DAP), number of examinations performed within the 3 month survey period, balance between the different modalities (radiology, cardiology, urology and gastroenterology) and the geographical distribution with in Switzerland.

The monitored examinations (coronary angiography, PTCA, cerebral angiography, angiography and PTA of lower limbs) were chosen by a panel of radiologists. Each of the 32 centers involved agreed to monitor 20 patients for each examination. Examinations of the digestive system and urology will be analyzed and presented at a later date.

B. Characterization of the installations

To compare the different DAP-meters of the installations and to get a reference point of the dose all installations in the survey have been characterized. In addition the entrance surface dose was determined using a patient equivalent phantom to characterize the skin dose and the image quality using a specific type of automatic exposure control system.

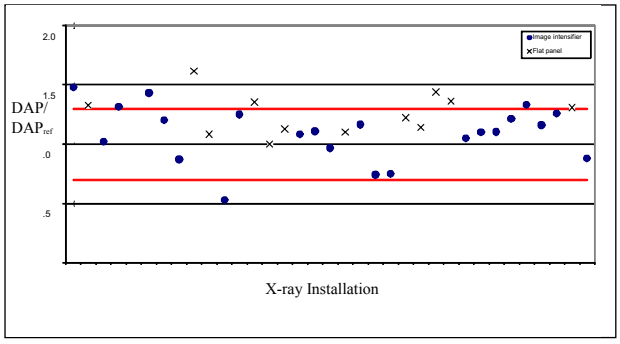

Fig. 1 Characterization of the DAP-meters of the x-ray installations to a reference chamber, red lines indicate ±30% of the reference

C. Determination of diagnostic reference levels DRL

The primary goal of this survey was the establishment of DRL (3. Quartile of the distribution). The DRL are primarily determined in fluoroscopic examinations for the DAP. Because each examinations is set together of a fluoroscopic part (Characterized by the fluoroscopic time: T) and another part of image acquisition (Characterized by the number of images: N), the DRL of these quantities are determined in addition.

D. Analysis of patient collective and patient size

In the questionnaire following data of the patients were collected: age, size, weight and sex. The information was used to determine for each examination the specific distribution of the patient collective.

For the examinations of the trunk, the delivered dose depends essentially on the size of the patient. For the establishment of DRL the measured dose values have to be corrected to a standard patient (height: 1.70m; weight: 70kg). A simple model for a correction factor to modify the measured DAP has been applied:

$$f = DAP_{standard}/DAP_{measured} = e^{\mu(d_a-d_r)}$$

With μ for the average attenuation coefficient ($0.3cm^{-1}$), d_a for diameter of the average patient and d_r the diameter of the real patient; d_r is calculated from the height h and the weight m with the formula

$$d_r = 2(m/\pi h\rho)^{-2}$$

With ρ for the density of the body (set to $1000kg/m^3$).

E. Effect of the complexity of the examination

The complexity of the examination is certainly an important factor for the dose delivered to the patient. The results were analyzed to determine this correlation. Three categories of the complexity were recorded in the questionnaire: simple, normal and difficult examination.

F. Effect of the experience of the operator

On the basis of years of experience of the radiologist or cardiologist, a classification in three groups has been applied: doctor-in-training (<1 year), junior doctor (1-5 years) and senior doctor (>5 years)

G. Influence of the detector type

The efficiency of the detector system has a mayor influence of the primary radiation needed and consequently to

the patient exposure. The survey was also analyzed in respect to the used detector type: flat panel detector or image intensifier.

H. Inter-center comparison

The selected centers represent private radiological institutes and hospitals of small and medium size. Therefore a analysis of the results in respect of the center type can show differences in clinical practice and possible systematic different patient exposure.

III. RESULTS

A. Diagnostic reference values DRL

The survey allowed to the establish DRL for five types of examinations. The values of the present study in small and medium hospitals are shown in the table 1 below and compared to those of the previous study in the university hospitals.

Table 1 Results for the DRL for the DAP (Gy·cm^2), the fluoroscopic time T (min) and the number of images N

Type		Small and medium hospitals	University hospitals	Ratio
coronary angiography	DAP	110	80	1.38
	T	10	7	1.43
	N	1500	1400	1.07
PTCA	DAP	150	110	1.36
	T	20	20	1.00
	N	1800	1500	1.20
cerebral angiography	DAP	160	125	1.28
	T	8	15	0.53
	N	240	480	0.50
angiography of lower limbs	DAP	70	210	0.33
	T	8	8	1.00
	N	150	150	1.00
PTA of lower limbs	DAP	70	460	0.15
	T	22	25	0.88
	N	180	200	0.9

In terms of the DAP, the values obtained for the DRL in the small and medium sized hospitals are 30-40% higher than the values of the university hospitals in the case of coronary angiography, PTCA and cerebral angiography. In contrary the values are 3 to 7 times smaller in the case of angiography ant PTA of the lower limbs.

B. Influence of the difficulty of the examination

The analysis of the data in respect of the difficulty of the examination has shown a clear dependency of the complexity of the case in all 5 examinations selected. In table 2 the results of the analysis for coronary angiography is shown:

Table 2 Influence of the complexity of the case in coronary angiography

Category of complexity of the case	Number of cases	DAP [Gy·cm^2] Average	DAP [Gy·cm^2] 3. Quartile
simple	47	49±6	69
normal	140	71±6	95
complex	69	200±9	233
all	256	94±6	110

The increase in patient exposure with the complexity of the examination is seen in all 5 examinations.

C. Influence of the experience of the operator

An effect of the experience of the radiologist or cardiologist is seen in coronary angiography, PTCA and the PTA of the lower limbs, while for the cerebral angiography and the angiography of the lower limbs the distribution of the cases were not sufficient enough to see any evidence. In table 3 the results of the analysis for coronary angiography is shown:

Table 3 Influence of the experience in coronary angiography

Experience of the medical doctor	Number of cases	DAP [Gy·cm^2] Average	DAP [Gy·cm^2] 3. Quartile
In-training	8	64±3	97
Junior	28	60±4	91
Senior	204	93±6	112
all	240	84±6	109

Due to the fact, that the more complex examinations are manly handled be senior doctors, the values for the average DAP ant the 3. quartile is higher than for juniors and trainees.

D. Influence of the detector type

The analysis of the effect of the detector type (flat panel or image intensifier) did not show a significant difference between the average DAP of the tow cases. In table 4 the results of the PTCA are shown:

Table 4 Influence of the type of detector in PTCA

Type of detector	Number of cases	DAP [Gy·cm^2] Average	DAP [Gy·cm^2] 3. Quartile
Flat panel	41	124±12	156
Image intensifier	48	108±13	166
all	89	115±9	109

The analysis with the Mann an Whitney test shows no significant difference for the PTCA examinations in the survey using flat panel detectors or image intensifier (p-value=0.14). An explanation could be that in the flat panel cases the radiation field is not optimized in a proper manner.

E. Inter-center comparison

To compare the different centers with each other, the average DAP of the centers were put in relation. The results are widely spread (up to a factor of 3) and indicate a high potential of optimization of the clinical practice. A significant higher average DAP (factor of 2) has been observed in private hospitals than in public hospitals.

IV. CONCLUSIONS

A strict control concerning the denomination of the examinations involved in such a study is mandatory to obtain reliable data. This can only be done through a close collaboration between physicians, radiographers and medical physicists. The values obtained in the study differ partly strongly from the study performed in the University Hospitals due to the different difficulty of the examinations and the due to degree of experience of the operator. The clinical practice in many hospitals seems to have a high potential to optimize patient exposure. Expertise of medical physics is needed in the hospitals as well as professional clinical audits.

ACKNOWLEDGMENT

The authors are grateful to all radiologists, cardiologists, physicists, radiographers and others who collaborated or provided assistance in the five participating hospitals during this survey.

REFERENCES

1. Nation-wide Survey on Radiation Doses in Diagnostic and Interventional Radiology in Switzerland in 1998. Aroua A, Burnand B, Decka I, Vader JP and Valley JF. Health Phys 83(1):46-55 (2002).
2. International Commission on Radiological Protection (ICRP). Avoidance of Radiation Injuries from Medical Interventional Procedures. Publication 85. 2000.
3. European Union, On Health Protection of Individuals Against the Dangers of Ionizing Radiation in Relation to Medical Exposure, Council Directive 97/43/Euratom, Official J. Eur. Commun. No L 180, 22-27 (1997).
4. Diagnostic Reference Levels in Medical Imaging, International Commission on Radiological Protection, ICRP Committee 3, Draft (5 February 2001).
5. Guidance on Diagnostic Reference Levels (DRLs) for Medical Exposures, European Commission, Radiation Protection 109 (1999).
6. International Atomic Energy Agency, International Basic Safety Standards for Protection against Ionising Radiation and for the Safety of Radiation Sources, Safety Series No. 115, Vienna 1996.
7. Adult Reference Levels in Diagnostic and Interventional Radiology for Temporary Use in Switzerland. Aroua A, Besançon A, Buchillier-Decka I, Trueb Ph, Valley JF, Verdun FR and Zeller W. Radiat Prot Dosim 111(3), 289-295(2004).
8. Diagnostische Referenzwerte bei dosisintensiven Untersuchungen in der Radiologie. Aroua A, Jung H, Theiler Th, Trueb PhR, Valley JF and Verdun FR, Strahlenschutz in Forschung und Praxis 46:301-310 (2005)
9. International Commission on Radiological Protection, ICRP Publication 73, Pergamon Press, Oxford (1996).
10. How to set up and apply reference levels in fluoroscopy at a national level? Aroua A, Rickli H, Stauffer JC, Schnyder P, Trueb Ph, Valley JF, Vock P and Verdun FR. Eur Radiol 17(6):1621-33 (2007).

Author: Philipp R. Trueb
Institute: Federal Office of Public Health
Radiation Protection Division
City: CH-3003 Berne
Country: Switzerland
Email: philipp.trueb@bag.admin.ch

Compensator for Advanced Radiation Field Homogeneity

K.-J. Dörner

Abteilung für Strahlentherapie, ALLGEMEINES KRANKENHAUS CELLE, Celle, Germany

Abstract— **To produce a homogenous dose distribution in a phantom depth just behind the depth of the dose maximum a compensator is drilled. The compensator is inserted into the block tray holder of the linear accelerator. With this easy to use solution irradiations of detectors and probes are possible with a new quality of dose homogeneity.**

Keywords— **Radiotherapy, Dosimetry**

I. Introduction

The flattening filters of commercial available treatment machines are optimized to give a homogeneous as possible beam flattening at a specified water depth. The basic idea of this paper is to realize a uniform beam intensity at a different phantom depth by inserting an additional flattening filter in the pathway of the beam. The motivation to produce a homogeneous dose distribution in an appropriate phantom arises for example from calibration and test measurements: Thinkable tasks are cross-calibration of ionisation chambers or calibration and sensitivity test of detector arrays (like PTW-seven29) or to expose special probes to well defined doses: For MR-gel-dosimetry a reference probe with the dimensions of e.g. 2 cm x 2 cm x 5 cm has to be exposed to a uniform dose distribution in a handsome procedure.

II. Material and Methods

A. Eequipment

The radiotherapy department in Celle is equipped with a linear accelerator PRIMUS (Siemens), a Somatom Emotion Computer Tomograph (Siemens), a treatment planning system Oncentra Masterplan (Nucletron / Theranostic), an afterloading microSelectron (Nucletron / Theranostic) with the corrsponding brachytherapy planning system Plato (Nucletron / Theranostic), an Oncologist Workspace (Siemens) for virtual simulation and the verify and record system LANTIS (Siemens). The images generated from these entities and the portal images generated by the BeamView (Siemens) are handled by a DICOM archive and viewing device called MagicView (Siemens). Additionally patient set up documentation photos and treatment plans are stored in this archive. With a MP3-water phantom controlled via Mephisto mc² software dose distributions are measured. A solid RW3 phantom with a farmer type ionisation chamber (Type 30001 PTW) is used for daily checks. Absolute dosimetry could be carried out in a small water phantom. UNIDOS (PTW), MULTIDOS (PTW) and tandem electrometer (PTW) are the calibrated dosemeters. Additional dose measurement devices are a linear array LA48 (PTW) and a two dimensional array *seven29* (PTW).

B. Theorie

In radiation therapy the gross tumour volume has to be hit by a sufficient dose to achieve a proper tumour control. Therefore the accelerated electron beam has to strike a target to produce high energy photons. The result in a pencil beam (2-3 mm diameter) that has to be opened to produce a field size in the patient plane of 40 cm x 40 cm: A flattening filter is inserted to make the beam intensity uniform across the field. Due to absorption and scatter the field homogeneity could not be achieved for all phantom depth. The incoming photon spectrum will change depending on depth in the irradiate matter and in regions with small distances to the field boundary. Close to the boundary radiation is scattered outwards of the field what causes a drop of the dose. Compared to the photons with higher energies in the spectrum those with lower energies will be stopped in a larger portion with growing depth. This has a direct influence on the cross beam profiles. As the flattening filter is optimized by the vendor of the linear accelerator to equalize a cross beam in a specified depth profiles upstream and downstream are altered depending on the spectral energy fluence. Close to the central beam axis the spectrum is hardened because the part of the photons with the lower energies is more scattered and absorbed than the higher energies. With growing distance to the central axis the portion of the out scattered photons with the lower energies raises and the spectrum becomes weaker.

C. Measurements

In a water phantom a dose matrix is measured with a spatial resolution of 5 mm. The collimator of the accelerator is set to an isocentric field size of 40 cm x 40 cm. The matrix is taken with a scan limit of 300 mm x 300 mm in a water depth of 20 mm. The nominal energy of the photon radiation is 06 MV.

O. Dössel and W.C. Schlegel (Eds.): WC 2009, IFMBE Proceedings 25/III, pp. 140–141, 2009.
www.springerlink.com

III. Results

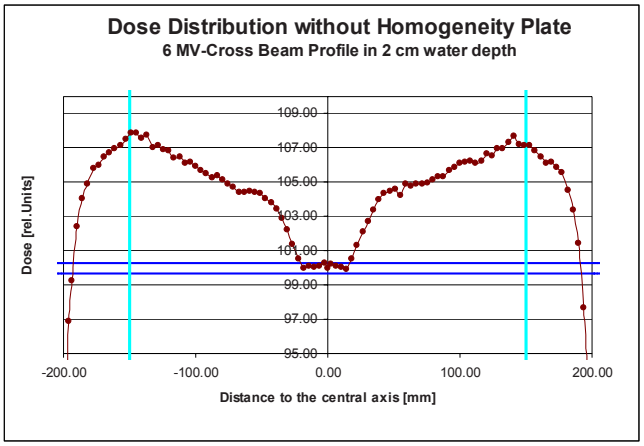

Fig. 1 Cross-Beam-Profile of the open beam

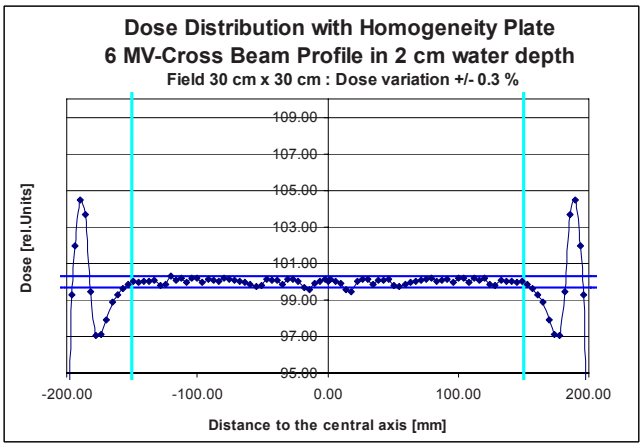

Fig. 2 Cross-Beam-Profile with compensator

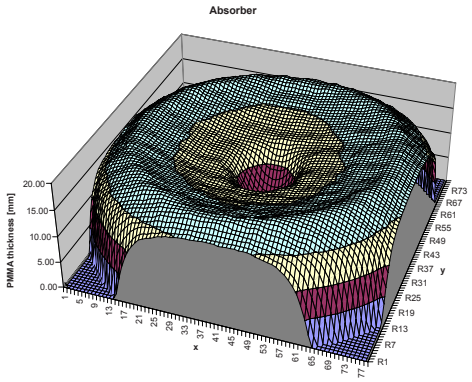

Fig. 3 Shape of the PMMA-Absorber

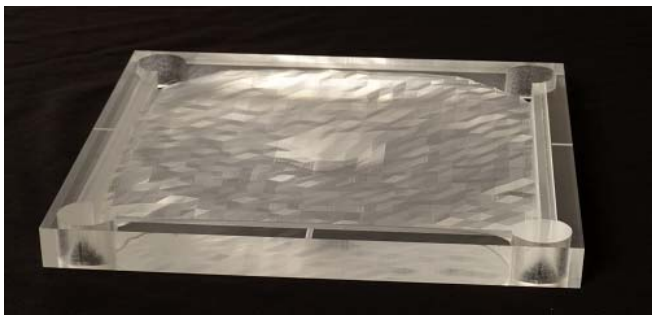

Fig. 4 Photo of the PMMA-Absorber

Similar to the manufacturing of a missing tissue compensator the shape of a PMMA-absorber is calculated from the measured dose distribution.. This absorber modifies the dose distribution as shown in figure 2.

IV. Conclusions

A very homogenous dose distribution is produced with the very easy to use solution: The insert of an additional low Z compensator into the block tray holder of the linear accelerator. The variation of the dose in the measuring plane is reduced from 8 % to +/- 0.3 %.

Acknowledgment

We wish to thank Mr. Armoneit (Positronic) for support, helpful discussions and manufacturing the compensator:
positronic beam service GmbH
Industriestraße 10E
25462 Rellingen
www.positronic.de/beam

References

1. Reich, H. (1990); Dosimetrie ionisierender Strahlung; Teubner Verlag Stuttgart 1990
2. ICRU 43 (1982) The Dosimetry of pulsed Radiation
3. DIN 6809-6 (2004) Klinische Dosimetrie – Teil 6: Anwendung hochenergetischer Photonen- und Elektronenstrahlung in der perkutanen Strahlentherapie; Beuth Verlag Berlin

Author: Dr. Karl-Joachim Dörner
Institute: Abteilung. Strahlentherapie
ALLGEMEINES KRANKENHAUS CELLE
Street: Siemensplatz 4
City: D-29227 Celle
Country: Germany
Email: kajo.doerner@AKH-Celle.

Differences in gamma-H2AX foci formation after irradiation with continuous and pulsed proton beams

O. Zlobinskaya[1], T.E. Schmid[1], G. Dollinger[2], V. Hable[2], C. Greubel[2], D. Michalski[1], J. Wilkens[1], G. Du[3], M. Molls[1] and B. Röper[1]

[1]Klinikum rechts der Isar, Department of Radiation Oncology, Technische Universitaet Muenchen, Muenchen, Germany,
[2]Institute for Applied Physics and Metrology, Universitaet der Bundeswehr Muenchen, Neubiberg, Germany,
[3]Technische Universitaet München, Physik Department E12, Garching, Germany

Abstract

Introduction: Classical particle accelerators offer proton pulses of some milliseconds duration. In contrast, the new technology of the high-intensity laser acceleration will produce ultimately shorter particle packages (up to one nanosecond) with substantially lower pulse frequency and higher pulse-dose achievement. Very little is known about the relative biological effectiveness (RBE) of this new beam quality, which could be a possible future application in radiation oncology. In our present study we investigate possible differences based on quantitative analysis of γ-H2AX fluorescence - a known marker of DNA double strand breaks (DSBs).

Methods: HeLa cells were irradiated with 1 Gy of 20 MeV protons at the Munich tandem accelerator, either at continuous mode (100 ms), or at pulsed mode with a single pulse of 1 ns duration. A dose-effect-curve based on five doses of 75 kV x-rays served for reference. The total number of γ -H2AX foci per cell was determined using a self-developed macro (ImageJ, NIH, USA).

Results: Quantitative analysis of γ-H2AX fluorescence revealed no significant difference (p=0.16) in yield of foci formation after irradiation with pulsed or continuous proton beams. γ-H2AX data for cell samples exposed to 1 Gy of 20 MeV protons at pulsed or continuous irradiation modes were 23.29 ± 2.04 and 26.54 ± 2.54 foci per cell, respectively. The corresponding RBE values for 20 MeV protons were 0.96 ± 0.18 and 1.13 ± 0.21 (p=0.21) for pulsed and continuous irradiation modes. However, the percentage of foci smaller than 5-10 pixels was slightly decreased and foci tended to cluster after irradiation with pulsed protons.

Conclusions: Based on γ-H2AX foci formation no significant difference in the RBE between pulsed and continuous proton irradiation beams in HeLa cells has been detected so far. These results are well in line with our data on micronucleus induction in HeLa cells.

.

Keywords— RBE, gamma-H2AX foci, protons, pulsed irradiation

I. Introduction

Classical particle accelerators generate proton irradiation with a typical pulse duration of some milliseconds. In contrast, the new technology of the high-intensity laser acceleration will produce ultimately shorter particle packages (up to one nanosecond) with substantially lower pulse frequency and higher pulse-dose achievement. One possible application may be radiotherapy of malignant tumors by high energy protons using laser driven accelerators (LDA) [1, 2]. Such laser accelerators will be very compact and the acceleration method may provide certain advantages for the radiation oncologist. Firstly, it reduces the overall system size and weight by more than one order of magnitude. In addition, the characteristics of the particle beams (protons) make them suitable for a kind of therapy that might not be possible with conventional accelerators, such as the ease for changing pulse intensity [3].

Thus, it is mandatory to investigate the relative biological effectiveness (RBE) of the new beam quality before its use in a radiotherapeutic setting is possible. The current subject of debate is the question of whether or not pulsed irradiation with high-energy particles or protons may induce a different amount of damage in cells or even changes in repair or apoptosis pathways relative to continuous irradiation. The short-pulse effects are subject to our current investigations utilising pulsed ion beams at the SNAKE (Superconducting Nanoprobe for Applied nuclear (Kern) physics Experiments) microprobe of the Munich tandem accelerator, where 10^5 high energy protons can be bunched into a single nanosecond pulse at a beam diameter of about 100 µm. These beam parameters are sufficient to irradiate cell cultures or tissue up to a dose of 5 Gy by a single pulse of protons.

The aim of the present experiments is to compare the RBE of continuous and pulsed modes of irradiation with high-energy protons at 20 MeV with 75 kV x-ray, using the γ-H2AX assay in HeLa cells. The cellular response to DSBs includes the very rapid phosphorylation of the histone H2AX [4]. Phosphorylated H2AX forms microscopically

O. Dössel and W.C. Schlegel (Eds.): WC 2009, IFMBE Proceedings 25/III, pp. 142–145, 2009.
www.springerlink.com

visible foci and the number of phosphorylated H2AX foci correlates well with the number of DSBs [5, 6]. Investigating such radiobiological effects at the Munich tandem accelerator is part of a series of research projects which are being performed in the framework of the DFG-cluster of excellence 'Munich-Centre for Advanced Photonics' (MAP).

II. Materials and Methods

Cell culture and irradiation conditions

HeLa cells were grown as monolayer cultures as described previously [7]. Shortly before irradiation experiments, cells were trypsinised, seeded in irradiation containers and allowed to adhere for 12 h. Since the construction of irradiation containers as well as the culture technique have been previously reported in detail [7, 8], only a brief description is given here. Irradiation containers are built by stretching and clamping a 6 µm Mylar foil between two stainless steel plates. Cells to be irradiated are grown on this carrier foil, which is part of the container developed specifically for irradiation at SNAKE. In order to obtain a dose-response curve for reference, HeLa cells were irradiated with doses in the range of 0 to 1.25 Gy with 75 kV x-ray (Philips RT100; Philips Medical Systems, Eindhoven, The Netherlands) with a dose rate of approximately 1 Gy per minute (10 mA, 2.0 mm Al) and a source–cell distance of 30 cm using a field of 20 cm x 20 cm. Cell irradiation experiments with 20 MeV protons were performed at the Munich tandem accelerator (LET of 2.6 keV/µm), each with three replicates of 1.0 Gy at either continuous or pulsed irradiation mode. In the pulsed irradiation mode the pulse length was 1.0 ns, the irradiation field was 1.5 x 2.0 mm². In continuous mode a 2.0 x 2.0 mm field was irradiated for 100 ms. After irradiation, the remaining culture medium was replaced with fresh medium and cells were incubated for 1 h at 37°C. A standard immunostaining protocol was applied to detect phosphorylated histone H2AX (γ-H2AX) according to the method of Hauptner *et al* [8]. From each sample (unirradiated or irradiated) at least 200 cells were analyzed.

Analysis of γ -H2AX

Microscopic γ-H2AX foci were immunolocalized and images were acquired using epifluorescence sectioning microscopy (Zeiss Axiovert 200M), utilizing immersion oil with 63x (N.A. 1.45) objective lens. The Alexa 488 and DAPI digital images were captured serially, at least 10 images were taken in Z plain, and 10 images (20 – 25 cells per image) were taken for each probe with Zeiss AxioVision Software. Data were analyzed on per nucleus basis using an NIH ImageJ software with a custom macro function designed to count particles. The macro was partially adopted from Kataoka *et al.* [9]. Briefly, maximum intensity projection was applied to convert stack images into 2D objects, then images were normalized and background noise was corrected. The noise suppression was performed with minimum reduction in focus detection sensitivity, according to Bocker and Iliakis [10]. Nuclear boundaries and foci were automatically identified in images by a threshold algorithm. Adjunct or overlapping nuclei were adequately segmented using watershed transformation. Details on the number of foci per cell, foci intensity and morphometry were subjected to final analysis and stored in an Excel file.

III. Results

Reference data from 75 kV x-rays

The sites of DNA damage can be visualized as discrete nuclear foci by immunofluorescence staining of phosphorylated H2AX, corresponding to the number of DSBs [6]. The dose-response curve for reference was established in a dose range from 0 to 1.25 Gy. The number of phosphorylated H2AX foci per cell followed a linear relationship with x-ray doses between 0.25 and 1.25 Gy of 75 kV x-rays (Fig. 1). In the sham-treated samples the average number of foci per cell was 3.8 ± 0.16. From the dose–response curve, a yield of 24.8 ± 2.01 foci per Gray was measured

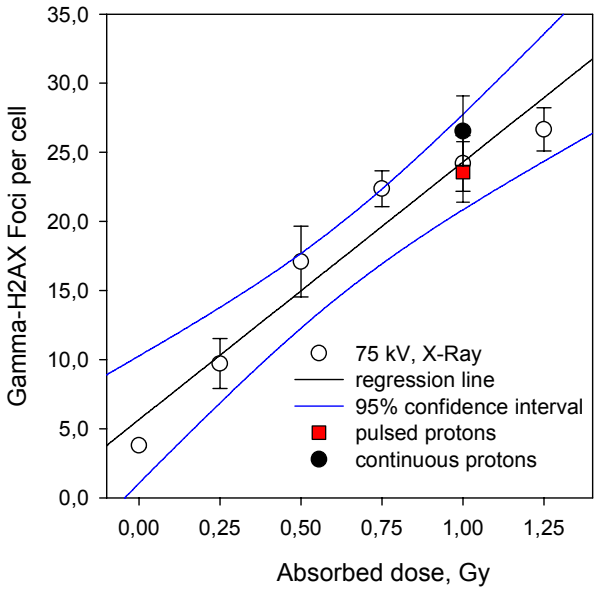

Fig. 1 Reference dose-response x-ray curve (○) and data for irradiation with 1 Gy continuous (●) and pulsed (■) proton beams

The control value obtained for γ-H2AX foci per cell in this experiment did not differ significantly from the control value of 4.1 ± 0.18, which was determined in the proton irradiation experiments.

Data from proton irradiation

Table 1 presents the mean values (± SD) of γ-H2AX foci data from single proton experiments, with three replicates (each at least 200 observations) of exposure of HeLa cells to 1 Gy of 20 MeV protons at pulsed or continuous irradiation modes. The mean value of 4.1 ± 0.18 for spontaneous induction of γ-H2AX foci in the control group is consistent with the corresponding experiment using 75 kV x-ray.

Table 1 Mean number of Foci per cell after proton irradiation

	Foci per cell, 3 independent samples (ca. 250 cells)	St.Dev
pulsed	23,69 25,12 21,08	
mean	23,29	2.04
continuous	29,16 26,36 24,10	
mean	26.54	2.54

The RBE of 20 MeV protons was calculated as the ratio between the dose of the reference radiation (75 kV X-ray) and the dose of protons (20 MeV) which produced equal response. In the proton experiments with a proton dose of 1 Gy at pulsed and continuous irradiation modes, mean numbers of γ-H2AX foci per cell of 23.29 ± 2.04 and 26.54 ± 2.54 were obtained (Table 1). The corresponding RBE values relative to the reference radiation of 75 kV x-ray were 0.96 ± 0.18 and 1.13 ± 0.21, respectively. RBE values were evaluated based on empirical data approximated with linear regression. Standard deviation for RBE values was calculated with help of bootstrap method. The difference between RBE values for pulsed and continuous modus was not significant ($p = 0.21$, t-test). Although absolute numbers of γ-H2AX foci formation per cell revealed no significant difference after irradiation with pulsed or continuous proton beams ($p = 0.16$, t-test), the percentage of foci smaller than 5-10 pixels was slightly reduced after irradiation with the pulsed proton beam. Instead, foci generated with pulsed irradiation tended to be bigger and more aggregated. Representative images of cells with visually different sizes of γ-H2AX foci are displayed in Fig 2. Further experiments are in progress to confirm these findings and to exclude the possibility of technical staining artifacts.

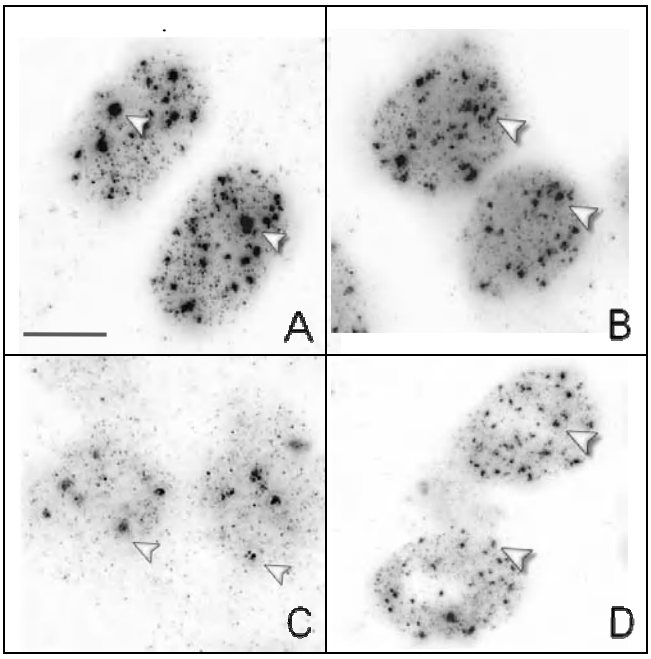

Fig. 2 Appearance of γ-H2AX foci in representative HeLa cells analyzed 1 hour after exposure to 1 Gy of proton irradiation in (**A**) pulsed mode (1 ns) or (**B**) continuous mode (100 ms). Images depicted in lower panel serve for comparison of foci number and size per cell between proton and reference x-ray irradiation. Reference x-ray irradiation with 0.25 Gy (**C**) and 1 Gy (**D**). Nuclei are indicated by DAPI staining with foci identified by antibody binding to γ-H2AX. Scale bar, 10 μm

IV. Discussion

In recent publications, a strong correlation between the number of microscopically detected γ−H2AX foci and the number of DSBs, which form after irradiation, was shown [11, 12]. Based on the micronuclei analysis in HeLa cells and 75 kV x–rays as reference, a RBE of 1.07±0.07 (pulsed) and 1.06±0.07 (continuous) was resulting for 3 Gy of 20 MeV protons [13]. Similarly, no significant difference in RBE for γ-H2AX foci formation could be found comparing pulsed and continuous proton irradiation (present study), although different endpoints were analyzed. The absolute numbers of foci formation per cell are well in line with previously published data [14-16]. Differences in foci size / intensity after pulsed irradiation compared to continuous mode need to be confirmed in further experiments. Still, they may indicate the persistence of more complex lesions after 1 hour of repair and therefore a possible difference in

repair kinetics of DSBs after irradiation with pulsed versus continuous proton beams. Our data support the idea, that the amount of DNA damage inflicted is not markedly effected by the ultrahigh dose-rate of a pulsed delivery mode when compared to irradiation times close to a second.

V. Conclusions

Based on the results of our experiments it can be concluded that there is no evidence for a different RBE in terms of γ−H2AX foci formation between pulsed and continuous irradiation in HeLa cells irradiated with 20 MeV protons. Our results are consistent with our previous findings (micronucleus assay). Therefore, our results add a new quality to the available knowledge about the radiobiological effects of pulsed proton beams, which is necessary before a clinical use of pulsed proton or heavy ion beams generated by high-intensity lasers is possible. Nevertheless, further experiments are necessary to evaluate their induction of further radiobiological endpoints covering aspects of radiation damage, repair, apoptosis and tissue reaction.

Acknowledgment

Supported by the DFG Cluster of Excellence: Munich-Centre for Advanced Photonics, by the EU-project Euro-Dyna and by the Maier Leibnitz Laboratory Munich.

References

1. Linz, U. and J. Alonso, (2007) What will it take for laser driven proton accelerators to be applied to tumor therapy? Physical Review Special Topics - Accelerators and Beams. 10(9): p. 094801.
2. Ma, C., I. Veltchev, E. Fourkal,et al., (2006) Development of a laser-driven proton accelerator for cancer therapy. Laser Physics. 16(4): p. 639-646.
3. Ma, C.-M.C., R.L. Maughan, and C.G. Orton, (2006) Within the next decade conventional cyclotrons for proton radiotherapy will become obsolete and replaced by far less expensive machines using compact laser systems for the acceleration of the protons. Medical Physics. 33(3): p. 571-573.
4. Rogakou, E.P., C. Boon, C. Redon, et al., (1999) Megabase chromatin domains involved in DNA double-strand breaks in vivo. J Cell Biol. 146(5): p. 905-16.
5. Ismail, I.H. and M.J. Hendzel, (2008) The gamma-H2A.X: is it just a surrogate marker of double-strand breaks or much more? Environ Mol Mutagen. 49(1): p. 73-82.
6. Kinner, A., W. Wu, C. Staudt, et al., (2008) Gamma-H2AX in recognition and signaling of DNA double-strand breaks in the context of chromatin. Nucleic Acids Res. 36(17): p. 5678-94.
7. Hauptner, A., R. Krucken, C. Greubel, et al., (2006) DNA-repair protein distribution along the tracks of energetic ions. Radiat Prot Dosimetry. 122(1-4): p. 147-9.
8. Hauptner, A., S. Dietzel, G.A. Drexler, et al., (2004) Microirradiation of cells with energetic heavy ions. Radiat Environ Biophys. 42(4): p. 237-45.
9. Kataoka, Y., V.P. Bindokas, R.C. Duggan, et al., (2006) Flow cytometric analysis of phosphorylated histone H2AX following exposure to ionizing radiation in human microvascular endothelial cells. J Radiat Res (Tokyo). 47(3-4): p. 245-57.
10. Bocker, W. and G. Iliakis, (2006) Computational Methods for analysis of foci: validation for radiation-induced gamma-H2AX foci in human cells. Radiat Res. 165(1): p. 113-24.
11. Whalen, M.K., S.K. Gurai, H. Zahed-Kargaran, et al., (2008) Specific ATM-mediated phosphorylation dependent on radiation quality. Radiat Res. 170(3): p. 353-64.
12. Sedelnikova, O.A., D.R. Pilch, C. Redon, et al., (2003) Histone H2AX in DNA damage and repair. Cancer Biol Ther. 2(3): p. 233-5.
13. Schmid, T., G. Dollinger, A. Hauptner, et al., (in press) No evidence for a different RBE between pulsed and continuous 20 MeV protons. Radiation Research.
14. Barber, P.R., R.J. Locke, G.P. Pierce, et al., Gamma-H2AX foci counting: image processing and control software for high-content screening. in Society of Photo-Optical Instrumentation Engineers (SPIE) Conference Series. 2007.
15. Kegel, P., E. Riballo, M. Kühne, et al., (2007) X-irradiation of cells on glass slides has a dose doubling impact. DNA Repair. 6(11): p. 1692-1697.
16. Schweinfurth, Y., B. Jakob, J. Rudolph, et al., Quantification of DNA double strand breaks in cancer therapy related experiments with carbon ions 2004, Biophysics, GSI Darmstadt, Germany Darmstadt.

Author: Olga Zlobinskaya

Institute: Klinikum rechts der Isar,
Department of Radiation Oncology,
Street: Ismaninger Strasse 22
City: 81675 Munich
Country: Germany
Email: olga.zlobinskaya@lrz.tum.de

Diagnostic Reference Levels in Computed Tomography in Switzerland

R. Treier[1], A. Aroua[2], F. Bochud[2], E. Samara[2], F.R. Verdun[2], A. Stuessi[1], Ph.R. Trueb[1] and W. Zeller[1]

[1] Radiation Protection Division, Federal Office of Public Health, Bern, Switzerland
[2] University Institute of Applied Radiation Physics, CHUV and University of Lausanne, Lausanne, Switzerland

Abstract— **Over the past few years the frequency of computed tomography (CT) examinations has dramatically increased. Simultaneously, there has been also a significant increase in CT patient dose due to high-resolution imaging and application of more complex scan techniques. Since no dose limit exists for patients, the International Commission on Radiological Protection introduced the concept of diagnostic reference levels (DRL) as a means of dose optimization. The aim of this project is to collect patient doses for the most frequently applied CT protocols and to provide a realistic basis for establishing DRL in CT in Switzerland. Starting in 2007, patient doses of every Swiss radiological institute operating a CT scanner were going to be collected. Volume computed tomography dose index ($CTDI_{vol}$) and dose-length product (DLP) for standard patients was collected for selected clinical CT protocols. The 75th percentile of the $CTDI_{vol}$ and DLP distribution was calculated and compared to the proposed DRL which is partly based on the Swiss survey in 1998 and recommendations of the European Union. For standard examination of the skull/brain the 75th percentiles are higher than the proposed DRL (72 mGy vs. 60 mGy; 1180 mGy·cm vs. 1000 mGy·cm). For examination of thorax and abdomen/pelvis the 75th percentiles are close to the proposed DRL (thorax: 15 mGy vs. 15 mGy; 511 mGy·cm vs. 450 mGy·cm; abdomen/pelvis: 16 mGy vs. 15 mGy; 701 mGy·cm vs. 700 mGy·cm). In conclusion, there is always a trade-off between dose reduction and diagnostic image quality. However, especially for skull/brain examinations, optimization is still feasible. The concept of DRL provides a valuable means for practitioners and manufacturers in optimizing CT protocols.**

Keywords— **Diagnostic Reference Level, Computed Tomography, Switzerland, CTDI, DLP.**

I. Introduction

Over the past few years the frequency of computed tomography (CT) examinations has dramatically increased [1]. While technical advances of state-of-the-art multi detector-row CT scanners have improved radiation efficiency, simultaneously there has been a significant increase in patient doses due to high-resolution imaging and the application of more complex scan techniques. In Switzerland, CT accounts for approximately 30 % of the collective dose of all X-ray examinations [2].

There is no dose limit for patients when applying ionizing radiation in medicine. However, X-ray examinations must be justified and optimized. Therefore, in 1996 the International Commission on Radiological Protection (ICRP) introduced the concept of diagnostic reference levels (DRL) as a means of dose optimization [3].

The aim of this project is to collect patient doses for the most frequently applied CT protocols and to provide a realistic basis for establishing DRL in CT in Switzerland.

II. Materials and methods

The project started at the beginning of the year 2007. Patient doses of every Swiss radiological institute operating a CT scanner were going to be collected. Volume computed tomography dose index ($CTDI_{vol}$) and dose-length product (DLP) for standard patients was collected for a selection of the most frequently applied clinical CT protocols (Table 1).

Table 1 Selected CT protocols with proposed DRL for $CTDI_{vol}$ and DLP

Examination	$CTDI_{vol}$ [mGy]	DLP [mGy·cm]
Skull/Brain (standard examination)	60	1000
Brain (vascular)	80	1000
Sinus	30	450
Petrosal Bone	30	150
Cervix, Cervical Spine (soft part, bony)	30	600
Cervix (vascular)	30	600
Shoulder	30	450
Thorax (tissue, bony)	10	350
Thorax (vascular)	15	450
Thorax + Upper Abdomen	15	600
Upper Abdomen	15	300
Upper Abdomen (vascular)	20	400
Abdomen/Pelvis (standard examination)	15	700
Abdomen/Pelvis (vascular)	20	650
Pelvis (bony)	10	200
Pelvis (vascular)	15	300
Thorax/Abdomen/Pelvis	15-20	1100
Lower Limbs (vascular)	10	700
Heart (cardiovascular)	50	1000
Heart (calcium scoring)	10	150

O. Dössel and W.C. Schlegel (Eds.): WC 2009, IFMBE Proceedings 25/III, pp. 146–149, 2009.
www.springerlink.com

The 75th percentile of the $CTDI_{vol}$ and DLP distribution was calculated and compared to the proposed DRL (Table 1) which is partly based on the Swiss survey performed in 1998 [4] and recommendations of the European Union [5].

III. Results

Up to now, patient doses of 168 of total 205 CT scanners were collected. More than 60 % of all 205 CT scanners are state-of-the-art multi detector-row CT scanners with a detector array configuration of 16 rows or more (Table 2).

Table 2 Detector array configuration of CT scanners

Detector configuration	Number of scanners [%]
1-row detector array	6
2-row detector array	2
4-row detector array	20
6-row detector array	6
8-row detector array	2
10-row detector array	2
16-row detector array	31
32-row detector array	2
40-row detector array	8
64-row detector array	21

Most of the CT scanners are installed and operated in small hospitals (46 %) and private radiology institutes (32 %) and only few CT scanners in university hospitals (9 %) and cantonal hospitals (13 %).

A. Standard examination of skull/brain

For a standard examination of the skull/brain the $CTDI_{vol}$ and DLP distribution is approximately normally distributed with a few outliers at high doses, as shown in Figures 1a and 1b. The 75th percentile of the $CTDI_{vol}$ and DLP distribution is higher than the proposed DRL (72 mGy vs. 60 mGy; 1180 mGy·cm vs. 1000 mGy·cm). 52 % of all $CTDI_{vol}$ values and 39 % of all DLP values are higher than the corresponding DRL.

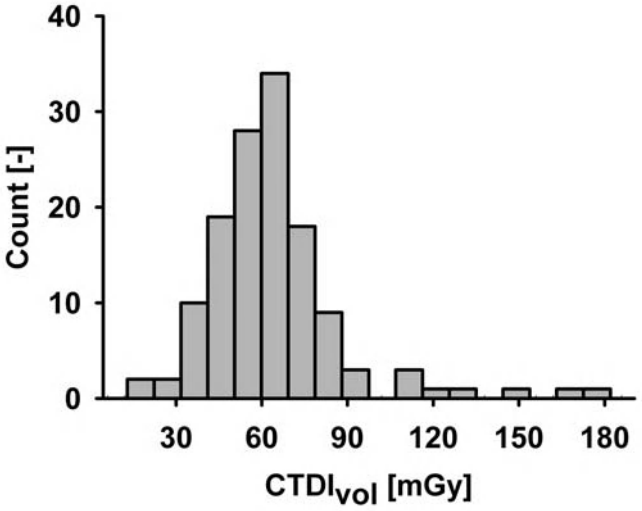

Figure 1a $CTDI_{vol}$ distribution for standard examination of the skull/brain

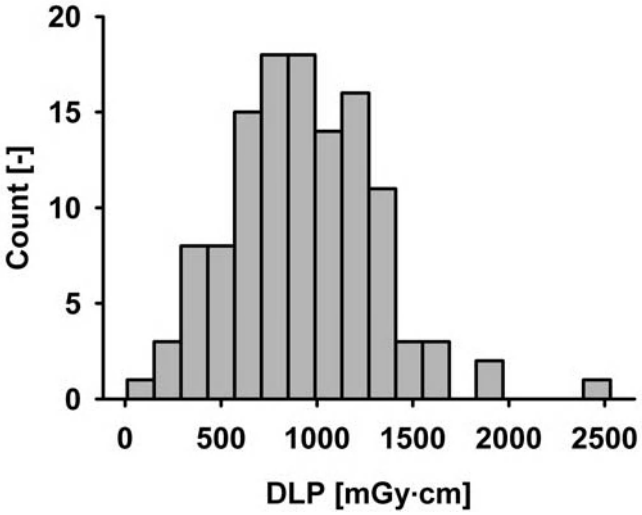

Figure 1b DLP distribution for standard examination of the skull/brain

B. Examination of thorax

The $CTDI_{vol}$ and DLP distribution for examination of the thorax is broader than those for standard examinations of the skull/brain (Figures 2a and 2b). However, the 75th percentiles are close to the proposed DRL (15 mGy vs. 15 mGy; 511 mGy·cm vs. 450 mGy·cm). 25 % of all $CTDI_{vol}$ values and 41 % of all DLP values are higher than the corresponding DRL.

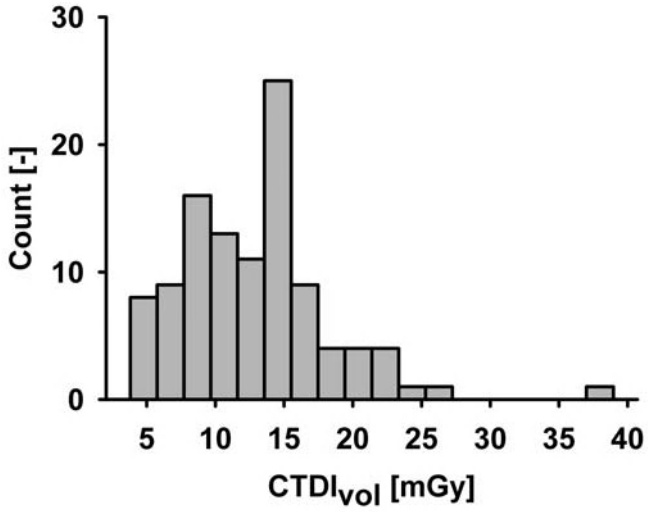

Figure 2a $CTDI_{vol}$ distribution for examination of the thorax

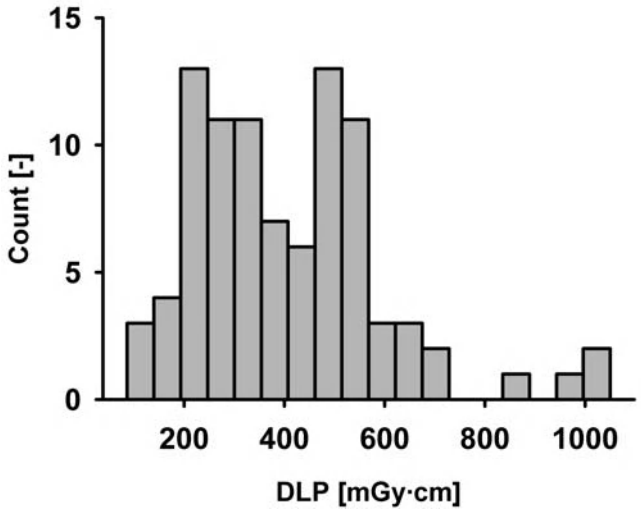

Figure 2b DLP distribution for examination of the thorax

C. Standard examination of abdomen/pelvis

The $CTDI_{vol}$ distribution is approximately normally distributed whereas the DLP distribution is more spread (Figures 3a and 3b). Similarly to examination of the thorax the 75th percentiles are close to the proposed DRL (16 mGy vs. 15 mGy; 701 mGy·cm vs. 700 mGy·cm). 32 % of all $CTDI_{vol}$ values and 25 % of all DLP values are higher than the corresponding DRL.

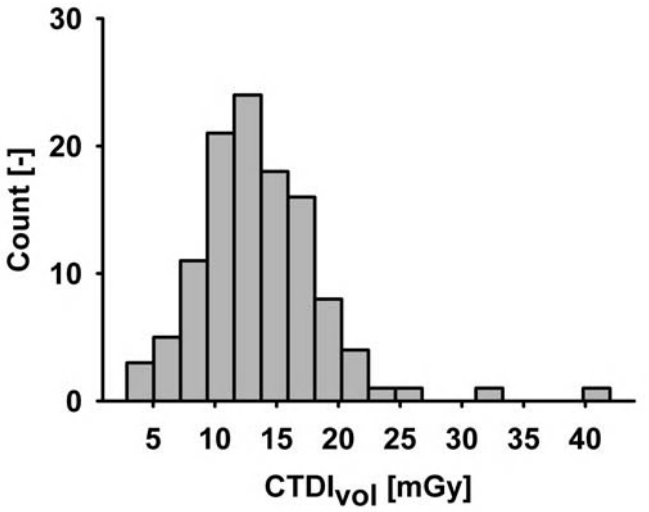

Figure 3a $CTDI_{vol}$ distribution for standard examination of the abdomen/pelvis

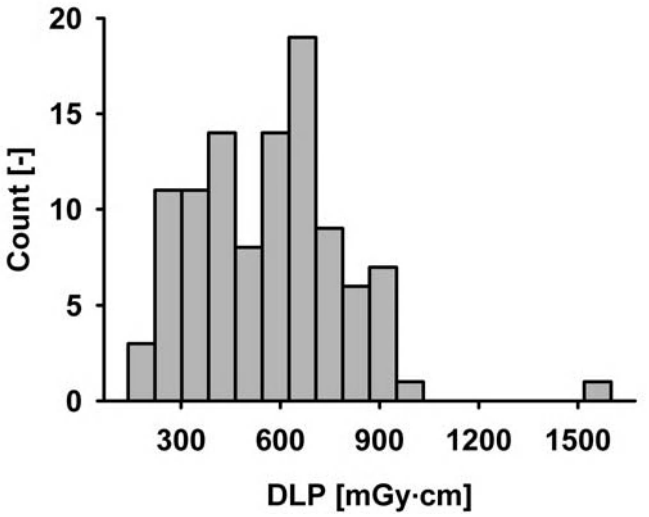

Figure 3b DLP distribution for standard examination of the abdomen/pelvis

IV. Discussion and conclusion

The amount of patient dose data collected so far varies strongly between the different CT examination protocols as defined in Table 1. In almost every radiological institute standard examinations of the skull/brain and abdomen/pelvis as well as examination of the vascular system of the thorax are performed in clinical routine. However, for establishing DRL in CT in Switzerland all of the acquired data must be carefully analyzed. Especially for cardiac CT, an examination that is being more and more frequently performed, the establishment of DRL is of major importance.

There is always a trade-off between dose reduction and sufficient diagnostic image quality. In the human brain a high spatial image resolution together with a high signal-to-noise ratio is essential for the detection of small anatomical structures. Nevertheless, results show that there is still a high potential of optimization.

The broad distributions of $CTDI_{vol}$ and DLP values indicate that the concept of DRL has not yet been correctly applied for CT examinations in clinical routine. Clinical audits will help the radiological institutes in controlling and optimizing their CT protocols in order to minimize patient doses.

References

1. Aroua A, Trueb P, Vader JP et al. (2007) Exposure of the Swiss population by radiodiagnostics; 2003 review. Health Phys 92(5):442–448
2. Trueb PR (2004) Kompendium für ärztliche Strahlenschutz-Sachverständige. Haupt Verlag, Bern
3. International Commission on Radiological Protection (1996) ICRP Publication 73: Radiological Protection and Safety in Medicine, 73. Pergamon Press, Oxford
4. Aroua A, Besançon A, Buchillier-Decka I et al (2004) Adult reference levels in diagnostic and interventional radiology for temporary use in Switzerland. Radiat Prot Dosimetry 111(3):289-295
5. European Commission, Radiation Protection Report 109 (1999) Guidance on Diagnostic Reference Levels (DRLs) for Medical Exposure

Author: Reto Treier
Institute: Federal Office of Public Health
Radiation Protection Division
Street: Schwarzenburgstrasse 165
City: CH-3097 Liebefeld
Country: Switzerland
Email: reto.treier@bag.admin.ch

A new method to measure shielding properties of protective clothing materials

L. Büermann

Physikalisch-Technische Bundesanstalt, Braunschweig, Germany

Abstract— **A new experimental method has been developed to measure the attenuation properties of materials used for radiation shielding garments worn by workers and patients during diagnostic x-ray imaging. In particular, the method is well suited for lead-free or lead-reduced composite materials because it includes the measurement of the secondary radiation generated by photon interactions inside the material. The new method is much easier to use than the classically applied "broad beam geometry" and is characterized by significantly lower standard uncertainties. The method was adopted in the German standard DIN 6857-1.**

Keywords— **radiation shielding garments, protective clothing, attenuation properties, lead equivalent value, broad-beam geometry.**

I. Introduction

Protective clothing for workers at medical x-ray facilities such as aprons, gloves and mittens, and protective devices for the patient, such as gonad aprons, scrotum, ovary and shadow shields shall comply with the requirements of the international standard IEC 61331-3 [1]. This standard deals with general requirements such as standard sizes, particular design features, minimum attenuation properties of materials, marking and standardized forms of statements of compliance with the standard. In particular, the attenuation properties of the protective materials shall be characterized by their values of the attenuation equivalent in defined thicknesses of lead of 0.25 mm, 0.35 mm, 0.5 mm and 1 mm.

Standardized methods for the determination of attenuation properties of materials are given in IEC 61331-1 [2]. According to the standard, the attenuation shall be measured in terms of the quantity air kerma rate in defined x-ray radiation qualities as given in the standard. Two different measuring arrangements are described in the standard, namely the "narrow-beam geometry" (NBG) and the "broad-beam geometry" (BBG) (see Fig. 1). The NBG is designed to measure the attenuation of the x-ray beam only due to primary photons. Therefore it is important that secondary photons such as fluorescence photons or Compton scattered photons from the test object cannot reach the detector. This is assured by the NBG sketched in Fig. 1. Attenuation values obtained in the NBG are close to those values which can be calculated by the linear attenuation law using photon mass attenuation coefficients of the material under test. In contrast, the BBG is specially designed to include the detection of secondary photons emitted by the material sample. Therefore the detector is positioned at a distance close to the test object, which is a large sheet of the sample material.

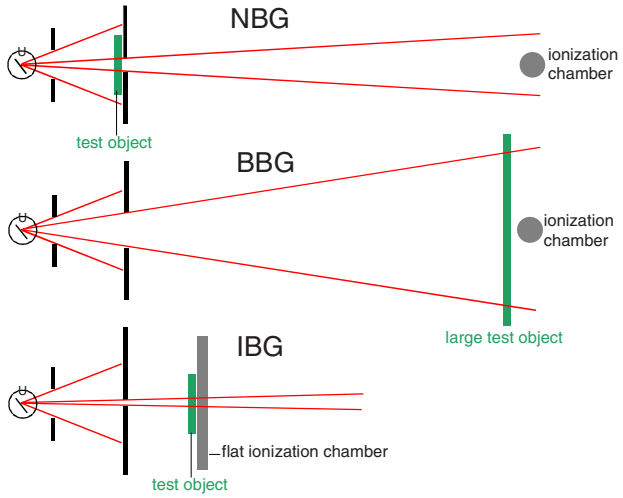

Fig. 1 Sketches of the narrow-beam geometry (NBG), the broad-beam geometry (BBG), and the inverse broad-beam geometry (IBG).

It is described in the standard that the lead equivalent thickness of materials used for radiation shielding garments shall be measured in the NBG. This measuring method is easy to use and can be performed with low standard uncertainties. As long as the material under test is composed of composites with atomic numbers Z close to that of lead (Z=82), it will have the same shielding effect as the lead equivalent thickness measured in the NBG. However, the vast majority of commercial shielding garments are made of lead-reduced or lead-free composites which contain large amounts of elements with atomic numbers close to Z=50 such as Cd, In, Sn, Sb, Cs, Ba or Ce. Eder *et al.* [3] and Schlattl *et al.* [4] were the first to point out that the lead equivalent value measured in NBG is not well suited for rating the protection properties of the lead-reduced or lead-free materials. They noticed that fluorescence radiation of

O. Dössel and W.C. Schlegel (Eds.): WC 2009, IFMBE Proceedings 25/III, pp. 150–153, 2009.
www.springerlink.com

the lower-*Z* materials can significantly reduce the shielding capabilities of such materials. Therefore, it is recommended that the characterization of the shielding potential of such materials should be done in the BBG in order to include the secondary radiations in the attenuation measurements.

II. The inverse broad-beam geometry

Unfortunately, it is difficult to realize the recommended BBG in practice. From Fig. 1 it becomes clear that large-sized material samples are needed, including thin sheets of lead which must be irradiated in a large homogeneous radiation field. Large homogeneous field sizes can only be realized far away from the focus of the x-ray tube which in turn reduces the available maximum air kerma rates. Low dose rates require high-sensitivity detectors which must be capable of measuring the dose rates in the attenuated beams. Moreover, the detector must have a low dependence on the air kerma response as a function of the photon energy and angle of incidence. Such demanding requirements can only be approximately fulfilled by spherical ionization chambers with air equivalent walls and a measuring volume large enough to yield a satisfying signal-to-noise ratio. On the other hand, the chamber should be as small as possible in order to be well suited for the principle of the measurements in BBG which requires a detector positioned close to the test object, as shown in Fig. 1.

In view of the numerous practical disadvantages of the BBG, a new measuring arrangement was designed and established at the Physikalisch-Technische Bundesanstalt (PTB) in Germany which is now called the “inverse broad-beam geometry” (IBG). In contrast to the classical BBG which uses a broad beam and a small detector, the IBG is characterized by a narrow beam and a large flat ionization chamber as shown in Fig. 1. The idea for such an arrangement originated from a well-known geometry frequently used in Monte Carlo simulations to obtain the spectral particle fluence at a reference point behind a large absorber plate irradiated with a broad parallel particle beam. Instead, to simulate the real situation which would demand long calculation times because most of the simulated particles would not reach the small detector volume, it is much more efficient to apply the radiation reciprocity principle [5], which in this case is a particle beam with an infinitesimally small diameter (“needle beam”) impinging on the absorber plate, and on the opposite side, there is an infinite plane counting all particles passing the plane. In the latter geometry, each primary and secondary particle leaving the absorber plate is counted. The equivalence of both situations can be made plausible when treating each point of the absorber plate, which faces the detector, as a new (secondary) source point with the same emission properties.

The use of the IBG arrangement has a lot of advantages over to the classical BBG. The experimental set-up is much easier. Only a small sheet of the sample material is needed and beams of small diameters are sufficient. There is no special requirement for the cross sectional homogeneity of the beam. The detector can be positioned closer to the focal spot of the x-ray tube and hence larger maximum dose rates can be achieved at the point of measurement. It can be expected that the standard uncertainties of measurements in the IBG arrangement are significantly lower than those in the BBG arrangement. The purpose of this paper was to verify the results obtained from attenuation measurements using the new method by comparison with Monte Carlo calculations. The IBG arrangement was realized and air kerma rate attenuation measurements were made in x-ray beams of known photon fluence spectra for thin lead sheets of different thicknesses and a silver sheet. The measured results were compared with Monte Carlo simulations.

III. Materials and methods

The radiation qualities recommended in the German standard DIN 6857-1 [5] shown in Table 1 were established.

Table 1 Standardized radiation qualities according to DIN 6857-1 [5]. The last digit in brackets of the total filtration is the standard uncertainty.

Tube voltage kV	Total filtration mm Cu	Half value layer mm Al	Mean energy keV
50	0.082(2)	1.23	32.70
60	0.101(2)	2.12	37.79
80	0.155(2)	4.18	47.83
100	0.256(2)	6.64	57.63
120	0.406(4)	8.93	66.62
150	0.717(5)	11.66	80.04

The photon fluence spectra of the radiation qualities were measured with a high-purity germanium spectrometer. Results are shown in Fig. 2. The half-value layers and mean energies listed in Table 1 were obtained from these measurements.

Air kerma rates in the IBG arrangement were measured with a flat cylindrical ionization chamber of type PTW TM34060 with an outer diameter and height of 10.3 cm and 1.3 cm, respectively. The wall consists of about 60 mg/cm^2 air equivalent material (corresponding to 50 cm of air at normal pressure). The dependence on the air kerma response of the TM34060 was measured for ISO 4037 [7] narrow beam radiation qualities for tube voltages between 10 kV and 150 kV. Results are presented in Fig. 3 which show that the response varies by less than 5 % in the range

from 20 keV to 150 keV and hence, the chamber is well suited for measurements in the IBG arrangement.

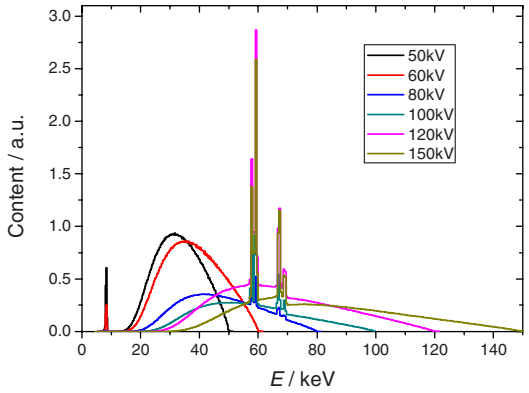

Fig. 2 Photon fluence spectra of the x-radiation qualities listed in Table1, measured with a high-purity germanium detector

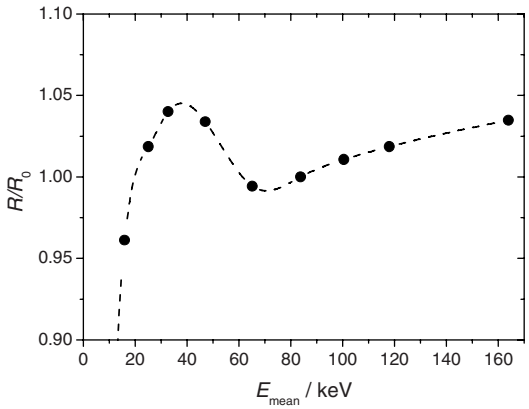

Fig. 3 Air kerma response, R, of the TM34060 chamber as a function of the mean energy, E_{mean}, of the ISO narrow qualities for tube voltages between 10 kV and 150 kV, normalized to the response R_0 at 100 kV.

Air kerma rates were measured in the non-attenuated and attenuated beams of the radiation qualities listed in Table 1 in the IBG arrangement for a set of thin lead sheets of thicknesses 100(2) µm, 244(4) µm and 297(5) µm and for a silver sheet of 200(5) µm thickness. The sheets were cut into squares of 5 cm x 5 cm. The beam diameter at the reference point of the chamber was 2 cm.

Monte Carlo (MC) simulations were made with the EGSnrc [8] user codes FLURZnrc and DOSRZnrc [9] to calculate photon fluence spectra behind the different absorbers in the IBG arrangement and to calculate the corresponding air kerma ratios of the non-attenuated and attenuated x-ray beams. MC input data for the materials were produced with the PEGS4 [8] preprocessor using the "XCOM" option, which generates interaction coefficients consistent with the NIST data base [10]. Photons were transported down to 1 keV and electrons down to 10 keV. The photon transport parameters were set to include bound-Compton and Rayleigh scattering and - more important for the current simulations – atomic relaxations. Sketches of the geometries used in the simulations are shown in Fig. 4.

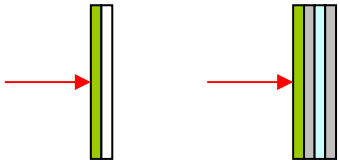

Fig. 4 Sketches of the geometries used in the FLURZnrc (left) and DOSRZnrc (right) simulations.

The FLURZnrc geometry was simply defined by a narrow photon beam impinging on the axis of two cylindrical discs of 40 cm diameter the first filled with the sample material and the other used for defining the volume in which the spectral photon fluence was calculated. The DOSRZnrc geometry was defined by a narrow beam of photons impinging on the axis of a set of four cylindrical discs of 10 cm diameter the first filled with the sample material, the second and fourth filled with "solid air" (air of density 1 g/cm^3), and the third filled with air at normal pressure (density 1.204 mg/cm^3). The latter geometry roughly models the attenuation properties of the TM34060 ionization chamber.

IV. Results and Conclusion

Two examples of calculated photon fluence spectra for the 100 kV quality behind 100 µm of lead and 200 µm of silver are shown in Fig. 5. The incident primary spectrum is shown in black, the attenuated primary in red, and the attenuated total (primary and secondary photons) in blue. Cleary visible are the W-K fluorescence peaks of the tube anode, the Pb-K and L fluorescence peaks behind the lead layer and the Ag-K-fluorescence peaks behind the silver layer. From these spectra it becomes clear that the fluorescence photons emitted from the absorber materials contribute significantly to the total spectrum.

Results of the comparison of measured (IBG) and calculated (DOSRZnrc) air kerma ratios of the non-attenuated and attenuated beams behind 244 µm of Pb and 200 µm of Ag normalized to the values obtained behind 100 µm of Pb are presented in Table 2. The normalization is necessary to

exclude uncertainties due to the very low energy part of the measured primary spectra shown in Fig. 2, especially those of the 50 kV and 60 kV qualities which have significant contributions below 10 keV. The data in Table 2 show that there is a reasonable agreement between experimental (IBG) and calculated (MC) values within a few percent, the maximum deviation being 5 %.

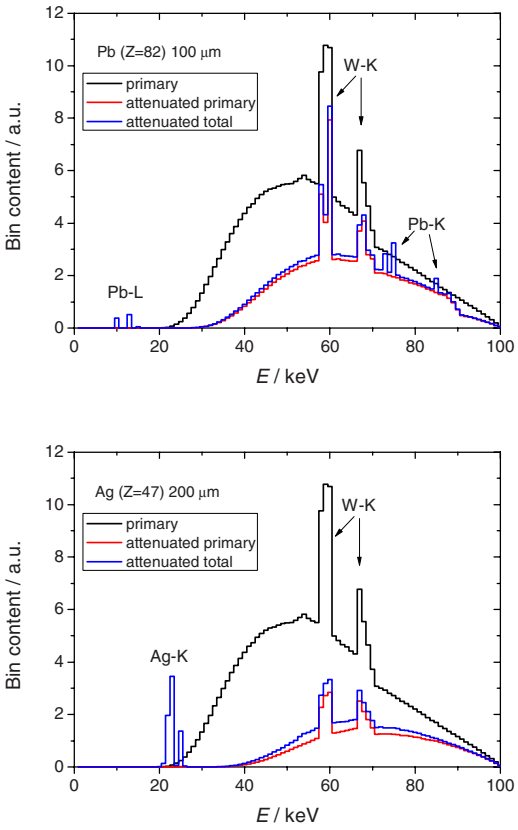

Fig. 5 Photon fluence spectra of the 100 kV primary and attenuated primary and total beams behind 100 µm of Pb (upper) and 200 µm of Ag as obtained with FLURZnrc using the geometry shown in Fig. 4.

Care has to be taken with uncertainties connected with spectral contributions below about 15 keV (e.g. Fig. 2 and Fig. 5), because ionization chambers suited to measure air kerma rates for photon energies up to 150 keV usually have a significant decrease in their response below about 20 keV (Fig. 3) due to photon absorption in the wall. On the other hand, it may not be necessary to include such low-energy photons into the attenuation measurements, because they may not be relevant to the practical shielding properties of the material due to their low penetrability. The general conclusion is that the inverse broad beam geometry yields reasonable results and is well suited for measurements of attenuation properties of materials irradiated by broad beams. Further studies are under way to examine the uncertainties of the method as to whether lead equivalent thicknesses of lead-free or lead-reduced materials have been determined.

Table 2 Comparison of the measured (IBG) and calculated (MC) air kerma ratios of the primary and attenuated beam and the ratio IBG/MC for the radiation qualities listed in Table 1 for 244 µm Pb and 200 µm Ag.

Qual.	Pb-244/Pb-100			Ag-200/Pb100		
kV	IBG	MC	**Ratio**	IBG	MC	**Ratio**
50	9.64	9.72	**0.99**	1.46	1.47	**0.99**
60	5.45	5.40	**1.01**	1.63	1.65	**0.99**
80	2.98	2.84	**1.05**	1.48	1.51	**0.98**
100	2.22	2.15	**1.03**	1.30	1.35	**0.96**
120	1.96	1.95	**1.01**	1.17	1.23	**0.95**
150	1.74	1.72	**1.01**	1.06	1.05	**1.00**

References

1. IEC, Protective devices against medical X-radiation-Part 3: Protective clothing and protective devices for gonads, IEC 61331-3 (1998)
2. IEC, Protective devices against medical X-radiation-Part 1: Determination of attenuation properties of materials, IEC IEC 61331-1 (1994)
3. Eder H, Panzer W, Schöfer H (2005) Ist der Bleigleichwert zur Beurteilung der Schutzwirkung bleifreier Röntgenschutzkleidung geeignet? Röfo Fortschr Röntgenstr 177: 399-404
4. Schlattl H, Zankl M, Eder H (2007) Shielding properties of lead-free protective clothing. Med Phys. 34(11): 4270-80
5. King L V (1912) Absorption problems in radioactivity. Philos. Mag. 23: 242-250
6. DIN, Strahlenschutzzubehör bei medizinischer Anwendung von Röntgenstrahlen – Teil 1: Bestimmung der Abschirmeigenschaften von bleifreier und bleireduzierter Schutzkleidung, DIN 6857-1 (2009)
7. ISO, X and gamma reference radiation for calibrating dosemeters and doserate meters and for determining their response as a function of photon energy – Part 1: Radiation characteristics and production methods, ISO 4037-1 (1996)
8. Kawrakow I and Rogers D W O (2000) The EGSnrc code system: Monte Carlo simulation of electron and photon transport. Technical Report PIRS-701 (Ottawa, Canada: National Research Council of Canada) http://www.irs.inms.nrc.ca/EGSnrc/pirs701.pdf
9. Rogers D W O, Kawrakow I, Seuntjens J P, Walters B R B (2000) NRC user codes for EGSnrc. Technical Report PIRS-702 (Ottawa, Canada: National Research Council of Canada) http://www.irs.inms.nrc.ca/EGSnrc/pirs702.pdf
10. XCOM: Photon Cross Sections Database, NIST Standard Reference Database 8 (XGAM), available at http://physics.nist.gov/PhysRefData/Xcom/Text/XCOM.html

Corresponding author:

Author: Ludwig Büermann
Institute: Physikalisch-Technische Bundesanstalt
Street: Bundesallee 100
City: Braunschweig
Country: Germany
E-mail: Ludwig.bueermann@ptb.de

Radiation Response of Normal Tissues and Tumors to Carbon Ion Irradiation

C.P. Karger[1], P. Peschke[2] M. Scholz[3], P. Huber[2], J. Debus[4]

[1] German Cancer Research Center/Dept. of Medical Physics in Radiation Oncology, Im Neuenheimer Feld 280, Heidelberg, Germany
[2] German Cancer Research Center/Clinical Cooperation Unit Radiation Oncology, Im Neuenheimer Feld 280, Heidelberg, Germany
[3] Gesellschaft für Schwerionenforschung/Dept. of Biophysics, Planckstr. 1, Darmstadt, Germany
[4] University Hospital of Heidelberg/Dept. Radiation Oncology, Im Neuenheimer Feld 400, Heidelberg, Germany

Abstract— **Carbon ions show an increased relative biological effectiveness, which increases with penetration depth. This differential RBE between peak and plateau may be used to increase the biological effective dose in the tumor while still sparing the surrounding normal tissue. For clinical application, a RBE-model such as the local effect model (LEM) is required to describe the dependence of RBE on dose and LET. To validate these models, experiments in normal tissues and tumors are necessary. The spinal cord and a prostate tumor in the rat were irradiated with photons and carbon ions using different fractionation schedules and dose response curves were determined. In the spinal cord experiment, the LEM overestimated the RBE in the plateau for small doses and underestimated the RBE in the Bragg-peak region over the whole dose range. A significant fractionation effect was found only for the plateau region. For the prostate tumor, local control could be achieved and significantly increased RBE-values were found for single and split doses. The acquired data contribute to the validation of the LEM and the quantification of the involved uncertainties.**

Keywords— **heavy ion radiotherapy, relative biological effectiveness (RBE), radiation tolerance, normal tissue, Tumors**

I. Introduction

Heavy ions show an inverted depth dose profile, the so-called Bragg-curve, which deposits most of the dose at the end of the particle range. By superimposing several monoenergetic Bragg-curves, a spread-out Bragg-Peak (SOBP) can be produced which covers the extension of the tumor in depth, while still preserving an advantageous dose ratio between tumor and normal tissue [1,2,3].

As the linear energy transfer (LET) of heavy ions increases significantly towards the end of their range, heavy ions are biological more effective in the peak- than in the plateau-region. This is considered by introducing the relative biological effectiveness (RBE), which is defined as the ratio of a photon dose to the corresponding iso-effective ion dose for a given endpoint:

$$RBE = \left.\frac{D_{photon}}{D_{ion}}\right|_{\text{samend point}} \quad (1)$$

Therefore, dose has to be prescribed in terms of biological equivalent dose (= absorbed Dose x RBE) rather than absorbed dose. It is the difference of the increased RBE between the peak and the plateau regions, which potentially increases the therapeutic effectiveness of heavy ion therapy relative to low LET radiation [3].

In clinical practice, biological homogeneous dose distribution are required and hence a RBE-model has to be included into the treatment planning system. One of these models is the so-called local effect model (LEM) [4], which has been clinically applied for more than 10 years at the carbon ion radiotherapy project at the Gesellschaft für Schwerionenforschung (GSI) in Darmstadt (Germany). The RBE-model must describe the rather complex dependence of the RBE on LET, dose per fraction, the fragment spectra of the projectiles, the cell or tissue type irradiated as well as on the regarded biological endpoint.

To investigate the dependence of RBE on dose per fraction and LET and to test the prediction of the LEM, the radiation response of the spinal cord and a prostate tumor model was investigated in the rat.

II. Materials and methods

A. Spinal cord

The cranial segment of the spinal cord of the rat was irradiated with 1, 2, 6 or 18 fractions of photons or ^{12}C-ions, respectively. Plateau irradiations were performed in the entrance region of a 270 MeV/u Bragg-peak, while for the peak irradiations a 10 mm spread-out-Bragg-Peak of 140 MeV/u was used (fig. 1). Animals were followed up for 300 days after irradiation. Biological endpoint was the onset of paresis grade II within 1 year after irradiation. Dose response curves were calculated for each irradiation experiment and D_{50}-values (dose at 50% complication probability) were determined.. Based on these D_{50}-values, the RBE and the α/β-parameters were calculated. The RBE-values were compared with predictions of the local effect model [5].

O. Dössel and W.C. Schlegel (Eds.): WC 2009, IFMBE Proceedings 25/III, pp. 154–157, 2009.
www.springerlink.com

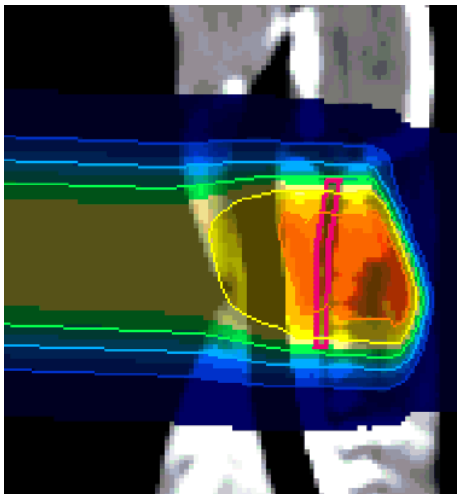

Fig. 1 Dose distribution for SOBP-irradiations of the spinal cord

B. Prostate carcinoma

To investigate the radiation response of tumors, an experimental prostate tumor (AT1-R3327, diameter 9 mm) transplanted to the hind limb of the rat was irradiated with 1, 2 or 6 fractions of photons or carbon ions, respectively. For carbon ions, the tumor was located in the middle of a 20 mm-SOBP. Aim of the experiment is to determine dose response curves for the endpoint "local control at 1 year" and to compare the derived RBE-values with predictions of the LEM.

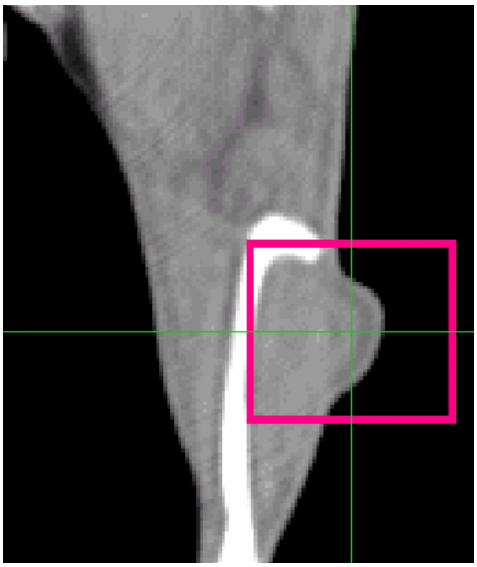

Fig. 2 Tumor and target volume for the carbon ion irradiations

III. Results

A. Spinal cord

Latency was found to be significantly shorter for the peak than for the plateau irradiations. For the peak irradiations, no dose dependence of the latency was observed while at least for some of the photon and carbon ion plateau irradiations, a decreasing latency with increasing dose was found.

The experimentally determined RBE-values for 1, 2, 6 and 18 fractions were 1.44±0.08, 1.37±0.05, 1.33±0.02 and 1.42±0.02 for the plateau- and 1.77±0.06, 2.17±0.06, 2.97±0.05, and 5.04±0.08 for the peak-irradiations. The respective predictions by the LEM were 1.14, 1.19, 1.37, and 1.72 for the plateau- and 1.28, 1.61, 2.35, and 3.80 for the peak irradiations. Fig. 3 shows the measured and calculated RBE-values as a function of the dose per fraction.

The measured α/β-values were 2.8±0.4 Gy for photons, 2.1±0.4 Gy for the plateau and 37.0±5.3 Gy for the peak-irradiations, respectively.

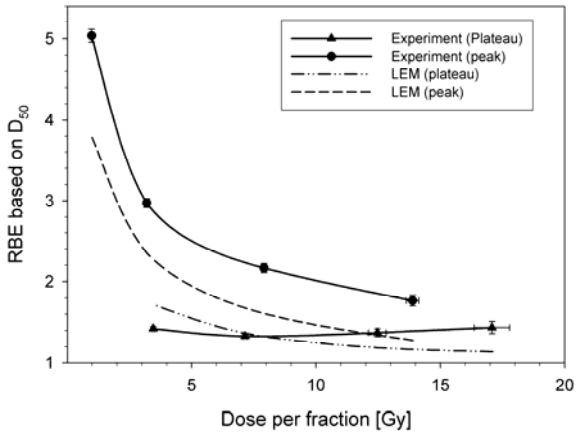

Fig. 3Comparison of measured and calculated RBE

B. Prostate carcinoma

First experiments show that it is possible to achieve local control for this experimental tumor system. For the tumor irradiations, three different types of radiation response was seen (fig. 4): i) uncontrolled growth for small irradiation doses, ii) temporary reduction of tumor size, followed by continuation of uncontrolled growth, and iii) reduction of tumor size and maintenance of control until the end of follow-up. Preliminary data show a significantly increased RBE larger than 2 for single and split doses.

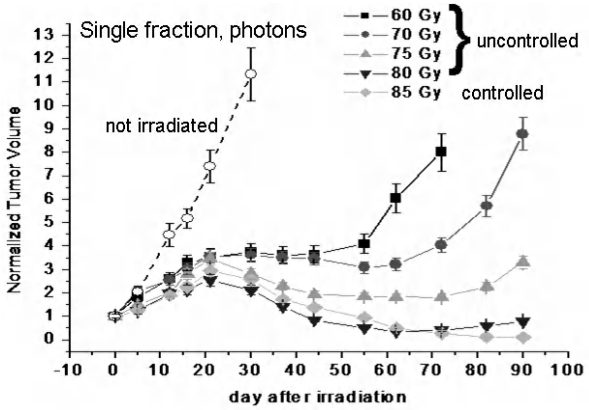

Fig. 4 Tumor growth curves after different irradiation doses

IV. Discussion

A. Spinal cord

High LET radiation is associated with a reduced latency time and with a lack of dose dependence. The latency for low-LET irradiation is significantly larger. Regarding the α/β-values, carbon ion plateau irradiations show a similar fractionation effect as photon irradiations while carbon ion peak irradiation exhibit no significant fractionation effect. With respect to LET, RBE-values for spinal cord and brain for single fraction are consistent (tab. 1).

Table 1 RBE-values for spinal cord and brain for single fractions

Endpoint	LET [keV/μm]	SOBP [cm]	RBE	Ref.
Rat brain (20 months)				
T1-w MRI	155 (60-245)	< 0.2	1.95±0.20	[6]
T2-w MRI			1.88±0.18	
Spinal cord of the rat (10 months)				
Myelopathy °II	125±25	1	1.77±0.06	[5]
	80	4	1.48±0.12	[7]
	70	6	1.38	[8]
	13	plateau	1.44±0.12	[5]
	10	plateau	1.45±0.17	[7]

For small doses per fraction, we found an overestimation of the RBE by the LEM, which appears to be safe for clinical application. In the peak, the calculated RBE was significantly underestimated suggesting that the biological effective dose in the tumor is higher than expected, although the different biological properties of tumors may lead to somewhat different RBEs and hence to different biological effective doses. Clinically, it is important to know, whether the RBE is over- or underestimated in the region proximal to the SOBP, where combinations of high physical doses and increased RBEs may occur. To investigate this, we started measuring a RBE-depth dose profile for a clinically relevant SOBP with 6 cm extension in depth.

Regarding the underestimation of the RBE in the peak region, an improved version of the LEM has been developed [9], which better describes these data. From a clinical point of view, however, there is no indication that the biological effective dose calculated on basis of the original LEM model is significantly wrong [10,11]. This discrepancy has to be further analyzed and one reason might be that different biological parameter-values may be needed to describe the radiation response of rats and humans. Nevertheless, the comparison of measured and calculated RBEs indicate that the LEM correctly describes the relative dependences of RBE on dose per fraction and LET and that biological optimization leads to rather homogeneous biological effective dose distributions..

B. Prostate carcinoma

With the established tumor model, it is possible to acquire dose response curves and RBE-values. In contrast to with growth-delay experiments, this represents a clinically more relevant endpoint. The currently investigated tumor model is an anaplastic, hormone-independent tumor. The investigations will be extended to a well differentiated hormone-dependent subline of the same tumor to investigate the impact of these biological parameters on RBE.

V. Conclusions

The dependence of the RBE on biological properties of the irradiated tissues means that the therapeutic benefit of high-LET radiation may depend on the combination of the normal- and tumor-tissue type. With the established animal models, it is possible to determine RBE-values and to investigate the differential RBE between normal and tumor tissues. In this way the therapeutic benefit of high-LET radiation might be experimentally shown as a prove of principle.

References

1. Jäkel O, Schulz-Ertner D, Karger CP et al. (2003) Heavy ion therapy: status and perspectives. *Technol Cancer Res Treat* 2:377-387
2. Karger CP, Jäkel O (2007) Current status and new developments in ion therapy. *Strahlenther Onkol* 183:295-300
3. Jäkel O, Karger CP, Debus J (2008) The Future of Heavy Ion Radiotherapy. Med Phys 35:5653-5663

4. Scholz M, Kellerer AM, Kraft-Weyrather W et al. (1997) Computation of cell survival in heavy ion beams for therapy. The model and its approximation. *Radiat Environ Biophys* 36:59-66
5. Karger CP, Peschke P, Sanchez-Brandelik R et al. (2006) Radiation tolerance of the rat spinal cord after 6 and 18 fractions of photons and carbon ions: Experimental results and clinical implications. *Int J Radiat Oncol Biol Phys* 66:1488-1497
6. Karger CP, Debus J, Peschke P et al. (2002) Dose-response curves for late functional changes in the normal rat brain after single carbon-on doses evaluated by magnetic resonance imaging: influence of follow-up time and calculation of relative biological effectiveness. *Radiat Res* 158:545-555
7. Leith JT, McDonald M, Powers-Risius P et al. (1982) Response of rat spinal cord to single and fractionated doses of accelerated heavy ions. *Radiat Res* 89:176-193
8. Okada S, Okeda R, Matsushita S et al. (1998) Histopathological and morphometric study of the late effects of heavy-ion irradiation on the spinal cord of the rat. *Radiat Res* 150:304-315
9. Elsässer T, Krämer M, Scholz M (2008) Accuracy of the local effect model for the prediction of biologic effects of carbon ion beams in vitro and in vivo. Int J Radiat Oncol Biol Phys 3:866-873
10. Schulz-Ertner D, Karger CP, Feuerhake A et al. (2007) Effectiveness of carbon ion radiotherapy in the treatment of skull-base chordomas. *Int J Radiat Oncol Biol Phys* 68:449-457
11. Schlampp I, Karger CP, Jäkel O et al. (2008) Clinical Validation of the Local Effect Model (LEM) in the Treatment Planning of Carbon Ion RT in Patients with Skull Base Tumors. *Int J Radiat Oncol Biol Phys* 72 (Suppl. 1):229

Address of the corresponding author:

Christian Karger
German Cancer Research Center (DKFZ)
Im Neuenheimer Feld 280
69120 Heidelberg
Germany
c.karger@dkfz.de

The Impact of the 2007 Recommendations of the International Commission on Radiological Protection (ICRP) in Medical Applications

C.H. Clement[1]

[1] Scientific Secretary, International Commission on Radiological Protection
PO Box 1046, Station B, 280 Slater Street, Ottawa, Canada K1P 5S9

Abstract— **The International Commission on Radiological Protection (ICRP) is an independent registered charity established in 1928 to advance for the public benefit the science of radiological protection, in particular by providing recommendations and guidance on all aspects of protection against ionizing radiation. Its system of protection is used by governments, practitioners, and other experts worldwide. Recently, ICRP produced a new set of fundamental recommendations, The 2007 Recommendations of ICRP, ICRP Publication 103, replacing those of 1990. ICRP Publication 105, Radiological Protection in Medicine, soon followed, to underpin the 2007 Recommendations with regard to the medical exposure of patients, including their comforters and carers, and volunteers in biomedical research. It addresses the proper application of the fundamental principles (justification, optimization of protection, and application of dose limits) of the 2007 Recommendations to these individuals. With regard to medical exposure of patients, it is not appropriate to apply dose limits or dose constraints, because such limits would often do more harm than good. Often, there are concurrent chronic, severe, or even life-threatening medical conditions that are more critical than the radiation exposure. The emphasis is then on justification of the medical procedures and on the optimization of radiological protection. In diagnostic and interventional procedures, justification of procedures (for a defined purpose and for an individual patient), and management of the patient dose commensurate with the medical task, are the appropriate mechanisms to avoid unnecessary or unproductive radiation exposure. Equipment features that facilitate patient dose management, and diagnostic reference levels de-rived at the appropriate national, regional, or local level, are likely to be the most effective approaches. In radiation therapy, the avoidance of accidents is a predominant issue. With regard to comforters and carers, and volunteers in biomedical research, dose constraints are appropriate.**

Keywords— **Radiological, Protection, Recommendations, ICRP, Medicine.**

I. Introduction

The International Commission on Radiological Protection (ICRP) is an independent registered charity established in 1928 to advance for the public benefit the science of radiological protection, in particular by providing recommendations and guidance on all aspects of protection against ionizing radiation. Its system of protection is used by governments, practitioners, and other experts worldwide.

Recently, ICRP produced a new set of fundamental recommendations, The 2007 Recommendations of the International Commission on Radiological Protection, ICRP Publication 103 [1], replacing those of 1990. ICRP Publication 105, Radiological Protection in Medicine [2], soon followed, to underpin the 2007 Recommendations with regard to the medical exposure of patients, including their comforters and carers, and volunteers in biomedical research.

ICRP Publication 105 addresses the proper application of the fundamental principles (justification, optimization of protection, and application of dose limits) of the 2007 Recommendations to these individuals. This paper is primarily a summary of ICRP Publication 105.

II. The use of ionising radiation in medicine

More people are exposed to ionising radiation from medical practice than from any other human activity. Recently, for the first time in history medical exposures in countries with advanced healthcare systems are as high as those from natural background radiation. In the United States, it has been estimated that as of 2006 medical doses made up 48% of the effective dose per individual, a six-fold increase from the early 1980's [3]. Furthermore, doses to patients for the same type of examination can vary considerably, suggesting that there is considerable scope for management of patient dose [4]. At the same time, accidental over (and under) medical exposures continue to take place, and there will always be room to reduce the frequency of these incidents.

III. Biological effects

The biological effects of radiation can be grouped into two types: deterministic effects (tissue reactions) and stochastic effects (cancer and heritable effects).

Deterministic effects result when many cells in an organ or tissue are killed, and are only clinically observable if the radiation dose is above some threshold. Above this threshold the severity of the effect increases with do

O. Dössel and W.C. Schlegel (Eds.): WC 2009, IFMBE Proceedings 25/III, pp. 158–161, 2009.
www.springerlink.com

Stochastic effects arise from DNA damage in individual cells that are still able to reproduce. There is a small probability that this damage may contribute to deleterious effects such as cancer induction. As dose increases, the number of damaged cells increases, thus increasing the probability of cancer induction. Although a single radiological examination only leads to a small increase in the probability of cancer induction in a patient, there are a large number of such examinations each year. Using the assumption of a linear non-threshold model, the proportion of cancer deaths that could be attributed to exposure from radiological procedures may reach a level from a fraction of one to a few percent of that cancer mortality [5].

IV. The System of Radiological Protection in the 2007 Recommendations

The primary aim of radiological protection is to provide an appropriate standard of protection for people and the environment without unduly limiting the beneficial practices giving rise to radiation exposure. In its 2007 Recommendations the Commission has described its latest system of protection with this aim in mind.

A. Exposure Types

The system of protection identifies three exposure types: occupational, public, and medical. It is medical exposures that are the focus of this paper.

Medical exposures are predominantly those received by patients undergoing diagnostic examinations, interventional procedures, or radiation therapy. However, in the ICRP system of protection medical exposures also includes exposures received by other individuals helping to support and comfort patients. These include parents holding children during diagnostic procedures, and family or close friends who may come close to patients following the administration of radiopharmaceuticals or during brachytherapy. Exposures of volunteers in biomedical research are also included. This paper focuses on medical exposures to patients, although advice on other medical exposures can be found in ICRP Publication 105.

B. Fundamental Principles

The foundation of the system of protection is a set of fundamental principles: justification, optimization, and application of dose limits. Although justification and optimization are applied in the case of medical exposures, dose limits are not relevant to the medical exposures of patients.

Justification is the process of determining whether a planned activity using radiation is beneficial overall. Optimization is the process of determining what level of protection and safety makes exposures, and the probability and magnitude of potential exposures, as low as reasonably achievable (ALARA), economic and societal factors being taken into account. Both of these are discussed in more detail below with respect to medical exposures to patients.

V. Appication of the System of Radiological Protection to the Medical Exposure of Patients

ICRP Publication 105 describes how the ICRP system of protection is applied in medicine. Specifically, it elaborates on the application of the principles of justification and optimization, and it describes the purpose and use of diagnostic references levels as an aid to optimization.

A. Justification

Justification of medical exposures is performed at three levels. At the first and most general level, the proper use of radiation in medicine is accepted as doing more good than harm to society. This general level of justification is now taken for granted.

At the second level, a specified procedure with a specified objective is defined and justified (e.g. chest x rays for patients showing relevant symptoms, or a group of individuals at risk for a condition that can be detected and treated). The aim of the second level of justification is to judge whether the radiological procedure will improve the diagnosis or treatment, or will provide necessary information about the exposed individuals.

At the third level, the application of the procedure to an individual patient should be justified (i.e. the particular application should be judged to do more good than harm to the individual patient). Hence all individual medical exposures should be justified in advance, taking into account the specific objectives of the exposure and the characteristics of the individual involved.

B. Optimization

In the medical exposure of patients, optimization is best described as management of the radiation dose to the patient commensurate with the medical purpose. In other words, the medical purpose (e.g. generating an image for diagnostic purposes or cancer cell killing in radiotherapy) must be achieved, while keeping doses to the patient (other than to the treatment volume in radiotherapy) as low as reasonably achievable.

Note that non-optimized doses can be too high, for example due to non-optimized diagnostic or therapeutic equipment or methods, or due to insufficient training. However, doses can also be too low. In imaging this may result in a need to redo the procedure, thus resulting in additional unnecessary dose. In therapy this may result in an ineffective treatment. Neither of these outcomes is desirable, and therefore optimization of doses in the medical exposure of patients can be a careful balancing act.

C. Diagnostic Reference Levels

Management of patient dose can often be facilitated for diagnostic and interventional procedures by use of a diagnostic reference level (DRL). DRLs are a key tool in evaluating whether the patient dose is unusually high or low for a particular medical procedure.

DRLs are not limits, but rather benchmarks to determine whether doses are in line with the same type of procedure performed under similar circumstances elsewhere. If not, the reasons should be investigated and understood. DRLs should be set by national, regional or local bodies as appropriate, and numerical values should be in units easily measured to facilitate their use.

VI. Preventing accidents in radiation therapy

Accident prevention in radiation therapy should be an integral part of the design of equipment, facilities, and procedures. A key feature of accident prevention is the use of multiple safeguards against the consequences of failures, or "defense in depth", which aims to prevent equipment failures and human errors, and mitigates their consequences should they happen.

VII. More specific guidance

In addition to the general guidance given in ICRP Publications 103 and 105, more specific guidance relating to the management of medical doses to patients is provided in a series of other ICRP publications:

- ICRP Publication 80: Radiation Dose to Patients from Radiopharmaceuticals [6]
- ICRP Publication 84: Pregnancy and Medical Radiation [7]
- ICRP Publication 85: Avoidance of Radiation Injuries from Medical Interventional Procedures [8]
- ICRP Publication 86: Prevention of accidental exposures to patients undergoing radiation therapy [9]
- ICRP Publication 87: Managing Patient Dose in Computed Tomography [10]
- ICRP Safety Guidance 2: Radiation and your patient: A guide for medical practitioners [11]
- ICRP Publication 93: Managing patient dose in digital radiology [12]
- ICRP Publication 97: Prevention of high-dose-rate brachytherapy accidents [13]
- ICRP Publication 98: Radiation safety aspects of brachytherapy for prostate cancer using permanently implanted sources [14]
- ICRP Publication 102: Managing Patient Dose in Multi-Detector Computed Tomography (MDCT) [15]
- ICRP Publication 106: Radiation Dose to Patients from Radiopharmaceuticals [16]

Additional ICRP guidance relating to the management of medical doses to patients is forthcoming, including several reports currently in progress on: minimizing unintended exposure in radiation therapy from new technologies, evaluation and management of secondary cancer risk in radiation therapy, and protecting children in pediatric radiology.

As well ICRP has and will continue to produce recommendations on the radiological protection of medical practitioners, comforters and carers of patients, and volunteers in biomedical research using radiation.

References

1. ICRP (2008) The 2007 Recommendations of the International Commission on Radiological Protection, ICRP Publication 103. JAICRP **37**(2-4)
2. ICRP (2008) Radiological Protection in Medicine, ICRP Publication 105. JAICRP **37**(6)
3. NCRP (2009) Ionizing Radiation Exposure of the Population of the United States, NCRP Report No. 160.
4. UNSCEAR (2000) Sources and Effects of Ionising Radiation. United Nations Scientific Committee on the Effects of Atomic Radiation Report to the General Assembly with Scientific Annexes. United Nations, New York, NY
5. NAS/NRC (2006). Health Risks from Exposure to Low Levels of Ionising Radiation: BEIR VII Phase 2. Board on Radiation Effects Research. National Research Council of the National Academies, Washington, D.C.
6. ICRP (1999) Radiation Dose to Patients from Radiopharmaceuticals, ICRP Publication 80. JAICRP **28**(3)
7. ICRP (2000) Pregnancy and Medical Radiation, ICRP Publication 84. JAICRP **30**(1)
8. ICRP (2000) Avoidance of Radiation Injuries from Medical Interventional Procedures, ICRP Publication 85. JAICRP **30**(2)
9. ICRP (2001) Prevention of accidental exposures to patients undergoing radiation therapy, ICRP Publication 86. JAICRP **30**(3)
10. ICRP (2001) Managing Patient Dose in Computed Tomography, ICRP Publication 87. JAICRP **30**(4)

11. ICRP (2002) Radiation and your patient: A guide for medical practitioners, ICRP Safety Guidance 2. JAICRP **31**(4)
12. ICRP (2004) Managing patient dose in digital radiology, ICRP Publication 93. JAICRP **34**(1)
13. ICRP (2005) Prevention of high-dose-rate brachytherapy accidents, ICRP Publication 97. JAICRP **35**(2)
14. ICRP (2005) Radiation safety aspects of brachytherapy for prostate cancer using permanently implanted sources, ICRP Publication 98. JAICRP **35**(3)
15. ICRP (2007) Managing Patient Dose in Multi-Detector Computed Tomography (MDCT), ICRP Publication 102. JAICRP **37**(1)
16. ICRP (2008) Radiation Dose to Patients from Radiopharmaceuticals, ICRP Publication 106. JAICRP **38**(1-2)

Estimation of Patient Doses from Interventional Radiology Procedures in Pakistan Result of IAEA Project RAS /9/047

Areesha Zaman[1], Aftab Ahmed[2], Hamid Naseer[1], Numair yunous[1], Mahboob Ali[3], and Maham Zaman[1]

[1]Institute of Nuclear Medicine and Oncology Lahore, Pakistan.
[2]Punjab Institute of Cardiology Lahore, Pakistan.
[3]Pakistan Nuclear Regulatory Authority, Islamabad, Pakistan.

Abstract— **To determine peak skin dose (PSD), a measure of the likelihood of radiation-induced skin effects, for a variety of common interventional radiology (IR) and IC procedures, and to identify procedures associated with a PSD greater than 2 Gy. IAEA project RAS/9/047 started. The study conducted in 10 hospitals of Pakistan with twenty cath labs over a period of 4years.**

For the measurements of peak skin doses 180 patients are included in the project. Aged between 10 to 60 years who underwent diagnostic or therapeutic interventional procedures, e.g. (PTCA), CF, VP, HE, RF,) with fluoro time more than 30 minutes and for which the highest peak skin dose values were expected .To estimate the peak skin doses during fluoroscopically guided procedures, Dosimetry films (Gafchromic films, EDR2 films) are used, demographic data and technical details of the procedures are gathered. Equipment parameters (dose area product, total air karma) are used to estimate the skin doses. For Dose area products measurements 300 patients are included in the study age range (10-70). Young Patients who received at least 3 interventional procedures their total peak skin dose is also calculated. . Incident of skin injuries is monitored in the patients where the calculated skin dose is more than 2Gy., wide variations in PSD were observed for different procedures.

Results

83.7%ptients received peak skin dose <1GY
10.45%patients received peak skin dose 1-2GY
4.4%patients received peak skin dose 2-4 GY
1.1patients received peak skin dose 4-6GY

In PTCA procedures highest skin doses are estimated and fluoro time was more than 30 min, to assess the repeated interventional procedures on the same patients,8 patients had repeated IR procedures with fluoro time more than 30min for each procedures and their skin dose was more than 4 GY .

Keywords— IC: Interventional Cardiology
IR: Interventional Radiology
Percutaneous Transluminal Coronary Angioplasty (PTCA)

I. Introduction

Interventional radiology is a rapidly growing area of medicine in Pakistan. Fluoroscopically –guided techniques are being used by an increasing number of clinicians and technicians not adequately trained in radiation safety or radiation biology. Interventional procedures in children are generally performed in children hospitals. No data is available related to radiation doses and skin injuries in adults/children during different IR procedures where fluoro time is more than 30 min. IAEA project "Strengthening Radiological Protection of Patients and Medical exposure Control RAS/9/047"started in 2005.All the clinics and hospitals where interventional procedures especially in children are performed included in the project to evaluate the radiation protection conditions.

Following conditions from radiation protection viewpoint are determined. Numbers of Procedures on same patient, skin doses to patients, number of patients suffering with radiation -induced skin injuries and in young patients increased risk of future cancer.

II. Metarial and Method

IAEA project protocol was comprised of two phases

Phase one

Selecting interventional cardiology (IC) and interventional radiology (IR) facilities to participate in the IAEA study.

Data collection on radiation protection tools used in the interventional rooms e.g. use of personnel monitoring badge by the operator and those assisting in the angiography room, lead apron, lead glass eye wear

Determining the work statistics separately for children and adults and

Becoming familiar with the use of gaf chromic dosimetry media (films) provided by the IAEA for peak skin dose (PSD) measurement

Phase two

Patient's dose estimation

Radiation protection data regarding to the use of personnel monitoring badge by the operator and those assisting in the angiography room, lead apron, and lead glass eye wear data was collected from 20 catheterization laboratories in 10 hospitals in large cities of Pakistan. Gafchromic films were used in 180 patients to measure the peak skin doses using

O. Dössel and W.C. Schlegel (Eds.): WC 2009, IFMBE Proceedings 25/III, pp. 162–165, 2009.
www.springerlink.com

semi quantitative method, films were placed on patients back before the procedure on the table underneath the patient for an under coach tube position and centered as close as possible to the most irradiated area of the patient. . Dose Area Product (DAP) measurements were also recorded.

To determine radiation doses for interventional procedures .where fluoro time is more than 30 min, and to identify procedures associated with higher radiation doses, and to determine the doses of repeated procedures on the same patients. A study was performed at 10 hospitals / clinics equipped with well established cath labs, with built in cumulative dose and dose-area product (DAP) meter. And follows the radiation protection conditions

A total of 180 interventional therapeutic procedures (Coronary Angioplasty, Percutaneous Transluminal Coronary Angioplasty (PTCA) with grafts, PTCA with LAD Stent, PTCA with CPP, Cerebral Stent, and Procedures) were included in the study for the measurements of peak skin doses with age group range (11-60 year), and fluoro time range (30-110 min). For each procedure the fluoro time and fluoroscopic and digital radiographic dose area product were recorded in a computer data base. There were wide variations in doses and significant difference in fluoroscopy time, number of images, DAP, and CD for different instance of same procedures depending upon the complexity of the procedures. Dose measurements were also done with semi quantitative method using Gafchromic films.

DAP measurements of 300 patients are recorded to see the high skin dose point.

Peak Skin Dose Evaluation

Peak skin dose evaluations are done in adult patients
With Gafchromic films, peak skin dose evaluations of 180 patients are performed with semi quantitative method. Using the calibration strip provided with the film lot.
Optimization of operational and technical parameters is achieved with the proper selections of filters and acquisition mode.

The mean DAP values are reduced for patients who under went the PTCA procedures with the optimization of exposure parameter and with the use of appropriate copper filter.

For the measurements of doses of repeated procedures on the same patient, intensive follow up is carried out.

Eight patients had repeated IR procedures. After first intervention procedures patients are followed up. Three patients have three repeated IR procedures and five patients have two repeated IR procedures.

III Results

Table 1 Peak Skin Dose Measurements Age (11-60 years)

Hospital /clinics	10
No of Cath Labs	20
Procedure	CA,PTCA,LAD,CCP,CEREBRAL STENT
Total No of Evaluation in 20cath labs	180
No of patients receiving < 1Gy	151
No of patients receiving 1-2 Gy	19
No of patients receiving 2 – 4 Gy	8
No of patients receiving 4 – 6 Gy	2
No of patients receiving 6 – 10 Gy	Nil
No of patients receiving > 10 Gy	Nil

In PTCA procedure highest skin doses were estimated were the fluoro time ranged (30- 110) minutes

Table 2 Dose Area Product (DAP) Measurements

Hospital /clinics	10
No of Cath Labs	20
Procedure	PTCA LAD,CCP,CEREBRAL STENT
Total No of measurements	300
No of patients receiving ≤ 100Gy. cm^2	The mean DAP value 48.3(213patients)
No of patients receiving 101-200 Gy.cm^2	The mean DAP value 173.7(73patients)
No of patients receiving 201 – 300Gy.cm^2	The mean DAP value, ,235(8patients)
No of patients receiving 301 – 400 Gy.cm^2	The mean DAP value 33.2(4patients)
No of patients receiving > 400 Gy.cm^2	2

Table 3 Repeated intervention procedures on the same patient Mean peak skin dose

1	HOSPITALS/CLINICS	10
2	CATH LABS	20
3	TYPE OF PROCEDURES PTCA, CAD	
4	TOTAL NO OF PATIENTS WITH REPEATED PROCEDURES	8
5	NO OF PATIENTS WITH THREE REPEATED PROCEDURES	3
6	NO OF PATIENTS WITH TWO REPEATED PROCEDURES	5
7	MEAN PEAK SKIN DOSE WITH THREE PROCEDURES	4Gy
8	MEAN PEAK SKIN DOSE WITH TWO PROCEDURES	2 Gy

Table 4 Repeated intervention procedures on the same patient DAP measurements

1	HOSPITALS/CLINICS	10
2	CATH LABS	20
3	TYPE OF PROCEDURES PTCA, CA	
4	TOTAL NO OF PATIENTS WITH REPEATED PROCEDURES	4
5	NO OF PATIENTS WITH THREE REPEATED PROCEDURES	3
6	NO OF PATIENTS WITH TWO REPEATED PROCEDURES	2
7	TOTAL DAP FOR REPEATED PROCEDURES)1,2	1 341+201=542 2 110+115=225

Table 5: Statistics No of procedures in adults

Year	Diagnostic Interventions only	Therapeutic Interventions only	Both diagnostic AND therapeutic Interventions
2005	10341	3570	1521
2006	11000	4233	1596
2007	14023	5214	1625
2008	16499	6359	1792

Table 6: Statistics No of procedures in children

Year	Diagnostic Interventions only	Therapeutic Interventions only	Both diagnostic AND therapeutic Interventions
2005	585	236	178
2006	723	413	210
2007	1200	521	425
2008	1450	635	479

IV Discussion

Table 1 summarizes the peak skin dose measurements of 180 patient's age range 11-60 years. For 20 cath lab patients who underwent IR and IC procedures. In most cases CA procedures are followed by PTCA. The DAP reading include exposure from both fluoroscopy and cine .the highest dose per procedure was found at right lateral and mid posterior positions. PSD measured values were found to be between 1- 4 Gy for PTCA procedures .And in two patients more than 4 Gy.

Peak skin doses of 180 patients were measured with Gafchromic films (151) patients had Peak Skin Dose (PSD) lower than 1Gy. (19) Patients had PSD of 1-2 Gy which is just below the threshold of erythema. (8) patients had PSD higher than the 2 Gy threshold and 2 of these patients had PSD in the range of 4-6Gy.Skin entrance dose measured with gafchromic film and it is a preferred tool to identify both entrance dose to the critical are of skin and the maximum entrance skin dose MSED.PSD evaluations with Gafchromic films is quick and of great clinical value particularly in patients undergoing complex IR procedures such as AF ablation ,but also among those patients undergoing repeat procedures in a relatively short perood of time .

Table 2 summarized the DAP measurements in 300 patients there is a wide variation found in DAP value measurements for the same procedures. These variations could arise from longer fluoroscopic time, variation in cine time, operator skill, field size severity of the case treated the mean DAP values of this study are comparable with mean DAP values of other study. In PTCA procedures the contribution of fluoroscopy dose to DAP was higher, where as in CA procedures the contribution of cine to DAP was high than in PTCA procedures. There is significant co relation between the MSED and DAP values for various IR procedures. It is observed that high –skin doses measured in IR procedures where fluoro time is greater than 60 min.

Table 3 and 4 summarized the results of repeated procedures on the same patients. Eight patients of the sample had 2 or more PTCAs with PSD value in each case above the threshold. One case of diagnostic Coronary Angiography (CA) that was repeated twice was also evaluated with PSD exceeding again the threshold of 2Gy. In two patients DAP exceed 400Gycm^2.

It is found in some IR procedures doses are very high due to very long fluoro time , and inadequate adjustments of machines technical parameters .in some of the cath lab the equipment is very old need immediate replacements .

V Conclusion

Interventional procedures are increasing in Pakistan not only in adult but also in pediatric patients radiation protection conditions are better with respect to use of personnel monitoring badges. use of lead glass eye wears is 70%. Use of lead apron is 100%. There is KAP availability in 50%cath lab but no use of it. None of the hospitals had previously measured or estimated PSD and most hospitals had no experience of recording KAP. Most hospitals did not have persons with skills to use dosimetry methods and therefore required very detailed instructions and training.

Radiations induced cancer is an important risk associated with diagnostic and therapeutic procedures that required fluoroscopic imaging. The data indicates that in some procedures the PSD is either near to threshold 2Gy and more than that and needs patients monitoring .even though it is not possible to reduce MSD dose below 2Gy in some IR procedures due to patient factors, procedure complexity.

Prolonged procedures with high radiation dose are unavoidable. Considering the increased number of IR, IC procedures per year in adults and children and monitoring conditions of radiation doses in interventional radiology in Pakistan, this study is of great importance and needs to developed specific methods for assessing and monitoring the resultant doses in IR procedures at national level. Dose can be minimized through the optimization of technical factors, training of staff old equipment should be replaced with new fluoroscopic that in corporate current reduction technology. IAEA SAFETY STANDARDS AND GUIDE LINES for interventional radiology should be implemented all over the country.

VI References

1. Smith IR, Rivers JT. Measures of Radiation Exposure in Cardiac Imaging and the Impact of Case Complexity. Heart Lung Circ. 2008 Jan 30 [Epub ahead of print].
2. Balter S, Moses J. Managing patient dose in Interventional Cardiology. Cath Card Inter 2007; 70: 244-249.
3. Chu R, Thomas G, Maqbool F. Skin radiation dose in an interventional radiology procedure. Health Phys 2006; 91(1): 41-46.
4. Koenig TR, Wolff D, Mettler FA, Wagner LK. Skin injuries from fluoroscopically guided procedures, Part I: Characteristics of radiation injury. Am J Roentgenol 2001; 177:3-11.
5. Schmoor P, Descamps V, Crickx B, Steg PG, Belaich S. Chronic radiodermatitis after cardiac catheterization. Cath and Cardiov Interv 2001; 52: 235-236.
6. Koenig TR, Mettler FA, Wagner LK. Skin injuries from fluoroscopically guided procedures: part 2, review of 73 cases and recommendations for minimizing dose delivered to patient. AJR Am J Roetgenol 2001; 177: 13-20.

Rehani M, Ortiz-Lopez P. Radiation effects in

Acknowledgement
Pakistan Nuclear Regulatory Authority.
Armed Force Institute of Cardiology Rawalpindi
Punjab Institute of Cardiology Lahore
Institute Of Nuclear Medicine and Oncology Lahore

Inhibiting survivin expression increases the radiosensitivity of human hepatoma HepG2 cells to high-LET carbon ions

X.D. Jin[1,2], Q. Li[1*], P. Li[1], Q.F. Wu[1], Z.Y. Dai[1]

[1] Institute of Modern Physics, Chinese Academy of Sciences, Lanzhou 730000, China
[2] Graduate School of Chinese Academy of Science, Beijing 100039, China

Abstract— **In this study, we investigated whether survivin plays a direct role in mediating high-LET radiosensitivity. We designed small interfering RNA (siRNA) targeting survivin mRNA, in vitro chemo-synthesized and transfected into HepG2 human hepatoma cells. Real-time PCR assay and western bolting were used to determine survivin expressions at transcriptional and post-transcriptional levels, respectively. The survivin expressions decreased at both the transcriptional and post-transcriptional levels after treatment with survivin-specific siRNA. This observation indicates that survivin-specific siRNA could make survivin gene silent effectively. After exposure to high-LET carbon ion radiation, a reduced clonogenic survival effect was observed in cells treated with siRNA compared with those untreated with siRNA. Furthermore, Annexin V assay was used to determine apoptotic rate. Compared with siRNA mismatch and irradiation alone, siRNA treated cells showed increased apoptotic rates. We also found that transfection with survivin siRNA increased levels of G_2/M arrest. These results suggest that the radiosensitivity of HepG2 cells to high-LET carbon ions is increased after inhibiting survivin expression and gene therapy for constitutive survivin may be effective for therapeutic improvement in radioresistant solid tumors by high-LET radiation.**

Keywords— **surviving, high LET radiation, siRNA, apoptosis, HepG2.**

I. Introduction

High LET radiation is a critical component in the space environment and is increasingly being used as an alternative for radiation cancer therapy [1, 2]. However, there has been limited information available regarding the cell apoptosis induced by high LET radiation. The inhibitor of apoptosis proteins such as survivin are expressed at high levels in many tumors including hepatoma and have been associated with refractory disease and poor prognosis in affected individuals, an increased rate of tumor recurrence, and resistance to certain anticancer agents [3-5].It was also reported that high survivin expression cells displayed radiation resistance by suppression cell apoptosis [6]. In order to further apply the crucial role of survivin in high LET beam (carbon ion) radiotherapy, we utilized RNA interference (RNAi) strategy in tumor radiosensitization. In this report, we demonstrate that the treatment of survivin siRNA significantly reduces messenger RNA (mRNA) and protein expression, leading to tumor radio-sensitization in vitro mainly through the spontaneous and radio-induced apoptosis increase and G_2/M arrest.

II. Materials and methods

A. Cell culture and irradiation

Human hepatoma HepG2 cells were obtained from the First Hospital of Lanzhou University and grown in DMEM supplemented with 10% fetal calf serum and antibiotics. Irradiation was performed using a carbon ion beam supplied by the Heavy Ion Research Facility in Lanzhou (HIRFL) at the Institute of Modern Physics (IMP), Chinese Academy of Sciences (CAS). The energy of the beam on cell samples was calculated to be 816 MeV (dose averaged LET=35 keV/μm), and the dose rate was adjusted to be about 4Gy min^{-1}.

B. siRNA treatment

Survivin siRNA (5'-TGT GCT ATT CTG TGA ATT-3') and mismatch control siRNA (5'-TAA GCT GTT CTA TGT GTT-3') were synthesized from SBS Genetech, China. 5×10^5 HepG2 cells were seeded with 20nM siRNA using so-fast transfection reagent (Sunma Biotech, China) according to the instructions of the manufacturer. Cells were then cultured in normal growth media for 12h before irradiation.

C. Realtime reverse transcription-polysmerase chain reaction(RT-PCR)

Total RNA was isolated from the cell line and the cells were directly lysed in Trizol reagent (Invitrogen, USA). mRNA silencing was quantified by realtime PCR using a Bio-rad icycler system. The mRNA value for each gene was normalized relative to β-action mRNA levels in RNA

O. Dössel and W.C. Schlegel (Eds.): WC 2009, IFMBE Proceedings 25/III, pp. 166–169, 2009.
www.springerlink.com

sample. All reagents necessary for running a TaqMan RT-PCR assay, including predesigned and optimized assays were purchased from TaKaRa biotechnology, China and used according to the manufacture's instruction. All the measurements and results were analyzed with the icycler detection software.

D. Western blotting

Western blot analysis was performed following standard methods. Cell lysates were resolved by SDS- PAGE under reducing conditions at a concentration of 30 μg protein of each sample per lane. PVDF membranes were incubated overnight with primary polyclonal surviving antibody (the rabbit anti-human survivin antibody, 1:1500 dilution, Abcam, UK), the immunodetection with a secondary peroxidase-conjugated antibody (the sheep anti-rabbit antibody, 1:4000 dilution, Abcam, UK) and chemiluminescence was performed according to the manufacturer's protocol (Beyotime Biotech, China). To confirm equal protein loading per lane, the membranes were subsequently reprobed with a 1:5000 dilution of an anti-β-actin antibody (Abcam, UK) and developed as described above.

E. Cell survival assay

Immediately after irradiation, the cells were washed with PBS buffer, trypsinized and counted using a hemacytometer. After diluting with fresh medium they were replated into 60 mm Petri dishes at various cell densities. After 10 days of growth at 37°C, the cells were fixed with methanol and acetic acid (v/v=3:1), stained with Giemas, and then the number of colonies with more than 50 cells was counted. Because of experimental limitations, data are from three replicates obtained in one experiment.

F. Detection of apoptosis

Apoptosis was quantified by a combined staining of Annexin V and PI using Annexin V-FITC Apoptosis Derection Kit(Keyfentec China). Briefly, cells were harvested and resuspended in 500 μl of Binding Buffer. After adding 2 μl of Annexin V-FITC solution and 5 μl of PI solution, cells were incubated for 15 min at room temperature in the dark. At the end of incubation, 10,000 cells were analyzed by flow cytometer (Becton Dickinson, USA). The apoptotic cells were quantified using the FlowJo 5.0 software.

G. Analysis of cell cycle

Cell cycle status was assessed by DNA content analysis. Cells were resuspended in 1 ml of fluorochrome solution (propidium iodide (PI) at 0.5mg/ml in 0.2mg/ml RNAase and 0.1% Triton X-100) and incubated at room temperature for 30 min in darkness.10,000 cells were measured per sample using flow cytometer (Becton Dickinson, USA). The arrested at G_2/M phase (4N) was quantified using cell-cycle data analysis software (FlowJo 5.0). Three replicates were assessed.

H. Statistical analysis.

Statistical comparison of mean values was performed using the Student's t-test. Differences with a P-value of <0.05 were considered statistically significant.

III. Results

A. Effect of siRNA on survivin expression

To examine whether siRNA treatment alters mRNA levels of survivin in HepG2 cells, a realtime PCR was done from total RNA. Results are displayed in Fig1 Up. Twelve hours after tranfection, the relative levels of survivin mRNA was decreased by 38%, ($P<0.01$ versus mismatch or nontreated), which was further reduced significantly at 24(by 51%, $p<0.01$) and 36 hours (by 56%, $p<0.01$), and increased again at 48 hours. Similarly, survivn protein expression was a markedly reduced at 24 and 36 hours after transfection as compared with nontransfection or mismatch siRNA transfected control cells.(Fig1 Down)

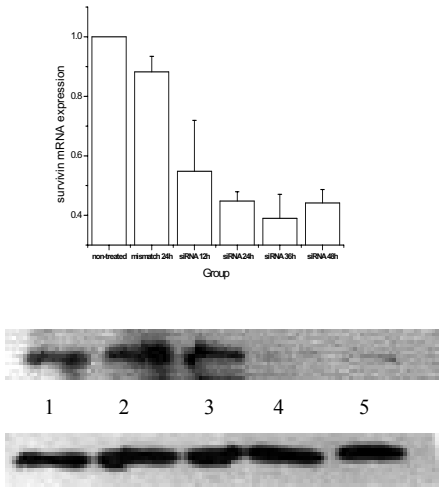

Fig 1. Down-regulation of survivin mRNA and protein in following transient transfection with survivin-specific siRNA. Up, total RNA was extracted at the indicated times after transfection and survivin mRNA was quantitated by a realtime PCR. Shown are the relative mRNA levels of survivin in reference to β-action expression. Down, Western immunoblots from total cellular proteins extracted12, 24, and 36 hours after transfection using antibodies against survivin(up) and β-action(down) as a loading control. 1 nontreated, 2 mismatch 24h, 3,4 and 5 siRNA 12,24 and 36h, respectively.

B. Survivin siRNA enhances radiosensitivity irradiation by high-LET

To establish the high-LET radiosensitizing ability of survivin siRNA, clonogenic survival assay has been done after treatment with survivin-siRNA in combination with high-LET radiation. The survival curves for the HepG2 cells by carbon ions are shown in Fig2. The survival fraction (SF) for siRNA transfected groups were significantly lower than those for the mismatch or non-transfected groups ($P<0.05$ at various doses).

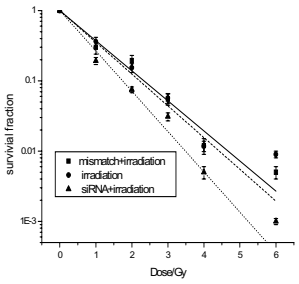

Fig 2. Effect of survivin on the clonogenic survival of HepG2 cells transfected with either survivin-specific or mismatch-control siRNA. Untreated cells served as a control. Twelve hours later, the cells were irradiated with the indicated doses. After 10 days, colonies greater than 50 cells were counted.

C. Down-regulation of survivin enhances apoptosis

To analyze whether down-regualtion of survivin by si-RNA affect spontaneous and radiation-induced apoptosis, we detected the proportion of apoptotic cells by annexin V-PI staining. The spontaneous apoptotic cells were significantly higher in survivin siRNA-treated as indicated by a 5- or 4.2-fold increase as compared with nontreated or mismatch siRNA treated cells, respectively. Furthermore, the apoptotic cells induced by the combination of high LET radiation at the same dose and survivin-siRNA transfection were greater than the other groups (Fig3).

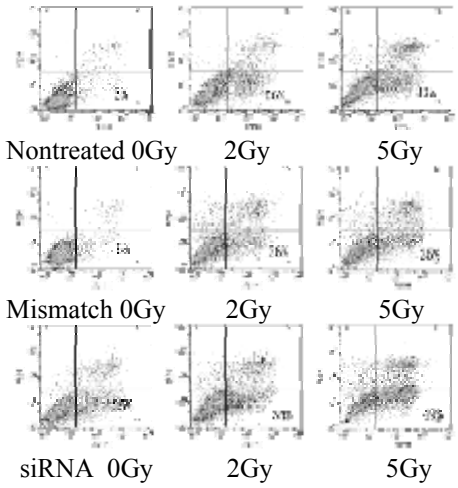

Fig3. Survivin attenuation by siRNA treatment affects spontaneous and radiation-induced apoptosis. The apoptotic cells were determined by Annexin V and PI -staining in nonirradiated cells as well as 48 hours after irradiation with 2 and 5 Gy.

D. Cell cycle anslysis after siRNA

To determine whether inhibition of survivin affect cell cycle distributing, cycle analyses were done. The results revealed an increase in the G_2/M fraction in survivin siRNA-treated cells 12 hours after transfection, indicating that a larger fraction cells was blocked in a more radio-sensitive stage as compared with nontreated or mismatch siRNA treated cells when the cells had been irradiated ($P<0.01$, Fig. 4).

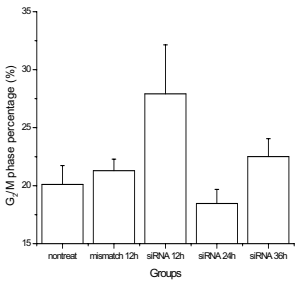

Fig4 Survivin attenuation by siRNA treatment affects cell cycle distribution. Various time after transfection, fixed HepG2 carcinoma cells were labeled with propidium iodide and flow cytometry was used to measure DNA content.

IV. Discussion

Recently, several groups showed that suppression of survivin by using synthetic ASO [7,8], ribozymes[9], small interfering RNA [10,11], or dominant-negative mutants [12] effectively radiosensitized in human tumor cells to low LET radiation. However, so far little information is available in tumor cells after exposure to high-LET radiation. Therefore, we hypothesized that survivin also plays a key role in mediating high-LET radiation resistance. As we expected, the cell survival experiments showed a clear radiosensitization by survivin siRNA to high-LET radiation in human tumor cells (Fig.2). This observation indicated that survivin functions as a factor conferring resistance against high-LET radiation.

Response to radiation is thought to have multifactorial etiologies. The possible underlying mechanisms by which inhibition of survivin may enhance cell radiosensitivity remain to be elucidated. Our results showed that survivin enhances survivial of apoptosis-related cell death. A significant increase of spontaneous and high LET radiation-induced apoptosis was observed in HepG2 cells transfected with survivin siRNA(Fig3), suggesting that survivin is playing an active role in cell apoptosis process. Furthermore, we also observed that survivin siRNA treatment altered the cell cycle distribution, resulting in an increased G_2/M fraction 12 hours after transfection. Thus, at the time of irradiation, the cells were blocked in a more radiosensitive stage of the cell cycle. We considered it had been seemed to be additional mechanisms to enhance sensitivity to high-LET radiation.

In summary, we demonstrated that survivin siRNA significantly enhanced the radio-sensitivity of tumor cells HepG2. The cause of radio-sensitization is likely to come from the spontaneous and radio-induced apoptosis increase and G_2/M arrest by siRNA.

*corresponding author address: Qiang Li, Nanchang Road 509, Lanzhou, Gansu Province, China 730000

REFERENCE

[1].Goodwin E, Blakely E, Ivery G et al. (1989) Repair and misrepair of heavyion-induced chromosomal damage, Adv. Space Res. 9: 83–89.
[2].Tsujii H, Mizoe J, Kamada T et al. (2007) Clinical results of carbon ion radiotherapy at NIRS, J. Radiat. Res. 48 (Suppl. A): A1–A13.
[3].Kountouras J, Zavos C, Chatzopoulos D.(2005) Apoptotic and anti-angiogenic strategies in liver and gastrointestinal malignancies. J Surg Oncol 90:249—59
[4].Chakravarti A, Noll E, Black P.M, et al (2002) Quantitatively determined survivin expression levels are of prognosticvalue in human gliomas, J. Clin. Oncol. 20:1063–1068.
[5].Tamm I, Wang Y, Sausville E, et al (1998) IAP-family protein survivin inhibits caspase activity and apoptosis induced by Fas (CD95), Bax, caspases, andanticancer drugs. Cancer Res 58:5315–5320
[6].Asanuma K, Kobayashi D, Furuya D, et al (2002) A role for survivin in radioresistance of pancreatic cancer cells. Jpn J Cancer Res 93:1057–1062,
[7].Lu B, Mu Y, Cao C, et al.(2004) Survivin as a therapeutic target for radiation sensitization in lung cancer. Cancer Res 64: 2840–2845.
[8].Guan HT, Xue XH, Dai ZJ, et al. (2006) Down-regulation of surviving expression by small interfering RNA induces pancreatic cancer cell apoptosis and enhances its radiosensitivity. World J Gastroenterol 12: 2901–2907.
[9].Pennati M, Binda M, Colella G, et al. (2003) Radiosensitization of human melanoma cells by ribozyme-mediated inhibition of survivin expression. J Invest Dermatol120: 648–654.
[10].Rodel F, Hoffmann J, Distel L, et al. (2005) Survivin as a radio-resistance factor, and prognostic and therapeutic target for radiotherapy in rectal cancer. Cancer Res 65:4881–4887.
[11].Kami K, Doi R, Koizumi M, et al. (2005) Downregulation of survivin by siRNA diminishes radioresistance of pancreatic cancer cells. Surgery 138:299–305.
[12].Chakravarti A, Zhai GG, Zhang M, et al. (2004) Survivin enhances radiation resistance in primary human glioblastoma cells via caspase-independent mechanisms. Oncogene 23:7494–7506.

Extremity and eye lens doses of the staff during interventional radiology procedures – First results

C. Koukorava[1], E. Carinou[1], J. Domienik[2], J. Jankowski[2], S. Krim[3], D. Nikodemova[4], L. Struelens[3] and F. Vanhavere[3]

[1] Greek Atomic Energy Commission (GAEC), Greece
[2] Nofer Institute of Occupational Medicine, (NIOM), Lodz, Poland
[3] Belgian Nuclear Research Centre (SCK•CEN), Belgium
[4] Slovak Medical University (SMU), Bratislava, Slovakia

Abstract— **Interventional radiology procedures have become more complex over the last years and new methods have been implemented in clinical practice. Taking into account the long fluoroscopy times and the large number of images needed for a good clinical outcome, the occupational exposure is an important issue that needs thorough investigation. So far many studies have been performed on this field but there is no systematic data analysis on the exposures of the medical staff. The ORAMED project started in order to fill the above gap and improve the standards of radiation protection.**

The procedures monitored in the present study are cardiac angiographies (CA) and angioplasties (PTCA), radiofrequency ablations (RFA), pacemaker implantations (PM), angiographies (DSA) and angioplasties (PTA) of the lower limbs (LL), the carotids (C) and the reins (R), embolisations and endoscopic retrograde cholangiopancreatographies (ERCP). All measurements are based on a common protocol so that all data can be compared.

The lowest Kerma-Air-Product (KAP) values were observed during PMs and ERCPs and the highest ones during embolisations and renal PTAs. The highest skin doses were measured on the left side of the physician. So far, doses up to 2.08 mSv were recorded on the left finger during CA/PTCA procedures. In the embolisations, the doses to the legs and the eyes were comparatively high as well, especially when protective equipment was not used. Finally for the PMs and ERCPs the doses were generally low due to the absence of image acquisitions.

Keywords— **extremity dosimetry, eye lens dosimetry, interventional radiology, occupational exposure.**

I. Introduction

The state-of-the-art analysis performed within the FP6 CONRAD project highlighted high extremity doses and a lack of systematic data analysis on exposures to the staff in interventional radiology [1,2].

A range of measurements have been reported in the literature, but several topics are still unclear. Routine monitoring of extremities is difficult, since "the most exposed area" -according to the ICRP recommendations [3]- cannot easily be found. Firstly, in most of the cases, only finger or hand doses are reported, while doses to the eye lens and legs are missing. It should be noted that there are cases where leg doses can be even higher than finger doses [4]. Moreover, it is almost impossible to get a clear view on the influence of parameters like experience of the physician and radiation protection measures with the present data.

The ORAMED (Optimization of RAdiation Protection for MEDical staff) project came into the scene to fill the above mentioned gaps and to improve standards of protection for medical staff. ORAMED is a new project (funded through the FP7) with main objective the safety and efficacy of the use of radiation in diagnostics and therapy. The project's main purpose is to develop methodologies for better assessing and reducing exposures to medical staff in nuclear medicine and interventional radiology, focusing in extremity and eye lens dosimetry and the use of active personal dosemeters.12 partners participate in the ORAMED project with different background, but all have been active in radiation protection in the medical field in recent years. The results presented in this study are part of WP1 of the project which has as main goal the study of extremity and eye lens doses in interventional cardiology and radiology.

To accomplish the above objective well coordinated measurement campaigns in European hospitals will be performed. The same measurements will be made and the same parameters will be recorded, based on a common protocol, so that all data can be compared and evaluated. Special attention will be given to eye lens and leg doses as there is a lack of data at the present time. Correlations with other parameters (such as KAP values) will be evaluated. Monte Carlo simulations will also be performed in order to better evaluate the influence of several parameters to the doses that are being studied. The present work shows the first studies done in this field and the first measurements that have been performed using the protocol established among the partners.

O. Dössel and W.C. Schlegel (Eds.): WC 2009, IFMBE Proceedings 25/III, pp. 170–173, 2009.
www.springerlink.com

II. Materials and methods

A. List of procedures

In order to decide the type of interventional procedures that will be studied within the framework of WP1 of the ORAMED project, a retrospective study from hospital data on the frequency of procedures and the respective KAP values was performed in many European hospitals. The final list of procedures includes 3 cardiac and 5 general interventional diagnostic and therapeutic examinations. More specifically, the list is composed of cardiac angiographies (CA) and angioplasties (PTCA), radiofrequency ablations (RFA), pacemaker implantations (PM), angiographies (DSA) and angioplasties (PTA) of the lower limbs (LL), the carotids (C) and the reins (R), embolisations and endoscopic retrograde cholangiopancreatographies (ERCP).

B. Measurement protocol

After preliminary studies a measurement protocol was established, according to which several parameters related to the angiographic system, the type and complexity of the procedure, the position of the physician and the protective equipment, the experience of the physician, some field parameters (kV values, filtration, projections, etc.) and finally the fluoroscopy time, the number of images acquired and the KAP values, should be recorded.

For the measurements it was decided to use TL dosemeters (LiF:Mg,Cu,P). The TLDs are sealed in small plastic bags and taped on the parts of the body to be monitored. Specifically 8 TLDs are used, 1 on each ring finger and wrist -on the palmar side when the tube is under the table and on the dorsal side for over-couch interventions- 2 on the legs about 5 cm below the lead apron, one between the eyes and one near the left/right eye depending if the tube is on the left/right side of the doctor respectively. Especially for the fingers, wrists and eyes, test measurements showed that the chosen positions indicate the most exposed area.

The measurement protocol is common for all partners and for all types of procedures so that all results are homogenized and can be analyzed and compared. Towards that purpose, an intercomparison exercise was performed in the very beginning in order to assure that all partners evaluate the doses the same way using each one their own calibration method. The TLDs were irradiated to ^{137}Cs and X-ray beams on the ISO slab phantom and the participants were asked to evaluate the $H_p(0.07)$ value.

III. Results

The results of the intercomparison showed that energy dependent correction factors are needed, due to the energy response of the TLDs. Every partner determined these factors according to the calibration method followed in each institute.

Up to now 137 procedures have been monitored in 7 European hospitals. The majority (77 procedures-56%) are CAs and PTCAs. However, there are 10 RFAs, 12 PMs, 15 DSA and PTAs, 8 embolisations and 10 ERCPs.

Figure 1 shows the distribution of the KAP median values for the various procedures. The KAP values vary from 0.46 Gycm^2, recorded in PM procedure, to 942 Gycm^2 in an embolisation one. The lowest values are presented in the ERCP and PM procedures, whereas the highest at the embolization and the renal PTA ones. Generally high KAP values are encountered when large number of images/frames is acquired. The KAP values present high distribution even within the same type of procedure, which shows the variation in the techniques and the experience of the physician.

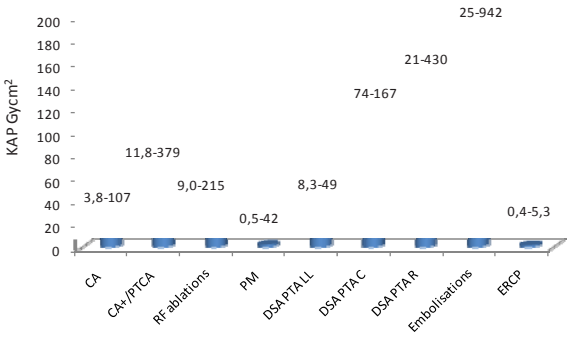

Fig. 1 The median KAP values of the various procedures are presented. Above each column the range in the respective values is noted.

The median values of $H_p(0.07)$ for each kind of procedure are shown in figure 2. Moreover, in figure 3 the median values of the ratio of the $H_p(0.07)$/KAP are presented. As far as the recorded doses are concerned, the only common characteristic in all these procedures is that the part of the body closer to the tube receives the highest dose (usually the left one). The maximum dose that was recorded was at the left finger in a CA and PTCA procedure (2.08 mSv, KAP=380 Gycm^2). The maximum eye dose (1.28 mSv) was recorded in the embolisation with the highest KAP value. The highest $H_p(0.07)$/KAP values are observed to the PM procedures. This can be explained by the fact that even though the doses are not very high as absolute values, they are high compared to the respective KAP values.

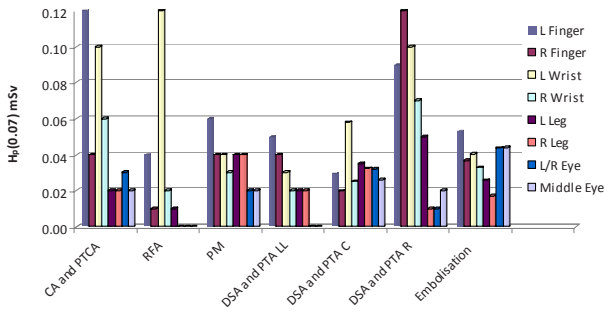

Fig. 2 The median values of Hp(0.07) for the various procedures in the different anatomic sites

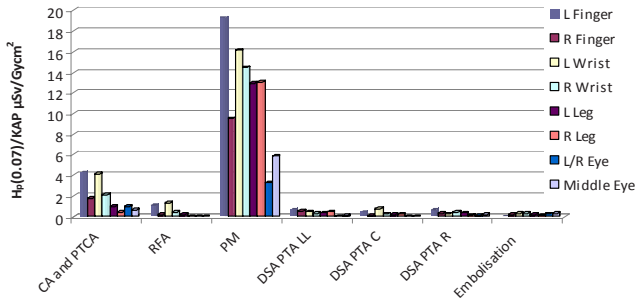

Fig. 3 The median values of the ratio Hp(0.07)/KAP for the various procedures in the different anatomic sites. The respective values for the ERCP were zeros

For CA and PTCA the left side of the operator received the highest dose. The fingers received slightly higher dose than the wrists and the legs higher than the eyes. In Martin et al. [5] hand doses in the range 0.16-0.76 mSv per procedure were recorded which are close to the wrist doses recorded in our study. Tsapaki et al.[6] recorded foot doses with a median value 0.04 mSv which is higher than the leg doses recorded in our study (0.02 mSv). For the RFA, the finger and wrist doses are higher than the leg and the eye ones as in the CA and PTCA procedures. It should be noted that in one hospital the operator was inside a special shielding cabin so the eyes and leg doses are very small. In McFadden et al [7] the hand doses (0.21-0.26 mSv per procedure) for RFA are higher than the wrist and ring doses recorded in the present study. For the PM interventions the $H_p(0.07)$ values are generally low due to the short fluoroscopy time and the absence of image acquisitions, although values up to 0.4 mSv/procedure were recorded in the finger region. In those cases the hands were very close or sometimes even inside the beam. The ratio of $H_p(0.07)$/KAP in this kind of procedures is higher compared to the rest of the procedures examined in this study. In PM implantations the primary doctor's position can be closer to the patient compared to other interventional procedures so it is not easy to use the protective equipment of the table and ceiling. In DSA, PTA of lower limbs and carotids the finger and wrist doses are higher than the leg ones. The doses to the eyes are the lowest. The absolute values for the $H_p(0.07)$ and the ratio $H_p(0.07)$/KAP in the DSA, PTA of lower limbs are slightly higher than in the DSA, PTA of carotid procedures. The situation in renal DSA, PTA procedures is different as the wrist doses are higher than the finger and the legs ones. Again the doses to the eyes are small (highest value 0.11 mSv). In the embolisations, the wrist doses are higher than the fingers which are in agreement with Whitby et al [5]. The doses to the legs and the eyes are comparatively high as well. Attention is paid to the fact that the KAP values are also high. In Whitby et al [4] mean doses to the tibia of 0.94 mSv have been recorded while in our study the mean value is only 0.06 mSv. This difference is explained by the fact that in Whitby's study there was no protective shield during embolisation procedures while in our case there was always a lead curtain attached to the table. In reference [6] the median hand doses are 0.13 mSv and in our case 0.05 mSv. Finally the doses recorded in the ERCP interventions are small varying from 0 to 0.03 mSv because protective equipment was used at all times.

IV. Discussion

There is a great difficulty in comparing the dosimetric results in the various studies mentioned in the literature because many different factors influence the doses. Harmonization of the calibration methodologies and positions used for monitoring is needed. When the ORAMED measurements are finished, more systematic analyses will be possible because all the relevant parameters are noted down. At that moment an in-depth analysis of the different protection measures will be done.

In these first results, higher doses are measured at the physician's wrist and ring due to their proximity to the scattered area, whereas the doses to the eyes are low due to the larger distance from the patient's body.

The large distribution of the $H_p(0.07)$ doses that is observed can be explained by the different X ray systems and the protective equipment that is used and by the differences in complexity and duration of the interventions.

The large variation that is observed in the ratio of the $H_p(0.07)$/KAP can be explained by the large variability of the work technique (position of the doctor, distance from

the tube, projections, etc), the protective devices that are used, the X ray characteristics. Furthermore, doctors switch positions during the procedures or they move away from the X ray tube or go behind a movable shield. In this way although the KAP is unchanged the dose to the staff decreases.

V. Conclusions

Further work is needed in the field taking into account all the parameters which can influence the extremity and eye lens doses. Detailed analysis and further conclusions on yearly doses will be performed when the number of procedures per group is larger. Moreover, numerical simulations that are also performed within the framework of WP1 of the ORAMED project will be a powerful tool in correlating the various parameters with the doses in the anatomic sites examined.

Acknowledgment

The research leading to these results has received funding from the European Atomic Energy Community's Seventh Framework Programme (FP7/2007-2011) under grant agreement n° 211361. The authors would also like to thank the staff of the hospitals for their help and collaboration.

References

1. Vanhavere F, Carinou E et al. (2008) An overview on extremity dosimetry in medical applications. Radiat Prot Dosim 129:350–355
2. Donadille L, Carinou E et al. (2008) An overview of the use of extremity dosemeters in some European countries for medical applications. Radiat Prot Dosim 13:62-66
3. International Commission on Radiation Units and Measurements (2007) The 2007 Recommendations of the International Commission on Radiological Protection. ICRP Publication 103.
4. Whitby M and Martin CJ (2003) Radiation doses to the legs of radiologists performing interventional procedures: are they a cause for concern? Br J Radiol 76:321-327
5. Whitby M and Martin CJ (2005) A study of the distribution of dose across the hands of interventional radiologists and cardiologists. Br J Radiol 78: 219-229
6. Tsapaki V, Kottou et al. (2004) Occupational dose constraints in interventional cardiology procedures: the DIMOND approach. Phys Med Biol 49:997-1005
7. McFadden SL, Moooney RB et al. (2002) X-ray dose and associated risks from radiofrequency catheter ablation procedures. Br. J. Radiol, 75:253-265.

Author: Christina Koukorava
Institute: Greek Atomic Energy Commission
Street: Patriarhou Grigoriou & Neapoleos, 15310
City: Agia Paraskevi, Athens
Country: Greece
Email: chkoukor@eeae.gr

GafChromic® film measurements for Microbeam Radiation Therapy (MRT)

E. Bräuer-Krisch[1], E. A. Siegbahn[2] , A. Bravin[1]

[1] ESRF, European Synchrotron Radiation Facility, B.P.220, 6, rue Horowitz, 38043 Grenoble Cedex, France
[2] Department of Hospital Physics, Karolinska Universitetssjukhuset, 17176 Stockholm, Sweden

Abstract— **Microbeam Radiation Therapy (MRT) is a preclinical synchrotron radiation based therapy technique in its preclinical stage with the potential to treat brain tumours in children when other kinds of radiotherapy would be excessively toxic to the developing normal brain. The most promising feature of MRT lies in its unusual resistance of MRT irradiated tissues to radioneurotoxicity even for peak doses of several hundreds of Gray. Results obtained with the spatially fractionated beams indicate a superior therapeutic effect compared to conventional radiotherapy. MRT, solely possible at SR sources with negligible beam divergence, is profiting from the dose volume effect and most probably from some differences in the tumour and the normal tissue responses, yet to be fully understood. This paper demonstrates that dosimetric measurements requiring a spatial resolution of a few microns is feasible with the use of GafChromic® films together with a high resolution scanner system. The data so obtained can be used to benchmark Monte Carlo calculations.**

Keywords— **Microbeam Radiation Therapy, Dosimetry, Synchrotron Radiation, GafChromic® film**

I. Introduction

Microbeam Radiation Therapy (MRT) uses typically 20-100 micron wide parallel beams, spatially fractionated by a centre-to-centre distance of about 100-400 micron. Such microbeams can only be produced at a 3rd generation synchrotron facility with a negligible divergence of the beam. Additionally, MRT requires dose rates in the order of several thousands of Gy/sec to cope with the internal movements of the brain, due to the pulsation of the heart, which, in case of too slow exposures could lead to a blurring of the microbeams. The indispensable sharp slopes between the peaks and the valleys can only be maintained by such high dose rates like at the ESRF, ID17 Biomedical beamline. One of the fundamental reasons why these PVDRs (ratios between the peak and the valley doses) are important and a minimum PVDR is required, lies in the simple fact that radiobiologically the cells in the path of the peak will be essentially destroyed, while the valley dose must remain low enough for the normal tissue to provide sufficient repair.

During the past decade, potential applications of Microbeam Radiation Therapy (MRT) have been studied experimentally at the National Synchrotron Light Source (NSLS) at Upton, New York, USA[1-3] and at the European Synchrotron Radiation Facility (ESRF) in Grenoble, France[4-7].The ESRF preclinical MRT program comprised irradiation of normal brain tissues in weanling piglets[4] and suckling rats followed by long-term (9-15 months) neurobehavioral observation, MRI imaging and finally histopathological studies. Several references describe surprisingly high tissue tolerances to multiple microbeams, which is especially remarkable for developing tissues, well known to be radiosensitive

The rectangular microbeams (with typical size 25 µm × 0.5 mm) used in these experiments are produced when a multi-slit collimator intercepts the sycnchrotron beam.The synchrotron beam is only 0.5 mm high but on the width of the beam there are no limitations. In order to irradiate with microbeams of a specific height (e.g. 1 cm instead of 0.5 mm) the target (phantom) is therefore vertically translated in the beam during irradiation.

Absolute microdosimetry for dose values between 5 – 1000 Gy with the spatial resolution in the range of one micron still remain a challenge, since no commercial detector can be bought off shelf. Several approaches using MOSFET edge-on detectors[8-9] haven proven to be useful, but are too time consuming (long alignment procedures) and absolute dosimetry within +/- 5% is not feasible. The spatially non-fractionated beam can be measured accurately enough by scanning an ionchamber through the beam, but a reliable dosimetric on-line system to measure PVDRs prior patient irradiation needs to be developed to insure perfect reproducibility when such microbeams are applied to treat patients. A potential candidate of such a detector system would be a MOSFET strip detector where accuracy of spatial resolution and high reproducibility of the measured signal are more important than measuring directly the quantity of absorbed dose, provided by a Monte Carlo based treatment planning system previously benchmarked with GafChromic® film dosimetry

O. Dössel and W.C. Schlegel (Eds.): WC 2009, IFMBE Proceedings 25/III, pp. 174–177, 2009.
www.springerlink.com

II. FILM ORIENTATION AND HANDLING

As reported by Niroomand-Rad[10], the orientation of the GafChromic® film does influence the level in optical densities. We have done a systematic analysis and observed that for homogenous exposures using linearly polarized Synchrotron Radiation, comparing the 90 degree rotated film with respect to the 0 degree irradiation direction, the maximum difference in optical densities for several series of MRT irradiated films is in the order of 10 % (10 mm x 10 mm radiation field).

Due to the fact that the Synchrotron wiggler insertion device delivers highly polarized photons the effect of the orientation of the exposed GafChromic® film, with vertical microbeams projected on them, on the densitometer readout is increased and our studies showed differences of up to 20 % in the measured absolute peak dose. To avoid these artefacts, a standard convention for the exposure and readout procedure was established, with the thin coated side facing the beam: an "R" is marked on the upper right corner when looking downstream with the Synchrotron light (beams-eye-view) and the "R" is visible on the lower right corner when the film is positioned onto the glass plate of the Epson scanner, used to digitalize the films. The optical density is then analysed using the ImageJ software.

Before irradiation, the films are kept in their light tight black envelope and at room temperature (20 degree Celsius and never exceeding 25 degree Celsius). They are cut and prepared in a relatively dark room and kept in Aluminium foil except during exposures. Due to the high dose rates at the ID17 beamline, the total exposure time to ambient light is never exceeding 5 minutes. The effect of this light has been described in different literature studies and our own tests showed no increase in optical densities for films exposed less than 15 minutes at our typical light conditions. The readout of all films was done not earlier than 2 days after the irradiation exposures, where the measured OD signal is perfectly stable.

In this paper, the Monte Carlo simulations with the Monte Carlo code PENELOPE[16] considers a perfect parallel beam as the primary source impinging on the PMMA phantom, which is not exactly the case due to the slight divergence of the beam, as well as the mechanical imperfections of the multislit collimator (MSC), used to produce the beams. Such a full calculation can only be done approximately, since the exact condition of the inner surface of the MSC can only be estimated and different surface effects, like total reflection can not be included into the calculations.

III. RESULTS

In this study we present results obtained with GafChromic® film dosimetry scanned and analysed using an Epson scanner V Pro 750. Due to the high dose rate and technical limitations, like the maximum possible goniometer speed of the motor used to scan the film through the spatially fractionated synchrotron radiation light, we are limited to a minimum peak dose of about 20 Gy, which is in the range of doses where the GafChromic® films HD-810 from ISP (Nuclear Associates)[11-12] show a rather linear dose response. To overcome the problem of the large dose range to be covered in MRT dosimetry, we applied a Monte Carlo pre-calculated PVDR to two separate exposures, one for the peak dose and one for the valley dose measurement. In the example presented below (see Fig. 1), the film was irradiated with 2000 Gy peak entrance dose for the valley dose measurement and the following microbeam parameters were used: the microbeam size was 50 micron FWHM (Full Width Half Maximum), 400 microbeam c-t-c (centre-to-centre) distance, 10 mm x 10 mm microbeam array size. The measurement was then done at 10 mm depth in a cubic PMMA phantom of approximately 16 cm x 16 cm x 16 cm. For the configuration described above, a pre-calculated PVDR of 28 corresponds to a valley dose of about 73 Gy at 10 mm depth. The second film was irradiated under exactly the same condition, but depositing a peak entrance dose reduced by the same PVDR, which can be directly translated to an increase in the speed with which the phantom is translated vertically through the beam from e.g. 3.63 mm/sec to 100 mm/sec. A reasonable match in the absolute doses (and measured ODs) of the peak and valley doses is obtained with this method as shown in Figure 1 below.

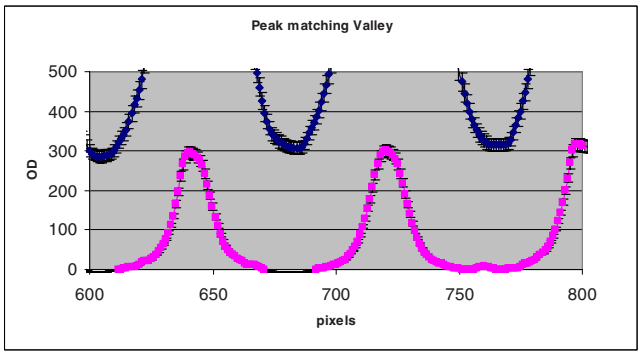

Figure 1: Two films exposed to doses which were corrected with a Monte Carlo pre-calculated dose ratio, in order to obtain similar valley and peak doses.

The depth dose profiles for the peaks and for the valleys have been described in previous publications [13-15] and special attention must be drawn to the variation of the valley dose with depth, since it is assumed that this is of crucial importance for the normal tissue tolerance. (The valley dose will give the lowest "background" dose like the constant dose level in broad beam irradiations.) Figure 2 shows an example of a measurement of the variation of the valley dose with depth within an approximately 16 cm diameter PMMA phantom, using the same parameters as mentioned above, resulting in a reasonable match with the Monte Carlo pre-calculated valley dose. An important build-up in valley dose over the first centimeter is seen which is typical for much harder X-ray spectra, but in the case of MRT with a white beam filtered spectrum peaked around 100 keV. This shape of the valley depth dose profiles is due to the build-up of laterally Compton scattered photons.

The associated error bars for absolute dosimetry using GafChromic® films in MRT are as high as 10 % due to the intrinsic fluctuation in OD for a given dose of the GafChromic® films. Nevertheless, the relative valley depth doses matches within 5 % the theoretical calculations beyond the dose maximum, making the GafChromic® film a valuable tool to check Monte Carlo calculated dose values in a phantom.

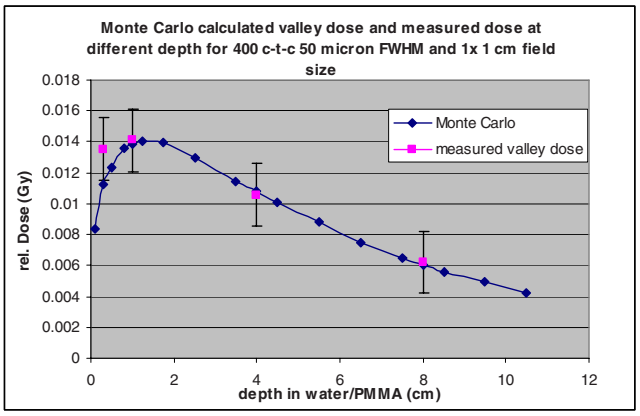

Figure 2: Comparison between the Monte Carlo calculated and GafChromic® film measured valley doses as a function of depth..

IV. CONCLUSIONS

GafChromic® film in combination with a commercial scanner is an adequate dosimeter to measure peak and valley doses in x-ray microbeams where micron resolution is required. Benchmarking of the Monte Carlo calculations with measurements is mandatory to verify the changes in dose due to variations in field size, spacing, point of interest in depth etc. predicted by the Monte Carlo calculations. This is a necessary step to provide the future accurate input data in the TPS (Treatment Planning System) used for clinical trials in MRT.

ACKNOWLEDGMENT

The authors would like to thank the entire team of the ID17 biomedical beamline for their valuable help and support.

REFERENCES

1. D. N. Slatkin, P. O. Spanne, F. A. Dilmanian, J-O. Gebbers, and J. A. Laissue, "Subacute neuropathological effects of microplanar beams of X-rays from a synchrotron wiggler," Proc. Natl. Acad. Sci. 92, 8783-8787 (1995)
2. D. N. Slatkin, P. O. Spanne, F. A. Dilmanian, and M. Sandborg, "Microbeam radiation therapy," Med. Phys. 19, 6, 1395-1400 (1992)
3. F. A. Dilmanian, G. M. Morris, G. Le Duc, X. Huang, B. Ren, T. Bacarian., J.C. Allen, J. Kalef-Ezra, I. Orion, E. M. Rosen, T. Sandhu, P. Sathé, X. Y. Wu, Z. Zhong, and H. L. Shivaprasad, "Response of avian embryonic brain to spatially segmented X-ray microbeams," Cell. Mol. Biol. 47, 485-494 (2001)
4. J. A. Laissue, N. Lyubimova, H.-P. Wagner, D. W. Archer, D. N. Slatkin, M. Di Michiel, C. Nemoz, M. Renier, E. Brauer, P. O. Spanne, J.-O. Gebbers, K. Dixon, and H. Blattmann, "Microbeam radiation therapy," Proceedings of SPIE Vol.3770, 38-45 (1999)
5. J. A. Laissue, G. Geiser, P. O. Spanne, F. A. Dilmanian, J-O. Gebbers, M. Geiser, X. Y. Wu, M. S. Makar,, P. L. Micca, M. M. Nawrocky, D. D. Joel, and D. N. Slatkin, "Neuropathology of ablation of rat gliosarcomas and contiguous-brain tissues using a microplanar beam of synchrotron-wiggler-generated x-rays," Int. J. Cancer 78, 654-660 (1998)
6. H. M. Smilowitz, H. Blattmann, E. Bräuer-Krisch, A. Bravin, M. Di Michiel, J.-O. Gebbers, A. L. Hanson, N. Lyubimova, D. N. Slatkin, J. Stepanek, and J. A. Laissue, "Synergy of Gene-Mediated Immunoprophylaxis and Unidirectional Microbeam Radiation Therapy for Advanced Intracerebral Rat 9L Gliosarcomas" J. of Neuro-oncology 78, 135–143 (2006).
7. M Miura, H Blattmann, E Brauer-Krisch, A Bravin, A L Hanson, M M Nawrocky, P L Micca, D N Slatkin, and J A LaissueRadiosurgical palliation of aggressive murine SCCVII squamous cell carcinomas using synchrotron-generated X-ray microbeams The British Journal of Radiology, 79 (2006), 71–75
8. A. B. Rosenfeld, E. A. Siegbahn, E. Brauer-Krish, A. Holmes-Siedle, M. L. F. Lerch, A. Bravin, I. M. Cornelius, G. J. Takacs, N. Painuly, H. Nettelbeck, and T. Kron, "Edge-on Face-to-Face MOSFET for Synchrotron Microbeam Dosimetry: MC Modeling," IEEE Trans. Nucl. Sci. 52, 2562-2569 (2005).
9. Brauer-Krisch E,BravinA, Lerch M, Rosenfeld A, Stepanek J, Di MichielMand Laissue JA2003MOSFETdosimetry for microbeam radiation therapy at the European Synchrotron Radiation Facility Med. Phys. 30 583–9
10. Niroomand-Rad A et al 1998 Radiochromic film dosimetry: recommendations of AAPM Radiation Therapy Committee Task Group 55. American Association of Physicists in Medicine Med. Phys. 25 2093–115

11. ISP 2007 GafChromic® EBT Product Brief. International Speciality Products (ISP) Technologies http://online1.ispcorp.com/ layouts/GafChromic®/index.html
12. ISP 2008 Technical Report GafChromic® HD-810 radiochromic dosimetry film and D-200 pre-formatted dosimeters for high energy photons; Configuration, specifications and performance data. International Specialty Products
13. Siegbahn E A, Stepanek J, Brauer-Krisch E and Bravin A 2006 Determination of dosimetrical quantities used in microbeam radiation therapy (MRT) with Monte Carlo simulations Med. Phys. 33 3248–59
14. Orion I, Rosenfeld A B, Dilmanian F A, Telang F, Ren B and Namito Y 2000 Monte Carlo simulation of dose distributions from a synchrotron-produced microplanar beam array using the EGS4 code system Phys. Med. Biol. 45 2497–508
15. J. Spiga, E. A. Siegbahn, E. Bräuer-Krisch, P. Randaccio, A. Bravin, "The GEANT4 toolkit for microdosimetry calculations: Application to microbeam radiation therapy "MRT"," Med. Phys. 34, 4322-4330 (2007).
16. F. Salvat, J. M. Fernández-Varea, and J. Sempau, PENELOPE, a Code System for Monte Carlo Simulation of Electron and Photon Transport, (OECD Nuclear Energy Agency, Issy-les-Moulineaux-France, 2003).

Author: E. Brauer-Krisch
Institute: ESRF
Street: 6, rue Horowitz
City: 38043 Grenoble
Country: France
Email: brauer@esrf.fr

Application of the New ICRP Reference Phantoms to Internal Dosimetry: Calculation of Specific Absorbed Fractions of Energy for Photons and Electrons

L. Hadid[1], A. Desbrée[1], H. Schlattl[2], D. Franck[1], E. Blanchardon[1], and M. Zankl[2]

[1] IRSN, French Institute for Radiological and Nuclear Safety, Fontenay-aux-roses, France
[2] Helmholtz Zentrum München, German Research Center for Environmental Health, Neuherberg, Germany

Abstract— **Introduction: Connecting the emission of radiation from a contaminated body region with the dose received by a radio-sensitive tissue, the specific absorbed fraction (SAF) of energy is an essential element of internal dose assessment. Here is reported a set of specific absorbed fractions calculated using the male and female reference computational phantoms recently published by the International Commission on Radiological Protection (ICRP). This work was performed simultaneously at the Helmholtz Zentrum München (HMGU, Germany) and IRSN (France) for quality assurance purpose. The results were then compared to the SAF values for mathematic phantoms.**

At IRSN, the Monte Carlo transport code MCNPX version 2.6f was used to simulate monoenergetic photons and electrons with energies ranging from 15 keV to 10 MeV. The OEDIPE software, developed by IRSN, was used to create the MCNPX input file describing the two voxel phantoms. The particles were emitted from three source organs: lungs, thyroid and liver. SAFs were calculated for several target regions in the body (lungs, colon wall, breast, stomach wall) and compared with the results obtained at HMGU using the EGSnrc Monte Carlo code.

The results show general agreement for photons and high-energy electrons with discrepancies less than 6%. Nevertheless, significant differences were found for electrons of lower energy due to statistical uncertainties larger than 10%. The comparison of the SAF values between the new ICRP voxel phantoms and the mathematic ones shows significant differences.

The present SAFs calculation for the new ICRP reference phantoms is validated by the intercomparison of results obtained by HGMU and IRSN and gives an insight into the evolution from the former SAFs derived from stylized phantoms.

Keywords— **SAF, ICRP reference computational phantoms, OEDIPE, Monte Carlo, internal dosimetry.**

I. Introduction

In nuclear medicine, a radiopharmaceutical administered to a patient is distributed in the body according to its biokinetics. Thus, several organs become sources of radiation delivering a fraction of emitted energy in each tissue of the human body. For radiation protection purpose, it is important to accurately and realistically determine the dose received by patients during either diagnostic or therapeutic procedures. From the biokinetics and energy emission spectrum of the incorporated radionuclide, the quantity needed to evaluate the patient dose is the specific absorbed fraction (SAF). It is defined as the fraction of the energy emitted from a source organ that is absorbed by a target organ, divided by the mass of the target organ.

So far, SAFs have been calculated by applying the equations of particle transport in matter to computational phantoms representing body organs by simple mathematical expressions providing a rough representation of the human anatomy. The development of more realistic anatomical models was desirable to achieve a better dose assessment. To do so, voxel phantoms were derived from computed tomography (CT) or magnetic resonance (MRI) image data of real persons and provide detailed information about the human anatomy. In its recent recommendations [1], the ICRP adopted adult male and female voxel phantoms, respectively RMCP and RFCP, for the forthcoming update of organ dose coefficients.

SAFs for monoenergetic photon and electron sources were computed simultaneously at the Helmholtz Zentrum München (HMGU, Germany) and Institut de Radioprotection et de Sûreté Nucléaire (IRSN, France) using RMCP and RFCP for application to internal dosimetry.

II. Materials and Methods

A. The new ICRP reference male and female phantoms

The new reference adult male and female computational phantoms shown in figure 1, RMCP and RFCP [2], were developed at HMGU on the basis of CT data of real persons

O. Dössel and W.C. Schlegel (Eds.): WC 2009, IFMBE Proceedings 25/III, pp. 178–180, 2009.
www.springerlink.com

[3]. The dimensions and masses of their 140 organs and tissues are consistent with the ICRP reference anatomical and physiological parameters [4].

B. OEDIPE

At IRSN, the software OEDIPE [5] was used to perform the SAF calculations. This software allows estimating the specific dose absorbed by the tissues of an internally exposed individual using voxel phantoms and the MCNPX Monte Carlo particle transport calculation code (LANL, USA) [6].

OEDIPE was elaborated as a user-friendly graphic interface developed under Interactive Data Language (Research Systems Inc. USA). Its global features are defined according the following stages:

- importation of CT or MRI data of the person,
- construction of a computational phantom or importation of an existing voxel phantom,
- definition of the sources of radiation (location, activity, energy and type of emissions),
- automatic creation of a MCNPX input file
- process of the MCNPX output file

OEDIPE can provide either the dose distribution either at the organ or voxel level (as isodose curves superimposed with the anatomical images).

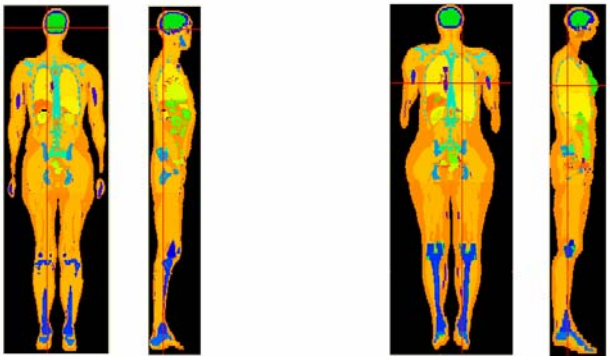

Fig. 1 Frontal and lateral slices of the new reference phantoms of the ICRP: adult male RMCP (left) and adult female RFCP (right).

C. Calculation of SAFs

Monoenergetic electron and photon sources were simulated by assuming that they were uniformly distributed inside each source organ of RMCP and RFCP. In the lungs, the source was distributed proportionally to the mass of the 4 lung regions. 3 source organs and tissues (lungs, thyroid and liver) have been simulated with initial photon and electron energies ranging between 15 keV and 10 MeV. With MCNPX, the energy deposit tally *f8 was used to score the energy absorbed by target tissues. The SAF values were then derived for each source and target region using equation (1):

$$SAF(r_k \leftarrow r_h) = \frac{E_k / E_h}{m} \qquad \text{Equation (1)}$$

Where r_h is a source organ, r_k is a target organ, E_k is the energy absorbed in r_k, E_h is the energy emitted from r_h and m is the mass of r_k.

The same SAF values were calculated at HMGU using the EGSnrc Monte Carlo code [7] and the results were compared for quality assurance purpose.

III. Results

The chosen source organs are the lungs, thyroid and liver. The colon wall, stomach wall, liver and breasts were selected as target tissues. For each phantom, source organ and photon/electron energy, 5 millions particle histories were simulated.

Selected examples are provided, illustrating the SAF values obtained for photons (figure 2) and electrons (figure 3) when the source is the liver and the target is the lung.

A general good agreement was obtained between SAF values assessed by MCNPX and EGSnrc codes. For photons, the discrepancies were less than 6 %. For high energy (>300 keV) electrons, slight differences between 0.1 % and 4.7 % were observed. However, at lower energies (<300 keV), more significant differences are seen, ranging from 1.3 % to 100 %. These discrepancies for low energy electrons are mainly attributable to statistical errors higher than 10 %.

These results for the voxel phantoms were then compared with the SAF values from the stylized ORNL reference adult male [8] and female [9] phantoms. For photon SAF, the differences between stylized and voxel phantoms are significant as illustrated in figure 2. For electrons, the MIRD committee formalism [10] considers only auto-irradiation of organs with no electron escape from a source organ. However, explicit calculations of SAF show that electron escape and cross irradiation of organs are not negligible at high energies.

IV. Conclusions

SAF results for the reference female and male computational phantoms recently adopted by the ICRP are presented here for the first time. For monoenergetic photons and electrons in the considered source (lungs, thyroid and liver) and

target regions (stomach wall, breast, colon wall and lungs), the calculation performed at HMGU and IRSN using EGSnrc and MCNPX codes are in overall good agreement, enabling the validation of the SAF values for internal dosimetry.

Nonetheless, statistical errors for both Monte Carlo codes induce significant differences for low energy electrons.

References

1. International Commission on Radiological Protection (2007) The 2007 recommendations of the International Commission on Radiological Protection. ICRP publication 103, Ann. ICRP 37(2-4).
2. International Commission on Radiological Protection (2009) ICRP reference computational phantoms of the adult male and female. ICRP supporting guidance 6. To be published in Ann. ICRP.
3. Zankl M, Eckerman KF, Bolch WE (2007) Voxel-based models representing the male and female ICRP reference adult—the skeleton. Radiat Prot Dosimetry 127:174-86.
4. International Commission on Radiological Protection (2002) Basic anatomical and physiological data for use in radiological protection: reference values. ICRP Publication 89, Ann. ICRP 32 (3-4).
5. Chiavassa S, Bardiès M, Jourdain J.R, Franck D et al., (2005). OEDIPE: A personalized Dosimetric Tool Associating Voxel-Based Models with MCNPX.
6. Hendricks JS. MCNPX, Version 2.5e. Los Alamos National Laboratory Report, LA-UR-04-0569.
7. Kawrakow I. and Rogers D.W.O. The EGSnrc Code System: Monte Carlo Simulation of Electron and Photon Transport - NRCC Report PIRS-701
8. Cristy and Eckerman, ORNL/TM-8381, 1987.
9. Stabin et al., ORNL/TM-12907, 1995.
10. Loevinger R, Budinger TF, Watson EE (1991) MIRD Primer for Absorbed Dose Calculation. Rev ed. New York, NY: Society of Nuclear Medicine.

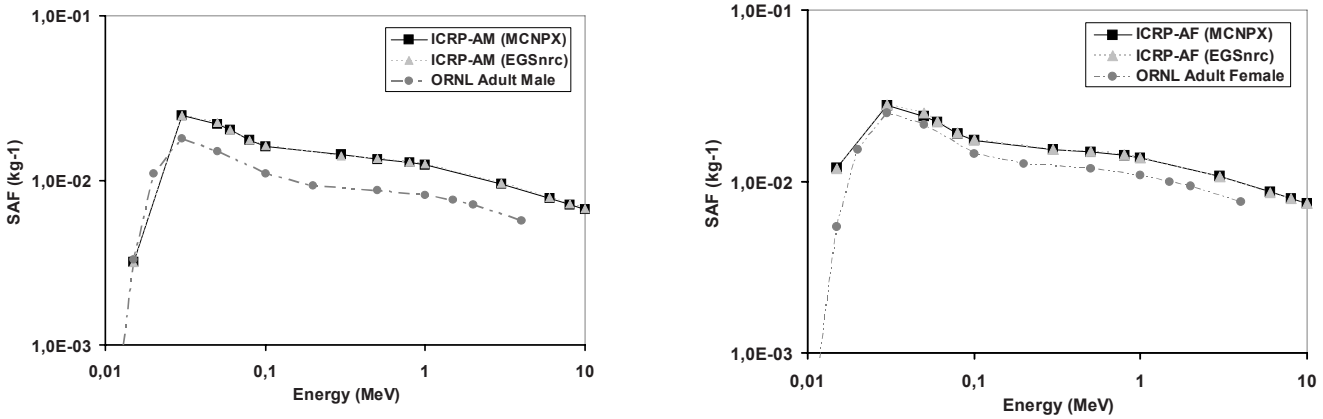

Fig. 2 Photon SAF evaluated at IRSN (MCNPX) and HMGU (EGSnrc) for the RMCP (left) and RFCP (right) phantoms compared to the ORNL Adult male (left) [7] and ORNL Adult Female (right) [8] phantoms. The source organ is the liver, the target is the lung

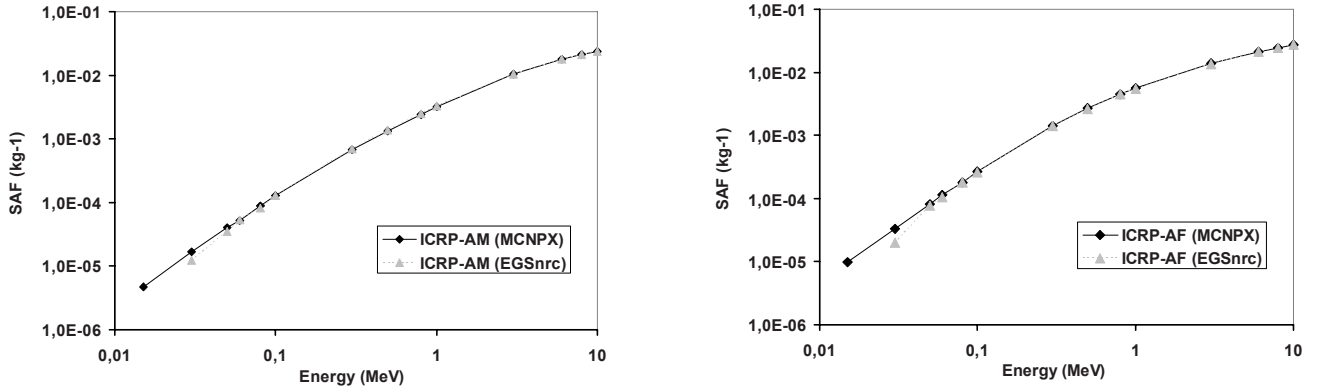

Fig. 3 Electron SAF evaluated at IRSN (MCNPX) and HMGU (EGSnrc) for the RMCP (left) and RFCP (right) phantoms. The source organ is the liver, the target is the lung.

Dose-Area-Product to Effective Dose in Interventional Cardiology and Radiology

L. Struelens[1], K. Bacher[2], M. Zankl[3]

[1] Belgian Nuclear Research Centre, SCK•CEN, Mol, Belgium
[2] University of Ghent, Department of Medical Physics, Ghent, Belgium
[3] Helmholtz Zentrum München – German Research Center for Environmental Health, Neuherberg, Germany

Abstract— **In this paper is explained how systematic tables are calculated for the determination of organ doses and effective dose from DAP values for interventional radiology and cardiology. This information is useful as an additional tool for dose optimization of patients for complex high-dose procedures. In the Monte Carlo calculation, 2 voxel based phantoms Golem and Laura are used.**

Keywords— **Interventional radiology and cardiology, organ dose, effective dose, conversion coefficients**

I. Introduction

The implementation of the European Directives (97/43/Euratom) [1] into the Belgian legislation introduced a number of new tasks to the radiology departments. It was stated that the determination of radiation doses are an important issue in the framework of radiation protection of the patient. And special attention is given to high-dose procedures, like interventional cardiology (IC) and interventional radiology (IR).

The need of dose auditing and patient dosimetry is emphasized in relation to optimization of radiological procedures. Moreover, radiological departments are legally obliged to register dose-area-product (DAP) values for every patient undergoing IR and IC procedures. As these procedures were considered as a priority, the Belgian Federal Agency of Nuclear Control financed a very large national multi-centre project on dose evaluations for IC and IR procedures a few years ago [2]. From this project, however, we learned that only DAP registration for optimization purposes is not always adequate. Measurements in almost 20 hospitals showed that centers with similar average DAP-values, could still result in significant different average effective dose values. This was caused by a different use in copper filtration during the procedures. With complex interventional procedures the risk of deterministic skin damage to the patient exists. To prevent this, the use of additional filtration is recommended. At new modern equipment, the amount of filtration is automatically introduced by the system, depending on the procedure and the patient. More and more also the use of other types of filtration is investigated for these kinds of procedures.

Simply register DAP-values is therefore not always the only and most adequate tool for optimization at interventional procedures. The additional calculation of effective dose could enable medical physicists to determine and evaluate dose values which will more connect to radiation risk evaluation, if necessary.

The effective dose can be calculated by multiplication of the registered DAP-values and appropriate conversion coefficients (CCs). In the past such coefficients have been calculated systematically for different anatomical regions and radiation projections for conventional radiological procedures. The use of these published CCs, however are not appropriate for the calculation of effective dose for IC and IR procedures. The irradiated field sizes and regions deviate from those in conventional radiology. Moreover, the requested CCs according to the beam qualities used for these complex procedures are not included in the published conversion tables. In literature [3], [4], [5], [6] some CCs can be found for specific interventional procedures, calculated according to the need of the specific study. In the framework of patient dose optimization, however, there is a need to the availability of systematic tables with CCs who will allow the calculation of the effective dose for the complete offer of IC and IR procedures, if needed.

In this paper is described how the CCs are calculated for the most common and used radiation fields in interventional cardiology and interventional radiology. The systematic tables with conversion coefficients can be obtained from the authors or at the Federal Agency of Nuclear Control (www.fanc.fgov.be).

II. Material and methods

A. Choice of Monte-Carlo code

The Monte Carlo code that is used in this project is *MCNP-X (v 2.5.0)* [7]. This code has been used frequently in medical physics and allows reliable dose calculations for photon radiation sources. The calculations are performed by 2 institutes: the department of medical Physics of the University of Ghent (UGent) performed the necessary calculations for the IC procedures and the Belgian Nuclear Research Centre (SCK•CEN) performed all calculations for

O. Dössel and W.C. Schlegel (Eds.): WC 2009, IFMBE Proceedings 25/III, pp. 181–184, 2009.
www.springerlink.com

the IR procedures. The same and most recent libraries, containing all cross sections and material data, are used by both institutes.

B. X-ray source definition

An important input parameter for the Monte-Carlo simulations is the X-ray source design. Different possibilities exist to model an X-ray source in the *MCNP-X* environment. A small intercomparison with a simplified geometry showed that the approach of both institutes resulted in the same values.

With respect to the definition of the X-ray spectrum, the "IPEM-78 – Catalogue of Diagnostic X-ray Spectra" [8] was used. This publication provides a valuable software tool for generating X-ray spectra based on parameters kVp, filtration, anode angle and kV signal ripple. In clinical practice a large variety of X-ray spectra are being used. For the interventional applications in this project, kVp-values typically range from 60 to 130 kVp. Filtrations can be based on a single aluminium filtration (2.5 – 6 mm Al) or on a combination with copper filtration (0.1 – 0.9 mm Cu). As it is practically impossible to simulate all possible kV/filtration combinations for all clinical projections, an alternative approach is used within the project. We have decided to use X-ray spectra definitions based on half-value layers (HVL). In fact, different kVp/filtration combinations may result in the same HVL-values as illustrated in figure 1.

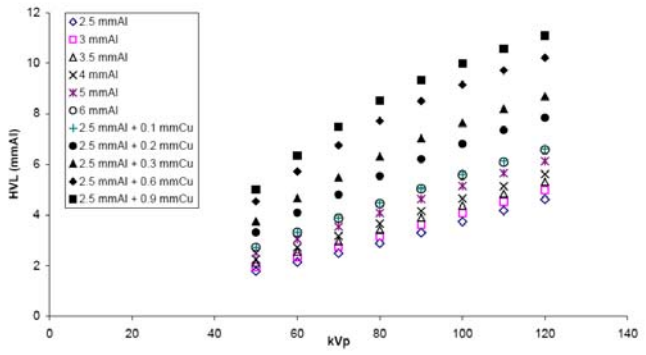

Fig. 1 Half-value layer values for different kVp and filter combinations

Therefore, simulations based on a HVL-range that is clinically relevant would be interesting. In order to test the feasibility of this approach, Monte Carlo calculations were performed on a mathematical anthropomorphic phantom using different kVp/filtration settings – all resulting in the same HVL. The latter simulations showed that DAP-to-effective dose conversion coefficients simulated with the "HVL method" deviated maximum 5% of the values simulated with the exact spectrum. For interventional radiology procedures, an anode angle of 14° was used, whereas for interventional cardiology procedures the spectra are generated based on an anode angle of 9°.

C. X-ray fields and projections

The X-ray field sizes and projections are other important factors to be taken into account for the simulations. In table 1 and 2, an overview of typical clinical settings is given for IR and IC, respectively.

Table 1 X-ray fields and projections considered for interventional radiology procedures

	Application	Projection	Field size at image intensifier (cm)
1	Head	LAO[1] 45°	28
2	Head	RAO[2] 45°	28
3	Head	PA[3]	28
4	Head	LLAT[4]	28
5	Head	RLAT[5]	28
6	Neck	LAO 45°	28
7	Neck	RAO 45°	28
8	Neck	PA	28
9	Thorax	LAO 45°	28
10	Thorax	RAO 45°	28
11	Abdomen	LAO 45°	40
12	Abdomen	RAO 45°	40
13	Abdomen	PA	40
14	Abdomen	LLAT	40
15	Abdomen	RLAT	40
16	Pelvis	LAO 45°	40
17	Pelvis	RAO 45°	40
18	Pelvis	PA	40
19	Upper legs	PA	40
20	Lower legs	PA	40

[1]LAO: Left Anterior Oblique / [2]RAO: Right Anterior Oblique
[3]PA: Posterior-Anterior / [4]LLAT: Left Lateral
[5]RLAT: Right Lateral

Table 2 X-ray fields and projections considered for interventional cardiology procedures

	Projection RAO/LAO	Projection CRAN[1]/CAUD[2]	Field size at image intensifier (cm)
1	RAO 30°	CAUD 25°	17
2	RAO 30°	CAUD 0°	17
3	RAO 30°	CRAN 25°	17
4	LAO 45°	CRAN 25°	17
5	LAO 45°	CAUD 0°	20
6	LAO 45°	CAUD 25°	17
7	LAO 90°	CAUD 0°	17
8	LAO 0°	CAUD 25°	17
9	LAO 0°	CAUD 0°	20
10	LAO 15°	CAUD 0°	17
11	LAO 30°	CAUD 0°	17
12	RAO 30°	CAUD 0°	20

[1]CRAN: cranial / [2]CAUD: Caudal

D. Choice of anthropomorphic phantom

In view of the new recommendations of ICRP [9] and the definition of additional radiation sensitive organs (salivary glands, adipose tissue, connective tissue, extra thoracic airways, heart wall and lymphatic nodes) for the calculations of the effective dose, the choice of an anthropomorphic phantom was not straightforward. Current mathematical phantoms are not appropriate for calculating the revised definition of the effective dose as they do not contain these 'new' organs. The choice of a voxel-phantom, for which a larger amount of organs are segmented, seemed more appropriate. At the start of the project, the standard ICRP voxel phantoms were not available. Other appropriate and available phantoms with standard dimensions are the MAX06 and FAX06 phantoms from Kramer et al [10]. These are very detailed phantoms constructed from voxels of 1.2 x 1.2 x 1.2 mm³. The total MAX06 phantom consists of 474 x 222 x 1359 = 143.004.582 voxel elements. All necessary organs are present and realistically segmented. However, when this phantom is converted into a format suitable for *MCNP-X*, input files are created from 20 to 30 MB. Such large input files require a lot of computer memory and some test calculations demonstrated that this memory capacity is not available in both UGent and SCK•CEN. Hence, the calculations could not be performed with these phantoms.

A large family of voxel phantoms is available at the Helmholtz Zentrum München – German Research Center for Environmental Health and we decided to test the Golem [11] and Laura phantoms. These phantoms have body characteristics similar to the reference persons. Golem is constructed from voxels of 2.08 x 2.08 x 8.0 mm³. His height is 176 cm and weight 68.9 kg. Laura is constructed from 1.875 x 1.875 x 5.0 mm³ voxels. Her height is 167 cm and weight 59 kg. A cross section of both phantoms is given in figure 2. Both phantoms have a realistic number of voxels that can be handled by *MCNP-X*. Test runs showed that CPU time of maximum 130 minutes are needed for the transport of 10E06 particles (for F6 and *F8 tallies) on the computer clusters of UGent and SCK•CEN, resulting in relative errors for the organs in the radiation field lower than 1%.

As red bone marrow and bone surface are not segmented within the Golem/Laura phantoms, correction factors to the mean skeleton dose were calculated based on the material composition and density of red bone marrow, yellow bone marrow and cortical bone structures throughout the human body [12]. For the gall bladder and small intestine no distinction is made between wall and contents in the Golem phantom. Golem does not have breast (glandular tissue) and salivary glands and both phantoms do not have oral mucosa nor lymphatic nodes. The dose to the oral mucosa was approximated by the dose to the tongue and the dose to the lymphatic nodes was approximated by that to other distributed tissue, like muscle or adipose tissue.

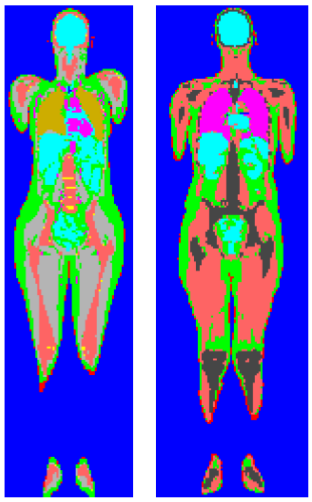

Fig 2 Cross sections of the Laura (left) and Golem (right) voxel phantoms

III. Results

For interventional radiology, the following spectra are considered:

- Head: from 80 to 100 kVp in steps of 10 kVp
  from 3 mm Al to 6 mm Al in steps of 1 mm
  from 0 to 0.3 mm Cu in steps of 0.1 mm
  This resulted in a HVL range from 3.5 – 8.5 mm Al
- Neck: from 60 to 100 kVp in steps of 10 kVp
  from 3 mm Al to 6 mm Al in steps of 1 mm
  from 0 to 0.3 mm Cu in steps of 0.1 mm
  This resulted in a HVL range from 2.5 – 8.5 mm Al
- Thorax, abdomen and pelvis: Idem as Neck
- Legs: from 60 to 80 kVp in steps of 10 kVp
  from 3 mm Al to 6 mm Al in steps of 1 mm
  from 0 to 0.3 mm Cu in steps of 0.1 mm
  This resulted in a HVL range from 2.5 – 6.5 mm Al

Spectra are considered in steps of 1 mm Al HVL for both the Golem and the Laura phantoms and each projection as given in table 1. This resulted in a total number of 262 calculations. For interventional cardiology, the following spectra are considered:

- Thorax: from 60 to 130 kVp in steps of 10 kVp
  2.5 mm Al, 3 mm Al and 4 mm Al
  from 0 to 0.9 mm Cu for 2.5 mmAl
  from 0 to 0.3 mm Cu for 3 and 4 mm Al
  in steps of 0.1 mm Cu

This resulted in a HVL range from 2.5 to 11.5 mm Al. For both phantoms and all projections considered in table 2, this resulted in a total number of 240 calculations.

Before the systematical calculation campaign started, a final intercomparison was performed between UGent and SCK•CEN. This should reveal possible differences in processing the voxel-based data. The simulations for this intercomparison was based on the same input file (PA thorax irradiation of the Golem phantom, field size 520 cm³, 70 kVp, 4 mm Al and 10E06 particles). The results are presented in table 3.

Table 3 Results of an intercomparison for one typical input file

	organ dose D/DAP SCK/CEN [Gy/Gy cm²]	organ dose D/DAP UGent [Sv/Gy cm²]
RBM	1,96E-05	1,98E-05
colon	7,56E-06	7,55E-06
lung	1,30E-04	1,31E-04
stomach	9,93E-05	9,92E-05
bladder	1,23E-07	1,22E-07
oesophagus	2,39E-04	2,39E-04
gonads	1,47E-08	1,45E-08
liver	1,04E-04	1,03E-04
thyroid	1,03E-04	1,04E-04
bone surface	4,46E-04	4,50E-04
brain	1,53E-06	1,54E-06
kidneys	1,87E-05	1,86E-05
salivary glands	4,41E-08	4,39E-08
skin	4,19E-05	4,20E-05
remainder:	8,99E-05	8,95E-05
effective dose/DAP	**6.72 Sv/Gycm²**	**6.72 Sv/Gycm²**

The results show an excellent agreement between the SCK•CEN and UGent simulations with respect to the effective dose/DAP. Individual organ doses show small deviations smaller than 1%. The latter simulation run had a CPU time of 55 min for the SCK•CEN simulations and of 79 min for the UGent simulations.

The results of the systematic calculation campaign are given in organ dose/DAP and effective dose/DAP for both phantoms separately. The tables can be obtained from the authors and from the Federal Agency of Nuclear Control (www.fanc.fgov.be).

IV. CONCLUSIONS

The possibility to calculate effective dose from online DAP measurements for interventional radiology and cardiology procedures can be a useful tool and completion for dose optimization purposes. In this project complete and systematic tables with organ dose and effective dose conversion coefficients are calculated from DAP values for these kinds of procedures

ACKNOWLEDGMENT

The research leading to these results has received funding from the Belgian Federal Agency of Nuclear Control.

REFERENCES

1. Council Directive 97/43/Euratom on Health Protection of Individuals against the Dangers of Ionizing radiation in relation to medical exposures and repealing Directive 84/166/Euratom, June 30th 1997. Official Journal No L 180, 09/07/1997
2. Bosmans H, et al (2006) First multi centre study to investigate high-dose X-ray procedures in Belgium. Final report funded by the Federal Agency of Nuclear Control.
3. Kemerinck GJ, De Haan MW et al. (2003) The effect of equipment set up on patient radiation dose in conventional and CT angiography of the renal arteries. BJR 76:625-630
4. Schultz FW, Geleijns J et al. (2003) Monte Carlo calculations for assessment of radiation dose to patients with congenital heart defects and to staff during cardiac catherizations. BJR 76:638-647
5. Kemerinck GJ, Kicken PJH et al. (1999) Patient dosimetry in abdominal arteriography. Phys. Med. Biol. 44:1133-1145
6. Kicken PJH, Zankl M and Kemerinck GJ (1999) Patient dosimetry in arteriography of the lower limbs. Part II: Dose conversion coefficients, organ doses and effective dose. RPD Vol. 81, No1:37-45
7. Pelowitz DB et al. MCNPX User's manual, version 2.5.0. Los Alamos National Laboratory. Report LA-CP-05-0369
8. Cranley K, Gilmore BJ, Fogarty GWA and Desponds L. Catalogue of Diagnostic X-ray Spectra & other Data .IPEM Report 78
9. ICRP Publication 105: Radiological Protection in Medicine, 105. Annals of the ICRP Volume 37 Issue 6
10. Kramer R, Khoury JH, Vieira JW and Lima VJM (2006) MAX06 and FAX06: update of two adult human phantoms for radiation protection dosimetry. Phys. Med. Biol. 51:3331-3346
11. Zankl M, Wittmann A (2001) The adult male voxel model "Golem" segmented from whole-body CT patient data. Radiat Environ Biophys 40:153-162
12. Zankl M, Eckerman KF, Bolch WE (2007) Voxel-based models representing the male and female ICRP reference adult – the skeleton. Radiat Prot Dosim 127(1-4), 174-186 doi:10.1093/rpd/ncm269

Author: Lara Struelens
Institute: Belgian Nuclear Research Institute SCK•CEN
Street: Boeretang 200
City: 2400 Mol
Country: Belgium
Email: lara.struelens@sckcen.be

The reference computational phantoms adopted by ICRP and ICRU

M. Zankl[1], J. Becker[1], N. Petoussi-Henss[1], H. Schlattl[1], W.E. Bolch[2], K.F. Eckerman[3], H.G. Menzel[4] and C. Hoeschen[1]

[1] Institute of Radiation Protection, Helmholtz Zentrum München – German Research Center for Environmental Health, Neuherberg, Germany
[2] Department of Nuclear & Radiological Engineering, University of Florida, Gainesville, Florida, USA
[3] Life Science Division, Oak Ridge National Laboratory, Oak Ridge, Tennessee, USA
[4] Radiation Protection Group, CERN European Organization for Nuclear Research, Genève, Switzerland

Abstract— **This paper summarizes the development of the computational phantoms of the Reference Male and Reference Female. In its recent recommendations, the ICRP adopted these computational phantoms for the forthcoming update of organ dose coefficients for internal and external radiation. The phantoms are based on medical image data of two individuals whose body height and mass closely resembled the reference data. The organ masses of both models were adjusted to the ICRP data on the adult Reference Male and Reference Female, without significantly altering their realistic anatomy. Thus, the phantoms are consistent with the information given in ICRP Publication 89 on the reference anatomical and physiological parameters for both male and female subjects. The paper describes the methods used for this process and the characteristics of the resulting voxel phantoms.**

Keywords— **Computational phantoms, voxel models, Reference Male, Reference Female.**

I. Introduction

Computational models of the human body have been used together with radiation transport codes for the evaluation of organ dose conversion coefficients in occupational, medical and environmental radiation protection. During the last two decades, the mathematical MIRD-type body models were replaced by voxel models that are derived mostly from medical image data of real persons. Among other laboratories, the Helmholtz Zentrum München – German Research Center for Environmental Health (i.e., the former GSF – National Research Center for Environment and Health) developed 12 voxel models of individuals of different stature and ages: 2 pediatric ones, 4 male and 6 female adult models [1-4]. It was shown that the simplified schematic organ shapes of the MIRD-type phantoms influence the resulting dose coefficients, which may deviate systematically from those calculated for voxel models in some cases [2, 5].

For external radiation, the parameters influencing the organ doses are mainly: depth of the organ below the body surface, trunk diameter relative to the incoming radiation, and exterior shape of the trunk. For internal dosimetry, the dominating parameters are the relative position of source and target organs (for organ cross-fire) and organ mass (for organ self-absorption). Hence, the International Commission on Radiological Protection (ICRP) and the International Commission of Radiation Units and Measurements (ICRU) decided to use voxel models for the update of organ dose conversion coefficients, following the recent revision of the ICRP Recommendations [6]. According to the ICRP, these voxel models should be representative of the adult Reference Male and Reference Female [7] with respect to their external dimensions and their organ masses.

To meet these requirements, at the Helmholtz Zentrum München two voxel adult reference models of a male and a female have been developed upon request of and in collaboration with the ICRP, based on the voxel models of two individuals whose body height and weight resembled the reference values. Approximately 140 organs and tissues were segmented, including also objects that were not previously contained in the MIRD-type phantoms, such as the main blood vessels, cartilage, muscles, and lymphatic nodes. The external dimensions and nearly all organ masses of both models were adjusted to the ICRP reference values. A detailed description of the reference computational phantoms is provided by the ICRP [8]. The construction process and the resulting voxel phantoms are shortly summarized in the following.

II. Construction of the Reference Computational Phantoms

A. Phantom properties requested by the ICRP

In order to use the voxel phantoms for calculations of organ dose conversion coefficients and SAFs following the new ICRP Recommendations [6] it is obvious that they should accommodate all organs and tissues relevant to radiation protection considerations. Furthermore, additional target regions have been identified in the Human Respiratory Tract [9] and Human Alimentary Tract [10] Models.

O. Dössel and W.C. Schlegel (Eds.): WC 2009, IFMBE Proceedings 25/III, pp. 185–188, 2009.
www.springerlink.com

When radioactive material is incorporated in the body, those organs, tissues, and body regions where this material is accumulated or passes through, become "source organs" that irradiate the radiation-sensitive "target organs". Most of the possible source regions are also target regions and as such already included due to the above considerations. Additional source regions are located especially in the alimentary and respiratory tracts as well as in the skeleton.

Due to the limited resolution of the medical image data used to construct the voxel phantoms (in the range of millimeters) and the very small dimensions of some source and target tissues (tens of micrometres), not all of them could be segmented directly. Therefore, for some source and target tissues, "surrogate" regions had to be found or correction factors have to be applied to the calculated doses. These limitations of the phantoms are discussed in more detail below.

B. Selection of suitable segmented data

In order to construct voxel models of the Reference Male and Reference Female, appropriate voxel models were used as a starting points, i.e. models with external dimensions close to the ICRP reference values [7] since then the required modifications remained moderate, and the danger of distorting the anatomical relations was small.

Male phantom: As a basis for the male reference computational phantom, the male adult voxel model "Golem" [11] was used that was constructed from whole-body CT images of a 38-year old single individual patient with a height of 176 cm and a whole body mass of slightly below 70 kg (Reference Male: 176 cm; 73 kg). The data set consisted of 220 slices of 256 x 256 pixels. The original voxel size was 8 mm in height with an in-plane resolution of 2.08 mm. 122 individual regions, i.e., organs, tissues and parts thereof, in the body were segmented.

Female phantom: The female reference computational phantom was constructed on the basis of the voxel model "Laura". The data were derived from a whole body CT scan of a 43-year old patient of 167 cm height and a mass of 59 kg (corresponding ICRP reference values: 163 cm and 60 kg). The data set consisted of 174 slices of 5 mm width (head and trunk) and 43 slices of 2 cm width (legs), each with 256 x 256 pixels. The 2-cm slice images were resampled to result also in slices of 5 mm width. The resulting data set consisted of 346 slices; the voxel size was then 5 mm height with an in-plane resolution of 1.875 mm. A total of 88 regions of the body were segmented in Laura [4].

C. Modifications of Golem and Laura to create the reference computational phantoms

The following steps were then followed: (1) adjustment of the body height and the skeleton mass of the segmented model to the reference data by voxel scaling, (2) adjustment of the single organ masses to the reference values by adding or subtracting appropriate numbers of organ voxels, and (3) adjustment of the whole body mass to the reference values by adding or subtracting an appropriate number of adipose tissue voxels.

It was the intention to keep the modifications to the skeleton shape to a minimum so as to preserve the 'frame' of the body. It was, however, not possible for both models to accommodate the requested brain mass within the skull. Therefore, it was necessary to increase the skulls of both phantoms. Furthermore, for the female phantom an outward movement of the ribs (as occurs also during breathing) was necessary to accommodate the liver.

Voxel scaling: Apart from the above modifications of the skeleton shape, the volume of the skeleton was adjusted to the reference value by voxel scaling. Since Golem's body height corresponds to the reference value, the original voxel height was kept unmodified. Laura was taller than the ICRP adult Reference Female, so the voxel height for the female reference computational phantom was reduced from 5.0 to 4.84 mm. The numbers of segmented skeleton voxels (including the segmented cartilage) are 211427 and 378204 for the male and female reference computational phantom, respectively. Using the ICRP reference mass values [7] and the ICRU mass density values [12] of the various bone constituents, total skeleton volumes of approximately 7730 cm^3 and 5770 cm^3 for the male and female reference computational phantoms were evaluated. This resulted in voxel volumes of 36.54 mm^3 and 15.25 mm^3, respectively. From this, in-plane resolutions of 2.137 mm for the male and 1.775 mm for the female reference computational phantom were calculated.

Individual organ volume modifications: The individual organs were adjusted to their reference masses one by one using a software package that was designed specifically for this purpose [13]. Some very fine structures could not be adjusted exactly to the reference values, due to limitations of voxel resolution, but for most organs a very close approximation of the reference values could be achieved.

Additional modifications: Going back to the original CT images, some effort was made to identify further anatomical details, such as smaller blood vessels and bronchi. Furthermore, since Laura was lying on her hands, the arms of the reference computational phantom were moved to the sides. After having fixed the internal organ topology, lymphatic nodes were incorporated on the basis of anatomical text-

books. The final step was to adjust the whole body masses to 73 kg and 60 kg, respectively, by adding additional voxel layers of adipose tissue.

Sub-segmentation of the skeleton: Since the dimensions of internal structures of the bones are in the order of tens of micrometers and cannot be resolved in a normal CT scan, direct segmentation of these structures was not possible. Therefore, the bones were sub-divided in an outer shell of cortical bone and the spongiosa volumes that are accommodating trabecular bone, red and yellow bone marrow, as well as endosteal tissues and some amount of cartilage. The long bones contain a medullary cavity as third component.

III. Description of the Reference Computational Phantoms

A. Main characteristics

The adult reference computational phantoms are defined in the form of a three-dimensional voxel array. The array entries are organ identification numbers that describe to which organ a specific voxel belongs. The columns correspond to the x co-ordinates, with numbers increasing from right to left side; the rows correspond to the y co-ordinates, increasing from front to back; and the slices correspond to the z co-ordinates, increasing from the toes to the vertex of the body.

The main characteristics of the adult reference computational models are summarized in the following table.

Table 1 Main characteristics of the adult male and female reference computational phantoms

Property	Male	Female
Mass (kg)	73	60
Height (m)	1.76	1.63
Voxel in-plane resolution (mm)	2.137	1.775
Slice thickness (mm)	8	4.84
Approximate number of tissue voxels (millions)	1.9	3.9
Number of columns	254	299
Number of rows	127	137
Number of slices	220	346

A graphical representation of both adult reference computational phantoms is shown in Fig. 1.

B. Skeleton

Nineteen bones and bone groups were identified and subdivided in cortical bone, spongiosa and – if applicable – medullary cavity. In total, 48 different identification numbers were assigned to the skeleton. To fully exploit the available data on red bone marrow distribution and marrow cellularity [14], the spongiosa regions of different bones are composed of different ratios of mineral bone, red and yellow bone marrow [15].

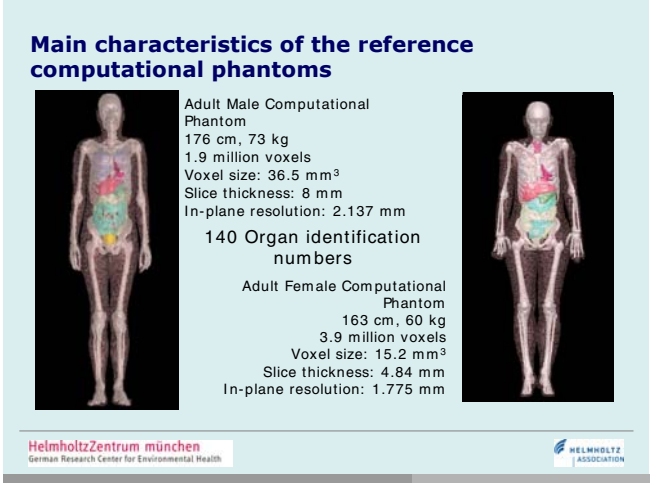

Fig. 1 Frontal view of the male (left) and female (right) reference computational phantoms representing the ICRP adult Reference Male and Reference Female

C. Blood

It is not possible to segment the entire blood pool of the body; the larger part of the blood volume is situated in the small vessels and capillaries inside the organs and cannot be segmented. On the other hand, the elemental compositions of tissues as listed in the relevant ICRP and ICRU publications [7, 12] are exclusive of blood. Therefore, the blood content in each organ as given in [7] was considered by including a blood portion in the elemental tissue composition of each organ.

D. Limitations due to image resolution

In addition to the skeletal fine structures, there are also other regions that could not be directly segmented or could not be adjusted to their reference values due to their small size or complex structure. These are:

- Extrathoracic airways (represented by an entire voxel layer lining the airways of nose, larynx and pharynx, whereas in reality they are only a few millimeters thick)
- Bronchi (not followed down further than the very first generations of branching)

- Bronchioles (too small for segmentation; represented by homogeneous lung tissue with a density that is the average of the densities of bronchiolar tissue and included air)
- Skin (represented by one voxel layer wrapping the exterior of the phantoms)
- Cartilage (only partly segmented; rest included in elemental composition of spongiosa regions)
- Gall bladder (sum of wall and contents have reference mass sum; otherwise not enough wall voxels to encompass the entire volume of the content)
- Adipose tissue ("residual tissue" used to adjust whole body mass to reference value; matching of reference adipose tissue mass approximately achieved)

The eye lens masses were adjusted to the reference values, but the shape of the lenses is somewhat coarse, due to their small size compared to the voxel dimensions.

IV. Conclusions

While in the past mathematical phantoms of the human body having simplified shapes of the body and its internal organs have been used for all types of organ dose calculations, a variety of voxel models became available in recent years that are based on medical image data of real persons. A series of studies performed by different research groups were able to show that the voxel models do not only have the advantage of a much more realistic anatomy, but that this difference has also a clear impact on the calculated organ doses. These findings have persuaded the ICRP and the ICRU to employ this new type of computational phantoms for the update of dose coefficients for external and internal exposures to ionising radiation that is planned following the new ICRP Recommendations issued recently.

The reference computational phantoms presented in this work are the closest existing representation of the ICRP reference individuals. As such they will be employed by the ICRP and ICRU to calculate dose coefficients for radiological protection quantities.

Although the organ masses have been adjusted to the reference values, it should be clear that these phantoms still have their individual anatomical relations based on the individuals whose medical image data have been used for their construction. Both models cannot represent any real individual, and they should not be used to assess doses for individuals, e.g. in medical applications. Especially for radiation treatment planning purposes, the reference computational phantoms cannot be applied.

Acknowledgment

We acknowledge the comments received from the ICRP committees, the ICRU, and selected expert reviewers.

References

1. Petoussi-Henss N, Zankl M, Fill U et al. (2002) The GSF family of voxel phantoms. Phys Med Biol 47:89-106
2. Zankl M, Fill U, Petoussi-Henss N et al. (2002) Organ dose conversion coefficients for external photon irradiation of male and female voxel models. Phys Med Biol 47:2367-2385
3. Fill U, Zankl M, Petoussi-Henss N et al. (2004) Adult female voxel models of different stature and photon conversion coefficients for radiation protection. Health Phys 86:253-272
4. Zankl M, Becker J, Fill U et al. (2005) GSF male and female adult voxel models representing ICRP Reference Man - the present status, The Monte Carlo Method: Versatility Unbounded in a Dynamic Computing World, Chattanooga, TN, pp
5. Zankl M, Petoussi-Henss N, Fill U et al. (2003) The application of voxel phantoms to the internal dosimetry of radionuclides. Radiat Prot Dosim 105:539-548
6. ICRP (2007) The 2007 Recommendations of the International Commission on Radiological Protection. ICRP Publication 103, Oxford, UK
7. ICRP (2002) Basic anatomical and physiological data for use in radiological protection: reference values. ICRP Publication 89, Oxford, UK
8. ICRP (in press) Adult reference computational phantoms. ICRP Publication 108, Oxford, UK
9. ICRP (1994) Human respiratory tract model for radiological protection. ICRP Publication 66, Oxford, UK
10. ICRP (2006) Human alimentary tract model for radiological protection. ICRP Publication 100, Oxford, UK
11. Zankl M, Wittmann A (2001) The adult male voxel model "Golem" segmented from whole body CT patient data. Radiat Environ Biophys 40:153-162
12. ICRU (1992) Photon, electron, proton and neutron interaction data for body tissues. ICRU Report 46, Bethesda, MD
13. Becker J, Zankl M, Petoussi N (2007) A software tool for modification of human voxel models used for application in radiation protection Phys Med Biol 52:N195-N205
14. ICRP (1995) Basic anatomical and physiological data for use in radiological protection: the skeleton. ICRP Publication 70, Oxford, UK
15. Zankl M, Eckerman K F, Bolch W E (2007) Voxel-based models representing the male and female ICRP reference adult – the skeleton. Radiat Prot Dosim 127:174-186 doi:10.1093/rpd/ncm269

Author: Maria Zankl
Institute: Helmholtz Zentrum München – German Research Center for Environmental Health, Institute of Radiation Protection
Street: Ingolstädter Landstr. 1
City: 85764 Neuherberg
Country: Germany
Email: Zankl@helmholtz-muenchen.de

Indoor Radon Measurement in Some Apartments of Mashhad City (Iran)

A. Binesh[1], A.A. Mowlavi[2], S. Mohammadi[3], and P. Parvaresh[3]

[1] Physics Department, Payam Nour University, Fariman, Iran
[2] Physics Department, Sabzevar Tarbiat Moallem University, Sabzevar, Iran
[3] Physics Department, Payam Nour University, Mashhad, Iran

Abstract— **Environmental monitoring and indoor radon measurement are important for health life to give advises to the people in order to reduce the cancer risk of respiratory system. In the present resarch, radon concentration in the air has been measured at indoor of 40 apartments in Mashhad city with PRASSI system. Most of people close the doors and windows during the cold days in winter and use natural gas as fuel and other household usage. So, the radon concentration level increases as we expect. The result demonstrates about 35% of apartments have radon level low than the normal level (48 Bq/m^3) and more than 65% have high radon concentration. We suggest reducing radon level at homes by suitable simple ventilation systems.**

Keywords— **Indoor Radon concentration, Respiratory cancer, Mashhad**

I. Introduction

Radon (^{220}Rn) and Thoron (^{222}Rn) in indoor space, such as houses and apartments, originate and emanation from the wall, floor and ceilings which are constructed of building material, rock or soil. Also, it release from materials brought into the room, such as radon-rich water or natural gas fuel, and by radon or thoron in inlet air, which may in turn have a normal concentration of the gases or an increased concentration derived from sources outside the room [1]. Radon is one of the most dangerous radioactive elements in the environment. The greatest fraction of natural radiation exposure in humans results from inhalation indoor and in work places of the decay products of radon which are short lived daughters such as ^{218}Po and ^{214}Po [2-6]. The radon progenies are solid isotopes that found in aerosol and when inhaled, they constitute the major source of health risk. In fact, they adhere to the internal wall of the respiratory tract, and can induce lung cancer [7]. It has been estimated that radon and its short-lived decay progenies contribute with three quarters of the annual effective dose received by man from natural terrestrial sources and is responsible for about half of the dose from total sources [1, 2].

In the last few years national authorities and the public in general have shown a renewed interest in natural radiation in the environment, particularly the concentration of radon gas in homes. During the cold days most of people close the doors and windows; so, air ventilation is minimized and the radon concentration level increases in indoor spaces. In the present research, radon concentration in the air has been measured at indoor some apartments in Mashhad-the second city after Tehran, located in north-east of Iran- with PRASSI system.

II. Indoor Radon Measurement

The PRASSI (Portable Radon Gas Surveyor SILENA) Model 5S has been use for indoor radon concentration measurement. This system is particularly well suited for this type of measurement. PRASSI pumping operates with constant fallow rate at 3 litters per minute and its detector is a scintillation cell coated with ZnS(Ag) 1830 cm^3 volume.

III. Results and Discussion

In this work, radon concentration in the air of some apartments in Mashhad city has been measured with PRASSI system. Most of people close the doors and windows during the cold days; so, the radon concentration level increases as we expect. Fig. 1 shows the histogram of radon concentration at 40 apartments. The result demonstrate about 35% of apartments have radon level low than the normal level (48 Bq/m^3), as shown in Fig. 2. Some of the apartments have radon level exceed the normal level up to 5-6 times! We must mention the mean outdoor radon was 15.2 Bq/m^3 in that time.

O. Dössel and W.C. Schlegel (Eds.): WC 2009, IFMBE Proceedings 25/III, pp. 189–190, 2009.
www.springerlink.com

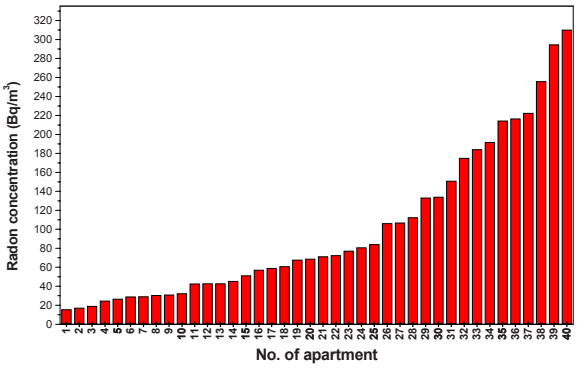

Fig. 1 The histogram of radon concentration in the air of 40 apartments.

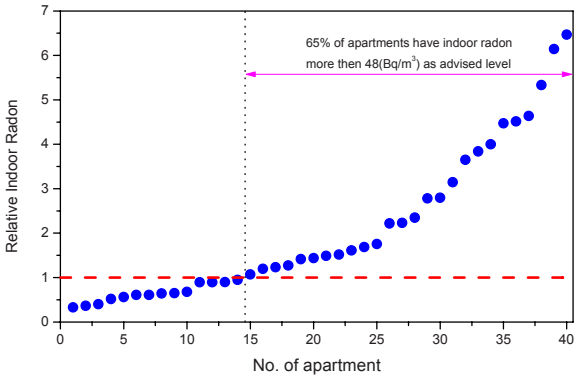

Fig. 2 Relative radon concentration of the 40 apartments (the measured data are normalized to 48 Bq/m^3 as normal indoor radon level).

IV. Conclusions

Nearly 50% of annually radiation dose absorption of human is due to radon which is one of the main cancers cause at respiratory and digestion systems. The result demonstrates about 35% of apartments have radon level low than the normal level (48 Bq/m^3) and more than 65% have high radon concentration! To improve the social health, it is necessary to training public people how they can reduce the indoor radon level by simply way such as using fans or air circulate systems.

Acknowledgment

This work has been done by support of Payam Nour University and authors would like to thanks for their contribution.

References

1. UNSCEAR (1982) United Nations Scientific committee on the Effects of Atomic Radiation. Ionizing Radiation: Sources and biological effects. United Nations, New York, USA.
2. Mansour HH, Khdar S, Abdulla HY, Muhamad NQ, Othman MM, Qader S (2005) Measurement of indoor radon levels in Erbil capital byusing solid state nuclear track detectors. *Radiat Meas* ***40:*** *544– 547.*
3. Abbady A, Abbady AGE, Rolf M (2004) Indoor radon measurement with The Lucas cell technique. *Applied Radiation and Isotopes* ***61:*** *1469–1475.*
4. Abu-Jarad F (1997) Indoor cigarette smoking: uranium contents and carrier of indoor radon products. *Nucl Tracks Radiat Meas* ***128:*** *579–584.*
5. Russel WM, James AR, Thomas WD (1984) Physics of the Atomic, Fourth edition, Addison-Wesley Publishing Company, Reading, MA.
6. Panatto D, Ferrari P, Lai P, Gallelli G (2006) Relevance of air conditioning for 222Radon concentration in shops of the Savona Province, Italy. *Science of the Total Environment* ***355:*** *25–30.*
7. Marley F, Denman AR, Philips PS (1998) Studies of radon and radon progeny in air conditioned rooms in hospitals. *Radiat Prot Dosim* ***5:*** *273– 276*Smith J, Jones M Jr, Houghton L et al. (1999) Future of health insurance. N Engl J Med ***965***:325–329.

Author: Alireza Binesh
Institute: Payam Nour University
Street:
City: Fariman
Country: Iran
Email: binesh_ar@yahoo.com

Mammodos – In-Vivo Dosimetry in Mammography

J.U. Wuerfel[1], C. Pychlau[1], C. Cappellini[2], A. Bulgheroni[3], F. Risigo[2], V. Chmill[2], M. Caccia[2], and A. Martemiyanov[4]

[1] PTW-Freiburg, Freiburg, Germany
[2] Department of Physics and Mathematics, University of Insubria, Como, Italy
[3] Istituto Nazionale di Fisica Nucleare – Sez. di Milano, Milano, Italy
[4] Institute for Theoretical and Experimental Physics (ITEP), Moscow, Russia

Abstract— **In the scope of the RAPSODI EU research project, a prototype detector for in-vivo dose measurements in Mammography was developed. We present and discuss first results on the system qualification, in particular on the linear dynamic range, the energy response and the radiological as well as optical transparency of the detector.**

Keywords— **In-vivo dosimetry, Mammography, Diagnostic instrumentation, Average glandular dose**

I. Introduction

An increasing number of countries in Europe are starting to introduce Mammography screening programs for the early detection of Breast Cancer [1]. To evaluate the radiation hazard these patients are exposed to, it is essential that the dose for each examination is well documented. For most modalities of classical diagnostic imaging in Germany, the dose of each examination has to be measured and recorded [2]. Dose measurements are also requested by the EC for any new radiological equipment [3]. Currently, there exists no device on the market that is able to measure the dose during a mammographic examination. In the scope of the RAPSODI EU-project a prototype, "Mammodos", to measure in-vivo dose in Mammography has been developed. Mammodos is designed to measure the surface dose on top of the breast during the examination. It consists of a flat sheet of transparent plastic and will be placed between breast and compression plate, see Fig. 1.

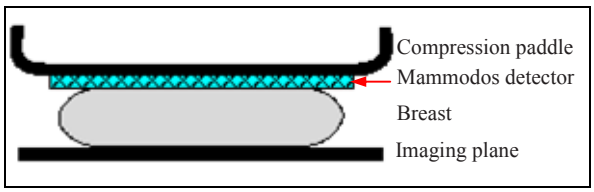

Fig. 1 In order to measure the surface dose on the breast, the Mammodos detector will be placed between compression paddle and the breast.

II. Materials and Methods

The X-ray dose is measured by an organic scintillator. Via a polymeroptical cable, the scintillated light is transported to a very sensitive semiconductor based light detector, called "Silicon Photo Multiplier" (SiPM). In order not to disturb the mammography image, the scintillator is embedded into a plastic sheet of X-ray equivalent material. This embedded detector is almost invisible on a mammogram. In addition, the embedding material is optically transparent to facilitate the handling of the detector in every day use.

SiPMs from Hamamatsu [4] and from SensL [5] have been used. In addition to the SiPMs, an Optidos dosemeter (type T10013, PTW-Freiburg, Germany [6]) employing a classical Hamamatsu photo multiplier tube, was used to measure the optical signals. The scintillation detectors were produced by ITEP and the light coupling to the SiPMs or the Optidos was done via FC optical connectors. The SiPM signals were read out using a transimpedence amplifier developed at SensL, effective gain 470 mV/mA, and digitized by a CAEN V792 Charge to Digital Converter. The resulting signal was typically sampled at a frequency of 30 kHz with integration times ranging between 500 and 5000 ns.

The radiological performance of the detectors was evaluated in the calibration lab of PTW.

III. Results

The linearity with dose rate of the detector was measured using a Pandoros X-ray (Siemens, Germany [7]) at 35 kV tube voltage with a Tungsten anode and 1.2 mm Aluminum equivalent self-filtering. In Fig. 2, the response of a non-embedded prototype to dose rates in the range of 5 to 200 mGy/s is shown. The signal was recorded using a Hamamatsu SiPM.

O. Dössel and W.C. Schlegel (Eds.): WC 2009, IFMBE Proceedings 25/III, pp. 191–193, 2009.
www.springerlink.com

The energy response of the same Mammodos prototype was evaluated for five standard radiation qualities stated in Table 1. The measurements were performed on a Mammomat (Siemens) using the Optidos as optical detector. The scintillator was placed on a plate of polyvinyl chloride (PVC). For each radiation quality, the response of the prototype was measured. The deviation of the response to each radiation quality from the mean response is depicted in Fig. 3.

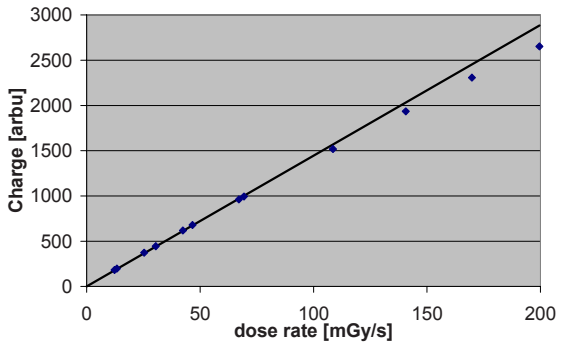

Fig. 2 Detector signal versus dose rate of the Mammodos prototype. The deviation from a linear dependence above 100 mGy/s is clearly visible. The dose rate of most Mammography machines is below 100 mGy/s, hence the linear dynamic range can be considered as very good.

Table 1 Radiation qualities used in this work

Radiation quality	Anode / Filter	Tube voltage range [kV]
MMV	Mo / 32 µm Mo	25–35
WRV	W / 54 µm Rh	25–35
MRV	Mo / 25 µm Rh	25–35
WMV	W / 60 µm Mo	25–35
WAV	W / 0.5 mm Al	25–35

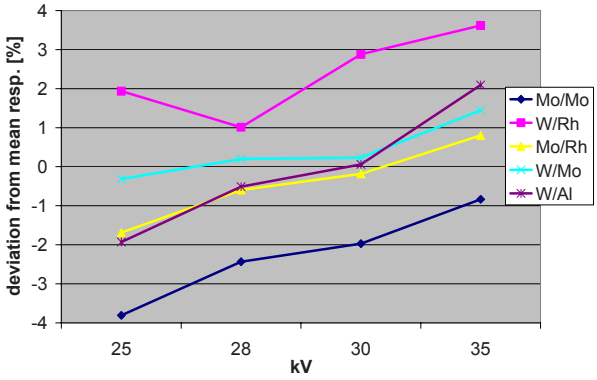

Fig. 3 Energy response of the Mammodos prototype using the Optidos as optical detector. For each radiation quality the deviation of the response to the mean response of all measurements is indicated.

The latest prototype consists of a scintillating fiber fully embedded in an organic matrix as depicted in Fig. 4.

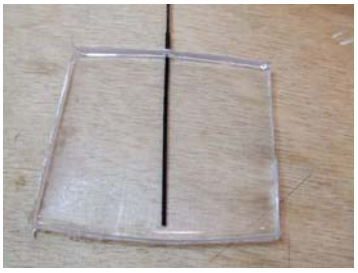

Fig. 4 Prototype of a fully embedded scintillating fiber detector. It is optically transparent, the grain of the wood is well visible.

Mammography images of this prototype were taken on top of an anthropomorphic breast phantom Rachel (Gammex, USA [8], 5 cm equivalent thickness) in the Radiology department of S. Anna hospital in Como, Italy. The resulting Mammogram is displayed in Fig. 5.

Fig. 5 Mammogram of the prototype depicted in Fig. 4 on an anthropomorphic breast phantom. The image was taken with an Essential Senographe (GE Healthcare, USA [9]) in maximum contrast mode. The exit of the fiber (see arrow) can be identified while the embedded part of the fiber is not visible in this Mammogram.

IV. Discussion

The dose rates of most Mammography machines are below 100 mGy/s. Hence the linear dynamic range of the prototype as shown in Fig. 2 can be considered as very good. The same is true for the energy response of the prototype. For comparison: an SFD-chamber (type 34069, PTW-Freiburg) having an excellent energy response exhibits

deviations of ±3 % over the full range of the radiation qualities listed in Table 1. It must be noted, however, that the energy response was measured on a non-embedded prototype. The final energy response will depend on the exact surrounding material of the detector.

The embedding procedure, as shown in Fig. 5, seems to work very well. Further research is necessary to thoroughly check whether the prototype might nevertheless degrade the image quality. The final prototype will be of the same size as the compression paddle, hence no naked fiber (as on the right hand side in Fig. 5) or edge will be visible.

V. Conclusions

In the presented work, we have shown that in-vivo dosimetry is conceivable in mammography. A detector was developed that has a very good linear dynamic range and energy response. In addition, it is almost invisible on a mammography image. The next step will be to perform a detailed analysis whether the detector might influence the image quality.

Acknowledgment

The presented research is supported by the European Commission under the contract COOP 32993 – RAPSODI.

References

1. J.P. De Landtsheer (2004) Breast Cancer Screening Program in Vaud – Quality Assurance Process and Results; in Veröffentlichungen der Strahlenschutzkommission Band 51, 2004, ISBN 3-437-21499-3
2. Deutsche Röntgenverordnung (RöV), §3 Clause 3 (2003).
3. Council directive 97/43 EURATOM, article 8, sub-clause 6 (1997)
4. Hamamatsu at http://www.hamamatsu.com
5. SensL at http://www.sensl.com
6. PTW-Freiburg at http://www.ptw.de
7. Siemens at http://www.siemens.com
8. Gammex at http://www.gammex.com
9. GE Healthcare at http://www.gehealthcare.com/worldwide.html

Investigation of the Specific Absorption Rate for a 7 Tesla T/R Body Array

T. Bolz[1], A. Bahr[1], J. Mosig[1], A. Bitz[2], and S. Orzada[2]

[1] RF&Dosimetry, IMST GmbH, Kamp-Lintfort, Germany
[2] Erwin L. Hahn Institute For Magnetic Resonance Imaging, Essen, Germany

Abstract— **High specific absorption rates (SAR) and B_1^+ field inhomogeneity are the major challenges in magnetic resonance imaging at ultra high fields. Transmit arrays are a promising approach for controlling the SAR and to improve the B_1^+ field homogeneity. In this study numerical results for the local SAR and the B_1^+ field homogeneity of an 8 channel T/R body array for 7 Tesla are presented. This body array is composed of novel meander microstrip elements. Two different excitation schemes (a birdcage and a shimming mode) are investigated. The numerical investigation shows that RF shimming has the potential to simultaneously minimize B_1^+ field inhomogeneity and SAR deposition.**

Keywords— **B_1^+ shimming, 7 T, stripline array, transmit array, receive array, FDTD, SAR.**

I. Introduction

Magnetic resonance imaging (MRI) at ultra high fields provides several advantages originating from an increased signal-to-noise ratio (SNR) in particular a higher spatial resolution and a higher sensitivity to analyze tissue metabolism and function. But at higher field strengths the corresponding RF wave length is lower than the body dimensions causing interferences between damped RF travelling waves. This leads to a B_1^+ field inhomogeneity and also in a highly heterogeneous SAR distribution and give rise to SAR hotspots at transitions between tissues with a high dielectric contrast [1]. Several methods for reducing transmit and receive interference have been presented. Transmit arrays are a promising approach to improve B_1^+ field homogeneity and to reduce the SAR deposition at the same time. Particularly microstrip transmission line (MTL) RF coils are attractive for RF-shimming and parallel imaging applications in ultra-high magnetic fields because of high decoupling between the coil elements. In the present study numerical results for the local SAR of a 8 channel body array at 7 T for two different excitation schemes (birdcage mode, shimming mode) are presented. The design of the body array is based on [2] and is modified by novel meander microstrip elements presented in [3].

II. Materials and Methods

A. Coil Design

The meander microstrip elements of the 8 channel body array are shown in Fig. 1. The substrate of the individual MTL elements (10 cm x 2 cm x 22 cm) consists of low loss ROHACELL ($\varepsilon_r \sim 1$, $\tan(\delta) \sim 0.0002$). The strip width of all coil elements is 1.5 cm. Each element was individually tuned to the Larmor frequency at 7 T and matched to 50 Ω. The posterior four-channel array comprises 4 MTL elements and is covered by a PMMA plate ($\varepsilon_r = 2.2$, $\tan(\delta) = 0.02$) of 1 cm thickness (Fig. 1 right) to prevent any contact of the electrical components by the subject. The MTL elements of the anterior four-channel array are enclosed by MAKROLON casings ($\varepsilon_r = 2.6$, $\tan(\delta) = 0.02$) and are connected with a NEOPREN coat (not shown in Fig. 1) to provide a flexible former. Due to the casing size the elements of the anterior four-channel array are placed 4 cm away from the chest of the subject. The smallest distance of the elements to the subject of the posterior four-channel array amounts to 2 cm.

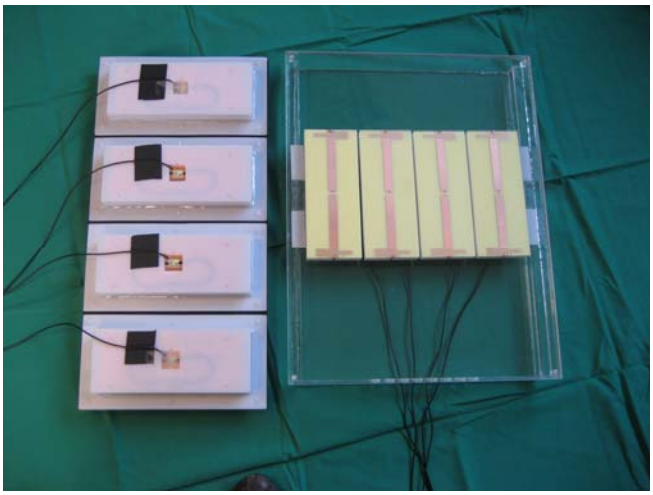

Fig. 1 Meander MTL elements of the 8 channel body array

O. Dössel and W.C. Schlegel (Eds.): WC 2009, IFMBE Proceedings 25/III, pp. 194–196, 2009.
www.springerlink.com

B. Excitation Scheme

Two kinds of excitation are investigated: For the first excitation scheme – a modified birdcage mode - constant magnitudes and geometrical phases are used (see Fig. 2). The phases are measured with respect to the middle of the MTL array from the reference element (coil 1) to the other elements [2]. In the second excitation scheme - a shimming mode - the B_1^+ homogeneity is maximized in a transversal plane of the region of interest (ROI) located in the liver. B_1^+ shimming is performed by altering the magnitudes and phases of the input signal of the individual channels based on B_1^+ maps obtained for each coil element by numerical simulations. The input magnitudes and phases are determined by a least squares solution. To accomplish RF shimming at 7 T a whole-body MR scanner (Magnetom 7 T, Siemens Healthcare, Erlangen, Germany) is modified [4]. The multiple transmit system is realized by splitting the excitation signal of a conventional single-channel system into 8 channels and adjusting the magnitude and phase of each channel using a vector modulator. It is notable that these components are incorporated in the small signal chain of the RF power system allowing low cost components.

C. Numerical Modeling

Numerical investigations are performed with the commercially available FDTD software package EMPIRE™. The numerical model of the MTL array is loaded with the visible human phantom which distinguishes more than 40 tissues. The resolution of the human model amounts to 2 mm. Fig. 3 shows the numerical model of the loaded 8 channel MTL array. For better visualization only the upper part of the visible human is depicted. The casings and the NEOPREN coat are also not shown. Each element of the body array is excited in the center of the microstrip by an independent RF current source.

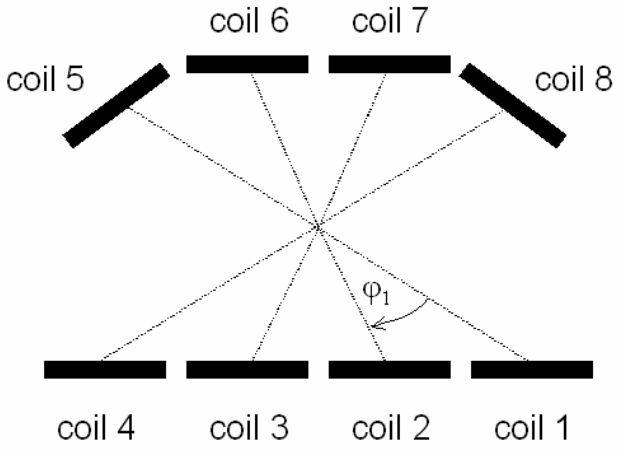

Fig. 2 Geometrical configuration of the MTL meander elements

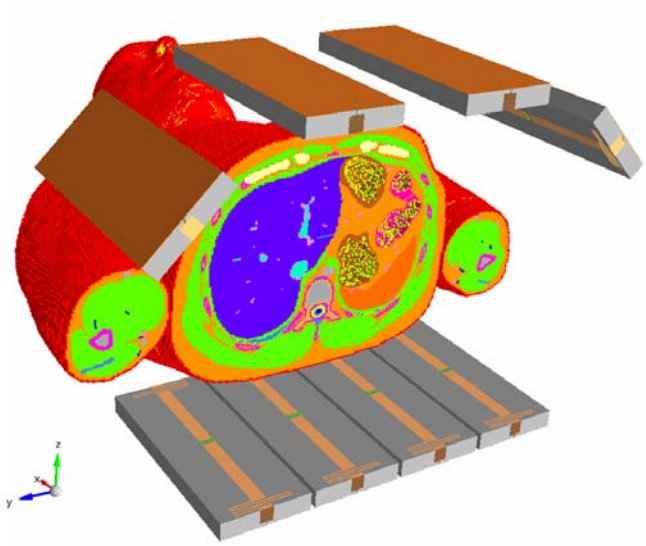

Fig. 3 Numerical model of the loaded 8 channel MTL array

III. Results and Discussion

Simulated and measured decoupling between adjacent elements of the loaded 8 channel meander MTL array is better than -20 dB. As a measure for B_1^+ field homogeneity the ratio of the standard deviation to the mean value of the B_1^+ field is used. For the investigated ROI simulated B_1^+ homogeneity for the shimming mode is 40 % better in comparison to the birdcage excitation scheme. Numerical results for the local SAR averaged over a 10 g tissue cube show that the limit of 10 W/kg is achieved for a total input power of 101 W in the case of the birdcage excitation scheme and for 90 W in the case of the shimming mode. The ratio of the local SAR to the square of the maximum value of the magnetic field within the ROI is 15.21 (W/kg)/(A/m)^2 for the birdcage mode and 12.57 (W/kg)/(A/m)^2 for the shimming mode. This means that for a given magnetic field in the ROI lower SAR deposition is expected for the shimming excitation scheme. Furthermore to achieve the desired magnetic field within the ROI 36 % less input power is necessary for the shimming mode in comparison to the birdcage mode. In Fig. 4 the non averaged SAR in a transversal slice containing the ROI for both excitation schemes is shown. It can be observed that for the shimming mode most power is dissipated at the right side of the body where the ROI is located.

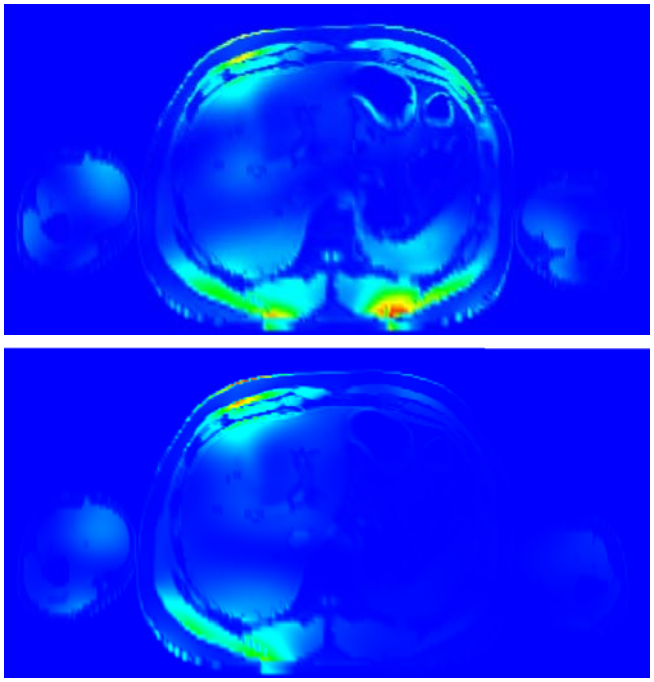

Fig. 4 Non averaged SAR in a transversal slice. Top: birdcage mode, Bottom: shimming mode

In Fig. 5 a reasonably homogeneous T1-weighted FLASH magnetic resonance image for the ROI in a transversal slice obtained by the shimming mode is depicted. This image is acquired in the trunk of a volunteer with 100 kg body mass by the modified 7 T whole-body MR scanner [4].

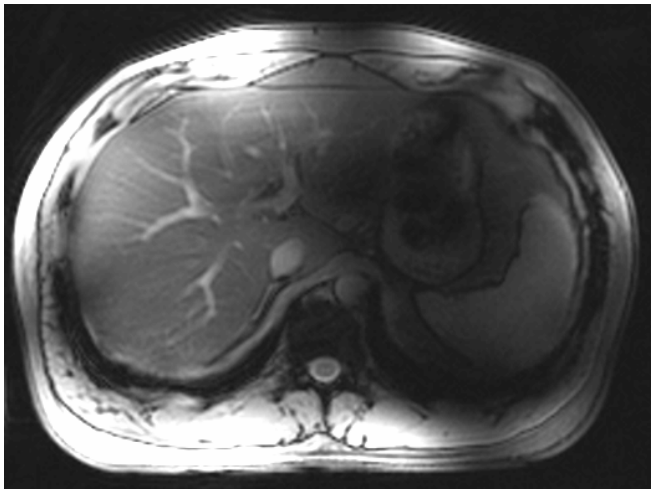

Fig. 5 T1-weighted FLASH image (in-phase, breath hold) acquired by the shimming mode [4]

IV. Conclusions

This study presents an 8 channel T/R body array for 7 T magnetic resonance imaging consisting of novel meander microstrip elements. A birdcage and a shimming excitation scheme are investigated. The numerical results show that RF shimming has the potential to simultaneously minimize B_1^+ field inhomogeneity and SAR deposition.

References

1. Cornelis A. T. Van den Berg et al. (2007) Simultaneous B_1^+ homogenization and specific absorption rate hot spot suppression using a magnetic resonance phased array transmit coil, Magn. Reson. Med. 2007, 57:577-582
2. Gregory J. Metzger et al. (2008) Local B_1^+shimming for prostate imaging with transceiver arrays at 7T based on subject-dependent transmit phase measurements, Magn. Reson. Med. 2008, 59:396-409
3. Achim Bahr et al. Characterization of a novel 8 channel microstrip head array at 7 T – Numerical simulations and experimental verification, ISMRM-16th annual meeting, Toronto 2008
4. Andreas K. Bitz et al. (2009) An 8-channel add-on RF shimming system for whole- body 7 Tesla MRI including real-time SAR monitoring, accepted for the ISMRM-17th annual meeting, Honolulu 2009

Lessons learned from 25 years in exploring Norwegian radiology practices from a radiation protection point of view

H.M.Olerud[1,2], L.Borgen[3,4], E.G.Friberg[1], K.B.Lysdahl [5,6], R.D.Silkoset[5] , A.Widmark[1] and G.Saxeböl[1]

[1] Norwegian Radiation Protection Authority, P.O.box 55, NO-1332 Østerås, Norway
[2]Institute of physics, Biophysics group, P.O Box 1072 Blindern, NO-0316 Oslo University of Oslo, Norway
[3] Department of Radiology, Buskerud University Hospital, Dronninggata 28, NO- 3004 Drammen, Norway
[4] Department of Health, Buskerud University College, Konggate 51, NO-3019 Drammen, Norway
[5] Radiography Programme, Faculty of Health Sciences, Oslo University College, P.O. Box 4, St. Olavs plass, NO-0130 Oslo, Norway
[6] Section for Medical Ethics, Faculty of Medicine, University of Oslo, P.O. Box 1130, Blindern, NO-0318 Oslo, Norway

Abstract— **The traditions in Norway in following trends in the use of radiology and exploring the national differences in examination frequencies and patient doses is reviewed. Norway has had a public founded healthcare system and early access to digital technology included MDCT. The first may explain a moderate examination frequency on the national level, and the second the relatively high collective effective dose (S_E) compared to other western countries (1.1 mSv/ per inhabitant; 59% from CT). There is substantial variation in examination frequency and doses between counties, radiology institutions and X-ray rooms. This may be explained by several factors: Accessibility and referral strategy (justification), focus on quality, skills and multidisciplinary approaches (optimization), together with equipment related factors. The implementation of diagnostic reference levels are presumed to be a useful tool for optimization locally, and also a source for updated national dose figures in the future. European guidelines on estimating population doses are recently provided [8], a new national survey will be performed accordingly this year.**

Keywords— **radiation protection, collective effective dose, radiology, X-ray diagnostics, DRL, CT**

I. Introduction

Norway has a centralized public founded health care system, and a population of about 4.5 million people. Imaging is performed in radiological departments in public hospitals or in private radiology institutes. Virtually all radiological examinations are submitted to a public reimbursement system. The Norwegian radiation protection regulation [1] is founded on the basic recommendations of the International Commission on Radiological Protection (ICRP). The Norwegian Radiation Protection Authority (NRPA) has the authorization to ask for information about examination frequency and patient doses and has made regular assessments of the use of diagnostic radiology in order to explore trends in the use of different imaging modalities, looking for possible regional variations and the effects from the introduction of digital technology. Recent developments in medical imaging, particularly with respect to computed tomography (CT), have had significant consequences for individual patient doses and for the collective dose (S_E) to the population. On the other hand, the use of non-ionizing modalities such as ultrasound (US) and magnetic resonance (MRI), as well as various scopy techniques, has provided diagnostic advantages at no costs concerning the S_E. The paper reviews the experiences based on the three latest nationwide population dose surveys in Norway [2-4], and also some regional studies [5-7], reflecting and analyzing the trends in diagnostic radiology during the past 25 years.

II. Materials and methods

A. Information about examination frequency in Norway

In Norway we have used the definition recently suggested in European guidelines, RP 154 [8]: 'An x-ray examination or interventional procedure is defined as one or a series of x-ray exposures of one anatomical region/organ/organ system, using a single imaging modality (i.e. radiography/fluoroscopy or CT), needed to answer a specific diagnostic problem or clinical question, during one visit to the radiology department, hospital or clinic'. Annual numbers of examinations have been obtained directly by questionnaires sent to all hospitals, clinics and practices, i.e. it has not been necessary to scale up to cover the whole country. The Norwegian College of Radiology has through more than twenty years developed a code system that has been used both for activity analysis and reimbursement. All enterprises in Norway have for a long time had radiological information systems (RIS), and the number of codes could just be gathered from the RIS systems in the departments. The codes had, however, to be interpreted into actual numbers of examinations, i.e. some problems of double-counting, particularly with examinations of double-sided organs had to be adjusted for, and likewise examinations which consisted of several contrast series that would create more than one radiological code in the system.

O. Dössel and W.C. Schlegel (Eds.): WC 2009, IFMBE Proceedings 25/III, pp. 197–200, 2009.
www.springerlink.com

B. Surveys on patient doses in Norway

For radiographic and fluoroscopic X-ray examinations the dosimetry in Norway has been based on the dose-area product, P_{KA}. During the eighties, the data were collected by site visits to all hospitals by the NRPA [2,3]. For CT examinations the CT dose indexes for the actual scanners, C_K, were either measured or looked up in the literature, while the technique parameters for standard protocols and for certain clinical indications were collected by questionnaires to all CT rooms [9]. The Monte Carlo based conversion coefficients published by the former NRPB in the UK (now part of the Health Protection Agency) were used to calculate the effective dose. According to ICRU [10]:

$$P_{KA} = \int_A K_a(A)\,dA \quad (1)$$

$$C_K = \frac{1}{N_i T_i} \int_{-50\,mm}^{+50\,mm} K_a(z)\,dz \quad (2)$$

Since 2004 we instead have collected information from the hospitals and X-ray institutes by asking for their local diagnostic reference levels (DRL's). These are the mean values for 20 representative patients in each X-ray or CT room. The practical dose quantities used for CT are now connected to measurements in standard CT dosimetry PMMA phantoms with diameters of 16 or 32 cm (head or body FOV), given as the weighted CT doseindex, $C_{K,PMMA,w}$ corrected for the pitch, and the dose length product, $P_{KL,CT}$.

III. Results

A. Trends in frequency and dose on a national level

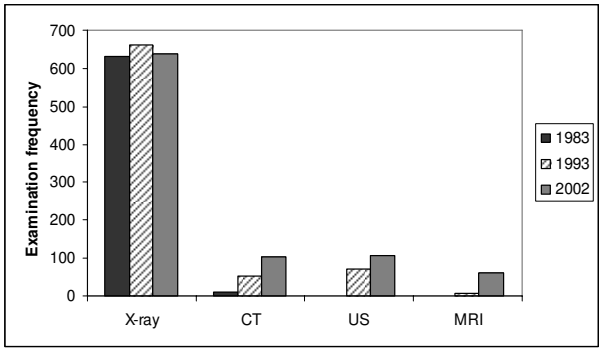

Fig. 1 The trends in examination frequencies, (no of examinations per 1000 inhabitants) for conventional X-rays, CT, MRI and ultrasound exams from 1983 to 2002. Frequencies of MRI and US are only available from 1993 and 2002 respectively.

In Norway, totally 910 radiological examinations per 1000 inhabitants were performed in 2002, a 15 % increase since 1993 (dental X-ray excluded). The frequencies of MRI, CT, and ultrasound did increase by a factor of 11, 2 and 0.5, respectively in that period, while the use of conventional X-ray examinations was almost unchanged (fig.1). Consequently the total collective effective dose increased with 40%, that gave 1.1 mSv per inhabitant in 2002 (fig.2).

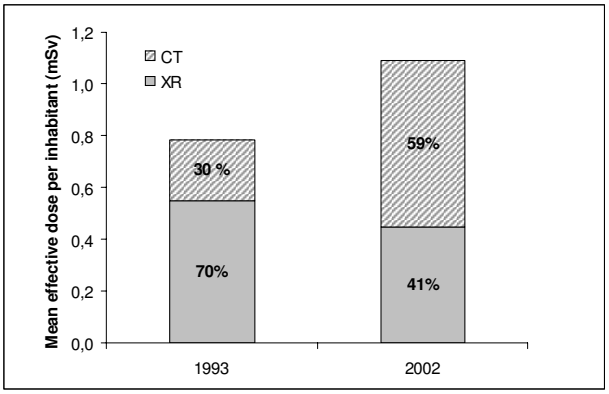

Fig. 2 The total collective effective dose per inhabitant in 1993 and 2002, with contributions from CT and conventional x-ray examinations [4].

B. National variations in doses and frequency

The variations in patient doses between different X-ray rooms are huge and typically Poisson distributed. Measurements through the eighties were basis for establishments of the first guidance levels [12, 13]; the interpretation of diagnostic reference levels (DRL) published by the radiation protection authorities in the Nordic countries (fig.3).

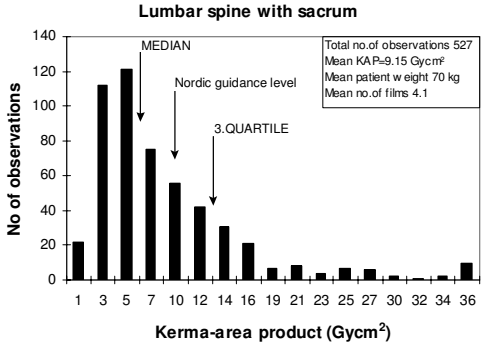

Fig. 3 Distribution of measured KAP values for conventional examinations of the lumbar spine in Norwegian hospitals. The first Nordic guidance level was set to 10 Gy·cm^2, which corresponds to an effective dose of 2.1 mSv

A recent national survey of local DRL values showed a general decrease in patient doses, and most of the current national DRLs are proposed lowered by 10-60% [14]. In particular the DRL values for CT, originally based on the European quality criteria for CT, seem too high to reflect current scan techniques in Norway: CT of the lumbar spine gives in mean about half the national DRL value (fig.4).

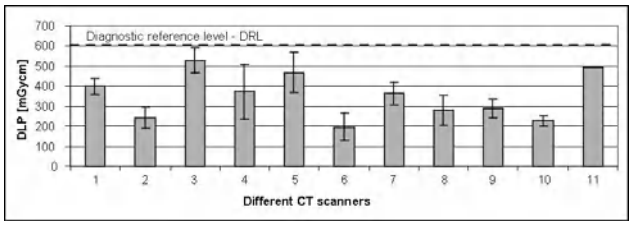

Fig. 4 Distribution of DLP values for CT examinations of the lumbar spine in the Oslo region. The current national DRL value of 600 mGy·cm corresponds to an effective dose of 10.2 mSv

The geographical variation in the total material between counties varied a factor of 2.4.The use of MRI varied from 170 to 2, and CT from 216 to 56 examinations per 1000 inhabitants (tab.1). Two plausible causes for these variations are differences in accessibility, and coexistence of public and private services [11].

Table 1 Examinations per 1000 inhabitants with conventional X-ray (RG), Computed Tomography (CT), Magnet resonance (MR) and Ultrasound (US) in all 21 counties in Norway (sorted after total frequency) [12]

County	RG	CT	MRI	US
Oslo	921	216	170	180
Telemark	823	97	80	135
Vest-Agder	754	114	98	101
Troms	778	108	65	113
Østfold	691	122	84	139
Sør Trøndelag	671	121	57	98
Buskerud	656	80	58	131
Vestfold	612	86	72	111
Nordland	576	106	60	94
Rogaland	589	89	34	95
Hordaland	573	95	25	88
Hedmark	565	83	12	102
Møre og Romsdal	544	72	29	103
Aksershus	522	77	40	69
Nord Trøndelag	533	78	33	62
Sogn og Fjordane	505	72	37	86
Aust Agder	484	61	34	71
Oppland	484	56	26	82
Finmark	459	72	2	80

C. Explanations for the differences in patient dose

A national CT survey in 1995 demonstrated mean effective doses in the range 2 mSv for CT of the head, 10 – 13 mSv for CT of the trunk region and 4.5 mSv for CT of the lumbar spine. For any examination type the ratio between the highest and lowest effective dose ranged from 8–20. The total scan length and scanner model were the two most important variables. Each of them did explain about 30% of the observed total spread in dose for a given examination type. Similar spreads in doses were found for examinations of a particular body region also when the clinical indication were specified, however, there were examples of significantly different mean doses for different clinical indications, for examples in CT of the head/brain [9].

Analyses of more recent collected local DRL's in CT rooms in Norway clearly demonstrate that dedicated multi disciplinary optimization work gives results [15]: In departments where radiologists, radiographers and medical physicists collaborate in working out the examination procedures and scan protocols, the local DRL's are significantly lower. Furthermore, departments having radiographers with postgraduate studies in CT also show significantly lower DRL's.

D. Approaches to decrease frequency of ionizing exams

Leading radiologists in the county Buskerud where some of the first to focus on the EU referral criteria in Norway, and made a deliberate strategy to use non ionizing modalities whenever possible. This strategy resulted in a shift in imaging modalities and collective effective dose between 1993 and 2003 in examinations of the spine [5], urinary tract [6] and gastrointestinal tract [7] respectively. Figure 5 demonstrates how increased use of MRI as opposed to CT for examinations of the spine resulted in a decreased collective effective dose in the county of Buskerud between 1994 and 2002, i.e. before the introduction of multidetector CT.

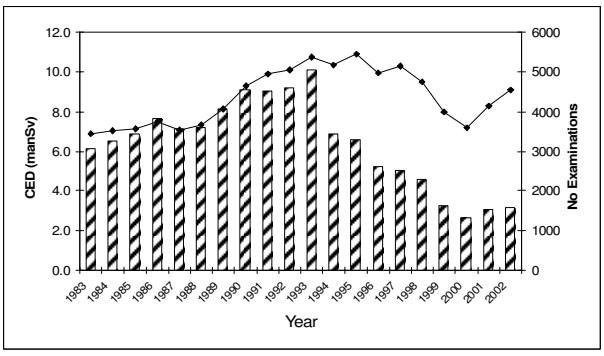

Fig. 5 The collective effective dose and the total number of examinations of the spine (RG, CT, MRI) between 1983 and 2003 in Buskerud county

IV. Conclusion and future aspects

Huge geographical variations in the use of radiology are seen in Norway. For the radiation protection of the patients the most effective measure would be to focus on adequate referral criteria that take into consideration the national resources available. Even though the principle of justification is addressed in the national regulations, it is not easy to manage from a legal point of view. At least it seems important to follow the trends and try to explain the differences as input to political priorities. An EU-funded project called DOSE DATAMED (2004 – 2007) was set up to develop mutually acceptable methods for future surveys of population exposure from medical x-rays, and have now been published as No 154 in the Radiation Protection Series issued by the European Commission [8]. A national survey based on the twenty examination types most contributing to the S_E is planned in 2009.

The variations in patient doses between X-ray rooms are also huge, that means there is a great potential for dose savings. The published national DRL values and the registration of local DRL's has shown to be a powerful tool in optimization. Focus on continuously review of the examination protocols, education and multidisciplinary work has been proven to give lower patient doses in the hospitals and clinics. It is expected that deliberate choices with respect to scan parameters and dose levels also will results in more adequate image quality and better clinical outcome.

Compliance with the latest standards from the International Electro technical Commission (IEC), the Digital Imaging and Communications in Medicine (DICOM) for radiation dose reporting in radiology and the profiles from Integrating the Healthcare Enterprise (IHE) should be included in purchasing specifications for x-ray equipment and RIS systems. Electronic information on patient doses from the RIS systems around the country may then be input to databases; for the maintenance of diagnostic reference levels, for future population dose estimates and for individual dose records. It would then be possible to focus on radiation protection efforts for subgroups of younger patients with chronic diseases or patients survived from cancer treatment in need of radiological follow up examinations. Databases of individual dose records would also open for future epidemiological studies on the relation dose versus risk.

References

1. Regulations no. 1362 of 21 November 2003 on radiation protection and use of radiation. Oslo: Ministry of Health, 2003. http://www.nrpa.no/archive/Internett/Publikasjoner/Annet/act_eng.pdf (10.02.2002)
2. Saxebøl G, Olerud HM, Lundgren LE (1990) Radiation hygiene analysis of radiological activities in Norway. In: Radiation and cancer risk. Eds: Brustad T, Langmark F, Reitan J. New York: Hemisphere Publishing Corporation, 1990, pp. 139 -147
3. Olerud HM, Saxebøl G (1997) Diagnostic radiology in Norway from 1983-1993 - Examination frequency and collective effective dose to patients. Radiat Prot Dosim 74: 247-260
4. Borretzen I, Lysdahl KB, Olerud HM (2007) Diagnostic radiology in Norway: trends in examination frequency and collective effective dose. Radiaton Protection Dosimetry 2007; doi: 10.1093/rpd/ncm204. http://rpd.oxfordjournals.org/cgi/reprint/ncm204?ijkey=8wBFzfgwJfzmzzp&keytype=ref'.
5. Borgen L, Østensen H, Stranden E, Olerud HM, Gudmundsen TE (2006) Shift in imaging modalities of the spine through 25 years and its impact on patient ionizing radiation doses. Eur Jour radiol 60:115 – 119
6. Borgen L, Østensen H, Stranden E, Olerud HM, Gudmundsen TE (2007) Shift in imaging modalities of gastrointestinal tract through 25 years and its impact on patient ionizing radiation doses. Clinical Imaging 31:189 – 193
7. Borgen L, Østensen H, Gudmundsen TE, Stranden E, Olerud HM (2007) Shift in imaging modalities of the urinary tract over a 25-year period and its impact on ionizing radiation doses given to patients. Scan Jour Urol Nephr 41:110 – 114
8. European guidance on estimating population doses from medical x-ray procedures and annexes. Radiation protection no. 154. Brussels: European Commission, Directorate General for Energy and Transport, 2008. http://ec.europa.eu/energy/nuclear/radioprotection/publication/doc/154_en.zip (06.10.2008)
9. Olerud HM (1997) Analysis of factors influencing patient doses from CT in Norway. Radiat Prot Dosim 71: 123-133
10. ICRU Report 74 Patient Dosimetry for X Rays used in Medical Imaging. Journal of the ICRU Volume 5 No 2 (2005). International Commission on Radiation Units and Measurements, ICRU, 2005
11. Lysdahl KB, Boerretzen I (2007). Geographical variation in radiological services: a nationwide survey. BMC Health Services Research 2007, 7:21 http://www.biomedcentral.com/1472-6963/7/21 (15.2.07)
12. Saxebøl G, Olerud HM, Hjardemaal O, Leitz W, Servoma A, Walderhaug T (1998) Nordic guidance levels for patient doses in diagnostic radiology. Radiat Prot Dosim 80: 99-101
13. Widmark A, Fosmark H, Einarsson G, Gundtoft P, Hjardemaal O, Leitz O, Pukkila O (2001) Guidance levels in the Nordic countries: A preliminary report for selected interventional procedures. Radiati Prot Dosim 94: 133-135
14. Friberg EG, Widmark A, Hauge IHR. National collection of local diagnostic reference levels in Norway and their role in optimization of X-ray examinations. In: IRPA 12: International Congress of the International Radiation Protection Association, Buenos Aires 2008. Strengthening radiation protection worldwide: proceedings. TS III 3.1, FP 0809.pdf. CD-Rom. Buenos Aires: IRPA, 2008
15. Silkoset RD (2009). Analysis of the variation in local reference dose levels from Computed-tomography examinations. StrålevernRapport 2009:3. Østerås: Norwegian Radiation Protection Authority, 2009. Language: Norwegian.

Author: Hilde M. Olerud
Institute: National Radiation protection Authority
Street: P.O.box 55
City: No-1332 Østerås
Country: Norway
Email: hilde.olerud@nrpa.no

Calibration of semiconductor detectors for dosimetry in diagnostic radiology

A.R. Petri[1], R. A. Terini[1] and M. A. G. Pereira[2]

[1] Departamento de Física, Pontifícia Universidade Católica de São Paulo (PUC-SP)), São Paulo, Brazil
[2] Instituto de Eletrotécnica e Energia, Universidade de São Paulo (IEE/USP), São Paulo, Brazil

Abstract—**The ionization chamber is the standard instrument for dosimetry in diagnostic radiology. Alternative detectors are those based on semiconductor technology. These dosimeters don´t require corrections for pressure, are rigid and smaller than ionization chambers, and provide real time information. The main disadvantage of these devices has been their energy dependence which differs considerably from that of ionization chambers. In Technical Report Series n° 457 the International Atomic Energy Agency (IAEA) proposed the 'substitution method' for calibration of dosimeters at secondary standard dosimetry laboratories (SSDL) based on a comparison between the measured air kerma with a reference ion chamber and a user dosimeter to be calibrated. The present study describes the results concerning the implementation of this method for semiconductor detectors calibration in a laboratory other than a SSDL. The overall uncertainty was better than 7.5 % (coverage factor k = 2), being the uncertainty of the reference chamber better than 5 %.**

Keywords— **Calibration, semiconductor detectors, dosimeters, X-ray, radiology, ionization chambers.**

I. Introduction

In diagnostic radiology most common dosimeters for performance testing of X-ray equipments and monitoring of patient dose are the ionization chambers, termoluminescence dosimeters (TLD) and semiconductor detectors [1].

TLDs are suitable for measurements in phantoms and even patients, but they do not provide real time information about patient exposure. Semiconductor detectors and ionization chambers respond instantaneously to their irradiation.

Semiconductor detectors produce large signals from modest amounts of radiation, are rigid and do not require pressure corrections, which makes them suitable for some field applications.

The simplest of semiconducting devices is the diode, based on a p–n junction. As ionizing radiation strikes the semiconductor, electron-hole pairs are induced. The current produced in the biased sensitive volume increases with ion production rate, and, thus, with radiation intensity.

Semiconductor detectors are smaller than ionization chambers, but they don´t have an inherent constant response with angle and incident photon energy. Thus, there may be some energy and directional dependence in these detectors. To compensate the energy dependence in commercial meters based on semiconductor detectors, manufacturers use mainly metal filters and electronic or computational correction methods.

The occurrence of structural damage is less probable for instruments used in diagnostic radiology, because doses are smaller than those in radiation therapy. However, it is recommended that the dosimeter response be checked at regular intervals through their calibration [1].

The International Atomic Energy Agency (IAEA) published in 2007 the Technical Report Series n° 457 [1]. In this document the IAEA pointed out specific procedures for calibration of dosimeters at SSDL (secondary standard dosimetry laboratory). Some of these procedures can be used also for calibration in lower level standard laboratories.

In this work, the calibration of semiconductor dosimeters was done by the 'substitution method', comparing the reading of a reference ionization chamber and detectors to be calibrated in the same diagnostic X-ray standard beams [2]. Beam quality could be described by the voltage applied to the X-ray tube in terms of Practical Peak Voltage (PPV) [3], first Half Value Layer (HVL) and homogeneity coefficient.

II. Materials and Methods

Previously, for semiconductor dosimeters calibration, the X-ray beams have been characterized according to the standard qualities defined by IEC 61267 [2]. Beam characterization was realized by two methods: by means of air kerma measurements with an ionization chamber and with spectrometry.

The reference instrument was a 6 cc ionization chamber with electrometer model 9095 (Radcal, Co., Monrovia, USA). The two systems based on semiconductor technology were a PMX III meter with R100 detector and ADI module 8/B (RTI Electronics, Molndal, Sweden) and an Unfors Xi meter with detector R/F (Unfors Instruments AB, Billdal, Sweden). The electrometers resolution were 1 mGy/h for Radcal, 1 μGy/s for PMX III as well as 0.1 μGy/s (50 and 70 kV) and 1μGy/s (90 – 150 kV) for Unfors Xi.

O. Dössel and W.C. Schlegel (Eds.): WC 2009, IFMBE Proceedings 25/III, pp. 201–204, 2009.
www.springerlink.com

Standard X-ray beam spectra have been directly measured by means of a CdTe spectrometer (Amptek, Inc.), utilizing 4-5 m in distance between tube focal spot and detector. Proper corrections have been applied for air absorption and detection efficiency.

The utilized X-ray generator was a Philips constant potential industrial system with 22° tungsten anode, beryllium window, MCN 323 tube, operated in continuous mode.

To minimize the contribution to the uncertainty of the calibration coefficient N_{K,Q_0}^{user} due to detector position and scattered radiation, the geometry adopted for calibration followed the recommendations of the TRS n°457 (Fig. 1).

Fig. 1 Calibration setup. Fo: focal spot; A: Pb apertures; F: added filtration; M: PTW monitor chamber; D: detector at the point of test.

The dosimeters were positioned 100 cm from the focal spot, at the point of test. Semiconductor detectors were positioned so that their element rows were perpendicular to the X-ray tube axis. Positioning devices used to position the apertures, dosimeters and monitor chamber were aligned between themselves and with the X-ray tube by laser beams and mirrors.

Before starting the calibration procedures, enough time (at least 2 hours) was spent for acclimatization of both the reference and the semiconductor dosimeters in the place where the calibration should be carried out.

TRS n°457 [1] determines that the calibration must be carried out with the same X-ray qualities with which the reference chamber was calibrated, in this case, RQR 3, 5, 7, 9 and 10. The method indicated for the calibration of dosimeters by IAEA is the substitution method. The steps adopted during the calibration in this work were:

- To position the reference ionization chamber or the semiconductor detector at the point of test.
- To measure temperature, atmosferic pressure and air humidity before each set of measurements.
- To take four measurements of air kerma rate for each dosimeter, as well as of background and leakage radiation.

The calibration coefficient of the semiconductor dosimeters has been determined as the ratio of the ionization chamber reading to the semiconductor detector reading.

Environmental conditions were controlled in both calibrations with the aid of an air-conditioning system; temperature varied between 19 – 21 ˚C, pressure kept constant (P = 93.1 kPa) and humidity oscillated between 45–48 %. In the range 30–80 % of relative humidity the measuring volume of the ionization chamber is not influenced by the humidity, and chamber response varies by less than 0.15 %. Therefore, the correction factor could be neglected.

Ionization chamber readings have been corrected for calibration coefficients and air density. The correction for temperature and pressure, which affect air density, has been applied, as usual, for any differences between the conditions during measurement and reference calibration conditions (reference pressure P_o = 101.325 kPa and temperature T_o = 20 °C). For semiconductor detectors, the correction factor for air density has been taken as k_{TP} = 1.

X-ray tube voltage was measured using an invasive method. The acquisition of voltage waveforms was carried out by a Tektronics digital oscilloscope model TDS 5104 connected to the internal voltage divider of the Philips x-ray system. Waveform voltage ripple was less than 2 %.

A computational routine developed by IEE/USP in LabVIEW (National Instruments) evaluates the quantities absolute peak voltage, average peak voltage, PPV and ripple from the waveform, during the data acquisition, allowing the adjustment of the rated tube voltage to obtain the values of the desired PPV. Tube voltage has been previously calibrated by comparison with the values determined through the “end point” of the measured beams spectra [4].

As a suitable alternative to ionization chambers, semiconductor dosimeters should present a linear response in relation to the chamber. For this purpose, dosimeters were compared in terms of the mean air kerma rate. The energy dependence of the two systems (RTI and Unfors) could be analyzed through the graph $N_{k,Q}^{user}$ x PPV.

III. Results and discussion

Table 1 presents the results obtained for the standard beams characterization with ionization chamber used for dosimeters calibration, according to IEC 61267 [2].

Values determined for the first HVL and homogeneity coefficient associated with each radiation quality RQR should lie within, respectively, 0.1 mmAl and 0.03 from the reference values [2], according to TRS n°457 [1]. Table 1 shows that differences obtained between the experimental values and the reference ones were in this range.

Spectral results for HVL and homogeneity coefficient were in close agreement with ionization chamber results, with larger deviations in RQR 10 obtained values.

Table 1 Standard X-ray beams characterization using Radcal 6 cc ionization chamber. Uncertainties are expressed with coverage factor k = 1.

RQR	PPV (kV)	First HVL (mmAl)	Homogeneity coefficient	Additional filtration (mmAl)
3	50.00 (9)	1.77 (8)	0.76 (6)	2.373 (5)
5	70.24 (11)	2.66 (13)	0.70 (5)	3.054 (5)
7	90.00(13)	3.38 (16)	0.66 (5)	3.054 (5)
9	120.06 (17)	4.96 (26)	0.67 (6)	3.691 (5)
10	149.98 (21)	6.59 (42)	0.69 (7)	4.489 (5)

The maximum deviation of the measured PPV relative to the reference PPV in IEC 61267 [2] was 0.34%. According to IEC 61267 and TRS n°457 (for invasive measurements), the uncertainty of high voltage measurements should not exceed 1.5% or 1.5 kV (coverage factor k = 2), whichever is greater. The maximum uncertainty in the determination of the PPV was 0.4% (RQR 3).

A. Calibration of PMX III with R100 detector

Table 2 presents corrected air kerma rates of the ionization chamber, $M_{k,Q}^{ref}$, and the semiconductor detector, $M_{k,Q}^{RTI}$, as well as the calibration coefficients, $N_{k,Q}^{RTI}$, for the RTI dosimeter.

Table 2 Calibration coefficients for the RTI PMX III dosimeter

RQR	$M_{k,Q}^{ref}$ (Gy/h)	$M_{k,Q}^{RTI}$ (Gy/h)	$N_{k,Q}^{RTI}$
3	1.58 (4)	1.60 (5)	0.987 (37)
5	3.16 (8)	3.11 (9)	1.015 (38)
7	4.60 (11)	4.69 (14)	0.981 (37)
9	7.77 (19)	7.55 (22)	1.030 (39)
10	11.35 (27)	11.05 (32)	1.028 (39)

Contributions for the uncertainty of calibration coefficients for beam qualities RQR 3, 7 and 10 are shown in Table 3.

B. Calibration of Unfors Xi with R/F detector

Table 4 presents corrected air kerma rates of the ionization chamber, $M_{k,Q}^{ref}$, and the semiconductor detector, $M_{k,Q}^{Unfors}$, as well as the calibration coefficients, $N_{k,Q}^{Unfors}$, for the Unfors dosimeter.

Table 3 Percent contribution of each main source of uncertainty in PMX III calibration coefficients (k=1)

Uncertainty sources	Considered values *	RQR 3 %	RQR 7 %	RQR 10 %
Reference chamber calibration	0.75 %	9.6	3.3	1.4
k_{TP}	0.005	6.9	7.2	7.7
PMX III accuracy	2.5%	47.0	51.8	54.1
Radcal electrometer accuracy	2.0%	31.6	35.9	36.0
PMX III resolution	1 µGy/s	3.8	1.4	0.6
Radcal electrometer resolution	1 mGy/h	1.1	0.4	0.2

* From calibration certificates and manuals.

Table 4 Calibration coefficients for the Unfors Xi dosimeter

RQR	$M_{k,Q}^{ref}$ (Gy/h)	$M_{k,Q}^{Unfors}$ (Gy/h)	$N_{k,Q}^{Unfors}$
3	1.47 (4)	1.39 (4)	1.052 (37)
5	2.80 (7)	2.76 (7)	1.014 (35)
7	4.31 (10)	4.35 (11)	0.990 (34)
9	7.24 (17)	7.11 (18)	1.016 (35)
10	10.42 (24)	9.91 (25)	1.051 (36)

As before, the contribution for the uncertainty of the calibration coefficients for beam qualities RQR 3, 7 and 10 are shown in Table 5.

Table 5 Percent contribution of each main source of uncertainty in Unfors Xi calibration coefficients (k = 1)

Uncertainty sources	Considered values *	RQR 3 %	RQR 7 %	RQR 10 %
Reference chamber calibration	0.75 %	10.5	3.5	1.6
k_{TP}	0.005	7.6	8.0	8.4
Unfors Xi accuracy	2.5%	45.7	48.0	50.2
Radcal electrometer accuracy	2.0%	34.6	38.4	38.9
Unfors Xi resolution	0.1 - 1 µGy/s	0.5	1.6	0.7
Radcal electrometer resolution	1 mGy/h	1.2	0.4	0.2

* From calibration certificates and manuals.

C. Repeatability and linearity of the semiconductor detectors response

Repeatability of dosimeters response was greater than 99.96% for Unfors Xi and RTI PMX III. The ionization chamber presented a repeatability of response in the range 99.92 – 99.99 %.

Linearity of semiconductor detectors response relative to ionization chamber can be analyzed by the graph in Fig. 2. Regression coefficients R in the linear fit were 0,998 for Unfors Xi dosimeter and 0,999 for PMX III dosimeter.

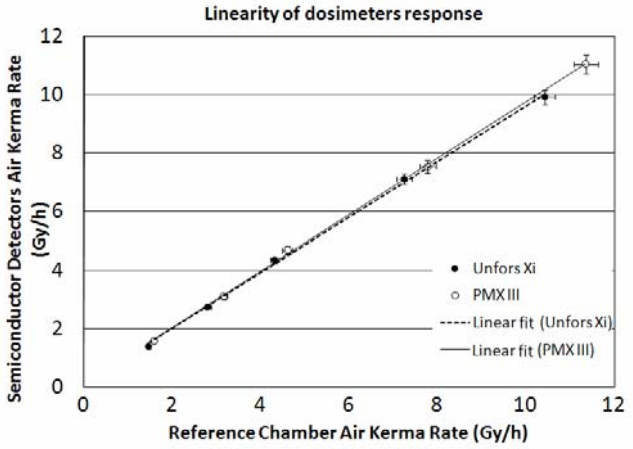

Fig. 2 Linearity of dosimeters response

D. Semiconductor dosimeters energy dependence

The analysis of energy dependence was performed comparing semiconductor devices and ion chamber responses. This dependence can be analyzed by means of the curve of calibration coefficients as a function of PPV, for the dosimetric system as a whole, that is, electrometer and semiconductor detectors (Fig. 3).

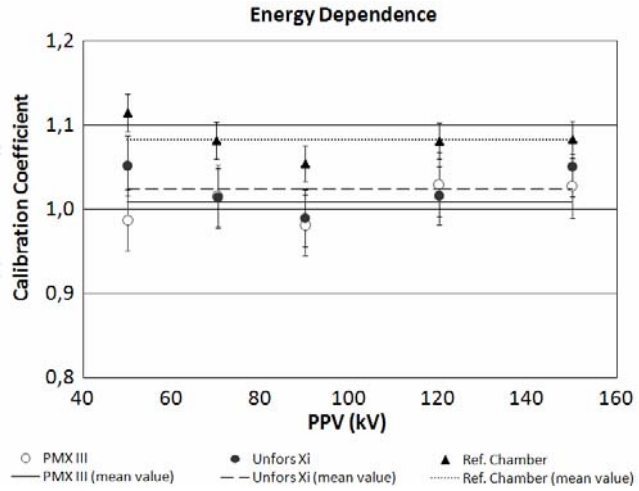

Fig. 3 Dosimeters energy dependence. For comparison the reference ionization chamber energy dependence is shown, based on its calibration.

Unfors Xi and RTI PMX II dosimeters have presented the largest deviation in calibration coefficients relative to the mean value for beam quality RQR 7 (90 kV): 3.4 % for Unfors Xi and 2.7 % for PMX III. For qualities other than RQR 7, the maximum deviation was 2.6% for Unfors Xi (50 and 150 kV) and 2.0% for PMX III.

IV. CONCLUSIONS

Keeping stable conditions during the calibration and using a reproducible geometry, the calibration of these commercial semiconductor dosimeters is possible. In this work, the standard expanded uncertainty associated with calibration factor was 7.0% for the Unfors Xi dosimeter and 7.4 – 7.6% for the PMX III dosimeter (k = 2). Variation in response of both dosimeters with PPV lies in the nominal range of ± 5%. Results have been in close agreement with those obtained by Martin [5]. Contribution of major sources of uncertainty has been explicited.

It's to be noted that this is a work in progress, and that both reference chamber and semiconductor detectors have been considered in the uncertainty evaluation. If one uses a PTW UNIDOS reference dosimeter, for example, overall uncertainty falls to around 5 % for Unfors dosimeter.

ACKNOWLEDGMENT

The authors would like to thank to PUC-SP and Brazilian agencies CNPq and FAPESP for partial financial support; to IEE – USP for staff help and utilization of infrastructure and to KONEX Acessórios Radiológicos for lending the Unfors Xi dosimeter for study.

REFERENCES

1. International Atomic Energy Agency (2007) Dosimetry in Radiology: An International Code of Practice, Technical Reports Series n° 457. IAEA,Vienna.
2. International Electrotechnical Commission (2005) Medical Diagnostic X-ray Equipment – Radiation Conditions for Use in the Determination of Characteristics, IEC 61267. IEC, Geneva.
3. Kramer H-M, Selbach H J, Iles W J (1998) The Practical Peak Voltage of diagnostic X-ray generators. Br. J. Radiol. 71:200-209.
4. Terini R A, Pereira M A G, Künzel R, Costa P R, Herdade S B (2004) Comprehensive analysis of the spectrometric determination of voltage applied to X-ray tubes in the radiography and mammography energy ranges using a silicon PIN photodiode. Br. J. Radiol. 77: 395-404.
5. Martin C J (2007) An evaluation of semiconductor and ionization chamber detector for diagnostic X-ray dosimetry measurements. Phys. Med. Biol. 52: 4465 - 4480.

Author: Ricardo A Terini
Institute: Pontifícia Universidade Católica de São Paulo – PUC/SP, Departamento de Física
Street: Marquês de Paranaguá, 111, Consolação, 01303-050
City: São Paulo
Country: Brazil
Email: rterini@pucsp.br

Charge Recombination Correction in the Dosimetry by Means Ionization Chambers of a High Dose-per-Pulse Electron Accelerator for Intraoperative Radiation Therapy (IORT)

E. Moretti, M.R. Malisan, K. Frisano, and R. Padovani

Medical Physics Department, University Hospital, Udine, Italy

Abstract - **The electron beams of some accelerators dedicated to *Intraoperative Radiation Therapy* (IORT) are characterized by a dose-rate of the order of some cGy/pulse, much higher than the typical values less than 1 mGy/pulse of conventional linacs. Thus dose-rates attain values of some tens of Gy/min reducing considerably the treatment time, but introducing a problem in the use of ionization chambers in beam calibration because of the significant lack of complete charge collection due to ion recombination. At very high dose-per-pulse values the standard "two voltage" [1] method for k_{sat} evaluation is no more valid and yields overestimates of k_{sat} up to 20% [2]. To overcome the problem, dose-rate independent dosimeters (such as chemical or radiochromic dosimeters) should be used. Indeed, the most commonly used chemical Fricke dosimeters have some disadvantages such as scarce spatial resolution, low sensitivity, high cost and post-irradiation reading process that limit their use in routine clinical dosimetry. Radiochromic film dosimeters seem more suitable to the purpose, but they are sensitive to temperature, time after irradiation and they need both a calibration procedure and a post-irradiation procedure to give the dose value. The ionization chamber has a very good sensitivity, it is practical to use, and, last but not least, it gives the dosimetric information on-line. The aim of this work is the determination of k_{sat} [1] for NACP (Scanditronix-Wellöhfer) parallel plate ionization chamber on the basis of the method proposed recently by Laitano et al. [3] exposed to high-dose-per pulse electron beams of a mobile accelerator (LIAC, Sordina, Italy). Dose estimates obtained with ionization chamber were compared with Fricke and radiochromic dosimetry.**

The good agreement among the dosimetric methods demonstrate that the ionization chamber maintains a key role in dosimetry of high-dose-per-pulse electron beams too.

Keywords — **iort, dose per pulse, k_{sat}, parallel plate ionisation chamber.**

I. Introduction

Intraoperative radiation therapy (IORT) is a treatment modality where a large single dose of radiation is delivered during a surgical intervention, after the removal of a neoplastic mass [4]. IORT uses the incision to direct radiation to the tumour bed, to the possible localisation of sub clinic illness or to macroscopic residue in the case of non- radical resection. IORT foresees a single session only. The dose delivered during IORT is typically 10–25 Gy. It allows the achievement of a selective radiation boost on the tumour volume. It can be chosen as a one- time/stand alone treatment in initial cancers of small volume, or in unresectable malignancies for palliative purpose. Recently, in Italy, mobile electron linear accelerators dedicated to IORT producing only electron beams of a maximum energy of 9-12 MeV have been manufactured which have promoted a local large diffusion of this radiotherapy modality. These linacs can be introduced directly into the operating theatre without particular needs for special fixed shielding barriers. The use of this type of equipment avoids the transport of patients outside the operating room, but presents more complex problems in terms of dosimetry.

The peculiar dosimetric feature of these dedicated linacs is the very high dose-per-pulse, ranging from 1.0 to 10 cGy/pulse values up to 100 times greater than the doses per pulse produced by a conventional medical accelerator. The dosimetry of such beams requires particular care when performed by ionization chambers. In fact, in electron beams with considerably larger values of dose per pulse, the traditional Boag's two-voltage analysis (TVA) [1] as recommended by dosimetry protocols [1] gives results for k_{sat} which are no longer consistent [2,4]. To avoid the problems with ion recombination, output calibrations are usually performed with independent dose-per-pulse dosimeters such ferrous sulfate dosimeters (Fricke dosimeters) or radiochromic films [6].

Recently Laitano, Guerra et al. [2] published a very interesting work in which they proposed a method to determine chamber collection efficiencies in high-per-pulse beams starting from the Boag et al. [7] expressions and not requiring any chamber calibration. The results of their study support the conclusion that one of the models for the charge collection efficiency is more adequate to correct for ion recombination, even in high-dose-per-pulse conditions, provided that the fraction of free electrons is properly assessed.

In occasion of the calibration procedure of our IORT machine, we made an intercomparison of dose estimates obtained by employing three different dosimeters: ionization chamber according to the method proposed by Laitano's group, the traditional Fricke dosimeter and the radiochromic film.

O. Dössel and W.C. Schlegel (Eds.): WC 2009, IFMBE Proceedings 25/III, pp. 205–208, 2009.
www.springerlink.com

II. MATERIALS AND METHODS

In our facilities, IORT is performed by a mobile linear accelerator specifically designed for IORT treatments in unshielded operating rooms. The machine used (LIAC, Sordina, Italy) is shown in Fig. 1, and its main characteristics and performances are reported in Table 1.

At the time of the current report, about one hundred patients had received IORT treatments: the principal disease considered is early-stage breast cancer as either a boost or a single treatment in the context of breast conserving surgery, without the combination with external beam radiotherapy, according to the European Institute of Oncology (IEO) protocol [5]. Additionally, our IORT experience regarded abdominal malignancies such as rectal and pancreatic tumours.

Table 1. LIAC main characteristics and performance.

Accelerating structure	Standing wave
Radiofrequency generator	Magnetron
Frequency	2998 MHz
Focusing	Automatic
Scattering filter	Brass (75 μm)
Pulse lenght	3.5 μs
Maximum Pulse Repetion Frequency	30 Hz
Nominal Electron Energy	4, 6, 8, 10 MeV
Dose-rate	range (10 - 38 Gy/min)
Dose/pulse	range (0.8 - 6 cGy/p)
Field diameter	30 – 120 mm

LIAC has both a mobile and a fixed unit. The mobile unit is a stand structure on a motorized base, which supports the accelerator and modulator.

Fig. 1. LIAC mobile linear accelerator (Sordina, Italy).

The beam collimation is performed through polymethyl methacrylate applicators consisting of two separated sections: the upper is fastened to the accelerator's head, with the lower in contact with the patient. These sections are aligned and hard-docked together before dose delivery. The applicators set consists of cylindrical tubes with a wall thickness of 5 mm, diameter ranging from 30 to 12 cm, and face angles of 0, 15, 30 and 45°.

The output calibrations were performed with three different dosimetric methodologies: ionization chamber (parallel-plate chamber, NACP, Scanditronix-Wellöhfer) with the compensation method for ion recombination defined by Laitano et al. [3], Fricke dosimeters, and radiochromic films (Gafchromic^{TM} EBT, ISP Tech. inc). All the measurements for a particular combination collimator-energy were done in the same session. The intercomparison study was limited to the most representative applicators of our routine clinical activity (i.e.: 4, 5, 6 cm-dia) and to the reference collimator for the daily quality checks (i.e: 10-cm-dia).

The parallel plate chamber NACP was irradiated in water at the depth of maximum dose (R_{max}) with a clinically significant dose value (about 10 Gy). The polarization voltage was set to +300 V. We calculated the k_{sat} factor value on the basis of the three models for the efficiency collection *f* discussed in the work by Laitano [3]. All of these three models incorporate the free-electron component in different modalities [6].

The Fricke dosimeters are chemical dosimeters (ferrous sulfate) and they consist of sealed glass ampoules with a volume of 1.1 cm^3. They have to be irradiated with a minimum dose of 40 Gy. The Fricke dosimeters are provided by the Italian Primary Standard Dosimetry Laboratory (PDSL ENEA-INMRI, Rome). The dosimeters (two for each combination of applicator-energy) were positioned in water with their center at R_{max}. Dose values ranged from 60-80 Gy. The value of the depth in water at which the dose is 50% of its maximal value (R_{50}), was communicated to the PSDL, which, furnished the dose estimates with an uncertainty of 3.2% (2σ). These dose values represented the mean absorbed dose and were then corrected, considering both the non-uniformity of the transversal profiles and the percentage of the depth dose (PDD) curves through the Fricke dosimeter's volume.

Finally, we exposed 3 EBT Gafchromic [7] film cutouts (2.0x2.0 cm^2 size), one at a time positioned at R_{max} depth in a solid water phantom (Virtual Water Phantom, VWP, Standard Imaging), at doses of the order of 5 Gy. An Epson Expression 1680 (Epson Seiko Corporation, Nagano, Japan), flatbed scanner was used to study the EBT response at 72 dpi resolution. The readout of the EBT films was delayed until at least 32 h after the irradiation in order to minimize effects of post-irradiation coloration. Images obtained were converted in dose with a Matlab home-made routine. Calibration curve was obtained by exposures at the 8 MeV electron beam of a conventional radiotherapy linac (ELEKTA SL18). Dose values ranged from 0 to 8 Gy. To improve the accuracy of EBT film as absolute dosimeter, we used a mask to position each piece always in the same

portion of the scanner bed and no correction for position and dose was needed.

In our study, Fricke dosimetry represented the gold standard to evaluate the goodness of the k_{sat} estimates by using Laitano's method and, secondary, the dosimetric performance of EBT film for IORT electron beams.

III. Results and Discussion

For the determination of dose by ionization chamber, the uncertainty level was derived using the parameters involved in dose calculation and using the uncertainty of the determination of k_{sat}. We estimated a total uncertainty of 6% (2σ).

Regarding radiochromic films, experimental data were fitted by a 4th degree polynomial function. The calibration curve is shown in Fig. 2. Dose uncertainty of 7% (2σ) was estimated.

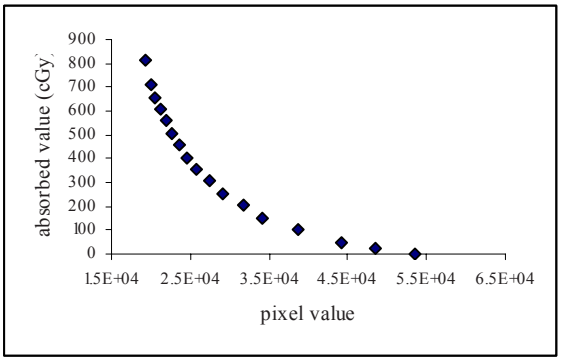

Fig. 2. EBT dosimetry - calibration curve.

In the table 2, k_{sat} values for 10 MeV energy determined according to the TVA method [1] and the three models proposed in the protocol of Laitano [3] are shown.

Table 2. k_{sat} values for the flat applicators (10 MeV energy). Columns 2 and 3 report the chamber voltages V_1 and V_2, respectively, used for TVA. k'_{sat}, k''_{sat}, k'''_{sat} refer to the three recombination models discussed in the Laitano paper [3].

dia (cm)	D/p (cGy)	V_1 (V)	V_2(V)	k^{TVA}_s	k'_s	k''_s	k'''_s
4	**5.56**	300	100	1.452	1.296	1.204	1.244
5	**5.28**	300	100	1.429	1.281	1.194	1.232
6	**4.86**	300	100	1.397	1.261	1.181	1.216
10	**3.39**	300	100	1.303	1.203	1.142	1.168

At this values of dose per pulse the results of k_{sat} are considerably different from those referring to the conventional pulse beam. The comparison between Fricke dosimetry results and ionisation chamber estimates of doses evidenced once more that k_{sat} derived by the dosimetric protocol TVA method is largely overestimated for such high dose rates, thus demanding more sophisticated corrections for ion recombination phenomenon. Of the three models analysed, the one providing a more accurate k_{sat} factor appears to be that denoted by k'''_{sat}.

The comparison of dosimetric data among the three methods adopted was made in terms of dose per pulse (cGy/p) and dose per MU (cGy/MU). In Fig. 3, the output expressed in cGy/p is plotted against the applicator diameter for all energies.

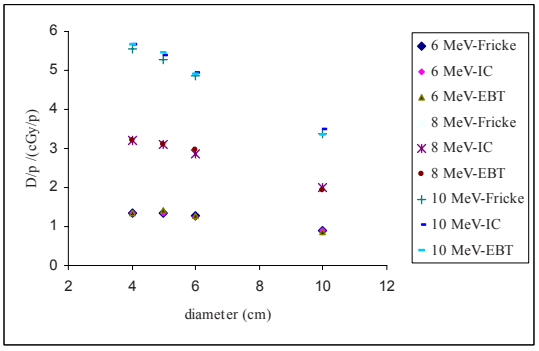

Fig. 3. Dose/p (cGy/p) in function of applicator size: comparison among the dosimetric procedures: Fricke, IC, EBT film.

The results with ionization chamber tend to overestimate the dose determined by Fricke dosimeter, that in this study, represent the reference dosimeter. The values of dose for EBT film appear to be randomly distributed around the Fricke measurements. However, the difference observed are not significant (within experimental uncertainties), also for the most critical set-up (the 4-cm-dia applicator).

IV. Conclusion

The most commonly recommended dosimeters used in the dosimetry of high dose-per-pulse electron beams produced by linac dedicated to IORT are the chemical Fricke dosimeters: they present some disadvantages such as their cost and post-irradiation process that limit the use in routine clinical dosimetry. Also radiochromic film dosimeters need a calibration step and a time consuming post-irradiation procedure to give the dose value. On the other side, the ionisation chamber has a very good sensitivity, it gives the dosimetric information on-line, and, it is practical to use also by users not acquainted with unconventional dosimetry methods.

Dose estimates of electron beams supplied by a linac dedicated to IORT (LIAC) obtained with parallel-plate ionization chamber NACP were compared with Fricke and Gafchromic™ EBT dosimetry. The good results obtained with may be considered a further experimental confirmation

of the formulation of Laitano et al. [1] for the collection efficiency in which the free-electron fraction is properly considered. In accordance with the conclusion of Laitano et al. [3], also our inter-comparison study confirms that the model labelled ''three'' appears more adequate to correct for ion recombination in high-dose-per-pulse conditions.

Combining the uncertainty on k'''_s s with the typical uncertainties for dose in water, we calculated an overall uncertainty 3% (1σ). As the peculiarity of output calibration of high-dose-per-pulse beams by LIAC, the uncertainty of 3% has to be considered an optimal uncertainty level.

In conclusion, the good agreement among the NACP-dosimetry and the dosimetry with Fricke dosimeters and EBT films demonstrate that the ionization chamber allows to carry out absolute dosimetry of high dose-per-pulse electron beams with sufficient accuracy and good ease of execution, giving again a central role in clinical dosimetry to ionization chamber.

References

1. International Atomic Energy Agency "Absorbed dose determination in external beam radiotherapy: an international code of practice for dosimetry" Technical Report Series No 398, Vienna, IAEA 2000.
2. A. Piermattei et al. "The saturation loss for plane parallel ionization chambers at high dose per pulse values", Phys. Med. Biol. Vol. 45, 1869-1883, 2000.
3. Laitano R. F. et al., "Charge collection efficiency in ionization chambers exposed to electron beams with high dose per pulse ", Phys. Med. Biol., 51, 6419-6436, 2006.
4. Rosi A. et al., "Guidelines for quality assurance in intra-operative radiation therapy", ISS, Rapporto ISTISAN, 03/1; 2003.
5. Orecchia R et al., "Intraoperative electrons" Semin Radiat Oncol, 15: 76-83, 2005.
6. Boag J W, Hochh¨auser E and Balk O A "The effect of free-electron collection on the recombination correction to ionization measurements of pulsed radiation" Phys. Med. Biol. 41 885–97, 1996.
7. Fan-Chi Su et al., "Dosimetry characteristics of GAFCHROMICs EBT film responding to therapeutic electron beams" Applied Radiation and Isotopes 65 1187–1192, 2007.

Doses to Patients in Interventional Cardiology

A. Benini, F. Pedersen, E. Jorgensen, S. Helqvist, L. Sondergaard, H. Kelbak, and K. Saunamaki

Cardiac Catheterization Laboratory, Dep. of Cardiology, Heart Centre, University Hospital Rigshospitalet, Copenhagen, Denmark

Abstract: **The growing number of interventional procedures in cardiology, as well as their increasing complexity level, require more attention to be paid to doses delivered to patients and to operators. In this paper the focus is on doses to patients. Due to an appropriate use of protective devices, the workers have kept their personal doses within the recommended levels. At the Cath. Lab. of the Heart Centre of Rigshospitalet in Copenhagen there are 7 angiography units of the latest model, all of them equipped with a dose area product meter (DAP). A computerized data base archive is operating from 1998.**

The DAP values of more than 51.000 coronary angiographies, more than 18.000 percutaneous coronary interventions (PCI) and more than 700 congenital heart diseases have been examined. DAP values have been evaluated versus intervention complexity levels, patients' body mass indexes and operators. Interventions with particularly high DAP values have been looked at separately. As expected there is correlation of DAP values with complexity indexes and patients body masses. There is also a clear difference related to the various operators, showing that there is room for improvement in the creation of awareness regarding radiation doses.

Keywords: **Dosimetry, Radiation protection, Radiation doses, Interventional procedures.**

I. Introduction

There is growing concern about doses delivered to patients in interventional cardiology and more effort should be put in limiting the probability of radiation injuries and stochastic effects, with particular attention paid to children. In fact, repeated procedures on the same patient, might be in the range of deterministic effect.

The aim of this study is to analyze doses, in order to increase awareness and discuss ways for optimization of procedures and, when possible, limiting the fluoroscopy time (FT). The Catheterization Laboratory (Cath Lab) of the Heart Centre at the University Hospital, Rigshospitalet, in Copenhagen, is equipped with seven angiography units, of most recent Philips and Siemens models. Each angiography unit has a dose area product (DAP) meter. A computerized clinical database of procedures is active as from 1998, including DAP values and FT. The Cath Lab is also well equipped with personal dosimeters, lead aprons, lead eye wears and lead glass shielding, for the workers.

II. Methods and Results

Data from 51.172 diagnostic coronary angiography procedures, 18.732 percutaneous coronary intervention (PCI) procedures, and 780 congenital heart disease procedures are available in the clinical database. In the diagnostic procedures 68% are men (average age: 61.6 ± 11.8 years, average BMI: 28.6 ± 29.4), and 32% are women (average age: 64.2 ± 12.6 years; average BMI: 27.9 ± 24.7) with average FT of 5.5 ± 6.4 min. Only, 1.1% of procedures has FT longer than 30 min. Average DAP: 49.2 ± 41.8 Gycm^2, only 3.7% of procedures has DAP value higher than 100 Gycm^2.

The average number of lesions in the PCIs is 1.5 ± 0.8 and the average number of stents implanted per procedure is 1.4 ± 1.0. Average FT: 13.8 ± 15.6 min, with average DAP: 71.5 ± 59.5 Gycm^2. Only, 7.7% of procedures have FT longer than 30 min; 78% have DAP less than 100, and 18% have DAP from 100 to 200, three percents have DAP from 200 to 300, and 0.8% has DAP more than 300 Gycm^2.

From the above data it appears that there are cases when, a crude estimation of the maximum skin dose, would indicate values within the range expected to produce some skin lesions. Anyhow, skin injuries have not been registered. The possibility exist that some minor erythema might have been overlooked, but certainly any significant lesions would have been reported and followed up.

Doses to patients during PCI, were statistically, significantly related to body mass index (BMI) of patients and number of PCI lesions (PCI complexity) as expected, but also to individual operators ($p<0.000$).

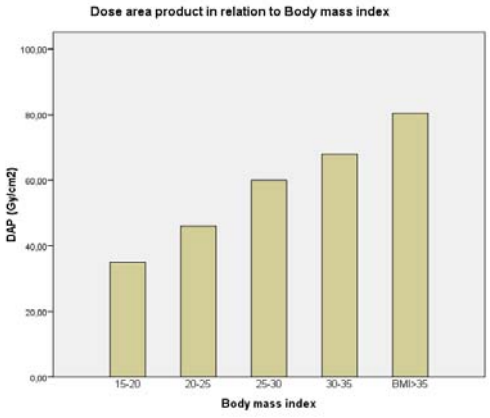

Figure 1: DAP values versus body mass index

O. Dössel and W.C. Schlegel (Eds.): WC 2009, IFMBE Proceedings 25/III, pp. 209–210, 2009.
www.springerlink.com

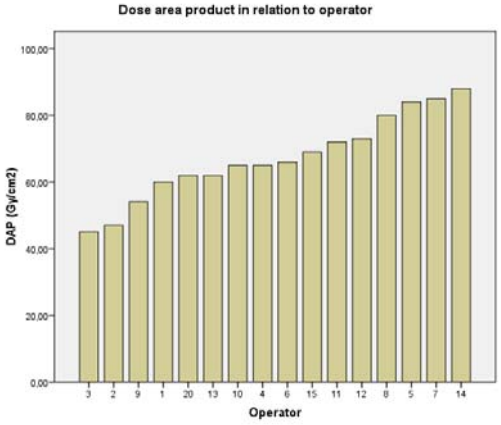

Figure 2: DAP values versus different operators.

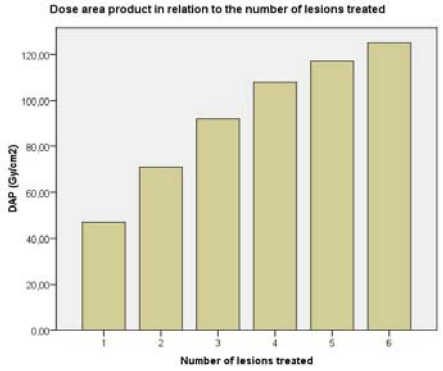

Figure 3: DAP values versus PCI complexity index.

In addition, 780 congenital heart disease procedures, performed on 595 patients, have been analyzed. Average age were: 4.6 ± 5.3 years (range 0-18), average FT: 9.6 ± 11.3 min, average DAP: 7.7 ± 17.7 Gycm^2.

The following age groups have been considered separately:

- Age group 1-364 days: 225 procedures, median weight: 6.1 kg, median FT: 9min, average DAP: 5.1 ± 11.1 Gycm^2, 5.3% of procedures has FT longer than 30 min.

- Age group 1-5 years: 306 procedures, median weight 13.6 Kg, median FT: 6 min, average DAP: 5.6± 18.7 Gycm^2, 1.3% of procedures has FT longer than 30 min.

- Age group 6-11 years: 123 procedures, median weight: 26 Kg, median FT: 7 min, average DAP: 5.4 ± 6.1 Gycm^2, 2% of procedures has FT longer than 30 min.

- Age group 12-18 years: 126 procedures, median weight: 55 Kg, median FT: 9 min, average DAP: 19.4 ± 23.0 Gycm^2, 9.5% procedures has FT longer than 30 min.

III. Conclusions

In general, doses to patients during cardiac interventional procedures seem to be within the "expected" dose range. However, a few percents of patients receive relatively high doses. Patients' BMI, procedures' complexity and operators' way-of-work are important factors to be taken into account. Clearly it is very difficult to evaluate all these aspects in connection with the clinical result of the treatments, which is, of course, the most important point.

Anyhow, it appears from the variability of DAP values in relation to the operators that there is room for improvement in the optimization of the procedures and reduction of doses to patients and staff. However, due to the correct use of protective devices, problems regarding doses to the workers have not been reported.

Criteria for Acceptability for Radiological, Nuclear Medicine and Radiotherapy Equipment – Part 2: Radiology Equipment

J.F.Malone[1], A. Schreiner[2], H. Zoetelief[3], I.D. Mclean[4], S. Balter[5], E. Vano[6], H. Bosmans[7], N. Bischof[9], R. Klausz[8], A. Dowling[1], U. O'Connor[1], C. Walsh[1], A. Gallagher[1], K. Faulkner[10]

[1] St James's Hospital and Trinity College, Dublin 8, Ireland
[2] Ministry of Health, Affiliation, Luxembourg
[3] Delft University of Technology, Delft, The Netherlands
[4] International Atomic Energy Agency, Vienna, Austria
[5] Columbia University Medical Center, New York, USA
[6] Complutense University of Madrid, Madrid, Spain
[7] University Hospitals of the KU Leuven, Leuven, Belgium
[8] GE Healthcare, France
[9] IEC, Siemens Ltd., Erlangen, Germany
[10] Quality Assurance Reference Centre, Wallsend, Newcastle, UK

Abstract— **In 2007, the European Commission has commissioned a group of Experts to undertake the revision of Report RP91 on "Criteria for Acceptability of Radiological (including Radiotherapy) and Nuclear Medicine Installations", which will be published soon. This paper introduces some of the concerns encountered in the diagnostic radiology section of the report and the approach adopted to establishing the criteria.**

Keywords— **Diagnostic Radiology, Criteria of Acceptability, Suspension Levels, Ionising Radiation.**

I. Introduction

As already detailed in Part 1 of this series of papers on the revision of the EC publication on the Criteria for Acceptability of Equipment, RP 91, the new criteria will be presented under three headings, one of which is (diagnostic) radiology equipment. The scope and form of the radiology equipment criteria are set out below, as are some features of their genesis and application that require more explicit presentation for radiology than for nuclear medicine and radiotherapy.

II. Scope of Radiology Equipment

Approximately 30 different types of equipment were assessed with a view to producing Criteria for Acceptability. These were grouped into 7 major categories as indicated in Table 1. This gives a considerably wider scope than that which prevailed in RP 91. Much of the change is due to the advances in digital technology, the development of new types of CT system, and the development and widespread deployment of Dual Energy X-ray Absorptiometry bone mineral assessment systems (DXA). In many instances the pace of development of the newer technologies has outstripped the pace of development of both industrial standards and regulatory performance limits. This gap is more acutely felt in the area of diagnostic radiology.

Table 1 Scope of Equipment Covered

Type of System	Some Subsystems Covered
X-Ray Generators, General Radiography	Mobiles, Tomography
Image Receptors and Viewing Facilities	Film, Screens, CR, DR, Viewing boxes, Monitors
Mammography	Screening and symptomatic diagnostic
Dental Radiography	Intra-oral, extra-oral
Fluoroscopic Systems	General purpose, interventional, mobiles
Computed Tomography	All types
DXA	All types

III. Methods

The methodology followed is for practical purposes that set out in Part 1. The expert group involved was the authors. Each area in the left hand column of Table 1 was lead by a member of the group, who produced drafts relating to performance and safety levels, at the remedial and suspension levels. The drafts were reviewed by the entire group and by additional reviewers who also made suggestions. These were incorporated and the scope narrowed on the basis of the reviewers' comments and other considerations, principally usefulness, practicality and the availability

O. Dössel and W.C. Schlegel (Eds.): WC 2009, IFMBE Proceedings 25/III, pp. 211–214, 2009.
www.springerlink.com

of other good sources of guidance. The principal narrowing of scope was the decision to confine the publication to suspension levels.

Considerable attention was given to how the criteria might be applied in practice in the area of diagnostic radiology, as a result of significant unease between the industry and standards approach on one side and the hospital and medical physics approach on the other. Guidance on the application and intended use of the criteria was produced with a view to reducing these difficulties, which should allow all involved to work more freely in the interests of the patients.

IV. Acceptability Criteria

The Criteria are presented in a series of Tables. These generally provide hard numerical values that are expected to be reached. They are, where possible, drawn from authoritative sources with a good level of consensus, and graded A to D as outlined in Part 1 of this series of papers. Examples of the criteria will be presented at the World Congress. Some concern has been expressed about the relationship between the criteria and international standards and/or the suppliers specified performance levels.

The MDD Directive, Standards, Criteria for Acceptability

Since 1993, safety aspects of design, manufacturing and placing on the market of medical devices have been dealt with by the "Council Directive 93/42/EEC concerning medical devices" (MDD) The MDD was substantially amended by Directive 2007/47/EC. When a device is in compliance with the Essential Requirements of the MDD, it can be "CE marked", which opens the full European market to the product. There are a number of ways with which manufacturers can demonstrate that their products meet the Essential Requirements of the MDD; the one of most interest here involves international standards., such as those issued by the International Electrotechnical Commission (IEC) or the Comité Européen de Normalisation Electrotechnique (CENELEC).

Although the MDD includes requirements for devices emitting ionising radiation, this does not affect the authorisations required by the directives adopted under the Euratom treaty when the device is brought into use. In this regard, the Euratom Treaty directives have precedence over the MDD. Conformity with the standard will frequently be included as part of the suppliers' specification and will be confirmed during contractual acceptance (acceptance testing) of the equipment by the purchaser. On the other hand the acceptability criteria must be met during the entire useful life of the equipment and its compliance with them will generally be regularly assessed.

In transposing these European directives into national law, the acceptability criteria required by the MED may be transposed using country specific approaches. It is clear that this may undermine the applicability of essential performance standards as required by the MDD or through compliance with the international standardisation system. Such an approach conflicts with the concept of free circulation and suppression of barriers to trade, which is one of the primary goals of the EU in general and the MDD in particular. To avoid these difficulties there is an urgent need for harmonisation between the requirements of the two directives (MDD and MED). Thus it is desirable that all EU countries both transpose the MED requirement for criteria of acceptability in a consistent fashion that will not harm the efforts under the MDD, the standards and CE marking systems, to ensure free circulation of goods and suppress trade barriers. We have tried to achieve this in the approach to criteria adopted.

Care must be exercised transposing the requirements of the MED to avoid inappropriate adoption of part of the criteria document as national legislation. Where this is envisaged, some caution is necessary and due discretion must be allowed in respect of the clinical situations envisaged in the introduction to the associated technology specific volumes. At a national level, the solution adopted should ensure patient safety while fostering a cooperative framework between industry, standards, end users and regulators. Internationally, there is a need for harmonization and a level of uniformity between countries in recognition of the global nature of the equipment supply industry.

V. Application of the Criteria

Advice is provided how the criteria may be applied or developed in some unusual circumstances which occur more frequently in diagnostic radiology than in other areas.

Special Considerations

The Medical Exposure Directive requires that special consideration be given to equipment in the following categories:

- Equipment for screening,

- Equipment for paediatrics and
- High dose equipment, such as that used for CT, interventional radiology, or radiotherapy.

The sections dealing with the high dose group (CT, interventional radiology or radiotherapy), deal comprehensively with this requirement. Equipment used for paediatrics and in screening programmes is often similar or possibly identical to general purpose equipment. Where this is the case, additional guidance for the special problems of paediatrics, such as the requirement for a removable grid and special needs with regard to CT exposure programmes are noted. The requirements for mammography are based on those appropriate to screening programmes.

Exceptions

Exceptions to the recommended criteria may arise in various circumstances. For example, where equipment compliant with safety and performance standards that predate the criteria for acceptability has to be assessed. In such cases, the Radiation Protection Adviser (RPA)/Medical Physics Expert (MPE) should make a recommendation to the end user or holder, on whether or not this level of compliance is sufficient to meet the intentions of the directive. These recommendations must take a balanced view of the overall situation, including the economic/social circumstances, older technology etc.; they may be nuanced in that he/she may recommend that the equipment be accepted subject to restrictions on its use. Likewise it is always well to remember that acceptability criteria, as already outlined, may depend on the use(s) for which equipment is deployed.

Exceptions: rapidly evolving technologies

Medical imaging is an area in which many new developments are occurring. Encouragement of development in such an environment is not well served by the imposition of rigid criteria of acceptability. Such criteria, when rigorously enforced, could become obstacles to development and thereby undermine the functionality and safety they were designed to protect. In such circumstances, the MPE should recommend to the end-user a set of criteria that are framed to be effective with the new technology and that takes account of related longer established technologies, any IEC/CEN/CENELEC standards available, the manufacturer's recommendations, the related scientific and professional opinion/published literature and the maxim that the new technology should aspire to be at least as safe as existing technology it is replacing.

Exclusions

The term "equipment" has been interpreted to mean the main types of equipment used in diagnostic radiology. This follows the precedent established in RP 91. It is important to be aware that the full installation is not treated. Thus, the requirements for an acceptable physical building and shielding that will adequately protect staff, the public and, on occasions, patients; power supplies and ventilation have not been addressed. However, this is an area of growing concern and one in which the requirements have changed considerably as both equipment and legislation have changed. In addition the acceptable solutions to the new problems, arising from both equipment development and legislation, in different parts of the world are different. Consequently, this area is now in need of focused attention in its own right.

Likewise, the contribution of IT networks to improving or compromising equipment functionality can bear on both justification and optimization. This can apply to either PACS or RIS networks in diagnostic radiology. The requirements for acceptability of such networks are generally beyond the scope of this initiative.

VI. Process to establish Criteria have been met

The criteria of acceptability will be applied by the competent authorities in each member state. The authorities for the MED are generally not the same as those for the MDD. In addition the criteria will be introduced and applied in the context of the unfolding requirements for clinical audit in healthcare in general and in the radiological world in particular. This is accompanied by a general increase in the requirements for individual and institutional accreditation. Thus the holder of radiological equipment should appoint a competent person to establish that the criteria of acceptability have been met. The person appointed should be an MPE or a person of similar standing. Who performs the tests to verify compliance is a matter for local arrangements. Thus the MPE may choose to perform the tests themselves, write them up, report on them and sign them off. Alternatively, he/she may accept results provided by the manufacturer's team. These may have been acquired, for example, during acceptance testing or commissioning. Results for tests performed to agreed methodology will be satisfactory in many cases. They provide the information on which the MPE can make a judgement on whether or not the equipment meets the criteria. These two approaches represent the extremes. Most institutions will establish a local practice somewhere between that allows the criteria to be verified with confi-

dence by a suitably qualified agent acting on behalf of the end user. In radiotherapy, joint acceptance testing by the manufacturer's team and the holder's MPE is commonplace.

In situations where the formally recommended criteria of acceptability are incomplete, lack precision, or where the equipment is very old, subject to exception, special arrangements or exemptions, the judgement and advice of the MPE becomes even more important. Additional, more complete, measurements may be needed to determine the cause of the change in performance. When equipment fails to meet the criteria, agreement must be established on how it will be withdrawn from use with patients. This must be done in association with the MPE whose advice must be obtained. The options, in practice, include those mentioned above and include the possibility of immediate withdrawal, where the failure of compliance is serious enough to warrant it. Alternatively a phased withdrawal or limitations on the range of use of the equipment may be considered. In the latter case, the specific circumstances under which the equipment may continue to be used must be carefully defined and documented. In addition, the advice of the MPE to the practitioner and/or the holder or the holder's representative must be made available in a prompt and timely way, consistent with the recommendations for action.

VII. CONCLUSIONS

The background to and framework for implementation of the revised criteria for acceptability of equipment in diagnostic radiology are described.

ACKNOWLEDGMENT

The authors thank all the reviewers for their helpful comments. This project has been undertaken via a contract with the European Union Commission, Directorate General for the Environment and Transport (DGTREN) under contract number TREN/07/NUCL/S07.7064

REFERENCES

1. K. Faulkner, J. Malone, S. Christofides, S Lillicrap. (2009) Criteria for acceptability for Radiological, Nuclear Medicine and Radiotherapy Equipment – Part 1: Introduction and Methodology, These Proceedings.
2. Council Directive 96/29/Euratom of 13 May 1996 laying down basic safety standards for the protection of the health of workers and the general public against the dangers arising from ionising radiation, OJ L 159, 29.6.1996 p. 1-114
3. Council Directive 97/43/Euratom of 30 June 1997 on health protection of individuals against the dangers of ionising radiation in relation to medical exposure, and repealing Directive 84/466/Euratom, OJ L180, 9.7.1997, p. 22-27
4. RP91Criteria for acceptability of radiological (including radiotherapy) and nuclear medicine installations, 1997.
5. Council Directive 93/42/EEC of 14 June 1993 concerning medical devices, OJ L169, 12.7.1993, p. 1–43

Author: J. F. Malone
Institute: Medical Physics, St James's Hospital,
City:Dublin 8
Country: IRELAND
Email: jifmal@gmail.com

TL Response study at dosimetry of ^{106} Ru/Rh ophthalmic applicator

D.P.F. Figueiredo[1], K.A.C.Daros[1] and R.B.Medeiros[1]

[1] Universidade Federal de Sao Paulo, Sao Paulo, Brazil.

Abstract— **The accuracy of the absorbed dose in the tumoral volume is essential for the success of the treatment. A non-uniformity of the beta dose rate of up to 30 % is considered acceptable by the Netherlands Commission of Radiation Dosimetry (NCS), however an uncertainty of 15 to 20 % may compromise the results of the treatment. The objective of this work is to verify the accuracy of the TL response of pellets of different characteristics in the beta dosimetry of the 106Ru ophthalmic applicator, through the dose rate distribution in simulated structures near the orbital cavity. A Nylon® phantom to simulating the orbital cavity and Thermoluminescent dosimeters were used. They are: CaSO4:Dy with graphite, CaSO4:Dy (TLD-900) e LiF (TLD-100). The relative errors resulting from the sensitivity correction factors were evaluated. O CaSO4:Dy with graphite presented proper sensitivity and higher accuracy compared with the others TLDs being an option for use in dosimetry of beta ophthalmic applicators. The phantom model used can help to estimate the absorbed doses in critical structures nearest to the ocular orbit with higher accuracy than the recommended value by NCS**.

Keywords— **Beta dosimetry, ophthalmic applicator, thermo luminescent dosimeters.**

I. Introduction

The opthalmic brachytherapy consists in the insertion of a beta emitter applicator in the ocular cavity for enough time until the prescribed dose in the pre-determined tumoral volume is absorbed. The applicators were specifically developed for the treatment of retinoblastoma in children [1] [2] and through the years, it has become an alternative for the enucleation in the treatment of ocular tumors such as malign melanoma and retinoblastoma [3] [4] [5].

The choosing of radioisotope for the treatment depends mainly on volume of the tumor and of dose distribution in it. [3] [6] [7]. Smaller tumors are treated with ^{106}Ru applicators for eye disorders. [8] [9].

Its tenth-value-layer is of 7 mm in the tissue, which makes possible the protection of sensitive tissues near the tumoral target and results in a better treatment for tumors of 5 to 6.5mm of height. [10] [11].

The accuracy of the dose in the tumoral volume is essential for the success of the treatment. A non-uniformity of the dose rate of up to 30 % is considered acceptable by the Netherlands Commission of Radiation Dosimetry (NCS), however an uncertainty of 15 to 20 % may compromise the results of the treatment. [12] [13]. From this comes the importance of the quality control in the dose distribution delivered by the ophthalmic applicators.

The thermoluminescent (TL) dosimetry was for a long time used to verify the accuracy of the absorbed dose in water, in ophthalmic plaques since it offers advantages due to its constructive characteristics and interaction process with the radiation [14]. However, the uncertainty of ± 30 % in the determination of this dose rate when the LiF (TLD-100) is used caused the other dosimetric methods to be studied for this purpose [12] [15].

In Brazil some TL dosimeters were studied for use with beta sources and, among them, the CaSO4:Dy with different graphite contents. These studies show a low energetic dependency and proper sensitivity for potential use in the skin beta dosimetry. [16] [17] [18].

The objective of this work is to verify the accuracy of the TL response of pellets of different characteristics in the beta dosimetry of the ^{106}Ru ophthalmic applicator, through the dose rate distribution in simulated structures near the orbitary cavity.

II. Materials and methods

A Nylon® phantom of the orbitary cavity and thermoluminescent dosimeters of 3 kinds were used: CaSO4:Dy with graphite, CaSO4:Dy (TLD-900) e LiF (TLD-100). The phantom is showed in the figure1. Twenty TLDs of each kind were previously selected in a batch pre-calibrated by the manufacturer and they were placed in groups of four, as shown in figure 1. The CaSO4:Dy + graphite pellet group was randomly irradiated 10 times while, on the other hand, the others were irradiated 3 times, maintaining their positions.

In the center of phantom cavity was disposed the ^{106}Ru ophthalmic applicator, CCB 909 model from Bebig manufacturer, and over it was used water in order to simulate the ocular orbit.

In a second step each pellet was sealed and irradiated in direct contact with the plaque in the center of phantom. The measurements were taking as reference values permitting to

O. Dössel and W.C. Schlegel (Eds.): WC 2009, IFMBE Proceedings 25/III, pp. 215–218, 2009.
www.springerlink.com

acquire the correction factor for sensitivity for each pellet of the 3 types of TLDs.

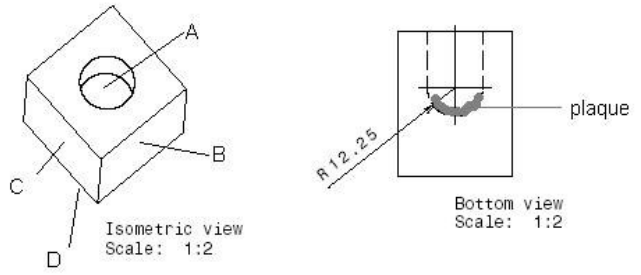

Fig. 1: Phantom of nylon®. Total stopping power (S/p) = 1,837 MeV cm^2/g.

The readings were done using the Harshaw Reader 4000, as the characteristics described in the table 1.

Table 1: Thermal treatment and TLDs readings characteristics used during the irradiation with 106Ru/Rh ophthalmic applicator

TLD	Annealing pre-irradiation	Reading Characteristics		
		pre-irradiation anneal	Heat rate	Tempera-ture max
Ca-SO4:Dy+ graphite	300^{0}C / 3h	180^{0}C	34^{0}C	340^{0}C
CaSO4:Dy	300^{0}C / 3h	180^{0}C	34^{0}C	340^{0}C
LiF	400^{0}C / 1h and 100^{0}C / 2h	100^{0}C	8^{0}C	220^{0}C

The readings values acquired in the Nylon ® phantom were corrected to the water using the total stopping power for 3.54 MeV (correction factor: 0.98).

III. RESULTS

The figure 2 shows the absorbed dose rate results in the water in the A, B, C and D points.

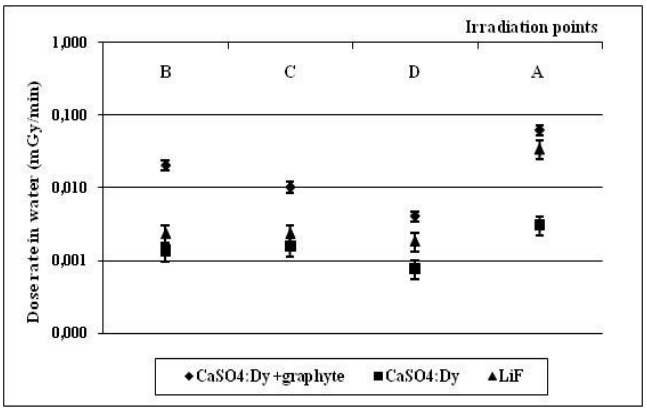

Fig. 2. Absorbed dose rates distribution in the water using the Nylon ® Phantom

The Figure 3 present the dose rate values in the water acquired with the TLDs in different phantom depths.

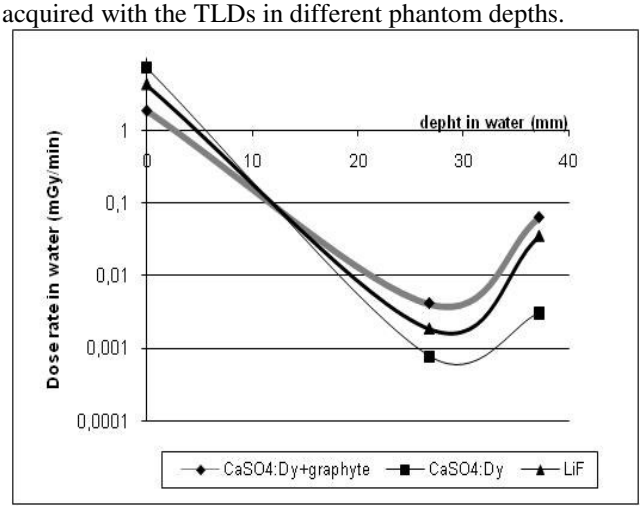

Fig. 3 TL response's comparison among depth dose values in water

The relative errors resulting from the sensitivity correction factors analyses of the individually irradiated pellets in the reference point and of the pellets irradiated in group were presented in the table 2.

Table 2: Relative error from individual irradiation and in group at reference point and in the points distributed in the 106Ru/Rh applicator

TLDs	TLD-900 +graphite	TLD-900	TLD-100
Pellets over the plaque	12.9%	14.3%	12.9%
Pellets in the points A, B, C e D	15.8%	28.8%	28.8%

IV. DISCUSSION

Severe side effects may occur if the irradiated target volume is near of important structures (e.g. cataracts and vitreous hemorrhage) [19].

The tumor location is correlated with observed complications and the risks of the treatment must be considered.

The side effects may be caused by specific factors, such as total absorbed dose, absorbed dose rate and imparted dose volume, among others.

The accuracy of the dose is relevant and can be influenced by factors related with tumor size, location and tumor resistance under irradiation or biological response [20].

With the applicator over the tumor, the distribution of absorbed dose varies due to its geometric aspects suggesting that the accuracy of dosimetry is relevant [15].

Treatments of tumors in the anterior region result in a higher absorbed dose for eye lens meanwhile the irradiation in the posterior region promotes an absorbed dose higher at macula. The accurate dosimetry of ophthalmic applicators can be useful at dose selection and can avoid undesirable secondary effect. [17].

The absorbed dose rate specified by the manufacturer present a variation of ± 30% and the relative dose distribution has an associate error of ± 6% [21]. These values were determined using LiF (TLD100) dosimeters. This kind of TLD is commonly used for ophthalmic applicators dosimetry since they have effective atomic number near to biological tissue (ZLiF=8,14, Ztecido=7,1) [21].

The TLD 900 presents high sensitivity and energetic dependence. It is considered a good thermoluminescent material due to its high sensitivity. This TLD has frequently been used in Brazil due to high benefit cost. The TLD 900 with graphite can be a good option as beta dosimeter since present high sensitivity and lower energetic dependence for beta emitters. Its lower variation at relative dose rate measurements and higher accuracy at dose distribution have taken it proper for use in ophthalmic applicator dosimetry.

There are several detectors for dosimetry but t is difficult to meet calibrated detectors with traceability of primary standard for beta sources. The sources have small depth of penetration, around 1 cm for water and a gradient steep of dose. This gradient is present in the detection volume and small disturbances at source-detector position (~0.1 mm) can result in a great variation of signals (~10%).

V. CONCLUSIONS

O CaSO4:Dy with graphite presented proper sensitivity and higher accuracy compared with the other TLDs being an option for use in dosimetry of beta ophthalmic applicators.

The phantom model used can help to estimate the absorbed doses in critical structures nearest to the ocular orbit with higher accuracy than that one accepted by NCS recommendation.

ACKNOWLEDGMENT

The authors are thankful to Capes by financial support and to the Radiotherapy Section of Hospital São Paulo by the operational support.

REFERENCES

1. Abouzeid, H., Moeckli, R., et al. (2008) ^{106}Ruthenium brachytherapy for retinoblastoma. Int. J. Radiation Oncology Biol. Phys.71, 821-828.
2. M.P Casebow, (1971) The calculation and measurement of exposure distributions from ^{60}Co ophthalmic applicators. Brit J. of Radiology 44, 618-624.
3. Reyes, A.S., Tello, J.J. et al. (1998) Monte Carlo calculation of the dose distributions of two ^{106}Ru eye applicators. Radiot. And Oncology 49, 191-196.
4. Luxton, G., Astrahan, M.A., et al. (1988) Dosimetric calculations and measurements of gold plaque ophthalmic irradiators using Iridim-192 and Iodine-125 seeds.IJROBP 15, 167-176.
5. Finger, P.T.(2000) Tumor location affects the incidence of cataract and retinopathy after ophthalmic plaque radiation. Br. J. Ophthalmol, 84, 1069-1070.
6. Nag, S., Quivey, J. M et al. (2003) The American Brachytherapy Society Recommendations for Brachytherapy of Uveal Melanomas. Int. J. Radiation Oncology Biol Phys, 56, 544-555.
7. Damato, B., Ophth, F.R.C., et al. (2005) Visual acuity after Ruthenium^{106} brachytherapy of choroidal melanomas. Int. J. Radiation Oncology Biol Phys, 63, 392-400.
8. Hokkanen, J., Heikkonen, J. et al. (1997) Theoretical calculations of dose distributions for beta –ray eye applicators. Med. Phys. 24 (2).
9. Schueler, A.O., Flühs, D. et al (2006). B-Ray rachytherapy with ^{106}Ru plaques for retinoblasmotma. Int. J. Radiation Oncology Biol Phys, 65, 1212-1221.
10. Laube, T.,Flühs D., et al. (2000) Determination of Surgeon's Absorved Dose in Iodine 125 and Ruthenium 106 Ophthalmic Plaque Surgery. Ophthalmology, (107), n.2,. 366-368.
11. BEBIG An Eckert & Ziegler Company.(2001) Ru-106 Ophthalmic Plaques.
12. Kollard R. P, et al, (2006) Recommendations on detectors and quality control procedures for brachytherapy beta sources, Radiotherapy and Oncology 7 223-229.
13. Develaar J. et al (1992) Dosimetry of ruthenium-106 eye applicators, Med. Phys. 19 691-694.
14. Kovacevic, N. et al (2005) A simple calibration method for 106 Ru-106 RH eye applicators. Radiology and Oncology 74 293-299.
15. Kaulich, T. W., Zurheide, J. (2005) Clinical quality assurance for ^{106}Ru ophthalmic applicators. Radiotherapy and, 76, 86-92.

16. Daros, K.A.C, et al (2001). TL Response study of the CaSO4:Dy pellets with graphite for dosimetry in beta radiation and low –energy photons fields. Applied Radiation and Isotopes 54 957-960.
17. da Rosa, L.A.R, Caldas, L.V.E. (1986) Skin beta-dose assessment with ultra-thin thermoluminescent detectors. Phys. Med. Biol.31, 677-682.
18. Oliveira, M.L., Caldas, L.V.E. (2007) Performance of thin CaSO4:Dy pellets for calibration of a 90Sr +90Y source. NuclearInstruments and Methods in Physics Research A580 293-295.
19. Binder, W. Chiart et al (1999). Determination of the dose distributions of an ophthalmic ^{106}Ru irradiator with TLDs and an eye phantom. Radiation Protection Dosimetry, (34), 275-278.
20. British Library Cataloguing in Publication Data. Applied thermoluminescence dosimetry. (1981) Published for the European Communities, Directorate- General Information Market and Innovation, Luxembourg.
21. Flühs, D, Anastassiou G., and Wening, J. et al (2004). The design and the dosimetry of bi-nuclide radioactive ophthalmic applicators. Med. Phys. (31)1481-1488.

Use macro [author address] to enter the address of the corresponding author:

Author: Daniela Figueiredo Pinto Ferreira
Institute: Federal University of São Paulo
Street: Mirassol, 313
City: São Paulo
Country: Brazil
Email: daniela@cfhr.epm.br

The Exposure Assessment of Pulsed Magnetic Fields – A Comparison between Physiological Backgrounds and Guidelines

Ch. S. Rueckerl[1], K. Fr. Eichhorn[2]

[1,2] HTWK Leipzig/ Institute of Electrical Power Engineering, Waechterstrasse 13, Leipzig, Germany

Abstract— **The exposure assessment of pulsed magnetic fields in the low frequency range is time consuming and needs a signal processing of recorded measurement data. Different methods are applied to compare the effects of pulsed and broadband fields with sinusoidal fields of one frequency. The exposure assessment of pulsed magnetic fields is based on current density as a restriction quantity. This can bring the effect of a very restrictive assessment of the exposure. A relation to physiology has to be established which can be used to introduce an evaluation assessment guide for pulsed fields. In this article two approaches taken from ICNIRP guidelines are compared with physiological basics of nerve excitation.**

Keywords— **Exposure Assessment, Magnetic Fields, Pulsed Fields, Exposure Limits**

I. Introduction

National and international restrictions to limit the exposure of general population and employees to low frequent electric and magnetic fields have been set up. The assessment of pulsed fields is debatable, whereas the assessment of sinusoidal fields is well established. The knowledge about sinusoidal currents and fields is used to evaluate pulsed fields by considering the frequency dependent nerve excitation and thermal effects. It is apparently useful to evaluate pulsed fields in the frequency domain by comparing the amplitude frequency response with reference levels. Physiological experiments resulted in the effect that nerve excitation does not only depend on the amplitude but also on the duration of induced current pulses. The processes on the level of the single nerve cell have to be considered. It is, therefore, useful to investigate the guidelines for exposure assessment for these basic relationships. Besides the Guidelines for Limiting the Exposure to Time-Varying Electric, Magnetic and Electromagnetic Fields [1] the International Commission on Non-Ionizing Radiation Protection (ICNIRP) has published a statement to test the compliance of exposure to pulsed and complex non-sinusoidal waveforms below 100 kHz [2]. This statement contains instructions to evaluate pulsed and non-sinusoidal fields. The assessment procedure shall ensure the protection of exposed people anyway and avoid a too restrictive evaluation. The guidelines are meant to aim at the suggestion of a method which is easy to apply and to automate. It should also be based on physiological knowledge. The third section of this paper demonstrates two simple examples of exposure assessment with the ICNIRP guidelines and compares them with the physiological background.

II. Physiological background

The basic effect of low frequent magnetic fields is the nerve excitation caused by induced body currents. With increasing frequency this phenomenon is replaced by thermal effects. Up to a frequency of 1 kHz a constant excitation threshold of current density can be assumed. Above this frequency the threshold level increases according to the frequency. When pulsed fields are considered it is intended to estimate the induced body current density which is not useful as a measurement quantity. Therefore the field quantities (B, H) have to be measured. The relationship between change in time of magnetic flux density and induced current density is given by Faraday's Law and a plain loop model of the human body [2].

$$J = K_B \frac{dB}{dt} \tag{1}$$

For sinusoidal fields the equation (1) can be used easily. For pulsed fields, however, the physiological background has to be considered separately. Nerve excitation is initiated by a polarization of the cell membrane. For this process in a single nerve cell not only the current density but also the pulse duration and thus the current density time integral is responsible. This behaviour can be transferred to the whole body. An example for the threshold level of current pulses induced via electrodes is shown in figure 1. The threshold level decreases according to pulse duration.

O. Dössel and W.C. Schlegel (Eds.): WC 2009, IFMBE Proceedings 25/III, pp. 219–222, 2009.
www.springerlink.com

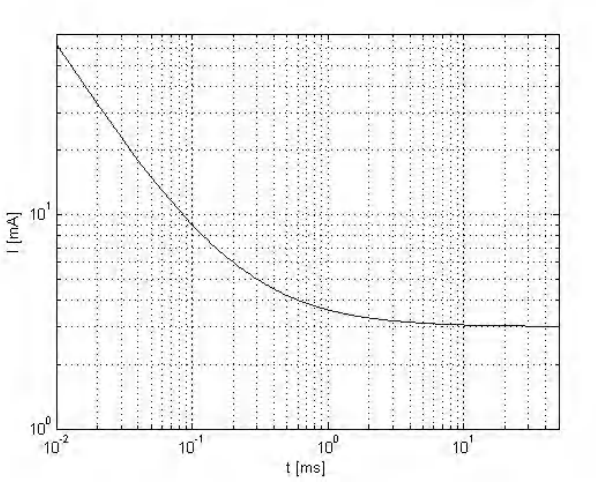

Fig 1 Example for the threshold level of current pulses

This relation can be described with the quantities rheobase I_0 and chronaxie τ. It results in an equation (2).

$$I(t) = I_0\left(1+\frac{\tau}{t}\right) \tag{2}$$

This equation is called Weiss' Law [3]. Lapicque introduced an electrical circuit which describes the behaiour of the polarization based on this insight [4]. Lapicques Law describes polarization according to the amplitude and the duration of single pulses with two parameters α and β (3) for the voltage.

$$V = \frac{\alpha}{1-e^{\beta t}} \tag{3}$$

As in Weiss' researches nearly the intensity-time-face is responsible for nerve excitation. Therefore, in a certain range short high pulses have the same impact as long low pulses. This insight should be considered in exposure assessment.

III. GUIDELINES AND ICNIRP STATEMENT

The ICNIRP guidelines [1] define the body current density as a quantity for basic restriction. The reference levels are derived from this quantity. Even when pulsed fields are evaluated it is recommended to determine the induced body current density. In the special case of a rectangular waveform of current density the ICNIRP guidelines suggest a method to convert such pulses to an equivalent sinusoidal waveform. With the duration of the pulse of half the period of the sinusoidal waveform t_p a frequency f can be determined with (4).

$$f = \frac{1}{2t_p} \tag{4}$$

The frequency and the rms value of this equivalent sinusoidal waveform can be used for an assessment. Therefore, these values are compared with the basic restrictions in the ICNIRP Guidelines ([1] Table 4).

For the general case of broadband fields there are two summation formulae for an assessment based on Fourier analysis in the frequency domain. With these equations the amplitude for each frequency is compared with the related reference level. The magnetic flux density or its time derivative is evaluated. The comparison to the reference value is realized by means of a weighting function WF_i for the i-*th* frequency.

$$\sum_i \left(WF\right)_i A_i \le 1 \tag{5}$$

This equation is very restrictive because the amplitude response is considered only. Thereby, the information of the phase angles (nearly 50% of the signal information) is neglected. A more exact and less restrictive assessment following to [2] is achieved with equation (6) which includes the phase angles for each frequency.

$$\left|\sum_i \left(WF\right)_i A_i \cos\left(2\pi f_i t + \vartheta_i + \varphi_i\right)\right| \le 1 \tag{6}$$

A_i is the peak value and ϑ_i the phase angle of the i-*th* frequency. With the angle φ_i the phase response of the weighting function is determined.

With this equation at least the peak value of the time derivative of the magnetic flux density considering the both fequency ranges ($f<820Hz$ and $f>820Hz$) is determined. A frequency evaluated peak value of current density is the result of this method. Especially when short pulses are concerned the neglect of the pulse duration can be followed by an assessment that would be too restrictive. The change of flux density should be evaluated for frequencies up to ca. 1 kHz, since the current density time integral of the time derivative of the magnetic flux density is responsible for the nerve excitation. This shall be demonstrated by an example of two magnetic field pulses with different slew rates.

IV. EXAMPLE

A. Equivalent Sinusoidal Waveform

In the following example two magnetic field pulses with different slew rates are considered. A measurement time of 0.5 s and a sampling frequency of 10 kHz were chosen for a simulation. The one-dimensional time series of magnetic

flux density for both pulses are shown in Fig. 2 (above). The time derivatives of the two pulses are shown in Fig 2 (below).

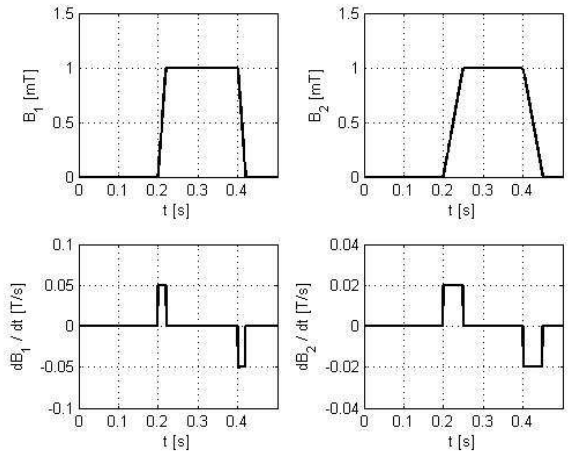

Fig. 2. Magnetic field pulses (above) and related time derivatives (below)

Since the time derivatives result in rectangular waveforms equivalent sinusoidal waveforms can be determined easily with pulse durations for both pulses. Induced body current can be calculated with the factor K_b (0.064 A/m² s/T from [2]) and compared with the ICNIRP guidelines [1]. Quantities and results are summarized in Table 1.

Table 1 Results for an assessment with equivalent sinusoidal waveforms.

	Pulse No 1	Pulse No 2
$\frac{dB}{dt}$ / T /s	0.05	0.02
t_p / s	0.02	0.05
f / Hz	25	10
J/ mA/m²	3.2	1.3
J (ICNIRP) / mA/m²	14.1[1]	14.1[1]

[1] peak value / rms = √2

These results show that basic restrictions comply with ICNIRP guidelines.

B. Summation Formula

For an evaluation with equation (6) the same pulses as in section *A* were chosen. With summation formulas the assessment is performed in the frequency domain. This method is useful for an automated assessment procedure. With the weighting function (general public) a time series results for all time steps *t* (Fig. 3).

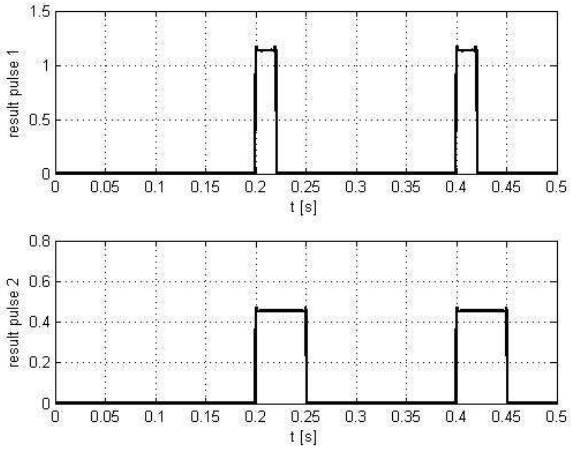

Fig. 3. Result of equation (6) for both pulses for the whole measurement time

A compliance with reference levels can be assumed if time series in Fig. 3. are below (or equal) 1 for every point in time *t*. For the pulse 1 the maximum of the function is higher than 1. The reference level is exceeded for this pulse. For a comparison the results (maxima of the time series in Fig. 3) are depicted in Fig. 4.

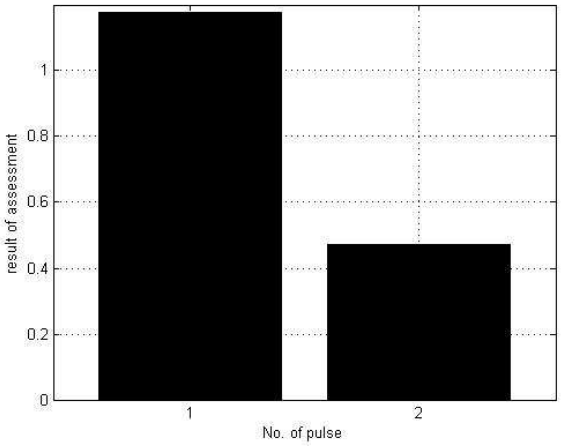

Fig.4. Maxima of the time series in Fig. 3 as the result of the assessment following to eq. (6) for both pulses.

Whereas pulse 1 exceeds the reference level pulse 2 is in compliance with the guidelines. These results show that both methods result in different evaluations of the exposition. At this point further methods could be compared as described in [5].

V. DISCUSSION

The assessment of pulsed magnetic fields with summation formulae in the frequency domain can easily be automated. Especially the application in measurement equipment is easy to implement. The method, however, can result in very restrictive assessments. Whereas both pulses induce the same current density time integral, the results of the assessments are different. In case of pulse 1 measures have to be adopted to limit the exposition of the public. This contradicts the result of the assessment with an equivalent sinusoidal waveform which results not in an exceeding exposition. This method is at least a comparison of the induced current density time integral with half sine waveform. This method is thus, in firmer accordance with physiological findings. It is useful to evaluate the change of the magnetic field instead of its time derivation in a frequency range up to 1 kHz. When the time derivative of the magnetic flux density is used it is useful to introduce a factor which involves the ratio of pulse duration. A too conservative assessment of short pulses with high slew rates can thus be avoided. Different assessment results for two methods should be excluded.

REFERENCES

1. International Commission on Non-Ionizing Radiation Protection (1998) Guidelines for Limiting Exposure to Time Varying Electric, Magnetic and Electromagnetic Fields. Health Physics. 74(4):494–522
2. International Commission on Non-Ionizing Radiation Protection (2003) Guidance on Determining Compliance of Exposure to Pulsed and Complex Non-Sinusoidal Waveforms Below 100kHz With ICNIRP Guidelines. Health Physics. 84(3):383-387
3. Weiss G. (1901) Sur la possibilite de render comparables entre eux les apareils servant a l'excitation electrique. Arch. Ital. Biol. 35:413-446
4. Lapicque L. (1907) Quantitative investigations of electrical nerve excitation treated as polarization. Biological Cybernetics. (2007) 97:341-349
5. Eichhorn, K.Fr. (2007) Bewertung breitbandiger niederfrequenter Feldexpositionen insbesondere durch gepulste Felder. Elektromagnetische Verträglichkeit EMV 2008, VDE Verlag, 2008, 405:412

Author: Christian Rueckerl
Institute: FTZ Leipzig
Street: Waechterstrasse 13
City: 04107 Leipzig
Country: Germany
Email: rueckerl@ftz.htwk-leipzig.de

Accelerated Hypo-fractionation by biological equivalent DVH for patients affected by gastric carcinoma in postoperative concomitant Radiochemotherapy

P. Pedicini[1], M. Mazziotta[1], S. Clemente[1], M. Cozzolino[1], L. Caporaso[2], P. Sanpaolo[3], V. Barbieri[3], L. Lapadula[3], G. Castaldo[3] and V. Fusco[3]

[1] Servizio Fisica Sanitaria, I.R.C.C.S. Ospedale Oncologico Regionale C.R.O.B., Rionero in Vulture (PZ), Italy
[2] Sezione Bioetica I.R.C.C.S, Casa Sollievo della Sofferenza, S. Giovanni Rotondo (FG), Italy
[3] U.O. Radioterapia, I.R.C.C.S. Ospedale Oncologico Regionale C.R.O.B., Rionero in Vulture (PZ), Italy

***Abstract* — Recent result of clinical trial on carcinoma of stomach demonstrate an advantage to adjuvant postoperative chemo-radiotherapy witch is now used more commonly for gastric cancer. However remain some doubt for toxicity as for the optimal chemotherapy regimen as for the optimal method of radiation delivery. To increase the biological effectiveness and, at same time, to reduce toxicity of conventional radiotherapy we tested many alternative fractionation schemes of dose radiation, using a biological equivalent Histogram Dose Volume (DVH) for prior analysis and as tool for the assessment and choice of fractionation dose biologically more effective.**

Keywords — **dose volume histogram, chemo-radiotherapy, tolerance dose, fractionation, biological equivalent dose.**

I. INTRODUCTION

Available data on failure after curative intent surgery suggest that the possibility of improving prognosis of gastric cancer, with radiation therapy alone, as an adjuvant treatment to surgery [1], may be quite limited because of systemic and peritoneal component of recurrence. Such evidence represent the rationale for the use of radiation therapy in combination with systemic treatment. In combination with chemotherapy, radiation therapy has been used either as a postoperative or as preoperative approach [2]. The results of these studies focused on the role of radiation therapy (RT) in the adjuvant treatment of gastric cancer and had like aim, in gastric cancer as well as in the other malignancies, that to increase local tumor control and thereby to improve patient survival rate. The probability of achieving these objectives is in general related to the actual incidence of loco-regional recurrence on survival [3]. However, because of significant toxicity of combined treatment, in this context was investigate, on radiobiological approach, the possibility of reducing the toxicity for all organs at risk (OARs) affected by radiation maintaining, at same time, the objective of equal effectiveness on the target volume.

II. MATERIALS AND METHOD

A. Standard Chemoradiotherapy

A total of 13 patients with stomach adenocarcinoma were treated with 3D-conformal RT to a dose of 45 Gy in 25 fractions with concurrent continuous infusional 5-fluorouracil (5-FU). The majority of patients received epirubicin, cisplatin and 5-FU (ECF) as the systemic component given before and after chemo-radiation [4].

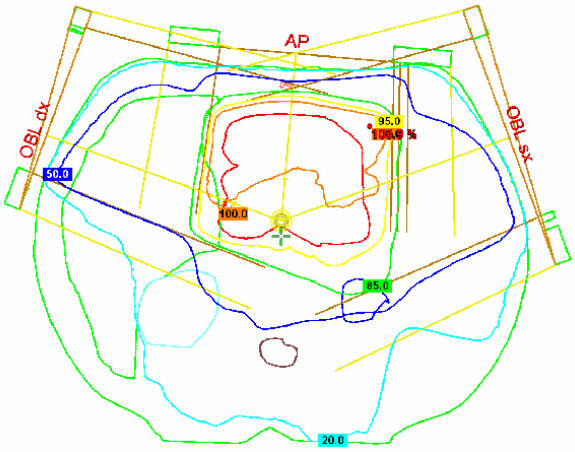

Fig. 1 Iso-center slice and iso-doses in 3D conformal radiotherapy technique with three 15 MeV fields of radiation.

For radiotherapy technique we used two 15 MeV shaped fields with gantry rotation about of 5°and 80° and a third 15 MeV field with a variable angle between 270° and 310°, depending on patient anatomy, to obtain a better saving of

O. Dössel and W.C. Schlegel (Eds.): WC 2009, IFMBE Proceedings 25/III, pp. 223–226, 2009.
www.springerlink.com

the oppose-lateral kidney (Fig. 1). Oblique left and right fields had both 45° wedge to obtain more deep in dose distribution. The average values for weights of radiation were: 30% for the anterior field; 34% for 80° field and 36% for third field.

The PTV has been obtained by fluoroscopic examinations at the time of the simulation, and once a week during RT, to evaluate inter- and intra-fractional gastric region variations. We identified the most superior, inferior, lateral, ventral, and dorsal points (by metallic clips) of the stomach on each films. Then, the appropriate treatment margins, as expansion on CTV, calculated from both systematic and random errors and adding homogeneous margin of 5 mm for setup error, was 15, 20, and 27 mm for the superior–inferior, lateral, and ventro-dorsal directions, respectively [5].

Dose constrains for OARs have been used in agreement with tolerance values used in our clinical experience: Liver, V40 < 30%; V30 < 51%; D_{mean} < 20Gy; Omo-lateral kidney, V30 < 30%; V25 < 31%; Oppose-lateral kidney, V30 < 22%; V25 < 33%; Spinal cord, D_{max} < 40 Gy; Heart, V40 < 33% (Fig. 2).

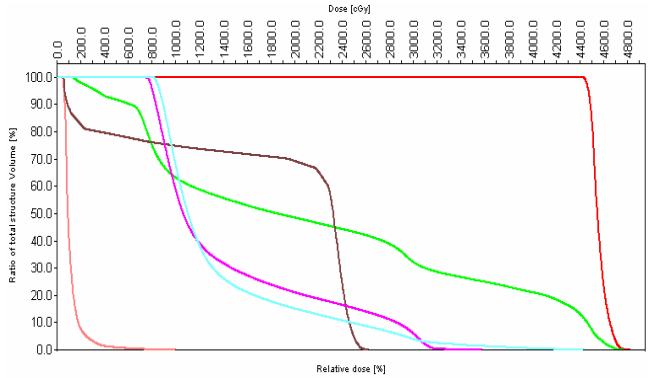

Fig. 2 Dose Volume Histogram in Standard Fractionation: Target, Liver, Spinal cord, Omo-lateral Kidney, Oppose-lateral Kidney, Heart.

B. Radiobiological analysis

The effects of changing for dose fractionation on serial and parallel components of an organ or different organs, can be evaluated directly on DVH transforming his in biological DVH [6], obtained by the "index of toxicity" *I* witch is defined for each OARs exposed to radiation as the ratio of modified ($E(d_m)$) from the standard fractionation effect ($E(d_s)$), evaluated with the linear quadratic model [7] with equal effect on the target volume:

$$ {}^{\alpha/\beta_t}_{\alpha/\beta_o} I = \frac{E(d_m)}{E(d_s)} = \frac{(\alpha/\beta_t + d_s)}{(\alpha/\beta_t + d_m)} \cdot \frac{(\alpha/\beta_o + d_m)}{(\alpha/\beta_o + d_s)} \qquad (1) $$

where α/β_t is reported for target and α/β_o for the OAR studied, d_m and d_s, represents the dose/fraction prescribed in modified and standard fractionation dose, respectively. Values such that I > 1, indicating an increase of toxicity on OAR, which occurs when

$$ (\alpha/\beta_t - \alpha/\beta_o) \cdot (d_m - d_s) > 0 \qquad (2) $$

so that, for example in a hypo-fractionation (d_m - d_s > 0), we have an increase in OAR toxicity, when the value α/β_t for neo-plastic target is greater that of the same OAR (ex. the low value of α/β for prostate, justifies the choice of a hypo-fractionation [8]). However, because of radiotherapy treatment usually involving the OARs by a inhomogeneous distribution dose [9], it is necessary to define a generalized index *I(d)* for each value of dose *d* equivalent to a variable fraction of the prescription dose "$d = f \cdot d_s$". For the volume fraction (ex. 60% V) corresponding at dose *d,* there is an increase of toxicity when

$$ (f \cdot \alpha/\beta_t - \alpha/\beta_o) \cdot (d_m - d_s) > 0 \qquad (3) $$

Therefore this inequality highlights the existence of a critical dose value $d^* = d_s \cdot (\alpha/\beta_o / \alpha/\beta_t)$ such that $I(d^*) = 1$ and for which the corresponding volume fraction suffering an invariant toxicity level with the change of the dose/fraction. If $\alpha/\beta_o > \alpha/\beta_t$, d^* result higher of prescription dose and this implies that for structures with α/β greater than target, hyper-fractionation becoming more toxic and hypo-fractionation less toxic than standard, for all sub-volume involved (fig.3).

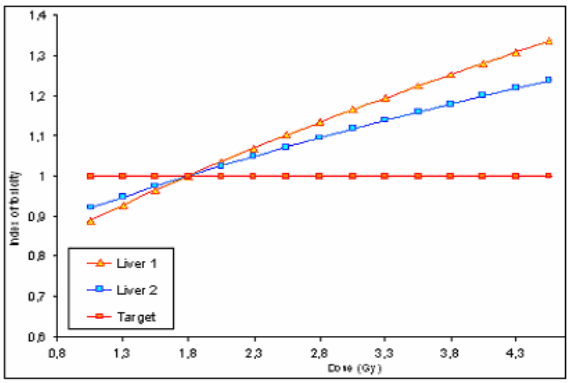

Fig. 3 Trend of toxicity Index as function of dose/fraction for two component of Liver (α/β = 3) and for target volume (α/β = 10) in the treatment of gastric cancer. The curves describes difference in behaviour for more serial component (Liver 1, 30% V) and for more parallel component (Liver 2, 51% V) in the form of hyper-fractionation ($d_m < d_s$) and hypo-fractionation ($d_m > d_s$).

If $\alpha/\beta_o < \alpha/\beta_t$, d^* result smaller than prescription dose hence, following increasing the dose/fraction with equal effect on T, sub-volumes corresponding at doses higher than critical dose for OAR (serial components) suffer increased toxicity while, at the same time, sub-volumes corresponding at doses smaller than critical dose for OAR (parallel components) benefiting from a reduction of toxicity.

Overall, applying the reasoning described above, there is the possibility of saving OARs at the same therapeutic result on the target (Equal value of Biological Equivalent Dose, BED) [10].

Table 1 α/β values, radiobiological end-point, average of DVH Volumes (V_{mean}) and tolerances doses (T_D) for OARs and CTV

OAR	α/β	End-point	V_{mean}	T_D
Liver	3 Gy	Hepatitis	$V_{40} = 20$ %	$V_{40} < 30$ %
			$V_{30} = 50$ %	$V_{30} < 51$ %
Heart	3 Gy	Cardiomiopathy	$V_{40} = 7$ %	$V_{40} < 33$ %
Kidney om.	2 Gy	Nephritis	$V_{30} = 17$ %	$V_{30} < 30$ %
			$V_{25} = 20$ %	$V_{25} < 31$ %
Kidney op.	2 Gy	Nephritis	$V_{30} = 2$ %	$V_{30} < 22$ %
			$V_{25} = 3$ %	$V_{25} < 33$ %
Spinal-cord	3,3 Gy	Myelitis	$D_{max} = 16$ Gy	$D_{max} < 40$ Gy
CTV	10 Gy	/	$V_{45} = 97$ %	/

III. RESULTS

The reference radiobiological values used in the planning fractionation analyzed (Table 1) are: α/β = 10 Gy for neoplastic target, α/β = 3 Gy for both liver and heart, α/β = 2 for kidneys and α/β = 3,3 for Spinal-cord [11]. As mentioned above being the value α/β_t considerably larger than those of OARs in question, would be choice a reduction of the dose/fraction, however, to maintain the condition of equivalent effect on target volume this type of schedule would require an elongation of the overall time of treatment which increases the effect because of beginning for an important phenomenon of the accelerated proliferation for clonogenic cells of neoplastic target. This drawback could be overcome by a awkward accelerated hyper-fractionation schedule, that provides more fractions per day separated by at least 8 hours to allow at all healthy tissue to obtain a complete repair in inter-fraction period. On the other hand, the reduction of total dose resulting from a reduction in the overall time of treatment with an hypo-fractionated treatment [12], obtain similar benefits in this last circumstance (Fig. 4).

The best fractionation obtained by analysis consist of hypo-fractionation accelerated scheme with 18 fractions at 2,25 Gy/fraction.

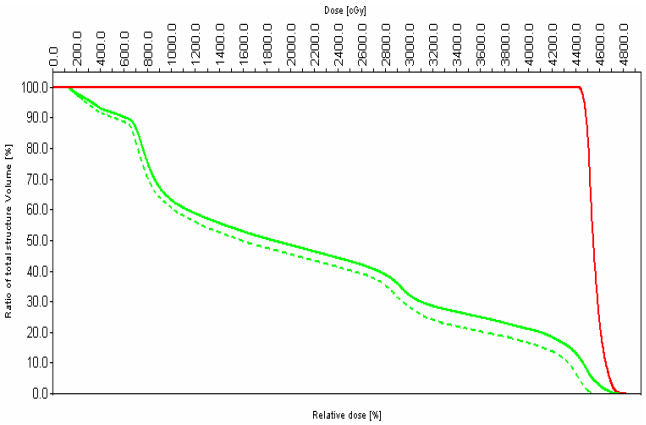

Fig. 4 Biological equivalent DVH, in the transition 1.8 (solid lines)-2.25 Gy/f (dashed line), in overall treatment for Target and Liver. Is apparent the reduction of toxicity, specially at high doses for the serial component of Liver (α/β = 3 Gy).

Comparison between standard and modified fractionations has been carried out introducing a constrain satisfaction index (CSI) as the average percentage difference between dose constrains for involved portions of the OARs and the corresponding values obtained in the planning phase on the modified equivalent DVH, considering, substantially, the same PTV covering (Table 2).

Table 2 Average of DVH doses; equivalent doses at 2 Gy/f in Standard fractionation (D_{eq} (Std)) with 1,8 Gy/f and in Modified fractionation (D_{eq} (Mod)) with 2,25 Gy/f; relative differences with tolerance doses and CSI values for all OARs. All values are expressed in Gy.

OAR	DVH dose	D_{eq} (Std)	D_{eq} (Mod)	$(T_D\text{-}D_{eq})_S$	$(T_D\text{-}D_{eq})_M$	CSI
Liver	$D_{(30\%}V) = 36$	$L_1 = 32$	$L_1 = 30$	8	10	5 %
	$D_{(51\%}V) = 29$	$L_2 = 24$	$L_2 = 22$	6	8	6,6 %
Heart	$D_{(33\%}V) = 13$	H = 10	H = 8	30	32	5 %
Kidney om.	$D_{(30\%}V) = 17$	$K_{om1} = 12$	$K_{om1} = 10$	18	20	6,6 %
	$D_{(31\%}V) = 10$	$K_{om2} = 10$	$K_{om2} = 10$	15	15	0 %
Kidney op.	$D_{(22\%}V) = 9$	$K_{op1} = 6$	$K_{op1} = 4$	24	26	6,6 %
	$D_{(33\%}V) = 4$	$K_{op2} = 2$	$K_{op2} = 1$	23	24	4 %
Spinal-cord	$D_{max} = 16$	Sc = 12	Sc = 10	28	30	5%

This schedule results equivalent in terms of local control probability and, at the same time, makes possible reduction of toxicity for OARs by follow improvement of CSI:

- Liver, 5% on 30% V and 6,6% on 51% V;
- Omo-lateral kidney, 6,6% on 30% V;
- Opp-lateral kidney, 6,6% on 22% V and 4% on 33% V;
- Heart, 5% on 33% V;
- Spinal cord, 5% on D_{max} (Fig. 5).

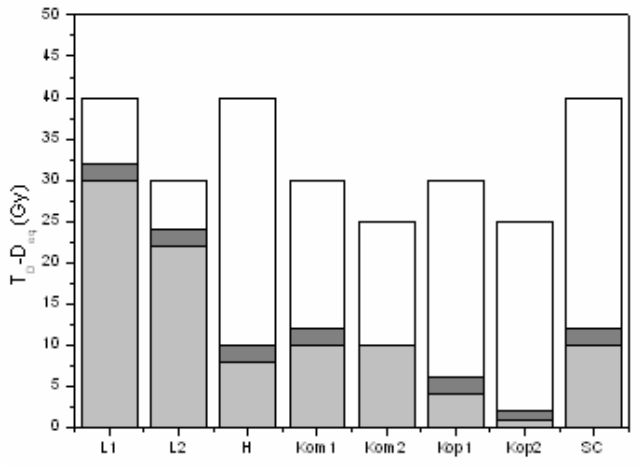

Fig. 5 Histogram for Tolerance doses (white bars), D_{eq} (Std) (dark grey bars) and D_{eq} (Mod) (grey bars), the CSI result by differences of grey bars.

IV. DISCUSSION

The identified accelerated hypo-fractionation schedule of radiation for treatment of gastric carcinoma in postoperative concomitant chemo-radiotherapy, appears considerably improvement compared to standard fractionation in terms of savings of OARs. The advantage is obtained mainly by the reduction in the number of fractions for the entire radiotherapy treatment and for consequent reduction of overall treatment time (accelerated fractionation) that minimizes the effect of an important phenomenon of neo-plastic accelerated proliferation [13].

In the final analysis it's clear that the purpose of addressing the study of complex biological systems, in which individual components are connected and coordinated with one another by morphologically differentiated structures, it's necessary to know the causal and the quantities relationships that exist between the different factors that come into play in order to provide the best approximation possible to the response expected from a biological system, following its exposure to radiation. To answer this need, in our view, the equivalent DVH can be used as a methodology that allows to provide a knowledge for the rational observation of the data collected in clinical practice.

V. CONCLUSION

The use of biological DVH allowed to study in advance the fractionation doses and intervenes in the planning phase of treatment in addition with the traditional planning based only on physical dose distributions. Our results suggest that this adjuvant regimen can be adopted to meet the goal of reducing the toxicity of combined treatment of adjuvant postoperative chemo-radiotherapy for gastric cancer.

References

1. Montalban C, Santon A, Redondo C, et al. Long-term persistence of molecular disease after histological remission in lowgrade gastric MALT lymphoma treated with H. pylori eradication. Lack of association with translocation t(11; 18): a 10-year updated follow-up of a prospective study. Ann Oncol (2005); 16: 1539–44.
2. Wydman´ski J, Suwinski R, Poltorak S et. al. The tolerance and efficacy of preoperative chemoradiotherapy followed by gastrectomy in operable gastric cancer, a phase II study. Radiotherapy and Oncology (2007); 82: 132–136
3. Park W, Chang SK, Yang WI, et al. Rationale for radiotherapy as a treatment modality in gastric mucosa-associated lymphoid tissue lymphoma. Int J Radiat Oncol Biol Phys (2004); 58: 1480–6.
4. Regine WF, Winter KA, Abrams RA, et al. Fluorouracil vs. gemcitabine chemotherapy before and after fluorouracilbased chemoradiation following resection of pancreatic adenocarcinoma. A randomized controlled trial. JAMA (2008); 299:1019–26.
5. Watanabe M, Isobe K , Takisima H, et al. Intrafractional gastric motion and interfractional stomach deformity during radiation therapy. Radiotherapy and Oncology (2008); 87: 425–431.
6. Kutcher GJ, Burman C, Brewster L, Goitin M, Mohan R. "Histogram reduction method for calculating complication probabilities for three-dimensional treatment planning evaluations". Int J Radiat Oncol Biol Phys (1991); 21.
7. Dale RG. The application of the linear-quadratic dose-effect equation to fractionated and protracted radiotherapy. Br J Radiol (1985); 58:515–28.
8. Fowler J., Chappel R. and Ritter M., "Is α/β for prostate tumors really low?" Int. J. Radiation Oncology Biol. Phys. (2001); 50: 4.
9. Kutcher G. J., Burman C., Brewster L. Gotein M. and Mohan R. Calculation of complication probability factors for nonuniform normal tissue irradiation: The effective volume method. Int. J. Radiation Oncology Biol. Phys. (1991); 21.
10. Lee SP, Leu MY, Smithers JB, et al. Biologically effective dose distribution based on the linear quadratic model and its clinical relevance. Int J Radiat Oncol Biol Phys (1995); 33:375–89.
11. Bentzen SM, Overgaard J. Clinical normal-tissue radiobiology. Current Radiation Oncology (1996); 2.
12. Jones B, Dale RG, Khaksar SJ. BED assessment of the consequences of hypofractionated radiotherapy. Int J Radiat Oncol Biol Phys. In press.
13. Thames HD, Bentzen SM, Turesson I, Overgaard M, Van den Bogaert W. Time-dose factors in radiotherapy: a review of the human data. Radiother Oncol (1990); 19.

Author: Piernicola Pedicini
Institute: I.R.C.C.S Ospedale Oncologico Regionale C.R.O.B.
Street: Via Strada Provinciale n.8, 85028
City: Rionero in Vulture (PZ)
Country: Italy
Email: ppiern@libero.it

Reducing Non-uniformity Error of Radiochromic Film in The Diagnostic Range by Ultraviolet Exposure: Preliminary Study

T Katsuda[1], R Gotanda[2], T Gotanda[2], A Tabuchi[2], K Yamamoto[2], H Yatake[2], K Kashiyama[2], T Kuwano[2].

[1] Department of Health Science, Himeji Dokkyo University. Hyogo, Japan
[2] Graduate School of Health Sciences, Okayama University, Okayama, Japan

Abstract— **Thickness irregularity of active layer is made to express density irregularity. True data by the X-rays are extracted by exposing Ultraviolet (UV) rays that prohibited exposure are exposed for radiochromic film (RF). When UV is exposed, the density irregularity is corrected. In addition, RF is initialized, thereby improving of data acquisition.**

GAFCHROMIC EBT (GAF-EBT) film was exposed to UV light at 360 nm twice with a 2 hour interval. The distance from the UV tube to the GAF-EBT film was 165 cm. The GAF-EBT films were scanned after the first and second UV exposure, using a flat bed scanner. Analyses were performed by the density profile curve of the short and long axes of the GAF-EBT.

The density irregularity of the active layer of the film was corrected to 2.19 ± 0.49 (pixel value) by subtracting the density obtained with the first UV exposure from that with the second UV exposure of GAF-EBT on the short axis. On the long axis, the density irregularity of the active layer of GAF-EBT was corrected to 2.67 ± 0.65 (pixel value).

Uniform UV exposure data was identified. The measurement precision of the GAF-EBT film and its usefulness are improved by this method.

Keywords— **Radiochromic Film, Active Layer, Irregularity, Ultraviolet Exposure.**

I. Introduction

Radiochromic film (RF) was developed to measure radiation dose during radiation therapy, as a film-type dosimeter. At present, however, it is used for X-ray measurements and for quality control of diagnostic X-ray equipment. The method uses a sheet roll type phantom and RF for dosimetry of computed tomography (CT), enabling the measurement of the three dimensional dose of X-rays in the phantom [1, 2, 3]. In addition, RF is beginning to be used for the measurement of slice thickness and pitch, as well as X-ray dosimetry, as a component of quality control for CT [4]. On the other hand, the half-value layer is being measured with a change in density, instead of measuring the radiation dose, because changes of radiation dose and film density are related linearly [5].

A flatbed scanner is used for data collection from the RF. Transmission type scans are produced using RFs, Gafchromatic EBT film (GAF-EBT: International Specialty Products (ISP), Wayne, NJ, USA) (6). There are two problems that must be addressed when using these films.

First, when data from transmission-type RF is acquired with a flatbed scanner, it is necessary to remove noise generated by the density difference among places of a RF of the visible light transmittance of the transparence region. There are non uniformity errors caused by the coating of the GAF-EBT are 0.5% to 1.0% (6). This noise can be bigger than the actual data, because there is only a small density increase of the X-ray in the diagnosis range. Therefore, the data correction is necessary, because the size of this noise is heterogeneous in each region of the sheet. This noise is constant, regardless of X-ray exposure. The subtraction method can extract true exposure data from the data on the RF acquired before and after X-ray exposure. Non-uniformity of the flatbed scanner was also corrected for each point on the scanner by the subtraction method.

The second problem with the RF is the irregularity of the active layer. When the thickness of the active layer is uneven, the density may show an increase at a certain position although the X-ray exposure may be uniform. While there is a linear relationship between the radiation dose and the film density, if an arbitrary area of the film is used, the linearity may be lost. However, the irregularity of the active layer is not apparent, because the active layer of the RF is transparent until the film density increases by exposure of X-rays. For this reason, even if a subtraction method is used, the irregularity of the active layer is not corrected.

Thickness irregularity of active layer is made to express density irregularity. True data by the X-rays are extracted by exposing Ultraviolet (UV) rays that prohibited exposure for RF. When uniform UV is exposed, the density irregularity is appeared. In addition, RF is initialized, thereby improving the data acquisition.

O. Dössel and W.C. Schlegel (Eds.): WC 2009, IFMBE Proceedings 25/III, pp. 227–230, 2009.
www.springerlink.com

II. Materials and Methods

A. GAFCHROMIC EBT Film (GAF-EBT)

GAF-EBT was used as a dosimeter. The GAF-EBT can measure doses in the range of 1-800 cGy. It is a transmitted type film, and an economical flatbed scanner can be used for the measurement of film density [6].

B. UV Exposure

First UV exposure: The GAF-EBT was cut into 4 pieces (size 20 cm x 10 cm) to enable scanning on a flatbed scanner. The density of the active layer increased following exposure to a 15 W UV light source (FL15BL-B, NEC, Tokyo, Japan) with a peak wavelength of 360 nm. The distance from the UV tube to the film was 165 cm (Figs. 1 and 2), and a digital UV strength meter (YK-34UV, Fuso Co., Ltd., Tokyo, Japan) was placed in the center of the field of exposure. The film was exposed to UV light for 5 min with a total intensity of about 0.018 mW/cm^2.

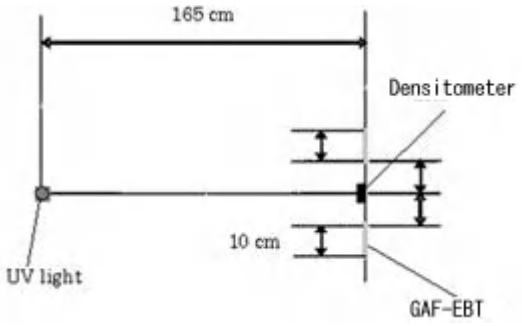

Fig. 1. Arrangement of ultraviolet (UV) exposure. Lateral view.

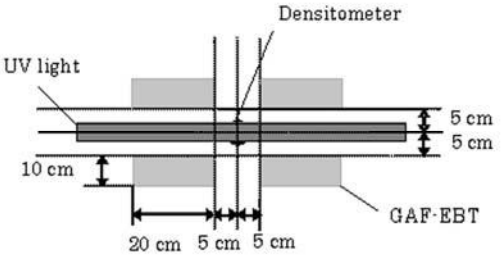

Fig. 2. Arrangement of ultraviolet (UV) exposure. Top view

Second UV exposure: The film was again exposed to the UV source, same condition as first exposure, instead of X-rays. The X-ray intensity is non uniform by an exposed area. Thus, a density irregularity of the GAF-EBT is occurred. The data of GAF-EBT which performed the second UV exposure is scanned by a flatbed scanner.

C. Analysis of the GAF-EBT

For image data acquisition, GAF-EBT films were scanned after the first and second UV exposures using an Epson ES-2200 flat bed scanner (Seiko Epson Co., Nagano, Japan) in RGB (48 bit) mode, 150 dpi, with a liquid crystal protection [7] (LCD-150; Sanwa Supply Inc., Okayama, Japan). The GAF-EBTs were placed on the scanner bed in the same orientation (with the active component coating parallel to the short dimension of the scanner bed). To eliminate any density errors due to time differences, films were scanned at a constant time (2 hours) after both the first and second UV exposures [4]. Image data of the GAF-EBTs were changed into Red mode with Adobe Photoshop 6.0 (Adobe Systems Incorporated, San Jose, CA, USA), and were changed 8-bit gray scale and analyzed with Image J 1.37 (National Institutes of Health, Bethesda, MD, USA). The data of the first UV exposure were subtracted from the data after the second UV exposure.

The analyses were performed using the profile curve of the short axis (Fig. 3 left, line A) and the long axis (Fig. 3 right, line B) intersecting at the center of the film.

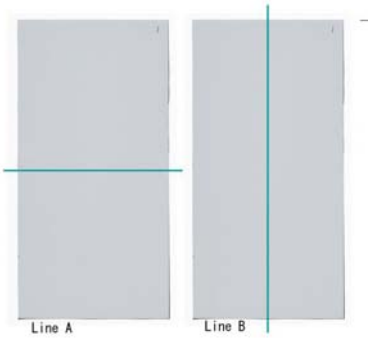

Fig. 3. The location of the profile curves. Line A: short axis, Line B: long axis

III. Results

Figures 4, 5 and 6 showed profile curves of the short axis at the center of the film. Figure 4 showed the profile curve 2 hours after the first UV exposure. The center of the curve had a low pixel value, while both sides of the film showed a high pixel value. The mean value ± standard deviation (SD) of the pixel value was 51.6 ± 0.9. Figure 5 showed the profile curve 2 hours after the second UV exposure. The center of the curve had a low pixel value, and both

sides of the film had high pixel values, similar to that obtained after the first UV exposure shown in Fig. 4. The mean value ± SD of the pixel value was 53.8 ± 1.0. Figure 6 showed the corrected profile curve of the data from the second UV exposure. The corrected profile curve was flat. The mean value ± SD of the pixel value was 2.19 ± 0.49.

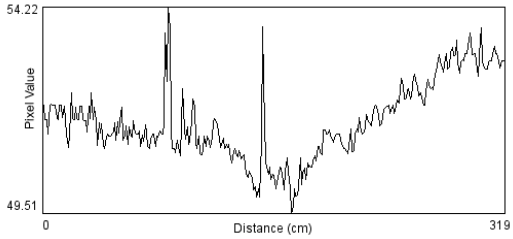

Figure 4. Profile curve of the first UV exposure 2 hours later. (short axis)

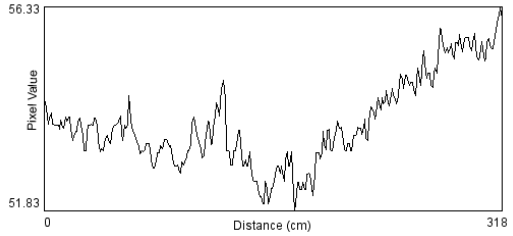

Fig. 5. Profile curve of the second UV exposure 2 hours later. (short axis)

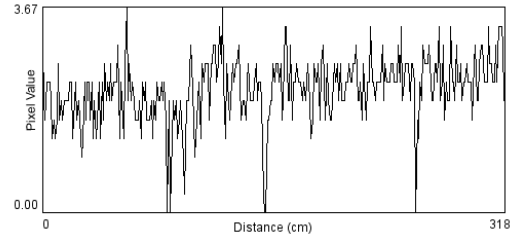

Fig. 6. Profile curve of the subtraction image. (short axis)

Figures 7, 8 and 9 showed the profile curves of the long axis at the film center. Figure 7 showed the profile curve of the data taken 2 hours after the first UV exposure. The center of the curve had a low pixel value, and both sides of the film had a high value. The mean value ± SD of the pixel value was 52.2 ± 0.81. Figure 8 showed the profile curve of the data obtained 2 hours after the second UV exposure. The center of the curve showed a low pixel value, and both sides of the film had relatively high pixel values similar to the result obtained with the first UV exposure shown in Figure 7. The mean value ± SD of the pixel value was 53.37 ± 0.87. The corrected profile curve of the second UV exposure is shown in Figure 9. The corrected profile curve was flat, and the mean value ± SD of the pixel value was 2.67 ± 0.65.

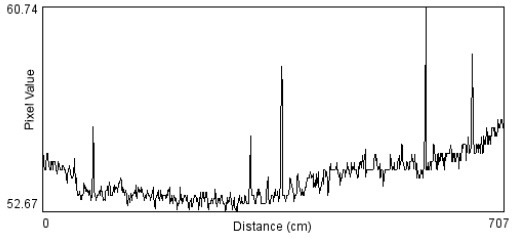

Fig. 7. Profile curve of the first UV exposure 2 hours later. (long axis)

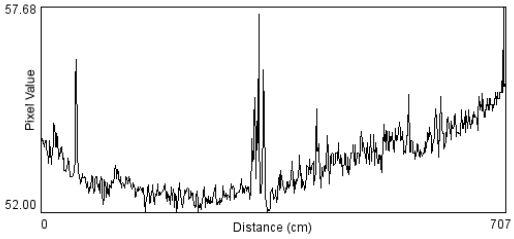

Fig. 8. Profile curve of second UV exposure 2 hours later. (long axis)

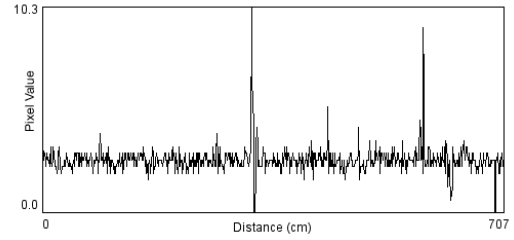

Fig. 9. Profile curve of subtraction image. (long axis)

IV. DISCUSSION

A. Noise in scanning

Since the GAF-EBT film is scanned with a flatbed scanner in this study, it is possible that dust and scratch of the surface of the film may appear as high frequency noise. However, this noise is showed extreme data. Thus, it is likely that the correction is comparatively simple. Nevertheless, this correction was not applied in this study.

B. Increase in density after UV exposure

The density increase of the GAF-EBT film is stable after a period of 2 hours following the UV exposure. Therefore, it is recommended to scan the film 2 hours after the

exposure is completed. The purpose of the first UV exposure is to reveal the thickness irregularity of the active layer, and not to provide data on the absorbed dose. Therefore, the factor of thickness irregularity of the active layer is removed by using the data obtained from scanning just after first the UV exposure. However, there will be an increase in the density data after the first UV exposure. Thus, it is useful to wait for 2 hours after the second UV exposure. The increase in density following the first UV exposure becomes the noise and is added to the data from the second UV exposure. On this account, it is considered that more than a 2-hour interval after the first UV exposure is necessary to obtain data from the first UV exposure. In addition, the influence of the light of the scanner at the time of image acquisition is ignored.

C. Second UV exposure

In this study, 360 nm UV was used as a substitute for X-ray exposure. This is because UV has an equivalent effect on the active layer of GAF-EBT with a uniform exposure. There is a possibility, however, that the second UV exposure was absorbed at the surface of the active layer by the density increase of active layer caused by the first UV exposure. Thus, it is possible that the pixel value of the actual second UV exposure data has become smaller. The density increase due to an irregularity of the thickness of the active layer is may not a linear change; this problem will be addressed in future studies.

D. Scan position and a subtraction image

It is difficult to scan the GAF-EBT film at the same position on a flatbed scanner surface every time. Thus, precise pixel by pixel subtraction is not possible. It is occurred misregistration when the subtraction images are obtained. The developed black radiographic film was placed on the surface of the flatbed scanner such that the two sides of the film were at a constant position. On this account, it is believed that the difference in position from scan to scan was small.

E. Wavelength and the exposure dose of ultraviolet rays

In this study, a commercial black light of 15 w of peak wavelength 360 nm was used. A sufficient increase in density was observed in the active layer. In addition, a relatively long time of exposure (5 minutes) was used. Nevertheless, in future studies it will be necessary to ascertain the most efficient UV peak wavelength and exposure time.

The distance from the UV tube to the GAF-EBT was set to 165 cm to expose the GAF-EBT uniformly. It may be possible to shorten the exposure time and the distance by considering an appropriate exposure dose and a uniform exposure method.

V. Conclusion

True exposure data were obtained by utilizing UV light at 360 nm without actual X-ray exposure. In other words, data initialization of the GAF-EBT is possible. When exposed to equal X-ray dose to arbitrary segments of GAF-EBT, the density data indicate equal value. Uniform X-ray exposed data was identified. The precision of the measurements on GAF-EBT as well as its usefulness are improved by this method.

VI. References

1. R. Gotanda, T. Katsuda, M. Eguchi, S. Takewa, A. Tabuchi, H. Yatake. Computed Tomography Phantom for Radiochromic Film Dosimetry. Australas Phys Eng Sci Med, 30, 194-199, 2007.
2. R. Gotanda, T. Katsuda, T. Gotanda, A. Tabuchi, H. Yatake, Y. Takeda. Dose Distribution in Pediatric CT Head Examination: Phantom Study. IFMBE Proceedings 22, 775-779, 2008.
3. R. Gotanda, T. Katsuda, T. Gotanda, A. Tabuchi, H. Yatake, Y. Takeda. Dose Distribution in Pediatric CT Head Examination using a New Phantom with Radiochromic Film Australas Phys Eng Sci Med, 31, 2008 (in press).
4. T. Gotanda, R. Gotanda, A. Tabuchi, T. Kuwano, H. Yatake, K. Yamamoto, T. Katsuda. Visualization of Radiation Exposure for Computed Tomography.Health Sciences, 24, 394-403, 2008.
5. T. Gotanda, T. Katsuda, R. Gotanda, A. Tabuchi, K. Yamamoto, T. Kuwano, H. Yatake, Y. Takeda. Measurement of Half-Value Layer for QA and QC: Simple Method Using Radiochromic Film Density. IFMBE Proceedings 22, 780-783, 2008.
6. http://www.ispcorp.com/products/dosimetry/content/gafchromic/content/products/ebt/pdfs/EBTwhitepaper.pdf. 2008.1.20

Author: Toshizo Katsuda
Institute: Department of Health Science, Dokkyo University
Street: 7. 2. 1. Ue-Ohno
City: Himeji
Country: Japan
Email: tkatsuda@yahoo.co.jp

Investigation of acceptance criteria for the gamma-index in scanned carbon ion radiotherapy

S. Lahrmann[1], O. Jäkel[1,2] and C.P. Karger[1]

[1] German Cancer Research Center/Dept. of Medical Physics in Radiation Oncology, Im Neuenheimer Feld 280, Heidelberg, Germany
[2] Heidelberg Ion Beam Therapy Center (HIT), Im Neuenheimer Feld 450, Heidelberg, Germany

Abstract— **In this work, several sets of acceptance criteria for the gamma-index (γ) were investigated for the dose verification of scanned carbon ion therapy. 40 verification measurements were retrospectively analyzed and the resulting measurement acceptance rate was compared to that based on the currently applied action levels for dose deviation to propose action levels for γ as well. Additionally, a correction of the measured dose values was performed and γ was recalculated to estimate acceptance criteria for an improved beam model.**

Using acceptance criteria of 7% for the dose deviation and 2 mm for the DTA, clinically acceptable results were obtained. Simulations showed that the acceptance criteria can be tightened, if the beam model is improved. To reproduce acceptance rates achieved with current action levels, two requirements for measurement acceptance are suggested for γ: First, the mean γ per measurement has to be below one. Second, less than 30% of the individual measurement positions per measurement are allowed to exceed a γ of one.

Keywords— **carbon ion radiotherapy, dose verification, gamma-index, acceptance criteria, action levels.**

I. Introduction

The gamma-index is a routinely used assessment criterion for patient specific dose verification in photon IMRT. It combines dose deviations and spatial deviations, which can be caused by detector misalignments as well as beam displacements, to one dimensionless parameter [1]. Acceptance criteria for both types of errors can be defined separately.

In photon IMRT, acceptance criteria of 3% as well as 5% of the maximum dose and 3mm for the distance to agreement (DTA) are widely accepted [2, 3, 4, 5]. In heavy ion radiotherapy (RT) the γ has not been applied yet, hence no suitable acceptance criteria have been established.

In this study, several sets of acceptance criteria have been retrospectively investigated for dose verification measurements in scanned carbon ion RT performed at the Gesellschaft für Schwerionenforschung (GSI, Darmstadt, Germany) and associated action levels for measurement points exhibiting $\gamma > 1$ are proposed. Furthermore, acceptance criteria as well as action levels were estimated for the case that the applied beam model is improved.

II. Materials and methods

At GSI dose verification is performed with a 3D stack of 24 ionization chambers. Action levels of 5% for the mean deviation as well as for the standard deviation of deviations between measured and calculated dose are currently applied. Only measurement positions in moderate dose gradients are taken into account. Treatment plans failing acceptance can only be applied after discussion with and approval by the responsible radio-oncologist.

A. Investigation for current beam model

For the GSI setup, a tool calculating γ in 3 dimensions has been implemented. Acceptance criteria of 3%/3mm (a), 5%/2mm (b), 6%/1mm (c) and 7%/2mm (d) have been retrospectively analyzed in 40 treatment fields verified and accepted at GSI. Subsequently, the resulting measurement acceptance rate was compared to that found with current criteria.

B. Estimation for future improved beam model

The beam model at GSI is known to systematically underestimate the planned dose for decreasing field size and increasing depth. Therefore, to estimate the acceptance criteria for the case of an optimized beam model, which is still under development, the measured dose value of each IC was individually corrected by the mean dose deviation of the respective measurement, before calculating γ again. For recalculation of γ the same acceptance criteria were used as before the correction.

III. Results

A. Investigation for the current beam model

A fraction of (a) 0.81, (b) 0.85, (c) 0.82 and (d) 0.89 of all measurement positions in all measurements yielded γ below 1. The mean γ was below 1 for all measurements,

O. Dössel and W.C. Schlegel (Eds.): WC 2009, IFMBE Proceedings 25/III, pp. 231–233, 2009.
www.springerlink.com

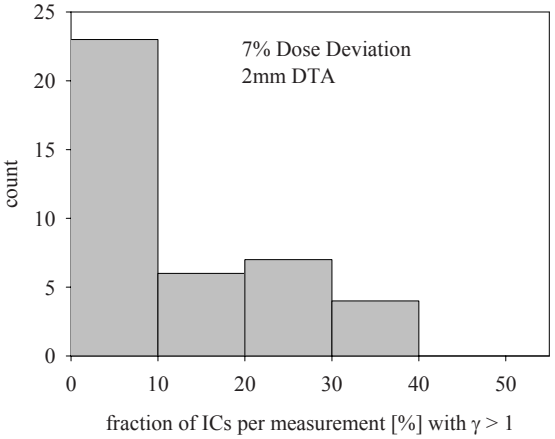

Fig. 1 Distribution of the fraction of ICs per measurement yielding $\gamma > 1$. *Note*: A fraction of 100% refers to 24 ICs. The histogram contains 40 entries corresponding to the 40 analyzed measurements.

when acceptance criteria sets (b), (c) or (d) were applied. Acceptance criteria (d) resulted in the smallest fraction of individual IC positions exhibiting $\gamma > 1$. With 10% (4 out of 40), this set also showed the smallest amount of measurements exceeding a fraction of 30% of ICs per measurement yielding $\gamma > 1$ (Fig. 1). A failing rate of 10% is in the same order of magnitude as the rate achieved with currently applied action levels (3 out of 40).

B. Estimation for a future improved beam model

Recalculation of γ after individual correction of each measured dose value resulted in fractions of (a) 0.84, (b) 0.89, (c) 0.88 and (d) 0.95 of all measurement positions in all measurements with $\gamma > 1$. The mean γ was again below 1 for all measurements, when acceptance criteria sets (b), (c) or (d) were applied. Acceptance criteria (b) and (c) resulted in similar fractions of individual IC positions exhibiting $\gamma > 1$ as the application of (d) before the correction. For both sets, 7.5% of the measurements exceeded a fraction of 30% of ICs per measurement yielding $\gamma > 1$ (Fig. 2), which is comparable to the result obtained previously with set (d).

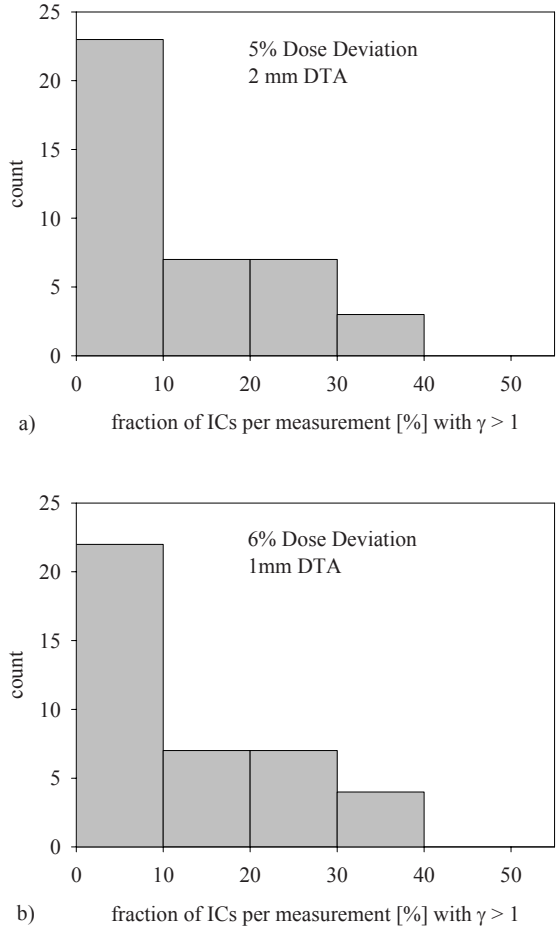

Fig. 2 Distribution of the fraction of ICs per measurement yielding $\gamma > 1$. *Note*: A fraction of 100% refers to 24 ICs. The histograms contain 40 entries corresponding to the 40 analyzed measurements. Before calculating γ, the measured dose for each IC was individually corrected for the mean dose deviation of the respective measurement (see methods and materials).

IV. Discussion

A. Investigation for the current beam model

With the currently applied beam model using acceptance criteria of 7%/2mm, clinically acceptable results could be obtained. Although the mean γ was below 1, some individual measurement positions exhibited $\gamma > 1$. If the fraction of measurement positions with $\gamma > 1$ was restricted to 30% per measurement, a measurement acceptance rate of 10% would be obtained, which is similar to the acceptance rate found in current clinical practice of scanned carbon ion radiotherapy.

Hence, for the current beam model, 7%/2mm are suggested as acceptance criteria and, applying this set, as further requirements the mean γ should be below 1 and less than 30% of individual positions per field should be allowed to show $\gamma > 1$. These requirements should define action levels for further investigations of these treatment plans rather than actual tolerance limits.

B. Estimation for an improved beam model

After correcting each individual measured dose by the mean dose deviation in the respective measurement, acceptance criteria of 5%/2mm and 6%/1mm showed similar results as those obtained with 7%/2mm before the correction. Therefore, it can be concluded that for an improved beam model the applied acceptance criteria can be tightened. Those tighter criteria would then be comparable to those used in photon IMRT.

V. Conclusions

The use of the gamma-index for dose verification requires action protocols for the case of failing the acceptance criteria. For scanned carbon ion RT, acceptance criteria of 7%/2 mm for the dose deviation and DTA are recommended. We further suggest requiring a mean $\gamma < 1$ and a maximum fraction of 30% of the individual measurements exhibiting $\gamma > 1$.

References

1. Low DA, Harms WB, Mutic S et al. (1998) A technique for the quantitative evaluation of dose distributions. Med Phys 25:656-661 DOI 10.1118/1.598248
2. Winkler P, Zurl B, Guss H et al. (2005) Performance analysis of a film dosimetric quality assurance procedure for IMRT with regard to the employment of quantitative evaluation methods. Phys Med Biol 50:643-654
3. Childress NL, White RA, Bloch C et al. (2005) Retrospective analysis of 2D patient-specific IMRT verifications. Med Phys 32:838-850 DOI 10.1118/1.1879272
4. Low DA, Dempsey JF (2003) Evaluation of the gamma dose distribution comparison method. Med Phys 30:2455-2464 DOI 10.1118/1.1598711
5. van Zijtveld M, Dirkx MLP, de Boer HCJ et al. (2006) Dosimetric pre-treatment verification of IMRT using an EPID; clinical experience. Radiother Oncol 81:168-175 DOI 10.1016/j.radonc.2006.09.008

Address of the corresponding author:

Sonja Lahrmann
German Cancer Research Center (DKFZ)
Im Neuenheimer Feld 280
69120 Heidelberg
Germany
s.lahrmann@dkfz.de

Feasibility of Polycrystalline Alanine-in-Glass Tubes as Gamma-Ray Dosimeters

Anan M. Al-Karmi[1] and M.A. Morsy[2]

[1] Physics Department, King Fahd University of Petroleum & Minerals, Dhahran 31261, Saudi Arabia
[2] Chemistry Department, King Fahd University of Petroleum & Minerals, Dhahran 31261, Saudi Arabia

Abstract— **This study examines the feasibility of utilizing pure polycrystalline alanine-in-glass tubes as commercial dosimeters. The design of the dosimeters avoids preparation complications such as mortaring, sieving, and/or binder addition. It also reduces several fabrication techniques of alanine dosimeters and hence it allows other laboratories to conduct similar electron paramagnetic resonance (EPR) measurements. The dosimeters were irradiated with gamma rays ranging from 0 to 20 Gy. The dosimeters were found to be more sensitive to low radiation doses than other types of alanine-with-binder dosimeters. They exhibited a linear response in the dose range from 0.1 to 20 Gy. These positive properties favor the pure polycrystalline alanine-in-glass tube as a radiation dosimeter for low gamma irradiation doses.**

Keywords— **EPR, dosimetry, gamma, irradiation, dose.**

I. Introduction

Alanine/EPR dosimetry is based on electron paramagnetic resonance spectroscopy of free radicals induced by ionizing radiation in the amino acid alanine [1]. It is a reliable technique for dose measurements in industrial as well as medical irradiation processes [2] [3].

Gel, film, and pellet are three familiar forms of alanine dosimeters, commercially available for the measurements of radiation doses. Alanine dosimeters are prepared by compressing, casting, or extruding a mixture of alanine and binder. Examples of such binders are paraffin, polyethylene, and polystyrene. However, the binding material may introduce a background signal due to radiation and/or thermal aging [4]. This expected background signal will definitely influence the EPR measurements of the irradiated alanine at different dose ranges. As an alternative, the use of pure alanine without a binder may be more reliable dosimetric material. However, only a limited number of prior studies have reported its usage in clinical dosimetry [5] [6].

In this study, we propose the use of pure polycrystalline alanine-in-glass tubes as commercial dosimeters. This simple design of the dosimeter overcomes the discrepancies in the alanine-EPR reproducibility reported by many research groups [2] [7] and it permits other laboratories to conduct similar EPR measurements.

II. Materials and Methods

A. Preparation of alanine dosimeters

The alanine-in-glass dosimeter is composed of a Pyrex glass tube (length: 40 mm; inner diameter: 3 mm; wall thickness: 0.5 mm) filled with 110 mg of high purity (>99%) polycrystalline L-α-alanine powder. Alanine is used as received from the manufacturer (Fluka AG, Switzerland). Cotton is used to keep the alanine in place inside the unsealed tube. The height of the alanine column in the tube covers the whole active region of the microwave cavity in the EPR spectrometer. To mimic commercially available alanine dosimeters, cylindrical pellets are prepared in accordance with the American Society for Testing and Material (ISO/ASTM 51607:2004). A homogenous mixture of 85% (w/w) alanine and 15% (w/w) paraffin as a binder material is pressed with a manual presser at room temperature to form cylindrical pellets having 3 mm diameter and 7 mm height.

B. Irradiation of dosimeters

All the alanine dosimeters are irradiated in air at room temperature to different doses from 0 to 20 Gy by using a 130 Ci ^{137}Cs gamma irradiation device (Shepherd, model 78-10). The dose rate of the source is 0.215 Gy/h as measured by ionization chambers calibrated by the National Institute of Standards and Technology, USA.

C. EPR measurements

To eliminate any possible contribution of the irradiated Pyrex glass to the EPR signal, the irradiated alanine is transferred to EPR quartz tubes (Model Q707, Wilmad LabGlass, Buena, NJ) having the same dimensions as the Pyrex tubes. The EPR spectra of irradiated alanine are recorded at room temperature by using an X-band EPR spectrometer (Model JES-RE1X, JEOL, Japan) equipped with a standard cylindrical microwave resonator cavity operating in a TE_{011} mode with a 100 kHz field modulation frequency. The EPR acquisition parameters that obtain the highest signal-to-noise ratio are as follows: 10 mW microwave power, 1.25 mT modulation amplitude, 366 mT center field, 20 mT

O. Dössel and W.C. Schlegel (Eds.): WC 2009, IFMBE Proceedings 25/III, pp. 234–236, 2009.
www.springerlink.com

sweep width, 100 ms time constant, and 4096 point resolution. The spectra are collected and analyzed by using EW-Win EPR software (Scientific Software Services, Northville, MI). The dose response of an irradiated alanine dosimeter is assessed by using the maximum peak-to-peak amplitude of the first-derivative EPR spectrum. An external standard reference (Mn^{2+}/MgO) is used to correct for sensitivity variations in the spectrometer response. To average out possible anisotropy of alanine dosimeters, the mean value of five repeated EPR measurements, obtained by taking out and randomly repositioning the dosimeter in the cavity, is taken for each dosimeter.

III. Results and Discussion

The pure polycrystalline alanine-in-glass dosimeter was evaluated against the alanine pellet dosimeter, which is commonly used in industrial and medical applications. Figure 1 shows the EPR spectra of the polycrystalline alanine-in-glass dosimeter and the pellet dosimeter irradiated to the same dose.

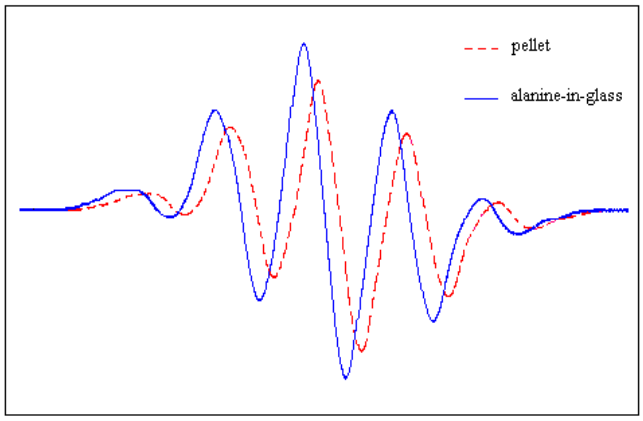

Fig. 1 EPR spectra of the pure polycrystalline alanine-in-glass dosimeter and the pellet dosimeter irradiated to 20 Gy. (Spectra were shifted intentionally for better presentation)

It is clearly seen that the alanine-in-glass dosimeter produces an EPR signal intensity that is about 5% higher than that of the pellet. Moreover, it is found that pellets are insensitive to radiation doses less than 2 Gy, due to the low signal-to-noise ratio. On the other hand, the alanine-in-glass dosimeter certainly improves the detection of radiation-induced signals down to 0.1 Gy. It is therefore concluded that the polycrystalline alanine-in-glass dosimeter is the best choice to obtain the most sensitive EPR response.

To determine the lower limit of detection (LLD) for the alanine-in-glass dosimeter, the EPR signal intensity of the central line of each irradiated alanine dosimeter is plotted as a function of the absorbed dose. The dose response of the alanine-in-glass dosimeter demonstrates excellent linearity ($R^2 = 0.999$) for doses ranging from 0.1 to 20 Gy with some deviation from the origin. This deviation may be attributed to a background signal from the quartz tube as well as the unirradiated alanine. By subtracting this zero-dose EPR signal, a "corrected" dose response curve is obtained with a linear fit of $Y = 0.1752X + 0.0164$, where Y is the EPR signal intensity and X is the absorbed dose as shown in Figure 2.

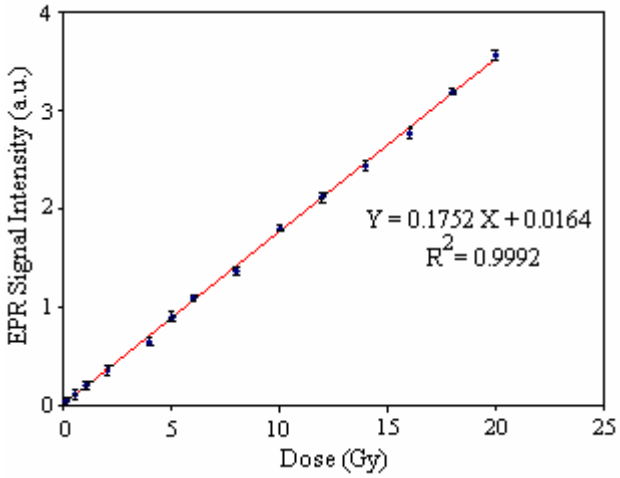

Fig. 2 Dose response curve for alanine dosimeters irradiated by gamma rays to doses in the range 0.1–20 Gy after subtracting the zero-dose EPR signal.

Following the procedure reported by Bartolotta et al. [8], the LLD for this EPR/alanine-in-glass system is estimated to be 0.3 Gy, which reflects its sensitivity as a radiation dosimeter. Therefore, there seems to be a large uncertainty in the measurement of the minimum dose (0.1 Gy) detected in this study due to the significant effect of the background signal. This uncertainty at low doses is attributed to the combined effect of a low signal with instrument noise, variation in background signal (zero dose), and signal anisotropy [7]. In previous studies, a low-dose detection limit near 0.6 Gy was obtained [9].

IV. Conclusions

A radiation dosimeter is developed for EPR dosimetry technique by using pure polycrystalline alanine in glass tubes. This dosimeter production scheme avoids any contribution to the EPR signal from a binding material. Gamma-ray irradiation produces a sharp EPR signal at

doses as low as 0.1 Gy. The dosimeter exhibits a linear dose response in the dose range from 0.1 Gy to 20 Gy. This dosimeter is found to be more sensitive to low radiation doses than dosimeters of alanine with binders. These favorable properties provide the potential of using polycrystalline alanine-in-glass as a commercial dosimeter for EPR dosimetry at low gamma irradiation doses.

Acknowledgement

The authors would like to acknowledge the support provided for this work by King Fahd University of Petroleum and Minerals, Dhahran, Saudi Arabia, through Fast Track project number FT-2004/18.

References

1. Regulla D F, Deffner U (1982) Dosimetry by ESP spectroscopy of alanine. Int J Appl Radiat Isot 33:1101–1114
2. Desrosiers M F, Schauer D A (2001) Electron paramagnetic resonance (EPR) biodosimetry. Nucl Instrum Methods B 184:219–228
3. Schauer D A, Iwasaki A, Romanyukha A A et al. (2007) Electron paramagnetic resonance (EPR) in medical dosimetry. Radiat Meas 41:S117–S123
4. Hayes R B, Haskell E H, Wieser A et al. (2000) Assessment of an alanine EPR dosimetry technique with enhanced precision and accuracy. Nucl Instrum Methods Phys Res A 440:453–461
5. Ciesielski B, Schultka K, Kobierska A et al. (2003) In vivo alanine/EPR dosimetry in daily clinical practice: a feasibility study. Int J Radiat Oncol Biol Phys 56:899–905
6. Schultka K, Ciesielski B, Serkies K et al. (2006) EPR/alanine dosimetry in LDR brachytherapy: a feasibility study. Radiat Prot Dosim 120:171–175
7. Nagy V, Sholom S V, Chumak V V et al. (2002) Uncertainties in alanine dosimetry in the therapeutic dose range. Appl Radiat Isot 56:917–929
8. Bartolotta A, Fattibene P, Onori S et al. (1993) Sources of uncertainty in therapy level alanine dosimetry. Appl Radiat Isot 44:13–17
9. Sharpe P H G, Rajendran K, Sephton J P (1996) Progress towards an alanine/ESR therapy level reference dosimetry service at NPL. Appl Radiat Isot 47:1171–1175

Address of the corresponding author:

Author: Anan M. Al-Karmi
Institute: King Fahd University of Petroleum & Minerals
Street: P O Box 1776
City: Dhahran 31261
Country: Saudi Arabia
Email: alkarmi@kfupm.edu.sa

The Risk for Secondary Cancers in Patients Treated for Prostate Carcinoma – An Analysis with the Competition Dose Response Model

A. Daşu[1], I. Toma-Daşu[2], L. Franzén[1], A. Widmark[1], and P. Nilsson[1,3]

[1] Department of Radiation Sciences, Umeå University, Umeå, Sweden
[2] Department of Medical Radiation Physics, Stockholm University and Karolinska Institutet, Stockholm, Sweden
[3] Department of Radiation Physics, Lund University Hospital, Lund, Sweden

Abstract— **The risk for radiation-induced cancers has become increasingly important as patient survival following radiotherapy has increased due to the advent of new methods for early detection and advanced treatment. Attempts have been made to quantify the risk of cancer that may be associated with various treatment approaches, but the accuracy of predictions is rather low due to the influence of many confounding factors. It is the aim of this paper to investigate the impact of dose heterogeneity and inter-patient anatomical heterogeneity that may be encountered in a population of patients undergoing radiotherapy and are thought to influence risk predictions. Dose volume histograms from patients treated with radiation for the carcinoma of the prostate have been used to calculate the risk for secondary malignancies using a competition dose-response model previously developed. Biologically-relevant parameters derived from clinical and experimental data have been used for the model. The results suggested that dose heterogeneity plays an important role in predicting the risk for secondary cancer and that it should be taken into account through the use of dose volume histograms. Consequently, dose-response relationships derived for uniform relationships should be used with care to predict the risk for secondary malignancies in heterogeneously irradiated tissues. Inter-patient differences could lead to considerable uncertainties in the shape of the relationship between predicted risk and average tissue dose, as seen in epidemiological studies. They also lead to rather weak correlations between the risk for secondary malignancies and target volumes. The results stress the importance of taking into account the details of the clinical delivery of dose in radiotherapy for treatment plan evaluation or for retrospective analyses of the induction of secondary cancers. Nevertheless, the levels of risks are generally low and they could be regarded as the price of success for the advances in the radiotherapy of the prostate.**

Keywords— **radiation induced cancers, risk estimations, radiation treatment, prostate cancer, heterogeneity**

I. Introduction

Radiation-induced cancers have become increasingly important since advances in detection and radiotherapy techniques have led to a significant increase of the patient survival. This issue is especially important for survivors of childhood cancers, but also for adult patients with good prognosis such as patients with prostate carcinomas. Consequently, a number of studies have been initiated in order to investigate the risk for radiation-induced secondary malignancies. Epidemiological studies concerned with the magnitude of this effect have shown that this risk is small, but significant [1,2]. It has therefore been proposed to estimate the risk for radiation-induced cancers and use it as an additional criterion for the evaluation of treatment plans or techniques [3-5]. Thus, experimental measurements and theoretical models have been used in order to investigate the modification of the risk with the irradiation technique used for treatment [4,6,7]. The accuracy of predictions is however rather low due to the influence of several confounding factors. It is the aim of this study to investigate the impact of some of them, namely the dose heterogeneity and inter-patient anatomical heterogeneity, that could be encountered in a population of patients.

II. Materials and Methods

A. Theoretical model

The model used for calculation has originally been proposed by Daşu et al. [5] and is based on the competition between induction of mutations and cell survival that has been postulated many years ago [8]. The model calculates the weighted average of the effects from partial irradiations described by dose volume histograms (equation 1).

$$Risk = \frac{\sum_i v_i \cdot \left(\alpha_1 D_i + \frac{\beta_1 D_i^2}{n} \right) \cdot \exp\left[-\left(\alpha_2 D_i + \frac{\beta_2 D_i^2}{n} \right) \right]}{\sum_i v_i} \quad (1)$$

where v_i is the volume of tissue receiving dose D_i given in n individual fractions, α_1 and β_1 are parameters that describe the induction of carcinogenic mutations in the irradiated cells and α_2 and β_2 are parameters describing the survival of cells in the irradiated tissues.

For uniform irradiations, the competition model predicts that the dose-response curve has a bell shape. Thus, at low doses the induction of mutations outweighs the cell kill and

O. Dössel and W.C. Schlegel (Eds.): WC 2009, IFMBE Proceedings 25/III, pp. 237–240, 2009.
www.springerlink.com

therefore the risk increases with increasing dose. However, at larger doses the model predicts that cell kill will prevail and therefore there will be fewer mutated cells that survive the irradiation which will translate into a decrease of the risk for increasing radiation doses. A similar behavior has indeed been observed in clinical studies of patients treated with radiotherapy that showed a significant number of secondary malignancies around the target volume, in tissues that have received radiation does less than about 6 Gy [9].

The risk coefficients α_1 were derived from ICRP Publication 60 [10]. Cell survival parameters were obtained from analyses of clinical and experimental data [5]. Thus, it was assumed that α/β is 7.5 Gy for the bladder and 5.4 Gy for rectum, while α_2 =0.25 Gy^{-1}. This latter value corresponds to a maximum effectiveness for cancer induction around 4 Gy [11] that is in agreement with the observations of Dörr and Herrmann [9] regarding the maximum effectiveness for cancer induction in clinically irradiated tissues.

B. Patient data

Treatment plans from 51 patients receiving radiotherapy for prostate carcinoma were included into the study. The patients followed the usual procedure for treatment. Conformal radiotherapy (CRT) plans were devised for the patients based on pre-treatment CT-images where target volumes and organs at risks were delineated according to the treatment protocol. Risk values were calculated only for the bladder and for the rectum as these organs close to the target were identified as the most significant contributors to the increased risk in the irradiated population [1].

III. RESULTS

Figure 1 shows the influence of dose heterogeneity on the predicted risk for secondary malignancies. Thus, the lines in the figure panels show the expected risk for uniform irradiations, while the points represent the predicted risk for individual patients calculated with equation 1. It can be seen that the individual risk levels follow the general shape predicted by the competition risk model. Indeed, for doses above the interval of maximum effectiveness, the risk decreases as the probability of the mutated cells to survive the treatment also decreases. However, there is a significant difference between the predictions of the model for uniform irradiations and the patient data with heterogeneous irradiations. Thus, it can be seen that the non-uniform irradiation of the organs leads to considerably shallower dependences between the predicted risk and the average organ dose. The explanation resides in the details of the risk model in relation to the distribution of partial doses given by the dose volume histograms (DVH) of the individual patients. Thus, according to the competition risk model the most effective in inducing cancers are the doses in a rather limited interval. This means that the risk in individual patients would be mainly given by the corresponding interval of the dose volume histograms, while in contrast the average dose for the organ would be heavily weighted by the large-dose component of the DVH. This might also explain the spread of the individual values since quite different DVH could lead to the same average dose.

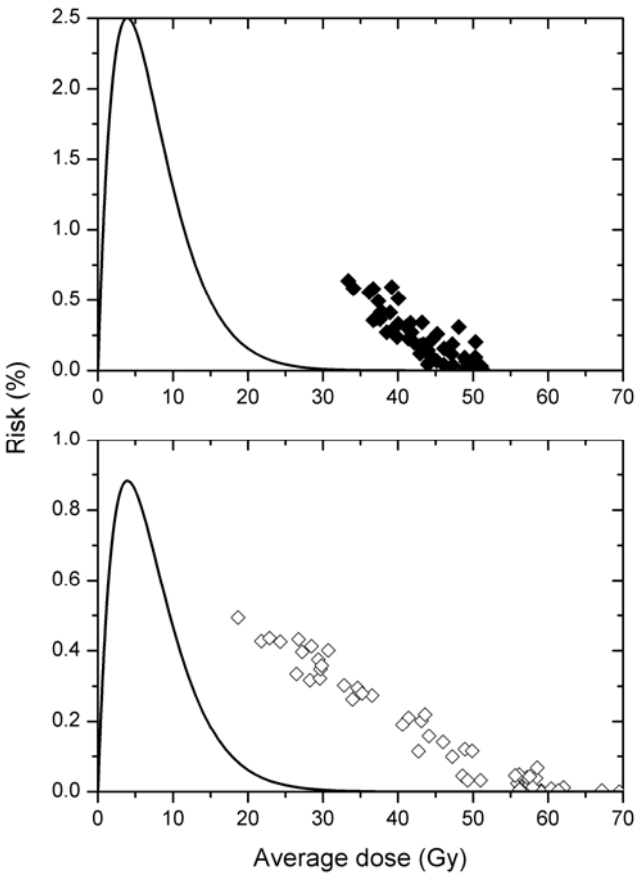

Fig. 1 Predicted risk levels in individual patients (points) compared to expectations from uniform irradiations (curves). Panel a – risks in the rectum. Panel b – risks in the bladder.

These results also indicate that for therapeutic irradiations the dose interval of maximum effectiveness for cancer induction may appear to extend to considerably higher values than predicted for uniform irradiations, if the average dose is taken as the reference. Nevertheless, dose-response relationships derived for uniform relationships should be used with care to predict the risk for secondary malignancies in heterogeneously irradiated tissues.

Figure 2 shows the correlation between individual risk levels and the size of clinical target volume (CTV). Such a correlation is sought on the grounds that the pattern of irradiation of the healthy organs nearby might be different for a larger target in comparison to a smaller one. However, the data in figure 2 appears to indicate that although a negative correlation cannot be excluded, the anatomical heterogeneity of the patients leads to a considerable spread of the risk values which in turn weakens the correlation, as it can be seen from the R^2 values.

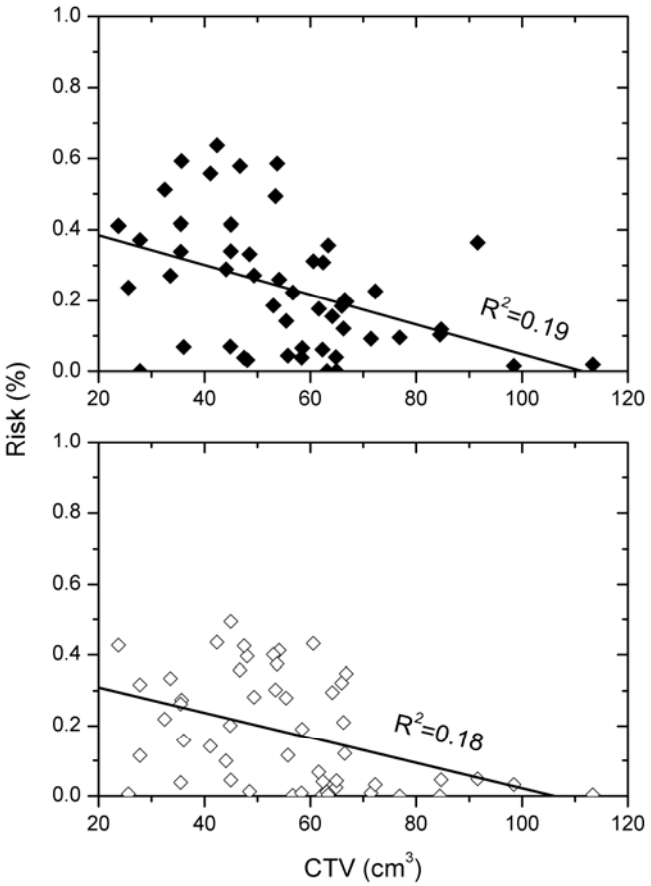

Fig. 2 Correlations between the predicted risk levels and the clinical target volume (CTV). Panel a – risks in the rectum. Panel b – risks in the bladder.

Similar correlations were also found when the planning target volume (PTV) was used instead of the CTV, but this was expected since the two target volumes are correlated.

It has to be mentioned that the risk values predicted by the competition model used in the present study are in agreement with risk levels that have been observed in clinical studies of patients receiving irradiation for pelvic tumors. Thus, a study of the long term survivors of pelvic irradiation [12] suggests that the risk for secondary cancers in the bladder is about 0.15-0.32% and 0.05-0.20% for the rectum. These values are comparable with the average values found in the present study, 0.18% for the bladder and 0.23% for the rectum.

IV. Discussion

The improvement of the cure rates for many tumors has brought again into the discussion the link between ionizing radiation and carcinogenesis. Indeed, it appears that radiation-induced cancers may be counted nowadays among the late complications of radiotherapy. Even though the risk levels that have been derived either from clinical studies or from theoretical simulations are rather small [13], radiation-induced carcinogenesis in long term survivors of radiotherapy should be taken into consideration for the choice of the treatment. The issue is not about radiotherapy versus other forms of therapy, because in many cases high cure rates cannot be achieved without treatment with ionizing radiation. The proposal however concerns the risks that may be associated with the irradiation techniques available or the treatment plans that could be generated.

In this respect there have been several studies which investigated the modification of the risk for secondary malignancies in patients undergoing conformal radiotherapy (CRT) versus intensity-modulated radiation therapy (IMRT) [4,6] or external beam radiotherapy versus brachytherapy [7]. The focus in these studies has been on the average risk levels that may be determined for the treatment technique considered and less on other factors that may influence them and could therefore be involved indirectly in the comparison. To our knowledge, the present study has been the first to address some of these issues, namely the patient heterogeneities that could lead to different patterns of irradiation in patients undergoing treatment with the same technique.

The simulations performed in the present study have shown that heterogeneities have to be carefully taken into consideration for the risk estimations. Indeed, linear transformations of the dose volume histograms like the average tissue dose may not be directly related to the risk for radiation-induced cancers since the relationship between dose and effect is non-linear. This is a very important aspect since full dose distributions are not available in many retrospective studies and correlations are attempted with average organ doses or similar simplifications. As the results in this study have shown, the shape of the dose-effect relationship in these conditions may be significantly different from that predicted from uniform irradiation. Furthermore, inter-patient heterogeneity leads to considerable scatter of the

individual risk predictions which in turn translate into large confidence intervals for the average risks that may characterise populations of patients, as seen in epidemiological studies.

V. Conclusions

The results presented in this paper suggested that dose-response relationships derived for uniform relationships should be used with care to predict the risk for secondary malignancies in heterogeneously irradiated tissues. The results also stress the importance of taking into account the details of the clinical delivery of dose in radiotherapy for treatment plan evaluation or for retrospective analyses of the induction of secondary cancers. Nevertheless, the predicted levels of risks are generally low and they could be regarded as the price of success for the advances in radiation therapy of the prostate.

Acknowledgments

The authors would like to acknowledge support from the Nordic Cancer Union, the Swedish Cancer Society (070604) and the Cancer Research Foundation in Northern Sweden.

References

1. Brenner DJ, Curtis RE, Hall EJ et al. (2000) Second malignancies in prostate carcinoma patients after radiotherapy compared with surgery. Cancer 88:398-406
2. Moon K, Stukenborg GJ, Keim J et al. (2006) Cancer incidence after localized therapy for prostate cancer. Cancer 107:991-998
3. Verellen D, Vanhavere F (1999) Risk assessment of radiation-induced malignancies based on whole-body equivalent dose estimates for IMRT treatment in the head and neck region. Radiother Oncol 53:199-203
4. Kry SF, Salehpour M, Followill DS et al. (2005) The calculated risk of fatal secondary malignancies from intensity-modulated radiation therapy. Int J Radiat Oncol Biol Phys 62:1195-1203
5. Daşu A, Toma-Daşu I, Olofsson J et al. (2005) The use of risk estimation models for the induction of secondary cancers following radiotherapy. Acta Oncol 44:339-347
6. Hall EJ, Wuu CS (2003) Radiation-induced second cancers: the impact of 3D-CRT and IMRT. Int J Radiat Oncol Biol Phys 56:83-88
7. Takam R, Bezak E, Yeoh EE (2009) Risk of second primary cancer following prostate cancer radiotherapy: DVH analysis using the competitive risk model. Phys Med Biol 54:611-625
8. Gray LH (1965) Radiation biology and cancer. in: Cellular Radiation Biology: A Symposium Considering Radiation Effects in the Cell and Possible Implications for Cancer Therapy. The Williams and Wilkins Company, Baltimore, pp. 7-25
9. Dörr W, Herrmann T (2002) Second primary tumors after radiotherapy for malignancies. Treatment-related parameters. Strahlenther Onkol 178:357-362
10. ICRP (1991) ICRP Publication 60: 1990 Recommendations of the International Commission on Radiological Protection. Annals of the ICRP 21:1-202
11. Daşu A, Toma-Daşu I (2005) Dose-effect models for risk-relationship to cell survival parameters. Acta Oncol 44:829-835
12. Boice Jr. JD, Day NE, Andersen A et al. (1985) Second cancers following radiation treatment for cervical cancer. An international collaboration among cancer registries. J Natl Cancer Inst 74:955-975
13. Dörr W, Herrmann T (2008) Second tumors after oncologic treatment. Strahlenther Onkol 184:67-72

Address of the corresponding author:

Author: Alexandru Daşu
Institute: Department of Radiation Sciences
Umeå University
City: 901 87 Umeå
Country: Sweden
Email: alexandru.dasu@radfys.umu.se

Evaluating the dosimetric effect of lack of side-scatter volume for measurements of large fields with an integration diode array

P. Ma[1], W.J. Cui[1] and J.R. Dai[1]

[1] Department of Radiation Oncology, Cancer Institute (Hospital),
Chinese Academy of Medical Sciences, Beijing, People's Republic of China

Abstract—**One method to verify IMRT fields larger than the maximum area that detector arrays can measure is by merging the different parts of the fields in multiple exposures. In this case, the measured dose is less than expected performance because of the lack of side-scatter volume. The purpose of this study is to quantitatively evaluate this dosimetric effect.**

Keywords—**Large field, lack of side-scatter volume, diode array.**

I. Introduction

Dosimetric verification of patient plans is a quality assurance procedure for intensity modulated radiation therapy [1-8]. One common method to perform this procedure is to measure dose maps for all treatment fields with a detector array that includes diode arrays, ionization chamber arrays and electronic portal imaging devices [9-12]. However, current designs of detector arrays have a measuring area smaller than the maximum field size encountered in radiation therapy applications. One solution to such scenarios is to move the detector array to measure different parts of the large field in multiple exposures, and then merge them into the single large field. This solution increases the maximum measuring area for detector arrays, but may cause lower dose reading due to lack of side scatter. According to dosimtric protocols such as IAEA Codes of Practice TRS-277[13], to assure enough scatter volume, the phantom should extend to at least 5 cm beyond all four sides of the largest field size at the measurement depth. There should also be a margin of at least 5 cm beyond the maximum measurement depth. The purpose of this study is to quantitatively evaluate the dosimetric effect of lack of side-scatter volume (LSSV effect) through comparing large fields' dose maps measured under the condition of full scatter volume and that of lack of side-scatter volume.

II. Materials and methods

A. Brief description of MapCheck merging function

We used a diode array, MapCheck, to measure dose maps for large fields. MapCheck has been demonstrated to be an accurate and reliable tool for the IMRT treatment verification[11-12]. It has 445 diodes distributed in an area of 22×22 cm^2. Because there are only a few diodes outside of the central 20×20 cm^2 area, we may assume the maximum measurable field size to be 20×20 cm^2. For fields larger than 20×20 cm^2, it provides a software function of merging to get a full dose map from multiple partial exposures. MapCheck can obtain the full dose map through merging dose maps of all exposures with the information of the orientation and offset. The dose at any diode location is equal to the average of all measured doses at the location. Fig.1 illustrates the setup of 4 exposures. The square formed by the dotted lines is the 40×40 cm^2 field. The intersection of the crosshairs is the center of the field. When the four exposures are taken, MapCheck is sequentially placed in the four quadrants.

B. Determination of field center in MapCheck coordinate system

MapCheck has a Cartesian coordinate system. The centre detector with coordinates (0, 0) is numbered (23, 23)[14]. If a detector's coordinates are (x, y), its numbering (D_x, D_y) can be calculated with equations 1 where the number "0.5" in the two equations is the minimum distance in unit of cm between any two detectors along X or Y direction.

$$\begin{cases} D_x = 23 + x/0.5 \\ D_y = 23 + y/0.5 \end{cases} \quad (1)$$

When doing measurements with merging function, we need to determine the position of field center in MapCheck coordinate system. In order to have scatter volume as much as possible, we should set the field center to be close to the center of MapCheck as much as possible.

O. Dössel and W.C. Schlegel (Eds.): WC 2009, IFMBE Proceedings 25/III, pp. 241–244, 2009.
www.springerlink.com

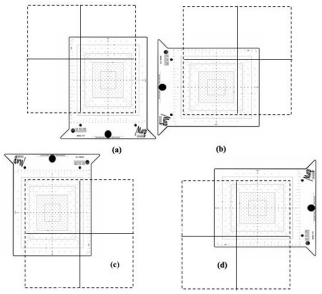

Fig. 1 Schematic drawing of MapCheck merging function.

When the field size is more than 20 cm only along one direction (X or Y direction), two-exposure merging is needed. For two-exposure merging, the field center would be on detector (D_x, D_y). D_x and D_y are calculated with the following equation:

$$\begin{cases} D_x = 23 \\ D_y = 23 + (\mathrm{Max}(y_1, y_2) - 10)/0.5 \end{cases}$$

or

$$\begin{cases} D_x = 23 + (\mathrm{Max}(x_1, x_2) - 10)/0.5 \\ D_y = 23 \end{cases} \quad (2)$$

Where, symbols x_1, x_2, y_1 and y_2 are collimator jaw positions defining the field.

When the field size is more than 20 cm along both directions, four-exposure merging is needed. For four-exposure merging, the field center would be on detector (D, D) to maintain rotational symmetry, where D is determined as follows:

$$D = \mathrm{Max}\left(D_x, D_y\right) \quad (3)$$

Where,

$$\begin{cases} D_x = 23 \pm (\mathrm{Max}(x_1, x_2) - 10)/0.5 \\ D_y = 23 + (\mathrm{Max}(y_1, y_2) - 10)/0.5 \end{cases} \quad (4)$$

The equation 4 shows that the field center can be in the 1st and 2nd quadrants rather than the 3rd and 4th ones of MapCheck coordinate system. This preference is for protecting the electronic section.

C. Test fields

Test fields included three regular fields (30×30 cm^2 and 40×40 cm^2 open fields, and 30×30 cm^2 wedge field with wedge angle of 60^0), and 19 IMRT fields. In terms of intensity-modulation, they changed from no modulation, to one dimensional modulation, and then to two dimensional modulation. According to Section II*B*, these regular fields needed four-exposure merging. 9 of 19 IMRT fields came from a lymphoma case, of which the width ranged from 12.1 cm to 25.3 cm, and length from 20 cm to 37 cm. Similarly to regular fields, they needed four-exposure merging. The other 10 IMRT fields came from two esophagus cancer cases, of which the width ranged from 9.5 cm to 11.7 cm, and the length ranged from 27 cm to 32 cm. According to II*B*, they only needed two-exposure merging.

For all test fields, measurement setup was the same as that for dosimetric verification of patient IMRT plans in our clinic. The setup was as follows: the detector array was located in the isocenter plane; beam irradiated downwards from a gantry angle of 0^0; the measurement depth was set to 5.33 cm equivalent water through adding 3 cm PMMA on the top of MapCheck. For the regular field, measurements were performed for both 6 MV and 18 MV X ray whereas for the IMRT field, measurements were performed only for 6MV X ray. The reason for this energy arrangement was that LSSV effect was found to be less severe for high beam energy when we did the measurements for regular fields.

D. Measurement procedure

For each field, measurement was performed twice, one under the condition of full scatter volume, and the other under the condition of lack of side-scatter volume. The former condition was satisfied through adding PMMA slabs by MapCheck while the latter condition was satisfied without adding PMMA slabs. For four-exposure merging, the full measurement procedure is demonstrated in Fig. 1 and described here:

1. Place MapCheck with the intersection of crosshairs on detector (D_x, D_y) and the front of the device pointing towards the gantry, and this is position A.
2. Expose the field.
3. Put PMMA slabs by MapCheck to form the full scatter volume.
4. Expose the field.
5. Remove PMMA slabs, and rotate MapCheck clockwise 90^0 around detector (*Dx*, *Dy*).
6. Expose the field.
7. Repeat Steps 3, 4 and 5, now the MapCheck should be rotated 180^0 from position A.
8. Repeat Steps 2, 3, 4 and 5, now the MapCheck should be rotated 270^0 from position A.
9. Repeat Steps 2, 3 and 4.

For two-exposure merging, the above procedure should be modified. MapCheck should be rotated clockwise 180^0 in Step 5 and just the first seven steps are needed.

E. Dose map comparison

For each field, we obtained two merged dose maps, one for full scatter volume (FSV map) and the other for lack of side-scatter volume (LSSV map). We used FSV map as reference, and compared LSSV map against it. The comparison was done with MapCheck software. For two measured dose maps, the software can calculate pass rate for a specified acceptance criterion and a threshold of relative dose difference. The location of normalization point affects pass rate, and should be selected in the high dose, low dose gradient region. Otherwise, the pass rate may not objectively reflect the dose maps' difference.

In this study, the acceptance criterion of relative dose difference was set to 0.5%, 1%, 2% and so on, and the threshold was fixed to 10%. For dosimetric verification of patient IMRT plans, the pass rate of dose points is usually required to be at least 95% when the acceptance criterion are 3% dose difference and 3 mm distance-to-agreement[15]. Considering that the LSSV effect will underestimate expected dose, and cause a systematic error in measurement results, we assumed in this study that this effect is clinically significant and can not be ignored if the pass rate is less than 95% when the acceptance criterion is 1% dose difference. We did not use distance-to-agreement, since MapCheck disables this criterion when comparing two measured dose maps.

III. Results and Discussions

A. Regular fields

Field size, beam energy, and adding wedge or not are found to be influence factors of LSSV effect. For low energy large open field, LSSV effect becomes significant. Among all the six measurement cases, the 40×40 cm^2 open field with 6MV X ray has the largest LSSV effect. In this case, PR was 92.7% for 1% acceptance criterion, and thus the LSSV effect is clinically significant and can not be ignored. For the other five cases, PR was always more than 95%, and the LSSV effect is negligible. The results of regular fields are consistent with physics principles that the bigger the field is and the lower the energy is, the more lateral scatter exists.

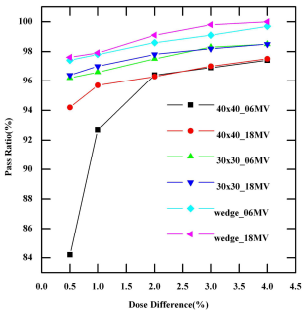

Fig. 2 Pass Rate (PR) curves for regular fields.

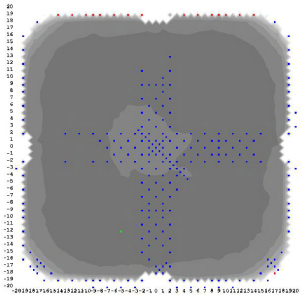

Fig. 3 Dose map comparison for the 40×40 cm^2 open field. A blue dot means the dose measured under the condition of lack of side-scatter volume is 0.5% less than that measured under the condition of full scatter volume. A red dot means the opposite.

Figure 3 displays the comparison result of LSSV map and FSV map with the 0.5% dose difference for the 40×40 cm^2 open field. A blue dot means that LSSV dose at this position is lower than FSV dose by more than 0.5% while a red dot means that LSSV dose is higher than FSV dose by more than 0.5%. We can see that blue dots form a clear cross shape inside the field, and few red and blue dots distributed along field edges. The cross shape means that this region lacks of scatter volume the most, and just like what we expected. But we did not expect the appearance of red and blue dots along field edges. We analyzed this phenomenon, and found two possible causes. One cause was that MapCheck might shift invisibly when we removed PMMA slabs in Step 5 of measurement procedure (see section II*C*). Another cause was that jaw positions might have changed by sub-millimeter during two measurements.

B. IMRT fields

All 19 IMRT fields, no matter whether they were

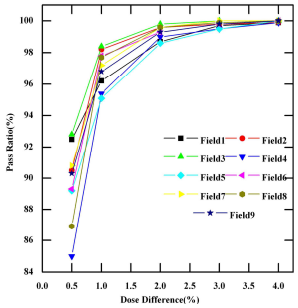

Fig. 4 Pass Rate (PR) curves for the IMRT fields needing four-exposure merging.

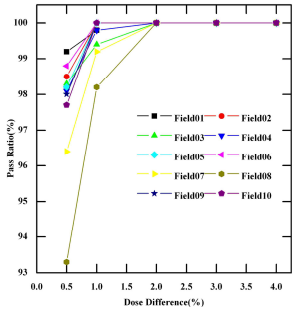

Fig. 5 Pass Rate (PR) curves for the IMRT fields needing two–exposure merging.

measured through four-exposure merging or two-exposure merging, their PRs were always more than 95% when the acceptance criterion was 1% or higher (Figs.4 and 5). Therefore, the LSSV effect can be concluded as clinically insignificant.

For the nine IMRT fields using four-exposure merging, PR ranged from 95.1% to 98.4% with an average of 97.0% when the acceptance criterion was 1%. Compared to the regular fields that also used four-exposure merging, IMRT fields had higher PRs. That means intensity modulation reduces LSSV effect.

Compared with the nine fields using four-exposure merging, the 10 fields using two-exposure merging had even higher PRs. Their average PR was 99.6% when the acceptance criterion was 1% (Fig.5). That means two-exposure merging has less LSSV effect than four-exposure merging.

IV. Conclusions

The LSSV effect happens when a large field is measured with a detector array of limited measuring area through merging multiple exposures. Field size, beam energy, intensity-modulation are influence factors of LSSV effect. For large open fields, the effect may be significant. But, for large wedge fields and IMRT fields, the effect is negligible.

References

1. Luo W, Li J S, Robert A. Price et al.(2006) Monte Carlo based IMRT dose verification using MLC log files and R/V outputs. Med Phys. 33:2557-2564.
2. Yan Y L, Papanikolaou N, Weng X J et al.(2005) Fast radiographic film calibration procedure for helical tomotherapy intensity modulated radiation therapy dose verification. Med Phys. 32:1566-1570.
3. Chen X, Yue N J, Chen W et al. (2005) A dose verification method using a monitor unit matrix for dynamic IMRT on Varian linear accelerators. Phys Med Biol. 50:2641-2645.
4. Winkler P, Zurl B, Guss H et al.(2005) Performance analysis of a film dosimetric quality assurance procedure for IMRT with regard to the employment of quantitative evaluation methods. Phys Med Biol. 50:643-654.
5. Lei X and Jonathan G. Li. (2000) Computer verification of fluence map for intensity modulated radiation therapy. Med Phys. 27:1566-1570.
6. Higgins P D , Alaei P , Gerbi B J et al.(2003) In vivo diode dosimetry for routine quality assurance in IMRT. Med Phys. 30:3118-3123.
7. Charland M P, Chetty I J, Yokoyama S et al. (2003) Dosimetric comparison of extended dose range film with ionization measurements in water and lung equivalent heterogeneous media exposed to megavoltage photons. J Appl Clin Med Phys. 4:25-39.
8. Arthur J. Olch. (2002) Dosimetric performance of an enhanced dose range radiographic film for intensity-modulated radiation therapy quality assurance. Med Phys. 29:2159-2168.
9. Yang Y, Xing L.(2004) Quantitative measurement of MLC leaf displacements using an electronic portal image device. Phys Med Biol. 49:1521-1533.
10. F. Banci Buonamici, A. Compagnucci, L. Marrazzo et al.(2007) An intercomparison between film dosimetry and diode matrix for IMRT quality assurance. Med Phys. 34:1372-1379.
11. Letourneau D, Gulam M, Yan D et al.(2004) Evaluation of a 2D diode array for IMRT quality assurance. Radiother Oncol. 70: 199-206.
12. Jursinic PA, Nelms BE. (2003) A 2-D diode array and analysis software for verification of intensity modulated radiation therapy delivery. Med Phys. 30:870-879.
13. IAEA.(1987) A Code of Practice for Absorbed Dose Determination in Photon and Electron Beams (TRS-277).
14. Sun Nuclear Corporation.(2004) MapCheck Model 1175 Manual. Melbourne (FL): Sun Nuclear Corporation.
15. Benjamin E. Nelms and Jeff A. Simon.(2007) A survey on planar IMRT QA analysis. J Appl Clin Med Phys. 8:2448.

Author: J.R. Dai
Institute: Department of Radiation Oncology
Cancer Institute (Hospital)
Chinese Academy of Medical Sciences
Street: Pan Jiayuan Nanli 17
City: Beijing
Country: People's Republic of China
Email: mpsophia@163.com

Radon Measurement in Drinking Water Samples of Mashhad City in Iran

A. Binesh[1], S. Mohammadi[2], A.A. Mowlavi[3], and P. Parvaresh[2]

[1] Physics Department, Payam Nour University, Fariman, Iran
[3] Physics Department, Payam Nour University, Mashhad, Iran
[2] Physics Department, Sabzevar Tarbiat Moallem University, Sabzevar, Iran

Abstract— **In the present work, radon concentrations in drinking water samples of Mashhad city with about 4 millions population has been measurement by PRASSI system. Water samples were collected from various places and supplies of public used water in Mashhad, and then radon concentration has been measured tree times for each sample. Result shows about 75% of water samples have radon concentration gather than 10Bq/lit which advised EPA as a normal level. According the measuring data, water used by people in most of regions is not low enough and below the EPA proposed limits. Since a main section of radon come in body is due to drinking and household water, and for improvement of the social health level, we suggest using the low radon level water source, or public water supplies authority reducing the radon in the drinkable water before public using.**

Keywords— **Radon concentrations; Drinking water; PRASSI system; Mashhad city.**

I. Introduction

Radon (^{222}Rn) is a naturally occurring radioactive noble gas with a half-life of 3.82 days, which is a member of the ^{238}U decay series [1]. Radon and its short-lived decay products such as ^{218}Po, ^{214}Pb, ^{214}Bi, and ^{214}Po at indoor places are recognized as the main sources of public exposure from the natural radioactivity, contributing to nearly 50% of the global mean effective dose to the public [2, 3]. The type of soil, building materials, and water used for drinking and other household uses can make variable contributions to the indoor radon level [1]. The available data indicate that the main source of the indoor radon is the soil underlying a building [2]. However, certain building materials with high concentrations of radium and even domestic water with high concentrations of radon can make major contributions to indoor radon exposure [4-6]. The most important aspect of radon in high concentrations can be health hazard for humans, mainly a cause of lung cancer [7]. However, a very high level of radon in drinking water can also lead to a significant risk of stomach and gastrointestinal cancer. Knowledge of the levels of radon in each source including household water, particularly water from groundwater sources, is necessary to protect public from consequences of excessive exposure to radiation, mainly from the risk of lung cancer.

In Iran, the household water is supplied from various sources. Due to the dry climate condition in the most parts of the country, drilled wells have provided the main section of drinking water used by public. In a few parts with high annual rain, surface water is the main source for public usages. In a number of cities, including Mashhad, both groundwater and surface water are the sources of household water. Domestic water of Mashhad, the second big city of Iran after Tehran, which has about 4 million fixed population and more than 12 million religion tourists and business persons, is supplied from two Torogh and Kardeh dams and more than 84 deep wells drilled in and around the city. Depending on raining condition the contribution of groundwater to the supplied domestic water, particularly in summer season, may increase. Depending on geographical situation of a specified region in the city, domestic water may be supplied from groundwater, surface water or a mixture of them. In addition, there are a number of large reservoirs in various parts of Mashhad for the collection and distribution of treated surface water and groundwater in the city.

In the presents research results of radon measurement in 50 water samples, sources and tap water actually used for drinking and other household uses in Mashhad. Radon of water samples that have been measured using PRASSI system include a ZnS(Ag) scintillation detector. This paper is organized as follows. In the next section, we describe the method which is used for radon measurements; in section 3 the results of radon concentration in various samples have been presented.

II. Materials and Methods

A. Water Sampling

The water samples were collected in various points distributed in and around the city of Mashhad; Fig. 1 shows the sampling sites. Water sampling has been done from each water supply; including wells, and surface water, as well as from household water. The samples were collected from the head ports of active wells selected for sampling, rivers and surface water reservoirs, as well as from domestic water

O. Dössel and W.C. Schlegel (Eds.): WC 2009, IFMBE Proceedings 25/III, pp. 245–247, 2009.
www.springerlink.com

taps of high consumption rates, using the standard procedure proposed by the USA Environmental Protection Agency, EPA [2, 8]. In this procedure a plastic funnel was connected via a short plastic hose to the water tap. After the water flowed for several minutes, the flow rate was slowed down and the water was allowed to be collected in the funnel. Then, three 150 ml water samples have been collected from each source or region. The collected samples were transferred to the laboratory of Payame Noor University for analysis.

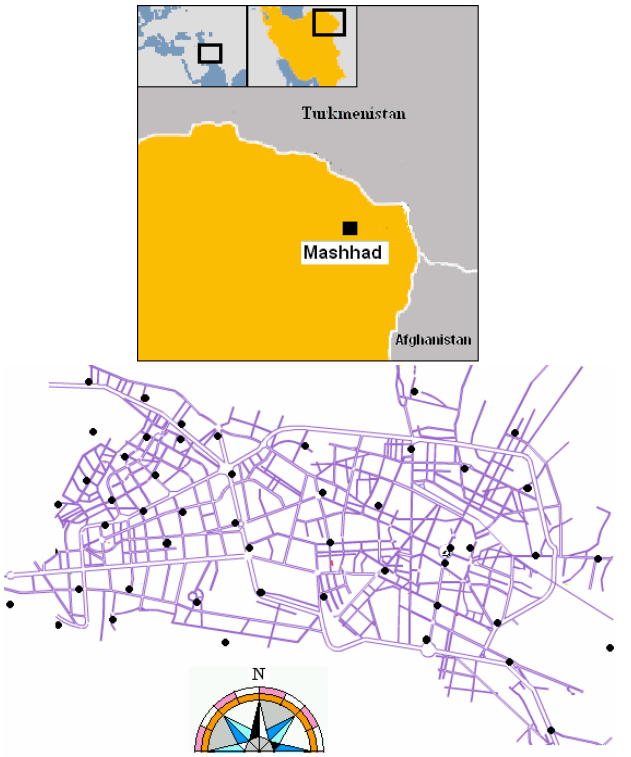

Fig. 1 Mashhad location in Iran, and he map of Mashhad city and • shows the sampling sites.

B. Radon Measurement

The PRASSI (Portable Radon Gas Surveyor SILENA) Model 5S has been used for radon concentration measurement in the water samples [9], which is particularly well suited for this type of measurement that must be performed in the closed loop circuit. Fig. 2 shows the system set up of measurement including bubbler and drier column. PRASSI pumping circuit operates with constant flow rate at 3 litters per minute in order to degassing the water sample properly. The sensitivity of this system in continuous mode is 4 Bq/m^3 during the integration time of 1 hour.

To measure the content of radon in water, we consider V_{sample}=150 ml of the water sample in bubbler and the PRASSI will read a concentration of:

$$Q_{PRASSI}[Bq/m^3] = \frac{A_{Rn}[Bq]}{V_{tot}[m^3]} \quad (1)$$

Where V_{tot} is the total volume of system equal $2.4\times10^{-3}\,m^3$ and A_{Rn} is the radon activity [9]. It follows that the concentration of radon in water is:

$$Q_{Ra}[Bq/m^3] = \frac{A_{Rn}[Bq]}{V_{sample}[m^3]} = Q_{PRASSI}\frac{V_{tot}[m^3]}{V_{sample}[m^3]} \quad (2)$$

The average value of three measurements was considered as the radon concentration in the water sample.

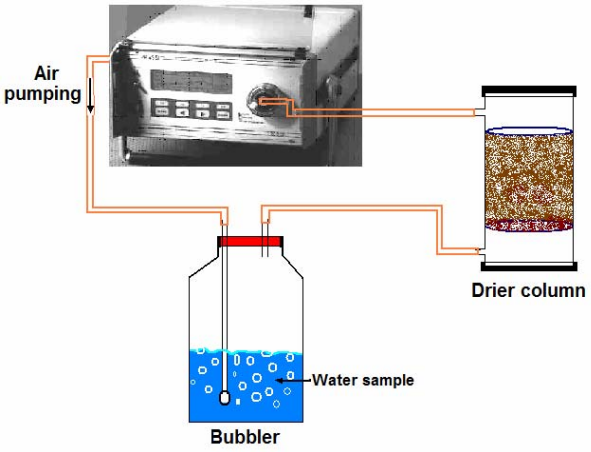

Fig. 2 The PRASSI system set up for radon measuring in the water sample.

III. Results and Discussion

In the present research, a total number of 50 water samples from groundwater of deep wells, surface water of rivers, tap water samples were collected and analyzed for radon concentrations. As the data shown in Fig. 3, the radon concentrations is about 75% for samples used by people in Mashhad which are greater than the EPA advised level, 10 Bq/L [8]. We must mention that we sorted the experimental data in ascending order. The main reasons for large differences of radon concentration in sample seems to be due to mixing of surface water with groundwater in proportions mentioned earlier, and storage of the mixed water in large reservoirs before distribution.

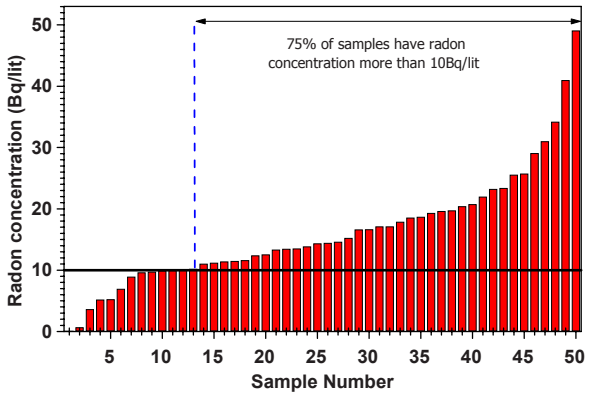

Fig. 2 Radon concentration for various samples of drinking water.

Unfortunately up to now, there is no specific national regulation for radioactivity concentrations in drinking water in Iran. Compared to maximum contaminant level of 10 Bq/L for radon in public drinking water, suggested by the EPA, the radon concentrations in most of the drinkable water samples in Mashhad, is significantly higher. In addition, the EPA requires that action be taken to reduce radon levels above an alternative maximum contaminant level of 150 Bq/L. A number of investigators have reported much higher radon concentrations in public drinking water [10-14]. Kusyk et al. has been reported the mean value of 74 Bq/L for tap water, and mean value of 207 Bq/L for wells, in southern of Poland [15].

The annual effective dose due to inhalation corresponding to the concentration of 1 Bq/L in tap water is 2.5μSv/y [7]. Therefore, waterborne radon concentration of 1 Bq/L causes total effective dose of about 2.68μSv/y for adults.

IV. Conclusions

The results of this study well indicate that the radon concentrations in public drinking water samples of Mashhad are mostly low enough and below the proposed concentration limits. Measuring radon results show about 75% of samples actually used by people in Mashhad are greater than the EPA advised level, 10 Bq/L. Although, according to the advised of WHO and the EU Council just 2 samples (No. 49 and 50) induced the total annual effective dose greater than 0.1mSv/y. Therefore, there is a radon problem for these two sources and requiring some action to reduce their radon level before public usage, such as mixing with surface water in large reservoirs or aerate water in order to allowing some radon removal from the water. It is evident that if the wells are to be the only water supply for some parts of Mashhad, the required remedial action should be taken to reduce radon concentrations consumed by people.

References

1. Sohrabi M (1990) Recent radiological studies of high background radiation areas of Ramsar. Proceeding of International Conference on High Levels of Natural Radiation (ICHLNR) Ramsar, Iran, 3-7.
2. UNSCEAR. United Nations Scientific Committee on the Effects of Atomic Radiations. The general assembly with scientific annex. United Nation, New York (2000).
3. United Nations Scientific Committee on the effect of Atomic Radiation (UNSCEAR). Sources effects and risks of ionizing radiation, United Nations, New York (1998).
4. Baykara O, Doğru M (2006) Measurements of radon and uranium concentration in water and soil samples from East Anatolian Active Fault Systems (Turkey). Radiat. Meas. 41:362–367.
5. Ghosh D, Deb A, Patra KK (2004) Measurements of alpha radioactivity in arsenic contaminated tubewell drinking water using CR-39 detector. Radiat. Meas. 38:19–22.
6. Alabdula'aly AI (1999) Occurrence of radon in the central region groundwater of Saudi Arabia. J. Environ. Radioactivity 44:85–95.
7. Tayyeb ZA, Kinsara AR, Farid SM (1998) A study on the radon concentrations in water in Jeddah (Saudi Arabia) and the associated health effects. J. Environ. Radioactivity 38(1):97-104.
8. EPA (1991) U.S. Environmental Protection Agency, www.epa.org. National primary drinking water regulations; radio nuclides; proposed rules. Fed. Regist. 56(138):33050.
9. SILENA (1995) PRASSI portable radon gas surveyor Model 5S, user's manual.
10. Soavi R (1994) Measurement of radium and radon in water and soil with the SILENA PRASSI monitor. ∑ SILENA Application note, Italy.
11. E. Vitz. Toward a standard method for determining waterborne radon. Health Phys., 60 817- 829 (1991).
12. WHO (1998) Guidelines for Drinking Water Quality, Second edition. Geneva, Switzerland.
13. EUC (1998) European Council Directive 98/83/EC of 3 November 1998 on quality of water intended for human consumption. Official Journal of the European Communitties, L 330/32.
14. Somlai K, Tokonami S, Ishikawa T, Vancsura P, Gáspár M, Jobbágy V, Somlai J, Kovács T (2007) ^{222}Rn concentration of water in the Balaton Highland and in the southern part of Hungary, and the assessment of the resulting dose. Radiation Measurements, 42:491-495.
15. Kusyk M, Ciesla KM (2002) Radon levels in household waters in southern Poland. NUKLEONIKA, 47:65- 68.

Author: Alireza Binesh
Institute: Payam Nour University
Street:
City: Fariman
Country: Iran
Email: binesh_ar@yahoo.com

Water-equivalent calibration of ^{192}Ir HDR Brachytherapy source Using MAGIC Gel Polymer

M. S. Alva, T. Marques, M. Schwarcke, O. Baffa, P. Nicolucci

Faculdade de Filosofia, Ciências e Letras de Ribeirão Preto-Universidade de São Paulo, FFCLRP-USP, Ribeirão Preto, SP, Brazil.

e-mail: nicol@ffclrp.usp.br

Abstract— **Treatments with high dose rate (HDR) ^{192}Ir sources deliver a high dose to tissues near the source. Due to the energy spectrum and the high gradient of dose delivered in these treatments, a proper calibration of the source is necessary. Calibration protocols for HDR brachytherapy sources recommend the use of reference air kerma rate measured using an ion chamber. Absorbed dose measurements in water have recently been proposed to be used to calibrate ^{192}Ir HDR brachytherapy sources. MAGIC gel dosimeter with characteristics of Z_{eff} equal to 7.41 (water-equivalent) and high spatial resolution has been shown as a potential dosimeter for many treatments in radiotherapy. The aim of the present work is to obtain percentage depth dose (PDD) and calibration parameters from ^{192}Ir HDR sources using MAGIC gel, thermoluminescent dosimeters (TLD), ionization chamber and Monte Carlo simulation. The results show that MAGIC polymer gel is an adequate dosimeter to routinely calibrate ^{192}Ir HDR sources for brachytherapy.**

Keywords— **^{192}Ir HDR, Brachytherapy, MAGIC Gel.**

I. Introduction

High dose rate brachytherapy is treatment technique that uses sealed radioactive sources to deliver high doses to treat prostate, colorectal cancer and some gynecological malignacies [Yan *et al* 2008, Takam *et al* 2009]. The most used implants are of ^{192}Ir sources with a half-life of 74 days, emitting beta rays ranging from 530 keV to 670 keV, and a main gamma ray emitted with an energy of 370 keV [Goggen 1988].

Due to the energy spectrum present in this source and the high gradient dose delivered, a proper source calibration is necessary although vendors use to assign large uncertainties to their calibration values (up to ± 10%). The calibration protocols for HDR brachytherapy sources recommend a specification in reference to air kerma rate using ionization chamber [Nath *et al* 1997**,** IAEA 2002]. Absorbed dose measurement in water has recently been proposed to calibrate ^{192}Ir HDR brachytherapy sources [Sarfehnia 2007].

MAGIC polymer gel dosimeter have been shown as a suitable dosimeter for many treatments in radiotherapy due to its characteristics of water equivalent (effective atomic number of 7.41) and a spatial resolution better than 1mm.

This work presents the percentage dose depth and calibration curve parameters of a ^{192}Ir HDR source using MAGIC gel dosimeter, TLDs, ionization chamber and Monte Carlo simulation.

From the parameters obtained it was shown that MAGIC polymer gel is a suitable dosimeter to routinely calibrate ^{192}Ir HDR sources used in radiotherapy.

II. Materials and Methods

For all experiments a water phantom of 50 x 50 x 50 cm^3 with electronic positioning holder (0.1mm precision) was used. The Gamma Med Plus 232 ^{192}Ir source with 5.43 Ci (200.91 GBq) was employed in this work. This source has an active cylindrical volume of 0.6 mm diameter and 3.5 mm height encapsulated in stainless steel welded to a steel cable. An esophageal catheter of 1.6 mm radius was used to guide the source inside the water phantom.

A. TLDs and ionization chamber

Measurements of PDD in water were carried out using TLDs (LiF-100 with dimensions: 0.9 x 0.9 x 3.1 mm^3) packed with plastic and a plane parallel ionization chamber (Markus type, 0.05cm³) properly calibrated. Both dosimeters were introduced in different depths (from 3 up to 12 mm) in a water phantom (figure 1). The catheter containing the HDR source was set parallel to the TLDs and the ionization chamber.

O. Dössel and W.C. Schlegel (Eds.): WC 2009, IFMBE Proceedings 25/III, pp. 248–251, 2009.
www.springerlink.com

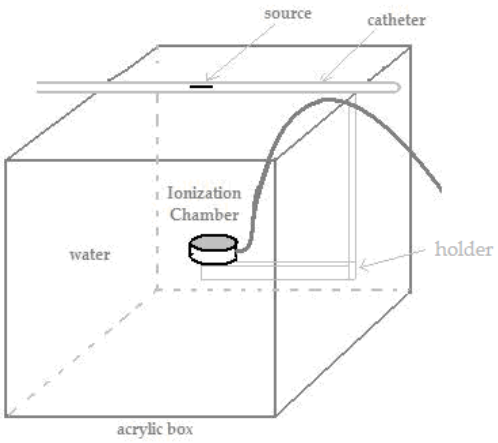

Figure 1– Measurements setup for ionization chamber and TLDs.

B. Magic gel procedures

The gel preparation was described elsewhere [Fernandes *et al* 2008]. After preparation the gel was poured in an acrylic cylindrical phantom of 6 cm diameter, 8 cm height and 0.5 cm thickness avoiding air penetration. During the PDD measurement the gel phantom was kept inside the water phantom and the source was positioned at a distance of 2 cm from the gel phantom wall.

For gel calibration, part of the gel was poured into three cylindrical glass tubes routinely used for blood sample collection (BD Vacutainer® with 5ml volume, 12mm diameter and 75 mm height, closed with a 20mm hermetic stopper inserted in a plastic cover).

Relaxometry images of the gel phantom were acquired using a 1.5 T scanner (Siemens, Magneton Vision from the Hospital das Clinicas –Faculdade de Medicina de Ribeirão Preto) one day after the irradiation to allow enough time for gel reaction completion and achievement of thermal equilibrium with the MRI scanner room temperature. A head coil and multi spin echo sequences with 16 echo times multiple of 22.5 ms, a repetition time of 3000 ms and a matrix size of 512 × 512 pixels were used during image acquisition. The slice thickness was 2mm and the FOV was 150 mm. Two acquisitions were averaged for each scan. The transverse relaxation rate R2 (=1/T2) was calculated by fitting the signal intensities versus the echo time pixel by pixel. The R2 maps were related to absorbed dose using a specific program developed by our group in MatLab® 6.5 (Mathworks Inc), which provides a volumetric dose distribution.

C. PENELOPE-Monte Carlo code

The Monte Carlo simulations were run with PENELOPE code. A user code was written to describe faithfully the geometry of the source and simulate all anisotropic properties of the brachytherapy extended source. Beta radiation of 240, 536 and 672 keV and an average energy of 376 keV for photons were used to represent the spectra source. The simulated cubic water phantom dimensions (30 cm) were assumed to be sufficient for obtaining full scattering conditions for the relevant range of distances. Simulation spatial resolution was set to1 mm

III. Results and Discussions

Calibration curves for HDR ^{192}Ir source using TLD, ionization chamber and MAGIC gel are shown in figure 2.

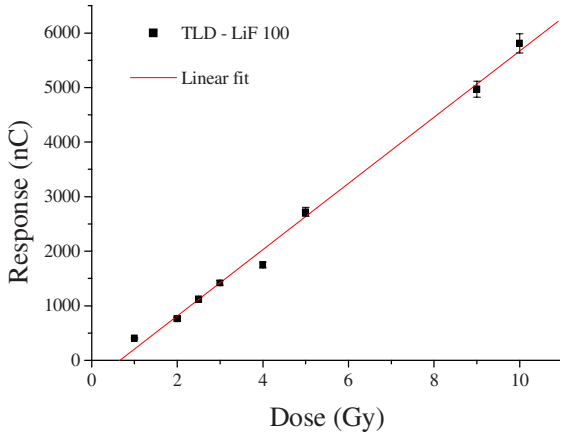

a)

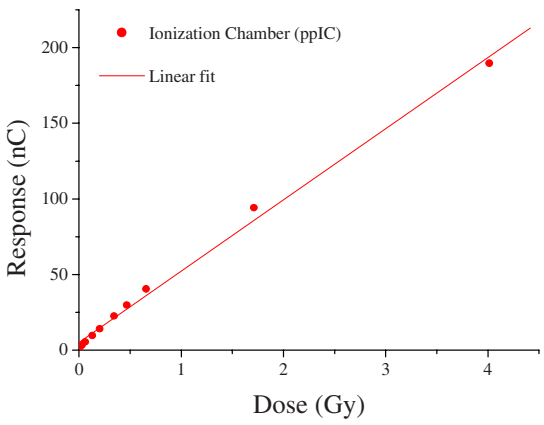

b)

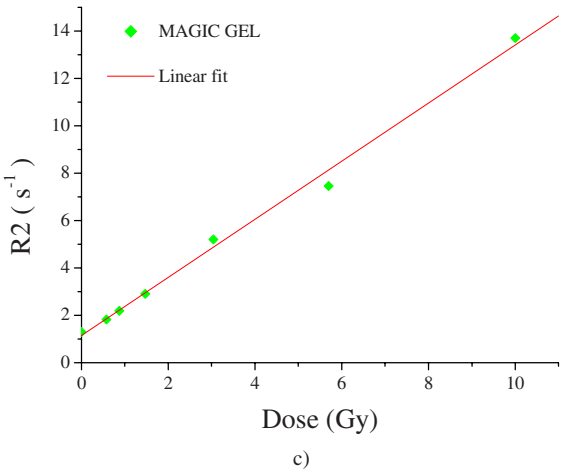

Figure 2 – HDR [192] Ir source calibration curves: a) LiF-100, b) IC and c) MAGIC polymer gel

The three dosimeters showed linearity with relative dose. The TLDs did not present sensitivity for low doses (0.5 Gy) and MAGIC gel presented a background dose that was subtracted for PDD measurements.

Dose map distributions were obtained with MAGIC polymer gel in some interesting planes like shown in figure 3.

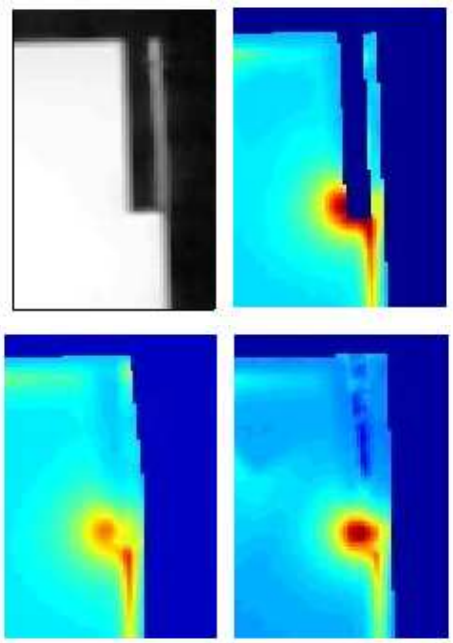

Figure 3 – Relaxometry image and dose maps around the HDR [192] Ir source obtained experimentally with MAGIC polymer gel.

The PDD curves obtained by TLD, ionization chamber, MAGIC gel and PENELOPE code are shown in figure 4.

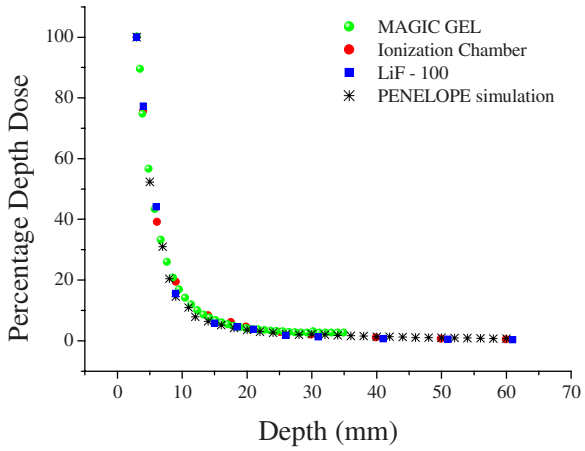

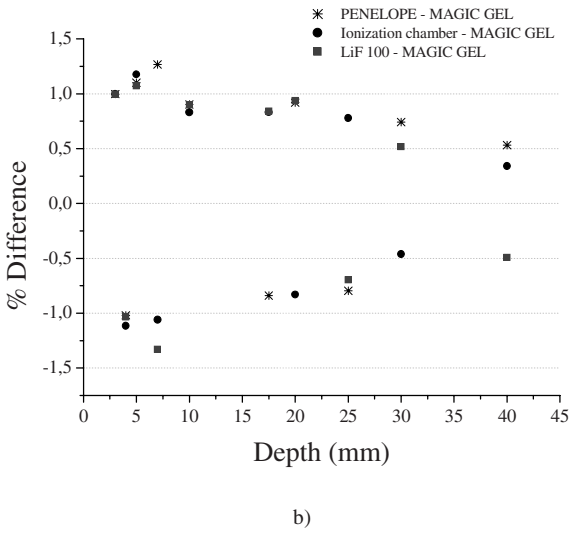

Figure 4 –a) Percentage depth dose differences for HDR [192] Ir with MAGIC polymer gel, ionization chamber, LiF-100, and PENELOPE code, b) differences between PENELOPE, IC and LiFs related to MAGIC gel PDDs.

Acknowledgments

We are grateful to Juliana Fernandes and Jose Luis Azianiby for technical support and the Brazilian agency CAPES for financial support.

Conclusions

From the percentage depth dose and calibration curve results it can be concluded that the MAGIC polymeric gel can be used as dosimeter in routinely clinical procedures and can be used to check the calibration of ^{192}I sources in an water-equivalent medium as part of the assurance quality in HDR brachytherapy.

Rererences

A Sarfehnia, K. Stewart, and J. Seuntjens. (2007) An absorbed dose to water standar for HDR 192 Ir brachytherapy sources based on water calorimetry: numerical and experimental proof-of-principle. Med Phys 34: 4957-61.

Fernandes J., Pastorello B., Araujo ., Baffa O. (2008) Formaldehyde increases MAGIC gel dosimeter melting point and sensitivity. Phys Med Biol 53: N53-8.

Goggen T. J. Physical Aspects of Brachytherapy. (1988) Medical Physics Handbooks, v.19, England.

International Atomic Energy Agency-IAEA. (2002) Calibration of photon and beta ray sources used in brachytherapy. IAEA-TECDOC 1274..

Nath R., Anderson L., Meli J. Olch A., Stitt J. And Williamsom J. (1997) Code of practice for brachytherapy physics: Report of the AAPMRadiation Therapy Committee Task Group No. 56. Med Phys 7, 24: 1557-98.

Takam R., Bezak E and Yeoh E. (2009) Risk of secondary primary cancer following prostate cancer radiotherapy: DVH analysis using the competitive risk model. Phys Med Biol 54**:** 611-25.

Yan X., Poon E, Reniers B., Voung T. And Verhaegen F. (2008) Comparison of dose calculation algorithms for colorectal cancer brachytherapy treatment with a shielde applicator. Med Phys 35: 4824-30.

Doses to patients for computed tomography in Sarajevo

A. Beganović[1], A. Skopljak-Beganović[1], A. Drljević[1], S. Džanić[2], J. Bošnjak[3], M. Gazdić-Šantić[1], B. Metlić[1], L. Lincender[4] and M. Ninković[5]

[1] Department of Medical Physics and Radiation Safety, Clinical Centre of Sarajevo University, Sarajevo, Bosnia and Herzegovina
[2] Radiation Protection Centre, Institute for Public Health of Federation of B&H, Sarajevo, Bosnia and Herzegovina
[3] Institute for Public Health of Republic of Srpska, Banja Luka, Bosnia and Herzegovina
[4] Institute of Radiology, Clinical Centre of Sarajevo University, Sarajevo, Bosnia and Herzegovina
[5] Institute »Vinča«, Belgrade, Serbia

Abstract— **Clinical Centre of Sarajevo University is the largest hospital in Bosnia and Herzegovina. Computed tomography (CT) examinations are performed at the Institute of Radiology. The purpose of this paper is to give overview of patient doses received for various CT examinations. Three CT scanners are in practical use – 2, 4 and 64-slice unit. Two scanners are equipped with automatic dose modulation. *CTDI* measurements are performed using 10 cm ionization chamber and dosimetry phantom. Data relevant for dose is collected for 10 patients per body part for each scanner. The measured values of $_nCTDI_w$ correspond to data shown on console. Mean effective doses for head examination range from 0.8–1.5, neck examination 0.5–2.8, thorax 2.5–10.5, abdomen 1.9–9.0, and pelvis 1.8–9.3. The total collective dose is 77 personSv. The results are below EU Diagnostic Reference Levels and are similar to doses in other European countries. Automatic dose modulation protocols show significant decrease in patient dose. The use of these protocols is recommended especially for non-standard patients such as children.**

Keywords— **CT, dose, CTDI, DRL**

I. Introduction

Since the first introduction of CT scanner in 1972 there is an increase in number of these units as well as workload per one unit. This increase is followed by higher collective dose to population due to computed tomography or diagnostic radiology in general. The data presented by the Organization for Economic Co-operation and Development in 2006 show that Japan has the largest number of CT scanners per 1.000.000 population – 92.6, while countries like the USA, South Korea and Austria have approximately 30 scanners per 1 million residents [1]. Large number of CT units mean high collective dose. Results from 2004 in Japan show evaluation of dose per caput due to computed tomography examinations to be 2.3 mSv [2]. Doses in Europe are lower [3]. Computed tomography can and should be optimized just like any other technique in diagnostic radiology. Patients should receive doses as low as reasonably achievable without losing relevant diagnostic information. The dose survey is a baseline for optimization.

II. Materials and methods

A. CT facilities

According to latest UN estimation population of Bosnia and Herzegovina (BiH) is approximately 4 million (UN estimate, 2007). The number of CT scanners is shown in Table 1. Number of CT units per 1 million is 11.6.

Institute of Radiology at the Clinical Centre of Sarajevo University uses 3 CT scanners for the purposes of diagnostic radiology. Table 2 shows name of the manufacturer and model, year of installation, number of channels (slices) and information on technical capabilities for automatic dose modulation (ADM).

Table 1 Number of CT units in Bosnia and Herzegovina

Town	Number of CT units
Sarajevo	9
Tuzla	5
Banja Luka	4
Mostar	4
Bihać	3
Zenica	3
Bijeljina	2
Brčko	2
Doboj	2
Foča	1
Gradiška	1
Kasindol	1
Konjic	1
Livno	1
Mrkonjić Grad	1
Orašje	1
Posušje	1
Prijedor	1
Travnik	1
Trebinje	1
Zavidovići	1
Total	46
Population of BiH	3,981,239
Number of CTs per million	11.6

O. Dössel and W.C. Schlegel (Eds.): WC 2009, IFMBE Proceedings 25/III, pp. 252–254, 2009.
www.springerlink.com

Table 2 CT scanners available at the Institute of Radiology in Sarajevo

Name	Year of installation	Number of channels/slices	ADM
Siemens Volume Zoom	2004	4	No
Siemens Emotion Duo	2006	2	Yes
GE LightSpeed VCT	2008	64	Yes

B. Patients

Table 3 shows number of CT examinations performed in 2008 on three available CT scanners. Patients under 15 are regarded as children.

Table 3 Number of CT examination of adults and children at the Institute of Radiology in Sarajevo

CT	Number of examinations			
	Adults	Children	Children (%)	Total
Siemens Volume Zoom	5011	388	7	5399
Siemens Emotion Duo	6574	348	5	6922
GE LightSpeed VCT[1]	446	3	0.7	449

[1]Data for 16.4–3.9.2008

For dosimetry purposes patients were divided into groups of ten according to body part exposed during examination. Ten patients were randomly chosen for body, neck, thorax, abdomen and pelvis examinations.

C. Dosimetry equipment

Measurement of CTDI was performed using 10 cm ionization chamber and dosimetry phantoms – head and body (Fig. 1).

III. Results

Dosimetry measurements have shown that *CTDI* reported on console is equal to the measured *CTDI*. Therefore, it was safe to use reported values of $CTDI_w$, $CTDI_{vol}$ and *DLP* for data collection.

Patient examinations were divided into 6 groups according to body part examined. Table 4 shows number and ratio of these examinations for all three CT. Collective dose to patients is 77 personSv.

Dosimetry data is similarly grouped. Periphery examinations are not taken into account since effective doses due to exposure in these regions are negligible (Table 5).

Siemens Emotion Duo is equipped with automatic dose modulation protocol (DoseCare4D). Table 6 shows how value of *It* is decreased when this protocol is in use. The image quality should not lower than image quality when reference *It* is used.

Table 4 Number of examinations per month of specific body parts at the Institute of Radiology, Sarajevo

Region	Emotion Duo		Volume Zoom		LightSpeed VCT	
Head	746	51%	118	18%	5	5%
Neck	90	6%	44	7%	7	7%
Thorax	43	3%	143	22%	67	63%
Abdomen	473	32%	224	35%	18	17%
Pelvis	113	8%	49	8%	7	7%
Periphery	0	0%	68	11%	3	3%
Total	1465		646		107	

Table 5 Mean values of $CTDI_{vol}$ (mGy) and effective dose, *E* (mSv), for CT examinations of specific body parts on three CT scanners at the Institute of Radiology, Sarajevo. Values in parenthesis are European diagnostic reference levels [4].

	Emotion Duo		Volume Zoom		LightSpeed VCT	
	$CTDI_{vol}$	*E*	$CTDI_{vol}$	*E*	$CTDI_{vol}$	*E*
Head (60)	56,04	1,5	58,67	1,9	24,18	0,8
Neck	4,18	0,5	11,69	1,5	24,18	2,8
Thorax (30)	4,84	2,5	19,15	9,3	21,76	10,5
Abdomen (35)	4,18	1,9	11,89	5,3	20,93	9,0
Pelvis (35)	3,86	1,8	14,81	7,2	19,71	9,3

Table 6 Reduction of *It* (mAs) when DoseCare4D automatic dose modulation protocol is used on Siemens Emotion Duo CT at the Institute of Radiolgy, Sarajevo

	Q_{ref} (mAs)	*It* (mAs)	Reduction
Head	260	260	0%
Neck	88	38	57%
Thorax	60	44	27%
Abdomen	90	62	31%
Pelvis	90	57	37%

IV. Discussion

Results presented in Table 5 show that mean values of $CTDI_{vol}$ are below European diagnostic reference levels [4]. Doses received on Siemens Emotion Duo are much lower than doses received on Siemens Volume Zoom CT scanner. It is the automatic dose modulation system that is responsible for this decrease.

It is noticed that doses at 64-slice CT are similar to doses received on Siemens Volume Zoom that is not equipped with ADM system. Doses could be lower. The possible reason for higher doses is higher image quality demanded when this CT scanner is used. This should be investigated for possible dose reduction.

The effect of ADM, such as DoseCare4D, is presented in Table 6. We could see that reduction of *It* (mAs), and con-

sequently the effective dose, is from 27% in thorax region up to 57% for the neck.

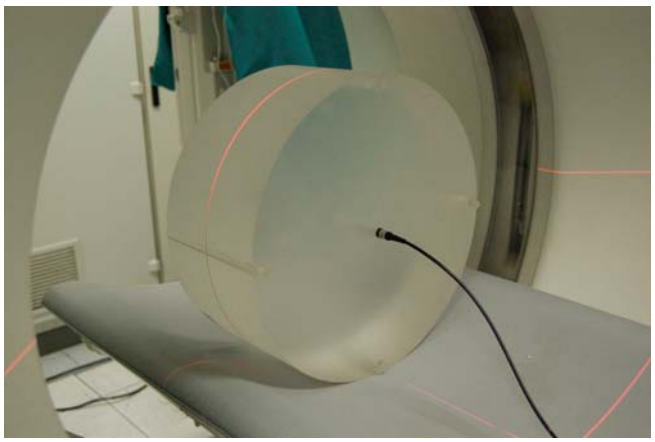

Fig. 1 CTDI measurements in 32 cm body phantom

When compared to results in other countries reported doses are similar [5].

V. Conclusions

Knowing doses for patients is the first step towards optimization. Patients undergoing CT examinations in the Clinical Centre of Sarajevo University receive doses similar to doses in Europe. The results are below European diagnostic reference levels.

The usage of automatic dose modulation systems is recommended since doses are significantly lower.

References

1. Organization for Economic Co-operation and Development (2006) OECD health data 2006. OECD, Paris, France.
2. Nishizawa K, Matsumoto M, Iwai K, Maruyama T (2004) Survey of CT practice in Japan and collective effective dose estimation. Nippon Igaku Hoshasen Gakkai Zasshi 64(3):151–158
3. Scanff P, Donadieu J, Pirard P, Aubert B (2008) Population exposure to ionizing radiation from medical examinations in France. Br J Radiol 81(963):204–213
4. European Commission (2000) European guidelines on quality criteria for computed tomography. EC, Luxembourg.
5. Muhogora WE, Ahmed NA, Beganović A, Benider A, Ciraj-Bjelac O, Geršan V, Gershkevitsh E, Grupetta E, Kharita MH, Omrane LO, Manatrakul N, Milaković M, Ohno K, Ptacek J, Rehani MM, Shabaan MS, Schandorf C, Toutaoui N, Vasileva J, Wambani JS (2009) CT patient doses in nineteen countries: Initial results from International Atomic Energy Agency projects. AJR, in press.

Author: Adnan Beganović
Institute: Department of Medical Physics and Radiation Safety, Clinical Centre of Sarajevo University
Street: Bolnička 25
City: Sarajevo
Country: Bosnia and Herzegovina
Email: adnanbeg@gmail.com

Biological Effects of Densely Ionizing Radiation

M. Durante [1, 2]

[1] GSI, Biophysics Department, Planckstraβe 1, 64291 Darmstadt, Germany (M.Durante@gsi.de)
[2] Institut für Festkörperphysik, Technische Universität Darmstadt, Hochschulestraβe 3, 64289 Darmstadt, Germany

Abstract— **Densely ionizing radiation, such as heavy ions, produce biological damage which is different from that normally produced by sparsely ionizing radiation, such as X- or γ-rays which are a large component of the natural radiation background. In fact, as a result of the different spatial distribution of the energy deposited, along the core and penumbra of the track, DNA lesions are exquisitely complex, and difficult to repair. RBE factors are normally used to scale from X-ray to heavy ion damage, but it should be kept in mind that RBE depends on several factors (dose, dose rate, endpoint, particle energy and charge, etc.) and sometimes heavy ions produce special damages that just cannot be scaled from X-ray damage. The special characteristics of heavy ions can be used to treat tumors efficiently, as it is currently done in Japan and Germany.**

Keywords— **Heavy ions, radiobiology, high LET, densely ionizing radiation, particle therapy**

I. Introduction

The biological effectiveness of ionizing radiation strongly depends on the linear energy transfer, or LET, and it is well known that it is, for many endpoints, higher than sparsely ionizing radiation for LET values between 50 and 200 keV/μm in water. This different biological effectiveness os normally attributed to the different spatial distribution of lesion density in the DNA. While physicists know very well, form nuclear emulsions, how different a track of a heavy ion is compared to photons, more recently this could be visualized directly in mammalian cells, exploiting markers of DNA lesions such as phosphorilated histone γH2AX (Fig. 1) [1] or the accumulation of GFP-tagged repair proteins, such as 53BP1 (Fig. 2) [2]. Clearly, heavy ions produce "streaks" of DNA lesions in the cell nucleus, and the density of lesions increase with LET (Fig. 1), and they can be hardly repaired or moved following exposure (Fig. 2). This observation begs the question of whether the damage induced by heavy ions is different from that produced by X-rays. The answer is unfortunately not simple: even if the DNA damage is more difficult to repair, this may lead to an increased cell killing, but not necessarily to increased late risk: a dead cell cannot represent a risk, although the bystander effect may play a dominant role in explaining the effectiveness of high-LET radiation for late effects.

II. Heavy Ion Radiobiology

Because heavy ions are not present on Earth, their study is not relevant for radiation protection, and neither it has been for radiation therapy for many years. However, heavy ions are now often used in therapy [3] and they represent a major risk for human space exploration [4] (Fig. 4).

A. Particle therapy

The rationale of oncological particle therapy is simply base don the different energy deposition of charged particles (the Bragg curve) and photons (exponential attenuation). Fig. 3 immediately suggests that charged particles have a better energy deposition pattern than X-rays for therapy, as recognized by Wilson already in 1946. Protontherapy is today widely spread in the world, and is considered a cutting-edge technology, with clinical results at least comparable to X-ray IMRT. However, apart from the favorable dose distribution, protons do nor really add biological advantages, as their RBE is close to 1. On the other hand, heavy ions combine an increased biological effectiveness to a high RBE, and reduced oxygen enhancement ratio (OER), in the Bragg peak. Carbon ions are for instance low-LET (about 10 keV/μm) in the entrance channel, but high-LET (up to 80 keV/μm) in the Bragg peak, thus providing sparing of the normal tissue and high effectiveness in the tumor. The clinical results, so far based on a fairly limited number of cancer patients (about 5000) are indeed very good, and after the clinical trials in NIRS (Japan) and GSI (Germany), several new centers are under constructions in Europe and Asia.

B. Radiation protection in space

Although protons are by far the most common particle in space radiation, heavy ions play a major role because energy deposition increase with z^2, and the RBE increases with LET. Therefore, heavy ions are nowadays acknowledged by space agencies as a major barrier to human space exploration. Cancer risk is of course the main concern, because it is well documented that radiation can induce

O. Dössel and W.C. Schlegel (Eds.): WC 2009, IFMBE Proceedings 25/III, pp. 255–257, 2009.
www.springerlink.com

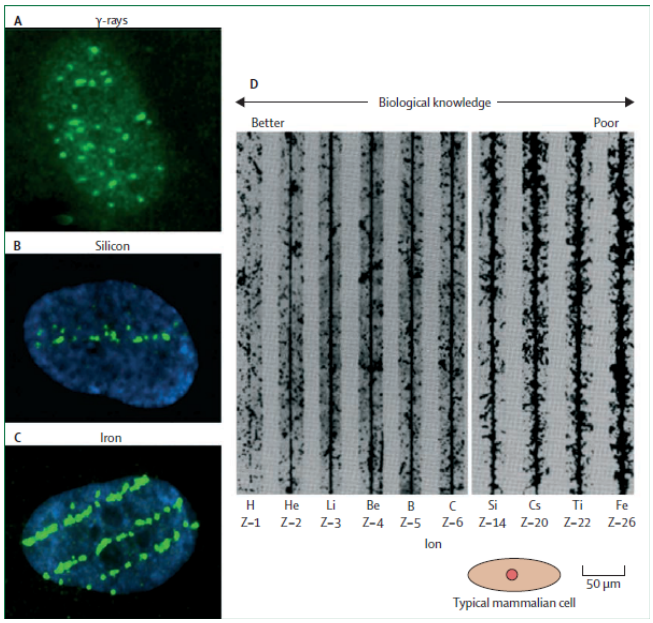

Fig. 1. Three nuclei of human fi broblasts exposed to (A) γ-rays, (B) silicon ions, or (C) iron ions; and immunostained for detection of γ-H2AX. Every green focus corresponds to a DNA double-strand break. In the cell exposed to sparsely ionising γ-rays (A), H2AX foci are uniformly distributed in the nucleus. Cells exposed to heavy ions show DNA damage along tracks—one silicon (B) and three iron (C) particles, respectively. Spacing between DNA double strand breaks is reduced at very high-LET. (D) Tracks of different ions, from protons to iron, in nuclear emulsions, show increasing LET as charge, Z, increases. From ref. [1].

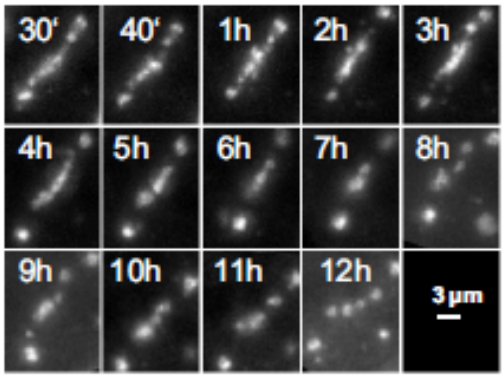

Fig. 2. Quantitative analysis of the motion of DNA double-strand breaks (DSBs) after high LET irradiation. Time-dependent changes of a single Ni-ion-induced 53BP1-GFP streak in a human tumor cell showing the typical motional behavior of individual proteins along the trajectory over the time course of 12 h after irradiation. Compared to Fig. 1, these pictures show the evolution of the damage in living cells, exploiting GFP-tagged proteins expressed in the cell, instead of fixing and staining the samples. From ref. [2].

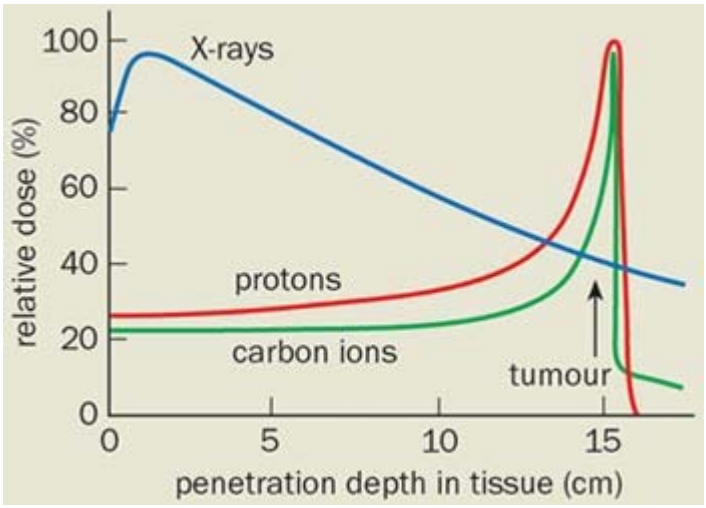

Fig. 3. Rationale of using charged particles for cancer therapy. While X-rays deposit more energy on the surface than in the tumor, the opposite holds for charged particles, such as protons and carbon ions.

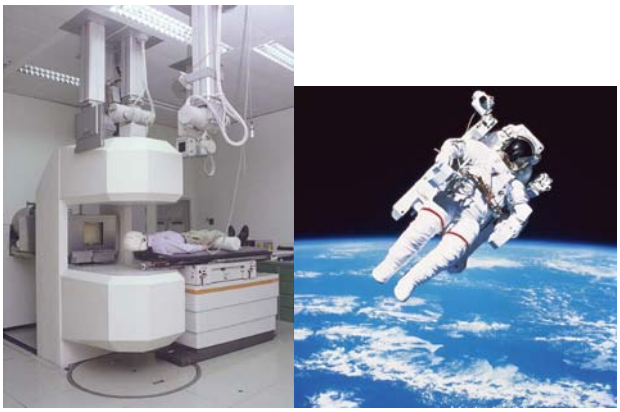

Fig. 4. Interest for radiobiology of heavy ions is linked to two main applications: cancer therapy (left) and protection of astronauts in long term space missions (right). In one case, we are interested to exploit the ability of heavy ions to kill cells; in the second, to protect the crews from long-term late effects. Although the exposure conditions are very different (high dose, fractionated, localized irradiation in therapy; low dose, chronic, whole body in space), the two topics share several research topics, such as studies on stochastic risk of heavy ions, or on radioprotectors (Table 1).

cancer, but the RBE of heavy ions is not known, due to the lack of epidemiological studies and the only limited animal studies, performed at particle accelerators [4]. In addition to cancer, several others late effects cause concern, including damage to the central nervous system, cataracts, risk of cardiovascular diseases, and hereditary effects. Both NASA and ESA support large experimental campaigns to study these effects, considering that space agencies are now shifting their programs to exploration. The NASA program is based at the Brookhaven National Laboratory (Upton, NY), whereas the European program is based at GSI (Darmstadt, Germany).

Notwithstanding the large differences in exposure conditions (high dose, fractionated acute partial-body exposure in therapy; low dose, chronic whole-body exposure in space), the two topics share several research topics as summarized in Table 1.

III. CONCLUSIONS

Biological effects of densely ionizing radiation are becoming a key topic in radiobiology, because of the interest for heavy ions coming from space radiation protection and particle therapy. Large experimental campaigns are currently under way at accelerators, and it is likely that they will lead to a reduction of the uncertainty on the late risk of heavy ions.

REFERENCES

1. Cucinotta FA, Durante M (2006) Cancer risk from exposure to galactic cosmic rays: implications for space exploration by human beings. Lancet Oncol. 7: 431-435.
2. Jakob B, Splinter J, Durante M, Taucher-Scholz G (2009) Live cell microscopy analysis of radiation-induced DNA double-strand break motion. Proc. Natl. Acad. Sci. USA, epub ahead of print (February)
3. Amaldi U, Kraft G (2005) Radiotherapy with beams of carbon ions. Rep. Prog. Phys. 68: 1861-1882
4. Durante M, Cucinotta FA (2008) Heavy ion carcinogenesis and human space exploration. Nature Rev. Cancer 8: 465-472.

	Hadrontherapy	**Space Radiation Protection**
Particles	H and C.	All ions from H to Ni.
Maximum energy	~ 400 MeV/n	~ 10 GeV/n
Dose	60-80 Gy-eq. in the target volume. Dose to the normal tissue depend on the treatment plan.	50-150 mSv on the Space Station, up to 1 Sv for the Mars mission
Exposure conditions	Partial-body, fractionation (2 Gy-eq./day in the target volume)	Total-body, low dose-rate (1-2 mSv/day)
Individual radiosensitivity	Patient selection, personalized treatment planning	Personalized medical surveillance of the crewmembers
Mixed radiation fields	Effects of primary particles and fragments for tumor cell killing and side effects	Cosmic radiation is a mixed field. Effects of shielding.
Late stochastic effects of heavy ions	Risk of secondary cancers in patients	Risk of cancer in astronauts
Normal tissue deterministic effects	Early and late morbidity	Cataracts, CNS damage, other late degenerative effects
Radioprotectors	Protection of the normal tissue, but not of the tumor. Drugs.	Protection from heavy ions at low doses and protons at high doses (solar particle event). Dietary supplements
Biomarkers	Predicting risk of secondary cancers or late morbidity	Reducing uncertainties in risk estimates
Bystander effect	Role in tumor cell killing	Role in stochastic risk at very low fluence

Table 1 – Some research topics relevant for both hadrontherapy and space radiation protection.

Track Structure and Biological Effects of Densely Ionizing Radiation

Hooshang Nikjoo PhD

Radiation Biophysics Group, Karolinska Institutet, Stockholm, Sweden

Abstract— **The paper provides a brief discussion of physical, biophysical and biological aspects of densely ionizing radiation tracks. Densely ionizing radiations include 'track ends' of electrons and Bragg peak area in the case of heavy ions where the energy loss is the highest. The paper examines features of radiation tracks, biophysical significance of energy loss in molecular targets and biological lesions induced by heavy ions.**

Keywords— **Track structure, Energy deposition, LET, DNA damage, damage complexity.**

I. Introduction

Ionizing radiations induce a variety of molecular and cellular types of damage in mammalian cells as the result of energy deposition by radiation track. In general, tracks are divided into two classes of sparsely ionizing such as electron tracks and densely ionising tracks such as heavy ions. Although heavy ions are defined as protons and heavier elements, in radiobiology proton, helium up to carbon ions are referred to as light particles. Tracks of heavier elements than carbon up to and including iron are referred to as heavy ions or HZE in space radiation research community. This presentation primarily discusses physical aspects and biological effects of densely ionizing radiations. In addition to the observed laboratory experiments, biophysical studies of radiation tracks have provided much of the insight in mechanistic understanding of the relationship between the initial physical events and observed biological responses. Sources of exposure to ionizing radiations include natural back ground radiations (82%) and man-made (18%) radiation sources. The worldwide background radiation is about 2.4 mSv/yr composed of nearly 61% high-LET exposures by radon (52%); ingestion (5%) and neutron component of cosmic radiation (4%). The remaining 31% is due to low-LET exposure from earth (20%); photon component of cosmic rays (12%) and ingestion (7%). The man-made radiation sources are mainly of low-LET type include medical sources (79%); consumer products (16%); occupational (2%); fallout (2%) and nuclear fuel cycle (1%).

Over the past decade we have seen increasing establishment of many radiotherapy centres using protons and carbon ions. The attraction of using heavy ions in preference to classical low-LET radiation therapy using electrons and photons is the presence of radiation resistance tumours, where the dose to the tumour cannot be sufficiently increased without severely damaging the normal healthy tissue. The treatment results have been improved considerably by using physically optimized intensity modulated photon therapy (IMRT) and also proton therapy using 3D spot scanning to maximize the tumour dose and minimize the side effects in normal tissues. To improve the treatment outcome further with severely hypoxic tumours, such as lung, bone, soft tissue sarcoma and prostate cancer use of heavier ions such carbon ions is essential. But the major disadvantage to use of heavy ions is the damage to normal tissue by high-LET radiation which is largely irreparable and the healthy tissue will not recover overnight as it does with low LET photon and electron radiations. Therefore the optimal modality in radiation therapy should be a very high LET radiation in the Bragg peak area which is placed in the tumour area and have a low LET component in the entrance and plateau regions. For this reason ions helium to carbon are most suitable for therapy. In addition to the physical aspects of therapy beam improved outcome should be sought as a function of particle LET and apoptotic properties of the tumour cells.

II. Features of radiation tracks

Track of ionizing radiations can be modelled and simulated in many forms including single parameter such as linear energy transfer (LET), quality factor (Q), lineal energy (y), and specific energy(z) [1], Amorphous model of track [2], condensed history technique [3], and the 3D or the full 4D(x,y,z,t) at molecular level [4]. Apart from the latter, the simpler forms of tracks fail to adequately describe the microscopic stochastic features of radiation track. It is generally thought the microscopic features of radiation tracks are responsible for the relative biological effectiveness of different types of radiations. To illustrate differences between tracks of different radiation qualities, Figure 1 shows a few examples of tracks of electron, proton, carbon ion and iron a HZE particle. There is a great diversity among these tracks. In general electron and proton tracks are of low-LET type with sparsely ionizations and excitations, while tracks of carbon and iron show much higher density of energy loss events per unit track length. Therefore, a question one can ask is whether biological effectiveness of radiations correlated with the quality of track?

O. Dössel and W.C. Schlegel (Eds.): WC 2009, IFMBE Proceedings 25/III, pp. 258–261, 2009.
www.springerlink.com

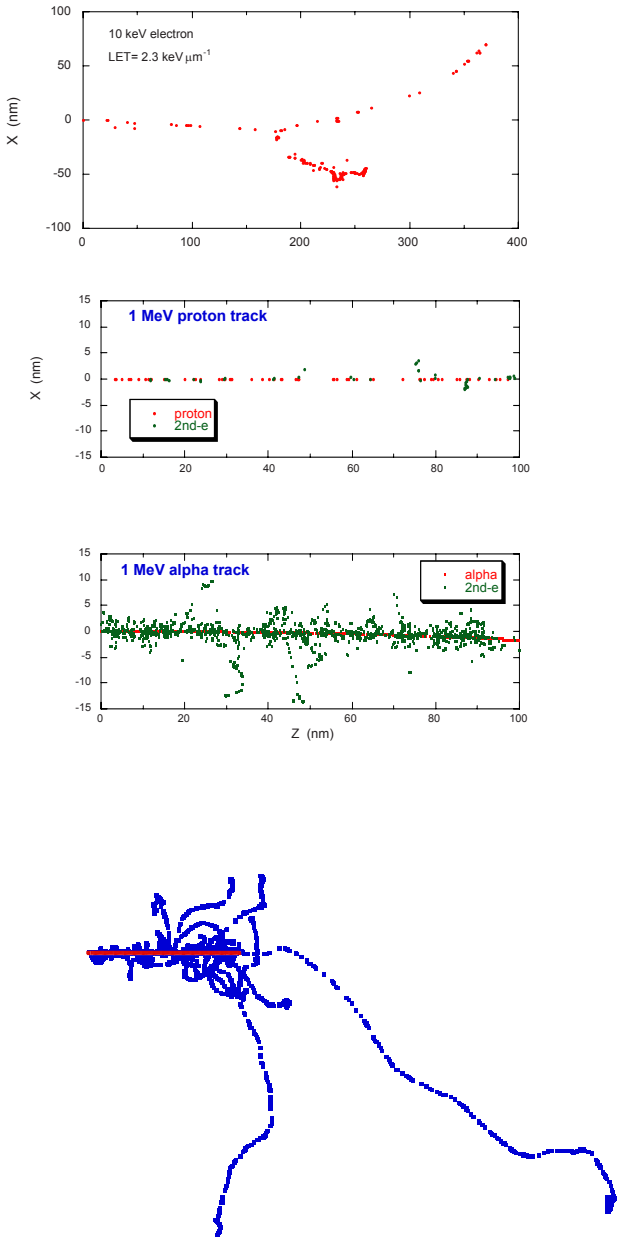

Figure 1 2D projection of a 10keV electron track, a segment of a 1 MeV proton, a segment of 1MeV alpha particle and a 1-μm segment of a 1GeV/u Fe ion track. For proton, alpha-particle and Fe ion, the red dots indicate primary ion interactions while green and blue are 2ndry delta electrons.

III. Tracks in Molecular Targets

The central parameter of radiation dosimetry is the absorbed dose in the volume of the target. Absorbed Dose is defined as the quotient of the local energy deposited in the volume of interest by radiation track(s) and the mass of the volume. In line with this, the differences in quality of radiations in terms of spatial and temporal distributions of radiation interactions in the volume of interest can be obtained as absolute frequency of energy deposition. Such data in particular for protons and heavier ions is a rich source for biophysical analysis. Such differences can only become meaningful when the dimensions of target volumes become sufficiently small, 1-100nm diameter of a sphere or a cylinder. Spheres and cylinders, in general, mimic most biological targets such as cells and linear segments of DNA or its macromolecular structures. By energy deposition events we mean inelastic events such as ionizations and excitations.

Energy transfer by electrons is a most important topic in radiation research as low energy electrons are released as the result of energy transfer in collision between ions and matter. To elucidate and quantify the prominent role of these electrons we calculate the frequency of energy depositions in target volumes irradiated by electrons and ions. The distributions are shown in targets 10 nm height by 5nm width. This target dimensions is similar to a nucleosome unit. Radiation tracks, electrons and ions, deposit their energy in the medium in the form of sparsely isolated interactions and partly in clusters of ionizations and excitations, in particular near the end of the track called 'track-ends'. By comparing the frequency distributions for energy depositions by radiations of different qualities with their relative effectiveness for biological effects, it has been suggested significant biological effects are due to clusters of energy depositions and the probability of final effect increase with increasing size of clusters or severity of the initial physical damage [5-6]. In electrons and photon irradiations these clusters of energy depositions are mainly due to low energy 'track-ends'.

A question one can ask here is: which of these protons are more effective in causing initial biological damage in a selected target of the size, for example, similar to DNA? The effectiveness of the protons mainly depends on the initial energy of the particle and the size of the energy deposition is considered. In above examples, for small energy depositions in a DNA size target, say 100eV equivalent on average to 4 ionizations in water, the 100 MeV proton track seems to be most effective, while for energy depositions greater than 100 eV, 1MeV protons have a greater probability of creating larger clusters.

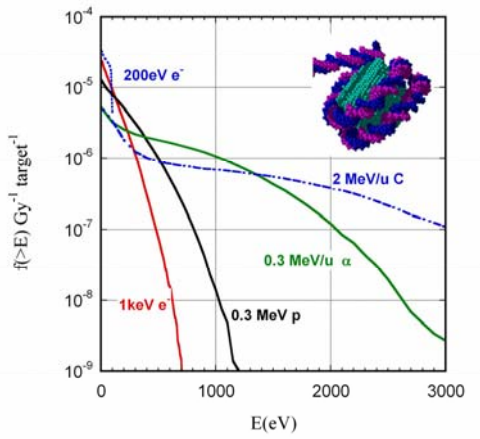

Figure 2 Distribution of absolute frequency of energy deposition events greater than energy E, in cylinder volumes in water irradiated with various radiations . The ordinate gives the absolute frequency of energy deposition greater than E(eV) randomly positioned in water irradiated with 1Gy of the given radiation.

This is the reason in the Bragg region of the full slowing of the proton track, the track becomes highly effective in killing of the tumour cells. Similarly, in panel B of Figure 4 which compares radiations of different qualities, the effectiveness of radiation measured as the size of energy deposition delivered in the target volume. For example, electron track ends, such as 200eV electrons (similar to photo electrons generated by ultrasoft Ck X-ray) and 1keV electrons, are seen to be most effective in depositing energies below 50 eV in DNA size volumes. But for generation of larger clusters of ionizations carbon ions and alpha-particles are most effective. So, general conclusions from these biophysical studies can be related to the production of initial biological lesions, for example production of simple and clustered DNA damage, it is seen that the lower energy electrons are most effective in producing complex damage (Goodhead and Nikjoo 1991 [5], Nikjoo and Goodhead 1989 [6], Nikjoo et al 2002 [7], Nikjoo and Uehara 2004 [8].

IV. Biological response to tracks of different radiation qualities

Double strand break DSB have been emphasized as the determinants of the fate of the irradiated cells because inadequate repair of the DSB is the root cause of cellular lethality, mutagenesis and carcinogenesis. Induction of DSB in cells are found to be linear with dose for all LET ranges. Values of the yield of double strand breaks and chromatin breaks per Gy per Dalton as a function of LET show much similarity except at very high LET values where the yields are reduced. For this reason there is the possibility that more complex double strand breaks are more difficult to process and repair but these have not yet fully proven because of experimental difficulties. Overall, the interrelationship between DSB, LET, lethality and Oxygen have not fully emerged despite considerable experimental efforts in these areas.

Table 1 below summarises biological lesions induced in mammalian cells after 1 Gy of irradiation by low-LET radiation such as Co^{60}- γ photons and 3MeV alpha-particles as a typical representative of a high-LET densely ionizing radiation. Data shows much similarity in initial lesions induced by low and high LET radiations. However, the

Approximate Yield of Damage in a Single Mammalian Cell after 1 Gy of Radiation

Radiation	*Low-LET*	*High-LET*
Tracks in nucleus	10^3	4
total SSB	10^3	10^3
total DSB	40	40
Complex SSB	4%	20%
Complex DSB	~20%	~70%
DSB per lethal lesion	87	22
Chrom. Aberration	1	3
Dicentric per cell	0.1	0.4
HPRT Muatation	10^{-5}	
Cell Inactivation	30%	85%
8-OxoG	700	

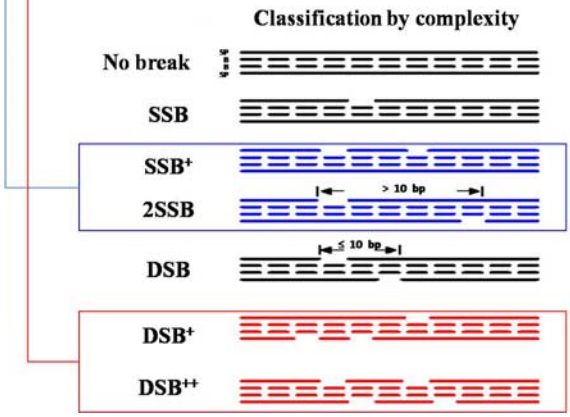

Table 1 DNA Damage & Lesions

frequency of complex single and double strand DNA damage produced by densely ionizing radiations are much more than

those by low LET radiations. Such differences also reflect in the residual numbers of DSB in mammalian cells after nearly 3 hours of repair. The lower part of the table shows classification of DNA damage by complexity [7]. This classification is done only in terms of the variety of different types of strand breaks.

In the middle part of the table 1 differences are seen between the sparsely and densely ionizing radiations. These include number of DSB per lethal lesions, numbers of chromosome aberrations, number of dicentrics per cell, frequency of HPRT mutation per survived cells, percentage of cell inactivated and lastly number of 8-Oxo G produced as a measure of induced base damages.

V. Conclusions

Biophysical modelling using Monte Carlo track structure simulations of tracks of photons, electrons and ions, molecular interaction by interaction, in space and time and models of DNA structures have provided a powerful tool to probe characteristics of ionizing radiation interactions in cellular DNA. Such calculations have provided the basis for generation of hypothesis such as clustered DNA damage. These calculations have provided a quantitative measure of frequencies of complex and simple SSB, DSB ad base damage induced by direct and indirect events in cell nucleus after exposure to ionizing radiations. With the more recent advances in understanding of the model and structure of cell nucleus in which chromosome loops are located and spread in the cell nucleus one has come a step closer to making more realistic estimation of risk of exposure to ionizing radiations.

References

1. Nikjoo H, S Uehara, D Emfietzoglou, A Brahme, (2008), Heavy charged particles in radiation biology and biophysics, *New Journal of Physics*, 10, 075006
2. Cucinotta FA, Nikjoo H, Goodhead DT (1999) Applications of amorphous track models in radiation biology. *Radiation and Environmental Biophysics* 38: 81-92
3. Nahum AE, (1999)Condensed-history Monte-Carlo simulation for charged particles:what can it do for us? *Radiation and Environmental Biophysics* 38: 163-173
4. Nikjoo H, S. Uehara, D. Emfietzoglou, F.A. Cucinotta, (2006), Track structure codes in radiation research. *Radiation Measurements*, 41(9-10), 1052-1074.
5. Goodhead DT, Nikjoo H (1989) Track structure analysis of ultrasoft X-rays compared to high- and low- LET radiations. *International Journal of Radiation Biology* 55: 513-529
6. Nikjoo H, Goodhead DT (1991) Track structure analysis illustrating the prominent role of low-energy electrons in radiobiological effects of low-LET radiations. *Physics in Medicine and Biology* 36: 229-238
7. Nikjoo H, O'Neill P, Wilson WE, Goodhead DT (2001) Computational approach for determining the spectrum of DNA damage by ionising radiation. *Radiation Research* 156: 577-583
8. Nikjoo h and Uehara S. (2004) Track structure studies of biological systems. In: Mosumder A, Hatano Y (Eds), Charged particle and photon interactions with matter: chemical, physicochemical, and biological consequences with applications. Marcel Decker, New York.

Author: Hooshang Nikjoo
Institute: Karolinska Institutet
Street: Box 260, SE-171 76
City: Stockholm
Country: Sweden
Email: Hooshang.nikjoo@ki.se

Patient radiation doses during cardiac angiography and implantations of cardiac resynchronization devices. Deriviation of local DRLs.

T. Topaltzikis[1], N. Papageorgiou[2], J. Skoularigis[2], F. Triposkiadis[2], C. Kappas[1], K. Theodorou[1].

[1]University Hospital of Larissa, Medical Physics Department, P.O.Box 1425, Larissa 41110, Hellas.
[2]University Hospital of Larissa , Cardiology Department, P.O.Box 1425, Larissa 41110, Hellas..

Abstract — **The Euratom directive 97/43 recommends the use of patient dose surveys in diagnostic and interventional cardiology and the establishment of diagnostic reference dose levels (DRLs).The objective of the present project was the determination of the dose received by patients during diagnostic coronary angiography (CA) and during cardiac resynchronization devises implantation in order to introduce local dose reference levels. Dose survey was performed during CA on 5900 patients since 2001, and on 955 patients since 2006 during cardiac resynchronization devises implantation. For the dose measurement a suitably calibrated dose-area product (DAP) meter was used. Mean value of DAP during CA was 50.01 Gycm^2 and 14.87 Gycm^2 during cardiac resynchronization devises implantation. The contribution of cinefluoro-graphy to the total DAP was 67.25% of the total DAP during CA. The mean duration of fluoroscopy during cardiac resynchronization devises implantation was 4.4 min. Mean values of effective dose equal to 10.1 mSv, for CA and 3 mSv for cardiac resynchronization devises implantation, were calculated applying conversation factors. A local DRLs was choosen to be 57.80 Gycm^2 for CA and 19.4 Gycm^2 for cardiac resynchronization devises implantation. A triggering level of 300 Gycm^2 is introduced, in order to avoid any possible injury.**

The results of the present study, due to the large number of the sample, can be used in for the establishment of national or international DRLs

Keywords— **Coronary angiography, Pacemaker, DRLs, Effective dose.**

I. Introduction

The largest man-made source of population dose from ionizing radiation is diagnostic radiology. The growing use of interventional radiology (IR) procedures combined with the fact that these procedures generally require prolonged fluoroscopy time and multiple X ray exposures, contribute to high doses and their associated risks. Interventional radiology procedures in cardiology include, among others, cardiac angiography (CA), as well as insertion of cardiac resynchronization devices. It is important to monitor patient doses from radiological procedures since a) the fluoroscopy time that the patient is irradiated can be long, b) the number of the acquired images can be high. The effect of the above is that the dose, both to the patient and the personnel can be relatively high. However, if practice and protection are optimized, the doses will be as low as is compatible with the medical purpose. The International Commission on Radiological Protection (ICRP) has recommended the use of reference dose levels (DRLs) in diagnostic radiology [1]. It has also proposed that DRLs should be the result of optimization in radiation protection and should be used as an aid to keeping doses as low as reasonably achievable [2]. Moreover the Euratom directive 97/43 [3], recommends the use of patient dose surveys and the proposal that all radiology departments have a legal obligation to promote and use the DRLs.

Two approaches to patient dose measurements are: (a) the measurement of dose on the patient's skin or organ doses using thermoluminescent dosemeters (TLDs), and (b) the measurement of the dose-area product (DAP). The DAP meter technique is the most reliable measurement technique for dynamic examinations such as fluoroscopy in which the projection direction and technique parameters are continually varying but also because it can give a real time reading.

The dose measurement is used for estimating the radiation risk. Thus, it is desirable to use a dose quantity that relates closely to the radiation risks associated with X-ray examinations. The effective dose is a suitable quantity and it is of great value in characterizing patient doses.

This study is intends to evaluate, the effective dose to the patient during CA and during insertion of cardiac resynchronization devices at Haemodynamic Laboratory, University Hospital of Larissa (UHL), Greece. Additionally, it is aimed to estimate the risk of the radiation dose, compare the obtained results with the results quoted in literature and finally to propose a local DRL for this investigation.

II. materials and methods

Since October 2001, dose measurement was performed during 4950 CA examinations, and since March 2006 the DAP meter value was recorded during 955 insertions of cardiac resynchronization devices. The selection was random and without any additional criteria. All the CA examinations were performed by the femoral access.

All the procedures were performed using a Philips Integris H 3000 C-arm x-ray unit with an undercouch tube/overcouch image intensifier configuration using filtration (HVL) of 3 mm Al. Quality assurance measurements were periodically performed, according to the national protocols, to ensure proper operation of the unit.

The DAP meter was built-in to the x-ray system and it was calibrated in situ. The calibration was done having a proper phantom and the beam was always intercepted with

O. Dössel and W.C. Schlegel (Eds.): WC 2009, IFMBE Proceedings 25/III, pp. 262–264, 2009.
www.springerlink.com

the table. The correction factor that was obtained was 0.9454. The overall uncertainty of DAP reading was estimated to be 8%.

For each patient all the exposure parameters total DAP value ($Gycm^2$), DAP value due to fluoroscopy, DAP value due to digital cine, fluoroscopy duration but also patient data (age, weight, height) were recorded.

Images were acquired at 12,5 frames/sec and only when it was necessary a frame rate of 25 frames/sec was used.

The total DAP value was used to calculate the effective dose. Estimation of the effective dose was done by the use of conversion factors. Such factors have been calculated to range between 0.183 and 0.220 mSv Gy^{-1} cm^{-2} for the thoracic region [4,5,6,7].

The risk of fatal cancer for patients life has been proposed by the International Commission on Radiological Protection (ICRP) [8] to be a value of $5.5x10^{-2}$ Sv^{-1} for the whole population and $4.1x5x10^{-2}$ Sv^{-1} for adults.

III. Results

Dose monitoring was performed during CA examinations, and during insertions of cardiac resynchronization devices. For patients monitored during CA, the mean age of the patients was 63.62 years, (range 7-98 years) and the mean height and weight were 167 cm and 79.12 kg respectively. For patients monitored during insertions of cardiac resynchronization devices, the mean age of the patients was 75.8 years, (range 14-95 years). The mean total DAP value during CA was 50.01 $Gycm^2$ (range 4.1-621.6). The mean DAP value due to fluoroscopy was 18.6 $Gycm^2$ (range 0.2-289.8), and the mean DAP value due to digital cine was 31.43 (range 1.4-412.3). The mean time of fluoroscopy during insertions of cardiac resynchronization devices was 4.4 minutes (range 0.1-40.5). The mean DAP value during insertions was 14.87 $Gycm^2$ (range 0.1-96.5). The effective dose was calculated to be equal to 10.1 mSv during CA and 3 mSv during insertions of cardiac resynchronization devices. The risk of fatal cancer for patients life was calculated to be equal to $5.54x10^{-4}$ and $1.65x10^{-4}$ for the two above mentioned examinations.

IV. Discussion

The values of DAP, 50.01 $Gycm^2$, during CA, is comparable to those referred by other authors. Betsou et al. [6] reported the mean value of DAP to be 30.4 $Cycm^2$. Bahreyni Toossi et al. [7] reported mean values for DAP 32.47 $Cycm^2$, which is almost the same with Betsou [6]. Clark et al. [9] report the mean value of DAP to be even fewer, around 20.3 $Cycm^2$. However many authors have reported bigger mean DAP value. Vano et al. [10] reported mean DAP value 66.5 $Gycm^2$, Bakalyar et al. [11] reported 95.2 $Gycm^2$, Cusma et al. [12] reported 74.4 $Gycm^2$, and van de Putte [13] reported 106.3 $Gycm^2$. Kuon et al. [14], calculated the mean value of DAP during CA from various authors and find it to be around 55.9 $Gycm^2$.

During insertions of cardiac resynchronization devices the fluoroscopy duration was 4.4 minutes and the mean DAP value was 14.87 $Gycm^2$. Trianni et al. [15] reported DAP value during pacemaker insertion 4.5 $Gycm^2$ and mean duration of fluoroscopy 3.8 minutes. Perisinakis et al. [16] reported the DAP value and time of fluoroscopy during cardiac resynchronization device implantation and convetional rhythm device implantation. The values were 47.65 $Gycm^2$, 11.06 $Gycm^2$ and 35.2 minutes and 8.2 minutes respectively.

Dragusin et al. [17] despite the small sample size, proposed local DRLs for CA to be the DAP value of 40 $Gycm^2$. Neofotistou et al. [18], collected data from six European countries and from a total sample size of 600 persons proposed preliminary DRLs. The RL for CA was for DAP, 57 $Gycm^2$, 6 min and 1270 frames.

To our knowledge no DRLs have been proposed for the procedure of insertions of cardiac resynchronization devices.

The effective dose to the patient during the two aforementioned procedures, can be obtained by multiplying the mean value of DAP with appropriate conversion factors [4,5,6,7] we can approach the effective dose to the patient during those two procedures. The conversion factors have been calculated to range between 0.183 and 0.220 mSv Gy^{-1} cm^{-2} for the thoracic region [4,5,6,7]. By application of the mean value of the factor, to the mean value of DAP we calculate the effective dose during CA to be equal to 10.1 mSv (range 9.1-11,0 mSv) and 3 mSv (range 2.7-3.2 mSv) during insertions of cardiac resynchronization devices.

Due to the large sample size we can propose DRLs for those two specific examinations in means of DAP value, that corresponds to 75 percentile of the values.

For CA the proposed RL is 57.8 $Gycm^2$, and during insertions of cardiac resynchronization devices 19.4 $Gycm^2$.

V. conclusions

A dose survey resulting from CA and insertions of cardiac resynchronization devices was carried out. The mean effective dose was calculated to be 10.1 mSv and 3 mSv respectively for CA and insertions of cardiac resynchronization devices. The lack of national or local DRLs in literature lead the research team to recommend a local DRL for DSA of the CA to be a DAP value of 57.8 $Gycm^2$ and 19.4 $Gycm^2$ for cardiac resynchronization devices. The differences on the doses may reflect technique variations among intervention lists, differences in training and the experience of cardiologist. Methods for minimizing dose include limitation of the number of images and decreasing fluoroscopy time whenever possible.

References

1. International Commission on Radiological Protection (1990). Recommendations of the International Commission on Radiological Protection. ICRP Publication 60. Pergamon Press, Oxford
2. International Commission on Radiological Protection (1996). Radiological protection and safety in medicine, ICRP Publication 73.Pergamon Press, Oxford
3. Council Directive 97/43/Euratom (1997). Health protection of individuals against the dangers of ionizing radiation in relation to medical exposure, and repealing Directive 84/466/Euratom. The European Commission.
4. Hart D, Jones DG, Wall BF. (1994) Normalised organ doses for medical X-ray examinations calculated using Monte Carlo Techniques. NRPB report NRPB-SR 262. HMSO, London.
5. KC Leung and CJ Martin (1996). Effective doses for coronary angiography. Br J Radiol 69:426-431.
6. S Betsou, EP Efstathopoulos, D Katritsis et al. (1998) Patient radiation doses during cardiac catheterization procedures. Br J Radiol 71: 634-639.
7. M. T. Bahreyni Toossi, H. Zare, S. Bayani et al. (2008) Organ and effective doses of patients arising from coronary angiography and percutaneous transluminal coronary angioplasty at two hospitals in Mashhad-Iran. Radiat Prot Dosim. 128(3):363-366.
8. International Commission on Radiological Protection (2007), Recommendations of the ICRP. ICRP Publication 103, Ann. ICRP 37 (2–4).
9. Clark AL, Brennan AG, Robertson LJ et al. (2000) Factors affecting patient radiation exposure during routine coronary angiography in a tertiary referral centre. Br J Radiol 73:184–189.
10. Vano E, Gonzalez L, Fernandez JM et al. (1995) Patient dose values in interventional radiology. Br J Radiol 68:1215– 1220.
11. Bakalyar DM, Castellani MD, Safian RD (1997) Radiation exposure to patients undergoing diagnostic and interventional cardiac catheterization procedures. Cathet Cardiovasc Diagn 42:121–125.
12. Cusma JT, Bell MR, Wondrow MA et al. (1999) Real-time measurement of radiation exposure to patients during diagnostic coronary angiography and percutaneous interventional procedures. J Am Coll Cardiol 33:427–435.
13. Van de Putte S, Verhaegen F, Taeymans Y et al. (2000) Correlation of patient skin doses in cardiac interventional radiology with dose-area product. Br J Radiol 73:504–513.
14. Eberhard Kuon, Christian Dorn, Moritz Schmitt et al. (2003) Radiation dose reduction in invasive cardiology by restriction to adequate instead of optimized picture quality. Health Phys. 84(5):626–631
15. A. Trianni, G. Chizzola, H. Toh et al. (2005) Patient skin dosimetry in haemodynamic and electrophysiology interventional cardiology. Radiat Prot Dosim 117:241–246.
16. Kostas Perisinakis, Nicholas Theocharopoulos, John Damilakis et al. (2005) Fluoroscopically Guided Implantation of Modern Cardiac Resynchronization Devices Radiation Burden to the Patient and Associated Risks. J Am Coll Cardiol DOI 10.1016/j.jacc.2005.01.070.
17. O. Dragusin, W. Desmet, H. Heidbuchel et al. (2005) Radiation dose levels during intervenional cardiology procedures in a tertiary care hospital. Radiat Prot Dosim 117:231–235.
18. Neofotistou V, Vano E, Padovani R et al. (2003) Preliminary reference levels in interventional cardiology. Eur Rad 13(10):2259-63.

Protection of Human Health and the Environment by Means of Predisposal Management of Medical Solid Radioactive Waste

A.P. Stefanoyiannis[1], I. Gerogiannis[2], S. Christofides[2], G. Koutroumpis[3], X. Geronikola-Trapali[1], S.N. Chatziioannou[1], A. Bakas[3], I. Armeniakos[1], A. Prentakis[1], and S. Bakalis[1]

[1]2nd Department of Radiology, Nuclear Medicine Division, University General Hospital of Athens "Attikon", Athens, Greece
[2]Department of Medical Physics, Nicosia General Hospital, Nicosia, Cyprus
[3]Department of Radiology, Highest Technological Educational Institution of Athens, Athens, Greece

Abstract— **Aim: A radioactive waste management programme is a well-established practice in clinical departments that utilize radioactivity for both diagnostic and therapeutic purposes. Such a programme must ensure the effective organization of all activities relating to radioactive waste management, the presence of internal procedures and the maintenance of records, in order to assure full compliance with radiation protection and safety requirements. A study was carried out to determine whether certain quantitative parameters describing medical radioactive waste are correlated with the level of training and experience of the operating personnel. Materials and methods: Data collected concerned medical radioactive waste generated during the first 48 months of operation of the Department of Nuclear Medicine, University General Hospital of Athens "Attikon". It was examined whether a correlation exists between released (A_r, in Bq) and utilized activity (A_u, in mCi), between released waste mass (m_r, in gr) and A_u, as well as between the ratio (A_r/A_u, in Bq/mCi) and time (t, in months). All parameters were calculated separately for short-lived (e.g. Tc-99m) and long-lived (e.g. Tl-201, Ga-67) γ-emitting isotopes. Results: The existence of correlation was examined by means of ANOVA. With respect to (A_r) vs (A_u), it was showed that there is a statistically significant increase of A_r with A_u for short-lived isotopes, whereas no correlation exists for long-lived isotopes. As far as (m_r) vs (A_u) is concerned, no correlation exists for both types of isotopes. Finally, no trend was observed in (A_r/A_u) vs (t) for short-lived isotopes, while for long-lived isotopes the relationship is that of a statistically significant decrease. Discussion: Good operating practice reduced significantly the value of A_r/A_u for long-lived isotopes. Additionally, there was no increase of m_r with time for both types of isotopes. In this way, both environmental risk and financial burden for our hospital were reduced.**

Keywords— **solid radioactive waste, statistical evaluation.**

I. Introduction

Modern Medicine is based on a plethora of diagnostic tools, for the prompt and reliable diagnosis of various diseases. Nuclear Medicine scans are among the foremost diagnostic procedures. Carrying out these scans is based on the selective concentration of special radioactive substances in organs under study. These substances are called radiopharmaceuticals and are delivered to the patients either through ingestion or intravenously. Additionally, utilization of radioactivity in clinical environment for therapeutic purposes is very common, with typical example the administration of high-dose I-131 for thyroid cancer therapy.

Clinical utilization of radioactivity for both diagnosis and therapy demands, apart from other measures for radiation protection of both patients and the personnel, special care for the minimization and optimum management of the produced radioactive waste [1]. Good operating practice assures significant benefits in multiple levels, such as:

- Minimization of radiation burden for the operating personnel.
- Minimization of radiation burden for the environment, taking into account the presence of an annual dose limitation for the members of the public of 300 μSv, deriving from any single facility.
- Minimization of the hospitals' financial burden, for radioactive waste management in disposal facilities.

The establishment of medical radioactive waste management systems is based on national and international legislation, as well as the guidelines of International Atomic Energy Agency (IAEA) [2-4]. Nevertheless, the presence of significant inter-hospital differences with respect to the level of released radioactive waste is possible, due to the inhomogeneity of practices. This fact can be attributed to the inhomogeneity of hospital interim storage space and equipment, the possibility of different levels of workload, as well as possible differences-even in an intra-hospital level-of the level of training and experience of the operating personnel.

The aim of the present study is the examination of possible correlation between the level of released solid radioactive waste and the level of training and experience of the operating personnel, on the basis of statistical evaluation of appropriate quantitative indicators.

O. Dössel and W.C. Schlegel (Eds.): WC 2009, IFMBE Proceedings 25/III, pp. 265–268, 2009.
www.springerlink.com

Table 1 Quantitative parameters examined

Parameter	Short-lived	Long-lived
Utilized activity (Au)	✓	✓
Released activity (Ar)	✓	✓
Released mass (mr)	✓	✓

Table 2 Correlation controls

Correlation control	Short-lived	Long-lived
(Ar) vs (Au)	✓	✓
(mr) vs (Au)	✓	✓
(Ar/Au) vs (t)	✓	✓

II. Materials and Methods

The study was based on data generated in the Department of Nuclear Medicine, University General Hospital of Athens "Attikon". The specific lab was considered as suitable for several reasons:

- It offered the possibility to study the internal procedures of radioactive waste management during the beginning of its operation, which is relatively recent (December 2003).
- During the beginning of its operation, the majority of the personnel had little or no professional experience in a Nuclear Medicine lab.
- The paramenter of interim storage space and equipment remained constant in the course of time.

Suitable parameters of radioactive waste management were selected from the records maintained, in the framework of the Quality Assurance Program carried out in the Department [5]. Afterwards, data were classified and subsequently analyzed, by means of appropriate statistical tests, in order to check for the presence of possible correlations.

Specifically, data utilized concerned medical solid radioactive waste, generated during the first 48 months of operation of the Department of Nuclear Medicine, University General Hospital of Athens "Attikon". The quantitative parameters under study, as well as the correlation controls, are presented in Tables 1 and 2, respectively. The parameters of released activity (A_r, in Bq), utilized activity (A_u, in mCi) and released waste mass (m_r, in gr) were exploited. It was examined whether a correlation exists between A_r and A_u, m_r and A_u, as well as between the ratio A_r/A_u (in Bq/mCi) and time t (in months). All parameters were calculated separately for short-lived (e.g. Tc-99m) and long-lived (e.g. Tl-201, Ga-67) γ-emitting isotopes. The study was based on the assumption that released radioactive waste of short-lived isotopes of a specific month is generated by radioactivity utilized during the same month, taking into account the small value of half-life time of these isotopes. On the same ground, it was assumed that released radioactive waste of long-lived isotopes of a specific month is generated by radioactivity utilized during the previous month.

Table 3 Results of statistical evaluation

Correlation Control	Short-lived Isotopes	Long-lived Isotopes
(Ar) vs (Au)	SS increase Ar=-44.8921 +0.48816Au	SNS
(mr) vs (Au)	SNS	SNS
(Ar/Au) vs (t)	SNS	SS decrease Ar/Au=48.5261-1.06918t

III. Results

The temporal variation of the quantitative parameters under study is depicted in the diagrams of Figures 1-6, whereas the results of statistical evaluation are presented in Table 3. A preliminary study of all data (calculation of skewness parameter) proved the normality of all populations, therefore the ANalysis Of VAriance (ANOVA) statistical test was considered to be suitable for further statistical evaluation.

With respect to the variation of Ar with Au for short-lived isotopes (Figure 1), a statistically significant (SS) increase is noticed ($p<0.05$). This fact demonstrates that, as the number of examinations and therefore Au increases in the course of time, Ar also increases. This can be attributed to the small value of half-life time of these isotopes, which restricts the measures that can be practically taken to reduce the level of the corresponding radioactive waste.

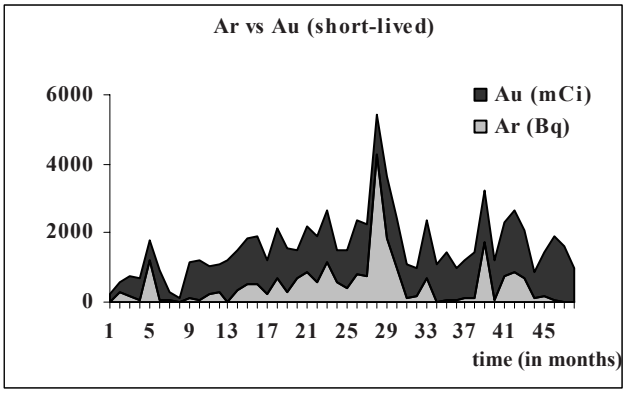

Fig. 1 Variation of Ar with Au for short-lived isotopes

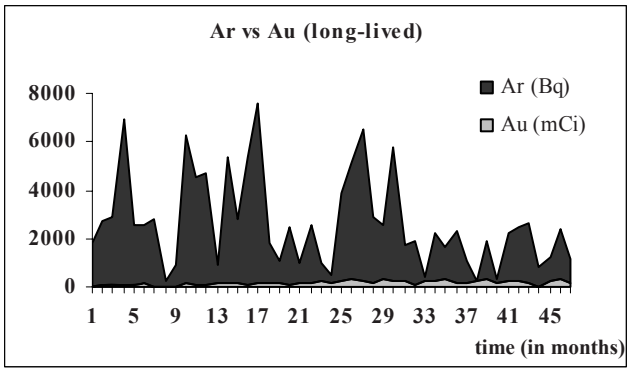

Fig. 2 Variation of Ar with Au for long-lived isotopes

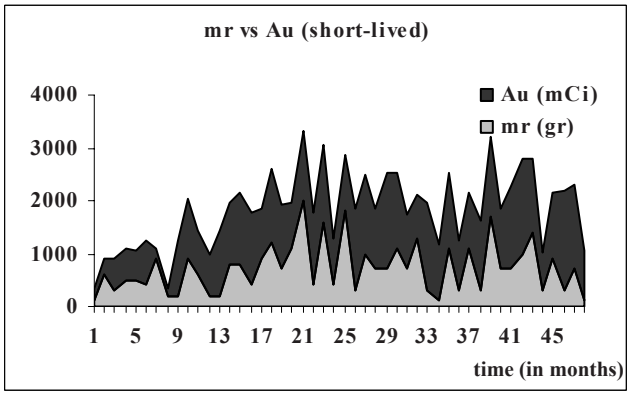

Fig. 3 Variation of mr with Au for short-lived isotopes

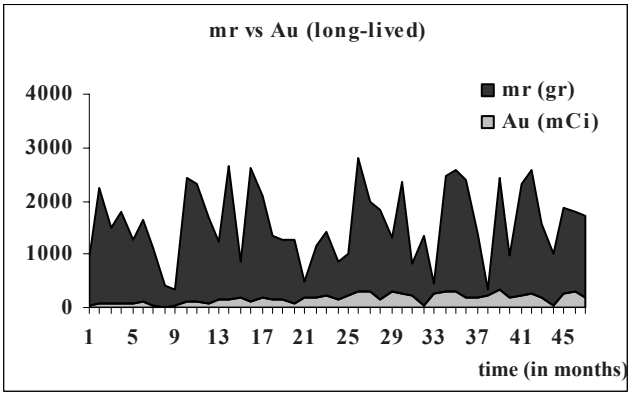

Fig. 4 Variation of mr with Au for long-lived isotopes

The results of the variation of Ar with Au for long-lived isotopes are more encouraging (Figure 2). A statistically non-significant variation is noticed (SNS, $p>0.05$). Although Au increases with time, a respective increase in the level of Ar does not take place. This can be attributed to the temporal improvement of radioactive waste management practices of long-lived isotopes adopted by the operating personnel.

The results of statistical evaluation are also positive with respect to the variation of mr with Au, for short-lived (Figure 3), as well as long-lived (Figure 4) isotopes. In both cases, the variation is found to be SNS. This fact demonstrates that the increase in the value of Au in the course of time is not followed by a similar increase in the value of mr for both types of isotopes, therefore the improvement in the level of training and experience of the operating personnel led to an improved management, with respect to the mass of the released waste.

A study of the temporal variation of the ratio Ar/Au for short-lived isotopes (Figure 5) shows that it is SNS. In accordance with the explanation of the variation of Ar with Au for short-lived isotopes, this can be attributed to the corresponding small value of half-life time, which restricts the possibilities of improvement of the initial practice.

On the contrary, in the case of the temporal variation of the ratio Ar/Au for short-lived isotopes (Figure 6), the reduction is found to be SS. This result is encouraging and offers an additional quantitative proof of improved long-lived radioactive waste management in the course of time.

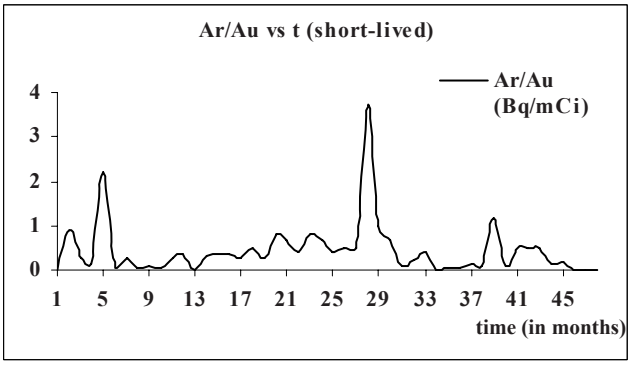

Fig. 5 Temporal variation of Ar/Au for short-lived isotopes

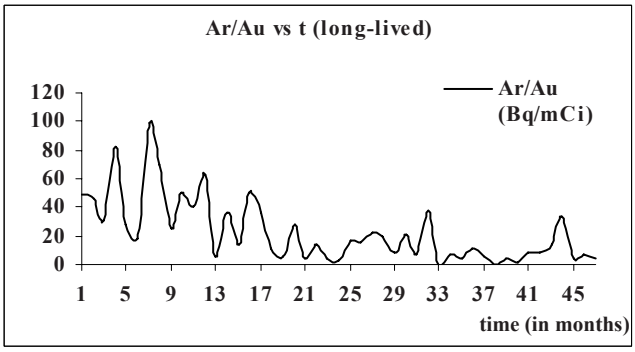

Fig. 6 Temporal variation of Ar/Au for long-lived isotopes

IV. Discussion

The present study proved quantitatively the presence of an improvement, with respect to the in-hospital solid radioactive waste management at the Department of Nuclear Medicine, University General Hospital of Athens "Attikon". Adequate training and experience of the operating personnel resulted in the development of radiation safety culture, especially concerning activities related to the production and management of radioactive waste. Good operating practice was beneficial, resulting in a significant reduction of the ratio A_r/A_u for long-lived isotopes. Additionally, m_r did not increase with time for both types of isotopes. In this way, both environmental risk and financial burden for our hospital were reduced.

As an open issue of this study, we mention the generation of additional quantitative parameters for our hospital, in order to further confirm our results. Furthermore, it would be useful to derive similar parameters for other hospitals, under a similar Quality Assurance Program. This would enable a comparative evaluation, as a basic optimization tool of regional practices.

References

1. Sundell-Bergman S, de la Cruz I, Avila R et al. (2008) A new approach to assessment of the impact from medical liquid radioactive waste. J Env Radioactivity 99: 1572-1577.
2. INTERNATIONAL ATOMIC ENERGY AGENCY. (2005) Management of waste from the use of radioactive material in Medicine, Industry, Agriculture, Research and Education. IAEA Safety Guide No. WS-G-2.7.
3. INTERNATIONAL ATOMIC ENERGY AGENCY. (2006) Storage of radioactive waste. IAEA Safety Guide No. WS-G-6.1.
4. Balonov M, Linsley G, Louvat D et al. (2005) The IAEA standards for the radioactive discharge control: present status and future development. Radioprotection suppl. 1, 40: S721-S726.
5. Stefanoyiannis A P, Geronikola-Trapali X, Armeniakos I et al. (2008) Level of released medical radioactive waste versus level of training and experience of the operating personnel: is there a correlation? Eur J Nucl Med Mol Imaging suppl. 2, 35: S210.

Author: Stelios Christofides
Institute: Nicosia General Hospital
Street: Old Road Nicosia-Limassol
City: Nicosia
Country: Cyprus
Email: cstelios@cytanet.com.cy

The Effect of Activated Water on Staphylococcal Infection *in Vivo* in Animal Model and *in Vitro* on Staphylococcus Aureus Culture

Vladimir I.Vysotskii[1], Lydia S.Kholodna[2] and Alla A.Kornilova[3]

Kiev National Shevchenko University, Radiophysical[1] and Biological[2] Departments, Kiev, Ukraine
[3]Moscow State University, Moscow, Russia

Abstract— **The results of detail investigation of the effect of water, activated by special nonionizing Molecular Resonance Effect Technology (MRET water), on staphylococcal infection is presented. Investigated activator is the stationary source of low-frequency resonant magnetic field with composite space structure and very weak amplitude (about 1 Oersted).**

The investigation of the effect of MRET activated water was conducted in two steps: the evaluation of the immune-stimulatory effect following the ingestion of MRET water on the immune-competent cells in the model of mice infected with *Staphylococcus aureus Wood-46* (*in vivo*) and the evaluation of the inhibition of growth of *Staphylococcus aureus Wood-46* culture in MRET activated nutrient mediums (*in vitro*).

MRET activation of the water based nutrient medium with suspended staphylococcal culture leads to the origination of the high bacteriostatic activity of such nutrient medium which depends on the time duration of activation and the initial concentration of culture cells. The bacteriostatic activity increases following the increase of time of activation (the times of activation up to 60 minutes were studied). The efficacy of bacteriostatic activity increases following the decrease of initial concentration of the suspension of staphylococcal culture

Keywords—**Activated Water, Staphylococcal Infection, Prophylactic Treatment, Therapeutic Treatment, Bacteriostatic Activity.**

1. PHYSICAL-MOLECULAR PROPERTIES OF MRET ACTIVATED WATER

In the work the results of detail investigation of the effect of water, activated by special nonionizing Molecular Resonance Effect Technology on staphylococcal infection is presented. The results of action of the same activated water on prophylaxis and treatment of two kind of oncology and on metabolic activity and growth of conditionally pathogenic *Escherichia coli K-12* microbiological culture were presented in [1,2].

Investigated activator of water is the stationary source of low-frequency resonant magnetic field with composite space structure and very weak amplitude (about 1 *Oersted*).

It was discovered in our detailed physical experiments that under the action of this irradiation there are very essential modifications of the basic physical-molecular properties of distilled water.

Of a great interest is the dependence of the viscosity coefficient on the applied mechanical stress for water being at a temperature of 36.6^0 C. In this case, we carried out the more detailed studies with regard for the influence of the water activation duration.

In Fig. 1, we present the results of studies of the viscosity coefficient for initial distillated nonactivated water and for the samples of water which were obtained for the duration of activation of 15, 30, 45, and 60 min and were at a temperature of 36.6^0C in the process of measurement. With regard for the fact that the anomalous properties of activated water relax rapidly with increase of the temperature, the measurements were carried out at once after the activation of water. It is seen from the obtained data that an increase of the water activation duration leads to a very significant decrease of the viscosity coefficient in the region of small mechanical stresses at this temperature (relative to the initial nonactivated water).

It was discovered also that influence of MRET activation on properties of distilled water very strongly depends on duration of activation. E.g., at very low velocity of motion of investigated activated water (tension less than 0.01 Pa) viscosity of water, activated during 60 min, decrease by 100 times at 20^0 C in relation to nonactivated water. Minimal viscosity at such temperature will be for water activated during 30 min. In this case viscosity decrease by 300 times!

These results are presented on Fig.1

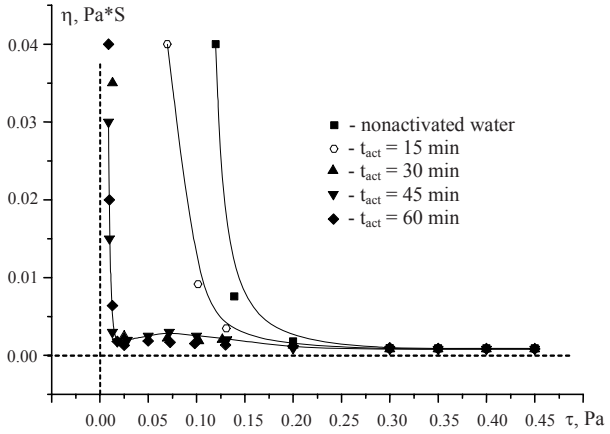

Fig.1. Influence of MRET activation on viscosity of distillated water at 36.6^0C .

It is necessary to note that the absolute values of the viscosities of nonactivated and activated water samples in the region of small mechanical stresses increase significantly with the temperature. For example, for the viscosity coefficient of nonactivated water equal to its minimum value $\eta \approx 0.7*10^{-3}$ Pa*s at 20^0C for $\tau \approx 0.015$ Pa, we determined at a temperature of 36.6^0 C for the same $\tau \approx 0.015$ Pa that $\eta \approx 5*10^{-3}$ Pa*s, which corresponds to the increase by 7 times. The close changes of the viscosity with increase of the temperature are also characteristic of activated water.

It is seen from Fig. 1 that a change (increase) of the duration of activation in the limits of 1 h leads to a monotonous displacement of the curve of the viscosity coefficient as a function of the applied mechanical stress to

O. Dössel and W.C. Schlegel (Eds.): WC 2009, IFMBE Proceedings 25/III, pp. 269–272, 2009.
www.springerlink.com

the side of less viscosities. The position of the minimum of the viscosity coefficient is also shifted with increase of the duration of activation from $\tau \approx 0.1$ Pa for the duration of activation of 30 min to $\tau \approx 0.05$-0.02 Pa for the duration of activation of 45-60 min.

Very important is the circumstance that the viscosity of activated water in the region of very small shear stresses at the vitally important temperature 36.6^0C, like the case of a lower temperature of 20^0 C, is by several orders less than that of ordinary (nonactivated) water.

The same strong influence of MRET activation on different electrical characteristics of activated water in the range of low frequencies was observed and presented on Fig.2.

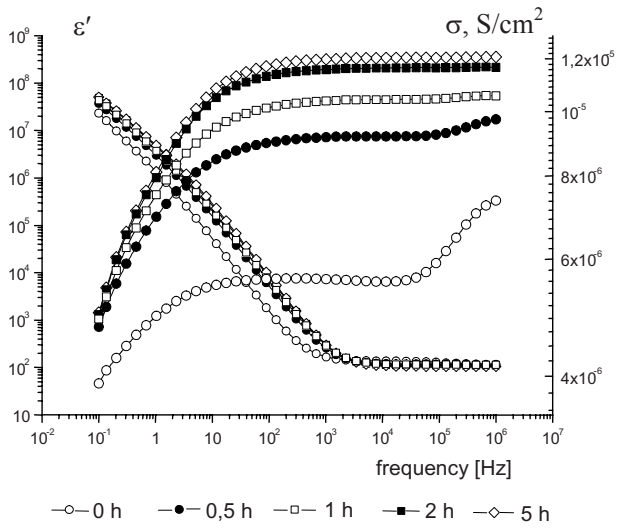

Fig.2. Influence of MRET activation on electrical conductivity (σ) and permittivity (ε′) of distillated water. Water was activated during 30 min and storage at 20 C during 0.5; 1, 2 and 5 hours.

It was discovered also that duration of internal storage of these abnormal characteristics of activated water equals several days or weeks at low temperature (close to 0^0 C). The problem and concrete mechanism of long time memory of activated water were studied earlier in [3,4].

11. FUNCTIONAL ACTIVITY OF CELLS OF THE IMMUNE SYSTEM OF MICE INFECTED WITH STAPHYLOCOCCAL CULTURE FOLLOWING PREVENTIVE CONSUMPTION OF MRET WATER

The investigation of the effect of MRET activated water on prophylaxis and treatment of staphylococcal infection was conducted in two steps: the evaluation of the immune-stimulatory effect following the ingestion of MRET water on the immune-competent cells in the model of mice infected with *Staphylococcus aureus* Wood-46 (*in vivo*) and the evaluation of the inhibition of growth of culture of *Staphylococcus aureus* Wood-46 in MRET activated nutrient mediums (*in vitro*). The *Staphylococcus aureus* Wood-46 culture was received from the Czechoslovak collection of microorganisms.

The 400 male mice of line BALB in the age of 11 – 13 weeks and of the weight 18 – 21 grams were used in the study *in vivo*. After preliminary experiments on the persistence of pathogen in homogenate of kidneys of mice conducted on five groups of mice (45 animals per each group) the optimal 30 minutes time of MRET water activation was chosen for the main line of the investigation. The main line of experiments was conducted on three groups of mice with 50 animals in each group and the following strategy of examinations was applied.

Prior to the inoculation of *Staphylococcus aureus* Wood-46 culture one group of mice (Group #1) consumed MRET activated distilled water during 4 weeks, another group (Group #2) consumed MRET water during 2 weeks, the control group consumed non-activated ordinary distilled water. During the following 2 weeks of experiment the first two groups continued to consume MRET water and the control group consumed ordinary distilled water.

The main results are the following.

a) The consumption of MRET activated water significantly enhances the factors of natural resistance of the body which constitute the first line of protection of an organism against the penetration and reproduction of pathogenic microorganisms.

The analysis of data in the beginning of experiment leads to the conclusion that significant changes in all studied parameters of mice on MRET water (decrease of pathogen colonies in homogenate of kidneys, increase of the weight and the cellularity of lymphoid organs, intensification of the phagocytic and bactericidal activity of macrophages and neutraphils) begins only after 24 hours following the inoculation of *Staphylococcus* culture. Another words the consumption of MRET water increases the potentials of immune capacities of the body to counteract the infections without any changes in the vital parameters of immune organs and functions prior to the penetration of infectious pathogens in the body.

At the end of two weeks of experiment the mean values of studied parameters in both groups of mice on MRET water (preventive for 4 and 2 weeks respectively) significantly increased compare to the control group. The differences in mean values of the studied parameters of the groups of mice consuming MRET water compare to the control group of mice on non-activated water were statistically significant with $p<0.05$ (for most of the parameters). These results confirm the significant intensification of phagocytic activity and of immune system response following the consumption of MRET water.

The differences in mean values of studied parameters for the groups of mice on MRET water compare to each other were statistically insignificant, which confirms the similarity of the level of the beneficial effect of MRET water in both groups. This fact also confirms that the

regular consumption of MRET water provides health benefits in rather short period of time (2 weeks in case of the animal mice model).

b). During the infection period in both groups of mice on MRET water there was observed the significant increase of the cellularity (quantity of cells) and the weight of a spleen and lymph nodes as well as the insignificant increase of the cellularity and the weight of thymus. These results confirm the fact of the intensification of immune system response in animals on MRET water subject to *Staphylococcus* infection.

c). MRET water stimulated the phagocytic capacities of neutrophils of the peripheral blood and peritoneal macrophages. It increased their phagocytic activity (intensity of engulfing of alien microorganisms) and stimulated the hyper activation of their oxygen-dependent bactericidal activity, particularly the increase of quantity of NBT-positive phagocytes. These results confirm the increase of effective potentials of phagocytes, which constitute one of the main factors of natural protection of an organism against infections and are essential for the initiation of immune response.

d). The consumption of MRET water has significant bactericidal effect that was confirmed by substantial decrease of *Staphylococcus* CFU (colony forming units) in homogenate of kidneys of mice. The consumption of MRET water also reduced the death rate from 30% (control group) to 0% (MRET groups) during the first 9 days of experiment.

f). The development of the local acute inflammation was significantly inhibited in case of preventive consumption of MRET activated water by animals.

111. THE EFFECT OF NUTRIENT MEDIUM ACTIVATION ON THE GROWTH OF STAPHILOCOCCAL CULTURE

The second step of investigations was conducted *in vitro* based on the analysis of the growth of staphylococcal culture on meat-peptone agar (MPA) at a temperature of 37˚C during 18 – 24 hours with different initial concentrations of cells (from 10 to 10^9 cells/ml). The samples were treated with the help of MRET activator during different periods of time (in the range of 15 to 60 minutes) right after the introduction of staphylococcal culture to MPA.

These examinations are related to the study of the effect of MRET activation process on the process of growth and development of *Staphylococcus aureus* Wood-46 culture *in vitro* in nutrient medium. The bacterial cultures were grown on meat-pepton agar (MPA) with different initial concentration of culture cells. They were introduced to MPA in the form of suspensions and the nutrient medium with culture was MRET activated during the different periods of time (activation for 15 minutes, 30 minutes, 45 minutes, and 60 minutes respectively) following the requirements of sterility.

Petri dishes with the activated medium and culture were covered with glass caps (aerobic environment) and placed in the thermostat for cultivation at a temperature of 37^{o}C during 18-24 hours. After the cultivation the morphological and tinctorial properties of cultures were observed and the concentrations of colonies grown on MPA surface were calculated. Then the bacteriostatic activity of MRET activated nutrient medium was defined with the help of appropriate statistical calculations.

The Index of Bacteriostatic Activity (IBA) is defined as a coefficient of the inhibition of growth and reproduction of pathogens in bacteriostatic medium, particularly in MRET activated nutrient medium. It is calculated as reduction of the concentration of colonies in MRET activated medium related to the control samples not exposed to the activation:

$$IBA = (N_{control} - N_{act})/N_{control}$$

where N – concentration of colonies calculated in control (non-activated) and MRET activated nutrient medium respectively.

In order to verify the sterility of experiments Petri dishes with nutrient medium (MPA) without staphylococcal culture were exposed to the process of activation and then were kept in the thermostat. No colonies of culture were observed that confirms the sterility of environment.

Following the investigation the direct correlations between the times of activation (t_{act}), the initial concentration of culture cells ($N_{0)}$ and the quantity of colonies grown on MRET activated medium were observed. The results are presented below in the form of a serie of photos of Petri dishes with the colonies grown on MPA surfaces and the following diagram based on the data of these experiments..

In the process of investigation the effect of MRET activation on the growth of staphylococcal culture at rather small initial concentration of culture cells was analyzed. The data corresponding to higher initial concentrations $N_0 > 10^3$ cells/ml were not analyzed due to the difficulties related to calculation of very high values of concentrations of colonies, despite the fact of the high bacteriostatic activity of MRET activated nutrient medium in case of high initial concentrations.

The highly significant bacteriostatic effect of 92 – 93% was observed after MRET activation for 30 minutes and more of cultures with initial concentration $N_0 = 10^3$ cells/ml (Fig 14) and of 70 – 90% with initial concentration of $N_0 = 10^2$ cells/ml. In case of cultures with low initial concentration $N_0 = 10$ cells/ml the bacteriostatic activity in 15 minutes activated nutrient medium exceeded 93% and in 30 minutes activated nutrient medium was observed 100% inhibition of staphylococcal colonies.

The last result confirms that the bacteriostatic effect of nutrient medium based on MRET activated water is caused by the effect of MRET water environment on each pathogenic cell. It is possible to assume that there is a zone of blocking bacteriostatic activity around each pathogenic cell (the germ of the future colony) where such activity is the most efficient. In case when such zones are not

overlapped the bacteriostatic activity of MRET activated medium is the most efficient.

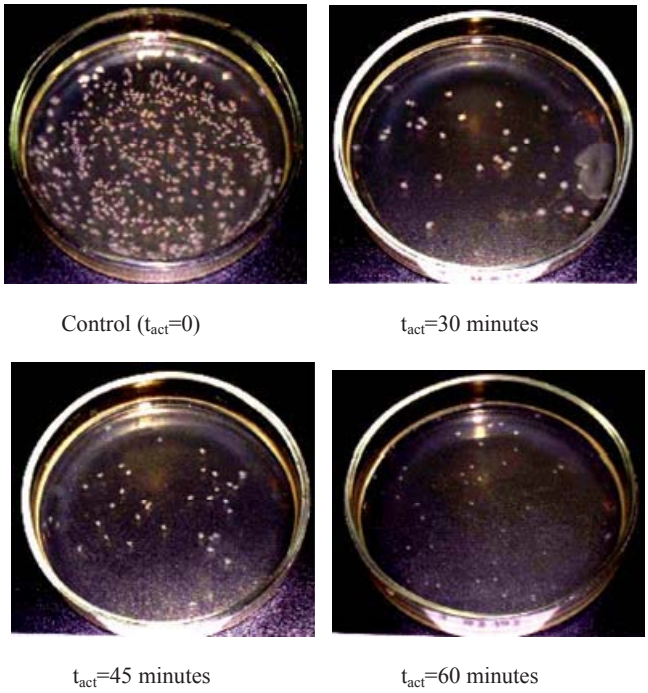

Fig. 3. The effect of time duration of MRET activation on the inhibition of growth of culture of *Staphylococcus aureus* Wood-46 with initial concentration of culture $N_0=10^3$ cells/ml. Duration of cultivation at 37°C was 24 hours.

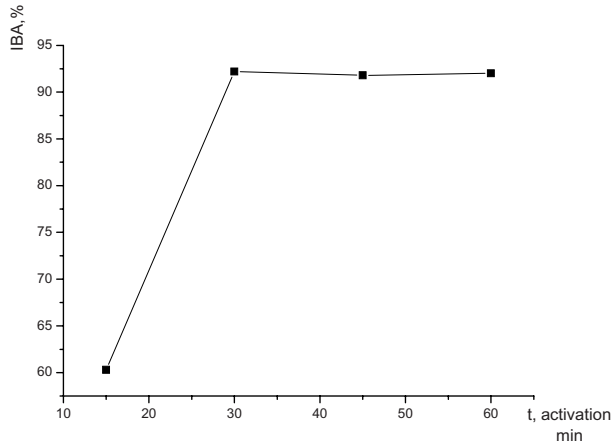

Fig 4: The effect of time duration of MRET activation on the inhibition of growth of culture of Staphylococcus aureus Wood-46 with initial concentration $N_0 = 10^3$ cells/ml.

In case there are several colonies in such zone the bacteriostatic activity is less efficient. Such assumption can explain the dependence of the bacteriostatic effect of MRET water based medium on the initial concentration of pathogenic cells.

IV. CONCLUSIONS

MRET activation of the water based nutrient medium with suspended staphylococcal culture leads to the origination of the high bacteriostatic activity of such nutrient medium which depends on the time duration of activation and the initial concentration of culture cells.

The bacteriostatic activity increases following the increase of time of activation (the times of activation up to 60 minutes were studied).

The efficacy of bacteriostatic activity increases following the decrease of initial concentration of the suspension of staphylococcal culture. The process of MRET activation is most effective on culture suspensions with the concentration not more than 10^3 cells/ml.

The results of the second part of investigation provide the evidence regarding the high efficacy of MRET activation on the inhibition of growth of colonies and reproduction of staphylococcal microorganisms *in vitro*.

The results of complex experimental and theoretical studies of the characteristics of activated water (e.g. mechanical, electrodynamics, optical, and other characteristics of activated water; theoretical analysis of a possible mechanism of the water memory and methods of its stimulation; influence of this water on higher plants sterile plants, and callus tissues; experiments on the influence of activated water on "pure" microbiological cultures and their natural associations; the results of studies of the use of activated water in the prophylaxis and treatment of oncologic tumors; possible biophysical molecular mechanisms of the direct influence of activated water on biological objects) are presented in the book [5].

ACKNOWLEDGMENT

The present work was conducted through a support from DBA Global Quantech Inc., San Marcos, CA, USA.

REFERENCES

1. Vysotskii V.I., Olishevsky S., Yanish Yu.V. A.B., Kornilova A.A. (2006) (IFMBE Proceedings, v. 14, p. 1788 - 1791,
2. Vysotskii V.I., Tashyrev A.B., Tashyreva A.B., Kornilova A.A. (2006) (IFMBE Proceedings, v. 14, p. 3093 - 3096,
3. Vysotskii V.I., Kornilova A.A. (2004). Physical foundation of long-time water memory, Moscow University Physics Bulletin, v.59, no.3, p.58-62.
4. Vysotskii V.I., Smirnov I.V., Kornilova A.A. Introduction to the Biophysics of Activated Water, Universal Publishiers, USA, 2005.
5. Vysotskii V.I., Kornilova A.A., Smirnov I.V. Applied Biophysics of Activated Water: the physical properties, biological effects and medical applications of MRET activated water, World Scientific Publishing, 2009.

Address of the corresponding author:
Prof. Vladimir Vysotskii,
Kiev National Shevchenko University., Radiophysical Faculty,
Vladimirskaya St. 64, 01033, Kiev, UKRAINE

Evaluation of SAR in a Finite Element Human Body Model Imposed to Magnetic Fields Generated by a MRI Bird Cage Coil

Sylvia Smajic-Peimann and Waldemar Zylka

Medical Physics Research Laboratory
Department of Physical Engineering, University of Applied Sciences Gelsenkirchen
Neidenburgerstr. 43, 45877 Gelsenkirchen, Germany

Abstract— **There has been increasing public concern about the adverse health effects of human exposure to electromagnetic (EM) waves in magnetic resonance imaging (MRI). The safety recommendations given in a number of general publications on EM radiation include the maximum permissible whole-body specific absorption rates (SAR). In this paper theoretical analysis indicates other factors that may have an even higher impact on the potential heating of tissue, e.g. in the vicinity of implanted devices.**

A new finite element human body at millimeter resolution has been used to estimate local SAR in MRI scanners. The radio frequency (RF) transmitter coil has been modelled to provide circular polarized B_1 field and E-field components based on tuned electrical circuits and on physical locations and values of the discrete capacitors distributed throughout the RF transmitter coil.

SAR values are calculated for all tissue types included in the human body model. The results presented at the surface of various organs SAR distribution are non-trivial functions of the irradiated frequency as well as the geometry, shape, homogeneity, and material properties of the tissue and organ under consideration. It has been found that the flexibility of grid sizing in finite elements calculations leads to an order of magnitude in time savings compared to FDTD algorithms used in other studies.

Keywords— **multi-physics modeling, magnetic resonance imaging, MRI, specific absorption rate, SAR, human body, finite element, RF, transmit coil, bird cage**

I. Introduction

According to the safety guidelines of the ICNIRP (International Commission on Non-Ionizing Radiation Protection) (1998) [1] and the IEEE standard (2006) [2], the whole-body-averaged specific absorption rate (WBSAR) is used as a metric of basic restriction for RF whole-body exposures. The basic restriction of the WBSAR is 0.4 Wkg^{-1} for occupational exposure or 0.08 Wkg^{-1} for public exposure.

SAR depends on the irradiated frequency. As the static magnetic field of MRI scanners, thus the frequency of operation, has been increasing over the years, the dimension of the RF components are becoming comparable to the wave length of the electromagnetic waves. Birdcage resonators are extensively used in MRI systems since they introduce a high SNR and a high homogeneity of RF magnetic field. In this contribution we apply a new highly efficient approach to design coils at arbitrary frequency, i.e. B_0, operating as high-pass resonators which comprise electrical circuit and field calculators [3].

In computational dosimetry in the 1980s, human modeling was highly simplified e.g. to a spheroid or a homogeneous block model. In recent years, with the development of computational resources, anatomically based human body voxel-models have been used for investigating the SAR using FDTD methods.

In the standards and guidelines, homogeneous and simple-shaped models have been used in order to determine the reference level or maximum permissible exposure against the basic restriction of the SAR. However, it is not clear that the SAR in the homogeneous and simple-shaped models could give a conservative estimate compared to that in anatomically based human models. In addition, such simplified models are in great demand for discussing the variability of

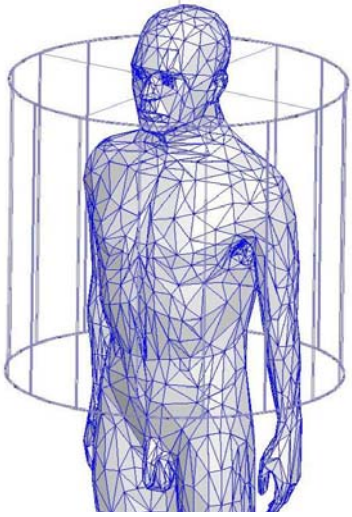

Fig. 1: A 16 rung RF coil operating as a high-pass resonator with finite element human body model inside. The capacitors locations are on the rings inbeteewn the ends of the rungs. The diameter and the height of the cylindrical coil are 60cm.

O. Dössel and W.C. Schlegel (Eds.): WC 2009, IFMBE Proceedings 25/III, pp. 273–276, 2009.
www.springerlink.com

the SAR, due to local effects of inhomogeneous organs and objects, e.g. implants.

In this contribution we present results based on two new model constituents shown in Fig. 1: A MRI RF transmit coil designed according to realistic dimensions and electrical properties of a MRI scanner. The coil is tuned, e.g. to 42,6MHz. Additionally, a finite element human body model is placed inside the designed MRI coil. To the knowledge of the authors, it is for the first time the finite element human body model is utilized to calculate local SAR values as output of finite element calculations.

II. Modelling and Calculation

Modeling and calculations were performed using electric and electromagnetic finite element tools. The electric simulator allows obtaining the complete frequency spectrum of the RF coil based on an electrical circuit scheme. These results are co-linked and transferred to an electromagnetic simulator calculating the relevant RF magnetic field pattern inside the coil.

As the static field B_0 pointing into the z-direction and the gradient field are not expected to induce deposition of energy, they have been neglected. In many publications, B_1 field is modelled as a circular-polarized wave approaching from infinity. In this paper, the transceiver coil was modelled as a birdcage coil operating as high-pass resonator at different frequencies, shown in Fig.1. The coil is driven in phase-optimized quadrature mode. The matching network has been build up with ports which define power sources. At two rungs feed port were created for electric sources having a phase difference of 90 degrees which was optimised to obtain the best circular polarized and homogeneous B_1 field within the volume of the coil.

The numerical investigation encompasses four steps: (1) development of electric circuits of the RF coil including matching network, (2) calculation of capacitors of the high-pass placed in the rings between the rungs, (3) the determination of frequency spectrum of the coil and (4) the calculation of electromagnetic and SAR fields giving a geometrical design, the electric circuit of the coil, and a human body model. While the electric circuit design (1)-(3) lacks any geometry of the coil, its output is forwarded to a full wave field simulator which in step (4) calculates of the distribution of electromagnetic fields based on geometry and shape..

The relevant output of the calculation was B_1 and E-fields, as well as spectrum and S parameters of the coil. The local SAR distribution was derived from this results using:

$$SAR = \sigma(\omega)E^2/(2\rho) \quad \text{with} \quad \sigma = \sigma_{bulk} + \omega\varepsilon_0\varepsilon_r \tan\delta\,.$$

The quantity tanδ is the dielectric loss tangent, i.e. the ratio of imaginary relative permittivity to the real relative permittivity, ε_0 and ε_r are the standard dielectric constants; σbulk describes impedance losses of the conductivity of the tissue. The symbol ρ describes the mass density and $\omega=2\pi f$ the frequency.

The corpus of the human body model and its organs placed inside the coil consists of more than 300 various organs with resolution at millimeter level. Mass density e.g. of muscle tissue is set to $\rho=1040$ kgm^{-3}. The mass of the body was set to m=70kg and the masses of organs of interest are chosen according to a standard body model, e.g. heart m_H=300g, lung m_L=4000g. Frequency dependent tissue dielectric parameters have been attributed to every par-

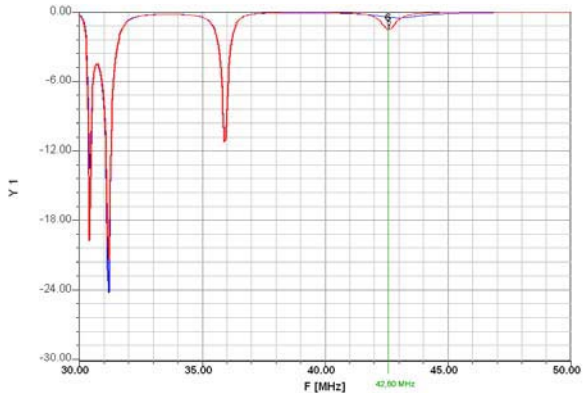

Fig. 2: Spectrum of a loaded coil. The desired frequency, f=42,6MHz mode, is marked green. Loaded with the human phantom model the coil has been tuned to the desired frequency of 42,6MHz by choosing an appropriate value of the discrete capacitor, i.e. C = 63,0pF.

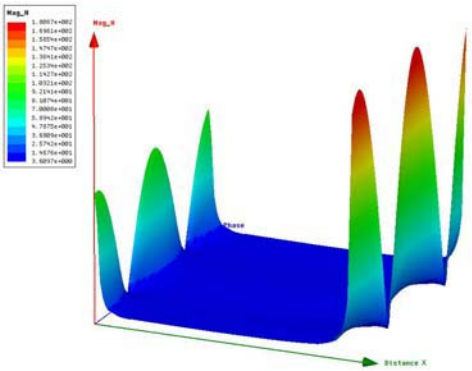

Fig. 3: B_1 field generated by the RF transmit coil model is zero along the x axis for all phases, as required.

ticular tissue type and all finite element cells [4]. SAR is calculated as an average over 10g of tissue.

Both, the numerical calculation of the spectra and a first approximation of the corresponding fields take only minutes. Also, the determination of the accurate electromagnetic fields requires only few minutes on a quad core processor 64GB RAM workstation. The inclusion of the human body model increases the number of tetrahedra to $3x10^5$, equivalent to 21GB memory. The calculation time rises to about six hours. The investigations of step (4) were done using HFSS while the electronic steps (1)-(3) were performed using Designer simulation software. Both packages are by Ansoft/Ansys, USA.

III. RESULTS AND DISCUSSION

Figure 2 presents the frequency spectrum of a loaded coil calculated in steps (1)-(3). The coil has been tuned to f = 42,6MHz, i.e. 1T, using capacitor value of C = 63,0pF. The subsequent calculation of electromagnetic fields in step (4) is done assuming the radius and the height of the 16 rung coil to be 60cm. The physical locations of the discrete capacitors are distributed throughout the RF transmitter coil according to the high-pass requirement, i.e. the capacitors are placed on the rings.

A key element in judging the quality of the model and numerical calculations is the homogeneity and uniformity of the B_1 field within the coil volume. Figure 3 presents results for B_1 magnitude for all phases along the z direction, indicating the requirement B_1=0 along z-direction to be satisfied. The homogeneity within the volume of the coil is excellent; B_1 filed is perpendicular to z-axes with circular polarization (not demonstrated here). The amplitude of B_1 can be adjusted by choosing the power applied to the ports of the transmit coil (equivalently by the magnitude of the current in the rungs of the coil). SAR scales with the amplitude of B_1 which itself scales with the power on the port. To generate the figures P=1W has been selected. An appropriate choice of the power value depends on the chosen sequence, MRI scanner vendor and other factors and becomes very important for the comparisons of SAR levels and with experiments.

SAR values are calculated for all tissue types included in the model. Mass density values and standard weights are taken into account for the organs. Figures 4-6 present SAR values at the surface of three various organs. It should be stressed that since the conductivity and mass density is assumed to be constant on the organ surface, the SAR distribution reflects the E-field distribution on this surface.

Figure 4 presents SAR distribution on the skin in lateral and sagittal views. Since the position of the human model is

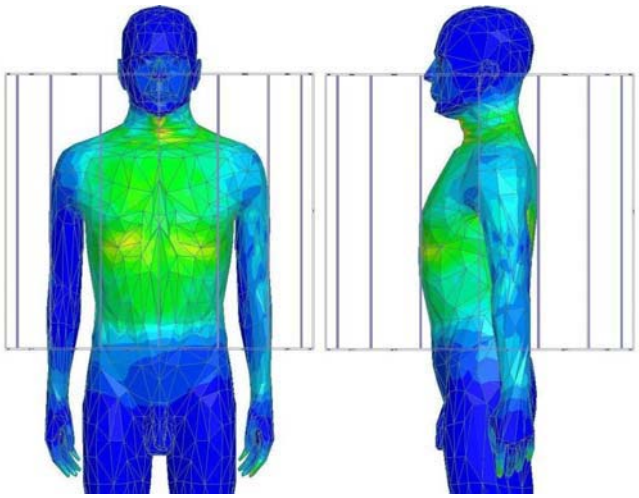

Fig. 4: Local absorbed power on the skin in terms of SAR. Max. (red) $3,3x10^{-3}$ Wkg^{-1}, Min. (blue) $4,0x10^{-8}$ Wkg^{-1}, linear scale.

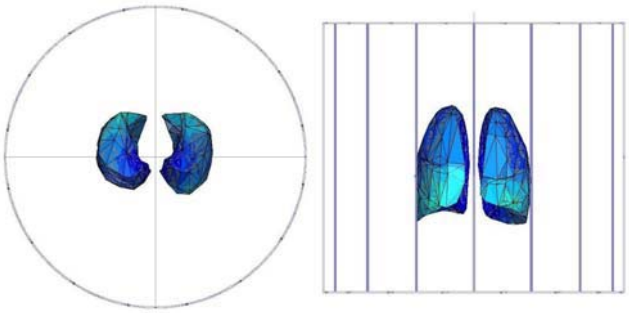

Fig. 6: Local absorbed power on lung surface in terms of SAR. Max. (red) $3,3x10^{-3}$ Wkg^{-1}, Min. (blue) $4,0x10^{-8}$ Wkg^{-1}, linear scale.

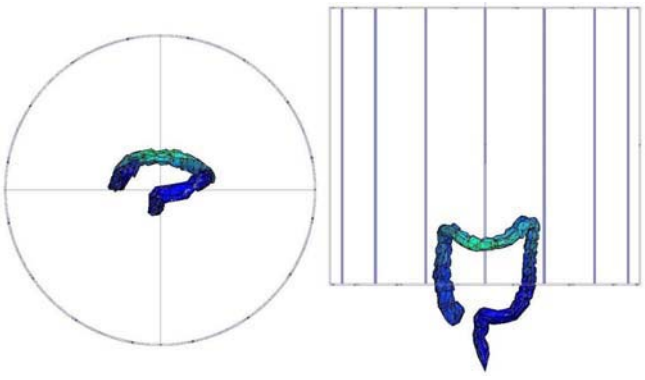

Fig. 5: Local absorbed power on colon surface in terms of SAR. Max. (red) $3,3x10^{-3}$ Wkg^{-1}, Min. (blue) $4,0x10^{-8}$ Wkg^{-1}, linear scale.

fixed with respect to the RF transmit coil, notable irradiation exposure is limited to the position and size of the coil.

It's worthwhile to stress that body parts being closer to the transmitting RF coil rungs are exposed stronger than those lying inside the coil.

Figure 5 and figure 6 show an axial and lateral view of SAR distribution at surfaces of two organs: lung and colon. Again, the color indicates SAR, the magnitude of which is decreased by factor of about 100 compared to the skin. This is due to central position of the organs within the body. Details of the scales are given in figure captions. Some parts of the colon are outside the coil, thus not irradiated at all. The front side of the lungs and the a small part of the colon are more exposed as others which is caused by the position of the organ relative to the coil, by its shape and by the B_1 filed within the coil.

IV. CONCLUSIONS AND DISCUSSION

In this study a new and highly efficient approach to design MR resonators which comprise the electrical and the physical points of view has been applied. We demonstrate the procedure for a birdcage coil operating as high-pass resonator and a human body model with resolution at millimetre level. The numerical approach is based on finite elements as this is more suitable and faster especially for inhomogeneous objects with irregular geometry, e.g. like organs or implants in human body. Especially in those situations the flexibility in grid sizing with finite elements is advantageous compared to FDTD methods. Changes and extensions are possible on short notice. Based on this a new approach for design and numerical calculations of coils 7T seems to be feasible as a daily task.

This study demonstrates that numerical investigations reflect electromagnetic field changes in the process of a MRI examination. Energy deposition, i.e. SAR values, and therefore temperature increases are subject to geometry, homogeneity and material properties. In addition local SAR distribution is a result of the irradiated frequency as well as shape and position of the object under consideration.

The paper collects numerical results at f=42,6MHz, i.e. B_0=1T MRI. It appears to be worthwhile to compare numerical predictions and measurements even for other strengths of the static field B_0. To achieve this goal it is necessary to improve the model and its experimental validation. This includes a detailed model of the MRI sequence and an improvement of the quality of measurements [5]. Attempts to ensure RF safety in high field MRI often rely on assumptions about levels of SAR as calculated in this publication. However, calculations of temperature may be preferable to calculations of SAR because of the more direct relationship between temperature and safety [6]. Achievements to these issues will be reported shortly.

ACKNOWLEDGMENT

The authors acknowledge continuous support by Ansoft/Ansys Germany, especially by Markus Laudien and colleagues for providing the finite element human body model, Thomas Hilbel, University of Applied Sciences Gelsenkirchen, for providing important data of organs.

REFERENCES

1. ICNIRP (1998) Guidelines for limiting exposure to time-varying electric, magnetic, and electromagnetic fields (up to 300 GHz)
2. IEEE Std C95. 1-2005 (Revision of IEEE Std C95.1-1991) (2006) Standard for safety levels with respect to human exposure to radio frequency electromagnetic fields, 3 kHz to 300 GHz
3. Smajic-Peimann S, Zylka W (2008) Co-simulation approach for the design of MRI RF coils and its application to local SAR distribution, ECIFMBE 2008, IFMBE Proc 22, pp. 2636–2639
4. Tissue dielectric parameters are computed according to the 4-Cole-Cole Model described in "COMPILATION OF THE DIELECTRIC PROPERTIES OF BODY TISSUES AT RF AND MICROWAVE FREQUENCIES" by Camelia Gabriel in the U.S. Air Force Report AFOSR-TR-96, Federal Communication Commission, at http://www.fcc.gov/fcc-bin/dielec.sh
5. Hakim BM, Beard , B B, Davis C C (2009) Precise dielectric property measurements and E-field probe calibration for specific absorption rate measurements using a rectangular waveguide, Meas. Sci. Technol. 20 045702
6. Stenschke J, Li D, Thomann M, Schaefers G, and Zylka W (2007) A numerical investigation of RF heating effects on implants during MRI compared to experimental measurements, in Advances of Medical Engineering, Springer Proceedings in Physics 114, Springer 2007, pp 53-59

Authors: Sylvia Samjic-Peimann
Waldemar Zylka
Institute: Medical Physics Research Laboratory
University of Applied Sciences Gelsenkirchen
Street: Neidenburger Str. 43
City: Gelsenkirchen
Country: Germany
Email: waldemar.zylka@fh-gelsenkirchen.de

Exploring the use of the Tarmed coding system for establishing the annual frequency of medical x-ray examinations in Switzerland

A. Aroua[1], F.O. Bochud[1], R. Le Coultre[2], E.-T. Samara[1], A. Stuessi[3], R. Treier[3], Ph.R. Trueb[3] J.-P. Vader[4], F.R. Verdun[1], W. Zeller[3]

[1] University Institute of Radiation Physics, CHUV/University of Lausanne, Lausanne, Switzerland
[2] Technical Branch of Medical Radiology, High School of Health of the Vaud Canton, Lausanne, Switzerland
[3] Radiation Protection Division, Federal Office of Public Health, Bern, Switzerland
[4] University Institute of Social and Preventive Medicine, CHUV/University of Lausanne, Lausanne, Switzerland

Abstract— **Surveying the frequency of medical x-ray examinations is of prime importance in the assessment of the collective detriment due to diagnostic and interventional radiology. In the past, this was performed using paper questionnaires, but today there is an increasing interest in the automatic collection of the frequency data for reasons related to reducing the work load and increasing the accuracy of the results. This paper present the work performed in Switzerland to explore the use of the Tarmed coding system for this purpose. The preliminary investigation covering a sample of examinations indicates that Tarmed coding can easily be used for the collection of radiography and CT examinations, but presents some difficulties for fluoroscopy, mainly in the case of complex angiography and interventional examinations.**

Keywords— **diagnostics, x-ray examinations, frequency surveys, coding systems, population exposure.**

I. Introduction

Surveying the population exposure by medical x-rays is a useful tool in radiation protection. Among the main objectives of population dose assessments are: "1) to observe trends in the annual collective dose and the annual average per caput dose from medical x-rays in a country with time; 2) to determine the contributions of different imaging modalities and types of examination to the total collective dose from all medical x-rays." [1]

At the international level, surveys on the exposure of the population by medical radiology are conducted with a periodicity of 5 to 10 years [2-10]. Nationwide surveys are conducted at more or less the same periodicity in several European countries [11] and particularly in Switzerland [12-18].

The proper design of a survey and the use of a validated methodology are of prime importance in order to obtain an accurate assessment of the level of exposure of the population. Two main methods have been used at the international level for assessing the annual frequency of x-ray examinations: "1) from the healthcare provides (hospitals, clinics or practices, etc.); 2) from central statistics held by government departments or insurance companies" [1]. Another method that could be used, although it is heavy to implement, is the patient-oriented method where a sample of the population is directly surveyed.

In the past the surveys have primarily used paper forms sent to participants who were asked to fill them in. This is not only time consuming and demands a heavy investment from the participants, but the recording of data on paper and then transcribing them into data processing software is a source of errors. Considering the acceleration of the information technology developments, the automation of the frequency and dose data collection is an objective followed by several European groups specialized in the periodic assessment of the irradiation of the population by medical x-rays [19-25]. In its recent recommendations the European Dose Datamed group predicts that "in the future the national authorities responsible population dose surveys may gather the electronic information on patient doses from RIS/PACS systems around the country as input to any national dose databases for the establishment of diagnostic reference levels and/or for future population dose estimates" and encourages them to explore these new avenues [1].

Obviously the use of coding systems has to be validated since it presents several difficulties: they are often designed for reimbursement and not for dosimetric purposes, they might vary with time (several countries have experienced that almost every year there are minor changes in the coding system), they differ between European countries which makes any intercomparison a tedious task, etc. But once validated this method will definitely bring several advantages: better accuracy, gain in time and resources, less work load for the practitioners.

In Switzerland a survey on the exposure of the population by medical x-rays in 2008 is being conducted. It updates the results obtained in 1998 [16] and 2003 [18]. The aim of this work is to explore the appropriateness of the Tarmed coding system as an automatic tool for surveying the frequency of diagnostic and interventional examinations in Switzerland to be used in this nationwide survey.

O. Dössel and W.C. Schlegel (Eds.): WC 2009, IFMBE Proceedings 25/III, pp. 277–279, 2009.
www.springerlink.com

II. Method

First the Tarmed positions that generate radiation dose to the patients were identified. All other positions related to non radiogenic medical acts were ignored.

For a sample of types of examinations belonging to the three radiological modalities: radiography, fluoroscopy and computed tomography (CT), the relationship between the common name of the examination and the Tarmed position (or set of positions) were analysed to explore the possibility to use the Tarmed information to identify a type of examination with a well defined dose to the patient.

III. Results

Table 1 shows a few types of x-ray examinations and their associated Tarmed codes, the analysis of the Tarmed positions for radiography examinations shows that a direct link can be established between a code and a radiograph. It is also possible to know the number of X-rays that have been performed since a specific code is given for the supplementary radiography. For CT the code system allows also to know which part of the body have been examined and a code is added if the examination is a vascular study. One of the main difficulties is the use of the code for fluoroscopy examinations (especially interventional or angiography procedures) where the codes are less specific. For these examinations the use of the hospitals statistics will be necessary to get a better picture of the actual frequency of the examinations.

Table 1 – Example of Tarmed examinations coding

Examination	Code number
Radiography of the humerus	390230 (2^{nd} x-ray 390235)
Radiography of the knee	390310
Radiography of the head	390100
CT of the shoulder	394110
CT of the head	394030
CT of the abdomen	39070
Vascular CT examination	394170

IV. Conclusion

The analysis of the Tarmed coding process used in Switzerland for invoice purposes will simplify the determination of the frequency of the most common radiological examinations (radiography and CT procedures). For fluoroscopy a different approach will have to be taken using in particular the statistics monitored by the hospitals.

Acknowledgment

This work was funded by the Swiss Federal Office of Public Health.

References

1. Wall B, Hart D, Mol H, Lecluyse A, Aroua A, Trueb P, Griebel J, Nekolla E, Gron P, Waltenburg H, Beauvais-March H, Aubert B, Scanff P, Pirard P, Sinno-Tellier S, Shannoun F, Brugmans M, Meeuwsen E, Stoop P, Olerud H, Borretzen I, Leitz W. (2008) Guidance on estimating population doses from medical radiology (as required by Article 12 of the EC Medical Exposure Directive). Publication de la Commission européenne, Luxembourg.
2. UNSCEAR (1958) Report of the United Nations Scientific Committee on the Effects of Atomic Radiation. General Assembly Official Records: Thirteenth session Supplement No. 17 (A/3838). United Nations, New York.
3. UNSCEAR (1962) Report of the United Nations Scientific Committee on the Effects of Atomic Radiation. General Assembly Official Records: Seventeenth Session Supplement No. 16 (A/5216). United Nations, New York.
4. UNSCEAR (1972) Ionizing Radiation: Levels and Effects. A Report of the United Nations Scientific Committee on the Effects of Atomic Radiation to the General Assembly, with annexes. United Nations, New York.
5. UNSCEAR (1977) Sources and Effects of Ionizing Radiation. United Nations Scientific Committee on the Effects of Atomic Radiation. 1977 Report to the General Assembly, with annexes. United Nations, New York.
6. UNSCEAR (1982) Ionizing Radiation: Sources and Biological Effects. United Nations Scientific Committee on the Effects of Atomic Radiation. 1982 Report to the General Assembly, with annexes. United Nations, New York.
7. UNSCEAR (1988) Sources, Effects and Risks of Ionizing Radiation. United Nations Scientific Committee on the Effects of Atomic Radiation. 1988 Report to the General Assembly, with Annexes. United Nations, New York.
8. UNSCEAR (1993) Sources and Effects of Ionizing Radiation. United Nations Scientific Committee on the Effects of Atomic Radiation. UNSCEAR 1993 Report to the General Assembly, with Scientific Annexes. United Nations, New York.
9. UNSCEAR (2000) Sources and Effects of Ionising Radiation. United Nations Scientific Committee on the Effects of Atomic Radiation. Report to the General Assembly, with scientific annexes. Vol 1: Sources. United Nations, New York.
10. UNSCEAR (in press, expected in 2009) Sources and Effects of Ionising Radiation. United Nations Scientific Committee on the Effects of Atomic Radiation. Report to the General Assembly, with scientific annexes. United Nations, New York.
11. Wall B, Hart D, Mol H, Lecluyse A, Aroua A, Trueb P, Griebel J, Nekolla E, Gron P, Waltenburg H, Beauvais-March H, Aubert B, Scanff P, Pirard P, Sinno-Tellier S, Shannoun F, Brugmans M, Meeuwsen E, Stoop P, Olerud H, Borretzen I, Leitz W. (2008) Review of recent national surveys of population exposure from medical x-rays in Europe. Publication de la Commission européenne, Luxembourg.
12. Zuppinger A, Minder W, Sarasin R, Schär M. (1961) Die Strahlenbelastung der schweizerischen Bevölkerung durch röntgendiagnostische Massnahmen. Radiol Clin 30:1-5.

13. Poretti G, Ionesco R, Lanz W. (1971) Erhebung über die Strahlenbelastung der Schweizer Bevölkerung infolge Röntgendiagnostischer Untersuchungen, Hrsg., Schweiz. Vereinigung für Atomenergie.
14. Mini RL, Poretti G. (1984) Die Bestimmung der Strahlenbelastung einer Bevölkerungsgruppe gemäss ICRP26. Tagungsbericht der Schweizerischen Gesellschaft für Strahlenbiologie und Strahlenphysik.
15. Mini RL. (1992) Dosisbestimmungen in der medizinischen Röntgendiagnostik. Kerzers: Verlag Max Huber.
16. Aroua A, Burnand B, Decka I, Vader JP and Valley JF. (2002) Nationwide Survey on Radiation Doses in Diagnostic and Interventional Radiology in Switzerland in 1998. Health Phys 83(1):46-55.
17. Aroua A, Decka I, Burnand B, Vader JP and Valley JF. (2002) Dosimetric Aspects of a National Survey of Diagnostic and Interventional Radiology in Switzerland. Medical Phys 29(10):2247:2259.
18. Aroua A, Vader JP, Valley JF and Verdun FR. (2007) Exposure of the Swiss population by radiodiagnostics: 2003 review. Health Phys 92(5):442-8.
19. Gron P. (2007) Private communication.
20. Brix G, Nekolla E, Griebel J. (2005) Strahlenexposition von Patienten durch diagnostische und interventionelle Röntgenanwendungen: Fakten, Bewertung und Trends. [Radiation exposure of patients from diagnostic and interventional X-ray procedures. Facts, assessment and trends]. Radiologe 45: 340-349.
21. Nekolla EA, Veit R, Griebel J, Brix G. (2005) Frequency and effective dose of diagnostic x-ray procedures in Germany, Proceedings of the jointly held Congresses ICMP 2005 and BMT 2005 (Editorial: W Kalender, EG Hahn, AM Schulte): Medical Physics 50, Suppl. 1-2: 1334-1335.
22. Brugmans MJP, Buijs CAM, Geleijns J, Lembrechts J. (2002) Population exposure to diagnostic use of ionizing radiation in the Netherlands. Health Phys. 82(4):500-509.
23. Shannoun F, Zeeb H, Back C, Blettner M. (2006) Medical exposure of the population from diagnostic use of ionizing radiation in Luxembourg between 1994 and 2002. Health Phys. 2006, 91:154-162.
24. Olerud, H.M. and Saxebøl G. (1997) Diagnostic radiology in Norway from 1983-1993- Examination frequency and collective effective dose to patients. Radiat.Prot. Dosim. 74 (4) 247-260.
25. Borretzen I, Lysdahl KB, Olerud HM. (2007) Diagnostic radiology in Norway: trends in examination frequency and collective effective dose. Radiat Prot Dosim 124(4):339-47.

Author: Abbas Aroua
Institute: University Institute of Radiation Physics
Street: Grand-Pré 1
City: 1007 Lausanne
Country: Switzerland
Email: abbas@aroua.com

Simulation of beta-emitters for radiopharmaceutical dosimetry using voxel phantoms and Monte Carlo calculations

N. Petoussi-Henss, M. Zankl, H. Schlattl, W.B. Li, C. Hoeschen

Helmholtz Zentrum München, German Research Center for Environmental Health (GmbH)
Institute of Radiation Protection, Ingolstaedter Landstr. 1, 85764 Neuherberg, Germany

***Abstract*— Radiation dose estimates are needed for assessment of the risk to patients associated with the use of radiopharmaceuticals both for comparison with the possible benefit of an investigation and to help giving adequate information to the patient. With respect to the physical aspects, one of the most crucial requirements is to establish values of so-called Specific Absorbed Fractions (SAF) which specify the fraction of penetrating energy emitted by radioactivity in a given organ which is absorbed in the source organ itself and in other organs. Until recently, photon SAFs were calculated on the basis of MIRD-type mathematical anthropomorphic phantoms and a whole range of data exists covering all ages. For electrons, the radiation was assumed to be absorbed entirely in the source region, except when the source was part of the skeleton or when the source is in the contents of a walled organ. For this work, photon SAFs and electron SAFs were derived with the Monte Carlo code EGSnrc for the new reference male and female voxel-based phantoms adopted by the ICRP. The present results of electron SAFs show that the previously applied assumption of electrons being fully absorbed in the source organ itself presents an over-simplification at higher energies. For organs in close vicinity, such as liver and stomach wall, high-energetic electrons escaping from the source organ may result in cross-fire SAF values that can reach the same order of magnitude as those from photons. Examples of organ absorbed doses per nuclear transformation will be given for some radiopharmaceuticals. The impact of the new electron SAFs used for the calculation of the absorbed doses instead of the previously used assumption, will be discussed.**

Keywords— **Voxel phantom, radiopharmaceuticals, SAF, particle transport.**

I. Introduction

The calculation of radiation dose from internally incorporated radionuclides is based on the knowledge of the so-called Specific Absorbed Fractions (SAF) which specify the fraction of penetrating energy emitted by radioactivity in a given organ which is absorbed in the source organ itself and in other organs. According to the MIRD formalism [1], the equations relating absorbed dose, S values and SAFs are as following:

$$D_T = \sum_S \tilde{A}_S \cdot S(T \leftarrow S) \tag{1}$$

$$S(T \leftarrow S) = \mathrm{k} \sum_i E_i \cdot \mathrm{Y}_i \cdot \Phi_i(T \leftarrow S) \tag{2}$$

where D_T is the absorbed dose in target organ T, $\tilde{A}_S$ is the cumulated activity, $S(T \leftarrow S)$ is the S value for target organ T and source organ S, E_i is the mean energy of radiation type i and Y_i is the yield per transformation, i.e. number of radiations with E_i, emitted per nuclear transition; Φ (acronym SAF) is the fraction of energy emitted in S and absorbed in T, divided by the corresponding target mass; k is a proportionality constant.

Until recently, SAFs were calculated on the basis of MIRD-type mathematical anthropomorphic phantoms and a whole range of data exists covering all ages [2]. The voxel phantoms, based on CT data of real persons, are now used for internal dosimetry and could significantly contribute to better dose assessments for patients.

The photon SAF values for the mathematical models, used as input data from many software tools for internal dosimetry, were calculated at the Oak Ridge National Laboratory [2]. For electrons, no SAFs values stemming from particle transport were available. Instead, the following assumptions were used [3]:

For solid regions:

$$\phi(T \leftarrow S) = \begin{cases} 1, \textit{if } T = S \\ 0, \textit{if } T \neq S \\ M_T / M_{WB}, \textit{if } S = WB \end{cases} \tag{3}$$

where T: Target organ, S: Source organ, WB: Whole Body, M_T , M_{WB}: Masses of the target organs and of the

O. Dössel and W.C. Schlegel (Eds.): WC 2009, IFMBE Proceedings 25/III, pp. 280–283, 2009.
www.springerlink.com

whole body respectively and $\phi(T \leftarrow S)$: is the fraction of energy emitted in *S* and absorbed in *T*.

For contents of walled organs, the assumption was used that the dose to the wall is the dose at the surface of a half-space, or half the equilibrium dose to the contents:

$$\Phi(wall \leftarrow contents) = \frac{0{,}5}{M_{content}} \quad (4)$$

For the present work, photon as well as electron SAFs were calculated and implemented for the calculation of doses due to radiopharmaceuticals. One of the aims of this work was to investigate the impact of the improved electron dosimetry, in comparison to the dosimetry using the simple assumptions described above.

II. The Voxel Phantoms

The phantoms used for the calculations are the new ICRP/ICRU reference voxel adult male and female computational phantoms [4]. These are based on medical image data of real persons, and are consistent with the information given in ICRP Publication 89 [5] on the reference anatomical and physiological parameters for both male and female subjects and represent, therefore, the reference Caucasian individual. The reference voxel phantoms were developed at the Helmholtz Zentrum München in collaboration with the ICRP Task Group Dose Calculations (DOCAL).

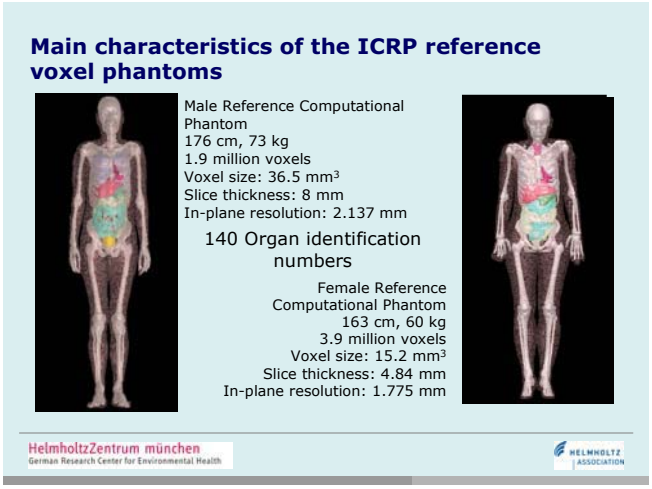

Fig. 1 The male (left) and female (right) voxel reference phantom

For the construction of the reference computational models, tomographic data sets were selected of individuals having external dimensions close to the reference data. From these data, voxel phantoms were segmented and then modified to the reference values given in ICRP Publication 89. Most relevant source and target regions are adjusted to their reference mass values without spoiling the realistic anatomical morphology and topology**.** These phantoms represent, therefore, the reference Caucasian individual, have "representative" organ masses and locations. Figure 1 shows a 3-dimensional representation of these phantoms and their main characteristics.

III. Specific Absorbed Fractions

Calculations of SAFs for monoenergetic photons and electrons for the new reference computational phantoms were performed for 55 source regions and more than 65 target organs. For photons, energies from 10 keV to 10 MeV were considered and for electrons, energies between 15 keV and 10 MeV. The radiation transport through the body was simulated using the EGSnrc code [6].

As example of the results, Figure 1 shows the photon SAFs for source organ liver and target organ stomach wall. For comparison purposes, the SAFs of ORNL are also shown.

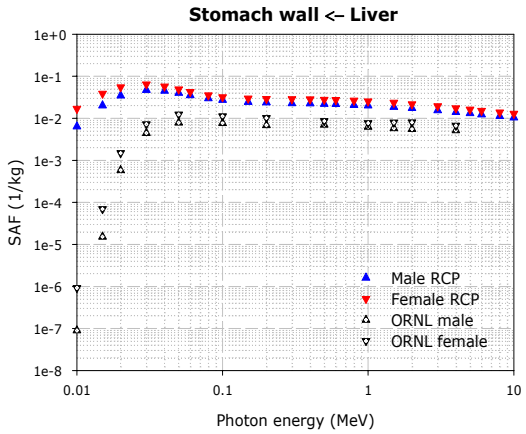

Fig. 2 Photon SAF for source organ liver, target organ stomach wall

For organ self-absorption there is a strong dependence of SAFs on organ mass which results in rather small differences between the MIRD values and the voxel SAF values. For organ cross-fire, larger discrepancies occur for some organ pairs between the reference voxel and MIRD-type models; these are due to the fact that inter-organ distances tend to be larger in the MIRD-type phantoms than in reality.

The following figures show some SAFs sets for electrons: Figure 3 for organ self-dose, Figure 4 for cross-fire from contents to a wall organ and Figure 5 for cross-fire for distant organs.

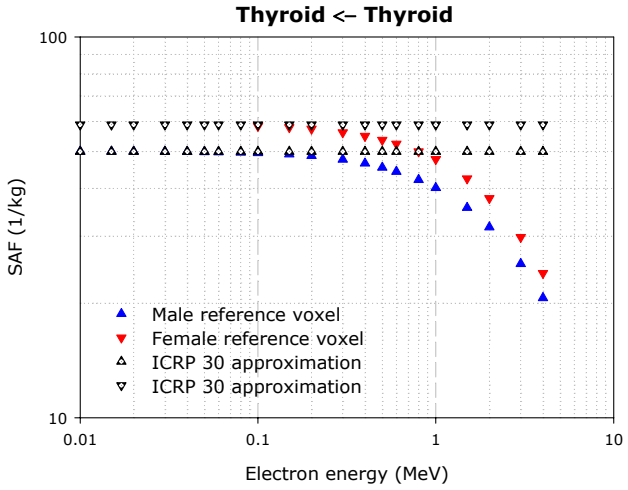

Fig. 3 Electron SAF for source and target thyroid

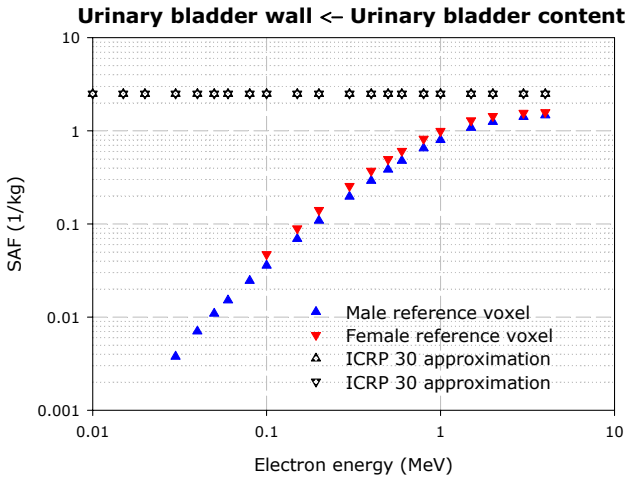

Fig.4 Electron SAF for source bladder contents and target bladder wall

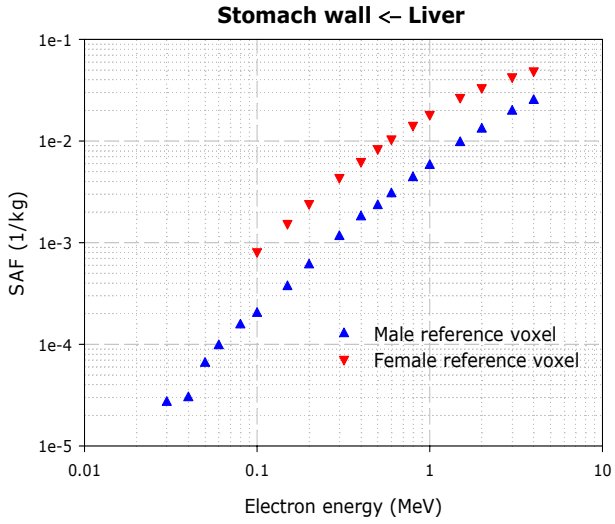

Fig. 5 Electron SAF for source liver and target stomach wall

The present results confirm earlier findings that the previously applied assumption of electrons being fully absorbed in the source organ itself presents an oversimplification at higher energies [7]. Higher-energetic electrons have the ability to escape from the source organ, as can bee seen, e.g., in figure 2 where SAFs for self-absorption in the thyroid are shown. For organs in close vicinity, such as liver and stomach wall, high-energetic electrons escaping from the source organ may result in cross-fire SAF values that can reach the same order of magnitude as those from photons. For distant organ pairs, however, such as thyroid and colon wall, electron SAF values can be considered negligible.

IV. Organ Absorbed Dose Coefficients for Radiopharmaceuticals

For the calculation of absorbed dose rates for radiopharmaceuticals, an in-house software was used which utilizes both photon and electron voxel SAFs [8]. The following standard formulation was used.

$$D_T = \sum A_S S_{T \leftarrow S} + A_{REM} [(m_{TB} S_{T \leftarrow TB} - \sum m_S S_{T \leftarrow S}) / m_{REM}] \quad (5)$$

where S = "S" or “SEE” factor (dose in target organ per unit of cumulated activity in source organ (mGy.MBq^{-1}.s^{-1})) ; S, T = source, target organs, TB = total body without contents of walled organs, m = mass (g), REM = remain-

ing tissues ($m_{REM} = m_{TB} - \sum m_S$); $A_S =$ is the time integrated or cumulated activity and is equal to the total number of transformations in S. The value of the expression in square brackets is the calculated "S" value for the remaining tissues (note that in this term of the equation the contents of walled organs are excluded from the summation over the source organs).

The resulting voxel photon SAFs were introduced as input to the program. Concerning the dosimetric method for the skeletal tissues: as source organ, the segmented cortical bone volume was taken as a surrogate of cortical bone surface. Similarly, a distribution of sources in the segmented spongiosa volume was taken as a surrogate of trabecular bone surface and trabecular bone volume sources. Concerning bone surface as a target organ, the spongiosa was taken as a surrogate organ. For red bone marrow as the target, specific correction factors were applied to the dose to spongiosa that account for the variations of RBM distribution among different bones, the different absorption by RBM compared to spongiosa, and the non-existence of secondary electron equilibrium between bone trabeculae and marrow cavities.

As an example, Fig. 6 shows some preliminary results for [99mTc] ECD.

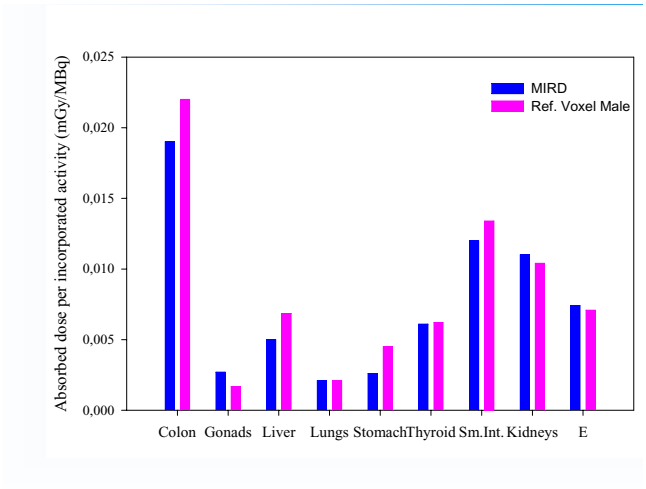

Fig.6 Organ absorbed doses per unit activity administered for [99mTc] ECD

V. Conclusions

Extensive tables of photon and electron specific absorbed fractions (SAF) are available for the reference computational voxel models mentioned above and photons and electrons of 10 keV to 10 MeV, for up to 55 source organs and more than 65 target organs. These were calculated using the Monte Carlo code EGSnrc. The present results of the electron SAFs demonstrate that the previously applied assumption of electrons being fully absorbed in the source organ itself presents an over-simplification.

References

1. Loevinger R, Budinger, T., Watson, E. (1988) MIRD primer for absorbed dose calculations. New York, NY: Society of Nuclear Medicine
2. Cristy, M., Eckerman, K. F. SEECAL 2.0(1993) Program to calculate age-dependent specific effective energies. RSICC compute code collection CCC-620. ORNL/TM-12351. Oak Ridge, TN: Oak Ridge National Laboratory
3. International Commission on Radiological Protection.. (1979) Limits of Intakes of radionuclides by workers. ICRP Publication 30 Part I, Pergamon Press, Oxford, UK
4. International Commission on Radiological Protection (in press). *Adult reference computational phantoms.* ICRP Publication 108, Pergamon Press, Oxford, UK
5. International Commission on Radiological Protection (2002). Basic anatomical and physiological data for use in radiological protection: reference values. ICRP 89, Pergamon Press, Oxford, UK
6. Kawrakow, I., Rogers, D.W.O. (2003) The EGSnrc code system: Monte Carlo simulation of electron and photon transport. PIRS Report 701, National Research Council of Canada (NRCC), Ottawa
7. Chao, T.C., Xu, X.G. (2001) Specific absorbed fractions from the image-based VIP-Man body model and EGS4-VLSI Monte Carlo code: internal electron emitters. Phys. Med. Biol. 46, 901-927
8. Petoussi-Henss N, Zankl M, Nosske D (2005) Estimation of patient dose from radiopharmaceuticals using voxel models. Cancer Biotherapy and Radiopharmaceuticals, 20, 103-109

Author: Nina Petoussi-Henss

Institute: Helmholtz Zentrum München, German Research Center for Environmental Health
Street: Ingolstaedter Landstr. 1
City: Neuherberg
Country: Germany
Email: petoussi@helmholtz-muenchen.de

Characterization of a Radiochromic Solid Polymer Dosimeter According to its' Composition

A. Mostaar[1], B. Hashemi[1], M.H. Zahmatkesh[2], S.M.R Aghamiri[3] and S.R. Mahdavi[4]

[1] Department of Medical Physics, Tarbiat Modares University, Tehran, Iran.
[2] Novin Medical Radiation Institute, Tehran, Iran.
[3] Department of Radiation Medicine, Shahid Beheshti University, Tehran, Iran.
[4] Department of Medical Physics, Iran University of Medical Sciences, Tehran, Iran.

Abstract—**Recently, a novel transparent polymer dosimeter, PRESAGE, has been introduced. Radical initiator and leuco dye are two main parts of this dosimeter influencing its' dose response. To study the effect of a solid polymer dosimeter compositions on its' response to therapeutic radiation, various amounts of a radical initiator and a leuco dye were investigated. The solid polymer was evaluated for its linearity, sensitivity, and stability for various compositions of its' main paerts. It was noted that as the concentration of the radical initiator is increased, its' sensitivity is increasesed while its' stability is decreased. On the other hand, we noted that as the concentration of the leuco dye is increased, its' sensitivity is not changed significantly while its' stability is decreased. For all of the concentrations of the radical initiator and leuco dye used in this tudy, the linearity of the dose response in the applied radiation dose range was good. Based on our results it can be concluded that the PRESAGE continues to represents a significant step forward in the developments towards a truly practical and convenient 3D dosimetry material. The attractiveness of this dosimeter lies in its' insensitivity to atmospheric exposure, radiochromic response sensitivity (absorbing rather than light-scattering), linearity, and lack of requirement for an external container.**

Keywords— **PRESAGE, radiation dosimetry, sensitivity, linearity, stability.**

I. Introduction

In order to minimize the dose to nearby critical organs, clinical applications of advanced radiation therapy techniques continue to progress rapidly, and applications of new modalities like three-dimensional (3D) conformal radiotherapy, intensity modulated radiation therapy and stereotactic radiosurgery have been realized [1]. These techniques have created an urgent need for 3D dosimetry with high resolution and assured quality. However, conventional dosimetry detectors do not meet this requirement because they are limited in the measurable dimensions (for example, films are planar, and diodes, thermoluminescence detectors and ion chambers are point measurement devices). Potential advantages of MRI gel dosimetry were recognized two decades ago. The basic fundamental principle of polymer gel dosimeters involves the radiation-induced polymerization of monomer (and often co-monomer) species suspended in a gelatin matrix. Radiation induced polymerization creates long-chained polymers that are spatially retained in the gelatin matrix, thus allowing for the extraction of 3D dose information from the polymer gel dosimeters[2-4]. However, these polymer gels did not become a practical tool because of the blurring of dose distributions and other problems [5, 6].

Without any doubt, one of the most exciting developments on 3D radiation dosimetry during recent years has been the introduction of PRESAGE, a novel transparent polymer dosimeter. PRESAGE is not a gel-dosimeter, but a polyurethane material doped with leuco dyes which undergo a peak radiochromic response at 633nm [7, 8]. A number of potential advantages of this dosimeter accrue over other 3D dosimeters includes its' lack of sensitivity to oxygen and diffusion [8, 9]. It is also rigid and easily machineable. Therefore, a variety of shapes and sizes without the requirement to an external container is achievable [10] for this solid polymer dosimeter. In this study, this type of solid polymer dosimeter was composed in the laboratory by focusing on therapeutic radiation applications. To investigate the effect of the main parts of the dosimeter composition on its' dose response, the amount of its' radical initiator and leuco dye were varied. The solid polymer with various combinations of the composition of its' main parts was evaluated for the linearity, sensitivity, and stability of its' dose response.

II. Materials and methods

A. PRESAGE preparation

The PRESAGE dosimeter based on polyurethane matrix is formed in two steps. In the first step, reacting an equivalent of commercially available polyol with two equivalents of a di-isocyanate forms a pre-polymer, referred to as "Part A". The second step consists of mixing the leuco dye, a free radical initiator, and a catalyst with "Part B" (a commercial-

O. Dössel and W.C. Schlegel (Eds.): WC 2009, IFMBE Proceedings 25/III, pp. 284–287, 2009.
www.springerlink.com

ly available polyol) then blending it with Part A in specific proportions, placing the blended material in an appropriate mold, and incubating at an optimal temperature under 60 psi to minimize out gassing.

The Part A and Part B were Crystal Clear 206 (Smooth-On, Inc.). The leuco dye used in this study was leucomalachite green (LMG, Sigma-Aldrich, St Louis, MO) and the free radical initiator was carbon tetrachloride (Merck Chemical Company).

In this paper, we used an efficient method to investigate the basic properties of the 3D dosimetry material that exhibits an optical dose response. We used the standard cuvetts of a spectrometer. The cuvetts were made of polystyrene with a wall thickness of 1 mm, and an internal dimension of $1\times 1\times 4.5$ cm^3.

Different formulations of PRESAGE dosimeters, containing different amount of leuco dye and free radical initiator, lead to different radiation sensitivity, stability and other basic properties. The PRESAGE dosimeters were grouped into three with varying ingredients ratios. The weight percent of each group is summarized in Table 1. The polyurethane used in this study had an elemental composition of C at 61 %, H at 9 %, N at 10 %, and O at 20% giving an effective atomic number (Z_{eff}) of 6.6. Depending on the weight percent of the halocarbon added to the polymer, as free radical initiators, the Z_{eff} can be increased. The effective atomic number of each composition was calculated by using the Mayneord equation [1] as shown in Table 1.

Table1. The weight percent of the elements and relevant Z_{eff} values in each PRESAGE group

Group	Radical initiator	Leuco dye	PartA+PartB +Catalyst	Z_{eff}
1	5	1	94	7.8
2	10	1	89	8.7
3	5	2	93	7.8

B. Irradiation of PRESAGE

The cuvetts filled by the PRESAGE material were placed at a fixed position in a water phantom and were irradiated to appropriate levels of Co-60 therapeutic radiation to deliver 0, 0.25, 0.5, 1, 2, 3, 5, 10, 15, 20, 35 and 50 Gray doses. The temperature of the water phantom was stabilized around the room temperature (22 °C) during the radiation exposure because the dosimeter dose response depends on the temperature [8].

C. Measurement of PRESAGE absorbance change

The absorbance of each PRESAGE sample was measured by using a spectrophotometer (T70+ UV-VIS Spectrophotometer, PG Instrument), in both of the pre and post-irradiation of the samples. The spectrophotometer wavelength was assigned at 633 nm and its' auto zeroing was done in air. All measurements were carried out in 30 minutes after the spectrophotometer was turned on for achieving its' stability. Subsequent absorbance acquisitions were measured at various post-irradiation times to ascertain the stability of absorbance changes in the dosimeters.

III. Results

The absorbance changes with post-irradiation time for the group 1 PRESAGE composition at different radiation doses are displayed in Figure 1. This composition exhibits good characteristics for practical use in 3D dosimetry with respect to its' initial sensitivity and stability. Plots of the measured absorbance change versus the dose for this group are shown in Figure 2. In general, a good linearity (R^2>0.99) was observed for this PRESAGE composition in the applied radiation dose range.

Plots of the measured absorbance changes versus dose for the group 2 and 3 PRESAGE compositions are shown in Figure 3 and 4 respectively. These compositions of the dosimeter also showed a good linearity whitin the applied radiation dose range but their absorbance at various post irradiation times differed and their stability was decreased.

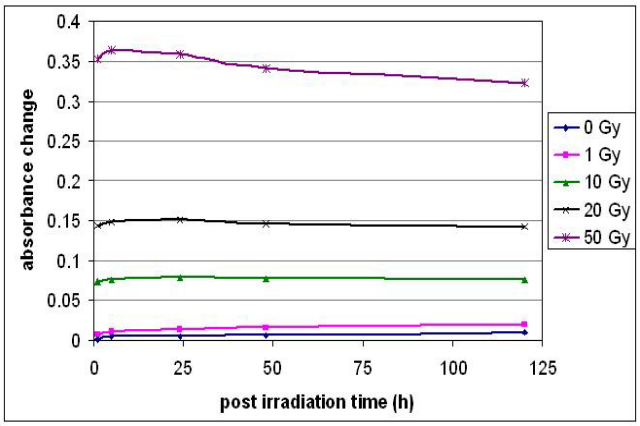

Fig 1. Absorbance changes of different doses as a function of post irradiation time. All presented data is for the group 1 PRESAGE composition. The radiation induced absorbance change in the PRESAGE was measured by using a spectrophotometer at the wavelength of 633 nm

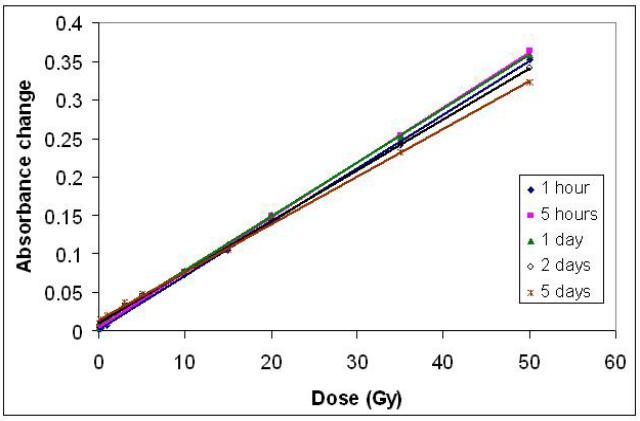

Fig 2. Absorbance changes of different post irradiation time as a function of the radiation dose. All presented data is for the group 1 PRESAGE composition.

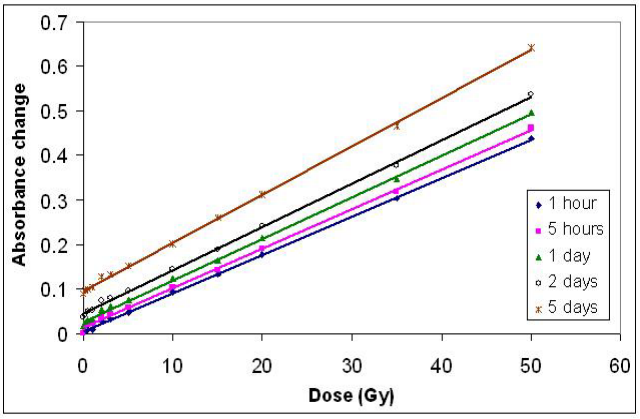

Fig 3. Absorbance changes of different post irradiation times as a function of dose. All presented data is for the group 2 PRESAGE composition.

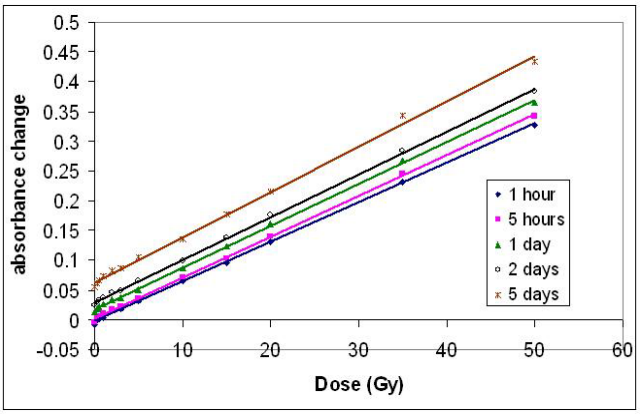

Fig 4. Absorbance changes of different post irradiation times as a function of dose. All presented data is for the group 3 PRESAGE composition.

IV. Discussion

The basic compositions of polyurethane polymer used in this study is a reasonably tissue equivalent material with a Z_{eff} = 6.6, which is nearly identical to adipose tissue. In order to make the material equivalent to muscle and bone, higher Z materials such as chlorohydrocarbons are added.

The results of the present study focusing on the properties of a new polymer dosimeter, PRESAGE, are noticeable in that a linear, stable, and sensitive dose response was achieved in the material compositions that were made and exposed to therapeutic radiation doses in the atmosphere conditions and had no special protective container. The sensitivity of the dosimeter is more when the weight percent of radical initiator is increased. But the sensitivity is not changed significantly when the weight percent of leuco dye is increased. It was noticed that with increasing the radical initiator the stability of the dosimeter response at various post irradiation times is decreased.

V. Conclusions

In summary, this work supports the conclusion that PRESAGE represents a significant step forward in the development towards a truly practical and convenient 3D dosimetry material. The principle attractiveness of this dosimeter lies in its' insensitivity to atmospheric conditions, radiochromic response sensitivity (absorbing rather than light-scattering), linearity, and lack of requirement for an external container.

Acknowledgment

The authors are grateful to Tarbiat Modares University for the financial support of the project. The autors would also like to express their appreciation to the staff of Novin Radiation Medicine Institute for their kind cooperation in carrying out this research using their technical facilties as well as their Co-60 machine.

References

1. Khan FM. (2004) The physics of radiation therapy. William and Wilkins, Maryland
2. McJury M, Oldham M, Cosgrove VP et al. (2000) Radiation dosimetry using polymer gels: methods and applications. Brit J Radiol 73: 919-929
3. Maryanski M J, Schulz RJ, Ibbott GS et al. (1994) Magnetic resonance imaging of radiation dose distributions using a polymer-gel dosimeter. Phys Med Biol 39:1437-1455

4. Gum F, Scherer J, Bogner L et al. (2002) Preliminary study on the use of an inhomogenous anthropomorphic Fricke gel phantom and 3D magnetic resonance dosimetry for verification of IMRT treatment plans. Phys Med Biol 47: N67-N77
5. De Deene Y, Hurley C, Venning A et al. (2002) A basic study of some normoxic polymer gel dosimeters. Phys Med Biol 47: 3441-3463
6. Venning A J, Hill B, Brindha S et al. (2005) Investigation of the PAGAT polymer gel dosimeter using magnetic resonance imaging. Phys Med Biol 50: 3875-3888
7. Adamovics J, Maryanski MJ. (2004) A new approach to radiochromic three-dimensional dosimetry-polyurethane. Journal of Physics: Conference Series 3: 172–175
8. Adamovics J, Maryanski MJ. (2006) Characterization of PRESAGE: a new 3-D radiochromic solid polymer dosimeter for ionizing radiation. Radiat Prot Dosim 120: 107–112
9. Guo PY, Adamovics JA, Oldham M. (2006) Characterization of a new radiochromic three-dimensional dosimeter. Med Phys 33: 1338-1345
10. Guo PY, Adamovics JA, Oldham M. (2006) A practical three-dimensional dosimetry system for radiation therapy. Med Phys 33: 3962-3972

Author: B. Hashemi
Institute: Tarbiat Modares University
Street: Al-Ahmad and Chamran Cross
City: Tehran
Country: Iran
Email: bhashemi@modares.ac.ir

Radiosensitizing Effect of IUdR Combined with Co-60 γ Radiation on Malignant Glioma Spheroids

H Khankeshizaeh[1], B. Hashemi[1], and A. Neshastehriz[2]

[1] Department of Medical Physics, Tarbiat Modares University, Tehran, Iran
[2] Department of Radiology, Iran University of Medical Sciences, Tehran, Iran

Abstract— **Glioma is recognized as one of the most common tumors in the central nervous system. This tumor is resistant to all usual treatments. Because of the anatomical positions of this tumor, the surgery, as a treatment modality, is not possible in all cases. Even in the cases suitable for the surgery, because of the indistinct boundaries of this tumor and normal cells, complete elimination of the tumor is impossible. Glioma cells are also resistant to cytotoxic drugs. So, chemotherapy, as another treatment modality has no effect on this tumor. Sufficient radiation doses to kill the tumor cancer cells are not endurable for normal cells. Therefore, investigators are looking for new approaches to treat this malignant disease. One of the approaches is to use radiosensitizers in combination with the radiotherapy. IUdR is a halogenated pyrimidine which its radiosensitizing effect has been proved. In this research we have studied the effect of IUdR combined with ^{60}Co γ radiation for two sizes of Glioma spheroids (100 and 300μm). The spheroid diameters were measured and analyzed to evaluate the level of radiation damages. Our results showed that the combination of IUdR with the ^{60}Co γ radiation can increase the radiation damage in both sizes of Glioma spheroids. The induced radiation damage in the greater spheroids was less than the lesser ones. This may be explained by the more hypoxic cells normally existed in greater spheroids. In addition, in greater spheroids more cells are in the G0 phase of the cell cycle and cannot uptake IUdR, so they will not be affected by the sensitizing effect of this radiosensitizer.**

Keywords—**Glioma, Spheroid, IUdR, Radiosensitizer, Co-60.**

I. Introduction

Nowadays, Cancer is known as one of the main causes of human mortality. Cancer treatment is usually done by three usual procedures: the surgery, chemotherapy and radiotherapy. Radiotherapy can be applied as a dedicated or supplementary treatment. Radiotherapy is aimed on killing cancer cells while protecting normal cells. Using radiosensitizers is a way to better achieve this goal. By using the radiosensitizers, tumor cells became more sensitive to radiation damage because of the differential effect of the radiosensitizer drugs. Theoretically, the best tumor to be treated in this way is Glioma [1]. More than 50% of malignant tumors of the CNS are Glioma. Survival of cancer patients after diagnosis is between 6 to 12 months [2]. Usual treatment methods are incapable to treat this tumor. Because of the tumor anatomical position, the surgery is not also possible in all cases. Even for the cases that surgery is possible, because of indistinct boundaries of tumor and normal cells, complete elimination of tumor is impossible [3]. Glioma cells are resistant to cytotoxic drugs. Therefore, chemotherapy has no effect on this tumor [4]. The most radiation endurance in brain normal cells is less than 6000 cGy and even this amount of radiation will lead to brain atrophy and ventricle enlargement in ⅓ of cases [5]. Hence, it is necessary to use other alternative methods like using radiosensitizers for the treatment of Glioma . In recent years many drugs have been either produced or discovered as radiosensitizers. But, most of these drugs have no differential effect between tumor and normal cells. Therefore they are not applicable. Considering all important factors, just halogenated pyrimidines and hypoxic cell sensitizers can be used in clinical radiotherapy. Halogenated pyrimidines are suitable for tumors with high rate duplication. These drugs are known as Iododeoxy uridine (IUdR) and Boromodeoxy uridine (BUdR). Because these are thymidine analogues, they act as thymidine in the body and in the synthesis phase of the cell cycle they lie in the DNA chain. One of the most applications of these drugs are for the of treatment of tumors which their adjacent normal cells have low duplication rate. Because a plenty amount of BUdR causes allergic reactions, most of investigations are done on IUdR [6]. Although the mechanism of the IUdR in sensitizing the cells is unknown, it is confirmed that the IUdR increases the number of SSB (Single Strand Break) and DSB (Double Strand Break) in DNA [7]. Available IUdR in DNA chain reacts with electrons which are produced by radiation and this reaction produces active Uracil radicals and halide ions. Then, these free radicals increase SSB and DSBs [7]. Finally the damages which are not repaired, lead to the cell death [8]. On the other hand, technically in the tumor treatment, the in vitro examinations will be ideal when the treatment factors in the tissue model response the same as that of the in vivo condition. So, a 3D cell culture is better than a mono layer cell culture [9]. In this research we used the Glioma spheroids with 100 and 300μm diameters as real tissue samples. Regarding the cells environment and form, spheroids are very similar to in vivo conditions. Spheroids with 300μm diameter were chosen to

O. Dössel and W.C. Schlegel (Eds.): WC 2009, IFMBE Proceedings 25/III, pp. 288–291, 2009.
www.springerlink.com

study the effect of radiation on hypoxic cells because in this size, spheroids contain hypoxic cells [10].

II. Materials and methods

Cell: U87MG cell line with Glioma origin was purchased from the cell bank of Iranian Institute of Pasteur.

Cell Culture Media (100cc): 0.96g MEM culture media (Gibco) containing L-Glutamine, 10 mg penicillin (Sigma), 0.22g NaHCO3 (Sigma) were solved in 80cc of deionized water and 100µl Fungizone (Gibco) was added to this solution. The solution pH was adjusted to 7-7.1. 10ml FBS (Gibco) was added to 90ml of this solution.

Tripsine/EDTA: To prepare 100ml of the solution, 0.25g tripsine powder and 0.03g EDTA powder were solved in 100ml PBS. This solution was then used to excide the cells of the Petri floor.

Agar 1%: Agar 1% was used as a layer to cover the floor of Petri to prepare the spheroids. A mixture made from 50% agar 2% and 50% 2X culture media was prepared. It was then poured into Petri dishes.

IUdR Solution: 3.5 mg IUdR powder was solved in 10ml PBS and a 1000µM solution was prepared. This solution was used for the cell incubation.

Monolayer Cell Culture: 5×10^3 cells/cm^2 were cultured in 25 ml flasks. The cells were used till 6 passages. They were cultured in MEM with 10% FBS. When the flask floor was completely covered by the cells, the flasks were taken out of the incubator. The culture media was outpoured and the flask floor was washed with PBS, then tripsine/EDTA was added to the flask. The flasks were put again in the incubator for 3-4 min to let the cells get apart from the flask floor. Then the culture media with 10% FBS was added to the flask and its contents was used for the experiment.

Calculating Growth Curve and Doubling Time (DT): 10^4 cells were cultured in each well of a 24 well micro plate with 500µl MEM and 10% FBS in each well. After 24 hour, the cells of each 3 wells were excided and counted every day. This was done for 10 continuous days. Every 3 day, half of the MEM was refreshed. Then, the growth curve was drawn in a semi logarithmic scale. The curve had 3 phases including the lag, linear or logarithmic, and plateau phase. In the logarithmic phase, the cells increased with the following equation:

$$N = N_0.e^{bt} \quad (1)$$

in which, N_0 represents the number of the primary cells, N is the number of cells after the time t, and b is the line slope in the logarithmic phase. The doubling time (DT) was calculated from the following equation:

$$DT = ln2/b \quad (2)$$

Spheroid Culture: 8ml agar 1% was poured in each 100 ml Petri dish. Then 500000 cells in 12ml MEM with 10% FBS were cultured on the agar.

Calculating Spheroid Growth Curve and Volume Doubling Time (VDT): 4 days after the beginning of the spheroids culture, they were transferred to a 24 well micro plate. There was just one spheroid in each well. The spheroids were kept in a 37^c incubator with 5% CO_2 and saturated humidity. Two crossed diameters of spheroids were measured by the scaled lens under a microscope every day for one month. The spheroid volume was calculated by the following equation:

$$V = a.b^2.\ \pi/6 \quad (3)$$

in which a and b are the lesser and greater spheroid diameters respectively. Then, the growth curve was drawn in a semi logarithmic scale. This curve had the same 3 phases described before. In the logarithmic phase, the spheroids grow by the following equation:

$$V = V_0.e^{kt} \quad (4)$$

in which V_0 is the primary volume, V is volume after the time t and k is the line slope of the curve in the logarithmic phase. Then the volume doubling time (VDT) was calculated from the following equation:

$$VDT = ln2/k \quad (5)$$

IUdR Incubation: 100µl IUdR solution with 100µM concentration was added in each 10 cc culture media. The spheroids were kept in the IUdR solution for one VDT. Then, they were washed with PBS and irradiated.

γ Ray Irradiation: A ^{60}Co machine (Teraton 760) was used for the irradiation of the spheroids. Because of their weight, the spheroids were located at the bottom of the flasks. The maximum dose of the γ radation of the ^{60}Co sources occurs at 5mm depth of the liquid surface. Therefore, the flasks were filled in a way there will be 5mm culture media above the spheroids. The dose rate of the ^{60}Co system at 70cm distance and 5×11 cm^2 field size was 1.14 cGy. Hence, the time chosen to deliver 2 Gy radiation dose was 176 s. Then, the spheroids were transferred to a micro plate (one spheroid in each well). Thereafter, two crossed diameter of the spheroids were measured every day for a period of 9 days. Then, the spheroids growth curve was drawn.

III. Results

A. Monolayer Cells:

As described in the previous section, the monolayer cell numbers were counted for a period of 10 days and then its growth curve was drawn. As can be seen in Figure 1, the lag, logarithmic and plateau phases correspond to 0-2, 2-5, and 5-10 days respectively. The Calculation made from the line slope of the logarithmic phase of the growth curve using Equations 1 and 2 lead to a value of 25 h as the DT of the monolayer cells.

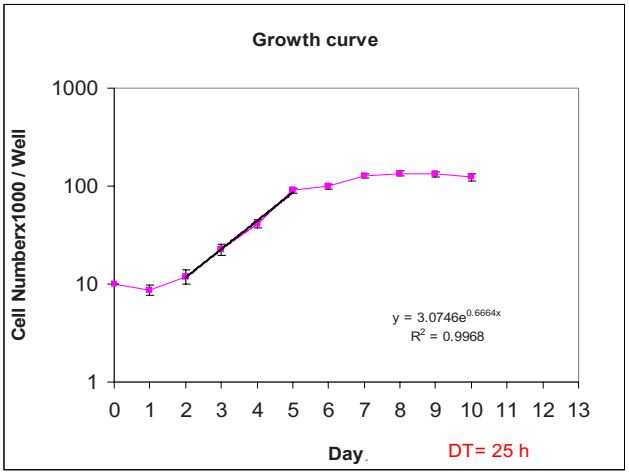

Fig. 1 Calculated growth curve and DT for the monolayer cells

B. Spheroid Volume Doubling Time

The calculated spheroid VDT is shown in Figure 2. The spheroid VDT was calculated from Equations 3, 4 and 5. The calculation resulted in a VDT of 63.48 h for the spheroids.

C. Radiation damage in the U87MG cells

100µm spheroids: The spheroids with a mean diameter of 100 µm were divided to 4 groups of: (1) the control; (2) the IUdR (these spheroids were incubated with the IUdR for one VDT without radiation); (3) ^{60}Co (these spheroids were irradiated to 2Gy of γ radiation from the ^{60}Co source); and (4) IUdR+^{60}Co (these spheroids were incubated with IUdR for one VDT, and they were then irradiated to 2Gy of γ ray from the ^{60}Co source. Thereafter, the diameters of all the four spheroid groups were measured for a period of 9 days from which their growth curve was determined as shown in Figure 3. As can be seen in this Figure, the control and IUdR groups show no damages. The ^{60}Co group shows significant damage but the most damages are seen in the IUdR+^{60}Co group. The difference between the group 3 and 4 was statistically significant.

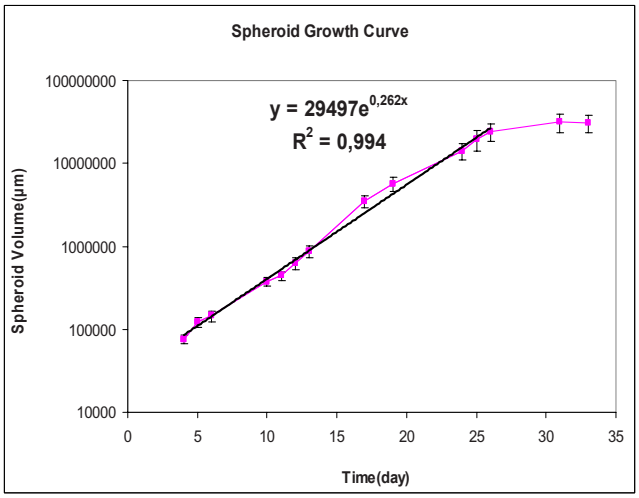

Fig. 2 Calculated growth curve for the spheroids

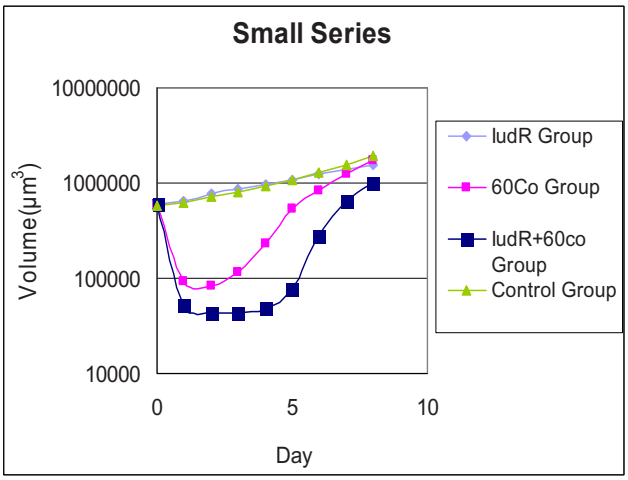

Fig. 3 The radiation damage of the U87MG cells (100µm spheroids)

300µm spheroids: The procedure for these spheroids was the same as that of the 100µm diameter spheroids. The relevant results obtained for these spheroids are shown in Figure 4. The control group shows no damage. In the IUdR group some damages are seen, The ^{60}Co group has more damages. However, the most damages are seen in the IUdR+^{60}Co group. It must be noted that the total damage for the 300µm spheroids are less than 100µm spheroids and it seems that for the larger spheroids, the repair mechanism is faster than the smaller ones.

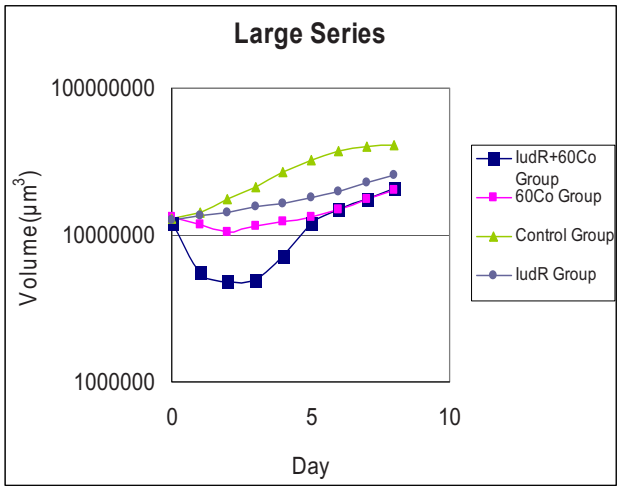

Fig. 4 The radiation damage of the U87MG cells (300μm spheroids)

IV. Conclusions

The goal of this research was to study the radiosensitizing effect of the IUdR in Glioma spheroids. We assumed that the IUdR can increase the radiation damages in the cancer cells. Our results obviously showed that in both sizes of the spheroids considered in this study, the IUdR+^{60}Co group showed much more damages compared with the ^{60}Co group. This indicates that the IUdR can increases the radiosensitivity of Glioma spheroids. Comparison between the two sizes of the spheroids shows more damage in the 100 μm spheroids. This can be explained by more hypoxic cells of greater spheroids which are resistant to ionizing radiation and the existence of some cells at the G0 cycle which do not uptake the IUdR.

Acknowledgment

The authors would like to acknowledge the financial support provided by Tarbiat Modares University. The authors would also like to thank the head and staff of the Department of Radiology of Iran University of Medical Sciences. We also like to acknowledge Dr Khoei for providing us access to her lab facilities and also for her scientific and technical assistance in performing the experimental measurements.

References

1. Kinsella TJ, Collins J, Rowland J, et al. (1988) Pharmacology and phase I/II study of continuous intravenous infusion of iododeoxyuridine and hyper fractionated radiotherapy in patients with glioblastoma multiform. J Clin Oncol. 6(5):871-879
2. Sullivan FJ, Herscher LL, Cook JA, et al. (1994) National Cancer Institute (phase II) study of high grade Glioma treated with accelerated hyper fractionated radiation and iododeoxyuridine: results in anaplastic astrocytoma. Int J Radiat Oncol Biol Phys 30 (3):454-460
3. Wrensch R, Bondy L. (2000) Central nervous system tumors. 2nd Edition. Churchill Livingstone, Edinburgh
4. Phillips PC. (1991) Antineoplastic drug resistance in brain tumors. Neurol Clin 9(2):383-404
5. Leibel SA, Scott CB, Loeffler JS. (1994) Contemporary approaches to the treatment of malignant Glioma with radiation therapy. Semin Oncol 21(2):198-219
6. Kalia VK. (1999) Optimizing radiation therapy of brain tumors by combination of 5-bromo-2-deoxy-uridine and 2-deoxy-D-glucouse. Indian J Med Res 10:182-187
7. Fornace AJ Jr, Dobson PP, Kinsella TJ. (1990) Enhancement of radiation damage in cellular DNA following unifilar substitution with iododeoxyuridine. Int J Radiat Oncol Biol Phys 18(4):873-878
8. Kinsella TJ, Dobson PP, Mitchell JB, Fornace AJ Jr. (1987) Enhancement of X ray induced DNA damage by pre-treatment with halogenated pyrimidine analogue. Int J Radiat Oncol Boil Phys 13(5):733-739
9. Hoffman RM. (1994) The three dimensional question: can clinically relevant tumor drug resistance be measured in vitro? Cancer Metastasis Rev 13(2):169-173
10. Neshastehriz A, Angerson WJ, Reeves JR, Smith G, Rampling R, Mairs RJ. (1997) Incorporation of iododeoxyuridine in multicellular Glioma spheroids: electron emitters. Br J Cancer 75(4):493-499

Author: Bijan Hashemi
Institute: Tarbiat Modares University
Street: Al-Ahmad and Chamran Cross
City: Tehran
Country: Iran
Email: bhashemi@modares.ac.ir

The use of radiobiological parameters and the evaluation of NTCP models. How do they affect the ability to estimate radiation induced complications?

P. Svolou, I. Tsougos, K. Theodorou, C. Kappas

Medical Physics Department, Medical School, University of Thessaly, Greece

Abstract— **Normal Tissue Complication Probability (NTCP) models currently used, provide a simplified representation of the clinical radiobiology since there are number of radiobiological mechanisms which affect the clinical outcome and are not taken into account by the models. The use of published radiobiological parameter sets in NTCP modeling introduce uncertainties on the dose-response curves due to the fact that each parameter set is accompanied by a certain standard deviation. Therefore, a model is represented by a dose-response bandwidth creating areas in which different models may coincide. The purpose of the present study is to evaluate the models and parameter sets determining the overlapping areas thus estimating the importance of parameter application.**

Keywords— **Radiobiological modeling, Radiotherapy, Breast cancer, NTCP**

I. Introduction

Despite the advanced treatment techniques applied in thoracic radiotherapy, radiation induced complications and toxicities of the respiratory system are relatively common after radiotherapy. Breast cancer patients treated with radiotherapy are vulnerable to such side effects (e. g Radiation Pneumonitis) because of the proximity of lung to the irradiated breast tissue [1]. The NTCP models used in literature provide a quantitative and qualitative approach of the clinical outcome, however radiation induced complications cannot be accurately evaluated by any model. This weakness derives from the fact that radiobiological factors (e.g intrinsic radiosensitivity) which influence the biological response to radiation, are not taken into account by the models [2,3,4]. Moreover, this weakness is enhanced when applying published parameter sets in radiobiological models in order to evaluate normal tissue complications on other patient groups. If the population examined is not adequate to extract parameter sets (from a statistical point of view), the selection of the appropriate published parameter set, is of great importance. Firstly, because published parameter sets derive from patient groups with specific clinical characteristics, which must be similar to the ones of the patient group examined, and secondly, each parameter value entering a model should be accompanied by a standard deviation. Therefore, each NTCP model is described by a group of dose-response curves, creating an area in which the model may vary. This generates areas of coincidence between the models, areas in which the models do not differentiate hence their predictive strength is constrained. In the present study, an extensive bibliographic research was conducted, in order to collect all published parameters sets used in NTCP models, so as to identify and evaluate these areas of coincidence [5,6,7,8,9,10,11,12,13].

II. Methods and materials

The models investigated were the Relative Seriality Model, the LKB and Parallel model. All parameter sets used in literature are shown in Table 1. There was a lack of available parameter sets used for the Parallel model. Only the set of Seppenwoolde et al. 2003 was available [7]. Therefore, there could be no model range established. In order to validate the existence of coincidence areas between the models, we selected a minimum and a maximum published parameter set, based on the D50 (or TD50) value. Table 2 shows the selected sets as well as a computed set of mean values for every model. Dose-response curves were plotted using DORES [14] for the minimum and maximum set for every model (Table 2), pointing out the range in which every model can vary depending on the parameter set choice, as well as the areas of coincidence between the models.

Table 1 Radiobiological parameters used in literature

Relative Seriality parameter sets				
Reference	*Case*	D50/TD50	γ/m	s/n
Mah et al.(1987)	Breast	26.0	2.00	0.031
Gagliardi et.al (2000)	Breast	30.1	0.97	0.010
Seppenwoolde et al.(2003)	Breast, Lung	34.0	0.90	0.060
Rancati et al. (2007)	Breast	16.3±1.1	1.08±0.28	0.15±0.11
LKB parameter sets				
Burman et al. (1991)	Breast	24.5	0.18	0.870
Martel et al. (1994)	Breast	28.0	0.18	0.870
Kwa et al. (1998)	Breast, Lung	30.5	0.30	1.000
Moiseenko et al. (2003)		30.5	0.26	1.020
Seppenwoolde et al. (2003)	Breast, Lung	30.8	0.37	0.990
Rancati et al.(2007)	Breast	16.4 ±1.1	0.36±0.08	0.86±0.10
Semenenko et al.(2007)		29.9	0.41	1.000
Parallel parameter sets				
Seppenwoolde et al.2003	Breast, Lung	30.8	0.37	0.99

O. Dössel and W.C. Schlegel (Eds.): WC 2009, IFMBE Proceedings 25/III, pp. 292–294, 2009.
www.springerlink.com

Table 2 Min/Max values of parameter sets

Relative Seriality Model		
Min	D50=15.1, γ=0.8, s=0.04	Rancati et al.(2007)
Max	D50=34.0, γ=0.9, s=0.06	Seppenwoolde et al(2003)
Mean	D50=24.6, γ=0.85, s=0.06	Present study
LKB Model		
Min	TD50=15.3,m=0.28,n=0.76	Rancati et al.(2007)
Max	TD50=30.8, m=0.37,n=0.99	Seppenwoolde et al(2003)
Mean	TD50=23.1, m=0.33,n=0.88	Present study
Parallel Model		
	TD50=30.8, m=0.37,n=0.99	Seppenwoolde et al(2003)

III. Results

Figure 1 and Figure 2 show the ranges of variance for the Relative Seriality and the LKB model, when applying the minimum and maximum parameter sets of every model. As it is evident from Fig. 3 a large overlapping area exists between the two models. In this area both models predict similar normal tissue complication probabilities. Observing the mean dose-response curve for each model (RS: D_{50}=24.6 Gy, γ=0.85, s=0.06 / LKB: TD_{50}=23.1 Gy, m=0.33, n=0.88) (Fig.3), up to the dose of 20 Gy the two models do not differentiate on their response. From 20 Gy and above the LKB model gives a steeper response to increasing dose than the Relative Seriality, however both models do not show great differences on their response behavior.

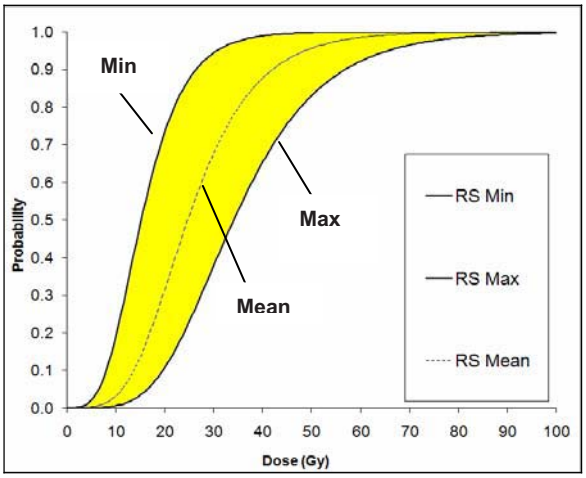

Fig.1 Yellow area depicts the range in which the Relative Seriality Model may vary, depending on the parameter set selection

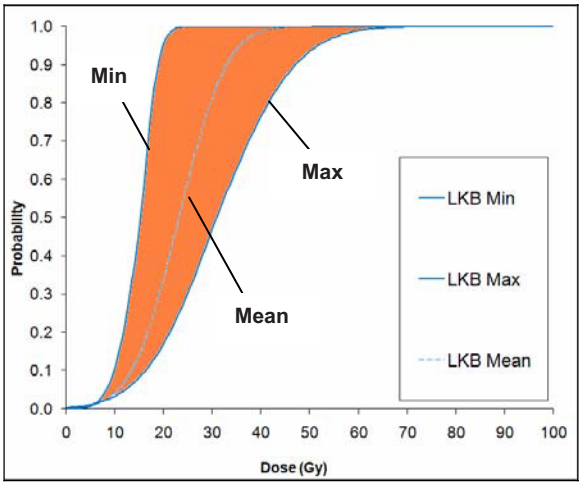

Fig. 2 Orange area depicts the range in which the LKB Model may vary, depending on the parameter set selection

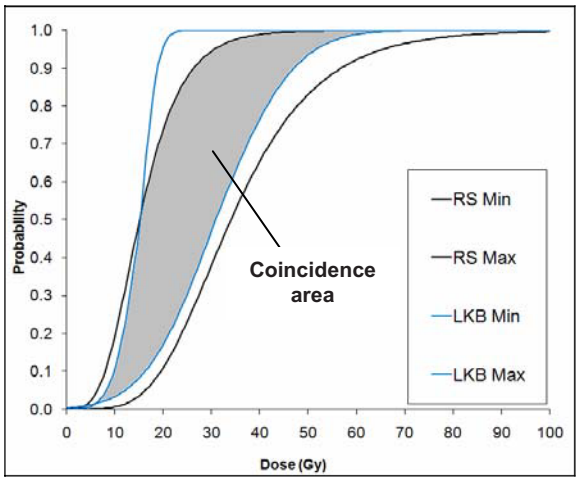

Fig. 3 Grey color depicts the area of coincidence of the models resulting from the use of non-specific radiobiological parameters

IV. Discussion

A matter of great importance is the selection of parameter sets entering a radiobiological model. The parametric values are usually accompanied by their standard deviation, therefore the models are represented by a group of dose-response curves, creating an area in which the model may vary. The optimum radiobiological evaluation would be

possible by using parameter sets extracted from patient groups with the same clinical characteristics as the ones examined. Nevertheless, when this is not possible, it is essential to select radiobiological parameters with the smallest standard deviation available, in order to avoid the aforementioned model coincidence. In conclusion, the dose-response curves used in NTCP modeling illustrate a simplified representation of the clinical radiobiology, because there are a number of radiobiological mechanisms and further related information that are not exclusively taken into account by the different NTCP models. The influence of the parameter uncertainties on the dose-response curves can be quite large and hence the use of published radiobiological parameter sets in NTCP modeling should be considered safe only when derived by similar clinical treatment.

References

1. Madani In, De Ruyck K, Goeminne H, De Neve W, MD, Thierens H, and Van Meerbeeck J, (2007) Predicting Risk of Radiation-Induced Lung Injury. Journal of Thoracic Oncology 9:864-874
2. Tsougos I, Mavroidis P, Rajala J, Theodorou K, J¨arvenp¨a¨a R, Pitk¨anen M.A, Holli K, OjalaA.T, Lind B, Hy¨odynmaa S and Kappas C (2005) Evaluation of dose–response models and parameters predicting radiation induced pneumonitis using clinical data from breast cancer radiotherapy. Phys Med Biol 50: 3535–3554
3. Tsougos I, Mavroidis P, Theodorou K, Rajala J, Pitk¨anen M A, Holli K, Ojala A T, Hy¨odynmaa S, J¨arvenp¨a¨a R, Lind B. and Kappas C (2006) Clinical validation of the LKB model and parameter sets for predicting radiation-induced pneumonitis from breast cancer radiotherapy, Phys Med Biol 51
4. Tsougos I, Nilsson P, Theodorou K, Kjell´en E, Borje Ewers S, Jarlman O, Lind B, Kappas C. and Mavroidis P (2007) NTCP modelling and pulmonary function tests evaluation for the prediction of radiation induced pneumonitis in non-small-cell lung cancer radiotherapy. Phys Med Biol 52:1055–1073
5. Mah K, Van Dyk, Keane T and Poon PY (1987) Acute radiation-induced pulmonary damage. A clinical study on the response to fractionated radiation therapy. Int J Radiat Oncol Biol Phys 13:179-188
6. Gagliardi G, Bjohle J, Lax I, Ottolenghi A, Eriksson F, Liedberg A, Lind P. and Rutqvist L (2000) Radiation Pneumonitis after breast cancer irradiation: Analysis of the complication probability using the relative seriality model. Int. J. Radiation Oncology Biol. Phys 46:373–381
7. Seppenwoolde Y, Lebesque J, Jaeger K, Belderbos J, Boersma L, Schilstra C, Henning T, Hayman J, Martel M. and Ten Haken R (2003) Comparing different NTCP models that predict the incidence of radiation pneumonitis. Int. J. Radiation Oncology Biol. Phys. 55:724–735
8. Rancati T, Wennberg B, Lind P, Svanee G. and Gagliardi G. (2007) Early clinical and radiological pulmonary complications following breast cancer radiation therapy: NTCP fit with four different models. Radiotherapy and Oncology 82:308-316
9. Burman C, Kutcher G J, Enami B et al. (1991) Fitting of normal tissue tolerance data to an analytic function. Int J Radiat Oncol Biol Phys 21:123-135
10. Martel M K, Ten Haken R K, Hazuka M B (1994) Dose Volume Histogramm and 3-D treatment planning evaluation of patients with pneumonitis. Int J Radiat Oncol Biol Phys 28:575-581
11. Kwa St, Theuws J, Wagenaar A, Damen E, Boersma L, Baas P, Muller S, Lebesque J. (1998) Evaluation of two dose–volume histogram reduction models for the prediction of radiation pneumonitis. Radiotherapy and Oncology 48:61–69
12. Moiseenko V, Craig T, Bezjak A, Van Dyk J (2003) Dose Volume analysis of lung complications in the radiation treatment of malignant thymoma: a retrospective review. Radiotherapy and Oncology 67:265-274
13. Semenenko V A, Li X A, (2008) Lyman-Kutcher-Burman NTCP model parameters for radiation pneumonitis and xerostomia based on combined analysis of published clinical data. Phys Med Biol 53:737-755
14. Tsougos I, Grout I, Theodorou K, Kappas C, (2009) A Free Software for the Evaluation and Comparison of Dose Response in Clinical Radiotherapy (DORES), International Journal of Radiation Biology, “in press”

Simulating dose and cancer risk due to low-dose neutron background in proton beam therapy

B. Athar[1] and H. Paganetti[1]

[1] Department of Radiation Oncology, Massachusetts General Hospital & Harvard Medical School, Boston, MA, USA

Abstract—**In proton therapy secondary neutrons are produced due to protons undergoing nuclear interactions with the treatment head and the patient. The neutron contribution to various organs is difficult to measure but can be simulated using Monte Carlo methods and whole-body computational phantoms.**

For this study we considered a proton therapy treatment field to treat a CTV in the central spine, thus exposing the whole body to a low-dose neutron background. In order to mimic the treatment of a pediatric case, we have implemented phantoms resembling an 11-year old and a 14-year old patient. We considered six treatment fields with varying treatment volumes and depths.

The results show that the cancer risk for most organs is lower than the natural baseline risk assuming risk models based on the BEIR VII report [1] and radiation weighting factors given by the ICRP [2].

Keywords— **Proton Therapy, Scattered Radiation, Second Cancers**

I. Introduction

There is a growing concern of increased risk of treatment complications among radiation therapy patients as the age of patients diagnosed with cancer is decreasing due to early cancer detection and treatment. Of concern are organs affected by the primary beams but also organs at a considerable distance to the target. The latter may experience low dose due to long-range neutons generated in proton-nucleus interactions. Neutrons are generated in the accelerator head (external neutrons) and inside the patient (internal neutrons). This work does focus on simulating the potential risk for developing a second cancer for a treatment of an 11-year old male and a 14-year old male patient with proton therapy to the central spine region.

II. Methods

The simulations were performed with the 8.1.p01 version of the Geant4 toolkit [3]. The physics settings for proton interactions are described elsewhere [4]. Whole-body computational phantoms were implemented as voxelized geometries as described elsewhere [5].

First, particles were tracked through the treatment head [6] to generate phase space files containing spatial, energy and angular information of the particles at the exit of the treatment nozzle, i.e. at the entrance of the phantom. Next, dose calculations in the phantom were done by sampling source particles from the phase space files. The starting point was defined to ensure irradiation of the virtual patient posteriorly, between vertebrae-t and vertebrae-l.

The scoring of the dose has to take into account the particle (and particle energy) specific radiation weighting factors. These can be determined on-the-fly during particle tracking as described elsewhere [7]. We applied the radiation weighting factors specified by the ICRP [2]. It is known that these are associated with considerable uncertainties. However, not enough experimental data exist to justify alternative settings.

Six treatment fields were considered as listed in Table 1.

Table 1 Diameter, range and modulation widths for each considered spread-out Bragg peak (SOBP) field

Field	Aperture Diameter [cm]	Beam Energy at Treatment Head Entrance [MeV]	SOBP Range [cm]	SOBP Width [cm]
1	3	169.2	10	5
2	6	169.2	10	5
3	9	169.2	10	5
4	3	178.3	15	10
5	6	178.3	15	10
6	9	178.3	15	10

Doses were scored for a variety of critical organs outside of the main radiation field. In addition, risks for developing a second cancer were estimated based on risk models published by the National Research Council in the BEIR VII report [1]. We decided to use the Lifetime Attributable Risk (LAR) as indicator (integrating excessive risks due to radiation to an attained age of 100 years). A dose and dose-rate effectiveness factor (DDREF) of 1 was used [8].

O. Dössel and W.C. Schlegel (Eds.): WC 2009, IFMBE Proceedings 25/III, pp. 295–297, 2009.
www.springerlink.com

III. Results

Our overall findings are that absorbed neutron equivalent doses to various anatomical organs decreases as the lateral distance from the target increases. Further, as the field size increases the scattered neutron doses (external) decrease due to less scattering in the aperture. External neutrons originating in the treatment head represent the main contribution

We found that with an increase in field size less primary protons are stopped in the aperture, which leads to a decrease in neutron fluence from the treatment head. On the other hand, an increased field size leads to a larger internal neutron dose because of higher proton fluence in the patient. Internal neutron doses scale with the target volume. As the modulation width increases, the neutron equivalent dose increases due to a larger treatment volume.

Figure 1 shows the neutron equivalent doses in mSv per treatment Gy in various organs as a function of lateral distance from the target for the 11-yer old patient treated for a spine lesion. The neutron doses from first three fields 1-3 (Table 1) are smaller compared to those from the fields 4-6 (Table 1) with larger range and modulation widths and also lower proton beam energies for the first three fields. Doses to organs farther away from the field have large statistical errors in tens of % for scattered doses, in particular for small organs. Close to the field the uncertainty is in the order of 1-3%. Due to large uncertainties associated with neutron weighting factors the uncertainty might even be as much as 50%.

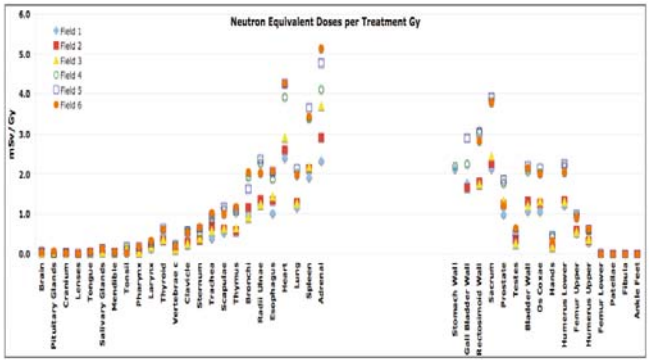

Fig. 1 Absorbed scattered (external + internal neutron doses in an 11 year old male phantom) neutron equivalent dose distribution at various organs as a function of the lateral distance from the PTV site. The diamonds (turquoise), solid squares (red), triangles (yellow), opened circles (green), open squares (blue), and solid circles (orange) denote dose distributions for fields 1, 2, 3, 4, 5, and 6, respectively.

Assuming a treatment dose of 70 Gy figure 2 shows the lifetime attributable risk for several organs assuming treatment with field #2 (Table 1) for both phantoms. The unexposed lifetime baseline risks used in this analysis are based on 2001-2005 [9]. Overall, the risk increases with decreasing patient age

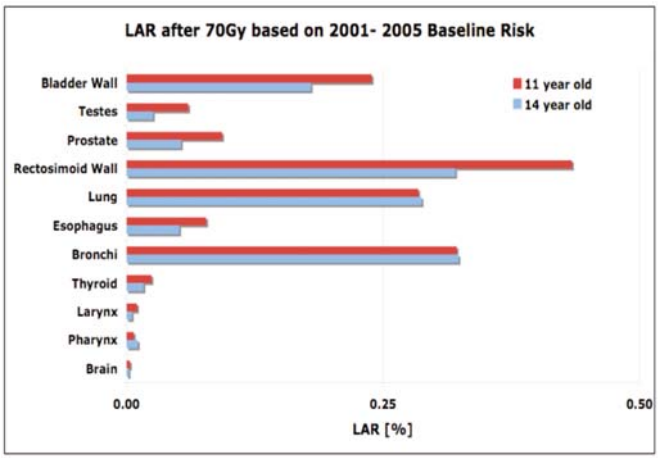

Fig. 2 Simulated lifetime attributable risk, LAR, [%] for an 11-year old male and a 14-year old male patient receiving 70 Gy to the central spine region using field #2.

There are major uncertainties in the applied risk models. First, they are based on data from atomic bomb survivors. Second, there is the assumption that the solid cancer risk dependence at low doses is linear. Due to these large uncertainties in these risk models the estimated LAR values are known at best within 50% error.

IV. Conclusions

This study does focus on scattered radiation. Further, the BEIR risk models are not necessarily applicable to medium dose levels. Consequently we have excluded organs from the study that were irradiated by the primary beam.

The variation among different organs is substantial due to the significant decrease in neutron dose with the increasing distance to the field edge.

Overall, we conclude that (given the large uncertainties associated with such risk estimations), that the lifetime risk for developing a second cancer is smaller or (at most) comparable with the baseline risk.

Acknowledgment

This work was supported in part by a grant from the National Cancer Institute: CO6 CA059267

REFERENCES

1. BEIR VII, 2006. Biological Effects of Ionizing Radiation Committee. Health risks from exposure to low level of ionizing radiation, National Research Council, National Academy of Science.
2. ICRP 2003 Relative Biological Effectiveness (RBE), Quality Factor (Q), and Radiation Weighting Factor (wR. International Commission on Radiological Protection (Oxford: Pergamon) ICRP Publication 92
3. Agostinelli S et al. 2003 GEANT4 - a simulation toolkit. Nuclear Instrum. Methds. Phys. Res. A 506 250-303.
4. Zacharatou Jarlskog C and Paganetti H: Physics settings for using the Geant4 toolkit in proton therapy. IEEE Trans Nucl Sci 2008: 55, 1018-1025
5. Zacharatou Jarlskog C et al 2008. Assessment of organ specific neutron doses in proton therapy using whole-body age-dependent voxel phantoms. Phys. Med. Biol. 53 693-717.
6. Paganetti H, Jiang H, Lee SY, and Kooy H 2004a. Accurate Monte Carlo simulations for nozze design, commissioning, and quality assurance in proton radiation therapy Med. Phys. 31 3107-18.
7. Zacharatou Jarlskog C and Paganetti H: Sensitivity of different dose scoring methods on organ specific neutron doses calculations in proton therapy. Phys Med Biol 2008: 53, 4523-4532
8. Kocher DC, Apostoei AI, and Hoffman FO 2005. Radiation effectiveness factors for use in calculating probability of causation of radiogenic cancers. Health Phys. 2005; 3-32.
9. SEER. Cancer Statistics Review 1975-2005. http://seer.cancer.gov/csr/1975-2005.

Author: Harald Paganetti
Institute: Massachusetts General Hospital, Radiation Oncology
Street: Fruit Street, Proton Therapy Center
City: Boston, MA 02114
Country: USA
Email: hpaganetti@partners.org

Characterization of barite and crystal glass as Attenuators in X-ray and gamma radiation Shielding

Almeida Jr., Airton T[1]., Pereira dos Santos M. A[2]., Nogueira Tavares, M. S[3]., Filho, J. A[4].

[1] FUNDACENTRO - Fundação Jorge Duprat Figueiredo, de Segurança e Medicina do Trabalho, Av. Guajajaras, 40, Centro, Belo Horizonte, Brazil, airton.almeida@fundacentro.gov.br
[2]CRCN/CNEN - Centro Regional de Ciências Nucleares. Av. Prof. Luiz Freire, 200, Cidade Universitária, Recife, Brazil, masantos@cnen.gov.br
[3]CDTN/CNEN - Centro de Desenvolvimento da Tecnologia Nuclear, Av. Antônio Carlos, 6.627, Campus da UFMG, Pampulha, Belo Horizonte, Brazil, mnogue@cdtn.br
[4]DEN/UFPE - Departamento de Energia Nuclear - Universidade Federal de Pernambuco, Av. Prof. Luiz Freire no 1000, 50740-540, Recife, Brazil, jaf@ufpe.br

Abstract— **Aiming to determine the barium sulphate ($BaSO_4$) ore and crystal glass attenuation features, both utilized as shieldings against ionizing X and gamma radiations in radiographic installations, a study of attenuation using barite plaster and barite concrete was carried out, which are used, respectively, on wall coverings and in block buildings. The crystal glass is utilized in screens and in windows. To do so, ten plates of barite plaster and three of barite concrete with 900 cm2 and with an average thickness ranging from 1 to 5 cm, and three plates of crystal glass with 323 cm2 and with thicknesses of 1, 2 and 4 cm were analyzed. The samples were irradiated with X-rays with potentials of 60, 80, 110 and 150 kilovolts, and also with 60Co gamma rays. Curves of attenuation were obtained for barite plaster and barite concrete (mGy/mA.min) and (mGy/h), both at 1 meter, as a function of thickness and curve of transmission through barite plaster and barite concrete as a function of the thickness. The equivalent thicknesses of half and tenth value layers for barite plaster, barite concrete and crystal glass for all X-Ray energies were also determined.**

Keywords— **shielding, radiation protection, Curves of attenuation, crystal glass**

I. Introduction

Crystal glass and the barite plaster and barite concrete has been largely used as shielding material in installations housing gamma radiation sources as well as x-ray generating equipment , in order to minimize exposure to individuals.

Crystal glass is a compound of nefetina, syenite, ferrous oxalate, petalita, pyrite, sodium nitrate, selenium, caustic soda, sodium sulfate, oxides of silicon, lead, antimony, cobalt, copper, nickel, zinc and the barite plaster and barite concrete are compounds of cement, sand, barium sulfate and water. The knowledge of the physical characteristics crystal glass and the barite such as density, the degree of radiation attenuation and composition, granulometry, plasticity, density, resistance to compression and the degree of radiation attenuation for the different types of barite plaster and barite concrete commercially available in Brazil respectively are very important when dealing with shielding calculations for both medical and industrial installations.

This work was carried out aiming to determine the transmission and attenuation factors as well as the thickness equivalent of a half value layer and deci value layer for different X – ray energies and gamma radiation of 60Co. Some physical characteristics, such as density, composition, granulometry, plasticity, resistance to compression and radiation attenuation for the different types of barite plaster, of crystal glass, commercially available in Brazil are not well known[1,2,3,4].

II. Material and Methods

Barium and sulphate concentrations in barite samples from the states of Bahia, Piauí and Minas Gerais, Brazil, were determined by using two different methods: a) the soil sulphur method, based on the use of acetic acid and sodium phosphate for extracting barium and sulphate forming a colourless, crystalline extract. The sulphur content of the solution was determined by absorption spectrophotometry in both the UV and visible regions as well as by atomic absorption spectrometry. b) The gravimetric method [5, 6] where the sulphate was obtained by precipitation with barium chloride, and then washed with chloridric acid.

In order to obtain data for the attenuation curves, 20 x 20 cm^2 barite slabs with different thicknesses (1 to 20 cm) were prepared. They were irradiated with x-rays generated by a diagnostic type x-ray equipment (Pantak 250) for accelerating potentials varying between 80 and 150 kV, while keeping the tube current constant at 10 mA (radiation qualities used were ISO 60, 80, 110 and 150). The air kerma rates

O. Dössel and W.C. Schlegel (Eds.): WC 2009, IFMBE Proceedings 25/III, pp. 298–300, 2009.
www.springerlink.com

were measured with a 0.6 cc ionization chamber coupled to a Farmer dosimeter. The focus to detector distance was fixed at 1 meter. Data for slab thicknesses higher than 20 cm were obtained by extrapolation.

III. Results

Table 1 and 2 presents the results the qualitative analysis for the plaster, as well as the granulometric analysis of the barite mineral (sand +$BaSO_4$) and their respective densities.

The chemistry composition of the crystal glass, the barite plaster and barite concrete are indicated in the table 3 and 4.

Table 1 - Chemical characteristics and composition of barite mineral ($BaSO_4$)

Origin	Mineral Composition		
	% Ba	% SO_4	% Soil
Piauí	33.7	24.7	41.6
Bahia	32.5	24.5	43.0
+*M.Gerais	44.3	31.0	24.7
+M.Gerais	46.2	32.4	21.3

+* Barium sulphate (gray); + barium sulphate (purple)

Table 2 - Chemical characteristics and composition of barite mineral (sand).

Origin	Sand Loam Soil Composition						
	% clay	% silt	% VFS	% FS	% MS	% CS	ρ(g•cm-3)
Piauí	1	46	35	16	2	0	1.6
Bahia	0	36	16	3	34	14	2.1
+*M.Gerais	2	46	46	6	-	-	1.6
+M.Gerais	2	47	41	10	-	-	1.9

VFS (very fine sand); FS (fine sand); MS(medium sand); CS (coarse sand).

Table 3 - Cristal glass characteristic

CRISTAL GLASS	THICKNESS (cm)				
% Ce	% other composition*	Crystal glass			
0.5	99.5	1.0	2.0	3.0	4.0

* Nefetina, syenite, Ferrous oxalate, Petalita, Pirita, sodium nitrate, Selêncio, caustic soda, sodium sulfate, oxides of silicon, lead, antimony, cobalt, copper, nickel, zinc.

Table 4 – Composition of barite plaster and concrete

Composition	$BaSO_4$ (g)	Cement (g)	Sand (g)	H_2O (ml)	Barite stones((g)
Mixture I	600	200	400	270	-
Mixture II	500	300	500	300	-
Mixture III	300	200	300	400	400

In figures 1, 2 and 3 the attenuation curves are presented in function of the thickness for different compositions of barite plaster – mixture I; mixture II; concrete – mixture III.

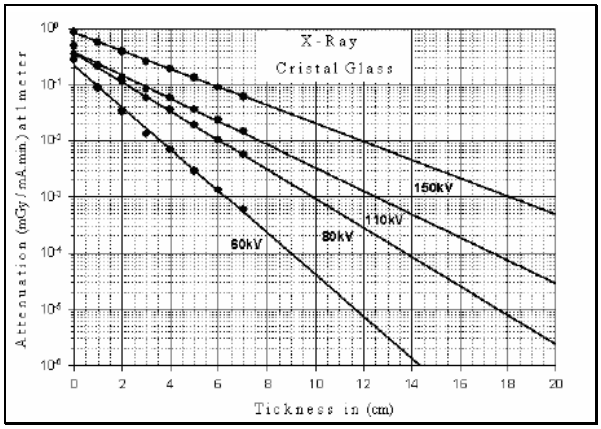

Figure 1 - Attenuation curves obtained for crystal Glass X-ray irradiated with potential constants of 60, 80, 110, 150 kV and density of ñ = 2,08 g/cm3 respectively.

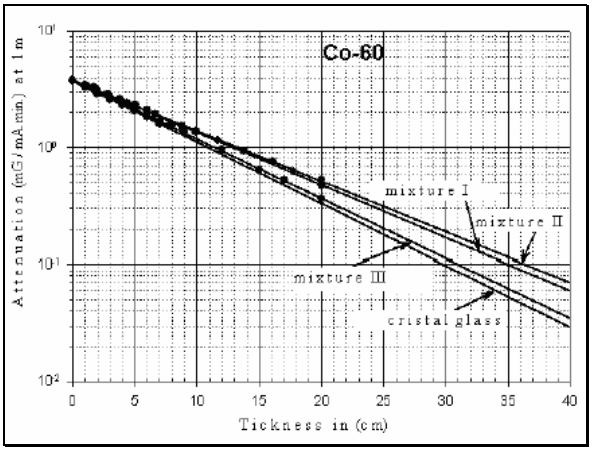

Figure 2 - Attenuation curves obtained for barite plaster X-ray and crystal glass, irradiated with 60Co, with density of 1.95 g/cm3 and 2.05 g/cm3 respectively.

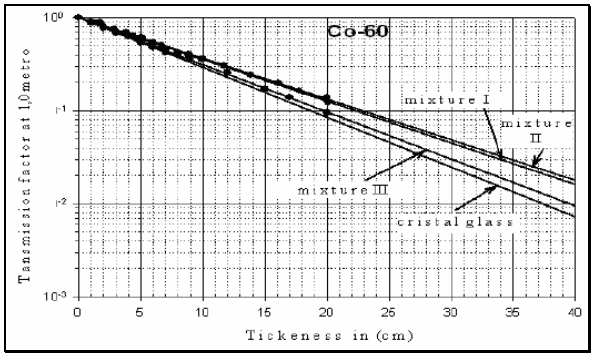

Figure 3 – Transmission curves obtained for barite plaster X-ray and crystal glass, irradiated with 60Co, with density of 1.95 g/cm3 and 2.05 g/cm3 respectively.

IV. Discussion

The analysis of the data on Table 1 for samples from Piauí and Bahia States show that there are no significant differences in their barium, sulphate and soil content. However, the data for the soil composition show that there are differences in the percent of fine sand, very fine sand and silt and that these differences affect the specific density of the barite mineral. The lower the percent of fine sand, very fine sand and silt the higher the specific density (Bahia: 2.12 g•cm^{-3}; Piauí: 1.60 g•cm^{-3}).

The curve of the Figures 1, 2 and 3 can be too used to determine the thickness of wall coverings facing the primary and secondary beams in order to conform to the desired level of radiation in a radio diagnostic installation.

V. Conclusions

The attenuation and transmission curves, and thicknesses of the semi and deci-reduced layers are rare for the barite plaster, barite concrete and crystal glass types of materials studied, although their use permits the dimensioning of the armor covering for external radiation whit precision and safety without elevating the cost of protection.

The results obtained in this study show that the barium content is higher than the sulphate content in the $BaSO_4$ compound regardless of its origin. The composition of soil rather than its proportion in the mixture is an important parameter in determining the specific density of the barite plaster.

Both the transmission and attenuation curves obtained in this study present characteristics that are similar to those published elsewhere for other materials.

Acknowledgment

The authors wish to thank the directors of the CRCN / CNEN and DEN / UFPE by supporting on the implementation of this experimental work.

References

1. Ralph C. C. Shielding calculation below 100 kVp in concrete-equivalent materials. Health Physics, 36 (January): 69-70, (1979).
2. DOUGLAS J. SIMPKIN. General solution to the shielding of medical X and x ray by the NCRP report 49 methods Health Physics, New York, v. 52, n.4, p. 431 - 436, 1987.
3. Kenneth R. KASE, Ph.D. Shielding of Medical Radiation Facilities – National Council on Radiation Protection and Measurements Reports No. 147 and No. 151. The Second All African IRPA Regional Radiation Protection Congress, Ismailia Egypt 22-26 April 2007.
4. S.M.J. Mortazavi, M.A. Mosleh-Shirazi, M.R. Maheri,H.Yousefnia, S. Zolghadri,A. Haji-pour. Production of an economic high-density concrete for shielding megavoltage radiotherapy rooms and nuclear reactors. Iran. J. Radiat. Res., 2007; 5 (3): 143-146.
5. Vogel, A. Análise Inorgânica Quantitativa. Guanabara S.A. 4th Edition, (1981).
6. Otto, A. Química Analítica Quantitativa. Ed. Técnicos e Científicos, 3rd Edition,V.1, (1981).

Population exposure from medical X-rays in Germany: time trends – 1996 to 2005

E.A. Nekolla[1], J. Griebel[1] and G. Brix[1]

[1] Federal Office for Radiation Protection, Department of Radiation Protection and Health, Neuherberg, Germany

Abstract— **Data on medical radiation exposure due to diagnostic X-ray procedures in Germany for 1996 to 2005 are presented. Information on annual frequencies of X-ray procedures was for the most part obtained from German health insurance companies. Effective doses per examination were taken from a recent nation-wide survey on CT practice, research projects, random samples of measurements in hospitals and medical practices, and the current literature. From frequency data and dose estimates the collective effective dose and the effective dose per inhabitant were computed, and trends in time series were investigated. In Germany, about 1.6 X-ray examinations per capita and year were performed in 2005. On the one hand, the frequency for X-ray examinations is decreasing during the 1996 to 2005 period. On the other hand, the mean annual per caput effective dose shows an increase from about 1.6 mSv in 1996 to about 1.8 mSv in 2005. This rise is mainly caused by the increased use of computed tomography (CT). CT contributes more than half of the total cumulative effective dose in 2005 albeit it contributes only about 7% to the overall frequency of X-ray procedures. Increasing trends in the annual per caput effective dose due to X-ray examinations are also observed in many other industrialised countries, reflecting the rising importance of diagnostic imaging procedures and the increasing use of new diagnostic techniques, especially of CT. However in international comparison, Germany is positioned in the upper range regarding the population exposure from medical X-rays.**

Keywords— **population exposure, diagnostic X-rays, frequency, dose survey, collective effective dose**

I. Introduction

Article 12 of the Medical Exposure Directive of 1997 [1], entitled "Estimates of population doses", requires Member States to ensure that the distribution of individual dose estimates from medical exposure is determined for the population and for relevant reference groups of the population, as may be deemed necessary by the Member State. With the amended "Röntgenverordnung" (X-ray Ordinance) coming into force in 2002, Germany has made the implementation of Article 12 of the Medical Exposure Directive a matter for national legislation: The Federal Office for Radiation Protection (BfS) was assigned the official task to regularly assess medical radiation exposures of the general population.

In the most recent evaluation, data of the years 1996 to 2005 were included.

II. Materials and methods

A standardised method has been developed to permit a consistent evaluation over time and thus a trend analysis. Beware of the fact that systematic errors cannot be completely avoided, the BfS method to estimate frequency and per caput dose aims at keeping these errors at least constant in order to be able to recognise trends as early and as reliable as possible.

A. Frequency data

Information on annual frequencies of X-ray diagnostic procedures was mainly obtained from German health insurance companies. In Germany, the statutory health insurance (SHI) is the main source of healthcare funding covering almost 90% of the population. About 9% of the population have full-cover Private Health Insurance (PHI). As a result of these parallel systems of statutory and private health insurance, there are two different medical fee schedules, i.e. reimbursement catalogues, in Germany, one for the statutory health insurance funds (EBM = **E**inheitlicher **B**ewertungs**m**aßstab [=valuation standard]) and one for the private health insurance funds (GOÄ = **G**ebühren**o**rdnung für **Ä**rzte [=medical fee schedule for physicians]).

In these reimbursement catalogues, a great number of the physicians´ services, i.e. the different kinds of medical attendance and thus also the radiological examinations, are accounted for via special codes (Example: GOÄ 5100 = two-view examination of cervical spine).

There are about 120 codes referring to GOÄ, and about 110 codes corresponding to EBM. Both, the GOÄ and the EBM codes were arranged according to the type of diagnostic procedure and/or the region of examination. To achieve a standardisation, 19 categories were created in total: dental examinations, exams of head, shoulder, thorax, abdomen, pelvis/hips, extremities, spine, mammography, exams of upper gastro-intestinal (GI) tract, lower GI tract, urinary tract, bile tract, osteodensitometry, computed tomography (CT), arteriography, venography, interventional procedures, other and non-assignable examinations.

O. Dössel and W.C. Schlegel (Eds.): WC 2009, IFMBE Proceedings 25/III, pp. 301–304, 2009.
www.springerlink.com

According to international standards, the term "examination" includes all X-ray applications which – referring to one organ – are required to answer a clinical question by means of an X-ray modality. E.g. a two-view chest X-ray examination combined with fluoroscopy is considered to be one examination.

Complete code numbers are obtained for SHI out-patients, i.e. for about 70% of all X-ray examinations. For privately insured patients, total frequencies are determined on the basis of random samples taken separately for in-patients and out-patients by the PKV. Sample sizes comprise for about 0.1% of the total account number. In 2005, X-ray applications paid by private health insurance funds account for about 15% of all X-ray diagnostics in Germany where about 2/3 refer to out-patients.

Code numbers for SHI in-patients have to be estimated from out-patient data. "In-patient to out-patient ratios" for the various examination categories were estimated by means of data from a recent research project which evaluated the frequency of X-ray diagnostics in German hospitals for the year 2002. Using these ratios, in-patient examination frequencies were extrapolated from out-patient numbers. Due to small numbers in the private in-patient sector, it was decided to use this approach for the total in-patient sector, not only for SHI in-patients. About 20% of X-ray applications in 2005 are assigned to German in-patient facilities.

In Germany, a clear allocation of codes to certain X-ray diagnostic procedures or to certain body regions or organ systems is not always possible since in certain cases the same code is used for different X-ray applications or various body regions. For example one single code (GOÄ 5030) refers to X-ray applications of the extremities, the shoulder and the pelvis. A recent research project has estimated the proportional fractions of allocations of body regions in these "accumulative codes" for in-patients. The estimates for in-patients are used for both, in-patients and out-patients.

B. Effective dose per examination type and collective effective dose

The effective doses per examination type for radiographic and radioscopic examinations were calculated using measured quantities and conversion factors from these measured quantities to effective dose. The conversion factors were either obtained from literature (e.g. [2]) or by using the software X-RAY DOSIMET-RG which is based on the results of Monte Carlo calculations with anthropomorphic phantoms [3]. The basic quantities measured were mainly kerma area product, KAP, but also air kerma, K_A, or values reported for tube current and voltage. These were collected for several examination types in selected German hospitals. For examination types, where measured data were not available, assumptions were made concerning e.g. fluoroscopy time and KAP per minute. Representative effective doses for CT examinations were estimated on the basis of data of a nation-wide CT survey in 1999 [4] using the software CT-EXPO. The dosimetric algorithm implemented in this program was validated for a number of CT scanner types by TLD measurements at an anthropomorphic Alderson phantom [5].

The annual collective effective doses from X-ray diagnostics were obtained by multiplication of the estimated effective doses per examination type (defined by code) with the corresponding annual frequency, and summation over all types of examination. For the entire period 1996 to 2005, dose values for the different X-ray procedures were assumed to be constant except for CT examinations. For CT examinations a model was postulated which uses a variable dose over the period to account for technical developments in the field of CT (in particular the availability of multi-slice CT systems).

III. Results

A. Frequency data

In Germany, the frequency of X-ray examinations per head of population was approximately 1.6 in the year 2005. A decreasing trend in the overall frequency of X-ray exams was observed during the period 1996 to 2005 (see figure 1).

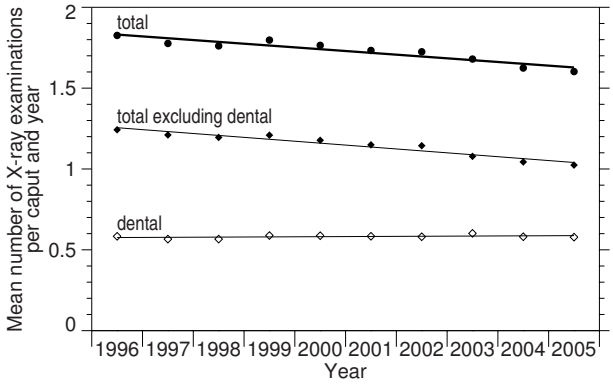

Fig. 1: Annual per caput number of medical and dental X-ray examinations in Germany for 1996 to 2005

Dental X-ray diagnostics account constantly for about one third of the total number of X-ray examinations (see figures 1 and 2).

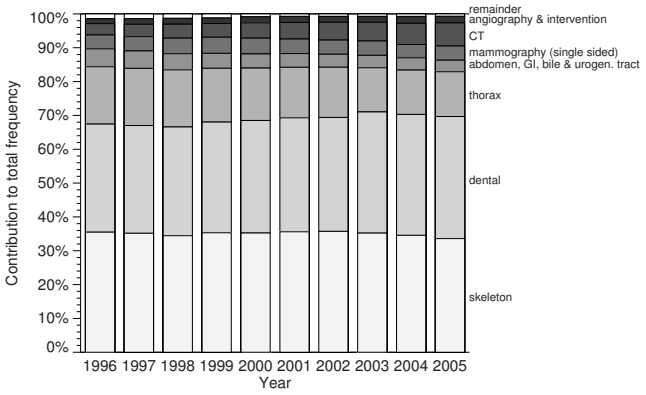

Fig. 2: Contribution of different examination types to the total frequency in dependence on calendar year in Germany

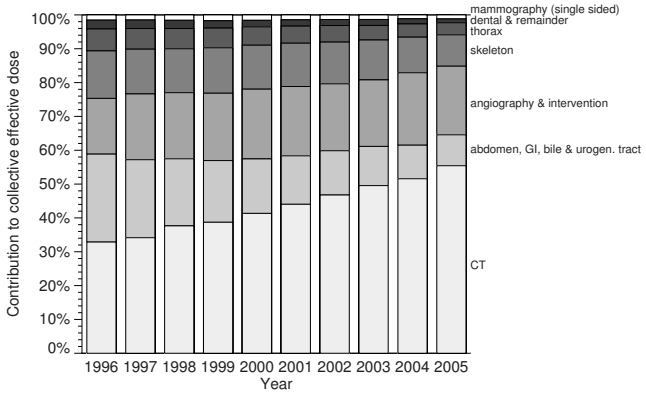

Fig. 4: Contribution of different examination types to the total collective effective dose in dependence on calendar year in Germany

Apart from dental X-ray examinations, X-ray examinations of the skeleton (i.e. head, shoulder, spine, pelvis/hip, extremities) and of the thorax are most frequent. The frequency of conventional X-ray examinations of the chest, spine and of the abdomen (including digestive, bile and urogenital tract) and of venographies is decreasing.

In contrast, the number of CT examinations is increasing, accounting for about 3% of the total X-ray frequency in 1996 and for about 7% in 2005 (see figure 2). Besides, the number of arteriographies and of interventional procedures is also on the increase.

B. Mean annual per caput effective doses

The mean annual per caput effective dose from X-ray examinations in Germany shows an increase from about 1.6 mSv in 1996 to about 1.8 mSv in 2005 (see figure 3). This rise can mainly be attributed to the increased application of CT.

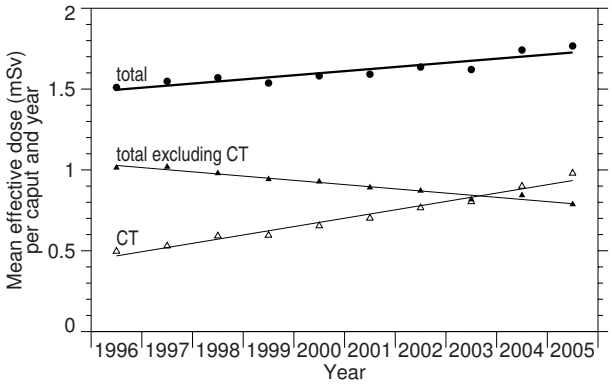

Fig. 3: Mean annual effective dose (mSv) per caput due to X-ray diagnostics in Germany for 1996 to 2005

CT contributes about half of the total cumulative effective dose in 2005 despite the fact that it contributes only about 7% to overall X-ray procedures (see figures 2 and 4).

IV. Discussion and conclusion

To assess population exposure from X-ray diagnostics in Germany, a standardized method has been developed to permit a consistent evaluation over time and thus a trend analysis. A decreasing trend in frequency and an increasing trend in the annual per caput effective dose due to X-ray diagnostics was observed for the decade 1996 to 2005. This increase in per caput dose can be observed in many industrialized countries, reflecting the increasing importance of diagnostic imaging procedures and the increasing use of new diagnostic techniques, especially the rising use of CT. In 2005, the frequency of X-ray examinations per head of population is about 1.6 and the mean per caput effective dose is 1.8 mSv. Nuclear medicine examinations contribute relatively little to population exposure compared to medical X-rays. On average, the annual per caput number of nuclear medicine exams is 0.05, and the annual per caput effective dose is 0.13 mSv [6].

A. International comparison

Compared to other industrialized countries, Germany is positioned in the upper range. UNSCEAR, the United Nations Scientific Committee on the Effects of Atomic Radiation, has regularly monitored the medical uses of radiation for a multitude of countries as part of its continuing review of sources of exposure [7]. It is striking that the reported estimates of population doses from medical procedures vary widely between countries with similar levels of health care.

However, interpreting the UNSCEAR data needs some caution because the methods of data collection and assessment vary substantially between different countries since there are no internationally accepted protocols for evaluating patient exposures from medical X-ray imaging procedures. For that reason, the European Commission initiated a study at the end of 2004 to review recent surveys of population exposure from medical X-rays, to understand the differences and sources of uncertainty, and to develop methods for future surveys. The multinational project (called DOSE DATAMED) involved partners from ten European countries [8]. The main result of the project was that there are, indeed, large differences in the population dose from all medical X-ray examinations between some of the ten European countries studied in this project. For example, a difference of about a factor of four in the mean per caput effective dose has been seen between the three countries with the highest estimates (Belgium, Germany, Luxemburg) and the three countries with the lowest estimates (Denmark, Netherlands, United Kingdom). These differences were thought to be real (i.e. much larger than the uncertainties) and primarily due to the different healthcare systems operating in each country.

In the United States the population exposure due to radiodiagnostics is estimated to be even higher than in European countries with an approximate per caput effective dose of 3 mSv in 2006 [9].

B. Assessing radiation risks for patients

Concerns about the continuous rise in population exposure due to the increasing use of radiological imaging arose in the US by the „American College of Radiology White Paper on Radiation Dose in Medicine“ [10] assuming that the current annual collective dose from medical exposure in the US “may likely result in an increase in the incidence of imaging-related cancer in the US population in the not-too-distant future.” However, a critical problem of this kind of radiation risk assessment is that it is based on collective effective dose estimates, i.e. does not take into account that medical exposures are not equally distributed among the population but rather cumulate to a considerable amount in certain groups of severely-ill patients, e.g. cancer patients whose life expectancy is markedly lower than that of the general population. Therefore, a reliable risk analysis of radiological imaging procedures has to be broken down to diagnosis-related groups of patients [11]. In risk assessments it is also important to note that the probability of a radiation induced cancer significantly decreases with increasing age at exposure. This must especially be accounted for when assessing radiation risk for patients since these are, in general, considerably older than the average population. Moreover, radiation risk estimates have been derived using the so-called linear, non-threshold (LNT) hypothesis, which is based on the assumption that the increase in cancer risk is proportional to dose. Yet, one has to be aware that the risks evaluated at low dose levels are hypothetical, i. e. that estimates of excess cancer cases do not refer to radiation induced cancer cases that can actually be observed.

In contrast to the hypothetical radiation risk supposed to interfere the patient many years later, diagnostic procedures benefit the patient immediately.

REFERENCES

1. Council Directive of 97/43/EURATOM. Health protection of individuals against the danger of ionising radiation in relation to medical exposures. O.J. No. L 180/22 (9.7.1997)
2. Hart D, Jones DG, Wall BF (1994) Estimation of effective dose in diagnostic radiology from entrance surface dose and dose-area product measurements, Report NRPB-R262. HMSO, London
3. Drexler G, Panzer W, Widenmann L, Williams G, Zankl M (1990) The calculation of dose from external photon exposures using reference human phantoms and Monte Carlo methods, Part III: Organ doses in X-ray diagnosis, GSF-Bericht 11/90. GSF, Neuherberg
4. Galanski M, Nagel HD, Stamm G (2001) CT-Expositionspraxis in der Bundesrepublik Deutschland. Ergebnisse einer bundesweiten Umfrage im Jahre 1999 (CT practice in the Federal Republic of Germany. Results of a nation-wide survey in 1999). Fortschr Röntgenstr 173: R1-R66
5. Brix G, Lechel U, Veit R, Truckenbrodt R, Stamm G, Coppenrath EM, Griebel J, Nagel HD (2004) Assessment of a theoretical formalism for dose estimation in CT: an anthropomorphic phantom study. Eur Radiol 14:1275-1284
6. Stamm-Meyer A, Nosske D, Schnell-Inderst P, Hacker M, Hahn K, Brix G (2006) Diagnostic nuclear medicine procedures in Germany between 1996 and 2002: application frequencies and collective effective doses. Nuklearmedizin 45:1-9
7. United Nations Scientific Committee on the Effects of Atomic Radiation (2000) UNSCEAR 2000 Report to the General Assembly, with scientific annexes. Volume I: Sources. United Nations, New York
8. European Commission (2008) Radiation Protection 154: European guidance on estimating population doses from medical X-ray procedures and annexes at http://ec.europa.eu/energy/nuclear/radiation_protection/publications_en.htm
9. Mettler FA Jr, Thomadsen BR, Bhargavan M, Gilley DB, Gray JE, Lipoti JA, McCrohan J, Yoshizumi TT, Mahesh M (2008) Medical radiation exposure in the U.S. in 2006: preliminary results. Health Phys 95:502-507
10. Amis ES Jr, Butler PF, Applegate KE, Birnbaum SB, Brateman LF, Hevezi JM, Mettler FA, Morin RL, Pentecost MJ, Smith GG, Strauss KJ, Zeman RK; American College of Radiology (2007) American College of Radiology white paper on radiation dose in medicine. J Am Coll Radiol 4:272–284
11. Brix G, Nissen-Meyer S, Lechel U, Nissen-Meyer J, Griebel J, Nekolla EA, Becker C, Reiser M (2008) Radiation exposures of cancer patients from medical X-rays: how relevant are they for individual patients and population exposure? Eur J Radiol [Epub ahead of print]

Author: E.A. Nekolla
Institute: Federal Office for Radiation Protection
Street: Ingolstädter Landstr. 1
City: D-85764 Neuherberg
Country: Germany
Email: ENekolla@BfS.de

Paediatric organ and effective doses in dental cone beam computed tomography

C. Theodorakou[1,2], K. Horner[2], K. Howard[1], A. Walker[1]

[1] North Western Medical Physics, The Christie NHS Foundation Trust, Manchester, United Kingdom
[2] School of Dentistry, University of Manchester, Manchester, United Kingdom

Abstract— **Cone beam computed tomography (CBCT) is an x-ray emerging technology with wide applications in the dental and maxillofacial disciplines. Dental CBCT has been associated with higher radiation risk to the patients compared to conventional dental x-ray imaging.**

Several studies have investigated the radiation doses involved in dental CBCT for adults but none has looked into paediatric doses. This study estimates the organ and effective doses to two paediatric tissue-equivalent phantoms using thermoluminescent dosimeters for three dental CBCT units and six imaging protocols. The doses to the thyroid, salivary glands and brain ranged from 0.068mSv to 1.131mSv, 0.708mSv to 2.009mSv and 0.031mSv to 1.584mSv respectively. The skin and red bone marrow have received much lower doses than the other three organs.

The effective doses ranged from 0.022 mSv to 0.081 mSv. The highest effective dose was calculated for the NewTom VG using the dental protocol and the lowest was observed for the Next Generation i-CAT using the 6cm maxilla protocol. The effective doses calculated in this study were much higher than these of panoramic x-ray imaging but lower than conventional CT.

Keywords— **dental cone beam CT, organ dose, effective dose, paediatric**

I. Introduction

Dental Cone Beam Computed Tomography (CBCT) is a cutting-edge X-ray technology applied in oral and maxillofacial disciplines. The ability of the CBCT systems to provide 3-dimensional (3D) high resolution images with diagnostic reliability resulted in a significant CBCT increase in areas such as orthodontics, endodontics, oral medicine and surgery, periodontics and restorative dentistry [1-6]. The radiation absorbed dose to the patient is two-fold lower than conventional medical CT but three to seven times higher than conventional panoramic imaging [1-2]. Therefore it is of major importance to assess the radiation risk imposed on the patient by performing dental CBCT examination. The radiation risk should also be evaluated for paediatric patients since orthodontics x-ray imaging is primarily carried out on children and teenagers.

Several studies have measured absorbed organ and effective doses for a range of dental CBCT examinations and units using thermoluminescent dosimeters (TLDs) and anthropomorphic phantoms [1-3, 7-10]. Although these studies have measured doses to adult patients for a range of CBCT units and imaging protocols, none has estimated the organ and effective doses to paediatric patients. In addition, for most of the studies the number of TLDs used for measuring the average organ doses was rather limited which might have led to underestimation or overestimation of the organ absorbed and effective dose. For large organs such as the brain or for small organs such as the salivary glands which are positioned along several phantom slices, a large number of TLDs should be placed to ensure that the mean absorbed dose is accurately measured.

The aim of this study is to estimate average organ absorbed and effective doses to two paediatric anthropomorphic phantoms for a range of CBCT units and imaging protocols using a large number of TLDs.

II. Methods and materials

A. Anthropomorphic phantoms

Two tissue-equivalent anthropomorphic phantoms (ATOM Model 702-C and ATOM Model 706-C, Computerized Imaging Systems, Inc, USA) were used in the measurement of radiation absorbed doses. Models 702-C and 706-C simulate an adult female and a 10 year old child respectively. An adult female phantom was used to simulate a teenager as there are no commercially available teenager tissue equivalent anthropomorphic phantoms. The ATOM phantoms are based on ICRP 23 [11] and ICRU 48 [12] and available anatomical data. The tissue simulated in the ATOM phantoms are average bone and soft tissue, cartilage, spinal cord, spinal disks, lung, brain, sinus, trachea and bronchial cavities. The paediatric simulated bone tissues match age related density. The bone tissue is an average of known cortical to trabecular ratios and age based mineral densities.

The ATOM phantoms are available in 25 mm slices and for the purposes of this study the head, neck and shoulders of both phantoms were used as shown in figure 1.

O. Dössel and W.C. Schlegel (Eds.): WC 2009, IFMBE Proceedings 25/III, pp. 305–308, 2009.
www.springerlink.com

B. Thermoluminescent dosimeters (TLDs)

The dose measurements were performed using thermoluinescent dosimeters chips TLD-100H, LiF:Mg,Cu,P (Harshaw Thermo Fisher Scientific Inc, USA). The TLDs were calibrated free in air against an ionisation chamber with calibration traceable to national standards. The calibration was performed using a conventional diagnostic x-ray tube at 80kV (HVL=3.02 mm Al). A flat energy TLD response was observed from 60 kV to 100 kV. Chips with a reproducibility error of less than 10% were used. The chips were read using an automatic TLD reader (Harshaw 5500, Harshaw Thermo Fisher Scientific Inc, USA). Five TLDs were kept outside the CBCT room to measure the background signal.

Fig. 1 ATOM Models 702-C and 706-C

C. Evaluation of organ and effective doses

Absorbed doses were measured in the brain, salivary glands, thyroid gland, red bone marrow, skin and lungs as these are the most radiosensitive organs in the head, neck and shoulders according to ICRP 103 [13]. Bone surface, oral mucosa and oesophagus are also listed as radiosensitive organs in the ICRP 103 [13]. It was assumed that the bone surface and oesophagus absorbed doses are equal to the red bone marrow and thyroid ones respectively. Multiplying the red bone marrow dose with the bone surface tissue weighting factor (w_T) resulted in an insignificant dose. The oral mucosa is listed as a 'remainder' organ and therefore its contribution to the average 'remainder' dose is insignificant since the rest of the 'remainder' organ doses are zero. Finally, the dose to the oesophagus was assumed to be small since it has to be fractionated over 14-16 slices. Therefore these three organs were not taken into account for the calculation of the effective dose.

For small organs such as the brain, salivary glands, thyroid gland, a uniform irradiation can be assumed and therefore the factors f_i which account for the fraction of the total mass of the specified organ in the phantoms slice i are reduced to unity. For large organs like the skin and the red bone marrow the average doses per slice were fractionated using the f_i values from the Huda *et al* study [14]. The effective dose was calculated as the product of the radiation weighted average organ doses and the relevant ICRP 103 [13] w_T summed over all of the tissues/organs exposed.

Table 1 Location and number of TLDs in the two ATOM phantoms

Organ	ATOM model 706-C		ATOM model 702-C	
	Number of TLDS	Slices	Number of TLDs	Slices
Brain	35	2-6	27	2-7
Right submandibular gland	2	8	2	7
Left submandibular gland	2	8	2	7
Right parotid gland	3	6-7	2	6
Left parotid gland	3	6-7	2	6
Sublingual gland	1	8	1	7
Thyroid gland	5	10	5	9
Red bone marrow	59	2-12	36	2-11
Skin	48	2-12	44	2-11

D. Dental CBCT units and imaging protocols

Table 2 shows the CBCT units and the imaging protocols used in this study while table 3 summarizes the exposure factors. The imaging protocols were the ones most frequently used by the dental practices.

Table 2 Dental CBCT units and Imaging protocols

Organ	Manufacturer	Imaging protocol
NewTom VG	QR s.r.l/AFP Imaging	Dental, Maxillofacial
Next Generation i-CAT	Imaging Sciences International	6 cm mandible, 6 cm maxilla, 10 cm
3D Accuitomo 170	Morita MFG. CORP	4x4 molar mandible

Table 3 Technical factors used in this study

	NewTom VG		Next Generation i-CAT (all protocols)		3D Accuitomo 170	
	702-C	706-C	702-C	706-C	702-C	706-C
kV	110	110	120	120	90	90
mA	2.5	2	5	5	5	3
mAs	8.2 (dental) 15.8 (max)	4.8 (dental) 11.7 (max)	18.5	18.5		
Scan time					17.5	17.5
FOV	9''	9''	6 x16 10x16	6 x16 10x16	4x4	4x4
Voxel size (mm)	0.3	0.3	0.4	0.4		

III. Results

Tables 4 and 5 summarise the organ absorbed doses to the five radiosensitive organs for both phantoms. Figure 2 shows the effective doses for the two phantoms.

Table 4 Organ absorbed doses for the 10 year old phantom

	Red bone marrow (mGy)	Skin (mGy)	Thyroid (mGy)	Salivary glands (mGy)	Brain (mGy)
NewTom VG-Maxillofacial	0.165	0.088	0.197	0.708	1.584
NewTom VG-Dental	0.103	0.052	1.131	1.901	0.381
Next Generation i-CAT-6cm Mandible	0.045	0.030	0.380	1.563	0.077
Next Generation i-CAT-6cm Maxilla	0.086	0.036	0.190	1.021	0.285
Next Generation i-CAT-10 cm	0.090	0.040	0.485	1.678	0.228
3D Accuitomo 170	0.024	0.021	0.217	1.333	0.031
Average (mGy)	0.085	0.044	0.433	1.367	0.431

Table 5 Organ absorbed doses for the teenager phantom

	Red bone marrow (mGy)	Skin (mGy)	Thyroid (mGy)	Salivary glands (mGy)	Brain (mGy)
NewTom VG-Maxillofacial	0.222	0.107	0.107	1.627	1.438
NewTom VG-Dental	0.108	0.063	0.297	1.970	0.228
Next Generation i-CAT-6cm Mandible	0.040	0.025	0.134	1.427	0.047
Next Generation i-CAT-6cm Maxilla	0.058	0.029	0.068	1.084	0128
Next Generation i-CAT-10 cm	0.123	0.052	0.194	1.813	0.167
3D Accuitomo 170	0.038	0.033	0.179	2.009	0.042
Average (mGy)	0.098	0.052	0.163	1.655	0.342

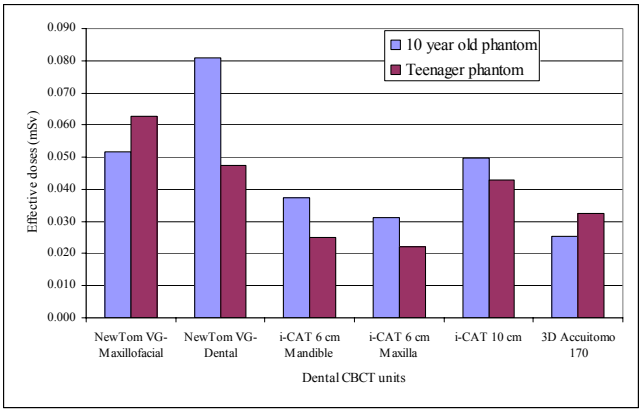

Fig. 2 Effective doses for the 706-C phantom (10 year old) and for the 702-C phantom (teenager)

IV. Discussion

Figure 2 shows that the effective doses range from 0.025 mSv to 0.081 mSv for the 10 year old phantom and from 0.022 mSv to 0.063 mSv for the teenager phantom. The maxilla imaging protocol of the Next Generation i-CAT unit and the 3D Accuitomo give the lowest effective doses for the two phantoms. The highest effective doses for both phantoms were observed for the NewTom VG unit due mainly to its fixed large FOV.

The effective doses for the 10 year old phantom are higher than these of the teenager phantom for most of the CBCT units and imaging protocols. This is mainly due to the positioning of the thyroid, salivary glands and brain with respect to the primary beam. As the 10 year old phantom is smaller in size than the teenager phantom and the beam field sizes on the phantoms are fixed for the same imaging protocols, organs such as the thyroid, salivary glands and brain are more likely to be positioned either in or closer to the primary beam for the 10 year old phantom than for the teenager phantom. For example, there is an almost two-fold difference between effective doses for the NewTom VG-Dental. Comparing the thyroid doses between the two phantoms shows that the dose to the thyroid for the 10 year old phantom is almost four times higher than the one for the teenager phantom due mainly to the field size and positioning. The thyroid gland for the 10 year old (slice 9) was fully covered by the primary beam while the thyroid gland for the teenager phantom (slice 10) was outside the primary beam.

Tables 4 and 5 show that the red bone marrow and skin absorbed doses are lower than the thyroid, salivary glands and brain absorbed doses. For the NewTom VG unit and for the maxillofacial protocol, the brain contributes the most to

the effective dose for the 10 year old phantom while for the teenager phantom the salivary glands contribute almost half of the effective dose. For the rest of the imaging protocols and units, the salivary glands contribute the most to the effective dose for the teenager phantom while for the 10 year old phantom there is an almost equal contribution from the salivary glands and thyroid gland to the effective dose.

Hayakawa *et al* [15] have calculated an average effective dose of 9.8 μSv from rotational panoramic radiograph. The average effective dose found in this study was 42 μSv. This study confirms that the effective doses involved in dental CBCT examinations are much higher than these involved in conventional dental x-ray imaging.

The % radiation-induced fatal cancer risk per Sv in a UK population for a 10 year old child is 11% and for a 15 year old is 10% [16]. This study has calculated an average effective dose of 0.046mSv for a 10 year old child and 0.039 mSv for a teenager. The % radiation-induced fatal cancer risk for a 10 year old child undergoing a dental CBCT exam is 0.0004% and for a teenager is 0.00028%.

V. Conclusions

This study has estimated the organ and effective doses to two paediatric tissue-equivalent anthropomorphic phantoms for three dental CBCT units and for six imaging protocols. It was found that the radiation doses to patients are significantly higher than the traditional x-ray imaging.

As children are more radiation sensitive than adults it is essential that the dental CBCT use is fully justified over conventional dental imaging techniques.

Acknowledgment

The research leading to these results has received funding from the European Atomic Energy Community's Seventh Framework Programme FP7/2007-2011 under grant agreement no 212246 (SEDENTEXCT: Safety and Efficacy of a New and Emerging Dental X-ray Modality).

The authors are grateful to Dr Fiona Carmichael and Mrs Lynda Sheard at the Leeds Dental Institute, Dr Jackie Brown, Dr Jonathan Davies, Mrs Nadine White and Mr Ben Johnson at the Department of Dental Radiological Imaging, Guy's Hospital and Dr Andrew Dawood and Dr Veronique Sauret-Jackson at the Cavendish Imaging for allowing us to use their facilities for this study.

References

1. Roberts JA, Drage NA, Davies J, Thomas DW (2009) Effective dose from cone beam CT examinations in dentistry. The British Journal of Radiology 82:35-40
2. Ludlow JB, Davies-Ludlow LE, Brooks SL and Howerton WB (2006) Dosimetry of 3 CBCT devices for oral and maxillofacial radiology: CB Mercuray, NewTom 3G and i-CAT. Dentomaxillofacial radiology 35:219-226
3. Hirch E, Wolf U, Heinicke F and Silva MAG (2008) Dosimetry of the cone beam computed tomography Veraviewepocs 3D compared with the 3D Accuitomo in different fields of view. Dentomaxillofacial Radiology 37:268-273
4. Guerrero ME, Reinhilde J, Loubele M, Schutyser F, Suetens P and van Steenberghe D (2006) State-of-the-art on cone beam CT imaging for preoperative planning of implant placement. Clinical Oral Investigations 10:1-7
5. Ziegler CM, Woertche R, Brief J, Hassfeld S (2002) Clinical indications for digital volume tomography in oral and maxillofacial surgery
6. Mah J, Enciso R, Jorgensen M (2003) Management of impacted cuspids using 3-D volumetric imaging. J Calif Dent Assoc 31:935-41
7. Ludlow JB, Davies-Ludlow LE, Brooks SL (2003) Dosimetry of two extraoral direct digital imaging devices: NewTom cone beam CT and Orthophos Plus DS panoramic unit. Dentomaxillofacial Radiology 32:229-34
8. Silva MAG, Wolf U, Heinicke F, Bumann A, Visser H and Hirch E (2008) Cone-beam computed tomography for routine orthodontic treatment planning: A radiation dose evaluation. American Journal of Orthodontics and Dentofacial Orthopedics 133:640.e1-e5
9. Hashimoto K, Arai Y, Iwai K, Araki M, Kawashima S, Terakado M (2003) A comparison of a new limited cone beam computed tomography machine for dental use with a multidetector row helical CT machine Oral Surg Oral Med Oral Pathol Oral Radiol Endod 95:371-77
10. Lofthag-Hansen S, Thilander-Klang A, Ekestubbe A, Helmrot E, Gröndahl K (2008) Calculating effective dose on a cone beam computed tomography device: 3D Accuitomo and 3D Accuitomo FPD. Dentomaxillofacial Radiology 37:72-79
11. International Commission on Radiological Protection (1975) ICRP Publication 23: Reference Man: Anatomical, physiological and metabolic characteristics, (1975) Pergammon Press, England
12. International Commission on Radiation Units and Measurements (1992) ICRU Report 48 Phantoms and computational models in therapy, diagnosis and protection.
13. International Commission on Radiological Protection ICRP Publication 103 (2007) Recommendations of the International Commission on Radiological Protection. Annals of the ICRP. Elsevier Ltd.
14. Huda W and Sandison (1984) Estimation of mean organ doses in diagnostic radiology from Rando phantom measurements. Helth Physics 47:463-467
15. Hayakawa Y, Kobayashi N, Kuroyanagi K, Nishizawa K (2001) Paediatric absorbed dose from rotational panoramic radiography. Dentomaxillofacial radiology 30:285-292
16. National Radiological Protection Board (1993) Board Statement on Diagnostic Medical Exposures to Ionising Radiation During Pregnancy and Estimates of Late Radiation Risks to the UK population

Author: Dr Chrysoula Theodorakou
Institute: North Western Medical Physics, The Christie NHS Foundation Trust
Street: Wilmslow Road
City: Manchester
Country: United Kingdom
Email: christie.theodorakou@physics.cr.man.ac.uk

Why No One Believes Us: Cognitive Neuroscience and Radiation Risk

R.E. Toohey, Ph.D., CHP

President, Health Physics Society
Oak Ridge Associated Universities
Oak Ridge, Tennessee, U.S.A. 37831-0117

Abstract— **Public perception of radiation risks and their acceptability remains far from the consensus of radiation protection specialists, despite decades of individual and organizational efforts at risk communication. We have eagerly adopted the guidance of risk communication specialists, and presented the facts in a non-threatening and understandable fashion. Nevertheless we continue to encounter intense opposition to the development of nuclear power plants, waste storage sites, food irradiation facilities, and other applications of radiation and radioactive materials. We have been told such opposition is an emotional reaction that we must allow to be expressed, and then calmly and coolly respond with our understandable facts. One understandable fact is that what we have been doing simply doesn't work. The rapid development of the cognitive neurosciences, particularly evolutionary psychology, over the past twenty years or so has provided remarkable insights into this situation. Human brains come into the world with certain genetically determined methods of classifying sensory inputs called "memes," a term adopted from cultural anthropology. The "contagion" meme is a key player in response to radiological issues, as is the "pattern-seeking" meme. Furthermore, the human decision-making faculty does not exist in Descartes' *res cogitans*, but in a hard-wired network of literal gut feelings and other body states we call emotions. Understanding and implementing these findings may lead us to more effective communication efforts, but also warn us that effecting significant behavioural changes will be a Sisyphean task.**

I. Introduction

Many radiation protection professionals are bewildered by the huge chasm between their own understanding of radiological risk and that of the general public. In meeting with stakeholders, we present scientific data and analyses which clearly demonstrate that radiation, particularly at low doses and dose rates, is a rather weak carcinogen, and yet we continue to encounter intense public opposition to radiation-based technologies. Although medical uses of radiation seem to have been exempt from public concern for many years, recent increases in public concern over medical exposures have been reported, coincident with an almost five-fold increase in the average medical radiation dose to the U.S. population. Despite over 100 years of data, we are still told there is no "safe" and therefore no "acceptable" radiation dose. Yet we continue to give science-based, quantitative presentations to the public, usually producing only mutual frustration. Recent developments in the cognitive neurosciences have shed light on this dichotomy in perception between health physicists ("us") and the public ("them"). These findings fall into four main categories: preferred thinking and communicating styles, innate behavior, individual experiences, and generational differences.

II. Differences between "Us" and "Them"

Volunteer testing of preferred thinking and communication styles of radiation scientists based on the Myers-Briggs Personality Type categories has shown that 51% of health physicists tested fell into four personality types which combined represent only 13% of the general population, and only 15% of health physicists fall into the six types that represent 57% of the general population. This difference has in fact been demonstrated in the "Star Trek" franchise of television shows and films: we tend to be much like Mr. Spock and Mr. Data, while our audience identifies much more with Dr. McCoy and Counselor Troi.

Human decision-making has been shaped by evolution to be primarily interested in self-preservation. This is accomplished by automated circuitry in the brain concentrated in the amygdala to detect danger signals in sensory input even before those signals reach the frontal cortex for analysis; because the amygdala has more neural connections to the rest of the brain than does the frontal cortex, its decisions are very difficult to override. In fact, our highly-evolved survival systems, based in the emotions, provide the foundation for all decision-making, despite our Cartesian mythology of "rational" decision-making. Thus, arguments based on scientific data carry very little weight. Some examples of subconscious decision-making templates include the contagion meme (any contact with a hazard is best avoided, so the dose-response curve is irrelevant) and pattern-seeking (if radiation caused injury to someone else,

O. Dössel and W.C. Schlegel (Eds.): WC 2009, IFMBE Proceedings 25/III, pp. 309–310, 2009.
www.springerlink.com

it will also injure me.) Learned behavior is most influential when it reinforces innate behavior (at the subconscious level) and personal expectations (confirmation bias). In addition, most people are uncomfortable with mathematical formalism, and interpret risk estimates solely by their numerators and not their denominators. Finally, generational differences also affect our communication. Each generation, as it comes to adulthood, interprets the world in terms of the world in which they were children. This produces cyclical patterns in history, politics, and technology acceptance.

III. Effective Communication

Spinoza taught that a negative emotion can only be changed if it is replaced with a positive emotion, and there must be a clear benefit to making the effort to do so. Consequently our communication efforts, if they are to effect changes in the audience's behavior, must focus on benefits rather than risks, be framed for emotional impact, and appeal to the whole brain, not merely to our preferred "rational" modes of thought.

Numerical Estimation of Peak/Average SAR Ratio for Different Thorax Models

V. Hartwig[1,2], G. Giovannetti[1], N. Vanello[3], M.F. Santarelli[1] and L. Landini[3]

[1] Institute of Clinical Physiology, CNR, Pisa, Italy
[2] Department of Electrical Systems and Automation, University of Pisa, Italy
[3] Department of Information Engineering, University of Pisa, Italy

Abstract— **The estimation of Specific Absorption Rate (SAR) during a Magnetic Resonance Imaging (MRI) scan is an important safety procedure. In this work, a birdcage body coil model is used for radiofrequency (RF) excitation of several inhomogeneous human thorax models with different sizes and weights. To study the peak/average SAR ratio correlation with sample metrics, numerical simulations using the Finite Difference Time Domain (FDTD) method are performed to estimate the peak and average SAR values on the entire sample volume. Results for 11 different thorax models indicate a strong correlation between the peak/average SAR value and the sample mass/height ratio.**

Keywords— **Magnetic Resonance, Specific Absorption Rate, FDTD, peak/average SAR ratio.**

I. Introduction

Magnetic Resonance Imaging (MRI) systems routinely used for clinical diagnosis can produce high quality images with relatively low static magnetic field (B_0) strengths ($\leq$ 3 T). However, to achieve greater signal to noise ratio (SNR) in images and improved resolution for spectroscopy applications, new generation MRI systems are designed to work with even higher B_0 fields. This increases the Lamor frequency of the imaging species, and leads to an associated increase in the frequency of the excitation radiofrequency (RF) magnetic field (B_1). As the shortened wavelength of the B_1 field approach the sample's dimensions, significant interaction between the field and the sample may occur [1]. This leads to undesired spatial variations of the B_1 field in the sample. Measurements of the effects of this interaction and the total absorbed power are very complex and dependent on many parameters related to experimental conditions, transmit RF coils, and subject geometry [1].

Specific Absorption Rate (SAR), which is normally measured in W/kg, is the most used parameter to monitor and quantify the power deposited on a subject that could cause dangerous local heating [2].

Classically, the SAR is given by

$$SAR = \frac{\sigma |\mathbf{E}|^2}{2\rho} \quad (1)$$

where σ is the tissue electrical conductivity, **E** is the electric field vector in the tissue, and, ρ is the tissue density.

There are several standards to regulate the limits for average SAR (whole body, head only, or body extremities) and peak SAR (maximum SAR in the entire sample) [2, 3]. Subsequent references to the phrase "radiofrequency dosimetry" will refer to the estimation of SAR in a human subject during a MR procedure.

It is possible to distinguish theoretical and experimental dosimetry. In the former, SAR is calculated using electromagnetic theory and a geometrical model of the transmission coil and human subject. The power deposition on the subject can be calculated by analytical equations [4], or numerical resolution of Maxwell's equations to estimate the electric field on the human subject [5].

In the second method, SAR is computed from experimental measurements of related quantities, such as the local temperature increment after the MR exam [6].

MRI systems estimate the power deposition in the subject occupying the bore area via software means. A simple model for the SAR calculation permits one to estimate the average SAR for each sequence, and is based on parameters in the scan prescription (patient weight, type of sequence, and sequence repetition time), and an empirical derivation of the energy deposited by a standard RF pulse. Peak SAR is then a function of the average SAR, coil type and patient weight, according to two different values for peak/average SAR ratio. This method does not evaluate local SAR and a possible presence of *hot spots* in the sample volume. Using numerical methods, however, it is possible to calculate the electric field *distribution* in a realistic model of the sample, which can then be used to calculate and visualize the local SAR in the entire sample.

Recent work has demonstrated that power deposition during a MR exam is strongly correlated with body geometry and subject size [5]. These results indicate that the simple model used by some MR systems to estimate SAR can underestimate the peak SAR value for some patients.

In this work, a FDTD algorithm is used to estimate the average and peak SAR values on human thorax models with different mass and size (covering newborn to adult subjects) to evaluate the correlation between the peak/average SAR ratio and sample geometry. The results indicate a strong

O. Dössel and W.C. Schlegel (Eds.): WC 2009, IFMBE Proceedings 25/III, pp. 311–314, 2009.
www.springerlink.com

correlation between this ratio and other model metrics, such as mass or mass/height ratio.

II. Materials and Methods

A. MR systems model for SAR calculation

Generally, MR scanners estimate the power deposition for each scan according to this model

$$SAR \propto \frac{RFpulse \cdot E_{RF}}{TR \cdot M_{pat}} \tag{2}$$

where *RFpulse* is the number of identical RF pulses in the sequence, E_{RF} is the energy deposited by each RF pulse, *TR* is the sequence repetition time and M_{pat} is the patient weight. Since a MR scan uses a variety of RF pulses with different transmit and/or receive coils, the RF pulses are not identical, nor is the energy deposition independent of scan prescription parameters. For this reason, the MR software converts the RF pulses into an equivalent number of standard RF pulses ($ST_{RFpulse}$) of known energy content (E_{STRF}). The average SAR value (*AvgSAR*) is then given by

$$AvgSAR = \frac{ST_{RFpulse} \cdot E_{STRF}}{TR \cdot M_{pat}} \tag{3}$$

Then, the MR scanner software computes the peak SAR of a sequence as a function of the average SAR, coil type and patient weight, e.g., with the body coil, the software approximates the subject as a cylindrical object and calculates the peak SAR as

$$PeakSAR = 2 \cdot AvgSAR \tag{4}$$

After calculating these SAR values, the MR scan compares them with the limits in the system configuration (e.g. 2 W/kg for the body average, 3.2 W/kg for the head average and 10 W/kg for the extremities average). If the estimated SAR values exceed these limits, the scan cannot begin until the operator changes some sequence parameters (e.g. TR or number of slices), to reduce the power deposition on the subject.

B. SAR numerical calculation with FDTD

FDTD methods facilitate the computation of electromagnetic fields at each point of the sample model for numerical evaluation of local SAR values [7]. This method, introduced for the first time in 1966 [8], is able to resolve the Maxwell's equations in the time domain by means of a discretization of the temporal and spatial derivates with the finite difference approximation. To solve the equation for the electric and magnetic fields in a volume, this volume must be enclosed in a computational domain that is divided into small cubic cells.

Given an excitation and initial values for the electric and magnetic fields, the process iteratively calculates the field values of each cell.

All the FDTD calculations in this work were set up and solved using commercially available software (GEMS, Computer and Communication Unlimited, USA) [9].

The calculation space (computational domain) was 80 x 80 x 80 cm and perfectly matched layer (PML) boundary condition [7] was used at all boundaries of the problem region. For RF transmission, a birdcage coil (16 rungs, 60 cm diameter, 64 cm length, high pass body coil) modeled with a 1 cm wide wire of perfect electric conducting material (PEC) was used.

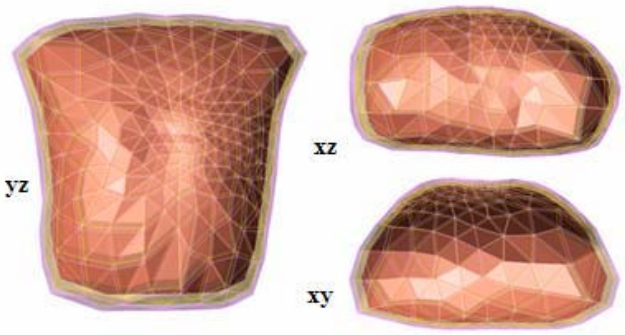

Fig. 1 Three layers human thorax CAD model (yz: coronal view, xz: sagittal view, xy: axial view)

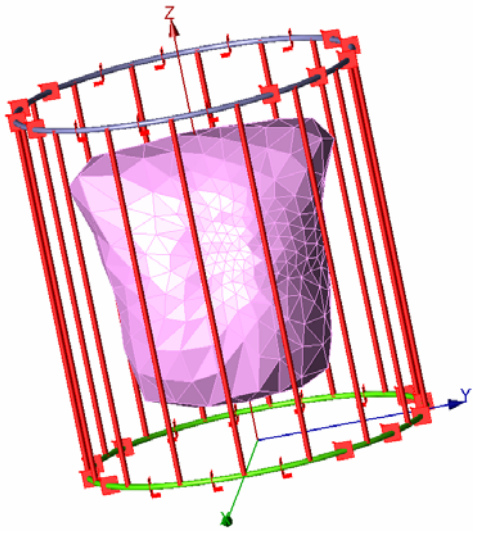

Fig. 2 Human thorax model placed in the RF body coil

To reduce computation time, we used a non-resonant coil with an ideal excitation using a sinusoidal current source (amplitude 1 A) placed in the middle of each end ring segment. Any two adjacent current sources have a 22.5° phase shift. In this way, the current in each rung follows the pattern that produces a homogeneous RF field in the empty coil. The excitation frequency was chosen as 128 MHz to simulate a MR exam on a 3 T MR scanner. Each simulation was run for twenty cycles to ensure the steady state was reached.

A model for the human thorax (Fig. 1) to use with FDTD method was created using CAD software (GID, International Center for Numerical Methods in Engineering, Spain) [10]. The model has three types of tissues (skin, fat and muscle) with proper values of relative permittivity, conductivity and mass density at 128 MHz [5]. We chose not to include the arms in the model to avoid hot spot near air gaps between the arms and the torso and in the arms near to coil conductors. To create 11 human thoraxes with different sizes, we scaled the CAD model in the x, y, z directions with different scaling factors in order to cover size for newborn (10.24 x 18.02 x 18.168 cm, 2.10 kg) to adult male thorax (29.11 x 51.81 x 52.23 cm, 48.45 kg). Each model was sampled onto the FDTD grid with a resolution of 2.5 x 2.5 x 2.5 mm. For each thorax model, placed at the centre of the birdcage coil (Fig. 2), the software calculated mass, average SAR and peak SAR. Differences in the relative proportions of the head, arm and leg lengths, and torso length, between adults and newborns are not accounted for at this time, but may be a topic for future work.

Using custom written Matlab scripts, we compared the average SAR and peak SAR values for all models. Finally, the peak/average SAR ratio was calculated for all models and correlated with sample metric parameters such as mass or mass/height ratio.

III. Results

Fig. 3 shows the average SAR values for 11 human thorax models with different size and weight covering from newborn to adult male. These results indicate that the average SAR value increase linearly with the thorax weight (R^2=0.9978).

Fig. 4 shows the simulation results for peak SAR values of all the thorax models. The peak SAR increases with the thorax weight according to a quadratic regression model (R^2= 0.9961).

Peak SAR / average SAR ratio is calculated for each model to verify a possible correlation between this ratio and metric of sample model exposed to the RF field. In Fig. 5 the peak SAR / average SAR ratio values are reported for different mass / height ratio of the human thorax models used in our simulations. With the term height we consider the maximum extension of the models (along the z axes).

IV. Discussions and Conclusions

In this work, the FDTD algorithm is used to estimate the average and peak SAR values for several human thorax models of different sizes and weights that are exposed to a RF electromagnetic field corresponding to a MR procedure at 3 T.

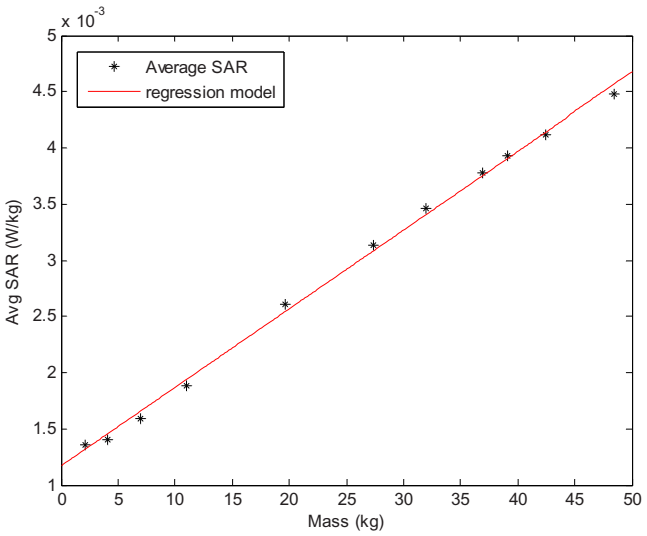

Fig. 3 Average SAR vs thorax model mass

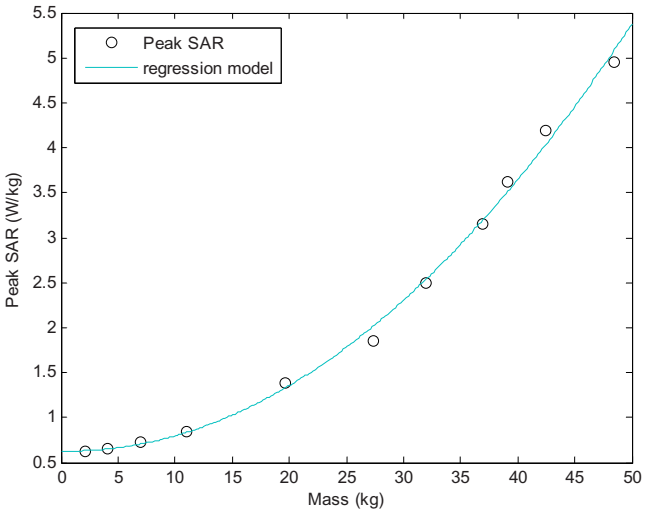

Fig. 4 Peak SAR vs thorax model mass

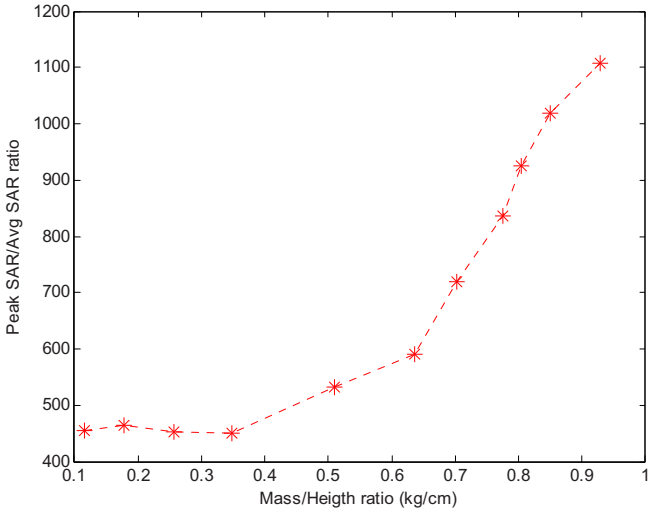

Fig. 5 Peak SAR / Average SAR ratio vs thorax model mass / height ratio

A birdcage body coil is chosen to transmit the RF field to the biological sample using an ideal excitation with a sinusoidal current source for each end ring segment. The thorax models used for the simulations cover a range of geometries and sizes, from a newborn to an adult male. The average SAR that we compute refers to the partial body SAR value, which is the average SAR respect to the mass inside the MR scanner imaging area. The peak SAR is defined as the maximum local SAR value inside the torso model. We chose not to include the arms in the model to avoid the hot spots near air gaps between the arms and the torso and in the arms near to coil conductors. These regions will be investigated in future work.

Results indicate a linear relationship between the average SAR and the sample weight.

A good correlation between the peak SAR values and the thorax model weight is found to indicate a quadratic dependence of maximum local SAR value from the sample mass.

Peak to average SAR ratio results for each thorax model show a strong correlation between this factor and the model metric. This result indicates the need for a more robust algorithm to estimate the peak SAR from the average SAR, one that accounts for the size and geometry of the subject exposed to the RF field during a MR exam. Typical MR scanners can only estimate average SAR using a model based on a cylindrical or spherical object, but they cannot directly estimate the peak SAR. They estimate this parameter by means of a simple model that is independent of the geometry and size of the object. Our results suggest that this approach is not robust in the estimation of real peak SAR values in human subjects. Further studies with more complex human subject models are needed to verify this hypothesis for whole body SAR value and to find a body metric, e.g., mass or mass/height, that correlates with the peak/average ratio. In this way, with prior knowledge of the patient body metrics, i.e., weight and height, and the precomputation of average SAR, the peak SAR could be correctly obtained by the MR scanner using the relationship between peak/average ratio and the body metric parameters.

In addition, further studies are needed to establish a possible relationship between the peak/average SAR ratio and the frequency of RF excitation.

Acknowledgment

The authors wish to thank Prof. P.A. Bottomley for his expert advice and Dr. D. Yeo for his helpful discussions.

References

1. Hoult DI (2000) Sensitivity and power deposition in a high field imaging experiment. J Magn Reson Imaging 12: 46-67
2. IEC International standard, medical equipment-part 2: particular requirements for the safety of magnetic resonance equipment for medical diagnosis, 2nd revision, 601-2-33. International Electrotechnical Commission, Geneva, 2002.
3. IEEE Std C95.3-2002 IEEE recommended practice for measurements and computations of radio frequency electromagnetic fields with respect to human exposure to such fields, 100 KHz-300 GHz, Inst of Electrical and Electronics Eng
4. Bottomley PA, Redington RW, Edelstein WA, Schenck JF 81985) Estimating radiofrequency power deposition in body NMR imaging. Magn Reson Med 2: 336–349
5. Liu W, Collins CM, Smith MB 2005 Calculations of B1 distribution, specific energy absorption rate, and intrinsic signal-to-noise ratio for a body-size birdcage coil loaded with different human subjects at 64 and 128 MHz. Appl Magn Reson 29: 5–18
6. Cline H, Mallozzi R, Li Z, McKinnon G, Barber W (2004) Radiofrequency power deposition utilizing thermal imaging. Magn Reson Med 51:1129–1137
7. Kunz KS, Luebbers RJ (1993) The finite difference time domain method for electromagnetics. CRC, Ann Arbor
8. Yee KS (1966) Numerical solution of initial boundary value problems involving Maxwell's equations in isotropic media. IEEE Trans Ant Propag 14:302–307
9. GEMS (2008) *Computer and Communication Unlimited*, PA, USA, at http://www.2comu.com
10. GID (2009) *International Center for Numerical Methods in Engineering*, Barcelona, Spain, at http://gid.cimne.upc.es/index.html

Author: Valentina Hartwig
Institute: Institute of Clinical Physiology, CNR
Street: Via Moruzzi 1
City: Pisa
Country: Italy
Email: valeh@ifc.cnr.it

The lower detection limit of GR-200A and MCP-100D thermoluminescence dosimeters at different readout and annealing temperatures

T. Stock[1], M. Lüpke[1] and H. Seifert[1]

[1] University of Veterinary Medicine Hannover, Foundation, Institute for General Radiology and Medical Physics, Hannover

Abstract— **The lower detection limit of two types of TLD rods (GR-200A and MCP-100D) based on LiF:Mg,Cu,P has been studied at different thermal treatments. Both materials showed considerably high, lower detection limits when readout and annealed at 260 °C. Irrespective of readout and annealing temperatures applied, the lower detection limits of GR-200A rods were much lower than the lower detection limits of MCP-100D rods.**

Keywords— **TLD, lower detection limit, annealing temperature, readout temperature**

I. Introduction

Thermoluminescent dosimeters (TLD) based on LiF:Mg,Cu,P have some significant advantages over the most widely accepted material, LiF:Mg,Ti for usage in low dose personal measurement (< 50 µSv). The lower detection limit of TLD depends on the applied readout and annealing procedure. In this study the lower detection limits at different annealing and readout procedures were investigated for two materials based on LiF:Mg,Cu,P. Several authors [1, 2, 3] recommend annealing and readout temperatures of no more than 260 °C, since this leads to a loss of sensitivity and can result in irreversible damage of the TL detector.

II. Materials and methods

The rods of LiF:Mg,Cu,P used in this study were GR-200A (Solid Dosimetric Detector and Method Laboratory, Beijing 102205, China) and MCP-100D (TLD Poland, Krakow).

Ten TLD of each material were treated at six different readout and annealing temperatures. The parameters of the readout and annealing procedures used in this study are listed in Table 1.

In order to estimate the lower detection limit untreated TLD were read out ten times in a TL reader (Harshaw 5500). After this procedure all samples were irradiated to the same dose of 600 µSv, then the rods went through the readout and annealing protocol (Table 1). The whole procedure was repeated ten times for each group of rods. The lower detection limit was calculated according to DIN 6818-6 [4], where the lower detection limit is defined as 2 times the standard deviation of the background readout value of ten unirradiated rods.

Table 1 Readout and annealing procedures in this study

	Temperature and plateau time during						
Group	Preheat		Readout		Annealing		Heating Rate
	[°C]	[s]	[°C]	[s]	[°C]	[s]	[K / s]
1	145	10	260	23.33	230	20	10
2	145	10	260	23.33	240	20	10
3	145	10	260	23.33	250	20	10
4	145	10	260	23.33	260	20	10
5	145	10	240	23.33	240	20	10
6	145	10	250	23.33	250	20	10

III. Results

The effects of different readout and annealing temperatures on the lower detection limit of GR-200A and MCP-100D samples are shown in Figure 2 and Figure 3. All results are displayed as boxplots. An example of a boxplot is shown in Figure 1.

The best results were achieved for rods of GR-200A readout at 260 °C with a subsequent annealing at 240 °C. The lower detection limit was 0.30 µSv. In comparison, the best result of MCP-100D rods was a lower detection limit of 0.68 µSv.

As shown in Figure 2 and Figure 3 the lower detection limit of both materials was affected by the readout and annealing temperature.

O. Dössel and W.C. Schlegel (Eds.): WC 2009, IFMBE Proceedings 25/III, pp. 315–317, 2009.
www.springerlink.com

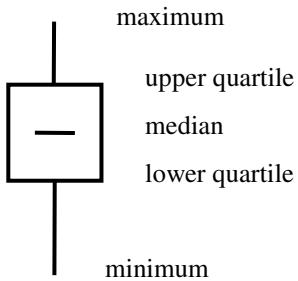

Fig. 1: Description of the boxplot symbol

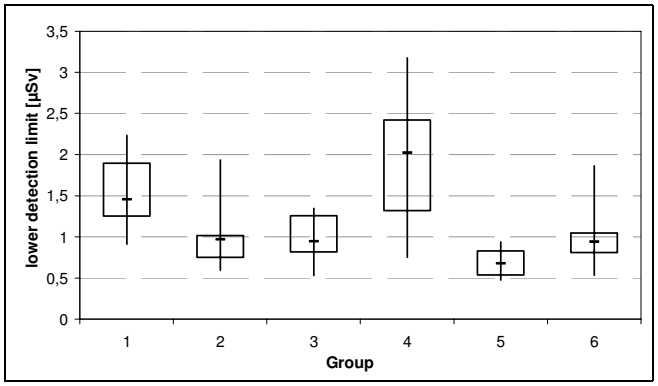

Fig. 2: Lower detection limit of MCP-100D at different readout and annealing temperatures. The parameters of the readout and annealing procedures are listed in Table 1.

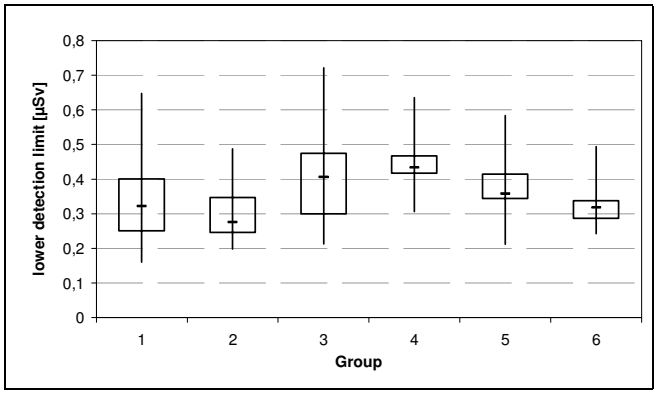

Fig. 3: Lower detection limit of GR-200A at different readout and annealing temperatures. The parameters of the readout and annealing procedures are listed in Table 1.

This behaviour was less prominent for the samples of GR-200A. For this material all applied readout and annealing programs lead to good results regarding the lower detection limit. When results of GR-200A were evaluated statistically using a Tukey Test there was only a significant difference ($p<0.05$) between group 2 and group 4. The highest recorded lower detection limit (0.45 µSv) was found for group 4 at a readout and annealing temperature of 260 °C. This is in agreement with the results of MCP-100D where a lower detection limit as high as 2.0 µSv was found for this group. Results in Figure 2 show that for all other readout and annealing temperatures samples of MCP-100D had lower detection limits of less than 1.0 µSv at all other readout and annealing procedures. The best result of these samples (0.68 µSv) were achieved when rods were readout and annealed at 240 °C. Compared to all other groups a statistically significant difference could only be found for group 4 (Tukey Test, $p<0.05$).

IV. Conclusions

The lower detection limit of GR-200A and MCP-100D samples shows a dependence on the applied readout and annealing temperatures. GR-200A rods lead to good results at all investigated readout and annealing procedures. The influence of readout and annealing temperatures is not very distinctive for this material. Irrespective of readout and annealing temperatures applied, the lower detection limits of GR-200A rods were much lower than the lower detection limits of MCP-100D rods. The range between minimal and maximal lower detection limits within a group of TL is smaller for GR-200A samples. MCP-100D is more dependent on readout and annealing temperatures and also the statistical spread within a group of TLD is much higher. The investigated readout and annealing temperatures lead to reasonably good results. As a result of this study a readout and annealing temperature of 260 °C can not be recommended.

V. References

1. Tang K, Hongying Z, Shen W (2000) Thermal loss and recovery of thermoluminescence sensitivity in LiF:Mg,Cu,P. Radiat. Prot. Dosim. 90: 449 – 452
2. Cai g, Fesquet J, Dusseau L, Martini M, Meinardi F, Huang B, Tang, K et al. (1996) Thermoluminescence of LiF:Mg,Cu,P (GR-200A) TLD after annealing between 200 and 400 °C. Radiat. Prot. Dosim. 65: 163 – 166

3. Oster L, Horowitz Y, Horowitz A (1993) Glow curve readout of LiF:Mg,Cu,P (GR-200) chips at maximum temperatures between 240 °C and 280 °C: elimination of the residual signal. Radiat. Prot. Dosim. 49: 407 – 411
4. DIN 6818-6, Ausgabe 1988-12, Strahlenschutzdosimeter, Thermolumineszenzdosimetriesysteme

Author: Matthias Lüpke
Institute: University of Veterinary Medicine Hannover, Foundation Institute for General Radiology and Medical Physics
Street: Bischofsholer Damm 15
City: 30173 Hannover
Country: Germany
Email: matthias.luepke@tiho-hannover.de

Air kerma-area product in pediatric x-ray examinations of paranasal sinuses: an indirect method of assessment

M. A. S. Lacerda[1], T. A. da Silva[1], H. J. Khoury[2]

[1] Development Centre of Nuclear Technology – Brazilian Commission of Nuclear Energy, Belo Horizonte, Brazil
[2] Nuclear Energy Department – Federal University of Pernambuco – Recife, Brazil

Abstract— **A survey of the air kerma-area product (P_{KA}) in pediatric x-ray examinations of paranasal sinuses was performed. Without interfering in the hospital routine, an indirect methodology for assessing P_{KA} with low uncertainty values was adopted. Results showed the influence on the PKA values of the characteristics and performance of one x-ray equipment in Belo Horizonte.**

Keywords— **Patient dosimetry, Pediatric radiology, Air kerma-area product**

I. Introduction

The assessment of doses delivered to patients in conventional diagnostic x-ray examinations is mandatory for optimization of the radiological protection practices. The comparison between patient doses and internationally recommended or nationally standardized diagnostic reference levels (DRLs) provides important information concerned with radiological procedures performed in the institution.

Special attention must be taken during radiographic examinations of children once they comprise the segment of the population more susceptible to deleterious effects of ionizing radiation [1]. The surveys in pediatric radiology are currently being done for chest radiographs and, in a minor instance, for abdomen, pelvis and skull radiographs [2]. An often procedure performed in children in Brazilian hospitals is paranasal sinuses in projections Caldwell and Waters. Some works have published data related to this kind of examinations [3, 4, 5].

Two practical dosimetric quantities were recommended for monitoring patient doses in diagnostic radiology: entrance surface air kerma (K_e) and air kerma-area product (P_{KA}) [6]. Although K_e is the most usual quantity used for dosimetric measurements in medical x-ray imaging, the P_{KA} presents a substantial advantage: it has a good correlation with the radiation risk, as the number of interactions within the patient is proportional to both the air kerma and field size [7].

The P_{KA} is defined as the integral of the air kerma over the area of the x-ray beam in a plane perpendicular to the beam axis. It has a useful property of being approximately invariant with the distance from the x-ray tube focus (if interactions in air and extrafocal radiation are neglected); it means that the plane of measurement should not be close to the patient or the phantom in order to avoid contribution from backscattered radiation [6]. P_{KA} can be measured with a KAP meter or estimated, indirectly, by the product of the incident air kerma (K_i) and the demagnified area of the exposed x-ray film from the focus to image receptor distance (d_{FID}) to the focus to patient surface distance (d_{FSD}) [4].

In this paper, it was carried out a survey of the P_{KA} in children submitted to diagnostic x-ray examinations of paranasal sinuses in a pediatric hospital of Belo Horizonte, Brazil. The indirect method of estimating this quantity was employed. Results are compared with other published data.

II. Methods

X-ray examinations of paranasal sinuses (projections Caldwell and Waters) carried out in a private pediatric hospital of Belo Horizonte were followed. Patient's age, weight (W), height (H) and parameters like tube voltage (kV), current-time product (mAs) and focus to patient surface distance (d_{FSD}) of 53 radiographs with acceptable diagnostic images were recorded. Patients were divided in 3 age range groups: 1 to 5, 5 to 10 and 10 to 16 years old. The quality of the radiograph images was evaluated by the technician in the x-ray room and by the doctor at the time the patient returned to the medical attendance.

The characteristics of the x-ray equipment are shown in the Table 1.

Table 1. Characteristics of the x-ray equipment of the pediatric hospital studied.

CHARACTERISTICS	
Manufacturer	VMI (Brazilian manufacturer)
Generator	Monophase full-wave rectified
HVL	(1.70 ± 5%) mm Al (70 kV)
X-ray Tube Output (70 kV)	28.0 μGy/mAs

Air kerma-area products (P_{KA}) were obtained through x-ray tube output measurements. The air kerma free-in-air was

O. Dössel and W.C. Schlegel (Eds.): WC 2009, IFMBE Proceedings 25/III, pp. 318–320, 2009.
www.springerlink.com

determined with a RADCAL/MDH 10X5-6 ionisation chamber traceable to a secondary national standard laboratory.

All x-ray examinations were performed using an x-ray field limitation cone (an indispensable device for radiological protection of patients). As the air kerma-area product is approximately invariant with distance from the x-ray tube focus, P_{KA} values were obtained by the product of the area of the cross-section of the cone exit (A_{CSC}) by the x-ray output measured at 1.0 m distance from the focus and corrected to the distance corresponding to the exit of the cone (d_{FEC}). Thus, the P_{KA}, per radiograph, was determined by the following equation:

$$P_{KA} = Y_{exam} \cdot Q_{exam} \cdot \left(\frac{d_{FEC}}{1} \right)^2 \cdot A_{CSC} \qquad (1)$$

Y_{exam} is the output of the x-ray tube, in $mGy.mAs^{-1}$, at 1 m distance, for the kV used in the examination (interpolated from a curve of the output "versus" tube voltage), Q_{exam} is the product of the tube current, in mA, and the exposure time, in s, used in the examination.

The uncertainty in the P_{KA} value, per radiograph, was based on the uncertainties in the output measurement and inaccuracies due to consideration of uniform x-ray exposure across the field.

III. Results and Discussions

Table 2 presents, for each age group, the statistical data for patient's features (height and weight), exposure parameters (kV, mAs) and P_{KA}. In the Table 3 is presented a comparison of the radiographic techniques (kV, mAs) and P_{KA} among the hospital studied and other published data.

It should be emphasized that the VMI x-ray machine of the hospital is not adapted for radiographic procedures of pediatric patients, since exposure times lower than 10 ms cannot be selected and it is not a high frequency or constant potential machine [2, 3]. Furthermore, two important performance parameters of the equipment: the HVL and the x-ray tube output are not adequate for pediatric radiography [8].

Results given in the Table 2 showed a low increment on kV compared to mAs for patients in different age groups. For patients in the age group 1-5, the P_{KA} show a high variation compared to values found for 10-16 age group. These results can be explained by the non-standardization of the use of the grid by technicians of the hospital.

The expanded uncertainty (coverage factor equals to 2) of the P_{KA} values, per radiograph, were estimated as 18.5%. This value was lower than the recommended maximum uncertainty value of 25% for patient dose measurements in diagnostic radiology.

Comparison with other published data presented in the Table 2 showed that despite kV and mAs were similar to those used by da Silva et. al. [5], P_{KA} were significantly high. Cook et. al. [3] used high values of kV and low values of mAs compared with other published data. This can be justified by the use of high focus-to-image receptor distances and the lack of utilization of grids in children less than 10 years by the mentioned authors.

Another important point is the unnecessary exposure of children less than 5 years old. Cook et. al. [3] did not recommend this kind of examination in patients within this age group.

Table 2. Statistical data for patient's features (height and weight), exposure parameters (kV, mAs) and P_{KA}.

Age group (years old)	H (cm)	W (kg)	kV	mAs	P_{KA} (cGy.cm^2)
1 to 5					
Min.	65	10	52	50	9.2
Mean	98.4	15	67.8	57.1	28.5
Max.	120	20	71	100	54.7
SD	11.5	2.6	3.5	13.4	9.5
N			28		
5 to 10					
Min.	102	17	60	50	15.5
Mean	121.2	22.7	68.5	65.3	33.7
Max.	143	34	71	100	57.6
SD	9.6	4.4	2.6	17.4	11.5
N			18		
10 to 16					
Min.	138	26	67	50	23.3
Mean	150	43	69.3	67.9	36.0
Max.	147.4	33.9	70	75	41.0
SD	4.5	6.5	1.1	12.2	7.9
N			7		

Table 3. Comparison of the exposure parameters and P_{KA} values among the hospital studied and other published data.

Reference		kV	mAs	P_{KA} (cGy.cm^2)
This work	1-5	67.8	57.1	28.5
	5-10	68.5	65.3	33.7
	10-16	69.3	67.9	36.0
Cook et. al. [3]	5-10	65.0	10.0	2.4
	10-15	78.0	16.0	7.0
Lacerda et. al. [4]	1-5	70.6	17.3	28.0
	5-10	69.0	20.2	35.8
	10-16	72.5	18.0	37.4
da Silva et. al. [5]	1-5	68.0	34.2	4.6
	5-10	61.3	47.9	5.2
	10-16	60.3	52.8	5.6

IV. Conclusion

The adopted methodology for assessing P_{KA} in x-ray examinations of paranasal sinuses showed low uncertainties and it can be used during the routine of any hospital with minimum interference.

The characteristics and performance of the x-ray equipment and the lack of standardization of exposure parameters by radiology technicians are the main causes for high P_{KA} values found in the hospital studied.

Acknowledgment

M. A. S. Lacerda and T. A. da Silva are thankful to CNPq and FAPEMIG for providing research fellowships and financial resources for presenting the results.

The scientific team is grateful to the Brazilian Science and Technology Minister (MCT) for supporting this work through the Institute of Science and Technology for Radiation Metrology in Medicine (INCT).

References

1. ICRP (2007). International Commission on Radiological Protection. The 2007 Recommendations of the ICRP. ICRP Publication 103. Ann ICRP 32 (3-4) Oxford, UK: Pergamon Press
2. EC (1996). European Commission. European Guidelines on Quality Criteria for Diagnostic Radiographic Images in Paediatrics. EUR 16261 En, Luxemburg
3. Cook, J. V., Shah, K., Pablot, S., et. al. (1998). Guidelines on best practice in the x-ray imaging of children; a manual for all x-ray departments. Queen Mary's Hospital for Children. Carshalton.
4. Lacerda, M A S, da Silva, T A, Khoury, H J (2008) Assessment of dosimetric quantities for patients undergoing x-ray examinations in a large public hospital in Brazil – a preliminary study. Radiat. Prot. Dosim. 132, 73-79.
5. da Silva, T A, Lacerda, M A S, Khoury, H J (2008) Radiation doses in children submitted to x-ray examinations of paranasal sinuses. Proc. International Congress of the International Radiation Protection Association. IRPA 12. Buenos Aires, Argentina.
6. IAEA (2007). International Atomic Energy Agency. Dosimetry in diagnostic radiology: an international code of practice. IAEA Technical Report Series 457. Vienna.
7. Faulkner, K, Broadhead, D A, Harrison, R M (1998). Patient dosimetry measurement methods. Appl. Radiat. Isot. 50, 113-123.
8. MS (2005). Ministério da Saúde – Brazil. Medical diagnostic radiology : equipment performance and safety [in Portuguese]. Brasília.

Corresponding author:

Author: Marco Aurélio de Sousa Lacerda
Institute: Centro de Desenvolvimento da Tecnologia Nuclear (CDTN/CNEN)
Street: Av. Antônio Carlos, 6627, Pampulha
City: Belo Horizonte
Country: Brazil
Email: masl@cdtn.br

Dosimetry Studies on a Fetus Model Combining Medical Image Information and a Synthetic Woman Body

L. Bibin[1], J. Anquez[1], A. Hadjem[2], E. Angelini[1], J. Wiart[2] and I. Bloch[1]

[1] Institut Telecom, Telecom ParisTech, CNRS UMR 5141 LTCI, Paris, France
[2] France Telecom, Orange Labs R&D, Issy les Moulineaux, France

Abstract— **Wireless systems are increasingly used and the electromagnetic fields (EMF) generated by these systems have induced a large public concern regarding potential sanitary effects, in particular on children and fetus during pregnancy. Few works have been performed to analyze the fetus exposure but additional studies are still needed, based on precise anatomical models. In this paper, we propose a new method to assess the fetus exposure, based on realistic anatomical models built from 3D MRI images at different gestational ages. The whole body specific absorption rate (SAR) and the maximum SAR over 10 grams have been estimated using finite differences in time domain (FDTD) simulation methods for five fetuses at different ages. Results show that the local and the whole body SAR are lower in the fetus than in the mother and that they depend on position and morphology but not on gestational age.**

Keywords— **"Dosimetry", "3D Modeling", "Segmentation", "Fetus", "Medical Imaging".**

I. Introduction

Nowadays, wireless systems are increasingly used. More than 3 billions of people are nowadays using worldwide GSM mobile phone and more and more people are using Wi-Fi systems. The electromagnetic fields (EMF) generated by these systems to communicate have induced a large public concern about potential sanitary effects. The World Health Organization (WHO) has set up in 1996 the EMF Project to promote and coordinate the worldwide research around this concern. In 2004, the WHO set up a workshop (Istanbul June 2004) dealing with the sensitivity of children to EMF. One of the outputs of the workshop led to the recommendation of improvements in dosimetry studies. Precise models of the human body are therefore needed, in particular children and pregnant woman models.

Human head models were previously developed by our group for adults [1] and children [2-3] in order to study the impact of the use of a mobile phone on the brain [4-6]. With new usages (e.g. body worn and hand-free kit) and permanent exposures in professional environment, fetal dosimetry needs to be investigated with more care. Up to now only few fetus models have been developed and all present several limitations, being incomplete, not representative or too much simplified.

The aim of this project is to analyze the specific absorption rate (SAR) induced by an incident EM plane wave in different fetuses with detailed, representative and realistic three-dimensional pregnant women models and their fetus at various stages of gestation and in different positions in order to simulate several radiation dosimetry studies. These models are created from the segmentation of magnetic resonance imaging (MRI) for the fetus and from a synthetic woman model created with the software DAZ Studio (www.daz3d.com) for the mother.

In this paper, after reviewing the state of the art, we describe the image database and the proposed methods to create the models. We then present visual illustrations of one generated model. Using these models and the well known finite difference in time domain (FDTD) simulation method, the SAR averaged over 10 g and the whole body averaged SAR of a pregnant woman and her fetus are assessed for a plane wave (vertical polarization) at 900 MHz. Our main contribution is to propose a set of five models, enabling for the first time the study of position influence on dosimetry.

II. State of the art

Adult computational models used in dosimetry studies are built using whole body MRI data, acquired on volunteers. Acquiring such data on a pregnant woman is impossible for ethical reasons. Therefore, hybrid models are built, merging stylized models (modeled with surface equations), synthetic models (issued from the computer graphics community) and/or voxelized models (extracted from medical images).

The first published pregnant woman model was a stylized model [7]. Even if unrealistic, it was useful as computational power was limited at this time and obstetric medical imaging could not provide suitable data to build voxelized models.

Recently, the advent of fast acquisition imaging protocols usable in routine obstetrical screening allows gathering data imaging the whole fetus without motion artifact. In [8], a voxelized model was built from computerized tomography (CT) images. The fetus model was coarse due to large slice thickness (7 mm) and only the fetal soft tissues and skeleton were differentiated. The pregnant woman model was truncated, the CT image including only the patient torso. The hybrid model SILVY was built combining an MRI of a malformed fetus with the model of [8], adding legs, arms and head models from computer graphics to this model [9]. It was a realistic whole body model, but the fetus and uterus modeling remained coarse. The uterus and fetus stylized model of [10] was embedded in the non-pregnant model

O. Dössel and W.C. Schlegel (Eds.): WC 2009, IFMBE Proceedings 25/III, pp. 321–324, 2009.
www.springerlink.com

NAOMI. This embedding involved voxel editing of NAOMI which induced variations in organs shapes and volumes. A highly detailed and realistic mother model was obtained, but the uterus and fetus model remained highly simplified. In [11], a voxelized model of the uterus and fetus was embedded in a women computer-aided design model. Using this interesting approach, a set of pregnant woman models at each month of gestation was generated, scaling the uterus and fetus models. Due to the complexity of fetal organs growth, scaling seems however inappropriate. A complex hybrid model using the CT images presented in [8], the VIP-MAN model [12] and computer aided design models were proposed in [13]. Three models were built at 3, 6 and 9 months of pregnancy. Anatomical realism is difficult to evaluate because the model building process involves many components and few fetal tissues are distinguished. In [14], a uterus and fetus model is merged within a non gravid woman model. The former model is morphed using free form deformation, yielding an anatomically correct model.

Each model presents advantages and drawbacks, considering realism and anatomical details. As no whole body woman model is freely available, we have adopted the approach presented in [11]. We create a set of hybrid models, merging uterus and fetus models extracted from medical imaging data, and a virtual woman body. In contrast with [11], uterus and fetus models are extracted from different medical images and are all realistic. The proposed set of hybrid models enables for the first time the study of the influence of the fetus position and morphology on dosimetry.

III. Image Database

In collaboration with pediatric radiologists from the Saint Vincent de Paul hospital (Paris, France), a study [15] was performed to select the best suited MRI imaging protocols for the segmentation of the fetus and the mother. The quality criteria included: large field of view in order to image the whole uterus, good global contrast, good spatial resolution ($1\times1\times4$ mm^3), fast acquisition (less than 30 seconds) and low sensitivity to fetal movements artifacts.

The MRI acquisition protocols FIESTA (Fast Imaging Employing Steady state Acquisition) for the General Electric systems and True FISP (Fast Imaging with Steady state Precession) for the Siemens system were chosen, corresponding to the generic sequence SSFP (Steady State Free Precession).

Figure 1 shows an MRI image and the outline of the fetus. The database gathered so far contains 22 cases between 30 and 34 weeks of amenorrhea.

IV. Models

A. Segmentation

From the image database, we segment the tissues playing an important role in dosimetry such as the uterus, the brain or the bladder. This has been done either manually for a number of data sets, or automatically, using the method described in [16]. An example of fetus segmentation on MRI data is shown in Figure 1.

Fig. 1 Fetus outline traced on a slice of a 3D MRI data set.

B. 3D reconstruction

A triangulation method is applied on the segmented surfaces to construct corresponding shape meshes. The segmented organs were filtered using a simple Gaussian filter to reduce the staircase effects due to the anisotropy of the images. Reducing these effects provides surfaces better suited to the algorithms used for dosimetry computation.

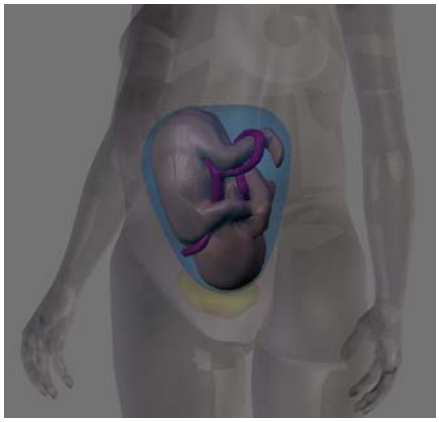

Fig. 2 A 3D fetus placed in the deformed virtual woman body.

C. Fetus placement in the virtual woman body

As the body of the mother is not entirely included in the field of view of the medical images, we use a synthetic

virtual woman body distributed with the DAZ studio software.

To obtain a realistic pregnant model, the synthetic woman model is fitted to the external envelope of the real maternal anatomy that is partially visible on the medical imaging data. The virtual body is reshaped using a lattice based free-form deformation with the software tool Blender (www.blender.org). The fetus and its internal organs are inserted into the virtual body using anatomical landmarks such as the pelvis.

To guarantee that our models are anatomically correct and depict a realistic maternal body, all this deformation work was done with the control of obstetricians and pediatric radiographers.

We have modeled so far five pregnant women with fetus segmented from MRI 3D images at 30, 32 (two models), 33 and 34 weeks of amenorrhea. Figure 2 shows a surface reconstruction of a fetus in the deformed virtual mother body.

Our models include anatomical variations to represent several typical pregnancy configurations. In particular, the set of models includes:

- a fetus in breach position. This position can have an impact on the dosimetry;
- a filled mother urinary bladder. This configuration elevates the fetus position and can also change the dosimetry;
- a model where the MRI was acquired with the mother in a lateral decubitus position whereas the others were acquired in dorsal decubitus positions; This position changes the shape of the mother abdomen and also the fetus position.

For dosimetry studies, we generate voxelized models from the surface models. Each tissue type is assigned a unique label in order to create the final 3D volumes that contain all the segmented tissues (see Figure 3).

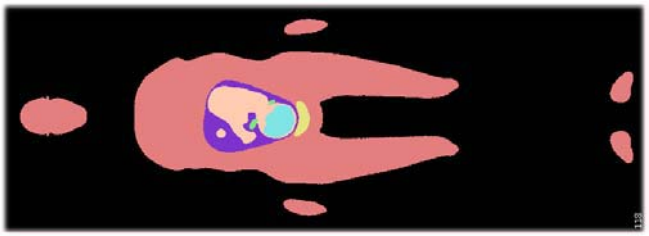

Fig. 3 3D Voxelized model of a mother and a fetus.

V. Exposure analysis

A. Specific Absorption Rate assessment

Using our models, we analyze the exposure of the fetus exposed to a plane wave.

The fetus is heterogeneous while the mother tissues are homogeneous. The dielectric properties of the fetus are those commonly used [17] while the dielectric properties of the mother tissue are those used in IEC [18].

The incident field at 900 MHz is vertically polarized and is arriving face to the pregnant women. The exposure is quantified by the well known (SAR) measure given by:

$$SAR = \frac{\sigma . E^2}{\rho} \tag{1}$$

where σ is the conductivity (S/m), ρ the mass density (Kg/m3) and E the rms electric field strength induced in tissues (V/m). In this study, the method used to assess electric field induced in the woman body is the finite difference in time domain (FDTD) [19]. To avoid spurious reflection at the boundary of the computational domain, we use the perfectly matched layer (PML) absorbing boundary conditions [20]. The exposure is characterized through the global SAR, averaged over the whole body and the local SAR averaged over 10 g of tissues. Most of the SAR studies that have been published are performed over a cube. To allow comparisons with previous studies, we decided to assess the maximum SAR over 10 g using a cube shape.

B. Results

The whole body (wb) SAR and the maximum SAR over 10 grams have been estimated for 5 fetuses at different ages from 30 weeks to 34 weeks. Table 1 shows that the local SAR and whole body SAR are lower in the fetus than in the mother. The table shows also that the exposure does not increase with the age of the fetus but depends on the position of the fetus and the fetus morphology (see e.g. the results for the two models at 32 weeks, where the main difference between the data sets is the position and morphology of the fetus). The mean ratio of the whole body SAR between the fetus and the pregnant woman is 0.21 with a standard deviation of 0.062. This means that the whole body exposure in fetus is 5 times below the whole body exposure induced in the maternal model.

Table 1 SAR in the fetus and the pregnant woman

Age (week)	30	32	32	33	34.5
SARwb (mW/kg/1W/m²) (fetus)	1	1.6	2	1	1.1
Ratio SAR wb (fetus / pregnant women)	0.16	0.25	0.31	0.18	0.18
Ratio SAR over 10g (fetus / pregnant women)	0.026	0.028	0.042	0.033	0.025
Maximum SAR over 10g (Fetus) mW/kg	5.8	7.8	10.7	8.1	6.2

These results are in accordance with those obtained in [21, 22] for the fetus. For the woman, the results differ since we assumed homogeneous tissues, which was sufficient here since we were mainly interested in the ratio between SAR values in the fetus and in the woman. The maximum SAR

values are interesting results too. This measure was not assessed before for the fetus, and is thus an additional contribution of the paper.

VI. Conclusions

In this paper, we have presented a methodology to construct hybrid pregnant women models with detailed fetal anatomy extracted from MRI image data, combined with a woman body from a synthetic model. Our models are detailed as we can segment several fetal organs. For the moment, we have created five models from MRI images at various stages of the gestation and in different positions. The placement of the fetus in the synthetic woman was performed under medical control. All our models were validated by clinical experts and anatomically corrected. These models will be made freely available to the scientific community, in a near future.

A comparison of SAR induced in a pregnant woman with different gestational stages was performed employing an incident plane wave having a vertical polarization and operating at 900 MHz. The SAR was numerically estimated using the FDTD method. The results show that the fetus exposure depends on the fetus morphology, fetus stages and on the position of the fetus, while it remains well below the local and whole body SAR of the mother. Further work is needed for definitive conclusion since these simulations have been carried out only for specific cases (specific fetus models and pregnant women with homogeneous tissues).

For fetus at earlier stages of gestation, we have already developed models issued from 3D ultrasound images [23], and simulations still be carried out on these models as well.

Acknowledgment

This work has been partially founded by a grant from the Fondation Santé et Radiofréquences and by Orange Labs.

References

1. Dokladal P, Bloch I, Couprie M, Ruijtersand D, Urtasun R, Garnero L (2003) Topologically Controlled Segmentation of 3DMagnetic Resonance Images of the Head by using Morphological Operators. Pattern Recognition, 36(10):2463-2478.
2. Burguet J, Bloch I (2004). Homotopic Labeling of Elements in a Tetrahedral Mesh for the Head Modeling. CIARP, Lecture Notes in Computer Science, Puebla, Mexico, 3287:566-573.
3. Burguet J, Gadi N, Bloch I (2004) Realistic Models of Children Heads from 3D MRI Segmentation and Tetrahedral Mesh Construction. 2nd International Symposium on 3D Data Processing, Visualization and Transmission, 3DPTV, Thessaloniki, Greece, 631-638.
4. Hadjem A, Lautru D, Dale C, Man Fai Wong, Hanna V F, Wiart J (2005) Study of specific absorption rate (SAR) induced in the two child head models and adult heads using a mobile phones IEEE Trans. Microw. Theory Tech. 53 4–11.
5. Wiart J, Hadjem A, Gadi N, Bloch I, Wong M F, Pradier A, Lautru D, Hanna V F, Dale C (2005) Modeling of RF exposure in children. Bioelectromagnetics 26:45–50.
6. Wiart J, Hadjem A, Wong M F, Bloch I (2008) Analysis of RF exposure in the head tissues of children and adults. Phys. Med. Biol. 53:3681–3695.
7. Stabin M G et al (1995) Mathematical Models and Specific Absorbed Fractions of Photon Energy in the Non pregnant Adult Females and at the End of Each Trimester of Pregnancy. Springfield, Va.: Oak Ridge National Laboratory; National Technical Information Service.
8. Shi C, Xu X G (2004) Development of a 30-week-pregnant female tomographic model from computed tomography (CT) images for Monte Carlo organ dose calculations. Medical Physics, 31:2491.
9. Cech R, Leitgeb N, Pediaditis M (2007) Fetal exposure to low frequency electric and magnetic fields. Physics in Medicine and Biology, 52(4):879-888.
10. Chen J (2004) Mathematical models of the embryo and fetus for use in radiological protection. Health Physics, 86(3):285–295.
11. Wu D, Shamsi S, Chen J, Kainz W (2006) Evaluations of Specific Absorption Rate and Temperature Increase Within Pregnant Female Models in Magnetic Resonance Imaging Birdcage Coils. IEEE Transactions on Microwave Theory and Techniques, 54(12):4472–4478.
12. Xu X G, Chao T C, Bozkurt A(2000) VIP-MAN: an image-based whole-body adult male model constructed from color photographs of the visible man project for multi-particle Monte Carlo calculations. Health Physics, 78(5):476.
13. Xu X G, Taranenko V, Zhang J, Shi C (2007) A boundary-representation method for designing wholebody radiation dosimetry models: pregnant females at the ends of three gestational periods-P3,-P6 and-P9. Physics in Medicine and Biology, 52(23):7023–7044.
14. Nagaoka T, Togashi T, Saito K, Takahashi M, Ito K, Watanabe S (2007) An anatomically realistic whole-body pregnant-woman model and specific absorption rates for pregnant-woman exposure to electromagnetic plane waves from 10 MHz to 2 GHz. Physics in Medicine and Biology, 52(22):6731-6745.
15. Anquez J, Angelini E, Bloch I, Merzoug V, Bellaiche-Millischer A E, and Adamsbaum C (2007) Interest of the Steady State Free Precession (SSFP) Sequence for 3D Modeling of the Whole Fetus. In Engineering in Medicine and Biology Conference, EMBC 2007, pages 771-774, Lyon, France.
16. Anquez J, Angelini E, Bloch I (2009) Automatic segmentation of head structures on fetal MRI. In IEEE International Symposium on Biomedical Imaging (ISBI'09) (submitted).
17. Gabriel C (1996) Compilation of the dielectric properties of body tissues at RF and microwave frequencies Brooks Air Force Technical Report AL/OE-TR-1996-0037.
18. IEC 2005 Human exposure to radio frequency fields from hand-held and body-mounted wireless communication devices—Human models, instrumentation, and procedures: Part 1. Procedure to determine the specific absorption rate (SAR) for hand-held devices used in close proximity to the ear (frequency range of 300 MHz to 3 GHz) Standard Int. Electrotechnical Commission (IEC) Std 62209-1.
19. Taflove A, Hagness S (2000) Computational Electrodynamics (Boston, MA: Artech House).
20. Berenger J P (1994) A perfectly matched layer for the absorption of electromagneticwaves J. Comput. Phys. 4 185–200.
21. Nagaoka T. et al. (2008) Postured voxel-based human models for electromagnetic dosimetry, Phys. Med. Biol,. 53:7047-7061.
22. Togashi T., Nagaoka T., Kikuchi S., Saito K., Watanabe S, Takahashi M., Ito K. (2008) FDTD Calculations of Specific Absorption Rate in Fetus Caused by ElectromagneticWaves From Mobile Radio Terminal Using Pregnant Woman Model, IEEE Transactions on Microwave Theory and Techniques 56(2):554-559.
23. Bibin L, Anquez J, Angelini A, Bloch I (2009) Hybrid 3D modeling of mother and fetus from medical imaging for dosimetry studies. CARS, 23rd International Congress and Exhibition, Berlin, Germany.

Author: Lazar Bibin
Institute: Telecom ParisTech, CNRS UMR 5141 LTCI
Street: 46, rue Barrault 75634
City: Paris Cedex 13
Country: France
Email: lazar.bibin@telecom-paristech.fr

Use of a Standard Ionization Chamber at Different Distances in Diagnostic Radiology Beams

M.T. Yoshizumi, L.C. Afonso and L.V.E. Caldas

Instituto de Pesquisas Energéticas e Nucleares, IPEN-CNEN/SP, São Paulo, Brazil

Abstract— **A secondary standard ionization chamber was calibrated, by a primary standard laboratory, at a determined distance. However, in the routine procedures of a calibration laboratory, sometimes the radiation detector cannot be positioned exactly at the calibration distance, for any reason. In this work, the response of a secondary standard ionization chamber was tested to verify the possibility of its use at different distances than at the calibration distance, using the same calibration factor.**

Keywords— **Ionization chamber, X-radiation, diagnostic radiology beam qualities.**

I. Introduction

All radiation detectors must be calibrated periodically [1]. The calibration frequency depends on the type of radiation detector. The calibration services are offered by calibration laboratories which may be classified as primary, secondary or regional laboratories.

The primary standard laboratories have primary standards, such as radiation sources and ionization chambers that are used to calibrate radiation detectors. For low- and medium-energy X-radiation, the primary standard is usually a free-air ionization chamber [2].

Secondary standard laboratories have equipment and/ or sources calibrated against primary standards. The secondary standards are calibrated under their usage conditions. These laboratories offer calibration service to clinics, hospitals and other medical services that use radiation detectors. In Brazil, the secondary standard laboratory is located in Rio de Janeiro and it is named National Laboratory of Metrology of the Ionizing Radiations (LNMRI).

The Calibration Laboratory of Instituto de Pesquisas Energéticas e Nucleares (IPEN) is a regional laboratory, and it offers calibration services using X, alpha, beta and gamma radiations. Sometimes, in the calibration laboratory routine, a specific radiation detector cannot be calibrated at the recommended distance. This situation may occur when, the radiation field is not large enough to cover the sensitive volume, or when the air kerma rate is too low that a large irradiation time is necessary or even when it is not possible to position the radiation detector because of geometrical problems.

In this work, a secondary standard ionization chamber was tested at different distances than the calibration distance of 100 cm to verify its utilization under several conditions.

II. Materials

For all tests performed in this work an industrial X-ray unit, Pantak/Seifert, model ISOVOLT 160HS was used. This system operates from 5 to 160 kV, 0.5 to 45.0 mA and presents 0.8 mmBe of inherent filtration. Its standardized beam qualities are shown in Table 1.

A secondary standard plane-parallel ionization chamber, *Physikalisch Technische Werksttäten*, PTW, model 77334-2052, traceable to the German primary standard laboratory *Physkalisch Technische Bundesanstalt* (PTB) [3], was used to establish the diagnostic radiology qualities [4] in the X-ray unit and it was used for the tests described in this work.

III. Results

A. Response stability tests

The short- and medium-term stability tests were performed using the quality beam RQR 4 of the X-ray unit, listed in table 1, that corresponds to 60 kV, 10 mA and 2.5 mmAl of total filtration. Over the period of tests, the leakage current of the ionization chamber was always negligible.

For the short-term stability test ten consecutive measurements of the collected charge were taken. The standard deviation of these measurements presented a maximum

O. Dössel and W.C. Schlegel (Eds.): WC 2009, IFMBE Proceedings 25/III, pp. 325–328, 2009.
www.springerlink.com

value of 1.5%. According to international recommendations this value shall not be higher than ±3% [5].

The medium-term stability test verifies the variation of the mean value of the measurements of the short-term stability test along the time. As can be seen in Figure 1, the maximum variation of the values was 1.6%, thus within the international recommendation of ±2% in a period of one year [5].

Table 1 Characteristics of the X-ray beam qualities of the Pantak/ Seifert unit defined at 100 cm.

Beam quality	Voltage (V)	Total filtration (mmAl)	Half-value layer (mmAl)	Energy (keV)	Air kerma rate (mGy.min^{-1})
Direct Beams					
RQR 3	50	2.5	1.79	27.2	22.82
RQR 4	60	2.5	2.09	28.8	33.98
RQR 5	70	2.5	2.35	30.2	45.59
RQR 6	80	2.5	2.65	31.7	58.49
RQR 7	90	2.5	2.95	33.1	72.67
RQR 8	100	2.5	3.24	34.4	87.56
RQR 9	120	2.5	3.84	37.1	119.59
RQR 10	150	2.5	4.73	40.8	172.44
Attenuated Beams					
RQA 3	50	12.5	3.91	37.3	3.46
RQA 4	60	18.5	5.34	43.3	3.11
RQA 5	70	23.5	6.86	49.4	3.45
RQA 6	80	28.5	8.13	54.8	4.04
RQA 7	90	32.5	9.22	59.7	5.00
RQA 8	100	36.5	10.09	64.0	5.94
RQA 9	120	42.5	11.39	71.2	8.06
RQA 10	150	47.5	13.20	82.1	13.48

B. Linearity of response

The linearity of the ionization chamber response was tested using the beam quality RQR 5, with characteristics shown in table 1. In this test the tube current was varied from 0.5 to 40.0 mA, with the ionization chamber positioned at 50, 100 and 250 cm from the X-ray tube. The results are shown in Figure 2. As expected, the ionization chamber response is linear with the tube current variation for all three distances. The maximum uncertainty of the measurements was 3%.

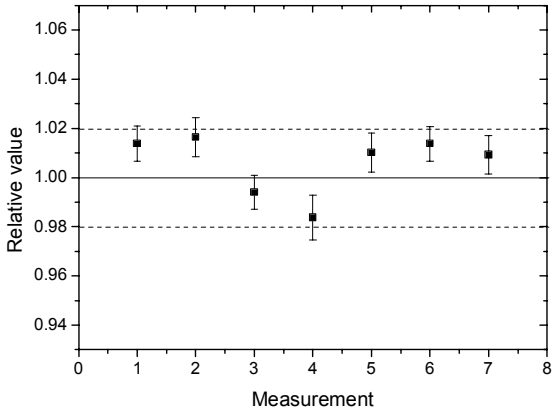

Fig. 1 Response stability of the ionization chamber.

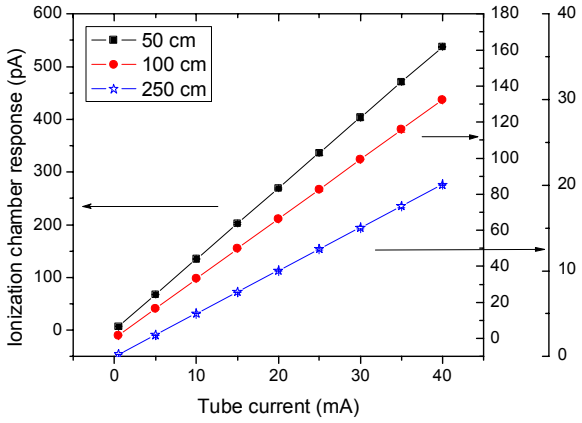

Fig. 2 Response linearity of the ionization chamber at 50, 100 and 250 cm from the X-ray tube.

C. Energy dependence

The energy dependence of the secondary standard ionization chamber was also studied at the distances of 50, 100 and 250 cm.

First of all, the ionization chamber was positioned at the calibration distance of 100 cm. Using the calibration and correction factors given by the primary laboratory [3], the air kerma rates for all X-ray beam quality, diagnostic radiology level, were calculated from the measurements of

collected charge. These values of air kerma rate are shown in Table 1.

The same procedure was followed with the ionization chamber positioned at the distances of 50 and 250 cm using the same calibration and correction factors determined for 100 cm. Using the inverse square law, the air kerma rates at these distances were also determined from the values obtained at the distance of 100 cm. The results of measured and calculated values are shown in Figures 3 and 4.

As can be seen in Figures 3 and 4, the measured and calculated values are similar. For direct beam qualities the maximum variations were 5.1% and 3.7% at the distances of 50 and 250 cm, respectively. For attenuated beam qualities the measured and calculated values presented maximum variations of 6.3% and 3.8% at the distances of 50 and 250 cm, respectively. These variations are probably due to the scattered radiation from the beam filtration. The maximum uncertainty of these measurements was only 2%.

In Figure 5 the inverse square law is showed for the radiation quality RQR 5.

IV. CONCLUSIONS

The secondary standard ionization chamber response showed to be stable over the test period.

For the distances of 50, 100 and 250 cm from the X-ray tube focal spot, the ionization chamber response is linear to the tube current range from 0.5 to 40.0 mA.

For the distances of 50 and 250 cm, the measured values of the ionization chamber response in energy were similar to the calculated values, using the inverse square law. The measured values were calculated using the same calibration and correction factors established for the distance of 100 cm by the primary standard laboratory; thus these factors may be used in other distances. The maximum variation was 6% for the attenuated beam quality RQA 10 at the distance of 50 cm.

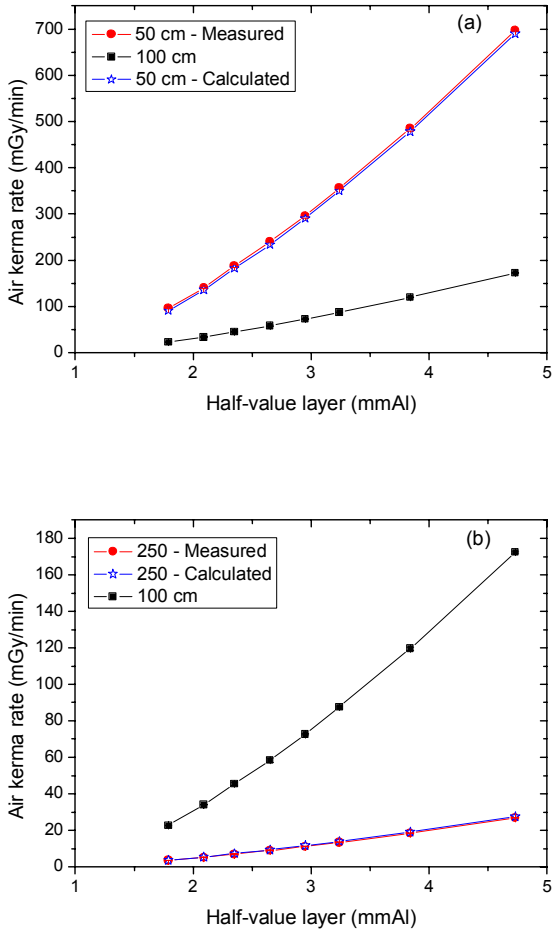

Fig. 3 Energy dependence of the ionization chamber at (a) 50 cm and (b) 250 cm from the X-ray tube for direct beam qualities RQR 3 to RQR 10.

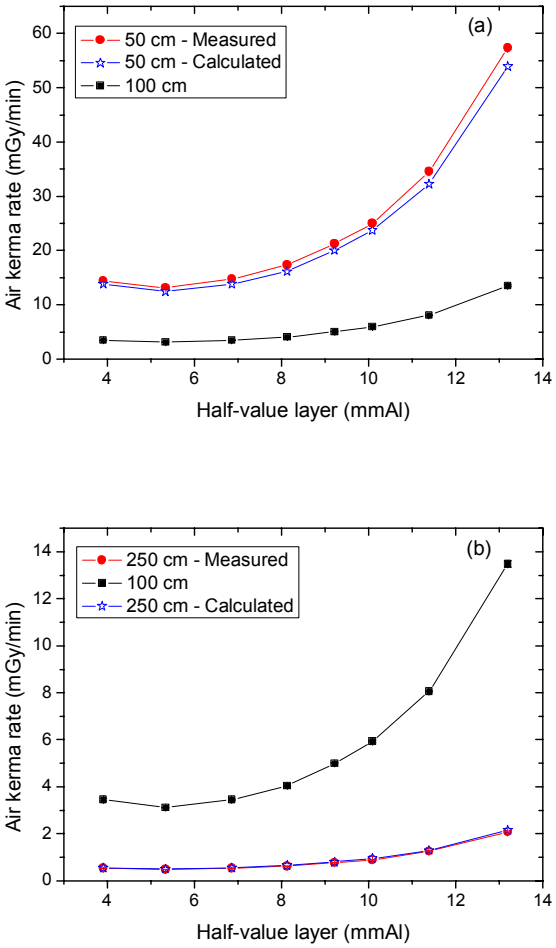

Fig. 4 Energy dependence of the ionization chamber at (a) 50 cm and (b) 250 cm from the X-ray tube for attenuated beam qualities RQA 3 to RQA 10.

In both cases, direct and attenuated beams, the measured values were higher than the calculated values at 50 cm of distance and the contrary occurred at 250 cm of distance. These facts are probably due to the increase in the ionization chamber response with the scattered radiation produced by the beam filtration at 50 cm, and the decrease in the ionization chamber response due to the air attenuation of the X-ray beam at the distance of 250 cm.

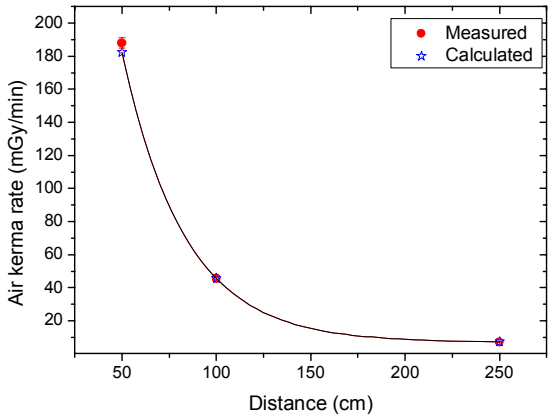

Fig. 5 Inverse square law for the diagnostic radiology beam quality RQR 5.

ACKNOWLEDGMENTS

The authors acknowledge Fundação de Amparo à Pesquisa do Estado de São Paulo (FAPESP) and Comissão Nacional de Desenvolvimento Científico e Tecnológico (CNPq), Brazil, for the partial financial support.

REFERENCES

1. IAEA (2000) Calibration of radiation protection monitoring instruments. Safety Reports Series 16 (Vienna: International Atomic Energy Agency)
2. IAEA (2007) Dosimetry in diagnostic radiology: an international code of practice. Technical Reports Series 457 (Vienna: International Atomic Energy Agency)
3. PTB (2004) Calibration certificate of the ionization chamber 77334-2052. (Munich: Physikalisch-Technische Bundesanstalt)
4. IEC (1994) Medical diagnostic X-ray equipment – Radiation conditions for use in the determination of characteristics. Report 1267 (Genève: International Electrotechnical Commission)
5. IEC (1997) Medical electrical equipment – Dosimeters with ionization chamber and/ or semi-conductor detectors as used in X-ray diagnostic imaging. Report 61674 (Genève: International Electrotechnical Commission)

Use macro [author address] to enter the address of the corresponding author:

Author: Luciana Caminha Afonso
Institute: Instituto de Pesquisas Energéticas e Nucleares
Street: Prof. Lineu Prestes, 2242
City: São Paulo
Country: Brazil
Email: lcafonso@usp.br

Implementation of tube current modulation in CT dose computations with voxel models

H. Schlattl, M. Zankl and C. Hoeschen

Helmholtz Zentrum München – German Research Center for Environmental Health, Institute of Radiation Protection, Ingolstädter Landstr. 1, 85764 Neuherberg, Germany

Abstract— **Automatic tube current modulation is meanwhile a standard procedure in modern CT devices to save radiation dose. The implementation of this method into Monte Carlo organ-dose calculations is described. A comparison of conversion coefficients obtained with and without tube current modulation is performed. A standard reliable procedure to compute conversion coefficients for any CT examination is to combine the pre-computed coefficients obtained in axial scans appropriately. The applicability of this procedure was validated for the case with tube current modulation, too.**

Keywords— **Organ dose conversion coefficients, voxel models, computed tomography.**

I. Introduction

The excellent diagnostic power of images obtained by computed tomography (CT) led to a strong increase in the application of this technique [1]. However, CT examinations are accompanied with relatively high radiation dose compared to simple projection radiography. One method to reduce the patients' radiation dose that has been implemented by the CT manufactures is the usage of an automatic tube current modulation (ATCM) [2, 3]. The basis of this method lies in the different attenuation of the human body along its height (z-modulation) and in different transverse directions (angular modulation). The first implementation in a CT device developed by GE systems ("smart scan") was using two additional localizer radiographs in lateral and antero-posterior direction to estimate the transverse attenuation profile [4]. Modern devices use the signal in the center of the detector of that projection that was taken either 180° or 360° before the current one [3]. Entrance dose reductions of up to 70% have been reported with such systems without loss of image quality [5].

For a detailed study of how the individual organ doses are affected by the tube current modulation, the implementation of this technique into numerical dose calculations is required. Thus, it has been incorporated into a Monte Carlo particle transport program that has been developed for the calculation of dose conversion coefficients for various cases [6, 7]. Moreover, most currently available conversion coefficients for CT examinations [8, 9], which relate entrance dose to organ or effective doses, are based on mathematical models of the human. A considerably better representation of the human anatomy is achieved with voxel-based models, which originate in CT images of real persons. The International Commission on Radiological Protection (ICRP) has currently been publishing new reference voxel models that are employed in the computations of the conversion coefficients in this work.

II. Methods

A. The CT system

In the simulations, properties similar to a Siemens Sensation Cardiac (Siemens AG, Medical Solutions, Forchheim, Germany) have been employed. The detector and source diameter are 57 cm. The bowtie filter has been apparently designed for cardiac imaging, as it leads to a strong reduction of the x-ray intensity at the body's edges.[1] Thus, the resulting organ doses might not be representative for real systems used for other body regions, but exact information on other bowtie filters was not made available. Nevertheless, organ dose conversion coefficients are presented normalized to $CTDI_{vol}$. Since this quantity is a weighted mean of air kerma at the edge and center of the field and thus accounts for differently shaped filters, the presented dose conversion coefficients depend probably only weakly on the exact filter shape.

B. Voxel models and Monte Carlo simulation

As human model serves the ICRP adult reference computational male phantom [10]. Its voxel dimensions are 2.137 × 2.137 × 8 mm³. The height and weight of the model are 176 cm and 73 kg, respectively. The simulations are performed with two user codes of the Monte Carlo particle transport package EGSnrc [11]. With the first one, the pho-

[1] Details of filter material and shape are proprietary information of the manufacturer and thus cannot be disclosed.

O. Dössel and W.C. Schlegel (Eds.): WC 2009, IFMBE Proceedings 25/III, pp. 329–332, 2009.
www.springerlink.com

tons transmitted by the body are recorded in a small field representing the central detector part in a real system. A measurement area of 5 x 1 cm² at the detector plane was assumed due to the lack of more detailed knowledge. The focus-to-detector and focus-to-isocenter distances were assumed to be 114 and 57 cm, respectively. The transmitted spectra are quite narrow, thus the energy-dependence of the detector signal is not crucial for determining relative changes in the photon number or air kerma during a scan. Therefore, a simple photon counting detector was simulated. The size of the x-ray beam in the plane through the isocenter was about 100 x 1 cm², similar to the field size in the actual CT scan.

Two different trajectories of the x-ray beam have been simulated, a helical one with a pitch of 1.4 representing a chest CT [12] and subsequent axial paths equally spaced with a distance of 5 mm. This leads to a detector signal in its central part $N(\varphi,z)$, where φ denotes the source angle around the body and z its height position, which for a helical trajectory also depends on φ. It has been shown [13] that the optimal pixel noise in the reconstructed image is obtained when the source intensity is modulated proportional to the square root of N^{-1}. Thus, we simulated with a second user code to EGSnrc the actual image acquisition process, where the x-ray intensity at each source position φ_S is modulated with the square root of N^{-1} obtained at $\varphi = \varphi_S - 180°$. During this simulation the energy deposited in each organ is recorded and thus the dose relative to air kerma in the entrance field is obtained. The total collimation in the helical scan was 0.4 cm, and for the axial trajectories 0.5 cm in the isocenter plane. With air kerma to $CTDI_{vol}$ conversion coefficients obtained by Monte Carlo simulations using a CTDI body phantom, the organ doses per air kerma are related to $CTDI_{vol}$.

III. Results and Discussion

A. Body attenuation

The number of transmitted photons during an axial scan is shown in Fig. 1 for two exemplary heights. The number of photon histories followed in each scan was 40 million. Clearly visible is the strong attenuation along lateral (0° and 180°) directions. The attenuation variation with body height can be recognized by the different maximal counts measured in the two slices. In a height of about 140 cm, i.e., at breast height, more than twice the number of photons are transmitted compared to those at the height of the liver (at about 123 cm). The reason of this difference is certainly the much smaller attenuation of the inflated lungs, where the air content leads to a mean density that is less than half of the density of soft tissue.

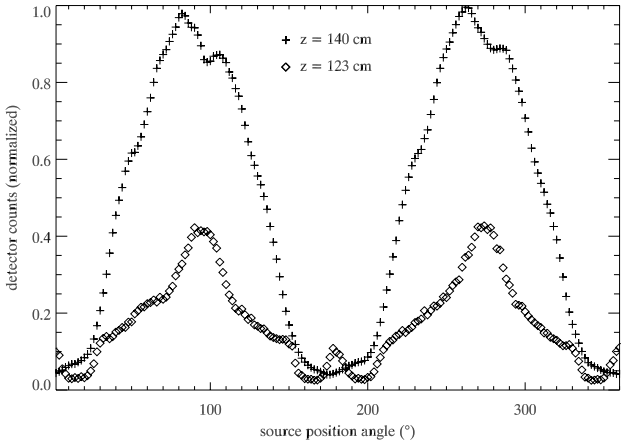

Fig. 1 The counting rates in the central detector region during two axial scans of the phantom in height of the breast (z=140 cm) and the liver (z=123 cm) The counts are normalized to the maximal counts in the two scans. Angles of 0° and 90° correspond to left lateral and postero-anterior view, respectively.

B. Dose conversion coefficients

A chest CT scan has been simulated without and with ATCM as described in II.B following the histories of 100 million photons. The equivalent doses relative to $CTDI_{vol}$ of the most exposed organs during this examination are provided in Table I. For a variety of organs the usage of ATCM leads to a considerable reduction of the dose conversion coefficients. In particular, for thyroid and thymus the dose conversion coefficients are almost halved. The reason is that they are relatively strongly shielded in lateral exposure, so that their dose is mostly caused by irradiation from the back or the front. The number of photons from these directions is, however, much smaller than from lateral directions when using ATCM (cf. Fig. 1). This yields a substantial reduction of the dose conversion coefficient of thyroid and thymus.

For some organs, like spleen, stomach or liver, the modulating source intensity can even lead to weakly increased dose conversion coefficients. These organs are located more or less at the side of the body, and thus ATCM causes just the opposite effect than for thyroid or thymus. It is, however, worth mentioning that with ATCM generally a lower

$CTDI_{vol}$ is required for the examination [3, 14, 15], such that the doses for organs like spleen, stomach and liver are probably smaller than without ATCM.

Table 1 Comparison of organ equivalent doses (H) per $CTDI_{vol}$ with and without employing ATCM in a chest CT scan.

Organ	$H/CTDI_{vol}$ (mSv/mGy)	
	without ATCM	with ATCM
Breast	1.29	1.21
Bronchial airways	1.62	1.28
Heart	1.64	1.39
Liver	0.82	0.86
Lungs	1.52	1.26
Oesophagus	1.32	0.98
Spleen	0.96	1.05
Stomach	0.77	0.85
Thymus	2.04	1.28
Thyroid	2.16	1.29

In the next step, the scan area for a chest CT is covered by equidistant axial scans, where in each case 40 million photon histories are pursued. The aim is to verify whether dose conversion coefficients obtained with such scans are comparable to those from following the exact spiral acquisition mode of modern CT devices. It is a widely used method to compute a set of axial scans at different heights (z), and combine the respective results appropriately to deduce conversion coefficients for various examinations that are actually made in spiral mode. By this method, it is avoided that for each examination new computations with spiral trajectories have to be performed.

The conversion coefficients from the axial scans are compared to those from the spiral acquisition mode for a chest CT investigation (Fig. 2). For organs in the center of the scan region like lungs, heart or oesophagus, the dose conversion coefficients obtained by the two acquisition modes are almost identical. Somewhat larger discrepancies can be observed for organs at the border of the scan region, in particular, liver and spleen. But even there, the differences in the conversion coefficients are at most 7-8%. Performing the same comparison of spiral and axial mode without the inclusion of ATCM, differences of the same order are obtained. Thus, no additional inaccuracy is introduced by using ATCM in the calculation, and the generally accepted method to combine conversion coefficients computed in axial mode remains valid.

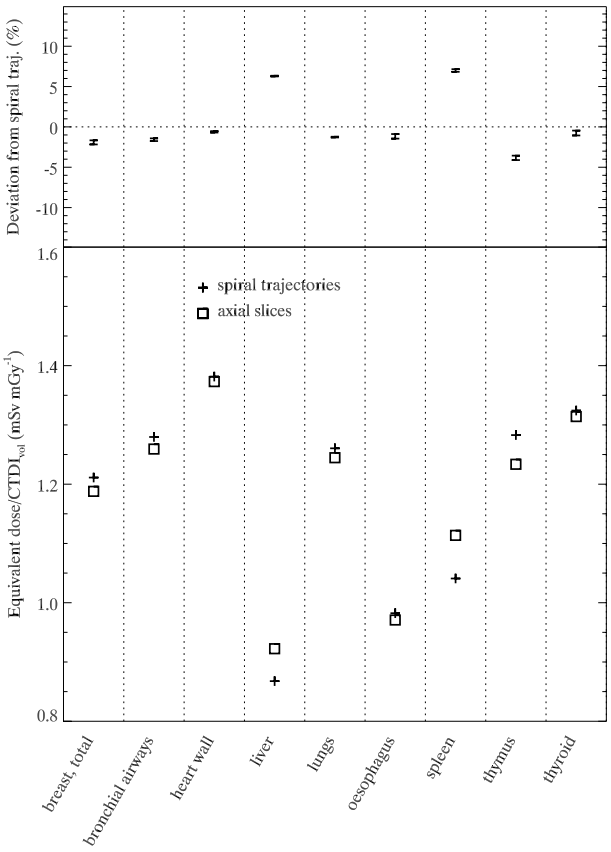

Fig. 2 Comparison of organ equivalent doses by either averaging over spirals with different starting angle ("+") or summing over the appropriate axial slices ("□").

IV. Conclusions

Adapted tube current modulation has been implemented in the computation of dose conversion coefficients for CT examinations. This technique is already standard in modern CT devices, because it allows a dose reduction by taking into account that x-rays are attenuated by the human body differently depending on the height and direction of the irradiation.

It has been demonstrated that ATCM should be included also in the numerical computations of patient organ doses, since otherwise errors of up to a factor 2 can be made. In addition, the widely used procedure to use conversion coefficients obtained by sets of axial trajectories to deduce the coefficients for various examinations in spiral mode, is still applicable. However, ATCM must then be considered in each of the circular scans.

Acknowledgment

This work has been financially supported by the German Federal Ministry for the Environment, Nature Conservation and Nuclear Safety under contract no. StSch4468.

References

1. Brix G, Nekolla E A, Griebel J (2005) Strahlenexposition von Patienten durch diagnostische und interventionelle Röntgenanwendungen: Fakten, Bewertung und Trends. Der Radiologe 45:340-349
2. Kopka L, Funke M, Breiter N et al. (1995) Anatomisch adaptierte Variation des Röhrenstroms bei der CT. RöFo - Fortschritte auf dem Gebiet der Röntgenstrahlen und der bildgebenden Verfahren 163:383-387
3. Kalender W A, Wolf H, Suess C (1999) Dose reduction in CT by anatomically adapted tube current modulation. II Phantom measurements. Med Phys 26:2248-2253
4. Giacomuzzi S M, Erckert B, Schöpf T et al. (1996) Das "Smart-Scan"-Verfahren der Spiral-Computertomographie: Eine neue Methode der Dosisreduktion. RöFo - Fortschritte auf dem Gebiet der Röntgenstrahlen und der bildgebenden Verfahren 165:10-16
5. Mulkens T H, Bellnick P, Baeyaert M et al. (2005) Use of an automatic exposure control mechanism for dose optimization in multi-detector row CT examinations: Clinical evaluation. Radiology 237:213-223
6. Schlattl H, Zankl M, Hausleiter J et al. (2007) Local organ dose conversion coefficients for angiographic examinations of coronary arteries. Phys Med Biol 52:4393-4408
7. Schlattl H, Zankl M, Petoussi-Henss N (2007) Organ dose conversion coefficients for voxel models of the reference male and female from idealized photon exposures. Phys Med Biol 52:2123-2145
8. Jones D G, Shrimpton P C (1993) Normalised organ doses for x-ray computed tomography calculated using Monte Carlo techniques. NRPB Software Report 250, Chilton, Didcot, Oxon, UK
9. European Commission (1999) European Guidelines on quality criteria for computed tomography. Report EUR 16262 EN, Bruxelles
10. ICRP (in press) Adult reference computational phantoms. ICRP Publication 108, Oxford, UK
11. Kawrakow I, Rogers D W O (2003) The EGSnrc code system: Monte Carlo simulation of electron and photon transport. PIRS Report 701, Ottawa
12. Brix G, Nagel H D, Stamm G et al. (2003) Radiation exposure in multi-slice versus single-slice spiral CT: results of a nationwide survey. Eur Radiol 13:1979 - 1991
13. Gies M, Kalender W A, Wolf H et al. (1999) Dose reduction in CT by anatomically adapted tube current modulation. I. Simulation studies. Med Phys 26:2235-2247
14. Kalender W A, Wolf H, Suess C et al. (1999) Dose reduction in CT by on-line tube current control: principles and validation on phantoms and cadavers. Eur Radiol 9:323-328 34/0218/CT
15. Greess H, Wolf H, Baum U et al. (2000) Dose reduction in computed tomography by attenuation-based on-line modulation of tube current: evaluation of six anatomical regions. Eur Radiol 10:391-394

Author: Helmut Schlattl
Institute: Helmholtz Zentrum München – German Research Center for Environmental Health, Institute of Radiation Protection
Street: Ingolstädter Landstr. 1
City: 85764 Neuherberg
Country: Germany
Email: helmut.schlattl@helmholtz-muenchen.de

Trends in dosimetry at the Neonatal Intensive Care Unit

J.W.A. Gutteling[1,3], S. Bambang Oetomo[2] and P.F.F. Wijn[1,3]

[1] Máxima Medical Center/Medical Physics, Veldhoven, Netherlands
[2] Máxima Medical Center/Neonatology, Veldhoven, Netherlands
[3] Eindhoven University of Technology, School of Medical Physics and Engineering, Eindhoven, Netherlands

Abstract— **Premature newborns frequently undergo radiographic examinations to assess the development of their lungs and/or other internal organs. Although this group may be extra sensitive to radiation, it is common that multiple examinations are performed.**

This study analyzes the usage of radiographic examinations in the neonatal intensive care unit in Veldhoven, Netherlands over the past years to investigate where additional actions can lead to improved dosimetry for this special group.

The average number of examinations per patient was lower than reported in previous other studies. Also, the amount of examinations decreased over three years, while admittance increased. The group of extremely premature newborns accounts for 1.8 times more examinations than other newborns, which should lead to extra caution for this group. Dose Reference Levels that specifically target them could be a solution.

Keywords— **NICU, Radiation Dosimetry, X-Ray, Thorax, Abdomen**

I. Introduction

Neonatal Intensive Care Units (NICU) provide care for those newborns that are either prematurely born or suffered complications during normal term delivery. A premature newborn is defined as being born before 37 weeks of gestation. A considerable amount of these infants may suffer from respiratory distress syndrome (RDS) or even worse, lunghypoplasia, which can be caused by underdeveloped lungs.

It is common medical practice to assess RDS severity by means of chest radiography (X-Ray) and follow-up this examination over the cause of stay of the newborn in the NICU. A few other diagnoses may also require either a combined thorax/abdominal radiograph, or a dedicated abdominal exam.

All in all, prematurely born infants may be subjected to multiple examinations in a matter of weeks. Although one X-Ray examination does not give rise to high patient doses, especially with adjusted voltage and current settings and compared to other medical risks in this fragile group, the examinations itself should be justified and the patient dose should be as low as reasonably achievable (ALARA)[1,2].

The group of newborns requires special attention as it is suggested [3] that their sensitivity for radiation is proportionally larger than even average children (factor 2-3 compared to average population). And of course the premature newborns are even more sensitive than term newborns.

Previous studies investigated dose levels [4], since knowing the patient dose is a first step of optimizing it. Even European multicenter comparisons were made as a first step towards diagnostic reference levels (DRL) for pediatric standard examinations[5].

Little is known however about the amount of examinations in general and trends in this regard, especially for newborns. Therefore, the goal of this study was to make an investigation of these trends to optimize radiation exposure of newborns.

Table 1 Measurement protocol for all X-Ray examinations on the NICU in MMC Veldhoven, based on the current weight of the newborn. Focus-Detector Distance is always 100 cm.

Current Weight (g)	kV	mAs	Output (mGy/mAs)	Absorbed Dose (µGy)
450	58.5	0.50	29,2	14.6
600	60	0.56	29,7	16.7
1000	61.5	0.56	34,1	19.1
1300	63	0.56	35,2	19.7
1700	64.5	0.56	38,6	21.6
2500	66	0.56	40,7	22.8
3200	68	0.63	42,7	26.9
3800	70	0.63	46,1	29.1
4200	70	0.63	48	30.2

II. Methods

At the Máxima Medical Center NICU in Veldhoven, Netherlands, the mobile X-Ray Mobilette II (Siemens Medical Solutions, Germany) was calibrated to check if its performance was comparable with literature [4]. The measurement protocol was similar to the one used in Leuven, with somewhat lower mAs values, see table 1.

O. Dössel and W.C. Schlegel (Eds.): WC 2009, IFMBE Proceedings 25/III, pp. 333–335, 2009.
www.springerlink.com

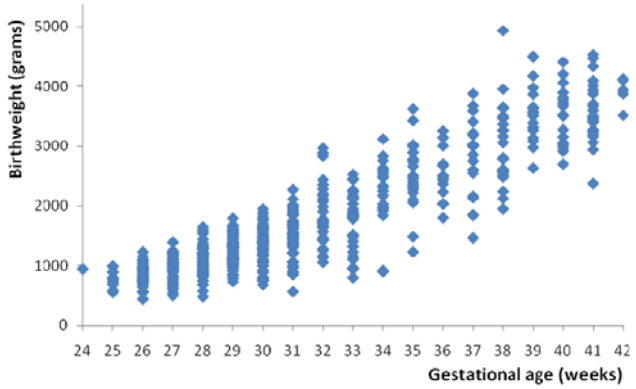

Fig. 1 Neonatal birth weight as a function of gestational age. Dotted lines represent extremely premature (<1000 gram), premature (1000-2500 gram) and term (normal weight).

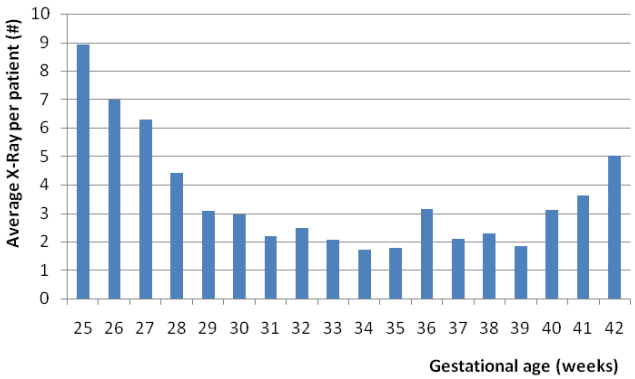

Fig. 2 Average number of examinations per patient as function of the gestational age. Critical is the large amount of examinations for the extremely premature.

Since patient doses or separate organ doses cannot be measured directly, X-ray tube output was measured with an external detector as a rough estimate of the total irradiation. This does not account for backscatter, which will attenuate the dose, or collimation, in which the irradiated field is adjusted and limited to the relevant region(s). Results are stated in table 1.

To acquire the typical numbers and types of examinations, extensive analysis was performed on patient records, PACS archive and radiology information system (RIS).

III. Results

First results show the amount of X-Ray examinations in Veldhoven has decreased since 2005, while the number of patients admitted to the NICU increased (see table 2). Also included is the average number of X-Rays per patient, this number will be further examined later on. To determine whether the acquisition protocol provides useful groups of weight, the birth weight of all patients was analyzed as a function of the gestational age at birth. Clinically, birth weight is used to separate newborns into three groups: extremely premature (<1000 gram), premature (1000-2500 gram) and term (normal, >2500 gram). From figure 1, it can be concluded that it makes sense to have subdivisions in irradiation parameters between 1000 and 2500 gram, as the majority of births is within this weight class during weeks 26 to 36. About 20% of the patients has birth weight lower than 1000 gram, so the subdivision here is useful as well.

Table 2 Overall results of admitted patients versus the amount of X-Rays in the last three years (2005-2007).

	2005	2006	2007
Patients admitted to NICU	298	300	325
Patients with X-Ray exam	193	185	180
Total X-Rays	924	791	743
Average number of X-Ray	4.8	4.3	4.1

Another result is that this group of extremely premature newborns accounts for significantly more X-Rays per patient than the premature and term newborns, as is displayed in figure 2. There are at least two explanations for this; either the extremely premature group has a larger chance to have severe forms of RDS, which seems logical as their lungs probably have not been able to fully develop. Another option is that since by definition the time between birth and the term newborns is largest for this group, that the number of follow-up X-Rays they need is just reflecting this time.

Table 3 Distribution of the number of examinations over the three groups of newborns, the lowest birth weight group clearly has a disproportionate share.

Birth weight (g)	Patients (#)	Patients %	Total X-Ray (#)	Total X-Ray %	Ratio (AU)
<1000	113	20.3	908	36.0	1.8
1000-2499	318	57.0	1192	47.3	0.8
>2500	127	22.8	420	16.7	0.7

Either way this group is responsible for a disproportional amount of the X-Rays taken, as summarized in table 3. Note that information on the timespan between examinations is not available, so it is uncertain for instance whether a newborn with gestational age of 25 weeks gets all examinations in its first week or spread out over the entire stay in the NICU.

The typical increase of X-Ray examinations for newborns between 40 and 42 weeks of gestational age that is

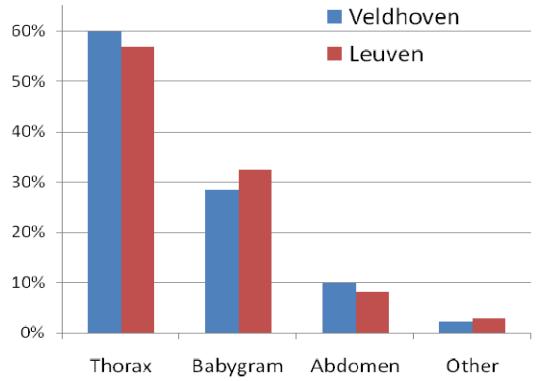

Fig. 3 Comparison of types of examinations between Veldhoven and Leuven. Babygram is a combined thorax/abdomen radiograph, the 'other' category mostly consists of fractures in fingers, legs, hips or skull.

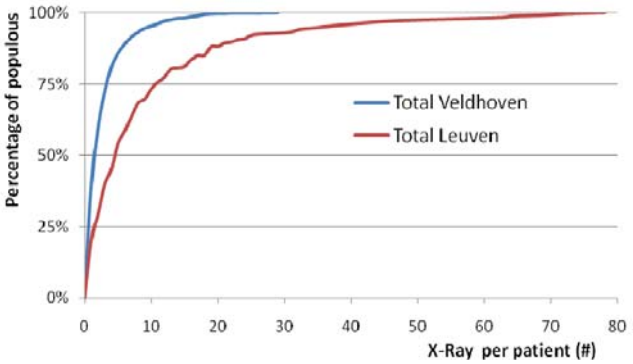

Fig. 4 Cumulative percentage of the newborn populous that is examined as a function of the number of X-Rays used. Median (50%) numbers are 4.5 for Veldhoven and 9.6 for Leuven. 95th percentile values are 12 examinations for Veldhoven and 38 for Leuven.

visible in figure 2 is an indication that that group consists of relatively ill patients, which makes sense as these term newborns would otherwise not be in the hospital.

In analogy with literature, the type of examinations was checked as well, results can be seen in figure 3. Data from our hospital was compared to data from the University Hospital in Leuven, Belgium, which was published before [4].

It turns out that both hospitals use similar amounts of each category. There is a small difference in the combined thorax/abdomen, but it is unclear if this has any impact on dose levels, as it might as well be a difference in population.

The most striking difference however, is the quantity of examinations, not their relative amounts. This can be appreciated from figure 4. On average, in Veldhoven 4.5 X-Rays are requested per newborn, while this is 9.6 for Leuven. Moreover, 95th percentile values are 12 examinations for Veldhoven and 38 for Leuven [4]. This is an indication that large differences exist between hospitals.

IV. Conclusions

The results from this study point out that dosimetry per examination is not the only point of attention when it concerns newborns. Although the data from Veldhoven suggest a downward trend in the number of X-Rays, as well as the average per patient, there is a skewed distribution within the group of newborns itself, where the extremely premature newborns receive 1.8 times more examinations than the others.

There seem to be differences between hospitals concerning the amount of examinations newborns receive on average, and even more so the subgroup that has to undergo a multiple amount of this. These finding were also true in earlier studies [4] regarding the radiation dose per X-Ray examination.

Future efforts should therefore not only center on Diagnostic Reference Levels for the radiation dose per radiographic examination, but the overall number of examinations a typical patient has to undergo, as well.

Acknowledgement

Kristien Smans from the University Hospital Leuven, Belgium.

References

1. Council Directive 97/43 EURATOM (1997) Medical Exposure. Directive of 30 June 1997, on health protection of individuals against the dangers of ionizing radiation in relation to medical exposures. Official J. Eur. Commun. No. L. 180/22.
2. International Commission on Radiological Protection (1991) Recommendations of the International Commission on Radiological Protection. ICRP Publication 60
3. International Commission on Radiological Protection (1996) Radiological Protection and Safety in Medicine, ICRP Publication 73. Ann. ICRP 26, 1–47
4. K. Smans et al. (2008) Patient dose in neonatal units. Rad. Prot. Dosim. 131(1), 143-147
5. K. Smans et al. (2008) Results of a European survey on patient doses in paediatric radiology. Rad. Prot. Dosim. 129, 204–210

Corresponding Author: Job W.A. Gutteling M.Sc.
Institute: Máxima Medical Center
Street: de Run 4600
City: Veldhoven
Country: Netherlands
Email: j.gutteling@mmc.nl

Evaluation of the radiological risk for premenopausic women in a Breast Cancer Early Detection Program

R. Tortosa[1], M. Ramos[2] , G. Verdú[2] , J.I. Villaescusa[1]

[1] Radiation Protection Service, La Fe University Hospital, Valencia, Spain
[2] Chemical and Nuclear Engineering Department, Polytechnic University of Valencia, Spain

Abstract— **In 1992, the Valencian Breast Cancer Early Detection Program (VBCEDP) started in the Valencian Community (Spain) . Up to now, 24 mammography units have been installed all over the region. Mammography is used to aid in the diagnosis of breast cancer diseases in women. There is a health risk in the studied women due to ionising radiation that has to be estimated and controlled. A methodology to calculate in an aproximate way the radiological detriment in the VBCEDP has been developed based on Monte Carlo techniques. As qualitative parameters in the Program, the average mean glandular dose from representative sample populations undergoing screening mammography (digital or screenfilm) from each of the twenty-four units in operation have been obtained. The American College of Radiology Imaging Network reached to conclusion that digital mammography performed significantly better than film for pre and perimenopausal women younger than 50 [1]. Women who are undergoing the program are between 45 and 69. This fact allows us to study premenopausic women. Our group uses the software SCREENRISK [2] to estimate induction and mortality rates in order to corroborate American conclusions in an European region. The obtained results confirm the american results about the application of digital mammography in pre and perimenopausal women younger than 50 years.**

Keywords— **Radiological detriment, premenopausic women, digital mammography.**

I. Introduction

Screening mammographic programs try to get an early diagnosis of the breast cancer in middle aged women. The European Protocol on Dosimetry in Mammography [3] is the document that regulates this practice, allowing quality on the diagnostic and the comparison between differents screening units.

Although screening for the early detection of breast diseases reduces breast cancer mortality, it is well known that the diagnosis by mammography presents risks for women undergoing screening due to the exposition to ionising radiation. At present, it is considered the mean glandular dose (MGD) in acquiring the mammography as a risk parameter. Then it is possible to use the MGD in order to obtain the risk of induced breast cancers in a screening programme. Risk projection models obtained from data of exposed populations, such as the survivors of the atomic bombs or patients exposed to high doses due to medical reasons have been used. This way of proceeding has many uncertainties but these indicators are right to compare how mammographic units act on different phases in a prevention program. That was the reason of the development of SCREENRISK. This software based on Matlab© gives us an easy way of quantifying risks in mammographic screening programs.

II. Methodology

A. Excess relative risk for incidence and mortality

The excess relative risk (ERR) is a parameter used to transport risks between populations which have been exposed to radiation and have different baseline rates. Risk projection models are used in epimediology in order to estimate incidence and mortality cancer rates in one population under study from data that has been obtained in other populations.

Different studies have been chosen to estimate risks in the Valencian Breast Cancer Early Detection Program. The mortality models are: (1a) Life Span Study cohort (LSS) that includes female bomb survivors between 1950 and 1985; (2a) and the LSS with follow-up until 1990 depending on age at exposure and (4a) depending on attained age. The incidence models for breast cancer are: (1b) the Life Span Study for incidence breast cancer (1958-1993); (2b) the Massachussets fluoroscopy study, for tuberculosis patients (TBO) and the extension (TBX); (3b) the New York acute post-partum mastitis cohort (APM); and (4b) the bening breast disease treatment in Sweden (BBD).

The excess relative risk is fitted with

$$ERR\left(\vec{z}^{(m)}\right)=\alpha^{(m)}\theta(s)\Phi(\vec{D}_g)\exp\left[\gamma^{(m)}(t_e-t^{(m)})\right]\left(\frac{t_k}{50}\right)^{\beta^{(m)}} \quad (1)$$

where $\Phi(d_g)$ is the dose response with dose d_g to the breast, s is the gender of the individual and $\theta(s)$ is a

O. Dössel and W.C. Schlegel (Eds.): WC 2009, IFMBE Proceedings 25/III, pp. 336–339, 2009.
www.springerlink.com

function that depends on gender and cancer type, equal to unity for breast cancer on female. The covariate vector for the *ERR* is the same for incidence and mortality, and it includes the variables $\vec{z} = \left[t_k, t_e, \vec{D}_g, s\right]$. Each model has its own parameters based on cases under study.

It has been considered in order to transport the risks an extension of Cox Proporcional Hazards to estimate the Excess Absolute Risk (EAR) as

$$EAR^{(m)}(t_k \mid \vec{z}^{(m)}) = \lambda(t_k)\left[ERR(\vec{z}^{(m)})\right] \quad t_k \geq t_e + L \qquad (2)$$

where $ERR^{(m)}$ is the excess relative risk of the model m for breast cancer. In (2), it is observed that $ERR^{(m)}$ is transported to a population with a risk base function $\lambda(t_k)$ for incidence or mortality.

B. Risk of exposure-induced cancer (REIC) and death (REID)

The risk of esposure induced cancer (REIC) is defined as the probability of an individual develops a radio-induced cancer, not necessarily mortal, all over his life. The risk of exposure induced death (REID) shows that an individual dies due to a radio-induced cancer. So, deriving a Markov process, REIC and REID can be obtained as

$$REID\ (t_e \mid \vec{z}_{fbc}) = \sum_{j=e+L}^{M} \hat{s}_1(t_j \mid \vec{z}_{fbc})\, EAR_{fbc}(t_j \mid \vec{z}_{fbc}) \qquad (3)$$

$$REIC\ (t_e \mid \vec{z}_{in}, \vec{z}_{fbc}) = \sum_{j=e+L}^{M} \hat{s}_1(t_j \mid \vec{z}_{fbc})\, EAR_{in}(t_j \mid \vec{z}_{in}) \qquad (4)$$

Where $\hat{s}_1(t_j \mid \vec{z}_{fbc})$ is the estimator of the survival function, EAR_{fbc} is the escess absolut risk for mortal breast cancer and EAR_{in} for incidence. $\vec{z}_{in}$ is the vector of covariates for breast cancer incidence.

C. The SCREENRISK software: simulation and implentation

In a breast screening program, women are invited to undergo mammography between an initial age (*a*) and a final age (*b*), with a constant screen interval (*s*) and receiving normally one exposure per breast at each time.

There are different indicators when evaluating the associated cancer risk during breast screening. These indicators are adequate to make comparisons between several programs. One of these is the average radiological detriment for breast cancer incidence and mortality, in a given instant of the screening and can be estimated as

$$\Pi_{in}^{(m)} = \sum_{j=a}^{b} \nu(t_j)\, REIC^{(m)}(t_j \mid \overrightarrow{d_{gj}}) \cdot \omega(t_j) \qquad (5)$$

$$\Pi_{fbc}^{(m)} = \sum_{j=a}^{b} \nu(t_j)\, REID^{(m)}(t_j \mid \overrightarrow{d_{gj}}) \cdot \omega(t_j) \qquad (6)$$

Where $\nu(t_j)$ is the number of views per breast in each visit , $\omega(t_j)$ is the fraction of population and $d_{g\,j}$ is the average mean glandular dose per film at an age-at-exposure t_j.

Using this methodology, it has been developed the SCREENRISK software, based on *Matlab© 6.5* which estimates the risk of exposure-induced cancer and fatal cancer for a specific cancer in a given population.

D. The Valencian Breast Cancer Early Detection Program and the digital mammography.

The Valencian Breast Cancer Early Detection Program started in 1992 and actually 24 units are working on that. Yearly quality controls are performed in all units with the recommendations of the European Protocol on Dosimetry in Mammography

The VBCEDP is directed towards asymptomatic women between 45 and 69 years old, with an initial age lower than other screening programs (i.e. UK Screening Program stars at the age of 50 years). The screening examination consist of two exposures per breast; craniocaudal (CC) and mediolateral oblique (OBL). The first time that the woman participates in the program (first round) receives two exposures per breast and a single mammogram OBL per breast in subsequent rounds. The screening rounds are spaced every two years and two independent radiologists read each mammogram.

Each six months population samples are taken from the screening units involved in the program in order to estimate and control the radiological risk.

In this work, we have analyzed the radiological detriment of premenopausic or perimenopausic women under 50 years and postmenopausic women that participate in the valencian screening program comparing those screened with a digital mammography versus screen-film mammography.

III. Results

The results have been calculated during the second semester of 2007 and the first semester of 2008. It was considered a sample of 1300 women for 2007 and 1200 women for 2008 who followed the screening program.

Table 1 shows the induced cancers calculated using SCREENRISK software where it is compared premenopausic and postmenopausic women for each incidence model. The values are presented as number of induced cancers per 100000 women. In the same way, results of fatal induced cancers per 10^5 women are showed in table 2. These tables correspond to the sample of 2007

Table 1 Induced cancers per 10^5 women 2007

Models	Premenopausic		Postmenopausic	
	Screenfilm	DM*	Screenfilm	DM
LSS Attained age	6.30 ±5.05	3.99±0.31	6.29 ±4.79	6.07±1.19
TBO Attained age	2.22 ± 1.77	1.41±0.12	2.22 ± 1.69	2.14±0.42
APM All ages	3.32 ± 2.57	1.98±0.15	3.40 ± 2.65	3.41±0.66
BBD Exposition age	1.07 ± 0.97	0.83±0.06	0.98 ± 0.66	0.73±0.15

*Digital mammography

Table 2 Fatal induced cancers per 10^5 women 2007

Models	Premenopausic		Postmenopausic	
	Screenfilm	DM	Screenfilm	DM
LSS (1950-1985) Exposition age	0.87 ± 0.73	0.61±0.04	0.83±0.61	0.74±0.15
LSS (1950-1990) Exposition age	1.73 ± 1.45	1.19±0.09	1.67±1.23	1.50±0.29
LSS (1950-1990) Attained age	4.15 ±3.29	2.59±0.20	4.17±3.19	4.07±0.79

Table 3 shows the induced cancers calculated using SCREENRISK software where it is compared premenopausic and postmenopausic women for each incidence model. The values are presented as number of induced cancers per 100000 women. In the same way, results of fatal induced cancers per 10^5 women are showed in table 4. These tables correspond to the sample of 2008.

Table 3 Induced cancers per 10^5 women 2008

Models	Premenopausic		Postmenopausic	
	Screenfilm	DM*	Screenfilm	DM
LSS Attained age	5.97 ±3.94	5.59±1.07	6.84±5.22	6.58±3.46
TBO Attained age	2.10±1.39	1.97±0.38	2.41±1.84	2.32±1.22
APM All ages	3.09±1.98	2.85±0.54	3.73±2.91	3.67±1.95
BBD Exposition age	1.07±0.78	1.06±0.19	1.01±0.67	0.85±0.43

Table 4 Fatal induced cancers per 10^5 women 2008

Models	Premenopausic		Postmenopausic	
	Screenfilm	DM	Screenfilm	DM
LSS (1950-1985) Exposition age	0.85±0.56	0.82±1.16	0.89±0.65	0.82±0.42
LSS (1950-1990) Exposition age	1.68±1.15	1.61±0.31	1.79±1.31	1.66±0.86
LSS (1950-1990) Attained age	3.92 ±2.56	3.66±0.69	4.55±3.49	4.40±2.32

IV. Conclusions

SCREENRISK provides an easy and fast way of calculating the radiological detriment in medical expositions due to ionising radiation, such as the Valencian Breast Screening Program. The obtained results for the VBCEDP shows a lower detriment in premenopausal women screened using digital mammography in front of screen-film mammography. It is also appreciated that the detriment in postmenopausal women is higher than premenopausic using digital mammography except for BBD model. This fact could be due to the higher uncertainties that models carry with.

According to the results, it is observed that the differences in detriment between premenopausic and postmenopausic women are not constant among models. It is difficult to reach to conclusion about it because population models concerning to fatal breast cancer due to radiation exposure are subjected to multiple uncertainties.

These results corroborate the work of Pisano et al. [1] but it is also recommended to increase the volume of screened women in order to achieve more confident values.

It is important to take into consideration that there are very few population models in order to study incidence and mortality cancers.

In spite of this, risk transport from any model is a good indicator to compare different screening units and programs.

Acknowledgment

This work is funded with the Project PI06/90502 of the Carlos III Health Institute (Spain). We are also grateful to the Valencian Breast Cancer Early Detection Program.

References

1. Pisano ED et al. (2005) Diagnostic performance of digital versus film mammography for breast cancer screening. N England Journal Med 353: 1773-1783.
2. Ramos M et al. (2005) Use of risk projection models to estimate mortality and incidence from radiation-induced breast cancer in screening programs. Phys Med Biol 50: 505-520.
3. European Commission 1996. European Protocol on Dosimetry in Mammography. European Commission Report EUR 16263 EN
4. MATLAB© 6.5. The MathWorks INC 2002

Author: Ricardo Tortosa
Institute: La Fe Hospital, Radiation Protection Department
Street: Avda Campanar 21
City: Valencia
Country: Spain
Email: tortosa_ric@gva.es

Study on local maximum skin doses to patients undergoing cardiac procedures

J. Domienik[1], S. Papierz[1], M. Brodecki[1,2], M. Tybor[1], J. Jankowski[1,2], A. Korejwo[2]

[1] Nofer Institute of Occupational Medicine, Radiation Protection Department, Lodz, Poland
[2] University of Lodz, Department of Nuclear Physics and Radiation Safety, Lodz, Poland

Abstract—**The local maximum skin doses (MSD) received by patients during the most commonly performed cardiac procedures were investigated. The distributions of radiation were measured with the method employing large-area films for extended dose range KODAK EDR2. The evaluated local maximum doses ranged from 105 mGy to 1507 mGy for coronary angiography (CA) procedures and from 84 mGy to 1555 mGy for percutaneous coronary intervention (PTCA) procedures. In neither of the analyzed procedures the local maximum dose exceeded the threshold dose (2 Gy) for deterministic effects. Additionally, the total irradiated areas as well as areas corresponding to the maximum skin dose were analyzed. The former ranged from 332 cm^2 to 1441 cm^2 and the latter ranged from 1 cm^2 to 132 cm^2. The concentration of dose on irradiated films was investigated in terms of concentration factor and dose index in some detail .**

For randomly selected procedures, simultaneously with films the self-made TL dosemeters arrays, were also used as optional measurement method. In the study the comparison of local maximum doses determined from the dose distribution registered on films and TLD arrays is presented. It was found that the discrepancies between both methods were not larger then 17%.

Keywords— **maximum skin doses, slow films, TLDs, concentration factor, dose index**

I. Introduction

The assessment of doses received by patient in rentgenodiagnostic procedures is the fundamental part of optimization process aiming at reducing the exposure to the level at which the costs and benefits are well balanced according to ALARA principle. In particular, in interventional radiology the evaluation of the doses during every single procedure is of priority concern due to the fact that the doses are relatively high and thus the deterministic injuries in some circumstances might occur. Such cases of patient's skin injuries have been reported and fully documented in scientific literature [1-5].

The present study aims at analyzing information on the MSD in a dedicated Polish cardiac center and comparing with corresponding data coming from other European centers. In order to assess the maximum skin doses (MSD), the measurements with large area films were performed for the coronary angiography (CA) and cardiac angioplasty (PTCA) procedures. Additionally, the self-made TLD arrays were used simultaneously with films and as a result the comparison of both methods is presented.

The detailed analysis of exposed films concerning the area of irradiation and dose concentration is put forward. In order to asses the scale of possible deterministic effects films were analyzed with respect to the area of maximum skin dose. The concentration of dose on irradiated films was investigated in terms of concentration factor and dose index in some detail as well.

Justification of this approach is explained in the paper [6], where we studied the relation between various dose indicators used for patient dosimetry purposes and the local maximum skin dose. We found no general and satisfactory correlation. The conclusion was that only dose area product (DAP) value can serve as a rough preliminary estimation. In the course of our study it appeared that the very problem of determination of the maximum skin dose deserves some direct attention. This problem is of more technical character than the one discussed in the mentioned paper [6] and it may appear to be important in wider context. Therefore, we decided to devote a separate short paper concerning the direct study of local maximum skin dose and related issues.

II. Materials and methods

The study on the local maximum skin doses was performed in one haemodynamic room in major cardiac center in Lodz. In all, 106 procedures (52 CA procedures and 54 PTCA ones) were analyzed with respect to entrance skin dose distribution.

The facility where the study was performed is equipped with C-arm angiography unit (GE Innova 2000) with flat panel digital system.

The maps of the patient skin doses were obtained with large-area films KODAK EDR2 (35 cm×43 cm). Additionally, the TLD arrays were used simultaneously with films for selected procedures. Both, films and TLD arrays were placed on the mattress of the medical table in contact with patient's back in such a way that part of the film was placed slightly over the patient's shoulders to reduce the effect of large angles for cranial and caudal projections.

O. Dössel and W.C. Schlegel (Eds.): WC 2009, IFMBE Proceedings 25/III, pp. 340–343, 2009.
www.springerlink.com

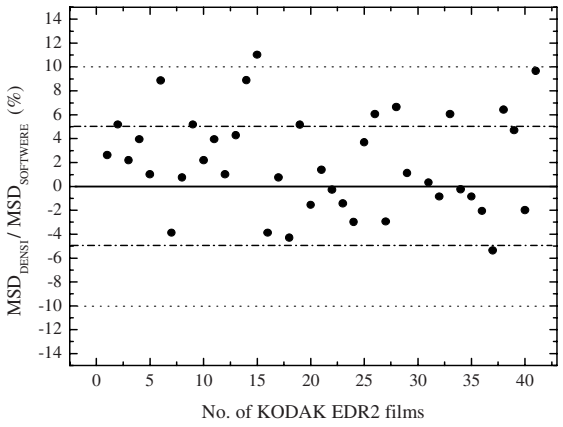

Fig. 1 The comparison of the densitometer and the software readings of the MSD value

In order to determine the exact response of the KODAK EDR2 film to the fluoroscopy beam qualities close to those used in clinical conditions, the dose calibration was performed in the Secondary Standard Dosimetric Laboratory of Nofer Institute of Occupational Medicine in Lodz. The contribution from backscatter radiation from the patient was included by placing the calibrated films in front of 20 cm PMMA phantom.

All films used in the study were read out manually with the densitometer. The optical density (OD) readings error due to the subjective localization of the region of maximum skin dose (evaluated on the basis of 12 measurements of MSD on various films and repeated by three different persons) was estimated to be less than 3%.

Independently, the appropriate software for film analysis was used. The 40 images coming from the most time consuming and thus delivering the highest dose to patient PTCA procedures were digitized with scanner (Epson Perfection V700) and analyzed with 'Pixel to Dose Converter' software. The reproducibility of the MSD readings was about 5%. The differences in the MSD read out made manually with densitometer and with the software tools were assessed as well. The results are presented in Figure 1.

Apart from the film-based method, the thermoluminescent dosemeters were used for independent determination of the MSD. The TLDs were spread over the polyethylene sheeting in 9 columns and 13 rows covering almost the same area as films; in all, 117 TL dosemeters were used in one exposure which allowed to obtain the reliable information about dose distribution. In the whole study seven TLD arrays were analyzed.

Dosemeters were calibrated in the above medium for the same geometry and beam quality conditions as for Kodak EDR2 films and read out in the manual thermoluminescence dosemeter reader (Fimel LTM, PTW FREIBURG). According to manufacturer the response of the TLD is linear with dose up to 5 Gy [7]. The dose measurement uncertainty with TL dosemeters was estimated to be 3%.

III. Results

The MSD estimated from the film calibration curve ranged from 105 mGy to 1507 mGy for CA procedures and from 84 mGy to 1555 mGy for PTCA ones. The upper values presented here are most close to the data reported in reference [8]; however, one has to take into account the upper calibration value 1250 mGy mentioned above which might make dose measurement uncertainty above this value significant. On the other hand, this fact does not influence our study too much because for the great majority of the analyzed cases (about 80%) the MSD value was below 1 Gy. The data obtained by other authors are collected for comparison in Table 1 [12-16].

Table 1 Comparison of MSD with other studies

References	Procedure	MSD [mGy]
Present study	CA	105–1507
	PTCA	84–1555
Van de Putte S. et al (2000)	PTCA	760
	PTCA+ST	1800
Vano E. et al (2001)	CA, PTCA	107–711
Waite J.C et al (2001)	PTCA	20–940
Delichas M.G. et al (2005)	CA	24–427.5
Trianni A. et al (2005)	PTCA	100–3400
Karambatsakidou A. et al (2005)	CA	1500
Morrell R. E. et al (2006)	CA	70–520

The data concerning mean, standard deviation, median and 3rd quartile of MSD presented in paper [6] are reminded here in Table 2.

Films digitized with scanner were carefully analyzed with respect to the field size of the most exposed area (area included dose above 90% MSD) and the total irradiated area.

Table 2 Statistical data concerning MSD for CA and PTCA procedures

MSD [mGy]	CA	PTCA
mean	365	917
Standard deviation	290	407
median	298	831
3rd quartile	373	1322
range	105–1507	84–1555

The areas of MSD vary from 1 cm^2 to 132 cm^2 where the maximum value corresponds to the 1.5 Gy. The total irradiated area was in the range from 332 cm^2 to 1441 cm^2.

Additionally, for films exposed during PTCA procedures, the two useful concepts related to the concentration of the dose on irradiated films were investigated and compared. These are concentration factor (CF) introduced by Vano et al. [9] and dose index (DI) (indicating the MSD contribution to the cumulative dose; DI=MSD/CD, were CD is the cumulative dose) analyzed in the paper [10] with regard to the peak skin dose reduction. The concentration factor, defined as quotient of the MSD to the mean dose calculated from DAP and total exposed area

$$CF \equiv \frac{MSD}{\left(DAP / A_{tot}\right)} \tag{1}$$

might be the measure of the homogeneity of radiation distribution on exposed film. In case of uniformly irradiated film area concentration factor is one while for nonuniformly distributed radiation it is greater than this value.

The obtained concentration factor ranged from 1.7 to 9.3. One is tempted to relate the value of concentration factor to the risk of deterministic effect. However, some care must be exercised here. Intuitively, for the larger concentration factor we expect part of irradiated area to be exposed to higher doses. This kind of reasoning is not fully justified unless the total irradiated area and total dose are taken into account. In the extreme case one can have the lowest concentration factor due to homogeneous distribution of radiation on small area resulting in high dose. Good example, corresponding to the most extreme concentration factors, is provided by PTCA procedure no. 49 (Fig. 2). In addition, it is instructive to compare the above mentioned procedure with procedure no. 34, where the concentration factor (for the similar DAP value) is much higher while the actual risk of the procedure is lower due to lower value of MSD.

We conclude that concentration factor may be some indicator of the deterministic risk, provided it is considered together with the total irradiated area and other available data like MSD and DAP. The latter can be illustrated by considering PTCA procedures no. 37 and no. 39 (fig. 3). Here, the total areas are similar and in spite of the fact that the DAP values differ by factor two, the MSD is lower for larger DAP, which is clearly indicated by the lower value of concentration factor. Thus, the procedure no. 39 might be considered as the example of better radiological practice.

As far as DI is concerned, its value for analyzed films, ranged from 14% to 75%. Figure 4 shows that there exists correlation between concentration factor and dose index.

However, there are 3 points which seem to spoil the correlation, therefore one cannot be sure that the latter is not an artifact related to the selection of points.

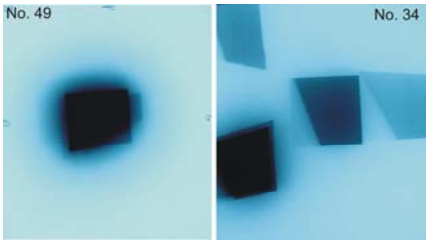

Fig. 2 Comparison of two PTCA procedures with similar DAP values but differing by the value of concentration factor

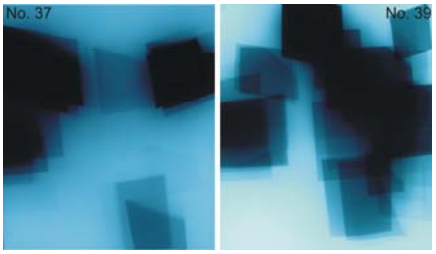

Fig. 3 The comparison of two PTCA procedures with similar total irradiated areas but differing in DAP values by factor two

This conclusion seems to be supported by the definition of dose index: the cumulative dose is assumed to be measured in interventional point (which is fixed in space), while the MSD is determined at the level of patient back (which varies both during the procedure and from procedure to procedure).

The comparison of MSD measurements with TL dosemeters against those performed with Kodak EDR2 films shows some discrepancies. The quotient q=MSD_{film}/MSD_{TLD} calculated for seven randomly selected procedures lies in the interval 0.83 to 1.17 which is in good agreement with other published data [9].

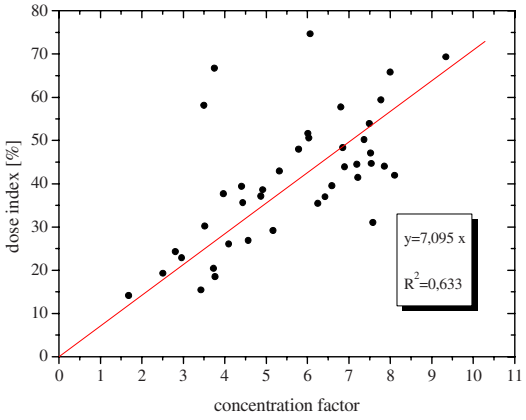

Fig. 4 Concentration factor and dose index correlation

Very good consistency of both methods was found for the case where the MSD was estimated to be 1507 mGy. The value of quotient q was 0.97. It is important to note that three from TL dosemeters localized in the area of maximum exposure received comparable doses, which seems to exclude accidental coincidence. This result might suggest that the Kodak EDR2 films, for the processing conditions used in the study, enable to estimate the doses up to the 1500 mGy, which is a slightly higher value than the one reported in reference [11], but still significantly lower than the threshold for deterministic effects (2 Gy). From the latter the saturation point is expected to appear at the OD greater than 3.5.

IV. Conclusions

The present study allows to provide careful analyses of various methods of evaluation of MSD. The cases of maximum skin doses exceeding 1 Gy were found for both CA and PTCA procedures. Further, it can be concluded from our study that in repeated procedures the doses may approach or exceed 3 Gy. Both these results make MSD assessment strongly recommended. The simultaneous measurements with TLD self-made arrays were compatible with the data obtained with Kodak films. Moreover, the measurements show the necessity of using, together with slow films, other alternative MSD assessment methods (TLDs) in order to measure in reliable way doses greater than those corresponding to the saturation point of the slow film.

The large variations in the MSDs reported in literature and in the present study support the conclusion that there are many parameters which can affect the doses delivered to the patient. However, the differences in various methods applied in order to assess the MSD should not be overlooked when comparing the data. Even if, generally speaking, the same methods were applied, the differences might occur depending on the type of detectors used in the studies (various saturation points for slow films or varying number and locations of TLDs).

Our study shows that for the case of films, the concentration factor is the useful concept for film analyzing as well as for evaluation of the irradiation risk when supplied with additional data (MSD, total area, DAP) of the irradiation risk. On the contrary, the dose index, from its very definition, does not provide the best estimator of the latter. Our study reveals that the areas subjected to MSD may be quite large -132 cm^2- which typically corresponds to the beam cross-section at the level of patient. Therefore, it is recommended that the operator should use various dose spreading techniques, like collimation which reduces the dose as well as the irradiated area and table moving.

References

1. Wagner, L. (1998) Typical doses and biological implications, 84th Scientific Assembly and Annual Meeting of the Radiological Society of North America, Chicago, pp.249-54
2. Wagner L, MacNeese M, Marx M et al. (1999) Sever skin reactions-from interventional fluoroscopy: case report and review of literature. Radiology 213:773–6
3. Koenig T, Wolff D, Mettler F et al. (2001) Skin Injuries from Fluoroscopically Guided Procedures. Am. J. Radiol 177:3–11
4. Vano E at al. (2001) Skin radiation injuries in patients following repeated coronary angioplasty procedures. Br.J. Radiol. 174:1023–31
5. International Commission on Radiological Protection (2002) , Avoidance of Radiation Injuries from Medical Interventional Procedures, ICRP Publication 85. Ann ICRP 30(2)
6. Domienik J, Papierz S, Jankowski J et al. (2008) Correlation of patient maximum skin doses in cardiac procedures with various dose indicators. Rad. Prot. Dos. 132:18–24
7. http://www.tld.com.pl/tld/mts.html
8. Karambatsakidou A, Tornvall P, Saleh N at al. (2005) Skin dose alarm levels in cardiac angiography procedures: is a single DAP value sufficient? Br. J. Radiol. 78:803–809
9. Vano E, Gonzalez L, Ten J at al. (2001) Skin dose and dose – area product values for interventional cardiology procedures. Br. J. Radiol. 74:48–55
10. Miller D, Balter S, Noonan P at al. (2002) Minimizing radiation-induced skin injury in interventional radiology procedures. Radiology 225:329–336
11. Guibelalde E, Vano E, Gonzalez at al. (2003) Practical aspect for the evaluation of skin doses in interventional cardiology using a new slow film. Br. J. Radiol. 76**:**332–336
12. Van de Putte S, Verhaegen F, Taeymans Y (2001) Correlation of patient skin doses in cardiac interventional radiology with dose-area product. Br. J. Radiol. 74:504–13
13. Waite J, and Fitzgerald M (2001) An assessment of methods for monitoring entrance surface dose in fluoroscopically guided interventional procedures. Radiat. Prot. Dosim. 94:89–92
14. Delichas M, Psarrakos K, Giannoglou G at al. (2005) Skin doses to patients undergoing coronary angiography in a Greek hospital. Radiat. Prot. Dosim. 113:449–452
15. Trianni A, Chizzola H, Toh E at al. (2005) Patient skin dosimetry in haemodynamic and electrophysiology interventional cardiology Radiat. Prot. Dosim., 117:241–246
16. Morell R, Rogers A (2006) Kodak EDR2 film for patient skin dose assessment in cardiac catheterization procedures. Br. J. Radiol. 79:603–607

Author: Joanna Domienik
Institute: Nofer Institute of Occupational Medicine
Street: Sw. Teresy 8 St.
City: Lodz, 91-348
Country: Poland
Email: jdom@imp.lodz.pl

Validation of a MC code to assess patient doses from cone beam CT in dentistry

J.J. Morant[1], M. Salvadó[2], I. Hernández[3], E. Velasco[4], A. Calzado[3]

[1]Universitat Rovira i Virgili. Servei de Protecció Radiològica, Reus, Spain
[2]Universitat Rovira i Virgili. Facultat de Medicina i Ciències de la Salut, Reus, Spain
[3]Universidad Complutense de Madrid. Facultad de Medicina, Spain
[4]Asigma S.A., Cartagena, Spain

Abstract— **A Monte Carlo (MC) -based method to calculate absorbed dose from cone beam CT examinations has been developed and applied. To simulate X-ray exposure, a code using the EGS4 package and different voxel models representing an ionization chamber, a dosimetry head phantom and an anthropomorphic phantom (Remab system) were employed. In order to validate the method, dose measurements free-in-air, and within the phantoms were performed using an ionization chamber and 58 thermoluminescence dosemeter (TLD) chips. TLD dosemeters were grouped in stacks of 5, 3 or 2 elements at 16 positions in the anthropomorphic phantom. A comparison of the dose outcomes from both methods gave relative differences below 9% for the dose free-in-air, below 4.5% for the dose in the 9 cavities of the head phantom. For TLD measurements, relative differences in dose between both methods were ≤ 15% for dosemeters in the primary beam. Differences in other TLD positions can be explained by critical dependence of the calculated dose on the geometrical accuracy. The MC code gives an acceptable description of the dose distribution for simple and anthropomorphic geometries in combination with voxel models of the object or the patient.**

From the simulation of the standard examination on the Remab phantom, values of average dose per slab (ADS), energy imparted and mean absorbed organ doses were calculated. ADS values in the pituitary area were about 2 mGy, well correlated with energy imparted per slab. Calculated mean absorbed doses for selected organs were in the range 0.076 mGy (thyroid) to 1.74 mGy (salivary glands).

In conclusion, the devised MC method has been validated and can be a robust tool to optimize protocols and estimate patient doses for a CBCT unit in maxillofacial radiology.

Keywords— **Cone beam, Monte Carlo, Dosimetry, Dental CT, I-CAT**

I. Introduction

Recently available cone beam CT (CBCT) specially designed to be applied in oral and maxillofacial radiology represents a lower cost and lower patient dose alternative to conventional CT. Since it produces 3D information adapted to the needs of many dental specialties, its use is continuously growing. Remarkably, a significant number of examinations are being performed on paediatric patients. These facts, along with the appearance of new ICRP recommendations that include new tissues and new weighting factors to compute effective dose, make it necessary to address studies useful to quantify risks and to progress in the dose optimisation process [1] [2].

Many dosimetric studies published so far have used thermoluminescence dosemeters (TLD) placed in anthropomorphic phantoms to assess effective dose or organ doses [3-5]. However, for CT scanners it is well known that organ doses can be accurately calculated by combining Monte Carlo simulations of the X-ray beam and realistic computer models of the human anatomy [6]. In particular, the technique reduces the uncertainties arising from the use of a limited number and positions of TLD dosemeters.

The primary aim of this work has been to validate a Monte Carlo (MC) -based method to estimate patient doses for a particular model of CBCT system, and to calculate organ doses for a standard maxillofacial radiology protocol on a tomographic anthropomorphic phantom.

II. Materials and Methods

The work was performed using an i-CAT cone beam dental CT scanner (Imaging Sciences International, Hatfield, PA) consisting of a standard high-frequency fixed anode X-ray tube (120 kVp, 3–8 mA) and a 20 x 25 cm amorphous silicon flat panel detector. The X-ray beam is pulsed with two different frequencies (23.05 or 34.9 pulses/s), which gives rise to two overlapping angles for a full rotation/acquisition (36.9º and 30.7º, respectively).

A thorough study the operating mode of the CBCT system was performed. Absorbed dose at different points of the radiation field, exposure time, half-value layer, high voltage generator waveform, and kVp accuracy were measured using an Unfors X-ray multimeter Xi model with external probe B Xi 822032-R/F (Unfors Instruments, Billdal, Sweden)

O. Dössel and W.C. Schlegel (Eds.): WC 2009, IFMBE Proceedings 25/III, pp. 344–347, 2009.
www.springerlink.com

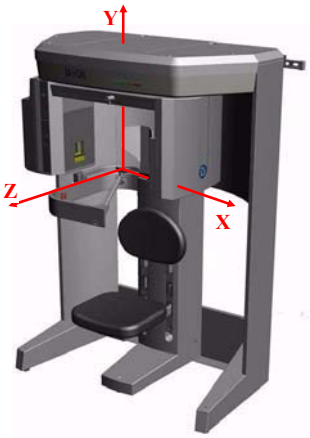

Fig. 1 i-CAT (Imaging Sciences International Inc., Hatfield, PA)

Two series of measurements were carried out to validate the simulation code: a) doses free-in-air at the Y-axis and within the peripheral, intermediate and central cavities of a standard head dosimetry phantom (16 cm diameter) were measured with a Radcal 20x5-3 CT ionization chamber + 2026 electrometer (Radcal, Monrovia, CA); and b) 58 TLD-100 dosemeter (Harshaw/Bicron, Solon, OH) chips were located at different positions inside and outside the bust of a Remab phantom (Alderson Research Laboratory). The chips, calibrated for an X-ray beam generated with 120 kVp, were grouped in stacks of 5, 3 or 2 elements and then located at 16 positions representative of the organs or tissues of interest in the anatomical region under study, such as salivary glands, cheek bones, nape, thyroid, eye lenses, spinal cord and pulmonary apex.

The evaluated dose quantities were the dose profile integral (DPI_{100}) [7] for ionization chamber measurements, and the absorbed dose for TLD measurements. Experimental values were compared to those estimated by simulating the exposures free-in-air and in the phantoms. All measurements and, consequently, the corresponding simulations in this study were performed for a standard examination protocol. Table 1 gives an overview of the values of the parameters used in the examination.

CT images of the ionization chamber and the phantoms (dosimetric and Remab system) were used to construct three-dimensional voxel objects. Each of the axial images was first reduced to a 256 x 256 matrix and the data were then stacked in a volume to obtain a 256x256x*N* object, where *N* is the number of slabs. A single 10 cm thick slab was used for chamber simulations free-in-air and inside the dosimetry phantom, and 301 slabs of 1.5 mm each formed the Remab Phantom voxel object. Thus, two different voxel sizes were used: 1.5x1.5x100 mm^3 or 1.37x1.37x1.5 mm^3.

TLD dosemeter images obtained from the examination of the Remab phantom were used to determine individual positions and to precisely locate them in the model. In addition, the images were segmented to classify CT numbers into four groups (air, lung, muscle and bone) by assigning the corresponding values according to their similarity to each group. A selected number of organs at risk (thyroid, salivary glands, brain, lymphatic nodes, oral mucosa, extrathoracic region, eye lenses) were segmented to calculate mean absorbed dose in them. Values of the mass absorption coefficients used for these standardised tissues were taken from the ICRU Report 46 [8].

Table 1 Overview of acquisition settings for the "Landscape 13 cm" examination

Parameter	Value
kVp	120
mA	5
mAs	18.54
Total acquisition time (s)	8.9
Voxel size (mm)	0.3
Size of reconstructed volume (cm)	13
Field size at the isocentre (cm)	16.6 x 13.3
Frequency (pulses/s)	34.8
No. pulses/full acquisition	310
Rotation speed (deg/s)	43.9
Starting angle	16.9 º
Ending angle	(360+47.5) º

Monte Carlo dosimetry was performed using an algorithm based on the Electron Gamma Shower V4 (EGS4) code [9, 10]. In combination with the Low Energy Photon Scattering Expansion (National Laboratory for High Energy Physics (KEK), Japan), EGS4 simulates transport of photons with energies of 1 keV and higher and electrons with energies of 10 keV and higher. In this study, a cutoff energy for photons of 5 keV and for electrons of 30 keV was used. Special attention was paid to simulate the cone X-ray beam, taking into account the beam spectral characteristics, the effect of the shaping filter, and penumbra effects caused by the focus and collimator. Since the radiation beam was found to be asymmetrical in the vertical direction (Y-axis), with the XZ plane matching the occlusal plane of the patient, this characteristic was also implemented in the simulation.

To calculate the absorbed dose in the volumes of interest, the total energy absorbed in the voxels of the volume was computed and divided by the corresponding mass. In this way we firstly calculated values of both DPI and absorbed dose to TLD chips. After validating the MC code, we simu-

lated the standard examination on the Remab voxel model to compute average dose in every slab (ADS) and mean absorbed dose in the selected organs or tissues.

III. RESULTS AND DISCUSSION

Concerning kVp accuracy, it has been verified that the differences between measured and nominal values were always below 10%. With regard to the time of irradiation, the difference between selected and measured values was always less than 1.5%. Measured half-value layer was 9.25±0.25 mm of Al, equivalent to a total filtration of 17 mm of Al at the beam axis. As a general conclusion in this point, the CBCT unit matched the manufacturer's specifications, making it possible a comparison between calculated and measured dose values to validate the simulation code.

Table 2 shows a comparison relative to DPI_{100} values obtained from both methods, experimental and simulated, free-in-air and within the head phantom. All DPI values are expressed as dose to air. There are two remarkable facts from the results: Firstly, differences between both methods were always lower than 9%, and, secondly, the values in all the phantom cavities were very similar (differences ≤ 9%). The former result indicates that the model and the code used in the simulation produced an acceptable description of the dose distribution for simple geometries, and the latter is caused by the high beam filtration.

Table 2 Comparison of measured and calculated DPI_{100} values (mGy·cm to air) free-in-air and within the head dosimetry phantom

Position	Measured	Calculated	Difference (%)
Isocenter (free-in-air)	23.7	25.8	8.8
C	20.0	19.3	-3.7
N	19.6	18.9	-3.8
S	20.1	20.5	2.0
E	20.6	21.4	3.8
W	19.4	18.8	-3.1
NE	20.7	20.2	-2.2
NW	20.1	19.2	-4.4
SE	21.2	21.6	2.0
SW	20.3	19.8	-2.6

An equivalent comparison of measured vs. calculated dose values (mGy to air) from the TLD dosemeters for the examination of the Remab phantom is shown in Figure 2. Experimental TLD doses correspond to the average value of 7 exposures, and a total number of $2.5 \cdot 10^7$ photon histories were simulated in the MC calculation.

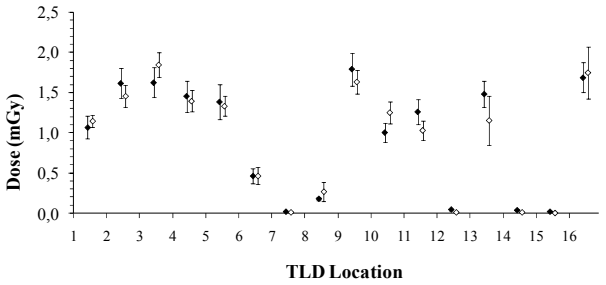

Fig. 2 Measured (♦) and simulated (◊) TLD dose values.

It can be noticed in Figure 2 that differences lower than 15% were obtained for most TLD positions. The largest relative differences correspond to dosemeters located far away from the field boundary but featuring very low dose values (positions 7, 12, 14 and 15). When dosemeters were placed in the thyroid, nape or in the eye lenses regions (positions 8, 9 and 13), differences in dose are strongly dependent on the location, due to their vicinity to the field margins. Additionally, the relative variation due to a ±5 mm displacement along the Y axis of the dosemeters in the thyroid has been estimated by simulations to be more than ±40%. Discrepancies in positions 10 and 11 were probably due to the difficulties to visualize the TLD package (3 chips) in the image, because they were inserted in the inner spinal cord location. Given the acceptable differences found for the dosemeters exposed to the primary beam, and that the highest differences for the TLD chips can be explained by geometrical variations in the radiation field, it can be concluded that the MC-based code is an accurate and useful tool to estimate radiation absorbed doses in homogeneous and anthropomorphic geometries.

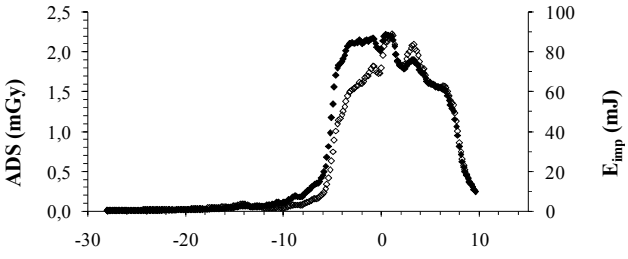

Fig. 3 Calculated values of ADS (♦) and E_{imp}, energy imparted per slab (◊), in the Remab model

After validating the MC method, the simulation of the standard examination on the Remab phantom enabled us to

calculate the ADS values, which are represented in Figure 3 and to assess the mean absorbed organ doses as well (see Table 3 below).

Table 3 Mean absorbed dose for selected organs at risk

Organ	Dose (mGy)
Thyroid	0.076
Salivary glands	1.74
Brain	0.70
Lymphatic nodes	0.50
Oral mucosa	1.43
Extrathoracic region	1.29
Eye lenses	1.73

The ADS values are well correlated with the energy imparted to each slab of the voxel phantom. Both quantities can be used in the future as a primary estimator of effective dose, because the involved organs at risk are basically the same for a range of examinations. With regard to organ doses, our values are lower than those obtained by other authors [4] and probably more alike to those from a recent publication [5] although the protocols used there are not completely equivalent. Organ doses, though one order of magnitude lower than those typically imparted in conventional CT, can be lowered if proper optimization programmes are applied.

IV. CONCLUSIONS

The devised MC method used to estimate doses for a CBCT unit has been validated and can be a robust tool to assess patient doses and to optimize protocols in the near future. In addition, the computation of the energy imparted and the average dose per slab might provide a simple method to estimate the effective dose to standard patients in maxillofacial radiology.

ACKNOWLEDGMENT

We are indebted to the Diagnostic Center in Granada for their facilities for using the i-CAT unit. Also the support from DI&B Company is very much appreciated.

REFERENCES

1. International Commission on Radiological Protection (2008). Recommendations of the International Commission on Radiological Protection. ICRP Publication 103. Ann ICRP 37
2. International Commission on Radiological Protection (1990). Recommendations of the International Commission on Radiological Protection. ICRP Publication 60. Ann ICRP 21
3. Ludlow JB, Davies-Ludlow LE, Brooks SL. Dosimetry of two extraoral direct digital imaging devices: NewTom cone beam CT and Orthophos Plus DS panoramic unit. Dentomaxillofac Radiol 2003;32:229–34
4. Ludlow JB, Davies-Ludlow LE, Brooks SL, Howerton WB. Dosimetry of 3 CBCT devices for oral and maxillofacial radiology: CB Mercuray, NewTom 3G and i-CAT. Dentomaxillofac Radiol 2006;35:219–26
5. Roberts JA, Drage NA, Davies J, Thomas DW. Effective dose from cone beam CT examinations in dentistry. Brit J Radiol 2009;82:35–40
6. Zaidi H, Ay MR. Current status and new horizons in Monte Carlo simulation of X-ray CT scanners. Med Bio Eng Comput 2007;45:809–817
7. Mori S, Endo M, Nishizawa K, Tsunoo T, Aoyama T, Fujiwara H, Murase K. Enlarged longitudinal dose profiles in cone-beam CT and the need for modified dosimetry. Med Phys 2005;32:1061-1069
8. International Commission on Radiation Units and Measurements (1992). Photon, electron, proton and neutron interaction data for body tissues. ICRU Report 46, Bethesda
9. Nelson WR, Hirayama H, Rogers DWO (1985). The EGS code system. Stanford Linear Accelerator Center. Report No.: Report SLAC-265
10. Salvado M, Lopez M, Morant JJ, Calzado A. Monte Carlo calculation of radiation dose in CT examinations using phantom and patient tomographic models. Radiat Prot Dosimetry 2005;114:364-368

Corresponding author:

Author: J.J. Morant
Institute: Servei de Protecció Radiològica, Rovira i Virgili University
Street: Sant Llorenç, 21
City: 43201 Reus
Country: Spain
Email: juanjose.morant@urv.cat

Design of an experimental set up for MRI induced heating measurement on biomedical implants

V. Hartwig[1,2], G. Antoniello[3], G. Giovannetti[1], N. Vanello[4], M.F. Santarelli[1] and L. Landini[4]

[1] Institute of Clinical Physiology, CNR, Pisa, Italy
[2] Department of Electrical Systems and Automation, University of Pisa, Italy
[3] Faculty of Engineering, University of Pisa, Italy
[4] Department of Information Engineering, University of Pisa, Italy

Abstract— **The radiofrequency (RF) field used during Magnetic Resonance Imaging (MRI) exams interacts with electrical conductor material exposed like as biological tissues and metallic medical implants. This interaction leads to temperature and specific absorption rate (SAR) increase at the implant position and could cause harmful *hot spots*. In this work an experimental set up for temperature and SAR measurements is presented. The measurements are performed by means of a laboratory reproduction of a general MRI RF transmission system, on a standard phantom with a typical cardiovascular stent implant.**

Keywords— **Biomedical implant, Radiofrequency field, Specific Absorption Rate, Temperature increase.**

I. Introduction

During MR procedures, the RF power transmitted from the transmission coil for imaging is transformed into heat within the patient's tissue. For this reason, the most important bioeffect associated with the RF radiation used during a MR exam is the tissue heating related to the absorbed power on the subject [1]. The presence of a metallic implant in an individual exposed to RF magnetic field may create a harmful situation due to the excessive magnetic field interactions. In fact, in presence of a metallic implant, like as pacemaker leads or stent, in spite of its nonferromagnetic nature, the potential RF heating can increase in the tissue immediately surrounding the implanted device [2]. Specific Absorption Rate (SAR) represents the current international dosimetric term used to characterize the thermogenic aspects of RF magnetic field [3]. Local SAR at the implant position can be calculated from the temperature increase due to RF power deposition, using the bioheat equation with the knowledge of the heat capacity of the surrounding tissues.

ASTM has developed a standard test method for measurement of RF induced heating near passive implants [3], based on temperature measurements with fiber optic probes on phantom placed in a MR scanner and exposed to RF field.

In this work we described an experimental set up designed for measurements of temperature increase and calculation of SAR in phantom with or without metallic implants, outside the MR scanner room. In our system the RF magnetic field transmission is reproduced using a birdcage coil: in this way the static magnetic field and the localization gradients are not present during the measure. The system is easy to use and permits to perform induced heating measure in a feasible way with no necessity of MR compatible probes.

Results of temperature increase and SAR value near a cardiovascular stent placed in a standard phantom are reported and discussed.

II. Materials and Methods

A. Exposure System

For the RF magnetic field transmission we realized a birdcage coil (diameter 13.2 cm, length 9.8 cm) with 8 legs in the classic low pass configuration. The coil is realized with a 1 cm wide copper strip placed on a plastic support.

Tuning capacitors are placed in the middle of each leg to obtain the desired resonance frequency. Using an IDL script [4], we simulated the frequency response of our coil with several capacitor values to set the tuning. We chose capacitors of 2 nF to obtain a resonance frequency of 8.26 MHz corresponding to a static magnetic field of 0.2 T.

Fig. 1 RF coil workbench test

O. Dössel and W.C. Schlegel (Eds.): WC 2009, IFMBE Proceedings 25/III, pp. 348–351, 2009.
www.springerlink.com

In order to evaluate the quality of our transmission coil we measured its frequency response by means of a dual loop probe and a network analyzer (HP 3577A) (Fig. 1) [5]: from the knowledge of the resonance frequency and the bandwidth we calculated the quality factor which is equal to 187 [5].

Finally, we measured the impedance (400 Ω) of the coil connected to the transmission shielded cable and loaded with the MR phantom used for the measurements, using the network analyzer S-parameter test set. In order to obtain the corrected power transmission from the generator to the coil, we realized a matching circuit with a 153 pF capacitor and a 2.7 μH custom designed coil. In this way the excitation signal generator is matched with a total impedance of 50 Ω.

The coil was fed by a waveform generator to produce a linear polarized B_1 field with a frequency of 8.26 MHz: the exposure was realized by a RF amplifier that delivers up to 50 W at this frequency.

Fig. 2 shows a block diagram of the entire exposure system.

B. Phantom and Implant

The phantom used for measurements was realized according to the specific of ASTM standard [3]: it was a gelled phantom made with 0.8 g/L NaCl and 5.85 g/L Polyacrilic acid into 0.5 L of distilled water. This formulation has an electrical conductivity of about 0.25 S/m and a viscosity sufficient to prevent convective heat transport.

As biomedical implant a cardiovascular stent was chosen and placed inside the phantom.

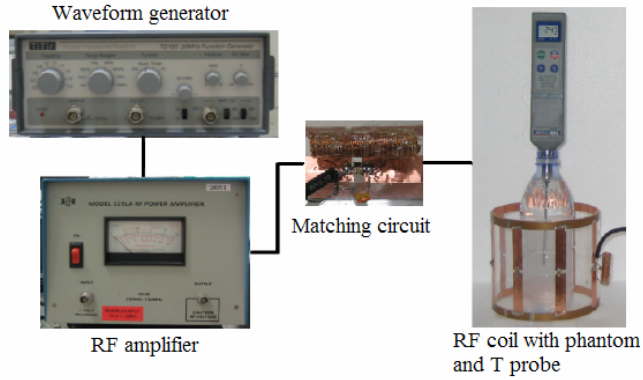

Fig. 2 Exposure system

The stent was constituted by a Nickel Titanium alloy (NITINOL) and had a diameter of 1 cm and a length of 4.5 cm: since this is a non ferromagnetic material, it is considered as compatible with MRI environment.

C. Temperature measurement and SAR calculation

Temperature at one location of interest was measured using a Pt 100 temperature probe (HD9215, Delta Ohm) with resolution of 0.1 °C. The terminal portion of the temperature probe was placed in contact with the stent using three plastic clamps.

The transmission RF coil loaded with the phantom and the temperature probe, were placed inside a thermal insulator box, to avoid measurement errors due to changes in the room temperature.

SAR values at the centre of the phantom without stent and at the location of the stent were calculated using the bioheat model according to the Pennes' equation [6], which can be expressed by:

$$c\frac{dT}{dt} = W_M + W_B + W_C + SAR \tag{1}$$

where c is the heat capacity, dT/dt is the temperature increment due to the exposure, W_M is the heat generated from the metabolic activity, W_B is the heat loss due to the blood perfusion and W_C is the heat loss due to the thermal conduction in tissue.

For SAR evaluations in vitro, that is on phantom simulating biological tissue properties, the heat exchanges W_M and W_B are not present. Moreover, using a phantom with a sufficient viscosity, which is achieved by inclusion of a gelling agent, it is possible to prevent the convective heat transport, so the W_C term is negligible. In this case the bioheat equation can be simplified as:

$$c\frac{dT}{dt} = SAR \tag{2}$$

Local SAR at the stent location was calculated by multiplying the initial slope of the temperature rise with the specific heat capacity of the phantom material. For our phantom the heat capacity was considered close to that of water, 4184 J/kg °C [3]. To avoid errors in the SAR estimation we selected the initial linear portion of the temperature rise, choosing as the starting point the first temperature increment step and using the number of samples that maximized the R-squared coefficient of the regression model (Pearson coefficient) [7].

Each sample represented the average of three temperature measurements. After the exposure, we observed an exponential cooling curve that persisted for many minutes.

After the first exposure, we started another irradiation when the cooling curve exhausted and the temperature returned to the initial value of 21.6 °C.

The first test regarded the temperature measurement in the phantom without the stent exposed at RF irradiation

with the maximum incident power (50 W): the initial temperature was 20.8 °C and the exposition length was 200 min. After, to estimate the SAR value in the phantom without the medical implant, we measured the temperature increase induced by 2600 seconds length irradiation with a power of 50 W.

Tests on the phantom with the stent were performed using different values of power (6.25, 12.5, 25, 50 W) for an exposition length of 1800 seconds; the initial temperature was 21.6°C. In all cases SAR values were calculated using the regression model.

III. Results

Results for test on the phantom without stent at 50 W of transmission power show an initial linear temperature increase followed from a quadratic rise with a saturation value for temperature equals to about 24.5°C (Fig. 3).

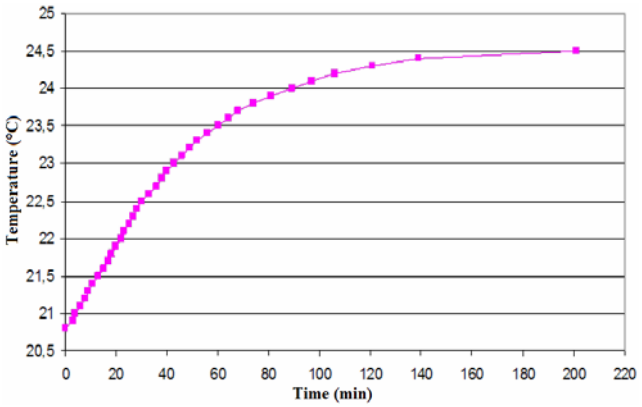

Fig. 3 Temperature vs Time during RF irradiation (50 W) on the phantom

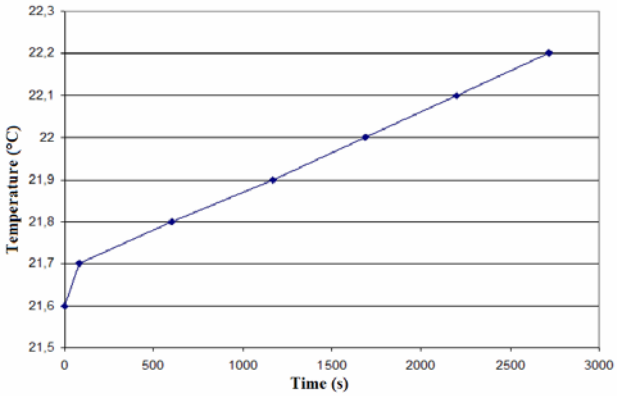

Fig. 4 Temperature vs Time during RF irradiation (50 W) on the phantom for SAR calculation

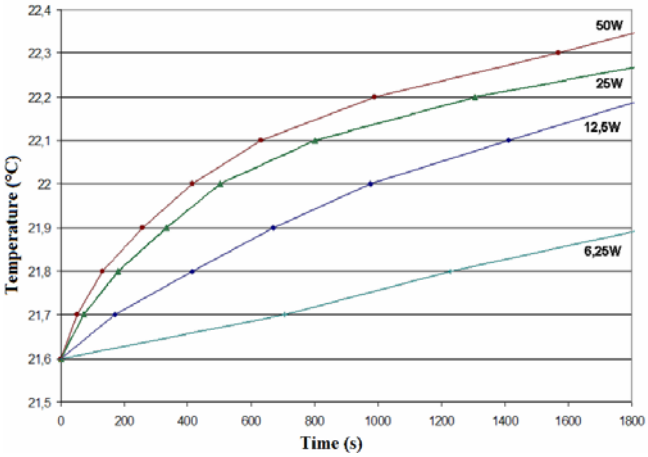

Fig. 5 Temperature vs Time during RF irradiation on the phantom with the stent for different transmission power

Table 1 SAR and R^2 in phantom+stent tests

RF transmission power (W)	R^2	SAR (W/kg)
6.25	0.9972	0.8398
12.5	0.9999	1.6736
25	0.9891	3.3472
50	0.9845	4.1840

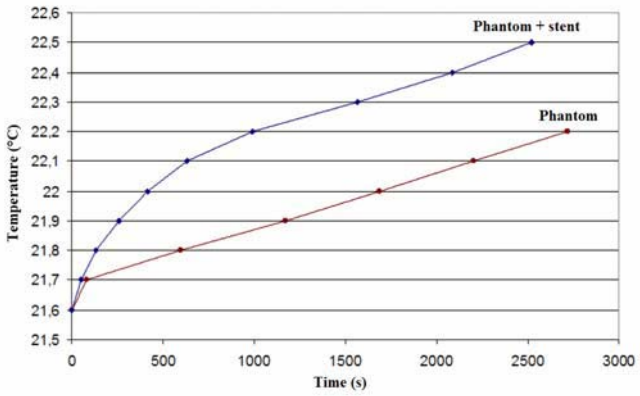

Fig. 6 Comparison of temperature time course for the phantom with/without stent

To calculated the SAR on the phantom without stent induced by the RF exposure (power = 50 W, exposure lenght = 2600 s) we used the initial linear slope of the curve shown in Fig. 4. We obtained a SAR value of 0.8368 W/kg (R^2 = 0.9997).

Results for tests on the phantom with the stent at four different values of RF transmission power are reported in Fig. 5. The exposition length was 1800 seconds and the initial temperature was 21.6°C for all cases.

Table 1 shows the calculated SAR for each RF transmission power value: the coefficient R^2 for each test is also reported to demonstrate the goodness of the used regression model.

Finally, in Fig. 6 we reported the temperature time course during the RF exposure for the phantom with and without the stent. The graphics are relative to a RF transmission power of 50 W and to an exposure length of 2600 seconds.

IV. Discussions and Conclusions

In this work, we present an experimental set up to MRI induced heating measurement on biomedical implants. RF magnetic field transmission was reproduced in laboratory using a custom designed birdcage coil, a signal generator and a power amplifier. Temperature measurements during exposure were performed on a standard phantom with or without a nonferromagnetic cardiovascular stent, using different values of RF transmission power. SAR values at interest location were calculated by multiplying the initial slope of the temperature rise with the specific heat capacity of the phantom material, according to the bioheat model for study on phantoms.

Results relative to the temperature increase due to a RF exposure at 50 W of the phantom without the stent reflect the expected time course: initial linear slope, quadratic rise and saturation at a certain temperature value.

In this case we obtained a SAR value of 0.8368 W/kg (R^2 = 0.9997): this value respects the minimum SAR value of 1 W/kg indicated by the ASTM standard for measurement of RF induced heating in presence of passive implants [3].

To validate our dosimetry system we performed temperature measurements on the phantom with the stent at four different values of RF transmission power are reported. As we expected, the results for these tests show that the SAR increase with the transmitted power.

To compare the results relative to the test on the phantom with or without the stent, we reported the temperature increase during the RF exposure (power = 50 W, length = 2600 seconds). The temperature slope obtained in the case of phantom with the stent is higher respect to that obtained for the phantom without the stent. Hence, we can conclude that in the stent location the RF exposure caused the presence of a *hot spot*, which it could damage the contiguous tissues. In confirmation of this conclusion, it is possible to observe that the SAR value for the phantom with the implant is five times higher than the SAR for the phantom without stent.

The proposed system is easy to use and permits to perform induced heating measure in a feasible way, with no necessity of MR compatible probes.

Moreover, changing the tuning of the RF transmission coil, it is possible to perform the tests with different frequencies, corresponding to different magnetic static field intensities. In this way, it is possible to evaluate the heating on biomedical implants induced by exposure to both magnetic static low and high field scanner.

Finally, using this experimental set up for the RF field generation system, the static magnetic field and the localization gradients are not present during the measure. This aspect could be important, for example, for study of MRI genotoxic effects, where could be necessary to identify which of the three magnetic field components is the cause of the biological effects [8].

References

1. Kangarlu A, Robitaille PML (2000) Biological effects and healt implications in Magnetic Resonance Imaging. Conc Magn Reson 12(5): 321-359
2. Schaefers G, Melzer A (2006) Testing methods for MR safety and compatibility of medical devices. Minim Invas Therapy 15(2): 71-75
3. ASTM F2182-02a (2002) Standard test method for measurement of Radio Frequency induced heating near passive implants during Magnetic Resonance Imaging. In ASTM International, PA, USA
4. Giovannetti G, Landini L, Santarelli MF, Positano V (2002) A fast accurate simulator for the design of birdcage coils in MRI. Magn Res Mat Phys, Biol Med 15: 36-44
5. Giovannetti G, Francesconi R, Landini L et al. (2004) Conductors geometry and capacitors quality for performance optimization of low frequency birdcage coils. Conc Magn Reson 20B: 9-16
6. Yeung CJ, Atalar E (2001) A Green's function approach to local RF heating in interventional MRI. Med Phys 28(5): 826-832
7. Mattei E, Triventi M, Calcagnini G et al. (2008) Complexity of MRI induced heating on metallic leads: Experimental measurements of 374 configurations. Biom Eng Online 7(11)
8. Simi S, Ballardin M, Casella M et al. (2008) Is the genotoxic effect of magnetic resonance negligible? Low persistence of micronucleus frequency in lymphocytes of individuals after cardiac scan. Mut Res/Fund Molec Mechan Mutag 645: 39-43

Use macro [author address] to enter the address of the corresponding author:

Author: Valentina Hartwig
Institute: Institute of Clinical Physiology, CNR
Street: Via Moruzzi, 1
City: Pisa
Country: Italy
Email: valeh@ifc.cnr.it

Simulating mammographic absorption imaging and its radiation protection properties

C. Hoeschen[1], H. Schlattl[1], M. Zankl[1], T. Seggebrock[2], L. Clemente[2] and F. Grüner[2]

[1] Helmholtz Zentrum München, German Research Center for Environmental Health, Institute of Radiation Protection, Neuherberg, Germany
[2] Ludwig-Maximilian-University, Department for Physics, Garching, Germany

Abstract— **There is a large number of optimization strategies for optimal relation between information and exposure in mammographic imaging procedures. This is especially due to the specific situations in screening programs. However, the variety of possibilities like breast CT, tomosynthesis absorption with photon counting or with energy integrating detectors and phase contrast mammography results in very difficult comparisons about pros and cons of different techniques. Simulation methods based on Monte-Carlo methods would be a useful tool for first approaches. However, such a simulateion approach requires suitable and useful phantoms of the female breast in typical imaging conditions. Voxel phantoms of real breasts would be an optimal solution. Mammographic specimen of female breasts from corps have been compressed and than fixated while being compressed as in a general mammographic application. Such kinds of specimen have been scanned using a flat panel imager system a holding unit and a rotation table. By that CT images could be gained with relatively low radiation qualities. These data sets have been transformed by segmentation into high resolution voxel models. We performed Monte-Carlo simulations of using such phantoms for simulating absorption based imaging procedures including monoenergetic and standard spectra images using EGSnrc and Geant4 codes to proof the feasibility of such phantoms and simulations in order to obtain a tool for radiation protection optimization.**

Keywords— **breast imaging, voxel phantoms, specimen, radiation protection optimization, Monte-Carlo simulations.**

I. INTRODUCTION

Mammographic imaging is an imaging task with increasing number of imaging procedures worldwide especially due to an increasing number of screening programms resulting in a lot of irradiated women. This is especially a topic for radiation protection properties since for mammographic screening programs the waste majority of the investigated women do not suffer from any cancer that can be diagnosed. Therefore the optimization of the mammographic absorption imaging which is still the most accurate and reliable method for early breast cancer diagnosis in terms of radiation protection is very crucial [1-5]. Radiation protection in this respect means the use of as low radiation exposure possible with the besdt possible diagnostic performance. This might mean an optimized image quality allowing better and more accurate diagnosis or it might mean an optimal tool for diagnosis presenting threedimensional (3D) image information. All this has to be investigated by means of relevant exposure to ionizing radiation and diagnostic properties. It is not feasible to do all kinds of investigations and especially it is difficult to measure the dose to the glandular tissue for a sufficient number of imaged breasts. Therefore it seems to be very useful alternative to simulate the whole process by means of Monte-Carlo simulations on suitable phantoms. However, these simulations have to take care about relevant dose properties and image quality or even image information content properties. This is so far not realized on real mammographic species. The aim of this particular work is therefore to develop a system of high resolution voxel models of real mammographic specimen and Monte-Carlo based image simulation for optimization of mammographic absorption imaging in the mammographic imaging field.

II. MATERIAL AND METHODS

The used methodology to achieve the goal of implementing a complete tool for simulating mammographic absorption imaging processes in terms of radiation dose properties and image information content is divided into two main aspects the first is the generation of the phantoms the second is the simulation with the Monte-Carlo codes of the imaging process.

A) The generation of the family of mammographic phantoms

First of all a unique set of mammographic specimen was created starting with specimen of female breasts from corps. Such specimen were fixated while being compressed showing the real status of the breasts during mammographic imaging procedures. The fixation procedure worked as follows: After resection of the breasts from the corps, theses were cleaned. Then they were fixated by the following steps:

O. Dössel and W.C. Schlegel (Eds.): WC 2009, IFMBE Proceedings 25/III, pp. 355–358, 2009.
www.springerlink.com

- perfused for about 6 months with formaldehyde solution
- maintenance in 60% alcohol for 1/2 year
- watered for 2 days
  compressed in between PVC plates
- fixation with formalin
- Impregnation with PEG 400:
  first : 4 weeks in 40% aqueous solution
  second : 4 weeks in 80% aqueous solution
  third : 2 weeks in 100% aqueous solution

With this techniques seven mammographic phantoms were generated by the anatomical institute of the Otto-von-Guericke- university of Magdeburg, Germany and its Department for Diagnostic Radiology [6]. One of the phantoms contains even a malignant tumor, which was diagnosed on the investigated ready prepared phantom. One of the pahntoms is shown as an example in figure 1:

figure 1: one of the physical compressed breast phantoms as used for the further procedures.

These phantoms have than been scanned in an CT like geometry using a flat panel detector and a fixation unit for the specimen together with a rotation table. Using these elements it was possible to generate a projection image darta set with a 40 kVp radiation quality and a relatively high resolution each projection representing pixel sizes of 200 µm squared. Due to small misalignments during the movement of the breast in its fixation unit we were able to generate a 3D data set of the breast specimen with a resolution of 400 µm by 400 µm by 1mm [7], which is to our knowledge the highest resolution 3D data set so far of real breast specimen for compressed breast.

This breast data set was then segmented into different breast tissues as it can be seen from figure 2.

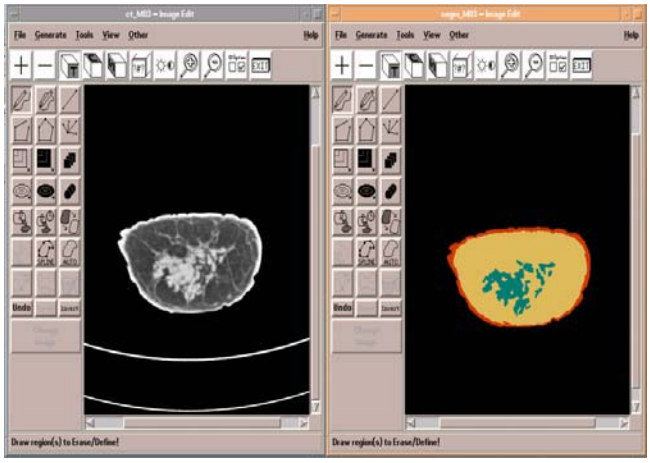

figure 2: One slice of the 3D data set of one of the breast specimen (left side) and its corresponding segmentation of such slice (right side)

Using this segmentation method we ended up with a 3D voxel model of the specimen with the same resolution properties as the 3D data sets. And representing mammographic phantoms in real imaging conditions. It should be noted here that in 3D applications like tomosynthesis and breast CT imaging the meaning of compression is discussed at the moment. New specimen without compression might be necessary to answer these questions. However for the standard optimization purposes these voxel models representing different sizes of breasts and different tissue composition are a useful tool for Monte-Carlo simulations.

B) The Monte-Carlo simulation process

For the Monte-Carlo simulations we used two different codes to be able to compare results and to choose the specific codes which are easier to implement for further optimisation tasks. We used EGSnrc [8] and GEANT4 [9]. We simulated as a first step standard mammographic imaging geometries to be also able to compare the results with test images we can perform from our physical test specimen. We simulated as a first task multi energy spectra imaging and compared it to monoenergetic imaging scenarios . For these monoenergetic input distributions of the X-ray we used different energies to be able to get results on optimal contrast-to-noise per dose ratios. We also investigated scatter effects by allowing scattering processes or avoid them in the simulation. We started with 10^9 photons incidenting the breasts but we increased the number by up to two orders of magnitude to get relevant results.

III. RESULTS

We generated the voxel phantoms with a resolution of 400 µm by 400µm by 1 mm voxel size. From these voxel phantoms we were able to calculate as well images by means of Monte-Carlo simulations as well as dose distributions in the phantoms. The results from the EGSnrc code and the GEANT4 code are comparable and within the range of the assumed accuracies due to the number of quanta used for the calculations. One of the resulting images is shown in figure 3:

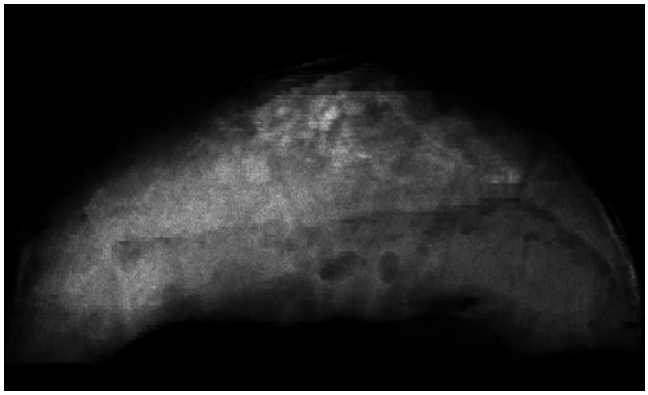

figure 3: The simulated image of one of the breast specimen with a monoenergetic incoming beam with 17keV photons.

It could be shown that the optimal contrast to noise ratio per dose could be achieved with a beam quality corresponding to the results presented by Schöfer et al for a slightly different task but a generalized model [10]. These results can be summarized in figure 4, showing an optimal contrast to noise ratio per absorbed dose if the main absorber allows 20% transmission.

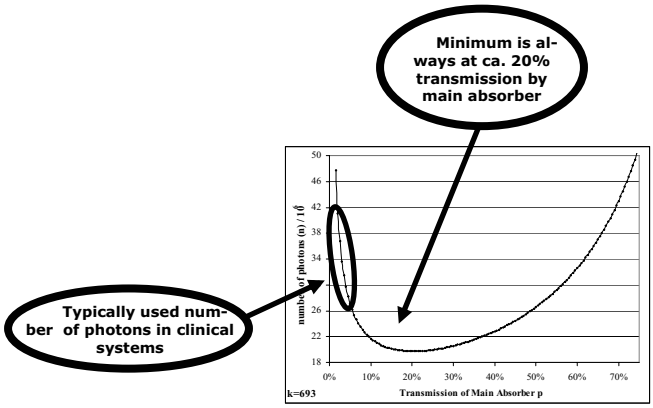

Figure 4: optimal dose efficiency dependent of absorption of main absorber. As shown in [10].

The results indicate that just due to the optimal beam quality adjustment a factor of two in dose to the glandular tissue could be saved compared to today's standard techniques.

IV DISCUSSION AND CONCLUSION

The work presented here did show that a generalized optimisation tool for mammographic absorption imaging by realistic simulation could be created. It can handle image quality / image information properties as well as dose properties.

To finalise the results for the topic of the advantage of monoenergetic beam qualities addressed in this paper it will be necessary to implement also more realistic detector properties compared to the assumptions made until now. It would be interesting in how far this will change the results gained so far regarding the potential optimization by monoenergetic beam qualities. Another aspect in this aspect might be the breast density and thickness. However, there might be an additional advantage in an easier access and therefore reduction potential of scatter for monoenergetic beam qualities when coupled to energy resolved detectors.

The variety of possible combinations will have to be simulated and evaluated by numbers as frequency dependent contrast to noise ratios per glandular dose.

We also want to try to gain voxel phantoms with even higher resolution. This should be possible due to the inherent information content of the specimen which have been proven before [6]. In this paper it had been shown, that the structures in the mammographic specimen contain frequency components of up to 20 mm^{-1} or even more This would result in necessary resolution of 25 µm resolution as a minimum. However, due to the fact of today's system resolution this might be unnecessary. A realistic approach seems to be a 50µm resolution in the final voxel model.

V. ACKNOWLEDGEMENT

This work was partly funded by the German Research Foundation due to projects within the Munich Advanced Photonics Excellence Cluster as part of the German Excellence Initiative.

VI. REFERENCES

1. Nyström, L., Andersson, I., Bjurstam, N., Frisell, J., Nordenskjöld, B., Rutqvist, L.E. Long-term effects of mammography screening: updated overview of the Swedish randomised trials. Lancet. 2002 Mar 16;359(9310):909-919.

2. Tabar, L., Yen, M.F., Vitak, B., Chen, H.H., Smith, R.A., Duffy, S.W. Mammography service screening and

mortality in breast cancer patients: 20-year follow-up before and after introduction of screening. Lancet. 2003 Apr 26;361(9367):1405-1410.

3. Ferrini, R., Mannino, E., Ramsdell, E., Hill, L. Screening mammography for breast cancer: American College of Preventive Medicine practice policy statement. Am J Prev Med. 1996 Sep-Oct;12(5):340-341.

4. Laming, D., Warren, R. Improving the detection of cancer in the screening of mammograms. J Med Screen. 2000;7(1):24-30.

5. Pisano, E.D., Gatsonis, C., Hendrick, E., Yaffe, M., Baum, J.K., Acharyya, S., Conant, E.F., Fajardo, L.L., Bassett, L., D'Orsi, C., Jong, R., Rebner, M. Diagnostic performance of digital versus film mammography for breast-cancer screening. N Engl J Med. 2005;353(17):1773-1783.

6. Hoeschen C, Fessel A, Buhr E, Döhring W: Determination of the x-ray intensity pattern in mammography with very high spatial resolution. SPIE 3977 (2000) 220 – 230

7. Hoeschen C, Fill U, Zankl M, Panzer W, Regulla D, Dohring W A high-resolution voxel phantom of the breast for dose calculations in mammography *Radiat Prot Dosimetry* 114, 406-9 2005

8. Kawrakow I, Rogers DWO The EGSnrc code system: Monte Carlo simulation of electron and photon transport PIRS Report 701 (Ottawa: National Research Council of Canada (NRCC)) 2003

9. S. Agostinelli, J. Allison, K. Amako, J. Apostolakis, H. Araujo, P. Arce, M. Asai, D. Axen, S. Banerjee, G. Barrand, F. Behner, L. Bellagamba, J. Boudreau, L. Broglia, A. Brunengo, H. Burkhardt, S. Chauvie, J. Chuma, R. Chytracek, G. Cooperman et al. G4—a simulation toolkit, Nuclear Instruments and Methods in Physics Research Section A: Accelerators, Spectrometers, Detectors and Associated Equipment, 506, 3, 1(2003), 250-303

10. Schöfer, F. H., Schneider, K., Hoeschen, C.: Minimum dose calculation for different imaging tasks in digital projection radiography SPIE 6510 (2009) 4E1-7

Author: Dr. Christoph Hoeschen
Institute: Helmholtz Zentrum München – Institute of radiation protection
Street: Ingolstädter Landstrasse 1
City: 85764 Neuherberg
Country: Germany
Email: christoph.hoeschen@helmholtz-muenchen.de

Approved Personal Dosimetry for Medical Personnel using Direct Ion Storage Dosimeters

M.R. Gårdestig[1], H.B.L. Pettersson[1]

[1] Radiation Physics Department, County Council of Östergötland, Linköping, Sweden

Abstract— **Dosimeters based on the Direct Ion Storage technology is used as the first approved electronic personal dosimeter in Sweden at the County Councils in Östergötland and Kalmar. TL dosimeters are replaced by DIS-1 dosimeters for all category A personnel at six hospitals with totally 300 dosimeter holders. The advantages are longer issue periods and instant read outs, appreciated by both the service and the holders.**

Keywords— **Personal dosimeter, direct ion storage, dosimetry service.**

I. Introduction

County Council in Östergötland, Sweden, has operated their personal dosimetry service since 1976. Film badges were replaced with TL dosimeters (2xLiF:Mg,Ti) in 1984, and is now, replacement started in 2002, as of April 2007, an approved [1] personal dosimetry service using the DIS-1 dosimeter.

Figure 1 illustrates the dose history and dose intervals at the University Hospital in Linköping from 1976 until 2008. The apparent decrease in 1984 is due to the improved accuracy and sensitivity of TL dosimeters over film badges and partly due to a decrease in number of dosimeter holders.

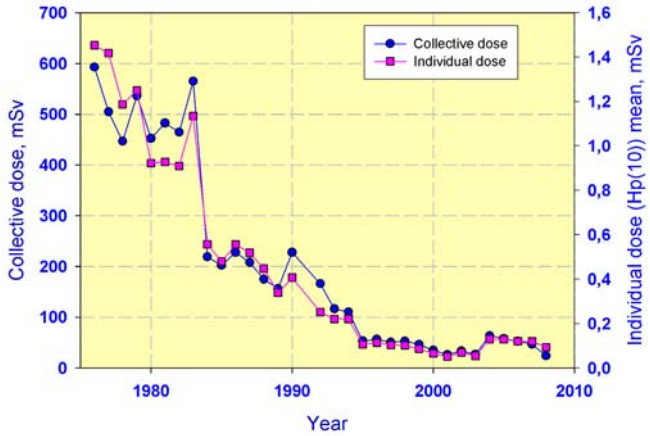

Fig. 1 Dose history of the University Hospital in Linköping over the years 1976 – 2008.

The Radiation Physics Department of the County Council of Östergötland is the first service in Sweden to receive an approval for legal personnel dosimetry using electronic dosimeters and all category A personnel now wear the DIS-1 dosimeter.

Eleven dosimeter badge readers (DBR) serve six hospitals and 20 different clinics ranging over interventional radiology, CT, nuclear medicine, radiation therapy, radiation physics, surgery, and laboratory work.

The dosimetry service distributes and evaluates DIS-1 dosimeters for 300 persons/year (15000 read outs so far)

II. Materials and methods

A. Description of the DIS system

The DIS-1 dosimeter is based on the DIS element [2,3], a small ion chamber mounted directly on a open floating gate non-volatile solid-state memory cell. Ionization in the airspace between the chamber wall and the gate, caused by electrons generated by photon interaction in the wall material, will alter the charge of the gate. At read out the conductivity over the transistor (proportional to the charge) is measured non-destructively. Two DIS elements measure the personal dose equivalent Hp(10) covering the dose ranges 1-4500 µSv and up to 1 Sv respectively. The software determines which element to use for dose report. One MOSFET transistor is used for high doses up to 40 Sv where the damage to the transistor itself is measured. Measurements of Hp(0.07) is provided by the third DIS element and a second MOSFET transistor behind a thin foil. Hp(0.07) doses are registered, but reports are not required by the Swedish Radiation Safety Authority.

Dosimeter Badge Readers (DBR) are connected using LAN (Local Area Network) adapters over the hospital intranet. The DBR can operate up to 8 hour on battery and store 256 read outs off-line. The readers are wall mounted and strategically placed where most holders pass daily. Any reader can be used by all holders.

A SQL server stores the data and the database management software, WinELD Pro, calculates and presents the dose information. Dose reports are sent to the clinics on

O. Dössel and W.C. Schlegel (Eds.): WC 2009, IFMBE Proceedings 25/III, pp. 352–354, 2009.
www.springerlink.com

monthly basis and, for category A personnel, reported to the Swedish Radiation Safety Authority.

Each dosimeter is individually assigned; a unique ID is stored in the memory of the dosimeter as well as in the database. On delivery, each holder receives an information sheet with instructions on how to wear and read the dosimeter. Information is also posted close to the readers and on the web. Natural background dose level for each relevant floor is established and stored in the database for subtraction on daily intervals.

Earlier, TL dosimeters were issued to individual holders on a monthly basis in order to meet the requirements from the legislation, but the holder of a DIS-1 dosimeter keep the same dosimeter as long as the most sensitive DIS element has enough charge left for registration of dose, typically about two years. The dosimeter is then reset at the service and reused. The holder is reminded by e-mail to read his dosimeter at least at the turning of each month. The reader gives instant dose information accumulated since last read out.

Dosimeter calibration is checked biennially in conjunction with the reset procedure. Calibration is made for ^{137}Cs quality with the dosimeter mounted on a ISO water slab phantom (30x30x15 cm) [4] yielding a Hp(10)-dose of 0,5-1 mSv.

The service handles about 350 DIS-1 dosimeters (10% surplus) in active service in 20 locations. Temporary, general purpose dosimeters are available at the clinics for teaching, visiting personnel or public, e.g. anaesthetic or accompanying personnel or family.

B. Field trial

A field trial was performed with control dosimeters worn by almost 100 holders during the approval process for testing of the procedures during a year-long period. Regular TL dosimeters were used in parallel with DIS-1. Holders were selected from the Nuclear Medicine, the Radiation Therapy and the Radiation Physics departments. Aspects of usability for the holders and handling of the system at the service were compared as well as dose data.

III. Results

The accuracy test done at the approval and biennial renewal procedure show that the DIS dosimeters register doses well inside the trumpet curve [1] over a broad range of doses, see figure 2. The approval from the Swedish Radiation Safety Authority for the dosimeter requires a minimum detectable dose equivalent of 0.17 mSv, an upper measure limit of at least 100 mSv, accuracy and linearity requirements according to the trumpet curve in figure 2 and angular dependency for 0º, 20º, 40º and 60º where dose measurements shall be within 40% from the 0º irradiation dose response. The DIS-1 dosimeter fulfilled these requirements with margin.

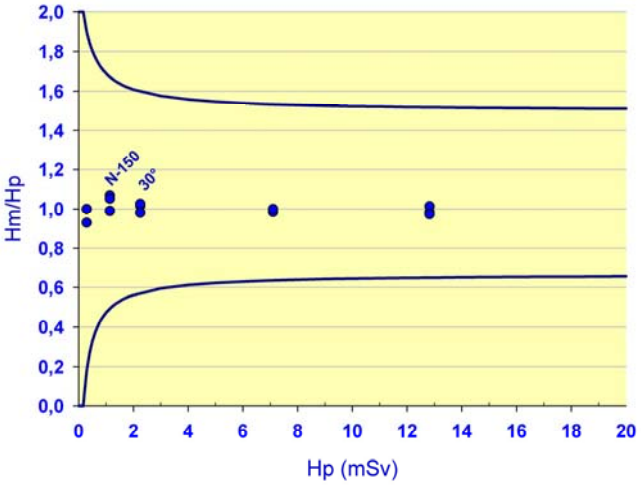

Fig. 2 Results from the blind test of the 2009 renewal of approval procedure. Hp is the given dose and Hm the measured value. Doses in Hp(10) in ^{137}Cs and N-150. 15 dosimeters in total.

User feedback during and after the field trial suggest appreciation of the instant readout and direct dose feedback, as well as appreciation of a modern device. Less handling due to the prolonged issue period, reminder in e-mail and more direct contact with the dosimetry service is also expressed benefits.

The handling of the dosimeters at the service was made easier due to the prolonged issue period. The timing of the procedures of read outs and evaluations is less important which makes the work flow easier.

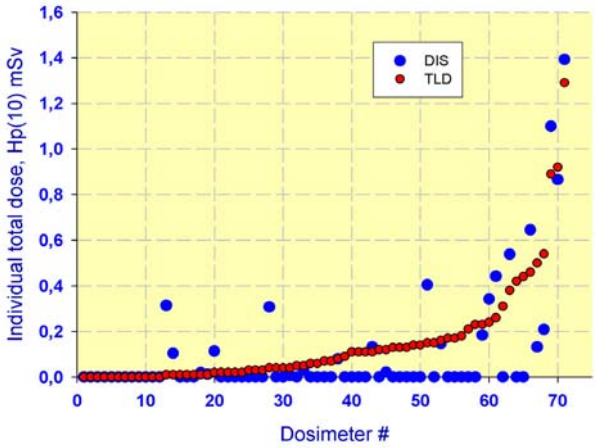

Fig. 3 Dose values from TLD and DIS usage during 14 months of field trial.

All evaluated doses during the field trial were moderate, as expected in hospital environment, see figure 3. Some doses differ due to more complicated handling of background correction when holders fail to hand in their TL dosimeter. The DIS system was found to be reliable and easier to evaluate the dose information.

A handful of DIS-1 dosimeters have malfunctioned and been taken out of service. The most common error is contact problem between dosimeter and reader which is easily solved by cleaning the contact surfaces. Regular preventative maintenance of dosimeters and readers is made by the service.

IV. Discussion

The new system was initiated because it was considered to demand less manpower, therefore cost effective, and give instant dose information directly to the customer/holder. The TLD system is not entirely obsolete due to the TL pellets small size and therefore versatile usage possibilities. TL dosimeters are still in use for finger, eye and phantom dose measurements, but the legal personal dosimetry is entirely covered by the DIS dosimeters. The DIS system may also replace direct displaying dosimeters in radiation protection investigations of new methods and buildings. Using the portable reader DBR-2, the system is suitable for emergency situations with first responders and decontamination personnel.

V. Conclusions

For legal dosimetry measurements of Hp(10), the TLD-system is replaced entirely by the DIS-system at six hospitals in the County Council in Östergötland and Kalmar County Council in Sweden.

References

1. SSI FS 1998:5 The Swedish Radiation Protection Institute´s Regulations on Monitoring and Reporting of Individual Radiation Doses. Now included in SSM FS 2008:51
2. Kahilainen, J (1996) The Direct Ion Storage Dosemeter. Radiat. Prot. Dosim. 66:459-462
3. DIS-1 Dosimeter User's Guide, version 1.02, RadosTechnology Oy
4. Alberts, W.G., et al (1994). International Standardization of Reference Radiations and Calibration Procedures for Radiation Protection Instruments. In: Strahlenschutz: Physik und Meßtechnik, band 1, Eds W. Kölzer and R. Maushart, pp. 181-188. Verlag TüV Rheinland GmbH

Author: Magnus Gårdestig
Institute: County Council in Östergötland
Street: University Hospital
City: Linköping
Country: Sweden
Email: magnus.gardestig@lio.se

Dosimetry and Quality Control in Medical Imaging Applications

B.M. Moores

Integrated Radiological Services Ltd, Liverpool, UK

Abstract— **Radiation exposure to medical diagnostic procedures is becoming a topic of increasing relevance and social interest. A primary aim of modern diagnostic procedures is to provide sufficient information for a particular diagnostic task with exposures kept as low as practicable. The ALARP principle (As Low As Reasonably Practicable) is the driving force behind a number of innovations and ongoing research activities over the past 30–40 years.**

To evaluate the performance of diagnostic imaging systems it is necessary to correlate image quality and dose and, therefore, be able to evaluate both. This can, on the one hand, involve advanced measurement tools and methods that attempt to measure imaging system parameters such as MTF, NPS, and NEQ as well as dose (quanta) dependent image/information quality parameters such DQE. However, whilst such measurements provide information concerning the physical performance capabilities of systems employed in diagnostic procedures under well defined exposure conditions, they do not permit us to verify optimal performance in daily clinical use. For this latter purpose it would be necessary to routinely perform measurements of image quality and associated dosimetric evaluations, ideally for every patient. Under such circumstances the ALARP principle could then be said to apply to each and every patient or group of patients.

In this paper the development of meaningful patient dosimetry methods and techniques for various patient specific radiological applications, as well as image quality control procedures will be reviewed. The importance of ongoing technological developments will be discussed in relation to the present situation and future progress that might be possible in the field of patient radiation protection. For example in the UK during the past 5 years there has been a complete transfer from film based to digital radiographic techniques. Equally, ongoing developments in CT technology continue to create increased imaging information albeit at much higher doses. The effects of these changes on scientific support to patient dosimetry and quality control in diagnostic radiology as well as future possibilities for improved application of the ALARP principle will be highlighted.

Keywords— **Radiation protection, patient dosimetry, quality control**

I. Introduction

Over the past 40 years collective effective doses arising from diagnostic radiology have risen consistently as the diagnostic power and availability of radiological imaging methods has continued to grow. Consequently increases in image quality (diagnostic power) rather than a reduction in patient dose continues to underpin modern practice. CT examinations, now considered to represent the "gold" standard for diagnostic outcomes continue to grow as a percentage of overall x-ray examinations as well as in terms of their overall contribution to population exposures [1]. Indeed a recent report released recently by the National Council on Radiation Protection and Measurements (NCRP) [2] indicates that in the US the population exposure to ionising radiation from medical procedures grew more than sevenfold between the early 1980's and 2006. This corresponds to a doubling time of roughly 8 years. What is the relevance and meaning of the fundamental aspects of radiation protection embodied in the ALARP and ALARA (As Low As Reasonably Achievable) principles in the face of such growth?

The field of general radiation protection is built upon the foundation of controlling exposures (minimisation of risks). However, in the field of healthcare, reduction of radiation exposures can be counterproductive and may actually lower benefits. The control of radiation exposure cannot be treated in isolation from the need to improve and/or maximize diagnostic outcomes. Thus we need to consider the total risk (R_T) arising from diagnostic radiology, given by:

$$R_T = R_R + R_D \quad (1)$$

Where R_R is the radiation risk and R_D is the diagnostic risk associated with false positive/false negative outcomes [3, 4]. Decreasing the radiation dose in order to reduce R_R may have a much greater deleterious effect on R_D. Also, both the diagnostic risks and benefits can vary from patient to patient (age, sex, weight) as well as disease process and anatomical region.

Given this extremely complex and varied situation medical scientists have attempted to create a scientific framework for radiation protection, including quality control and patient dosimetry. This framework has largely been driven by ongoing technical developments within the field of diagnostic radiology as well as the integration of developments from outside. Before attempting to indicate how such a scientific framework might continue to evolve it is worthwhile considering historical developments in this field over the past 50 years.

O. Dössel and W.C. Schlegel (Eds.): WC 2009, IFMBE Proceedings 25/III, pp. 359–362, 2009.
www.springerlink.com

II Development of Test Procedures and Standardisation of Practices (1950 – 1980)

The roots of quality assurance in diagnostic radiology, including quality control, radiation protection and patient dose, may be traced back to the 1950s. At this time there was just three X-ray imaging modalities; radiography, fluoroscopy and conventional tomography. A growing interest was developing throughout Europe and North America in developing a more scientific framework for diagnostic radiology including an improved understanding of its limitations. There was also a growing awareness of the need to quantify and assess the levels of radiation employed diagnostically.

These early initiatives were pursued by a relatively small group of radiologists, physicists and engineers working in industry and healthcare throughout Europe and North America. Concepts such as noise, resolution and visual performance that had been developed elsewhere for quantifying/assessing system performance, were being applied to the radiological image [5,6,7,8]. Also technical developments in image intensification for medical applications were receiving increased attention [9,10].

As well as the scientific and technical aspects of X-ray image production, interest was growing in the levels of radiation employed in diagnostic radiology and dosimetric measurement methods [11,12]. During the late 1950s in the UK the Adrian Committee organized a survey of the extent of medical and dental radiology in Great Britain in order to assess the levels of radiation dose employed and make recommendations for its reduction. The findings of the committee were published in three parts between 1959 and 1966 [13,14,15]. The reports included recommendations for reducing the genetically significant doses from diagnostic radiological practices since genetic risks were considered, at this time to be, the major hazard.

The early initiatives led to three meetings held in Washington [16] and Chicago [17,18]. These meetings brought together experts, from both Europe and North America and included radiologists, engineers and scientists and involved a transfer of information between the manufacturers and users of X-ray equipment. Also, the meetings were not only concerned with the technical basis of X-ray imaging methods but also methods for reducing patient dose by instrumentation and technological developments. However, over the intervening 40-year period, technological developments have led to the completely opposite outcome based upon a desire and capability for improved information.

Whilst these more fundamental initiatives were underway, interested individuals, who were working within the healthcare sector, continued to develop methods for assessing the performance of radiological systems and the application of imaging sciences to diagnostic radiology. Research, including methods for making measurements on X-ray beams, radiological imaging systems, image quality and perception, were all pursued. In 1974 the Hospital Physicist's Association (HPA) in the UK published in a single document what had previously been four individual reports dealing with the physical aspects of the important imaging components [19]. This has been subsequently revised on a number of occasions. Particular attention was paid to those aspects of performance that could be quantified. The transfer of basic research on systems performance and methods of measurement, into routine application within the clinical domain had now begun. However, test methods were extremely varied and in most instances test equipment was manufactured locally to personal design so that results could not easily be compared.

The momentum was maintained throughout the 1970s as individuals continued to develop, implement and refine methods for measuring X-ray system performance. Results of this effort in the UK led to the publication by the Hospital Physicists' Association (HPA) of standard test protocols of methods and procedures, for assessing the performance of radiological systems. The first protocol dealing with X-ray tubes and generators was published in 1980 [20]. This was followed almost immediately by protocols dealing with image intensifier/TV systems, screen-films and automatic processors, CT scanners and conventional tomographic units.

However, whilst these activities were underway, there was continued technological development and ongoing basic research in diagnostic imaging methods being pursued including rare earth intensifying screens, CsI image intensifiers, digital (subtraction) fluoroscopy, mammography, xeroradiography and ionography. There was a need for a dynamic scientific process within quality assurance in diagnostic radiology based upon the application of research and development methods. Also, up until this point the routine application of patient dose measurements was somewhat peripheral to the assessments of equipment performance.

III Harmonisation of Initiatives and Creation of a European Dimension (1980 – Present)

The beginning of a truly European dimension to quality assurance in diagnostic radiology can be traced to a meeting held in Munich-Neuherberg in April 1981 organized by the Commission of European Communities. The purpose of this meeting was to discuss with a group of European experts the possibility of reducing patient doses from medical X-ray diagnosis [21]. This meeting highlighted the need for a separate EU Directive on radiological protection of the

patient and the need for an EC research effort to reduce patient exposure.

Following this preliminary meeting a Council Directive concerned with protection of the patient was issued in 1984 (84/466/EURATOM). As part of the underpinning initiatives to support the Directive experts from research, industry and public health services involved in medicine came together to participate in a seminar on "Criteria and methods for quality assurance in medical X-ray diagnosis" held in Udine, Italy [22]. This meeting coincided with the commencement of an extended research programme in the field of radiation protection in diagnostic radiology. Prior to this contractors had been representatives from Government Laboratories and major University Hospitals. However, much of the expertise in this area lay with individuals working in routine medical practice and these were now included in the programme. A comprehensive radiation protection research programme including quality assurance and patient dosimetry has been ongoing throughout Europe over the past 20 years and has produced many notable outcomes.

Findings and outcomes from the European research programme in the field of radiation protection, including quality assurance and patient dosimetry, have been published in the proceedings of numerous meetings over the years, for example [23,24,25]. However, such programmes have had to constantly cope with and reflect the ongoing technological changes that are being implemented within the field of diagnostic radiology. For example in the UK there has been a complete replacement of film based radiographic imaging by digital technology. This has led to a completely electronic radiological environment that itself offers a number of exciting possibilities for developing more patient oriented scientific support mechanisms.

IV Current Status and Future Needs

There is no doubt that quality assurance including quality control, radiation protection and patient dose measurement in diagnostic radiology has evolved significantly both philosophically and practically over the past 50 years. It is now an accepted part of routine radiological practice and has helped to introduce a more scientific approach to this activity. It has led the way in terms of the application of quality assurance in healthcare. Also, given the increasing importance of imaging in therapeutic applications it is influencing scientific practice outside diagnostic radiology.

Research based activities in the field of quality assurance continue to underpin the ongoing development of the field. Thus new test methods are continuously being required to evaluate and assess new forms of X-ray imaging particularly in the field of 3 dimensional imaging methods such as tomosynthesis. This includes new techniques and methods for assessing patient dose. The impact of IT on the diagnostic imaging process, through the introduction of new detectors and PACS systems continues to open up new possibilities for automated quality assurance processes including improved data analysis and centralized management systems. The use of clinical images in routine quality control methods driven by the application of computer aided diagnostic methods [26] is also becoming a reality. These developments can have a major impact on the optimization of radiological practices throughout Europe.

Of particular interest is a web-based approach to the centralized collection, analysis, management and storage of x-ray exposure information accessed from a Hospital's Radiology Information System (RIS) [27]. Such an approach can permit ongoing patient dose audits as part of a routine automated QA programme [28]. For example the differences in mean dose for male and female patient populations provides valuable information on the performance of AEC devices. This approach can permit more detailed assessments of radiological practices as part of an optimization programme involving all patient records. It can also form the basis for ongoing international collection and comparison exercises of patient doses and radiological practices. Where data is collected to a standard format.

The application of IT to radiation protection in diagnostic radiology can provide new and improved scientific support mechanisms. Information generated can underpin the development of a more quantitative risk-benefit framework for diagnostic radiology as well as optimized feedback loops or expert system support for operators.

References

1. Regulla D, Wahl W and Hoeschen C. Current radiation exposure of man – A comparison between digital imaging and environmental, work place and accidental radiation burden. Proc IRPA 12, Buenos Aires, Argentina. October 2008
2. NCRP Report 160. Ionizing radiation exposure of the population of the United States. http://NCRPpublications.org.2009
3. Langlotz CP. Fundamental measures of diagnostic examination performance: usefulness for clinical decision-making and research. Radiology, 2003:228: 3-9
4. NG NS and Palmer CR. Analysis of diagnostic confidence and diagnostic accuracy: a united framework. Brit J Radiol, 2007:80:152-160
5. Sturm R.E. and Morgan R.H. Screen intensification systems and their limitations. Am. J. Roentgen. 62, 617, 1949.
6. Schade O. Image structure and transfer characteristics. Journ. S.M.P.T.E., 56, 137, 1951.
7. Mertz P. Perception of television random noise. Journ. S.M.P.T.E., 1950:54:8.
8. Burger G.C.E. Phantom tests with X-rays. Philips Technical Rev. 11, 291, 1950.

9. Hay G. A. X-ray image intensification using optical television methods. Advances in electronics and electron physics. New York, Academic Press, 363, 1960.
10. Hay G.A. Quantitative aspects of television techniques in diagnostic radiology. Br. J. Radiol., 1958:31: 611.
11. Osborn S.B. and Burrows R.G. An ionization chamber for diagnostic X-radiation. Phys Med Biol, 3, 37, 1958.
12. Stuart S. and Osborn S.B. A wide-range direct reading X-ray dosemeter. Phys Med Biol, 1959:3:255.
13. Adrian Committee. Radiological hazards to patients. Interim report. Her Majesty's Stationery Office (HMSO), London, 1959.
14. Ibid. Second report. HMSO, London, 1960
15. Ibid. Final report. HMSO, London, 1969.
16. Janower M.L. Technological needs for reduction of patient dosage from diagnostic radiology. Charles C. Thomas, Springfield Illinois, 1963.
17. Moseley R.D. and Rust J.H. The reduction of patient dose by diagnostic radiologic instrumentation. Charles C. Thomas, Springfield, Illinois 1964.
18. Moseley R.D. and Rust J.H. Diagnostic radiologic instrumentation. Charles C. Thomas, Springfield, Illinois, 1965.
19. HPA. The Physics of Radiodiagnosis. (First edition) SRS-6 (Hospital Physicists' Association, London) 1974.
20. HPA. Measurement of the performance characteristics of diagnostic X-ray systems used in medicine. Part 1 – X-ray tubes and generators. (Topic Group Report 32) Hospital Physicists' Association, London, 1980.
21. Drexler G., Eriskat H. and Schibilla H. Patient exposure to radiation in medical X-ray diagnosis-possibilities for dose reduction. EUR 7438, Luxembourg 1981.
22. Br. J. Radiol. Criteria and methods for quality assurance in medical X-ray diagnosis. Supplement 18, 1985.
23. Radiat. Protect. Dosim., Medical X-ray imaging: potential impact of the new directive. Radiation Protection Dosimetry. 90, Nos 1-3, (2000)
24. Radiat. Protect. Dosim.,. Optimization strategies in medical X-ray imaging. Rad Prot Dos. 114, Nos 1-3, (2005)
25. Radiat. Protect. Dosim., Optimization of dose and performance in interventional and digital imaging. Radiation Protection Dosimetry, 117, nos 1-3, (2005)
26. Br. J. Radiol., Computer-aided diagnosis. Edited by Gilbert FJ and Lemke H. vol 78, 2005
27. Ward M et al, Central dose data management and analysis in IT driven radiation protection strategies. Radiat. Protect. Dosim., 2005: 114(1-3): 135-142
28. Fazakerley J et al. The development of a 'gold standard' patient dose audit data set. IPEM Proceedings of the 14th Annual Scientific Meeting, Bath, UK, pp61

Author: B.Michael Moores
Institute: IRS Ltd
Street: Brunswick Business Park
City: Liverpool
Country: UK
Email: mikemoores@irs-limited.com

Patient Dose Measurements in Full Field Digital Mammography and Comparison with Dose to the Standard Breast

N.J. Tyler, C. Strudley, P. Hollaway, and D.J. Peet

Regional Radiation Protection Service, Department of Medical Physics, Royal Surrey County Hospital, Guildford, UK

Abstract— **Full field digital mammography is now becoming widespread in both the NHS and private healthcare sectors in the UK. In order to gain the most from the switch from film-/screen to digital imaging, optimization of these systems has become of vital importance and even more so with the introduction of exotic spectra such as tungsten targets and silver filters.**

Protocols have now been published that give guidance on the commissioning and routine testing of full field digital mammography systems. These documents include remedial levels for the mean glandular dose to equivalent breasts for thicknesses of polymethylmethacrylate (PMMA) from 20 -70 mm and acceptable and achievable levels of image quality. At our site initial set-up of digital mammography systems is therefore based on dose measurements made with PMMA and image quality assessed with a contrast detail phantom and comparison with these limits. In order to confirm that these set-ups are appropriate patient dose surveys are also undertaken.

We present results from a number of manufacturers' mammography systems comparing mean glandular doses to the standard breast measured with PMMA and clinical breast doses from patient dose surveys. Results show a different correlation for each manufacturer's system assessed between the two types of mean glandular dose measurement. Results from a GE system show less than 1% difference between the doses for 50 - 57 mm compressed breast thickness, whilst results for a Hologic system show a 50% difference.

The work highlights how, for digital mammography systems, PMMA measurements of mean glandular dose alone give little information on the doses to real breasts and highlights the importance of carrying out a patient dose survey as soon as possible following the installation of a digital mammography system.

Keywords— **digital mammography, patient dose, mean glandular dose.**

I. Introduction

Full field digital mammography is now becoming widespread in both the NHS and private healthcare sectors in the UK. Commissioning of the systems is of vital importance to ensure that they are set-up correctly, particularly with the recent introduction by some manufacturers of exotic spectra such as tungsten x-ray tubes with silver filters.

Mean glandular dose is used as the measure of risk for mammography exposures. Guidance for film/screen mammography provides a remedial level of mean glandular dose for 45 mm thickness of polymethylmethacrylate (PMMA) of 2.5 mGy [1]. This is equivalent to 53 mm of compressed breast tissue with a glandularity of 29% in the central region. This is close to the average compressed breast thickness and glandularity for a typical screened population in the UK [2]. To aid in the optimization process the NHSBSP [3] and EUREF [4] guidelines for the commissioning and routine testing of full field digital mammography systems also provide remedial values of mean glandular dose for equivalent breast thicknesses of 20 to 90 mm as well as levels of acceptable and achievable image quality.

In addition the UK has recently adopted a national diagnostic reference level (NDRL) of 3.5 mGy for mediolateral mammograms for breasts with a compressed breast thickness of 55±5 mm [5]. The NHSBSP protocol recommends that patient dose surveys are carried out at commissioning and then at least on a three yearly basis.

For most film/screen mammography systems the automatic exposure control (AEC) is based on the use of a radiation detector placed behind the cassette which terminates the exposure when a certain level of dose is reached, corresponding to the level needed to achieve the required film density. As this method is relatively simple and uses only the radiation reaching the detector from behind a single area of the breast, in most cases uniform blocks of PMMA could be used as breast substitutes for routine physics testing. Hence routine surveys would only look at the mean glandular dose measured with PMMA with a three yearly survey of clinical breast doses.

With the introduction of digital mammography with solid state detectors, manufacturers no longer use a single radiation detector to control the AEC exposure; rather each manufacturer may use the signal from the image detector in a different manner in order to determine when to halt the exposure. Signal measurements could also be taken from a variety of positions across the surface of the image detector. As the density of real breast tissue is going to vary across the image detector the system is unlikely to perform in exactly the same way with uniform PMMA blocks.

To date, tests on systems at our site have been based on image quality measurements using the CDMAM contrast detail test object (Artinis Medical Systems, The Netherlands) and comparison with the acceptable and achievable

O. Dössel and W.C. Schlegel (Eds.): WC 2009, IFMBE Proceedings 25/III, pp. 363–365, 2009.
www.springerlink.com

image quality limits given in the protocols. AEC settings can then be optimized to ensure that image quality meets the achievable levels and mean glandular dose measured with PMMA is within the remedial levels. However, the complex performance of the AEC on digital mammography units means that optimization based on PMMA measurements may be underestimating the mean glandular dose to the breast for real patients.

The aim of this work was to carry out standard patient dose surveys on a variety of manufacturers' systems and to compare the results of these surveys with mean glandular dose measurements made with PMMA during commissioning and routine physics surveys.

II. Materials and Methods

A. Dose to the Standard Breast

Physics surveys are carried out at our site on a six-monthly basis for all mammography equipment. Mean glandular dose to the standard breast is measured using PMMA blocks of 2, 3, 4, 4.5, 5, 6 and 7 cm thickness according the NHSBSP protocol. Measurements are made in the clinical AEC mode with each thickness of PMMA and sufficient expanded polystyrene spacers to make the total thickness the same as the equivalent thickness of compressed breast tissue. This ensures that the system selects the same kV, target and filter materials as it would for real breasts.

Measurements of X-ray tube output are made for the same combinations of kV, target and filter using a calibrated solid state detector.

Half value layer measurements are made on each unit for a range of kV values for each target filter combination available using a calibrated ionization chamber.

The mean glandular dose, D, to the standard breast equivalent to a 45 mm thickness of PMMA is calculated using the equation (1) below:

$$D = K_{45}.g_{53}.c_{53}.s \quad (1)$$

Where K is the incident air kerma (without backscatter) at the upper surface of a 45 mm thickness of PMMA, the factor g_{53} corresponds to a 53 mm thick breast with glandularity 50% and converts from incident air kerma to mean glandular dose, the factor c_{53} corrects for the difference in composition from 50% glandularity, the factor s corrects for differences in X-ray spectrum. Tables of these factors are provided in the NHSBSP protocol.

B. Clinical Breast Doses

Mean glandular doses are determined for at least 50 breast examinations on each unit according to the protocols given in IPEM report 89 [6]. Software provided by the NHSBSP [7] is used to calculate the doses. Doses for mediolateral views with compressed breast thicknesses between 50 and 60 mm were compared against the NDRL of 3.5 mGy. Data was also grouped by thickness for comparison with the measurements to the standard breast made with PMMA.

III. Results

To date data has been analyzed for a Hologic Selenia system, a GE 2000DS and a Siemens Novation. Data is still being collated for a further 2 GE 2000DS systems, a further Siemens Novation and a Siemens Inspiration.

Tables 1, 2 and 3 show mean glandular doses deduced for measurements using PMMA and mean glandular doses calculated for clinical examinations.

Table 1 Mean Glandular Dose to the Standard Breast and Clinical Breast Doses for a Hologic Selenia Mammography unit

Equivalent thickness of Breast (cm)		MGD calculated from PMMA measurements (mGy)	Average MGD for clinical breast examinations (mGy)
2.1	(0-2.7)	0.78	1.60
3.2	(2.7-3.9)		2.31
4.5	(3.9-4.9)		2.24
5.3	(5.0-5.7)	1.33	2.00
6	(5.7-6.8)		2.41
7.5	(6.8-8.3)		3.07
9	(8.3+)	2.54	-

Table 2 Mean Glandular Dose to the Standard Breast and Clinical Breast Doses for a GE 2000DS Mammography unit

Equivalent thickness of Breast (cm)		MGD calculated from PMMA measurements (mGy)	Average MGD for clinical breast examinations (mGy)
2.1	(0-2.7)	0.82	0.83
3.2	(2.7-3.9)	0.83	1.08
4.5	(3.9-4.9)	1.01	1.18
5.3	(5.0-5.7)	1.13	1.12
6	(5.7-6.8)	1.15	1.31
7.5	(6.8-8.3)	1.45	1.55
9	(8.3+)	1.8	1.9

Table 3 Mean Glandular Dose to the Standard Breast and Clinical Breast Doses for a Siemens Novation Mammography unit

Equivalent thickness of Breast (cm)	MGD calculated from PMMA measurements (mGy)	Average MGD for clinical breast examinations (mGy)
2.1 (0-2.7)	0.36	-
3.2 (2.7-3.9)	0.47	0.6
4.5 (3.9-4.9)	0.7	0.75
5.3 (5.0-5.7)	0.72	0.94
6 (5.7-6.8)	0.73	0.95
7.5 (6.8-8.3)	0.97	1.15
9 (8.3+)	1.26	1.28

IV. Discussion

Whilst clinical breast doses from the patient dose surveys on each unit were well within the NDRL level of 3.5 mGy and mean glandular doses to equivalent breasts measured with PMMA were all within the remedial levels published in the NHSBSP protocols, results so far show that there is little correlation between the 2 types of dose measurement for different digital mammography systems.

This appears to be due to differences in AEC design but may also be influenced by the choice of X-ray spectra. Differences at the 50-57 mm compressed breast thickness range from 50% for the Hologic Selenia to 0.9% for the GE 2000DS.

V. Conclusions

Patient dose surveys provide important data for the optimization of digital mammography systems. Results highlight the importance of carrying out surveys as soon as possible after installation of the unit and show that the correlation between measurements of mean glandular dose with PMMA and clinical breast doses appears to vary between manufacturers' units. This means that two systems that appear well optimized at commissioning, giving the same image quality and dose to the standard breast could, in clinical use, give widely different patient doses. In addition, cooperation between the system engineer, physics and the mammographers using the equipment is essential in ensuring the system is well optimized.

References

1. Recommended Standards for the Routine Performance Testing of Diagnostic X-ray Imaging Systems. York, Institute of Physics and Engineering in Medicine, Report 91, 2006.
2. Young KC. (2002) Radiation Doses in the United Kingdom trial of breast screening in women aged 40-48 years. Br. J. Radiol. 73 pp. 362-370.
3. Commissioning and Routine Testing of Full Field Digital Mammography Systems. (2006) NHSBSP Equipment Report 0604, Version 2, NHS Cancer Screening Programmes at http://www.cancerscreening.nhs.uk.
4. European protocol for the quality control of the physical and technical aspects of mammography screening. Part B: Digital Mammography. In: European Guidelines for Quality Assurance in Breast Cancer Screening and Diagnosis, 4th edition. Luxembourg: European Commission, 2006.
5. Department of Health, Guidance on the Establishment and Use of "Diagnostic Reference Levels" (DRLs) as the term is applied in the Ionising Radiation (Medical Exposure) Regulations 2000
6. Moore AC, Dance DR, Evans DS et al. (2005) The Commissioning and Routine Testing of Mammographic X-ray Systems. Institute of Physics and Engineering in Medicine, Report 89, York.
7. Young KC (2004) Breast Dose Surveys in the NHSBSP: Software and Instruction Manual Version 2.0. NHS Cancer Screening Programmes (NHSBSP Report 0405).

- Author: Nicola Tyler
- Institute: Royal Surrey County Hospital
- Street: Egerton Road
- City: Guildford
- Country: UK
- Email: n.tyler@nhs.net

Implementation on Methodology for TLD Postal Dosimetry Audit of Radiotherapy Photon Beams in Non-reference Conditions in Cuba

Stefan Gutiérrez Lores and Gonzalo Walwyn Salas

Centro de Protección e Higiene de las Radiaciones, Cuba
stefan@cphr.edu.cu , sglcu@yahoo.es

Abstract—**Purpose: This report presents the methodology and experience of the Cuban's Secondary Standard Dosimetry Laboratory for the implementation of postal dosimetry audit of radiotherapy photon beams in non-reference conditions, using powder TLD under IAEA Coordinated Research Project E2.40.12.**

I. Methods and materials

Under coordinated research project E2.40.12 a lot of approximately 50 g of LiF powder, type TLD-100 (Hasrhaw) was characterized. The Tl dosimeter consists of about 165 mg of LiF powder filled into a watertight polyethylene capsule with dimensions of 20 mm inner length and 3 mm inner diameter. A HARSHAW 2000C/B manual reader is used for the measurements. Based on the IAEA standard holder for photon beams, a TLD holder was developed with horizontal arm to enable measurements 5 cm off the central axis. New procedures for TLD irradiation hospitals were developed.

II. Results

Successful results in a external trial carried out using the IAEA TLD service in the year 2006 were obtained. Three facilities were considered to be included in the Pilot Audits in Radiotherapy for Co-60 in non-reference conditions (on - and off axis).

III. Conclusions

The TLD powder method has been successfully implemented by Cuban SSDL. The instructions and forms for non-reference conditions on axis and off axis were understood by participating hospital. Extend the postal dose audits to the rest of the hospitals around the country. The methodology of TLD audits in non reference conditions with a modified IAEA TLD holder has been shown to be feasible. The participation in these results audits promotes a major understanding of the physicists in their dosimetry procedures and TPS limitations.

O. Dössel and W.C. Schlegel (Eds.): WC 2009, IFMBE Proceedings 25/III, p. 366, 2009.
www.springerlink.com

A tissue-equivalent radioluminescent fiberoptic probe for in-vivo dosimetry based on Mn-doped lithium tetraborate

M. Santiago[1,2], M. Prokic[3], P. Molina[1,2], J. Marcazzó[1,2] and E. Caselli[1,4]

[1] Instituto de Física Arroyo Seco, Universidad Nacional del Centro de la Provincia de Buenos Aires, Pinto 399, 7000 Tandil, Argentina
[2] Consejo Nacional de Investigaciones Científicas y Técnicas (CONICET), Rivadavia 1917, 1033 Buenos Aires, Argentina
[3] Institute of Nuclear Sciences, Vinca, P.O. Box 522, 11000 Belgrade, Serbia
[4] Comisión de Investigaciones Científicas de la Provincia de Buenos Aires (CICPBA), calle 526 entre 10 y 11, 1900 La Plata, Argentina

Abstract— **The fiberoptic (FO) dosimetry concept, which relies on the assessment of dose by measuring the intensity of the light emitted by a tiny sample of a radioluminescent (RL) compound coupled to an optical fiber cable, is gaining importance as a promising dosimetry technique for in-vivo dosimetry. In this work the design, construction and test of a tissue-equivalent RL probe is described. The intensity of the RL emission of Mn-doped Lithium Tetraborate samples during irradiation is used as an estimate of the relative dose. The influence of spurious luminescence is discussed and a removing method based on simple optical filtering is implemented. Finally, the response of the probe in the context of a typical depth-dose experiment in a ^{60}Co radiotherapy facility is analyzed and compared to the response of a standard ionizing chamber.**

Keywords— **radioluminescence, radiotherapy, fiberoptic dosimetry, tissue-equivalent detector.**

I. Introduction

The development of new radiation-based treatments for cancer claims for dosimetry systems accomplishing more and more demanding characteristics. Among them, the possibility of performing in-vivo dosimetry has shown to be an increasing necessity in the different radiotherapy contexts [1]. Among the different approaches developed so far to achieve this goal, the recently established *fiberoptic dosimetry* method offers interesting potentialities. This technique is based on the use of an efficient, either organic or inorganic, scintillating material, which is placed in the point where dose or dose-rate is to be assessed. During irradiation, part of the energy absorbed by the scintillator is re-emitted as light of characteristic wavelength. This light is collected by means of an optical fiber to which the scintillator is glued or mechanically coupled, and taken outside the irradiation room up to a suitable high-gain detector. Generally the scintillation yield is proportional to the dose-rate, what makes the system suitable for dosimetry. Overall, the FO technique shows interesting characteristics: a) the small size of the detector permits accurate dose measurements in regions of high dose gradients, b) the system does not use any external high-voltage bias, c) its rugged design makes is suitable for the routine tasks carried out by radiotherapy technicians, d) since the reading is obtained during irradiation, the FO technique allows for in-vivo dosimetry, etc.

Many materials have been tested as FO scintillators: rare-earth oxides [2,3], Cu^{1+}-doped quartz [4], plastic scintillators [5], scintillating fibers [6], Ce^{3+}-doped SiO_2 optical fibres [7], Tb^{3+}-doped fluorides [8], NaI(Tl), CsI(Tl) and ZnS(Ag) [9], carbon-doped Al_2O_3 [10,11,12], etc. Although all of them show promising performances, Al_2O_3:C is one of the most investigated compounds in the context of this application probably due to its commercial availability (by Landauer, Inc.), besides its outstanding properties as RL phosphor. As to the optical fiber component, both plastic, polymethyl methacrylate (PMMA) [11,13] and fused silica [9, 12, 14] fibers have been used. Although PMMA fibers have higher attenuation, they are cheaper, have lower bending radius and are more tissue-equivalent than silica fibers [15,16], what is important from the point of view of their application in dosimetry practice. Besides, PMMA fibers show lower spurious intrinsic luminescence than silica fibers [17].

The intrinsic RL of the scintillator at the sensitive end of the optical fiber is not the only source of light during the irradiation of the FO probe. Spurious light produced in the fiber by Cherenkov effect and the intrinsic luminescence of the fiber also reaches the detector. The Cherenkov radiation is emitted whenever charged particles pass through dielectric matter with a velocity beyond the velocity of light in the medium (fiber). The intensity of Cherenkov light increases inverse to the third power of the wavelength. Consequently, in the visible spectrum the blue color dominates. On the other hand, the intrinsic luminescence of the optical fiber depends on the characteristics of the kind of fiber being used. Several methods have been proposed in the literature to get rid of the spurious luminescence, also dubbed *stem effect*: simple optical filtering, subtraction of the background signal, and time gating. In the first case long-pass filters remove the short wavelength components of the light reaching the detector, which are supposed to be more affected by the Cherenkov emission. In the second case, the

O. Dössel and W.C. Schlegel (Eds.): WC 2009, IFMBE Proceedings 25/III, pp. 367–370, 2009.
www.springerlink.com

signal of a blank optical fiber having no detector at its end is used to estimate the contribution of the stem effect. In the third case, which is only useful for measurements at linear accelerators (LINAC), the spurious contribution of the stem effect is avoided by measuring the RL signal from the detector between the LINAC pulses, when the stem effect luminescence is negligible [5].

In the field of radiotherapy dosimetry, the possibility of relying on tissue-equivalent detectors, say, detectors having an energy-dependent response similar to water, has been always welcome. For this reason several researchers have used plastic scintillators when developing FO dosimetry systems [14]. However, many inorganic materials showing also tissue-equivalent response to photons should not be dismissed. Among them, lithium tetraborate (LTB), which has been extensively investigated as thermoluminescent dosimeter for its nearly tissue-equivalent effective atomic number (Z_{eff} = 7.3) clearly constitutes an interesting alternative for RL dosimetry [18]. Although the RL of LTB doped with different activators, such as Cu, Eu, Mn and Ag, has been reported [19,20], its application to FO dosimetry has been never explored.

In this article first results on the performance of a FO probe featuring a doped LTB scintillator are reported. The most suitable dopant has been chosen by taking into account the corresponding RL spectra and the spectrum of the stem effect. As a test evaluating the response of the system under tissue-equivalent conditions, a percent depth dose (PDD) curve in a water phantom has been recorded and compared to that obtained with a standard ionization chamber.

II. Materials and methods

Lithium tetraborate samples doped with Mn, Cu and Cu,Ag,P have been used in this work. They have been developed by M.P at the Institute of Nuclear Sciences, Belgrade. These compounds have been prepared by a sintering technique reported in Ref. [18,21,22], which renders pellets (4.5 mm dia and 0.95 mm thickness) made by cold-pressed polycrystalline powder having grain sizes between 75 and 200 microns, which were sintered at 880ºC for Mn activated, and at 850ºC for Cu and Cu,Ag,P activated LTB phosphors. The sintered LTB:Mn pellets are semitransparent, and pale blue-colored for LTB:Cu and LTB:Cu,Ag,P. The activator concentrations for LTB:Mn was 0.1 wt%, for LTB:Cu was 0.03 wt% and for LTB Cu,Ag,P samples were 0.03 wt%, 0.03 wt% and 0.8 wt% respectively. As described in the references cited before, the optimal stoichiometric ratio of the reagents has been carefully chosen in order to eliminate the effect of moisture on the prepared lithium borate phosphor.

Solid sintered LTB phosphors are relatively complex materials with characteristics strongly influenced by the preparation method, the phases of the Li_2O-B_2O_3 system present, the basic chemical used, the sintering temperature, and the proper choice of the chemical form of activators and co-activators, etc. [18].

In-lab RL spectra have been obtained at room-temperature by means of an Acton Research VM-504 0.39 m monochromator featuring an Electron Tubes P25PC-02 photon counting head as detector. This detector has a sensitivity window that goes from 250 up to 650 nm. The measurements have been made with a resolution of approximately 5 nm. In order to perform the spectral measurement the pellets were placed onto the entrance slit and irradiated from their back side by means of a 3.7×10^8 Bq ophthalmic ^{90}Sr beta-source located 1 cm away from the sample.

In order to build the FO probe, a 1mm^3 piece has been cut from a LTB:Mn pellet and glued to the end of a PMMA fiber (1mm dia core, 2mm outer jacket). The sensitive end has been coated with three layers of opaque, water resistant painting.

In-situ measurements with the FO probe have been made at room temperature in a Theratron 80 ^{60}Co radiotherapy facility rendering 0.3 Gy/min at 5 mm water depth (80 cm SSD, source-surface distance). The emission of the FO probe has been measured by means of a Hamamatsu H9319 photon counting head having sensitivity between 300 and 850 nm. A long-pass colored-glass filter Schott OG530 has been placed between the end of the fiber and the detector in order to cut off the spurious contribution of the stem effect emission. To obtain the PDD with the FO probe a 40×40×40 cm^3 water phantom has been employed. During the measurements the SSD and the field size have been set to 80 cm and 10×10 cm^2 respectively. PDD readings have been made starting from the water surface up to 34 mm water depth. Measurements performed in the water phantom with the FO probe have been checked with a 0.6 cm^3 PTW Farmer chamber model 30013 and a PTW UNIDOS E electrometer.

In-situ spectral measurements have been made at room temperature with a resolution of approximately 10 nm employing an Acton Research SP-2155 0.150 m monochromator equipped with a Hamamatsu H9319 photon counting head.

III. Results and discussions

In Fig. 1 the RL spectra of LTB:Cu, LTB:Cu,Ag,P and LTB:Mn under beta irradiation are shown. The RL spectrum of Cu:LTB shows a single peak at 380 nm, what matches very well the RL spectrum of LTB:Cu single crystals reported in Ref. [19]. On the other hand, the spectrum

of Cu,Ag,P:LTB presents a peak at approximately 435 nm. Similar results have been obtained by Can *et al.* [23] when they irradiate Cu,Ag,P:LTB pellets with X-rays at room temperature. The RL emission of LTB:Mn shows a broad peak stretching between 300 and 500 nm and a minor, longer-wavelength peak centered at 590 nm, what resembles the spectrum obtained by Holovey *et al.* for LTB:Mn single crystals under X-ray irradiation [24]. By taking into account the previous results, we have chosen LTB:Mn as the best candidate to build a FO probe, since it shows intense RL beyond the short-wavelength region where the stem effect is usually important.

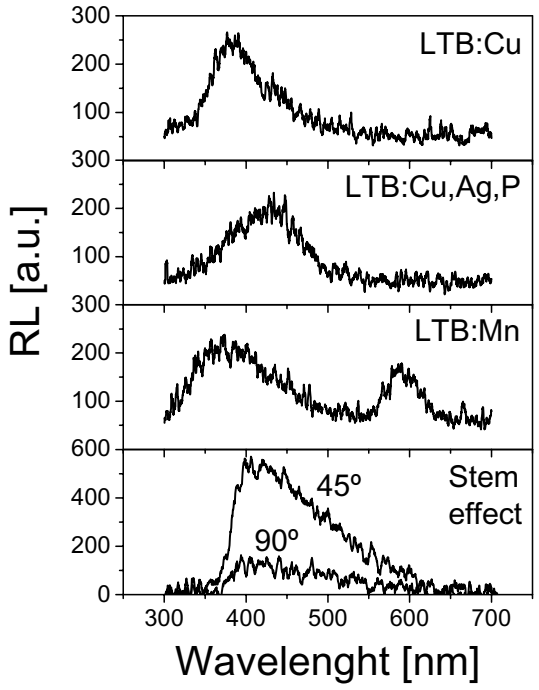

Fig. 1 In-lab spectra corresponding to the RL emission of the different doped LTB samples and to the spurious luminescence (stem effect) produced in a blank fiber under ^{60}Co irradiation at different angles between the beam and fiber axes

When a FO probe is planned to be employed for in-situ measurements, it is important to determine the actual influence of the stem effect for the particular setup being used. Indeed, if the simple optical-filtering technique will be used to remove the spurious luminescence produced in the fiber, it is necessary to learn about the spectrum of the stem effect. For this reason, we irradiated in the ^{60}Co radiotherapy facility a blank PMMA fiber, say, a fiber having no sample at its end, and recorded the resulting spectrum. The end of the fiber was placed at 5 mm depth in the water-phantom (SSD = 80 cm, field 10×10 cm^2) while the angle spanned by the fiber axis and the beam axis was set to 90 and 45º. In principle, it is expected that approximately at 45º the contribution of the Cherenkov emission reaches its maximum value [14]. The results of the spectral measurement are shown in Fig. 1. For our setup the contribution of the stem effect spans a wide wavelength range, which goes from 375 up to about 600 nm with maximum at 400 nm. The strong dependence of the intensity on the angle confirms that the stem effect is made up mainly of Cherenkov emission. By taking into account this information and the RL spectrum of LTB:Mn shown in Fig. 1, a OG530 Schott long-pass filter has been used in the rest of the measurements between the FO probe and the detector head in order to suppress by simple optical filtering the stem effect contribution.

The typical response of the Mn:LTB probe under ^{60}Co irradiation as function of time is illustrated in Fig. 2. The emission curve shows an abrupt rise as soon as irradiation is switched-on and a decaying behavior when irradiation is turned off. This so-called *afterglow* is usually linked to the presence of defects, which trap and release free charge carriers at room temperature during irradiation [11].

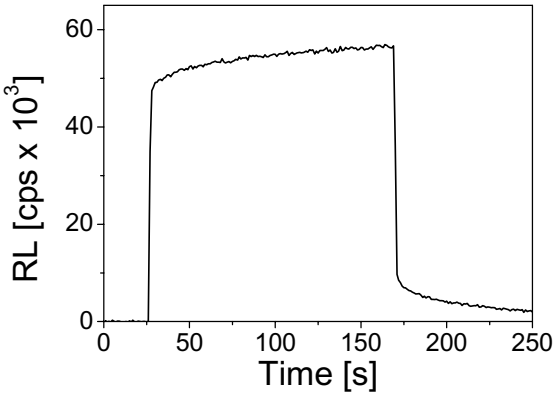

Fig. 2 Radioluminescent curve of the Mn:LTB FO probe obtained at 5mm water-depth in ^{60}Co (dark counts have been previously subtracted).

In Fig. 3 the PDD obtained by using the Mn:LTB probe is compared to that obtained in identical conditions with the ionizing chamber. As a relative estimate of the dose absorbed by the FO probe, the integral under the RL curve between switch-on and switch-off instants has been used. As can be seen from the figure both curves reach their maxima at 5 mm water depth, as expected [25]. Besides, they match each other fairly well within the whole depth range of interest (5-35 mm). Within the build-up region differences between the response of the FO probe and the chamber are observed mainly due to the different effective

volumes and materials and the fact that there is no electronic equilibrium. These results imply that in principle and at ^{60}Co photon energies, the Mn:LTB FO probe has an energy response similar to water. A second PDD reading (not shown in Fig. 3) performed with the Mn:LTB probe by going back up to the water surface rendered similar results to those depicted in the figure.

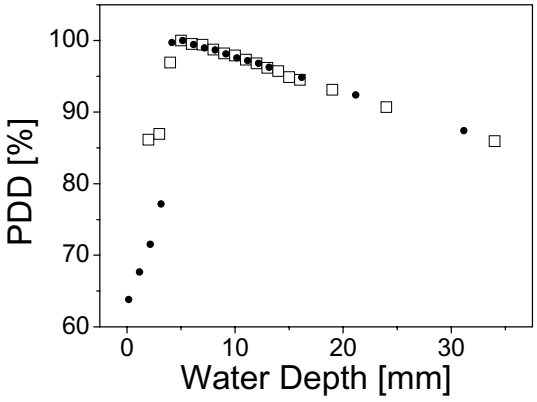

Fig 3 Percent depth dose curve obtained with the Mn:LTB probe (hollow squares) and a standard ionizing chamber (filled circles)

IV. CONCLUSIONS

Samples of tissue-equivalent LTB doped with different activators have been investigated in order to determine the most suitable compound to be used as detector in a FO dosimetry system. Mn-doped LTB has been finally chosen because of its RL spectral component centered at 600 nm, which allows to remove the contribution of the spurious luminescence showing up at shorter wavelengths by means of a long-pass optical filter having cut-off wavelength at 530 nm. A FO probe featuring a piece of Mn-activated LTB at its sensitive end has been built and successfully tested against the response of a standard ionizing chamber in a water phantom experiment.

The results of the present work demonstrate the feasibility of using LTB as a base for developing tissue-equivalent FO dosimetry probes, which could be employed for absolute dosimetry after calibration. The physical characteristics of the FO method make it ideal to perform in-vivo measurements in the context of radiotherapy treatments.

REFERENCES

1. Dixon P, O'Sullivan B (2003) Radiotherapy quality assurance: time for everyone to take it seriously, Eur J Cancer 39:423–429
2. Shikama T, Toh K, Nagata S et al (2006) Optical dosimetry for ionizing radiation fields by infrared radiolumines-cence, Meas. Sci. Technol. 17:1103–1106 DOI:10.1088/0957-0233/17/5/S27
3. Toh K, Shikama T, Nagata S et al (2003) Search for radioluminiscent materials working at elevated temperatures, Fus Sci Technol 44:475
4. Justus B, Falkenstein P, Huston A et al (2004) Gated fiber-optic-coupled detector for in vivo real-time radiation dosimetry, Appl Opt 43:1663.
5. Archambault L, Beddar A, Gingras L et al (2006) Measurement accuracy and Cerenkov re-moval for high performance, high spatial resolution scintillation dosimetry, Med. Phys. 33:128
6. Frelin A, Fontbonne J, Ban G et al (2006) A New Scintillating Fiber Dosimeter Using a Single Optical Fiber and a CCD Camera, IEEE Trans Nucl Sci 53:1113
7. Mones E, Veronese I, Moretti F et al (2006) Feasibility study for the use of Ce^{3+}-doped optical fibres in radiotherapy, Nucl Instr Meth Phys Res A 562:449–455
8. Marcazzó J, Henniger J, Khaidukov NM et al (2007) Efficient crystal radiation detectors based on Tb^{3+}-doped fluorides for radioluminescence dosimetry, J Phys D: Appl Phys 40:5055-5060.
9. Bondarenko AV, Dyad'kin AP, Kashchuk YA et al (2006) Testing a Fiber-Optic Ionizing-Radiation Detector, Instr Exp Tech 49:187–189
10. Aznar M, Hemdal B, Medin J et al (2005) In vivo absorbed dose measurements in mammography using a new real-time luminescence technique, Brit J Radiol 78:328–334 DOI: 10.1259/bjr/22554286
11. Damkjær S, Andersen C, Aznar M (2008) Improved real-time dosimetry using the radioluminescence signal from Al_2O_3:C, Rad Meas 43:893 – 897
12. Marckmann C, Aznar M, Andersen C et al (2006) Influence of the stem effect on radioluminescence signals from optical fibre Al_2O_3:C dosemeters, Rad Prot Dosim 119:363–367 DOI:10.1093/rpd/nci507
13. Suchowerska N, Lambert J, Nakano T et al (2007) A fibre optic dosimeter customised for brachytherapy, Rad Meas 42: 929-932 (LUMDETR 2006) DOI:10.1016/j.radmeas.2007.02.042.
14. Beddar A, Kinsella T, Ikhlef A et al (2001) A Miniature "Scintillator-Fiberoptic-PMT" Detector System for the Dosimetry of Small Fields in Stereotactic Radiosurgery, IEEE Trans Nucl Sci 48: 924-928
15. Zubia J, Arrue J (2001) Plastic Optical Fibers: An Introduction to Their Technological Processes and Applications, Opt Fiber Technol 7:101-140 DOI:10.1006/ofte.2000.0355
16. Fontbonne J, Iltis G, Ban G et al (2002) Scintillating Fiber Dosimeter for Radiation Therapy Accelerator, IEEE Trans Nucl Sci 49:2223
17. Nowotny R (2007) Radioluminescence of some optical fibres, Phys. Med. Biol. 52:N67–N73 doi:10.1088/0031-9155/52/4/N01
18. Prokic M (2001) Lithium borate solid TL detectors, Rad Meas 33:393
19. Ignatovych M, Holovey V, Watterich A et al (2003) UV and electron radiation-induced luminescence of Cu- and Eu-doped lithium tetraborates, Rad Phys Chem 67:587–591.
20. Kelemen A, Holovey V, Ignatovych M (2008) Relative yields of radioluminescence and thermoluminescence in manganese- and silver-doped lithium tetraborate phosphors, Rad Meas 43:375-378
21. Prokic M (2002) Dosimetric Characteristics of $Li_2B_4O_7$:Cu,Ag,P Solid TL Detectors, Rad Prot Dosim 100:265-268.
22. Prokic M (1990) Progress in Thermoluminescence Dosimetry at the Institute of Nuclear Sciences, Vinca, Rad Prot Dosim 33:99-102.
23. Can N, Karali T, Townsend P et al (2006) TL and EPR studies of Cu, Ag and P doped $Li_2B_4O_7$ phosphor, J. Phys. D: Appl. Phys. 39:2038–2043 DOI:10.1088/0022-3727/39/10/009
24. Holovey V, Sidey V, Lyamayev V et al (2007) Influence of different annealing conditions on the luminescent properties of $Li_2B_4O_7$:Mn single crystals, J Phys Chem Sol 68:1305–1310
25. Johns H E, Cunningham J R (1983) The physics of radiology. Fourth Edition. Charles C Thomas Publisher.

Applicability of Imaging Plates for Individual Monitoring

M.B. Greiter, D. Regulla, and C. Hoeschen

Helmholtz Zentrum München, German Research Center for Environmental Health, Neuherberg, Germany

Abstract— **Imaging plates commonly replace analogue film in radiography, yet not in individual monitoring. One reason for this is the temporal instability of the optically stimulated luminescence signal over prolonged storage time, termed 'fading'.**

The present investigation comprises measurements of non-commercially available imaging plate prototypes of the BaFBr:Eu type in order to test their applicability to individual monitoring. Results are included for relative luminescence yield, reusability, dose response, photon energy-dependence of response, and fading.

Keywords— **imaging plate, individual monitoring, optically stimulated luminescence**

I. Introduction

By recording a two-dimensional image instead of a single dose value, radiographic film badges as dosimeters provide information on exposure conditions beyond pure accumulated dose. When exposed to a radiation field, a film package encased in a set of metal and polymer filters may allow evaluating the radiation quality from the differences of the optical density in the areas covered by the filters. Furthermore, radiation incidence direction, source or dosimeter movement during irradiation, distance to a point source, and/or backscatter from a person or object can eventually be derived from the edge profiles of the filter shadows.

Imaging plates based on optically stimulated luminescence (OSL) [1] commonly replace films in radiographic applications. Current imaging plates are optimized concerning high sensitivity to ionizing radiation and good spatial resolution, but the application in radiography does not need stable long-term storage of recorded latent images. The latter is a severe problem in medium- to long-term individual monitoring, since a temporal change in the dose response cannot be corrected from the image data alone if the time of exposure is unknown. Loss of luminescence intensity over prolonged storage time, termed fading, is caused by thermal release of electrons from trap states which could otherwise be stimulated optically and contribute to OSL.

We investigated several slightly different, non-commercially available samples of imaging plates concerning the values and variabilities of properties relevant to individual monitoring, including dose response, irradiation energy dependence, and fading. Our aim is to assess whether slight variations in chemical composition or manufacture processes can provide imaging plates suitable for individual monitoring.

II. Methods

Imaging plate samples provided by Agfa Healthcare N.V., Mortsel, Belgium were subjected to several test cycles of irradiation, (optional) storage and thermal pretreatment, readout, and bleaching. All 32 investigated samples consisted of a BaFBr:Eu-containing lacquer coating on a transparent polyethylene terephthalate (PET) carrier, with slight differences in chemical composition and manufacture process. Overall sample thickness was 0.47 – 0.48 mm, whereof 0.21 mm were taken up by the PET carrier. The samples were cut to a size of 30 mm x 41 mm, similar to type 2 imaging plates for dental radiography. 28 of the 32 samples were paired, i.e. identical in composition and manufacture, resulting in 18 different types of imaging plates.

Irradiations were performed with the following sources of the Secondary Standard Dosimetry Laboratory (SSDL) of the Helmholtz Zentrum München:

- Four ^{137}Cs gamma radiation sources (662 keV) with dose rates ranging from 1.9 mGy·h^{-1} to 2.2 Gy·h^{-1}.
- A ^{60}Co gamma radiation source (1.17 MeV and 1.33 MeV) with a dose rate of 4.67 mGy·h^{-1}.
- Two filtered x-ray sources with ISO narrow spectrum series radiation qualities, ranging from N30 (additional filtration ~4 mm Al; half-value layer (HVL) 1.2 mm Al; 26 keV mean energy) to N300 (additional filtration of ~5 mm Pb, ~3 mm Sb, and 4 mm Al; HVL 6.2 mm Cu; 248 keV mean energy). Due to stronger filtering, N series radiation qualities have higher effective energies and narrower spectral peaks in comparison to RQA radiation qualities of equal tube voltage.

Doses are reported as air kerma free in air. All samples were irradiated behind a layer of 3 mm PMMA, achieving dose build-up for gamma radiation.

During the time between start of irradiation and scanning process, samples were kept in envelopes protecting them against ambient light (Gendex size 2 barrier envelopes). Samples were stored and transported in light-tight plastic casings. Irradiated samples were exposed to a maximum illuminance of 5 lux in ambient light while being handled in envelopes, and to less than 2 lux in green light during

O. Dössel and W.C. Schlegel (Eds.): WC 2009, IFMBE Proceedings 25/III, pp. 371–374, 2009.
www.springerlink.com

sample mounting onto the scanner drum. After scanning, samples were exposed to > 500 lux for at least 10 min before reuse. After irradiation with 10 mGy Cs gamma radiation, no image could be recorded by the scanner system following this bleaching procedure.

The recorded temperature range during irradiation, transport and storage was 21 – 26 °C. The time between irradiation and first readout was in the range of 7 - 29 min, except in the fading experiments.

Sample readout was performed with a commercial scanner for dental image plates (DenOptix™ USB; Gendex Dental Systems / KaVo Dental GmbH, Hamburg, Germany). Image resolution was set to 300 dpi, equivalent to ~12 mm^{-1} or a pixel length and width of 85 µm. Images were evaluated with IDL 6.3 (Research Systems Inc./ITT Visual Information Solutions). A central area of 200 x 200 pixels was used for evaluation.

III. Results and Discussion

A. Dose response and reusability

A subset of samples was irradiated with doses in the range of 10 µGy to 10 mGy from ^{137}Cs sources (662 keV). The observed dose response is strictly linear in this dose range, as shown in Figure 1. The observable dose range is limited by the scanner through its 16 bit grayscale depth. Although the current hardware prevented evaluation of higher doses, imaging plates in general have been reported to feature a linear dose response up to 10 Gy [2].

The relative standard deviation of the evaluated pixel values was 25 – 36 % for the lowest detectable dose of 10 µGy, and decreased to 2 – 3 % for doses ≥ 2.5 mGy.

Luminescence intensity after exposure to 1 mGy of 662 keV gamma radiation differs by a factor of 2.4 between the most extreme samples. The intensity differences between members of sample pairs belonging to the same homogenous original imaging plate are comparatively small (< 7 %; 2.7 % on average).

Five repeated cycles of exposure to 5 mGy 662 keV gamma radiation, readout, and bleaching showed no sign of sample ageing or memory effects up to a cumulative dose of 25 mGy. The measured doses agreed to within ± 4 % of the mean of all 5 cycles.

In a dosimetric application, a single imaging plate could thus be reused several times. Individual calibration would be possible either per plate or per batch, if all individual plates from a single batch were sufficiently similar.

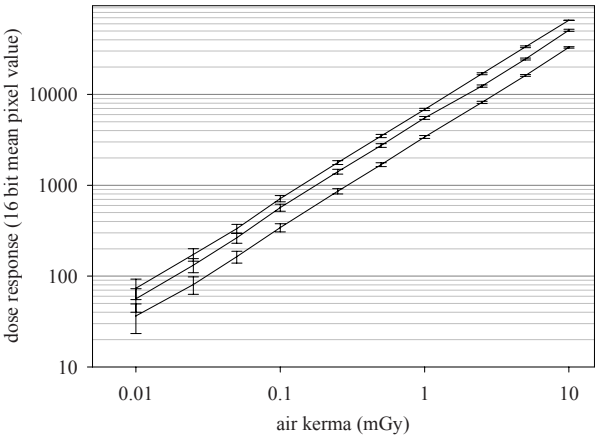

Fig. 1 Dose response for 662 keV gamma radiation. Error bars represent single standard deviations of pixel values in the evaluated image area. The three selected imaging plates represent the range of observed relative responses.

B. Photon energy dependence

Figure 2 shows the energy dependence of the OSL signal after exposure to 75 µGy for various effective energies in the range between 26 keV (ISO N30 radiation quality) and 1.25 MeV (mean energy of ^{60}Co gamma rays). The figure comprises only the four samples with the largest deviation from the mean normalized response in order to illustrate the small intersample variation.

All investigated samples feature a similar range of two orders of magnitude of conversion efficiency between radiation dose and OSL intensity. The maximal efficiency is reached at ~ 50 - 60 keV, slightly above the K edges of Ba (37.4 keV) and Eu (48.5 keV)[3]. The drop in yield is also in accordance with the energy dependence of the x-ray attenuation coefficients of Ba (atomic number Z = 56), F (Z = 9), and Br (Z = 35) in a mixture of roughly 1:1:1. For a bare image caused by moderate energy x-rays, the minimal detectable dose is as low as 0.1 – 0.2 µGy.

In a routine dosimetric application, this pronounced energy dependence must be compensated for, since the radiation quality will likely not be known for any exposure. A similar problem is known from conventional film, which contains a large amount of Ag (Z = 47). It is countered by a filtering approach with several fields of different metal and/or polymer plates. A similar approach has been shown to be applicable for imaging plate-based dosimetry [4].

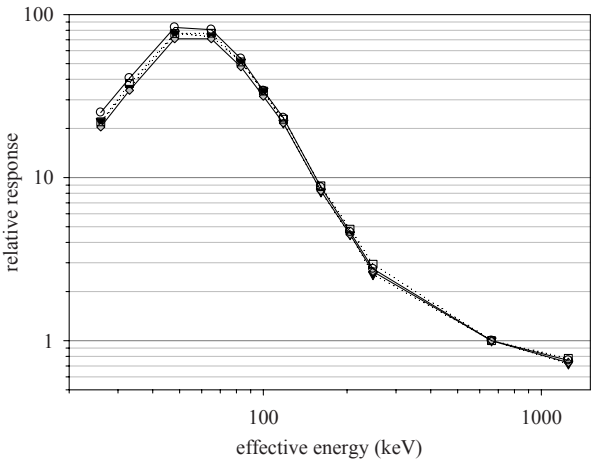

Fig. 2 Energy dependence of OSL response, normalized to gamma radiation from a ^{137}Cs source (662 keV).

C. Fading

Signal fading is attributed to thermal excitation and depletion of shallow trap states during storage. Annealing, i.e. short-term storage at elevated temperature, between irradiation and measurement was found to reduce fading [5]. The expected effect of annealing is the controlled depletion of shallow trap states which can be both thermally and optically emptied, and contribute to OSL; the remaining OSL signal then originates from deeper, thermally more stable traps.

Fading can bias dose determination if the time of exposure is unknown during a monitoring period. The maximum duration of a monitoring period is in principle arbitrary according to the German type test requirements of the Physikalisch-Technische Bundesanstalt (PTB) [6]; however, current film badge dosimeters are typically evaluated once per month. Therefore, fading over up to 30 d was examined for the investigated sample variety.

During the annealing procedure, samples were placed on a preheated metal plate in an oven at ~ 80 °C for 30 min. The signal loss caused by this procedure was sample-dependent, but similar within pairs; it ranged from about 50 % to 80 %.

For the fading experiments, samples were exposed to 10 mGy of 662 keV gamma radiation. Annealing and OSL measurements were performed for storage periods up to 30 d. After correction for annealing, the signal loss over 30 d in relation to immediate readout reaches 20 % to 80 %. The overall signal loss over 30 d, including annealing, lies between 40 % and 95 %.

Without further correction methods, none of the investigated samples features an OSL signal sufficiently stable for individual monitoring over a 1 month-period. Even the best sample with 20 % loss after annealing correction lies beyond the dose-dependent upper limit of the dose variation coefficient of 5 – 15 % as set by the aforementioned type test requirements. However, the large variation between samples gives hope for future optimizations.

IV. Conclusion

The investigated variety of imaging plates presents a highly sensitive radiation detector, especially for x-rays of moderate energy. Their strictly linear dose response, good reproducibility, as well as their mechanical flexibility and imaging properties allow them to be used for various applications in passive short-term dosimetry.

In contrast, their pronounced energy dependence and fading properties prevent their adoption in medium- to long-term individual monitoring as a surrogate for radiographic film. While filtering approaches can compensate for energy dependence, two alternatives could help to alleviate the fading problem.

First, as was the initial intention of this test, further variation in chemical composition and manufacture processes will possibly provide an improved imaging plate concerning the fading aspect. Such a plate could be used similar to film.

Second, imaging plates and any other suitably stable detectors (e.g. TLD or active dosimeters) could be combined, the latter accounting for an accurate cumulative dose estimate. In this case, the filtered OSL image would provide the additional information now reserved to film badges, such as movement during exposure, angle of incidence, and radiation quality.

Acknowledgment

The authors are grateful to P. Leblans (Agfa) for providing the imaging plate samples as well as for an extended discussion. We would like to thank M. Keusch and F. Wagner for their assistance in the measurements. This project was funded by resources from W. Wahl from the ‘Auswertungsstelle’ (personnel monitoring service) of the Helmholtz Zentrum München.

References

1. McKeever S W S (2001) Optically stimulated luminescence dosimetry. Nucl Instrum Meth B 184:29-54
2. Pradhan A, Lee J, Kim J (2008) Recent developments of optically stimulated luminescence materials and techniques for radiation dosimetry and clinical applications. J Med Phys 33:85-99

3. Hubbell J H, Seltzer S M (2004) Tables of X-Ray Mass Attenuation Coefficients and Mass Energy-Absorption Coefficients (version 1.4). [Online available at http://physics.nist.gov/xaamdi]
4. Taniguchi S, Yamadera A, Nakamura T et al. (1999) Development of a New Personal Dosemeter for Low Energy X Rays by Using an Imaging Plate. Radiat Prot Dosim 85:7-10
5. Ohuchi H, Yamadera A, Baba M (2003) Development of a new passive integral dosemeter for gamma ray monitoring using an imaging plate. Radiat Prot Dosim 107:239-246
6. PTB (2007) PTB-Anforderungen: Strahlenschutzmessgeräte - Personendosimeter zur Messung der Tiefen- und Oberflächen-Personendosis; PTB-A 23.2. [Online available at http://www.ptb.de/de/org/q/q3/q31/ptb-a/ptb-a.htm]

Corresponding author:

Author: Dr. Matthias Greiter
Institute: Helmholtz Zentrum München
Street: Ingolstädter Landstraße 1
City: 85764 Neuherberg
Country: Germany
Email: matthias.greiter@helmholtz-muenchen.de

Evaluation of radiation doses inside a phantom of mammography utilizing Compton spectrometry

J.N. Almeida Jr.[1], R.A. Terini[1], S.B. Herdade[2], T.C. Furquim[2].

[1] Departamento de Física, Pontifícia Universidade Católica (PUC-SP), São Paulo, SP, Brasil
[2] Instituto de Eletrotécnica e Energia, Universidade de São Paulo (IEE/USP), São Paulo, SP, Brasil

Abstract – **Absorbed dose in breast cannot be measured directly in mammography equipments. Therefore, methods based on Compton spectrometry are alternatives to evaluate dose distributions in a simulator of human breast material. In this work, a CdTe detector was used for the Compton spectrometry measurements of radiation scattered at approximately 90º by a PMMA cylinder. To reach the objective, the necessary reconstruction of primary spectra (in units of photon fluence) has been made using Klein-Nishina and Compton theories, followed by a determination of air kerma and, finally, of absorbed dose values in the breast phantom. Incident X-ray spectra and depth-dose distributions in a BR-12 phantom were determined. Results presented here were obtained for mammography range (28 to 35 kV) and show good agreement with literature data.**

Keywords - **Compton spectrometry, mammography, depth-dose, CdTe detector, BR-12 phantom.**

I. Introduction

For the screening of patients, in the prevention of breast cancer, X-ray mammography is widely used. Nevertheless, in this procedure, there is a small but significant risk of radiation induced carcinogenesis. Therefore, dosimetry in mammography is mandatory.

From the measured incident air kerma, conversion factors can be applied to evaluate the mean glandular dose (MGD), a quantity relevant for the cancer risk estimation in mammography. These conversion factors may be obtained by Monte Carlo calculations or from depth-dose measurements in homogeneous breast phantoms [1-2].

In the past, depth-dose measurements have been carried out by utilizing TLD chips or ionization chambers [1]. In this work, results of in-phantom depth-dose distributions and X-ray spectra in mammography determined by means of a Compton spectrometer are presented. For this purpose, plates of a breast simulator material were used, located in the incident X-ray beam of a clinical mammographic equipment, for voltages in the range 28 to 35 kV. A radiation scatterer was utilized in some depths inside the phantom, for the spectrometric measurements.

II. Materials and methods

A CdTe spectrometer (Amptek, Inc.) was used for the measurement of the spectra of scattered photons. X-rays produced by a GE Senographe 700T mammography equipment Mo/30μmMo anode/filter combination were measured, after scattering by a 6 mm diameter Lucite (PMMA) cylinder, located in the primary beam, under certain thickness of a BR-12 (50% glandular-50% fat) breast phantom (Nuclear Associates, NY, USA). This phantom is formed by rectangular plates, being utilized 6 cm as the total thickness, for 30 and 35 kV and 4cm, for 28kV. Data were obtained for 100mAs, adapting a Pb diaphragm (1cm in hole diameter) in the tube output. The distance from the phantom surface to the tube focal spot was 58cm (for 30 and 35kV) and 60 cm (for 28 kV).

Previously, the spectrometer was calibrated by means of X and γ-rays of known energies emitted from radioactive sources of ^{241}Am and ^{133}Ba. In sequence, from each measured spectrum of the scattered and energy calibrated mammographic beam, the scattering angle (in degrees) was determined by the Compton's theory, utilizing measured energies of Mo characteristic X-rays (K_α–17.48keV, and K_β – 19.61keV[3]) incident and scattered, through eq. (1), with E and E' in keV:

$$\theta = \cos^{-1}\left(1-511.\left(\frac{E-E'}{E.E'}\right)\right) \quad (1)$$

To obtain the scattered beam energy E', lorentzian curves have been fitted to the spectrum peaks, by means of a least square method, for analysis of multiple peaks. For each calibrated spectrum, five peaks have been considered: the greatest of them was related to the shift of K_α X-rays, and the second one, to the shift of K_β X-rays. Between these peaks, there was a peak referring to the original energy of Molybdenum K_α rays and, after the smaller peak, the original energy of K_β rays. Figure 1 shows the fit, for a spectrum of a scattered beam that undergone attenuation from 3cm of BR-12, for 30kV.

Thus, using equation 1, one gets the scattering angle θ, calculated for each thickness of attenuation in the breast phantom, for 28, 30 and 35kV. All spectra of scattered X-

O. Dössel and W.C. Schlegel (Eds.): WC 2009, IFMBE Proceedings 25/III, pp. 375–378, 2009.
www.springerlink.com

ray beams were corrected for the detector intrinsic full energy efficiency, K-escape and photon attenuation by the absorbers between scatterer and detector sensitive region.

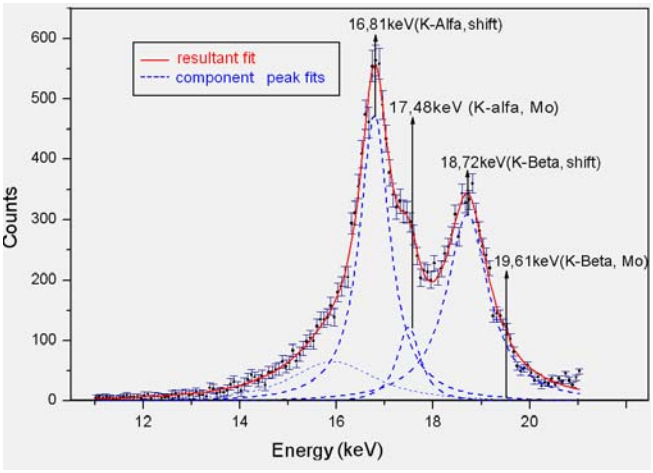

Fig. 1 Spectrum (ROI) of scattered and calibrated X-ray beam, for Mo-Mo combination, with 3cm of BR-12 attenuation, for 30kV.

Figure 2 shows the equipment used in the measurement of spectra of the beams scattered by the PMMA cylinder, including the Compton spectrometer and BR-12 plates.

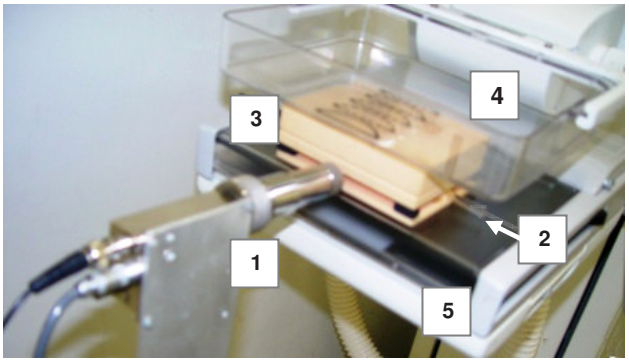

Fig. 2 Experimental setup showing (1) the CdTe spectrometer, with collimator, support and preamplifier, (2) the PMMA scatterer rod between (3) plates of the BR-12 phantom, which is placed between (4) the compression paddle and (5) the image receptor, at the mammography equipment.

For the reconstruction of primary beam spectra, from the scattered beams, Compton and Klein-Nishina theories have been used. The contribution of the coherent scattering should be subtracted, because it is relevant in the mammography energy range (up to 18%)

In this procedure, a method based on that proposed by Yaffe *et al.* [4] and Matscheko *et al.* [5] was used. Then, it was determined the fluence rate, Φ_{inc} (E, θ), of the beam incident on the scatterer, from the rate of photons undergoing Compton scattering, $N_{d,incoh}$ (E,θ), using the incoherent scattering cross section, $d\sigma/d\Omega$ (E, θ), in [m²molec^{-1}.sr^{-1}] units, as in Eq. (2):

$$\left(\frac{d\sigma}{d\Omega}(E,\theta)\right)_{incoh} = \left(\frac{r_0^2}{2}\right).(1+\cos^2\theta).(F_{KN}(E,\theta)).(S(\chi,Z)) \quad (2)$$

Eq. 2 is corrected for electrons binding energy in atoms of the scatterer [3], through the incoherent scattering function, S (χ, Z) [6], as well as parameters related to the experimental setup. Moreover, r_0 = 2,81794 x 10^{-13} cm is the electron classic radius; $\chi = [\text{sen}(\theta/2)]/\lambda$, is the photon momentum transferred to the electron; λ is the photon wavelength; Z is the PMMA effective atomic number and F_{KN} is the Klein-Nishina factor [4], given by

$$F_{KN}(E,\theta) = \left[\frac{1}{1+\alpha(1-\cos\theta)}\right]^2 \cdot \left[1+\frac{\alpha^2(1-\cos\theta)^2}{1+\alpha(1-\cos\theta)(1+\cos^2\theta)}\right] \quad (3)$$

being $\alpha = \frac{E(keV)}{511}$.

Thus, the incident photon fluence rate $\Phi_{inc}(E,\theta)$, has been finally obtained by equation (4):

$$\Phi_{inc}(E,\theta) = \frac{N_{d,incoh}(E',\theta)}{M.\left(\frac{d\sigma}{d\Omega}(E,\theta)\right)_{incoh}.d\Omega.f(E,E',t).na} \quad (4)$$

where $N_{d,incoh}(E',\theta)$ is the photon rate incident on the detector, scattered by Compton process (in the Lucite cylinder), and corrected by detector intrinsic efficiency; $M = \rho.V$, is the irradiated mass of the scatterer, being ρ, the PMMA density, $V = \pi.r^2.h$, with r = 0,3 cm, the radius of the PMMA cylinder, and h, the cylinder length that scatters photons which reach the detector; na is the number of molecules.g^{-1} in PMMA; $d\Omega$ is the detection solid angle for the scattered radiation [5]; $f(E, E',t)$ is a correction factor for absorption of photons in the scatterer, before and after scattering, which depends on E and E', as well as on the scatterer effective thickness (t).

Air kerma spectrum (K_{air}), in [mGy.mAs^{-1}.keV^{-1}] units, could be obtained from the primary beam fluence spectrum as a function of energy, (Φ_{inc} (E, θ)), by equation (5):

$$K_{Air}(E) = \Phi_{inc}(E,\theta) \cdot \left(\frac{\mu_{Tr}}{\rho}\right)_{Air} \cdot 1{,}602 \cdot 10^{-19} \cdot \left[\frac{10^3}{mAs}\right] \quad (5)$$

where $(\mu_{Tr}/\rho)_{Air}$ is the air mass coefficient for energy transferred.

Dose spectrum could be determined utilizing experimentally measured coefficients for energy absorption in BR-12 ($(\mu_{Ab}/\rho)_{BR\text{-}12}$), obtaining (also in [mGy.mAs^{-1}.keV^{-1}] units) the absorbed dose in BR-12 breast phantom, as shown in eq. (6):

$$D_{BR\text{-}12}(E) = \Phi_{inc}(E,\theta) \cdot \left(\frac{\mu_{Ab}}{\rho}\right)_{BR\text{-}12} \cdot 1{,}602 \cdot 10^{-19} \cdot \left[\frac{10^3}{mAs}\right] \quad (6)$$

With the air kerma and BR-12 absorbed dose spectra, one determines each quantity integrating the respective obtained spectra, in [mGy.mAs^{-1}] units. If the product current-time is known, the respective values, in [mGy] units, are found.

Relative absorbed doses in BR-12, estimated by the spectrometric method, from 28 to 35kV, have been compared with data gotten with an ionization chamber (6M, Radcal, Co.), and with TLD [1].

III. Results

Values of depth-dose, as well as half-value layers and scattering angles, obtained for 28, 30 and 35kV are listed in Table 1, for unattenuated case and for BR-12 thickness of 1, 2, 3 and 4 cm (only for 30 and 35 kV) above the PMMA scatterer. Values of HVL obtained with an ionization chamber are presented in Table 2. Data, in Table 2, were obtained at the same distance from the phantom surface to the tube focal spot used in spectrometric measurements.

Table 1 Results from Compton spectrometry of absorbed dose in BR-12 ($D_{BR\text{-}12}$), air kerma (K_{air}) –corrected by depth, half-value layer (HVL) and scattering angles obtained using the Compton spectrometry method.

Voltage (kV)	Depth in BR-12 (cm)	Scattering angle (degree)	$D_{BR\text{-}12}$ (mGy)	K_{air} (mGy)	HVL (mm Al)
28	**0**	**103.05(5)**	**15.81**	**18.93**	**0.39**
	1	102.10(4)	6,91	8,21	0.44
	2	98.00(4)	3.85	4,57	0.46
	3	97.31(4)	1.67	1,96	0.49
30	**0**	**102.38(5)**	**22.83**	**27.14**	**0.40**
	1	101.28(5)	10,27	12.14	0.44
	2	99.67(4)	5,74	6.77	0.48
	3	99.47(4)	2,47	2.54	0.50
	4	98.67(4)	1,21	1.41	0.53
35	**0**	**100.68(5)**	**41.90**	**45.69**	**0.44**
	1	99.02(4)	18.33	19.76	0.48
	2	98.10(4)	8.98	10.12	0.52
	3	97.31(4)	4.49	5.01	0.55
	4	96.80(4)	2.70	2.98	0.58

Table 2 Results obtained with ionization chamber for absorbed dose in BR-12 surface ($D_{BR\text{-}12}$), incident air kerma (K_{air}) and half-value layer (HVL) obtained using a mammography ionization chamber. Uncertainties are expressed with coverage factor k = 1.

Voltage (kV)	$D_{BR\text{-}12}$ (mGy)	K_{air} (mGy)	HVL (mm Al)
28	9.46(34)	8.68(28)	0.38(1)
30	12.57(44)	11.54(37)	0.40(3)
35	19.42(69)	17.82(58)	0.44(1)

In Table 1, for comparison, values of air kerma and absorbed dose, in each phantom depth, were found correcting the actual values by the inverse square law, for each position of the PMMA scatterer, relative to the BR-12 surface.

In Figure 3, for example, a comparison among the primary spectra is shown, for 30 kV, in photon fluence units [photons.cm^{-2}.keV^{-1}], for all phantom attenuations. The influence of attenuation can be perceived, as is observed an intensity reduction and a change in the ratio between the intensities of K-alpha and K-beta X-ray peaks.

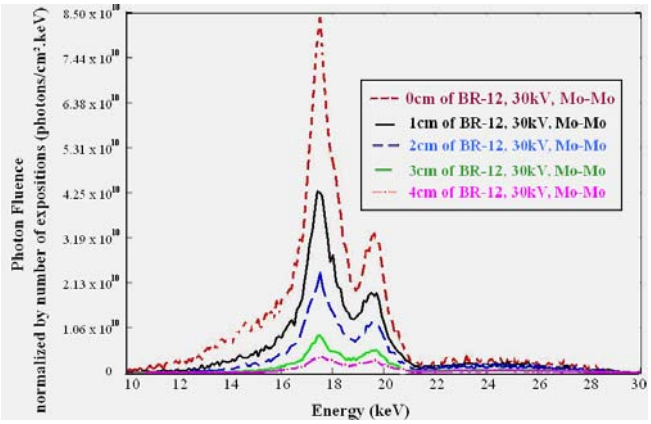

Figure 3 Spectra of photon fluence (normalized to the number of expositions of the spectrum obtained without attenuation), for all BR-12 thickness, for 30kV.

Influence of voltage can be noted in Figure 4. Photon fluence spectra of incident beams can be observed (at BR-12 surface), from 28 to 35kV. The largest difference among these spectra is at the end of the continuous region.

Figure 5 shows BR-12 depth-dose distributions obtained for 28, 30 and 35 keV. Values were fitted to first order exponential curves, with very close results. In this figure, dashed line, solid line and short-dash line represent, respectively, the relative dose (in units of incident air kerma) for 35kV, 30kV and 28 kV.

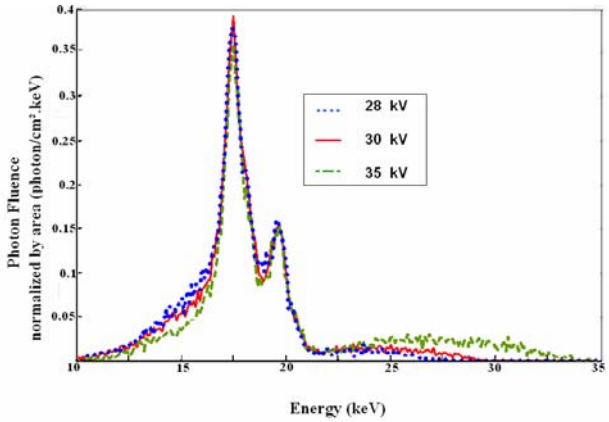

Figure 4 Comparison among spectra of photon fluence (normalized by areas) in the mammography range (28, 30 and 35 kV).

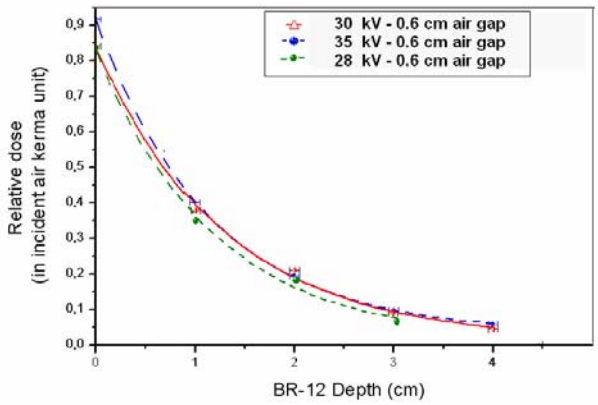

Figure 5 Relative dose as a function of different thicknesses of BR-12, for 28, 30 and 35kV.

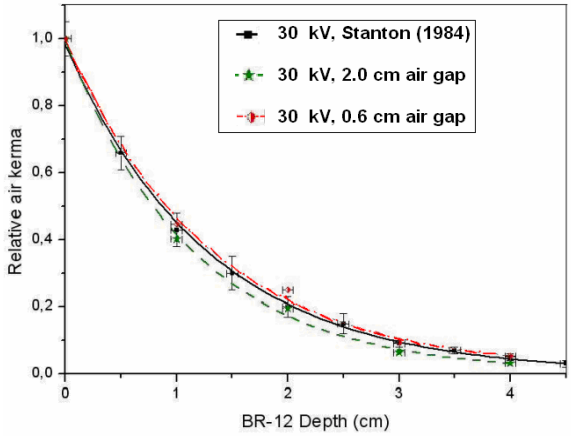

Figure 6 Comparison between dose curves as a function of the BR-12 depth, with scatterer space having 2.0 cm (dashed line) and 0.6 cm (dot-dash line) of air gap, and with data found in literature (solid line) [1].

IV. Analysis

During the analysis of the influence quantities that affect the proposed method, spectrometric measurements have been carried out adjusting two different air gaps (2.0 and 0.6 cm) between the plates where PMMA scatterer is situated (inside the phantom).

Plotting the curve of relative air kerma as a function of BR-12 depth, such values fitted to a first order exponential curve, in a similar way as in Stanton et al [1], with TLD. This can be seen in Figure 6, for 30 kV, with scatterer air gap of 2.0 cm and 0.6 cm (with better agreement).

V. Conclusions

In this work the results of in-depth distributions of dose and X-ray spectra are presented, for a mammography equipment, obtained using a BR-12 breast phantom.

The described method is a good alternative for determination of relative depth-dose in breast phantoms and beam spectra in clinical environments, through spectrometric measurements, utilizing Compton effect with the respective reconstruction of the primary beam incident on the scatterer.

In the near future, the method should be also utilized with other anode/filter combinations and in the evaluation of the mean glandular dose (MGD).

Acknowledgment

We would like to thank to Brazilian agencies CNPq and FAPESP, by the financial support; to IAEA, for providing the mammography X-ray equipment, and to IEE/USP, for the use of infra-structure and staff help.

References

1. Stanton L et al. (1984) Dosage Evaluation in Mammography. Radiology 150: 577-584.
2. Dance D R et al. (1999) Breast dosimetry. Appl. Rad. Isot. 50:185-203.
3. Johns H E et al. (1986) The physics if radiology, 4th ed. Charles C. Thomas, Springfield, IL, USA.
4. Yaffe M et al. (1976) Spectroscopy of diagnostic X-rays by a Compton-scatter method. Med. Phys. 3: 328-334.
5. Matscheko G et al. (1987) A Compton scattering spectrometer for determining X-ray photon spectra, Phys. Med. Biol. 32: 577-594.
6. Tartari A, Casnati E, Bonifazzi C, Baraldi C (1997) Molecular differential cross section for x-ray coherent scattering in fat and polymethyl methacrylate. Phys. Med. Biol. 42: 2551-2560.

Author: Ricardo Andrade Terini
Institute: Pontifícia Universidade Católica (PUC-SP)
Street: R. Marquês de Paranaguá, 111, Consolação, 01303-050
City: São Paulo, SP
Country: Brasil
Email: rterini@pucsp.br

Comparison of dose distribution of ionizing radiation in a water phantom with frequency of cytogenetic damage in a human bronchial cells

M. Konopacka[1], J. Rogoliński[1], K. Ślosarek[2]

[1] Maria Sklodowska-Curie Memorial Cancer Center and Institute of Oncology Gliwice Branch, Department of Experimental and Clinical Radiobiology, Gliwice, Poland
[2] Maria Sklodowska-Curie Memorial Cancer Center and Institute of Oncology Gliwice Branch, Department of Radiotherapy and Brachytherapy Treatment Planning, Gliwice, Poland

Abstract— **In this study we compare dose distribution of photon and electron radiation in a water phantom with a frequency of occurrence of apoptotic and micronucleated cells from human bronchial BEAS-2B and lung cancer A549 cell lines. Formation of micronuclei and apoptotic like bodies were evaluated by the cytokinesis-block micronucleus test. Measurements were performed on a five depths (3-20 cm) in a water phantom. Cells were irradiated in a beam axis or beyond field. As the irradiation source, a linear accelerator was used. Results indicate discrepancy between physical dose distribution observed on different depths in a water environment and biological effects (frequency of apoptosis and micronuclei formation). This discrepancy is specially significant for cells placed outside the field during exposure to radiation. Evaluation of these effects could be useful for modeling low-dose radiation risk and for radiotherapy protocols.**

Keywords— **Micronuclei, apoptosis, ionizing radiation, dose distribution, water phantom**

I. Introduction

Ionizing radiation consists of streams of photons or charged particles, which interact with biological molecules by depositing energy by ionisation or excitation. Interaction of ionising radiation with cellular DNA induces a wide variety of biological effects, from cell death to induction of mutations, chromosomal damage, genetic instability and carcinogenesis. It is well established that the efficiency of inducing biological effects vary not only with the absorbed dose but also with the type of radiation and its energy [1].
During radiotherapy the bunch of radiation at determined dose is directed on tumour. The inevitable effects of radiation is its penetration through body to cells placed below appropriate tumour cells. With penetration depth in the irradiated medium increases energy broadening, and the number of interactions with the fraction of scattered radiation having decreased energy becomes larger at increased depth. A larger portion of scattered radiation with energy lower than that of the incident beam, should change the biological response of irradiated cells in manner different than that predicted by dosimetric methodologies.

The aim of present work was to assess the biological effect of electron and photon radiation used commonly in radiotherapy upon cultured cells placed at various depths inside a water phantom and irradiated in different conditions: in a beam axis or outside irradiation field. The biological effects were determined using the cytokinesis-block micronucleus test. For the experiments, we selected normal human bronchial cells and a cancer cell line. To answer the question whether change of energetical spectre of radiation influence the biological response of cells we previously tested the effect of medium depth on radiation-induced genetic damage of human melanoma Sk-mel cells [2]. We have shown that in the cells exposed to 5 Gy of X radiation at either 5 or 25 cm depth in water phantom, approximately 30% more damaged cells were detected at depth of 25 cm as compared to depth of 5 cm. Next, we compared the biological response of cells with response expected based on the doses received at different depth in water phantom [3]. Our measurements showed that, the for electron radiation, with increasing medium depth the number of damaged cells were greater than expected from the corresponding received dose. In present work we exposed cells not only in a beam axis but also beyond irradiation field.

II. Material and methods

BEAS-2B (a human bronchial epithelial cell line) and A549 (a human bronchial cancer cell line) were used in experiments. The cells (10^5) in test tube suspended in culture medium were placed in a special stand on a fife depths between 3 – 20 cm. The stand with cells was placed in a water phantom and irradiated in a different conditions: in a beam axis and 4 cm outside the field. Experiments were performed for photon (6MV) and electron (22MeV) radiation generated in a linear accelerator Clinac series Varian System Company, for 300MU/min dose rate with radiation dose of 5 Gy in build-up (3 cm) depth. At least nine samples from three independent experiments were examined for each depth.

O. Dössel and W.C. Schlegel (Eds.): WC 2009, IFMBE Proceedings 25/III, pp. 379–382, 2009.
www.springerlink.com

Micronuclei were assessed *in situ* by using the cytokinesis-block technique [4]. After irradiation, the experimental and the control cells were transferred into plastic plates and supplemented with medium up to 5 ml. Next, cytochalasin B (Sigma, final concentration 2µg/ml) was added and cultures were incubated at 37^0 C. To get on optimum frequency of binucleated cells, the cultures were maintained for 46 and 48 h for BEAS-2B and A549 cells, respectively. Next, cells were washed with PBS and fixed in situ for 20 min in a cold solution of 1% glutaraldehyde (Sigma) in phosphate buffer (pH=7.5). Cells were stained by Feulgen reaction and examined under microscope. Micronuclei were scored in 500 binucleate cells per plate using standard criteria. On the same plate the cells showing condensation of chromatin characteristic for processes of apoptosis were also scored.

III. Results

The dose depth of photon or electron radiation was estimated in a water phantom and compared with the measured biological effectiveness for induction of micronuclei and apoptosis in normal (BEAS-2B) and cancer (A549) cells. The values of the micronucleated and apoptotic cells found at the depth corresponding to maximum dose (5 Gy in build up = 3 cm) was accepted as 100% and the numbers of damaged cells irradiated in higher depth were normalised to this value (relative effect).

A. Cells irradiated in axis

In a beam axis dose of radiation measured dosimetrically in water phantom decreased characteristically for photon and electron radiation, respectively. The frequency of micronucleated and apoptotic cells placed in different depth in water phantom and irradiated in axis of electron radiation as well as dosimetric curve are presented in Fig 1A. With increasing medium depth the numbers of micronucleated and apoptotic cells were greater than expected from the corresponding received dose. This discrepancy between the observed numbers of damaged cells in relation to dosimetric curve becomes visible in greater medium depth. This effect was observed for both cell lines.

For photon radiation the discrepancy between the number of micronucleated cells was visible only in BEAS-2B cells, as is showed in Fig 1B. The differences with physical dose and relative biological effect were not visible in A549 cells and apoptosis formation in BEAS -2B cells.

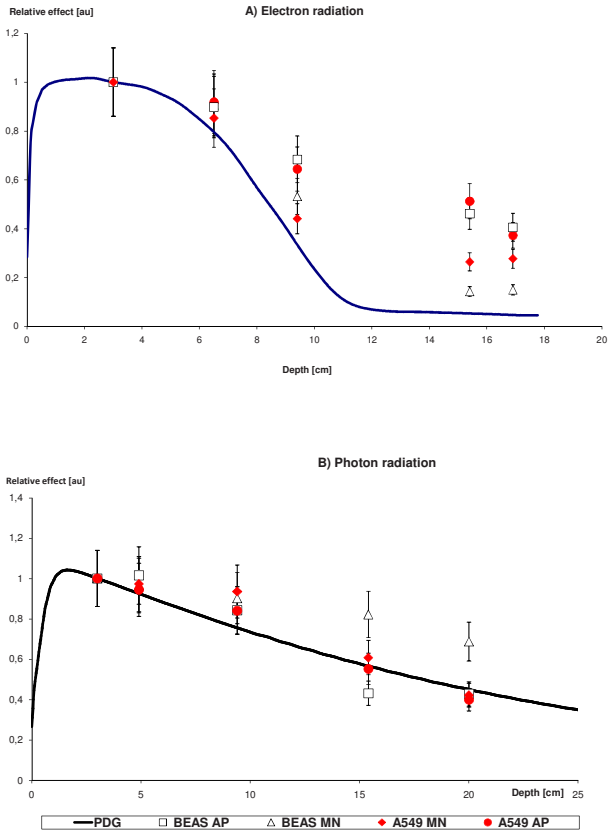

Fig.1 Comparison of the yields of micronucleated and apoptotic-like BEAS-2B and A549 cells irradiated in a beam axis, with value of electron radiation (A) and photon radiation (B) dose received in increasing medium depth in water phantom. Shown are means from three independent determination ±SD. PDG – percentage dose depth, MN – micronucleated cells, AP – apoptotic cells.

B. Cells exposed beyond irradiation field

In the next experiments cells were placed 4 cm outside the field during exposure to radiation. The numbers of micronucleated and apoptotic cells as well as dosimetric curves are presented in Fig 2A (electron radiation) and Fig 2B (photon radiation), respectively. For both types of radiation, the frequency of damaged cells placed in different depth in water phantom was higher than expected from the radiation dose calculated for these physical conditions, but independent of depth.

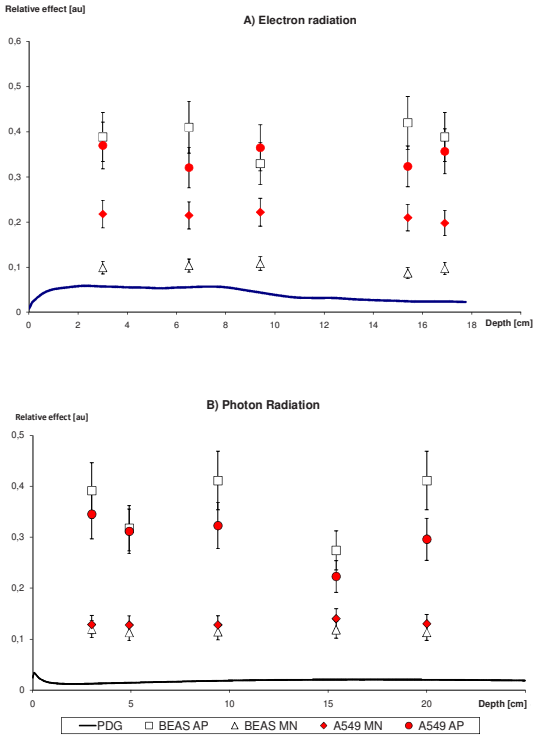

Fig.2 Comparison of the yields of micronucleated and apoptotic-like BEAS-2B and A549 cells irradiated outside field, with value of electron radiation (A) and photon radiation (B) dose received in increasing medium depth in water phantom. Shown are means from three independent determination ±SD. PDG – percentage dose depth, MN – micronucleated cells, AP – apoptotic cells.

IV. Discusson

The dose depth of photon and electron radiation emitted from accelerators used in radiotherapy was estimated in a water phantom and compared with experimentally measured biological effectiveness for induction of micronuclei and apoptosis in human normal and cancer cells. Our measurements showed that for electron radiation, at various depths, both the numbers of apoptotic and micronucleated cells were greater than expected from the corresponding received radiation dose as is presented in Fig.1. This discrepancy between observed and expected numbers of damaged cells based on the dosimetric curve becomes greater with increased medium depth. For photon radiation the relationship between penetration depth was less visible for induction of micronuclei and the number of apoptotic cells did not differ from expected value. This difference between results for electron and photon radiation can be due to better medium penetrability characteristic for photon radiation (see dosimetric curves, Fig 1 and 2). In the case of cells placed 4 cm beyond irradiation field we observed differences between physical dose distribution for both, photon as well as electron radiation and biological effects, although there was no dependence of depth.

The effects reported herein is likely to result from scattered radiation, since with increasing medium depth as well as distance of beam of axis, its proportion to the incident radiation becomes greater. It has been known that RBE (relative biological effectiveness) increase with decreasing X-ray energy and decreasing electron track length [5]. The low energy electron track produced by X-rays have large RBE. Physical calculations have shown that approximately 40% of the absorbed dose from common low LET radiations such as X-ray is deposited by low energy (0.1-5 keV) secondary electron [6]. These low energy secondary electrons responsible for the increase of RBE are the predominant agent causing of different cellular effects such as increase in the initial yield of DSBs [7].

Our results are consistent with the described above data and indicate that with increased medium depth, the radiation energy decreases and causes more biological damage in cells than could be predicted by dosimetric curve of absorbed dose. This is probably responsible for the observed effect and should be taken into consideration in both clinical practice and in treatment planning.

V. Conclusions

The discrepancy between the physical dose distribution and biological response of cells exposed at higher depth or outside radiation field may be important for modeling low-dose radiation risk for radiotherapy protocols.

Acknowledgment

This study was supported by a grant from the Ministry of Science and Higher Education, No. NN 402 4447 33.

References

1. Hill MA (1999) Radiation damage to DNA, Radiat Measurements 31:15-23
2. Ślosarek K, Konopacka M, Rogoliński J et al (2005) Effect of depth on radiation-induced cell damage in a water phantom, Rep Pract Oncol Radiother 10:37-41
3. Rogoliński J, Konopacka M, Sochanik A et al (2006) Effect of water phantom depth upon radiation-induced cytogenetical damage of cells, Polish J Environ Stud 15(4A):198-201

4. Fenech M (1993) The cytokinesis-block micronucleus technique and its application to genotoxicity studies in human populations, Environ Health Perspect 101(suppl.3): 101-107
5. Barendsen GW (1982) Dose fractionation, dose rate and iso-effect relationship for normal tissue responses, Int J Radiat Oncol Biol Phys 8(II): 1981-1997
6. Nikjoo H, Goodhead DT (1991) Track structure analysis illustrating the prominent role of low-energy electrons in radiobiological effects of low-LET radiations, Phys Med Biol 36:229-238
7. Botchway SW, Stevens DL, Hill MA et al (1997) Induction and rejoining of DNA double-strand breaks in Chinese hamster V79-4 cells irradiated with characteristic aluminum K and copper L ultrasoft X ray. Radiat Res 148: 317-324

The address of the corresponding author:

Author: Maria Konopacka
Institute: Comprehensive Cancer Centre, Maria Sklodowska-Curie Memorial Institute, Branch Gliwice, Department of Experimental and Clinical Radiobiology
Street: Wybrzeże Armii Krajowej 15
City: Gliwice
Country: Poland
Email: m_konopacka@epf.pl

Comprehensive Evaluation of On-position Leakage from Source Head of Bhabhatron-II Telecobalt Unit

S. D. Sharma[1], Rajesh Kumar[1], D. C. Kar[2]

[1]Radiological Physics & Advisory Division, Bhabha Atomic Research Centre, CTCRS, Anushaktinagar, Mumbai, India
[2]Division of Remote Handling and Robotics, Bhabha Atomic Research Centre, Trombay, Mumbai, India

Abstract - **Bhabhatron-II is a new model of telecobalt machine introduced for external beam therapy of cancer patients. It is a fully computer controlled new generation telecobalt machine which has a number of unique features such as 0.5x0.5 cm^2 treatment field, auto patient set-up, remote diagnosis, automatic closure of collimator to 0x0 field in case of functional abnormality. The source head of this telecobalt machine consists of a cast steel shell filled with lead and depleted uranium which can house ^{60}Co source of strength up to 250 RMM (250 Roentgen per minute at 1 meter ≈ 15,000 Ci). Measurement of on-position leakage from the source head of this telecobalt unit was carried out using a specially designed couch mountable tool. PTW 40 cm^3 ionization chamber along with PTW UNIDOS dosimeter (PTW Freiberg, Germany) was used in this work. Measurements were carried out for points located both in-patient plane and other than patient planes. The measured values are much less than the IEC-60601-2-11 recommended tolerances. The measurement results indicate high degree of on-position radiation safety status of the Bhabhatron-II telecobalt machine.**

Keywords – **Bhabhatron, telecobalt unit, head leakage, patient safety, occupational safety**

I. Introduction

Telecobalt machines are prominently used as external beam delivery equipment in almost all the developing countries of the world including India. About 1-million new cancer cases are detected in India per annum. To cope with the increasing burden of cancer patients about 1000 teletherapy machines are required as against currently available 392 teletherapy units (282 telecobalt machines and 110 medical linear accelerators) [1,2]. Considering the large requirements of teletherapy machines, a new model of indigenously developed telecobalt unit, named Bhabhatron-II, was introduced for cancer treatment. For the safety of patients and occupational workers, the design and shielding of the telecobalt machine shall adhere to the radiological safety requirements stipulated in IEC-60601-2-11 in addition to general safety requirements [3-5]. This paper describes a method which was used for comprehensive evaluation of on-position leakage radiation from source head of Bhabhatron-II telecobalt machine.

II. Materials and methods

A. Bhabhatron-II telecobalt machine

Bhabhatron-II is an isocentric (source to isocentre distance = 80 cm) telecobalt machine which incorporates various unique features such as (i) availability of 0.5x0.5 cm^2 treatment field size (ii) fully software controlled operation with record of operation history (iii) automatic closure of collimator to 0x0 field in case of functional abnormality (iv) software controlled collimator, couch and gantry movement (v) auto patient set-up (vi) remote diagnosis (vii) iso-wedge, and (viii) asymmetric collimator. Source head of Bhabhatron-II consists of a stainless steel shell filled with lead and depleted uranium which can house ^{60}Co source of strength up to 250 RMM (250 Roentgen per minute at 1 meter ≈ 15,000 Ci). Cylindrical source capsule of nominal diameter 2.0 cm mounted on a standard source drawer can be loaded in this telecobalt unit. Source movement is controlled by pneumatic drive system. Field limiting devices contains fixed opening primary as well as variable opening secondary collimators. Secondary collimator of this unit includes two pairs of collimating jaws made up of depleted uranium. Two pairs of trimmer bars made up of depleted uranium are also provided beneath lower jaws (X-jaws) to limit the radiation beam penumbra. The collimator jaws are motor driven and can define square/rectangular field sizes at the isocentre in the range of 0x0 to 35x35 cm^2. In case of source stuck, the collimator jaws/trimmers closes to zero automatically which is an improved design aspect towards radiation safety concerns of patients and occupational workers. All movements of the couch, collimator, gantry and field defining jaws are controlled by push-buttons located at couch panel. This unit has a dedicated dual window display monitor installed in the treatment room where mechanical positions of all the systems/ subsystems of the unit are displayed. Control console consists of graphical user interface (GUI) type software. Treatment prescriptions of patients can be loaded on the control console with their distinct identification numbers which can be recalled routinely for treatment delivery. Treatment delivery of a patient by this machine is possible only when the set (or prescribed) values and actual values are within the given tolerances. The machine has been certified by IEC ERTL (Eastern Region Test Laboratory) for its electromagnetic compatibility as stipulated in IEC-60601-1-2 [6]. Further details about

O. Dössel and W.C. Schlegel (Eds.): WC 2009, IFMBE Proceedings 25/III, pp. 383–385, 2009.
www.springerlink.com

the Bhabhatron telecobalt unit are available elsewhere [7].

B. Measurement of on-position leakage

A specially designed tool for measurement of on-position leakage from source head of teletherapy machine was fabricated using aluminium and heavy metal. The tool consists of an aluminium semi circular arc of diameter 2 meter. This arc is mounted on an heavy metal base plate that can be attached to the treatment couch of a teletherapy machine. T-type vertical support is also provided to the aluminium arc to make stable in a given standing position. There are provisions over the circumference of the aluminium arc to hold the various types of detectors such as TLDs (chips/ rods/ powder filled pouches), pocket dosimeter, large volume ion chamber at an angular interval of 30°. Using this tool, seven detectors can be irradiated simultaneously. For the source head leakage measurement of Bhabhatron-II, the tool was positioned at its couch in such a fashion that the centre of the semi circle was in coincidence with the position of the source in its on-position (Fig. 1). In this arrangement, all the seven detector positions were at 1-meter distance from the source. PTW 40 cm^3 ionisation chamber with its ^{60}Co build cap along with PTW UNIDOS dosimeter (PTW Freiburg, Germany) was used in this work.

Fig. 1 Photograph showing experimental arrangement used for leakage measurement from source head of Bhabhatron-II telecobalt unit (couch angle is 0° in this case).

For a given couch angle (say 0°), the ion chamber was positioned at five different locations over the circumference of the aluminium arc one by one and irradiated for 5 minute. The seventh position was in line with the radiation beam axis (designated 180° position of the detector with respect to source On-position) and it was inside collimator zone. Measurement at seventh detector positions was not carried out because the aim of this work was to determine leakage from the source head. In addition, sixth detector position on this tool was the point inside the patient plane. The experiment was repeated for seven different angular positions of the couch namely 135, 90, 45, 0, 315, 270 and 225°. The measurement at 0° detector position was carried out for 0° couch angle only once as this point was fixed in space at all the angular positions of the couch. The data so obtained was the source head leakage in other than patient plane.

The source head leakage in the patient plane was measured at 65 and 155 cm distance from the radiation beam axis. Fig. 2 is the schematic diagram showing measurement positions in patient plane. The black shaded region at the centre of this figure is the collimator transmission zone. In this case, the ionisation chamber was positioned at the given distance and the readings were recorded for seven different angular positions (135, 90, 45, 0, 315, 270 and 225°) of the couch. The gantry of Bhabhatron-II was stationary at 0° and the secondary collimator was fully closed during all the measurements.

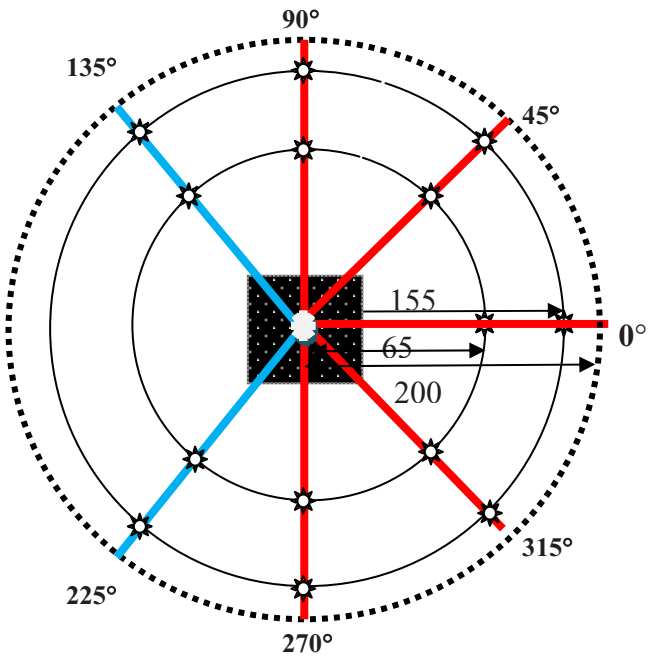

Fig. 2 Schematic diagram showing measurements positions in patient plane at 65 and 155 cm from the radiation beam axis. Black shaded region indicates area under the collimator zone. Indicated angular positions are the couch positions.

The dose rate at 1-meter distance from the source along the radiation beam axis corresponding to depth of dose maximum from the Bhabhatron-II was also measured using the same dosimetry

system. In this case, field size of 20x20 cm^2 was used for irradiating the ion chamber and dose rate for reference field of 10x10 cm^2 was calculated using the output factor of 20x20 cm^2 field determined using a secondary standard dosimeter. Percentage source head leakage at a point was calculated using absorbed dose value determined at this point and the dose rate along the radiation beam axis for10x10 cm^2 field.

III. Results and discussion

Table 1 presents the percentage on-position leakage from the source head of Bhabhatron-II telecobalt unit in other than patient plane measured with the help of specially designed tool. All the values shown in this table are less than 0.1% except one value at 270° couch position and 90° detector position. But all the values are much less than 0.5% (maximum value) which is the IEC-60601-2-11 recommended tolerance for this case. The determination of leakage radiation in a plane other than patient plane is important for the safety of occupational workers.

Table 1. On-position leakage (%) from source head of Bhabhatron-II telecobalt unit in other than patient plane.

Couch position	% source head leakage in other patient plane at source to detector angle				
	0^0	30^0	60^0	90^0	120^0
225^0	---	0.022	0.019	0.026	0.055
270^0	---	0.040	0.077	0.100	0.079
315^0	---	0.062	0.091	0.086	0.046
0^0	0.116	0.046	0.025	0.032	0.099
45^0	---	0.056	0.076	0.076	0.043
90^0	---	0.039	0.055	0.070	0.083
135^0	---	0.022	0.019	0.026	0.055

Measured percentage leakage radiation from the source head of Bhabhatron-II telecobalt unit at different angular positions in patient plane (the plane perpendicular to radiation beam axis) at 65 and 155 cm distance from the radiation beam axis are shown in Table 2. All the values in this table are much less than the IEC-60601-2-11 recommended tolerance of 0.2% (maximum value) in this case. The measurement of leakage radiation in patient plane is important for the safety of the patient during the treatment.

Table 2. On-position leakage (%) from source head of Bhabhatron-II telecobalt unit in patient plane.

Couch position	% source head leakage in patient plane at a distance from radiation beam axis of	
	65 cm	155 cm
225^0	0.012	0.002
270^0	0.015	0.003
315^0	0.010	0.002
0^0	0.022	0.003
45^0	0.009	0.002
90^0	0.016	0.003
135^0	0.010	0.002

IV. Conclusions

Percentage on-position leakage from the source head of Bhabhatron-II was determined both in patient plane and other than patient planes at a number of points. The measured values are much less than the IEC-60601-2-11 recommended tolerances. The measurement results indicate high degree of on-position radiation safety status of the telecobalt machine.

Acknowledgements

The authors wish to express their gratitude to Shri H. S. Kushwaha, Director, Health Safety and Environment Group, Dr. Y. S. Mayya, Head, Radiological Physics & Advisory Division (RP&AD), and Dr. G. Chourasiya, Head, Medical Physics & Training Section, RP&AD, Bhabha Atomic Research Centre, Mumbai for their encouragement and support during this work.

References

1. International Atomic Energy Agency (2008) Setting-up a radiotherapy programme: Clinical, medical physics, radiation protection and safety aspects, STI/PUB/1296, IAEA, Vienna
2. International Atomic Energy Agency (1998) Design and implementation of a radiotherapy programme: clinical, medical physics, radiation protection and safety aspects. IAEA-TECDOC-1040, IAEA, Vienna
3. International Electrotechnical Commission (1988) Medical Electrical Equipment: General Requirement for Safety, IEC 601-1
4. International Electrotechnical Commission (1997) Medical Electrical Equipment: Part 2: Particular requirements for the safety of gamma beam therapy equipment, IEC 60601-2-11
5. International Electrotechnical Commission (2004) Medical electrical equipment - Part 2-11: Amendment 1: Particular requirements for the safety of gamma beam therapy equipment, IEC 60601-2-11- am1
6. International Electrotechnical Commission (2001) Medical Electrical Equipment: Electromagnetic Compatibility-Requirement and Test, IEC 60601-1-2
7. Kumar R., Sharma S. D., Reena P., Deshpande D.D. and Kannan S. (2005) Performance characteristics of indigenously developed Bhbahtron-I telecobalt unit. J. Med. Phys. 30(2): 41 - 47

Address of the corresponding author:

Author: Dr. S. D. Sharma
Institute: RP&AD, BARC
Street: CT&CRS, Anushaktinagar
City: Mumbai - 400094
Country: India
Email: sdsharma_barc@rediffmail.com
sdsbarc@gmail.com

Patient Exposure from Interventional Cardiology Procedures in Slovenia

D. Žontar[1,2], V. Kanič[3], D. Kuhelj[4], D. Škrk[1], and U. Zdešar[5]

[1] Slovenian Radiation Protection Administration, Ljubljana, Slovenia
[2] Jožef Stefan Institute, Ljubljana, Slovenia
[3] Department of Cardiology and Angiology, University Hospital Maribor, Maribor, Slovenia
[4] Clinical Radiology Institute, University Hospital Ljubljana, Ljubljana, Slovenia
[5] Institute of Occupational Safety, Ljubljana, Slovenia

Abstract— **A country-wide study aimed to determine patient exposure from interventional cardiology procedures in Slovenia was carried out. All five cardiology rooms in four public hospitals have been included in the study. Results of dosimetric measurements of the involved X-ray units are presented. Dosimetric data were collected for 860 procedures: 416 coronary angiography (CA) procedures and 444 angioplasty procedures. Significant differences between centers have been observed, with the third quartile values for air kerma-area product (KAP) between 21 Gy cm^2 and 32 Gy cm^2 for CA and between 47 Gy cm^2 and 118 Gy cm^2 for CA+PTCA procedures. Gathered data will increase awareness about patient doses and will be used to develop corrective actions in centers where procedures are not optimized.**

Keywords— **interventional cardiology, patient exposure, dosimetry, radiation protection.**

I. Introduction

Interventional cardiology procedures can be a cause of one of the highest patient exposures from medical use of X-rays. They not only lead to significant dose to the patient [1-5] but are one of the rare medical procedures that can potentially cause deterministic effects on the patient's skin [6-9].

An increasing interest in patient exposure from interventional cardiology procedures can be observed in the last decade, providing a rising pool of data and suggesting guidelines and reference levels for particular procedures [10-18]. Until recently patient exposure for those procedures in Slovenia has been mostly unknown. Thus the objective of this study was to obtain information about patient exposure from the most frequent cardiac interventional procedures in Slovenia. In addition, dose levels from different institutions were compared to each other and to international values.

II. Materials and Methods

The study encompasses all four public hospitals in Slovenia that are performing cardiac interventional procedures and includes all 5 cardiology rooms and X-ray systems in use. Radiation doses from 860 interventional cardiology procedures have been collected, 416 coronary angiography (CA) and 444 percutaneous transluminal coronary angioplasty (PTCA) or CA and *ad hoc* PTCA (CA+PTCA).

A. X-ray equipment

The X-ray units involved in the study were Siemens Axiom Artis FC, Siemens Coroscop, GE Innova 2100, Philips Allura XPER FD 20 and Philips Allura XPER FD 10. All units are using C-arm configuration. The first two units are equipped with an image intensifier (II) and the latter three with a flat panel (FP) detector. All units are equipped with a Kerma Area Product (KAP) meter and three of them provide information about cumulative dose at the interventional reference point (CD_{IRP}).

B. Dosimetric measurements

Dosimetric measurements using water phantoms were performed on all five units. They included measurements of entrance skin air kerma (ESAK) rate and air kerma rate at the image detector (DAK) for all standard fluoroscopy and cine-angiography settings (all combinations of field sizes and dose rate settings). To simulate thin, normal and thick patient 16 cm, 20 cm and 24 cm thick water phantoms were used. Measurements of ESAK were performed using electrometer (UNIDOS E, PTW, Germany) with two different calibrated ionization chambers (TW77337 and TW34069-2,5, PTW, Germany). Chamber was placed at the entrance of the water phantom so that the measured ESAK rate includes the contribution from backscattered radiation. For measurements of DAK a calibrated semiconductor detector (R-100B, RTI Electronics, Sweden) connected to digital dosimeter (Barracuda, RTI Electronics, Sweden) was used. Detector is constructed so to exclude backscatter. Built-in KAP meters were calibrated from direct measurements of air-kerma free-in-air and measurements of the beam area using radiographic film. Correction factors (varying from 0.65 to 0.90) were used to normalize the collected KAP readings. No calibration was performed for CD_{IRP} readings.

O. Dössel and W.C. Schlegel (Eds.): WC 2009, IFMBE Proceedings 25/III, pp. 386–389, 2009.
www.springerlink.com

Results of dosimetric measurements are summarized in Tables 1 and 2, giving values for the most frequently used settings as well as minimal and maximal values for a 20 cm thick water phantom for each unit. One can note poor correlation between ESAK and DAK values for different units, indicating differences in beam quality.

Table 1 Entrance skin air kerma (ESAK) rate and air kerma rate at the detector (DAK) during fluoroscopy measured with a 20 cm thick water phantom. Values for the most frequently used settings (Typical) and settings with the lowest (Min.) and highest (Max.) dose rates are given for all X-ray units. Information about dose rate setting (low, medium or high) and filed size (in cm) for the listed settings is given.

Room	Typical		Min.		Max	
	ESAK mGy/min	DAK µGy/s	ESAK mGy/min	DAK µGy/s	ESAK mGy/min	DAK µGy/s
1	7.1	1.74	2.7	0.72	27.5	4.40
	med., 17 cm		low, 23 cm		high, 15 cm	
2	2.8	0.92	2.2	0.84	6.3	1.47
	low, 17 cm		low, 20 cm		high, 12 cm	
3	7.5	1.80	5.6	1.00	20.6	4.10
	low, 17 cm		low, 23 cm		high, 13 cm	
4	8.7	1.79	7.9	1.71	30.0	3.76
	low, 19 cm		low, 22 cm		high, 15 cm	
5	15.6	2.27	12.8	2.02	52.5	3.86
	low, 20 cm		low, 25 cm		high, 15 cm	

Table 2 Entrance skin air kerma (ESAK) rate and air kerma rate at the detector (DAK) during cine-angiography measured with a 20 cm thick water phantom. Values for the most frequently used settings (Typical) and settings with the lowest (Min.) and highest (Max.) dose rates are given for all X-ray units. Information about dose rate setting (low, medium or high) and filed size (in cm) for the listed settings is given.

Room	Typical		Min.		Max	
	ESAK mGy/min	DAK µGy/s	ESAK mGy/min	DAK µGy/s	ESAK mGy/min	DAK µGy/s
1	75.2	12.7	38.9	9.02	319	35.9
	low, 17 cm		low, 23 cm		high, 15 cm	
2	34.6	8.06	27.2	6.28	78.0	13.6
	low, 17 cm		low, 20 cm		high, 12 cm	
3	102	8.60	74.3	6.50	276	27.0
	low, 17 cm		low, 23 cm		high, 13 cm	
4	134	9.70	126	9.58	278	20.5
	low, 19 cm		low, 22 cm		high, 15 cm	
5	178	9.44	145	8.61	460	20.7
	low, 20 cm		low, 25 cm		high, 15 cm	

C. *Patient doses*

Collected data include patients age, sex, weight, height, fluoroscopy time (FT), number of frames, total KAP reading and CD_{IRP} where available. Unfortunately data on number of frames were in some cases missing, incomplete and/or presented in an inconsistent manner so they could only be used for three rooms.

Due to significant differences in the workload of the four centers and because they were included at different stages of the project, at this time there are large differences in the amount of data gathered from different centers. In most centers PTCA procedures (and stent implantation), if required, are generally performed immediately after CA. Taking into account the relatively low number of pure PTCA procedures and the fact that the doses from (elective) PTCA procedures were comparable to those from CA and *ad hoc* PTCA, we combined data from both types of procedures ((CA+)PTCA).

III. Results and Discussion

Results of the dose survey for CA and (CA+)PTCA are summarized in Tables 3 and 4 respectively. Number of patients, third quartiles for FT, no. of frames and CD_{IRP} (where available) together with third quartile and average of KAP are listed for each catheter lab. Differences between the rooms are up to ~50% in most parameters but the maximal difference for fluorography time in CA procedures and KAP values in PTCA is more than twofold.

Although unit 2 has by far the lowest dose rates, effects of the low settings are much less pronounced in the total KAP values. It should also be noted that the highest total KAP values for both CA and (CA+)PTCA procedures were measured on unit 1, although its dose rates at the most frequently used settings are on the low side.

Table 3 CA procedures: a summary of the third quartile values for fluoroscopy time (FT), number of frames, total KAP reading and cumulative dose at the interventional reference point CD_{IRP}. For each unit number of procedures and average values of KAP are also given.

Room	No. of patients	FT [min]	No. of frames	KAP [Gy cm^2]		CD_{IRP} [Gy]
		3rd quart	3rd quart	Aver.	3rd quartile	3rd quart.
1	18	1.9	/	24.9	27.2	/
2	81	3.2	661	18.1	23.6	0.31
3	230	4.4	/	21.8	27.4	/
4	44	2.6	349	19.5	21.4	0.24
5	43	1.9	489	24.6	32.0	0.37

Table 4 (CA+)PTCA procedures: a summary of the third quartile values for fluoroscopy time (FT), number of frames, total KAP reading and cumulative dose at the interventional reference point CD_{IRP}. For each unit number of procedures and average values of KAP are also given.

Room	No. of patients	FT [min]	No. of frames	KAP [Gy cm^2]		CD_{IRP} [Gy]
		3rd quart	3rd quart	Aver.	3rd quartile	3rd quart.
1	64	12.1	/	92.7	117.8	/
2	97	14.1	1139	43.0	46.7	0.80
3	225	10.6	/	54.3	67.7	/
4	37	11.8	1042	66.4	84.2	1.37
5	21	11.0	720	55.8	61.3	1.04

Figure 1 shows the distributions of KAP values for (CA+)PTCA procedures for all five cardiology rooms. Similar distribution is found for all rooms, although for two rooms one can notice a large broadening. For room 4 the broadening of the peak is likely a fluctuation due to the low number of entries. It will be investigated if confirmed on a larger data set. For room 1 the broadening of the distribution is also reflected in longer tails, represented as an increased number of entries in the last bin (>200 Gy cm^2). Since the data gathering is still in progress a discussion about possible reasons for increased doses in room 1 has been initiated.

Results of the study were compared to the reference levels as proposed by SENTINEL project [9]. The proposed reference levels for CA and PTCA procedures are: 6.5 min and 15.5 min respectively for fluoroscopy time, 700 and 1000 for number of frames, 45 Gy cm^2 and 85 Gy cm^2 for KAP, and 0.65 Gy and 1.5 Gy for CD_{IRP}. Applying them to the five cardio rooms in Slovenia we find that for CA procedures, the third quartile values for all four parameters are below the SENTINEL reference levels in all rooms. For (CA+)PTCA procedures, fluorography times and CD_{IRP} are below the reference levels in all rooms, KAP reference level is exceeded in one of them, while the reference level for number of frames is exceeded in two out of three rooms for which the data are available.

Using organ dose conversion coefficient for skin as proposed by Schlatti [5] (22 mGy (Gy cm^2) $^{-1}$), a reasonably good agreement between KAP and CD_{IRP} values is observed for (CA+)PTCA procedures. The agreement is much worse in case of CA procedures.

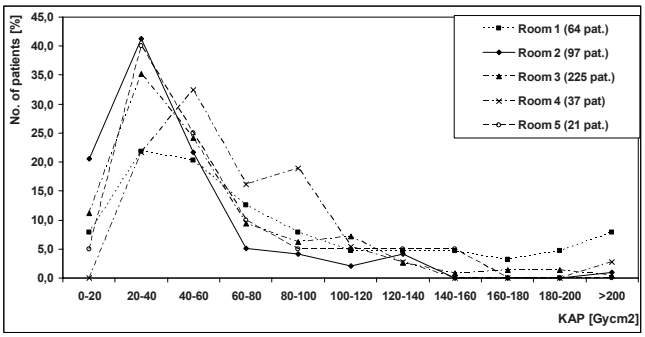

Fig. 1 Distributions of KAP values for (CA+)PTCA procedures for all five cardiology rooms.

IV. Conclusion

A study with a goal to determine patient exposure from cardiac interventional procedures on a national level has been initiated. Data from all public hospitals performing these procedures have been collected and despite large differences in the amount of data obtained so far the first comparisons were made.

For most parameters variations between the cardiac catheter labs were within 50%. Although large differences in entrance dose rates were found between X-ray units, the differences in measured patient doses (KAP) seem to be only weakly related to them. The third quartile values for air kerma-area product (KAP) were between 21 Gy cm^2 and 32 Gy cm^2 for CA and between 47 Gy cm^2 and 118 Gy cm^2 for (CA+)PTCA procedures. Except for (CA+)PTCA procedures in one catheter lab, determined third quartile values for KAP are below the reference levels as proposed by the SENTINEL project [9].

The data gathered in the first stage of the project should prove a valuable input to the process of optimization of cardiac interventional procedures in Slovenia, leading to reduced patient doses from these procedures.

Acknowledgment

The work was undertaken as part of technical cooperation project RER/9093 of the International Atomic Energy Agency. The authors are grateful to all staff of the interventional cardiology departments of the University Hospital Ljubljana, University Hospital Maribor, General Hospital "Dr. Franca Derganca" Nova Gorica and General Hospital Celje.

REFERENCES

1. Faulkner K, WerduchA (2008) An estimate of the collective dose to the European population from cardiac X-ray procedures. Br J Radiol 81: 634–639
2. Bedetti G, Botto N, Andreassi MG, Traino C, Vano E, Picano E. (2008) Cumulative patient effective dose in cardiology. Br J Radiol 81: 699-705
3. Betsou S, Efstathopoulos EP, Katritsis D, Faulkner K, Panayiotakis G. (1998) Patient radiation doses during cardiac catheterization procedures. Br J Radiol 71: 634–639
4. Smith IR, Rivers JT (2008) Measures of Radiation Exposure in Cardiac Imaging and the Impact of Case Complexity. Heart Lung Circ. 17:224-231
5. Schlatti H, Zankl M, Hausleiter J, Hoeschen C (2007) Local organ dose conversion coefficients for angiographic examinations of coronary arteries. Phys Med Biol 52(15):4393-408
6. US Food and Drug Administration (1994) Avoidance of serious X-ray induced skin injuries to patients during fluorosopically-guided procedures. Med Bull 24:7-17
7. Koenig TR, Wolff D, Mettler FA, Wagner LK (2001) Skin injuries from fluoroscopically guided procedures, Part I: Characteristics of radiation injury. Am J Roentgenol 177:3-11
8. Koenig TR, Mettler FA, Wagner LK. (2001) Skin injuries from fluoroscopically guided procedures: part 2, review of 73 cases and recommendations for minimizing dose delivered to patient. AJR Am J Roetgenol. 177: 13-20
9. Rehani M, Ortiz-Lopez P. (2006) Radiation effects in fluoroscopically guided cardiac interventions—keeping them under control. Inter J Cardiol 109(2):147-51
10. Tsapaki, V, et al (2009) Radiation exposure to patients during interventional procedures in 20 countries: Initial IAEA project results. Am J Roentgenol (in press)
11. Vano E, Jarvinen H, et al. (2008) Reference levels at European level for cardiac interventional procedures. Radiat Prot Dosimetry 129 (1–3): 104–107
12. Kuon E, Empen K, Rohde D, Dahm JB. (2004) Radiation exposure to patients undergoing percutaneous coronary interventions—are current reference values too high? Herz 29 (2): 208–217
13. Chu RY, Thomas G, Maqbool F. (2006) Skin entrance radiation dose in an interventional radiology procedure. Health Phys 91 (1): 41–46
14. Padovani R, Bernardi G, Malisan MR, Vano E, Morocutti G, Fioretti PM. (2001) Patient dose related to the complexity of interventional cardiology procedures. Radiat Prot Dosimetry 94 (1/2): 189–192
15. Peterzol A, Quai E, Padovani R, Bernardi G, Kotre CJ, Dowling A. (2005) Reference levels in PTCA as a function of procedure complexity, Radiat Prot Dosimetry 117 (1–3): 54–58
16. Neofotistou V, Vano E, Padovani R, Kotre J, Dowling A, Toivonen M, Kottou S, Tsapaki V, Willis S, Bernardi G, Faulkner K. (2003) Preliminary reference levels in interventional cardiology. Eur Radiol 13 (10): 2259–2263
17. Padovani R, Quai E. (2005) Patient dosimetry approaches in interventional cardiology and literature dose data review. Radiat Prot Dosimetry 117 (1–3): 217–221
18. Dragusin O, Desmet W, Heidbuchel H, Padovani R, Bosmans H. (2005) Radiation dose levels during interventional cardiology procedures in tertiary care hospital. Radiat Prot Dosimetry 117 (1–3): 231–235

Author: Dejan Žontar
Institute: Slovenian Radiation Protection Administration
Street: Ajdovščina 4
City: Ljubljana
Country: Slovenia
Email: dejan.zontar@gov.si

Measurement of Entrance Skin Dose Due the Imaging Systems for Treatment Planning of Stereotactic Radiosurgery of Arteriovenous Malformations

O.O. Galván De la Cruz[1], O.A. García-Garduño[2,1], B. Hernández Reyes[3], S. Moreno Jiménez[1], M.A. Célis López[1], and J.M. Lárraga-Gutiérrez[2,1]

[1] Unidad de Radioneurocirugía, Instituto Nacional de Neurología y Neurocirugía. Insurgentes Sur 3677, Col. La Fama, C.P. 14269 Tlalpan, D.F., México
[2] Laboratorio de Física Médica, Instituto Nacional de Neurología y Neurocirugía. Insurgentes Sur 3677, Col. La Fama, C.P. 14269 Tlalpan, D.F., México
[3] Unidad de Neuroimagen, Instituto Nacional de Neurología y Neurocirugía. Insurgentes Sur 3677, Col. La Fama, C.P. 14269 Tlalpan, D.F., México

Abstract— **This work presents measurements of entrance skin dose (ESD) delivered by the imaging systems that are needed for treatment planning of arteriovenous malformations (AVM) by stereotactic radiosurgery (SRS). Measured ESD values are in agreement with measurements reported in the literature, and their magnitudes are less than the threshold ESD for the deterministic effects. This project pretends to establish a protocol for the quantity of image acquisitions for AVM treatment by SRS.**

Keywords— **AVM, stereotactic radiosurgery, digital subtraction angiography, computed tomography, film dosimetry.**

I. Introduction

The delimitation of the target in stereotactic radiosurgery (SRS) is done, routinely, with images generated by magnetic resonance and computed tomography (CT). Depending on the kind of lesion to be treated, another set of useful images could be, as positron emission tomography (PET), or X-ray planar angiographies. The CT images, in the treatment planning system (TPS), are used to establish the stereotactic reference frame, and it is the source of radiologic information for the calculation of dose distribution [1]. In the special case of arteriovenous malformations (AVMs), magnetic resonance and CT images are enhanced with contrast media. Also images generated by digital subtraction angiography (DSA) help to define more accurately the AVM nidus and increase the probability of obliteration [2]. AVMs were the second more frequently pathology treated by (SRS) in the National Neurology and Neurosurgery Institute (INNN) in Mexico during 2007 [3]. If the treatment plan is done with the contrast enhanced CT, the electronic density of the target will be higher than what actually is, and these could end in an erroneous calculation. The solution found to this problem is to take two CT scans, one prior and one enhanced with contrast media [1]. However, it is possible that skin-overexposure to X-ray ionizing radiation delivered by the imaging systems occurs for this special pathology.

In this work we measure the ESD due to the image generating systems with radiochromic film. *In vivo* ESD measurements with patients that have a diagnose of an AVM were performed for DSA SRS planning. ESD measurements of CT with an anthropomorphic phantom are reported for both scans (prior and enhanced contrast images).

II. Material and methods

A. Dosemeter calibration

Gafchromic EBT® (International Specialty Products, USA) radiochromic film has been used for patients and for the anthropomorphic phantom ESD measurements. The EBT radiochromic film has a dose useful range from 0 cGy to 800 cGy. This film does not need any chemical process for the reading, just needs hours for color stabilization [4].

Film calibration was carried out using a high energy photon beam of a dedicated SRS linear accelerator with a nominal energy of 6 MV (Novalis, BrainLAB, Germany). The calibration interval used was from 0 cGy to 34 cGy.

Film digitalization was performed with a flat bed color scanner (Epson perfection V750 PRO) in the transmission mode at 300 dpi spatial resolution, and 48 RGB bit color depth (16 bit per channel). Only the red component was used for reading and analysis. A cubic polynomial has been adjusted to the measurement.

B. In vivo measurements

Two films were placed, one at beam entrance on the lateral and in the front for postanterior projection of the DSA on the head of the patient. The same radiochromic films were collocated in the same position for 4 different patients, who were treated by SRS with the diagnostic of an AVM in different cerebral regions. Dose measurements were done for the complete imaging process needed for the TPS for the

O. Dössel and W.C. Schlegel (Eds.): WC 2009, IFMBE Proceedings 25/III, pp. 390–392, 2009.
www.springerlink.com

planning of the AVM SRS treatment. The dose detected by the radiochromic films included the ESD during the angiography procedure and the 2 CT scans (prior contrast and with contrast enhanced). The digitalization has been done with the same parameters and conditions of the films used for the calibration curve. ESD due the CT scans has been subtracted from the dose measured of the complete image process.

C. CT ESD measurements

At the surface of a water anthropomorphic phantom (RSVP phantom, The Phantom Laboratory) a set of new radiochromic films has been placed, simulating the position of the films on the patients, to measure the entrance dose of a CT study (SOMATOM Sensation 64, Siemens, USA) with SRS scanning protocol (512x512 matrix size, voxel size of 0.7 mm^3 and H30 reconstruction filter)

Four complete CT scans protocols for the treatment of AVMs were performed to the phantom, so the lecture of the film has to be divided by 8 to get the entrance dose per scan. The measurements include phantom backscatter.

III. Results

A. Dosemeter calibration

The calibration curve of the EBT radiochromic film is presented in Figure 1. The correlation coefficient between the adjustment and the measured points was 0.997. The polynomial curve has been applied to all the red component of color density of the films.

B. In vivo measurements

In vivo measurements are presented in table 1. An important point that has to be considered is that the front film (AP projection) was not the entrance measurement of the angiography projection. The X-ray tube was under the patient, so this value is the measurement of the output of the X-ray beam thru the patient (exit skin dose). The lateral measurement has been placed at the entrance of the beam on the DSA procedure.

Table 1.- Measurements of the entrance dose by the DSA procedure

Film position	Entrance dose (cGy)
Lateral (entrance)	3.7 ± 0.1
AP (output)	1.6 ± 0.3

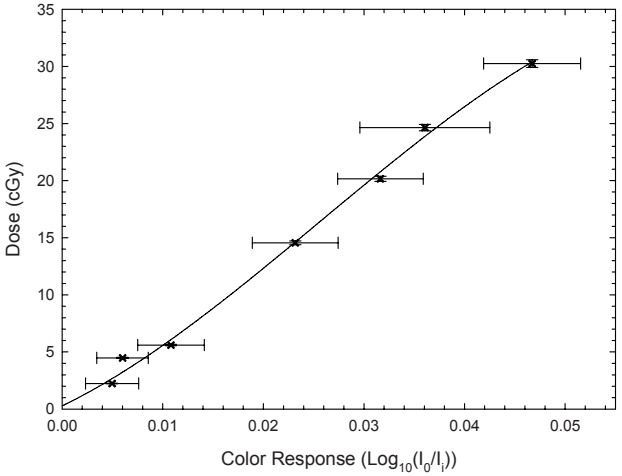

Figure 1.- Dose calibration of EBT radiochromic film. A cubic polynomial has been adjusted

The measurements of the CT scans were subtracted from the angiography measurements.

C. CT ESD measurements

Measured dose with the anthropomorphic phantom (that was full of water) gave an entrance dose per scan of 2.1 cGy ±0.1 cGy. So, the entrance dose in an AVM CT protocol is the double of the quantity given above.

IV. Discussion

The maximum ESD of the images needed for a SRS planning of an AVM is approximately 5.8 cGy ± 0.2 cGy. But, this value shall not be taken as a rule, the entrance dose generated by the DSA is variable, it depends on the patient anatomy, the radiologist, among other factors.

The measured values for CT scans are not as high as others reported in the literature (3-7 cGy) [5]. The concern of ESD measurements of these imaging systems is because there has been a considerable increment on collective dose deposited by radiologic studies, in some populations over the world [5].

The goal is to reduce as low as possible the ESD in SRS imaging planning procedures. This objective is very important, since there is not a threshold dose for stochastic effects. Also, is probable that the patients that are having SRS have had already at least one CT scan for the initial diagnosis of the AVM. During the AVM management, in order to recommend the treatment procedure, and to establish the Spetzler-Martin grade of AVM an angiography

needs to be done [6]. So, by the time the SRS is performed, a considerable dose has been deposited to the patient just for the diagnosis and treatment decision.

It is well accepted that angiography is the imaging procedure where more dose is deposited to the patients. There are recommendations for neurological angiography procedures to measure the entrance skin dose, in order to communicate to the patient the possible deterministic effects (temporary epilation, and erythema) [7,8]. The food and drug administration (FDA) recommends that if there is a possibility of exceeding more that 1 Gy to the skin, there is needed to communicate to the patient of possible deterministic effects [7].

Besides the possibility of exceed the threshold dose, the ALARA philosophy should be followed and try to minimize the dose deposition of the image generating systems. To do so, a study of the effect the CT contrast media in the dose calculation of the TPS is being carried out. Approaches of these problem can be found in the literature [9, 10]. To determine if the prior contrast CT scan is necessary, it has to be established if there is any discrepancy, and its value, in the calculation of dose deposition and distribution is considerable if the treatment plan is done in the CT with contrast.

Gafchromic EBT radiochromic film, is a useful dosemeter for the dose measurement in radiodiagnostic. The possible inconvience is that it needs to be irradiated several times (to repeat the study) to have a good interval of measured dose.

V. Conclusions

By these preliminary results, the dose deposited by the CT scan and DSA procedure is not as high as another interventional neurological procedures. They also agree with other reported in the literature, [5, 7, 11, 8].

Further studies need to be done to establish if the CT scan prior contrast is necessary. The considerations needed to make a decision are the uncertainties of the accelerator, of the TPS, and the dosimetry equipment. Also measurements to evaluate the TPS calculation are needed to be done for further conclusions.

Acknowledgment

Part of this work is supported by project CONACYT-SALUD-2005-01-14012

To M. Sc. Paola Ballesteros Zebadúa for the revision and useful comments of this paper.

References

1. Software Guide Manual Brainscan v5.31, *Brainlab* (2004) 138
2. Flickinger, J. *et al* (2002) An analysis of the dose-response for atreriovenous malformation radiosurgery and other factors affecting obliteration. Radiother Oncol 63: 347-354
3. Annual activity report of the Radioneurosurgery unit *Internal report* INNN, 2007
4. Cheung, T *et al* (2005) Post-irradiation colouration of Gafchormic EBT radiochromic film. Phys Med Biol 50: 281-285
5. Nickoloff E, Alderson P.(2001) Radiation Exposures to patients from CT: Reality, public perception, and policy. American J. Roentgenology 117: 285-287
6. Spetzler, R. Martin, N (1986) A proposed grading system for atreriovenous malformations. J. Neurosurg 65: 476-483.
7. O'Dea, T. *et al* (1999) The potential for radiation-induced skin damage in interventional neuroradiological procedures: A review of 522 cases using automated dosimetry. Med Phys 26(9): 2027-2033
8. Huda, W. Peters, K. (1994) Radiation-induced temporary epilation after a neuroradiologically guided embolization procedure. Radiology 193: 642-644
9. Burridge N. et al (2006) Effect of contrast-enhanced CT scans on heterogeneity corrected dose computations in the lung. J. Appl. Clin. Med. Phys. 7(4):1-12
10. Ulla R. et al (2001) Influence of CT contrast agents on dose calculations in a 3D treatment planning system. Phys. Med. Biol. 46:2631-2635.
11. Schueler, B et al (2005) 3D Cerebral angiography: radiation dose comparison with digital subtraction angiography. Am J Neuroradiol 26: 1898-1901.

Corresponding author:

Author: J.M. Lárraga-Gutiérrez
Institute:Instituto Nacional de Neurología y Neurocirugía
Street: Insurgentes sur 3877, La Fama, Tlalpan
City: México
Country: México
Email: jlarraga@innn.edu.mx

Gamma Dose Rate Measurement and Dose Rate Calculation of Sensitive Organs in the Vicinity of Hot Springs in Kerman Province, Southeastern Iran

A. Jomehzadeh [1*], Z. Jomehzadeh[2]

[1] Rafsanjan University of Medical Sciences, Medical Physics Dept, M.Sc, Rafsanjan, Iran.

[2] Kerman University of Medical Sciences, Medical Physics Dept, M.Sc, Kerman, Iran.

Abstract— **Measurement of background radiation is very important from different points of view especially to human health. In some cases exposure rate near hot springs are higher than those of normal areas. The high background radiation of hot springs is primarily due to the presence of very high amounts of Ra-226 and its decay products. The aim of this paper was to measure environmental gamma radiation of 19 hot springs in Kerman province with RDS-110 surveymeter and sensitive organs dose rates were calculated. Measurements were carried out at one meter above water level in the vicinity of hot springs. The results indicate that annual gamma-ray dose rate in the vicinity of 19 hot springs ranged from 0.53 ± 0.23mSv/y to 1.65 ± 0.54 mSv/y. Also the annual bone marrow and sexual organs dose rates are in ranged from 0.42 ± 0.18 mSv/y to 1.32 ± 0.43 mSv/y and 0.43 ± 0.19 mSv/y to 1.34 ± 0.44 mSv/y, respectively. This study showed that the The doses obtained by our study are significantly below that recommended dose for all categories of water.**

Keywords— **Gamma Dose Rate, Hot Spring, Environmental Monitoring, Kerman**

I. INTRODUCTION

In Kerman province, southeastern Iran, a lot of thermal water occurrences providing thermal water for spas are used for curative therapeutic purposes in cases of locomotors and gastrointestinal diseases. Besides, spas attract many local visitors and tourists as recreational facilities [1]. The geological origin of thermal water sources is different; accordingly the radioactivity levels of the waters vary widely. Treatment by spa water in the special atmosphere of the spa is proven by physicians to be beneficial [2]. In spite of that at spas having high radon in the air particular attention should be played to the exposure of the workers. Patients and visitors usually spend limited time in spas, therefore less affected by radon exposure, but certainly have to be informed about the potential effects [3].

Measurement of background radiation is very important from different points of view especially to human health [4,5]. In some cases exposure rate near hot springs are higher than those of normal areas. The high background radiation of hot springs is primarily due to the presence of very high amounts of Ra-226 and its decay products. The aim of this paper was to measure environmental gamma radiation of 19 hot springs in Kerman province and sensitive organs dose rates were calculated.

II. MATERIALS AND METHODS

Equipments used in this work included: a surveymeter (RDS-110), a tripod and an aluminum frame to hold the survey meter horizontally. RDS-110 is a microprocessor controlled detector. This survey meter has been designed for monitoring X and γ rays and β radiation. Measurements were carried out at one meter above water level in the vicinity of hot springs. Dose rates were recorded for one hour. The average of all recorded dose rates over one hour period was taken as the exposure rate for each station [6, 7, 8]. Then, bone marrow and sexual organs dose rates using the following equations are calculated [9]:

$$\begin{aligned} &\textit{Bone marrow dose arte} = \textit{Absorbed dose rate (in air)} \times 0.80 \\ &\textit{Sexual organs dose rate} = \textit{Absorbed dose rate (in air)} \times 0.81 \end{aligned} \quad (1)$$

In order to comparing the averages, independent T test and variance analysis were used.

III. RESULTS

Measurements were carried out from October 2008 until December 2008. In Table 1 the annual gamma-ray dose rate, with standard deviations, from 19 hot springs in Kerman province, measured with RDS-110 surveymeter, are presented.

It is evidence from this table that annual gamma-ray dose rate in the vicinity of 19 hot springs ranged from 0.53 ± 0.23mSv/y to 1.65 ± 0.54 mSv/y.

* Corresponding author: Tel. +98 391 8220019; Fax: +98 391 8220019.
E-mail address: ali_jomehzadeh@yahoo.com

O. Dössel and W.C. Schlegel (Eds.): WC 2009, IFMBE Proceedings 25/III, pp. 393–395, 2009.
www.springerlink.com

Table 1 Annual gamma-ray dose rate, with standard deviation, in vicinity of 19 hot springs in Kerman province

Region	Height from sea level (m)	Temperature (C^0)	Annual dose rate (mSv/y)
Abghanat	1750	29	1.53 ± 0.68
Abgarmoo	220	28	1.06 ± 0.33
Amire-keykhosravi	2750	28	1.65 ± 0.54
Bahadora-bad	440	27	1.09 ± 0.46
Joshan	1545	25	0.70 ± 0.25
Chegery	2100	36	0.56 ± 0.23
Chaharfar-sakh	1020	37	0.68 ± 0.23
Hormok	1220	29	1.38 ± 0.21
Khaneghah	1845	27	0.60 ± 21
Khodadadi	2605	19	1.25 ± 0.51
Dehzey	1830	30	1.45 ± 0.49
Rang	2290	39	1.13 ± 0.40
Sofla	1640	19	1.01 ± 0.26
Shirinak	2535	30	1.39 ± 0.32
Gharayoob	550	28	0.53 ± 0.23
Gholgholoo	2135	20	1.36 ± 0.25
Gisheki	1530	40	1.14 ± 0.40
Mohamma-dabad	2110	35	0.93 ± 0.30
Maskoon	1835	39	1.13 ± 0.38

Table 2 calculated annual sensitive organs dose rate, with standard deviations, are presented. As shown in Table 2, the annual bone marrow and sexual organs dose rates are in ranged from 0.42 ± 0.18 mSv/y to 1.32 ± 0.43 mSv/y and 0.43 ± 0.19 mSv/y to 1.34 ± 0.44 mSv/y, respectively.

Table 2 Annual bone marrow and sexual organs dose rates, with standard deviation, over 19 hot springs of Kerman province

Region	Bone Marrow Dose Rate (mSv/y)	Sexual Organs Dose Rate (mSv/y)
Abghanat	1.22 ± 0.54	1.24 ± 0.55
Abgarmoo	0.85 ± 0.26	0.86 ± 0.27
Amirekeykhosravi	1.32 ± 0.43	1.34 ± 0.44
Bahadorabad	0.87 ± 0.37	0.88 ± 0.37
Joshan	0.56 ± 0.20	0.57 ± 0.20
Chegery	0.45 ± 0.18	0.45 ± 0.19
Chaharfarsakh	0.54 ± 0.18	0.55 ± 0.19
Hormok	1.10 ± 0.17	1.12 ± 0.17
Khaneghah	0.48 ± 0.17	0.49 ± 0.17
Khodadadi	1.00 ± 0.41	1.01 ± 0.41
Dehzey	1.16 ± 0.39	1.17 ± 0.40
Rang	0.90 ± 0.32	0.92 ± 0.32
Sofla	0.81 ± 0.21	0.81 ± 0.21
Shirinak	1.11 ± 0.26	1.13 ± 0.26
Gharayoob	0.42 ± 0.18	0.43 ± 0.19
Gholgholoo	1.09 ± 0.20	1.10 ± 0.20
Gisheki	0.91 ± 0.32	0.92 ± 0.32
Mohammadabad	0.74 ± 0.24	0.75 ± 0.24
Maskoon	0.90 ± 0.30	0.92 ± 0.31

IV. DISCUSSION AND CONCLUSION

According to ICRP recommendations the limit for public exposure should be expressed as an effective dose of 1 mSv in a year [10]. The doses obtained by our study are significantly below that recommended dose for all categories of water. This supports the conclusion that in Croatia thermal spring waters can be used without any restrictions (for bathing, drinking for medical therapy, recreation and rehabilitation), on the assumption that the 5- year average does not exceed 1 mSv per year and that other sources of exposure are also taken into account. According to UNSCEAR (2000) the worldwide annual effective dose for normal areas is 2.4 mSv/y[9]. This study showed that the maximum annual dose rate in vicinity of hot springs in Kerman province was 120% higher than annual outdoors dose rate for normal areas [10]. It is because of the existence of the radioactive elements in spring water and high altitude of spring from the sea level. Due to the high dose rate of sensitive organs of the human who are close to the spring in comparison with the normal dose rate in outdoors, it is suggested that it is better to use Chegeri, Ghaneghah, Gharayoob, Joshan and Chaharfarsakh springs for spas and ventilation of spring baths with relatively high concentrations of indoor radon is highly recommended to reduce risk. Also, according to the results, there is no relation between the gamma dose rate and temperature of springs.

ACKNOWLEDGMENT

The authors would like to thank the Kerman University of Medical Sciences for the financial support.

REFERENCES

1. Shojaei MR, Information of the hydrozoas chemical around the hot springs of Kermn province. Global water organization of Kerman province 2003; 1-477.
2. Hadad K, Doulatdar R, U-series concentration in surface and ground water resources of Ardabil province. Radiat. Prot. Dosim. 2008; 128(3): 55-75.
3. Bahreyni toosi MT, Aghamir SA. Evaluation of the Gamma doses in the cities an hot springs of Mazandaran, M.Sc. Thesis. Mashhad University of medical sciences 2003.
4. Bahreyni toossi MT, Jomehzadeh A, A comparison study on the indoor Gamma radiation in Kerman province using the Termoluminescence and survey meter RDS-110, Hormozgan Medical Journal. 2005; 3: 174-175.
5. Ghiassi-nejad M, Mortazavi SMJ, Cameron JR, Niroomand-rad A. Karam PA, Very high background radiation areas of ramsar, Iran: preliminary biological studies. Health Phys. 2002; 82 (1): 87-89.
6. Beitollahi M, Ghiassi-Nejad M, Esmaily A, Dunker R, Radiological studies in the hot spring region of Mahallat, central Iran. Radiat. Prot. Dosim. 2007; 123(4): 505-508.
7. Shahbazi-Gahrouei D. Saeb M. Dose assessment and radioactivity of the mineral water resources of Dimeh springs in the Chaharmahal and Bakhtiari province, Iran. Nuleonika 2008; 53(1): 31-34.
8. Isinkaye MO, Ajayi IR, Natural background dose and radium equivalent measurements at Ikogosi warm spring, Nigeria. Radiat. Prot. Dosim. 2006; 121(4): 466-468.
9. United Nations scientific committee on the effects of atomic radiation. Sources and effects of ionizing radiation. Report to the general assembly united nations, New York 2000.
10. ICRP Publication 60. 1990 *Recommendations of the International Commission on Radiological Protection*. Pergamon Press. Oxford. (1991).

Effect of Varying Phantom Size in Dosimetry of Iridium-192: A Comparison of Experimental Data with EGSnrc Monte Carlo Calculation

H. Seo[1], M. Haque[2], R. Hill[1,2], and C. Baldock[1]

[1] Institute of Medical Physics, The University of Sydney, Sydney, Australia
[2] Department of Radiation Oncology, Royal Prince Alfred Hospital, Sydney, Australia

Abstract— **There have been increasing numbers of studies in high dose-rate (HDR) brachytherapy dosimetry, which have shown that the phantom size has significant effect on the dose delivered. The most frequently used methodology consisted of verifying the Monte Carlo calculations with the experimental measurements. This paper primarily reports the effects of varying scatter material thickness above an Iridium-192 (^{192}Ir) HDR source by using a PTW Roos chamber (PTW, Germany) and the EGSnrc Monte Carlo code (National Research Council Canada, Canada). Virtual Water (Med-Cal, USA) was utilized as a scatter material. A microSelectron remote afterloader unit (Nucletron, Netherlands) was utilized to deliver ^{192}Ir source. The Roos chamber placed in the recess of a 20 mm thick Virtual Water slab was positioned above the backscatter material. A catheter attached to the treatment tube from the remote afterloader unit was fixed above the central axis of a Roos chamber. Secondly, the position dependence of a Roos chamber with respect to the source has been investigated. This was achieved by placing two different thick scatter materials between the planes of the source and a Roos chamber. The results from both experimental measurements and Monte Carlo calculations has shown increased dose with increasing scatter material thickness above ^{192}Ir source, with Monte Carlo calculated results showing less variation in dose. The dose output reduced considerably with increasing thickness of scatter materials between the chamber and the source.**

Keywords— **brachytherapy, high dose-rate, EGSnrc Monte Carlo, dosimetry, iridium-192**

I. Introduction

Most brachytherapy treatments involve insertion of a radionuclide into the body under full scatter conditions. However one possible brachytherapy use is the treatment of *squamous cell carcinoma* or *angiosarcoma* on the skin using a HDR radionuclide, typically on the limbs and head and neck regions [1, 2]. In these cases, the use of a surface mould allows one to deliver the dose on a curved contour. In order to deliver the HDR treatment of up to 6 Gy per minute, a radionuclide must have a strong source activity with appropriate energy. ^{192}Ir satisfies the above noted criteria with specific activity of about 450 Ci/g and an effective gamma ray energy of 0.38 MeV [3], and thus it has become indispensable radionuclide for superficial HDR brachytherapy treatments.

The most well known treatment planning system for brachytherapy is the PLATO brachytherapy planning system (BPS), (Nucletron, Netherlands). The dose calculation formalism based on AAPM Task Group 43 [4], allows calculation of a uniform dose distribution at a specified depth from the surface, which is effectively surrounded by subcutaneous tissue. Since skin surface lacks this surrounding tissue, skin dose has to be carefully evaluated. One should also be aware that the BPS assumes full scatter conditions and tissue homogeneity, both of which will have an effect on the dose to patient. There have been increasing numbers of studies in HDR brachytherapy dosimetry, which have shown that the phantom size has significant effect on the dose delivered [5]. The most frequently used methodology consisted of verifying the Monte Carlo calculations with the experimental measurements using ionization chambers or thermoluminescence dosimeters (TLDs) [6]. This involves modeling of a phantom geometry and designing of the source within the Monte Carlo code.

This paper reports the effect of varying the phantom size in dosimetry of ^{192}Ir source using a Roos chamber and the EGSnrc Monte Carlo code. Two aspects were investigated. First, the effect of varying the phantom thickness above ^{192}Ir source was studied. Furthermore, the position dependency of the source to the chamber was investigated by varying the separation between the source and the chamber.

II. Materials and Methods

A. Materials

A microSelectron HDR remote afterloader unit was utilized to deliver ^{192}Ir source through a catheter by means of stepping with varying dwell times. Indexer length was measured using the Source Position Simulator (Nucletron, Netherlands) and verified by measuring the position of the maximum chamber response in the plane of the measurement. Virtual Water slabs of dimension 30×30 cm were used to provide the scattering material. Virtual Water is claimed by the manufacturer (CNMC, USA) to have water equivalence to within 0.5% [7]. Virtual Water is almost

O. Dössel and W.C. Schlegel (Eds.): WC 2009, IFMBE Proceedings 25/III, pp. 396–399, 2009.
www.springerlink.com

identical to RMI-457 Solid Water (Radiation Measurements Inc., Middleton, Wisconsin) in composition and as such is suitable for dosimetry of low energy photon beams [8-10]. Several different thicknesses ranging from 2 to 50 mm were utilized for the measurement. A PTW Roos chamber was connected to the UNIDOS electrometer (PTW, Germany) for all dose output measurements. The experimental setup was modeled within the EGSnrc Monte Carlo code. The PLATO BPS (version 14.3) was used for treatment planning based on planar distributions.

B. Experimental method

A 50 mm thick Virtual Water slab was positioned on the patient couch to provide backscatter material. The Roos chamber placed in the recess of a 20 mm thick Virtual Water slab was positioned above the backscatter material. A catheter was fixed firmly above the central axis of a Roos chamber by a micropore tape and encompassed by layers of dental wax to provide a flat base for scatter materials above. ^{192}Ir source was programmed to travel to the position of maximum chamber response within the catheter.

The dose output was measured as a function of thickness of the scatter material. 2, 3, 10 and 50 mm thick Virtual Water slabs were positioned above the catheter consecutively. Measurements were repeated four times and averaged. Uncertainties were considered type A, which is represented by an estimated standard deviation [11]. The measurements were repeated with varying the separation between a Roos chamber and ^{192}Ir source. This separation was achieved by placing an additional scatter material between the source and the chamber. 5 and 10 mm thick Virtual Water slabs were utilized for this purpose.

C. Monte Carlo method

The EGSnrc Monte Carlo package for modeling radiation transport was used for all calculations [12]. EGSnrcMP GUI (graphical user interface) is a geometrical simulation package within the EGSnrc code, which enables the user to create a geometrical configuration of simple mathematical objects such as cylinders or spheres that are commonly modeled phantom shapes in Monte Carlo dosimetry. Our experimental setup was modeled assuming a cylindrical phantom of radius 150 mm. The DOSRZnrc based on the EGS4 code system was used for cylindrical geometry dose evaluation. The PEGS4 program within the EGSnrc code generates the cross section data for the media used in the calculations. However the database did not incorporate composition data for some of the phantom materials such as the Virtual Water and the RMI-457 Solid Water. The composition details of various water equivalent media were updated from published data [11].

Simplified geometric modeling of a Roos chamber and ^{192}Ir source was designed within the EGSnrc code. The thickness of a Roos chamber was assumed to be 3 mm, based on the depth of the sensitive volume and the water equivalent window thickness as per manufacturer's manual [13]. For the purpose of optimizing the calculation efficiency ^{192}Ir was assumed to be an isotropic point source within the central axis of a cylindrical phantom and for this reason, the source length was approximated to the length of the source diameter (1 mm) instead of 3.5 mm from previously published data [14]. The active source diameter was set to 0.90 mm as per the same published data. The electron and photon transport cut-off energies were set to 0.561 and 0.010 MeV respectively. The *^{192}Ir microSelectron spectrum* within the EGSnrc code was programmed to incident on this virtual setup. A total of 2×10^8 initial histories were used to achieve good statistical uncertainty. The dose was evaluated at different detector depths as a function of the scatter material thickness ranging from 2 to 50 mm.

III. RESULTS

D. Results from experimental method

Fig. 1 indicates the dose output for different thicknesses of scatter materials placed consecutively above ^{192}Ir source measured by a Roos chamber. The dose at the effective depth of a Roos chamber has shown to increase with increasing thickness of the scatter material above ^{192}Ir source. The maximum variation in dose output for scatter materials ranging from 2 to 50 mm was of the order of 1.3%. The uncertainty of the measurements derived from standard deviation of the overall mean was 0.6%.

Fig. 2 indicates measured dose output with placement of additional scatter material between the source and the chamber. The average dose output was reduced to an order of 2.4 and 5.1 for the separations of 5 and 10 mm between the source and the chamber, which demonstrates that the dose fall off is large close to the source. The maximum variations in dose output for scatter materials ranging from 2 to 50 mm were 1.5% and 2.7% for 5 and 10 mm separations respectively.

E. Results from Monte Carlo simulation

As shown in Fig. 3 the dose scored on the central axis of a cylindrical phantom is reasonably consistent with the experimental result. The Monte Carlo calculations indicate the maximum variation in dose due to different thicknesses

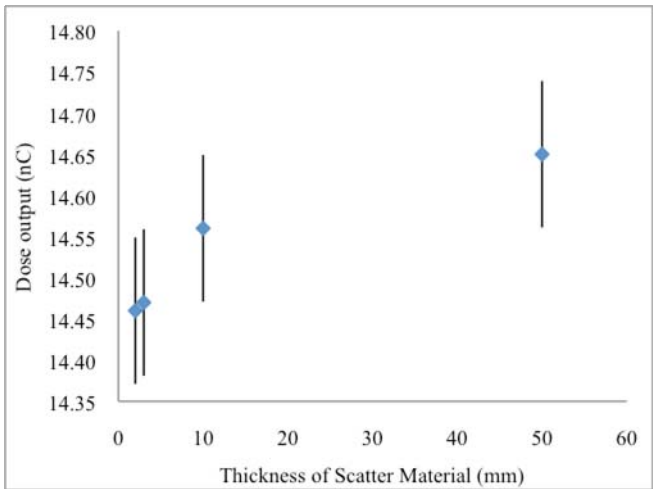

Fig. 1 Dose output measured by a Roos chamber with 2, 3, 10 and 50 mm thick scatter materials positioned above ^{192}Ir source.

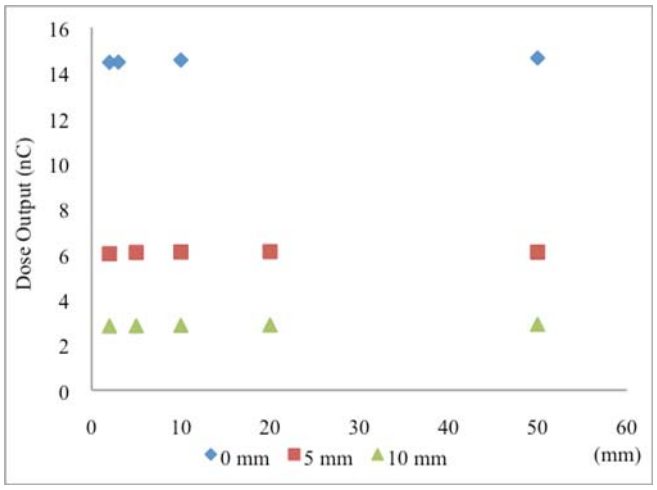

Fig. 2 Dose output measured by a Roos chamber with 0 (rhombus), 5 (square) and 10 mm (triangle) thick scatter materials placed between the planes of ^{192}Ir source and a Roos chamber.

ranging from 2 to 50 mm of scatter material was 0.5%. Calculated doses with 4, 10 and 50 mm thick Virtual Water slabs were slightly lower than anticipated in the order of 0.03%. The uncertainty in the Monte Carlo calculations as evaluated by the DOSRZnrc was generally less than 0.07%.

IV. Discussion

Fig. 4 summarizes the measured and calculated doses. The maximum variation in measured dose for scatter materials ranging from 2 to 50 mm was of the order of 1.3%.

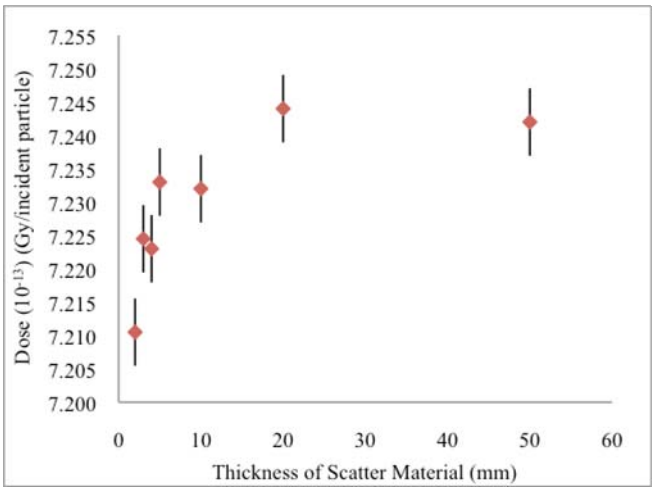

Fig. 3 Dose calculated by the EGSnrc Monte Carlo code for the scatter material thicknesses 2, 3, 4, 5, 10, 20 and 50 mm above ^{192}Ir source.

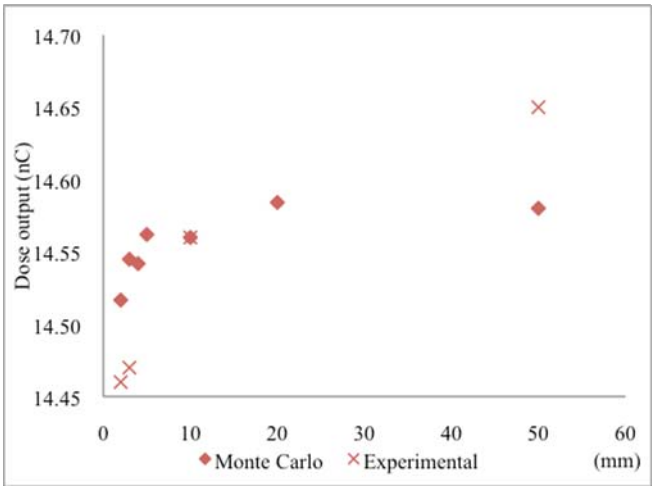

Fig. 4 Comparison of the dose output measured by a Roos chamber (cross) and the dose calculated by the EGSnrc Monte Carlo normalized to 10 mm detector depth from the surface (rhombus).

The Monte Carlo calculated results have shown that for the same range of scatter material thicknesses, the maximum variation was 0.5%. The increase in both measured and calculated doses over increasing scatter material thicknesses is consistent with the greater amount of scattering material causing dose to be scored in the region of the chamber. The Monte Carlo calculated doses were normalized to the measured doses at 10 mm detector depth from the surface. A depth of 10 mm was chosen to be a normalization point for a consistency with our in vivo measurement on a surface mould brachytherapy patient diagnosed with *hemangiosarcoma* (affecting the dorsal surface of the

scalp), whose treatment depth was also 10 mm from ^{192}Ir source [15].

In this paper, our modeling of ^{192}Ir source assumed an isotropic point source instead of an anisotropic seed for the purpose of optimizing the calculation efficiency. It is speculated that simplification of source modeling and phantom geometry could have affected the Monte Carlo calculations causing less variation in dose over compared scatter material thicknesses. It was also noted that the Monte Carlo results showed a small degree of dose decline with positioning of 4, 10 and 50 mm thick scatter materials. The reason remains obscured, however the decrease was regarded as negligible, being of the order of 0.03%.

This paper also predicted the likely consequences of misplacement of a detector in HDR brachytherapy dosimetry. 5 mm separation of the chamber from an isotropic point source resulted in the dose output decline to the order of 2.4. With 10 mm separation, the reduction was greater. The consequences will be even more critical for *in vivo* dosimetry of superficial brachytherapy treatments as the dose distribution of clinically available anisotropic ^{192}Ir seeds significantly differ to that of an isotropic point source's. Furthermore, ionization chambers are not regarded as the dosimeter of choice for in vivo dose verification and are usually replaced by compact sized TLD chips. However, compact sized dosimeters incorporate considerably smaller sensitive volume. Thus misplacement of the dosimeter or inaccurate verification of sensitive volume within the dosimeter, even by a fraction of a millimeter is well expected to result in inaccurate dose verification on patient surface.

High dose gradient of brachytherapy undoubtedly offers definite advantage in patient treatments. At the same time, it is also a critical drawback, which makes dosimetry difficult. Therefore it is crucial that user to accurately verify the effective point of measurement both on the regions of interest around patients and on the dosimeters.

V. Conclusions

The results from our Roos chamber measurements and Monte Carlo calculations are consistent and indicate that the thickness of the scatter material around ^{192}Ir source alters dose considerably with the Monte Carlo calculated results showing less variation in dose.

Given the complexity of HDR brachytherapy dosimetry due to the high dose gradients, there remain a number of options for further research. One issue would be to investigate the dosimetry closer to ^{192}Ir source, since the measurements indicated a large dose drop off close to the point source, as indicated by the isodoses. The ultimate goal of our research is to define a sophisticated model of ^{192}Ir source and a Roos chamber within the EGSnrc code.

Acknowledgment

The first author would like to acknowledge the following persons for their contributions. Dr. Benedict L Seo, Ms. Isla Nixon, Ms. Christine Thompson and Dr. Sivananthan Sarasanandarajah for their valuable advice and critical review of a paper.

References

1. C Palma, A Martinez, J R Guix, R Guix (2000) Treatment of skin carcinomas of the face by high-dose-rate brachytherapy and custom made surface moulds. *Int. J. Radiation Oncology Biol. Phys.* **47**:95-102
2. B V Sormanchi, A Stanton, M Webb, J Loncaster, E Allan, L.T.S.W Muir (2008) Hand function after high dose rate brachytherapy for squamous cell carcinoma of the skin of the hand. *Clinical Oncology* **20**:691-7
3. R K Das, B R Thomassen (2005) High dose rate sources and delivery systems. *Brachytherapy Physics Second Edition* Chapter 6, pp 59-74
4. R Nath, L Anderson, G Luxton, K A Weaver, J F Williamson, A S Meigooni (1995) Dosimetry of Interstitial Brachytherapy sources: Recommendation of AAPM Radiation Therapy Committee Task Group No. 43. *Med. Phys.* **22**:209-34
5. J Pérez-Calatayud, D Granero, F Ballester (2004) Phantom size in brachytherapy source dosimetric studies. *Med. Phys.* **31**:2075-81
6. P Karaiskos, A Angelopoulos, L Sakelliou, P Sandilos, C Antypas, L Vlachos, E Koutsouveli (1998) Monte Carlo and TLD dosimetry of an 192Ir high dose-rate brachytherapy source. *Med. Phys.* **25**:1975-84
7. CNMC at http://www.cnmcco.com
8. R Hill, L Holloway, C Baldock (2005) A dosimetric evaluation of water equivalent phantoms for kilovoltage x-ray beams. *Phys. Med. Biol.* **50**:331-44
9. R F Hill, S Brown, C Baldock (2008) Evaluation of the water equivalence of solid phantoms using gamma ray transmission measurements. *Radiation Measurements* **43**:1258-64
10. A S Meigooni, Z Li, V Mishra, J F Williamson (1994) A comparative study of dosimetric properties of Plastic Water and Solid Water in brachytherapy applications. *Med. Phys.* **21**:1983-7
11. Absorbed dose determination in external beam radiotherapy. In: *Technical Report Series No. 398.* pp 211, 40
12. I Kawrakow (2000) Accurate condensed history Monte Carlo simulation of electron transport. I. EGSnrc, the new EGS4 version. *Med. Phys.* **27**:485-98
13. Ionizing Radiation Detector Catalog at http://www.ptw.de
14. G M Daskalov, E Loffler, J F Williamson (1998) Monte Carlo-aided dosimetry of a new high dose-rate brachytherapy source. *Med. Phys.* **25**:2200-8
15. H Seo, M Haque, R Hill, C Baldock (2008) In-vivo dosimetric verification of a HDR brachytherapy surface mould. *Australas. Phys. Eng. Med.* **31**:519

Author: Hyong Seo
Institute: Auckland District Health Board
Street: 2 Park Road, Building 8, Level 4, Graton 1010
Country: New Zealand
Email: hyongs@adhb.govt.nz

Validating methodologies for evaluation of patient doses submitted to chest x-ray examinations

P. M. C. de Oliveira[1], P. L. Squair[2], V. L. S. de Oliveira[1], M. E. S. Abrantes[1], T.C.Alonso[2], T. A. da Silva[1,2]

[1]Nuclear Sciences and Techniques Post-Graduation Course, Nuclear Engineering Department-
Federal University of Minas Gerais – UFMG, Belo Horizonte, MG, Brazil
[2]Development Center of Nuclear Technology – CDTN
Brazilian Commission of Nuclear Energy, CNEN, Belo Horizonte, MG, Brazil

Abstract—. **Reliability of methodologies for assessing patient doses is achieved through validation process. Absorbed dose in selected organs were measured in a Rando-Alderson phantom under chest examination conditions. Results were compared to dose values that were obtained by simulating the same conditions in the PCXMC® computational software. Both methodologies agreed in an acceptable manner.**

Keywords— **patient dose, chest examination, Rando-Alderson phantom, PCXMC®**

I. Introduction

Radiodiagnostic with x-rays provides the highest dose contribution to the population due to exposures to man-made radiation sources [1]. Benefits and risks of medical procedures with radiation are required to be known; patient doses are also expected to be optimized without reducing the image quality [2].

Dosimetric studies of patients submitted to diagnostic x-rays have got a special attention in Brazil although they are not required in Brazilian legislation [3].

Dosimetry based on direct measurements in patients undergoing x-ray examinations cannot be easily performed. Experimental measurements with physical phantoms and theoretical calculations with computational software are widely used instead [4].

Reliable methodologies for patient dose assessment are expected to be validated under many conditions. This work compared two methodologies used for evaluating the organ absorbed doses in patients undergoing chest x-rays.

II. Materials and Methods

Absorbed doses in selected organs were experimentally determined in an anthropomorphic Rando-Alderson phantom with thermoluminescent dosemeters [5]. The Rando-Alderson phantom was positioned as in a typical chest examination (one lateral and one posteroanterior (PA) geometry).

Radiation exposures were done in the CDTN Dosemeter Calibration Laboratory with a VMI Pulsar 800 Plus medical x-ray machine (10 to 125 kV, 50 to 800 mA, 2.1 mmAl inherent filtration, 2.48 mmAl half-value layer and 4.65 mGy/mA.min output at 80 kV.

Figure 1 shows the phantom under the lateral exposure geometry during x-ray exposures.

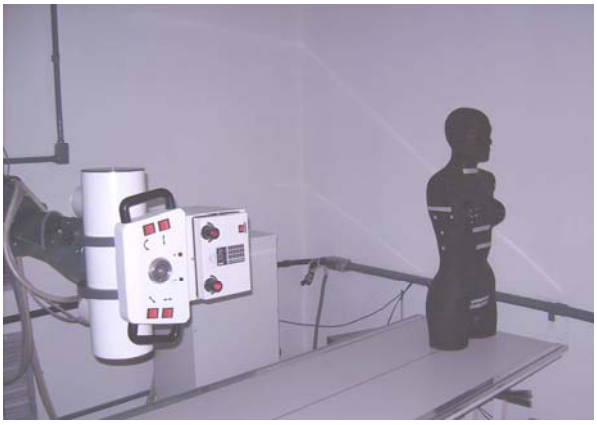

Fig. 1. Lateral geometry used during the exposure of the Rando-Alderson phantom in an x-ray beam.

Harshaw/Bicron LiF:Mg,Ti (TLD-100) dosemeters were used after being selected in terms of reproducibility and homogeneity and calibrated in an x-ray reference radiation of 54 keV (similar to the W80 ISO series) to reduce uncertainties [6]. Calibration was done in terms of air kerma against a 9015 Radcal Corporation ionization chamber traceable to the national standard laboratory as internally recommended [7].

Two hundred TL dosemeters were distributed inside then the Rando-Alderson phantom; the precise position of the

O. Dössel and W.C. Schlegel (Eds.): WC 2009, IFMBE Proceedings 25/III, pp. 400–402, 2009.
www.springerlink.com

organs was determined by CT of the phantom with the help of radiologists. Fig.2 shows the Rando-Alderson phantom and its CT image.

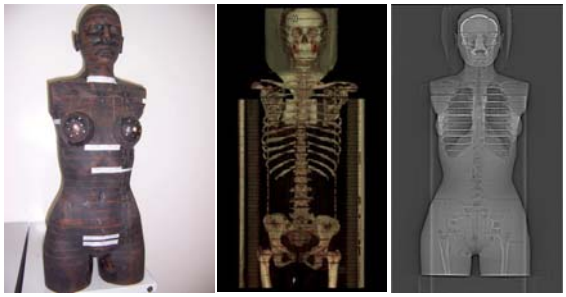

Fig. 2. The Rando-Alderson phantom and its CT to establish the organ positions.

Many exposures under the same conditions were needed to get TL readings above the lower detection limit in a reliable 4500 Harshaw/Bicron reading system. Some TL dosemeters were put on the phantom for measuring the entrance surface dose (ESD).

The PCXMC® Monte Carlo based software was used to estimate the organ doses [8]. The same x-ray beam parameters, the positioning geometry, the phantom biotype (1.67 m height, 65 kg weight, 30 years-old) and exposure conditions given to Rando-Alderson phantom were input to the software. Figure 3 shows the first entrance datum window of the PCXMC®.

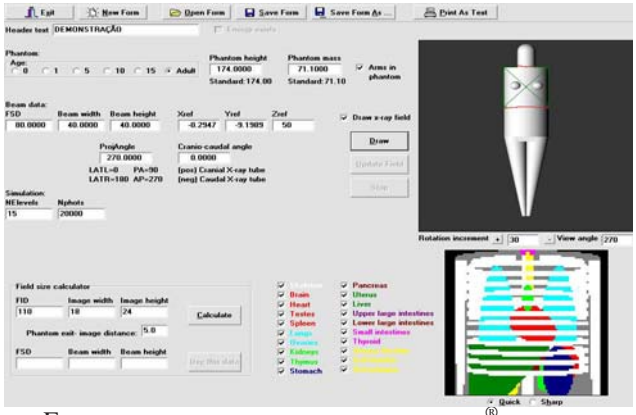

Fig. 3. The entrance datum window of the PCXMC® software.

III. Results

Table 1 and Fig. 4 show the absorbed dose values determined by the two methodologies: the Rando-Alderson phantom and the PCXMC®, in selected organs due to both exposures lateral and PA. Expanded uncertainties in the experimental dose values were assessed to be lower than 15% (coverage factor equals to 2) except for low dose values (ovaries); the PCXMC® provided the uncertainties due to statistical calculations that are directly related to the number of photon histories.

Table 1 - Organ absorbed doses in the Rando-Alderson phantom and determined by PCXMC® software.

Organ	Absorbed Dose (μGy)		Difference
	Experimental	PCXMC	(%)
Lungs	394±59	269±13	32
Bone Marrow	143±21	99±5	30
Liver	227±34	231±12	-2
Spleen	184±28	178±,9	3
Ovaries	0.25±0.20	1.0±0.3	-296

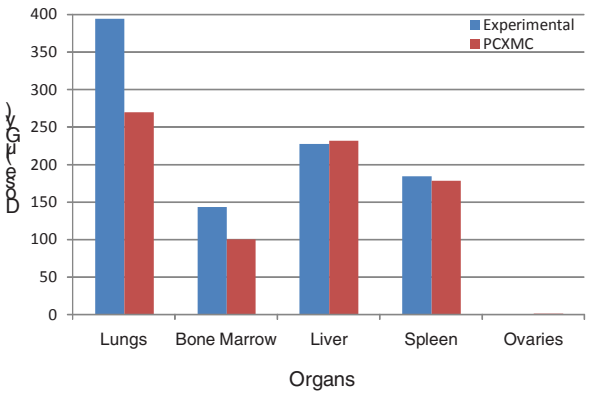

Fig. 4 Comparison between absorbed dose values in selected organs as determined by experimental and computational methodologies.

Results showed that absorbed doses experimentally determined in the Rando-Alderson phantom and by the PCXMC® methodology agreed acceptably for the lungs, bone marrow, liver and spleen. Results could be influenced by differences between localization and anatomic shape of the organ in the phantom and in the PCXMC® model.

As the ovaries were outside the primary radiation field they showed very low dose values with high uncertainties.

The entrance surface dose were found as (1222±183)μGy and (506± 760) μGy for lateral and PA geometry, respectively; they complied with the ESD values of 1500 and 400μGy established by Brazilian regulation.

IV. Conclusions

Although the x-ray parameters used in this work did not represent a standard technique used in the medical field, it is possible to state that both methodologies (experimental measurements and the PCXMC®) were validated for chest examination. It should be considered that organs that were not within the primary radiation field might show unreliable dose values.

As experimental phantom measurements require a hard and timely consuming work, validated software as the PCXMC® should be recommended to be used for routine patient dosimetry in a large scale.

Acknowledgment

T. A. da Silva is thankful to CNPq and FAPEMIG for providing research fellowships and financial resources for the development the project.

All team is grateful to get this work supported by the Ministério de Ciência e Tecnologia - MCT/Brazil, through the Brazilian Institute of Science and Technology for Radiation Metrology in Medicine.

References

1. IAEA. INTERNATIONAL ATOMIC ENERGY AGENCY, Radiological Protection for Medical Exposure to ionizing Radiation, *Safety Standards*. Series no. RS-G-1.5, 2002.
2. IAEA - International Atomic Energy Agency, Radiological Protection of Patients in Diagnostic and Interventional Radiology. Proceedings of an International Conference held in Malaga, (2001).
3. Health Minister – Brazil – Radiological Protection Directives for Medical and Dental Radiodiagnostic [in Portuguese]. D.O.U. June 1998.
4. ICRU. INTERNATIONAL COMMISSION ON RADIATION UNITS E MEASUREMENTS. Patient dosimetry for x rays used in medical imaging. Bethesda, Maryland: ICRU publications, Report 74, 2005.
5. ALDERSON RANDO© - Copyright (1995), The Phantom Laboratory. © Copyright (1973) ARL Inc. Departament of Radiology, The University of Chicago – Chicago, Illinois.
6. INTERNATIONAL ORGANIZATION FOR STANDARDIZATION. ISO 4037: X and gamma reference radiation for calibrating dosemeters and doserate meters and for determining their response as a function of photon energy, Geneva, (1996)
7. INTERNATIONAL ATOMIC ENERGY AGENCY. Dosimetry in Diagnostic Radiology: An International Code of Practice.: Vienna: IAEA 2007. 359 p. (Technical reports series, 457) (2007).
8. STUK-139 Tapiovaara M, Lakkisto M, Servomaa A. PCXMC – A PC-based Monte Carlo program for calculating patient doses in medical x-ray examinations. Helsinki (1997).

Author: Da Silva, Teógenes Augusto
Institute: Development Center of Nuclear Technology – CDTN/CNEN
Street: Av.Pres.Antonio Carlos 6627 – Pampulha – UFMG Campus
City: Belo Horizonte, Minas Gerais
Country: Brazil
Email: silvata@cdtn.br

Scattering Medium Depth and Cell Monolayer Positioning with Respect to Beam Field Affect Cell Viability

J. Rogoliński[1], M. Konopacka[1], A. Sochanik[2], and K. Ślosarek[3]

[1] Maria Sklodowska-Curie Memorial Cancer Center and Institute of Oncology, Gliwice Branch/Department of Experimental and Clinical Radiobiology, Wybrzeże Armii Krajowej 15, 44-100 Gliwice, Poland

[2] Maria Sklodowska-Curie Memorial Cancer Center and Institute of Oncology, Gliwice Branch/Department of Molecular Biology, Wybrzeże Armii Krajowej 15, 44-100 Gliwice, Poland

[3] Maria Sklodowska-Curie Memorial Cancer Center and Institute of Oncology, Gliwice Branch/Department of Radiotherapy and Brachytherapy Treatment Planning, Wybrzeże Armii Krajowej 15, 44-100 Gliwice, Poland

Abstract— **The purpose of this study was test the cytotoxic effect of scattered radiation generated with penetration of medium depth upon cells placed inside a water phantom with respect to beam field.**

We tested the viability of A549 cells exposed to photon radiation, both within the beam field or outside of it.

Our measurements show that cells placed within the beam field show decreased viability as compared to non-irradiated control ones, and scale of this effect depends of medium depth.

Surprisingly was done, that comparing to non-irradiated cells, the cells placed during exposure outside of the beam field showed decreased viability too.

This finding suggests that healthy cells lying outside of the beam field might die as a result of irradiation during radiotherapy.

Keywords— **Scattered radiation, water phantom, cell viability, medium depth, human A549 cells.**

I. Introduction

Linear electron accelerators used for cancer radiotherapeutic purposes generate photon and electron radiation having nonmonenergetic spectrum. During passage through an absorbing medium this radiation is scattered and its energy spectrum is altered with increasing penetration depth the contribution of incident radiation decreases whereas that of scattered radiation becomes greater [1]. Since biological effectiveness of radiation depends on its energy, this alteration in energy spectrum may affect biological processes [2]. Our previews work on the electron radiation [3] showed that with increasing medium depth the number of cells with chromosomal damage was greater than expected from received physical dose used in routine procedure in radiotherapy. In present study we tested relationship between the cell viability and the mode of cell monolayer exposure (cell within beam field or outside in different depth) to photon irradiation.

II. Materials and Methods

The study was performed using human A549 cell line (lung adenocarcinoma). As the irradiation source, a linear electron accelerator was used (Clinac 2300 CD); 6 MV photon radiation was applied at 100 MU/min accelerator mode. A 5 Gy dose was applied at the maximum dose depth. Tests were performed at two medium depth: 5,4 and 15 cm as presented in Fig.1.

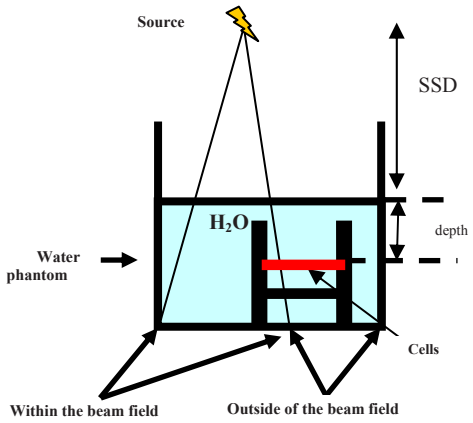

Fig.1 Schema of plates irradiation (SSD – source surface distance)

To assess viability we scored the percentage of dead cells (trypan blue exclusion test) and measured cells' ability to metabolize MTS (a tetrazolium salt) to a spectrophotometically-identifiable formazan. For the latter measurements we made use of 96-well plates placed horizontally in the water phantom in such a way that part of wells was within the irradiation beam field whereas the rest was outside of it.

O. Dössel and W.C. Schlegel (Eds.): WC 2009, IFMBE Proceedings 25/III, pp. 403–405, 2009.
www.springerlink.com

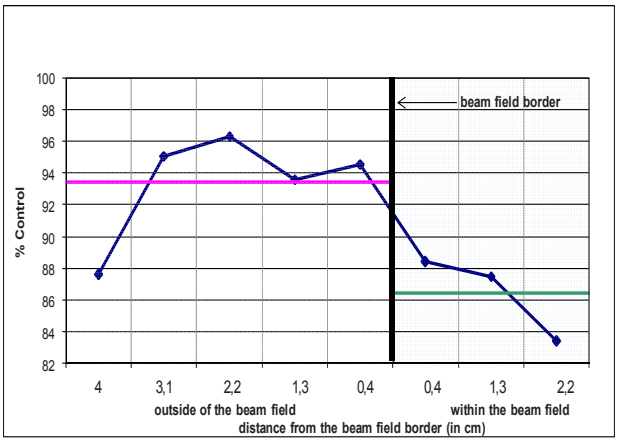

Fig.2. Viability of cells irradiated in water phantom (depth 5,4 cm) within or outside of the beam field.

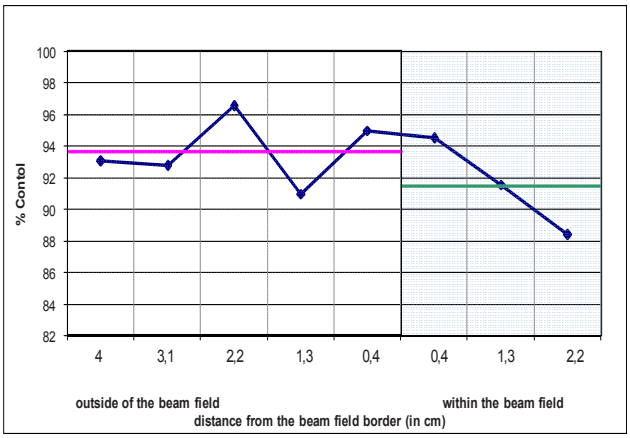

Fig.3. Viability of cells irradiated in water phantom (depth 15 cm) within or outside of the beam field.

Each well contained 5000 cells in 200 µl DMEM F12 medium supplemented with FCS. In each row lying at given distance from the beam field border were 8 repeated wells. After irradiation, the plates were incubated for 48 hours at 37° C in a humidified, 5% CO_2 atmosphere. Next we removed the medium, added diluted MTS (1:10 in colorless medium) and recorded the absorbance at 490 nm.

III. Results and Discussion

MTS test results have indicated that cells exposed within the beam field or outside of the field show decreased viability as compared to controls. As is presented in Fig. 2 and Fig.3 respectively, this effect is diminished at 15 cm of depth in comparison to 5,4 cm. Viability of cells outsider of the beam field is lower than that of control cells and, to practical purposes, independent of medium depth.

Identification of dead cells by trypan blue exclusion confirmed the MTS test results.

Our results can be explain by the action of scattered irradiation that is present either within the beam field (in all depths of medium, especially in greater depth) or outside the beam field.

It has been showed that the effects of very low doses, such as a low-dose hypersensitivity and bystander effects are greater than would be predicted by conventional radiobiology [4]. Although these observations show that very low irradiation can damage and/or die the cells but radiotherapy procedures don't take this into consideration.

V. Conclusions

Cells placed not only within the beam field but also outside of it show decreased viability as compared to non-irradiated cells. This suggests that a fraction of cells in healthy tissues lying outside of the beam field and independently of depth might die as a result of irradiation.

Acknowledgement

This study was supported by a grant from the Ministry of Science and Higher Education No. NN402 4447 33.

References

1. Briot E (1982).:Etude dosimetrique et comparaison des faisceaux d'electrons de 4 a 32 MeV issus de deux types d'accelerateurs lineaires avec balayage et diffuseurs multiples, Universite Paul Sabatier, Toulouse
2. Malicki J. Łobodziec W., Ślosarek K (1990).: Dose rate distribution under partially shielded beams. Strahlentherapie Onkol., 66: 733-737.
3. Rogoliński J., Konopacka M., Sochanik A., Ślosarek K. (2006) Effect of water phantom depth upon radiation-induced cytogenetical damage of cells. Polish Journal of Environmental Studies, 15 (4A): 198-201.
4. Mothersill C., Seymour C.B., Joiner M.C. (2002): Relationship between radiation-induced low-dose hypersensitivity at the bystander effect. Radiation Research. 257: 526-532.

The address of the corresponding author:

Author: Jacek Rogoliński
Institute: Comprehensive Cancer Centre, Maria Skłodowska-Curie Memorial Institute, Gliwice Branch
Street: Wybrzeże Armii Krajowej 15
City: Gliwice
Country: Poland
Email: rogolinski@io.gliwice.pl

Effect of Modulated Microwave Exposure on Spectral Asymmetry of Human EEG

A. Suhhova, H. Hinrikus, M. Bachmann, J. Lass

Department of Biomedical Engineering, Technomedicum of the Tallinn University of Technology, Tallinn, Estonia

Abstract— **This study was aimed to investigate the effect of modulated low-level microwave radiation on the human electroencephalographic (EEG) signal. The 450 MHz microwave exposure 100% pulse-modulated at 40 Hz frequency was applied to a group of 14 volunteers. The field power density at the scalp was 0.16 mW/cm^2. Ten cycles of the exposure (1 min on and 1 min off) were applied. The resting 9 channels EEG was recorded during 20 minutes in exposed and sham conditions. The EEG spectral asymmetry index was calculated as a relative difference in powers of high and low EEG frequency bands. The analysis revealed statistically significant changes caused by microwave exposure for the whole group in temporal, parietal and occipital EEG channels. The exposure caused increase in the calculated EEG spectral asymmetry index values related to increase in the EEG beta power.**

Keywords— **non-ionizing radiation, microwave effect, human EEG, spectral asymmetry.**

I. Introduction

Wide use of telecommunication equipment causes increasing interest to the effects of low-level modulated microwave radiation on human brain. A number of investigators have reported that exposure to a low-level microwave radiation produces alterations in the resting electroencephalographic (EEG) signal and/or brain behaviors [1 – 7]. Despite of many investigations, the observed effects of low-level microwave were subtle and the underlying mechanisms remain still unknown. Difficulties experienced in replication of experimental findings have caused doubts concerning these effects. Therefore new and more sensitive measures for detection of the microwave effect on EEG would be useful.

In our previous studies the modulated at different low frequencies microwave exposure was shown to increase the EEG power in the EEG alpha and beta frequency bands in all EEG channels. Most regular increase occurred in the EEG beta band power and no significant changes were revealed in the EEG theta band power [3, 7]. Based on these findings, we can assume that relative changes in the EEG power spectrum can characterize the effect of microwave exposure. On the other hand, a new indicator for depressive disorder, spectral asymmetry index (SASI), was recently proposed and investigated [8].

The aim of this study was to apply the spectral asymmetry index SASI to evaluate the specific changes produced by microwave exposure in human resting EEG.

II. Materials and methods

A. Subjects

Experiments were carried out on a group of healthy volunteers, consisting of 14 young healthy persons (aged 21–24): eight male and six female. All the subjects selected had no medical or psychiatric disorders. During the experiments, the experimenter and the subjects were in the dark laboratory room. The subjects were lying in a relaxed position, eyes closed and ears blocked during the experiments. All the subjects passed two recording sessions — with microwave exposure and sham exposure. For each recording session, the exposure conditions were randomly assigned. The subjects were not informed of their exposure during a session, however, they were aware of the possibility of being exposed.

The study was conducted in accordance with the Declaration of Helsinki and has formally approved by the local Medical Research Ethics Committee.

B. Microwave exposure

Electromagnetic radiation of 450 MHz was generated by a Rhode & Swartz signal generator (model SML02), The microwave radiation was 100% pulse-modulated at 40 Hz frequency (duty cycle 50%). The output power of 1 W was guided by a coaxial lead to the 13 cm quarter-wave antenna located at 10 cm from skin on the left side of head.

The spatial distribution of the electromagnetic radiation power density was measured by the Fieldmeter C.A 43 field strength meter. The measurements were performed by the Central Physical Laboratory of the Estonian Health Protection Inspection. The calibration curves of the dependence of field power density on the distance from the radiating antenna were obtained from these measurements, performed under real experimental conditions. Estimated

O. Dössel and W.C. Schlegel (Eds.): WC 2009, IFMBE Proceedings 25/III, pp. 406–409, 2009.
www.springerlink.com

from the measured calibration curves field power density at skin was 0.16 mW/cm^2. During the experiments a Digi Field C field strength meter was used to monitor the stability of the electromagnetic radiation level. The specific absorption rate (SAR) was calculated using SEMCAD software. The calculated spatial peak SAR averaged over 1 g was 0.303 W/kg.

C. Experimental procedure and EEG recording equipment

Our experimental study was performed according to the recording protocol identical for all subjects. All subjects completed the session with microwave exposure and sham.

In exposed recordings for the duration of every even minute of the recording the subject was exposed to microwave. The pair of successive reference minute followed by exposed minute was an exposure cycle. All subjects passed 10 cycles of exposure. EEG was continuously recorded during 20 minutes. Sham recording session used the same protocol, except that the microwave power was switched off. For each recording session, the exposure conditions (exposed or sham) were randomly assigned between subjects.

The Cadwell Easy II EEG measurement equipment was used for the EEG recordings. The EEG was recorded using 9 electrodes, which were placed on the subject's head according to the international 10-20-electrode position classification system. The channels for analysis were chosen to cover the entire head: frontal – FP1, FP2; parietal – P3, P4, temporal – T3, T4; occipital – O1, O2 and the reference electrode Cz. The EEG recordings were stored on a computer at a 400 Hz sampling frequency.

Artifacts can be induced by parasitic demodulation of the radio-frequency electromagnetic components on the EEG electrodes and equipment. To detect possible parasitic interaction between the recording and radio-frequency equipment, the set-up was validated before the experiments. The recordings on phantom were conducted in accordance with the procedure of the study. Multichannel recordings in frequency band 0.5-48 Hz detected spectral components at the modulation frequency 40 Hz. No other spectral components were detected. The artifacts at the modulation frequencies were removed from the EEG signals by off-line filtering during the pre-processing of the signals in the LabVIEW programming and signal-processing environment. Elliptic bandstop filters with an attenuation of 50 dB in the stopband were used.

The pre-processing of the signals was performed in the LabVIEW programming and signal-processing environment. The EEG spectrum 0.5 - 39 Hz was selected for the analysis. Such a selection excluded possible modulation frequency artifacts.

D. EEG analysis

The spectral asymmetry index was calculated using comparison of EEG powers in two selected EEG frequency bands. The EEG analysis comprises of four main operations: 1) estimation of power spectral density of the recorded EEG signal; 2) selection of boundary frequencies of high and low EEG frequency bands; 3) calculation of the EEG power in the selected bands; and finally 4) calculation of spectral asymmetry as a combination of the EEG powers in the selected frequency bands.

1) The power spectral density of the recorded EEG signal was estimated by means of Welch's averaged periodogram method. The signal was divided into overlapping sections (50%), with the length of 1024 points and windowed by the Hanning window.

2) The frequency limits of the high and low EEG frequency bands were selected as follows. The first step was estimating the central frequency band with the maximum spectral power f_{max} in the region of alpha band 8-13Hz of the recorded EEG signal. Thereafter the best parabolic fit was calculated to the ($f_{max} \pm a$) Hz spectrum, where a was half-width of the EEG central frequency (alpha) band. The maximum point of the fitted parabola fp_{max} was taken as a centre of the central band. This frequency is different for individual subjects.

The frequency limits for low and high frequency bands for an individual subject were determined as follows: low frequency band from F1= (fp_{max} – 6) Hz to F2= (fp_{max} – 2) Hz and high frequency band from F3= (fp_{max} + 2) Hz to F4= (fp_{max} + 26) Hz.

In this study the fixed boundary frequencies averaged for the whole group were applied: low frequency band from F1=4 Hz to F2=8 Hz and high frequency band from F3=14 Hz to F4=38 Hz.

3) Afterwards, the EEG signal power W_{lmn} in the low EEG frequency band (F1-F2) Hz and the power W_{hmn} in the high EEG frequency band (F3-F4) Hz was computed for each subject (indexed by $n \in [1,14]$) and channel (indexed by m=1,8) as the area under the spectrum for the corresponding frequency band (integral of the power spectral density over the band).

4) Finally, the spectral asymmetry index SASI was calculated as relative difference between powers of the high and low frequency bands

$$SASI = \frac{W_{hmn} - W_{lmn}}{W_{hmn} + W_{lmn}} \quad (1)$$

The Student t-test was applied for statistical comparison of the results between depressed and healthy subjects

separately in each EEG channel. The Bonferroni correction for multiple comparisons was used. The confidence level of 0.05 was considered statistically significant to the Bonferroni corrected *p*-values.

III. Results and discussion

Parameter SASI values were calculated in each EEG channel (8) for all subjects.

Calculated SASI values averaged over a group for recordings in microwave exposure and sham conditions are presented in Fig.1.

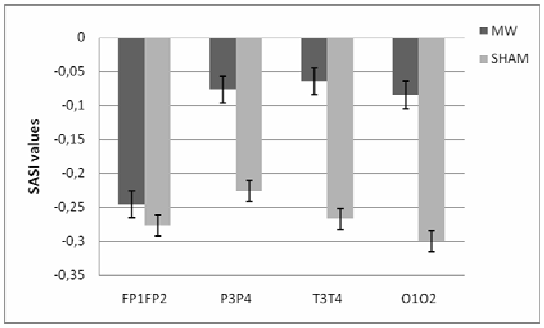

Figure.1. The calculated SASI values averaged over 10 exposure cycles, 14 subjects and 2 symmetric EEG channels in frontal, temporal, parietal and occipital brain regions for recordings in microwave exposure (MW) and sham condition.

Table 1. Results of *t*-test performed for evaluation of differences between the calculated SASI values in microwave exposure and sham conditions

Channel	FP1	FP2	T3	T4	P3	P4	O1	O2
P-values	0,91	0,36	0,03	0,02	0,02	0,03	0,01	0,02

As can be seen in Fig.1 the microwave exposure reduces averaged SASI parameter values in all analyzed channels compared to sham condition. The biggest differences occur in occipital channels, the changes in frontal channels are minimal.

The Student t-test performed for sham and microwave conditions reveals the changes to be statistically significant in all analyzed channel, except FP1 and FP2. (Table1).

Calculation of SASI values performed for exposed and reference minutes during recordings in microwave exposed conditions showed also negative SASI values averaged over 10 cycles in exposed compared to reference minutes. The biggest differences occur in P3 channels. No significant differences in SASI values during recordings in sham conditions.

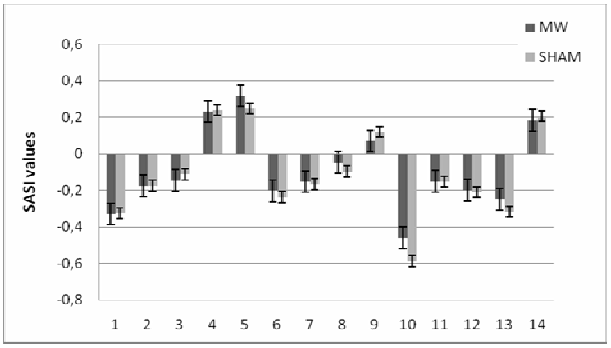

Fig.2. The calculated SASI values for individual subjects in P3 channels averaged over 10 exposure cycles.

The changes in SASI produced by microwave exposure for individual subjects are shown in Fig.2.

The results show negative average values of SASI in both microwave expose and sham conditions, but average SASI values are more positive in the case of microwave exposure.

The applied in this study spectral asymmetry index becomes more positive in the case of increased power in the high EEG (beta) band. Our experimental results showed more positive average SASI values in microwave exposed conditions (Fig. 1). The SASI values calculated for individual subjects are also more positive with exposure for majority of subjects (Fig. 2). These findings confirm increase in the power of higher EEG frequency bands in microwave exposed conditions and are in a good agreement with the results reported in other studies [2, 3, 6].

On the other hand, higher beta power has been shown characteristic for depressive disorder [9, 10]. Microwave exposure seems to disturb brain activity but only by a soft manner.

As can be seen from Fig. 2, about 28% of subjects involved in experiment showed positive SASI parameter values and are not affected by microwave exposure. The percentage of subjects not affected by microwave exposure was the same for all analyzed channels. Individual sensitivity to microwave exposure has been shown to be different [7]. Correlation of polarity of the SASI parameter with individual sensitivity to microwave exposure would be of interest and need further investigation.

IV. Conclusion

Our results suggest that the spectral asymmetry index as a combination of powers of high and low EEG frequency bands is promising for distinction of the effect of microwave radiation on the EEG. The proposed SASI parameter differs significantly between exposed and sham exposed conditions. The increase in the calculated EEG spectral asymmetry index values is related to increase in the EEG beta power.

Acknowledgement

This study was supported by the Estonian Science Foundation Grant No 6632, by the Estonian targeted financing project SF0140027s07, and by the European Union through the European Regional Development Fund.

References

1. Cook C, Saucier D, Thomas A, Prato F (2006) Exposure to ELF magnetic and ELF-modulated radiofrequency fields: the time course of physiological and cognitive effects observed in recent studies. Bioelectromagnetics 27: 613-627
2. Huber R, Treyer V, Schuderer J et al (2005) Exposure to pulse-modulated radio frequency electromagnetic fields affects regional cerebral blood flow. Eur J Neurosci 21:1000–1006
3. Hinrikus H, Bachmann M, Lass J et al (2008) Effect of 7, 14 and 21 Hz modulated 450 MHz microwave radiation on human electroencephalographic rhythms. International Journal of Radiation Biology 84:69-79
4. Bachmann M, Säkki M, Kalda .J et al (2005) Effect of 450 MHz microwave modulated with 217 Hz on human EEG in rest. The Environmentalist 25: 165-171
5. Huber R, Treyer V, Borbely A et al (2002) Electromagnetic fields, such as those from mobile phones, alter regional cerebral blood flow and sleep and waking EEG. J Sleep Res 11: 289–295
6. Curcio G, Ferrara M, Moroni F et al (2005). Is the brain influenced by a phone call? An EEG study of resting wakefulness. Neurosci Res 53: 265–270
7. Hinrikus H, Bachmann M, Lass J et al (2008) Effect of low frequency modulated microwave exposure on human EEG: Individual sensitivity. Bioelectromagnetics 29: 527-538
8. Hinrikus H, Bachmann M, Lass J et al (2008) Method and device for determining depressive disorders by measuring bioelectromagnetic signals of the brain. US12/196335
9. Knott V, Mahoney C, Kennedy S, Evans K (2001) EEG power, frequency, asymmetry and coherence in male depression. Psychiatry Research: Neuroimaging. 106:123 – 140
10. Sun Y, Li Y, Zhu Y et al (2008) Electroencephalographic differences between depressed and control subjects: an aspect of interdependence analysis. Brain Res Bull 76:559-564

Author: Anna Suhhova

- Institute: Technomedicum of the Tallinn University of Technology
- Street: Ehitajate road 5
- City: Tallinn
- Country: Estonia
- Email: anna@cb.ttu.ee

Trigger Levels to Prevent Tissue Reaction in Interventional Radiology Procedures

A. Trianni[1], D. Gasparini[2], and R. Padovani[1]

[1] Medical Physics Department, University Hospital, Udine, Italy
[2] Radiology Department, University Hospital, Udine, Italy

Abstract— **It is well known that the large use of fluoroscopy in interventional radiology procedures may induce unintended patients' skin injuries. For that reason assessment of skin dose for these procedures is getting more and more important.**

Aim of the study is to investigate the role of cumulative air kerma (CK) as on-line dose indicator and to evaluate the possibility to define a local CK trigger level which can help operators to identify situations with high probability to exceed a peak skin dose of 2 Gy, the threshold dose for transient skin erythema. Cerebral angiography, aneurysm embolisation and chemoembolisation of liver cancer have been identified as the interventional procedures where high skin doses could be delivered.

Dosimetric data (CK, air kerma area product (KAP) and fluoroscopy time) have been collected in a sample of procedures and peak skin dose (PSD) have been measured from dose distributions measured with large area radiochromic films (Gafchromic, IPS, USA) located between table top and patient.

PSD varied in very wide range and in a few cases were close to the threshold for main erythema and epilation (6 Gy). The correlations between PSD and CK have been successfully assessed for each procedure type and a trigger level for CK has been derived to alert the interventionalist on the probability to have reached a PSD of 2 Gy.

In our center trigger levels of 5200 mGy and 2500 mGy has been established for brain aneurysm embolisation and chemoembolisation procedures respectively.

As suggested by ICRP in the publication No. 85, a follow-up for patients whose estimated peak skin dose was 3 Gy or greater has been implemented as a routine practice.

Keywords— **Interventional radiology, maximum skin dose, cumulative dose, trigger level.**

I. Introduction

The extensive use of fluoroscopy in interventional radiology procedures may induce unintended patients' skin injuries varying from erythema to necrosis. Some cases have been described in a review paper by Koenig et al. [1,2].

As stated by the European regulation 97/43/Euratom patient dose should be periodically evaluated to guarantee optimisa-tion and justification of the practice. Moreover the ICRP (International Commission on Radiological Protection) recom-mends to provide an adequate follow-up and eventual treatment of these injuries, for patients whose skin dose has been 3 Gy or greater [3].

Maximum skin dose (MSD) could be directly measured using film or thermoluminescent dosimeters (TLDs) [4,5]. In this way the operator doesn't have an immediate knowledge on the amount of dose received by patient. It is important to perform an "on-line" evaluation (e.g.: during the procedure) of patient's skin dose to individuate those procedure in which it could be greater than threshold for deterministic effects. Therefore dosimetric indicators for estimating and monitoring patient skin dose in routinely practice should be individuated.

For interventional radiology procedures kerma-air product (KAP) and cumulative air kerma (CK) at the interventional reference point (IRP) could be used as dosimetric indicators for skin dose.

Aim of this work is investigating the correlation between these parameters and the skin dose directly measured in a sam-ple of procedure.

The dosimetric indicator that better correlate with the MSD could then be used to define trigger levels that indicate the overcoming of threshold for deterministic effects and necessity of medical follow-up for possible radiation injuries, respectively.

II. Materials and Methods

In the period October 2007 – October 2008 data from procedures, both diagnostic and interventional, performed in two interventional rooms in Udine university hospital (Udine, Italy) have been collected.

The procedures were performed with two angiographic system equipped with a digital flat panel detector by four experi-enced radiologists.

The peak skin dose (PSD) has been measured with radiochromic films (Gafchromic XR-typeR, IPS, USA), placed between patient and couch in a sample of 61 procedures. Radiochromic films have been calibrated under an angiographic beam for comparison with an ionisation chamber (Radcal, Model 2026C 6cc ion cahmber).

Films were read with a flatbed scanner (Epson 1680pro) in reflective mode. Images obtained were evaluated in terms of dose with a Matlab home-made routine.

The correlations between PSD and KAP and PSD and CK have been investigated for each procedure type.

O. Dössel and W.C. Schlegel (Eds.): WC 2009, IFMBE Proceedings 25/III, pp. 410–413, 2009.
www.springerlink.com

III. RESULTS

Data collected are summarized in Table 1, in which are reported: type of procedure, number of patients, mean values of fluoroscopy time (FT), kerma-area product (KAP) and cumulative air kerma (CK) at IRP.

Table 1. Mean and SD fluoroscopy time (FT), air kerma-area product (KAP) and cumulative air kerma (CK) for a sample of interventional procedure performed at Udine University Hospital in the period October 2007- October 2008.

Procedure	No	FT (min)	KAP ($Gycm^2$)	CK (mGy)
Cerebral Angiography	197	6.1 ± 8.2	71.1 ± 49.2	770.9 ± 887.4
Aneurysm Embolization	76	26.6 ± 13.5	135.4 ± 60.8	2153.7 ± 1345.3
Chemo-embolization	144	14.1 ± 7.7	210.5 ± 138.6	1136.3 ± 767.9
Embolizations	57	26.2 ± 41.6	269.7 ± 320.8	1384.7 ± 1472.0
Peripheral Angiography	145	1.4 ± 1.9	43.4 ± 29.3	154.5 ± 106.1
Lower limb angioplasty	44	15.6 ± 9.9	24.7 ± 37.6	149.0 ± 237.6
Carotid angioplasty	73	9.4 ± 5.5	53.7 ± 26.0	247.3 ± 135.7
Iliac angioplasty	45	11.4 ± 9.8	80.5 ± 89.5	401.9 ± 293.8
Below-knee angioplasty	27	17.9 ± 10.4	8.9 ± 14.3	101.8 ± 326.0
Renal angioplasty	12	7.7 ± 3.5	48.8 ± 54.8	308.6 ± 270.3
AAA/AAT	13	11.6 ± 5.1	87.6 ± 50.3	495.7 ± 248.6
Brachyteraphy	9	22.6 ± 19.8	16.4 ± 14.6	104.1 ± 94.5
Cavography	7	7.5 ± 6.5	66.1 ± 53.8	273.3 ± 216.4
Fibrinolysis	10	19.9 ± 11.0	28.1 ± 29.6	113.2 ± 102.9
Caval Filter	10	7.0 ± 7.3	64.1 ± 98.3	236.7 ± 282.7
Fistolography	10	4.6 ± 4.0	4.5 ± 14.6	28.4 ± 109.2
Flebography	26	6.5 ± 16.1	28.4 ± 58.9	300.2 ± 803.9
HVPG measurement	10	9.1 ± 7.1	29.2 ± 18.1	167.0 ± 100.1
TIPS	13	20.5 ± 13.3	117.3 ± 74.1	827.5 ± 609.5
Epiaortic trunk angiography	13	3.6 ± 3.3	40.9 ± 30.5	221.3 ± 150.4
Vertebroplasty	13	13.0 ± 16.1	51.4 ± 26.0	392.7 ± 157.3

Mean values of FT, KAP and CK indicate that cerebral angiography, aneurysm embolisation and chemoembolisation of liver cancer are procedure where high skin doses could be delivered. PSD has been measured in a sample of these procedures: results are summarised in Table 2.

Table 2. Peak skin dose (PSD) (mean values, SD and range) for a sample of selected interventional procedures.

Procedure	No	PSD (mGy)	Range (mGy)
Cerebral Angiography	25	352.4 ± 145.4	98.8 ÷ 561.9
Aneurysm Embolization	18	1072.5 ± 1085.2	332.2 ± 4941.9
Chemo-embolization	38	1343.8 ± 915.7	343.4 ± 4135.5

The correlation between PSD and KAP and CK was investigated. Results for cerebral angiography are represented in figures 1 and 2 for KAP and CK respectively.

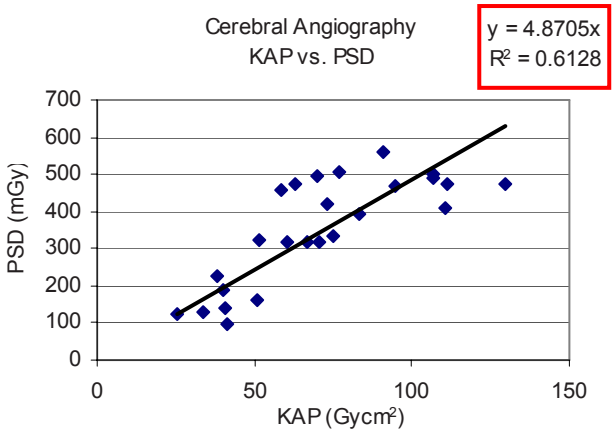

Fig. 1. Correlation between KAP and PSD for cerebral angiography

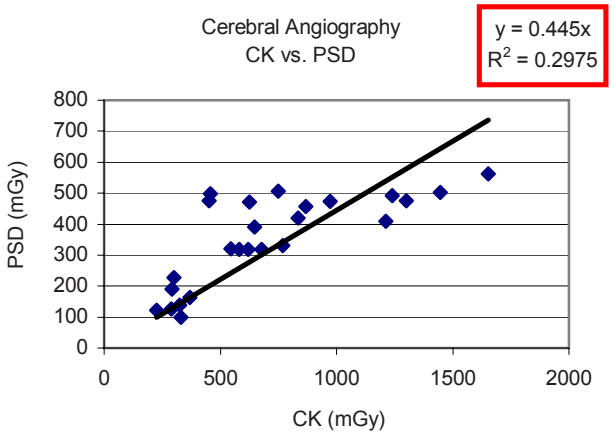

Fig. 2. Correlation between CK and PSD for cerebral angiography

Results for aneurysm embolisation are reported in figures 3 and 4 for KAP and CK respectively.

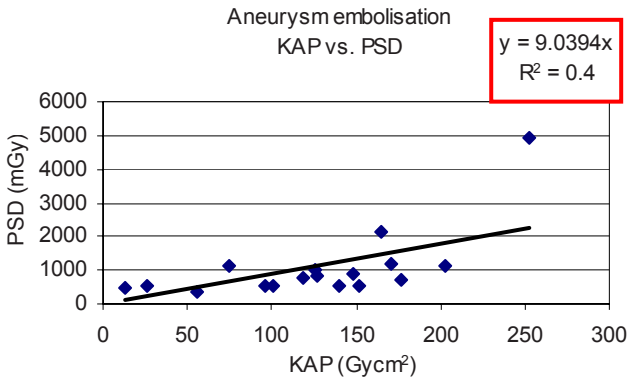

Fig. 3. Correlation between KAP and PSD for aneurysm embolisation

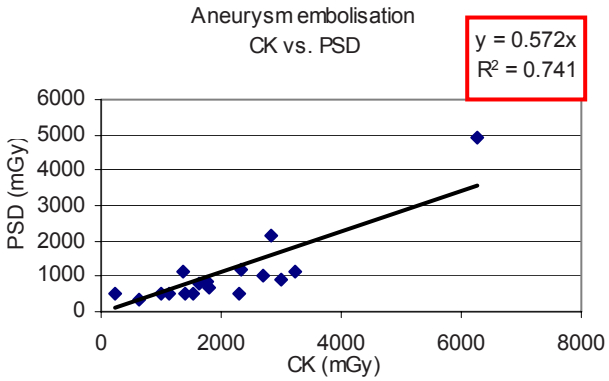

Fig. 4. Correlation between KAP and PSD for aneurysm embolisation

Results for chemoembolisation are reported in figures 5 and 6 for KAP and CK respectively.

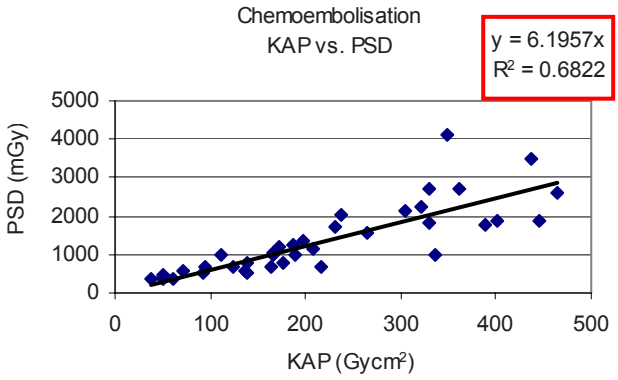

Fig. 5. Correlation between KAP and PSD for chemoembolisation

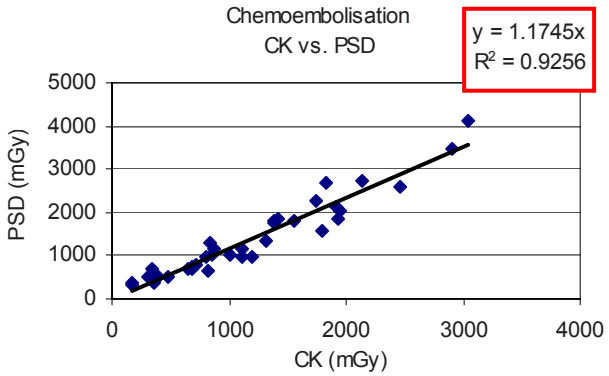

Fig. 6. Correlation between CK and PSD for chemoembolisation

IV. Discussion

Registered values of KAP, CD and FT are high and suggest high doses to patient' skin, in particular for cerebral angiography, aneurysm embolisation and chemoembolisation for liver cancer.

Therefore it's important to understand the meaning of these values in terms of skin dose. Moreover it's important to allow the operator to have an immediate knowledge of the amount of dose received by patient and to recognize those procedures in which the dose could be greater than the threshold for deterministic effects.

For that reasons the correlation between dosimetric indicators as KAP and CK given by the equipment and PSD directly measured has been assessed and the possibility to establish trigger levels to be used in routinely practice has been investigated for cerebral angiography, aneurysm embolisation and chemoembolisation.

A. Cerebral angiography

For cerebral angiography procedures, correlation between PSD and both dosimetric indicators is weak (R^2=0.61 and R^2=0.3 respectively for KAP and CK). This is probably due to the high number the projections at different angles used in these procedures.

As a consequence the definition of a trigger level wasn't possible.

However doses measured in the sample are quite low (maximum value of 561.9 mGy).

A comparison between FT, KAP and CK of the sample in which PSD has been measured and the values of the entire database October 2007 - October 2008 was performed: mean values were not statistically different.

This allow to assert that doses delivered in this type of procedure are generally not high and the definition of trigger levels in this case is not relevant

B. Aneurysm embolisation

For aneurysm embolisation procedures, correlation between PSD and KAP is weak ($R^2 = 0.4$), instead correlation between PSD and CK is quite strong ($R^2 = 0.74$), as reported in figures 3 and 4.

A retrospective analysis on the entire database was done using the linear coefficient to estimate PSD from CK. Estimated PSD exceeded the threshold for transient erythema (2 Gy) 10 times (13% of procedures) and 2 times the threshold for temporary epilation (3 Gy).

Therefore it's necessary in this case define a trigger level that indicate the possible overcoming of 3 Gy for PSD.

The value established in terms of CK for that type of procedure in our center is 5200 mGy.

C. Chemoembolisation for liver cancer

For chemoembolisation procedures, correlation of PSD resulted good ($R^2 = 0.68$) with KAP and very strong with CK ($R^2 = 0.93$).

Also for these procedures, a retrospective analysis on the entire database, using the linear coefficient between PSD and CK found, was done. PSD exceeded the threshold for transient erythema (2 Gy) in 25 procedures (17% of the total number) and in one time PSD was estimated to be higher thet 5 Gy.

Therefore, also in his case, it's necessary to define a trigger level that indicate the possible overcoming of 3 Gy for PSD.

The value established in terms of CK for chemoembolisation procedures in our center is 2500 mGy.

V. Conclusion

Doses delivered to patient' skin during some interventional procedures could be very high and overcome the threshold for tissue reactions.

For procedures at highest doses it's opportune to define trigger levels based on cumulative air kerma values (CK) measured by the equipment to inform the operators that the dose delivered in a procedure could be higher than the threshold for skin damage.

Skin doses measured for cerebral angioplasty were well below the threshold for deterministic effects and no trigger level has been established.

For aneurysm embolisation and chemoembolisation PSD measured were quite high. For that reason trigger levels have been established in terms of CK. In our center these levels are *5200 mGy* and *2500 mGy*, respectively for aneurysm embolisation and chemoebolsatiion.

As suggested by ICRP in the publication No. 85, a follow-up for patients whose estimated peak skin dose was 3 Gy or greater has been implemented as a routine practice.

References

1. Koenig TR, Wolff D, Mettler FA, Wagner LK (2001). Skin injuries from fluoroscopically guided procedures: part I, characteristics of radiation injury. Am J Roentgenol 177:3–11.
2. Koenig TR, Mettler FA, Wagner LK. (2001). Skin injuries from fluoroscopically guided procedures: part 2, review of 73 cases and recommendations for minimizing dose delivered to patient. Am J Roentgenol 177:13–20.
3. ICRP (2000). Recommendations of the International Commission on Radiological Protection. Publication 85: Avoidance of radiation injuries from medical interventional procedures. Ann. ICRP. Oxford, UK: Pergamon Press.
4. Vano E, Gonzalez L, Ten JI, Fernandez JM, Guibelalde E, Macaya C. (2001). Skin dose and dose-area product values for interventional cardiology procedures. Br J Radiol. 74:48–55.
5. A. Trianni, G. Chizzola, H. Toh, E. Quai, E. Cragnolini, G. Bernardi, A. Proclemer, and R. Padovani (2005). Patient skin dosimetry in haemodynamic and electrophysiology interventional cardiology. Radiat Prot Dosimetry 117: 241 - 246.

Absorbed dose enhancement caused by gold particles in polymer gels

L.C. Afonso, F. Schöfer and C. Hoeschen

Institute of Radiation Protection, Helmholtz Zentrum, Munich, Germany

Abstract— **Previous studies showed that the presence of high-Z materials adjacent to soft tissues, when submitted to irradiation, enhances the absorbed dose in these tissues. This effect is due to the outscattering of photoelectrons from the high-Z materials. The aim of the present work was to measure the absorbed dose enhancement caused by the presence of different concentrations of gold particles in polymeric gels.**

Keywords— **polymer gel, three-dimensional dosimetry, NMR, gold particles.**

I. Introduction

It is known from previous studies that the presence of high-Z materials adjacent to soft tissues, when submitted to irradiation, enhances the absorbed dose in these soft tissues. This is due to the outscattering of photoelectrons from the high-Z materials. [1, 2]

The concern about the effect of dose enhancement arose after discovering that oral cavity radiation therapy treatments on patients that had golden tooth replacements resulted in an increased damage of the soft tissues surrounding these gold replacements. It was found that the absorbed dose could reach an enhancement of two orders of magnitude in the microscope vicinity of gold replacements, when exposing the patient to diagnostic X-ray examinations. [1]

In experiments with human lymphocytes covered with a thin gold film and then irradiated with diagnostic X-ray beams, it was found that the dose absorbed by the cells was increased by a factor of 45.4. The number of chromosomic aberrations was also in accordance to this dose enhancement. [2]

Thereby, the aim of the present work was to measure the absorbed dose enhancement caused by the presence of different concentrations of gold particles in polymeric gels, which the main characteristic is the soft tissue equivalence. The polymer gel dosimetry technique allows the absorbed dose to be measured with high three-dimensional resolution, which is essential to analyze the enhancement distribution due to photoelectrons outscattered by the gold particles.

II. Dosimetric method

A. Polymer gel

Polymeric Systems began to be studied in relation to their dosimetric capacity in the fifties, by evaluating the radiation effects in poly-methyl-methacrylate [3]; and studying radio-induced polymerization in liquids [4]. Later, works combined these properties as the first polymer gel developed by Maryanski et al [5, 6], which had formulation that was composed by acrylamide, bis-acrylamide and nitrous oxide diluted in an agarose aqueous matrix. The polymerization reaction in this gel was based on the crosslinking of acrylamide monomers.

Further gel formulations were developed by changing the gel matrix (agarose to gelatin), the monomer (acrylamide to methacrylic acid, for example), etc. However, the working principle of any polymer gel dosimeter is based on the radiation-induced polymerization of the monomers present in the gel. When the gel is irradiated, the water radiolysis is induced. The polymerization process is mainly initiated by free radical reactions. The polymerization degree depends on the number of free radicals created by the incident radiation, which depends on the absorbed dose; therefore, originating spatial dose resolution. [7, 8]

The polymer gel used for this work is known as MAGIC (Methacrylic Ascorbic in Gelatin Initiated by Copper), foremost developed by Fong et al [9]. Its formulation is composed by methacrylic acid, ascorbic acid, gelatin and copper sulfate. As the gel polymerization process is initiated by free radical reactions, and molecular oxygen is an efficient "scavenger" of free radicals, its presence inhibits gel polymerization. Therefore, the ascorbic acid, in a process initiated by the copper sulfate, is responsible for capturing oxygen in the gel solution.

B. Nuclear Magnetic Resonance

Nuclear Magnetic Resonance (NMR) is a technique that allows determining the properties of a substance by correlating the absorbed energy and the frequency, in the radiofrequency range of the electromagnetic spectrum. The technique uses the transitions between the rotational energy

O. Dössel and W.C. Schlegel (Eds.): WC 2009, IFMBE Proceedings 25/III, pp. 414–415, 2009.
www.springerlink.com

levels of the compound's nucleus (atoms or ions) contained in the sample. This occurs necessarily under a magnetic field influence and under the concomitant irradiation with radiofrequency waves.

In dosimetric gels, the scanning process is based on the measurement of the longitudinal and the transversal relaxation rates (R1 and R2), from which dose maps may be determined. Traditionally, the corresponding relaxation times (T1 and T2) are measured, then, the rates are determined. The longitudinal relaxation time, T1, or spin-net relaxation time, is associated with the interaction of the spins with the net. The longitudinal relaxation is responsible for the return of the magnetization to the thermal equilibrium state. The transversal relaxation time, T2, or spin-spin relaxation time, is associated to the interactions between the spins. Due to the transversal relaxation, the magnetic moments lose coherence, which makes them precess with lightly different frequencies. The relaxation times are measured by applying radiofrequency pulses to excite the magnetization of the spin system, and then, samples are collected during the return to equilibrium. The transversal relaxation time (T2=1/R2) is measured by adjusting the collected data of the transversal relaxation curve after excitation. [10, 11]

III. METHODOLOGY

The samples of polymeric gels (30 ml flasks), with and without gold particles were irradiated with X-rays and γ rays beams. Then, these samples were scanned with a Nuclear Magnetic Resonance system and the resultant transversal relaxation rate (T2) distribution was analyzed and associated to the absorbed dose.

Further results are under analysis.

REFERENCES

1. Regulla D, Friedland W, Hieber L et al (2000) Spatially Limited Effects of Dose and LET Enhancement Near Tissue/Gold Interfaces at Diagnostic X Ray Qualities. Radiation Protection Dosimetry, 90, Nos 1–2, pp. 159–163
2. Regulla D, Panzer W, Schmid E et al (2001) Detection of Elevated RBE in Human Lymphocytes Exposed to Secondary Electrons Released from X-Irradiated Metal Surfaces. Ratiation Research, 155, pp. 744–747
3. Alexander P, Charlesby A, Ross M (1954) The Degradation of Solid Polymethyl-methacrylate by Ionizing Radiations. Proceedings of the Royal Society, pp. 392-404
4. Hoecker FE, Watkins IW (1958) Radiation Polymerization Dosimetry. International Journal of Applied Radiation and Isotopes, 3, pp. 31-36
5. Maryanski MJ, Gore JC, Schulz RJ (1992) 3-D Radiation Dosimetry by MRI: Solvent Proton Relaxation Enhancement by Radiation-Controlled Polymerisation and Cross-Linking in Gels. Proc. Intl. Soc. Mag. Reson. Med.
6. Maryanski MJ, Gore JC, Kennan RP et al (1993) NMR Relaxation Enhancement in Gels Polymerized and Cross-Linked by Ionizing Radiation: a New Approach to 3D Dosimetry by MRI. Magn. Reson. Imaging, 11, pp. 253-258
7. Berg A, Ertl A, Moser E (2001) High Resolution Polymer Gel Dosimetry by Parameter Selective MR-Microimaging on a Whole Body Scanner at 3 T. Medical Physics, 28(5), pp. 833-843
8. Bayreder C, Georg D, Moser E et al (2006) The spatial resolution in dosimetry with normoxic polymer-gels investigated with the dose modulation transfer approach. Medical Physics, 35(5), pp. 1756-1769
9. Fong PM, Keil DC, Does MD, Gore JC (2001) Polymer Gels for Magnetic Resonance Imaging of Radiation Dose Distributions at Normal Room Atmosphere. Physics in Medicine and Biology, 46, pp. 3105-3113
10. Baustert IC, Oldham M, Smith TAD et al (2000) Optimized MR Imaging for Polyacrylamide Gel Dosimetry. Physics in Medicine and Biology, 45, pp. 847-858
11. McJury M, Oldham M, Cosgrove VP et al (2000) Radiation Dosimetry Using Polymer Gels: Methods and Applications. The British Journal of Radiology, 73, pp. 919-929

Author: L. C. Afonso
Institute: Helmholtz Zentrum München
Street: Ingolstaedter Landstrasse 1
City: Neuherberg
Country: Germany
Email: Luciana.afonso@helmholtz-muenchen.de

Assessment of the self-developing films usefulness in interventional radiology

A. Werduch[1], M. Brodecki[1,2], J. Jankowski[1,2], A. Korejwo[1]

[1] University of Lodz, Department of Nuclear Physics and Radiation Safety, Lodz, Poland
[2] Nofer Institute of Occupational Medicine, Radiation Protection Department, Lodz, Poland

Abstract— **Complex interventional radiology (IR) procedures deliver high radiation doses to patients. This may result in skin injury inducted by exceeding deterministic effects threshold. Monitoring and mapping the radiation entrance to the patients is very important to secure patients from medical follow up in case of radiation injury. Basing only on the dose area product (DAP) meters, commonly used in haemodynamic centers, it is impossible to obtain sufficient information about entrance skin dose (ESD) and dose distribution on a patient skin. From this point of view, application of other types of detectors e.g. radiochromic films is suggested.**

A Gafchromic XR-RV2 film was tested to determine its potential usage for patient skin dose and dose distribution monitoring in a fluoroscopically guided interventional radiology procedures. Films' dosimetric characteristic i.e. dose, dose rate, energy and time dependencies in the applied range, were tested. The dose response in different color components of standard RGB color space image and film positioning during scanning were also determined.

This work shows that radiochromic films are a simple and pretty useful method that leads to localize and estimating patients' skin dose received during interventional radiology procedures. These films can be an alternative for the well-known dosimetric methods.

Keywords— **radiation doses, radiochromic films, calibration**

I. Introduction

Various methods of patients radiation doses measurements were presented in literature [1]. The most commonly used dose-area product (DAP) meters do not provide sufficient information about entrance skin dose (ESD) and about the distribution of ESD.

Direct method using thermoluminescent (TL) dosemeters seems to be very good to estimate radiation risk skin injury, but in reality it is very difficult to position small TL detectors correctly to cover all irradiated area on a patient skin. This fact results in underestimating information about ESD. The similar situation appears during work with electronic dosemeters.

Monte Carlo calculations based on theoretical phantoms deliver some data about organ doses. Unfortunately, these methods do not treat every patient separately, but calculations are provided for standard man, thus estimated ESD is burdened with a considerable uncertainty [2].

Recently, slow radiotherapy KODAK EDR2 films were used [3]. Films are positioned between table top and patient body and they theoretically deliver information about ESD distribution with good accuracy. Unfortunately, similarly like methods above, KODAK EDR2 is not a perfect dosimetric instrument for IR. In this case dose uncertainty is first and foremost connected with the arduous film chemical treatment and with calibration curve fitting.

First look at the Gafchromic XR-RV2 specification suggests that these films could present a golden means for IR dosimetric aplication. This paper presents physical and practical characteristic of the radiochromic films and tries to assess their usefulness in haemodynamic room.

II. Materials and methods

Gafchromic XR-RV2 film is a self-developing, non screen slow speed film and does not require use a film processor. The film consists of an active layer sandwiched between two sheets of 97 μm polyester; one clear-yellow film substrate and one opaque, white film substrate. The active layer is approximately 17 μm thick and it comprises sub micron sized crystal of a radiation-sensitive monomer. When the film is exposed to ionizing radiation, a polymerization reaction is initiated, resulting in the production of a blue-colored dye-polymer. The amount of polymer produced and the depth of the color change is proportional to the dose absorbed in the active layer [4-6].

Dose, dose rate and energy dependence measurements of Gafchromic XR-RV2 were performed on a Pantak HF320 Callibration System with reference class dosemeter Unidos type 10002 connected with air ionizing chamber (LS-01, PTW Freiburg) in Secondary Standard Dosimetric Laboratory (SSDL) in Nofer Institute of Occupational Medicine in Lodz, using typical haemodynamic procedures beams with mean energies ranged from 45 keV up to 137 keV. The 6 cm^2 pieces of Gafchromic XR-RV2 film were exposed with attainable dose rate 28.57 mGy/min, 21.46 mGy/min and 14.30 mGy/min from 100 mGy up to 1500 mGy. After the film irradiating, optical density analysis was performed using flatbed scanner (Epson Perfection V700 Photo) in reflection mode and appropriately designed "pixel value-to-dose converter" software. Pixel value was attributed to the dose value and calibration curve was established. Every

O. Dössel and W.C. Schlegel (Eds.): WC 2009, IFMBE Proceedings 25/III, pp. 416–419, 2009.
www.springerlink.com

sheet of radiochromic films originated from the same batch i.e. the same emulsion number. Films were stored and analyzed in temperature 20 ºC ± 2 ºC to avoid temperature dependence and were removed from tight envelope only during irradiation and scanning to reduce the effects of light.

III. Results and discussion

A. Color spectra dependence

Each pixel of the irradiated film scan consists of the red, blue and green components (RBG standard). The pixel value depends on these components directly. Figure 1 illustrated the response of the irradiated Gafchromic XR-RV2 film (80 kVp, HVL = 0.35 mm Cu) for three different color spectra as an absorbed dose function. The sensitivity was maximized when the red channel component was applied.

B. Geometry (irradiating and scanning) dependence

Due to the various layers material construction of the Gafchromic XR-RV2, these films are sensitive to the varying rotational position during their scanning. This is connected with variations in scattering effects of light [7]. This fact is visible in the Figure 3, presenting the set of calibration films which were scanned in three selected orientations 0°, 90° and 180°.

Perceptible changes of the pixel value are produced by the different orientation of scanning film and the orientation of a light source and detector.

The layers construction of Gafchromic XR-RV2 is also responsible for the pixel value differences in the case of the same scanning orientation but the opposite side (front and back) films irradiation [Fig. 4].

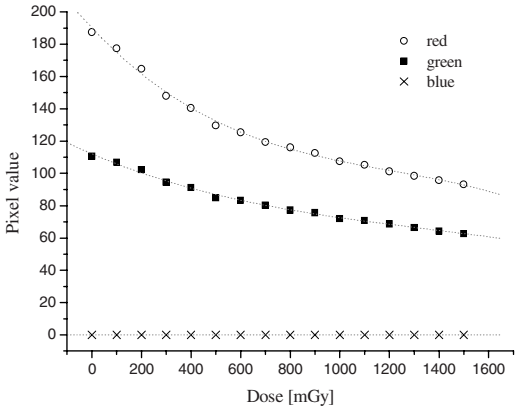

Fig. 1 Comparison of responses in various color components (RGB mode)

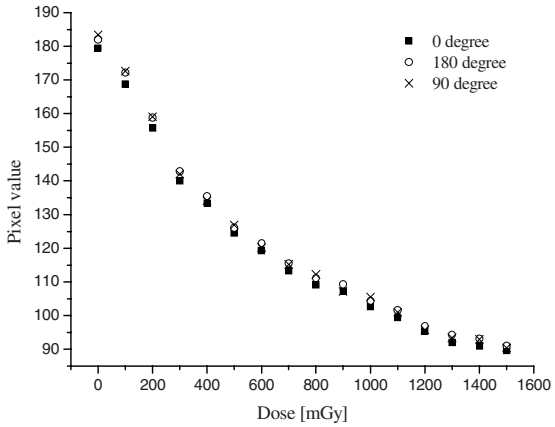

Fig. 2 Gafchromic XR-RV2 response depending on the scanning orientation

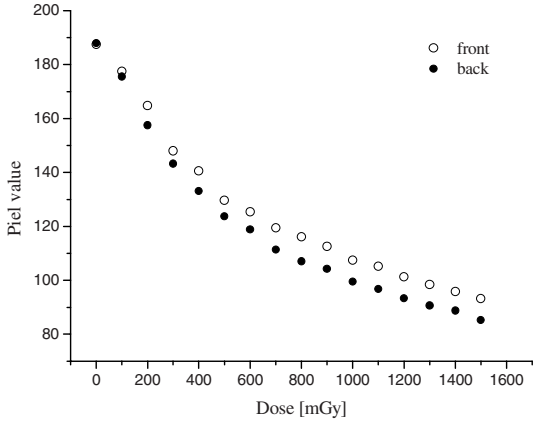

Fig. 3 Gafchromic XR-RV2 response depending on the side of the film irradiated

In both cases even insignificant pixel value disagreements lead to changing the calibration curves. For the different side film irradiation the geometry dependence is more visible.

C. Dose rate dependence

For the specific doses from 100 mGy to 1500 mGy the pixel value responses for different dose rates were evaluated. Figure 4 shows the variation of the film response as a function of dose rate.

As seen in this figure, the pixel values change with dose rate and dose rate dependence is insignificantly visible for the low doses, especially that the measuring range of the dose rates was not very wide. Similarly like in geometry dependence case, the dose rate dependence affects the dose calibration curve insignificantly.

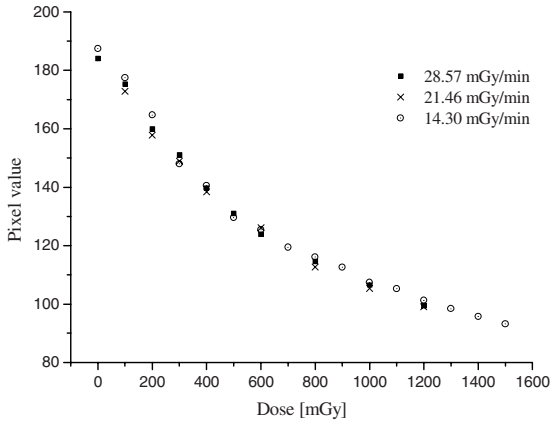

Fig. 4 Variation of the pixel value as a function of dose rate

D. Energy dependence

Especially in interventional radiology procedures the kVp value changing frequently causes that the flat energy characteristic of films is desirable. For that reason, the Gafchromic XR-RV2 energy dependence was measured for energies ranging from 45 keV up to 137 keV (X-ray energy using in interventional radiology), according to ISO X-ray beam [8] (Table 1). All of the analyzed films were exposed to a fixed total dose of 200 mGy in a front geometry and for the tube current 20 mA at the same focus-film distance.

Table 1 Characteristics of the wide X-ray spectrum series

Mean energy [keV]	Tube voltage [kV]	Filtration [mm Sn]	Filtration [mm Cu]	HVL [mm Cu]
45	60	-	0.3	0.18
57	80	-	0.5	0.35
79	110	-	2.0	0.96
104	150	1	-	1.86
137	200	2	-	3.08

Figure 5 illustrated the relative energy film response normalized to the 57 keV (mean X-ray energy generated from the angiograph tube – data analyzed from 20 procedures), which decreases and then increases along with energy increases, with a minimum value at 80 keV. The measurement shows that deviation of energy response in the applied range is not higher than 5%.

Additionally, the time influence on the energy characteristic was studied. The results consist of two tests performed with 27 hours interval (the same films were scanned 3 and 30 hours after exposition). Figure 6 shows that the pixel value is changing in the time but the shape of energy dependence is still preserved.

IV. Conclusions

The analysis of the Gafchromic XR-RV2 dosimetry film proved that these films are a valuable tool in the monitoring of patient skin exposure during the interventional radiology procedures.

From a practical standpoint, the Gafchromic XR-RV2 films can be easily placed between the table and the patient. The large size of films (14" x 17") would be helpful in many IR cases.

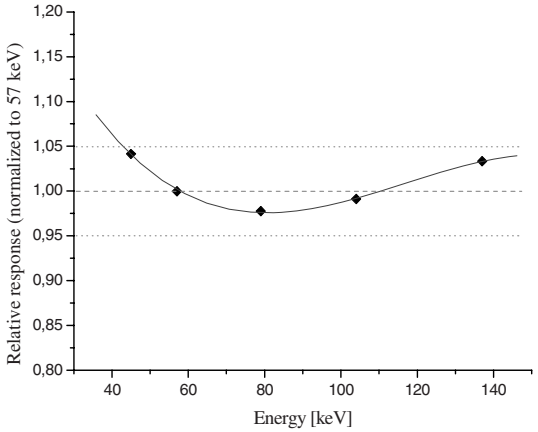

Fig. 5 Gafchromic XR-RV2 energy characteristic

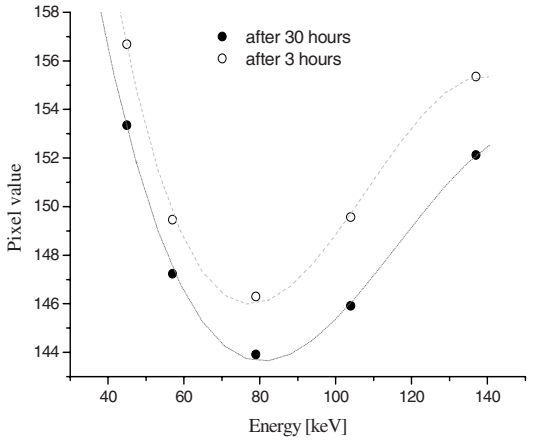

Fig. 6 Time dependence of mean energy characteristic

But the most practical characteristic is yet the self-developing of the exposured films.

The dose, dose rate, time, energy and geometry responses were tested on film samples. All measurements support the conclusion that the Gafchromic XR-RV2 is a quite simple, passive method to identify skin regions at risk from high X-ray doses.

The red color component of the RGB scan mode is the optimal choice in measuring film response. The dose response curve of radiochromic film is simple to fitting by exponential curve.

Work characteristic of angiograph X-ray tube, where the parameters like voltage, tube current, added filtration, and consequently dose rate, still changing during procedure, brings in this way some problems with the choice of the best calibration curve. Thus, the methods of irradiating and scanning the film have crucial meaning for pixel value.

Taking into the measuring characteristic and dependencies consideration, accuracy of measurements was deemed acceptable to estimate the localized skin dose to patients at risk for radiation induced skin injury.

Among a wide range of clinical applications using the Gafchromic XR-RV2 films, they could be used for interventional radiology as well.

References

1. Padovani R, Quai E (2005) Patient dosimetry approaches in interventional cardiology and literature dose data review. Rad Prot Dos 117:217–221
2. Tsapaki V (2001) Patient and staff dosimetry problems in interventional radiology. Rad Prot Dos 94:113–116
3. Morel R, Rogers T (2006) Kodak EDR2 film for patient skin dose assessment in cardiac catheterization procedures. Brit J Radiol 73:603–607
4. Dini S, Konna R (2005) Dosimetric evaluation of GAFCHROMIC XR type T and XR type R films. Am Coll Med Phys 6:114–134
5. http://online1.ispcorp.com/_layouts/Gafchromic/index.html
6. Bustom M, Yu P, Cheung T at al. (2002) High sensitivity radiochromic film dose comparisons. Phys Med Biol 47:291–295
7. Butson M, Cheung T, Yu1 P (2006) Scanning orientation effects on Gafchromic EBT film dosimetry. Austral Phys Engin Scien in Med 29:281–284
8. ISO 4037-1 (1996) X and gamma reference radiation for calibrating dosemeters and doserate meters and for determining their response as a function of photon energy – Part 1: Radiation characteristics and production methods

Author: Marcin Brodecki
Institute: Nofer Institute of Occupational Medicine
Street: Sw. Teresy 8
City: Lodz
Country: Poland
Email: marbrod@imp.lodz.pl

Biology of high dose-high precision radiotherapy – experience from brachytherapy of cervix cancer

C. Kirisits and D. Georg

Medical University Vienna/AKH Wien, Div. Medical Radiation Physics, Department of Radiotherapy, Vienna, Austria

Abstract— **Brachytherapy treatments deliver high doses in only few fractions to target volumes and healthy tissues. These high dose values to target cells might be the reason for very successful brachytherapy concepts. With the integration of 3D based treatment planning into brachytherapy the spatial dose distribution in relation to topography can be investigated and taken into account during treatment plan optimization. An analysis of cervix cancer patients treated at the Department of Radiotherapy, Medical University of Vienna, with intracavitary brachytherapy for cervix cancer illustrate dose and volume relations focused to high dose regions. In particular, a D_{2cc} of the rectum or sigmoid >75 Gy EQD2 was associated with a significantly higher incidence of late toxicity compared to a D_{2cc} ≤75 Gy (EQD2). No clear cut off point for bladder late effects could be demonstrated. Clinically, the dose D_{2cc} ≤ 90 Gy EQD2 can be recommended for clinical use to minimize side effects for bladder. The current clinical experiences in cervix cancer brachytherapy are based on forward planning. The integration of DVH parameters for treatment planning of image guided brachytherapy results in the wish to include inverse planning optimization concepts. Other current research activities aim at non-rigid image registration and voxel tracing in order to refine existing radiobiological knowledge and data, respectively, on dose volume relations for targets and organs at risk.**

Keywords— **brachytherapy, dose volume relations, cervix cancer.**

I. Introduction

Brachytherapy (BT) is an essential component of radiotherapy for patients with gynaecological malignancies, especially cervix cancer. Brachytherapy treatments deliver high doses in only few fractions to target volumes and healthy tissues. The advantage of brachytherapy is the rapid dose fall-off allowing the delivery of very high dose to the tumor, while sparing organs at risk (OAR). These high dose values to target cells might be the reason for very successful brachytherapy concepts. On the other hand, BT is inherently associated with inhomogeneous dose distribution due to the steep dose fall-off. Therefore, healthy tissues and OARs adjacent to the target structures (e.g. the anterior rectal wall, sigmoid walls or the posterior bladder wall) can receive high doses to small volumes, while organ walls further away from the tumour (e.g. the posterior recto-sigmoid walls, or the anterior bladder wall) are exposed to much lower doses.

With the integration of 3D based treatment planning into brachytherapy the spatial dose distribution in relation to topography can be investigated and taken into account during treatment plan optimization compared to simple radiography based methods for treatment planning [1,2]. As consequence of typical brachytherapy dose distributions and the shape of a given organ, a high dose region may be contiguous or non-contiguous. Non-contiguous high dose volumes are typically seen in the bladder wall, due to its concave form in filled status.

When assessing late effects from brachytherapy, small organ (wall) volumes irradiated to a high dose have been identified as the most critical parameter and are of major interest. It is recommended to report and record the minimum dose in the most irradiated 2, 1 and 0.1 cm^3 of a respective OAR [3,4]. Current research activities aim at establishing dose response curves or complication probabilities for these volumes [5,6]. This analysis of cervix cancer patients treated at the Department of Radiotherapy, Medical University of Vienna, with intracavitary brachytherapy illustrate dose and volume relations focused to high dose regions.

II. Methods and materials

Dose distributions of clinically used high dose regions were evaluated. Dosimetric and follow-up data is available for 145 patients treated from 1997 to 2003. Favourable clinical results have been reported for the patient cohort [7]. Dose volume histogram (DVH) data are reported for 22 patients with tandem/ring applicator to irradiate the clinical target volume for cervix cancer [1]. The prescribed dose per brachytherapy fraction was 7 Gy. Four fractions have been applied after an external beam dose of 45 Gy in 25 fractions.

An MRI with the applicator in place was directly scanned after implantation, prior to planning and irradiation. Target volumes according to the GYN GEC ESTRO recommendations were contoured [3]. The organs at risk bladder, rectum, and sigmoid were delineated. DVH calculations were

O. Dössel and W.C. Schlegel (Eds.): WC 2009, IFMBE Proceedings 25/III, pp. 420–422, 2009.
www.springerlink.com

performed to estimate high dose volumes. These high dose areas were later on identified on the dose distribution directly visible on the MRI scans. The dose delivered to OAR could be reduced and target coverage could be improved through treatment plan optimization.

For the assessment of the total dose to OAR, each fraction has to be evaluated and biologically weighted. In current clinical practice a "worst case assumption" is usually made, i.e. for calculating the total dose from brachytherapy the location of the DVH parameters is assumed to be identical for each fraction. For all patients the cumulative value from brachytherapy was added to the dose from external beam therapy (EBT) and normalized to conventional 2 Gy per fraction using the linear quadratic model. An α/β=10 Gy was used for target and α/β=3 Gy for OAR structures (EQD2) [8]. This adds a source of uncertainty in the overall dose assessment due to the anatomical changes and radiobiological differences between EBT and BT.

III. Results

The volume receiving the prescribed dose was on average 85 cm³. This was equivalent to a volume receiving an EQD2 normalized dose of 84 Gy. The volume receiving twice the prescribed dose was 25 cm³. Using the same simple straightforward EQD2 normalization results in a minimum dose of 156 Gy (α/β=10 Gy) for this volume. This very high dose was located around the vicinity of the applicators, but also partially inside the applicators. 90% of the contoured High Risk Clinical Target Volume (HR-CTV) was covered with at least 87 Gy (D90), while the GTV showed a D90 of 121 Gy.

For bladder the dose varied from at least mean 121 Gy for the most exposed 0.1 cm³ ($D_{0.1cc}$) to 83 Gy for the most exposed 2 cm³ (D_{2cc}). The Rectum $D_{0.1cc}$ was 77 Gy versus 64 Gy for D_{2cc}. Sigmoid dose was $D_{0.1cc}$ of 79 Gy and D_{2cc} of 63 Gy.

The localization of telangiectasia in the rectal wall corresponded to the 2cm^3 high dose rectal volume, while the development of ulceration was limited to the small high dose volumes of 0.1 cm³ at the anterior rectal wall segment [6]. A D_{2cc} of the rectum or sigmoid >75 Gy EQD2 was associated with a significantly higher incidence of late toxicity compared to a D_{2cc} ≤75 Gy EQD2. Given the inexact nature of the entire treatment planning and delivery process, in order to minimize high grade late effects of the rectum, we recommend a rectal dose constraint of $D_{2cc} \leq 70$ Gy EQD2. It can be expected that such a constraint should limit the rate of adverse side effects for the rectum to below 5%. Despite the fact, that a similar dose response could be observed for the sigmoid, due to the lack of a sufficient data (i.e. only 3 adverse events noted), we cannot recommend a reliable dose volume constraint at this point. In addition, no clear cut off point could be demonstrated for the sigmoid effects. Clinically, the dose $D_{2cc} \leq 90$ Gy EQD2 can be recommended for clinical use to minimize side effects.

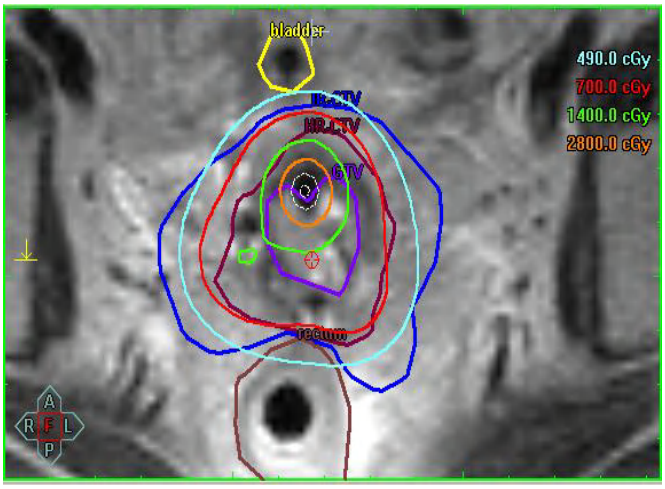

Fig. 1 Example of a typical dose distribution obtained with MR based BT of cervix cancer. The dose distribution was optimized with adaptation of application technique and dwell time settings.

IV. Discussion

During the last years optimization in brachytherapy of cervix cancer has been improved substantially. The integration of new applicators allowed increasing the coverage for larger tumour volumes [9,10]. New treatment planning systems provide tools for DVH parameter guided dose shaping using sophisticated forward planning algorithms. Nowadays the dose to the D90 is often exceeding 90 Gy for the HR-CTV. The volume receiving twice the prescribed dose is limited to not more than 40 cm³. The dose to bladder, rectum, and sigmoid is limited to 90 Gy, 70 Gy and 70 Gy for the D_{2cc}, respectively.

The current clinical experiences in cervix cancer brachytherapy are based on forward planning [2,7,9-11]. Clinical data show that using of 3D-MRI based BT in cervix cancer patients the dose delivered to OAR can be reduced and target coverage can be improved [7]. This leads to reduced treatment related acute and late toxicities and to the establishment of dose volume relations for OARs. In a recent study by Koom et al. a strong correlation was found between DVH parameters and endoscopic changes of the rectosigmoidal mucosa, although the location of the mucosal lesion could not be exactly matched with the position of the high-dose volume from which the DVH parameters

were calculated [12]. The outcome of side effect analysis in 35 patients treated with 3D-MRI based brachytherapy at the Medical University Vienna showed a significant dose dependent change of rectal mucosis [5,6].

On the other hand, the integration of DVH parameters for treatment planning of MRI based cervix cancer brachytherapy results in the wish to include inverse planning optimization concepts. However, the current experience is limited to simple measures for the dose distribution within the target and healthy tissue structures. Much more important seems the spatial distribution of high dose regions [13]. For intracavitary treatments a very high dose located around the intrauterine source arrangements has been accepted for all common treatment concepts by now, without major complications. 3D treatment plan optimization must not increase morbidity, high dose region have to be watched carefully. Not only the total high dose volume, but also its distribution is essential [14]. A high dose region around the intrauterine channel has a different impact on clinical outcome then high dose spots in the parametrium with a different situation of tissue types, nerves and blood vessels.

Current research activities aim at non-rigid image registration and voxel tracing to refine existing radiobiological knowledge and data, respectively, on dose volume relations for targets and organs at risk. However, more validation work needs to be done with respect to these models.

V. Conclusions

Intracavitary brachytherapy for cervix cancer results in high dose regions within target structures and organs at risk. DVH parameters are not sufficient to control the spatial distribution of these high dose volumes and have to be carefully observed, especially when integrating inverse planning optimization. Several centers in Europe and worldwide are implementing and evaluating 3D based gynaecologic brachytherapy at present. According to the first clinical experience, DVH parameters seem to correlate with morbidity. However, there are still open questions to be addressed to further prospective clinical research.

References

1. Kirisits C, Pötter R, Lang S, *et al*. Dose and volume parameters for MRI-based treatment planning in intracavitary brachytherapy for cervical cancer. *Int J Radiat Oncol Biol Phys* 2005;62:901-911.
2. De Brabandere M, Mousa AG, Nulens A, Swinnen A, and Van Limbergen E. Potential of dose optimisation in MRI-based PDR brachytherapy of cervix carcinoma. *Radiother Oncol* 2008; 88:217-226.
3. Haie-Meder C, Potter R, Van Limbergen E, et al., Recommendations from Gynaecological (GYN) GEC-ESTRO Working Group (I): concepts and terms in 3D image based 3D treatment planning in cervix cancer brachytherapy with emphasis on MRI assessment of GTV and CTV. Radiother Oncol, 2005. 74(3): p. 235-45.
4. Pötter R, Haie-Meder C, Van Limbergen E, et al., Recommendations from gynaecological (GYN) GEC ESTRO working group (II): concepts and terms in 3D image-based treatment planning in cervix cancer brachytherapy-3D dose volume parameters and aspects of 3D image-based anatomy, radiation physics, radiobiology. Radiother Oncol, 2006. 78(1): p. 67-77.
5. Georg P, Kirisits C, Hammer J, et al. Correlation of dose volume parameters, rectoscopy findings and rectal side effects in cervix cancer patients treated with definitive radiotherapy including MRI based brachytherapy [Abstract]. *Brachytherapy* 2006;5(2): 81.
6. Georg P, Dimopoulos J, Kirisits C, et al. Dose volume parameters in cervical cancer patients treated with MRI based brachytherapy and their predictive value for late adverse side effects in rectum, sigmoid, bladder [Abstract]. *Radiother Oncol* 2006;81:S38-S39.
7. Pötter R, Dimopoulos J, Georg P, et al. Clinical impact of MRI assisted dose volume adaptation and dose escalation in brachytherapy of locally advanced cervix cancer *Radiother Oncol* 2007;83(2):148-155.
8. Lang S, Kirisits C, Dimopoulos J, Georg D, and Potter R, Treatment planning for MRI assisted brachytherapy of gynecologic malignancies based on total dose constraints. Int J Radiat Oncol Biol Phys, 2007. 69(2): p. 619-27.
9. Kirisits C, Lang S, Dimopoulos J, et al., The Vienna applicator for combined intracavitary and interstitial brachytherapy of cervical cancer: design, application, treatment planning, and dosimetric results. Int J Radiat Oncol Biol Phys, 2006. 65(2): p. 624-30.
10. Dimopoulos JC, Kirisits C, Petric P, et al. The Vienna applicator for combined intracavitary and interstitial barchytherapy of cervical cancer: clinical feasibility and preliminary results. Int J Radiat Oncol Biol Phys 2006;66(1):83-90.
11. Lindegaard JC, Tanderup K, Nielsen SK, Haack S, and Gelineck J. MRI-guided 3D optimization significantly improves DVH parameters of pulsed-dose-rate brachytherapy in locally advanced cervical cancer. *Int J Radiat Oncol Biol Phys* 2008;71:756-764.
12. Koom WS, Sohn DY, Kim JY, et al. Computed tomography-based high-dose-rate intracavitary brachytherapy for uterine cervical cancer: preliminary demonstration of correlation between dose-volume parameters and rectal mucosal changes observed by flexible sigmoidoscopy. *Int J Radiat Oncol Biol Phys* 2007;68(5):1446-1454.
13. Chajon E, Dumas I, Touleimat M, et al., Inverse planning approach for 3-D MRI-based pulse-dose rate intracavitary brachytherapy in cervix cancer. Int J Radiat Oncol Biol Phys, 2007. 69(3): p. 955-61.
14. Kirisits C, Trnkova P, Baltas D, Dimopoulos J, and Potter R, Inverse optimization for cervix cancer brachytherapy including automatic loading, DVH optimization and modification restriction adapted from manual planning. Medical Physics, 2008. 35(6): p. 2726.

Author: Dr. Christian Kirisits
Institute: Department of Radiotherapy, Medical University Vienna
Street: Währinger Gürtel 18-20
City: 1090 Vienna
Country: Austria
Email: Christian.Kirisits@meduniwien.ac.at

Evaluation of dose dependent structural changes in 3D brain micro-vasculature in response to heavy particle radiation exposure

C. Hintermüller[1],J. S Coats[2],A. Obenaus[2],G Nelson[2],T Krucker[3] and M Stampanoni[1,4]

[1]Swiss Light Source, Paul Scherrer Institut, CH-5232 Villigen, Switzerland

[2]Loma Linda University, Dept of Radiation Medicine, CSP A-1010 Loma Linda, CA, USA

[3]Novartis Institutes for Biomedical Research, Cambridge, MA, USA

[4]Institute for Biomedical Engineering, University and ETH Zürich, 8092 Zürich, Switzerland

Abstract— **Space radiation with high energy particles (cosmic rays) presents a significant hazard to spaceflight crews. Recent reviews of the health risk to astronauts from ionizing radiation concluded that there is a need to establish a level of risk which may indicate the possible performance decrements and decreased latency of late dysfunction syndromes of the brain. A hierarchical imaging approach developed at ETH Zürich and PSI, which relies on synchrotron based X-ray Tomographic Microscopy (SRXTM), was used to visualize and analyze 3D vascular structures down to the capillary level. Various morphological parameters, such as overall vessel volume, thickness and spacing, are extracted to characterize the vascular structure within a region of interest. Three weeks after irradiation a first quantification of the effect of high energy particles on the vasculature was done on a set of 14 animals, all the same age. The animals were irradiated head-only with 1Gy, 2Gy and 4Gy of 600MeV/n ^{56}Fe heavy particles simulating the space radiation environment. We found that with increasing dose the diameter of vessels and the overall vessel volume are decreased whereas the vessel spacing is increased. As these parameters reflect blood flow in three-dimensional space they can be used as indicators for the degree of vascular efficiency which is thought to have an impact on the function and development of the central nervous system.**

Keywords—**Space radiation exposure, 3D vascular structure, morphometric analysis**

Introduction

Space radiation with high energy particles and cosmic rays presents significant health hazards to spaceflight crews. There is a need to establish a level of risk associated with exposure to space radiation and the potential development of late neurodegeneration such as Alzheimer's Disease (AD) and stroke. This risk assessment is similar to increases found for carcinogenesis after radiation exposure.

Little is known about the impact of radiation on the central nervous system (CNS). It is thought to be sensitive to radiation effects that may occur during space flight exploration. The hippocampal formation and the cortex are two main regions which are involved in formation, processing and storage of memory. These functions are altered in various disease states like AD and so may be affected by heavy particle radiation.

To evaluate the structural changes in the CNS microvasculature after radiation exposures similar to those expected in long term space flight we use an established genetic model of Alzheimer disease.

Methods

The temporal progression of the vascular changes was studied using a transgenic (tg) Alzheimer disease mouse model overexpressing the amyloid percussor protein (APP). The vascular architecture was accessed by imaging vascular corrosion casts (VCC) with synchrotron based x-ray tomographic microscopy. In total we analyze the data acquired for 60 animals irradiated with 1, 2 or

O. Dössel and W.C. Schlegel (Eds.): WC 2009, IFMBE Proceedings 25/III, pp. 423–426, 2009.
www.springerlink.com

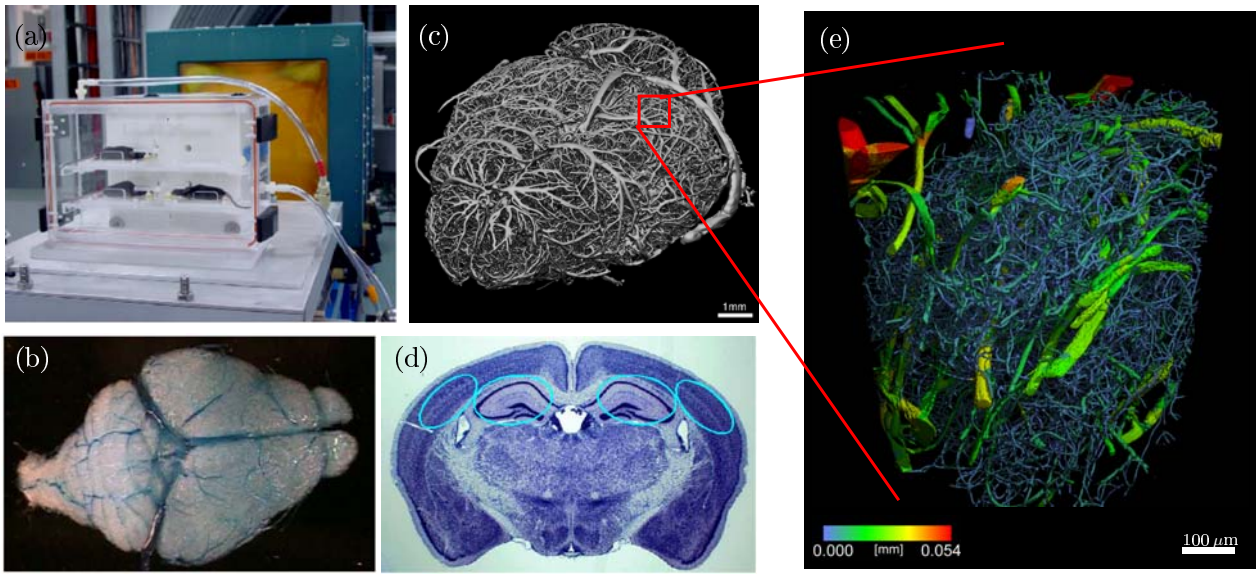

Figure 1: (a) Irradiation of animals at Nasa Space Radiation Laboratory at Brookhaven National Laboratory; (b) Vascular corrosion cast produced 3 weeks after irradiation; (c) 3D rendering of the brain vasculature scanned with a pixel size of 12 μm at the TOMCAT beamline of the Swiss Light Source (SLS) at Paul Scherrer Institute; (d) Regions targeted for morphometric evaluation of the vasculature; (e) 3D rendering of region from left posterior hippocampus with a pixelsize of 0.74 μm scanned at the TOMCAT beamline. Vessel thickness has been color coded.

4 Gy at the age of 5 weeks and 20 controls. The first 20 vascular corrosion casts (VCC) (fig. 1.b), were produced three weeks after 1–4 Gy ^{56}Fe radiation exposure (fig. 1.a) at the age of 2 month. Further samples were casted after 19 weeks, age 4 month, 32 weeks, age 6 month, and 54 weeks, age 1 year.

A hierarchical imaging approach (fig. 1.c, 1.e) allowed the visualization and analysis of 3D vascular structures down to the capillary level within their anatomical context. This is achieved by aligning regions of interest (ROI), giving access to micro-structures down to 0.74μm (fig. 1.e) within a field of view of 750x750 μm, on an overview scan obtained at a pixelsize of 12 μm and a field of view of 14x5 mm (fig. 1.c). The field of view on the overviews is vertically limited by the beam only and thus can be extended by combining two or more vertically adjacent scans into one data set. For both the overviews and the ROI we recorded 1001 X-ray projections over 180 ° at 13.5 keV and 80 ms exposure per image. All data were acquired at the TOmographic Microscopy and Coherent rAdiology experimenTs (TOMCAT) beamline [1] of the Swiss Light Source (SLS) at the Paul Scherrer Institute.

Hippocampal and cortical (fig. 1.d) morphological parameters including vessel thickness, volume and spacing were calculated in APP mice for 10 ROI, 4 cortical and 6 hippocampus. These parameters were calculated using distance transform and voxel counting based methods from the image processing language IPL^{TM} provided by SCANCO Medical (SCANCO Medical AG, Fabrikweg 2, 8306 Brüttisellen, Switzerland). Additional parameters such as number of vessels per mm^3, vessel length and tortuosity were computed using a network based hierarchical analysis system developed by Heinzer et al. [2, 3]. For each group of samples irradiated with 1–4 Gy and the controls we calculated the mean and standard deviation of the parameters and histograms for the vessel diameter, spacing and length.

Results

A previous study [2] has shown significant alterations in the micro-vasculature structures of APP tg mice. In our work, we quantify the effects of heavy particle (^{56}Fe) irradiation on the cortical micro-vasculature three weeks after exposure. It revealed that, three weeks after irradiation, as dose increased the vessel diameter and the volume of vessels with diameters >30 μm is decreased (fig. 2),

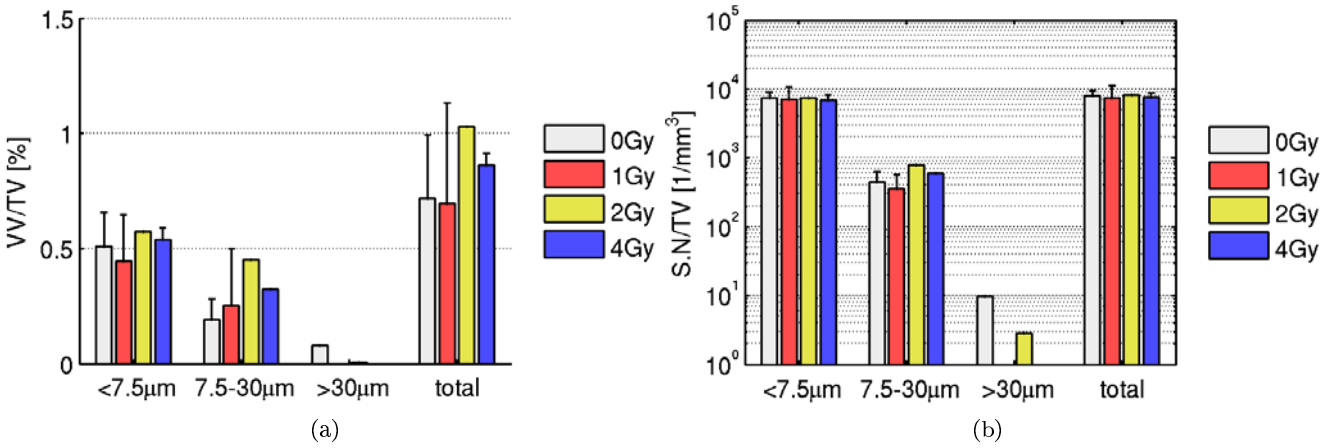

Figure 2: Plot (a) depicts the ratios between the vessel volume (VV) and the tissue volume (TV) for a region of interest (ROI) located in the right lateral cortex (RCTX). The corresponding numbers of vessels (S.N) per TV are plotted in (b) for RCTX. For the animals irradiated with 1 Gy and 2 Gy ^{56}Fe the volume of vessels with a diameter of 7-30 μm is increased whereas their number remains nearly constant. It appears that part of the loss of vessels $>30\,\mu$m is compensated by processes like angiogenesis and vascular remodeling. This is supported by the relative vessel volume and number of vessels being lower in the non irradiated controls.

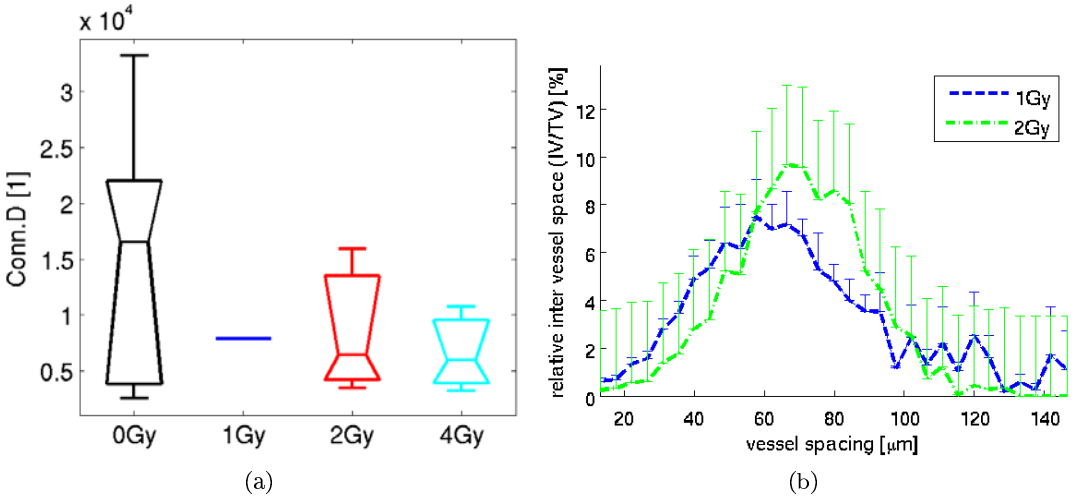

Figure 3: (a) The density of branching points is decreasing with dose for a region of interest in the right lateral cortex (RCTX). We think that this indicates inadequate compensation by processes like angiogenesis which are part of the response to the radiation event. When the dose is further increased to 4 Gy the connectivity density drops again, which is thought to be a result of insufficient replacement of lost vessels. (b) The histogram of the distribution of the vessel spacing reveals an increase in vessel spacing at distances between 40-90μm with increased dose.

thus increasing the inter-vessel spacing (fig. 3(b)). An initial quantitative analysis on 6 animals irradiated with 1, 2 and 4 Gy, done in [4] indicated that with increasing irradiation dose more vessels with diameters of $7-30\,\mu$m are lost in hippocampus. In contrast, in the cortex we found, through analyzing the data of 14 samples, that the number and volume of those vessels (fig. 2) is increased in animals irradiated with 1 and 2 Gy compared to animals exposed to 4 Gy and controls.

Discussion and Outlook

The dose dependent increment in vessel density (Fig. 2) and vessel spacing (Fig 3(b)) is likely to be caused by processes like angiogenesis and vascular remodeling. At the same time the density of branching points (Fig 2) was decreased with dose. We think the dose dependent alterations are related to the response triggered by the radiation event. This tissue response is a complex combination of cell death, cell division, inflammatory processes, signaling and reorganization of cellular components. In particular the decreased number of vessel junctions seems to be an indication for the inadequate compensation of the radiation induced damages. Further support to this assumption is given by the fact that the vessel spacing is increased at distances between 40–90 μm in irradiated animals compared to the controls.

The three week time point may be one of active tissue remodeling following endothelial cell apoptosis and later time points will provide insight into the long term steady state of the tissue. Thus, alterations in the vasculature after exposure to radiation can be important factors of neuro-degenerative diseases. How the radiation induced changes evolve over time is part of the ongoing research.

Acknowledgement

Supported by a NASA NSCOR # NNJ04HC9OG

References

[1] Stampanoni M, Marone M, Hintermüller C, Mikuljan G, Isenegger A and Abela R 2007 *Swiss Physical Society, Annual Meeting, Zurich, Switzerland* (Swiss Physical Society)

[2] Heinzer S, Krucker T, Stampanoni M, Abela R, Meyer E P, Schuler A, Schneider P and Müller R 2006 *NeuroImage* **32** 626–636

[3] Heinzer S, Müller R, Stampanoni M, Abela R, Meyer E P, Ulmann-Schuler A and Krucker T 2007 *Medical Imaging 2007: Physiology, Function, and Structure from Medical Images. Edited by Manduca, Armando; Hu, Xiaoping P.. Proceedings of the SPIE, Volume 6511, pp. 651104 (2007).* (*Presented at the Society of Photo-Optical Instrumentation Engineers (SPIE) Conference* vol 6511)

[4] Hintermüller C, Coats J S, Obenaus A, Nelson G, Krucker T and Stampanoni M 2008 *Journal of Physics: 9th International Conference on X-Ray Microscopy* Accepted

Author:	Dr. Christoph Hintermüller
Institute	Swiss Light Source, Paul Scherrer Institute
Address:	WLGA/133
City:	5232 Villigen PSI
Country:	Switzerland
Email:	christoph.hintermueller@psi.ch

Simultaneous measurements of electrical and optical properties of radiochromic films exposed to UV radiation as a function of temperature

F Gómez-Galván and H Mercado-Uribe

Cinvestav-Monterrey, PIIT, Vía del Conocimiento 201, Apodaca NL 66600, Mexico

Abstract— **By more than a decade, radiochromic films (RCF) have been used extensively in medical physics for evaluating uniformity of radiation beams and measuring dose distributions. Optical methods are usually the only ones used in the study of the response of these films. In this work, we have investigated the use of dielectric measurements as an alternative method to evaluate RCF exposed to ultraviolet (UV) radiation. We have developed an experimental device that allows us to measure simultaneously their electrical and optical properties. We performed the measurements in real-time to temperature increases from 27 to 48°C for EBT and MD-55 radiochromic films previously exposed to UV. We found that in both cases the spectra shifted towards shorter wavelengths. On the other hand, dielectric permittivity decreases but the dielectric loss increases in EBT films and decreases in MD-55.**

Keywords— **Radiochromic film, dielectric, optical density, radiation, temperature dependence.**

I. Introduction

Radiochromic films (RCF) are materials extensively used in medical physics as dosimeters. They are used to evaluate their response to radiation coming from electron [1,2], γ-ray [1,3], UV [4], proton [5,6] and heavy ion [7] sources. It is known that in general, radiation causes degradation of polymers, which can become apparent in the change of some properties [8]. In the case of RCF, they change their colour (optical density (OD)) when exposed to radiation. This change is correlated with the absorbed dose [9].

Until now, the effect of radiation in RCF has been evaluated using optical methods and devices as densitometers, scanners and spectrophotometers [10-14]. These methods use frequencies around 10^{16} Hz. The mechanism of response is electronic; the electric field causes a slight displacement of the electrons with respect to the nucleus [15]. Then, this assessment method permits to study microscopically one part of the film. On the other hand, at lower frequencies (for instance, around 1 MHz), the electric field causes the alignment of the dipoles in direction of the field. This orientation is strongly influenced by the temperature of the system. Therefore, the dielectric method is useful to study the films macroscopically. In this work, we use simultaneously these two complementary methods to evaluate the effect of the temperature in RCF after being exposed to UV radiation. We have developed an experimental device to measure simultaneously these electrical and optical properties. We performed the measurements in real-time in the temperature range of 27-48°C.

II. Materials and methods

We have studied two types of radiochromic films, EBT and MD-55. The EBT film consists in two polyester layers, each having a width of 97 μm. Between these layers there are two sensitive layers of 17 μm each, separated by a third layer of 6 μm. The MD-55 film consists in two sensitive layers of 16 μm separated by a region of two adhesive layers and polyester. The active layers are coated by polyester of 67 μm thick. These films are originally nearly transparent and turn to blue progressively according to the energy absorbed by radiation. The EBT film has two main absorption peaks located in the visible region, around 585 nm and 636 nm. In the case of MD-55, the peaks are at about 615 nm and 675 nm [9,16]. The batches we used were 47277-01I and N2519MD55, respectively.

The experimental device is a sample holder made up of two equal rectangular aluminum pieces with dimensions of 30 cm long, 6.3 cm high and 8 cm wide. Each piece has inside an electrically isolated circular steel disk with diameter and thickness of 2.0 cm and 0.5 cm, respectively. Once the pieces are joined together, the disks form a capacitor with a 0.4 mm of separation. A thin copper wire is connected to each disk and these wires to a Hewlett Packard LCR meter controlled by a computer. The film was laterally inserted inside the block holder for its evaluation. Two optical fibers were placed symmetrically in the two long sides of the aluminum blocks. One fiber is connected to an Ocean Optics HR4000CG-UV-NIR spectrometer. It is operated by a computer in a wavelength range of 200-1050 nm, with an optical resolution of 0.75 nm FWHM. The other optical fiber was placed in front of a halogen lamp. A thermocouple was placed at the top of the holder. The temperature of the system was controlled by a flux of water (using a Thermo Electron heater, model HAACKE DC10). The liquid flew through cylindrical chambers made along the

O. Dössel and W.C. Schlegel (Eds.): WC 2009, IFMBE Proceedings 25/III, pp. 427–430, 2009.
www.springerlink.com

aluminum pieces. The measurements were performed from 27 to 48°C. The dielectric permittivity (ε') and dielectric loss (ε'') measurements of the films were obtained by a LCR meter model 4284A, which operates in the range of 20 Hz-1 MHz, with a accuracy of ± 0.05% and ± 0.0005 in ε' and ε'', respectively. The frequency used was 1 MHz. The films were irradiated at different irradiances with an HP-120 UV point source, which generates UV and visible radiation (300-600 nm). A 7-59 Corning filter was placed at 4 cm above the film and at 10.5 below to the light guide. The filter transmits only the wavelengths from 300 to 495 nm of the full spectrum. Calibration was performed using a RM-21 radiometer from 200-700 nm connected a PC and an UVA sensor. The irradiances for EBT were 34, 137 and 205 mW/cm^2, and for MD-55, 34, 171 and 273 mW/cm^2. The experiment was carried out in dim atmosphere.

III. Results and discussion

Figures 1 and 2 show the optical spectra of the EBT and MD-55 films irradiated at 137 and 171 mW/cm^2 respectively, measured at temperatures from 27 to 48°C. Note that in both cases, as the temperature increases, the spectrum shifts to shorter wavelengths as previously reported in the past [1, 17]. For the EBT film, the main peak shifts 0.53 nm/°C and for the MD-55, 0.72 nm/°C (see insets of Figures 1 and 2).

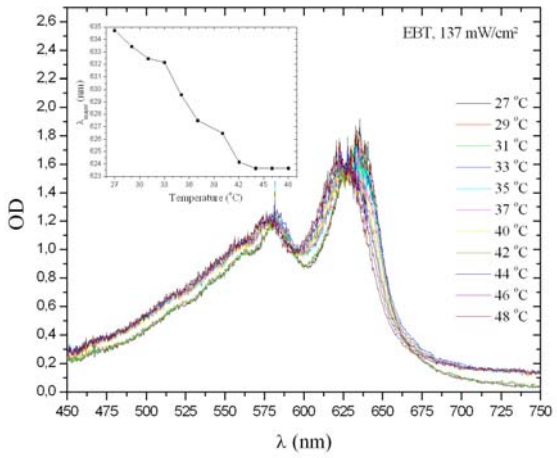

Fig. 1 Optical spectrum and wavelength of maximum optical density as a function of temperature of EBT RCF exposed to UV radiation.

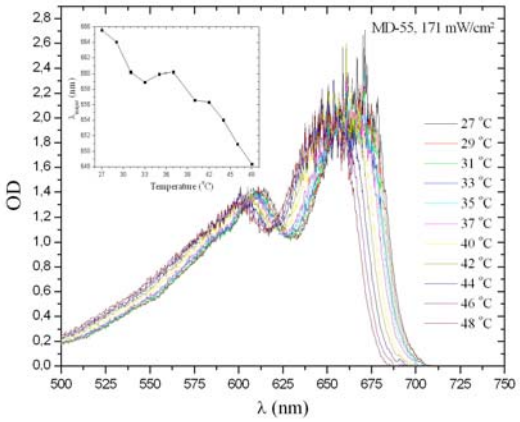

Fig. 2 Optical spectrum and wavelength of maximum optical density as a function of temperature of MD-55 RCF irradiated to 171 mW/cm^2.

Figures 3 and 4 show the temperature dependence of the dielectric permittivity (ε') for the EBT and MD-55 films. These plots show in both cases a decrease of ε' as the temperature increases, indicating the decrease of polarizability. On the other hand, Figures 5 and 6 show the dielectric loss ε''. It can be seen an evident difference between the two cases; for the EBT film, ε'' increases with temperature while for the other film, ε'' decreases. In the first case (EBT) there are three clear shoulders, indicating relaxation polymeric processes, possibly due to the stick-like morphology of the monomer crystals [18]. It is worth mentioning that relaxation mechanisms are normally observed at very high temperatures. Moreover, the existence of these relaxation processes seems to be correlated to the way λ_{max} shifts; it stops decreasing from 42 to 48°C (see inset to Fig. 1). In the case of the MD-55 film, both λ_{max} and ε'' drop continuously in the studied temperature range.

IV. Conclusions

We have measured simultaneously the dielectric and optical properties as the temperature increases from 27 to 48°C of EBT and MD-55 radiochromic films previously exposed to UV radiation. We have found, in both cases, that the optical density of the main peak decreases as a function of the temperature and the spectrum shifts toward shorter wavelengths. For the EBT film, the shift is 0.53 nm/°C and for the MD-55 is 0.72 nm/°C. We have also observed relaxation processes in the first film that may explain the plateau in λ_{max} at high temperatures.

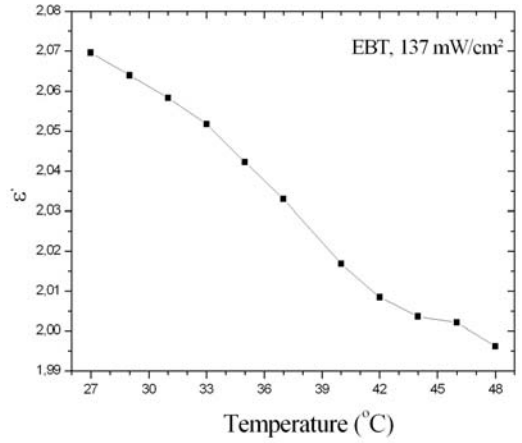

Fig. 3 Dielectric permittivity (ε') as a function of temperature of EBT RCF exposed to UV radiation.

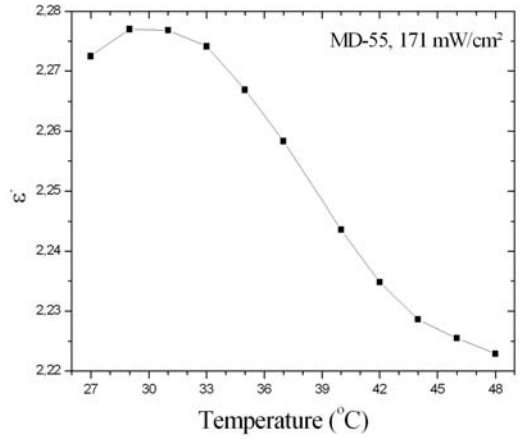

Fig. 4 Dielectric permittivity (ε') as a function of temperature of MD-55 RCF exposed to UV radiation.

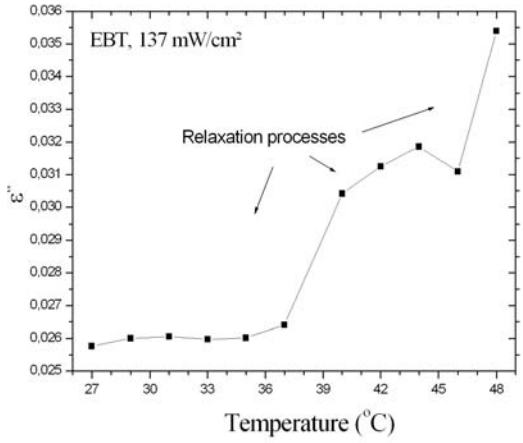

Fig. 5 Dielectric loss (ε'') as a function of temperature of EBT RCF exposed to UV radiation.

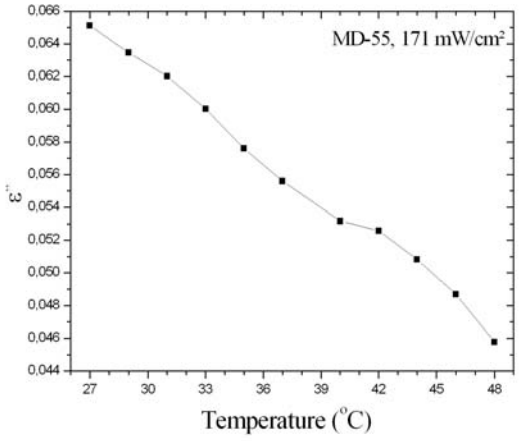

Fig. 6 Dielectric loss (ε'') as a function of temperature of MD-55 RCF exposed to UV radiation.

Acknowledgment

The authors want to thank C. Ruiz for valuable comments received. This work has been partially supported by CONACYT grant 81451.

References

1. McLaughlin W L, Yun-Dong C, Soares C G et al (1991) Sensitometry of the response of a new radiochromic film dosimeter to gamma radiation and electron beams. Nucl Instr and Meth A 302:165-176
2. Mercado-Uribe H, Brandan M E (2004) Thermoluminescent response of TLD-100 irradiated with 20 keV electrons and the use of radiochromic dye films for the fluence determination. Nucl Instr and Meth B 222: 210-212
3. McLaughlin W L, Puhl J M, Al-Sheikhly M et al (1996) Novel radiochromic films for clinical dosimetry. Radiat. Prot. Dosim 66:263-268
4. Butson M J, Cheung T, Yu P K N et al (2000) Ultraviolet radiation dosimetry with radiochromic film. Phys Med Biol 45:1863-1868

5. Vatnitsky S M (1997) Radiochromic film dosimetry for clinical proton beams. Appl. Radiat Isot 48:643-651
6. Piermattei A, Miceli R, Azario L et al (2000) Radiochromic film dosimetry of a low proton beam. Med Phys 27:1655-1660
7. Buenfil A E, Ruiz-Trejo C, Gamboa-deBuen I et al (2002) Response of radiochromic dye films to low energy heavy charged particles. Nucl Instr and Meth B 197:317-322
8. Dissado L A, Fothergill J C (2008) Electrical degradation and breakdown in polymers. The Institution of Engineering and Technology, London
9. Niroomand-Rad A, Blackwell C R, Coursey B M et al (1998) Radiochromic film dosimetry: Recommendations of AAPM Radation Therapy Committee Task Group 55. Med Phys 25:2093-2115
10. Stevens M A, Turner J R, Hugtenburg R P et al (1996) High resolution dosimetry using radiochromic film and a document scanner. Phys Med Biol 41:2357-2365
11. Reinstein L E, Gluckman G R (1997) Predicting optical densitometer response as a function of light source characteristics for radiochromic film dosimetry. Med Phys 24:1935-1942
12. Aydarous A Sh, Darley P J, Charles M W (2001) A wide dynamic range, high-spatial-resolution scanning system dye radiochromic dye films. Phys Med Biol 46:1379-1389
13. Alva H, Mercado-Uribe H, Rodríguez-Villafuerte M et al (2002) The use of a reflective scanner to study radiochromic film response. Phys Med Biol 47:2925-2933
14. Butson M J, Cheung T, Yu P K N et al (2005) Absorption spectra variations of EBT radiochromic film from radiation exposure. Phys Med Biol 50:N135-N140
15. Blythe T, Bloor D (2005) Electrical properties of polymers. Cambridge, New York
16. ISP at http://www.gafchromic.com
17. Rink A, Lewis D F, Varma S et al (2008) Temperature and hydration effects on absorbance spectra and radiation sensitivity of a radiochromic medium. Med Phys 35:4545-4555
18. Rink A, Vitkin I A, Jaffray D A (2005) Characterization and real-time optical measurements of the ionizing radiation dose response for a new radiochromic medium. Med Phys 32:2510-2516

Author: Hilda Mercado Uribe
Institute: Cinvestav-Monterrey
Street: Via del conocimiento 201, PIIT, Autopista al aeropuerto km. 9.5
City: Apodaca, NL
Country: Mexico
Email: hmercado@cinvestav.mx

Linear Accelerator Direct Shielded Doors – An Approach for Calculating the Specialized Shielding Required Adjacent to the Door

M.C. Martin[1]

[1] Therapy Physics, Inc., Gardena, California, USA

Abstract— **Medical linear accelerator vaults occupy less space when constructed with a direct shielded door instead of a maze. The door is a secondary barrier, with a straightforward shielding calculation required to determine the required material. However, because of the limited overlap between the door and the entrance, additional specialized shielding is required next to the door. This paper describes an approach to determine the amount of specialized shielding required.**

Keywords— **Radiotherapy, shielding.**

I. Introduction

Medical linear accelerator vaults have traditionally been constructed with a maze between the entrance to the vault and the machine [1]. The size required for the vault is reduced if this maze is eliminated and replaced with a direct shielded door. A direct shielded door must shield not only X-rays (with lead) but also leakage neutrons (with borated polyethylene) for machine energies at and above 10 MV. The door itself is simply a secondary barrier, with straightforward shielding calculations described in both a textbook [2] and an NCRP standard [3]. Section II describes this calculation.

A direct-shielded door will typically be designed to have a minimum 6 mm gap at the vertical location on the wall having least clearance. A maximum gap of 12 mm between wall and door is expected after allowing for fit-and-finish in the wall construction. The door design will typically provide a 19 cm minimum overlap beyond the inside surface of the shielding at in the entrance walls.

The limited overlap of the door with the entrance to the accelerator room requires additional specialized shielding. While approaches to provide this additional shielding are described in references [2] and [3], no specific calculations are included to quantify the shielding required. This paper describes an approach to provide this specialized shielding and a method for calculating the time-averaged dose rate expected beyond the entrance resulting from the design. Section III describes the shielding at the far side of the door, which is a secondary barrier calculation with a specialized geometry. Section IV describes a method for adapting maze calculations to determine the shielding required at the near side of the entrance.

II. Shielding design for the door

A shielding design goal (P) of 0.1 mSv/wk is appropriate for the vault entrance, assuming it is located in a controlled area. The dose rate reaching the protected location is directly proportional to the linear accelerator workload (W). A 3 Gy workload per treatment is a reasonably conservative value that is sufficient to include quality and maintenance use of the machine for a typical facility. This corresponds to a weekly workload of 450 Gy, assuming a patient workload of 30 patients per day with a 5 day work week.

The secondary radiation at the entrance includes leakage from the shielding around the target and scattered radiation from the patient. For accelerators ≥10 MV, both x-ray and neutron leakage must be considered. The secondary barrier unshielded dose is calculated using the geometry in Figure 1. The x-ray leakage unshielded dose rate due to leakage from the target (H_{UL}) in Sv/wk is given by Equation 1.

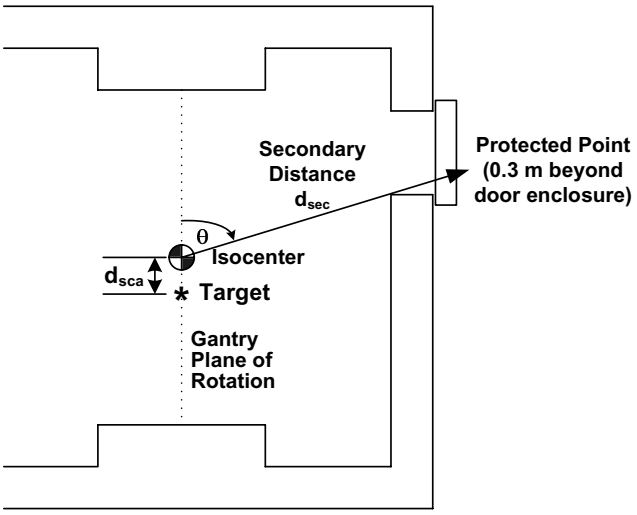

Fig. 1 Direct Shielded Door Geometry

$$H_{UL} = \frac{W_L \, 10^{-3}}{d_{\text{sec}}^2} \quad (1)$$

O. Dössel and W.C. Schlegel (Eds.): WC 2009, IFMBE Proceedings 25/III, pp. 431–434, 2009.
www.springerlink.com

The 10^{-3} factor (the x-ray leakage fraction) reflects the standard manufacturer's requirement that the average x-ray leakage outside the beam must be less than 0.1% of the dose rate at isocenter. Note that x-ray leakage is typically on the order of a factor of 4 to 5 lower than the requirement. The x-ray leakage workload (W_L) is equal to the conventional workload (W) if IMRT is not used.

Intensity Modulated Radiation Therapy (IMRT) requires an increase in monitor units (MU) compared to conventional radiation therapy. The IMRT ratio is defined to be the ratio of MU to cGy at isocenter when IMRT is used. The IMRT factor is the average IMRT ratio, given by:

$$\text{X-Ray IMRT Factor} = \text{IMRT Ratio} \times \%\text{IMRT} + (1-\%\text{IMRT}) \quad (2)$$

The x-ray leakage workload (W_L) is then given by:

$$W_L = W \times \text{X-Ray IMRT Factor} \quad (3)$$

The x-ray leakage shielded dose rate (H_L) is given by Equation 4.

$$H_L = H_{UL} \; B_L \quad (4)$$

Here B_L is the leakage transmission calculated from slant thickness and the x-ray leakage first and equilibrium tenth-value layers TVL_1 and TVL_e. The concrete leakage TVL values are given in NCRP 151 Table B.7 [3]. Lead and steel leakage TVL values are not as well documented, but 57 mm and 96 mm, respectively, are reasonable values. The borated polyethylene (BPE) leakage TVL values can be estimated based on a density of 0.95 g/cm^3 for BPE vs. 2.35 g/cm^3 for concrete.

Energies 10 MV and greater require a neutron leakage calculation also. Neutron leakage is calculated using the same approach as for x-ray leakage (Equations 1 through 4), except with an appropriate neutron leakage fraction (vs. 0.1% for x-rays), neutron IMRT factor, and tenth value layers. A lower neutron IMRT factor than x-ray IMRT factor is appropriate for a dual energy accelerator if the shielding calculations are performed only the higher energy. Appropriate neutron tenth value layers are 211 and 96 mm for concrete and borated polyethylene, respectively, assuming 1 one MV neutron energy [4].

Typical neutron leakage fractions for Varian are 0.004%, 0.07%, 0.15%, 0.19%, and 0.20% for 10, 15, 18, 20, and 24 MV, respectively. Typical neutron leakage fractions for Siemens are 0.002%, 0.04%, 0.10%, 0.14%, and 0.23% for 10, 15, 18, 20, and 24 MV, respectively. Typical neutron leakage fractions for Elekta are 0.03%, 0.07%, 0.15%, 0.20%, and 0.30% for 10, 15, 18, 20, and 24 MV, respectively.

The unshielded patient scatter dose rate (H_{UPS}) in Sv/wk is given by Equation 5.

$$H_{UPS} = \frac{a\,W\,U\,(F/400)}{d_{sca}^2\; d_{\text{sec}}^2} \quad (5)$$

As shown in in Figure 1, d_{sca} (meters) is the target to isocenter distance (typically 1 meter), d_{sec} (meters) is the secondary distance from isocenter to the point protected, W is the workload in Gy/wk, U is use factor (1 in this case),

- a = Patient scatter fraction relative to primary at 1 m distance for a 400 cm^2 field (Table B.4 of NCRP 151)
- F =Field area in cm^2 (e.g., 1600 for 40 x 40 cm maximum field size with no IMRT).

The patient scatter shielded dose rate (H_{PS}) is given by Equation 6.

$$H_{PS} = H_{UPS}\; B_{PS} \quad (6)$$

Here B_{PS} is the patient scatter transmission calculated from door slant thickness and patient scatter tenth value layers, which vary with MV and scatter angle. NCRP 151 Table B.5 and Figure A.1 give these tenth value layers [3].

A factor a two margin below P is recommended to account for capture gamma rays. If an HVAC duct located in wall near the door, increasing the margin to on the order of a factor of 3 below P is recommended.

III. Shielding the Far Side of the Entrance

As illustrated in Figure 2, a direct leakage path occurs at the far lateral edge of the door. To compensate for the short slant thickness at corner of the entrance, additional material is can be added at the two locations shown in Figure 3.

The slant thickness through the wall at the corner (d_C) is given by Equation 7.

$$d_C = \frac{d_o}{\cos(\theta)} - \frac{d_g}{\sin(\theta)} \quad (7)$$

where d_o is the door overlap beyond the entrance and d_g is the gap between the concrete wall and the door.

The slant thickness through the concrete is then given by d_C minus the slant thickness through the lead added to the wall, $d_L/\sin(\theta)$, where d_L is the lead thickness. Borated polyethylene is then added beyond the wall to reduce neutrons to the desired level. The shielding calculation uses the same secondary calculation methodology used for the door.

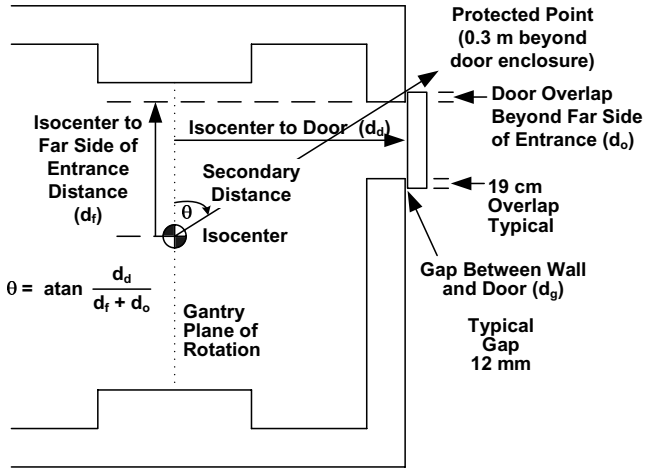

Fig. 2 Slant Thickness at Far Side of Direct Shielded Door

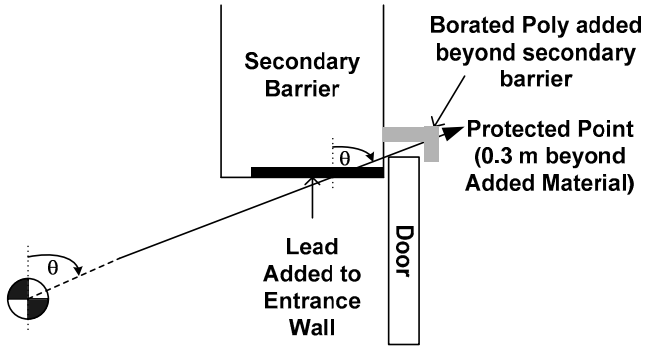

Fig. 3 Material Added to Entrance on Far Side of Direct Shielded Door

IV. Shielding the Near Side of the Entrance

The geometry at the near side of the entrance is similar to that of a maze, implying the same sources of leakage, scatter, and neutron-related radiation are present. Unlike a maze, single-bounce wall scatter from one lateral primary barrier has a direct path to the near side of the door, making the shielding requirements for the other sources of scattered radiation negligible in comparison.

A. Wall Scatter to Near Side of Door

The wall scatter unshielded dose rate at the near side of the entrance is calculated using the geometry in Figure 4. The unshielded dose rate due to wall scatter (H_{US}) in Sv/wk is given by Equation 8.

$$H_{US} = \frac{f\,W\,U\,\alpha_0\,A_0}{d_0^2\,d_Z^2} \quad (8)$$

As shown in Figure 4, d_0 (meters) is the target to primary barrier distance, d_Z (meters) is the distance from the primary barrier to the protected location, W is the workload in Gy/wk, U is the use factor (1),

- f = patient transmission factor (0.23 for 4 or 6 MV, 0.27 for ≥10 MV)
- α_0 = Reflection coefficient at linac MV with 0º incidence 75º reflection (NCRP 151 Table B.8a), and
- A_0 = beam area at first reflection = $(0.4\ d_0)^2$ for a 40 x 40 cm field at 1 meter

Because the wall scatter undergoes only a single bounce, the tenth value layer is based on the primary TVL at 0.5 MV in NCRP 151. A slant thickness of 45 degrees to normal is assumed at the corner.

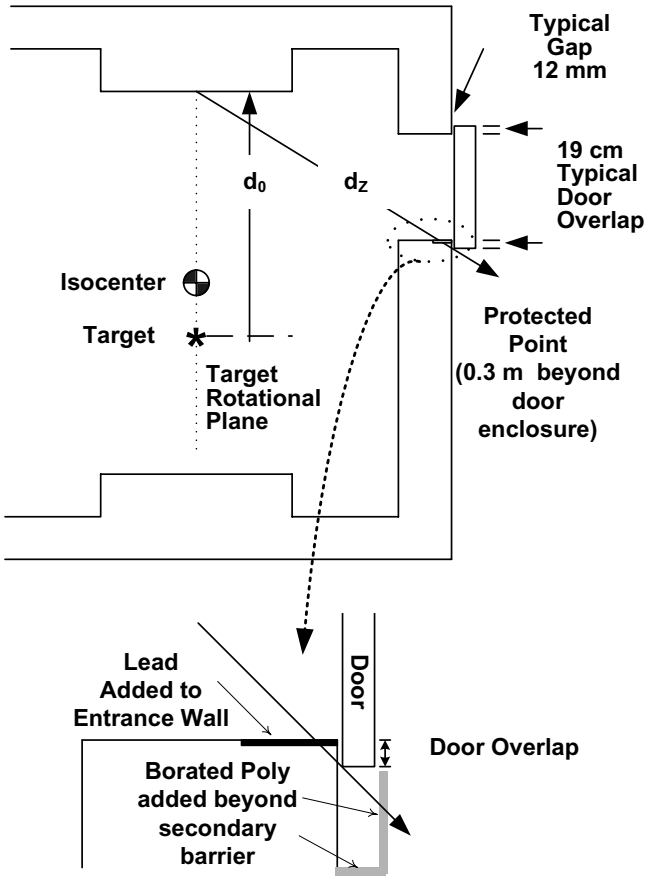

Fig. 4 Material Added to Entrance on Near Side of Direct Shielded Door

B. Neutrons and Capture Gammas at Near Side of Door

For accelerators 10 MV and greater, neutron transmission through the near side of the door must be included in the

dose equivalent rate calculation. This dose equivalent rate must include not only neutrons, but also gamma rays associated with neutron capture. This calculation is based on the modified Kersey method described in NCRP 151 Section 2.4.2 [3].

The first step is to calculate the Total Neutron Fluence (neutrons/m^2) at Point A per Gy Workload (φ_A). The calculation is given by Equation 9 and uses the geometry illustrated in Figure 5.

$$\varphi_A = \frac{\beta Q_n}{4\pi d_1^2} + \frac{5.4\,\beta Q_n}{2\pi S_r} + \frac{1.3\,Q_n}{2\pi S_r} \quad (9)$$

where β is the head shielding transmission factor (1 for lead, 0.85 for tungsten), Q_n is the neutron source strength from NCRP 151 Table B.9, h is the room height, and

$$S_r = 2\,(d_L\,d_W + h\,d_L + h\,d_W). \quad (10)$$

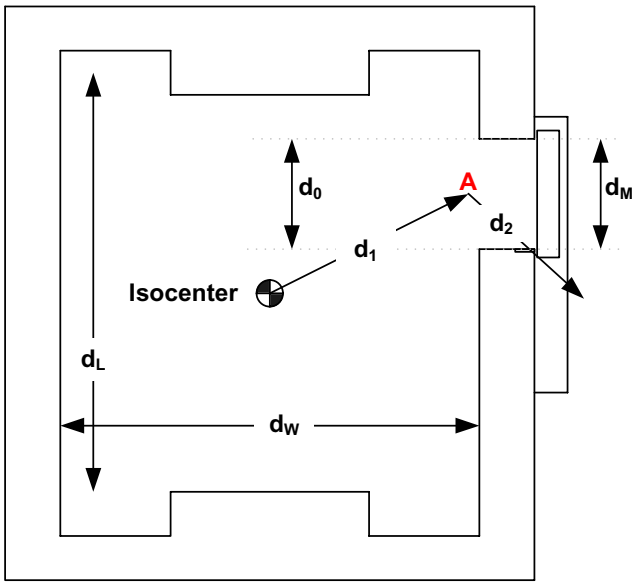

Fig. 5 Neutron Fluence Calculation at Near Side of Direct-Shielded Door

Equation 11 gives the Capture Gamma Unshielded Dose at Door per Dose at Isocenter (h_φ).

$$h_\varphi = K\,\varphi_A\,10^{-d_2/TVD} \quad (11)$$

In Equation 11, TVD is the tenth-value distance assumed to be 5.4 meters at 18 MV and above and 3.9 meters below 18 MV per NCRP 151. The constant K in Equation 11 is the ratio of capture gamma dose equivalent at point A, assumed to be 6.9 x 10^{-16} m^2 Sv per unit neutron fluence. The unshielded dose rate at the door is h_φ times the neutron leakage workload (W × neutron IMRT factor) [3].

Equation 12 gives the Neutron Unshielded Dose-Equivalent at Door per Dose at Isocenter ($H_{n,D}$).

$$H_{n,D} = 2.4\times10^{15}\varphi_A\left(\frac{S_0}{S}\right)^{\frac{1}{2}}\left(1.64\times10^{-(d_2/1.9)} + 10^{-(d_2/TVD)}\right) \quad (12)$$

where S_0/S is ratio of inner maze entrance cross-section area ($S_0 = d_0$ h) to maze cross-section area ($S = d_M$ h) and TVD is 2.06 × S$^{1/2}$. The unshielded dose rate at the door is $H_{n,D}$ × neutron leakage workload. Neutron and capture gamma radiation (for 10 MV and above) are calculated using the geometry in Figure 5, which is similar to a conventional maze calculation.

Based on NCRP 151, a TVL of 45 mm is assumed for borated polyethylene for neutron shielding. For the concrete at the wall adjacent to the door, a neutron TVL of 161 mm is assumed based on NCRP 79 at 0.1 MV neutron energy [4]. For capture gammas, the TVL values from NCRP 151 Figure A.1 are applied for materials other than lead, assuming average capture gamma energy of 10 MeV (consistent with a short maze). For lead, a 61 mm lead TVL is assumed for capture gammas.

V. Conclusions

For an 18 MV linear accelerator, a direct shielded door typically contains 12 to 15 cm lead and 23 to 28 cm borated polyethylene with 6 mm steel covers. To maintain the same shielded dose rate at the far side of the door (as beyond the door) requires 7 to 10 cm lead added to the far wall at the entrance and on the order of 15 cm borated polyethylene beyond the wall. Because there is no direct leakage at the corner of the near side of the door, approximately half as much lead and borated polyethylene is needed.

References

1. Stedeford B, Morgan H, Mayles W (2002) The Design of Radiotherapy Treatment Room Facilities. Institute of Physics and Engineering in Medicine, York, England
2. McGinley P (2002) Shielding Techniques for Radiation Oncology Facilities. Medical Physics Publishing, Madison WI USA
3. NCRP Report 151 (2005) Structural Shielding Design and Evaluation for Megavoltage X- and Gamma-Ray Radiotherapy Facilities. National Council on Radiation Protection and Measurements, Bethesda, MD, USA
4. NCRP Report 79 (1984) Neutron Contamination from Medical Electron Accelerators. National Council on Radiation Protection and Measurements, Bethesda, MD, USA

Database MAMOLIT for mammography screening patients in Lithuania

D. Adliene[1], M. Laurikaitis[2], J.Laurikaitiene[1,2], I. Cibulskaite[1,3] and A. Urboniene[4]

[1] Kaunas University of Technology/ Physics Department, Kaunas, Lithuania
[2] Kaunas Medical University Hospital/ Radiation Protection Service, Kaunas, Lithuania
[3] Kaunas Medical University Division Oncology Hospital, Kaunas, Lithuania
[4] Radiation Protection Centre, Kalvariju g. 153, Vilnius, Lithuania

Abstract— **Patient doses in mammography screening examinations in Lithuania have been investigated within a period between 2003 and 2009. *In vivo* dose measurements were performed using thermoluminescence dosimetry (TLD) technique. Interactive database MAMOLIT was created, which allowed calculating of patient's doses, documenting of measured and calculated doses and other parameters of the mammography screening examination, following up of the frequency of patient related X-ray examinations, and analysing of the collected data from different points of view. Reference level of 2.4 mGy of the average glandular dose was set for mammography screening in Lithuania on the base of the obtained results. Present paper summarises gathered experience and outlines some problems which may occur when performing dose measurements during mammography screening examinations of patients.**

Keywords— **mammography, thermoluminescence dosimetry, entrance surface dose, average glandular dose, dose reference level.**

I. Introduction

Breast cancer still remains one of the most common cancer diseases among the women in Lithuania (Fig.1). A number of the new breast cancer cases increases slowly year by year [1].

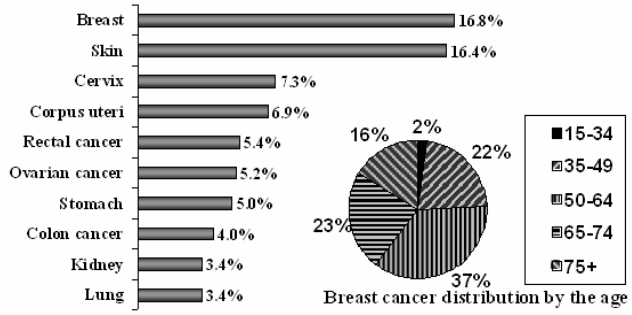

Fig.1. Breast cancer in Lithuania 2007-2008

National mammography screening program has been started in September 2005 with the aim to detect breast cancer in the early stage and to prevent women against fatal outcome of this disease. Mammography screening program was addressed to the women in the age of 50-69 years, the number of whose according the database of the Health Ministry of Lithuania was ~ 413200 in Lithuania. It was planned to apply breast screening procedure to 60% of all mentioned women during 5 years. 14 mammography screening centres were involved in this project (4 centres in Vilnius, 4 centres in Kaunas, 1 centre in each of hospitals in Klaipėda, Šiauliai, Panevėžys, Alytus, Marijampolė and Utena) in 2005. Only 11 of these centres are continuing this work until now.

Four X-ray examinations (Cranio-Caudal (CC) projection, Medio-Lateral-Oblique (MLO) for each breast of the patient) were planned as usual for the mammography screening procedure. Two independent radiologists-reviewers evaluated mammograms according to the standard BI-RADS evaluation system.

The efficiency of the National screening program was not that good as it was expected. An average outcome per year was only 72.3% of a planned number of women until now. The main factor influencing this figure was not a lack of screening equipment, but rather the minimal number of radiologists-evaluators in Lithuania. Due to the lack of high professionally skilled radiologists, it was not possible to continue the screening program in three institutions. Another shortness of this project was a performance of the screening examinations in parallel to diagnostic examinations of patients. Such praxis limited the number of mammography screening examinations in the biggest medical centres: in Vilnius (47%) and in Kaunas (60%), but was very effective (119%) in centres where in fact only screening examinations were undertaken ("Salvija Medical Centre" in Klaipėda, for example).

Despite of the quality checking of the procedure and installation of quality assurance programme in all mammography screening centres according to the requirements of Lithuanian HN-94-2004, assessment of patient's doses was not set as one of the high priority objectives in mammography examinations.

The first attempt to investigate systematically patient's doses during mammography examinations in Lithuania was made in 2003-2004 [2]. Gathered experience was used

O. Dössel and W.C. Schlegel (Eds.): WC 2009, IFMBE Proceedings 25/III, pp. 435–438, 2009.
www.springerlink.com

starting a new investigation of patient' doses, which runs now parallel to the National mammography screening program. The aim of this work was to establish interactive database for the patient's doses obtained during mammography examinations (both, screening and diagnostic), to identify and discuss the problems and to implement patient's dose optimization measures.

II. Investigation

A. Applicants

Investigation of patients doses during mammography examinations were performed in 15 health care institutions in Lithuania: S.Kudirka Hospital (Alytus), Clinic "Bendrosios medicinos praktika" (Kaunas), Dainava Outpatient department (Kaunas), Kaunas Medical University Hospital, Division of the Kaunas Medical University Hospital Oncology Hospital, Šančiai Outpatient Department (Kaunas), Klaipėda University Hospital, Marijampolė Hospital, Panevėžys Hospital, Salvija medical centre (Kaunas), Šiauliai Hospital, Utena Health Care Centre, Antakalnis Outpatient Department (Vilnius), Centre Outpatient Department (Vilnius), Vilnius University Oncology Institute.

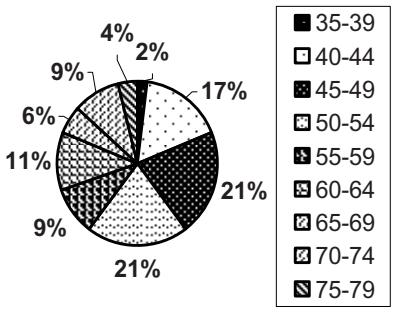

Fig.2. Applicants by the age

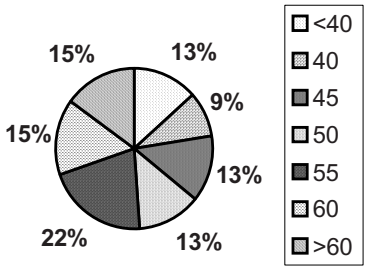

Fig.3. Applicants by the compressed breast thickness

Randomly selected groups consisting of 13-20 patients of different age and with different breast density and size were chosen for each investigation in each institution. Statistics on investigated applicants is provided in Fig.2 and Fig.3.

Approximately 400 patient's dose measurements were performed in the period of 2003-2004 and another 2000 dose measurements - in the period of 2006 - 2008.

B. Experimental

Dose to the breast of an individual patient depends on the characteristics of the equipment being used for the examination; technological factors, selected for the examination (X-ray tube voltage, X-ray tube output, anode/filter combination, X-ray attenuation, film/screen system, focal spot to the target distance, compression force); size and density of the patient's breast. Dosimetry method used for the measurements and estimation of the possible impact of human factor to the performed measurements are of great importance too.

Mammography units "ALPHA RT" (Instrumentarium), "MAMMOMAT 100" (Siemens) or "MAMMO DIAGNOST U-M", "PHILIPS MAMMO DIAGNOST" with a grid, Mo/Mo or Mo/Rh anode / filter combination; Kodak Min-RD, Cawo Mammo R200 film cassettes and Kodak X-Omat, Konica Minolta, CEA films were used for the screening procedures.

Exposure parameters were registered for each patient in a line with values of the compression force and the compressed breast thickness, age of the patient and other individual data.

Termoluminescence dosimetry method (TLD) was chosen for the patient's dose measurements.

Entrance surface doses to patients breast were measured using LiF:Mg,Ti TLD dosimeters: a)pellets having size of (3.2x3.2x0.9) mm^3, calibrated and red out using a Harshaw TLD5500 (Harshaw Bicron Radiation measurement products, Ohio, US) at the Department of Medical Radiation Physics, Malmö University Hospital and b) tablets with a diameter of ø5mm, which were calibrated at the representative energy and beam quality at the Second Standard Laboratory in Latvia and red out using Rados TLD system at Lithuanian Radiation Protection Centre. Depending on the type of the investigation, one to four dosimeters were placed on the breast surface at the reference point (central position, upper quadrant of the breast, 5-6 cm distance from the chest wall).

Average glandular dose (AGD), which is the main dosimetrical parameter in mammography examinations, expresses the dose absorbed in the patient's breast tissue and is described as [3]:

$$AGD = ESAKgcs\,, \tag{1}$$

ESAK is entrance surface air kerma; g is entrance air kerma to mean glandular dose conversion factor (corresponds to a breast glandularity of 50%); *c* is correction factor for any difference in breast composition from 50% glandularity; *s* is correction factor for different X-ray spectra [4, 5].

Value of the entrance surface air kerma (*ESAK*) could be obtained dividing the value of measured entrance surface dose (*ESD*) by backscattering factor, *B*, which corresponds to the dosimeter used (European protocol on dosimetry in mammography. EUR 16263EN) [3]:

$$ESD = B \cdot ESAK \tag{2}$$

Measured values of ESD were used as an input data for further investigation of patient's doses received during mammography examinations.

III. Results

A. Database MAMOLIT

Interactive database MAMOLIT was created, which allows calculating of patient's average glandular doses according to the input data, documenting measured (ESD) and calculated (AGD) doses and other related parameters of the mammography screening examination; following up of the frequency of patient related X-ray examinations; and analysing collected data (Fig.4).

Fig.4. Front page of the database

Different types of information about the mammography procedure are included into database MAMOLIT: patient related data (name, age, compressed breast thickness, identification number in a database, assigned dosimeter registration numbers); institution related data (name of institution, date of the performed examination, name of the person responsible for the performance of dose measurements), equipment related data (mammography unit, equipment, exposure parameters, compression force, exposure projections, film parameters); and dose related data (conversion coefficients, measured ESD, calculated AGD). It is possible to analyze and compare patient's doses using different data cross sections and to present dose distributions in a graphical form.

B. Doses

It was found, that a majority of the calculated average glandular doses for the particular compressed breast thickness was within acceptable levels, which are mostly used for the quality control measurements of the mammography system [6]. However analysis of dose distribution data in each hospital has shown significant differences as it is indicated in Fig.5 and Fig. 6. (Plots are taken from the database)

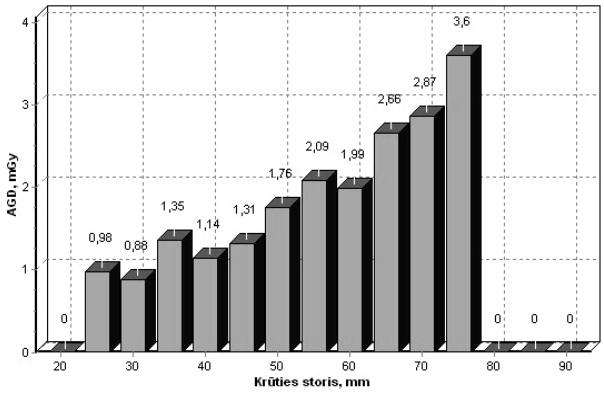

Fig. 5. AGD versus compressed breast thickness in hospital A

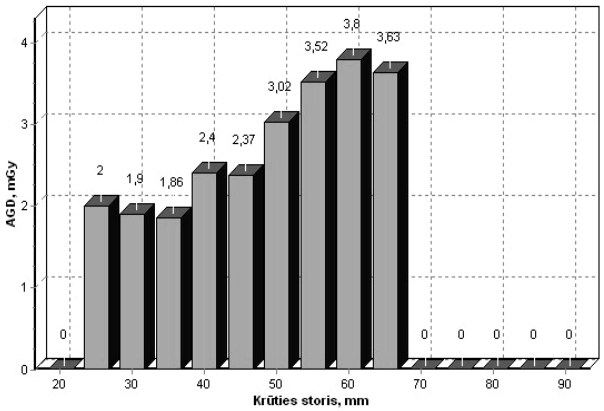

Fig. 6. AGD versus compressed breast thickness in hospital B

The improvement of the results in some hospitals has been achieved after regular quality control program was introduced and optimization of mammography screening procedure was performed. Comparison of the results before and after the optimization in the same hospital is presented in Fig. 7 and Fig. 8. (Plots are taken from the database)

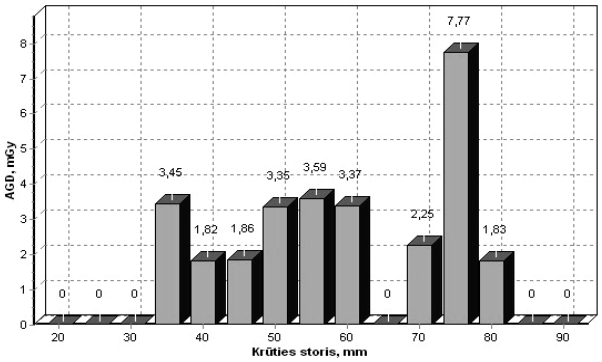

Fig. 7. AGD versus compressed breast thickness in hospital C (2006)

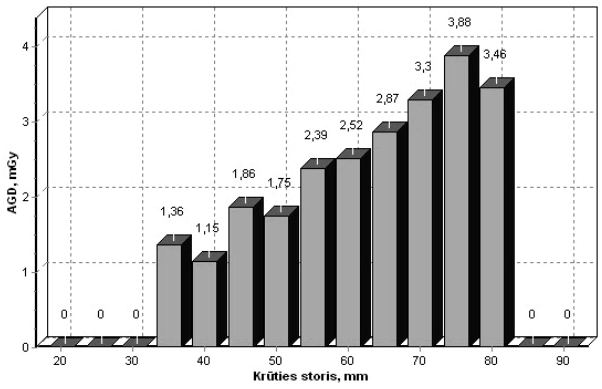

Fig. 8. AGD versus compressed breast thickness in hospital C (2008)

The primary idea of patient's dose measurements during mammography examinations was setting of the national dose reference levels in Lithuania and in each health care institution separately.

Due to this reason values of average glandular doses estimated for a "standard" 55 mm compressed breast thickness (as for Lithuania) in different hospitals were compared (Fig.9). According to the results of measurements national reference level of 2.4 mGy with the certainty of the third quartile was proposed for the average glandular dose absorbed in the patient's breast during mammography screening examination. The level of 2.4 mGy is well promising result, since it means possible reduction of the existing 3 mGy reference level, which was recommended for mammography screening examinations in Lithuania.

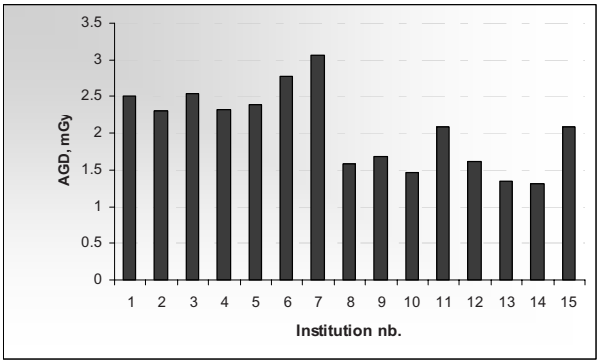

Fig. 7.. Comparison of AGD estimated for the compressed breast thickness of 55 mm in different hospitals

IV. CONCLUSIONS

Patient doses during mammography screening examinations have been investigated in the period of 2003 -2008. Case sensitive interactive database MAMOLIT was created, which enables calculation, comparison and analysis of mammography patient's doses using different data cross sections and presentation of the results in graphical form.

Reference level of 2.4 mGy was set for patient doses in mammography screening examinations in Lithuania.

ACKNOWLEDGMENT

This work was supported by Lithuanian State Science and Studies Foundation.

REFERENCES

1. Adliene D, Adlys G.A, Cerapaite R. et al. (2005) Optimization of the X-ray examinations in Lithuania: start of the implementation in mammography. Rad.Prot.Dos. V114, No 1-3: 399-402
2. http://www.is.lt/cancer_reg/moterys/MSL2005
3. European protocol on dosimetry in mammography. EUR 16263EN. ISBN 92-827-7289-6. Luxemburg.
4. Dance D., Skiner C., Young et al. (2000) Additional factors for the estimation of mean glandular breast dose using UK mammography dosimetry protocol. Phys.Med.Biol. 45: 3225-3240
5. Dance D.R., Skinner C.L., Alm Carlsson.G. (1999) Breast dosimetry. Applied Radiation and isotopes 50: 185-203.
6. Faulkner K. (2004) Screening Mammography including quality assurance. Proceedings of the 11th International Congress of the International Radiation Protection Association, Madrid, Spain, 2004:pp. 789–792.

Author: Diana Adline
Institute: Kaunas University of Technology
Addrress: Studentu g. 50, LT-51368 Kaunas
Country: Lithuania
Email: diana.adliene@ktu.lt

The effects of hydrogenous medium on MRI image of MAGICA gel dosimeter

S.M.Abtahi[1]-M.Shahriari[1]-M.H.Zahmatkesh[2]

[1]Shahid Beheshti University, Nuclear Engineering Faculty, Tehran, Iran
[2] Novin Medical Radiation Inc., Tehran, Iran

Abstract— **however the resolution of gel dosimeter is strongly dependant to gel composition, The proper parameters and selection of optimum method in dose response readout can reduce noise and improve some important features such as contrast and spatial resolution considerably. One method for dose response readout in gel dosimetry is variation of magnetic properties of proton using magnetic resonance imaging (MRI). A major problem in this method, is the serious reduction of contrast in edges when results in lost of dose in those region. In this study a new method contrast enhancement of gel dosimeter with MR image is presented. in doses lower than 17 Gy with imaging in water medium, a small reduction in spatial resolution is exchange to considerable increase of contrast in R2 map is important.**

Keywords— **gel dosimeter- MAGICA- contrast- resolution- MRI.**

I. Introduction

Polymer gel dosimeters in fact are monomers that distributed in a gelling matrix. Ionizing radiations convert these monomers to polymers via distinguished mechanism [1]. The polymerization degree is dependant on the absorbed dose in gel dosimeter.

In this study a new type of gel dosimeter with acronym MAGICA was used. This type of gel dosimeter was manufactured by adding of agarose to the ingredient of MAGIC gel dosimeter [2] and MAGICA gel dosimeter was manufactured in Novin Radiation Medicine Inc. (I. R. Iran) in 2004 [3].

In this study contrast enhancement of MAGICA gel dosimeters with MRI in water environment and noise in the dose map was investigated. contrast and noise of R2(=1/T2) in gel MRI images in water and air were also compared and optimum condition for MAGICA gel dosimeters MR imaging for best contrast and resolution was obtained.

II. Materials and Methods

A. Gel production

The composition of MAGICA gel dosimeter is given in table (1) [3]

Table1. Composition of 1000g MAGICA gel dosimeter

Component	Amount (g)
Gelatin	80
Agarose	5
Methacrylic acid	90
Ascorbic acid	0.352
CuSO4·5H2O	0.015
Hydroquinone	2
Ultra-pure Water (HPLC grade)	823

B. irradiation

Gels were irradiated with a clinical ^{60}Co system (Terathron II 780C, Canada). To create scattered radiation same as human body, the gels were put under 5 cm water in irradiation duration. The radiation field is $20\times 20cm^2$ and dose rate is $80^{cGy}\!\!\diagup_{\min}$. Dosimetry of Gamma source was done by ionization chamber (Farmer, Nuclear enterprise co., U.K.).

C. imaging and R2 map preparing

There are several method for dose response readout in gel dosimetry [4,5]. In this study the proton magnetic properties variation was exhibited by magnetic resonance imaging (MRI). Gels were imaged using a 0.5T MRI system (Philips). An MRI protocol that minimized the noise in 0.5T MR image was found which is given in table 2.

Container was centered in the head coil. Gel phantom were put in head coil had a higher signal to noise ratio in compare to body coil. To ensure that the obtained R2 values were not influenced by possible temperature gradients in the gel, phantoms were left in MRI room 24 h before scanning.

R2(=1/T2) maps were computed using modified radiotherapy gel dosimetry image processing software coded in MATLAB.

O. Dössel and W.C. Schlegel (Eds.): WC 2009, IFMBE Proceedings 25/III, pp. 439–442, 2009.
www.springerlink.com

Table2. Optimum imaging protocol used in a Philips 0.5T MRI systems

TE(ms)	20
TR(ms)	1500
ES(ms)	20
Echo No.	8
NEX	3
FOV(mm)	256×256
Slice thickness(mm)	3
No. slice	1

D. Dose error calculation and minimum detectable dose

In many point method the R2 map is obtained by fitting the MRI signals in different echoes in equation (1).

$$S = S_0 \exp(-R_2 TE) \qquad (1)$$

Where *S*0 is the signal corresponding with the unrelaxated magnetization

Gel dose response vs. absorbed dose is linear in the different ranges and follows the equation (2).

$$R_{2i} = R_{2,0} + \alpha D_i \qquad (2)$$

The standard deviation of the *R*2 values in an ROI is also determined. We call this value σ_{call}. if N_{ROI} is the number of pixels in ROI then the error of calibration points are assumed to have the same value (it has a little difference and we use the mean value of stds). The calibration dose error will be [6]

$$\sigma_{D^*} = \frac{\sigma_{call}}{\alpha\sqrt{N_{ROI}}}\sqrt{\frac{(D^* - \overline{D})^2}{\sum_{1}^{N_{ROI}}(D_i - \overline{D})^2} + \frac{1}{N_{call}}} \qquad (3)$$

The minimal detectable dose (MDD) is D_Δ^p as the dose approach to zero. D_Δ^p Can be written as

$$D_\Delta^p = k_p\sqrt{2}\sigma_D \qquad (4)$$

Where K_p is the coverage factor that is given in ISO 1995 [7].

E. result

As it can be seen in figure 1 and 2, imaging in water environment has increased the contrast noticeably. When small phantom is used this contrast enhancement for real boundary of R2 map determination is very important.

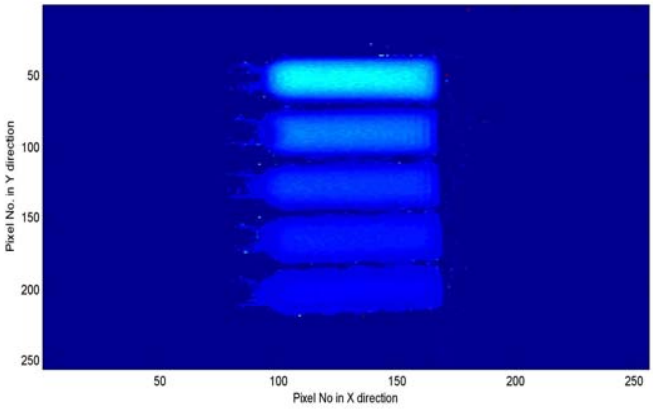

Figure1- R2 map from imaging in air

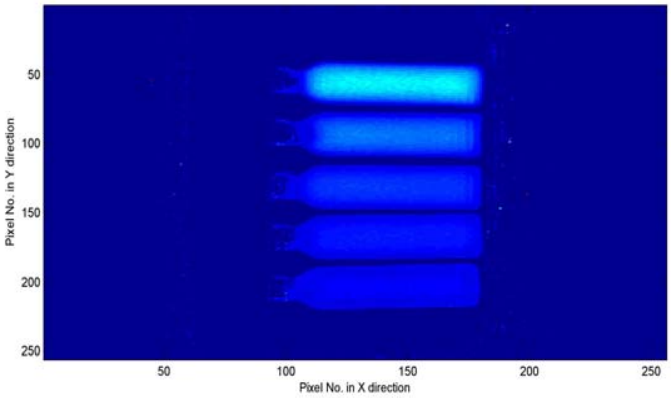

Figure2- R2 map from imaging in water; imaging in water environment has increased the contrast noticeably.

Figures 3 illustrate the change of R2[=1/T2] as a function of absorbed dose by imaging in air and water.

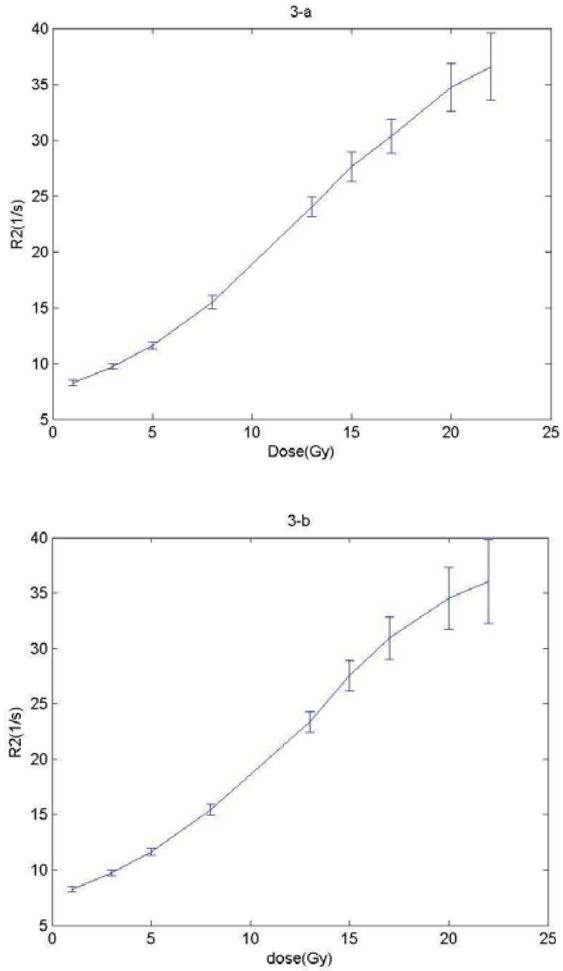

Figure3- The change of R2[=1/T2] as a function of absorbed dose for MAGICA gel dosimeter by imaging in air (a) and water(b)

Mean value of the slops of dose response curves in two method of imaging is given in table 4.

Figure 5 illustrates the values of calibration dose error in two images for different dose ranges.

Table4. the slope compression for two methods of imaging

Dose range	The slope for imaging in water	The slope for imaging in air
1-8Gy	1.039	1.032
8-17Gy	1.671	1.729
17-22Gy	**1.260**	**1.037**

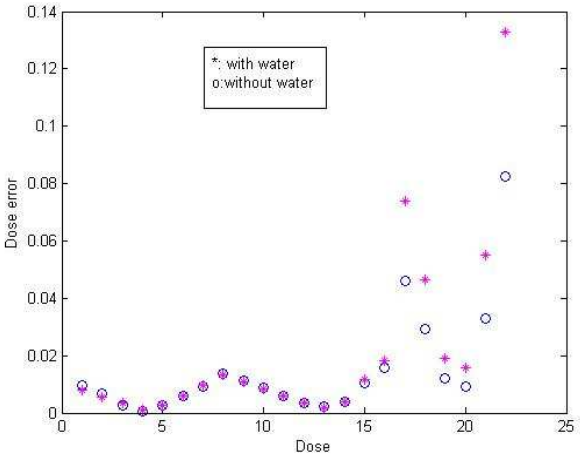

Fig.5- the compression of calibration error for tow imaging method

III. CONCLUSIONS

As it is shown in figure 1 and 2 by imaging in water environment R2 map contrast is enhanced noticeably. This contrast enhancement can referred to susceptibility artifact removing. Susceptibility artifact occurs as the result of microscopic gradients or variation in the magnetic field strength that occur near the interface of substance of different magnetic susceptibility. This gradient causes dephasing at the interface and signal loss [8]. Since magnetic property of gel is very similar to water this artifact is reduced and contrast enhanced noticeably when imaging is performed in water environment.

As it can be seen in figure 5 calibration dose error values are very similar up to 17 Gy but for range of 17-22 Gy imaging in water environment, increased error noticeably.

However object related geometrical distortions may be compensated by first measuring or simulating the local magnetic field distortions caused by susceptibility differences and chemical shift artifacts. These magnetic field maps can then be used to construct a correction template that can be used to correct the parametric images. Another method to correct for local magnetic field distortions is by view angle-tilting. This method has the advantage that no post-processing is needed but has the disadvantage that the point-spread function is broadened. Important to emphasize is that the artifacts act on a pixel-related scale instead of a geometrical scale. Increasing the resolution will decrease the artifact on a geometrical scale. Another important parameter is the receiver bandwidth. The distortions are inversely proportional to the receiver bandwidth. However increasing the bandwidth will decrease the signal-to-noise ratio [9]. All of these methods are complicated and time

consuming but using of water environment for MR imaging is simple and effective for phantom shape preservation.

In small sample of gel dosimeters, determination of dose boundary has a great importance imaging in water medium is recommended. As it can be seen in figure 5 imaging in water medium with high rang doses result in a high value of error which results in increase of minimal detectable dose difference within a given level of confidence, p (D_{Δ}^{p}) and this will causes reduction of dose spatial resolution. However reduction of spatial resolution in doses lower than 17 Gy is not considerable, therefore with imaging in water medium, a small reduction in spatial resolution is exchange to considerable increase of contrast inR2 map is important. In doses upper than17 Gy and importance of contrast and spatial resolution imaging in water is preferred.

ACKNOWLEDGMENT

Useful discussions with Mr. A Rahimi are highly appreciated. The authors also are thankful to Mrs. A. Madahian and Mr. H. Shahabian for their kind efforts in imaging process.

REFERENCES.

1. De Deene Y, Hurley C, Venning A, Vergote K, Mather M, Healy BJ, et al. (2002) A basic study of some normoxic polymer gel dosimeters. Physics in Medicine and Biology, **47**:3441-3463.
2. Fong PM, Keil DC, Does MD, Gore JC (2001) Polymer gels for magnetic resonance imaging of radiation dose distributions at normal room atmosphere. Physics in Medicine and Biology, **46**(12):3105-3113.
3. Zahmatkesh MH, Kousari R, Akhlaghpour S, Bagheri SA. MRI gel dosimetry with Methacrylic acid, Ascorbic acid, Hydroquinon and Copper in Agarose(MAGICA) gel. In: Preliminary Proceedings of DOSGEL 2004; 2004; Ghent, Belgium; 2004.
4. Ibbott GS (2004) Application of gel dosimetry. Journal of Physics, **Conference Series 3**:58-77.
5. Watanabe Y. 3D Dosimetry with polymer gel. In: MN- NCCAAPM Meeting; 2006 april 28; Minneapolis; 2006.
6. De Deene Y, Van de Walle R, Achten E, De Wagter C (1998) Mathematical analysis and experimental investigation of noise in quantitative magnetic resonance imaging applied in polymer gel dosimetry. Signal Processing, **70**:85-101.
7. Baldock C, Lepage M, Back SA, Murry PJ, Jayasekera PM, Porter D, et al. (2001) Dose resolution in radiotherapy gel dosimetry: effect of echo spacing in MRI pulse sequence. Physics in Medicine and Biology, **46**:449-460
8. WESTBROOK C, KAUT C. (1993) MRI in Practice. First ed., BLACKWELL, Londan.
9. De Deene Y (2004) Fundamentals of MRI measurements for gel dosimetry. Journal of Physics, **Conference Series 3**:87-114.

Author: Sayed Mohammad Mahdi Abtahi
Institute: Shahid Beheshti University
Street: Evin
City: Tehran
Country: Iran
Email: sm_abtahi@sbu.ac.ir

Overview of Dosimetry and Self-shielding Models in Ultraviolet Phototherapy

D.R. Grimes[1] and N.J. O'Hare[2]

[1] Dublin City University, Dublin, Ireland
[2] St. James's Hospital, Dublin, Ireland

Abstract— **Ultraviolet phototherapy is widely used in the treatment of skin disease and the benefits of such therapy are widely known. There are risks associated with such treatments, chiefly possible DNA damage leading to skin cancers, so it is imperative to reduce potential detrimental effects whilst keeping the treatment dose biologically effective. UV Dosimetry methods such as the ScUVido protocol are useful for providing a local calibration but there remains much ambiguity regarding dosimetry practices and the effects of patient self-shielding. In this work, we examine building a model of patient dose and in particular methods for predicting the self shielding factor of patients in a treatment cabin.**

Keywords— **Ultraviolet Phototherapy, dosimetry, modeling, self-shielding**

Introduction

Ultraviolet phototherapy and photochemotherapy have been used for decades in the treatment of skin diseases such as psoriasis and eczema as well as numerous other dermal conditions [1]. Treatment effectiveness is well documented and widely used in medical physics and dermatology worldwide, but problems with dosimetry remain. To quantify dose, phototherapy operators generally use the ScUVido method [2], where a UV-protected operator makes a series of 12 measurements at different body points with a personal dosimeter calibrated for the spectrum of the UV treatment in question. These points are the anterior, posterior and sides at shoulder height, hip height and knee height. The recorded dose is then averaged and this value is taken as cabin irradiance. Patient dosage is then the time integral of this irradiance.

Whilst this method is practical for local calibrations, it has several inherent weaknesses. Primarily that the operator build and size has a large effect on patient self-shielding and proximity to the emitting tubes in the cabin. Different operators making the calibration can have widely differing results [3]. Thus, it is not possible to achieve global or objective estimates for cabin irradiance using this method alone, which leads to uncertainty in patient dose.

This work is part of a series wherein an attempt is made to model the irradiance and self-shielding of various cabins geometries from first principles to improve current dosimetry methods and aid in patient treatment.

Simple cylindrical radiator model

UV phototherapy cabins consist of banks of fluorescent emitting tubes arranged in a particular geometry. A patient stands in the centre of the treatment cabin and in clinical practice may be asked to rotate 90 degrees during treatment. There is a wide range of phototherapy cabins available on the market with differing shapes and tube layout. The Waldmann UV1000 for example, consists of 26 tubes in a roughly hexagonal arrangement while the Waldmann UV7001 is a square cabin consisting of 40 tubes. These tubes are typically Phillips TL-01 models for UVB therapy.

Passing reference has been made to tubes as line sources [4] rather than point sources, and in this work we shall start with the assumption that the UV tubes can be treated as idealised cylindrical radiators. In such a simplified model, the irradiance is inversely proportional to the radial displacement from the tube, and essentially irradiance becomes a function of position.

$$I = P/2\pi r h \tag{1}$$

where P is the optical power emitted in the UV and h is the tube length. For multiple tubes, the principle of superposition can be applied and equation 1 adapted for multiple tubes

$$I_{total} = \frac{1}{2\pi h}\sum \frac{P_1}{r_1} + \frac{P_2}{r_2} .... + \frac{P_n}{r_n} \tag{2}$$

where the tube height is assumed to be the same, though this can also be easily modified. Figure 1 shows the effects on irradiance of modeling 40 emitting tubes of equal length (1.75 m) and output power (100 W) evenly spaced over an empty 1 metre squared area cabin.

O. Dössel and W.C. Schlegel (Eds.): WC 2009, IFMBE Proceedings 25/III, pp. 443–446, 2009.
www.springerlink.com

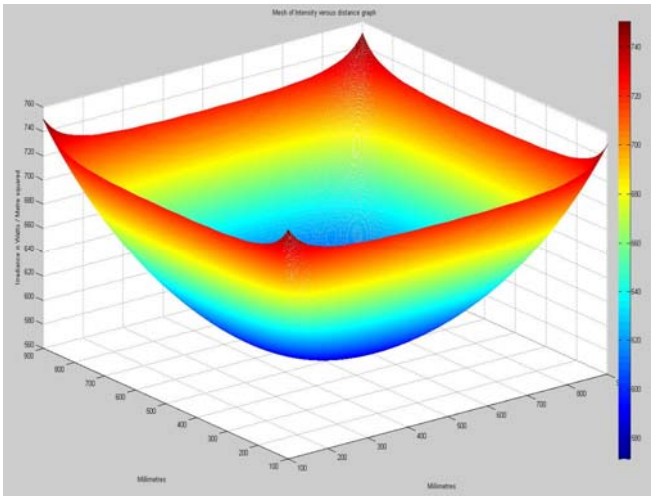

Fig. 1 Irradiance due to 40 free-standing cyclindrical radiating tubes

PATIENT SELF-SHIELDING

Patient self-shielding has a great effect on irradiance and hence dose received by the patient [5]. This occurs when part of a patient that is opaque to UV radiation effectively stops the transmission, so only certain points are irradiated by certain tubes. There is of course great variation in human build, which leads to equally great variation in the self-shielding factor. Table 1 shows the average measurement of a typical human being. Data in this table is from the DIN-Belg [6] survey on Belgian population dimensions except the data marked with an asterisk which was obtained by measuring the averaging patients.

Table 1 Typical patient attributes

Attribute	Typical value
Head Length	188mm
Head Breath	145mm
Shoulder Breath	438mm
Hip Breath	387mm
Abdominal depth	237mm
Knee Radius *	57.3mm
Knee Spacing *	110mm

This data indicates that 'slices' of a patient along some vertical extent can be approximated to one of two conic sections, namely a circle or ellipse. The head, for example, could be modeled by an ellipse with a semi-major axis of length 94mm and a semi-minor axis of 72.5, giving an eccentricity of 0.6365 whereas the knees could be modeled by two circles separated by a gap.

Modeling a circular obstruction is relatively straight forward and computationally not overly intensive. Figure 2 shows an example of the effects from a circular obstruction on the total irradiance due to 20 100 W 1.75m cyclindrical radiator tubes over a 1 metre squared area.

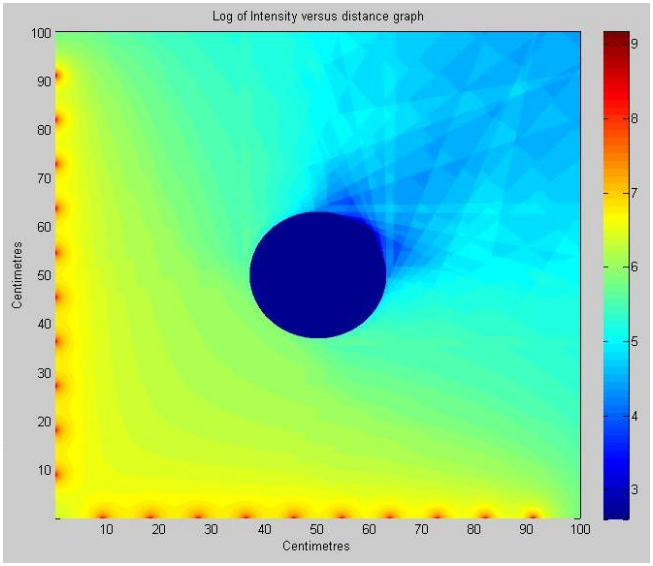

Fig. 2 Circular obstruction illuminated by 20 tubes

Elliptical modeling is many times more difficult to model and an order of magnitude more computationally intensive, due in part of the far more convoluted methods required. Elliptical models though are possible. Figure 3. shows an example of a single tube illuminating an ellipse with a semi-major axis of 20 cm and a semi-minor axis of 5 cm, giving an eccentricity of 0.9682.

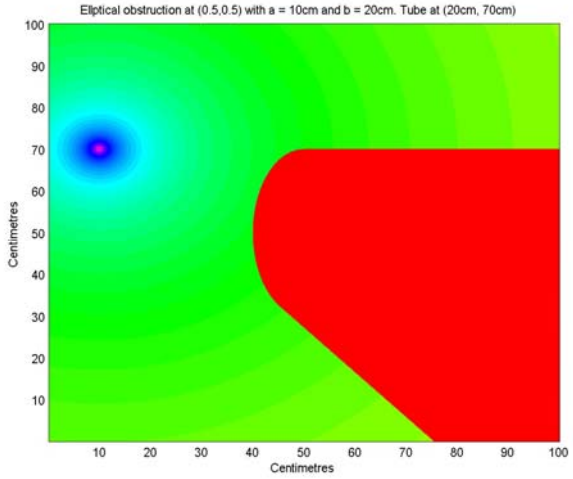

Fig. 3 Elliptical obstruction illuminated by tube

The mathematics of modeling both circular and elliptical obstructions have been left out for the sake of brevity, but will be available in other publications by these authors. For the purposes of this work, it is sufficient to see how these self-shielding models work in practice by taking simulation results.

Model Simulation for Realistic Cabin

For the purposes of model testing, we selected a commonly used full body phototherapy cabin. The Waldmann UV1000 is of a roughly hexagonal shape consisting of 26 tubes in total. The cabin splits into two halves, both of which are symmetrical and consist of 13 tubes per side. The engineering data for the cabin from Waldmann [7] is shown in figure 4.

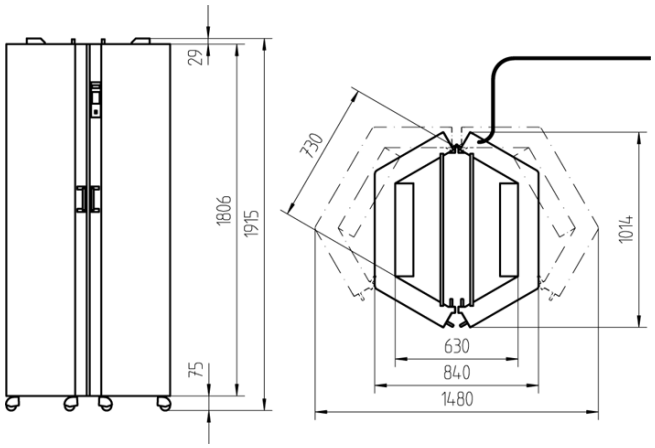

Fig. 4 UV1000 technical engineering diagram

The tube positions inside the cabin were calculated and entered into the model. Simulations were then run on the effects of irradiance in this particular cabin at head height, shoulder height, hip height and knee height, the latter three corresponding to typical areas for ScUVido measurement. The results of all four simulations are shown together in figure 5 for an average patient with typical dimensions.

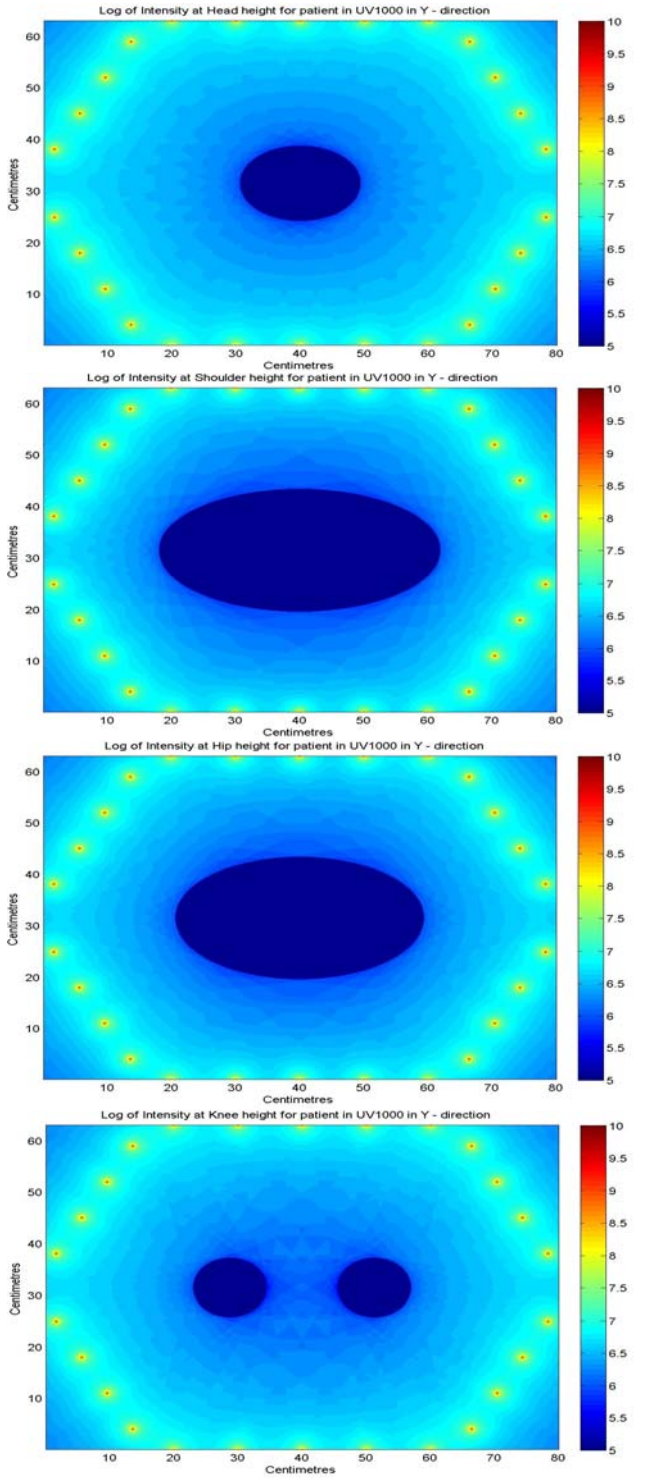

Fig. 5 UV1000 patient self-shielding model log plots at head, shoulder, hip and knee height respectively.

Comment and Conclusion

The model shows great promise is calculating the effects of patient self-shielding and improving dose, as a better understanding of patient effects can lead to a more effective treatment. The model also has the advantage of being easily adapted to specific patient builds which differ greatly from the normal, such a pediatric or obese patients. It is important to note that currently the model does not allow for reflectors, assuming instead that contributions from all reflectors will be equal and a simple scaling factor can be applied. This is currently being investigated to clarify the issue.

While the conic section model for patient shielding is very promising, questions remain about the validity of approximating the tubes to cyclindrical radiators and even line sources; certainly, it is a reasonable assumption at certain regimes and distances, but whether it is truly applicable at the distances of therapy remain to be seen. Current research by the authors is directed towards characterizing individual UV tubes as a means to better understanding emission behavior and then factoring elements like non-uniform emission and tube irregularities into future models, and subsequent work will concentrate on these aspects. Other work includes the detailed investigation of tube behavior under a full line source approximation, and a contrast of this to the data acquired in experimental measurement.

Acknowledgment

Many thanks to Una O'Connor at St. James's hospital for the irradiance data, David Taylor (Gloucestershire Royal Hospital) for his kind donation of a UV-1000 cabin, and to Tony Cafolla and Caroline Banahan at DCU for their MATLAB expertise and input. This worked was funded by IRCSET through the EMBARK initiative.

References

1. Green C, Diffey B L, and Hawk J L M (1992) Ultraviolet Radiation in the treatment of Skin disease. Phys. Med. Biol. 37: 1-20
2. Moseley H (2001) Scottish UV Dosimetry guidelines "ScUVido" Photodermatol Photoimmunol Photomed . 17: 230-233
3. Lalor N. (2008) Dosimetry In Paediatric Ultraviolet Phototherapy,; Masters thesis, TCD. Accepted in Nov 2008
4. Pye S D and Martin C J (2000) A study of the directional response of Ultraviolet radiometers: I. Practical evaluation and implications for ultraviolet measurement standards. Phys. Med. Biol. 44: 2701 – 2712
5. Langmack K A (1998) An insight into the contributions of self-shielding and lamp reflectors to patient exposure in phototherapy units Phy. Med. Biol. 43: 207 - 214
6. DINBelg at http://www.dinbelg.be/anthropometry.htm
7. Waldmann at http://www.waldmann.com

Low cost alternative to lead glass shielding in PET/CT control/scanner room window

J.A.M. Santos[1,2], A.L. Bastos[3], J. Lencart[1,2], A.G. Dias[1,2] and M.F. Carrasco[1,2]

[1] Centro de Investigação do Instituto Português de Oncologia Francisco Gentil, EPE, Porto, Portugal
[2] Serviço de Física Médica do Instituto Português de Oncologia Francisco Gentil, EPE, Porto, Portugal
[3] Serviço de Medicina Nuclear do Instituto Português de Oncologia Francisco Gentil, EPE, Porto, Portugal

Abstract— **The aim of this work is to propose a reasonably priced alternative to expensive lead glass used in PET/CT windows connecting the control room and the scanner room. These windows can be extremely useful to detect if the patient needs quickly to be assisted, for anesthesia surveillance when needed, among several other purposes and is mandatory to exist in these facilities. The window must provide also radiation protection to the worker inside the control room. One way to accomplish this task is to use lead glass. However, lead glass is expensive and is usually manufactured as predetermined lead equivalent thicknesses (frequently 2 mm or more). It is also designed to be lead equivalent with nominal thicknesses specified for radiology energy ranges. Depending on the distances involved and on the workload, since the photon energy irradiating from PET patients is significantly higher (511 keV) than other nuclear medicine and radiology procedures, it is usually necessary to protect the professionally exposed worker with a high thickness of lead or lead equivalent glass. For a big area window, a lead glass plate can be quite expensive. In this work it is presented a less expensive solution using common glass with thickness higher than 15 cm. Calculations are presented for typical situations and workloads, assuring protection both from PET and CT.**

Keywords— **PET/CT, nuclear medicine, radiation shielding, radiation protection**

I. Introduction

When designing a positron emission tomography/computer tomography (PET/CT) scanner room, besides close circuit television cameras (CCTV) assessment and acoustic communication between the technologist and the patient, it is necessary to assure the existence of a direct visual assessment glass window, as in conventional CT facilities, from where all the space inside the scanner room can be immediately observed.

Typically, the distance between the patient body and the control room (workplace) can be no less than 2 m due to the space for the scanner. Usually, it ranges from a minimum distance of 2.5 m, to a maximum of 4 or more meters. The effective dose equivalent rate constant for F-18 is 0.143 μSv m^2 MBq^{-1} h^{-1} [1] and the patient is considered to be the source. For simplicity, the patient is approximated by a point source and the activity during the exam is considered exactly the administered activity, which is a very conservative approach.

If one expresses the glass transmission as function of glass thickness between the source and the detector, t^{glass}, and as function of energy E, by T^{glass}, one can write:

$$T^{glass}(t^{glass}) = e^{-\left(\frac{\mu(E)}{\rho}\right)^{glass} \rho^{glass} t} \quad (1)$$

For lead one uses the same expression:

$$T^{Pb}(t^{Pb}) = e^{-\left(\frac{\mu(E)}{\rho}\right)^{Pb} \rho^{Pb} t} \quad (2)$$

The values of the mass attenuation coefficients $\mu(E)/\rho$ both for glass (borosilicate - "pyrex") and lead were taken from the literature [2].

These expressions can be written also as function of the half value layer (HVL), which is also a function of energy, for these two materials:

$$T^{glass/Pb}(t^{glass/Pb}) = e^{-\ln 2\left(\frac{t^{glass/Pb}}{HVL(E)^{glass/Pb}}\right)} \quad (3)$$

Thus, if a specific shielding thickness of lead (t^{Pb}) is required for a given energy E, the following expression can be used for the calculation of its equivalent in glass:

$$t^{glass} = t^{Pb} \frac{HVL^{glass}(E)}{HVL^{Pb}(E)} \quad (4)$$

As an example, in Figure 1 one can see the glass thickness equivalent to 8 mm of lead, as function of energy, directly calculated from the values obtained in [NIST1, NIST2]. As can be observed from the figure, there is no thickness of glass equivalent to a given thickness of lead for all energies. This is highly dependent on the energy under

O. Dössel and W.C. Schlegel (Eds.): WC 2009, IFMBE Proceedings 25/III, pp. 447–450, 2009.
www.springerlink.com

consideration and is particularly critical below 300-400 keV.

The problem thus is to obtain a glass thickness capable of assuring the necessary shielding both for the 511 keV required by PET and for the CT continuous spectra typically peaked around 50-70 keV.

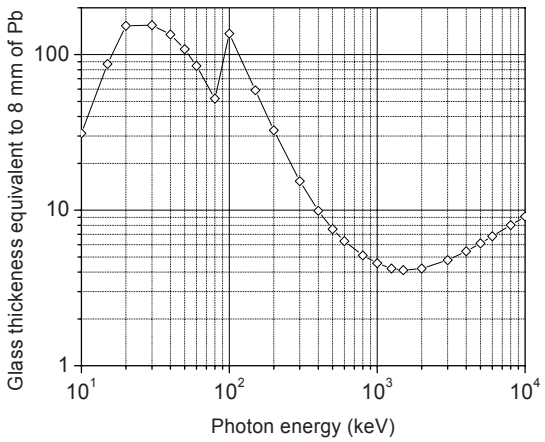

Fig. 1 Glass thickness equivalent to 8 mm of lead, where it is shown that the equivalence of the two materials depends strongly on the incident photon energy and that this is more pronounced for energies below and above 300-400 keV.

II. Shielding calculations for PET and CT

A. Shielding design for PET

The example presented here is an estimation and depends on the number of patients scanned per week. A conservative 8 hour working day (16 patients per day) will be assumed, with all the scans made by the same technologist and an occupancy factor of 1. If a limit of 0.4 mSv/week for the working place is permitted [3], and a maximum activity of 370 MBq/patient (740MBq/hour) is assumed during scan (very conservative assumption; does not take into account physical decay and F-18 elimination before the exam) and the dose equivalent rate constant of 18-F to be 0.143 $\mu Sv\ m^2\ MBq^{-1}\ h^{-1}$, the equivalent dose rate at the place to be protected at 2.5 m from the patient will be 0.646 mSv/week. The transmission of the shielding window to protect this place during acquisition (approximately 20 min for each PET acquisition) is thus 0.62. However, a dose constraint of 10% can be imposed for this particular source, since this is not the only source of exposure for a technologist in nuclear medicine (handling the patient between acquisitions, laboratory work, and scattered radiation from the patient body during the CT acquisition, etc.). In this case, a transmission coefficient of 0.062 (6 %) would be reasonably acceptable. Based on the HVL values for 500 keV of reference [2], the thickness of glass necessary would be 14.4 cm

B. Shielding design for CT

The shielding for the CT scanner scatter radiation is not as critical as the 511 keV shielding for the PET scanner where the patients constitute the radiation source. Additionally, it depends largely on the workload (number of patients, quality of CT image acquisition, etc).

The example presented here is for a typical and conservative use of the CT [4] and can be modified as local PET/CT workload and schedule can change from place to place. In this particular case, to control a given point 2.5 m away from the CT isocenter, in a system under heavy use (140kVp; 20,000 mA-min/wk), assuming an occupancy factor of 1, the lead thickness necessary to shield the area, where the controlled point is situated, is 0.118 cm.

C. Commercial glass transmission measurement (511 keV)

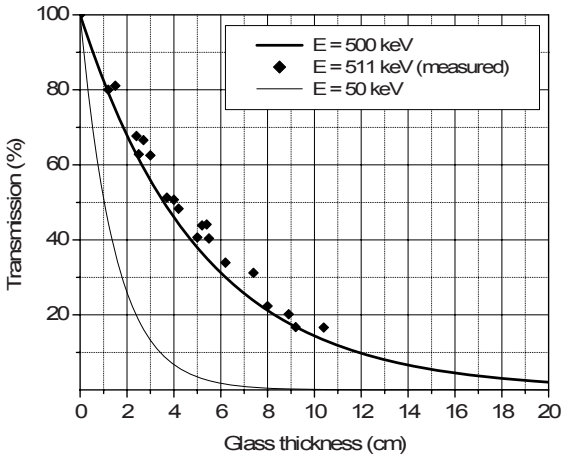

Fig. 2 .Transmission of borosilicate glass both for 50 and 500 keV (lines) compared with measured transmission data obtained from commercial soda-lime glass (dots).

For comparison of the HVL values obtained from the published mass attenuation coefficients for several energies [2], the attenuation from a common commercial soda-lime glass (ρ = 2.4 g/cm^3) was determined by measuring the equivalent dose rate obtained from the exposure at a source of 18-F with several glass thicknesses between the source and the detector. The results can be seen in Figure 2, compared with the transmission obtained from the above men-

tioned mass attenuation coefficients (500 keV; ρ = 2.23 g/cm^3) of borosilicate ("pyrex") glass.

From the experimental data, a value of HVL = 4.0 cm was found for the commercial soda-lime glass for 511 keV, while for the borosilicate was calculated a HVL = 3.5 cm (a difference of 12.5% in the HVL was observed between them).

D. Commercial glass composition determination

Since the results from reference [2] are obtained from borosilicate ("pyrex") glass, and in order to compare the compositions of both glasses, the commercially soda-lime glass used was characterized with a scanning electronic microscopy (SEM) provided with energy dispersive X-Rays (EDX) spectroscopy. The obtained stoiquiometry of the glass constituents is: SiO_2 - 61%, Na_2O - 21%, CaO - 10%, MgO - 5.5%, Al_2O_3 - 1.5%, K_2O - 1% as can be seen in Table 1.

Table 1 Composition of the commercially obtained glass as well as typical values for common soda-lime glass

Composite	Composition %	Usual ranges %
CaO	10	5-12
SiO_2	61	60-75
Na_2O	21	12-18
MgO	5.5	-
Al_2O_3	1.5	-
K_2O	1	-

The composition of the analyzed glass was found to be very similar to other soda-lime glasses. The composition analysis confirms the soda-lime characteristics of the glass, with typical compositions of SiO_2 and CaO, with just a slightly increased value of Na_2O.

III. Discussion and conclusions

From section II.B it was found that an approximated thickness of lead of 0.118 cm (or its equivalent in glass for the CT energy range) is necessary to obtain enough protection for the control room from the CT only. From the HVL values of lead and glass for CT energies calculated from [2], it is obtained a value of 16 cm of borosilicate glass to provide a similar degree of protection.

This value is higher than the value obtained in section II.A necessary to protect the control room for the PET energy (14.4 cm) with a dose constraint of 10%, which is approximately 11% less that the 16 cm necessary for the CT protection.

Fig. 3 . Photograph of a 16 cm soda-lime glass window from inside a PET/CT scanner room, where one notices that light and luminosity are not seriously compromised.

From the above, it is shown that a glass thickness window of 16 cm between the control room and the scanner room in a PET/CT facility can provide enough protection both for PET and CT energy ranges (both calculations were assumed under very conservative assumptions).

One should notice that all the calculations were done based on very conservative assumptions. Usually, in standard PET/CT facilities, the distance is larger than 2.5 m and there are several working shifts along the week and even along the day. The CT workload is also very small, since only one CT is made for each PET scan (approximately 2 per hour).

The light transmission can also present another problem when considering glass thicknesses such as 16 cm. It can however be optimized using laminated glass constituted by several glass plates of maximum thickness commercially available (typically 2.5 cm), and using a transparent interlayer, typically of polyvinyl butyral (PVB) to consolidate the assemblage and to optimize light transmission by optical impedance adaptation. An example can be seen in Figure 3.

The proposed shielding method is a cost-effective solution and can straightforwardly be implemented in any PET/CT control room, maintaining the individual doses of the workers within the permissible limits for category A staff such as nuclear medicine professional exposed workers even when assuring restrictive dose constraints [3]

References

1. Madsen, Mark T., Anderson Jon A., et al. (2006) AAPM Task Group 108: PET and PET/CT Shielding Requirements. Med. Phys. 33:4-15

2. Hubbell, J.H., Seltzer S.M. (1996) Tables of X-Ray Mass Attenuation Coefficients and Mass Energy-Absorption Coefficients from 1 keV to 20 MeV for Elements Z = 1 to 92 and 48. Additional Substances of Dosimetric Interest, accessed on-line 1st February, 2009
3. ICRP Publication 103, Annals of the ICRP, 2007
4. Pei-Jan, Paul Lin,, et al. (1993) AAPM report 39: Specification and acceptance testing of computed tomography scanners. American Association of Physicists in Medicine, 1993, ISBN 1-56396-230-6

Author: Joao A Miranda dos Santos
Institute: Instituto Português de Oncologia do Porto Francisco Gentil, E.P.E.
Street: Rua Bernardino de Almeida
City: Porto
Country: Portugal
Email: a.miranda@portugalmail.pt

Magnetic-Resonance-Imaging Based Polymer Gel Dosimetry: Methodology, Spatial Resolution, Applications

A. Berg[1]

[1] Medical University of Vienna, Center for Biomedical Engineering and Physics & MR-Center of Excellence, Vienna, Austria

Abstract — **Modern radiation techniques aim on improved 3-dimensional (3D) spatial selectivity of the dose application sparing dose from organs-at-risk (e.g. IMRT with micro-multi-leaf collimation, γ-knife-, Brachy- and heavy-ion therapy). The corresponding 3D-dose distributions exhibit high dose gradients above 4 Gy/mm, which are difficult to be investigated using standard single-point dosimetric detectors as ionization chambers, which cover a minimum size of few mm.**

Parameter selective Magnetic Resonance (MR) based dosimetry (*MRPD*) represents a 3D detection method, capable of high spatial resolution. Moreover tissue equivalence of the detector material (a polymer-gel) is offered. This review is focused on polymer-gels using the polymerization of monomers during ionizing radiation. The change in the mobility of the detected molecules is detected via parameter-selective (T2) MR-imaging.

A manufacturing recipe for the actually used "normoxic" polymer gels, which allow simple processing at normal oxygen pressure in atmosphere, is listed. Data on sensitivity, precision, accuracy, spatial resolution and sensitivity to different radiation quality (i.e. energy, particle type) is presented.

Dosimetric images for two highly-spatially selective radiation applications (i.e. a 2 mm electron-beam and a mixed 11 mm γ-knife collimation) from our lab demonstrate the capabilities of high-resolution *MRPD* at voxel size of 0,2 x 0,2 x 1 mm^3. Finally limitations of *MRPD* for actual clinical applications are discussed.

Keywords— **Dosimetry, MRI, Polymer, Gel, Review**

I. Introduction

The new developments in radiation therapy for cancer treatment are mainly related to the improvement in conformity and smaller margins. The high dose gradients available, e.g. 4 Gy/mm for a γ-knife radiotherapy unit [1] demand for 3-dimensional dosimetric methods at high spatial resolution in order to avoid partial volume detection. However, most dosimetric methods - e.g ionization chambers, TLD arrangements or silicon detectors - are not capable of detecting sub-mm dose variations due to their size or do not allow for simple 3D-dose imaging. 3D-arrangements of ionization chambers [2] ("Magic Cube" weighing about 40 kg) for Hadron therapy are limited in the number of lateral measurement points (32 x 32) and achieve smallest voxel volumes of about 4x4x5 mm^3.

High resolution silver halide film dosimetry is limited mainly due to difficulties in reproducibility as a consequence of changing conditions in the chemical development process and varying response of the optical density (OD) with photon energy and inhomogeneities in the dose response. Radiochromic films perform better. 3D-dosimetric images might be obtained from sets of several distant films, however each film is to be scanned separately; the 3D-interslice data has to be interpolated. In addition errors in lateral positioning during scanning may enter the evaluation process.

The development of non-invasive 3D-imaging methods based on MR in radio-diagnostics stimulated ideas for 3D-reading out of dosimetric changes in chemical dosimeters [3]. Fricke already showed in 1927 [4] that the change in the ion charge status of ferric ions during irradiation might be used for quantitative dosimetry. The longitudinal relaxation rate T1 in MR is sensitive to the corresponding changes in magnetic moment and magnetic susceptibility. However the spatial resolution is restricted by the diffusion path of the ferric ions after radiation.

There had already been several reports on the sensitivity of MR-parameters to the radiation dose applied to polymers. when the development and research in MRPD was strongly pushed in 1993 by Gore and Maryanski [5], who showed that MRI-T2 mapping may be used for high resolution dosimetric imaging. The polymerization process, induced by radiation in a mixture of momomer agarose-or gelatin and water, changed the mobility of the MR-detected molecules, which results in a linear increase of the transverse relaxation rate 1/T2 in MRI. The investigated polymer gel is based on acryl amide, a crosslinker (NN' Bis-acryl amide), water and agarose-gel. Oxygen had to be removed by bubbling Nitrogen through the polymer gel in order to avoid the suppression of the polymerization process by the very reactive oxygen molecules. Subsequently several modifications for improving sensitivity, linearity dose range and stability had been proposed [6]. Besides from T2 in MRI also other physical properties appeared to be sensitive to the polymerization process, i.e. the electron density via CT [7], high frequency stiffness as visualized by ultrasound [8], optical absorption with regard to the change of monomer double bound density during polymerization [9]. The change of color in polymers combined with colored leuco–dyes during

O. Dössel and W.C. Schlegel (Eds.): WC 2009, IFMBE Proceedings 25/III, pp. 451–454, 2009.
www.springerlink.com

irradiation represents the basis for a new class of dosimeters (Presage^{TM})[10]. Finally optical scattering coefficients, are changing significantly as the lateral distance in the polymer network structure approaches the optical wavelength: the polymer gel is becoming turbid during polymerization. Optical scanning allows for highly resolved dosimetric imaging after calibration [11]. Optical scanners are commercially available now at significant lower prices than MR-scanners but do not reach the 3D-spatial resolution or accuracy available in custom designed MR-apparatus, the focus of this short review.

A main disadvantage of polymer gel dosimetry is represented by the necessity to remove oxygen completely from the polymer gel. This main drawback has been overcome by using oxygen scavengers, at first announced by Fong et al [12]. A small amount of ascorbic acid along with a Copper-sulfate complex has proven to effectively avoid oxygen suppression of polymerization in a polymer gel called "MAGIC"(**M**ethacrylic **A**cid **G**el **I**nitiated by **C**opper). Thus the preparation and manufacturing of polymer gels became possible at normal oxygen (atmosphere) conditions ("normoxic" polymer gels). They can easily be produced in a simply equipped laboratory.

Several other oxygen scavengers have been proposed, the most effective one being the toxic **T**etrakis-**H**ydroxy-**M**ethyl-**P**hosphonium **C**hloride (THPC) [13]. A good overview of actual methodological work in polymer gel dosimetry, its advantages and limitations are presented at DOSGEL 2008 [IOP Conference Proceedings 2009]. In the following some relevant characteristics of polymer gels are outlined based mainly on the experience in our own laboratory.

II. Characteristics of Polymer Gel Dosimetry

A. Detection mechanism

During radiation radicals are produced which represent the initiating factor for a polymerization process in the monomer gel. The chemically reactive radical group interacts with a monomer carrying a double bound, as a result of which the monomer again will present an open binding in form of a radical. This monomer radical will interact with another monomer resulting in a Dimer, again carrying an open binding, which is capable of catching the next monomer. This step represents the first in a series resulting in a multi- or polymer. The process will stop, when a radical carrying multimer meets another radical carrying molecule. Polymer aggregates are built up, networks if an additional cross-linker is present. The immobilization of the monomers and the surrounding water molecules results in a reduction of the transverse relaxation time T2[5,6,13] in MRI due to less averaging of the dipolar magnetic interactions of the 1H-nuclear magnetic moments (BPP-theory). A linear increase of 1/T2 (fig. 1) is observed within a limited dose interval proposing the simple use of such polymer gels for relative dosimetry. Dependent on the specific polymer gel composition, an offset at low dose levels might be observed due to the underlying limitation of the relaxation rate of mobile protons interacting with the stiff gelatin matrix or polymers. At high dose levels usually a saturation domain with increasingly less sensitivity is observed. This domain is dominated by the consumption of monomers or the stop of polymerization due to recombining of two radical carrying partners at high radical concentrations.

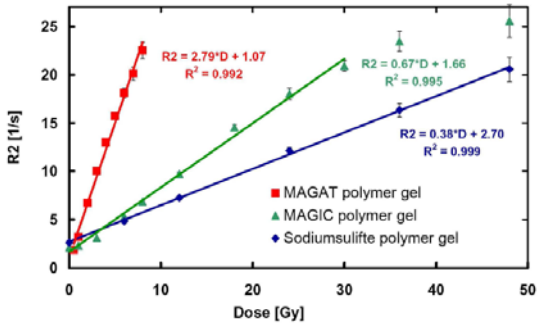

B. Type of polymer gels and dose response (sensitivity)

Fig. 1 Dose range and sensitivity ΔR2/ΔD for Methacrylic acid based polymer gels [15]. The sensitivity strongly depends on the oxygen scavenger.

Multifold recipes for polymer gels have been developed covering a wide range of different sensitivities and linear dose response regions [5,6,14]. The linearity domain might be increased by one order of magnitude, simply changing the oxygen scavenging composition from the very efficient THPC to ascorbic acid with copper-sulfate (fig. 1).

B. Composition and Manufacturing

As an example for manufacturing we present in the following the composition of MAGIC and MAGAT-type polymer gels (table 1). The manufacturing process is described in detail in ref. [16]. We prefer a comparably high concentration of gelatin for temperature stability and reduced diffusivity in order to improve spatial resolution. Please note the necessity of an oxygen dense container material, i.e. for instance BAREX (BP Amoco, UK) or glass, as the capacity of oxygen scavenging might be quickly overwhelmed by newly inflowing oxygen from outside.

Table 1: Composition of MAGIC and MAGAT type polymer gels as used in our laboratory

Composition for 1000 g polymer gel	*MAGAT-Gel*	MAGIC-Gel
deionised water	87% (w/w)	80%(w/w)
gelatin	8% (w/w)	14% (w/w)
methacrylic acid	5% (w/w)	6% (w/w)
copper(II)sulfate-penta-hydrate		0.025 g
ascorbic acid		0.3522g (2mM)
THPC	0.332g (2 mM)	

B. Precision and Accuracy

As an example we present data on MAGAT type polymer gels in the low dose (2Gy) medium (4Gy) and high dose domain (6Gy). MAGIC type performs better (4%) for accuracy in the middle dose range due to improved linearity [15,16]. Precision is defined here as the coefficient of variation in T2-values for the 6 gels irradiated. The calibration curve is obtained after irradiating 10 vials of polymer gel with dose.

Accuracy is termed as the difference between the absorbed dose measured in a gel using a calibration curve, compared to the „true“ dose, as measured by a calibrated ionization chamber (percentage of the true dose)[17].

Table 2 Precision, accuracy, dose uncertainty and dose error (confidence interval 95%) for a MAGAT type polymer gel[15,16].

standard resolution	linear fit			bi-exponential fitting function		
protocol	*2 Gy*	*4 Gy*	*6 Gy*	*2 Gy*	*4 Gy*	*6 Gy*
precision	1.3%	1.5%	1.2%	1.3%	1.5%	1.2%
accuracy	1.3%	9.0%	4.2%	1.5%	4.1%	2.8%
$u_c(D)/D$	1.5 %	1.4%	1.7%	1.5 %	1.4%	1.8%
D_Δ^p/D	4.2%	3.9%	4.7%	4.2%	3.9%	5.0%

D. Spatial Resolution

Oldham et al. defined criteria for modern dosimetric tools involving spatial **r**esolution, **t**ime of measurement, **a**ccuracy and **p**recision (RTAP-criterion) [18]. According to the RTAP-criterion a spatial resolution of about 1 mm should be strived for. Resolution and measurement time in MRPD with difference to Fricke dosimetry are mainly determined by the sensitivity of the detector and - for micro-imaging based MRPD($\Delta x \leq 1000$ µm) - also by gradient strength[19] and the diffusivity of monomers[20]. Whilst a spatial resolution of about 1 mm is sufficient in most cases in clinical radio-therapy and a voxel of that size can be achieved with clinical MR-scanners in several minutes now, the requirements on the spatial resolution increase for e.g. stereotactic irradiation, IMRT with micro-multi-leaf collimation, γ-knife- Brachy- [21] and heavy ion therapy [22], where easily dose gradients above 4Gy/mm are obtained. Systematic investigations on inherent spatial resolution might be based on the point spread function of the imaging system or the dose modulation transfer (DMTF) concept [23]. This contribution restricts to the newest data based on the DMTF concept from our laboratory [24](Fig.2).

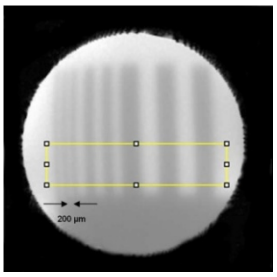

Fig 2a *Dose image below an absorption grid. Also the finest dose fingers at a/2 = 200 µm (a: spatial period) can be differentiated (voxel size: (ΔV = 0,047 x 0,094 x 1 mm³).*

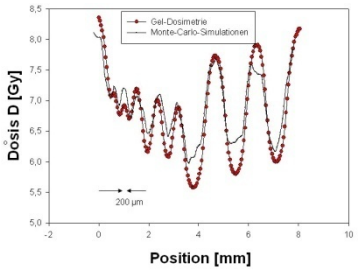

Fig. 2b *Dose-modulations across the absorption structures: red: gel dosimetry; black: Monte-Carlo-simulations. The relative reduction in dose modulation between MCS and MRPD at very fine periods (a/2 =200 µm) is indicating the limit in spatial resolution.*

E. Applications

As an example of the high spatial resolution possible with MRPD we present [25] results for the dose image for a 2 mm electron beam (Fig. 3) and a comparison [19] of lateral dose profiles on a mixed 8 and 14 mm γ-knife collimation (Fig. 4). Polymer gels have proven to offer unique 3D-visualization chances for dosimetry.

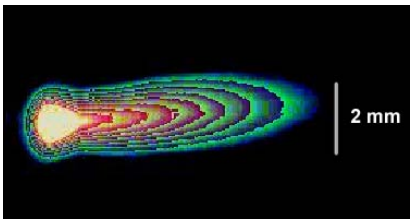

Fig. 3 Coronal projection of the dose distribution of a 2 mm electron beam in polymer gel. (Voxel size: 199x199x1000 µm³, MTX: 128x128x40). Note that the diameter of small ionization chambers as gold standard for dosimetry is about 5 mm.

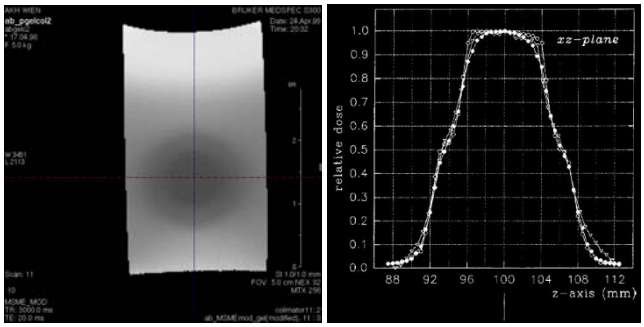

Fig. 4 a Left: T2 MR micro-image of BANG-type polymer gel after irradiation with γ-knife using two different collimators: 8 and 14 mm. **Fig. 4b Right:** Dose profiles. Open circles denote diode measurements, triangle polymer gel, closed circles indicate treatment planning system (Gammaplan 5.2)[19].

III. Discussion with regard to clinical application

Polymer gel dosimetry has proven to offer unique 3D-visualization for dosimetry. The gel dosimeter combines tissue equivalence, an integrative dose measurement concept and high spatial resolution, close to that of film dosimetry, dependent on the MR-equipment available. Sensitivity and dose range can be adjusted to the dosimetric demands in a wide range. The measurement time for 3D-clinical routine IMRT (resolution of 1 mm at slice thickness of 3 mm. Mtx: 256 x 128 x 20) with relative dosimetry is tolerable (about 30 min using Turbo-spin-echo-sequences). However its application is mainly focused on research investigations. Routine clinical dosimetry using polymer gels is rather rare. As a consumable it cannot be refreshed or read out and used again like an ionization chamber. Its practical use is therefore comparable to that of films. The manyfold variability of variations has not yet led to a standardized, commercial product, which can be easily applied and evaluated at low cost. The lack of standardization and cheaply available polymer gels also requires experienced applicants involving polymer gel manufacturing know-how and some MRI experience. The access to MR-scanners in radio-therapeutics is usually limited and therefore cooperation between different clinical departments is necessary. Cheaper available optical scanners might improve this limitation. In near future the application of polymer gel dosimetry will therefore - according to the authors view – be limited to research investigations and demanding high resolution complex 3D-dose distributions as first proof of principles in the introduction of new therapeutic applicant schemes. It is no method for daily routine QC. In research the combination of 3D-visualization possibilities, adjustable dose domains, tissue equivalence and spatial resolution mainly limited by the MR-scanner signal-to-noise-ratio, are unique. Principle methodological limitations in the application are mainly represented by the sensitivity of polymer gels to the linear energy transfer (LET) of ionizing radiation (similar to other dosimetric techniques e.g. film dosimetry). As a consequence, the fine Bragg-peak in single proton particle depth dose distribution is suppressed in MRPD even at very high spatial resolution[26], which might limit its application to Hadron dosimetry. Some polymer gels are also sensitive to the dose rate as available on clinical linear accelerators especially in the high dose domain [16]. However these limitations might be overcome in future by research and discovery of new recipe amendments or concepts in polymer gel dosimetry.

References

1. Tseng,-Y-J; Chu,-W-C; Chung et al (2002) Magn. Res. Imag. 20(6): 495-502
2. Cirio R, Garelli E et al. (2004) Phys. Med. Biol. 49: 3713-3724.
3. Gore J C, Kang Y S and Schulz R J (1984) Phys. Med. Biol. 29: 1189–97
4. Fricke H and Morse S (1927) Am. J. Roentgenol. Radium Therapy Nucl. Med. 18: 430–2
5. Maryanski M J, Gore J C et al (1993) Magn. Res. Imag. 11: 253-58
6. Lepage M, Jayasekera M, Bäck S Å J et al (2001) Phys. Med. Biol. 46: 2665-80
7. Hilts M, Audet C, Duzenli C et al. (2000) Phys. Med. Biol. 45: 2559-2571
8. Mather, M L, Whittaker A K and C. Baldock (2002) Phys. Med. Biol. 47: 1449–1458
9. Baldock C, Rintoul L, et al. (1998) Phys. Med. Biol. 43: 3617-27
10. Adamovics J. and Maryanski M (2003) Med. Phys. 30: 1349
11. Gore J C, Ranade M, Maryanski M J et al (1996) Phys. Med. Biol. 41: 2695-704
12. Fong P M, Keil D C, Does M D and Gore J C (2001) Phys. Med. Biol. 46: 3105-3113.
13. De Deene Y, Hurley C, Venning A et al (2002) Phys. Med. Biol. 47: 3441–63.
14. Senden R J, De Jean P, McAuley K B and Schreiner L J (2006) Phys. Med. Biol. 51: 3301–14
15. Bayreder C (2008) PhD thesis, Medical University of Vienna.
16. Bayreder C, Berg A, Georg D, Moser E. (2006) Med. Phys. 33 (7): 2506-2518
17. MacDougall N D, Pitchford W G, and Smith M A (2002) Phys. Med. Biol. 47: 107-121.
18. Oldham M and Siewerdsen J H (2001) Med. Phys. 28: 1436–45
19. Berg A, Ertl A, Moser E (2001) Med. Phys. 28: 833-843
20. Maryanski M J, Schulz R J, Ibbot G S et al (1994) Phys. Med. Biol. 39: 1437–55
21. Kipouros, P, Papagiannis,P.; Sakelliou,L et al. (2003) 30(8): 2031-9
22. Ramm U, Weber U, Bock M et al (2000) Phys. Med. Biol. 45: 95–102
23. Berg A, Pernkopf M, Fellner C et al (2004) Phys. Med. Biol. 49: 4087-4108
24. Berg A, Wieland M, Bayreder C et al. (2008) MAGMA 21 S1: 788
25. Berg A G, Bayreder C, Schmid P et al. (2004) MAGMA, 17 suppl. 1, 428: 254
26. Berg A, Bayreder C, Naumann I et al. (2005) Biomedizinische Technik/Biomedical Engineering 50 S1: 118-119.

Effective dose contribution of cone-beam CT acquisition during uterine artery embolization: a phantom study

A. De Crop[1], K. Bacher[1], L. Defreyne[2]; H. Thierens[1]

[1] Ghent University/Department of Medical Physics, Ghent, Belgium
[2] Ghent University Hospital/Department of Vascular and Interventional Radiology, Ghent, Belgium

Abstract— **Uterine artery embolization (UAE) is an efficient option for the treatment of uterine fibroids. Recently, cone-beam CT (CBCT) acquisitions are being introduced during these procedures. The purpose of current study was to evaluate the radiation dose contribution of these cone-beam CT runs. Therefore an anthropomorphic Rando phantom study was set up. The phantom was filled with 156 thermoluminescent dosemeters. Organ and effective dose conversion factors were determined for three different set-ups: cone-beam CT acquisitions, digital subtraction angiography (DSA) PA and DSA oblique. Using these factors, the ovarian and effective doses for the first two subsequent patient procedures were calculated. The contribution of the CBCT runs was determined.**

For the two patient procedures, equivalent ovarian doses of 140 and 91 mSv were found. 63% and 40% of the ovarian dose could be attributed to the CBCT runs, respectively. The total genetic risks involved in both procedures was estimated to be 6/10000 and 3/10000. Using the ICRP 103 tissue weighting factors, the effective dose of the entire procedure was calculated to be 48.3 mSv and 28.9 mSv. The 3D CBCT acquisitions were responsible for 71% and 47% of this effective dose. As a result, further optimization will be needed to reduce the CBCT dose contribution.

Keywords— **Interventional radiology, uterine artery embolization, cone-beam CT, organ dose, effective dose**

I. Introduction

Uterine leiomyoma or uterine fibroids are very common benign tumors in women. They can cause pelvic pain and excessive uterine bleeding that can lead to anemia.

Up to now, the conventional treatment for uterine fibroids was hysterectomy [1]. The main disadvantages of this technique are related to possible complications associated with surgery, psychological issues associated with uterus removal and the loss of childbearing potential.

A less invasive, but very efficient treatment is uterine artery embolization. Via the right common femoral artery, both left and right uterine arteries are cannulated. Embolization is performed by injecting polyvinyl alcohol particles until there is a cessation of vascular flow. This results in the infarction of the fibroids and temporary ischemia of the uterus [1]. The embolization procedure is performed using fluoroscopy and digital subtraction angiography runs.

Recently, the cone-beam CT (CBCT) technique became available on flat panel systems for interventional radiology [2]. CBCT images can be used for a more accurate 3D evaluation of the blood flow to the fibroids after embolization. However, when implementing this new technique into clinical practice, patient radiation exposure and corresponding risks have to be considered. This is of particular importance as different radiation-sensitive organs are located within the X-ray field. Moreover, an important fraction of the patients are still in childbearing age. Therefore, the ovarian dose should be kept as low as possible.

II. Material and Methods

In order to estimate the radiation burden of the DSA runs and the CBCT acquisitions during UAE procedures, an anthropomorphic Rando phantom (The Phantom Laboratory) study was set up. The phantom was filled with a total of 156 calibrated MTS-N thermoluminescent dosimeters (TLDs – TLD Poland, Krakow, Poland) in positions representative for the radiosensitive organs and tissues that are included in the concept of effective dose [3,4]. The choice of the TLD locations was based on a complete CT scan of the phantom.

DSA PA, DSA 30° oblique and CBCT acquisitions of the Rando phantom were obtained using pre-programmed settings of the X-ray installation (Siemens Artis bi-plane system with DynaCT option). Positioning and collimation of the X-ray beam was performed in a similar way as for patients. An example of a CBCT acquisition of the Rando phantom is presented in Figure 1. For each of the phantom acquisitions, the corresponding DAP values were registered, in order to be able to calculate corresponding DAP to effective dose conversion factors. To obtain dose measurements well above the background radiation, a total of 10 exposures were performed for each of the experiments.

O. Dössel and W.C. Schlegel (Eds.): WC 2009, IFMBE Proceedings 25/III, pp. 455–457, 2009.
www.springerlink.com

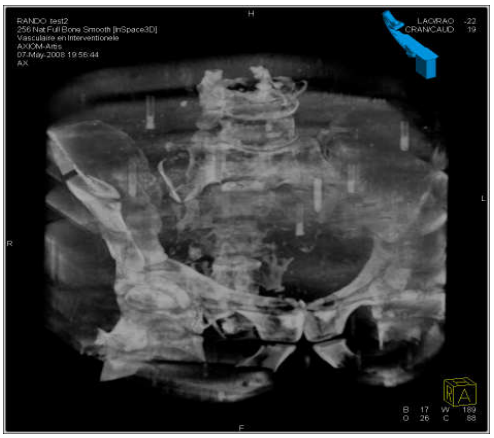

Fig. 1 Cone-beam CT image of the Rando phantom

After the irradiation of the Rando phantom, TLDs were read out using a Harshaw 3500 TLD reader (Thermo electron, Solon, OH). The background-corrected phantom TLD readings were converted into absorbed dose values after applying the corresponding calibration factor. Based on the latter dose values, the mean equivalent organ doses per unit of DAP were calculated as described by Huda et al. [5]. By combining these results with the corresponding tissue-weighting factors, the effective dose per unit of DAP could be calculated [3,4]. In this study, effective doses were calculated using the tissue weighting factors of both ICRP 60 and ICRP 103 (Table 1).

Table 1 ICRP tissue weighting factors

Organ	ICRP 60	ICRP 103
Gonads	0.20	0.08
Bone marrow	0.12	0.12
Colon	0.12	0.12
Lung	0.12	0.12
Stomach	0.12	0.12
Bladder	0.05	0.04
Breast	0.05	0.12
Liver	0.05	0.04
Esophagus	0.05	0.04
Thyroid	0.05	0.04
Skin	0.01	0.01
Bone surface	0.01	0.01
Brain	/	0.01
Salivary glands	/	0.01
Remainder	0.05	0.12

For the first two subsequent UAE procedures using the CBCT technique, the cumulated DAP of the DSA PA, the DSA oblique and the CBCT runs were registered. The latter values were multiplied with the previously derived organ and effective dose conversion factors.

III. Results

The measured equivalent organ dose conversion factors per unit of DAP (μSv/cGycm²) are summarized in Table 2.

For all acquisitions, the bladder, uterus, ovaries and small intestine are among the organs receiving the highest radiation dose. Using the DAP data from the patient procedures, equivalent ovarian doses of 140 and 91 mSv were found. 63% and 40% of the ovarian dose could be attributed to the CBCT runs, respectively. The total genetic risks (0.4%/Sv) involved in both procedures was estimated to be 6/10000 and 3/10000.

Table 2 Equivalent organ dose per DAP

	Equivalent organ dose (μSv/cGycm²)		
	CBCT	DSA PA	DSA oblique
Bladder	1.67	6.75	3.74
Colon	4.07	4.33	2.91
Uterus	2.55	5.26	3.03
Ovaries	3.67	8.70	6.10
Small intestine	3.58	3.39	2.25
Liver	1.21	0.48	0.45
Stomach	1.17	0.38	0.32
Kidney	0.91	0.60	0.53
Pancreas	1.24	0.84	0.74
Spleen	0.31	0.25	0.19
Lung	0.02	0.02	0.01
Hart	0.05	0.06	0.04
Remainder	0.61	0.95	0.60
Esophagus	0.01	0.01	0.01
Thyroid	<0.01	<0.01	<0.01
Bone marrow	2.03	5.53	4.46
Bone	4.10	11.12	8.96
Skin	1.06	1.06	0.33
Breast	<0.01	<0.01	<0.01

The measured effective dose conversion factors for CBCT, DSA PA and DSA oblique runs, using the different tissue weighting factors, are listed in Table 3.

Table 3 Effective dose per DAP

	Dose conversion factors (μSv/cGycm²)	
	ICRP 60	ICRP 103
CBCT	1.84	1.41
DSA PA	3.43	2.38
DSA oblique	2.43	1.70

Table 4 Patient effective dose calculations

	Effective dose (mSv)	
	Patient 1	Patient 2
CBCT	34.3	13.7
DSA PA	10.9	13.3
DSA oblique	3.1	1.9
Entire procedure	48.3	28.9

Using the registered DAP data of both patients, the effective doses of the different acquisition parts of the UAE procedure were found (Table 4). For the entire procedure, an effective dose of 48.3 mSv and 28.9 mSv was found, respectively. The corresponding risk of stochastic effects such as leukemia and cancer (5%/Sv) for these procedure was 2.4/1000 and 1.4/1000. The CBCT acquisitions were responsible for 71% and 47% of the total effective dose.

IV. DISCUSSION

An UAE procedure is an interesting alternative for the treatment of uterine fibroids as it can replace surgery [1]. In the conventional UAE procedures a series of 2D projections are acquired to investigate the blood flow in the fibroids and to follow the embolization procedure. Only recently, CBCT became available in interventional radiology rooms. As the CBCT acquisitions result in 3D images, a more accurate evaluation of the blood flow is possible. However, up to now, no data is available with respect to the patient radiation doses due to this CBCT technique.

In present study, organ and effective dose conversion factors were measured using an anthropomorphic Rando phantom (Table 2 and 3). The obtained effective dose conversion factors for the DSA PA and oblique directions are in agreement with previously published data, when comparing our conversion factors based on the ICRP 60 tissue weighting factors [7]. When we adapt the ICRP 103 recommendations, considerably lower conversion factors were found. The latter can be attributed to the lower tissue weighting factors of the gonads in ICRP 103.

Since an important fraction of the patients is still in childbearing age, the radiation dose to the ovaries is of particular interest. In the two patient cases, ovarian doses of 91 and 140 mSv were found. In both cases, the contribution of the cone-beam CT acquisitions was very high. In other studies using the conventional UAE procedure without CBCT, ovarian doses of 95 and 28 mSv were calculated [6,7].

The obtained effective dose values of both patients are considerably higher than the previously published value of 12.5 mSv by Vetter et al. (without CBCT) [7].

V. CONCLUSIONS

Cone-beam CT acquisitions are a valuable contribution to an UAE-procedure due to the 3D image information. However, the preliminary patient dose results showed that the CBCT runs will be responsible for a significant increase of the patient radiation dose. Therefore, further optimization will be needed to reduce the CBCT dose contribution.

REFERENCES

1. Siskin G (2006) New treatments for uterine fibroids. Techniques in vascular and interventional radiology 9:12-18
2. Kalender WA, Kyriakou Y (2007) Flat-detector computed tomography (FD-CT). Eur Radiol 17:2767-2779
3. ICRP (1991) Recommendations of the International Commission of Radiological Protection. ICRP Publication 60. Pergamon Press, Oxford
4. ICRP (2008) Recommendations of the International Commission of Radiological Protection. ICRP Publication 103. Pergamon Press, Oxford
5. Huda W, Sandisaon GA (1984) Estimation of mean organ doses in diagnostic radiology from Rando phantom measurements. Health Phys. 47:463-467
6. Nikolic B, Spies JB, Campbell L et al. (2001) Uterine artery embolization: reduced radiation with refined technique. J Vasc Interv Radiol 12:39–44
7. Vetter S, Schultz FW, Strecker EP, et al. (2004) Patient radiation exposure in uterine artery embolization of leiomyomata: calculation of organ doses and effective dose. Eur Radiol 14:842-848

Author: An De Crop
Institute: Ghent University
Street: Proeftuinstraat 86
City: 9000 Ghent
Country: Belgium
Email: an.decrop@ugent.be

Evaluation of effective patient dose in paranasal sinus imaging: comparison of Cone Beam CT, Digital Tomosynthesis and multi slice CT

K. Bacher[1], K. Mermuys[2], J. Casselman[2], H. Thierens[1]

[1] Ghent University/Department of Medical Physics, Ghent, Belgium
[2] A.Z. St.-Jan Hospital/Department of Radiology, Bruges, Belgium

Abstract— **Cone-beam CT (CBCT) and digital tomosynthesis are becoming interesting tools for paranasal sinus imaging. In present study, the effective dose of these new techniques was compared with the effective dose of multi slice CT (MSCT) acquisitions.**

An anthropomorphic Rando phantom was fitted with 156 calibrated thermoluminescent dosimeters (TLD) in positions representative for the radiosensitive organs and tissues according to the 2007 recommendations of the International Commission of Radiological Protection. CBCT (Imaging Sciences International, I-CAT), digital tomosynthesis (GE, Definium 8000/VolumeRAD), low-dose and standard dose MSCT (GE, Lightspeed 16) acquisitions of the Rando phantom were obtained. For all imaging systems, the Rando phantom was positioned and exposed in a similar way as for patient paranasal sinus imaging on that specific system. Afterwards exposure, TLDs were read out and TLD readings were converted into organ doses.

Independent of the applied imaging techniques, the salivary glands, the brain and the thyroid are receiving the highest equivalent doses for the paranasal sinus imaging. The effective dose for the CBCT and the digital tomosynthesis examinations were 30µSv and 65 µSv respectively. For the MSCT examination, effective doses of 200µSv and 1400 µSv were found for the low-dose and the standard CT protocol.

Paranasal sinus imaging with CBCT and digital tomosynthesis showed a large dose reduction compared to low-dose and standard MSCT. When comparing the two new imaging techniques, CBCT could acquire high quality images at less than half the dose of the digital tomosynthesis system.

Keywords— **Effective dose, paranasal sinus imaging, cone-beam CT, digital tomosynthesis, CT**

I. Introduction

Cone-Beam CT (CBCT) is an emerging technology for oral and maxillofacial applications with very low radiation dose exposure [1]. Recently, since the introduction of large imaging fields in CBCT, there has been an increasing interest in the use of CBCT as a substitute for paranasal sinus imaging.

Digital tomosynthesis is a relatively new technique for producing an arbitrary number of slice images generated retrospectively from a sequence of projections acquired during a single motion of the x-ray tube [1]. This technique has already been described for mammographic, skeletal and thoracic applications to reduce overlap of tissues and could also have advantages in paranasal sinus imaging

So far, the gold standard for routine radiological examination in the diagnosis of acute sinusitis was multi slice computed tomography (MSCT). In present study the mean effective doses of standard and low dose MDCT of the paranasal sinuses are compared with the effective dose of CBCT and digital tomosynthesis imaging.

II. Material and Methods

In order to compare the radiation burden of the selected paranasal sinus imaging techniques, an anthropomorphic Rando phantom (The Phantom Laboratory) experiment was set up. The phantom was filled with a total of 156 calibrated MTS-N thermoluminescent dosimeters (TLDs – TLD Poland, Krakow, Poland) in positions representative for the radiosensitive organs and tissues that are included in the concept of effective dose [3]. The choice of the TLD locations was based on a complete CT scan of the phantom.

CBCT (Imaging Sciences International, I-CAT), digital tomosynthesis (GE, Definium 8000 -VolumeRAD), low-dose and standard dose MSCT (GE, Lightspeed 16) acquisitions of the Rando phantom were obtained using selected protocols for paranasal sinus imaging. Positioning and collimation of the X-ray beam was performed in a similar way as in patients. To obtain dose measurements well above the background radiation, a total of 10 exposures were performed. After the irradiation of the Rando phantom, TLDs were read out using a Harshaw 3500 TLD reader (Thermo electron, Solon, OH). The background-corrected phantom TLD readings were converted into equivalent organ doses per acquisition. By combining these results with the corresponding tissue-weighting factors [3], the effective dose could be calculated.

O. Dössel and W.C. Schlegel (Eds.): WC 2009, IFMBE Proceedings 25/III, pp. 458–460, 2009.
www.springerlink.com

III. Results

In Table 1, an overview is presented of the equivalent organ doses for the four paranasal sinus imaging techniques. Independent of the applied techniques, the salivary glands, the brain and the thyroid are receiving the highest radiation doses.

Table 1 Equivalent organ dose of the imaging techniques

	Equivalent organ dose (μSv)			
	CBCT	Digital tomosynthesis	Standard CT	Low-dose CT
Brain	987	1570	58849	8610
Salivary glands	742	1650	37809	5100
Breast	<0.1	<0.1	<0.1	<0.1
Lungs	8	16	230	35
Esophagus	7	17	169	27
Thyroid	94	398	3750	544
Bone marrow	16	29	321	47
Bone	38	93	1106	158
Skin	20	38	1480	214
Remainder	43	79	1540	221

Summation of the equivalent organ doses with the corresponding weighting factors resulted in an effective dose value of 30 μSv for the CBCT acquisition. The digital tomosynthesis showed an effective dose of 65 μSv. MDCT images resulted in high effective radiation dose values of 200 and 1400 μSv for the low and the high dose protocol respectively.

In Figure 1 and Figure 2 typical coronal reconstructed images of the paranasal sinus region are presented. Figure 1 compares a CBCT reconstruction with a low-dose CT image. In Figure 2, a CBCT image is compared with a digital tomosynthesis acquisition. Both CBCT and digital tomosynthesis provide sufficient image quality for diagnosis of sinusitis.

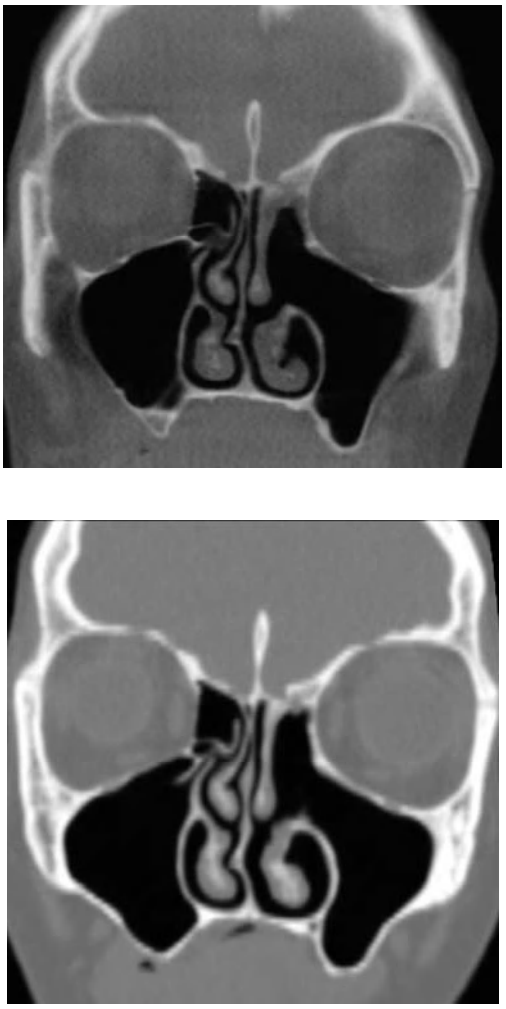

Fig. 1 Coronal reconstructed CBCT image (upper) and low-dose MDCT image in the same coronal plane of the same patient (lower)

Fig. 2 Coronal reconstructed CBCT image (upper) and digital tomosynthesis image (lower) obtained in the same coronal plane of the same patient

IV. DISCUSSION

Up to now, the gold standard imaging technique for paranasal sinus imaging is CT. Unfortunately, the latter technique is associated with high patient radiation doses, even with low-dose settings [4]. In present study, two new imaging modalities are introduced for sinus imaging: CBCT and digital tomosynthesis. Both new modalities provide sufficient image quality for diagnosis (Figure 1 and Figure 2) but achieve the images with significant lower radiation dose levels.

The use of digital tomosynthesis in paranasal sinus imaging resulted in an effective dose reduction in comparison with standard and low-dose MSCT of respectively 95% and 67%. However, a limitation inherent to the digital tomosynthesis technique is the fact that one can only reconstruct slice images parallel to the detector plane (coronal plane).

With a CBCT technique there are no such limitations in image reconstruction. Moreover, the effective dose of the CBCT acquisitions was found to be about 50% lower compared to the digital tomosynthesis technique. In the absence of CBCT, digital tomosynthesis could be a valuable screening tool in patients for with suspected paranasal sinus disease.

V. CONCLUSIONS

Both CBCT as digital tomosynthesis provide adequate paranasal sinus imaging at very low patient radiation doses compared to low-dose CT.

REFERENCES

1. Tsiklakis K, Donta C, Gavala S, et al. (2005) Dose reduction in maxillofacial imaging using low dose Cone Beam CT. Eur J Radiol. 56(3): 413-7
2. McAdams HP, Samei E, Dobbins J, et al. (2006) Recent advances in chest radiography. Radiology 241: 663-683
3. ICRP (2008) Recommendations of the International Commission of Radiological Protection. ICRP Publication 103. Pergamon Press, Oxford
4. Hein E, Rogalla P, Klingebiel R, et al. (2002) Low-dose CT for the paranasal sinuses with eye lens protection: effect on image quality and radiation dose. Eur Radiol 12: 1693-1696

Author: Klaus Bacher
Institute: Ghent University
Street: Proeftuinstraat 86
City: 9000 Ghent
Country: Belgium
Email: klaus.bacher@ugent.be

Exploring the techniques for radiation leakage measurements of a telegamma machine

G Sahani[1], DN Sharma[2], PK Dash Sharma[1], and SP Agarwal[1]

[1]Radiological Safety Division, Atomic Energy Regulatory Board, Mumbai- 94, India.
[2]Radiation Safety & Systems Division, Bhabha Atomic Research Centre, Mumbai-85, India

Abstract— **Radiation leakage measurements in source ON/OFF position of a telegamma (teletherapy) unit head is required in various conditions to check the compliance of the unit head adequacy with the IEC standard ((IEC-60601-2-11 for telegamma). Radiation leakage measurements of a telegamma unit head in various conditions of measurements are easy except in the other than patient plane during source ON position. Authors have tried different approaches for this purpose. It is described that how the radiation leakage measurement can be performed without any specialized gadget designed for holding the detector at various desired location and also exploring to design & develop an specific QA gadget for easy and accurate measurement.**

Key words— Telegamma unit, radiation leakage ,IEC, radiation safety standards, QA gadget

I. INTRODUCTION

It is mandatory that before the unit is used for clinical applications, it shall comply with various standards such as electrical, mechanical, dosimetric and radiation safety etc, In India, Atomic Energy Regulatory Board (AERB) ensures that the unit complies with national/international standards before granting type approval certificate to the manufacturer. The Chairman, AERB is the competent authority for issuance of type approval certificate. Moreover, for obtaining commissioning approval even of a type approved model of the telegamma machine for clinical applications, it shall be tested for compliance with the prevailing National/International standard apart from the other regulatory requirements. The electrical, mechanical and dosimetric tests are beyond the scope this paper and hence focus is on the method of radiation leakage measurement of the machine head. The radiation leakage measurements in source ON/OFF position of a telegamma (teletherapy) unit head is required in various conditions to check the compliance of the unit head adequacy with the IEC standard. As per IEC 60601-2-11 requirements, the following tests need to be carried out as far as radiation leakage/transmission is concerned[(1)]:

1. Leakage radiation in the patient plane during source ON position
2. Leakage radiation in other than patient plane during source ON position
3. Leakage radiation through beam limiting devices (secondary collimator) during irradiation in source ON position
4. Leakage radiation from the source head in source OFF position

Radiation leakage measurements of a telegamma unit head in various conditions of measurements as described above are easy except in the other than patient plane during source ON position. Therefore, authors have tried to explore various techniques for locating the 13 points of measurement, which are distributed evenly over a spherical surface as per IEC requirements[1]. The two different approaches for this purpose are:

1. Measurement of radiation leakage without availability of any specialized gadget for the purpose.
2. Exploring to develop a specialized gadget for holding detector with proper build up so that radiation leakage measurement at 13 points as needed (as explained above) during source ON position in the other than patient plane can be measured.

II. MATERIALS AND METHODS

A. Measurement of the radiation leakage in other than patient plane during source ON position — without availability of a specific gadget for the purpose

Radiation leakage measurement of a telegamma unit head is carried as per IEC-60601-2-11 requirements. It is very easy to carry out radiation leakage measurements of a telegamma unit head in the patient plane[2] . However, it is tedious to perform radiation leakage measurements of a telegamma unit head in

O. Dössel and W.C. Schlegel (Eds.): WC 2009, IFMBE Proceedings 25/III, pp. 461–463, 2009.
www.springerlink.com

the other than patient plane. Radiation leakage measurements of a telegamma unit head in the other than patient plane need to be performed at 13 points of measurement. These 13 measurement points distributed evenly over the spherical surface of radius r (here r = 1 m) with source at the centre of the sphere as explained in Fig. 1. Out of 13 measurement points, 4 points are on the equatorial plane, 8 points at the centre of the 8 spherical triangles as explained in the figure and remaining 13th point on the pole P (above the source head where central beam axis PQ intersects the spherical surface) . Locating these 13 measurement points is tedious. However, these points can be easily located if the coordinates of the points measurement are known in terms of Cartesian co-ordinates. By referring Fig. 1, we have three great circles E1-E2-E3-E4, P-E2-Q-E4 and P-E3-Q-E1, which are perpendicular to each other and passing through the centre of the sphere. Points P & Q are the poles of the sphere. PQ is the central axis of the radiation beam. The equator is equally divided into four points by the great circles P-E2-Q-E4 and P-E3-Q-E1 passing through poles P and Q. Thus creating eight identical spherical triangles. If A (x, y, z) be any point on the spherical triangle E2-E3-P and A' be its projection on the XY plane (equator plane) then we can have the following relations between polar and Cartesian co-ordinates:

$x = r \sin\theta \sin\phi$, $y = r \sin\theta \cos\phi$ and $z = r \cos\theta$

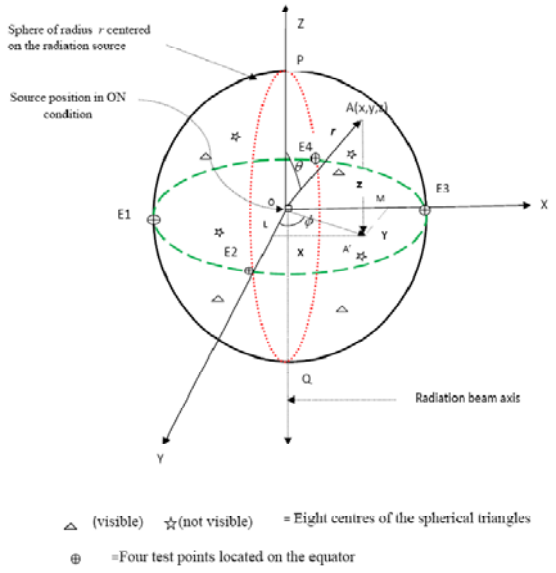

Figure 1 - Location of 13 points for radiation head leakage measurement in source ON condition.

Where θ = angle between radius OA (r) and Z axis,

ϕ = angle between OA' and Y axis

For center of the spherical triangle E2-E3-P we have

$\theta = 45^0$, $\phi = 45^0$ and r =1 m, then the value of the Cartesian co-ordinates for the centre of the spherical triangle E2-E3-P will be:

$x = 1 \sin 45^0 \sin 45^0$ m = 0.5 m, $y = 1 \sin 45^0 \cos 45^0$ m = 0.5 m, $z = 1 \cos 45^0$ m = 0.707 m

Similarly, one can also locate the centers of the other seven spherical triangles. The appropriate dosimeter can be placed with proper build up thickness at above 13 points and measurement can be performed. Thus percentage radiation leakage of the maximum dose rate on central axis at 1m can be calculated so as to ensure compliance of the unit head as per IEC standard as far as radiation leakage of the unit head is concerned.

B. Exploring to design and develop a specific gadget for radiation leakage measurement in source ON position

The measurement of leakage radiation of a telegamma unit head in the other than patient plane during source ON position can further be made easy as compared to the technique described in section A, if a specific gadget is developed for the purpose. The proposed specific gadget is shown in the Figure 2, can easily serve the purpose. The gadget should have semicircular arc, supporting assembly for the semicircular arc and base with pivot at the center. The radius of the semicircular arc should be 1m with provision for holding the dosimeter at various points as described in the Figure 2. The material for the semicircular arc as well as for the supporting assembly to it should be of light weight such as aluminum or any other similar material for easy transportation to the site and rotation around the pivot, fixed at the base of the gadget. The semicircular arc should be able to rotate throughout 360^0 around the pivot at the base so that measurement can be carried out at desired locations on the spherical surface. The base of the gadget should be either rectangular or circular disc having pivot fixed at the center with angular scale. This base can be clamped on the treatment table of the unit so that the semicircular arc could be rotated at the desired places for measurement. There should be a clamping device for holding the detector on the semicircular arc at various locations so that the radiation leakage measurement can be carried out as per IEC requirements. The center of the semicircular arc should coincide with the source center during source ON

position while performing the radiation leakage measurement. This gadget can also be used for the radiation leakage measurement at 1 m from the source in the source OFF position.

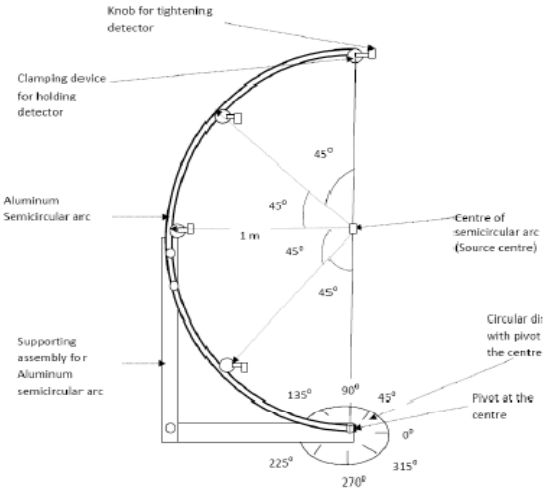

Figure 2- QA gadget for radiation leakage measurement during source ON position

III. Discussion

The result title is not justified here as the present paper deals with the two different techniques for radiation leakage measurement of a telegamma machine head during source ON position. The above techniques would be very helpful for the telegamma machine users, manufacturer and regulatory body for easy measurement so as they can ensure the compliance of the telegamma machine with relevant IEC standard as far as radiation leakage is concerned during source ON position.

IV. Conclusions

The above techniques will be helpful to the regulatory body for evaluating type approval of the unit of as well as the user and manufacturer of a telegamma machine for carry out the radiation leakage measurement.

Acknowledgements

Shri S.K. Sharma, Chairman, AERB is the guiding force behind this work and the authors are thankful to him for his encouragement.

Reference:

1. International Electro technical Commission; Part2: Particular requirements for the safety of gamma beam therapy equipment. 1997; IEC-60601-2-11.

2. International Electrotechnical Commission; Part2-1: Particular requirements for the safety of electron accelerators in the range 1 MeV to 50 MeV. 1998; IEC-60601-2-1.

Address of the corresponding author:

Author: G. Sahani
Atomic Energy Regulatory Board
Government of India
Niyamak Bhavan
Anushaktinagar
Mumbai- 400 094
India
Email: gsahani@gmail.com, gsahani@aerb.gov.in

Measurements and EGSnrc Monte Carlo Simulations for Thimble Ion Chambers with Various Metal Caps at ^{60}Co Beams

A. Toussaint, J. Wulff, K. Zink

University of Applied Sciences Giessen-Friedberg, Institut für Medizinische Physik und Strahlenschutz – IMPS, Giessen, Germany

Abstract— **This paper presents the direct comparison between measurements and Monte Carlo ion chamber simulations employing the EGSnrc Monte Carlo code.**

Surrounding metal caps for a 1 cm³ ionization chamber (PTW30015) were varied both, in measurements and simulations. Absorbing caps made of iron, copper and aluminum alloy were manufactured each with wall thickness between 2 and 30 mm. As a radiation source, a Siemens Gammatron S ^{60}Co machine was used. Normalized dose values were compared and changes to the cross-sections used in the Monte Carlo simulations investigated.

Results agreed within the range of the measurement uncertainties of ~0.5%. Still, variations in photon cross-sections lead to significant changes in the results, highlighting the need of accurate input data for this type of investigation.

Keywords— **Monte Carlo, EGSnrc, ionization chambers, systematic uncertainties**

I. Introduction

Reference dosimetry in radiation therapy is based on correction factors which in some cases can be obtained from Monte Carlo (MC) simulations [1]. Therefore knowledge of the reliability of the MC codes is mandatory.

The EGSnrc code system is known to accurately simulate ion chamber response and was demonstrated theoretically to be accurate at the 0.1% level, normalized to own cross-sections [2]. In a recent publication La Russa et al. [3] compared measurement data sets at ^{60}Co energies for various wall materials and cavity dimensions to simulations and found agreement within a few percent or less. There is still a lack of accurate comparisons available, confirming the reliability of MC codes to calculate ion chamber response.

The aim of this study was therefore to design a simple test setup which allows direct reproduction within MC simulations employing the EGSnrc system. Further, the principle influence cross-section uncertainty was investigated.

II. Methods

A. Experimental measurements

All measurements were performed with the thimble ionization chamber PTW30015 with an active air volume of 1 cm³. Charge was measured, with an accumulation time of 60 s and taken as the mean of 10 single measurements.

Absorption caps made of iron, copper and an aluminum alloy were manufactured, each with wall thickness of 2, 10, 20 and 30 mm ±0.01 mm.

A Siemens Gammatron S ^{60}Co therapy machine equipped with nickel plated ^{60}Co pellets was used as radiation source. The chamber was positioned free in air at the isocenter with the aid of a patient positioning laser system. A special, scatter-free assembly was developed, which allowed the chamber to be accurately mounted. The field size was 10x10 cm² each and a focus-chamber distance of 80 cm was chosen.

B. Simulation of the measurements

For simulations the EGSnrc system was employed in conjunction with the CAVITY user code [4]. This application allows the calculation of ion chamber dose in an arbitrary geometry such as an ion chamber. Particle transport thresholds were set to 10 keV and all transport defaults were used.

The geometry implementation of the ion chamber was taken from the study of Ubrich et al. [5], demonstrated to be accurate in the energy range of therapeutically kV beam qualities, and extended by the different metal caps. A collimated point source was used with the spectrum of a ^{60}Co machine, included in the EGSnrc distribution. Deposited dose was calculated in the sensitive air-volume of the ion chamber models, equipped with the different metal caps.

In order to compare the simulation results with the measurements both, the dose calculated and charge measured, were normalized to the values of the 2 mm aluminum cap.

All simulations were run until a statistical uncertainty below 0.1% was achieved.

O. Dössel and W.C. Schlegel (Eds.): WC 2009, IFMBE Proceedings 25/III, pp. 464–465, 2009.
www.springerlink.com

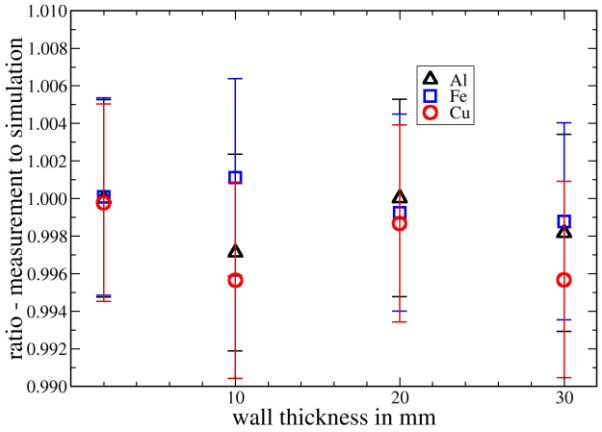

Figure 1 Comparison between measurement and simulation for the different metal caps. The error bars represent the combined uncertainty of measurement and statistical uncertainty of the simulations (±0.5%).

To investigate the influence of systematic uncertainties in photon cross-sections, their values were scaled by +1% for the metals used in the caps for additional simulations.

III. Results.

The changed response of the ion chamber with varying metal caps leads to a dose reduction of up to 53% for the thickest copper cap. The reproducibility of the charge measurements was influenced by the rotation of the source capsule when turning on and off the beam. The variation leads to an estimated measurement uncertainty of ±0.5%. It was assumed that the nickel plated pellets of the source are able to move in the cylinder, resulting in a small distribution variation of the pellets and therefore in dose rate variations due to self-absorption.

Figure 1 shows the comparison of the calculated response to the corresponding measured values, given as a ratio. Within the combined measurement and statistical ±0.5% uncertainties of the simulations, all results agree.

The severe +1% change in the cross sections led to a change in the calculated response of up to 0.7% for the thickest copper cap.

IV. Discussion and conclusion

The presented results show an excellent match between measurements and simulations for all materials and thicknesses of the caps within the measurement uncertainty of ±0.5%.

The good match between measurement and simulation allow the conclusion, that the uncertainty of photon cross-sections is presumably smaller than 1%. Still, the variations due to changed photon cross-sections point to the need for accurate input data for this type of investigation.

The original intentions for choosing ^{60}Co as a source, was to get a reproducible source with a stable dose rate. Unfortunately it turned out, that this source was the largest contribution to measurement uncertainty. Future experiments should therefore be performed with a more stable ^{60}Co machine.

V. Aknowlegement

The measurements were performed at the German Cancer Research Center (Deutsches Krebsforschungszentrum, DKFZ) located at Heidelberg. We wish to acknowledge their and especially the support of Prof. Dr. G. Hartmann.

References

1. Rogers, D W O; (2006) Fifty years of Monte Carlo simulations for medical physics. Phys. Med. Biol. 51, R287-R301
2. Kawrakow, I. (2000) Accurate condensed history Monte Carlo simulation of electron transport. II Application to ion chamber response simulations. Med. Phys 27:3, 499-513.
3. La Russa, D J; Rogers, D W O; (2008) Accuracy of EGSnrc calculations at ^{60}Co energies for the response of ion chambers configured with various wall materials and cavity dimensions. Med. Phys. 35:12, 5629-5640
4. Kawrakow I and Rogers D W O (2003) The EGSnrc code system: Monte Carlo simulation of electron and photon transport PIRS-701 National Research Council of Canada, Ottawa
5. Ubrich F, Wulff J, Kranzer R, Zink K. (2008); Thimble ionization chambers in medium energy X-rays and the role of constructive details of the central electrode: Monte Carlo simulations and measurements. Phys. Med. Biol. 53, 4893-4906

Author: André Toussaint
Institute: University of Applied Sciences Giessen,
Institut für Medizinische Physik und Strahlenschutz, IMPS
Street: Wiesenstraße 14
City: 35390 Giessen
Country: Germany
Email: Andre.Toussaint@tg.fh-giessen.de

Monte Carlo calculations of the perturbation factor p_{cav} for various Air cavities and guard ring widths in clinical electron beams

F. Rosam, J. Wulff and K. Zink

Institut für Medizinische Physik und Strahlenschutz – IMPS, University of Applied Sciences Giessen, Germany

Abstract— **The aim of this work was to examine the behavior of the perturbation factor p_{cav} for various cavity dimensions and guard ring widths of parallel-plate chambers using Monte Carlo simulation. The simulations revealed a depth dependence of the perturbation factor p_{cav} as well as an influence of the guard ring width on the fluence inside the air cavity. In contrast to the conventional view that the guard ring should prevent the in-scattering of electrons into the sensitive volume, a sufficiently wide guard ring contributes to the compensation of obliquity effect at larger depth.**

Keywords— **perturbation factor p_{cav}, cavity theory, guard ring, Monte Carlo simulation**

I. Introduction

In the current dosimetry protocols DIN 6800-2 and in the IAEA TRS-398 the perturbation factor p_{cav} corrects the fluence perturbation due to the air volume of an ionization chamber compared to the fluence in water when the chamber is absent. In practice, for well-guarded parallel-plate chambers p_{cav} is assumed to be unity and independent of depth [1, 2].

Because of the experimentally investigated and proven effect of in-scattering of electrons through the phantom material with high density inside the cavity gas with low density, a guard ring is recommended. The guard ring should prevent the in-scattering of electrons through the side walls of the cavity into the sensitive volume, and thus counteracts a perturbation of the electron fluence [3, 4].

Previous works supported by Monte Carlo simulations of Buckley and Rogers *et al.* as well as Verhaegen *et al.* revealed a depth dependence of the perturbation factor p_{cav} [5, 6]. These facts were the motivation to get a closer look at the behaviour of the perturbation factor p_{cav} by varying the dimensions of the air cavity and to investigate the dependence on the fluence when varying the guard ring width employing Monte Carlo simulations.

Locally resolved fluence calculations and the perturbation factor p_{cav} can be calculated according to Bragg-Gray or Spencer-Attix cavity theory [7] with the following equation:

$$p_{cav} = \frac{D_w(z)}{\bar{D}_{cav} \cdot s_{w,a}} = \frac{\int_\Delta \phi_w(z) \cdot (L/\rho)_a dE + \left[\phi_w^\Delta(z)\left(S(\Delta)/\rho\right)_a \Delta\right]}{\int_\Delta \bar{\phi}_{cav}(z) \cdot (L/\rho)_a dE + \left[\bar{\phi}_{cav}^\Delta \left(S(\Delta)/\rho\right)_a \Delta\right]} \quad (1)$$

where $D_w(z)$ is the absorbed dose to water in the depth z, $\bar{D}_{cav}$ the mean dose in the air filled cavity with walls entirely made of water and $s_{w,a}$ is the stopping power ratio of water to air. $\phi_w(z)$ denotes the fluence in water, $\bar{\phi}_{cav}(z)$ is the fluence in the air filled cavity averaged over the cavity volume, $(L/\rho)_a$ is the restricted mass stopping power of air and Δ the cut off energy of the electron spectra. The term outside the integral both numerator and denominator is the dose due to the track-ends of electrons falling below the cut-off energy Δ [7].

Neglecting the track-end terms which cancels out, the perturbation factor p_{cav} may be written as:

$$p_{cav} = \frac{D_w(z)}{\bar{D}_{cav} \cdot s_{w,a}} \approx \frac{\int_\Delta \phi_w(z) \cdot (L/\rho)_a dE}{\int_\Delta \bar{\phi}_{cav}(z) \cdot (L/\rho)_a dE} \quad (2)$$

From equation (2) it follows:

$$p_{cav} - 1 \approx \frac{\int (\phi_w - \bar{\phi}_{cav}) \cdot (L/\rho)_a dE}{\int \bar{\phi}_{cav} \cdot (L/\rho)_a dE} = \frac{\int \delta D_E dE}{\int \bar{\phi}_{cav} (L/\rho)_a dE} \quad (3)$$

with $\delta D_E = \left(\phi_w(z) - \bar{\phi}_{cav}(z + \Delta z)\right) \cdot (L/\rho)_a$ (4)

A good way to visualize the different contributions of the fluence spectra to D_w and $\bar{D}_{cav}$, is to calculate their difference according to eq. 4. If δD_E is further normalized, i.e.

$$XD_E = \frac{\delta D_E}{\int \bar{\phi}_{cav} \cdot (L/\rho) dE} \quad (5)$$

the total area under the spectral distribution of XD_E represents the magnitude of the perturbation. For balanced fluences the area is zero, hence $p_{cav}-1 = 0$ and $p_{cav} = 1$.

O. Dössel and W.C. Schlegel (Eds.): WC 2009, IFMBE Proceedings 25/III, pp. 466–469, 2009.
www.springerlink.com

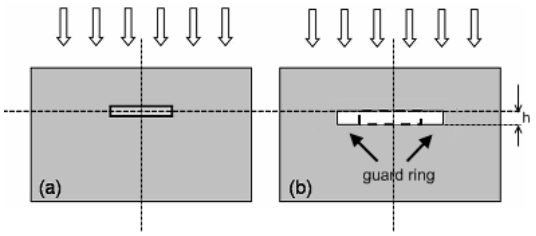

Fig. 1: simulation geometries. In fig. (a) the absorbed dose to water D_w and the fluence Φ were determined in a rotationally symmetric thin water layer with the dimensions r = 0.78 cm and h = 0.02 cm at various depths. In fig. (b) the dose D_{cav} as well as the fluence $\phi_{cav}(z)$ in the air filled cavity (dashed line) was scored. The width of the guard ring as well as the height of the cavity was varied.

II. Materials and methods

All Monte Carlo simulations in this study were performed with the EGSnrc Monte Carlo code system [8] of the National Research Council of Canada. With the use of the EGSnrc code system it is possible to determine the fluence and dose in the simulation geometries according to fig. 1 with high precision. For calculation of the fluences the FLURZnrc user code and for the dose calculations the DOSRZnrc user code was used [9].

As simulation geometry (fig. 1) for the fluence- and dose calculations, a water phantom with a diameter and a depth of 30 cm was used. In order to calculate the dose to water D_w and the fluence Φ, a thin water layer with radius r = 0.78 cm and height h = 0.02 cm was arranged in a rotational symmetry in the water phantom as illustrated in fig. 1(a). The restricted mass stopping powers of air $(L/\rho)_a$ were extracted from the EXAMIN user code [8], included in the EGSnrc package. As an electron source a spectrum of a Siemens KD2 accelerator with energy of 6 MeV and a half value depth R_{50} = 2.31 cm was used [10]. The radius of the parallel beam was 5 cm. Because fluence perturbations are largest for low electron energies [11], the present study is restricted on this electron energy.

To obtain a sufficient small statistical uncertainty of less than 0.3% for the Monte Carlo simulations 10^9 electron histories were calculated.

III. Results

The values of p_{cav} in fig. 2 were calculated according to eq. 2. The fluences used in the equation were calculated from the ratio of the fluence values with the FLURZnrc user code. The perturbation factor p_{cav} is smaller than unity at the depth z = 0.7cm which is caused by a higher dose within the

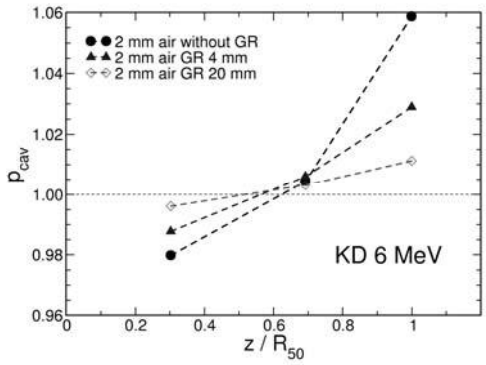

Fig. 2: Perturbation factor p_{cav} as a function of the scaled depth for various guard ring widths (GR). Height of the air cavity h = 2mm. Depth in water z = 0.7 cm, 1.6 cm and 2.31 cm. R_{50} is the depth in water in which the absorbed dose amounts to 50% of the dose maximum.

cavity compared to the dose in water. Increasing the guard ring width reduces the effect. At the depth z = 1.6 cm which is near the reference depth z_{ref} = 1.29 cm, p_{cav} is approximately unity. Beyond the reference depth there is a strong increase of p_{cav} indicating a lower dose within the cavity compared to the dose in water. This effect is also reduced by increasing the guard ring width.

The different values of p_{cav} in fig. 2 are attributed to different effects in the various depths.

At the depth z = 0.7 cm there is an excess of low energy electrons inside the cavity (fig. 3). This is the result of the in-scattering effect, by which electrons are more likely to be scattered into the cavity by the surrounding water than to be scattered out by the air of the chamber. This effect results in a value for p_{cav} less than unity [3].

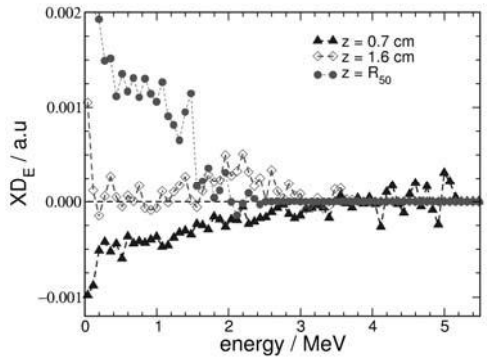

Fig. 3: Spectral difference XD_E (see eq.5) for the clinical 6 MeV electron spectrum for three different depths in water. Height of the air cavity h = 2mm. guard ring width GR = 4mm.

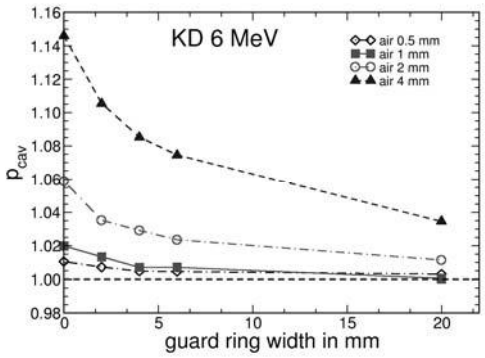

Fig. 4: Perturbation factor p_{cav} as a function of the guard ring width at the depth $z = R_{50} = 2.31$ cm, for various cavity thicknesses.

Close to the reference depth the excess of low energy electrons inside the air cavity is balanced by a miss of high energy electrons which results in a value p_{cav} of approximately unity (fig. 3).

A shortage of low energy electrons at the depth $z = R_{50}$ results in a value p_{cav} greater than 1 (fig 3). This is because of the path length effect, which results from the greater path length of the electron crossing the cavity when it is filled with water than when filled with gas. The dose in the cavity gas is less than that in the water. This effect is also known as obliquity effect [3].

Fig. 4 was also calculated with the data from the FLURZnrc user code to investigate the effect of an enlarged guard ring and the variation of the cavity thickness on the perturbation factor p_{cav}. As described, a descending value of p_{cav} by widening the guard ring can be observed. This observation allows the conclusion that a sufficiently wide guard ring contributes to the compensation of obliquity effect at larger depth.

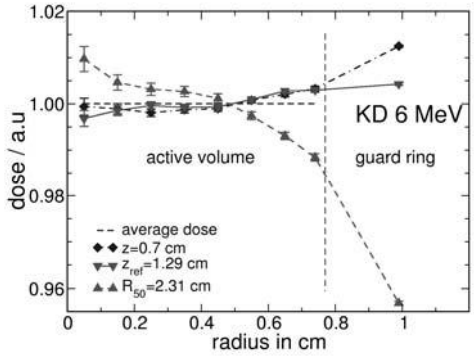

Fig. 5: Dose distribution in the air cavity (h = 0.4 cm) at various depths and the average dose in the active volume. Total radius of the air cavity = 0.78 cm + 0.4 cm guard ring. The horizontal line represents the average of the scaled absorbed dose in every depth of the active volume.

To get a deeper insight into the fluence perturbations, the air cavity was divided into several circular rings and for each of these rings the dose was calculated. Fig. 5 shows the locally absorbed dose in the air cavity at various depths z = 0.7 cm, $z_{ref} = 1.29$ cm and $z = R_{50} = 2.31$ cm. At the depth z = 0.7 cm an increase of the dose in the outer region of the active volume from the air cavity and the guard ring is noticeable confirming the findings of various experimental studies [3,4] and supporting the assumption of in-scattering. The dose at the reference depth $z_{ref} = 1.29$ cm is balanced over the entire active volume of the cavity and in the region of the guard ring, as was demonstrated in fig. 3.

At the depth $z = R_{50} = 2.31$ cm a clear decrease of the dose in the outer region of the active volume from the air cavity and in the region of the guard ring is visible.

Further observations of the fluence in the inner and outer radius of the air cavity in the depth z = 0.7 cm and $z = R_{50} = 2.31$ cm revealed that there is an excess of electrons in the depth z = 0.7 cm of about 1.3%, and a lack of electrons of about 5% in the area of the outer radius in contrast to the inner radius. This coincides with the dose difference from the inner to the outer radius in fig. 5.

IV. Discussion

The conventional view is that a guard ring must be wide enough to prevent the in-scattering of electrons in the sensitive volume, and because of this opinion the perturbation factor p_{cav} is assumed to be unity [1, 2, 3, 4].

With the present simulations a dependence of the perturbation factor p_{cav} on the depth and thus a deviation from unity could be revealed. p_{cav} approaches the value of 1 with increasing depth and width of the guard ring. The conclusion can be drawn that a wider guard ring in larger depths encourages the in-scattering of the electrons into the cavity and thus balances the fluence in the sensitive volume of the air cavity.

The results show that the Monte Carlo simulation is a useful aid for the optimization of ionization chamber designs, allowing for small perturbation factors.

References

1. DIN 6800-2 (März 2008): Dosismessverfahren nach der Sondenmethode für Photonen- und Elektronenstrahlung – Teil 2: Dosimetrie hochenergetischer Photonen- und Elektronenstrahlung mit Ionisationskammern
2. IAEA: Absorbed dose determination in external beam radiotherapy: An international code of practice for dosimetry based on standards of absorbed dose to water. Technical Report Series TRS-398 (International Atomic Energy Agency, Vienna 23.04.2004)

3. Harder, D.(1968). Einfluss der Vielfachstreuung von Elektronen auf die Ionisation in gasgefüllten Hohlräumen. *Biophysik* 5, 157.
4. Mattson, L. O., Johansson K.-A. and Svensson, H. (1981), Calibration and use of plane-parallel ionization chambers for the determination of absorbed dose in electron beams. Acta Radiologica Oncology 20, 385-399
5. Buckley, L. A. and Rogers, D. W. O. (2006), Wall correction factors, p_{wall}, for parallel plate ionization chambers. Med Phys 33 (6), 1788-1796.
6. Verhaegen, F., Zakikhani, R., Dusautoy, A., Palmans, H., Bostock, G., Shipley, D. and Seuntjens, J. (2006), Perturbation correction factors for the NACP-02 plane parallel ionization chamber in water in high-energy electron beams. Phys Med Biol 51 (5), 1221-1235.
7. Nahum, A. E. (1996), Perturbation effects in dosimetry: Part I. Kilovoltage x-rays and electrons. Phys Med Biol 41 (9), 1531-1580.
8. Kawrakow I, Rogers D, Report PIRS-701 - The EGSnrc Code System: Monte Carlo Simulation of Electron and Photon Transport. National Research Council of Canada, Ottawa, 2006
9. Rogers D, Kawrakow I, Seuntjens J, Walters B and Mainegra-Hing E, Report PIRS-702 NRC User Code for EGSnrc. National Research Council of Canada, Ottawa, 2005
10. G.X. Ding and D.W.O. Rogers, Report PIRS-0439, Energy spectra, angular spread and dose distributions of electron beams from various accelerators used in radiotherapy. National Research Council of Canada, Ottawa, 1995
11. Zink, K. and Wulff J. (2008), Monte Carlo calculations of beam quality factor k_Q for electron dosimetry with a parallel-plate Roos chamber. Phys Med Biol 53 (6), 1595-1607.

The ORAMED project: Optimisation of Radiation Protection for Medical Staff

F. Vanhavere[1], E. Carinou[2], G. Gualdrini[3], I. Clairand[4], M. Sans Merce[5] and M. Ginjaume[6]

[1] Belgian Nuclear Research Centre (SCK•CEN), Mol, Belgium
[2] Greek Atomic Energy Commission (GAEC), Athens, Greece
[3] ENEA Radiation Protection Institute, Bologna, Italy
[4] Institute for Radiological Protection and Nuclear Safety (IRSN), Fontenay-aux-Roses, France
[5] University Hospital Centre Vaudois (CHUV), Geneva, Switzerland
[6] Institute of Energy Technology - Universitat Politècnica de Catalunya (UPC), Barcelona, Spain

***Abstract*— The state-of-the-art analysis performed in the FP6 CONRAD project highlighted high extremity doses and a lack of systematic data analysis on exposures to the staff in interventional radiology (IR) and nuclear medicine (NM)[1,2]. To optimize the working procedures in the medical field with respect to radiation protection, a project called ORAMED focusses on improving the knowledge on extremity and eye lens exposures, combined with an optimization in the use of active personal dosemeters. The outline of this project is described in this paper.**

***Keywords*— radiation protection, eye lens dosimetry, extremity dosesimetry, active personal dosemeters, medical workplace fields**.

I. Introduction

The staff that carries out interventional procedures is likely to receive significant radiation doses to their hands, or parts of their body not covered with a protective apron, as they are close to X-rays tubes. The dose ranges for the same kind of procedures vary a lot, since there are many factors affecting extremity doses such as protective devices, X-ray geometry and spectra, the scattered radiation from the patient, etc.

Routine monitoring of extremities is difficult, since "the most exposed area" according to ICRP recommendations cannot easily be found. In most cases only finger or hand doses are reported; doses to the eye lens, legs or thyroid have not been evaluated. And this while (especially when no protective shielding on the couch is used) doses to the legs can be even higher than doses to the hands. There is evidence that eye lens doses are high in interventional radiology, and cases of cataracts have been reported in recent years. However, eye lens doses are never measured in routine applications, and also very few data can be found in the literature. There is no suitable dosemeter available and the standards for the operational quantity measurements are not complete. This situation is partly due to the lack of conversion coefficient and suitable calibration procedure.

A lack of appropriate equipment is also identified in the field of active personal dosemeters (APD) for typical fields in interventional radiology. Very few devices can detect low energy fields, and none of them are really designed for working in pulsed radiation fields.

In summary, in interventional radiology, there is an insufficient knowledge about which is the most exposed part of the body in the different procedures and the influence and effectiveness of protection measurements. Furthermore, there are no suitable eye-lens dosemeters or active personal dosemeters.

The literature concerning radiation exposure and protection of nuclear medicine staff mostly refers to conventional diagnostic nuclear medicine.

As a consequence of the definition that the dose limit for the skin has to be applied to 'the dose averaged over any area of 1 cm² regardless of the area exposed' it is advisable to measure the local skin dose at the location with presumably the highest exposure. This requirement is the central dilemma of extremity dosimetry and causes severe practical difficulties. In daily practice in nuclear medicine it is often not known which part of the hand will receive the highest dose. Moreover, the dose distribution over the hand may vary during a single process as well as when various persons perform the same procedure.

Unsealed radiation sources are being increasingly used in nuclear medicine for radiation therapy, in particular, nuclides that emit beta or mixed beta/gamma radiation. Considering the preferential use of beta emitters, the dosemeters must be appropriate for beta radiation, taking into account both the energy spectra of the nuclides and the spectral dose response of the dosemeter.

In nuclear medicine therapy, staff may be exposed to high doses, even exceeding the annual limit of the dose to the skin of 500 mSv. Thus, adequate safety measures including monitoring of personnel are a strict requirement.

In summary, in nuclear medicine one can highlight the difficulties in estimating the dose distribution across the hands, the need for greater knowledge of doses received

O. Dössel and W.C. Schlegel (Eds.): WC 2009, IFMBE Proceedings 25/III, pp. 470–473, 2009.
www.springerlink.com

during the main tasks of a nuclear medicine department and the effectiveness of the available protection measures.
To tackle these problems the ORAMED project was started in the beginning of 2008. In total 12 partners, among which two commercial companies, are working together to improve the knwoledge on the radiation exposures of medical staff.

The project is structured in 5 different work packages. The major tasks in every work package will be described below, together with the status after one year of the project.

II. GENERAL SET-UP OF THE PROJECT

A. Work package 1: Extremity dosimetry and eye lens dosimetry in interventional radiology and cardiology

The WP1 objective is to obtain a set of standardized data on doses for staff in interventional radiology and cardiology and to optimize staff protection. A coordinated measurement program in different hospitals in Europe is presently on-going. Moreover, simulations of the most representative workplaces/procedures in interventional radiology and cardiology will be performed to determine the main parameters that influence the extremity and eye lens doses.

For the measurement part, a retrospective study from hospital data on the frequency of procedures was performed in many European hospitals in order to decide the type of interventional procedures that are studied. The final list of procedures includes: cardiac angiographies (CA) and angioplasties (PTCA), radiofrequency ablations (RFA), pacemaker and cardiac defibrillator implantations (PM, ICD), angiographies (DSA) and angioplasties (PTA) of the lower limbs (LL), the carotids (C) and the reins (R), embolisations and endoscopic retrograde cholangiopancreatographies (ERCP).

After preliminary studies a measurement protocol was established according to which several parameters related to the system, the type and complexity of the procedure, the position of the physician and the protective equipment, the experience of the physician, the field parameters (kV values, filtration, projections, etc.) and finally the KAP values should be recorded. TL dosemeters will be used for the measurements. Up to now 137 procedures have been monitored in 7 European hospitals. The majority (56%) of the procedures are CAs and PTCAs. Doses up to 2.08 mSv were recorded on the left finger during CA/PTCA procedures. In the embolisations, the doses to the legs and the eyes were comparatively high as well, especially when protective equipment around the table was not used. Finally for the PMs and ERCPs the doses were generally low due to the absence of image acquisitions.

In order to perform the numerical calculations, a simulation protocol has been established. The input file contains the ORNL anthropomorphic phantom as a patient and the same one at the medical doctor's position. Eyes, hands, a thyroid collar and a lead apron have been added to the medical doctor phantom in order to better simulate the real situation. The list with the combinations of the different parameters (tube voltage, filtration, protective equipment, position of doctor, etc) has already been finalised. For the validation of the numerical methodology some simulations and measurements of a set-up at an X-ray equipment in a hospital has been performed. The results of the measurements were in good agreement with the simulation ones. Since the number of the simulations is too high, a sensitivity study on a simplified geometry is first started.

B. Work package 2:Development of practical eye lens dosimetry

Working Package 2 deals with eye lens dosimetry issues. The task is to better define and calculate the conversion coefficients from air kerma to $H_p(3)$. For this purpose, a cylindrical theoretical tissue equivalent phantom was judged to better reproduce the behaviour of the photon radiation within the human head.

Type test procedures are being planned to be elaborated. Also the backscattering properties of a new calibration phantom (PMMA water filled cylindrical 20x20cm^2 section) were numerically evaluated. A prototype of the plastic calibration phantom was designed and built

Relying on the computed conversion coefficients as well as the backscatter factor measurements and calculations, one partner is carrying out an optimization procedure for the design and construction of a dosemeter characterizad by a suitable response in terms of $H_p(3)$.

C. Work package 3: Optimization of the use of active personal dosemeters in interventional radiology and cardiology

The objective of WP3 is to optimize the use of active personal dosemeters (APDs) in interventional radiology. Interventional radiology procedures can be very complex and they can lead to relatively high doses to medical staff that stand close to the primary radiation field and are mostly exposed to radiation scattered by the patient. For the adequate dosimetry of these scattered photons, APDs must be able to respond to low-energy [10-100 keV] and pulsed radiation with relatively high instantaneous dose rates. Very few devices can detect low energy radiation fields and none of them are specially designed for working in pulsed radia-

tion fields. In this context, the tasks planned during this project are:

- make a study of the behaviour of commercial APDs under laboratory conditions (angular and energy response, effect of dose rate) and in real hospital conditions
- prepare guidelines for the use of APDs in interventional radiology, to define corrections for the APDs that are currently in use.
- work on a prototype of an improved APD for interventional radiology. The new developments are performed together with the manufacturer MGPInstruments

The work achieved so far consisted in first studying the real radiation field characteristics encountered in interventional radiology in terms of energy, angular distribution, dose rate and pulse characteristics. These data were gathered through questionnaires sent to hospitals, literature and quality control outputs. Second, a selection of APDs deemed suitable for application in interventional radiology was made. Thirdly, the behaviour of these selected APDs was studied by measurements under laboratory conditions, in continuous fields. The tests in continuous mode show that the response of the tested APDs fulfils the ISO 61526 standard requirements. Most of them present a satisfactory response at low energies from 24 keV, which is sufficient for interventional radiology. Most APDs can stand high dose rates up to 10 $Sv.h^{-1}$.

D. Work package 4: Extremity dosimetry in nuclear medicine

To evaluate extremity doses and dose distributions across the hands of medical staff working in nuclear medicine departments, an extensive measurement program has started in various hospitals in Europe. A measurement protocol elaborated by the WP4 members covers the fields of nuclear medicine diagnostics and therapy, including two different phases: preparation and injection. Preliminary data are already available from several European hospitals. Most measurements have been done for Tc^{99m} and F^{18} isotopes.
Analogous to the measuring protocol, a simulation protocol has been elaborated covering again diagnostic and therapeutic procedures, as well as both processes, preparation and injection.
Simulations are based on different scenarios with different hand phantoms representing most typical hand positions during preparation and/or injection. Some of these hand phantoms were produced out of paraffin. They were scanned, voxelized and introduced in the simulation code input file.
MCNPX-based simulations using the same scenario were performed by different institutes. As expected, similar results were obtained. Within WP4, two simulations codes are used, MCNPX and PENELOPE. Results obtained with both codes were consistent.
A program has been established to validate simulations with measurements. Three different institutes performed the measurements for the different scenarios with the hand phantoms. The same scenarios will be simulated. Preliminary results showed a good agreement between the measurements and simulations.

E. Work package 5: Training and dissemination

One of the main general objectives of ORAMED is to disseminate the work in progress in the project and to make the developed knowledge accessible and usable to stakeholders. This task is coordinated from Work package 5. One of the first milestones has been to set up a project website, which includes a public and a restricted part: www.oramed-fp7.eu. The public part contains the description of the research objectives and activities, the list of participants, the main events in the field and the training activities. A periodic up-date of the progress of the work is foreseen.

III. CONCLUSIONS

The ORAMED project will run untill the beginning of 2011. The outcome of the project will improve the radiation protection standards for medical staff. The systematic measurements and simulations will be compared to the existing scattered data, so that conclusions can be reached on the occupational doses and protection measures. In particular, the developments on the eye-lens dosimetry and the active personal dosemeters will result in an improvement of the practical measurement capabilities in the field.

ACKNOWLEDGMENT

The research leading to these results has received funding from the European Atomic Energy Community's Seventh Framework Programme (FP7/2007-2011) under grant agreement n° 211361.

REFERENCES

1. Vanhavere F, Carinou E et al. (2008) An overview on extremity dosimetry in medical applications. Radiat Prot Dosim 129:350–355

2. Donadille L, Carinou E et al. (2008) An overview of the use of extremity dosemeters in some European countries for medical applications. Radiat Prot Dosim 13:62-66

Use macro [author address] to enter the address of the corresponding author:

Author: Filip Vanhavere
Institute: Belgian Nuclear Research Centre SCK-CEN
Street: Boeretang 200
City: 2400 Mol
Country: Belgium
Email: filip.vanhavere@sckcen.be

Radiation Dose to Patients from Radiopharmaceuticals

S.Mattsson[1], L.Johansson[2], J.Liniecki[3], D.Nosske[4], M.Stabin[5], S.Leide-Svegborn[1], D.Taylor[6]

ICRP Task Group on Radiation Dose to Patients from Radiopharmaceuticals

[1]Medical Radiation Physics, Dept of Clinical Sciences, Malmö, Lund University, Malmö University Hospital, SE-205 02 Malmö, Sweden

[2] Radiation Physics, Department of Radiation Sciences, Umeå University, Norrland University Hospital, SE-901 87 Umeå, Sweden

[3]Department of Nuclear Medicine, Medical University, PL-92216 Lodz, Poland

[4]Bundesamt für Strahlenschutz, Institut für Strahlenhygiene, DE-85758 Oberschleißheim, Germany

[5]Department of Radiology and Radiological Sciences, Vanderbilt University, Nashville, TN 37232-2675, USA

[6]School of Chemistry, Cardiff University, Cardiff, CF10 3TB Wales, UK

***Abstract*— A Task Group within ICRP Committee 2 and 3 is continuously working to improve absorbed dose estimates to patients investigated with radiopharmaceuticals. The work deals with reviews of the literature, the initiation of new studies – and often to carry them out in-house.**

Dose calculations have up to now been done using the MIRD formalism. Recently, a new addendum to ICRP Publication 53 has been published under the name of ICRP Publication 106. This paper presents the ongoing work within the Task Group.

Keywords— **Radiation dose, Patients, Radiopharmaceuticals, Nuclear Medicine**

I. Introduction

This paper describes the work within the International Commission on Radiological Protection (ICRP) Task Group "Radiation Dose to Patients from Radiopharmaceuticals". In view of the importance of absorbed dose estimates in diagnostic nuclear medicine, this group was appointed early in the 1980s as a Task Group of ICRP Committee 2 and later converted to a Joint Task Group with Committee 3:

_ to provide biokinetic models, absorbed doses, and effective doses using ICRP dosimetry for current and new radiopharmaceuticals which have come into use since Publication 17 [1]; and

_ to supply estimated absorbed and effective doses to patients, including the range of variation to be expected in pathological states, for adults, children, and the embryo and foetus.

In 1987, ICRP published a report entitled 'Radiation dose to patients from radiopharmaceuticals' (Publication 53) [2]. This report contained calculations of absorbed doses per unit activity administered for some 120 radiopharmaceuticals in regular use at the time. A first addendum to Publication 53 was included in ICRP Publication 62 [3]. This contained biokinetic and dosimetric data for six new radiopharmaceuticals, and a table of effective doses per unit administered activity for those radiopharmaceuticals that had been discussed in Publication 53. In the second addendum to Publication 53 (ICRP Publication 80) [4], the Task Group presented biokinetic and dosimetric data on 10 new radiopharmaceuticals, and recalculations of dose data for 19 of the most frequently used radiopharmaceuticals in Publication 53. A number of minor corrections and recalculations of older data were also provided at that time. In a third printed amendment [5] to Publication 53, dosimetric and biokinetic data are provided for 33 radiopharmaceuticals in current use. The report also includes recommendations relating to breast-feeding for mothers who have undergone nuclear medicine procedures.

II. Methodology

The data on each substance are presented in three subsections: biokinetic model, biokinetic data, and table of ab-

O. Dössel and W.C. Schlegel (Eds.): WC 2009, IFMBE Proceedings 25/III, pp. 474–477, 2009.
www.springerlink.com

sorbed dose per unit of activity administered. Unless otherwise stated, the model refers to intravenous administration.
The calculations were based on biokinetic models and best estimates of biokinetic data for individual radiopharmaceuticals. Furthermore for consistency, standardised biokinetic or dosimetric models were used for the dose calculations. For the bladder, a voiding period of 3.5 hours was used. For the G-I tract, the former ICRP G-I tract model [6] was applied. Also a kinetic model for substances excreted via the liver and gallbladder was introduced and used in this report. For activity distributed in circulating blood, the fractional blood volume, or, for short-lived radionuclides, the fractional cardiac output was considered for assessing the distribution of the radioactive source in the body [7].
The rates of the biological processes, for example uptake, metabolism, and excretion, are usually given as the half-time of the corresponding exponential function (see example, Table 1). If the process is assumed to be multi-exponential, the fraction of the organ content belonging to each exponential component is given in brackets immediately after the half-time figure. When rates are given as fractions per time unit (k) as reported in the cited publications, they are transformed into half-times; T = 0.693/k.
The following abbreviations have been used:
S - Source organ or tissue
F_s - Fractional distribution to organ or tissue S
T - Biological half-time for an uptake or elimination component
a - Fraction of F_s taken up or eliminated with the corresponding half-time. A negative value indicates an uptake phase.
$\tilde{A}_s=A_o$ Cumulated activity in organ or tissue S per unit of administered activity.

The tables sometimes contain empty spaces under the headings T and a, usually because the kinetics are described by complex exponential, or non-exponential, expressions, which cannot easily be defined in the table. This is the case, for example, for activity in the gastrointestinal tract, the gallbladder, and the urinary bladder. In these cases, the tables present only the cumulated activities together with the fractional distributions.
The relative cumulated activities are presented in hours (h). Average organ or tissue absorbed doses are given as milligrays (mGy) per megabecquerel (MBq).
The effective dose is given as millisieverts (mSv) per MBq.
Dose calculations have been performed for adults and 15-, 10-, 5-, and 1-year-old children (see example, Table 2). The organs (or tissues) are presented in alphabetical order except 'Remaining organs', which is placed at the end. The dose to organs or tissues not mentioned in the table can usually be approximated with the value given for 'Remaining organs'.

For the dose calculations, the MIRD method has been used based on the mathematical phantom and hence S-values from MIRD Pamphlet 11 [8]. For children, absorbed fractions from Cristy and Eckerman [9] were utilised for the dose calculations. For bone tissue dosimetry, a refined model from Eckerman and Stabin [10] was used.

Table 1. Example of biokinetic tables for a radiopharmaceutical (^{111}In octreotide)

Organ (S)	F_s	T (h)	a	$\tilde{A}_s/A_0$(h)
Thyroid	0.001	60	1.0	0.046
Kidneys	0.06	60	1.0	2.8
Liver	0.06	2.0	0.40	2.6
		60	0.30	
		1680	0.30	
Spleen	0.05	60	1.0	2.3
Other organs and tissues	0.829	3.0	0.90	6.9
		60	0.10	
Urinary bladder contents	1.0			
Adult, 15 years, 10 years				1.7
5 years				1.4
1 year				0.91

Table 2. Example of dosimetric tables for a radiopharmaceutical (^{111}In octreotide)

	Absorbed dose per unit activity administered (mGy/MBq)				
Organ	Adult	15 years	10 years	5 years	1 year
Adrenals	5.8E-02	7.5E-02	1.1E-01	1.7E-01	2.9E-01
Bladder	2.0E-01	2.5E-01	3.7E-01	4.6E-01	5.6E-01
Bone surfaces	2.7E-02	3.3E-02	5.0E-02	7.5E-02	1.4E-01
Brain	9.6E-03	1.2E-02	2.0E-02	3.2E-02	5.7E-02
Breasts	1.2E-02	1.5E-02	2.3E-02	3.7E-02	6.7E-02
Gallbladder	5.2E-02	6.3E-02	9.2E-02	1.4E-01	2.2E-01
Gastrointestinal tract					
Stomach	4.3E-02	5.0E-02	7.7E-02	1.1E-01	1.8E-01
Small intestine	2.9E-02	3.7E-02	5.9E-02	9.0E-02	1.5E-01
Colon	2.9E-02	3.5E-02	5.5E-02	8.6E-02	1.4E-01
(Upper large intestine	3.0E-02	3.7E-02	5.8E-02	9.4E-02	1.5E-01)
(Lower large intestine	2.7E-02	3.3E-02	5.2E-02	7.5E-02	1.2E-01)
Heart	2.5E-02	3.2E-02	4.8E-02	7.0E-02	1.2E-01
Kidneys	4.1E-01	4.9E-01	6.7E-01	9.6E-01	1.6E+00
Liver	1.0E-01	1.3E-01	2.0E-01	2.7E-01	4.8E-01
Lungs	2.3E-02	3.0E-02	4.4E-02	6.7E-02	1.2E-01
Muscles	2.0E-02	2.6E-02	3.8E-02	5.6E-02	1.0E-01
Oesophagus	1.4E-02	1.8E-02	2.7E-02	4.3E-02	7.7E-02
Ovaries	2.7E-02	3.5E-02	5.3E-02	8.0E-02	1.3E-01
Pancreas	7.2E-02	8.8E-02	1.3E-01	2.0E-01	3.2E-01
Red marrow	2.2E-02	2.6E-02	3.9E-02	5.3E-02	8.5E-02
Skin	1.1E-02	1.3E-02	2.1E-02	3.2E-02	5.9E-02
Spleen	5.7E-01	7.9E-01	1.2E+00	1.8E+00	3.1E+00
Testes	1.7E-02	2.2E-02	3.7E-02	5.4E-02	8.7E-02
Thymus	1.4E-02	1.8E-02	2.7E-02	4.3E-02	7.7E-02
Thyroid	7.5E-02	1.2E-01	1.8E-01	3.7E-01	6.8E-01
Uterus	3.9E-02	4.9E-02	7.7E-02	1.1E-01	1.6E-01
Remaining organs	2.4E-02	3.2E-02	4.9E-02	8.0E-02	1.3E-01
Effective dose (mSv/MBq)	5.4E-02	7.1E-02	1.1E-01	1.6E-01	2.6E-01

III. RESULTS

Table 3 shows where to find the most recent ICRP information about a specific substance.

Table 3. Location of the most recent information for specific compounds in the relevant ICRP publications.

Radiopharmaceutical	*Publication 106*	*Publication 80*	*Publication 53*
^{3}H-neutral fat, free fatty acids		x	
^{11}C-acetate	x		
^{11}C-amino acids (generic model)	x		
^{11}C-brain receptor substances (generic model)	x		
^{11}C-methionine	x		
^{11}C-thymidine		x	
^{11}C (realistic maximum model)	x		
^{14}C-neutral fat, free fatty acids		x	
^{14}C-urea		x	
^{15}O-water	x		
^{18}F-amino acids (generic model)	x		
^{18}F-brain receptor substances (generic model)	x		
^{18}F-FDG	x		
^{18}F-L-dopa	x		
^{51}Cr-EDTA		x	
^{67}Ga-citrate		x	
^{68}Ga-EDTA		x	
^{75}Se-amino acids	x		
^{75}Se-HCAT		x	
^{99m}Tc-apticide	x		
^{99m}Tc-colloids (small) (intratumoral injection)	x		
^{99m}Tc-EC (normal renal funkt)	x		
^{99m}Tc-ECD	x		
^{99m}Tc-furifosmin	x		
^{99m}Tc-HIG		x	
^{99m}Tc-HM-PAO		x	
^{99m}Tc-IDA derivatives		x	
^{99m}Tc-MAA (normal renal funkt)		x	
^{99m}Tc-MAG3		x	
^{99m}Tc-markers, non-absorbable		x	
^{99m}Tc-MIBI		x	
^{99m}Tc-monoclonal antibodies/fragments	x		
^{99m}Tc-pertechnegas		x	
^{99m}Tc-pertechnetate		x	
^{99m}Tc-phosphates and phosphonates		x	
^{99m}Tc-RBC		x	
^{99m}Tc-Technegas		x	
^{99m}Tc-tetrofosmin (rest/exercise)	x		
^{99m}Tc-WBC		x	
^{111}In-HIG		x	
^{111}In-monoclonal antibodies/fragments	x		
^{111}In-octreotide	x		
^{123}I-iodide			x
^{123}I-iodo hippurate		x	
^{123}I-fatty acids (BMIPP/IPPA)	x		
^{123}I-brain receptor substances (generic model)	x		
^{123}I-MIBG		x	
^{123}I-monoclonal antibodies/fragments	x		
^{124}I-iodide			x
^{125}I-iodide			x
^{131}I-iodide			x
^{131}I-iodo hippurate		x	
^{131}I-monoclonal antibodies/fragments	x		
^{131}I-norcholesterol		x	
^{201}Tl-ion	x		

Effective dose from various radiopharmaceuticals

The quantity 'Effective dose' [11] can be of practical value for comparing the relative doses related to stochastic effects from: different diagnostic examinations and interventional procedures; the use of similar technologies and procedures in different hospitals and countries; and the use of different technologies for the same medical examination provided that the representative patients or patient populations for which the effective doses are derived are similar with regard to age and gender. However, comparisons of effective doses are inappropriate when there are significant dissimilarities between the age and gender distributions of the representative patients or patient populations being compared (e.g. children, all females, elderly populations) and the Commission's reference distribution of both genders and all ages. This is a consequence of the fact that the magnitudes of risk for stochastic effects are dependent on age and gender. Risk assessment for medical uses of ionising radiation is best evaluated using appropriate risk values for the individual tissues at risk, and for the age and gender distribution of the population groups undergoing the medical procedures.

For the exposure of young children, the risk would be higher, perhaps by a factor of two or three [12]. For many common types of diagnostic examinations, the higher risk will be offset by the reduction in administered activity relative to that to an adult. For an age at exposure of approximately 60 years, the risk would be lower, perhaps by a factor of three and will decrease somewhat thereafter [12]. The specific demographics of the medically exposed population raise issues related to the application of the concept of effective dose as a tool for comparing doses from medical irradiation with other sources of exposure to humans. Nonetheless, the quantity continues to be calculated for diagnostic pharmaceuticals and its use for summarizing and comparing dose between radiopharmaceuticals and other procedures involving ionising radiation has been widely accepted in the scientific and clinical communities.

Table 4. Eff dose per unit activity administered (for adults)

Radiopharmaceutical	*mSv/MBq*
^{3}H-neutral fat, free fatty acids	0.22
^{11}C-acetate	0.0035
^{11}C-amino acids (generic model)	0.0056
^{11}C-brain receptor substances (generic model)	0.0043

^{11}C-methionine	0.0084
^{11}C-thymidine [methyl-^{11}C]thymidine	0.0035
^{11}C-thymidine [2-^{11}C]thymidine	0.0027
^{11}C (realistic maximum model)	0.011
^{14}C-neutral fat, free fatty acids	0.21
^{14}C-urea (normal/*Helicobacter* positive)	0.031/0.081
^{15}O-water	0.0011
^{18}F-amino acids (generic model)	0.023
^{18}F-brain receptor substances (generic model)	0.028
^{18}F-FDG	0.019
^{18}F-L-dopa	0.025
^{51}Cr-EDTA	0.0020
^{67}Ga-citrate	0.10
^{68}Ga-EDTA	0.040
^{75}Se-amino acids	2.2
^{75}Se-HCAT	0.69
^{99m}Tc-apticide	0.0047
^{99m}Tc-colloids (large)	0.0094
^{99m}Tc-colloids (small), intratumoral inj	0.0012
^{99m}Tc-DMSA	0.0088
^{99m}Tc-DTPA	0.0049
^{99m}Tc-EC	0.0063
^{99m}Tc-ECD	0.0077
^{99m}Tc-furifosmin (rest/exercise)	0.010/0.0089
^{99m}Tc-HIG	0.0070
^{99m}Tc-HM-PAO	0.0093
^{99m}Tc-IDA derivatives	0.017
^{99m}Tc-MAA	0.011
^{99m}Tc-MAG3	0.0070
^{99m}Tc-markers, non-absorbable (fluids/solids) *per os*	0.019/0.024
^{99m}Tc-MIBI (rest/exercise)	0.0090/0.0079
^{99m}Tc-monoclonal antibodies Intact ab/F(ab´)$_2$-fragm/F(ab´)-fragm	0.0098/0.0097/0.011
^{99m}Tc-pertechnegas	0.012
^{99m}Tc-pertechnetate (without/with blocking)	0.013/0.0042
^{99m}Tc-phosphates and phosphonates	0.0057
^{99m}Tc-RBC	0.0070
^{99m}Tc-Technegas	0.015
^{99m}Tc-tetrofosmin (rest/exercise)	0.0069/0.0069
^{99m}Tc-WBC	0.011
^{111}In-HIG	0.017
^{111}In-monoclonal antibodies Intact ab/F(ab´)$_2$-fragm/F(ab´)-fragm	0.22/0.20/0.20
^{111}In-octreotide	0.054
^{123}I-iodide, 35% thyr up (without/with blocking)	0.22/0.01
^{123}I-iodo hippurate	0.012
^{123}I-fatty acids (BMIPP/IPPA)	0.016/0.016
^{123}I-brain receptor substances (generic model)	0.050
^{123}I-MIBG	0.013
^{123}I-monoclonal antibodies Intact ab/F(ab´)$_2$-fragm/F(ab´)-fragm	0.026/0.019/0.017
^{124}I-iodide, 35% thyr up (without/with blocking)	15/0.1
^{125}I-iodide, 35% thyr up (without/with blocking)	14/0.01
^{131}I-iodide, 35% thyr up (without/with blocking)	24/0.06
^{131}I-iodo hippurate	0.052
^{131}I-monoclonal antibodies Intact ab/F(ab´)$_2$-fragm/F(ab´)-fragm	0.42/0.14/0.11
^{131}I-norcholesterol	1.8
^{201}Tl-ion	0.14

IV. CONCLUSIONS

Updated information about mean absorbed doses to organs and tissues of patients of various ages are now available for over 40 radiopharmaceuticals in common use. There are also a number of generic models and realistic maximum models covering other large groups of substances (e.g. "^{11}C labeled fatty acids").

ACKNOWLEDGMENT

This project has been supported by ICRP and the Swedish Radiation Safety Authority. It was partially carried out within the Collaborative Project "MADEIRA", cofounded by the European Commission through EURATOM Seventh Framework Programme (Grant Agreement FP7-212100).

REFERENCES

1. ICRP, 1971. Protection of the patient in radionuclide investigations. ICRP Publ 17. Pergamon Press, Oxford.
2. ICRP, 1987. Radiation dose to patients from radiopharmaceuticals. ICRP Publ 53. Ann. ICRP 18(1-4).
3. ICRP, 1991. Radiation dose to patients from radiopharmaceuticals. Addendum 1 to ICRP Publication 53, in: Radiological protection in biomedical research. ICRP Publ 62. Ann. ICRP 22(3).
4. ICRP, 1998. Radiation dose to patients from radiopharmaceuticals. Addendum 2 to ICRP Publication 53., ICRP Publ 80. Ann. ICRP 28(3).
5. ICRP, 2008. Radiation dose to patients from radiopharmaceuticals. A third amendment to ICRP Publication 53. ICRP Publ 106. Ann. ICRP 38(1-2).
6. ICRP 1979. Limits for intakes of radionuclides by workers. ICRP Publ 30, Part 1. Ann ICRP 2(3-4).
7. ICRP 2002. Basic anatomical and physiological data for use in radiological protection: reference values. ICRP Publ 89. Ann ICRP 31(3-4).
8. Snyder W S, Ford M R, Warner G G, Watson S B, 1975. S absorbed dose per unit cumulated activity for selected radionuclides and organs. MIRD Pamphl 11, New York, USA, Society of Nuclear Medicine.
9. Cristy M, Eckerman K. Specific absorbed fractions of energy at various ages from internal photon sources. Oak Ridge National Laboratory, Oak Ridge, TN, USA, 1987, ORNL/TM-8381.
10. Eckerman K, Stabin M, 2000. Electron absorbed fractions and dose conversion factors for marrow and bone by selected regions. Health Phys 78, 199-214.
11. ICRP 2007. The 2007 recommendations of the international commission on radiological protection. ICRP Publ 103. Ann ICRP 37(1-3).
12. ICRP, 1991. 1990 Recommendations of the International Commission on Radiological Protection. ICRP Publ 60. Ann. ICRP 21(1–3).

Author: S. Mattsson
Institute: Medical Radiation Physics, IKVM, Lund University
Street: Malmö University Hospital
City: SE-205 02 Malmö
Country: Sweden
Email: soren.mattsson@med.lu.se

Alanine Dosimetry – A Versatile Dosimetric Tool

D. Regulla

Institute of Radiation Protection, Helmholtz Zentrum München – German Research Center for Environmental Health, Neuherberg, Germany

Abstract—**ESR spectroscopy using amino acid alanine as sensor material has developed ability, in the recent past, for outstanding and versatile dosimetry. Physically the method makes use of the radiation induced generation of free radicals in alanine: ESR spectroscopy serves for identification of the free radical type and for quantification of its concentration which corresponds linearly to the given radiation dose, in a wide dose range. Alanine/ESR dosimetry has reached acceptance as a leading technology in high-dose standardisation, world-wide. Currently it is high-ranking in therapy level dosimetry for clinical applications and used for reference metrology in postal dose intercomparisons aiming at both high-energy photon and electron radiation. Alanine/ESR dosimetry has qualified to compete Fricke dosimetry and complement ionization chamber dosimetry, with respect to high reliability, low uncertainty, small size and easy handling. The present review reports on the evolution of alanine/ESR dosimetry and on its established dosimetric properties up to the current state-of-the-art. The review has an eye also on international reports and recommendations dealing with alanine/ESR dosimetry, e.g. published by ICRU, ISO, IAEA.**

Keywords— **ESR spectroscopy, dosimetry, alanine, metrology.**

I. INTRODUCTION

In the current situation of a changing research world, creative ideas and new applications are most essential and valuable, also in dosimetry. It has been electron spin resonance spectroscopy (ESR) that, soon after its invention at Kazan State University by the Soviet physicist Yevgeny Zavoisky in 1944, was found to detect radiation effects in ferromagnetic media accessible for measurement. Measurements have first been applied to date geological, archaeological, and paleontological materials back millions of years, useful also for hominid and animal fossils. In the seventies, the growing field of industrial radiation application, under the aspects of health, safety and economy, has soon been recognised to require a reliable and accurate measuring technique to identify irradiated food, determine the dose applied and reproduce radiation effects.

At the same time a novel alanine based ESR method has been developed at Helmholtz Zentrum München for precision dosimetry capable to meet the requirements of IAEA to high-level transfer dosimetry and later on to therapy level metrology [1]. This method offered measurement reliability, precision and easy use, from the very beginning. ESR became soon a decisive scientific tool for dosimetric application in routine and metrology [2-6].

Half a decade later the Agency established the International Dose Assurance Service (IDAS) to the member states of IAEA based on a meanwhile standardised alanine/ESR technique, operated as a joint project between IAEA and Helmholtz Zentrum München [7]. Since 1991 the Agency continues to offer IDAS successfully as an exclusive service supplier.

II. ALANINE/ESR SYSTEM

Alanine/ESR dosimetry uses organic crystalline amino acids (e.g. alanine, CH_3-$CHNH_2$-COOH) as a measuring material and free radicals as the radiation effect accessible for measurement [8]. It has become an important tool in low to high range radiation dosimetry of low and high LET (linear energy transfer) ionizing radiation. The method is applicable to different types of radiation as well as, within limits, in mixed radiation fields, e.g. x and gamma rays, beta radiation, accelerator electrons, as well as protons, neutrons, and ions.

The free radicals in crystalline bio molecules are relatively stable interim products in a chain of events, that similar to tissue start with the absorption of radiation energy. Since free radicals take key positions in the chain of events which lead to biological damage in cell structures, the quantification of free radicals can even be considered a biologically relevant dosimetry.

A. Instrumentation

The alanine dosimetry system is operated using sophisticated research ESR spectrometers in the X band microwaves with the samples positioned inside a Suprasil quartz tube. Routine dosimetry can make use of still large table-top ESR spectrometers with permanent magnets. A pitch-activated alanine detector type or the use of an in-cavity Mn^{++} standard offer approaches to introduce individual calibration factors for alanine samples. The use of a constant rotation goniometer reduces the effect of response anisotropy and results in reduced detection limits. Large-scale alanine dosimetry services in national or international

O. Dössel and W.C. Schlegel (Eds.): WC 2009, IFMBE Proceedings 25/III, pp. 478–481, 2009.
www.springerlink.com

quality control can profit from automated sample changers by robot or magazine type mechanisms.

Most of the ESR spectrometers used in dosimetry are of high metrological quality and hence settled at high cost levels. Sufficiently precise table top spectrometers at a cost level affordable for clinical use in radiotherapy departments are not yet available. But future ESR applications, e.g. for in situ oriented biological or human based ESR dosimetry techniques, will probably provide the economical availability of even differing types of ESR spectrometers, potentially applying different microwave bands and magnetic field strengths. With the development of compact ESR spectrometers for these purposes, alanine/ESR will become more attractive for use also in routine clinical dosimetry.

B. Alanine probes

The alanine probes should be of high analytical-grade purity for sufficient metrological quality, e.g. L or DL alanine. Already the pure alanine powder without further processing may be used for dosimetry. To be used as a measuring probe, the polycrystalline powders are encapsulated or imbedded in paraffin wax with the melting point at sufficiently high-temperature. The wax-based probes allow the production of pellets (e.g. cylinders of 5 mm dia. x 5 mm length) and films (e.g. 5 mm dia. x 0.2 mm thickness) fitting the type of radiation or the dimensions of the microwave measurement cavity.

C. System components

The alanine/ESR measuring system provides the availability of an appropriate "system" as well as of qualified personnel with know-how, experience and care. The essential system components are:

- Appropriate alanine probes
- High performance ESR spectrometer operated in a temperature and humidity controlled laboratory by a skilled operator
- Calibration facilities providing radiation sources for the respective dose range and ensuring sufficient precision in dose application
- Software to control the ESR spectrometer and the ancillary equipment as well as to evaluate the doses
- Dosimeters of secondary standard or reference quality level, whose calibration is traceable to the primary standards of national laboratories (Fricke dosimetry, calorimetry, ionisation chamber dosimetry).

Prototypes of automatic sample changers for commercial ESR spectrometers are under development.

D. Data analysis

Both the reaction mechanism and the ESR spectrum of irradiated alanine are complex and neither has yet been fully elucidated. There are five main peaks in the ESR alanine spectrum. Usually, the central peak amplitude is chosen to perform dose measurements because it is the largest accessible signal. This method is fast and has a good precision when relatively high-doses are used, but has a higher degree of uncertainty when low-doses are concerned, due to essentially the low signal-to-noise and the influence of the baseline distortions.

ESR spectra of alanine irradiated to doses below 5 Gy are affected by a varying non-linear background which mainly influences the lower limit of detection in alanine/ESR dosimetry. A mathematical method based on Fast Fourier Transform has meanwhile been developed capable to filter background and simultaneously noise in the frequency domain of ESR spectra [9]; it provides significantly higher resolved alanine/ESR signals and this down to about 50 mGy. A linear increase of the ESR signal was found above 200 mGy when plotted versus absorbed dose, after correction for background and predose due to environmental exposure.

E. Dosimetric properties

The following data on dosimetric properties of alanine /ESR dosimetry are given for orientation: There is a linear, at dose levels above about 10 Gy exponentially saturating relationship between the concentration of radicals or spins in irradiated alanine and the absorbed dose. With an effective atomic number of roughly 7.2 (for comparison, soft tissue ≈ 7.4) the response of alanine to photon radiation was found to be independent of photon energy above 100 keV, and above 1 MeV for electron radiation. No dose rate effect has been detected at 1 kGy up to 10^{11} Gyh^{-1}; detectable dose rate effects have been found only above 20 kGy. Alanine probes are re-readable, and thus allow a kind of signal documentation, apart from measuring single and cumulating dose fractions; they can be used as reference probes for spectrometer settings over long periods of storage time, provided they are kept at room temperature or in a fridge. There is negligible influence of irradiation temperature on radical yield up to 70 °C ($k_\theta = 0.0018$ $°C^{-1}$ up to doses of 40 kGy). The fading of the alanine/EPR response depends on radiation quality and is negligibly small at room temperature for low-LET radiation, but more pronounced for high-LET radiation. Batch homogeneity can be achieved with ≤ 0.5 % (1 s.d.), re-read of an individual probe is as low as 0.1 % (1 s.d.). More details on dosimetric properties can be found in ICRU Report 80 [10].

Precision of ≤ ± 0.5% (1 s.d.) has been achieved in the dose range from 10 Gy up to 100 kGy. Poorer precision at doses ≤ 10 Gy was found to be due to a variable non-radiation induced ESR background signal from the alanine probes within a batch, provided modern X-band ESR spectrometers are used.

F. Reference and transfer dosimetry

Because of the earlier absence of relevant high-level dosimetry techniques at national and primary standard dosimetry laboratories, it has been the IAEA that, for long time, has played a central role in stipulating research and development for high-dose standardisation and alanine/ESR dosimetry. The Agency supported moreover the co-ordination, organisation and operation of alanine/ESR based international dose intercomparison programs, serving for accredited UN member states who asked for dosimetric guidance in radiation processing aimed at product finishing, sterilization and food preservation.

A remarkable number of acknowledged metrology institutions world-wide has meanwhile started to use the alanine/ESR technique for quality control programs in radiation processing. To the author's knowledge, it is at least Denmark, England, Germany, France, Italy, the Nordic countries, further Australia, Canada, China, Japan, Ukraine, USA, and a concerted action of Asian countries. All the mentioned activities have made use of the alanine/ESR technique similar to the IAEA/IDAS programme, i.e. they apply this technique for reference and transfer metrology.

G. Calibration

Alanine is capable of being used either as reference or as routine dosimeter and should be calibrated accordingly. At lower energies, dosimeters should be calibrated for the type and energy of radiation in which they will be used routinely. Calibration curves are fixed with a number of reference alanine probes; the curves are independent of the type of ESR spectrometer. Hence the curves are transferable; the respective yield can be fixed by mailing just one alanine probe only, irradiated with an appropriate reference dose.

H. Therapy-level dosimetry

The dosimetric properties of the alanine/ESR dosimetry have always been investigated with an eye on application in radiation therapy. Today, this meets well the requirements of modern conformal radiotherapy techniques, e.g. brachy therapy, helical tomotherapy and intensity modulated radiation therapy. These techniques represent a particular challenge for novel dosimetry solutions complementing the established dosimetry techniques. The advantages of alanine/ESR dosimetry in this field are evident, e.g. the dynamic dose range, the archival character of dose information based on a non-destructive readout that allows for repeated ESR measurements and sample storage, the tissue equivalency of probe material and the small probe size. The latter property makes the method applicable also in high-energy radiation dosimetry without the impact of perturbation and displacement effects as known from ionisation chamber dosimetry.

It is again the Agency which at an early stage has organised alanine/ESR intercomparisons in the therapy-level dose range and has later established a Co-ordinated Research Project aimed to implement alanine/ESR dosimetry into an IDAS-type quality assurance service [11]. Complementary investigations are reported on the use of alanine ESR dosimetry in proton therapy.

Today, a number of metrology laboratories use ESR/alanine dosimetry as a secondary standard for the dose to water, because of good water equivalence and small probe size.

I. Standards and recommendations

Principles, quantities and procedures used in the alanine/ESR dosimetric technology are described in an ASTM standard which has later been converted into an ISO standard [12]. ICRU has recently published a document on "Dosimetry systems for use in radiation processing" dealing with alanine/ESR dosimetry at full length [10]. It will be of great interest and need for public acceptance, benefit and health as far as dosimetry in radiation preserved food, sterilised pharmaceuticals, medical and health care products and in quality assurance of radiation therapy is concerned. The international and national bodies should initiate further recommendations and technical documents, on the basis of available international expertise.

III. Conclusions

Thirty years of research have substantiated ESR spectrometry to encompass reliably major key sector areas in quantifying radiation, e.g. transfer and secondary standard dosimetry, cancer treatment and radiation processing, dosimetry control of food irradiation and retrospective dosimetry of accidentally exposed humans or animals using natural body tissues. The potential and diversity of ESR in physical and biophysical dosimetry appears unrivalled, world-wide, by any of the other established traditional dosimetry methods; this was highlighted at the ESR Conference on Biodosimetry, Obninsk 1998, by both famous

Co-Presidents, Anatoly Tsyb and Leonid Ilyin: “ESR spectrometry provides the possibility to look into the past of our Earth, the evolution of mankind and its civilization, but also promises to open new landmarks in biophysical and biomedical research as well as prognosis focused to fields of public health and risk”.

Despite the great potential of ESR in dosimetry, the number of research centers engaged worldwide in this field is still relatively small. This may change in future when ESR dosimetry will succeed to offer an individual human *in vivo* and *in situ* dosimetry, or when national laboratories, probably within the global initiative of SSDL networking operated by IAEA/WHO, will decide to expand ESR dosimetry to quality control in medical tumour therapy as well as to radiological or nuclear emergencies. The role of alanine/ESR dosimetry complementing or replacing Fricke dosimetry and other high-level dosimetry techniques in cancer therapy and industrial radiation processing will rise accordingly. Alanine/ESR dosimetry fits dose delivery from clinical accelerators to patients and is ready to serve for implication to mailed transfer dosimetry.

References

1. Regulla DF, Deffner U (1982) Dosimetry by ESR spectroscopy of alanine. Appl. Radiat. Isot. 33: 1101-1114.
2. Sharpe P, Sephton J (2006) Therapy level alanine at the NPL. In: PTB-Dos-51 (M. Anton, Ed.) pp 3-8.
3. Lin M, Ding Y, Cui Y, Chen K (2006) Study of CIAE alanine dosimeter for radiotherapy level. In: PTB-Dos-51 (M. Anton, Ed.) pp 29-34.
4. de Angelis C, Onori S (2006) Alanine dosimetry at ISS. In: PTB-Dos-51 (M. Anton, Ed.) pp 3-8.
5. Desrosiers M, Puhl J, Cooper S (2006) Next-generation services for e-traceability to ionizing radiation national standards. In: PTB-Dos-51 (M. Anton, Ed.) pp 41-45.
6. Anton M (2005) Development of a secondary standard for absorbed dose to water based on the alanine EPR dosimetry system. Appl. Radiat. Isot. 62/5:779-795.
7. Nam WJ, Regulla DF (1989) The significance of the International Dose Assurance Service for radiation processing. Appl Radiat Isot. 40: 953-956.
8. Sagstuen E, Hole EO (2009) Radiation produced radicals. Chapter 9 in Electron Paramagnetic Resonance; A Practitioner's Toolkit (M. Brustolon and E. Giamello, Eds.), J. Wiley & Sons, 2009. ISBN: 978-0-470-25882-8.
9. Ruckerbauer F, Sprunck M, Regulla DF (1996) Numerical signal treatment for optimized alanine/ESR dosimetry in the therapy-level dose range. Appl. Radiat. Isot. 47, 1263-1268.
10. ICRU (2008) Dosimetry systems for use in radiation processing, Journal of the ICRU Vol 8 No 2, Report 80, Oxford University Press, UK, pp 29-33.
11. Nette H.P, Onori S, Fattibene P, Regulla D, Wieser A (1993) Coordinated research efforts for establishing an international radiotherapy dose intercomparison service based on the alanine/ESR system. Appl. Radiat. Isot. 44, 7-11.
12. American Society for Testing and Materials, Standard Practice for Use of the Alanine-EPR Dosimetry System, International Standards Organization & American Society for Testing and Materials, Designation ISO/ASTM 51607: 2004(E).

Bibliography

A condensed review on the development and achievements of EPR dosimetry and applications in the past two and a half decades can be found in the proceedings of the "International Conferences on Biodosimetry and International Symposia on ESR Dosimetry and Applications" held in 1985 (Ube University, Japan: EPR Dating and Dosimetry, Ionics Publ. Co, Ltd., Japan, pp 1-538), 1988 (GSF Neuherberg, Germany: Appl. Radiat. Isot. 40 (1989) pp 829-1246), 1991 (NIST, Gaithersburg, USA: Appl. Radiat. Isot. 44 (1993) pp 1-468), 1995 (GSF Neuherberg, Germany: Appl. Radiat. Isot. 47 (1996) pp 1151-1687), 1998 (MRRC/RAMS, Obninsk, Russia: Appl. Radiat. Isot. 52/5 (2000) pp 1019-1392), 2002 (University Sao Paulo, Brazil: Appl. Radiat. Isot. 62 (2005) pp 115-381), 2006 (USUHS, Bethesda MA, USA: Radiat. Meas. 42/6-7 (2007) pp 945-1264) and 2008 (Medical School, Dartmouth, USA: Health Phys., in print). Further review can be found compiled in: "Retrospective Dosimetry - Physical and Biological Aspects", Radiat. Prot. Dosim. 77 (1998) pp 1-138 and in "Alanine Dosimetry for Clinical Application" (M. Anton, Ed.), Report of the 216th PTB Seminar, Report PTB-Dos-51 (2006) pp 1-79.

Author: Dr. Dieter Regulla
Institute: Helmholtz Zentrum München – German Research Center for Environmental Health, Institute of Radiation Protection
Street: Ingolstädter Landstrasse 1
City: 85764 Neuherberg
Country: Germany
Email: regulla@helmholtz-muenchen.de

Three Dimensional Dose Verification of Intensity Modulated Radiosurgery Using Polymer-Gel Dosimetry

Dong-Joon Lee[1], Hyun-Tai Chung[2], Moon-Jun Sohn[1]

[1]Inje University/Dept. of Neurosurgery, Goyang, Korea
[2]Seoul National University, /Dept. of Neurosurgery, Seoul, Korea

Abstract- **Polymer gel 3D dosimetry was used to confirm the accuracy of treatment plans produced by the treatment planning software and assess the dosimetric uncertainties of the radiosurgery procedures. The aim of this study is to investigate the 3D dose distribution of intensity-modulated radiosurgery(IMRS) treatment using polymer gel dosimeter for a selected radiosurgery case. A spherical glass flask(160mm-radius) filled with the polymer gel dosimeter was fixed with in the stereotactic head frame. And the intensity-modulated radiosurgery(IMRS) treatment procedure was simulated to a selected preclinical concave shaped pituitary tumor closed to the optic pathway. Images of the gel dosimeter were acquired using a Simens 1.5T MR imager. The images transferred to a planning computer for which a data analysis and compare to dose distribution produced by planning software. Reasonable agreement was observed at medium and high doses (50%-80% isodose lines) although differences of up to 10% were observed at low doses (30% isodose line) between the treat-ment planning system calculation of relative dose distribution and the gel measured data. The gel dosimeter measured dose profiles of pre-planned beams agree within 3% with the beam profiles produced by planning software. The polymer gel dosimeter in combination with MR imaging has been shown to be a valuable devices for verifying three-dimensional IMRS dose distribution.**

Keywords- **3D, Dose verification, IMRS, Gel-dosimetry**

I. Introduction

Stereotactic radiosurgery or hypo-fractionated radiotherapy is used for the treatment of small volume lesions in intra-cranial and body region. Several QA programs for evaluate the dosimetric accuracy of the radiosurgery have been proposed, but dosimetry techniques are limited to point/2D dose measurement by ion chamber, diodes, solid state dosimeter such as TLDs or 2D dose mapping by planar film, 2D array diodes etc.

II. Writing the paper

Purpose

In this study, polymer-gel 3D dosimetry was used to confirm the accuracy of treatment plans produced by the treatment planning software and assess the dosimetric uncertainties of the radiosurgery procedures.

The aim of this study is to investigate the 3D dose distribution of intensity-modulated radiosurgery(IMRS) treatment using polymer gel dosimeter for a selected radiosurgery case.

Material and Methods

A spherical glass flask (160mm-radius) filled with the tissue equivalent polymer gel dosimeter was fixed with in the stereotactic head frame. And the intensity-modulated radiosurgery(IMRS) treatment procedure was simulated to a spherical polymer gel phantom as same as a selected preclinical concave shaped pituitary tumor closed to the optic pathway. Dosimetric verification was performed using commercial polymer gel phantoms from MGS Research, Inc. To irradiate the target in glass flask, Novalis radiosurgery system was used. It was commissioned at 6 MV and its collimators shape the beam field by means of 26 pairs of leaves. The maximal field size at isocenter is 10cm x 10cm Dose of 18 Gy was delivered to spherical glass flask as same as treatment dose to pituitary tumor of selected patient. MR imaging study was performed 24 hours after post irradiation. Images of the gel dosimeter were acquired using a Simens 1.5T MR imager. The images transferred to a planning computer for which a data analysis and compare to dose distribution produced by planning software. In order to direct comparison between gel-dosimeter measured and pre-planned selected patient data to be feasible, 2mm thickness image slices were acquired at the same position.

O. Dössel and W.C. Schlegel (Eds.): WC 2009, IFMBE Proceedings 25/III, pp. 482–483, 2009.
www.springerlink.com

Fig. 1. Experimental set up for verify the 3D dose distribution using gel-dosimeter

Results

3D dose verification using gel-dosimeter shows Reasonable agreement. It was observed at medium and high doses (50%-80% isodose lines) although differences of up to 10% were observed at low doses (30% isodose line). The gel dosimeter measured dose profiles of pre-planned beams agree within 3% at 80% isodose line with the beam profiles produced by planning software.

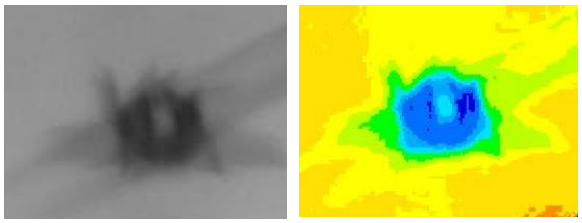

Fig. 2. MR scanned isodose image from Gel-dosimeter.

Discussion

Two dose distributions are compared between the computer planned dosimetry of selected patient' tumor and gel dosimeter measured axial, coronal, sagittal images.

Root mean square differences between the dose profile measured with gel dosimeter and computational pre-planned beams profiles by planning software were within 3% in the high dose gradient regions of 80% isodose line. And spatial deviations were not more than 2.5mm. The 3D dose profile using gel dosimeter shows complied with the pre-determined dose volume constrains.

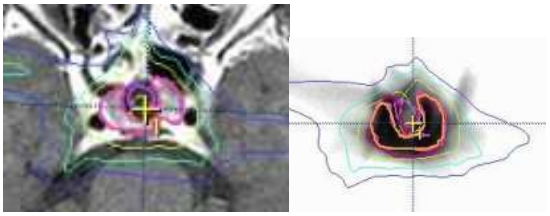

Fig. 3. Computer planned dosimetry of the selected patient' tumor and gel-dosimeter measured its axial image.

III. Conclusions

The polymer gel dosimeter in combination with MR imaging has been shown to be a valuable devices for verifying three-dimensional IMRS dose distribution. IMRS achieve good agreement between pre-computer planned and gel-measured dose distribution for complicated concave shape target volume planning.

References

1. Karaiskos P, Petrokokkinos L, Tatsis E et al. (2005) Dose verifyication of single shot gamma knife applixations using VIPAR polymer gel and MRI. Phys.Med.Biol 50:1235-1250
2. Baras P et al. (2002) The Polymer gel dosimetry using a three-dimensional MRI acquisition technique Med. Phys.29:2506-2516

RADEM - recombination ambient dose equivalent meter for neutron dosimetry around medical accelerators

N. Golnik[1], P. Tulik[2] and W. Bulski[3]

[1] Institute of Metrology and Biomedical Engineering, Warsaw University of Technology, Warsaw, Poland.
[2] Institute of Atomic Energy, Świerk, Poland
[3] Centre of Oncology, Medical Physics Department, Warsaw, Poland

Abstract— **A dose equivalent meter based on a recombination principle has been designed for routine measurements of ambient dose equivalent in mixed (gamma + neutrons) radiation fields outside the irradiation fields of linear medical accelerators. Two recombination chambers were used as detectors. The device applies sequentially four different voltages to the chamber electrodes and measures the ionization current values for each voltage. The absorbed dose rate and ambient dose equivalent are calculated taking into account the relationship between the initial recombination of ions and radiation quality factor. Tests at 15 MV Varian Clinac 2300C/D accelerator confirmed that the ambient dose equivalent of mixed radiation in clinical conditions could be determined with accuracy of about 10%.**

Keywords— **photoneutrons, recombination chambers, dosimetric methods.**

I. Introduction

Radiation fields around medical accelerators, are slightly contaminated with neutrons, generated by photon-neutron nuclear reactions. This concerns practically all the accelerators operating at maximum photon energy of 15 MeV or higher. The photoneutron energy spectrum has a peak around 1 MeV, however, at the patient's plane, after the transmission through the accelerator head, neutrons have a distribution similar to that of the heavily shielded fission source.

The level of neutron production and its unwanted whole-body dose to the patient vary around different treatment units between 1 and 5 $mSvGy^{-1}$ (neutron dose equivalent per tissue dose at isocentre), depending on accelerator characteristics and the distance from the isocentre. The total neutron dose equivalent evaluated for a complete therapeutic treatment of 60 Gy photon dose is between 60 mSv and almost 300 mSv.

The International Electrotechnical Commission (IEC) recommended limits for the neutron absorbed dose in the patient plan [1], but practically almost no measurements are performed in radiotherapy departments, The main reason which discouraged medical physicists from making the measurements is the lack of convenient measuring equipment for the routine use.

Relatively simple measuring methods, with a recombination chamber, have been recently proposed in our previous papers [2,3,4]. The methods are suitable for radiation protection measurements along the treatment couch outside the irradiation field. Among them, the method based on the determination of the recombination index of radiation quality seems to be the most convenient for the routine measurements.

The paper presents a short overview of the method and a model of the device for automatic measurements of ambient dose equivalent at the medical accelerators. Results obtained with the laboratory system and the new device were compared for the same measuring conditions.

II. Method

A. Measuring method

Recombination chambers are high-pressure, usually tissue-equivalent, ionization chambers operating under condition of initial recombination of ions. This kind of recombination occurs within tracks of single ionizing particles. It does not depend on the dose rate and depends on local ionization density within the tracks of ionizing particles i.e. on radiation quality.

The use of recombination chambers makes it possible to determine the total absorbed dose, which is proportional to the saturation current, and recombination index of radiation quality, Q_4 [5], which can be used as an approximation of the radiation quality factor. Ambient dose equivalent $H^*(10)$ can be well approximated [6] by the product of the ambient absorbed dose $D^*(10)$ and Q_4.

$$H^*(10) = D^*(10) \times Q_4 \tag{1}$$

The definition of the recombination index of radiation quality, Q_4 and the method how to determine this quantity were described earlier [5,6], so only the main points of the method are briefly sketched here. First, the special voltage U_R has to be determined, for a given chamber, in a reference

O. Dössel and W.C. Schlegel (Eds.): WC 2009, IFMBE Proceedings 25/III, pp. 484–486, 2009.
www.springerlink.com

field of gamma radiation. Usually, a ^{137}Cs radiation source is used for this reason. U_R is the voltage which ensures 96% of saturation in such field. Then, in the radiation field under investigation, one has to determine the saturation current and the ionization current at the voltage U_R. Then, the Q_4 is determined as:

$$Q_4 = (1 - f_R)/0.04 \tag{2}$$

where $f_R = f(U_R)$ is the ion collection efficiency (ratio of the ionization current to the saturation current), measured at the voltage U_R in the investigated radiation field.

By definition, Q_4 for gamma radiation of ^{137}Cs, $Q_{4\gamma} = 1$. For high energy photons and relativistic electrons Q_4 is slightly lower than one. The exact value for the conditions of the measurements at medical accelerators is not known, so basing on our earlier measurements, performed in several radiation fields [7], the value of $Q_{4\gamma} = 0.98 \pm 0.02$ was used in this work. Any excess of the measured Q_4 over unity in the vicinity of a medical accelerator, would indicate some presence of neutrons. Then, the H*(10) value can be calculated, from the equation (1) and used for radiation protection purposes.

If there is an interest in the value of neutron absorbed dose, D_n, it can be derived using the fact that Q_4 is an additive quantity i.e.

$$DQ_4 = D_\gamma Q_{4\gamma} + D_n Q_{4n} = (D - D_n) Q_{4\gamma} + D_n Q_{4n} \tag{3}$$

$$D_n = D \frac{Q_4 - Q_{4\gamma}}{Q_{4n} - Q_{4\gamma}} \tag{4}$$

where
D_γ - photon absorbed dose,
D_n - neutron absorbed dose,
D - total absorbed dose,
$Q_{4\gamma}$ - recombination index of quality for photons alone
Q_{4n} - recombination index of quality for neutrons alone.

The value of Q_{4n} in the equation (3) is not known, if not determined by an independent method. An approximate value of Q_{4n}. can be assumed, basing on general knowledge of the neutron spectra at medical accelerators. The uncertainty of such estimation is usually of about 15%. Combining the measurements performed with different recombination methods it was possible to determine the value of Q_{4n}=12.5±0.6 for the measuring conditions described below [3] but the measurements are time consuming and usually not needed for radiation protection.

B. Recombination chambers

A recombination chamber of F1 type [2] was used as a main detector in this work. The F1 chamber is in - phantom, parallel-plate chamber with volume of 3.8 cm^3. It was filled with ethane (C_2H_6) up to a pressure of 0.7 MPa. The chamber has three TE electrodes, 34 mm in diameter. The wall thickness is 0.6 g/cm^2. The distance between electrodes is equal to 1.75 mm. The F-1 chamber is well sealed and its sensitivity usually does not change more than 0.5% per year. The chambers were connected to the electronics by electrometric cables, type T3295 BICC (2 mm in diameter, PTFE insulation covered by graphite).

At small distances from the isocentre, the accuracy of the measurements could be influenced by volume recombination of ions in the recombination chamber. In our measurements, the correction for volume recombination was estimated to be of order of 1% of total ion collection efficiency at the distances below 30 cm from the isocentre. In order to improve the accuracy, a special cylindrical recombination chamber, denoted as T7, has been designed [3,4]. The chamber has a small distance between electrodes (0.5 mm), so the volume recombination is strongly reduced, comparing to the F1 chamber.

A high-pressure graphite ionization chamber, filled with carbon dioxide, served as a monitor of photon radiation dose rate. The monitoring chamber was supplied with the constant voltage of 300 V.

III. Measurements

Measurements were performed in the treatment room of the Varian Clinac 2300C/D at the Oncology Centre in Warsaw, with the accelerator producing 15 MV photons. The photon beam was collimated to the area of 10×10 cm^2 at the distance of one meter from the target.

The recombination chambers were placed on the treatment bed, in the distances of 17 cm (only T7 chamber), 50 cm, 100 cm and 300 cm from the isocentre.

The chambers were placed on the 30×30×30 cm PMMA slab phantom.

In both, laboratory and RADEM circuits, the measuring system involved two ionization chambers (main detector and monitoring chamber), connected to a two channel automated electronic circuit, controlled from a PC.

In the laboratory system each channel of the electronic circuit included an electrometer (Keithley 642), connected to the computer via IEEE 488 bus, a power supply and necessary interfaces [8]. The measuring results were normalized to the monitor readings after completing the measuring series.

The ionization currents of the main chamber were measured at a number of polarizing voltages. In order to achieve a better accuracy, the ionization current was measured for both polarities of each voltage and averaged. The high-

stability voltage supply ZSWN2 (designed at the IAE) was used.

The RADEM [6] device contains four multiplex AD channels with resolution of ±15 bit. Two of them are electrometric with measuring ranges of 2,5 nC and 25 nC for the measurements of the electrical charge and of 25 pA and 250 pA for the measurements of the ionization current. Two other channels are provided for the measurements of temperature and voltage in the range ±2,5 V and they have not been used in this work. AD conversion time for each channel is 25 μsek. The device contains also two stabilized high-voltage supplies. One is digitally controlled with resolution of 0,4 V in the range ±1638 V. The second one provides voltages in the range from 0 to 1600 V, with the step of 200 V and is controlled from the front panel. RADEM is controlled by a parallel port of a PC computer. With such solution, it can be used with different computer control systems.

The chambers with the measuring systems were calibrated at the Institute of Atomic Energy in reference radiation fields of ^{137}Cs, in terms of ambient dose equivalent. The calibration involved determination of the recombination voltage U_R.

IV. Results and discussion

The values obtained for the 10×10 cm^2 irradiation field are summarized in the Table 1. The value of the Q_4 increases with the distance from the isocentre. This clearly indicates that also neutron contribution to the ambient dose equivalent increases.

Table 1 Comparison of the results

Distance from isocentre	Q_4		$H^*(10)$	
	Lab	RADEM	Lab	RADEM
17	1.4	1.5	476	462
50	1.75	1.7	138	134
100	4.82	4.96	36.8	38

The measurements of H*(10) at the irradiation field of 4×4 cm^2 resulted in the values of 60 mSvh^{-1} at 50 cm and 35 mSvh^{-1} at 100 cm from the isocentre.

Determination of H*(10) is, in principle, sufficient from the point of view of radiation protection. Neutron absorbed dose can be also of interest, for comparison with the internationally recommended limits. The uncertainty of the neutron absorbed dose determined from the Eq. (4) can be large, when the Q_4 value is small (close to 1), but such values of Q_4 indicate that the neutron dose is small and can be neglected. In other cases the uncertainty depends mostly on the uncertainty of Q_{4n}. It can be expected that the overall uncertainty does not exceed 30%, if Q_{4n} of about 12 is assumed. Therefore, the results can be used for comparison with the recommendations, if the measured value is far enough from the limits. In other cases more precise measurements should be performed.

Ambient dose equivalent can be determined with much better accuracy, which depends mostly on the accuracy of Q_4 (usually 5-10%, in dependence of the measuring conditions). The estimated overall uncertainty is below 20%.

V. conclusions

The main idea of the present study was to create an automated measuring system with a recombination chamber, for the direct determination of the total $H^*(10)$ at medical accelerators outside the irradiation field. It was proved that the measurements could be performed in reasonable time of about 20 - 30 minutes and with accuracy better than 20%. The significant advantage of using the recombination chamber is the direct reading of the result and relatively short time of the measurements.

References

1. International Electrotechnical Commission (1998) Medical electrical equipment - Part 2-1: particular requirements for the safety of electron accelerators in the range 1 MeV to 50 MeV. IEC 60601-2-1
2. Golnik N, Kamiński P, Zielczyński M (2004) A measuring system with a recombination chamber for neutron dosimetry around medical accelerators. Radiat Prot Dosim 110: 271-274
3. Golnik N, Zielczynski M, Bulski W et al. (2005) Recombination methods for determination of neutron contribution to H*(10) at medical accelerators. Pol J Med Phys Eng 11: 61-73.
4. Golnik N, Zielczynski M, Bulski W et al. (2007) Measurements of the neutron dose near a 15 MV medical linear accelerator. Radiat Prot Dosim 126: 619-622
5. Zielczyński M, Golnik N (1994) Recombination index of radiation quality - measuring and applications. Radiat Prot Dosim 52: 419-422
6. Golnik N (1996) Recombination methods in the dosimetry of mixed radiation. Report IAE -20/A, Institute of Atomic Energy Świerk (PL)
7. Golnik N, Mayer S, Zielczyński M (2004) Recombination index of radiation quality of low-LET radiation. Nucl Instr Meth. in Phys Res B 213C: 650-653
8. Zielczyński M, Golnik N, Rusinowski Z (1996) A computer controlled ambient dose equivalent meter based on a recombination chamber. Nucl. Instr. Meth. in Phys Res A. 370: 563 567

Author: Natalia Golnik
Institute: Institute of Metrology and Biomedical Engineering, WUT
Street: Sw. A. Boboli 8
City: 02-525 Warsaw
Country: Poland
Email: Golnik@mchtr.pw.edu.pl

How far old technology and practices are in use in radiology?

O. Ciraj-Bjelac[1], M. Rehani[2]

[1] Vinca Institute of Nuclear Science, Radiation and Environmental Protection Department, Belgrade, Serbia
[2] International Atomic Energy Agency, Vienna, Austria

Abstract— **Diagnostic radiology has been undergoing fast changes in technology and practices that have implications on radiation safety of the patient. Some of the changes have well established role in patient protection like use of rare earth intensifying screens in radiography, low attenuating material in patient's table, and use of image intensifiers rather than conventional dark room fluoroscopy. For many countries in West, it may be unimaginable that older technologies are still in use or the practices such as use of fluoroscopy for positioning in radiography. A survey was conducted covering large number of developing countries in order to assess the use of old technology and practices. The survey included: age of the machine (>31 years, 21-30 yrs, 11-20 and ≤ 10 yrs), generator type for adult and pediatric radiography (single phase, three phase or high frequency), availability of minimum filtration of 2.5 mm of Al, low attenuating material in cassettes and patient table, speed of the screens in the cassettes (200, 400 or more), use of mass screening for chest, use of fluoroscopy for positioning in radiography, use of low kV technique in chest radiography, appropriate awareness about radiation exposures in pregnancy and when termination is not necessary and availability of single slice CT scanners. The most striking features of the survey were: there are number of countries where calcium tungstate screens are still in use rather than rare earth screens that implies patient doses almost double than those in developed countries, many hospitals still use 200 screen speed, manual processing is used frequently, dark room fluoroscopy is still in use in very many hospitals although there are clear recommendations to replace these units, use of low kV technique for chest radiography is rather rampant, there are hospitals where adult exposure factors are in use for CT scans of children.**

Keywords— **diagnostic radiology, old technologies, safety, patient protection**

O. Dössel and W.C. Schlegel (Eds.): WC 2009, IFMBE Proceedings 25/III, p. 487, 2009.
www.springerlink.com

Effective Dose – A Flawed Concept That Could and Should Be Replaced

D. J. Brenner

Center for Radiological Research, Columbia University, New York, USA

Abstract— **Effective dose is used to characterize the generic risk of a total body radiation-induced stochastic health detriment. The effective dose represents flawed science: two of the most important reasons are that the tissue-specific weighting factors used to calculate effective dose are a subjective mix of different endpoints, and that the marked and differing age dependencies for different health detriment endpoints are not taken into account. Effective dose is prone to misuse, particularly in the field of radiology. It is suggested that effective dose could be replaced by a new quantity, effective risk, which, like effective dose, is a weighted sum of equivalent doses to different tissues; unlike effective dose, where the tissue-dependent weighting factors are a set of generic, subjective committee-defined numbers, the weighting factors for effective risk would simply be evaluated tissue-specific lifetime cancer risks per unit equivalent dose. The resulting "effective risk", which has the potential to be age- and gender-specific if desired, would perform the same comparative role as effective dose, be just as easy to estimate, be less prone to misuse, be more directly understandable, and would be based on solid science.**

Keywords— **Effective dose, Effective risk**

I. Introduction

Effective dose aims to provide a single number proportional to the radiobiological "detriment" from a particular, often inhomogeneous, radiation exposure – detriment representing a balance between carcinogenesis, life shortening, and hereditary effects. It is commonly used to allow comparisons of the risks associated with different spatial dose distributions produced by different imaging techniques.

The effective dose represents questionable science: two of the most important reasons are that the tissue-specific weighting factors used to calculate effective dose are a subjective mix of different endpoints, and that the marked and differing age dependencies for different endpoints are not taken into account. Importantly, the effective dose is prone to misuse, with widespread confusion between effective dose, equivalent dose, and absorbed dose.

It is suggested here that effective dose could and should be replaced by a new quantity which does not have these problems. An appropriate new quantity would be "effective risk", which, like effective dose, is a weighted sum of equivalent doses to different tissues; unlike effective dose, where the tissue-dependent weighting factors are a set of subjective, committee-defined numbers, the weighting factors for effective risk would simply be evaluated tissue-specific lifetime cancer risks per unit equivalent dose. The resulting quantity would perform the same comparative role as effective dose; it would have the potential to be age- and, if desired, gender-specific, be just as easy to estimate, be less prone to misuse, be more directly interpretable, and would be based on more defensible science.

II. Effective Risk

There appears to be no disagreement that the concept of effective dose lacks scientific rigour; nor is there any disagreement that the concept of effective dose is "often misused". Given that it is agreed that some quantity is needed in order to compare different partial-body exposure scenarios, the issue is what to do about this.

One suggestion [1] is to replace effective dose (i.e., summed organ doses, each weighted with a set of committee-generated numbers), with "effective risk" (i.e., summed organ doses, each weighted with actual epidemiologically-based cancer risks). The logic is that effective risk would perform all the comparative functions that we agree are needed, but 1) would eliminate the subjectivity associated with committee-generated weighting factors, 2) would provide a more intuitively interpretable quantity relating to risk, leading in turn to 3) less potential for misuse.

The currently-used effective dose is defined as

$$\textit{Effective Dose} = E = \sum_{\mathrm{T}} w_{\mathrm{T}} \, H_{\mathrm{T}}, \qquad (1)$$

where H_T are the tissue-specific equivalent doses in tissues T, and w_T are committee-defined dimensionless tissue-specific weighting factors. The proposal is simply to replace the subjective committee-generated tissue weighting factors, w_{T}, with objective epidemiologically-based organ-specific radiation-induced cancer risk estimates. The resulting "effective risk" is thus

$$\textit{Effective Risk} = R = \sum_{\mathrm{T}} r_{\mathrm{T}} \, H_{\mathrm{T}}, \qquad 2)$$

where r_{T} are lifetime radiation-attributable organ-specific cancer risk estimates (per unit equivalent dose to tissue T). The effective risk, R, is thus a generic lifetime radiation-attributable cancer risk.

It can be seen that the two equations are structurally the same (and both inherently assume an LNT (linear no threshold) model), so that effective risk would fulfil all the same comparative functions as effective dose. But it would have the major advantages of objectivity, interpretability, and less potential for misuse, as is now discussed:

O. Dössel and W.C. Schlegel (Eds.): WC 2009, IFMBE Proceedings 25/III, pp. 488–490, 2009.
www.springerlink.com

1. Objectivity

The suggestion [1] is that the tissue weighting factors should no longer reflect subjective committee-generated judgements, but would be objective epidemiologically-based quantities. That the ICRP tissue weighting factors are highly subjective can hardly be disputed. Considering, for example, one of the major changes in tissue weighting factors adopted by the ICRP in 2005 [2], which is the increase in the weighting factor for the breast: in fact the motivation for this change was not so much because our knowledge of radiation-induced breast disease advanced in the intervening ten years, but in significant part because of a committee-based change in policy, now relying more on cancer incidence rather than cancer mortality.

This is not to suggest that the use of cancer incidence, or cancer incidence adjusted for mortality, is not reasonable, but rather to illustrate that the changes in tissue weighting factors every decade or so reflect, to a considerable extent, different groups of people making different subjective judgements.

Another example of the subjective nature of present tissue weighting factors relates to the fact they currently represent a balance between radiation-induced cancer and hereditary effects. *Any* methodology for combining the risks of cancer and hereditary effects into a single number must be inherently subjective – resulting again in weighting factors changing not so much because the science changes, but because committee memberships change.

This is the basis for the suggestion that objective epidemiologically-based radiation-induced cancer risk estimates be used for tissue weighting factors - the point being to remove the subjectivity inherent in committee-determined weighting factors. For sure such objective weighting factors might still change over time, but in such a case it would really be because of "relevant scientific advances".

2. Interpretability

The goal is to have a generic quantity reflecting radiobiological detriment or risk, so the choice of a quantity that has units of Sieverts is, to say the least, puzzling.

A major advantage of the use of Eq. 2 is the desire to have a quantity which is more directly interpretable as a risk. It is surely true that an effective risk of (say) 4 per 100,000 individuals is intuitively interpretable to the user in a way that an effective dose of (say) 1 mSv is not. As we struggle with the rapidly increasing man-made contribution to the overall population exposure [3], it is surely advantageous to have a measure of the radiological detriment which actually means something to most users.

3. Less Potential for Confusion

The confusion between organ dose and effective dose is widespread in the field of radiology; it is probably true that this confusion is "inevitable" if we stick with a quantity which a) has dose in its name, b) has units of dose, but c) is actually a measure of radiological detriment. The confusion would be entirely avoided if measures of radiobiological detriment were in units of (for example) "per 10,000 individuals" (as in effective risk), rather than in Sieverts (as in effective dose).

4. Radiation Protection *vs.* Patient Dosimetry

The original motivation for the effective dose concept was for external radiation protection, not for clinical patient dosimetry. Perhaps one could make the case for the continued use of effective dose in non-clinical radiation protection situations: here, the relevant population is often over 18 and under 70, so ignoring the differing age sensitivities of different organs may be acceptable. But the predominant use of effective dose is now for describing the doses delivered during radiological examinations - less than 1/3 of the 2008 PubMed citations on radiation "effective dose" refer to radiation protection, the rest relate to clinical patient dosimetry. For such clinical applications, where we are particularly concerned about pediatric exposures, one cannot justify the use of age-independent weighting factors.

III Conclusions

In summary, for radiation protection one could perhaps make an argument for the continued use of effective dose, flawed and confusing as it is. In practice, however, effective dose is now largely used for patient dosimetry, and there its use cannot be justified. Effective risk which would have the potential to be age- and gender-specific if desired, would perform the same comparative role as effective dose, be just as easy to estimate, be less prone to misuse, be more directly understandable, and would be based on solid science.

IV. References

1. Brenner DJ. Effective dose: A flawed concept that could and should be replaced. Br J Radiol 2008;81:521-3
2. International Commission on Radiological Protection. Recommendations of the ICRP: ICRP Publication 103. Annals of the ICRP 2007;37
3. Mettler FA Jr, Thomadsen BR, Bhargavan M, Gilley DB, Gray JE, Lipoti JA, McCrohan J, Yoshizumi TT, Mahesh M. Medical radiation exposure in the U.S. in 2006: Preliminary results. Hlth Phys. 2008;95:502-7

Corresponding author:

Author:	David J Brenner	City:	New York, NY 10032
Institute:	Center for Radiological Research, Columbia University Medical Center	Country:	USA
		Email:	djb3@columbia.edu
Street:	630 West 168th Street		

Status of Radiation Protection of Patients in Developing Countries

Madan M. Rehani

International Atomic Energy Agency, Vienna, Austria

Abstract— **How safe is the patient in developing countries and making patient safer has been the objective of the International Action Plan on Radiological Protection of Patients launched by the IAEA in 2002. This requires assessment and comparison of radiation doses to the patients undergoing diagnostic radiological examinations with reference levels without compromising on quality, finding how many patients are getting peak skin dose exceeding the threshold for erythema in interventional procedures (IP) and through this process creating awareness on radiation protection. A number of tools have been used namely; training courses, providing free training material developed in cooperation with international organizations and professional bodies, establishing a new website on radiation protection of patients (http://rpop.iaea.org), guidance documents, establishing networks and launching projects in over 80 countries. It is becoming clear that the patient doses (ESAK) in radiography examinations in many developing countries are generally within established diagnostic reference levels (DRL) but poor image quality is the root cause of higher patient doses, the situation with regard to computed tomography (CT) is different as many patients are receiving higher doses (DLP) than DRLs, in the case of interventional procedures like PTCA, many patients receive higher dose (KAP) than the currently known DRL and in mammography also there is need to achieve better optimization. There have been a number of success stories of optimization demonstrating reduction in patient doses in developing countries without compromising on image quality. With increased usage of high dose procedures in developing countries such as CT & IP and with fast changing technology that poses great challenge in implementing patient dose management, there is a greater need today to focus on patient protection.**

Keywords— **Radiation protection developing countries, patient protection, diagnostic radiology, interventional procedures, mammography, computed tomography.**

I. Introduction

We envision that a patient in developing country should not be exposed to radiation more than necessary as per international standards and the deterministic injuries are avoided without hampering the clinical purpose. This requires concerted actions, not only regulations, but dose monitoring and dose management.

Many assumptions are made when thinking about the situation in developing countries as there is generally lack of published information. This is all the more true regarding radiation protection of patients where there is lack of information about the type of equipment and technology in use, training of personnel, workload of diagnostic radiological and interventional procedures, availability and use of radiation protection tools and surveys of radiation doses to patients. It is not uncommon to hear people say that radiation doses to patients in some countries in (say) Africa might be 3 times or more than the figures in developed countries. It is true that many developing countries have not followed the path of a) wide scale survey of patient doses, b) comparing them with international standards and c) performing optimization and repeating measurements to estimate impact. Of course there have been a number of scattered reports of radiation doses primarily in radiographic examinations, but gross lack of data on doses in computed tomography, mammography and interventional procedures. To attend to this lacuna, the IAEA initiated an International Action Plan on Radiological Protection of Patients in 2002 which was followed by establishment in 2005 of regional projects in large part of the world with the objectives of "Estimating how safe is the patient in developing countries and making him safer". This approach was a deviation from the often used approach of utilizing tools and assuming that results will be achieved. For example, it is common to focus project activities on tools such as training and providing QC equipment to countries in international projects with the purpose of capacity and capability building. However, we decided to focus on assessing the impact – safety of the patient and that evaluates if the capability building in patient protection really happened. This presentation shares our experience with the hope that it may help many not only with the provision of information that was lacking but also on the effectiveness of the approach that was utilized.

II. Methodology

While dealing with large part of the world covering more than 80 countries with diverse conditions, we decided to have a uniform and consistent approach to patient protection. We identified 5 Tasks in diagnostic and interventional radiology as

O. Dössel and W.C. Schlegel (Eds.): WC 2009, IFMBE Proceedings 25/III, pp. 491–494, 2009.
www.springerlink.com

Task 1. Avoidance of radiation injuries in interventional procedures using X rays, and limiting probability of stochastic effects, especially in children;
Task 2. Surveys of image quality and patient doses in simple radiographic examinations: establishing Diagnostic Reference Levels and comparison with international standards;
Task 3. Exercising dose reduction in conventional radiography by using rare earth intensifying screens;
Task 4. Survey of mammography practice from the optimization of radiation protection viewpoint;
Task 5. Patient dose management in computed tomography with special emphasis on pediatric patients;

In addition, there is one Task each for nuclear medicine and radiotherapy as:

Task 6. Providing guidelines on the release of patients after radionuclide therapy based on current recommendations of the International Commission on Radiological Protection (ICRP); and
Task 7. Taking steps to avoiding accidental exposure in radiotherapy.

But this paper covers only diagnostic and interventional and thus Task 6 and 7 are not covered here.

Fairly detailed work plan covering instructions on what to do, why to do and how to do were prepared and passed on to project counterparts in Member States. Some countries have been able to show results as presented here.

III. RESULTS

A. Radiography

The results so far available from about 20 countries, some of which covering 45 hospitals in 12 countries were included in a recent publication [1] indicated that poor image quality constitutes a major source of unnecessary dose to patients in developing countries. Comparison with other surveys indicates that patient dose levels in these countries are not higher than those in developed countries. The fraction of images rated as poor was as high as 53%. The image quality improved up to 16 percentage points in Africa, 13 in Asia and 22 in Eastern Europe after implementation of a QC program. Patient doses varied by a factor of up to 88 although the majorities were below DRLs. The mean ESAK values in mGy were 0.33 (chest PA), 4.07 (lumbar spine AP), 8.53 (lumbar spine LAT), 3.64 (abdomen AP), 3.68 (pelvis AP) and 2.41 (skull AP). Patient dose reductions ranging from 1.4% to 85% were achieved.

B. Interventional procedures

It is desirable to include information on staff protection when it comes to interventional group and compare the level of patient and staff protection. The available results from 61 hospitals in 20 mainly developing countries (9 mostly in Eastern Europe, 5 in Africa and 6 in Asia) indicate that nearly 40% of the interventional rooms had annual workload of over 2000 patients. It is remarkable that work load of pediatric interventional procedures can reach the levels of adult even in developing countries. About 30% of participating countries have shown 100% increase in workload in 3 years. Lead apron are used in all participating rooms. Even though KAP was available in almost half of the facilities, none had experience in its use. Many patients exceeded the dose threshold for erythema. One hundred out of 505 patients monitored for PSD (20%) were above the 2 Gy threshold for deterministic effects. A substantial number (62%) of PTCA procedures performed in developing countries in this study are above the currently known DRL of 100 Gy.cm2 and thus could be optimized [2].

C. Computed Tomography (CT)

The results from CT facilities in 18 countries in Africa, Asia and Eastern Europe covering 73 CT facilities indicate that eleven CT facilities in six countries were found to use adult CT exposure parameters for pediatric patients thus indicating lack of awareness and optimization. Except in one case, the mean CTDIw values for adult patients were below DRLs, but the mean DLP values for adult patients in 17% of situations were above DRLs [3]. The resulting CT images were of adequate quality for diagnosis. The frequency of pediatric CT examinations was 21 %, 20% and 5% of all CT examinations in participating centers in Africa, Asia and Eastern Europe respectively. There is stronger need in many developing countries to justify CT examinations in children with relatively higher frequencies observed in this study more so when optimization is lacking. Poor technique, more than poor machine is the cause for higher radiation doses to the patients. Awareness, training and monitoring of radiation doses provides the way forward.

D. Mammography

Initial data available from about 20 countries in Asia, Africa and East European countries indicates large variation in Entrance Surface Air Karma (ESAK), for a standard breast,

ranging form 3.5 to 16 mGy. Also, suboptimal optical density (OD) was a common finding, as gross OD ranged from 0.84 to 1.78 and OD above 1.5 was observed in just a few centres. This could result in suboptimal visualisation of clinically relevant details. High contrast ratio was 10 to 16 lp/mm. In two cases it was below the threshold of 12 lp/mm, and only few units operated above achievable 15 lp/mm. The percentage of poor image quality before implementation of corrective actions ranged from 1% to 78% for both CC and MLO projections. Simple corrective actions pertained to film processing and darkroom conditions. Also, there were cases where more complex maintenance interventions were necessary, as Automatic Exposure Control adjustment and image receptor replacement. After implementation of corrective actions significant improvement in image quality were observed. Lower ESAK with lower optical density and with suboptimal viewing conditions was observed. In such situations increase in ESAK was required to improve image quality.

IV. Making Patients Safer

The tools that the IAEA has used are initially focused at health professionals who perform studies and thus deliver radiation doses to patients

Training activities cover a significant part of the IAEA's support programme [4]. The training actions in the area of radiation protection of patients are grouped into the following:

- Development of a standardized syllabus
- Development of training CDs containing power point slides of lectures,
- Organization of regional training courses
- Support to countries in organizing national training courses through training material and provision of experts

The training material on following areas is available for free download from

http://rpop.iaea.org/RPoP/RPoP/Content/AdditionalResources/Training/1_TrainingMaterial/index.htm

Radiation Protection in
Diagnostic and Interventional Radiology
Radiotherapy
Nuclear Medicine
Cardiology
PER/CT
Prevention of Accidental exposure in radiotherapy

Almost 60 training courses (regional and national) have been organized and information about these is available at the IAEA website. More than 3000 participants at these courses have benefited

V. Discussion

Many countries participating in the project have expressed that it is for the first time now that they have data on patient doses. The process has resulted in skills in patient dosimetry. It attains importance as there are hardly few medical physicists in developing countries who are involved in diagnostic and interventional radiology. Either one had to wait for years for the situation to improve which looked not likely in near future, or just start with actions utilizing the human resource that is available in the country wherever it may be- in radiotherapy, regulatory body, university or using radiographers. In fact this project helped to bring regulatory body closer to the hospitals in a cooperative manner to work together rather than acting as regulator. Also this created the need to seek medical physics support. After reaching the stage of patient dose estimations many country are now actively pursuing the development of medical physics program.

VI. Conclusions

The information that is becoming available from the IAEA studies shall have great impact in making patients safer in large part of the developing world. The project is not just about patient dose assessment and dose management but the actions are directed at developing leadership in countries on patient protection. It is expected that the changes documented at small level shall result in safety culture.

Acknowledgment

The author wishes to thank IAEA for the support to the activities pertaining to radiation protection of patients. The TC projects of the IAEA in different regions on medical exposure have been responsible for implanting the program. Thanks to Mr. Pedro Ortiz Lopez and Ms. Czarwinski for support to the program. The contribution of participants in the projects from large number of countries is gratefully acknowledged.

REFERENCES

1. Muhogora WE, Ahmed NA, Almosabihi A, Alsuwaidi JS, Beganovic A, Ciraj-Bjelic O,. Kabuya FK, Krisanachinda A, Milakovic M, Mukwada G, Ramanandraibe MJ, Rehani MM, Rouzitalab J, Shandorf C (2008). Patient doses in radiographic examinations in 12 countries of Asia, Africa and Eastern Europe: Initial results from IAEA projects. Am J Roentgenology 190: 1453-1461.
2. Virginia Tsapaki, Nada A Ahmed, Jamila Salem AlSuwaidi, Adnan Beganovic, Abdelkader Benider, Latifa BenOmrane, Rada Borisova, Sotirios Economides, Leila El-Nachef, Dario Faj, Ashot Hovhannesyan, Mohammad Hassan Kharita, Nadia Khelassi-Toutaoui, Nisakorn Manatrakul, Ilkhom Mirsaidov, Mohamed Shaaban, Ion Ursulean, Jeska Sidika Wambani, Areesha Zaman, Julius Ziliukas, Dejan Žontar, Madan Rehani (2009) Radiation exposure to patients during interventional procedures in 20 countries: Initial IAEA project results. AJR (to be published in August 2009 issue).
3. Wilbroad E Muhogora, Nada A. Ahmed, Adnan Beganovic, Abdelkader Benider, Olivera Ciraj-Bjelac, Vesna Gershan, Eduard Gershkevitsh, Edward Grupetta, Mohammad H Kharita, Nisakorn Manatrakul, Milomir Milakovic, Kazuko Ohno, Latifa Ben Omrane, Jaroslav Ptacek, Cyril Schandorf, Mohamed S. Shabaan, Desislav Stoyanov, Nadiakhelassi Toutaoui, Jessica S. Wambani, Madan M. Rehani. CT patient doses in ct examinations in eighteen eighteen countries: initial results from international atomic energy agency projects, (communicated to Rad Prot Dosim)
4. Rehani MM. IAEA activities on radiological protection in digital imaging. Rad Prot Dosimetry 2008; 129: 22-28. doi: 10.1093/rpd/ncn155

Author: Madan M. Rehani
Institute: International Atomic Energy Agency
Street: Wagramer Str. 5
City: Vienna
Country: Austria
Email: M.Rehani@iaea.org

Training of Doctors Using Fluoroscopy

Madan M. Rehani

International Atomic Energy Agency, Vienna, Austria

Abstract— **Increasing number of medical specialists are using fluoroscopic guided procedures for diagnostic applications and for interventions. Many of these specialists have either no training or inadequate training in radiation protection. These include interventional cardiologists, electro-physiologists and vascular surgeons in one group who make extensive use of catheterization procedures and orthopedic surgeons, urologists, gastroenterologists, gynecologists and anesthesiologists in second group with relatively lesser use of X ray based techniques as compared to former group. The IAEA has established training programmes for these two groups separately. So far about a thousand doctors from more than 50 countries have been trained using the standardized syllabus and training material The training material in the form of power point slides is available for free download from the website (http://rpop.iaea.org) for the first group and on a CD on request from patient.protection@iaea.org for the second group. It is very encouraging to report that the IAEA has established a lead in the world in training such doctors. An Asian network of cardiologist in radiation protection has been established and the network has started a newsletter which, to the best of our information, is first newsletter on radiation protection by any cardiologists' body in the world. The IAEA trained cardiologists are organizing sessions on radiation protection in various cardiology conferences. The follow up actions and surveys conducted have shown improvement in the level of staff and patient protection demonstrating that training programmes have resulted in skill development and implementation of radiation protection in clinical practice.**

Keywords— **radiation protection fluoroscopy, cardiac catheterization, training in radiation protection.**

I. Introduction

For many years in the past the focus of training actions in radiation protection to doctors, in many countries, has been on training those who work full time with radiation like radiologists, radiation oncologists and nuclear medicine physicians. While this was a natural course that received attention of most medical physicists, it became apparent in recent years that there are other groups of medical specialists who are currently actively using ionizing radiation in diagnosis and fluoroscopic guided interventional procedures, even if they are not full time involved in radiation work. A large part of the radiation injuries reported in recent years to patients have been in interventional procedures and mostly performed by those who lacked the foundation and any training in radiation protection. These include interventional cardiologists, electro-physiologists and vascular surgeons in one group (referred to as Group A in this paper and with brief title of cardiologists) who make extensive use of catheterization procedures. Another group consists of orthopedic surgeons, urologists, gastroenterologists, gynecologists and anesthesiologists (to name a few), referred to as Group B in this paper and titled as non-cardiologists, non-radiologists, with relatively lesser use of X ray fluoroscopy as compared to Group A. With a view to attend to this problem, actions were initiated by the IAEA in 2003 and this presentation summarizes the actions for the benefit of medical physicists who are involved in training activities in radiation protection.

II. Curriculum Development

A. Topics

It was decided not to follow the normal structure of training programme that typically consists of atomic structure, types of radiation, radiation units, radiation measurements, interaction of radiation with matter etc. as starting topics. Rather the very first lecture should be that catches the attention of participants and makes them feel that yes they need to be sitting in this course for their benefit rather than for requirements of regulations or certification. Thus the first lecture is titled as Why talk about radiation protection. The educational objectives of the topic are

a. Review of severity & frequency of radiation injuries
b. What do these injuries teach us regarding the cardiologist's role-for Group A (Lessons learnt)
c. Points-of-view about law suits of severe injury
d. Recognizing radiation injury & effects

Since the lecture involves units like Gy, it was deemed appropriate to let participants know that the feel of quantity is more important than the definition of the unit like not many can define temperature, pressure and length which one uses everyday. All the titles of the lectures are so designed to give a practical orientation to the situations in which doctors' work, rather than looking as physics teaching. This created acceptability and the participants were receptive. The list of topics, educational objectives of each topic and the contents of the talk for the curriculum

O. Dössel and W.C. Schlegel (Eds.): WC 2009, IFMBE Proceedings 25/III, pp. 495–497, 2009.
www.springerlink.com

standardized for Group A is available [1]. Based on successful feedback as described in C below, similar approach was followed for Group B professionals, but with lesser emphasis to deterministic effects such as radiation induced skin injuries which are largely found in procedures performed by Group A professionals rather than Group B.

B. Level of existing training and practice of radiation protection

The first course for Group A professionals was conducted in May 2004 with 29 cardiologists from 25 countries. The response to questionnaire distributed among participants of the training course indicated that for 88% of participants this was the first time that they were attending a structured program on training in radiation protection. 85% stated that they have not attended a cardiology conference where a lecture on radiation protection was included. 96% stated that they do not measure radiation dose to patients. It must be stated that the target audience for the IAEA training courses is developing countries.

Subsequently 7 more regional training courses have been organized with participation of cardiologists from about 56 countries as per further details available on the webpage at: http://rpop.iaea.org/RPOP/RPoP/Content/AdditionalResources/Training/2_TrainingEvents/Cardiology.htm. The webpage also contains information on feedback from participants.

The first course for Group B professionals' was conducted in Sept. 2006 and a total of 4 regional training courses have been conducted so far covering doctors from 34 countries. The survey of existing level of training and practice of radiation protection, similar to those for Group A, were conducted among participants in training courses for Group B professionals and the results are available at: http://rpop.iaea.org/RPOP/RPoP/Content/AdditionalResources/Training/2_TrainingEvents/Doctorstraining.htm. As is evident from the Table on the webpage, for more that 95% participants it was for the first time that they were attending a structured program on radiation protection, 87-100% stated that they never attended a conference where there was a lecture on radiation protection, 89-100% stated that they do not record radiation dose to patient and 100% stated that the course was relevant to them.

C. Training duration

This is an important issue. After considerable thoughts, deliberations and review of recommendations from various bodies e.g. EC [2], ICRP [3], WHO [4], Joint statements from professional bodies in USA [5], it was apparent that most recommendations pertained to interventional radiologists and much fewer for Group A professionals and hardly any for Group B professionals. Moreover, some recommendations only provided list of topics whereas others also recommended duration also. However, based on review it was deemed appropriate to design a 2 days program and test it [6]. The feedback from participants in first course indicated that 92% preferred 2 days duration, 4% felt it was short and another 4% stating that it was long. Nearly similar response has been apparent in other training courses for Group A as well as for Group B.

III. TRAINING RESOURCES

There was certainly lack of customized training material and its access to medical physicists. Realizing this lacuna, the IAEA took a bold step of making available power point slides of the standardized training material through its website on radiation protection of patients, for free download: http://rpop.iaea.org/RPOP/RPoP/Content/AdditionalResources/Training/1_TrainingMaterial/index.htm. This has tremendously helped medical physicists and other professionals including concerned medical specialists and radiographers to freely download training material and use them in training activities. In fact this happens to be the only resource in the world on the dedicated topic of radiation protection in specialized area such as cardiology. Every training material is initially brought out as a draft material on a CD, tested for couple of years in number of training courses, reviewed by professional societies at international level such as IOMP and concerned medical society and the finalized version after approval by different bodies is then made available through the website. The CD containing training material is freely made available to whosoever sends request to patient.protection@iaea.org. The permission is granted to conference organizers who request us at patient.protectionn@iaea.org to make copies of the CDs and distribute to all participants and also to professional societies to make copies for distribution to their members. While the training material for Group A is available at the above website for free download, the material for Group B is currently available only on CD which can be obtained by sending email as given above.

IV. DISCUSSION

For medical physicists it is a challenging area of professional activity- the education of medical specialists with no or little training in radiation protection. The conventional training topics as used for radiologists and the duration of training do not apply to this group of specialists. Unfortunately not many medical physicists, particularly in developing countries have engaged themselves with training of such

doctors. Even in developed countries, it is only for the last few years that some have gained experience in dealing with such group and thus there are not many with good deal of experience and expertise. There is certainly gross lack of experience sharing in published literature [7,8,9]. There seem to be good number of research papers published each year in clinical journals with contribution of medical physicists and dealing with issues of radiation dose estimations, both to staff and to the patients but not much on training issues. Our experience has shown fulfilling results. The interest generated among the participants is based on how simple and practically oriented one can make the curriculum and presentations. It requires a great deal of compromise with ego. It is encouraging to sate that a large number of cardiologists trained by the IAEA have followed up with actions in their country and in their region. The most significant is the Asian network of cardiologists on radiation protection, probably the only such network currently in the world: http://rpop.iaea.org/RPOP/RPoP/Content/AdditionalResources/Training/2_TrainingEvents/asian-network.htm. The network has its own Newsletter which is available for free download on the above website. The IAEA trained cardiologists are organizing sessions on radiation protection in various cardiology conferences and delivering lectures http://rpop.iaea.org/RPOP/RPoP/Content/Documents/Whitepapers/RP-lectures-cadiologists.pdf. This is in contrast to the situation depicted in IIB above which indicated that there were no cardiology conferences with a lecture on radiation protection.

The follow up actions and surveys conducted have shown improvement in the level of staff and patient protection: http://rpop.iaea.org/RPOP/RPoP/Content/Documents/Whitepapers/2nd_issue_Newsletter.pdf. This demonstrates that training programmes have resulted in skill development and implementation of radiation protection in clinical practice.

V. Conclusions

Training of medical specialists involved in fluoroscopy but without formal education in radiation protection is a relatively a newer area for medical physicists with vast potential to make improvement in practice that can lead to enhanced radiation safety of patients and staff. With the availability of a standardized and tested training material for free download; the situation can be improved much faster than otherwise.

Acknowledgment

The author acknowledges the support provided by the IAEA management in NSRW and in TC.

References

1. Rehani MM (2007) Training of interventional cardiologists in radiation protection--the IAEA's initiatives. Int J Cardiol 114:256-260
2. EC (2000) Guidelines on education and training in radiation protection for medical exposures. Radiation Protection 116. Office for Official Publications of the European Communities, Luxembourg
3. ICRP (2000) Avoidance of radiation injuries from medical interventional procedures. ICRP Publication 85, Annals of the ICRP 30 (2).
4. WHO (2000) Efficacy and radiation safety in interventional radiology. World Health Organization, Geneva.
5. ACCF/AHA/HRS/SCAI (2005) Clinical competence statement on physician knowledge to optimize patient safety and image quality in fluoroscopically guided invasive cardiovascular procedures. A report of the American College of Cardiology Foundation/American Heart Association/American College of Physicians Task Force on Clinical Competence and Training. Circulation 111:511-532.
6. Rehani MM (2007) The IAEA's activities on radiation protection in interventional cardiology. Biomed Imaging Interven J (BIIJ) 3(2): e31. http://www.biij.org/2007/2/e31/e31.pdf
7. Rehani MM, Ortiz-Lopez P (2006) Radiation effects in fluoroscopically guided cardiac interventions - keeping them under control. Int J Cardiol 109:147-151.
8. Vañó E, Gonzalez L, Canis M et al. (2003) Training in radiological protection for interventionalists. Initial Spanish experience. BJR 76:217-219.
9. Rehani MM (2008) IAEA activities on radiological protection in digital imaging. Rad Prot Dosimetry 129:22-28. DOI 10.1093/rpd/ncn155

Author: Madan M. Rehani
Institute: International Atomic Energy Agency (IAEA)
Street: Wagramer Str. 5
City: Vienna
Country: Austria
Email: M.Rehani@iaea.org

WHO's Role in the Assessment of Medical Radiation Exposures and Devices

F. Shannoun[1], M. Perez[1], N. Pendse[2], A. Velazquez Berumen[2], B. Fahlgren[2], S. Groth[2], and E. van Deventer[1]

[1] World Health Organization/Department of Public Health and Environment, Geneva, Switzerland
[2] World Health Organization/Department of Essential Health Technologies, Geneva, Switzerland

Abstract— **About 15% of the ionizing radiation exposure to the general public comes from artificial sources, and almost all of this exposure is due to medical radiation, largely from diagnostic procedures. Although radiological diagnostics provide great benefits, it is generally accepted that the use of radiation involves some risk. The large number of people exposed annually means that even the small individual risks associated with diagnostic exposures could cumulate into a public health concern. Assessment of population exposures resulting from medical uses of radiation is mainly available in industrialized countries, while in developing countries this information is scarce. The World Health Organization (WHO) seeks to mobilize the health sector towards safe use of radiation in medicine and to improve implementation of radiation safety standards in health care facilities. The United Nations Scientific Committee on the Effects of Atomic Radiation (UNSCEAR) has the mandate to assess and report levels and effects of exposure to ionizing radiation. Its reports constitute the most comprehensive source of compiled information on distribution of medical radiological devices and on frequency of medical procedures involving the use of radiation, as well as associated doses.**

WHO, jointly with UNSCEAR, have planned to conduct surveys on practice and availability of human and material resources in diagnostic radiology, nuclear medicine and radiotherapy and to act as a clearinghouse for collecting and sharing information on the use of radiation in health care. Earlier evaluations have demonstrated wide variations among countries in the frequency of diagnostic examinations performed. This could be explained by the imbalance in availability of equipment, health workforce and health care provision and also due to differences in the ability to obtain complete data on medical radiological. WHO urges Member States to conduct regularly such surveys and offers a platform for implementing a practical approach and standardized method .

Keywords— **medical radiation exposure, collective effective dose, medical dose survey, medical devices survey**

I. Introduction

About 15% of the ionizing radiation exposure to the general public comes from artificial sources, and almost all of this exposure is due to medical radiation, largely from diagnostic procedures [1]. However, diagnostic X-rays provide great benefits is generally accepted, that their use involves some risk of developing cancer. The individual risk is probably small because radiation doses are usually below 10 mGy, but the large number of people exposed means that even small individual risks could translate into a considerable number of cancer cases [2].

The World Health Organization (WHO) work with Member States to mobilize the health sector towards safe use of radiological devices In this context, information on the availability of such equipments have been used to analyse and to deduce temporal trends, to evaluate the collective population dose due to medical exposure and to determine the distribution of medical radiological devices. The United Nations Scientific Committee on the Effects of Atomic Radiation (UNSCEAR) has the mandate to assess and report levels and effects of exposure to ionizing radiation. With respect to medical exposures the objective has been to establish the frequency of medical examinations and procedures involving the use of radiation, as well as their associated doses. Public health authorities throughout the world rely on UNSCEAR's estimates as the scientific basis for evaluating radiation risks [1].

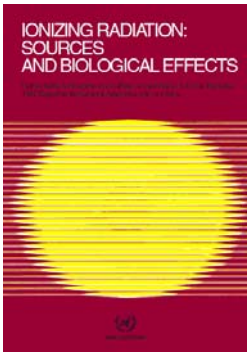

Fig. 1 UNSCEAR Report 1982

In 1982, UNSCEAR developed with WHO a survey to obtain information on the availability of radiological equipment and the frequency of diagnostic and therapeutic procedures in various countries. This report (Figure 1) presented data, which had been based upon surveys in a limited number of countries worldwide. This survey was the first to include an assessment of exposures from computed tomography (CT) [3].

O. Dössel and W.C. Schlegel (Eds.): WC 2009, IFMBE Proceedings 25/III, pp. 498–501, 2009.
www.springerlink.com

II. METHODOLOGY TO CONDUCT THE SURVEY

The evaluation of medical exposures consists of assessing the frequency and type of procedures being undertaken as well as an evaluation of the radiation doses for each type of procedure. Frequency and dose data are derived from three main sources: peer reviewed scientific literature, official reports published by Member States and surveys conducted especially for this purpose. UNSCEAR classifies Member States following a four level health care (HCL) model based on the number of physicians per population.

- Health Care Level I: > 1 physician / 1000
- Health Care Level II: 1 physician / 1000-3000
- Health Care Level III: 1 physician / 3000-10000
- Health Care Level IV: < 1 physician / 10000.

The number of physicians per population has been shown to correlate well with the number of medical radiological examinations performed [4]. Trend analysis and comparison between the different health care levels by means of UNSCEAR data are difficult due to the limited number of survey returns and their incompleteness in some countries. Since 1993, UNSCEAR [5] has used the effective dose as a convenient indicator of overall risk-related exposure of the patient from an X-ray examination, and population doses were expressed in terms of the annual collective effective dose (S) or the annual average per capita effective dose. The age and sex distribution of patients undergoing some types of x-ray examination in terms of three broad age bands (0-15 years, 16-40 years, >40 years) have also been reported for both sexes combined as well as the overall distribution between male and female patients.

There are no internationally standardized protocols for estimating the radiation exposures from medical imaging procedures. Therefore in 2004, the European Commission initiated the DOSE DATAMED project to review recent surveys of population exposure from medical radiological examinations, to understand the differences and sources of uncertainty, and to develop a harmonized and simplified method for future surveys [6]. The majority of radiological examinations make only a minimal contribution to the collective population dose, so that priority should be given to those examinations which contribute most to the dose S. Table 1 shows the 20 types of diagnostic examinations or procedures which are the highest contributors to the dose S [6]. These 20 exams contribute together between 50-70% to the total frequency (F) and between 70-90% of the total collective effective dose from all medical X-ray procedures (excluding dental). The average effective doses for each of the 20 exams obtained from DOSE DATAMED are indicated in the last column of Table 1.

Table 1 Frequency (F) and contribution to the collective dose (S) of the Top 20 exams and the related average effective dose (E) per exam obtained from the 10 DOSE DATAMED countries [6]

Exam type or category	% of total F	% of total S	Average E per examination (mSv)
Plain film radiography			
1. Chest/thorax	12 - 29	0.7 - 5.2	0.10
2. Cervical spine	2.0 - 5.4	0.1 - 2.3	0.27
3. Thoracic spine	1.0 - 3.1	0.5 - 3.7	1.00
4. Lumbar spine	2.8 - 9.6	2.0 - 17	1.90
5. Mammography	0.3 - 15	0.6 - 4.7	0.33
6. Abdomen	1.1 - 4.3	1.1 - 4.7	1.50
7. Pelvis & hip	6.3 - 10	2.8 - 9.4	0.90
Radiography/Fluoroscopy			
8. Barium meal	0.3 - 0.9	0.8 - 5.9	7.7
9. Barium enema	0.1 - 2.0	0.5 - 13	8.6
10. Barium follow	0.1 - 0.3	0.2 - 1.6	10.0
11. IVU	0.3 - 2.0	1.2 - 8.7	4.0
12. Cardiac angiography	0.2 - 1.3	1.0 - 9.9	9.1
All angiography	1.1 - 2.4	6.4 - 16	9.2
Computed Tomography (CT)			
13. CT head	1.8 - 5.4	3.0 - 7.9	2.0
14. CT neck	0.1 - 0.9	0.1 - 1.1	2.5
15. CT chest	0.5 - 1.5	6.1 - 12	8.0
16. CT spine	0.3 - 2.8	1.5 - 13	5.3
17. CT abdomen	0.1 - 3.0	1.9 - 26	12.0
18. CT pelvis	0.1 - 1.5	0.3 - 9.7	8.7
19. CT trunk	0.1 - 5.6	1.1 - 27	14.0
All CT	4.5 - 15	28 - 59	6.1
Interventional			
20. PTCA	0.1 - 0.3	0.5 - 3.6	14.0
All interventional	0.2 - 1.3	3.5 - 14	10.7
TOTAL 1-20	**50 - 70**	**70 - 90**	

Thus, the average annual effective dose per capita could be calculated from the frequency, the size of the population and the effective dose per examination.

The contribution of nuclear medicine (NM) examinations to the collective population dose from diagnostic medical exposures ranges from 4 to 14% [6]. Figure 2 depicts the five groups of examinations with the main contribution to the total dose S which could additionally be included in the estimation. The main medical devices used in nuclear medicine are gamma-cameras, Single Photon Emission Computed Tomography (SPECT) and more recently Positron Emission Tomography (PET) Systems.

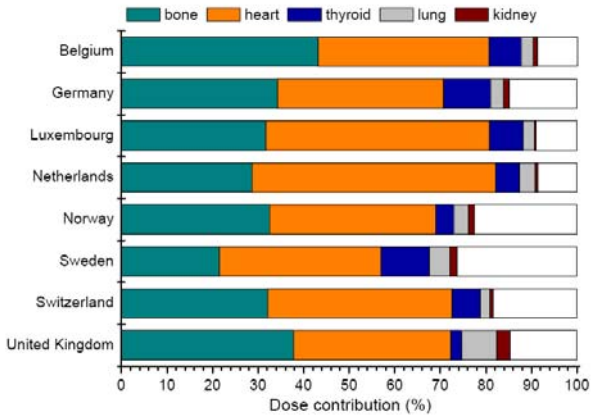

Fig. 2 The five main contributors to the population dose from nuclear medicine examinations [6]

Also information on the number of diagnostic radiology equipment has been obtained regularly as part of the surveys conducted by UNSCEAR. The number of equipment are presented normalized to the size of the population and usually are well correlated with the mean effective dose per capita as demonstrated in Table 2. The comparison of the four HCLs shows that the radiological devices are concentrated in HCL I countries.

Table 2 Comparison of some values for the usage of radiation in medical diagnostic per health care level from UNSCEAR 2000 [1]

Quantity*	HCL I	HCL II	HCL III	HCL IV	World
All Physicians	2800	710	210	45	1100
Radiologists	110	80	5	0.1	70
X-ray equipment	290	60	40	4	110
Dental equipment	440	60	10	0.1	150
CT scanner	17	2	0.4	0.1	6
Gamma camera	7.2	0.3	0.1	0.03	2.1
PET scanner	0.2	0.002	0	0	0.05
X-ray frequency	920k	150k	20k		330k
Effective dose per capita from RD**	1.2	0.14	0.02		0.4
Effective dose per capita from NM**	0.08	0.008	0.0063		0.03

* The values are given per million population
** The values are given in mSV

As shown in Table 3 the frequency of CT exams per population is proportional to the number of CT scanners per population and likewise to the CT dose per capita. Consequently, CT is the main contributor to the dose from medical exposures in HCL I countries.

Table 3 Comparison of CT frequency and CT dose per capita for six countries in 2000 and CT scanners [7, 8, 9]

Country	CT exams per 1000 habitants	CT dose per capita (mSv)	CT scanners per million habitants
Germany	90	0.73	14
USA	200	1.60	32
Japan	290	2.30	93
Luxembourg	115	0.84	26
Canada	88	-	11
Belgium	115	0.90	29

III. Discussion and Conclusions

Doses for a single examination have tended to decrease in the last years because of continuing improvements in equipment design and performance. However, the overall trend is an increased collective effective dose because the frequency of diagnostic radiological procedures has been rising worldwide. Especially, the number of CT scanners and the related doses per capita has increased significantly. Japan, for example, has with 93 CT-scanners per million population the highest density worldwide, and with 2.3 mSv per capita also the highest contribution to the collective effective dose [9]. Regular surveys on the use of medical radiological devices and the delivered doses to patients represent an important public health tool to monitor the effective and safe use of radiation in medicine.

Since 2005, WHO annually publishes the World Health Statistics including over 70 selected key health indicators. The density of physicians per 10 000 population is reported in the World Health Statistics which usually is used for the classification of countries into the different levels of health care. Additionally, a grouping into low, lower middle, upper middle and high income countries is provided which better reflect the influence of the economical situation of a country on its health system. Information on medical imaging devices and radiation exposures should be considered as health indicators reflecting the usage of radiological devices and the frequency of radiological examinations.

The Organization for Economic Co-operation and Development (OECD) reports regularly on the distribution of medical imaging devices of OECD countries. This approach may be extended through cooperation with UNSCEAR, WHO, and other relevant organizations. Manufacturers have an very important role as they can provide estimates of the equipment stock of radiological devices worldwide.

WHO urges Member States to conduct regularly surveys on the use of medical radiological devices and offers a platform for implementing a practical and standardized method.

References

1. United Nations Scientific Committee on the Effects of Atomic Radiation (2000): UNSCEAR 2000 Report to the General Assembly, with scientific annexes. Volume I: Sources. United Nations, New York
2. Ron E. (2003) Cancer risks from medical radiation, Health Phys: pp. 47-59
3. United Nations Scientific Committee on the Effects of Atomic Radiation (1982): Ionizing Radiation: Sources and Biological Effects. Report to the General Assembly, with annexes. United Nations, New York
4. J. Valentin (1995): UNSCEAR Data Collections on Medical Radiation Exposures: Trends and Consequences; Radiat Prot Dosimetry. 57: p. 85-90
5. United Nations Scientific Committee on the Effects of Atomic Radiation (1993) Sources and Effects of Ionizing Radiation, Annex C: Medical Radiation Exposures. United Nation, New York
6. European Commission (2008) Radiation Protection 154: European guidance on estimating population doses from medical X-ray procedures and annexes: http://ec.europa.eu/energy/nuclear/radiation_protection/publications_en.htm
7. Shannoun F., Blettner M., Schmidberger H., Zeeb H. (2008) Radiation protection in diagnostic radiology; Dtsch Arztebl, 105(3): p. 41-6
8. Canadian Institute for Health Information (2005) Medical Imaging in Canada. CIHI, Ottowa
9. Nishizawa K, Matsumoto M, Iwai K, Maruyama T (2004) Nishizawa survey of CT practice in Japan and collective effective dose estimation. Nippon Acta Radiol; 64: 151-158

Author: Dr. Ferid Shannoun
Institute: World Health Organization
Street: 20, Avenue Appia
City: CH-1211 Geneva
Country: Switzerland
Email: shannounf@who.int

Laser Particle Acceleration for Radiotherapy: A first radiobiological characterization of laser accelerated electrons

J. Pawelke[1,2], E. Beyreuther[2], W. Enghardt[1,2], M. Kaluza[3], L. Karsch[1], L. Laschinsky[1], E. Leßmann[2], D. Naumburger[1], M. Nicolai[3], C. Richter[1,2], R. Sauerbrey[2], H.-P. Schlenvoigt[3], M. Baumann[1]

[1] OncoRay – Center for Radiation Research in Oncology, Technische Universität Dresden, Medical Faculty, Dresden, Germany
[2] Forschungszentrum Dresden-Rossendorf, Institute of Radiation Physics, Dresden, Germany
[3] Friedrich-Schiller-Universität Jena, Institute of Optics and Quantumelectronics, Jena, Germany

Abstract— **In recent years, the technology of laser-based particle acceleration has developed at such a rate that compact and potentially more cost-effective accelerators are promised for medical application, e.g. for high precision hadron radiotherapy. Necessary requirements are the supply of stable and reliable particle beams with reproducible properties, sufficient particle intensities and monoenergetic spectra. Additionally, a precise dose delivery in an appropriate time and the exposure of a desired irradiation field are needed. Beside these physical demands, the consequences on detection and dosimetry as well as the radiobiological effect on living cells have to be investigated for the ultra-short pulsed laser-based particle beams.**

As a first step, the laser accelerator facility at the Jena Titanium:Sapphire system was customized for *in vitro* cell irradiation experiments and the delivered electron beam was improved with regard to its spectrum, diameter, dose rate and dose homogeneity. Furthermore, a custom-designed beam and dose monitoring system was established that enables real-time monitoring of the irradiation experiments and a precise determination of the dose delivered to the cells. Moreover, stable and reproducible beam properties were achieved during the whole three month experiment campaign.

Dose-effect-curves were obtained for four cell lines and two endpoints, generally displaying a lower biological effectiveness for short-pulsed laser-accelerated electrons relative to the continuous 200 kV X-ray reference irradiation. Possible reasons will be discussed.

Keywords— **laser-based particle acceleration, radiotherapy, *in vitro* cell experiments, biological effectiveness**

I. Introduction

Over the past years, the technological progress in high-power laser technology results in increasing peak powers and intensities associated with substantial reductions in system size, which enables the realization of table-top laser-based particle accelerators. This novel technology of particle acceleration promises accelerators of compact size and reasonable costs that may contribute to a widespread use of high precision hadron radiotherapy.

Some basic properties of laser acceleration are reasonably well known from theory, simulations and fundamental physical experiments [1-5], but considering medical application several further requirements have to be fulfilled. The particle beam should be stable and reliable with reproducible properties; the intensity and with it the dose rate should be high enough to guarantee appropriate irradiation times. Likewise, a precise and controlled dose delivery and the exposure of a desired irradiation field are required.

In addition to the physical demands, the radiobiological properties of these particle beams have to be characterized. Compared to conventional electromagnetic accelerators, the ultra-short pulse durations (in the order of 100 fs) of laser-accelerated particle beams result in 10^9 – 10^{11} times higher peak dose rates and peak currents of some thousand Ampere [3]. These differences in time structure and dose delivery could lead to different radiobiological effects, although both kinds of accelerators will administer the same dose to the patient. Consequently, the biological effectiveness of laser-accelerated particle beams have to be investigated starting from human cells and end up with clinical studies.

As a first step in this chain, laser-accelerated electrons were applied for *in vitro* cell irradiations in order to investigate the dose-dependent induction of radiation damage. For that reason, the experimental setup at the Jena Titanium:Sapphire (JeTi) laser system [6] as well as the generated electron beam were customized with regard to radiobiological requirements. In addition, a custom-designed beam and dose monitoring system was established. Subsequently, dose-effect-curves for four cell lines and two endpoints were obtained and compared to the results of a conventional 200 kV X-ray tube.

II. Material and methods

A. The Jena Titanium:Sapphire laser system (JeTi)

Electron pulses were generated using the 10 TW laser system JeTi that delivers 80 fs pulses (800 mJ energy, 800 nm central wave length, [6]) at a repetition rate of

O. Dössel and W.C. Schlegel (Eds.): WC 2009, IFMBE Proceedings 25/III, pp. 502–504, 2009.
www.springerlink.com

2.5 Hz. Focused into a subsonic helium gas jet the laser pulses produce plasma and accelerate electrons in the forward direction. The generated electron beam exited the vacuum system through a 1 mm thin aluminum window and propagated in air by reason of the living cell samples that demand for atmospheric pressure. In the following, the laser system, the beamline and the electron beam itself had to be optimized in order to perform radiobiological experiments.

B. Setup of the beam monitoring and dosimetry system

A beam monitoring and dosimetry system, consisting of a Faraday cup, a Roos ionization chamber (sensitive volume of 0.35 cm², PTW, Germany) and Gafchromic® EBT dosimetry films (ISP, USA) were established at the JeTi system. Firstly used for beam optimization, the system was employed later on for a careful control of the cell irradiation experiments. Here, the Faraday cup and the ionization chamber provide an online dose-information, whereas the radiochromic films were applied for retrospective precise dosimetry.

C. Cell irradiation experiments

Samples of two squamous cell carcinoma (FaDu, SKX) and two normal tissue (mammary gland epithelial cells 184A1, human skin fibroblasts HSF2) cell lines were irradiated with prescribed doses in the range of 0.3 to 10 Gy at several experiment days over a period of three months. During irradiation each sample was equipped with two EBT radiochromic films, one in front of and one behind the cell monolayer, providing a retrospective precise dose determination.

Following irradiation the dose-dependent cellular survival was measured using the clonogenic survival assay. Additionally, the immunochemical detection of co-localized γH2AX and 53BP1 molecules [7] was applied to analyze DNA double-strand breaks which remain in the cells 24 hours post-irradiation. Parallel to the experiments at the JeTi electron accelerator reference irradiations were performed with a conventional 200 kV X-ray tube.

III. Results

A. Adjusted setup for radiobiological experiments

The measured exponential energy spectrum of the JeTi electron beam was limited to a minimum energy of 3 MeV using a pair of permanent magnets for energetic filtration. Additionally, the beam spot size was adjusted by means of a lead collimator (10 x 10 x 10 cm³) with an aperture of 35 mm. As a result, a MeV electron beam of 35 mm diameter was achieved sufficient to irradiate common cell sample vessels like petri dishes (32 mm inner diameter). The dose homogeneity was improved resulting in less than 10 % inhomogeneity over the cell sample as proven by radiochromic films.

The electron yield and with it the mean dose rate of the pulsed electron beam was increased gradually with laser power using the Faraday cup to monitor the delivered bunch charge. In the end, a mean dose rate of 0.36 Gy/min or 2.4 mGy per pulse was achieved for cell irradiation.

B. Beam monitoring, stability and reproducibility

Basic requirements for radiobiological experiments are a stable beam with reproducible properties as well as a beam monitoring system that ensures a controlled dose delivery to the cells.

The beam stability and reproducibility were checked by comparing the actual dose, determined retrospectively with EBT radiochromic films, to the parameters monitored during the experimental period of ten weeks. As result, clear linear dependencies were achieved for all three parameters – the number of laser pulses, the accumulated dose (Roos ionization chamber) and the bunch charge (Faraday cup) – recorded. Hence, the beam properties were stable and reproducible over the time and the parameters can be deployed to control the dose delivery to the cells. Exemplary, the correlation of the doses measured with the Roos ionization chamber and the EBT radiochromic films were displayed in Figure 1.

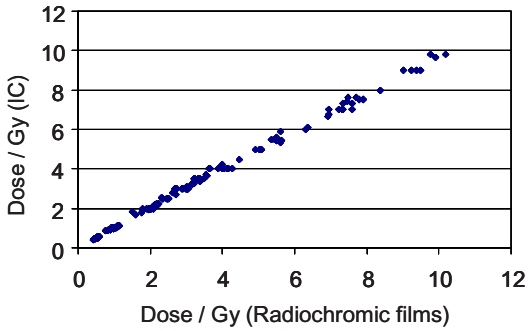

Figure 1: The accumulated dose measured online with the Roos ionization chamber compared to the dose determined retrospectively by EBT dosimetry films for the irradiation of 163 cell samples.

Regarding the beam intensity, variations of up to 40 % or 130 % were observed taken into account one day or all days of the experiment, respectively. These variations were compensated by means of the established online dose monitoring system.

C. The biological effectiveness of laser-accelerated electrons

The dose-effect-curves obtained for both endpoints and all cell lines investigated show in general a lower biological effectiveness for the ultra-short pulsed laser-accelerated electron beams relative to continuous 200 kV X-ray irradiation. Possible reasons are differences in time structure, mean dose rate and energy spectrum of both radiation qualities. The results of current investigations dealing with this topic will be discussed.

IV. Conclusion

The successful realization of the presented *in vitro* cell experiments demonstrates that the application of prescribed doses, a controlled dose delivery and accurate dosimetric measurements are feasible at laser-based electron accelerators. All technical requirements were established and all components and methods have proven their stability and reliability in systematic radiobiological cell studies over months. Obtained differences in the biological effectiveness of laser-accelerated electrons and conventional 200 kV X-rays can be explained by means of physical properties of radiation.

In a second step, experiments are prepared at a 100 terawatt laser system, which will provide laser accelerated proton beams for radiobiological cell irradiation studies.

Acknowledgment

This work has been supported by the German Federal Ministry of Education and Research (BMBF) under contract 03ZIK445.

References

1. Mangles SPD, Murphy CD, Najmudin Z et al. (2004) Monoenergetic beams of relativistic electrons from intense laser-plasma interactions. Nature 431: 535-538
2. Geddes CGR, Toth C, Tilborg Jv et al. (2004) High-quality electron beams from a laser wakefield accelerator using plasma-channel guiding. Nature 431: 538-541
3. Faure J, Glinec Y, Pukhov A et al. (2004) A laser-plasma accelerator producing monoenergetic electron beams. Nature 431: 541-544
4. Schwoerer H, Pfotenhauer S, Jäckel O et al. (2006) Laser-plasma acceleration of quasi-monoenergetic protons from microstructured targets. Nature 439: 445-448
5. Hegelich B, Albright B, Cobble J et al. (2006) Laser acceleration of quasi-monoenergetic MeV ion beams. Nature 439:441-444
6. Schlenvoigt HP, Haupt K, Debus A et al. (2006) A compact synchrotron radiation source driven by a laser-plasma wakefield accelerator. Nat Phys 4(2): 130-133
7. Eke I, Sandfort V, Storch K et al. (2007) Pharmacological inhibition of EGFR tyrosine kinase affects ILK-mediated cellular radiosensitization in vitro. Int J Radiat Biol. 83(11-12):793-802

Medical Exposure Issues in the Revision of the *International Basic Safety Standards for Protection against Ionization Radiation and for the Safety of Radiation Sources*

C. Borrás[1]

[1] Chair, Science Committee, International Organization for Medical Physics
Dosimetry and Nuclear Instrumentation Group/Department of Nuclear Energy, Universidade Federal de Pernambuco, Recife, PE, Brazil

Abstract— **The 1996 version of the *International Basic Safety Standards for Protection against Ionizing Radiation and for the Safety of Radiation Sources* is being revised by several international organizations led by the International Atomic Energy Agency. One of the main reasons for the revision is to make the Standards consistent with the most recent recommendations of the International Commission on Radiological Protection. Particular attention is given to the use of radiation in medical applications, in particular concerning patient protection, a subject mostly spearheaded by the Pan American Health Organization and the World Health Organization. Issues involved in the redrafting of the medical exposures section include assigning responsibilities to the appropriate parties and establishing requirements for the education, training and competence of those persons with responsibilities for patient radiation protection.**

Keywords— **Regulations, radiation, protection, safety, medicine.**

I. Introduction

The International Atomic Energy Agency (IAEA) published the first set of basic safety standards in June 1962 as *Safety Series No. 9* [1], following the guidance of their Board of Governors in 1960 that "The Agency's basic safety standards ... will be based, to the extent possible, on the recommendations of the International Commission on Radiological Protection (ICRP)". A revised version was published in 1967 and a third revision in 1982. This edition, titled the *1982 Edition of Safety Series No. 9* [2], was jointly sponsored by the IAEA, the International Labour Organisation (ILO), the Nuclear Energy Agency of the Organisation for Economic Co-operation and Development (OECD/NEA), and the World Health Organization (WHO). The revision of these Standards started in 1991 with two additional cosponsors: the Food and Agriculture Organization of the United Nations (FAO), which had just published jointly with WHO the *Codex Alimentarius*, and the Pan American Health Organization (PAHO), which had had a radiological health program since 1960 with strong emphasis on patient protection [3].

An interim version of the new Standards, with the title *International Basic Safety Standards for Protection against Ionizing Radiation and for the Safety of Radiation Sources* (BSS) was published in 1994 by the IAEA as *Safety Series 115-I*, following the approval or endorsement of the governing bodies of all the cosponsoring organizations, a consensus of 192 countries. The final version was published in 1996 [4]. Since then, the BSS, promoted by the cosponsoring organizations, has been used as the basis for radiation protection legislation/regulations world-wide.

A review of the 1996 BSS, carried out in 2006 by the then cosponsoring organizations, concluded that, while there was no single major reason for a revision, a number of factors–including the then imminent publication of the new ICRP recommendations–justified preparing a new edition. The revision process started in 2007, with the European Commission and the United Nations Environment Program as potential additional cosponsors**.**

The Standards under revision [5] draw upon information derived from experiences of the member states in applying the requirements of the previous BSS, and from experience in many countries in the use of radiation and nuclear techniques. They also draw upon extensive research and development work by national and international scientific and engineering organizations on the health effects of radiation and on techniques for the safe design and operation of sources.

This paper addresses issues related to medical exposures only –that is exposure incurred by patients for the purpose of medical or dental diagnosis or treatment; by carers and comforters; and by volunteers in a program of biomedical research involving their exposure.

II. Main Issues

A. Responsibilities

The ICRP, especially its Recommendations [6], articulate radiation protection principles for everybody involved with ionizing radiation in all situations: planned, existing and emergency situations. The intergovernmental organizations with responsibilities in radiation protection, which are cosponsoring the BSS, elaborate standards to be adapted/adopted by the competent authorities in their member states as part of the countries' regulatory systems. It is

O. Dössel and W.C. Schlegel (Eds.): WC 2009, IFMBE Proceedings 25/III, pp. 505–507, 2009.
www.springerlink.com

therefore important that the requirements be very explicit in assigning responsibilities. Because radiological procedures involve a multidisciplinary team led by a physician who often is not the registrant or licensee of an authorized practice, responsibilities in medical exposures are shared by several individuals. At the higher level, the draft revised BSS is identifying requirements for the government, the regulatory body (for radiation protection) and, in the case of medical exposures, the health authority and professional bodies. This is particularly important not only regarding the justification of medical practices, but also regarding the establishment of diagnostic reference levels (called guidance levels in the 1996 BSS) for patients, and of dose constraints for carers and comforters and for volunteers in biomedical research. The draft revised BSS is also assigning individual responsibilities, in medical exposures, to the registrant or licensee the radiological medical practitioner; the manufacturers, suppliers of sources, equipment, or software; the workers; the referring medical practitioners; the medical physicists; the medical radiation technologists; and the ethics committees. A distinction is made between the roles and responsibilities of the radiological medical practitioner, i.e. the medical practitioner involved in the use of the radiation, and the referring medical practitioner, the physician or dentist referring or requesting the radiological procedure.

The term "medical physicist" is included for the first time in the draft revised BSS, replacing the expressions in the 1996 version of "expert" in "radiotherapy physics", "radiodiagnostic physics" and/or "nuclear medicine physics". Medical physicist, as defined by the International Organization of Medical Physics (IOMP), is "a health professional, with education and specialist training in the concepts and techniques of applying physics in medicine, competent to practice independently in one or more of the subfields (specialties) of medical physics".

In the draft revised BSS, medical physicists are responsible for requirements concerning imaging, calibration, dosimetry and quality assurance, including medical radiological equipment acceptance and commissioning. For therapeutic uses of radiation, these activities shall be "conducted by or under the supervision of a medical physicist specialized in the relevant field". "For diagnostic and image-guided interventional uses of radiation", they shall be "fulfilled by, or under the oversight of or with the advice of, a medical physicist specialized in the relevant field, where the degree of involvement of the medical physicist is determined by the complexity of the particular use of radiation and the ensuing radiation risks".

The 1996 BSS had similar requirements, but without identifying the individuals responsible for their implementation. The draft revised BSS is intended to be very explicit in allocating responsibilities. In the case of medical exposures, the functions of the radiological medical practitioners and the need for them to work with medical physicists and medical radiation technologists are made very clear in order to ensure that roles and responsibilities are properly assumed. This may become very important in the case of an unintended or an accidental medical exposure, to prevent medical physicists from being made solely responsible for a dosimetry error they have made without any consideration of the role the medical staff played or should have played in the patient management.

B. Education, training and competence

Radiological practices involve physicians, physicists and technologists, whose education and training vary considerably from country to country. It is not up to the (radiation protection) regulatory body to decide whether they are competent to perform the medical acts for which they seek an authorization. All the regulatory body can demand is that they meet certain standards with respect to radiation protection and safety. Yet, unless these individuals are proficient in the performance of their duties, patient protection may be compromised. A solution is to demand that only professionals accredited in the relevant specialty (such as diagnostic radiology, image-guided interventional procedures, radiotherapy or nuclear medicine (diagnostic, therapeutic or both)) by the relevant professional body, health authority or appropriate organization be allowed to be involved in medical exposures in the appropriate areas.

Unfortunately, many developing countries do not have a specialty accreditation process. There are many physicians who call themselves radiation oncologists, or technicians working as professionals in diagnostic radiology, nuclear medicine or radiation therapy without any formal education or professional recognition. A particularly difficult situation is that of medical physicists. Even though the IOMP has adhering national medical physics organizations in 79 countries, the governments in some of these countries do not acknowledge medical physicists as health professionals. Such situations could lead to member states rejecting the revised Standards claiming that they cannot meet the requirements involving medical physicists because "there are no medical physicists" in their countries.

Could the solution to the problem be an explanatory note appended to the definition of medical physicist that clarifies that those member states that have yet to develop a formal mechanism for accreditation or certification of medical physicists in the various specialties, "could assess the education, training and competence of any individual proposed by the licensee to act as a medical physicist and decide, based either on international accreditation standards or standards from another country where such an accreditation

system exists, whether such an individual can undertake the functions of a medical physicist, within the required specialty, in these Standards"? Should this proposal be accepted, it is hoped that the IOMP's international accreditation program currently in progress will be accepted as the international standard.

III. Conclusions

The advisory bodies and the member states of the cosponsoring organizations will be heavily involved in the approval of the revised BSS [7]. Given the significant increase in dose arising from medical procedures, published by the United Nations Scientific Committee on the Effects of Atomic Radiation (UNSCEAR) [8], the section of medical exposures in the revised BSS will be rigorously scrutinized. It can only be hoped that the government in each member state ensures good coordination among the various governmental agencies involved in medical exposures: especially the (radiation protection) Regulatory Body, the Ministry of Health and the Ministry of Labour, as well as with the relevant professional bodies. Among the last, the IOMP has to play a key role in clarifying the functions of the medical physicists and defending their (our) unique contribution towards ensuring patient protection.

Acknowledgments

The efforts of the staff of the cosponsoring organizations involved in the BSS revision are acknowledged. Particular thanks go to John Le Heron from the IAEA, in charge of drafting the medical exposure section, and to Pablo Jiménez from PAHO and Maria del Rosario Perez and Zhanat Carr from WHO, main contributors to the section.

References

1. International Atomic Energy Agency (1962) Basic Safety Standards for Radiation Protection, Safety series No. 9. IAEA, Vienna.
2. International Atomic Energy Agency (1982), Basic Safety Standards for Radiation Protection (1982 Edition), Safety Series No. 9. IAEA, Vienna.
3. Hanson H, Borrás C, Jiménez P (2006) History of the radiological health program of the Pan American Health Organization. Pan Am J Public Health 20(2/3):87-98
4. Food and Agriculture Organization of the United Nations, International Atomic Energy Agency, International Labour Organisation, OECD Nuclear Energy Agency, Pan American Health Organization, World Health Organization (1996) International Basic Safety Standards for Protection against Ionizing Radiation and for the Safety of Radiation Sources, Safety Series No. 115, IAEA, Vienna.
5. IAEA Basic Safety Standards Web Folder at: http://www-ns.iaea.org/committees/comments/default.asp?fd=804
6. International Commission on Radiological Protection (2008) ICRP Publication 103: Recommendations of the ICRP. JAICRP 37(2-4)
7. IAEA Draft Standards for Comment Web Folder at: http://www-ns.iaea.org/committees/comments/default.asp?fd=699
8. United Nations Scientific Committee on the Effects of Atomic Radiation (2009) Sources and effects of ionizing radiation: UNSCEAR Report to the General Assembly, with Scientific Annexes. New York: United Nations.

Author: Cari Borrás
Institute: Dosimetry and Nuclear Instrumentation Group/Department of Nuclear Energy, Universidade Federal de Pernambuco
Street: Av. Prof. Luiz Freire, 1000
City: 50730-540 Recife, Pernambuco
Country: Brazil
Email: cariborras@starpower.net

A Kinetic Model for Tumor Survival Curves: Its Relation to the Linear-Quadratic Model

R. Martín-Landrove[1,2], N. Guillén[1], and M. Martín-Landrove[1]

[1] Laboratorio de Física Médica, Centro de Física Molecular y Médica
and
[2] Laboratorio de Física Estadística y Fenómenos Colectivos, Centro de Física Teórica y Computacional,
Escuela de Física, Facultad de Ciencias, Universidad Central de Venezuela, Caracas, Venezuela

Abstract— **The linear-quadratic model has been widely used to describe tumor survival curves for doses under 10 Gy. The absence of a proposed mechanism [1] behind the linear-quadratic model is an important limitation for the proper interpretation of clinical results. Models based on a detailed mechanism have the unpleasant feature of a large number of parameters, which makes also the interpretation and use in quantitative radiobiology a very hard task [2,3,4,5,6]. In this work a simple microscopic model based on reversible and irreversible DNA damage is proposed. The model is able to describe the survival curves at high and low LET for V-79 cells in late S phase of Chinese hamsters [7]. The new set of parameters can be related to the ones of the linear-quadratic model and in this way a connection with DNA damage and repair mechanisms is made. At the same time the evolution equations open the possibility for continuous and fractionated treatment plans.**

Keywords— **Tumor survival curves, linear-quadratic model, DNA repair, evolution equations for treatment, high and low LET.**

I. Introduction

The linear-quadratic model has been widely used in the literature to describe the behavior of tumor survival curves (that is, a survival fraction S as a function of applied radiation dose D) up to 10 Gy with a reasonable degree of success. It is characterized by a simple function given by

$$S = \exp\left(-\alpha D - \beta D^2\right) \tag{1}$$

where α and β are the fundamental parameters commonly used in treatment analysis. In principle the mechanistic basis is completely absent and the relation of this parameter set with particular effects in tumor tissue is unknown [1]. On the other hand, models based on detailed mechanisms are characterized by a large set of parameters which normally leads to a difficult extraction and use of these quantities for quantitative radiobiological applications [2,3]. Then in clinical practice there is a need for models of intermediate complexity where the relation between the effects in tumor tissue and linear-quadratic parameter set can be establish easily. This is the main motivation for our proposal which is discussed in the next section.

II. The Proposed Kinetic Model

A. Essential Features

From the clinical point of view it is important to have a model that allows the study of the system evolution and at the same time is able to provide its relation to the absorbed dose. For cellular death the effect to be considered is the irreversibility of DNA damage and it could happen in a single direct step or in a two-step process where the generation of an intermediate reversible DNA damage could take place and it does not interfere with the tumor proliferation process [4,5]. Under the assumption that the number of DNA chains is proportional to the number of cells, the equations which govern the evolution of the system are given by

$$\frac{dN}{dt} = \left[-\alpha_0 \ln\left(N/N_\infty\right) - (1+\gamma)\kappa_{RAD}(t)\right]N + \kappa_{REP} N_R \tag{2a}$$

$$\frac{dN_R}{dt} = \kappa_{RAD}(t)\left(N - N_R\right) - \kappa_{REP} N_R \tag{2b}$$

$$\frac{dN_{NR}}{dt} = \kappa_{RAD}(t)\left(N_R + \gamma N\right) \tag{2c}$$

where N is the number of clonogenic cells with undamaged DNA, N_R is the number of cells with reversible DNA damage and N_{NR} is the number of cells with irreversible DNA damage. At the same time α_0 and N_∞ are Gompertz model parameters [6] and κ_{REP} is the probability per unit time for DNA repair. The probability per unit time for radiation reversible damage of DNA is given by κ_0, as well as $\gamma\kappa_0$ is the probability per unit time for radiation irreversible DNA damage, t_0 is the treatment or fraction elapsed time and

O. Dössel and W.C. Schlegel (Eds.): WC 2009, IFMBE Proceedings 25/III, pp. 508–511, 2009.
www.springerlink.com

$$\kappa_{RAD}(t) \equiv \kappa_0 \theta(t)\theta(t_0 - t) \tag{3}$$

The initial conditions are given by

$$N(t=0) = N_0 \qquad N_R(t=0) = 0 \qquad N_{NR}(t=0) = 0 \tag{4}$$

Equations (2) allow the description of fractionated as well as continuous irradiation [8,9]. Since it is convenient to handle dimensionless quantities for the analysis, the relevant transformation is given by

$$\xi \equiv \frac{N_R}{N} \qquad \zeta \equiv \frac{N_{NR}}{N} \qquad \phi \equiv \ln(N/N_\infty) \tag{5a}$$

$$\tau \equiv \kappa_0 t \qquad \tau_0 \equiv \kappa_0 t_0 \tag{5b}$$

$$\nu \equiv \frac{\alpha_0}{\kappa_0} \qquad \sigma \equiv \frac{\kappa_{REP}}{\kappa_0} \tag{5c}$$

where τ_0 and τ can be regarded as the probabilities for reversible DNA damage for elapsed times t_0 and t, as well as those times measured in κ_0^{-1} units. Then for $0 \le \tau \le \tau_0$, when irradiation is taking place, the evolution is described by

$$\frac{d\phi}{d\tau} = -(1+\gamma) - \nu\phi + \sigma\xi \qquad \phi(\tau=0) = \phi_0 \equiv \ln(N_0/N_\infty) < 0 \tag{6a}$$

$$\frac{d\xi}{d\tau} = 1 + (\gamma - \sigma + \nu\phi - \sigma\xi)\xi \qquad \xi(\tau=0) = 0 \tag{6b}$$

$$\frac{d\zeta}{d\tau} = \gamma + \xi + [1 + \gamma + \nu\phi - \sigma\xi]\zeta \qquad \zeta(\tau=0) = 0 \tag{6c}$$

For $\tau > \tau_0$ the post-irradiation evolution is described by

$$\frac{d\phi}{d\tau} = -\nu\phi + \sigma\xi \qquad \phi(\tau=\tau_0) \equiv \phi_c \tag{7a}$$

$$\frac{d\xi}{d\tau} = (-\sigma + \nu\phi - \sigma\xi)\xi \qquad \xi(\tau=\tau_0) \equiv \xi_c \tag{7b}$$

$$\frac{d\zeta}{d\tau} = [\nu\phi - \sigma\xi]\zeta \qquad \zeta(\tau=\tau_0) \equiv \zeta_c \tag{7c}$$

B. The $\tau_0 \to \infty$ Limit

In order to relate parameters the limit $\tau_0 \to \infty$ could be considered first (i. e., there is no upper boundary for the treatment time). In that case equations (6a) and (6b) can be reduced to (it should be noticed that $N(\tau \to \infty) < N_\infty$)

$$\left.\frac{d\phi}{d\tau}\right|_{\tau\to\infty} = 0 = -(1+\gamma) - \nu\phi_\infty + \sigma\xi_\infty \tag{8a}$$

$$\left.\frac{d\xi}{d\tau}\right|_{\tau\to\infty} = 0 = 1 + (\gamma - \sigma + \nu\phi_\infty - \sigma\xi_\infty)\xi_\infty \tag{8b}$$

$$\phi(\tau\to\infty) \equiv \phi_\infty = \ln(N(\tau\to\infty)/N_\infty) < 0 \tag{8c}$$

$$\xi(\tau\to\infty) = \xi_\infty \tag{8d}$$

From equation (8a) it is immediate to obtain the relation

$$\sigma\xi_\infty = 1 + \gamma + \nu\phi_\infty \tag{9a}$$

and by replacing it in (8b), the following results can be obtained

$$\xi_\infty = \frac{1}{1+\sigma} = \frac{1+\gamma+\nu\phi_\infty}{\sigma} \tag{9b}$$

$$\Rightarrow \quad \sigma = -\frac{1+\gamma+\nu\phi_\infty}{\gamma+\nu\phi_\infty} = \frac{\nu|\phi_\infty| - (1+\gamma)}{\gamma - \nu|\phi_\infty|}$$

$$\sigma \ge 0 \quad \Rightarrow \quad |\phi_\infty| \ge \frac{1}{\nu}\left(\gamma + \frac{1}{2}\right) \tag{9c}$$

$$\xi_\infty = \nu|\phi_\infty| - \gamma \ge \frac{1}{2} \tag{9d}$$

In the high LET limit the repair mechanisms should be totally absent and these parameters become

$$\sigma = 0 \qquad \xi_\infty = \frac{1}{2} \qquad |\phi_\infty| = \frac{1}{\nu}\left(\gamma + \frac{1}{2}\right) \tag{10}$$

and then in this case the number of cells with reversible DNA damage is going to be a half of the number of clonogenic cells which is still present. At the same time the resulting depletion in the number of clonogenic cells is given by the fraction

$$\Delta \equiv \frac{N(\tau\to\infty)}{N_0} = \exp(\phi_\infty - \phi_0) = \exp\left[|\phi_0| - \frac{1}{\nu}\left(\gamma + \frac{1}{2}\right)\right] = \frac{N_\infty}{N_0}\exp\left[-\frac{\kappa_0}{\alpha_0}\left(\gamma + \frac{1}{2}\right)\right] \tag{11}$$

On the other hand from equation (6c) it can be notice that

$$\left.\frac{d\zeta}{d\tau}\right|_{\tau\to\infty} = \gamma + \xi_\infty = \nu|\phi_\infty| \ge \gamma + \frac{1}{2} \tag{12}$$

Equation (12) tells us that ζ does not have an upper boundary.

III. The Survival Fraction and The Linear-Quadratic Model

C. Low Dose Limit

The survival fraction S can be defined as

$$S = \frac{N + N_R}{N + N_R + N_{NR}} = \frac{1+\xi}{1+\xi+\zeta} \tag{13}$$

and in the low dose limit $D \to 0$ it should match the relation given by the linear-quadratic model

$$S = \exp\left(-\alpha D - \beta D^2\right) \to 1 - \alpha D + \left(\frac{\alpha^2}{2} - \beta\right) D^2 + \mathcal{O}\left(D^3\right) \tag{14}$$

If the absorbed dose rate dD/dt is taken as constant (which is very frequent in several modalities of radiation therapy), there is a simple linear relation in order to get the connection with the evolution parameters

$$\omega D \equiv \kappa_0 t_0 = \tau_0 = \omega \frac{dD}{dt} t_0 \qquad \kappa_0 \equiv \omega \frac{dD}{dt} \tag{15}$$

For the reversible and non-reversible damaged fractions in the $\tau_0 \to 0$ limit the behaviour is described by

$$\begin{aligned} \xi(\tau_0) &= \tau_0 + \frac{1}{2}\left[\gamma - \sigma + \nu\phi_0\right]\tau_0^2 + \mathcal{O}\left(\tau_0^3\right) \\ &= \omega D + \frac{\omega^2}{2}\left[\gamma - \sigma + \nu\phi_0\right] D^2 + \mathcal{O}\left(D^3\right) \end{aligned} \tag{16a}$$

$$\begin{aligned} \zeta(\tau_0) &= \gamma\tau_0 + \frac{1}{2}\left[1 + \gamma^2 + \gamma\nu\phi_0\right]\tau_0^2 + \mathcal{O}\left(\tau_0^3\right) \\ &= \gamma\omega D + \frac{\omega^2}{2}\left[1 + \gamma^2 + \gamma\nu\phi_0\right] D^2 + \mathcal{O}\left(D^3\right) \end{aligned} \tag{16b}$$

Up to second order in ξ and ζ, the survival fraction S can be written as

$$S = \frac{1+\xi}{1+\xi+\zeta} = 1 - \zeta + \xi\zeta + \zeta^2 + \ldots \tag{17}$$

and it should match the low dose limit for the linear-quadratic model, which means that

$$\begin{aligned} S &= 1 - \gamma\omega D - \frac{\omega^2}{2}\left[1 - 2\gamma - \gamma^2 + \gamma\nu\phi_0\right] D^2 + \mathcal{O}\left(D^3\right) \\ &= 1 - \alpha D + \left(\frac{\alpha^2}{2} - \beta\right) D^2 + \mathcal{O}\left(D^3\right) \end{aligned} \tag{18}$$

By using equation (18) the parameters of our proposal can be related to the ones of the linear-quadratic model in a very simple way (they do not depend on σ)

$$\begin{aligned} \alpha &= \gamma\omega \qquad \beta = \frac{\omega^2}{2}\left[1 - 2\gamma + \gamma\nu\phi_0\right] \\ \frac{\alpha}{\beta} &= \frac{2\gamma}{\omega\left[1 - 2\gamma + \gamma\nu\phi_0\right]} \end{aligned} \tag{19}$$

D. High LET Limit

In the high LET limit the main assumption is that no repair mechanism is working and then $\sigma = 0$. In this case equation (7a) becomes

$$\frac{d\phi}{d\tau} = -(1+\gamma) - \nu\phi \qquad \phi(\tau = 0) = \phi_0 \equiv \ln\left(N_0/N_\infty\right) < 0 \tag{20}$$

and its integration leads to

$$\phi = \phi_0 e^{-\nu\tau} - \frac{1+\gamma}{\nu}\left(1 - e^{-\nu\tau}\right) \qquad \lim_{\tau\to\infty}\phi(\tau) = -\frac{(1+\gamma)}{\nu} = \phi_\infty \tag{21a}$$

At the same time we have

$$\frac{d\xi}{d\tau} = 1 + (\gamma + \nu\phi)\xi \qquad \xi(\tau = 0) = 0 \tag{21b}$$

$$\frac{d\zeta}{d\tau} = \gamma + \xi + [1 + \gamma + \nu\phi]\zeta \qquad \zeta(\tau = 0) = 0 \tag{21c}$$

In what follows the asymptotic behavior of ξ and ζ is examined in the $\tau_0 \to \infty$ limit, which is equivalent to the $D \to \infty$ limit and where the survival curve observed behavior follows an exponential law, i. e., $S \to \exp(-\lambda D)$, where λ can be determined in the experiment. Since

$$\lim_{\tau\to\infty}\phi(\tau) = -\frac{(1+\gamma)}{\nu} = \phi_\infty \tag{22}$$

equations (21) can be reduced to

$$\frac{d\xi}{d\tau} = 1 - \xi \qquad \frac{d\zeta}{d\tau} = \gamma + \xi \tag{23}$$

and they can be integrated around $\tau = \tau_0$ in order to obtain

$$\xi(\tau) = [\xi(\tau_0)+1]e^{(\tau_0-\tau)} - 1 \quad (24a)$$

$$\zeta(\tau) = \zeta(\tau_0) + [\xi(\tau_0)+1]\left(1-e^{(\tau_0-\tau)}\right) + (1-\gamma)(\tau_0-\tau) \quad (24b)$$

With the extrapolation (a pure high LET behaviour) of this result to $\tau = 0$, it can be obtained

$$\tilde{\xi}_0 = [\xi(\tau_0)+1]e^{\tau_0} - 1 \quad (25a)$$

$$\tilde{\zeta}_0 = \zeta(\tau_0) + [\xi(\tau_0)+1]\left(1-e^{\tau_0}\right) + (1-\gamma)\tau_0 \quad (25b)$$

and then for $\tau_0 \to \infty$ and $D \to \infty$ limits, the result is

$$\xi(\tau_0) = \left[\tilde{\xi}_0 + 1\right]e^{-\tau_0} - 1 \quad (26a)$$

$$\zeta(\tau_0) = \tilde{\zeta}_0 + \left[\tilde{\xi}_0 + 1\right]\left(1-e^{-\tau_0}\right) + (\gamma-1)\tau_0 \quad (26b)$$

$$S = \frac{1+\xi}{1+\xi+\zeta} \to \frac{\left[\tilde{\xi}_0+1\right]e^{-\omega D}}{1+\tilde{\xi}_0+\tilde{\zeta}_0+(\gamma-1)\omega D} \quad (26c)$$

If the experimental behavior at $D \to \infty$ for high LET is given by $S \to \exp(-\lambda D)$, then by equation (26c) it implies $\gamma = 1$ and

$$\lambda = \omega = \alpha \qquad \beta = \frac{\omega^2}{2}[\nu\phi_0 - 1] \to 0 \qquad \phi_0 = \frac{1}{\nu} \quad (27)$$

For $20\, keV/\mu m$ (low LET) in the case of V-79 cells in late S phase [7], the parameters for the linear-quadratic model are $\alpha = 0.0933\, Gy^{-1}$ and $\beta = 0.04\, Gy^{-2}$. For the same set of cells at $127\, keV/\mu m$ (high LET) the parameters are $\alpha = 0.822\, Gy^{-1}$ and $\beta = 0$ (exponential behavior). Under the assumption that ω does not depend on LET, the following ratio can be found

$$\gamma_{\text{Low LET}}/\gamma_{\text{High LET}} = \alpha_{\text{Low LET}}/\alpha_{\text{High LET}} = 0.1135... \quad (28)$$

and then

$$\gamma_{\text{High LET}} \to 1 \quad \Rightarrow \quad \gamma_{\text{Low LET}} = 0.1135...$$
$$\omega = \alpha_{\text{Low LET}}/\gamma_{\text{High LET}} = \alpha_{\text{Low LET}}/\gamma_{\text{High LET}} = 0.822\, Gy^{-1} \quad (29)$$

The $\gamma_{\text{Low LET}}$ value is one order of magnitude lower than $\gamma_{\text{high LET}}$ as expected for irreversible DNA damage. For Gompertz parameters there are relations given by

$$[\nu \ln(N_\infty/N_0)]_{\text{High LET}} = 1 \quad (30a)$$

$$[\nu \ln(N_\infty/N_0)]_{\text{Low LET}} = \left(1-2\beta_{\text{Low LET}}/\omega^2\right)/\gamma_{\text{Low LET}} = 7.767 \quad (30b)$$

IV. Conclusions

They can be summarized as follows: (1) It is possible to develop simple models based on basic mechanisms of DNA damage and repair. (2) It seems to be essential to consider DNA damage in two steps, one reversible and another irreversible. (3) The α and β parameters of linear-quadratic model are independent of σ in the new model, which is related to the DNA repair mechanism. (4) The proposed model is able to describe the proper behavior at low and high LET for V-79 cells in late S phase.

Acknowledgment

Authors are grateful to Consejo de Desarrollo Científico y Humanístico of Universidad Central de Venezuela for its valuable support in the development of this work.

References

1. Zaider M (1998) There is No Mechanistic Basis for the Use of the Linear-Quadratic Expression in Cellular Survival Analysis. Med Phys 25:791-792.
2. Curtis S (1986) Lethal or Potentially Lethal Model. Radiat Res 106:252-270.
3. Stewart R (2001) Two Lesion Kinetic Model. Radiat. Res. 156:365-378.
4. Brenner DJ (1990) Track Structure, Lesion Development and Cell Survival. Rad Res 124: S29-S37.
5. Fertil B, Reydellet I and Deschavanne PJ (1994) A Benchmark of Cell Survival Models Using Survival Curves for Human Cells after Completion of Repair of Potentially Lethal Damage. Rad Res 138; 61-69.
6. Wheldon TE (1988) Mathematical Models in Cancer Research. Adam Hilger, Philadelphia.
7. Bird RP, Rohrig N, Colvett, RD, Geard CR and Marino SA (1980) Inactivation of Synchronized Chinese Hamster V-79 Cells with Charged-Particle Track Segments. Rad Res 82: 277-289.
8. Wigg DR (2001) Applied Radiobiology and Bioeffect Planning. Medical Physics Publishing, Madison.
9. Wigg DR (2008) Applied Radiobiology – Continuous Irradiation and Brachytherapy. Medical Physics Publishing, Madison.

Corresponding author:

Rafael Martín-Landrove
Centro de Física Molecular y Médica, UCV
Paseo los Ilustres, Los Chaguaramos
Caracas
Venezuela
rmartinlandrove@yahoo.es

Induction of DNA doublestrand-breaks along the tracks of low energy protons

Philipp Schrögel[1], Lukas Kober[1], Cecilia Pizzolotto[1], Andreas Teufel[1], Christian Vogel[1], Luitpold Distel[2] and Wolfgang Eyrich[1]

[1] University Erlangen-Nuremberg, Erlangen Centre for Astroparticle Physics, Erlangen, Germany
[2] University Hospital, Dept. of Radiation Oncology, Erlangen, Germany

Abstract— **With the setup presented here, it is possible to investigate the effects of densely ionising protons in the range of their bragg peak and the repair of the induced concentrated DNA damage. Primary human fibroblasts were irradiated with low energy protons at the Erlangen Tandem Van-de-Graaff accelerator. The DNA damage along the paths of the protons in the cell nuclei was visualised by immunostaining and fluorescence microscopy. The marker protein for the detection of doublestrand breaks was the phosphorylated histon γ-H2AX. Clearly identifiable particle tracks could be induced, allowing further investigations of the repair kinetics. While other experiments in this field mostly make use of heavy ions, this works allows the comparison of the results with the effects of densely ionising protons.**

Keywords— **DNA-damage, γ-H2AX, proton irradiation, doublestrandbreak, repair kinetic**

I. Introduction

The understanding of the mechanisms of DNA repair is important for the estimation of the effects of ionising radiation in therapy or natural situations. Densely ionising radiation like low energy protons or, even more, heavy ions creates clustered damage along their path. For this concentrated damage, the so called bulky lesions, cellular repair mechanisms have to meet higher requirements. The question about the repair kinetics of these bulky lesions and the involved proteins was posed in Erlangen some time ago and is also subject of actual experiments of other groups using heavy ions [1, 2].

II. Material and Methods

Primary human fibroblasts were irradiated at the vertical beam of the Erlangen Tandem Van-de-Graaff accelerator with low energy protons ($4 - 8$ MeV). The initial narrow proton beam is widened by a scatter-foil to generate a homogenous beamfield and cover the whole biological sample. The spatial proton distribution is controlled before cell irradiations with a beamprofile-detector consisting of 16 scintillating fibers. As the low energy protons are stopped inside the samples, the applied dose has to be measured with an indirect dosimetry system and to be counted back [3]. The system is formed by 4 monitor scintillation detecors arranged at the side of the beam. The signals are read out with VME-based QDC and scaler modules. The readout software is integrated in the data analysis framework ROOT, allowing an online-analysis of the data. For the energy calibration of the measured spectra, the data was compared with simulations (SRIM).

To induce tracks inside the cell nuclei, the cells had to be irradiated in a small angle to the beam (1°- 5°). Therefore, the cells were grown on coverglasses and placed headfirst in foil-base dishes ($2\mu m$ hostaphan) for the irradiation. This solution reduces the amount of water, the protons have to pass before entering the cells, to a minimum. The cells are furthermore protected from desiccation and can easily be placed back in culture medium after the irradiation. A schematic view of the setup is shown in figure 1. The dishes were mounted vertical on a rotable plate to allow an automated irradiation of up to 7 samples.

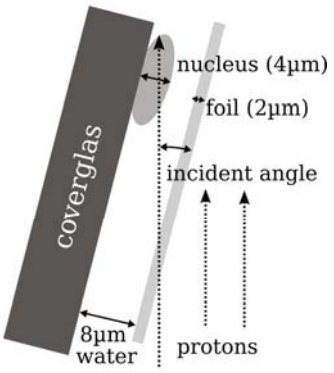

Fig. 1: Schema of the irradiation of the cells headfirst in foil-base dishes in a small angle to the proton beam

We used the phosphorylated histon γ-H2AX as marker for double-strand breaks [4], although it is possible that sometimes more than one double-strand break is located inside the phosphorylated area (foci) that appears in the fluorescence

O. Dössel and W.C. Schlegel (Eds.): WC 2009, IFMBE Proceedings 25/III, pp. 512–514, 2009.
www.springerlink.com

image. To ensure that only foci in the nucleus are considered, the nuclei are marked with DAPI to identify the dimension of the particular nucleus.

III. Results

The protons reach high LET values and are able to induce concentrated DNA damage in a narrow region along their path The trajectories are parallel in the range of the angular straggling of the protons through the scatter-foil and the beam-exit window (see figure 2a). We could observe proton tracks extending over two cells next to each other (see figure 2b) and nuclei with several damage tracks inside (see figure 2c and 2d). In some cells we found γ-H2AX foci, that could not be identified as tracks due to their position. They could have been produced by stochastical interactions of some protons or by secondary delta-electrons or gamma photons. These observations correspond with the results of Jakob et al. [5] for cell irradiations with heavy ions (Carbon and Bismuth).

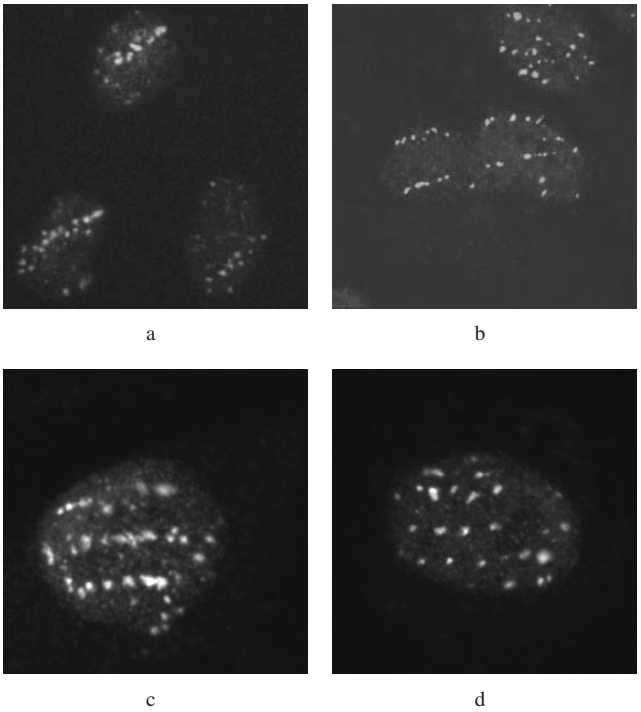

Fig. 2: γ-H2AX foci along proton trajectories in cell nuclei 1h after the irradiation. a) parallel trajectories in 3 cells b) trajectory through 2 cells c) and d) nuclei with multiple tracks

The mean distance of foci along a track was 1.8 μm (see distribution in figure 3). The measured distances accumulate between 1 and 2 μm along the trajectories. This result is in good agreement with the results of Hauptner et al. [2] for heavier ions (Lithium and Carbon), confirming that we reached the high LET region of the protons. The tracks consisted on average of 6 γ-H2AX foci, mainly varying from 4 to 8 (see distribution in figure 4). In the first measurements only short repair times ($<$ 2h) were given to the cells to verify the ability to produce clear particle tracks. Therefore, we cannot provide any data for the blurring of the tracks with time through diffusion or active transport processes at the moment.

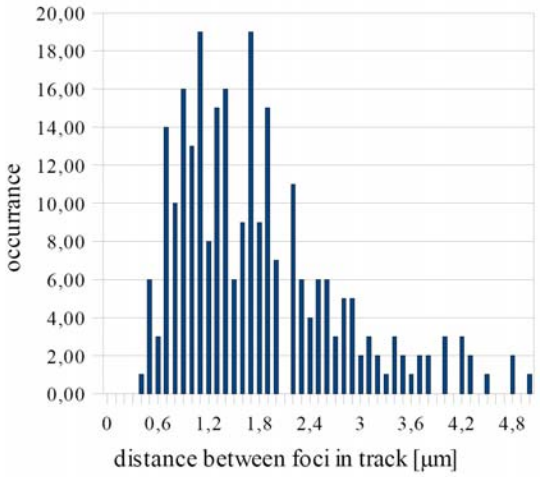

Fig. 3: Measured distance between the foci in the proton trajectories after a repair time of 30 minutes. 56 tracks are considered in this statistics.

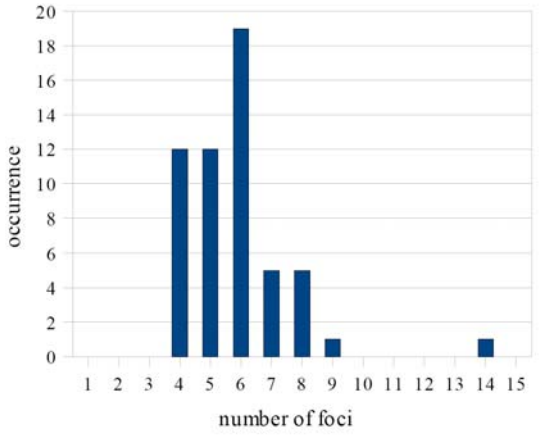

Fig. 4: Distribution of the total number of foci in the trajectories after a repair time of 30 minutes. 56 tracks are considered in this statistics.

IV. Conclusion

With the method presented here, it is possible to investigate the kinetics of DNA-repair and marker proteins after irradiation with densely ionising protons. As the DNA damage by protons is located in linear tracks, it is possible to determine the time-dependent movement of repair proteins and damage sites relative to each other and their colocalisation. It is still undetermined, whether double-strand breaks and bulky lesions are repaired at their point of origin by allocating repair proteins, or if the damage DNA parts are transported to special repair-sites inside the nucleus with a high repair-protein density. We are aiming to answer this open question: we expect either a strong blurring of the tracks or a linear alignement of the repair-proteins with advancing time parallel to an increasing colocalisation of the damage sites and repair proteins.

Acknowledgements

The authors wish to thank the staff of the Tandem accelerator for their cooperation as well as Elisabeth Müller from the radiation biology laboratory for her technical support.

References

1. Stap Jan, Krawczyk Przemek M, Oven Carel H Van, et al. Induction of linear tracks of DNA double-strand breaks by alpha-particle irradiation of cells *Nature Methods.* 2008;5:261-266.
2. Hauptner A., Krücken R., Greubel C., et al. DNA-repair protein distribution along the tracks of energetic ions *Radiation Protection Dosimetry.* 2006;122:147-149.
3. Mörtel Heiner, Georgi J., Eyrich W., Fritsch M., Distel L.. Automation of the particle dosimetry and the dose application for radiobiological experiments at a vertical proton beam *Nuclear Instruments and Methods in Physics Research A.* 2002;489:503-508.
4. Modesti M., Kanaar R.. DNA repair: Spot(light)s on chromatin *Current Biology.* 2001;11:R229-R232.
5. Jakob B., Scholz M., Taucher-Scholz G.. Biological Imaging of Heavy Charged-Particle Tracks *Radiation Research.* 2003;159:676-684.

Author: Philipp Schrögel
Institute: University Erlangen-Nuremberg, ECAP
Street: Erwin-Rommel-Str.1
City: 91054 Erlangen
Country: Germany
Email: schroegel@pi4.physik.uni-erlangen.de

New Materials for Radiation Protection Buildings

Monte Carlo-Simulations and Measurements for X-rays Protons and Carbon Ions

R.G. Mueller[1], J. Forster[2] , R. Forster[2], N. Achterberg[1], J. Karg[1] and O. Pravida[3]

[1] Strahlenklinik, IMP, University Erlangen, Germany
[2] Forster-Bau Ingenieurgesellschaft, Ingolstadt, Germany
[3] Pravida Bau, Pressath, Germany

Abstract— **For establishing sandwich technology in radiation protection constructions new filling materials were fixed and their attenuation characteristics in relation to X-rays (6-15 MV), protons (150-600 MeV) and carbon ions (150-430 MeV/u) were checked by Monte Carlo simulations and even so by direct measurements of transmitted dose at suitable sources.**

Keywords— **radiation shielding, radiation protection costruction, DIN 6847-2 [1]; PAS 1078; NCRP 151 [2], sandwich construction, neutron attenuation**

I. Introduction

The Sandwich technology for radiation protection construction has become a recognized technique for the shielding of Linacs in medical use in Germany. The technology is vastly superior to in situ concrete. Erection in sandwich reduces the time necessary for move-in readiness to less than half of usual. The walls are immediately dry after erecting. And last not least the costs are reduced at a fraction of before.

The Sandwich technology in radiation protection construction is so benefiting that it should in consequence be available for most radiation sources producing electrons, photons, protons, heavier ions, neutrons, and all their secondary particles.

Sandwich technology turns out to be suitable for all known radiation sources up to the highest energies which can be produced today. The most important component in this connection is the fluency and energy distribution of generated neutrons. Thus neutron attenuation capacity becomes the most important attribute of the radiation protecting material. In addition long term activation of the material must be avoided – e.g. no tracers like natural Co and Cs.

Measuring neutron attenuation in relation to protecting constructions makes large areas and thick layers necessary. So we decided to do this by installation of a special igloo with three windows in three directions in relation to the primary beam. The total mass which had to be installed and moved was about 240 t. Attenuation path length was up to 250 cm in different filling materials.

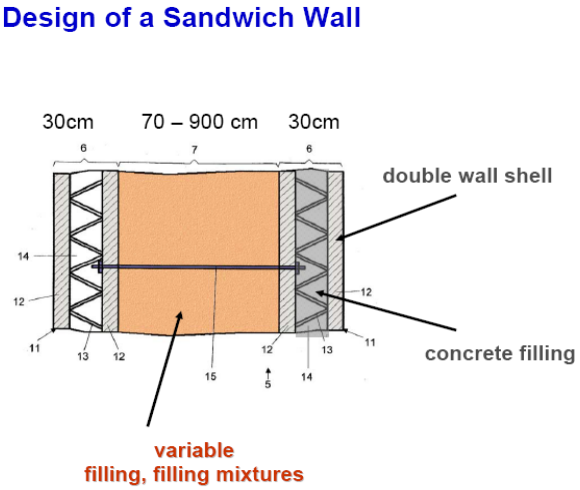

Fig. 1 Sandwich construction with inner and outer double wall shells (6) which will be filled with concrete, in between compacted filling material e.g. mixtures of different material or different material in vertical and horizontal layers.

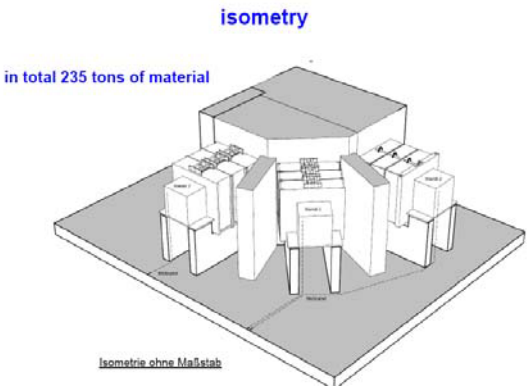

Fig. 2 Igloo with three windows of 0°, 45°, and 90° in relation to the primary particle beam. The cases with test materials are still in position.

O. Dössel and W.C. Schlegel (Eds.): WC 2009, IFMBE Proceedings 25/III, pp. 515–518, 2009.
www.springerlink.com

II. Monte carlo simulation

Starting with Linacs for medical use MC simulation using EGS4 was accomplished. For validation of the model results measurements were performed inside a treatment room of the radiation oncology in Erlangen. Measured data were done for 3 X-ray energies (6, 10 and 15 MV) and for about 10 different materials. Measured and simulated data were identical in between the estimated errors with one exception for natural gypsum, where the measured data for the tenth value layer of area density [g/cm²] e.g. were about ten percent worth than by simulation. Up to now we could find no sensible reason for this discrepancy besides the questionable purity and /or humidity of the material.

Some results of our endeavors were introduced in the German regulations DIN 6847-2 (Sept. 2008). Meanwhile more than 40 vaults were designed using our data.

During that MC simulations started for protons in use of radiation therapy up to 220 MeV. For the particle simulations we used GEANT4 [3]. The simulated data for concrete are part of the German regulations PAS 1078 (Jan. 2008). Covering the demands of clinical use MC simulations and measurements for carbon ions became necessary. After realizing the funding of the program it could be started October 2008.

In contrast to medical Linacs the dose relevant component behind shielding for particle therapy are the secondary neutrons. Hence the effective dose becomes relevant for the purpose of radiation protection. This makes a double convolution of the physical dose in Gy necessary. At first absorbed energy per volume will be calculated, than the neutron fluency and energy spectrum must be calculated dependent on position. The neutron spectra will be convolved with the biological effectiveness. At the end effective dose H*(10) behind a shielding wall will result.

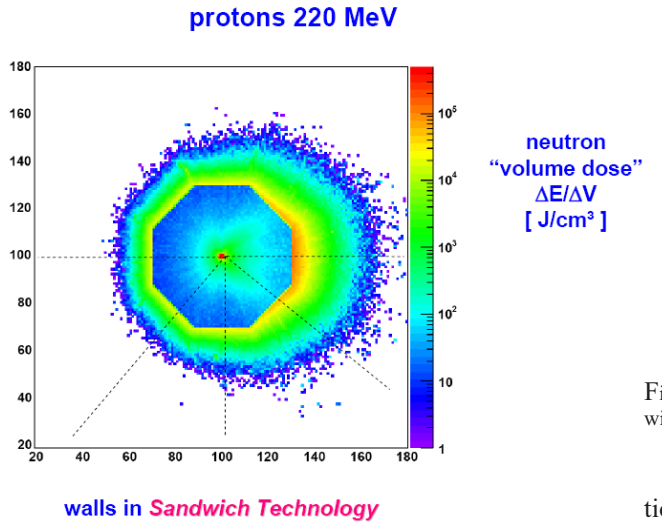

Fig. 3 Octagonal "treatment" room for MC simulation. Easy calculation along 5 axis (0°;45°;90°;135°;180°)

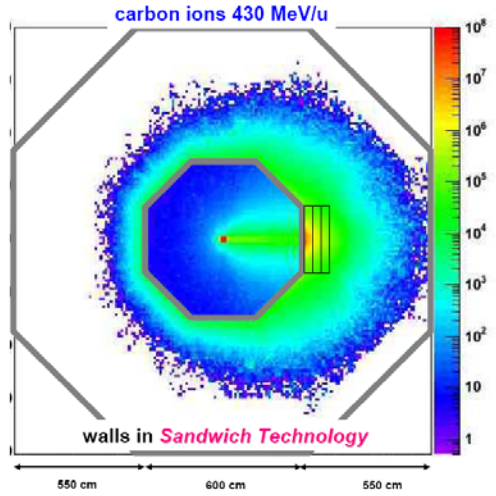

Fig. 4 Same situation as fig.3 but for 430 MeV/u carbon ions, including 100cm spalation layer in 0° direction.

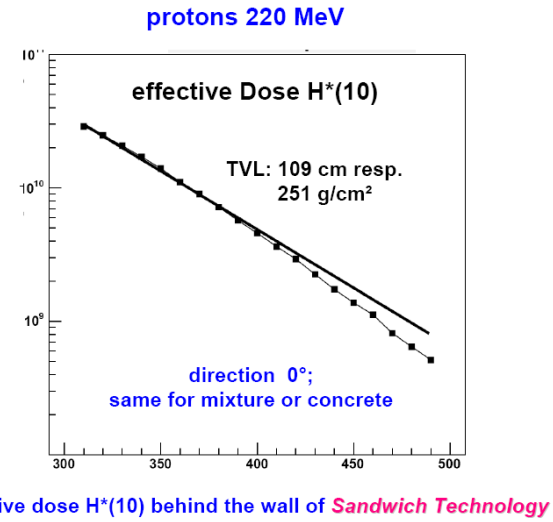

Fig. 5 Calculated effective dose H*(10) for 220 MeV protons and a sandwich wall.

Because of the nearly logarithmic dependency of attenuation the slope of e.g. fig. 5 offers a good estimate for radiation protection calculations passing MC simulation.

III. Measurement

In contrast to the measurement with X-rays particle measurement demand much bigger operating and financial expenses. The measurement for protons and carbon ions were performed at GSI (Darmstadt, Germany). The material to be transported there was more than 240 tons. Fortunately we had the opportunity to get for each particle a time slot of 2 days minimum for measurement.

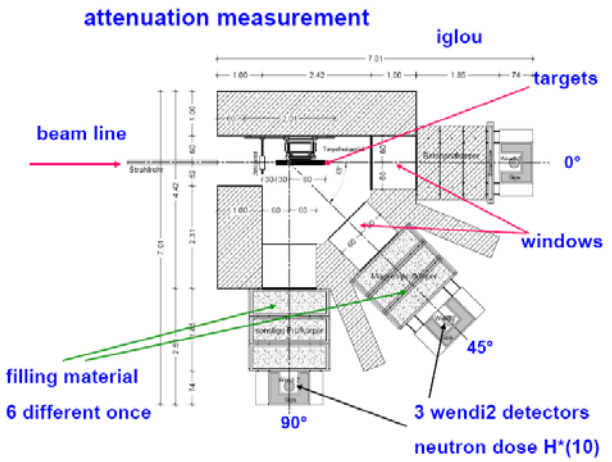

Fig. 6 A sketch of the experimental setting. Measurements were performed in three directions at once. For four energies three different targets were used. Material of the target was pure graphite, target length up to 110 cm. As direct reading dosimeter 3 Wendi2 (Thermo Fisher Scientific) was used.

Fig. 7 Real situation. The Wendi2 were shielded against backscattered radiation within the orange boxes filled with gypsum.

IV. Results

MC simulated and really measured data are in concordance. There are no systematic deviations to be seen

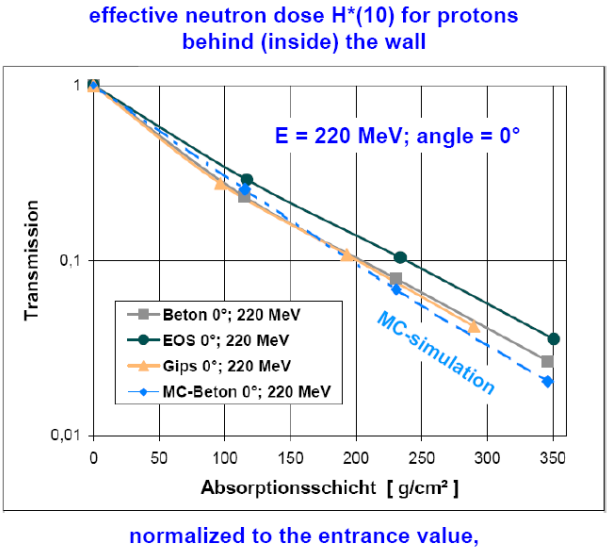

Fig. 8 Neutron attenuation for 220 MeV protons using different material: concrete (grey), electro furnace slag (green) gypsum (beige); dashed curve results from MC simulation for concrete.

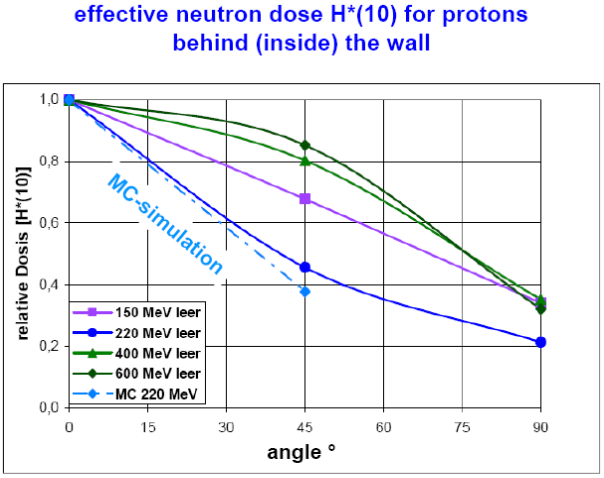

Fig. 9 Dependency of effective dose depending on proton energy and angle in relation to the primary beam. The curves are normalized at zero angle.

Fig. 8 shows the excellent concordance between simulation and measurement in relation to the attenuation in concrete. Obviously the iron content of the slag EOS shows no benefit for this moderate neutron energies produced by protons. This changes considerably using high energy carbon ions. There the spallation effect of high Z material becomes obvious.

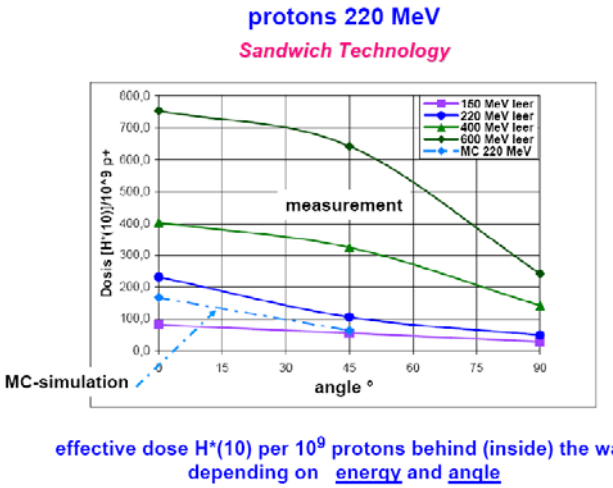

Fig. 10 Absolute effective dose depending on proton energy and angle. Here the MC simulation shows more than 10 % lower values than the measurement. This must be weighed by the fact that the read out of the Wendi2 for this broad neutron energy spectra has an uncertainty of up to 30%.

With fig. 10 it becomes clear that it may be very difficult to fix absolute values of H*(10) with an accuracy better than ± 20 % for these broad energy spectra of neutrons.

V. Conclusions

Monte Carlo simulation and measurement for radiation attenuation in shielding materials were performed. The data are in good agreement and all the experience with radiation protection design using this data had been positive. It turned out that sandwich technology is superior to normal concrete by erection time, wall dimensioning, price and sustainability. So we can be sure in using both, MC simulation and measurement, and the combination of both for dimensioning radiation protection buildings for even high energies of X-rays but also for particles.

Acknowledgment

We are very grateful to Prof. Dr. Horst Stöcker, scientific director of GSI, Darmstadt, and his colleagues for allowance and time slots for particle measurement. Also many thanks to the sponsors who made the measurement possible. We accentuate the help of our colleagues in the medical radiation physics team MSP Strahlenklinik of the Universitätsklinikum Erlangen for their support: Stefan Gebhardt, Markus Kellermeier, Stephan Kreppner, Ulrike Lambrecht, Michael Lotter, Manfred Schmidt, Stefan Speer, and Willi Stillkrieg.

References

1. DIN 6847-2 Sep. 2008: Medical electron accelerators – Rules for construction of structural radiation protection
2. PAS 1078 Jan. 2008: Accelerator systems for proton therapy – Rules for construction of structural radiation protection
3. Agostinelli S et al. GEANT4 7.1 2003, Nucl.Instrum.Methods A 506 250-303

Author: Prof. Dr. Reinhold Müller
Institute: Strahlenklinik-Universitätsklinikum Erlangen;IMP
Street: Universitätstraße 27
City: 91054 Erlangen
Country: Germany
Email: reinhold.mueller@uk-erlangen.de

Fetal Dose Evaluation in X-Ray Radiotherapy in Cases of Advanced Gestation

D. Filipov[1], K.C. Mafra[1], H.R. Schelin[1], D.S. Soboll[1,2]

[1] Federal University of Technology – Paraná, UTFPR-CPGEI, Curitiba, Brazil
[2] Erasto Gaertner Hospital, Radiotherapy Sector, Curitiba, Brazil

Abstract — **When pregnant women are submitted to x-ray radiotherapy, the fetus can be seriously affected by the scattered radiation dose. With the purpose of verifying this dose, an anthropomorphic phantom from a commercial mannequin was constructed to be irradiated in the left breast. The simulator was built with materials of density close to water and filled with water. The irradiation was made using x-ray beams of 6 MeV energy, from a linear accelerator Clinac 2100C. Using a cylindrical ionization chamber positioned in the fetal region of the simulator, it was verified that at the end of the breast treatment the dose of scattered radiation is around 136 cGy in all fetal area. These values are harmful to the fetus and thus, the use of radiological protection procedures is recommended.**

Keywords— **radiotherapy, fetus, dose, chamber.**

I. Introduction

Breast cancer is the second most common type of cancer in pregnancy. Its incidence increases due to the fact that women are getting pregnant at a later age nowadays as well as due to the development of technologies of illness diagnosis. [1] According to the *American Association of Physicists in Medicine – AAPM*, each year, in the United States, approximately 4,000 pregnant women get some kind of cancer, and x-ray treatment is chosen in most cases [2]. AAPM considers that the fetus can be harmed should the fetal area be irradiated with doses higher than 10 cGy [3]. According to AAPM in case the fetus is irradiated during the second trimester of pregnancy, doses lower than 100 cGy can cause sterility. In addition, there is a 14% probability for each 100 cGy that cancer will develop during his/her life, and a risk of growth retardation for doses larger than 50 cGy [4]. Furthermore, cell killing can appear (whose severity depends on the received dose) [3]. The effects caused by cell killing are: abnormalities of the central nervous system, cataracts, and behavior disorders [3]. With the purpose of verifying the dose that the fetus can receive during a breast radiotherapy treatment, an anthropomorphic phantom was constructed. The phantom was irradiated in the left breast and the scattered doses in several points of the abdominal region were measured.

II. Materials and methods

The phantom was constructed using a commercial polyethylene mannequin. It was adapted so that the dose of scattered radiation could be measured through a fixed acrylic component on the womb. In this component, three holes were made, inside of which a cylindrical ionization chamber Farmer (Exradin A12) was located, as shown in figure 1.

Fig. 1 A) nylon rod; B) the rod being placed in one of the holes C) all the rods (drilled internally) placed in the holes.

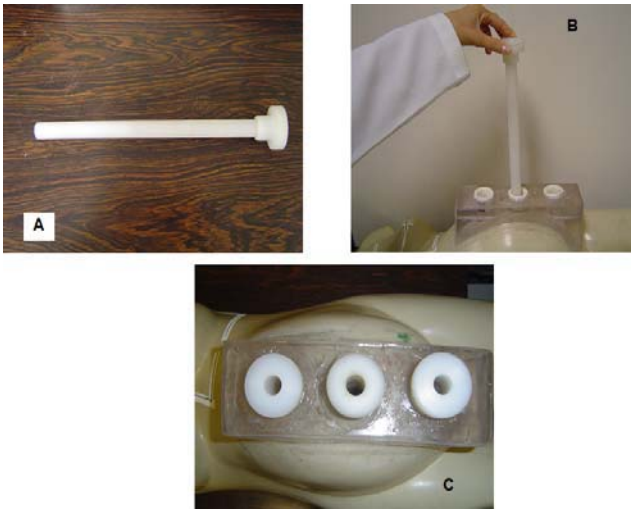

The mannequin was filled with water and imaged in a CT. A helical scan was made (which generated images with 7 mm distance between them and 7 mm step), with a FOV of 35.7 cm, resulting a total of 87 images. When the exam was finished, the images were transferred to the planning system through a DICOM system. Figure 2 shows the phantom located in the CT.

O. Dössel and W.C. Schlegel (Eds.): WC 2009, IFMBE Proceedings 25/III, pp. 519–522, 2009.
www.springerlink.com

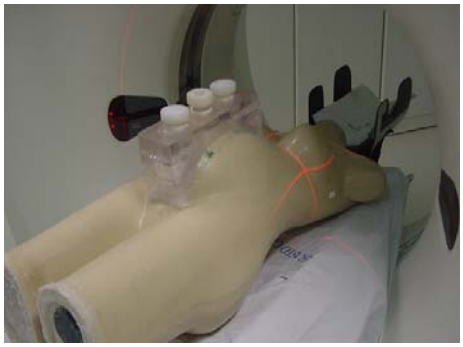

Fig 2 The phantom positioned in the CT.

The system of Three-dimensional Planning Cadplan-Somavision of the Varian Medical Systems was chosen, which is used in the Medical Physics Department of the Erasto Gaertner Hospital. The system is used to carry out the three dimension planning that makes the conformational radiotherapy possible. The "CadPlan" facilitates the reconstruction of the isodose distribution inside an antropomorphus virtual environment in three dimensions [5]. The images originated from the CT were sent digitally to the SomaVision Treatment Prescription planning program and later the contour of the phantom was drawn cut by cut. The PTV (planning target volume) represents all the breast of the phantom and was drawn in red. Finally, the rods were marked in orange. Once the marks were ready, the reconstruction in three dimensions was made. After this stage, the images were sent to the CadPlan planning system and the fields normally used in a breast treatment were inserted, as shown figure 3.

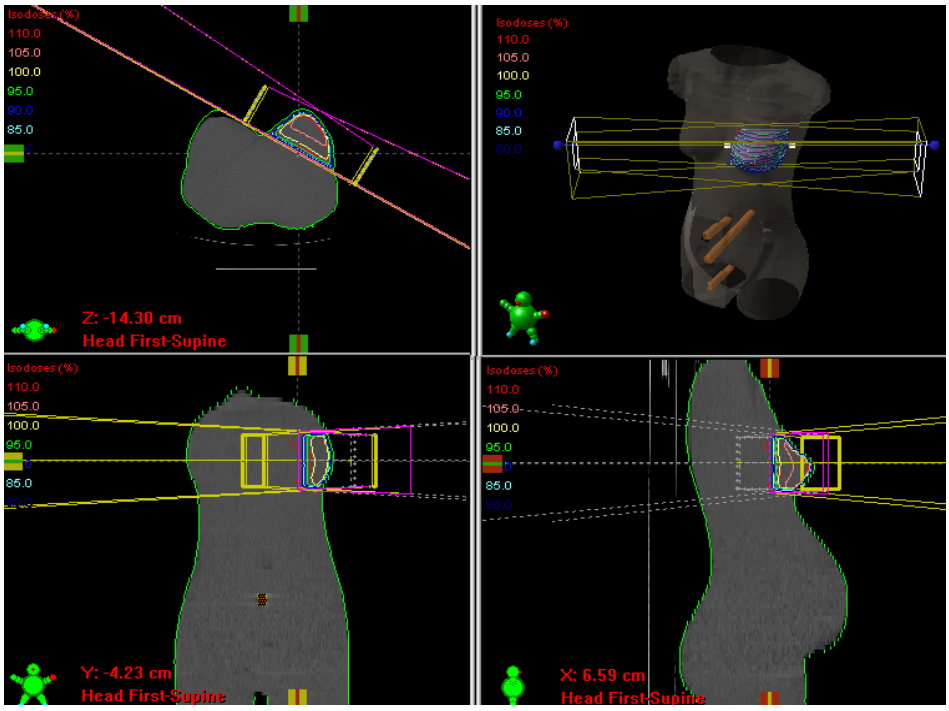

Fig 3 Radiotherapic breast treatment planning. Note in the first quadrant the breast being irradiated with two angulated fields.

The measurement of the absorbed dose by the fetus was made by irradiating the phantom in the CLINAC 2100C Medical Varian Systems accelerator. This accelerator produces beams of bremsstrahlung x-rays from electrons that reach potentials of 6 MV or 10 MV. The 6 MV beam was chosen for the dosimetry because it is the one which is clinically used for breast treatments. In order that the electric charges measured could be associated to dose values, initially measurements of the collected charge were made by the electrometer of the ionization chamber in a cubic phantom of 40x40x40 cm ^{3}, in reference conditions. In this way, the chamber was irradiated with a known dose, whose value was associated to the corresponding collected charge. The cubic phantom was irradiated with monitoring doses of 100 MU (monitoring units) - in a 10 x 10 cm^2 field - and the electrometer ("CDX - 2000B" of Standard Imaging) collected the charges of the ionization chamber, for a polarization voltage of 300 V.

The average value of three readings of the ionization chamber was 15.67 nC. According to the tables used in the accelerator, with 10 x 10 cm^2 field and at 5 cm, the percentage of deep dose is 86.0% of the dose of the maximum depth. As 100 MU were applied, the dose received in the maximum depth was 100 cGy, but at 5cm it was 86 cGy. Consequently, 86 cGy of absorbed dose is obtained when the electrometer shows 15.67 nC

After these measurements were made with the cubical phantom, additional measurements were done with the anthropomorphic phantom in the three connecting rods. The mannequin, filled with water, was located on the table of the linear accelerator. A field of 10 cm (x axis) by 16.5 cm (y axis) was projected in the left breast.

The anthropomorphic phantom was irradiated with a monitoring dose of 500 MU. Although the monitoring dose is not usually applied for breast treatment (in general it is a little bit more than 100 MU for each application), a larger value was chosen because the connecting rods are in a distant region of the breast and perhaps with only 100 MU would be difficult to collect the charges, due to the attenuation of the dose.

Figure 4 shows the three regions of the connecting rod where the chamber was located to collect the charges. The positions, according to the anatomy of the mannequin, were called anterior region, medial region and posterior region and are distant from the posterior extremity of the connecting rod, respectively, 23 cm, 15.6 cm and 2.6 cm. To carry out the measures in each region, the empty spaces of the connecting rods were filled with water.

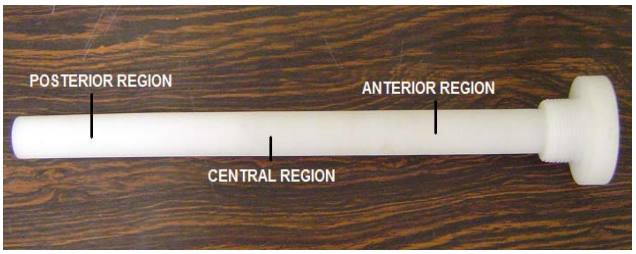

Fig 4 Connecting rod with the indications of the regions where the measurements were made.

III. Results and Discussion

The mannequin (used in commerce as expositor of adult clothes) modified and filled with water had a mass of 54 kg. The measurements were obtained based on the fact that, for the breast treatment in the Erasto Gaertner Hospital, usually a total of around 6000 MU are applied and the measurements of collected charge for electrometer shown on Table 1 were obtained.

Table 1 Ionization chamber readings with the connecting rod localization and the depth of the connecting rod inside the chamber.

Superior Rod		Central Rod		Inferior Rod	
Region	Reading (nC)	Region	Reading (nC)	Region	Reading (nC)
Anterior	0.55	Anterior	0.26	Anterior	0.13
	0.56		0.26		0.13
Central	0.33	Central	0.19	Central	0.11
	0.33		0.19		0.10
Posterior	0.25	Posterior	0.15	Posterior	0.08
	0.25		0.5		0.08

As the 15.67 nC reading corresponds to 86.0 cGy, then for each nC the dose absorbed in the region of the chamber is of 5.5 cGy. Considering this fact and that, clinically, in the Hospital Erasto Gaertner, for the treatment of breast usually a total of around 6000 MU is applied, we multiplied the values of table 1 by 5.5 cGy and by the rate 6000 MU/500 MU, in order to estimate the dose in the fetal region at the end of the treatment. The results are shown in Table 2.

Table 2 Doses obtained in each position of the ionization chamber at the end of the treatment of breast irradiation.

Superior Rod		Central Rod		Inferior Rod	
Region	Dose (cGy)	Region	Dose (cGy)	Region	Dose (cGy)
Anterior	36.3	Anterior	17.2	Anterior	8.6
	37.0		17.2		8.6
Central	21.8	Central	12.5	Central	7.3
	21.8		12.5		6.6

Posterior	16.5	Posterior	9.9	Posterior	5.3
	16.5		9.9		5.3

The lowest doses were observed in a more distant regions (next to the genital region) of the irradiated breast. The attenuation of the dose in this region is due, along with the biggest distance, to the acrylic part on the womb of the mannequin. It was also verified, that in deeper regions of the belly of the mannequin the doses are lower than in more superficial regions.

The relation of the doses estimated with the risks cited in the literature, were observed. According to theoretical data, at the final phase of the fetal period there is a risk of 14 % for each 100 cGy to develop cancer after the birth. In accordance with the obtained values in table 2, the received dose for the fetus, at the end of the radiotherapic treatment (around 136 cGy) is enough to offer risk to the development of cancer in the embryo after the birth.

IV. Conclusions

According to the results of the measurements, it is estimated that the dose measured in the fetal region is enough to develop sterility in the fetus, as well as a probability of 14% for each 100 cGy to develop some type of cancer during his life. The doses measured in the fetal region are due to the scattered radiation coming from the room and from inside the simulator object, and the leak radiations of the head of the tube. Therefore, we conclude that there is a necessity to protect the fetal region radiologically through the construction of a specific shield for this area.

V. References

1. Stewart A, *Brigham and Women's Hospital, Dana Faber Cancer Institute - Radiation Oncology, Boston – USA*. Fetal radiation dose: a phantom study of potential dose to the uterus at 12 and 24 weeks gestation with accelerated intracavitary partial breast irradiation.
2. Wierinqen N. van, Koedooder C, Tienhoven G. van, Blank L.E.C.M. *Academic Medical Center, Radiotherapy, Amsterdam, The Netherlands.* Estimations and limitations of the fetal dose during radiotherapy of the thoracic wall and regional lymph nodes of a pregnant patient.
3. Bednarz B, George X. *Nuclear Engineering and Engineering Physics Program, Rensselaer Polytechnic Institute,Troy, New York 12180*. A feasibility study to calculate unshielded fetal doses to pregnant patients in 6-MV photon treatments using Monte Carlo methods and anatomically realistic phantoms.
4. Stovall M, Blackwell C.R, Cundiff J, Novack D.H, Palta J.R, Wagner L.K, Webster E.W, Shalek R.J. (1995) Fetal dose from radiotherapy with photon beams: Report of AAPM Radiation Therapy Committee Task Group No. 36. MEDICAL PHYSICS, Vol. 22, Issue 1

Neutron spectrometry and determination of neutron ambient doses in radiotherapy treatments under different exposure conditions

C. Domingo[1], M.J. García-Fusté[1], E. Morales[1], K. Amgarou[1], J.A. Terrón[2], J. Roselló[3], L. Brualla[3], L. Nuñez[4], R. Colmenares[5], F. Gómez[6], G.H. Hartmann[7], F. Sánchez-Doblado[2,8] and F. Fernández[9]

[1] Dpto. de Física, Univ. Aut. Barcelona, Barcelona, Spain.
[2]H. V. Macarena, Sevilla, Spain
[3]ERESA, Valencia, Spain
[4]H. Puerta Hierro, Majadahonda, Spain
[5]H. Ramón Cajal, Madrid, Spain
[6] Dpto. de Partículas, Área de Física Atómica, Molecular y Nuclear, Univ. Santiago Compostela, Santiago de Compostela, Spain
[7] Deutsches Krebsforschungszentrum (DKFZ), Heidelberg, Germany
[8]Dpto. de Fisiología Médica y Biofísica, Univ. Sevilla, Sevilla, Spain
[9]CSN, Madrid, Spain

Abstract— **A project has been set up to study the effect on a radiotherapy patient of the neutrons produced around the LINAC accelerator head by photonuclear reactions induced by the gamma radiation above ~8 MeV. These neutrons may reach directly the patient, or they may interact with the surrounding materials until they become thermalised, scattering all over the treatment room and affecting the patient as well, contributing to the peripherical dose. Spectrometry was performed with a set of Bonner spheres at 50 cm from the isocenter and at the place where a digital device for measuring neutrons will be located the treatment room. Exposures have taken place in six linac accelerators with different energies (from 6 to 23 MV). A summary of the spectrometry results and of the neutron doses received by the patient is presented.**

Keywords— **photoneutrons, neutron spectrometry, ambient dose equivalent**

I. Introduction

The photon beam of appropriate energy and intensity for a localised radiotherapy treatment of a given organ is produced in electron linear accelerators (LINACs) from Bremstrahlung of a monoenergetic electron beam in a suitable target, made of a combination of heavy metals. A flattening filter, situated after the target and made also of heavy metals, has the purpose of giving a uniform photon irradiation all over the complete square irradiation field, which size is set by means of adequate collimators, made also of heavy metals.

The constant improvement and evolution of the methodology used in radiotherapy because of the advances on Physics and Engineering has the outcome of a better confinement of the radiation dose around the clinical target. In this way, techniques like Radiosurgery, Intensity Modulated Radiation Therapy (IMRT) or Hadrontherapy have an increasing role in the treatment of cancer.

If photons with energies above ~ 8 MeV are present, photoproduction of neutrons in any of the heavy metals present at the LINAC structure or shielding, in particular in the target, the flattening filter, the collimators and the multileaf collimators for IMRT if present, is possible [1]. Typical neutron spectra inside LINAC treatment rooms have a peak around 1 MeV (direct or primary component), another peak around 0.025 eV (thermal component) and a much less abundant epithermal component of neutrons with intermediate energies. All these neutrons contribute to the peripheral dose delivered to the patient.

ICRP publication 103 [2] deals, among other subjects, with radioprotection of patients and, in particular, of those being exposed to radiotherapy treatments, stating that *"… in radiation therapy it requires delivery of the required dose to the volume to be treated, avoiding unnecessary exposure of healthy tissues."* Although photon doses have been deeply studied, following well known experimental procedures, the neutron contamination from high energy photon beams is still a subject of research and discussion. Nevertheless, it seems clear that, when high energy linear accelerators are used for the treatment of deep-seated tumours, the patients may receive a large total body dose of scattered x-ray and photoneutrons. It should be expected, therefore, that patients might show a higher incidence of second malignancies [3-7].

A project has been set up with the final goal of estimating, from the readings of a digital device located inside the treatment room, the neutron equivalent doses that a patient subject to a given radiotherapy treatment has received in several relevant organs in a given session. During the first phase of the project, an anthropomorphic female phantom (tissue equivalent for photon irradiation) is filled with sev-

O. Dössel and W.C. Schlegel (Eds.): WC 2009, IFMBE Proceedings 25/III, pp. 523–526, 2009.
www.springerlink.com

eral types of passive neutron detectors (TLDs, PADCs, gold foils, …) at 16 different places (plus two extra places at the location of the digital device) and irradiated to several "standard" radiotherapy treatments at a number of LINAC accelerators of different energies (between 6 and 23 MV) and makes. Readings from these detectors will be correlated to those obtained from the digital device, and equivalent doses in organs will be calculated from these readings and computer reconstruction.

In addition, neutron spectrometry was performed with the UAB passive Bonner Sphere System (BSS) [8] at two reference points (at 50 cm from the isocenter and at the place where the digital device stands) in each treatment room. This passive BSS was calibrated and validated experimentally in reference metrological neutron fields, as recommended by the International Standards Organisation (ISO) [9,10]. Because of this reason, fluences and doses obtained from the BSS may be used as absolute reference, so measurements at the place of the digital device allow correlating the absolute neutron fluence and ambient dose equivalent with the response of the digital device itself and with the readings of the passive neutron detectors. This paper summarises the results obtained from the BSS spectrometry system in five different linacs of different energies and types

II. Material and method

Among the many available neutron spectrometry techniques, the multisphere or Bonner sphere spectrometer (BSS) is the most used for radiation protection purposes [11], due to advantageous characteristics as wide energy range (from thermal to GeV neutrons), large variety of active or passive thermal sensors allowing adapting the sensitivity to the specific workplace, good photon discrimination and simple signal management. The passive UAB Bonner sphere spectrometer (BSS) is described in [8].

Provided a well-established response matrix and adequate irradiation conditions [12], the most delicate part of the BSS-based spectrometry is the unfolding process. The response matrix of the passive UAB-BSS system was calculated by Monte Carlo simulation for a broad range of neutron energies (from thermal up to 20 MeV), using the MCNPX-2.4.0 [13] transport code. Simulation was performed with statistical uncertainties <1% at all points. The response matrix was verified by unfolding the data obtained from irradiation with the ISO ^{252}Cf source at the IRSN (Cadarache) calibration facility. The FRUIT code [14] has been used for unfolding, in order to obtain the energy distribution of the neutron fluence from the readings of the detectors at the center of the Bonner spheres and from the evaluated response matrix.

Spectrometric measurements have been made at all irradiation with a static (10×10) cm^2 field at 0°, in a reference point located at 50 cm from the isocenter (without the presence of the anthropomorphic phantom at the couch), at its same height, and at the place where the digital device is located (with the phantom at the couch).

Irradiations were performed at six linac accelerators: two 15 MV Siemens Primus linac (Hospital Universitario Virgen de la Macarena, Sevilla, Spain), an 18 MV Siemens Primus linac (Hospital General Universitario de Valencia, Spain), a 23 MV Siemens Mevatron linac (Universitätsklinikum Heidelberg, Germany), a 15 MV Varian Clinac 2100 (Hospital Puerta de Hierro, Majadahonda (Madrid), Spain) and a 15 MV Elekta Synergy linac (Hospital Ramón y Cajal, Madrid, Spain)

All standard treatments are set to 1000 *"monitor units"* (MU), as specified and measured in the control console. One *monitor unit* corresponds to a photon dose of 1 cGy measured at the depth of maximum dose (source to surface distance, *SSD* = 100 cm). The dose rate, related to the accelerator beam intensity, ranged from 300 to 600 MU/min. Expressing the results "*per MU"* or *"per Gy"* enables to compare results obtained in treatments and accelerators that have resulted on different X-ray doses.

III. Results

Figure 1 represents the lethargy neutron spectra per unit fluence at 50 cm from the isocenter at the different linacs. In all cases the fast neutron component is the dominant one close to the isocenter, with relatively small thermal component. Unit spectra do not seem to depend on the energy of the accelerator It is worth noting that no thermal component appears for the Elekta linac (Ramón y Cajal) probably due to its building characteristics. For the remaining accelerators, the presence of bigger thermal components is related to smaller treatment rooms.

Figure 2 displays the neutron lethargy spectra per unit fluence at the place where the digital device is located in the treatment rooms. It is apparent that, in this place, the thermal component dominates over the less abundant fast component as the place where neutrons originate is far from the measurement point. Small differences in the spectra are due to differences in the geometry of irradiation.

Table 1 shows a summary of the global dosimetric quantities (neutron *fluence*, neutron *dose equivalent*, *mean energy* of the neutron spectrum –energy averaged over fluence–, and *effective energy* of the spectrum –energy averaged over dose–) characterizing the neutron field at

50 cm from the isocenter and at the place of the digital device obtained from the Bonner sphere spectrometer (BSS) measurements. It is apparent that both the neutron fluence and dose equivalent per monitor unit increase for increasing accelerator energies, indicating that neutron photoproduction rises with energy for constant photon production, as expected. Nevertheless, the fact that unit spectra close to the isocenter (fig. 1) are machine independent, with a maximum around 0.2 MeV, indicate that the neutron production mechanism is energy independent, confirming the prominence of an evaporation process in front of a direct neutron emission. In addition, the fact that effective energies are always bigger than mean energies puts into evidence that the dose contribution of low energy neutrons is small in front of that of higher energy neutrons, as inferred from the values of the fluence to dose conversion coefficients.

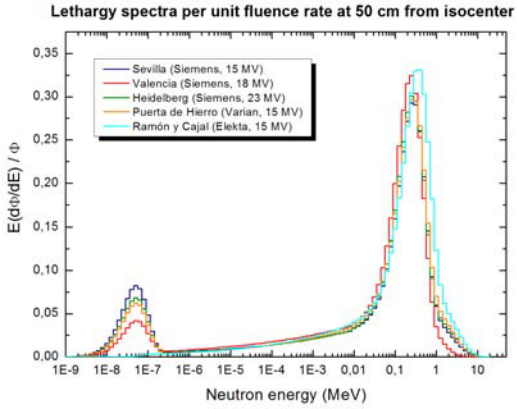

Fig. 1 Neutron spectra per unit fluence at 50 cm from the isocenter of the Siemens linacs under study.

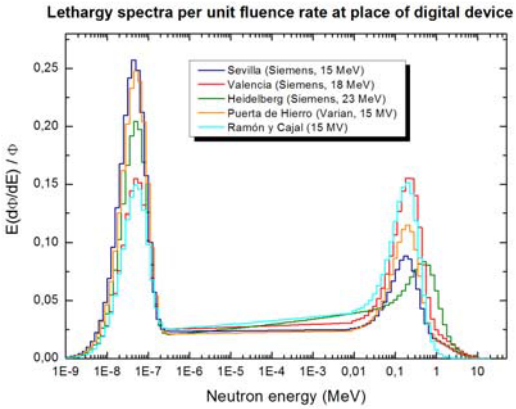

Fig. 2 Neutron spectra per unit fluence at the place where the digital device is located for the irradiation rooms of the Siemens linacs

Table 1 Global dosimetric quantities characterizing the neutron field at 50 cm from the isocenter and at the place of the digital device obtained from BSS measurements. Fluence and dose equivalent are given *per monitor unit* to make results from different irradiation conditions comparable. One *monitor unit* corresponds to a photon dose of 1 cGy measured at the depth of maximum dose (see text)

	50 cm from isocenter	Place of digital device
Sevilla bunker 1 (15 MV, Siemens Primus)		
Fluence per monitor unit ($cm^{-2}·MU^{-1}$)	$(3.797 \pm 0.043) \times 10^4$	$(1.001 \pm 0.015) \times 10^4$
Dose equivalent per monitor unit ($mSv·MU^{-1}$)	$(0.532 \pm 0.019) \times 10^{-2}$	$(0.04876 \pm 0.0073) \times 10^{-2}$
Fluence averaged energy (MeV)	0.27	0.086
Dose averaged energy (MeV)	0.61	0.57
Valencia (18 MV, Siemens Primus)		
Fluence per monitor unit ($cm^{-2}·MU^{-1}$)	$(4.632 \pm 0.044) \times 10^4$	$(1.605 \pm 0.020) \times 10^{-2}$
Dose equivalent per monitor unit ($mSv·MU^{-1}$)	$(0.595 \pm 0.016) \times 10^{-2}$	$(0.1188 \pm 0.0015) \times 10^{-2}$
Fluence averaged energy (MeV)	0.19	0.14
Dose averaged energy (MeV)	0.40	0.57
Heidelberg (23 MV, Siemens Mevatron)		
Fluence per monitor unit ($cm^{-2}·MU^{-1}$)	$(1.277 \pm 0.013) \times 10^5$	$(3.446 \pm 0.044) \times 10^5$
Dose equivalent per monitor unit ($mSv·MU^{-1}$)	$(1.846 \pm 0.053) \times 10^{-2}$	$(0.2323 \pm 0.0030) \times 10^{-2}$
Fluence averaged energy (MeV)	0.29	0.13
Dose averaged energy (MeV)	0.66	0.70
Puerta de Hierro (15 MV,Varian)		
Fluence per monitor unit ($cm^{-2}·MU^{-1}$)	$(5.157 \pm 0.15) \times 10^4$	$(1.630 \pm 0.068) \times 10^4$
Dose equivalent per monitor unit ($mSv·MU^{-1}$)	$(0.769 \pm 0.040) \times 10^{-2}$	$(0.0873 \pm 0.0067) \times 10^{-2}$
Fluence averaged energy (MeV)	0.30	0.086
Dose averaged energy (MeV)	0.67	0.48
Ramón y Cajal (15 MV, Elekta)		
Fluence per monitor unit ($cm^{-2}·MU^{-1}$)	$(2.131 \pm 0.028) \times 10^4$	$(0.518 \pm 0.028) \times 10^4$
Dose equivalent per monitor unit ($mSv·MU^{-1}$)	$(0.403 \pm 0.012) \times 10^{-2}$	$(0.0292 \pm 0.0028) \times 10^{-2}$
Fluence averaged energy (MeV)	0.42	0.067
Dose averaged energy (MeV)	0.77	0.27

IV. Conclusions

A project has been set up with the final goal of estimating, from the readings of a digital device located inside the treatment room, the neutron equivalent doses that a patient subject to a radiotherapy treatment receives in several relevant organs. Neutron spectra have been measured at several linacs, under different irradiation conditions, in two points inside the treatment room: at 50 cm from the isocenter and at the place where a digital device is located. Global dosimetric quantities (fluence and ambient dose equivalent) have been obtained from these measurements. As measurements are performed with a Bonner sphere spectrometric system calibrated and validated according to the ISO specifications, they may be used as absolute reference to obtain dose and fluence values from the readings of the digital device and of the passive neutron detectors used in the project. It has been found that unit neutron spectra near the isocenter do not depend on the accelerator energy, having a maximum around 0.2 MeV, and that neutron photoproduction increases with energy, as expected.

Acknowledgment

The authors would like to acknowledge the collaboration of the radiotherapy staff in the different hospitals.

References

1. National Council on Radiation Protection and Measurements (NCRP), 1984, Neutron Contamination from Medical Electron Accelerators, NCRP Report 79
2. ICRP, 2007, The 2007 Recommendations of the International Commission on Radiological Protection.ICRP Publication 103. Annals of the ICRP 37:1-332.
3. Hall E J, Martin S G, Amols H et al. (1995) Photoneutrons from medical linear accelerators - radiobiological measurements and risk estimates. Int J Radiat Oncol Biol Phys 33:225-230
4. Hall E J (2006) The inaugural Frank Ellis Lecture - Iatrogenic cancer: the impact of intensity modulated radiotherapy. Clinic Oncol 18:277-282
5. Mansur D B, Klein E E, Maserang B P (2007) Measured peripheral dose in pediatric radiation therapy: a comparison of intensity-modulated and conformal techniques. Radiother Oncol 82:179-184
6. Ruben J D, Davies S, Evans C et al. (2008) The effect of intensity-modulated radiotherapy on radiation-induced second malignancies. Int J Radiat Oncol Biol Phys 70(5):1598-1606
7. Verellen D, Vanhaver F (1999) Risk assessment of radiation-induced malignancies based on whole-body equivalent dose estimates for IMRT treatment in the head and neck region. Radiother Oncol 53:199-203
8. Fernández F, Bouassoule T, Amgarou K, et al. (2007) Monte Carlo calculations and validation of a gold-foil based Bonner sphere system. Radiat Prot Dosim 126:366-370
9. International Organisation for Standardisation (1989). Neutron reference radiations for calibrating neutron-measuring devices used for radiation protection purposes and for determining their response as a function of neutron energy. ISO-8529
10. International Organisation for Standardisation (2000) Reference neutron radiations — Characteristics and methods of production of simulated workplace neutron fields. ISO-12789
11. Thomas D J, Alevra A V (2002) Bonner sphere spectrometers–a critical review. Nucl Inst. and Meth in Phys Res A476:12-20
12. Alevra A V, Thomas, D J (2003) Neutron spectrometry in mixed fields: multisphere spectrometers. Radiat Prot Dosim 107:37-72.
13. Waters L S (ed.) (2002) MCNPX™ Users Manual, ECI, Version 2.4.0, Los Alamos National Laboratory report LA-CP-02-408.
14. Bedogni R, Domingo C, Esposito A, Fernández F (2007) FRUIT: An operational tool for multisphere neutron spectrometry in workplaces. Nucl Instr and Meth in Phys Res A580:1301-1309

Author: C. Domingo
Institute: Grup de Física de les Radiacions. Departament de Física. Universitat Autònoma de Barcelona
Street: Edifici C. Campus UAB
City: E-08193 Bellaterra
Country: Spain
Email: carles.domingo@uab.cat

First Results of a Multi Centre Study about Reduction of X-ray Exposure due to Surgical Navigation for Pedicel Screw Placement in Spine Surgery

A.B. König[1], C. Coauthor[2] and D.E. Othercoauthor[1]

[1] Institution/Department, Affiliation, City, Country
[2] Institution/Department, Affiliation, City, Country

Abstract— **In the AGROP of the DGU a multi centre study was initiated to evidence the reduction of X-ray exposure for the surgeon during implementation of pedicel screws in spine surgery. The comparison was done between navigated and non navigated operations for pedicel screw placement in spine surgery. In this first part of the multi centre study of AGROP of the DGU no statistical significant differences could be shown. But important manifestations for reduction of X-ray exposure by use of navigation systems for pedicel screw placement were seen.**

Keywords— **surgical navigation, spine surgery, reduction of X-ray exposure.**

I. Introduction

The percentage of navigated surgical procedures increases continuously in orthopaedic and trauma OR. Beside the increase of surgical precision the main aim of development of surgical navigation systems is the reduction of X-ray exposure for the surgeon and the patient. Actually literature doesn't show this advantage clearly. In the AGROP of the DGU a multi centre study was initiated to evidence the reduction of X-ray exposure for the surgeon during implementation of pedicel screws in spine surgery.

II. Material and Methods

In this multi centre study of the AGROP of the DGU following departments were included: Centrum für Muskuloskeletale Chirurgie of the Charité Berlin, Klinik für Unfallchirurgie of the Medizinische Hochschule Hannover, Berufsgenossenschaftliche Unfallklinik Ludwigshafen and the Abteilung für Unfallchirurgie, Hand- und Wiederherstellungschirurgie of the University Ulm.

From the first of June to the 30th of September 2005 about 35 navigated dorsal spine stabilisations with 206 pedicel screw placements in 103 segments were implemented. In 42 percent of the navigated operations the new 3D- C-arm based navigation was used. In 29 percent 2D- C- arm-based systems and in another 29 percent CT- based navigations systems were used.

In the group of conventional operated patients without surgical navigation 15 patients were implemented. This includes 74 screw placements in 37 segments.

By use of finger ring dosimeters type HARSHAW BTKD 2001 the X-ray exposure was measured cumulative during the operations. The sterile dosimeter was covered by the gloves.
In the dosimeters the X-ray dose was cumulative summarized. For comparison between navigated and non navigated pedicel screw placements the needed time was isolated mathematically out of the complete operation data set. Therefore the dose-plane-product of the image intensifier screen was used, after evaluation of this method in a foregoing study. The results of the study were statistical evaluated by use of the Mann-Whitney-U-Test.

III. Results

The analysis of the data shows a dose of 0,01242 mSv for navigated implementation of a pedicel screw. For non navigated pedicel screw implementation a dose of 0,0784 mSv per screw.

The average dose per screw by use of the 3D C-arm based navigation with one scan procedure for 4 screw implementations was between 0,00385 mSv and 0,00352 mSv.

For CT based navigation the average dose was 0,00257 mSv per screw.

The statistical analysis didn't show significant differences, because limited number of cases per group. Other cause was loss of data because of different units of the severe image intensifiers in the involved departments. Furthermore incomplete intraoperative documentation and loss of ring dosimeters reduced the data set. The last problem based on removal of ring dosimeter together with the used glove.

The high precision of the measuring method could be shown with the accordance of measured dose in different departments with the comparable 3D C-arm navigation system.

O. Dössel and W.C. Schlegel (Eds.): WC 2009, IFMBE Proceedings 25/III, pp. 527–528, 2009.
www.springerlink.com

IV. CONCLUSIONS

In this first part of the multi centre study of AGROP of the DGU no statistical significant differences could be shown.

However we found important manifestations for reduction of X-ray exposure by use of navigation systems for pedicel screw placement.

The problems of data acquisition were defined for the next enlarged multi centre study to generate clear results.

Fig. 1: Screen shot of navigated pedicel screw implementation with red plan and green visualisation of actually instrument position.

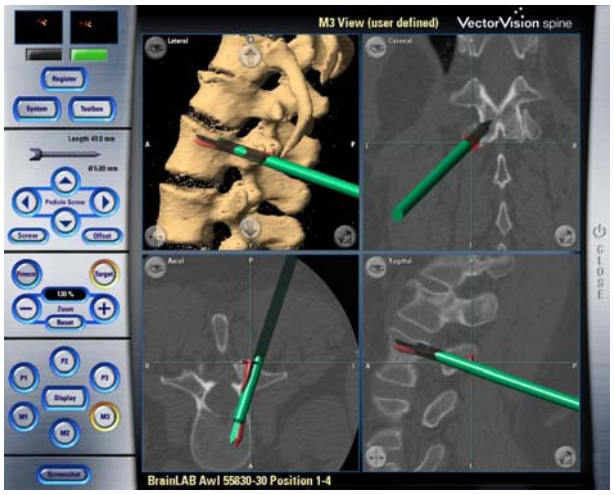

Fig. 2: The finger ring dosimeter is sterile covered under the glove.

REFERENCES

1. Eu ler E, Hei ning S et al. (2002) Ers te kli ni sche Er fahrungen mit dem SIREMOBIL Iso-C3D. elec tromedica 70: 64–67
2. Eu ler E, Wirth S et al. (2001) Ver gleichende Untersuchung zur Qualität der C-Bogen-basier ten3D-Bildgebung am Talus. Unfallchirurg 104: 839–846
3. Geb hard F, Kraus M et al. (2003) Strah len do sis im OP – ein Ver gleich computerassistier ter Ver fahren. Unfallchirurg 106: 492–497
4. Rock C, Kot sia nos D et al. (2002). Un ter su chun gen zur Bildqualität, Hochkontrastauflösung und Dosis am Stamm- und Glied ma ßenske lett mit ei nem neuen dedizier ten CT-System (ISO-C3D). Rofo Fortschr Geb Ront genstr Neuen Bildgeb Ver fahr 174: 170–176
5. Rock C, Linsenmaier U et al. (2001) Vorstellung eines neuen mobilen C-Bogen-/CT-Kombina tionsgerät (ISO-C3D). Unfallchirurg 104: 827–833
6. Wieners G, Pech M, et al (2005). Comparison of Radiation Dose and Image Quality of Siremobil-IsoC3D with a 16-Slice Spiral CT for Diagnosis and Intervention in the Human Pelvic Bone. Rofo. Februar;177 (2):258-264
7. König B, Erdmenger U et al (2005). Evaluation der Bildqualität des Iso-C3D-Bildwandlers im Vergleich mit dem CT - Diagnostik und Therapie im Beckenbereich. Unfallchirurg. Mai;108(5):378-86
8. König B, Schäffler A et al (2006). Accuracy of pedicle screw placement by use of Arcadis Orbic 3D C arm based navigation in comparison to 2D C arm based navigation and CT based navigation technique. Computer Assisted Orthopaedic Surgery. 6th Annual Meeting of CAOS International Proceedings. ISBN 3-939000-90-6. 301-302

Author: Dr. A. Benjamin König
Institute: Unfallchirurgie, Klinikum Rechts der Isar, TU München
Street: Ismaninger Strasse 22
City: 81675 München
Country: Germany
Email: koenig@uchir.me.tum.de

Patient Doses in Latin American Countries

Helen Khoury[1], Patricia Mora[2], Simone Kodlulovich[3], Maria Yolanda Defaz[4], Susana Blanco[5], Fernando Leyton[6], Tony Benavente[7], Daniel Blanco[8], Norma Roas[9], Juan Cardenas[10], and Raul Ramirez[11]

[1] Departamento de Energia Nuclear-UFPE, Recife, Brazil
[2] Centro de Investigación en Ciencias Atómicas, Nucleares y Moleculares, Universidad de Costa Rica, Costa Rica
[3] Instituto de Radioproteção e Dosimetria,CNEN Rio de Janeiro, Brazil
[4] Comisión Ecuatoriana de Energía Atómica, Quito, Ecuador
[5] Consejo Nacional de Investigaciones Científicas y Técnicas (CONICET, Argentina
[6] Instituto de Salud Publica de Chile, Santiago, Chile
[7] Instituto Peruano de Energía Nuclear, Lima, Perú
[8] Centro De Investigaciones Nucleares, Montevideo, Uruguay
[9] Laboratorio de Física de Radiaciones y Metrología, Universidad Nacional Autónoma de Nicaragua
[10] Centro de Protección e Higiene de las Radiaciones (CPHR), Cuba
[11] International Atomic Energy Agency Vienna, Austria

Abstract— **This paper discusses the results of patient doses evaluated in the following countries in Latin American Argentina, Brazil, Chile, Costa Rica, Cuba, Ecuador, Nicaragua, Peru and Uruguay. The entrance air kerma values for PA/AP pediatric chest examinations and the average glandular dose in mammography projections are presented, as well as doses from CT procedures for pediatric and adult patients. The results of the PA/AP chest adult and pediatric procedures demonstrated a large variation of the exposure parameters used in the different countries of Latin America. Many were outside the recommend values of the European Commission. For chest pediatric examinations, the K_e values ranged from 0,01 to 0,16 mGy for the newborns and from 0,020 to 0,24 mGy for the infants. In mammography, the mean value of the average glandular dose was 2.28mGy, with a range of 0.5 to 6.42 mGy for the cranio-caudal projection; and 2.71 mGy, with a range of 0.55 to 10.65 mGy, for the medio-lateral-oblique projection. In CT, the C_w mean value for the head exam was approximately 25% higher for adults than for children. However in the other procedures, the C_W for adults was 3% lower than for children. The adult mean values of C_w and PKL for all procedures were lower than the DRL values recommended in the European guidelines**

Keywords— **patient dosimetry, radiology, quality image**

I. Introduction

Over the last several decades, technological advances in medical imaging have placed imaging at the centre of patient management. This fact has resulted in an increase of the exposure of the population to ionizing radiation. Diagnostic radiology is by far the largest man-made source of radiation exposure for the population in most of the industrialized countries [1]

The effective use of ionising radiation in diagnostic radiology involves the interplay of three factors: image quality, radiographic technique and patient dose. A good radiographic technique should produce an image containing all the information essential to a diagnosis and should result in the minimum dose to the patient.

The analysis of health systems in Latin America shows that few countries have policies for the development of the imaging area. Most radiology services in this region are regulated from the viewpoint of radiation safety, but not of clinical efficacy. The national authorities responsible for radiation control are often located in nuclear or atomic-energy commissions, which usually monitor the adequacy of structural shielding, equipment safety, and occupational exposure. Few of these regulatory authorities control patient exposure [2].

A PAHO/WHO research project to assess the quality of radiology services[3], developed in 2001, concluded that because of the costs involved, many radiology services in Latin America were inappropriately equipped, inadequately staffed, insufficiently maintained and operated without consideration for the health risks to staff and patients. What has changed in the last eight years?

Some countries have made investments and have renewed the equipment. Digital radiology and sophisticated CT equipment has been introduced in the region. However, these new technologies have been incorporated without much preparation in the diagnostic radiology departments. This lack of preparation indicates the necessity of specific training of the health professionals including the medical physicists and on the need to perform dosimetry and image quality evaluation of the new equipment.

O. Dössel and W.C. Schlegel (Eds.): WC 2009, IFMBE Proceedings 25/III, pp. 529–532, 2009.
www.springerlink.com

On other hand, most of the modern facilities are concentrated in large cities. There are big differences between public and private services. In some countries, the main part of the population does not have adequate access to the medical .imaging services.

Motivated by the *International Action Plan for the Radiological Protection of Patients,* 13 countries of Latin America under the IAEA Regional Project RLA/9/057 initiated, in 2007, a project to optimize the radiological protection of patients in the areas of diagnostic and interventional radiology, nuclear medicine and radiotherapy. In this paper we will discuss some results of patient doses obtained for mammography, conventional radiology (adult and pediatric) and computed tomography examinations

II. Individual Studies

A. Pediatric Radiology

To evaluate the Entrance Air Kerma values (K_e) in pediatric chest examinations, a study was performed in nine hospitals from the following countries: Argentina (AR) (1), Brazil (BR)(4), Chile(CH)(1), Costa Rica (CR) (1), Peru (PE) (1) and Ecuador (EC) (1). The study group consisted of 462 pediatric patients (Group I- from two days to one year, Group II- from four to six years of age). At the time of the examination, the exposure parameters (kVp, mAs, focal-spot-to-film distance, etc.) and patient information (gender, height, weight and age) were recorded. The radiographic image quality was evaluated by the local radiologist based on the European Guidelines on Quality Criteria for Diagnostic Radiographic Images in Pediatrics.

The results show that the newborn PA chest projection examinations were performed with tube potential values that ranged from 40 to 105 kV, with many institutions using kVp values outside the 60-65 kV interval that is recommended in CEC guidelines [5]. Argentina and Institution A from Brazil used the lowest tube voltages (kV) values, while Chile used the highest values. It is interesting to observe that in all the countries, except Argentina, the examinations were performed using the anti-scatter grid. The use of anti-scatter grids in newborn patients is not in accordance with the European guidelines and is known to have a large influence on patient dose [5]. This study demonstrated a large variation of the exposure parameters used in the different countries of Latin America, many of which were found to be outside the recommend values of the European Commission. This survey has also shown that the image quality can be improved with the use of immobilization devices, and that the entrance surface air kerma is not fully optimized. Figure 1 shows the distribution of the K_e for patients 4-6 years old.

Similar results were obtained for the exams of newborn patients, with the K_e ranging from 20 to 220 μGy. The large variation in the exposure parameters and in the Entrance Surface Air Kerma indicates that much can be done to reduce patient doses and improve the image quality. It is also necessary to review the convenience of using (or not) antiscatter grids according to the age of the patient and the type of radiograph to be performed

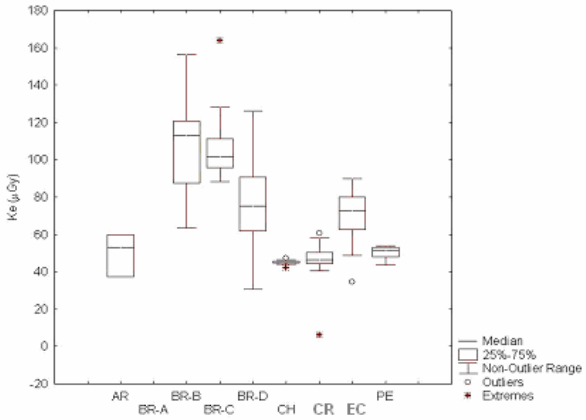

Fig. 1 Distribution of the Entrance Surface Air Kerma for chest examinations in AP projections of patients 4 to 6 years old.

B.- Mammography

A total of 30 hospitals from the following countries participated: Argentina (1), Brazil (11), Chile (6), Costa Rica (4), Cuba (1), Ecuador (2), Nicaragua (1), Paraguay (1), Peru (2) and Uruguay (4). The quality of 1275 CC and 1270 MLO images and the mean glandular doses for 538 CC and 534 MLO images were evaluated.

Regarding the brand of mammography equipment that participated in the survey: 11 were GE Senographe, 2 were Siemens, 3 Lorad, 2 Bennett Profile, 1 Planmed Sophie, 1 ELSCINT-MAN and 1 Fisher Imaging Athena. The processors were: 7 Agfa, 7 Kodak X-Omatic, 4 Konica, 2 Macrotec MX and 1 Fuji. The different types of screen-film combinations used are showed on Figure 2**.** For 28 kVp, the output for 20% of the equipments was below the 30 $\mu Gy.mAs^{-1}$ recommended value and one machine had a half

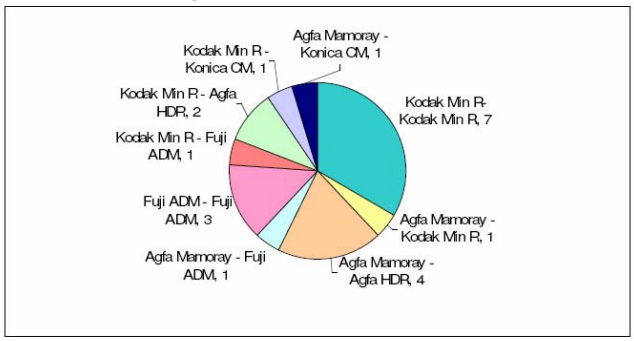

Fig. 2- Screen-film combinations used in Latin America

value layer (HVL) outside the recommended range for Mo/Mo. [6].

Figures 3 and Figure 4 show the distribution of the mean glandular doses for all the patients studied in the eight participating countries for the CC and the MLO projections respectively. The 3 mGy reference value [4], is shown as a red line. For the CC, the average glandular dose was 2,28 mGy with a range of 0.5 – 6.42 and for the MLO, the average glandular dose was 2.71 mGy with a range of 0.55 to 10.65. The 75% percentiles were 2.92 mGy and 3.46 mGy respectively. The cranio-caudal projection was just below the 3 mGy international dose level

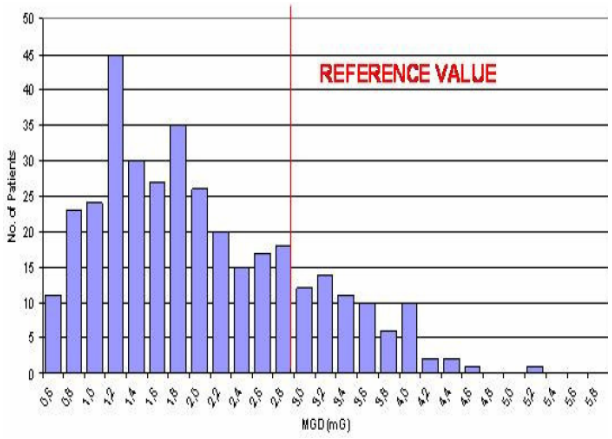

Fig. 3 Distribution of Mean Glandular Dose for CC projections

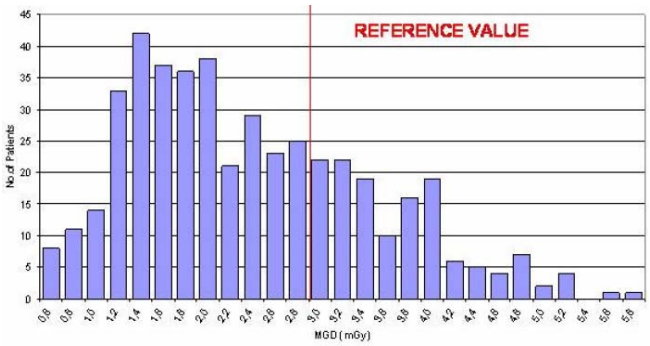

Fig. 4 Distribution of Mean Glandular Dose for MLO projection

C- Computed Tomography

In Latin America, there has been an exponential increase in the number of CT scanners installed in the last five years. Many facilities have acquired multi-slice CT scanners (MDCT) creating the possibility of new clinical application such as CT angiography and virtual endoscopy [7].

The present survey is based on data collected from 30 hospitals from Latin America countries. Each hospital voluntarily submitted a standard questionnaire, aimed to collect information on the practice in order to characterize the techniques and allow the calculation of relevant dose quantities. In the survey, the scanners models varied, approximately 46% were single-slice, 22% were dual systems and 31 % were multi-slice.

The C_w and PKL mean values obtained for adults and children for each procedure are shown in Figure 5.

For head scans, the C_w mean value for adults (40mGy) was approximately 25% higher than for children. However, in the other procedures, the C_w value for adults was 33% lower than for children. The adult mean values of C_w and PKL for all procedures were lower than the DRL value recommended in the European guidelines [8]. The majority of the centers performed the head examination using the axial mode. It can be observed that except for head procedures, the C_w value obtained for children is higher than the adult values, indicating no specific pediatric protocols. Even considering the large difference between the scan length for adults and children, it was observed that in many cases the doses were very similar.

The 75 percentiles in the distribution of C_w and PKL obtained in this survey was lower that the DRL European guidelines. However in all CT procedures, substantial differences were observed in patient radiation doses, for the same anatomic structure, in the different centers, even in the same country. The large range of results reported reveals the

differences in the techniques used at the centers of all participating countries.

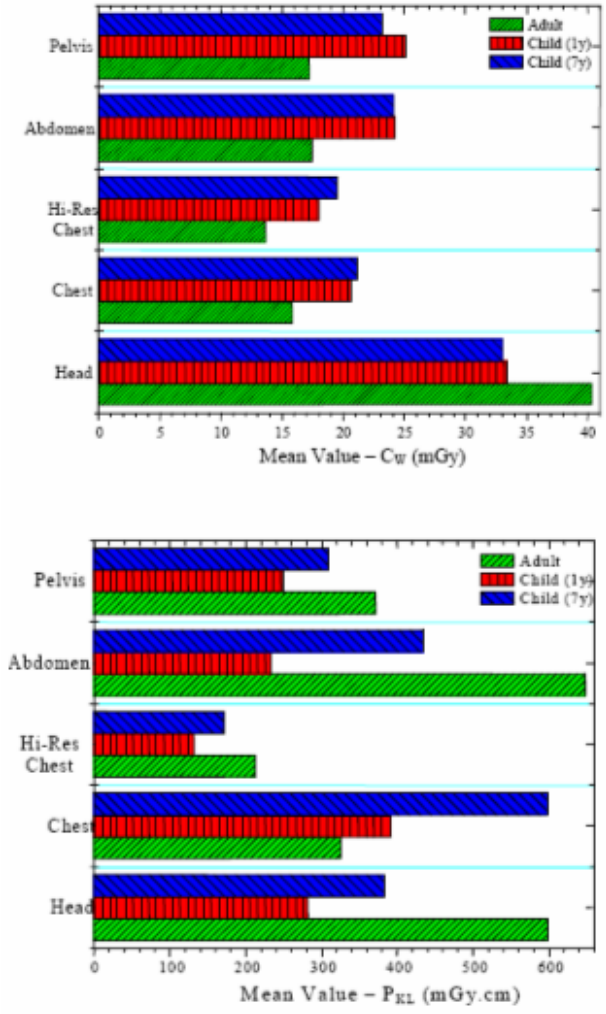

Fig. 5 Mean value of C_w and PKL for routine procedures on adult and children patients

III. Conclusions

Important actions in the region can be started to optimize patient radiation protection with the goal of obtaining high quality images, such as the implementation of quality control programs. It was observed that adult CT protocols are used for pediatric patients in Latin American centers. Special actions should be quickly implemented considering the higher sensitivity of children to the harmful effects of radiation

Latin American countries have to optimize the radiographic techniques in order to reduce patient dose. Actions have to be implemented soon, because the region is facing a new challenge which is the introduction of digital radiology

Acknowledgements

The authors would like to thank the staff of all hospitals participating in this study and the IAEA for the financial support.

References

1. United National Scientific Committee on the Effects of Atomic Radiation (UNSCEAR) (2000) Reports to the General Assembly, with Scientific Annexes, Source and Effects of Ionizing Radiation (Vols. I-II, Sources and Effects). New York: United Nations
2. Borrás C (ed.) (1997) Organization, Development, Quality-assurance and Radiation Protection in Radiology Services: Imaging and Radiation Therapy. Washington, DC: Pan American Health Organization / World Health Organization (PAHO/WHO)
3. Borrás C, Aguilar Serrano L, Barrientos Z et al (2001) Quality Assessment of Diagnostic Radiology Services in Five Latin American Countries- XXXVI Meeting of the Advisory Committee on Health Research, Kingston, Jamaica - 9-11 of July
4. European Commission (1996) European Guidelines on Quality Criteria for Diagnostic Radiographic Images in Paediatrics. EUR 16261EN
5. Cook, JV, Shah K, Pablot S, Kyriou J, Pettett A, Fitzgerals M (1998) Guidelines on best practice in the x-ray imaging of children; a manual for all x-ray departments. Queen Mary's Hospital for Children, Carshalton, UK
6. International Atomic Energy Agency (2006) Tec Doc 1517 Control de Calidad en Mamografía, IAEA:Viena
7. Torp C, Olerud H, Einarson G, Gron P, Leitz W, Servoma A (2001) Use of the EC quality criteria as a common method of inspecting CT laboratories: a pilot study by the Nordic Radiation Protection Authorities—radiological protection of patients in diagnostic and interventional radiology, nuclear medicine and radiotherapy. Document IAEA-CN-85-175. Vienna, Austria

.ï

Author: Helen Jamil Khoury
Institute: Nuclear Energy Department- UFPE
Street: Av. Prof. Luiz Freire 1000
City: Recife
Country: Brazil
Email: hjkhoury@gmail.com

Slowing the increase in the collective dose resulting from CT scans

D. J. Brenner
Center for Radiological Research, Columbia University, New York, USA

Abstract— **There has been a rapid increase in the collective dose from medical radiation within the last 20 years, mostly due to CT. Diagnostic radiation exposure should always operate under the ALARA (As Low As Reasonably Achievable) principle and opportunities do exist in the CT field for collective dose reduction through reducing the numbers of CT scans performed, or at least by slowing the rate of increase. It is argued that clinical decision rules for CT usage represent a potentially powerful tool for slowing down the increase in CT usage, because they have the potential to overcome some of the major factors that result in some CT scans being undertaken when they unlikely to be clinically helpful.**

Keywords—**Reducing CT usage; Clinical Decision Rules**

I. INTRODUCTION

The use of CT as a diagnostic tool is so well established that it is hard to imagine contemporary medicine without it. At the same time, x rays are a known and proven human carcinogen. Clearly the goal is to balance these two observations to provide the maximum benefit / risk balance, both on an individual and on a population basis.

While CT usage is most frequent in Japan, the USA and Australia, the rates of increase of CT usage are quite similar in many other countries. For example, over the past quarter century, CT usage has risen about 12 fold in the UK and more that 20 fold in the US [1-3]. The current annual usage is estimated to be more than 3 million per year in the UK and more than 65 million per year in the US. Overall, the mean effective dose in the US from all medical x rays has increased approximately seven fold over this period [4], with the result that medical exposures, for the first time, now represent the majority of the effective dose to which individuals in the US are exposed.

The various CT-based health screening applications are not yet quite ready for mass use, but some may be soon, resulting in an expected further jump in CT usage.

These increases are a reflection of the fact that CT is such a rapid, simple, and accurate diagnostic tool. Concerns arise because a CT scan results in organ radiation doses that are very much larger than those from conventional radiologic procedures such as chest x rays.

The second issue is that there is now direct credible epidemiological evidence of small risk of radiation-associated cancer at doses comparable to a few CT scans [5-8]. Indeed, as early as 2002, the International Commission on Radiological Protection (ICRP) commented that: "The absorbed dose to tissue from CT can often approach or exceed the levels known to increase the probability of cancer" [9].

The issues here are particularly pertinent for pediatric CT, in that there is compelling evidence that children are considerably more sensitive than adults to radiation-induced cancer. While early CT scanners were rarely used for children because they were comparatively slow, and thus required anesthesia, pediatric CT usage is now increasing rapidly [10], in significant part because typical CT scans now take less than 1 s, and thus do not require sedation.

Diagnostic radiation exposure should always operate under the ALARA (As Low As Reasonably Achievable) principle and, as we discuss, opportunities do exist in the CT field for collective dose reduction, both through reducing the numbers of CT scans, and through reducing the doses per scan. An important goal here is to promote ongoing dialogues among radiologists, emergency room, and other physicians, medical physicists, and indeed the public, as to practical ways to slow the increase in CT usage and CT doses, without compromising patient care.

II. APPROACHES TO REDUCING THE COLLECTIVE DOSE FROM CT

There are three ways to reduce, or at least stem the increase in the collective dose resulting from CT usage, without compromising patient care. These are

1. reducing the dose per CT scan,
2. replacing CT scans with other imaging modalities, where possible,
3. minimizing the number of prescribed CT scans that have a low probability of being clinically helpful.

There have been considerable technological advances in reducing the dose per scan, which is especially important for children. This can be dose either by manually adjusting the mAs settings for individuals of different sizes or, as pioneered by Kalender and colleagues [11], by automated current modulation. These automated techniques are now built in to most of the newer CT scanners, though how much they are being used is less certain.

We discuss here another important approach to collective dose reduction, namely minimizing the number of CT scans delivered which are unlikely to be clinically useful.

O. Dössel and W.C. Schlegel (Eds.): WC 2009, IFMBE Proceedings 25/III, pp. 533–535, 2009.
www.springerlink.com

III. LIMITING THE INCREASE IN CT USAGE: CLINICAL DECISION RULES

A significant fraction of CT scans, perhaps as many as 1/3 [12], could practically be replaced by alternate approaches, or need not be performed at all. This estimate is consistent with earlier studies of radiological examination utility [13], the difference being the higher doses associated with CT scans. Common situations where there may be considerable scope for reduction in CT usage are:

- CT for renal colic
- CT for abdominal pain
- CT for abdominal and chest trauma
- CT for minor head injury
- CT angiography for pulmonary embolus.

Whatever the actual proportion of CT scans that could potentially be eliminated, reducing or even slowing down the increase in CT usage will be an extremely hard task, for a variety of reasons. In particular the issues of patient throughput, legal issues, economic issues, as well as pressures from patients and parents to have the best available treatment, all tend towards increasing CT usage.

This having been said, there clearly are approaches to reducing CT usage which are practical, and will not compromise patient care. An example is in the assessment of appendicitis – typically a young person's disease. Until a few years ago, clinical observation and / or ultrasound were the standard tools to confirm the diagnosis prior to surgery. Currently, CT is clearly the gold standard for diagnosing appendicitis, and in many institutions all patients get a CT scan prior to an appendectomy.

An alternative approach is first to use ultrasound (US); if the US is positive, then an appendectomy follows, whilst if it is negative or equivocal, then a CT is given. As shown by Garcia Pena [14], this can reduce CT usage by about 30%.

More complex selective imaging schemes are feasible, with correspondingly greater potential reductions in CT usage. For example, the Alvarado scoring system, which is solely based on history, clinical exam, and routine lab tests, is a sensitive and specific tool for identifying high-risk patients who can go to surgery without imaging, as well as low risk patients who can appropriately undergo just observation, again without imaging [15]. Intermediate risk patients would be imaged by the sequential US/ CT approach described above. This selective imaging approach has the potential to cut the number of CT scans used to diagnose appendicitis by more than a factor of two [14].

These alternate schemes for diagnosing appendicitis represent examples of the potential use of clinical decision rules. As another example, published decision rules [16,17] have demonstrated a potential reduction of 25 to 50% in the use of head CT for minor head injury by applying a set of clinical criteria to decide whether CT is necessary.

Both the American College of Radiology (ACR) and the Royal College of Radiologists have published appropriateness criteria (decision rules) involving CT [18,19]. As an example of their application, Hadley *et al* [20] recently published a retrospective study of the ACR appropriateness criteria for trauma. They studied 200 trauma patients who had some radiation imaging, the imaging decisions having been made without the use of decision rules. 169 had CT scans, for a total number of 660 scans, and a total cost of $838K. Had the ACR Appropriateness Criteria been applied, 44% of the CT scans would not have been carried out. None of the major injuries would have been excluded from CT imaging, and 11 minor injuries, none of which required follow up, would have been excluded from CT imaging. There would also have been a 38% decrease in cost.

IV. CONCLUSIONS

Clinical decision rules represent a potentially powerful tool for slowing down the increase in CT usage, because they have the potential to "trump" some, though not all, of the major factors that result in CT scans being prescribed when they are unlikely to be clinically useful.

Of course, the factors that feed into a decision rule are complex, and the data often incomplete - and the rules need to be constantly adjusted to take into account new evidence. However, in the examples given here, and in other cases reported in the literature, clinical decision rules would be effective in reducing the number of CT scans (as well as the cost), without adversely effecting diagnostic efficacy.

In fact, in the example cited above [20], clinical decision rules were not part of the CT decision process, and this situation is often the norm. For example, the results of a recent study [21] of the percentage of respondents who reported awareness of, and use of, the Canadian CT Head Decision Rule (awareness: 66% in the UK, 31% in the USA; use of rule: 21% in the UK, 12% in the US), suggest that there is considerable room for improvement in CT decision rule awareness and utilization.

Two practical approaches towards increased utilization of CT decision rules are 1) to build them into a managed care preauthorization program [22], and 2) to incorporate them into a computerized radiology order entry system [23]. Both these approaches have proved successful in slowing CT usage rates [22,23].

These considerations points to the desirability of a greater focus on the utilization of clinical decision rules for CT, which represents one of the more practical approaches to limiting the rapid increase in CT usage.

V. REFERENCES

1. International Marketing Ventures. 2007 CT Market Summary Report. www.imvinfo.com. Rockville, MD, 2008.
2. UK Department of Health Hospital Activity Statistics: Imaging and Radiodiagnostics data files. www.performance.doh.gov.uk/hospitalactivity/ data_requests/imaging_and_radiodiagnostics.htm
3. Brenner DJ, Hall EJ. Computed tomography--an increasing source of radiation exposure. N Engl J Med 2007;357:2277-84.
4. Mettler FA, Jr., Thomadsen BR, Bhargavan M, Gilley DB, Gray JE, Lipoti JA, et al. Medical radiation exposure in the U.S. in 2006: preliminary results. Health Phys 2008;95:502-7.
5. Pierce DA, Preston DL. Radiation-related cancer risks at low doses among atomic bomb survivors. Radiat Res 2000;154:178-86.
6. Preston DL, Ron E, Tokuoka S, Funamoto S, Nishi N, Soda M, et al. Solid cancer incidence in Atomic Bomb survivors: 1958-1998. Radiat Res 2007;168:1-64.
7. Brenner DJ, Doll R, Goodhead DT, Hall EJ, Land CE, Little JB, et al. Cancer risks attributable to low doses of ionizing radiation: assessing what we really know. Proc Natl Acad Sci USA 2003;100:13761-6.
8. National Council on Radiation Protection and Measurements. Uncertainties in fatal cancer risk estimates used in radiation protection. NCRP Report 126. Bethesda MD, 1997.
9. International Commission on Radiological Protection. Managing patient dose in computed tomography, ICRP Publication 87. ICRP, Oxford: Elsevier Science, 2002.
10. Broder J, Fordham LA, Warshauer DM. Increasing utilization of computed tomography in the pediatric emergency department, 2000-2006. Emerg Radiol 2007;14:227-32.
11. Kalender WA, Buchenau S, Deak P, Kellermeier M, Langner O, van Straten M, et al. Technical approaches to the optimisation of CT. Phys Med 2008;24:71-9.
12. Slovis TL, Berdon WE. Panel Discussion. Pediatr Radiol 2002;32:242-4.
13. Royal College of Radiologists Working Party. Influence of the Royal College of Radiologists' guidelines on hospital practice: A multicentre study. BMJ 1992;304:740-3.
14. Garcia Pena BM, Cook EF, Mandl KD. Selective imaging strategies for the diagnosis of appendicitis in children. Pediatrics 2004;113:24-8.
15. McKay R, Shepherd J. The use of the clinical scoring system by Alvarado in the decision to perform computed tomography for acute appendicitis in the ED. Am J Emerg Med 2007;25:489-93.
16. Haydel MJ, Preston CA, Mills TJ, Luber S, Blaudeau E, DeBlieux PM. Indications for computed tomography in patients with minor head injury. N Engl J Med 2000;343:100-5.
17. Stiell IG, Wells GA, Vandemheen K, Clement C, Lesiuk H, Laupacis A, et al. The Canadian CT Head Rule for patients with minor head injury. Lancet 2001;357:1391-6.
18. Amis ES, Jr., Butler PF, Applegate KE, Birnbaum SB, Brateman LF, Hevezi JM, et al. American College of Radiology white paper on radiation dose in medicine. J Am Coll Radiol 2007;4:272-84.
19. The Royal College of Radiologists. Making the best use of clinical radiology services: Referral guidelines. 6th Edition. Royal College of Radiologists, London, 2007.
20. Hadley JL, Agola J, Wong P. Potential impact of the American College of Radiology appropriateness criteria on CT for trauma. AJR Am J Roentgenol 2006;186:937-42.
21. Eagles D, Stiell IG, Clement CM, Brehaut J, Taljaard M, Kelly AM, et al. International survey of emergency physicians' awareness and use of the Canadian Cervical-Spine Rule and the Canadian Computed Tomography Head Rule. Acad Emerg Med 2008;15:177-82.
22. Blachar A, Tal S, Mandel A, Novikov I, Polliack G, Sosna J, et al. Preauthorization of CT and MRI examinations: assessment of a managed care preauthorization program based on the ACR Appropriateness Criteria and the Royal College of Radiology guidelines. J Am Coll Radiol. 2006;3:851-9.
23. Sistrom CL, Dang PA, Weilburg JB, Dreyer KJ, Rosenthal DI, Thrall JH. Effect of computerized order entry with integrated decision support on the growth of outpatient procedure volumes: Seven-year time series analysis. Radiology Feb 2009, Epub ahead of print.

Corresponding author:

Author:	David J Brenner
Institute:	Center for Radiological Research, Columbia University Medical Center
Street:	630 West 168th Street
City:	New York, NY 10032
Country:	USA
Email:	djb3@columbia.edu

Patient Doses in CT and Radiography in Africa

W.E. Muhogora[1] and M.M. Rehani[2]

[1]Tanzania Atomic Energy Commission
P.O Box 743, Arusha, Tanzania
[2]International Atomic Energy Agency,
Wagramerstrasse 5, P.O.Box 100 A-1400, Vienna, Austria

Abstract—**There is increasing use of computed tomography (CT) scanning in Africa. However, there had been lack of information on patient doses in CT scanning and radiography in large part of Africa. Through the projects of the International Atomic Energy Agency (IAEA) and some independent work, significant information is now available from many countries. The first multinational dose survey in radiography from the countries from which information is currently available showed that doses to adult patients (in terms of ESAK) are not higher than the currently established DRLs. The data with regard to radiation doses in CT indicates that there are some hospitals where adult exposure factors are being used for scanning of children. Further to that, many hospitals have $CTDI_w$ values below DRLs while some DLP values exceeded DRLs. The CT machines vary from single slice to multi-slice with limited maintenance and QC routines. This study has created awareness, provided training on monitoring of radiation doses as the most challenging issues in many countries in Africa**

Keywords—**Patient protection in Africa, projection radiography, Computed tomography.**

I. Introduction

Medical diagnostic radiography has been practiced in Africa for a number of decades now. Modern technology such as computed tomography (CT) scanning and magnetic resonance imaging (MRI) are also in practice. However, such growth in usage has not matched radiological protection of patients according to the international standards. Under the projects supported by International Atomic Energy Agency (IAEA), programs in radiological protection of patients are currently been implemented in African countries. The motivations behind the CT project were of two fold. Firstly, it is increasingly being documented that patient doses are higher than necessary and image quality in CT often exceeds the needed confident diagnosis [(1).] There was a need to initiate radiation protection programs that ensure that principles of justification and optimization, which are fundamentals of radiation protection, are applied in Africa. Secondly, report from some developed countries have shown that exposure parameters used for CT examination of children are similar to those of adult patients [(2, 3)]. It is likely that a similar situation exist in African countries, prompting timely intervention.

In projection radiography, also two radiation protection concerns motivated this study. The first concern was the increasingly recognition of tremendous amount of waste of resources particularly in developing countries because of poor quality images [(4, 5)]. Therefore there was a need to examine the extent of poor radiographs in Africa. Secondly, is the reported wide variation in patient doses for patients of similar size undergoing the same type of radiographic technique, which could vary up to the factor of 2 to 10 [(6)]. Therefore, a need was further seen to investigate the extent of typical dose variations in Africa. The overall aim of this study was to survey the patient dose levels and image quality in CT procedures and projection radiography and compare patient doses with the recommended diagnostic reference levels (DRLs). Details of the IAEA projects can be found at http://rpop.iaea.org/RPOP/RPoP/content/InformationFor/MemberStates/1_RegionalProjects/index.htm. This paper presents the status results and identifies the way forward.

II. Materials and Methods

CT scanning

In CT scanning, data are currently available from 6 countries in Africa namely Algeria, Ghana, Morocco, Kenya, Sudan, Tanzania and Tunisia. A survey of exposure parameters in CT procedures was performed at all participating centres in different countries. The CT machines varied from single slice to multi slice

O. Dössel and W.C. Schlegel (Eds.): WC 2009, IFMBE Proceedings 25/III, pp. 536–539, 2009.
www.springerlink.com

with limited maintenance and quality control (QC) routines. For each examination, information was collected on the tube voltage employed, the tube current displayed, the scan rotation time and the type of scanning (axial or helical). The aim of this investigation was to find out if the selection of CT parameters takes into account the patient size. For dosimetry purposes, the weighted computed tomography dose index ($CTDI_w$) and the dose length product (DLP) for a complete examination in mGy.cm, which are well accepted dose descriptors in CT were used in the survey as recommended elsewhere [7,8].

Projection radiography

In radiography also data are currently available from 6 countries, which are Democratic Republic of Congo (hereinafter referred to as Congo), Ghana, Madagascar, Sudan, Tanzania and Zimbabwe. Patient dose surveys were undertaken in two phases. The work on phase 1 involved dose assessment by using entrance surface air kerma (ESAK) obtained from incident air kerma measurements [9]. For this purpose, at least 10 adult patients were selected for each x-ray projection. Before commencing with phase 2 of the survey, quality control (QC) tests were performed to identify equipment malfunctions and apply appropriate corrective actions based on exposure charts in use and equipment performance. Data on second phase of dose assessment are currently being collected.

III. Results and Discussion

CT scanning

Selection of exposure parameters for paediatric CT

The number of CT rooms where CT parameters for adults are used for scanning children is presented in Table 1. This can be an indication of limited awareness on radiation protection issues in CT. However, the centres were informed about the need to tailor exposure parameters according to patient size and feedback from the centres indicated that the situation has been rectified [10]. The mean $CTDI_w$ values for adult patients in different countries are presented in Table 2. The results indicate that all $CTDI_w$ values were below DRLs. $CTDI_w$ variation for individual patients are not shown but ranged from a factor of 2.6 -11.7 (chest), 1.7-3 (chest HR), 3.2-10 (lumbar spine), 1.5-11.2 (abdomen) and 1.9-10.3 (pelvis). Such variations indicate the need to carry out optimization studies. Table 3 presents the mean DLP values for adult patients. It can be seen that some mean DLP values were above DRLs. The DLP variations ranged from a factor of 2.3-8.4 (chest), 1.1-3.5 (chest HR), 3-6.3 (lumbar spine), 3-8 (abdomen) and 1.8-10.2 (pelvis). The DLP variations were largely due to variations of CT parameters in use such as scan lengths.

Projection radiography

The results of mean ESAK values to adult patients before implementing a QC program are presented in Table 4. It can be seen that all mean ESAK values were below DRLs as also previously reported [11]. However, further studies may be necessary to rule out whether such low doses are not related to poor quality of radiographs.

IV. Conclusion

The results of this first multinational study in Africa for CT scanning and projection radiography indicate a need to raise the awareness of radiology staff on radiation dose management in CT. There is also a need to continue and extend optimization studies both in CT

TABLE 1. Use of adult CT exposure parameters for paediatric patients in some countries

CT centres	Number of CT rooms	Use of adult exposure parameters in paediatric examinations
Ghana	2	all CT examinations
Sudan	2	all CT examinations

TABLE 2. Mean $CTDI_w$ values for adult patients in different countries. The determination method is indicated as based on phantom measurements (P), calculation by internet data (I) or display of console (C). The diagnostic reference level (DRL) [7] is shown in brackets.

Country	Method	Mean $CTDI_w$ (mGy)				
	DRL	Chest (30)	Chest HR (35)	Lumbar spine (35)	Abdomen (35)	Pelvis (35)
Algeria	P	9.2	6.8	16.2	15.4	19.1
Ghana	P or I	17.1	17.2	20.4	20.4	20.4
Kenya	P	20	-	-	13	20
Morocco	P	10	25.8	11.9	11.9	10.6
Sudan	P, I or C	19.2	14.1	-	20.5	7.3
Tanzania	I	16.8	13.9	38.8	22.7	26
Tunisia	C	24.3	-	-	-	25.4

TABLE 3. Mean DLP values for adult patients in different countries. The diagnostic reference level (DRL) [7] is shown in brackets.

Country	Mean DLP (mGy•cm)				
DRL	Chest (650)	Chest HR (280)	Lumbar spine (780)	Abdomen (780)	Pelvis (570)
Algeria	347	194	646	554	604
Ghana	396	348	523	496	415
Kenya	933	-	-	1314	837
Morocco	256	121	341	341	271
Sudan	423	171	-	725	163
Tanzania	382	366	363	602	494
Tunisia	874	-	-	-	599

.

TABLE 4. Mean entrance surface air kerma (ESAK) to adult patients before implementing a QC program. Diagnostic reference level is indicated as DRL1 (400 film-screen) and DRL2 (200 film screen) [12]

X-ray projection	ESAK (in mGy)							
	Congo	Ghana	Madagascar	Sudan	Tanzania	Zimbabwe	DRL1	DRL2
Chest PA	0.3	0.1	1.05	0.21	0.3	0.2	0.2	0.4
Lumbar spine AP	0.4	8.3	3.92	1.63	2.1	0.7	5	10
Lumbar spine LAT	-	14.4	6.61	3.29	4.7	2	15	30
Abdomen AP	0.3	10.3	3.92	1.5	0.9	0.6	5	10
Pelvis AP	0.1	7	3.92	0.9	1.5	1.1	5	10
Skull AP	-	-	2.95	1.02	-	0.9	2.5	5

as well as in projection radiography. In summary, this study has created awareness, provided training on monitoring of radiation doses as the most challenging issues in many countries in Africa

ACKNOWLEDGEMENT

This work was undertaken as part of Technical Co-operation projects of the International Atomic Energy Agency (IAEA), RAF/9/033.

REFERENCES

1. European Commission. *European Quality Criteria for Multislice CT*. Luxemborg (2004) (available at http://www.msct.eu/CT_Quality_Criteria.htm). Accessed on 16 May 2005
2. Donnelly LF, Emery KH, Brody AS, Laor T, Glylys-Monin VM, Thomas SR et al. Minimizing radiation dose for pediatric body applications of single-detector helical CT: Strategies at a large children's hospital. Am. J. Roentgenol. 176, 303-306 (2001).
3. Siegel MJ, Schmidt B, Bradley D, Suess C, Hildebolt C. Radiation dose and image quality in pediatric CT: Effect of technical factors and phantom size and shape. Radiology 233: 515-522 (2004).
4. Rehani MM. Diagnostic imaging quality assurance, 1st ed. Jaypee Brothers Medical Publishers (P) LTD, 1995:14-23, 43
5. Rehani M.M, Kaul R, Kumar P and Berry M. Does bridging the gap between knowledge and practice help? Example of patient dose reduction in radiology *Journal of Medical Physics* 1995; 20(2):18-22
6. International Commission on Radiological Protection (ICRP).Protection of the patients in diagnostic radiology. ICRP publication 34, Oxford, United Kingdom: Pergamon Press, 1982.
7. European Commission. European *Guidelines on quality criteria for computed tomography*. EUR 16262 EN, Luxembourg (1999).
8. Imaging Performance and Assessment of CT scanners (ImPACT). CT patient dosimetry Excel spreadsheet (version 0.99x 20/01/06) available at http://www.impactscan.org/ctdosimetry.htm)
9. International Commission for Radiation Units and Measurements. Patient dosimetry for x-ray used in medical imaging *Journal of ICRU* 2005; 5(2) Report 74 Oxford University Press
10. Muhogora, W.E., Ahmed, N.A.,Beganovic,A., Benider, A., Ciraj-Bjelac,0., Gershan,V., Gershkevitsh,E., Grupetta,E., Kharita, M.H., Manatrakul,N., Milakovic,M., Ohno, K., Omrane, L.B., Ptacek, J., Schandorf,C., Shabaan,M.S., Stoyanov,D., Toutaoui, N., Wambani,J.S., Rehani, M.M. *CT patient doses in ct examinations in eighteen countries*: initial results from international atomic energy agency projects, (communicated to Rad Prot Dosim)
11. Muhogora WE, Ahmed NA, Almosabihi A, Alsuwaidi JS, Beganovic A, Ciraj-Bjelic O,. Kabuya FK, Krisanachinda A, Milakovic M, Mukwada G, Ramanandraibe MJ, Rehani MM, Rouzitalab J, Schandorf C. *Patient doses in radiographic examinations in 12 countries of Asia, Africa and Eastern Europe: Initial results from IAEA projects*. Am J Roentgenology **190,** 1453-1461 (2008).
12. Rehani M.M. *Protection of patients in general radiography*. In: International Atomic Energy Agency. Proceedings of the international Conference, 26-30 march 2001, Malaga. Vienna, Austria: International Atomic Energy Agency, 169-180 (2001).

Authors: Wilbroad E. Muhogora/Madan M. Rehani
Institute: Tanzania Atomic Energy Commission/IAEA
Street: TPRI Head Office/Wagramerstrasse 5
City: Arusha/Vienna
Country: Tanzania/Austria
Email: w.muhogora@yahoo.com/M.Rehani@iaea.orrg

Melatonin modulates the expression of "vascular endothelial growth factor" gene in irradiated rat cervical spinal cord

G.H. Haddadi[1,2], A. Shirazi[1], Z. Sepehrizadeh[3] , M. Ghazi- khansari[3], B.Minaee[4] A. Farzaneh-Nejad[5], M. Haddadi[6], M. Meshkibaf[1]

[1] Department of Biophysics/Faculty of Medicine, Fasa University of Medical Sciences , Fasa, Iran
[2] Department of Biophysics/ Faculty of Medicine, Tehran University of Medical Sciences , Tehran, Iran
[3]Department of Pharmaceutical Biotechnology/ Faculty of pharmacy, Tehran University of Medical Sciences
[4]Department of Anatomy/ Faculty of Medicine, Tehran University of Medical Sciences, Tehran, Iran
[5]School of Allied Medical Sciences,Tehran University of Medical Sciences, Tehran, Iran.
[6]Faculty of Medicine, Iran University of Medical Sciences, Tehran, Iran.

Abstract— **It is suggested that vascular endothelial growth factor (VEGF) gene expression has an important role in inducing radiation injury to the spinal cord. In this study, the radioprotective effect of melatonin on the VEGF expression was assessed after localized irradiation of cervical spinal cord.**

A number of rats were divided into four groups: 1. Control group; 2. Group that was given an intraperitonial injection of melatonin (100 mg/kg body weight); 3. Group of rats which got melatonin and cervical spinal cord irradiation with 22 Gy gamma irradiation 30 minutes later; and 4. Group that was given an intraperitonial injection of vehicle and radiation to the spinal cord.

The changes in VEGF expression were assessed using real-time reverse transcription-polymerase chain reaction (RT-PCR). Upregulation of VEGF expression was observed from 8 to 22 weeks after irradiation ($P<0.05$). Paralysis and other radiation myelopathy manifestations developed within 22 weeks after irradiation. VEGF gene expression in melatonin pretreatment group compared with radiation group was significantly down-regulated in the 20th and 22nd weeks after irradiation.

The present researchers tried to outline the variations in the expresion profile of VEGF gene within the rats' cervical spinal cords in the periods of 4 hours to 22 weeks after 22 Gy single dose gamma irradiation.

The results support the hypothesis that modulation of VEGF gene expression by melatonin administration may increase the survival rate of irradiated animals.

Keywords— **VEGF, spinal cord, radiation myelopathy**

I. Introduction

Radiation therapy plays an important role in the treatment of head and neck malignant tumors. The effect of radiation on healthy spinal cord is one of the most important dose-limiting factors resulting in myelopathy that often greatly impairs the quality of life of the affected patients [1,2]. Many authors have suggested that vascular endothelial growth factor (VEGF) has a determining role in the disruption of blood-spinal cord barrier (BSCB), vascular alteration, and the development of tissue necrosis [3]. In the last decade, there have been reports on the radioprotective effect of melatonin [4]. Some in vitro studies have shown that melatonin can modulate the expression of VEGF induced by toxic agents [5]. A previous study has shown the protective effect of melatonin in radiation-induced toxicity of the spinal cord [6]. In the present study, the researchers aim at assessing whether melatonin administration can modulate VEGF gene expression after localized irradiation of cervical spinal cord.

II Materials and methods

A. Chemicals

Melatonin (N-acetyl-5-methyoxytryptamine) was obtained from Sigma-Aldrich. It was prepared at a concentration of 1% dissolved in ethanol and diluted with physiological saline. All the other reagents were also obtained from Sigma (St. Louis, MO) and Merck (Germany) companies.

B. Experimental design

Adult male Wistar rats weighing 180–220 g, were selected and housed in conventional rodent facilities.

The rats were divided into four groups. The first group (vehicle treatment) served as control. The second group

O. Dössel and W.C. Schlegel (Eds.): WC 2009, IFMBE Proceedings 25/III, pp. 540–543, 2009.
www.springerlink.com

(radiation) was treated with vehicle and 30 min later, the rats were exposed to radiation, which will be detailed in the following section. The third group (radiation+melatonin) was given an intraperitonial (i.p.) injection of melatonin (100 mg/kg body weight) and 30 min later exposed to radiadion in the same manner as in the second group. The fourth group (melatonin-only) was also given an i.p. injection of melatonin (100 mg/kg body weight). Throughout the experiment, 5mg/kg of melatonin were administered daily to rats in groups three and four and the vehicle were administered daily to rats in group one and two. We certify that all applicable institutional and governmental regulations concerning the ethical use of animals were followed during the course of this research

C. Irradiation

The rats of groups 2 and 3 were irradiated with the gamma beam of Cobalt-60 teletherapy unit (theratron 760-C) to the 1.8 cm cervical segment of the spinal cord (C1-T2). A single dose of 22 Gy was administered to the depth of 0.5 cm based on lateral simulation radiographs. Sham irradiation was also performed for control and melatonin-only groups.

D. Sample preparations

The animals were killed under ketamine and xylazine injection chronologically in 4 and 24 hours, and 1, 3, 8, 16, 20, and 22 weeks after radiation therapy. One centimeter of spinal cord was dissected and used for real time RT-PCR study.

Twenty rats from each of the control, irradiated, and irradiated + melatonin groups were kept for the late evaluation of melatonin effect on clinical symptoms of radiation myelopathy. The rats were monitored every other day for the development of any clinical signs of spinal cord myelopathy (clinical endpoint).

E. Statistical analysis

The data are presented as mean ±SEM. The differences among the groups were analyzed using the analysis of variance (ANOVA) followed by Tukey's multiple comparisons test. Survival data were analyzed in an actuarial fashion by means of Kaplan-Meier analysis and compared with the log-rank test. Significance was accepted at $p < 0.05$.

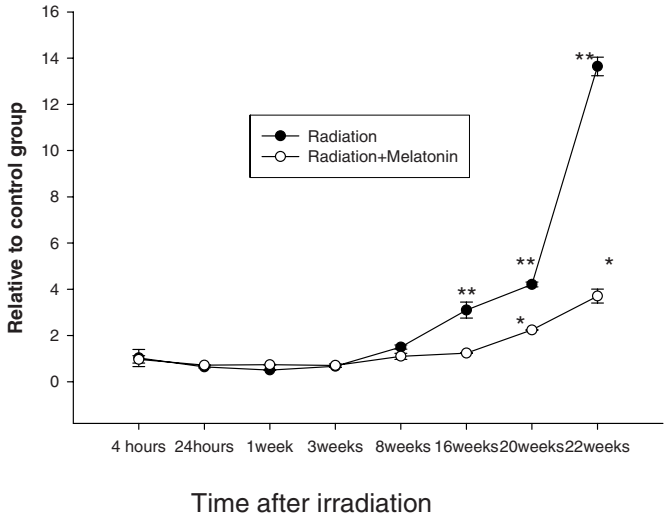

Fig.1.The profile of VEGF gene expression changes as a function of time after 22 Gy gamma irradiation-only and melatonin administration. VEGF gene expression increased rapidly in the weeks immediately preceding paralysis (**p<0.05 radiation vs control groups). Melatonin administration modulates the expression of this gene (*p<0.05 radiation+melatonin vs radiation groups). The data are presented as mean ±SEM.

III. Results

A. Change in VEGF expression

Within 8 weeks after irradiation, VEGF gene upregulated 1.5 fold in the irradiated group compared with the normal group. Within 16 and 20 weeks after irradiation, the expression of VEGF gene in the irradiated group was 3 and 4 fold, respectively as compared with the control group ($p<0.05$). However, the VEGF expression increased rapidly in the 22nd week after irradiation and reached 14 fold in the irradiated group as compared with the control group ($p<0.01$). VEGF expression in melatonin pretreatment group compared with the radiation group is significantly down-regulated in 16, 20, and 22 weeks after irradiation ($p<0.05$). There is not any difference between the control and melatonin-only groups (Fig 1).

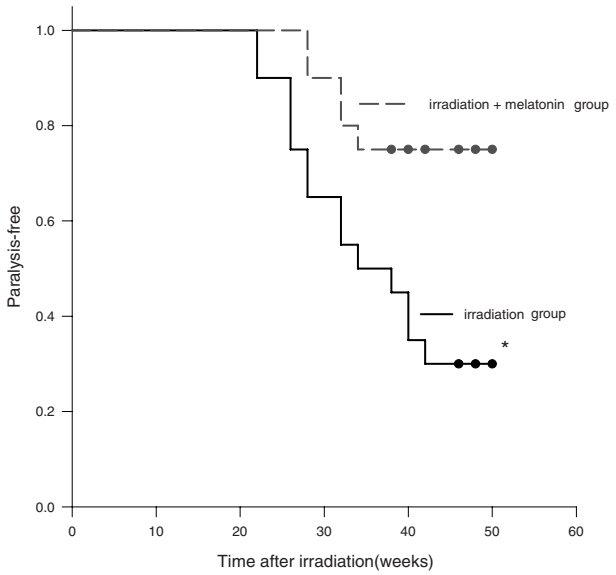

Fig.2. Kaplan-Meier curve of paralysis because of myelopathy for the two groups. The Irradiation +Melatonin group did considerably better than the Irradiation group in terms of paralysis-free (*p<0.05 vs Irradiation group)

B. Frequency and onset of myelopathy

None of the irradiated animals developed typical manifestations of RM after a short-term study. The onset of paresis occurred 22 weeks after irradiation in the irradiated group. Paresis occurred 6 weeks later in melatonin plus radiation group than the irradiated group. There were significant differences in the incidence of RM between the irradiated and irradiated plus melatonin groups ($p<0.01$) (Fig 2).

IIII. Discussion

Myelopathy seems to be a serious complication of spinal cord irradiation. Studies show that vascular damage from radiation is one of the mechanisms involved in the radiation myelopathy[2]. While the exact molecular mechanisms leading to late injury are not fully understood, VEGF, an important determinant of microvascular permeability, has been proposed to play a role in radiation myelopathy[7]. Li et al. assert that "in the irradiated rat's spinal cord, endothelial cell death or damage leads to blood-spinal cord disruption, vasogenic edema, vascular compromise, and hence, tissue hypoxia. In response to hypoxia, astrocytes produce VEGF that further compromises BSCB integrity[8]. This may trigger an avalanche effect, resulting in white matter necrosis. Melatonin has been reported to have radioprotective effects in addition to its known hormonal activities. This agent crosses the blood-brain barrier, and is a highly effective antioxidant in the brain[9]. Since there were some reports asserting that melatonin could modulate the expression of VEGF in vitro [5], it is speculated that melatonin may have radioprotective effect via VEGF down regulation.

The present researchers tried to outline the variations in the expression profile of VEGF within the rat cervical spinal cord in the periods of 4 hours to 22 weeks after 22 Gy irradiation. As the second step, the effect of melatonin on this profile was investigated.

The results indicate that VEGF expression is not an early response to irradiation, but its expression is a delayed reaction. VEGF over-expression has been shown in other CNS injuries due to focal ischemia. Abrupt release of excessive amounts of intracellular and extracellular oxygen-free radicals may initiate many chain reactions, leading to the release of cytokines and VEGF.

There is a strong relationship between VEGF gene expression and paralysis rate. Recently, some investigations have shown that melatonin suppresses the VEGF level in vivo [9]. The results of the present study suggest that the radioprotective effect of melatonin involves the down-regulation of VEGF gene because decreased VEGF mRNA levels were found to be associated with the increased paralysis-free rate of irradiated + melatonin group.

The findings also showed that the prophylactic administration of melatonin significantly increased the latency period by the delay in the onset of paralysis and reduced RM incidence in the irradiated animals. This is in agreement with Blickenstaff et al. study that reported when mice were pretreated with melatonin, 43% of the irradiated ones survived at least 30 days after being exposed to a lethal dose of ionizing radiation.

Although more investigation in this field is needed to better clarify the mechanisms of melatonin in VEGF down-regulation and its relation to histopathological alterations, the data of the present study suggest that melatonin administration may be useful in late radiation-induced toxicity via VEGF down-regulation.

The precise role of melatonin in VEGF down-regulation and neuroprotection after irradiation remain to be determined.

Acknowledgements This study was supported by a grant number 5722 of the TUMS Vice Chancellor for Research. We also express our gratitude to the staff of the Radiotherapy Department at Cancer Institute especially Mr Amir Hooshang Sedigh for the great help.

References

1 Nieder C, Atman F, Price R.E, Ang KK. (1999) Radiation Myelopathy: New perspective on an old problem. Radiation Oncology Investigation **7**: 193-203.

2 Shirazi A, Mahdavi SR, Trott KR. (2004) Radiation mylopathy: a radiobiological review**.** Report of Practical Oncology and Radiother **4**: 273-279.

3 Wong CS, Vander Kogel J.(2004) Mechanisms of radiation injury to the central nervous system**.** Molecular Interventions 4 (5): 273- 284.

4 Shirazi A, Ghobadi G, Ghazi-Khansari M. (2007) A radiobiological review on melatonin: a novel radioprotector. J Radiation Res; 48: 263-272.

5 Dai M, Cui P, Yu M, Han J, Li H, Xiu R. (2008) Melatonin modulates the expression of VEGF and HIF-a induced by $COCL_2$ in cultured cancer cells. J Pineal Res; **44**: 121-126.

6 Shirazi A, Haddadi G H, Ghazi-Khansari M, et al. (2009) Evaluation of Melatonin for prevention of Radiation Myelopathy in Irradiated Cervical Spinal Cord. Yakhteh Medical Journal 11,1: 41-46.

7 Nordal RA, Nagy A, Pintillie M, Wong CH. (2004) Hypoxia and Hypoxia-inducible factor-1 target genes in central nervous system radiation injury: a role for vascular endothelial growth factor. Clinical Cancer Research 10: 3342-3353.

8 Li UQ, Ballinger JR, Nordal RA, Su ZF, Wong CS. (2001) Hypoxia in radiation-induced blood-spinal cord barrier breakdown. Cancer Research; **61**: 3348-3354.

9 Chen TY, Lee MY, Kuo YL et al. (2006) Melatonin attenuates the postischemic increase in blood-brain permeability and decreases hemorrhagic transformation of tissue-plasminogen activator therapy following ischemic strock in mice. *J Pineal Res* 40: 242-250.

10 Marti HJ, Bernaudin M, Bellali A. (2000) Hypoxia-induced vascular endothelial growth factor expression precedes neovascularization after cerebral ischemia. Am J Path 156: 965-976

Author: Gholamhassan Haddadi
Institute: Tehran University of Medical Sciences
Street: Pursina
City: Tehran
Country: Iran
Email: ghadadi@razi.tums.ac.ir

Comparison of Lead-free and Conventional x-ray aprons for Diagnostic Radiology

N. Papadopoulos, C. Papaefstathiou, P.A. Kaplanis, G. Menikou, G. Kokona, D. Kaolis, C. Yiannakkaras and S. Christofides

Medical Physics Department/Nicosia General Hospital, Nicosia, Cyprus

Abstract— **Radiology personnel demand alternatives to lead x-ray aprons, as the weight of lead aprons often causes discomfort, fatigue and musculoskeletal problems. There is also a necessity to change the composition of x-ray protective aprons with environmentally friendly materials, as great concern exists worldwide, about health effects arising from lead exposure. Therefore, lead is being replaced by lightweight materials. The Medical Physics Department of Nicosia General Hospital, conducted a study to evaluate radiation transmission through commercially available lead-free aprons from different manufacturers. The study concluded that these aprons provide less lead equivalent thickness than what is stated on the lead aprons and their manufacturing certificates. This paper describes the methodology used and the results obtained.**

Keywords— **Lead-Free Aprons, Transmission, Lead-Equivalent materials, Attenuation, Radiation protection.**

I. Introduction

Lead is considered to be the most suitable material for protection against x-ray exposure due to its high mass attenuation coefficient for a wide energy range. It is the most effective element for the production of aprons worn by Radiology personnel to minimize x-ray transmissions and protect them from unintentional exposure to radiation during diagnostic examinations.

Simultaneously, lead aprons due to their heavy weight are considered inconvenient, as they can cause discomfort and fatigue to their users, especially during prolonged examinations. Conventional aprons are also associated with cervical/lumbar spine and other neurological health problems. In addition, lead is considered a hazardous material. When a significant amount of lead accumulates in the body, long term health effects may develop due to its toxicity [1].

In the last few years, lightweight environmentally freandly composite materials have been developed to replace lead in the production of lead-free aprons that are able to compete with conventional lead x-ray aprons [2]. These aprons are composed with high atomic number materials ($Z > 50$), such as tin (Sn^{50}), antimony (Sb^{51}), or tungsten (W^{74}) and when exposed to diagnostic x-rays, should perform similar with standard lead aprons. The evaluation of the protective effects of lead-free materials, is their rating exclusively in terms of lead equivalent (LE) value, which refers at a single value of the tube voltage and not for the complete diagnostic energy range. Some manufacturers use a double layer of material and some others a single layer in order to achieve the required lead equivalence [3].

The Medical Physics Department of the Nicosia General Hospital carried out a study to evaluate whether lead-free aprons are as effective as conventional lead aprons in protecting Radiology personnel against diagnostic x-ray exposure. The methodology used and the results obtained are presented below.

II. Materials and methods

Lead aprons of 0.5/0.25 mm thickness and lead-free aprons with the same lead equivalent thickness were used in the study. A fluoroscopic x-ray system (Model Mecall Superix 180N), in a radiographic mode was used. A series of transmission measurements over the energy range used clinically for diagnostic X-ray imaging (60-120 kVp), were performed on each apron. All measurements were repeated twice to improve precision. Broad beam geometry, instead of narrow beam was used, to include the contribution of secondary radiation (scattered and fluorescent), generated within the lead-free materials. The lead-free materials especially with atomic numbers below 60 generate significant fluorescent radiation and therefore only with broad beam set up, the full scale secondary radiation can be detected [4]. Transmissions were measured with the use of a 30x30x20 cm water phantom to simulate the patient [5]. The effective attenuation of both conventional lead and lead-free aprons across the examined energy range was calculated using the following formula:

$$Attenuation(\%) = [1 - \left(\frac{measurement\ with\ apron}{measurement\ without\ apron)}\right)]x100$$

Figure 1 shows the set up used to measure the dose from scattered x-rays with and without an apron. Exposure measurements were recorded with a calibrated Radcal 2026C electrometer plus 180cc ionization chamber. The dose from scattered x-rays was measured with the ionisation chamber placed at 33cm from the phantom's edge.

O. Dössel and W.C. Schlegel (Eds.): WC 2009, IFMBE Proceedings 25/III, pp. 544–546, 2009.
www.springerlink.com

The exposures were taken at a tube potential of 60, 80, 100, 120 kVp, with a 32 mAs. The exposure area (radiation field size) was 30x30 cm.

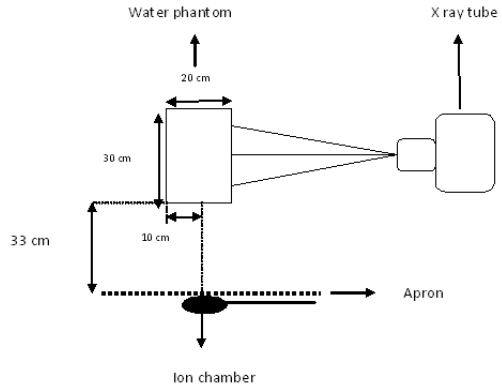

Figure 1 Experimental set-up

III. Results

Lead-free aprons from five different vendors participated in the study. Table 1 shows the attenuation (%) of each apron brand at different beam qualities for scattered x-rays. The average attenuation for conventional lead aprons is 98.4%, while the average attenuation for lead-free aprons varies from 87.2% to 97.8%.

Table 1 Attenuation at different beam qualities for scattered x-rays

Apron Brand	Attenuation (%)				Average attenuation (%)
kV_p	60	80	100	120	
HVL mmAl	2.5	3	4	5	
Lead-free 1	99.3	98.0	96.3	94.7	97.1
Lead-free 2	99.3	98.1	96.5	94.8	97.2
Lead-free 3	99.5	98.7	97.3	95.7	97.8
Lead-free 4	99.4	98.4	97.0	95.4	97.6
Lead-free 5	95.3	89.6	84.2	79.6	87.2
Conventional	100	99.2	97.8	96.4	98.4

Table 2, shows the Coefficient of Variation (CV) and the corresponding Standard Error of the Mean (SEM) of the attenuation (%), at the energies tested between the various brands.

Table 3 shows the weight of each brand's apron. All lead-free aprons were lightweight (weighting between 40-46 % less than conventional lead).

Table 4 shows the ratios of average attenuation over weight for all lead-free aprons.

Table 2 Coefficient of Variation (%CV) and Standard Error of the Mean (SEM), at the energies tested, between the various brands

Energy	%CV	SEM
60 kVp	1.75	0.70
80 kVp	3.25	1,28
100 kVp	5.46	2.11
120 kVp	7.72	2.93
Average of all energies	4.94	1.93

Table 3 Weight of each apron (110 cm length)

Apron Brand	Weight (kg)
Lead-free 1	4.4
Lead-free 2	4.4
Lead-free 3	3.9
Lead-free 4	4.0
Lead-free 5	4.0
Conventional	7.3

Table 4 Average attenuation over weight for lead-free aprons

Apron Brand	Average Attenuation (%)/Weight (kg)
Lead-free 1	22.1
Lead-free 2	22.1
Lead-free 3	25.1
Lead-free 4	24.4
Lead-free 5	21.8

IV. Discussion

The results obtained indicated that the lead free aprons tested, did not present the same attenuation efficiency as the one stated on their manufacturing certificates.

Furthermore, the coefficient of variation (CV) of the attenuation values increases with energy, with the highest value being 7.72% at 120 kVp.

The best lead free apron is the Lead-free 3 because:

- It was the lightest apron tested (<4kg).
- It attenuates radiation most effectively from 60-120 kV, even though the radiation protection provided by conventional lead aprons was somewhat higher for the same energy range (~0.6%).
- It exhibited consistent shielding protection over the diagnostic energy range (average attenuation), even

over 100 kV, where the shielding protection of lead is dominant.

V. Conclusions

1. None of the lead-free aprons provide lead equivalency (LE) of 0.5mm as stated by their manufacturers. The nominal LE values labeled on the aprons are not compatible with the measured actual values, leading to higher transmissions of radiation [6].
2. Even though lead-free aprons of different vendors have the same weight, they exhibit different levels of attenuation at the same beam quality. This is because the attenuation effect of each constituent material varies significantly with energy. Due to this, it is impossible for the manufacturers to state lead equivalency across the entire diagnostic energy range (usually lead equivalency is stated at 100 kV), indicating the necessity for the establishment of acceptable tolerance levels at each beam quality [7, 8].
3. The density and the K-absorption edge of each lead-free material are two significant factors that affect the attenuation efficiency of each material [7]. Hence, materials with high atomic numbers and low densities provide the best attenuation and proved to be the most effective for the production of lightweight lead-free aprons.
4. For a particular manufacturer the protection efficiency of its product is completely inefficient, especially at energies above 100 kV which is reduced by up to 20%.

Finally the study showed that the acceptance testing of lead-free aprons is essential to ensure that lead-free aprons meet their manufacturer's specifications and provide the necessary radiation protection for their indented use.

ACKNOWLEDGMENT

The authors, wish to thank the personnel of the Radiology Department of the Nicosia General Hospital for their assistance during this study.

References

1. 2-Health Effects of Lead at http//www.ccohs.ca/oshanswers/chemicals/chem._profiles/lead/he.
2. Are Today's Non-lead Lightweight Apron Safe? At http://www.xrayapron.com.
3. Muir S, Mcleod R, Dove R (2005). Light-weight lead aprons-light on weight, protection or labeling accuracy? Australas Phys Eng Sci Med Jun; 28(2):128-30.
4. Eder H, Panzer W, Schöfer H (2005). Is the lead-equivalent suited for rating protection properties of lead-free radiation protective clothing? ,Rofo, Mar 177(3):399-404.
5. Masayuki Z, Koichi C, Masaaki T et al (2008). Usefulness of non-lead aprons in radiation protection for physicians performing interventional procedures, Radiation Protection Dosimetry 2008 131(4):531-534.
6. Finnetry M, Bernnan P C, (2005). Protective aprons in imaging departments: manufacturer stated lead equivalence values require validation, Eur Radiol 15: 1477-1488.
7. McCaffrey J P, Downton B, Shein H (2007). The attenuation effects of lead and non-lead materials used in radiation shielding garments. Med Phys. 34, 530-537.
8. Christodoulou E G, Goodsitt M M, Larson S C et al (2003). Evaluation of the transmitted exposure through lead equivalent aprons used in a radiology department, including the contribution from backscatter, Med. Phys. Volume 30, Issue 6, pp. 1033-1038.

Author: Nicolaos Papadopoulos
Institute: Medical Physics Department, Nicosia General Hospital
Street: 215 Old Nicosia Limassol Road
City: Nicosia 2029
Country: Cyprus
Email: nicolaos.papadopoulos@gmail.com

Regulatory Aspects in Industrial Gamma Radiography in Iran

M.R.Deevband[1], B.Samimi [1],H.R.Khosravi[1,2],M.R.Kardan[1, 2], M.M.Hormozi[1],H. Karimi Ashtiani [1], Gh.H. Heravi[1,2]

[1] National Radiation Protection Department, Tehran, Iran
[2] Nuclear sciences and technology research institute, Tehran, Iran

Abstract— **Industrial radiography is one of the essential methods in the modern technology to guarantee the quality control of many types of devices, pieces and machines operation, and usually involves intense radiation sources, which can expose people at work to significant amounts of radiation. The aim of this research is to assess the level of dose to the industrial radiographers and the level of radiation safety regulations and radiation protection programme implemented in Iranian industries. In Iran, there are 650 mobile Gamma Radiography Projectors (GRP) containing ^{192}Ir radioactive sources. These GRP belong to 220 Industrial Radiography Companies (IRC). Approximately 1889 radiographer's works in these IRC. According to the latest data presented by United Nations Scientific Committee on the Effects of Atomic Radiation (UNSCEAR 2000), the average annual effective dose to the industrial radiographers is 3.37mSv/y. Based on this workk; average effective dose and collective effective dose to the radiographers are 3.49mSv/y and 6.41 Man.Sv, respectively due to 2008.**

Keywords— **Industrial Exposure, Industrial Radiography, collective dose, gamma projector, radiation protection programme.**

I. Introduction

Industrial radiography is an important method of quality control of welding and castings of products used in various spheres of industrial activity. Widespread use of radiography sources call for meticulous radiation safety programme so that radiation exposures received by industrial radiographers as well as members of public are in conformity with the ALARA concept. Industrial radiography usually involves using intense radiation sources. Generally, workers in industrial radiography have received higher doses than those working in other sectors using ionizing radiation. According to the latest data presented by United Nations Scientific Committee on the Effects of Atomic Radiation (UNSCEAR 2000), the average annual effective dose to the industrial radiographers is 3.37mSv/y [1]. Over the years several serious incidents have been caused by the failure to maintain equipment, to carry out routine monitoring or to employ proper emergency Procedures [2]. Potential risks associated with sources used in industrial radiography include acute radiation exposure which can produce immediate effects and genetic and delayed effects of long term low exposures.

Industrial gamma radiography activity is the most difficult area for regulatory control throughout the world as the radiation sources are used in construction sites and workshops where built – in safety systems are not available as in other uses of ionizing radiations. Regulatory control is mainly achieved through instituting proper work practices, effective radiation surveillance programme and inculcating healthy awareness for radiation safety in the work force operating the gamma radiography exposure devices.

II. Materials and Methods

A. Radiation Safety Legislation

The Radiation Protection (RP) in Iran dating back to 1957, when the Nuclear Center of Tehran University (NCTU) was established [3].The infrastructure of a nationwide RP programme was formally established in Atomic Energy Organization of Iran (AEOI), when the Atomic Energy Act of Iran was legislated and ratified in 1974. The Radiation Protection Act of Iran proposed to the parliament and legislated in 1989. The act precisely formulated responsibilities and clearly empowered the with authority to regulate and control the entire range of radiation protection activities in different disciplines [4].

According to The Radiation protection Act of Iran and its Regulations, the IRCs are obligated to get license from the Iranian Nuclear Regulatory Authority (INRA) before commensuration of their work with radiation. Based on the Basic Safety Standard 115, the INRA provided the Basic Radiation Safety Standards (BRSS) [5] in October 1999 and the Code of Practice for Industrial Radiographies (CPIR) in January 2001 and its revised version in April 2005.

O. Dössel and W.C. Schlegel (Eds.): WC 2009, IFMBE Proceedings 25/III, pp. 547–550, 2009.
www.springerlink.com

B. Regulatory Control

The following prerequisites are required to be complied by an applicant procuring an industrial radiography source.

1. Radiography equipment and sources

The industrial radiography equipment shall be capable of remote operation and control and their limits of leakage radiation levels and various built-in design safety features have undergone stringent tests for radiographic exposure devices under ISO3999 international standard [6], and also isotope sources comply with ISO 2919 sealed sources requirement. The sources, equipment and accessories are subjected to type approval by regulatory authority also can be employed.

2. Personnel requirements

The radiography institutions should have the following requisite qualified staff, in addition to radiation monitoring instruments and safety accessories as stipulated in the industrial radiography code of practice.

1. Responsible person
2. Radiation protection officer (RPO)
3. Certified Radiographer (Operators)

They should have the basic qualification and training in radiation safety aspects as stipulated in the industrial radiography code of practice.

3- Administrative control measures

Following administrative measures should be taken by licensees:

- When not in use, radiography sources and devices should be stored in an approved and secure storage facility.
- The inventory of radiography sources should be limited to those required for operation. Sources that are not in use or decayed to below their useful activity should be disposed off.
- All regulation and procedures for safe transport of radioactive material should be followed for transport of radioactive sources for disposal or for movement of sources from one location to another.
- Comprehensive records should be maintained in respect of use, location, storage and movement of all radiation sources.
- Adequate radiation monitoring program should be carried out as necessary. It is therefore essential that dose rate meter devices are in working order; have been type tested; have a valid test certificate and are within their calibration date.
- Appropriate area monitoring and personnel monitoring devices should be provided and used. In addition, personal direct dosimeter such as pen dosimeter and personal indirect dosimeter (TLD) and personal electronic alarming dosimeters give immediate warning of high dose rates, so wearing these are mandatory and useful to radiographers. However, this should not replace the use of portable dose rate meters.
- Adequate protection devices such as shielding barriers, collimators, remote handling devices should be provided and used when required.
- Adequate radiation warning symbols should be displayed when required.
- Appropriate safe working rules and emergency procedures should be prepared and followed.
- All accident involving radiation sources and equipment should be reported and investigated and actions to prevent recurrence should be taken.
- All relevant legislative requirements should be complied with.

4. Radiation safety in field radiography

In field operations, the source should be adequately shielded when in the fully closed or retracted position. The operator must ensure that unauthorized persons do not approach the exposed source. This is generally achieved by the following methods:

- An area around the source must be physically cordoned / Barriered to prevent access and warning notices/symbols must be provided at all points of access to the barrier.
- The operator must be available and must positively police the barrier throughout all exposures.

5. Emergency planning and preparedness

The centers should have action plans, clearly specify persons and responsibility and functions, line of authority and line of communication, initial and periodic training, appropriate tools, radiation safety accessory, radiation monitoring, personnel monitoring devices for possible accident scenarios.

C. Steps of Authorization

Step 1. Construction

When application form and all documents are submitted and complied with regulatory requirements, Authorization for construction is issued by NRPD.

Step 2. Source Authorization

When all the pre-requisites for source procurement are complied with regulatory requirements, Authorization for source procurement is issued by NRPD.

The authorization is issued with specific conditions of use for one source and for one year validity.

Step 3. Pre- authorization Inspection

Pre-authorization inspection of the radiography company or site is conducted by National Radiation Protection Department (RPD), to ensure that the facilities stated by the applicant in the application are actually available at the company as well the site and also to assess the site condition for carrying out radiography work in a safe manner with the radiography equipment and the activity of the radiography source by the applicant.

Step 4. License

When all documents for license are complied with regulatory requirements, the assessment report of the inspector with the recommendations is reviewed; license is issued with specific conditions of use for three years validity by NRPD.

D. Radiation Surveillance

1- Declaration for Source Movement

The radiography sources are initially authorized for use, if the users want to move the radiography source to another site; they should inform NRPD, furnishing details about the operating conditions and storage facility available at the new site.

This enables the regulatory body to have a check on the proper and safe use of radiography sources inverse parts of the country.

2- Specific Authorization for Replacement Sources

Authorization should be obtained for each and every replacement source for gamma radiography equipments. All remote operated exposure devices are inspected to ensure its smooth functioning by center approved and supervised by RPD, before loading of the replacement source in the equipment.

3- Periodic, Announced and Unannounced Inspections

Periodic radiological surveys are conducted by RPD, to evaluate the safety Status and the work practice of the radiography institutions. Unannounced inspections are also carried out to find out the actual working conditions at field radiography sites and to evaluate the authenticity of the information provided by the user institutions. Generally unsafe work practices and use of radiography sources at unauthorized area by uncertified persons are observed during such unannounced inspections.

E. Violations and penalties

Penalties are imposed for observed violations of the stipulated safety procedure by the user institutions in the form of recommendation, limitation and revocation/ suspension of license issued for operating the certificate holder are clearly mentioned by official letter. The certificates are liable to be withdrawn if serious violations of work practices are observed during inspections.

III. Results and Discussion

In Iran, industrial radiography contributes to about 69.5% of the total work force and above 90% of the total collective dose equivalent of all industrial applications of radiation sources. The annual average dose received by an industrial radiographer is nearly 5 times higher than the dose received by workers engaged in other industrial applications of radiation. Industrial radiography installations can be briefly classified into 3 categories namely (i) field radiography installations, (ii) enclosed installations and (iii) x-ray installations (where only x-ray machine are used).

Figure 1 and figure 2 shows the comparative dose distribution data for these three categories. Among the three categories, radiography at project sites (field radiography) contributes significantly to the collective dose equivalent.

When the exposure recorded by the personnel monitoring badge is more than 4 mSv for the period of its usage (generally two months), the case is investigated to assess the genuineness of reasons for the same. If exposure is appointed by the 50 mSv and higher, the individual is subjected to biological dosemetric test (CA test) and are not allowed to continue his\her job, until, medical doctor allow his\her. Statistical data of excessive exposures in the industrial exposures for the period 2005-2008 is given in Table 1.

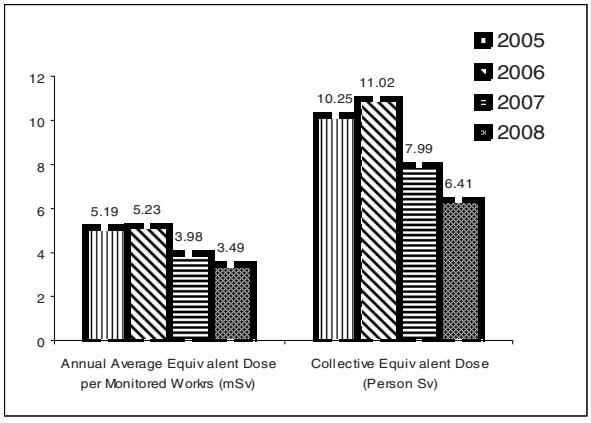

Fig. 1, Dose Distribution Data in Field Radiography

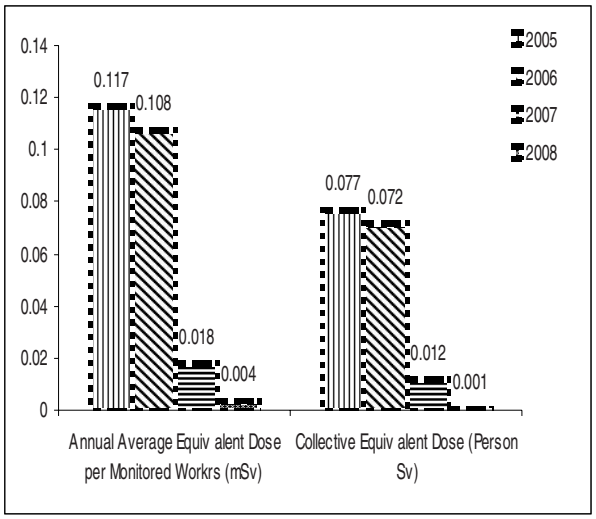

Fig. 2, Dose Distribution Data in Enclosed and X-ray Installation

Table 1, Analysis of Radiation Overexposures

Year	4-50 mSv	50-100 mSv	≥ 100 mSv	Total
2005	351	15	10	376
2006	368	13	8	389
2007	289	8	5	302
2008	233	6	6	245

Maximum levels of leakage of different type of GRDs are measured and it's equal to 620 μSv/h, So that the results of this study were less than 2 mSv/h.

Radiation safety status in industrial radiography reviewed through an analysis of dose distribution of industrial radiographers revealed that certain important factors such as the type of radiography equipment used, availability of trained man power, proper safety management and effective regulatory control can greatly help in minimizing the individual as well as collective dose in industrial radiography operations. It was observed that field radiography operations contributed to more than 90% of the total collective dose in the industrial radiography operations, Hence radiation surveillance was concentrated mainly on these institutions and this helped to improve the overall radiation safety status in industrial institutions. Availability of trained man power in an institution helped to minimize the individual and collective dose values. Trainee radiographers are not permitted to operate the radiography exposure devices.

IV. Conclusion

The mean dose equivalent to the radiographers was 3.49mSv/y and 6.41 Man.Sv, respectively due to 2008. 88% of them are received less than 5 mSv/y and only 1% more than 20 mSv/y. The 22% of companies had no adequate medical records for their radiographers, 47% had no emergency instruction but 35% had no enough emergency instruments, and 29.5% had no suitable temporary storage and transporting facilities.

References

1. United Nations Scientific Committee on the Effects of Atomic Radiation Sources and Effects of Ionizing Radiation. Report to General Assembly, with Scientific Annexes. United Nations Sales Publication E.00.IX.3 United Nations, New York, (2000).
2. M.R.Deevband, M.Ghiasi-Nejad, S.Borhan- Azad, The evaluation of parameters affecting accidents in companies using industrial radioactive sources in Iran. Radiation Protection Dosimetry (2004), Vol.109, No. 3, pp. 253-256.
3. M.Sohrabi, IAEA-SM-309/53, International Symposium on Radiation Protection Infrastructure, Munich, (1990).
4. M.Ghiasi-Nejad, S.Borhan Azad, M.R.Deevband, Status of Operational Implementation of Basic Safety Standards in Iran, IAEA-CN-91/35, Geneva (2002), pp.89.
5. Basic Radiation Safety Standards (nrpd-brss-1), Iranian Nuclear Regulatory Authority, (October 1999).
6. ISO," Apparatus for Industrial Gamma Radiography-Design and Test Criteria", ISO 3999,(1977).

- Author: M.R.Deevband
- Institute: National Radiation Protection Department
- Street: North of Kargar
- City: Tehran
- Country: IRAN

Email: mdeevband@aeoi.org.ir

Relation between Childhood Leukemia and High Power Lines in Tehran – Iran

Navid Khaledi, Moloud Dabaghi, Nima Khaledi, and Dr. Darush Sardari

Science and Research Campus, Young Researchers Club of Islamic Azad University, Tehran, Iran

*Abstract*__ **Up to the best of our knowledge, the first report on the relationship between childhood cancer and electromagnetic field emitted from power lines dates back to 1979. In our research, a group of 202 children suffering from leukemia has been studied (as case group). Map of Tehran was divided to 921600 square regions using AUTOCAD software. Using random number generator 4000 square regions were selected of which 86 were located 100 meters or less from the power line (as simulated control group) , corresponding to 0.2 μT. Out of 202 children 7 were living in these selected area. Statistical analysis shows that odds ratio is equal to 1.63 (95% CI = 0.8-3.6) that shows a causal relationship between electromagnetic field and childhood leukemia.**

Keywords— **Leukemia, High power lines, Simulation**

I. Introduction

Wertheimer and Leeper[1] were of the pioneer that researched about the effect of electromagnetic fields on the occurrence to childhood leukemia. After that, other researchers like Savitz[2] and M.Feychting[3] in different countries such as US, Sweden and Denmark surveyed this topic. All named researcher showed that being in front of the magnetic field of power lines increase risk of childhood leukemia. Also some more effects reported for magnetic fields, that we can mention nervous system tumors for example. But nervous system tumors, was not subject of this research.

Two prevalent type of leukemia is Acute Lymphoblastic Leukemia (ALL) and Acute Myelogenous Leukemia (AML). Percent of suffering from ALL is 78% and from AML is 19%[4].

We enrolled randomly 202 children with acute lymphoblastic leukemia (ALL) who were under 9 years of age, in Tehran as case group. Mathematical simulation has been applied for control group, too. So, this research based on case-control study.

II. Materials and Methods

The average of magnetic field in 100 meters, for power lines, is about 0.2μT[5].

In case group, those children their houses was in distance of up to 100 meters from 230kv and 400kv cables, were considered "exposed case group". As described above, mathematical simulation for control group has been used. In the way that, map of Tehran was divided to (921600=)960×960 squares by using AutoCad software and with this software earmarked a number for every square, and generated random number between 0 and 921600, then we selected 4000 first numbers (squares) as control group, if this number showed residential point. This 4000 numbers was our control group. In this 4000 squares, those numbers (squares) was in 100 meters region, named "exposed control group". In fact, this squares, shown children's habitat. Dwelling place of children can be expanded to their population. This election and expand is true, because number of children suffering from leukemia is too smaller than healthy children. Since afoul to leukemia in children is 3 in 100,000 per year[6], so with excellent approximation all children of a city can be assumed healthy. Notice, showing 92,1600 squares on letter sheet or in this article is impossible, because showing this number of squares in bounded size of this paper, redound to a black picture. Thus, only for presentation this method, showed just very lesser number of squares in fig.1. But in fig.2, an arbitrary region of Tehran is selected. And in this case squares size is real.

O. Dössel and W.C. Schlegel (Eds.): WC 2009, IFMBE Proceedings 25/III, pp. 551–553, 2009.
www.springerlink.com

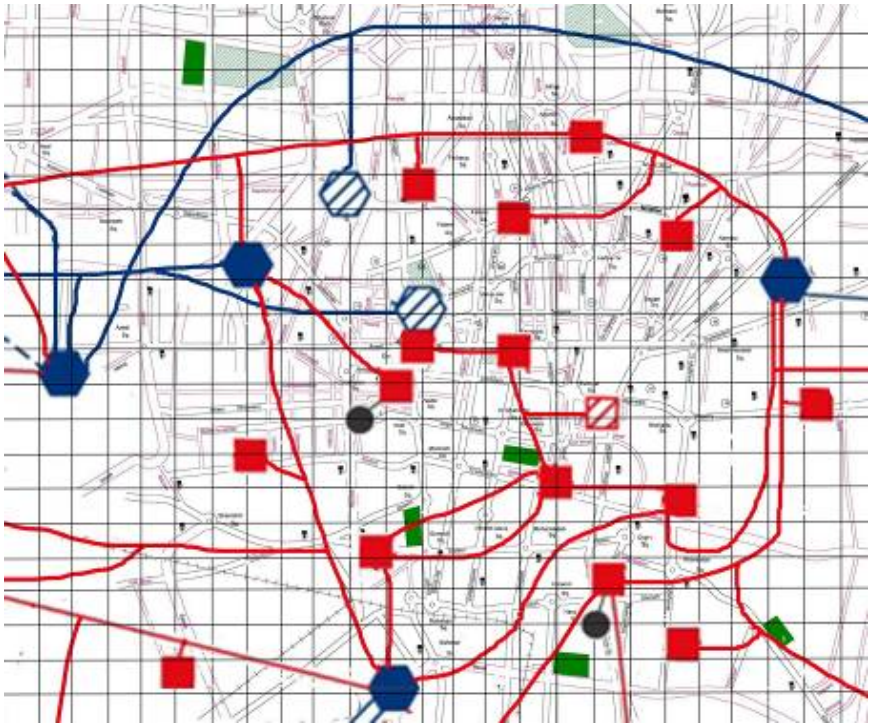

Fig.1
The divided map of Tehran (squares size is not real)
Blue lines indicate 230kv power lines.
Red lines indicate 400kv power lines.

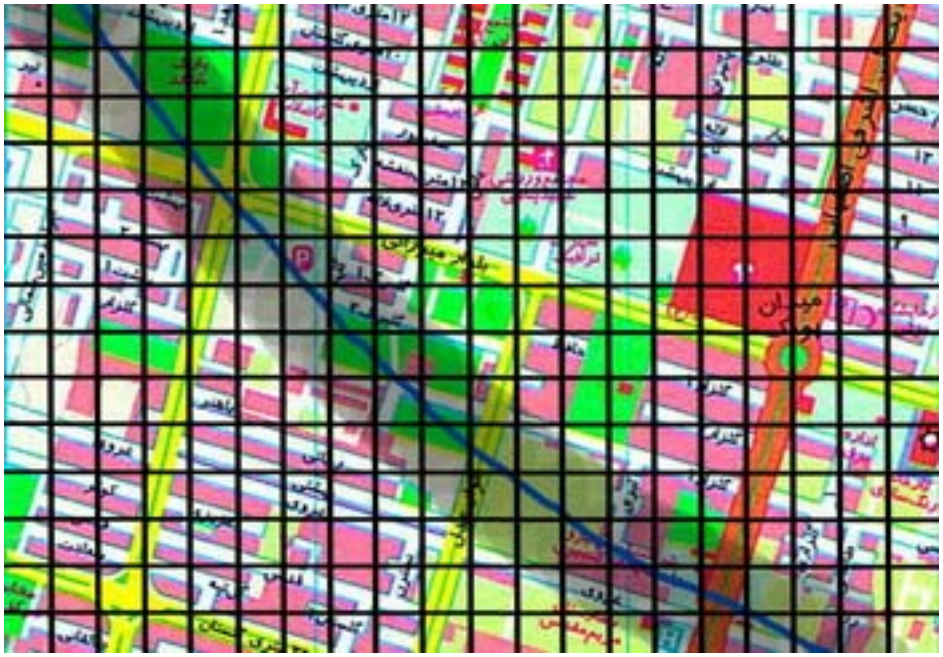

Fig.2
230kv power lines transition, in arbitrary region of Tehran (squares size is real)
Gray shadow shows the 100 meters border in per side of cable.

We should not forget effect of exposure from internal sources in the house. But this effect equal for every peoples, thus can neglect that.

A. Statistical calculation

Relation existence between power lines magnetic field and childhood leukemia, done by statistical calculations. This association calculated by odds Ratio (OR) and the random variability was assessed by 95% confidence intervals (95% CI). Being little number of leukemia patients was one of reasons that we chose OR.

The calculations indicated in table 2.

Table 1 Exposed and unexposed case and control group.

Groups	Total population	Exposed No.	Exposed (%)	Confidence Interval (95%CI)	Unexposed No.
Case group	202	7	3.46	1.52-7.3	195
Control group	4000	86	2.15	1.73-2.66	3914

III. Conclusions

By using content of table 1 odds ratio was calculated. As shown, this value equal to 1.63 (95%CI 0.8_3.6) which is greater than 1. Hence, can deduced, magnetic field of power lines can be influence on the increase of leukemia risk. This result had accordance on other researches done by Savitz, Martha, or Feychting and other researchers. The difference was only on OR value. They acquired OR respectively: 1.93, 1.53, 2.49[7] . This difference, arise from various conditions.

Table 2 Calculated odds ratio and confidence interval.

	OR	Confidence Interval (95%CI)
Value	**1.63**	0.8-3.6

Acknowledgment

By thanks of Mr. Sobhan Sajoodi, for helping in edition of this passage.

References

1. Wertheimer N, Leeper E. "Electrical wiring configurations and childhood cancer". AmJ Epidemiol 1979,109,273-284.
2. Savitz DA, Wachtel H, Barnes FA, John EM, Tvrdik JG. "Case-control study of childhood cancer and exposure to 60-Hz magnetic fields". Am J Epidemiol 1988;128:21-38.
3. M. Feychting,' G. Schulgen,2 J.H. Olsen3 and A. Ahlboml "Magnetic Fields and Childhood Cancer-a Pooled Analysis of Two Scandinavian Studies" European journal of Cancer Vol. 31A, No. 12, pp. 20335-2039,1995
4. www.envirohealthpolicy.net , Children, Cancer, and the Environment
5. www.wapa.gov , Electric and Magnetic Fields FACTS , WESTERN AREA POWER ADMINISTRATION
6. Frank S Barnes, Ben Greenebaum , " Handbook of Biological Effects of Electromagnetic Fields" , CRC Press , 2007
7. Daniel Wartenberg , " Residential EMF Exposure and Childhood Leukemia:Meta-Analysis and Population Attributable Risk" , Bioelectromagnetics Supplement 5:S86^S104 (2001)

Survey of Image Quality and Patient Dose in Simple Radiographic Examinations in Madagascar: Initial Results

Marie Jeanne Ramanandraibe[1], Raoelina Andriambololona[1], Eloïm Rakotoson[2], VirginiaTsapaki[3], Hans Gfinter[4], and Madan Rehani[5]

[1] Institut National des Sciences et Techniques Nucléaires, Antananarivo, Madagascar
[2] Centre de Soins et de Santé, Service de radiologie, Antananarivo, Madagascar
[3] Konstantopoulio Hospital, Athens, Greece
[4] Graf Tiemo Str. 16, D-94127 Neuburg
[5] International Atomic Energy Agency, Vienna, Austria

Abstract- **In the first ever survey of patient doses in Madagascar, image quality and patient doses were evaluated in 3 rooms of 2 hospitals in Madagascar as part of an International Atomic energy Agency (IAEA) project (RAF/9/033) using protocols and instructions by IAEA experts. Corrective actions were taken mainly in terms of field size and exposure parameters adjustment and data were recollected. Image quality improved in all 3 rooms (increase: 2-35%). Dose reductions in the range of 1 to 66% in terms of ESAK were found in different examinations investigated. The max reduction was found in chest examination. The comparison with IAEA guidance levels (GL) showed that patient doses (ESAK values) are lower than international values except for chest exam in one of the rooms of the hospital. Actions are being taken to extend measurements to a national level in the near future.**

Keywords— Radiography, patient dose, optimization

I. Introduction

The Basic Safety Standards require attention to the image quality and consideration of corrective actions [1]. There is tremendous amount of wastage of resources, particularly in developing countries, on images of poor quality [2]. In many situations poor quality images constitute as much as 15-40%. This results in unnecessary radiation exposure to patients, loss of diagnostic information, increased social costs besides the economical aspects on health care. Experience from national surveys in some countries such as UK has shown the possibility of large variation in patient doses for common examinations to the tune of 20 or more in different hospitals or even in different rooms in the same hospital. Unfortunately, more often than not, quality assurance (QA) in diagnostic radiology implies just testing X-ray equipment for possible malfunction without any consideration of image quality However, the emphasis has to be both on image quality and patient dose rather than simply testing equipment performance.

In 1998, Madagascar formed new legislation and regulation related to the basic principles of radiation protection especially in the medical field. Since no patient dose survey was ever performed in the country before, a study was performed under the International Atomic Energy Agency (IAEA) project RAF/9/033. The objective of this study was to assess image quality and radiation dose received by patients for common radiographic examinations in 3 rooms of 2 selected hospitals in the capital of Madagascar.

II. Materials and Methods

For the purpose of this study, one private hospital, "Centre de Soins et de Santé (CSS)" with 1 X-ray room and one public hospital CHU-HJRA Antananarivo (CHU) with 2 X-ray rooms were selected. The X-ray system in CSS hospital was a Bennet X-ray machine installed in 1995. The 2 X-ray systems in the CHU hospital were installed in 2002 (a Stephanix machine by Stephen technologies and a MT Lab IAE machine IAE SPA Cormanao technologies). Entrance surface air kerma (ESAK) was evaluated for a sample of 10 adult patients in the most common radiographic examinations. ESAK was calculated from machine output by taking into account the exposure parameters and focus to patient distance. Output measurements were conducted under standardized protocols prepared by IAEA experts using a Ratemeter-Timer, Model 3036, with an internal chamber (Radcal Corporation Company), calibrated at the Secondary Standard Dosimetry Laboratory of Institut National des Sciences et Techniques Nucléaires. Patient dose calculations were performed for chest AP, lumbar spine AP and lateral, pelvis AP, abdomen AP and skull AP. Dose evaluation was done for 10 patients of each of these examinations in all three x-ray rooms before and after quality actions. Basic quality control checks were performed: 1) reproducibility of delivered dose, 2) accuracy of tube potential and 3) half value layer determination. Image quality assessment was also performed for 2 weeks in radiology rooms. More

O. Dössel and W.C. Schlegel (Eds.): WC 2009, IFMBE Proceedings 25/III, pp. 554–556, 2009.
www.springerlink.com

specifically, a radiologist observed all X-ray films and assigned an A, B or C grade to each of the films (A: clearly accepted without any remark, B: accepted with some remarks and C: rejected). For B & C grade films a reason should be assigned (under/over exposed, artefact, field size misplacement, processing problem). If required, appropriate corrective actions were then made on the basis of quality control and adjustment of technical parameters used in X-ray exam.

Finally, a second series of dose measurements and image quality assessment was taken, after having implemented corrective actions to investigate possible patient dose optimization. ESAK measurements were compared with and IAEA guidance levels (GL).

III. Results

The following 5 tables summarize the results of the study:

Table 1 Corrective actions taken after initial image quality and patient dose assessment are shown in this table.

Corrective action	CSS	CHU room 1	CHU room 2
Field size adjustment	Y	Y	Y
Change in expos parameters	Y	Y	Y
Change of focus to film distance in chest exam	Y		

Table 2. Image quality (IQ) assessment as % of the films in A, B and C category before corrective actions.

Grade	CSS	CHU room 1	CHU room 2
A	96	41	40
B	3	56	56
C	1	3	4

Table 3. IQ assessment results as % of the films after corrective actions were applied.

Grade	CSS	CHU room 1	CHU room 2
A	98	52	54
B	2	47	45
C	0	1	1

Table 4. Mean ESAK values in mGy before corrective actions.

Exam	CSS	CHU room 1	CHU room 2
Chest	0.29	1.81	
Lumbar spine AP	3.92		
Lumbar spine LAT	6.61		
Pelvis	3.92		16.61
Abdomen	3.92	8.91	
Skull	2.95	6.89	11.08

Table 5. Mean ESAK values after corrective actions in mGy.

	CSS	CHU R 1	R2
	ESAK	ESAK	ESAK
Chest	0.19	0.53	
L/S AP	3.25		
L/ LAT	6.52		
Pelvis	3.10		5.22
Abdomen	3.10	3.53	
Skull	2.78	2.42	4.54

The analysis of B and C grade films showed that the most frequent problem was the existence of artefacts (75%, 79% and 78% in CSS, CHU room1 and 2 respectively), followed by field misplacement (25% in CSS hospital) and over or underexposure (17% in both rooms of CHU hospital). The quality control tests confirmed that the performance of the X ray systems was according to the manufacturer's specifications. Image quality assessment after the introduction of corrective actions showed a reduction of over and under exposure in CHU hospital (14 % in room 1 and 10% in room 2).

IV. Discusssion

The initial results of the study in 2 major Hospitals in Madagascar show that image quality improved and patient doses were optimized after corrective actions in both hospitals. Image quality was improved in all 3 rooms. Grade A films increases ranged between 2-35%.

Dose reductions range was 1%-71%. The max reduction was found in chest examination. The common cause of B grade film was possibly due to the long storage of films before use. Table 6 shows mean ESAK values of all hospitals before (ESAKb) and after corrective actions (ESAKa) in mGy as well as the percentage of dose reduction. The table presents also IAEA guidance levels (GL) for comparison purposes (200 film screen combination). The comparison showed that patient doses are lower than international values except chest exam in one of the rooms of CHU hospital and skull exam in the second room of CHU hospital (Table 5 for each hospital separately and Table 6 for all hospitals). In these rooms, further investigation is needed.

Table 6. Mean ESAK values, in mGy, before (ESAKb) and after (ESAKa) corrective actions as well as % of dose reduction are shown in this Table. IAEA guidance levels (GL) are also presented for comparison purposes.

Exam	ESAKb	ESAKa	% Change	GL
Chest PA	1.05	0.36	66	0.4
Lumbar spine AP	3.92	3.25	17	10
Lumbar spine LAT	6.61	6.52	1	30
Pelvis	10.27	4.16	59	10
Abdomen	6.42	3.32	48	10
Skull	7.0	3.25	54	5

V. Conclusions

This was the first patient dose survey ever performed in Madagascar. Initial results showed that image quality can be improved and patient doses can be reduced simply by changing exposure parameters and adjusting field size. In one of the hospitals, increasing the focus to film distance in the chest exam further optimized patient doses.

Acknowledgment

The work was supported by the IAEA through the TC project number RAF/9/033 “Strengthening on Radiation Protection of patients and Medical Exposure Control”. Thanks are due to the Staff of the hospital CHU-HJRA and the CSS for providing data on image quality assessment.

References

1. IAEA/PAHO/WHO/FAO/ILO/OECD-NEA.International Basic Safety Standards for protection against ionizing radiation and for the safety of radiation sources, IAEA Safety Series No. 115, Vienna (1996).
2. Rehani M. The IAEA’s activities in radiological protection in digital imaging. Radiat Prot Dosim 2008: doi:10.1093/rpd/ncn155.
3. European guidelines on quality criteria for radiographic images. EUR 16260 (European Commission) (1996).
4. International Atomic Energy Agency. Dosimetry in diagnostic radiology: an international code of practice. Technical reports series no. 457 (Vienna: IAEA) (2007).

Author: Virginia Tsapaki
Institute: Konstantopoulio Hospital
Street: 1 Ifaistou, 14569 Anixi,
City: Athens
Country: Greece
Email: virginia@otenet.gr

In-Phantom Peripheral Organ Doses from Prostate Irradiation Using 18 MV External Beam Radiotherapy Measured with ^{6}LiF:Mg,Cu,P & ^{7}LiF:Mg,Cu,P Glass-Rod TLDs

R. Takam[1,2], E. Bezak[2,1], E. Yeoh[3,4], and G. Liu[2,1]

[1] School of Chemistry and Physics, The University of Adelaide, Adelaide, Australia
[2] Medical Physics Department, Royal Adelaide Hospital, Adelaide, Australia
[3] School of Medicine, The University of Adelaide, Adelaide, Australia
[4] Radiation Oncology Department, Royal Adelaide Hospital, Adelaide, Australia

Abstract— **A radiation dosimetry technique based on pairs of ^{6}LiF:Mg,Cu,P and ^{7}LiF:Mg,Cu,P glass-rod TLDs was developed for measuring peripheral photon and neutron doses in the humanoid Rando phantom as a result of prostate irradiation using the 18 MV three-dimensional conformal radiotherapy (3D-CRT). The peripheral doses for different organs were estimated from TLD measurements and the risks of radiation-induced second malignancy were estimated using the competitive risk and linear no-threshold models. It was observed that following 80 Gy prostate irradiation using 18 MV 3D-CRT technique, both photons and neutrons doses ranged from approximately 97 mSv (in thyroid) to 807 mSv (in colon). Using the competitive risk model, the estimated risk of second malignancy was found to be ranging from 0.5% (for lungs) to 3.3% (for colon). Due to low doses (<2 Gy) exposure, estimation of the risk of second malignancy using the linear no-threshold model resulted in similar values as obtained with the competitive risk model. In conclusion, ^{6}LiF:Mg,Cu,P and ^{7}LiF:Mg,Cu,P glass-rod TLDs can be used in pairs to enable determination of photon and neutron doses simultaneously in a Rando phantom and to evaluate the impact of prostate cancer irradiation with high-energy (18 MV) 3D-CRT technique on the risk of second malignancy in various organs.**

Keywords— **Glass-rod TLDs, peripheral dose, second cancer.**

I. Introduction

The use of Dose-Volume Histograms (DVHs) of the prostate surrounding Organs-At-Risk (OARs), i.e. rectum, bladder, and urethra, incorporation with the competitive risk model to estimate the risk of second malignancy has been demonstrated recently [1]. It was observed that irradiation of these organs to high radiation doses from the prostate radiotherapy led to small risk of developing second malignancy. However, it is well acknowledged that irradiation of the prostate using medical linear accelerator (linac) at treatment energies at or above 10 MV is associated with production of out-of-field photons as well as neutrons. The patient's whole body outside the target region will be exposed to these radiations as a result of the prostate External Beam Radiotherapy (EBRT) using high-energy linac. This may result in elevated risk of developing radiation-induced second malignancy in organs distal to prostate. Therefore, it is also necessary to evaluate the risk of second malignancy for these organs. However, DVHs of the organs located outside PTV, i.e. liver, stomach, lungs, and thyroid, are not generally available for the risk estimation using such approach. Therefore, it is necessary to evaluate the dose to the patient from secondary radiations (peripheral dose) by means of radiation dose measurement in the anthropomorphic Rando phantom simulation prostate 3D-CRT with high-energy (>10 MV) linac. The measured peripheral doses can be used to evaluate the risk of second malignancy in the irradiated distant organs. In this study, a radiation dosimetry technique based on novel ^{6}LiF;Mg,Cu,P and ^{7}LiF:Mg,Cu,P glass-rod thermoluminescence dosimeters (TLDs) has been developed to carry out measurements of peripheral photon and neutron doses simultaneously in the Rando phantom irradiated to 80 Gy dose using 4-field 3D-CRT delivered by the 18 MV Varian iX linac.

II. Materials and Methods

A. ^{6}LiF:Mg,Cu,P and ^{7}LiF:Mg,Cu,P glass-rod TLDs and calibrations

General properties, of ^{6}LiF:Mg,Cu,P and ^{7}LiF:Mg,Cu,P glass-rod TLDs are described in Table 1. In these TLDs, the response to neutrons is enhanced by enrichment of ^{6}Li (high neutron cross-section) in ^{6}LiF:Mg,Cu,P or suppressed by using lithium consisting entirely of ^{7}Li (low neutron cross-section) in ^{7}LiF:Mg,Cu,P [2].

Calibrations of ^{7}LiF:Mg,Cu,P TLDs (35 in total) were performed using the 18 MV beam from the Varian iX linac. These TLDs were placed in a perspex phantom and covered with build-up plates to ensure that they were located at the depth of maximum dose. Source-to-Skin Distance (SSD) of 100 cm and a field size of 10 x 10 cm^2 were used in measurement. Radiation dose of 1 Gy was delivered to the TLDs.

O. Dössel and W.C. Schlegel (Eds.): WC 2009, IFMBE Proceedings 25/III, pp. 557–560, 2009.
www.springerlink.com

Table 1 General properties of ^{6}LiF:Mg,Cu,P and ^{7}LiF:Mg,Cu,P TLDs (Shanghai Renri Radiation Protection Equipment Co., Ltd.).

TLD	Dimension	Use	Capability
^{6}LiF: Mg,Cu,P	Φ 2.0 x 12 mm Glass-rod	Measures neutron and photon doses (^{6}Li has neutron cross-section of 9.42 x 10^{2} barns [3])	High sensitivity: up to 50 times higher than TLD-100 Repeatability: sensitivity decreases less than ±5% after 50 – 100 times Threshold: ≈200 nGy Linearity range: 0.01 mGy – 12 Gy Dispersity: ≤ 2.5% Photons Hp(10) energy response: ±20% between 15 keV – 1.25 MeV Neutrons Hp(10) energy response: ±50% between thermal – 20 MeV
^{7}LiF: Mg,Cu,P	Φ 2.0 x 12 mm Glass-rod	Measures photon dose only (^{7}Li has neutron cross-section of 8.6 x 10^{-2} barns [3])	

To determine the sensitivity of ^{7}LiF:Mg,Cu,P TLDs, four separate irradiations of 1 Gy dose were given. The average normalized readout of TLD# x for all four irradiations ($\overline{{}^{norm}_{x}R_{7LiF}}$) is given as:

$$\overline{{}^{norm}_{x}R_{7LiF}} = \frac{\sum_{I=1}^{4} {}^{norm}_{x}R^{I}_{7LiF}}{4}. \quad (1)$$

Then, a sensitivity correction factor (SCF) of TLD# x (SCF_x) was determined using the following formalism:

$$SCF_x = \overline{R_{7LiF}} \Big/ {}^{norm}_{x}R_{7LiF}. \quad (2)$$

where, $\overline{R_{7LiF}}$ is the average readout of all TLDs from all four irradiations.

This SCF represents the response of each ^{7}LiF:Mg,Cu,P TLD rod to photons relative to the whole batch of TLDs. This factor corrects for the variations in response of the TLDs to the same radiation dose as a result of variations in TLD powder contained within the glass rods.

In addition, the dose response linearity of ^{7}LiF:Mg,Cu,P TLDs was also determined. This was done by delivering radiation doses of up to 6 Gy to the TLD rods. The dependence of the TLD readout on delivered dose was plotted.

TLD reading temperature profile was modified to accommodate for glass encasing. Therefore, following temperature setups were used in this study: pre-heating at 135 ^{o}C for 45 seconds; and reading at 280 ^{o}C for 120 seconds, the heating rate being kept constant at 2 ^{o}C per second for both steps. Annealing of used TLDs was done in an oven at 240 ^{o}C for 10 minutes (as recommended by the manufacturer) which is sufficient to erase any residual signals from TLDs. This temperature treatment was applied to both ^{6}LiF:Mg,Cu,P and ^{7}LiF:Mg,Cu,P TLDs.

Calibrations of ^{6}LiF:Mg,Cu,P glass-rod TLDs were also done using 18 MV Varian iX linac which produces a mixed photon and neutron field at this energy. Hence, signals detected from these ^{6}LiF:Mg,Cu,P TLDs corresponded to both photons and neutrons. Identical setups as used for calibration of the ^{7}LiF:Mg,Cu,P TLDs were employed with the ^{6}LiF:Mg,Cu,P TLDs. Without the prior data about the actual neutrons sensitivity of the ^{6}LiF:Mg,Cu,P TLDs, the radiation dose of 2 Gy was given to the TLDs to enhance the neutron signals generated by the TLDs. Reading and annealing procedures of these TLDs were the same as those applied to the ^{7}LiF:Mg,Cu,P TLDs described previously. The same calculation procedures as ^{7}LiF:Mg,Cu,P TLDs for the sensitivity correction factor and reproducibility of ^{6}LiF:Mg,Cu,P TLDs were performed following three consecutive irradiations. In addition, the neutron measuring results obtained with AN/PDR-70 neutron survey meter and CR-39 etch-track neutron detector were used to cross-reference with TLDs corrected readouts to derive the readout-to-dose conversion factor for neutron irradiation.

Prior to the Rando phantom irradiation, eight TLD rods (4 each of ^{6}LiF:Mg,Cu,P and ^{7}LiF:Mg,Cu,P) were randomly selected. They were placed on a perspex plate and given a 2 Gy dose using 6 MV beam to be used as control TLDs providing a Batch Correction Factor (BCF) for each irradiation in subsequent measurements. Corrected readouts were calculated for these control TLDs. In addition, a ratio of average corrected readout of the ^{7}LiF:Mg,Cu,P TLDs ($^{corr}R^{\gamma}_{7LiF}$) to that of the ^{6}LiF:Mg,Cu,P TLDs ($^{corr}R^{\gamma}_{6LiF}$) following 6 MV beam irradiation (k) was calculated using equation (4) as shown below, the ratio representing the difference in response of ^{7}LiF:Mg,Cu,P TLDs to photons relative to ^{6}LiF:Mg,Cu,P TLDs [4]):

$$k = \overline{{}^{corr}R^{\gamma}_{7LiF}} \Big/ {}^{corr}R^{\gamma}_{6LiF}, \quad (3)$$

where, $\overline{{}^{corr}R^{\gamma}_{7LiF}}$ is the average corrected readout of ^{7}LiF:Mg,Cu,P TLDs exposed to 6 MV photon beam and $\overline{{}^{corr}R^{\gamma}_{6LiF}}$ is the average corrected readout of ^{6}LiF:Mg,Cu,P TLDs exposed to the same radiation beam.

Raw reading results were corrected for background, SCF, and BCF to obtain the corrected readouts. Photon dose

equivalent was derived from corrected readout of the ^{7}LiF:Mg,Cu,P TLDs ($^{corr}R^{\gamma}_{7LiF}$) using readout-to-dose conversion coefficient obtained from dose response linearity calibration.

For neutron doses, the background was subtracted from readouts obtained from non-irradiated ^{6}LiF:Mg,Cu,P TLDs ($R^{n+\gamma}_{6LiF}$) TLDs. The readouts were then corrected for SCF and BCF to obtain readouts corresponding to photon and neutron exposures. Finally, corrected readout of the ^{6}LiF:Mg,Cu,P TLDs corresponding to neutron exposure only ($^{corr}R^{n}_{6LiF}$) was obtained from the following equation:

$$^{corr}R^{n}_{6LiF} = \left[\left(R^{n+\gamma}_{6LiF} - B.G.\right) * SCF * BCF\right] - \left[\frac{^{corr}R^{\gamma}_{7LiF}}{k}\right]. \quad (4)$$

To obtain the neutron dose equivalent, $^{corr}R^{n}_{6LiF}(\mu C)$ calculated from equation (5) was converted to dose by cross-referencing to neutron dose rate (mSv/hr) measured with the neutron survey meter and the dose was calculated for the irradiation time. In case of the neutron survey meter, with 1,000 MU (300 MU/minute) delivered to the irradiation target, the neutron dose rate N (mrem/hour) detected at measuring location corresponds to neutron equivalent dose H_n as in the equation below:

$$H_n(mSv) = \left[\left(\frac{1{,}000\ (MU)}{300\ (MU/minute)}\right)/\ 60\right] * N\ (\frac{mrem}{hour}) * 0.01\ (\frac{mSv}{mrem}). \quad (5)$$

Assuming that $\overline{^{corr}R^{n}_{6LiF}}$ (in μC) is the average corrected readout of the ^{6}LiF:Mg,Cu,P TLDs as a result of irradiation to the same radiation field as the neutron survey meter. Therefore, the neutron equivalent dose (H_n, in mSv) of the neutron survey meter calculated from equation (5) is proportionally correlated to $\overline{^{corr}R^{n}_{6LiF}}$ making a readout-to-dose conversion factor (mSv/μC) for neutrons based on the AN/PDR-70 neutron survey meter.

Similarly, assuming that $\overline{^{corr}R^{n}_{6LiF}}$ (μC) is the average corrected readout of the ^{6}LiF:Mg,Cu,P TLDs as a result of irradiation to the same radiation field as the CR-39 etch-track detector. Correlation of the neutron equivalent dose (mSv) measured with the CR-39 etch-track detector to the $\overline{^{corr}R^{n}_{6LiF}}$ (μC) of ^{6}LiF:Mg,Cu,P TLDs also provides a neutron readout-to-dose conversion factor. Both AN/PDR-70 neutron survey meter and CR-39 etch-track detector were calibrated against known standard neutron sources.

B. Peripheral photon and neutron doses measurements and estimation of second malignancy

For lungs, TLD plugs were inserted in the Rando phantom at the designated positions according to the CT scan images of the phantom. A DVH of the lungs was constructed using volumetric data computed from Pinnacle^{3} treatment planning system and for other organs, their locations in the Rando phantom were approximated using data from published literature [5]. Organ peripheral photon and neutron doses were estimated from TLD measurements. After the TLDs were loaded, prostate irradiation was simulated in the Rando phantom by delivering 80 Gy radiation dose to the pelvic isocentre using 4-field 3D-CRT technique with the 18 MV Varian iX linac. The TLDs were then analyzed using Harshaw 3500 TLD Reader.

Estimations of second malignancy risk for each organ were performed using the competitive risk model as showing below [6]:

$$Total\ Effect = \left(\alpha_1 D + \frac{\beta_1 D^2}{n}\right) \times e^{-\left(\alpha_2 D + \frac{\beta_2 D^2}{n}\right)}. \quad (6)$$

The general model parameters as presented in [6] were used in risk estimations. The values of α_1, α_2, and α/β ratio for the lung are 0.017 Gy^{-1}, 0.25 Gy^{-1}, and 4.5 Gy, respectively. The values of α_1, α_2, and α/β ratio for other organs/tissues are 0.05 Gy^{-1}, 0.25 Gy^{-1}, and 5 Gy, respectively. The dose data obtained from the radiation dosimetry in the Rando phantom in combination with the approximated positions of organs/tissues in the phantom as described in [4] were applied to determine the photon, neutron, and total equivalent doses delivered to each organ/tissue as the results of the prostate irradiation using 4-field standard fractionated 3D-CRT technique with the 18 MV Varian iX linear accelerator for the total target dose of 80 Gy.

III. Results and Conclusions

It was observed that the neutron readout-to-dose conversion factor based on the AN/PDR-70 neutron survey meter differed from that based on the CR-39 etch-track detector. The CR-39 etch-track detector which is highly sensitive to fast neutrons provides a larger readout-to-dose conversion factor (49.4 mSv/μC) than that of AN/PDR-70 neutron survey meter (3.9 mSv/μC). Both of these values however, lie within the neutron dose ranges reported in the literature. As a result, an average value derived from these two factors was used in our analysis. Namely, a neutron readout-to-dose conversion factor of 26.7 mSv/μC (the average of above two factors) is used in conversion of the ^{6}LiF:Mg,Cu,P TLD corrected readout to a neutron dose in this study.

The distributions of photons and neutrons in the Rando phantom as a function of distance from the isocentre are shown in Figure 1 and 2, respectively. It was shown that outside the treatment field the photon doses decrease exponentially with distances whilst neutron doses were relatively constant.

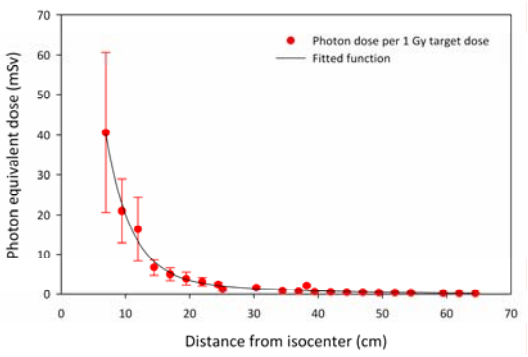

Fig. 1 Photon dose equivalent in the Rando phantom per 1 Gy target dose plotted against the distance (cm) from isocentre.

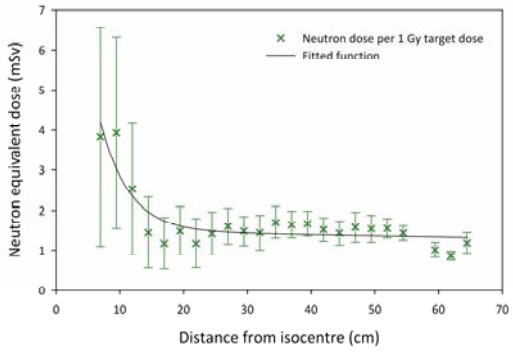

Fig. 2 Neutron dose equivalent in the Rando phantom per 1 Gy target dose plotted against the distance (cm) from isocentre.

The total dose equivalent in each organ corresponding to peripheral photon and neutron doses and associated risk of second malignancy are shown in Table 2. The dose was the results of exposure to both leakage radiations from the linac head and radiations which were scattered from the treatment volume in the patient. It was shown that the organs close to the PTV received larger dose equivalents than the organs locate further away from the PTV. In addition, it was found that the dose equivalents received by these distant organs were lower than 2 Gy allowing the use of linear no-threshold model to estimate the risk of second malignancy. Similar estimated risks of second malignancy were obtained from linear-quadratic and linear no-threshold models for most of the distant organs except those located close to the PTV.

Table 2 The total (photon + neutron) organ dose equivalent per 80 Gy target dose (H_{tot}^{80Gy}) and the risks of second malignancy of various organs.

Organ/tissue	Equivalent dose per 80 Gy prostate radiotherapy H_{tot}^{80Gy} ± S.D (mSv)	Risk of second malignancy (%) ± SD	
		Linear No-Threshold	Linear-quadratic
Thyroid	96.9 ± 18.4	0.5 ± 0.1	0.5 ± 0.1
Oesophagus	159.3 ± 38.1	0.8 ± 0.2	0.8 ± 0.2
Lungs	172.7 ± 34.0	0.3 ± 0.1	0.3 ± 0.1
Liver	254.4 ± 86.5	1.3 ± 0.4	1.2 ± 0.4
Spleen	215.2 ± 52.4	1.1 ± 0.3	1.0 ± 0.3
Stomach	258.5 ± 76.5	1.3 ± 0.4	1.2 ± 0.4
Kidney	286.9 ± 91.9	1.4 ± 0.5	1.3 ± 0.4
Pancreas	274.3 ± 56.2	1.4 ± 0.3	1.3 ± 0.3
Colon (and upper large intestine)	807.4 ± 870.2	4.1 ± 4.4	3.3 ± 3.5
Small intestine	667.6 ± 522.3	3.4 ± 2.6	2.8 ± 2.3

References

1. Takam R, Bezak E, Yeoh E et al. (2009) Risk of second primary cancer following prostate cancer radiotherapy: DVH analysis using the competitive risk model. Phys Med Biol Phys 54: 611 – 625
2. Obryk B, Bilski P, Budzanowski M et al. (2008) The response of different types of TL lithium fluoride detectors to high-energy mixed radiation fields. Radiat Meas 43: 1144 – 1148
3. Itoh M, Yamada Y, Kiriyama N et al. (1993) Neutron activation analysis of low level lithium in water samples. JRNC 172: 289 – 298
4. Harrison R, Wilkinson M, Shemilt A et al. (2006) Organ doses from prostate radiotherapy and associated concomitant exposures. BJR 79: 487 – 496.
5. Gregori B, Papadopulos S, Cruzate J et al. (2002) Multisphere neutron spectrometric system with thermoluminescence dosimeters: sensitive improvement. Radiat Prot Dosimetry 101: 133 – 136.
6. Dasu A, Toma-Dasu I, Olofsson J et al. (2005) The use of risk estimation models for the induction of secondary cancers following radiotherapy. Acta Oncol 44: 339 – 347

Corresponding author:
Author: Rungdham Takam
Institute: Medical Physics Department, Royal Adelaide Hospital
Street: North Terrace
City: Adelaide
Country: Australia

Email: Rungdham.Takam@health.sa.gov.au

Optimization of radiation protection in mammography in Lithuania

J.Ziliukas[1], R.Brediene[2] , E.Jonaitiene[3] V. Tsapaki [4],

[1] Radiation Protection Centre, Kalvariju 153, Vilnius, Lithuania
[2] Vilnius University Oncology Institute, Santariskiu 1, Vilnius, Lithuania
[3] Kaunas Medical University Hospital, Eiveniu 2, Kaunas, Lithuania
[4] Konstantopoulio Hospital, 3-5 Agias Olgas Str., Athens, Greece

Abstract—**Mammography is an effective and widely used method for breast diagnostics and early detection of breast cancer (screening). In order to obtain high quality mammograms at an acceptable breast dose, it is essential to use the correct equipment and perform regular quality control tests on mammography equipment. The aim of this work was to optimize radiation protection of patient and improve quality of mammography examinations by evaluating clinical image quality and measuring the entrance surface air-kerma for standard 4.5 cm breast thickness and the optical density of films herewith identifying problems and taking correction actions for optimization. The evaluation of mammography images of more than 180 patients was done according to selected image quality criteria and overall image quality assessment on a 5 point scale. The evaluation was performed in two hospitals. The results showed that up to 48% of cranio-caudal and 26% of medio-lateral oblique mammograms didn't fulfill all quality criteria, but only about 4 % of images were unacceptable or of suboptimal quality. The repeated (after corrective actions) image quality evaluation revealed the improvement of image quality up to 30%. The entrance surface air-kerma values were in range of 3.1-11.6 mGy and optical densities of films were in range of 1.11-1.86. The survey exhibited the potentiality to optimize radiation protection during mammography procedures by performing periodical image quality assessments and monitoring of doses.**

Keywords— **Entrance surface air-kerma; image quality; mammography; optimization.**

I. Introduction

The mammography examination is an effective and widely used method for breast diagnostics and early detection of breast cancer (screening). Mammography screening program in Lithuania has started three years ago. The diagnostic effectiveness of mammography screening is highly dependent on image quality and the lowest possible radiation dose to glandular tissue is mandatory. In order to obtain high quality mammograms at an acceptable breast dose, it is essential to use the correct equipment and perform regular quality control tests on mammography systems. According to the national legal basis, mammography departments should implement quality control programs that cover kV accuracy, kV and dose reproducibility, filtration, automatic exposure control, compression, technical image quality (spatial resolution and contrast), film processing and other checks and measurements. This program does not include clinical image quality evaluation and entrance surface air kerma (ESAK) measurements or average glandular dose calculations. The number of mammography systems increased from 21 machines at the end of 2005, to 30 systems at the end of 2008. It should be noted that of these 30 machines, only 18 are used for screening.

The aim of this work was to reveal the possibilities of optimizing radiation protection of patient and improving quality of mammography examinations by evaluating the clinical image quality and measuring the ESAK for standard 4.5 cm breast thickness and the optical density of films, trying to ascertain main problems and to take correction actions. The measurements of optical densities and ESAK were done and compared in more hospitals of Lithuania at the same time but not participated in this survey. This work was done under the International Atomic Energy Agency (IAEA) regional technical cooperation project RER/9/093 "Strengthening Radiological Protection of Patients and Medical Exposure Control", task 4 on "Survey of mammography practice from the optimization of radiation

O. Dössel and W.C. Schlegel (Eds.): WC 2009, IFMBE Proceedings 25/III, pp. 561–563, 2009.
www.springerlink.com

protection viewpoint and optimization in mammography".

II. Method

The X-ray departments of Kaunas Medical University Hospital and Vilnius University Oncology Institute were selected for the survey. These hospitals perform the largest part of diagnostic and screening mammography examinations in Lithuania and provide education and training of radiologists and radiographers. The quality control, ESAK and optical density measurements were performed by Radiation Protection Centre which is a regulatory authority institution and is accredited according to ISO 17025 standards [1].

The first phase of the survey was image quality evaluation, data collection and evaluation, arrangement of corrective actions and repeated image quality evaluation. It was done according to prepared forms by performing peer review of the quality of medio-lateral oblique (MLO) and cranio-caudal (CC) mammograms, following selected image criteria and evaluating clinical image quality. The grading was done by the radiologist on a 5 point scale: unacceptable, suboptimal, acceptable, high quality and too little noise, too high quality. The image quality criteria applied were taken from a list of image criteria suggested by IAEA [2]. The MLO mammograms were evaluated according to the following criteria: over/under exposure, artifacts, visually not sharp skin structure, visually not sharp all vessels and fibrous strands and pectoral muscle margin and visually not sharp cranial-lateral glandular tissue. The CC mammograms were evaluated according to criteria: over/under exposure, artifacts, breast misplacement, visually not sharp skin structure along the pectoral muscle, visually not sharp vascular structures seen through the most densest parenchyma, visually not sharp medial breast tissue and visually not sharp all vessels and fibrous strands and pectoral muscle margin. The evaluation was performed in all mammograms done in one week.

The second phase was the quality control testing of mammography unit, measuring ESAK and optical density for compressed breast thickness of 4.5 cm, taking correction actions if necessary and comparing results between the hospitals. For quality control test and ESAK measurements, the set of Barracuda Cabinet and a PMMA phantom of 4.5 cm thickness were used. The multipurpose detector MPD of Barracuda Cabinet was calibrated in terms of air kerma for Mo/Mo and Mo/Rh beam qualities.

The ESAK was measured as followed: The cassette with film was placed into cassette holder. The PMMA phantom of 4.5 cm thickness was placed on the breast support table, the compression paddle was put in position and the phantom was exposed using the automatic exposure control (AEC) system. The kV, mAs and filter target combination readings after exposure were putted down into protocol and the film was developed. The PMMA phantom was removed, the MPD detector was placed at the level of PMMA phantom surface, i.e. 4.5 cm above the breast support, 4 cm from the chest wall edge and centered with respect to the lateral direction on the breast support table. The mammography unit was switched to manual mode and exposure parameters were set as in previous exposure. mAs setting was selected to be as close as possible to the value of previous exposure. After the exposure and reading out the air kerma value, the right ESAK was recalculated taking into account the real mAs indicated by AEC system.

The optical density of the exposed and developed film was measured at the 4 cm from the chest wall edge and at the center, with a PTW DensiX densitometer.

III. Results

The results were obtained after analysis of mammography films performed in two X-ray departments with two (room 1 and room 2) and one mammography room (room 3) respectively, during a one week period. The total number of evaluated images of CC projection was 78, 198 and 143 in the three different mammography rooms. The same numbers of MLO projection images were evaluated.

The CC projection mammograms with image quality not fulfilling all selected image criteria were 48 % of all in room 1, 9 % in room 2 and 33 % in room 3. For MLO projection corresponding values were 26 %, 8% and 24 %, respectively. In Table I, the results of image quality evaluation in the three mammography rooms are presented.

Table 1 Results of image quality evaluation in three mammography rooms

Image criteria	Cases of poor images in %		
CC -projection	1-room	2-room	3-room
Over & under exposure	7.7	1	21.1
Artifacts	20.5	4.5	2.7
Breast misplacement	3.8	2.5	6
Visually not sharp skin structure along the pectoral muscle	8.9	1	
Visually not sharp vascular structures	7.7		1.4
Visually not sharp medial breast tissue			
Visually not sharp all vessels and fibrous stands and pectoral muscle margin			10.8
Totally from all evaluated films	48	9	33.1
MLO -projection	1-room	2-room	3-room

Over & under exposure	5.1	1.5	10.1
Artifacts	17.8	5	3.4
Visually not sharp skin structure	2.5	1	
Visually not sharp all vessels and fibrous stands and pectoral muscle margin			10.1
Visually not sharp cranial-lateral glandular tissue			
Totally from all evaluated films	25.6	7.5	23.6

The most frequent problem of poor images in the 2 rooms X-ray department was the existence of artifacts on the images in both projections. This was found in 42% of CC images and 70% of MLO images performed in room 1 and 50% and 67% respectively in room 2. The most frequent problems in both projections in room 3 were over/under exposure and visually not sharp all vessels, fibrous stands and pectoral muscle margin.

Then, the overall image quality evaluation of each image was performed by the radiologist, using a 5 point scale grading. The images of 99 patients in rooms 1 and 2 and 74 patients in room 3 were evaluated. The radiologist evaluating images in rooms 1 and 2 did not find any unacceptable or suboptimal images. On the other hand, unacceptable or suboptimal images of 4 %, were found in room 3. The main identified problems were because of film processing, artifacts and wrong positioning of mammograms.

After taking corrective actions, the repeated evaluation of image quality showed that only 4-5 % of images had problems with poor image quality criteria and about 99 % were assessed as high quality images. Totally 572 mammography images of both projections were evaluated. The image quality survey and corrective actions actually helped to improve image quality for approximately 30 % of images performed in both X-ray departments.

The quality control of mammography units and film processing was performed. Some problems with compression devices and stability of film processing were found. The troubles were corrected immediately. The other parameters of all the three mammography units complied with national requirements. The measured ESAK values in rooms 1 and 2 were 8.9 and 4.7 mGy and optical densities 1.15 and 1.2 respectively. Mo/Mo anode-filter combination and 27-28 kV were used in both mammography systems. The reason for the different doses apparently relies on differences in film screen combinations (cassettes Min-R *Kodak* 1997 and Fuji UM-MA 2004 and films *CEA* MA New). The measured ESAK room 3 was 5.7 mGy and optical density 1.7 using an anode-filter combination of Mo/Mo and 24 kV (cassettes Cawo Mammo R200 and films *Konica Minolta* CM-H were used).

The ESAKs need for getting image of phantom the same thickness in different hospitals vary in range of 3.1 – 11.6 mGy. The optical densities vary in range of 1.11 – 1.86 OD units. According to recommendations of European Commission [3] optical density in the range of 1.4-1.9 is recommended. The differences of doses and optical densities are comparably big. It should be optimized, taking to account the image quality.

IV. CONCLUSIONS

The survey of clinical image quality in mammography showed that up to 48 % of images CC projection and up 26% of images MLO projection did not comply with selected image quality criteria. After corrective actions repeated assessment of image quality showed that image quality was improved approximately up to 30 %. The survey exhibited the potentiality to optimize radiation protection during mammography procedures by performing periodical image quality assessments and monitoring of doses.

The ESAK and OD measurements showed that differences between hospitals are big and should be optimized taking into account quality of images.

ACKNOWLEDGMENT

We acknowledge the help of the staff of Lithuanian hospitals that participated in the survey in measuring patient doses and collecting data. We also acknowledge the help of International Atomic Energy Agency in calibrating measurement equipment, providing the methodologies and consultations of experts.

REFERENCES

1. ISO/IEC 17025:2005 General requirements for the competence of testing and calibration laboratories
2. Optimization of the radiological protection of patients: Image quality and dose in mammography (coordinated research in Europe) (2005), IAEA-TECDOC-1447, IAEA, Austria.
3. European Guidelines for Quality Assurance in Breast Cancer Screening and Diagnosis, Fourth Edition (2006), European Commission, Belgium

Patient Dose and Image Quality Evaluation in Common Radiographic Examinations in Sudan

N. A. Ahmed[1], I.I. Suliman[1], V.Tsapaki[2], M.M. Rehani[3]

[1] Sudan Atomic Energy Commission/Radiation Safety Institute, Khartoum, Sudan
[2] Konstantopoulio Hospital, Athens, Greece
[3] International Atomic Energy Agency, Vienna, Austria

Abstract- **Image quality and radiation dose were evaluated in 8radiography rooms in 5 several hospitals in Sudan as part of an International Atomic Energy Agency (IAEA) project RAF/9/033. Entrance Skin Air Kerma (ESAK) was measured in 452 patients in five Sudanese hospitals. The six most common X-ray examinations were selected: Chest posterior-anterior (PA), abdomen, lumbar spine anterior-posterior (AP), lumbar spine lateral (LAT), pelvis AP and skull. Exposure factors such as kVp, mAs and focal to skin distance (FSD) were recorded. Output measurements were conducted under standardized protocols prepared by IAEA experts and they were used together with corresponding technical data to calculate each patient ESAK. Patient effective doses (E) were also obtained from ESAK values. Reject analysis was conducted in 959 films in 8 X-ray rooms for 12 days. Corrective actions were applied and a second analysis was again performed in 1803 films. The results of the ESAKs revealed large variations not only between hospitals but also within the same hospital. The kVp settings applied in chest exams were almost half than kVp recommended by EC guidelines. ESAKs are within IAEA GL for all types of examinations except for chest. The reject analysis showed a repeat rate range of 4.5-24.27% at the radiographer level. The accepted films ranged between 51.4-90.4%. Corrective actions were taken. The reject analysis after these actions showed a reduction % of repeat in the range of 2.6-19.3% at the radiographer level. The accepted films ranged between 70.4-94.4%. Significant improvement in image quality was observed. The measurement of patient doses is continued in more hospitals in Khartoum, the capital of Sudan and other states in order to establish national dose reference levels.**

Keywords— Entrance skin dose, Effective dose, reject analysis

I. Introduction

One of the most important problems regarding radiation protection in X-ray diagnostic radiology is the unnecessary radiation dose to patients. The use of ionizing radiation and the associated health hazards dictate the justification, optimization and respect of rules as recommended by Basic Safety Standards (BSS) [1]. The basic principle when optimization is attempted is the reduction of patient dose to minimum possible while still obtaining all the necessary diagnostic information (ALARA principal). Furthermore, retake analysis and image quality grading are good indicators of practice and should be considered together with patient dose. The estimation of Entrance Skin Air kerma (ESAK) is currently recommended for patient dose assessment and for comparing patient dose levels with diagnostic reference levels in general radiography [2].

In Sudan, the Radiation Safety Institute of the Sudanese Atomic Energy Commission controls the use of X-ray equipment. In a recent routine testing of X-ray systems, it was found that rectification actions are rarely done due to a number of reasons: a) unqualified engineers, b) carelessness about corrective actions which is enhanced by the non enforcement of actions and finally c) lack of financial resources for maintenance. Furthermore, image quality assessment or evaluation is rarely done in X-ray departments. Taking into account all these factors, a study was performed under the International Atomic Energy Agency (IAEA) project RAF/9/033. As part of this study, image quality and radiation dose received by patients for common radiographic examinations were evaluated in several hospitals in Sudan and optimization was attempted. The initial results of this survey are presented here.

II. Materials and Methods

Output measurements were conducted under standardized protocols prepared by IAEA experts. They were used together with corresponding technical data to calculate each patient ESAK. ESAKs were estimated in 452 patients in five Sudanese hospitals, three of which were public hospitals and two were private clinics. The measurements were performed in six most common X-ray examinations, namely: Chest posterior-anterior (PA), abdomen, lumbar spine anterior-posterior (AP), lumbar spine lateral (LAT), pelvis AP and skull. Exposure factors such as kVp, mAs and focal to skin distance (FSD) were recorded. Mean ESAK values were compared with guidance levels (GL) recommended by IAEA [1]. Patient effective doses (E) were also obtained

O. Dössel and W.C. Schlegel (Eds.): WC 2009, IFMBE Proceedings 25/III, pp. 564–566, 2009.
www.springerlink.com

from ESAK values using special computer program [3]. Reject analysis and image quality grading was conducted in the three most occupied hospitals in Sudan. Initially, a total number of 959 films in eight X-ray rooms were evaluated for a period of 12 days. The repeat causes were evaluated by radiographers at first level. At second level radiologist observed all X-ray films and assigned an A, B or C grade to each of the films (A: clearly accepted without any remark, B: accepted with some remarks and C: rejected). For B & C grade films, reasons were assigned (under/over exposed, artefact, field size misplacement, processing problem). Corrective actions were applied for B and C grade films. A second analysis was then done once again by analyzing a total number of 1803 films for the same period of 12 days to reevaluate image quality after corrective actions.

III. RESULTS

Initial results revealed variations not only between the hospitals but also within the same hospital, as shown in Table 1.

Table 1. Mean values of kVp, mAs, FSD and weight (W) in all rooms (R) of 5 hospitals (H). The recommended kVp by European Commission (EC) guidelines are also shown.

	H 1	Hospital 2			Hospital 3		H 4	H 5	EC
		R 1	R 2	R 3	R 1	R 2			
		Chest PA							
W	59	55	72	62	67	55	54	64	
kVp	65	63	70	76	68	70	61	66	125
mAs	12	12	12	30	15	19	12	13	
FSD	157	178	176	106	87	135	210	142	
		Lumbar Spine PA							
W	74	70	72	59	82	68	60	67	
kVp	71	74	78	85	74	89	80	71	75-90
mAs	42	33	36	45	37	41	24	29	
FSD	106	122	125	121	96	109	121	122	
		Lumbar Spine LAT							
W	69	71	83	55	79	68	53	68	
kVp	81	82	84	91	81	89	88	86	80-95
mAs	54	41	42	46	56	97	24	43	
FSD	108	143	136	142	97	107	131	126	
		Abdomen						--	
W	69	61	58	62	57	62	61	--	
kVp	72	71	70	71	60	74	81	--	75-90
mAs	49	29	23	31	86	85	22	--	
FSD	135	121	124	129	106	105	120	--	
		Pelvis						--	
W	57	64	59	62	63	64	60	67	
kVp	67	71	69	80	68	75	81	72	75-90
mAs	28	30	23	26	38	41	23	22	
FSD	125	123	123	130	112	102	121	108	
		SKULL							
W	53	57	67	51	66	69	52	63	
kVp	64	68	70	65	72	76	73	64	70-85
mAs	27	36	25	16	34	40	16	14	
FSD	133	139	117	120	117	106	119	93	

Table 2 shows mean ESAK values as well as guidance levels (GL) proposed by IAEA. The results are within IAEA GL for all types of examinations except for chest radiography probably due to much lower kVp values (highlighted values).

Table 2.Mean ESAK values as well as Guidance Levels (GL) proposed by IAEA are shown here. R=Room, H=Hospital

Exam	R	H 1	H 2	H 3	H 4	H 5	IAEA
Chest AP	R 1	0.19	0.14	0.27	0.21	**0.57**	0.4
	R 2		0.22	**0.72**			
	R 3		0.3				
L/S AP	R 1	2.8	1.17	0.45	1.67	2.21	10
	R 2		1.6	3.76			
	R 3		2.12				
L/S LAT	R 1	5.4	2.31	2.57	2.38	5.14	30
	R 2		2.01	11.5			
	R 3		2.04				
Abdomen	R 1	2.1	0.95	1.92	1.64		10
	R 2		0.8	5.41			
	R 3		0.81				
Pelvis	R 1	0.78	4.24	1.28	1.72	2.27	10
	R 2		0.82	2.73			
	R 3		1.32				
Skull	R 1	0.59	1.8	5.12	0.84	0.99	5
	R 2		1.12	3.26			
	R 3		0.32				

Table 3. This table presents the results of E in participating hospitals. The last row shows typical values of effective dose (Et) [5].

	R	Chest	L/S AP	L/S LAT	Abdomen	Skull	Pelvis
H 1	1	0.017	0.269	0.008	0.24	0.005	0.108
H 2	1	0.013	0.132	0.044	0.121	0.018	0.672
	2	**0.023**	0.185	0.038	0.098	0.012	0.125
	3	**0.031**	0.243	0.044	0.098	0.003	0.209
H 3	1	**0.028**	0.051	0.049	0.206	0.056	0.197
	2	**0.067**	0.445	0.209	0.627	0.033	0.407
H 4	1	**0.046**	0.18	0.043	0.211	0.008	0.274
Et [5]		0.02	1.3	1.3	1.0	0.07	1.0

Table 3 presents the results of E in participating hospitals. The last row shows typical values of effective dose (Et) as given in the referral criteria [5]. Except chest exam, all other types of examination are lower than typical E values (highlighted values).

The reject analysis showed a repeat rate range of 4.5-24.27% at the radiographer level. The A grade films ranged between 51.4-90.4%. The main causes of B and C grade films were over/under exposure, wrong positioning and processing problems. Corrective actions were taken. The reject analysis after these actions showed a % of repeat in the range of 2.6-19.3% at the radiographer level. The A grade films ranged between 70.4-94.4% thus indicating improvement in image quality.

IV. DISCUSSSION

The results show that kVp adjustment is necessary for effective dose optimization in chest examination (both in terms of ESAK and E). The reject analysis showed that simple corrective actions at the level of radiographer (choice of exposure parameters, wrong positioning and processing problems) can have a great impact in improving image quality. It is encouraging that Sudan, a developing country, follows international recommendations (except chest exam). However, the sizeable differences between rooms show that more efforts should be done for better standardization of techniques. The measurement of patient doses is continued in more hospitals in Khartoum, the capital of Sudan and other states in order to establish national dose reference levels.

V. CONCLUSIONS

The results of this study showed that significant image quality improvement can be achieved with simple steps and ESAK values are within the guidance levels except for chest examination. Courses on radiation protection are planned in the near future and are going to be conducted by the Ministry of Health in collaboration with the radiation safety institutes. They will be targeted to the medical and paramedical staff and hopefully they will play a great role in increasing awareness to the staff.

ACKNOWLEDGMENT

The work was supported by the IAEA through the TC project number RAF/9/033 “Strengthening on Radiation Protection of patients and Medical Exposure Control”. The authors are grateful to the IAEA and to the staff of the hospitals and Radiation Safety Institute of Sudan Atomic Energy Commission (Esra, Andera, Zahra, Rasha, Lubna, Omima, Etidal, gazaly, Nahla, mohammed, Hiba and Ali) for their help and assistance.

REFERENCES

1. IAEA/PAHO/WHO/FAO/ILO/OECD-NEA. International Basic Safety Standards for protection against ionizing radiation and for the safety of radiation sources, IAEA Safety Series No. 115, Vienna (1996).
2. International Atomic Energy Agency. Dosimetry in diagnostic radiology: an international code of practice. Technical reports series no. 457 (Vienna: IAEA) (2007).
3. Hart D, Jones DG, Wall BF. Estimation of effective dose in diagnostic radiology from entrance surface dose and dose–area product measurements, NRPB Report 262. London: HMSO (1994).
4. Referral Criteria for Imaging. Radiation Protection 118. Luxembourg, 2000.[Please quote proper reference]

Author: Nada Abbas Ahmed
Institute: Sudan Atomic Energy Commission
Street: Aljamaa street,
City: Khartoum
Country: Sudan
Email: nadaabbasa@ogmail.com

Spectra Determination for a Cone Beam Computed Tomography System through the Employment of a CdTe Detector

B. Spyropoulos[1], G. Manousaridis[2,1], M. Varvatos[1], and K. Tsiklakis[3]

[1] Technological Educational Institute (TEI) of Athens, Medical Instrumentation Technology Department, Athens, Greece
[2] Greek Atomic Energy Commission (GAEC), Athens, Greece, [3] University of Athens, School of Dentistry, Athens, Greece

Abstract— **Individual Energy spectra determination in and around a Newtom 9000 (QR Verona) Cone Beam Computed Tomography (CBCT) system may contribute significantly to the improvement of routine patient dose monitoring. The purpose of this study was to investigate the Energy spectrum and the scattered radiation Intensity distribution of a CBCT system, through the employment of a CdTe detector.**

Keywords— **CdTe-detector, Cone Beam Computed Tomography (CBCT) Energy Spectrum.**

I. Introduction

Cone Beam Computed Tomography (CBCT) scanners have been available for craniofacial imaging since 1999 in Europe and since 2001 in the United States. The scanner uses a cone shaped x-ray beam rather than a conventional linear fan beam to provide images of the bony structures of the skull. Presently employed Cone Beam CT scanners use different detection systems to capture the cone shaped beam, resulting in a rather big volume of data. Subsequently reconstruction software is applied on the cone beam CT volumetric data to produce a stack of 2D gray scale level images of the anatomy. The compactness of the Cone Beam CT scanner makes it ideally suited for imaging the craniofacial region, including dental structures. With the increasing accessibility of Cone Beam CT imaging, this modality is emerging as the imaging "standard of care" for the number of diagnostic assessments of the bony components of the face.

In craniofacial imaging, applications have been identified by many medical specialties and there are multiple indications for the use of CBCT in maxillofacial imaging, such as assessment of the facial bones for infection, trauma, congenital and developmental deformities, assessment of residual bone for implant placement localization and identification of important anatomic structures, Temporomandibular Joint pathology, and finally evaluation of sinus disease and airway space analysis.

Although the delivered dose is significantly lower than standard medical CT [1], daily use of imaging procedures, such as cone-beam computed tomography (CBCT) may significantly increase the collective dose.

Individual Energy spectra determination in and around every Cone Beam Computed Tomography system, may contribute significantly to the improvement of shielding parameters.

It may also provide a means for determination of off-beam, non-invasive measurement of tube kVp even in clinical conditions.

Therefore it is the purpose of this study to investigate the Energy spectrum of a Cone Beam Computed Tomography system through the employment of a CdTe detector.

II. Instrumentation

Cadmium telluride (CdTe) detectors belong to a new "family" of semiconductor crystals employed in photon spectroscopy (as GaAs and HgI2) [2]. These detectors are constituted of elements with high atomic number (Cd: 48 and Te: 52), when compared to Germanium (Ge: 32) and Silicon (Si: 14), allowing for a good efficiency for energies of tens of keV with relatively small crystals (a few cubic millimeters). Many surveys have been published about these detectors [5-11]. As a cryogenic cooling system is not necessary to their operation, the experimental apparatus becomes simpler, allowing measurements out of the laboratory, e.g., under clinical conditions [12]. The main drawbacks of these new detectors are the incomplete collection of charge together with the relatively high probability of escape of fluorescence x-rays, due to the small dimensions.

With the advent of new crystal growth techniques and the improvement of electronic signal processing, the resolution these detectors have become closer to the germanium detectors. For the energy of 122 keV (^{57}Co), FWHM of 1.3 keV [7] and 0.9 keV [13] are obtained for CdZnTe and Ge, respectively. The use of Peltier cooler [4] and rise time discrimination circuit (RTD), and the incorporation of electronic processing for reduction of leakage current and noise were also important refinements to this detection system.

The hermetic package of the detector has a light tight, vacuum tight 4 mil (100 μm) Beryllium window. All the critical connections between the detector and the preamplifier have been made internally to the XR-100T-CdTe and it is provided complete with BNC connectors and power

O. Dössel and W.C. Schlegel (Eds.): WC 2009, IFMBE Proceedings 25/III, pp. 567–570, 2009.
www.springerlink.com

cable. The XR-100T-CdTe is capable of detecting energies from a few keV to several hundreds of keV.

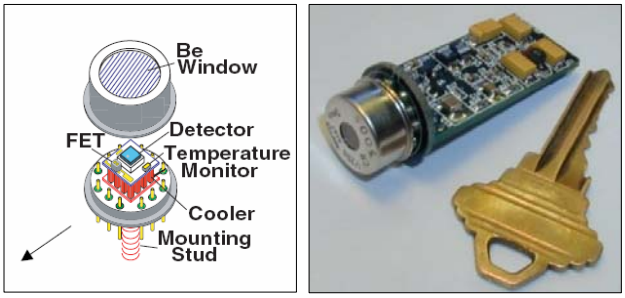

Fig. 1 Structure and size of the employed XR-100T-CdTe system [6].

X-rays & gamma rays interact with CdTe atoms to create an average of one electron/hole pair for every 4.43 eV of energy lost in the CdTe. Depending on the energy of the incoming radiation, this energy loss is dominated by either the photoelectric effect or Compton scattering.

The probability or efficiency of the detector to "stop" the incoming radiation and create electron/hole pairs increases with the thickness of CdTe. In order to facilitate the electron/hole collection process in the CdTe detector, a 400 volt potential is applied. This voltage is too high for operation at room temperature, as it will cause excessive leakage, and eventually a breakdown. Since the detector in the XR-100T-CdTe is cooled, the leakage current is reduced considerably, thus permitting the high bias voltage.

Electron/hole pairs created by radiation, which interact with the CdTe near the back contact of the detector, result in fluctuations of charge collection times. These fluctuations are observed as rise time variations of the voltage step at the output of the charge sensitive preamplifier. As a result, the acquired spectra suffer from increased background counts and degraded energy resolution.

To reduce these effects, a Rise Time Discrimination (RTD) circuit has been developed for the PX2T amplifier. When the RTD is active, the shaped pulses are internally gated and only pulses corresponding to "full charge collection" events are allowed to be sent to the Multi-channel Analyzer (MCA) for analysis.

III. METHODS

If we consider an ideal, noiseless detector system, then all pulses from the full-energy absorption of gamma rays of a given energy will appear in one channel of a spectrum, rather than as a broadened distribution. Energy degrading effects, such as small-angle Compton scattering and incomplete charge collection, inevitably produce pulses of lower energy. The result is a discontinuity or step in the background continuum at the peak. This ideal peak shape cannot be realized because several sources of energy dispersion are always present in gamma- and X-ray detector systems. The principal sources are electronic noise, statistical processes in the detector associated with the conversion of gamma-ray energy into electron-hole pairs, and various charge-loss processes in the detector. They largely determine the shape of the peak observed and of the underlying background.

We have developed a simple Method to determine, under clinical conditions, the diagnostic Dental X-ray equipment emitted spectra, by employing a high-resolution Schottky CdTe detector, in order to accurately determine the High Voltage actually applied on the X-ray tube. The Molybdenum 17.5 keV and 19.6 keV characteristic spectral lines from a Mammography System and the ^{241}Am isotope 59.5 keV line have been employed for the Energy Calibration of the system. Dental X-ray equipment of various types and manufacturers has already been tested with the developed method [14], and in this paper are presented the results of the employment of the method in a CBCT system.

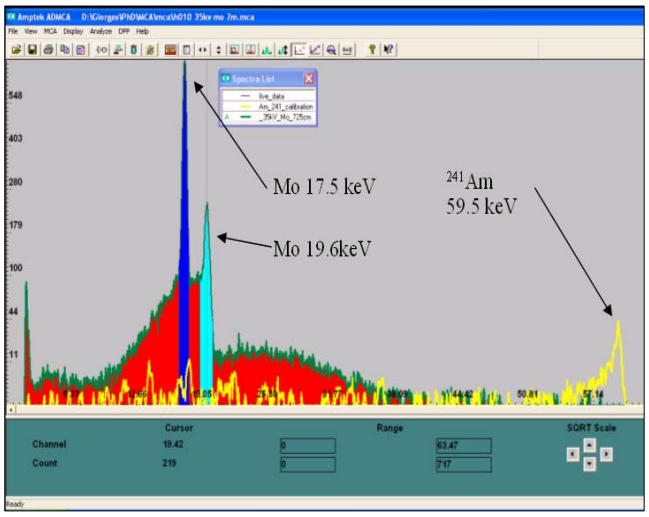

Fig. 2 Energy Calibration of the system

Fig. 3 The CBCT experimental set-up.

The "full-energy" peaks in a spectrum are also superimposed on a "background" continuum. This continuum is primarily due to Compton scattering of higher energy gamma rays, to Bremsstrahlung radiation, and to room background. To obtain the "net" channel counts in a region of interest, a channel-by-channel subtraction process is usually used to remove the background. The net-count intensity is then analyzed to yield peak positions and areas by a simple or more accurate, but complex, peak fitting process. However, for the purposes of our project, an adequate approach was to employ the voltage-equivalent energy at which the high-energy end of the spectrum, assumed to be linear and approximated by a straight line for the last few keV, intersects the background, and define it as the end-point energy.

IV. RESULTS

The Newtom 9000 (QR Verona) Cone Beam Computed Tomography system of the Dental School of the University of Athens was laboratory-tested with the developed method, and spectra from the same X-ray unit were taken repeatedly to check the influence of counting statistics. The accuracy of the calibration was examined by altering the above mentioned reference X- and Gamma spectral-lines considered and verifying the final Energy Spectrum variation.

The cut-off channel-defined Energy confirmed the nominal kVp value, within the two Standard Deviation (±2 SD) intervals. Since the aim of the developed method is the determination of the emitted spectra under clinical conditions, it is important to study the angular dependence of scattered radiation, both, its intensity (counts) and its energy (keV), because it will not always be possible, to perform the measurement, under optimal geometry.

Therefore, additional measurements have been carried out for angles of 15 °, 30° 45 °, and 60 °, beyond the typical 0° alignment. Further, the angular dependence of the intensity (counts) of the scattered radiation has been measured at a distance of 1m from the scatter phantom in order to attain comparable quantitative measurements.

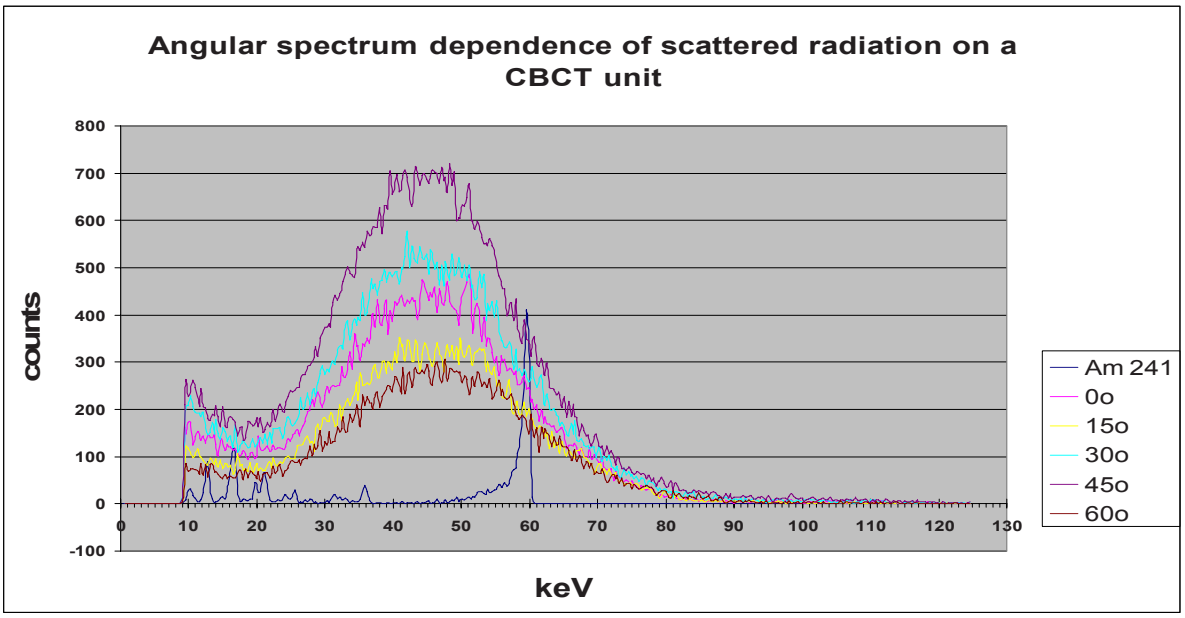

Fig. 4 The angular dependence of the scattered radiation on a CBCT unit.

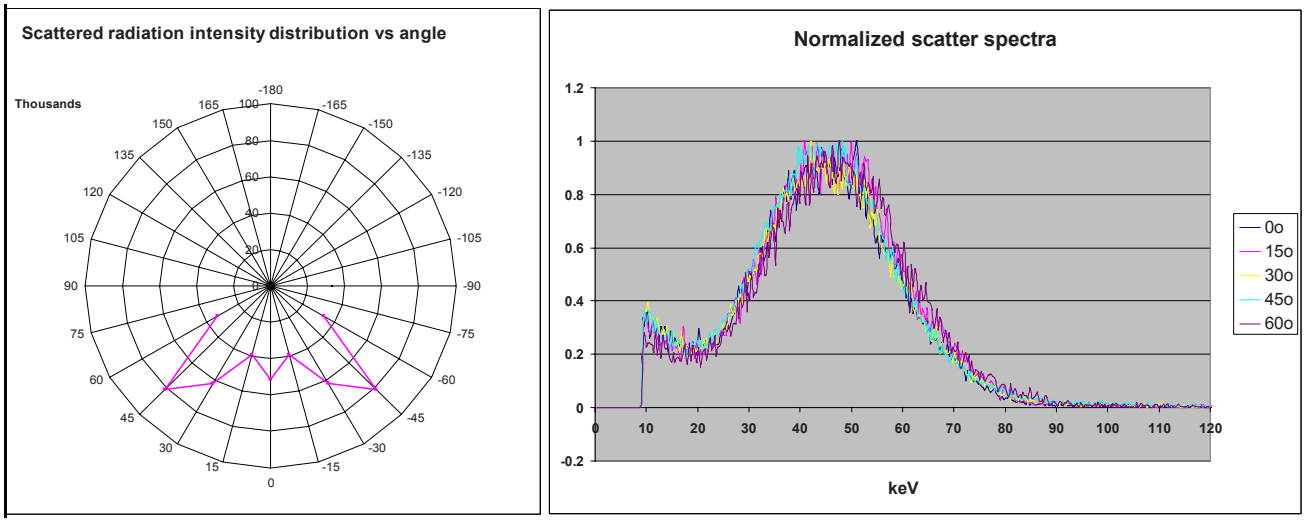

Fig. 5. Angular dependence of the CBCT scattered radiation Intensity (L) and the normalized scatter spectra for angles of 0^{o} to 60^{o} from rotation axis(R).

V. Conclusions

The method offers a fast, accurate and convenient way to inspect the CBCT spectra. The employment of the Molybdenum 17.5 keV and 19.6 keV characteristic spectral lines from a Mammography System and the Isotope ^{241}Am 59.5 keV line, allow for superimposing the measured spectra with the reference spectra. These spectra have been acquired under the same conditions, however, in laboratory environment, and have been stored in a spectra database. Still ongoing measurements lead to the conclusion that the method can be extended to provide for spectral information also about traditional CT, PET-CT and SPECT-CT.

Acknowledgment

We would like to express our appreciation for their valuable feedback and cooperation to the staff of the Oral Diagnosis and Radiology Clinic the Dental School of the University of Athens, Athens, Greece.

References

1. Ludlow J.B. and Ivanovic M, (2008) Comparative dosimetry of dental CBCT devices and 64-slice CT, Surg Oral Med Oral Pathol Oral Radiol Endod 2008; July 2008, Volume 106, Issue 1,930-938.
2. AAPM Report 4, 1977. Basic Quality Control in Diagnostic Radiology.
3. AAPM Report 74, 2002. Quality Control in Diagnostic Radiology, Diagnostic X-ray Imaging Committee Task Group #12.
4. Guidelines on Radiation Protection in dental Radiology (Directorate-General for Energy and Transport, Directorate H, Nuclear Safety and Safeguards, Unit H.4, Radiation Protection, Radiation Protection Issue N° 136/2004).
5. Anderson D W, Moore, G J, Lester, P D (1986) Absolute kVp calibration using characteristic X-ray yields. Med. Phys. 13, 663–666.
6. http://www.amptek.com/medical.html.
7. Deslattes R D, Levin, J C, Walker M D, Henins A (1994) Noninvasive high-voltage measurement in mammography by crystal diffraction spectrometry. Med. Phys. 21: 123–126.
8. Matsumoto M, Yamamoto A, Honda I, Taniguchi A, Kanamori H (2000) Direct measurement of mammographic X-ray spectra using a CdZnTe detector. Med. Phys. 27: 1490–1502.
9. Gunnink R, Arlt R (2001) Methods for evaluating and analyzing CdTe and CdZnTe spectra, Nuclear Instruments and Methods in Physics Research A 458: 196-205.
10. Miyajima S (2003) Thin CdTe detector in diagnostic X-ray spectroscopy, Med. Phys. 30: 771–777.
11. Krmar M, Shukla S, Ganezer K (2006) Some aspects involving the use of CdTe for finding end-point energies in Diagnostic Radiology, Applied Radiation and Isotopes, 64: 584–587.
12. Aoki K, Koyama M, (1989) Measurement of diagnostic X-ray spectra using a silicon photodiode. Med. Phys. 16: 529–536.
13. Kunzel R, Herdade S B, Terini R A, Costa P R (2004) X-ray spectroscopy in mammography with a silicon PIN photodiode with application to the measurement of tube voltage. Med. Phys. 31: 2996–3003.
14. Spyropoulos B, Manousaridis G, Papathymiou A, A high-resolution Schottky CdTe detector based spectrometric determination method of the kilovoltage applied to dental X-ray tubes, IFMB Proceedings, Springer, 2008, Vol. 22, pp.1479-1483.

Author: Professor Basile Spyropoulos.
Institute: Technological Educational Institute of Athens, Medical Instrumentation Technology Department
Street: TEI Athens, Agiou Spyridonos & Dimitsanas, Egaleo.
City: 12210 Athens
Country: Greece.
Email: basile@teiath.gr.

INFORMED CONSENT: COMMUNICATING RADIATION RISK

S. Balter[1], D. Brenner[1] , R. Balter[2]

[1]Columbia University Medical Center, New York City, USA
[2]John Jay College of Criminal Justice, New York City, USA

Abstract— **The benefits and risks of any medical procedure must be understood by patients or research volunteers so that they can make personally appropriate decisions. The method of communicating this information is called "informed consent". This process requires dialog between patient and provider that is documented by notes in the medical record as well as a specific consent document.**

Radiation induced stochastic or deterministic injuries are seldom the only high-severity risks associated with a clinical or research procedure. Radiation risks should be neither under nor over emphasized. All applicable risks need to be put into perspective, adjusted to the patient's individual health status, and presented in a way that both the practitioner and patient can understand.

Keywords— **Informed Consent; Radiation Risk Evaluation; Risk; Research**

I. Introduction

Medical procedures of any type should not be performed on patients or research volunteers until they have sufficient understanding of the benefits and risks of; the proposed procedure, alternative procedures, or doing nothing. The method of communicating this information and obtaining a response from the patient is called informed consent. This process requires an adequate dialog between patient and provider. The results of this discussion are documented by notes in the medical record as well as in specific consent documents.

It is impossible to list all of the possible risks associated with any procedure. The informed consent discussion is usually limited to high-probability events of any severity and high-severity events even if they have a low-probability of occurrence.

Radiation usage in X-ray guided interventional procedures can seldom be confidently predicted in advance. This is due to issues such as patient variability and clinical complexity. A discussion of the possibility of deterministic injuries should be included in the pre-procedure consent process. Post-procedure discussions with the patient should occur when significant amounts of radiation are used.

In most procedures, radiation is used as an imaging tool rather than for its direct effects. Practitioners who use these tools may have minimal understanding of radiation effects. This might reduce the effectiveness of both the oral and written components of the consent process.

II. Estimating radiation risks

A. Stochastic Risks.

A stochastic risk estimate usually starts with a model of the procedure and patient. A simple way to do this is to obtain the Effective Dose (E) for the closest similar procedure from the published literature (1) Dosimetric software is available from IMPACTSCAN (2) and STUK (3) that will calculate a set of organ doses as well as E when a more specific "dose" estimate is required.

Procedural radiation risk can be estimated once the "dose" is at hand. This conversion has explicit dependencies on the sex and age of the patient (4, 5) Unfortunately; dependencies on the patient's condition (e.g. short expected life-span) are seldom analyzed or applied.

B. Risks of Deterministic Injuries

The risk of a deterministic radiation injury includes factors such as the planned procedure, patient size, and previous irradiation of potential X-ray beam ports. Where appropriate, it is possible to include a general warning along with some specific information in the consent process. The patient also should know in advance that a further discussion may be necessary on this topic after the procedure is completed.

Post-procedure discussions with the patient are indicated when the physical dose delivered to the patient is high enough to suggest the possibility of a reaction. The threshold for initiating this discussion should be low enough to make missing a reaction highly unlikely.

III. Communicating radiation risks

Radiation and other risks must be communicated in a way that is understandable by the patient. This understanding can come from the health-care-provider, written consent materials, or a combination of the two.

O. Dössel and W.C. Schlegel (Eds.): WC 2009, IFMBE Proceedings 25/III, pp. 571–572, 2009.
www.springerlink.com

The written risk explanation is often produced by an automated system. The radiation section is often derived from a standardized template with risk expressed in dose units and translated into "everyday" topics such as transatlantic flights or days of natural background. Educational information such as the sources of background radiation is often included in the template. The actual risk (presumably cancer) and its probability are often omitted. The existence of uncertainty in the estimate is seldom mentioned. The resulting statements still typically contain a few hundred words. The overall form of the statement hardly differs with risk level. One prominent university's risk generator only changes the name of the procedure(s) and background days with increasing risk. When tested in 2009 using cardiac CT angiography as the procedure, it asked for the sex of the patient as input data but did not sex-adjust the risk even though this procedure produces a high breast dose. The NIH intramural process provides three risk based templates. The text in each of these fills most of a printed page.

IV. Consent scenarios

A. Pure Clinical

Procedures are only proposed in such situations where there is an expectation that the benefits of the procedure will outweigh the risks (including the risks of alternative procedures or doing nothing). In some circumstances, both expected benefits and procedural risks can be very high. When properly disclosed and discussed, the certainty of radiation injury (e.g. skin toxicity from radiotherapy) may be accepted by patients as being in their best interest.

B. Pure Research

Much of the current process for disclosing radiation risks derives from safeguards instituted after the "human radiation experimentation" era. An optimized version of the consent process described above works best when radiation is the only real risk associated with the procedure (e.g. a tracer experiment on food metabolism).

C. Research Add-On to a Clinical Procedure

Ideally, consent is simultaneously obtained for both the clinical procedure and the additional research component. In most cases, research adds little extra radiation to a clinical procedure. Special attention should be directed toward situations where the clinical procedure is not expected to produce deterministic injuries and where the additional research radiation may cross thresholds.

V. Discussion

A relatively simple list of non-radiation risks is found on most consent forms. Numerical or "everyday" estimates of these risks are infrequently provided on the form. A typical list has a dozen or more items, each described in very few words. The practitioner obtaining consent can usually provided an expanded explanation of most of these risks. However, many are not comfortable with providing additional information regarding the printed radiation risk statement.

Difficulties may arise when risks are presented to a patient in a visually unbalanced manner. Excessive focus on a long radiation risk statement might divert attention away from other serious risks. People tend to ascribe greater importance to longer texts than shorter ones even when the longer texts may not be as relevant as the shorter ones. Conversely, the long radiation statement may be ignored simply because of its size and the meaning subjects ascribe to "radiation."

A potentially valuable tool here would be nationally and / or internationally accepted standard descriptors of different radiation procedures, which could be used or adapted for individual consent forms.

The radiation elements of clinical or research consent must place this risk into an appropriate context relative to the other risks associated with the procedure. Under or over emphasis on radiation risk is not in the patient's or research subject's best interest.

VI. References

1. Mettler, F.A., Jr., et al., *Effective doses in radiology and diagnostic nuclear medicine: a catalog.* Radiology, 2008. **248:** 254-63.
2. IMPACTSCAN http://www.impactscan.org
3. STUK http://www.stuk.fi/
4. BEIR, *Health Risks from Exposure to Low Levels of Ionizing Radiation: BEIR VII – Phase 2 Committee to Assess Health Risks from Exposure*. 2006, The National Academies: Washington DC.
5. ICRP, *Report 103: The 2007 Recommendations of the International Commission on Radiological Protection*. 2007.

Author: Stephen Balter, Ph.D.
Institute: Columbia University Medical Center
City: New York, New York
Country: United States
Email: sb2455@columbia.edu

Calculation of Radiation Dose from a Cloud of Radioactive Iodine Using Voxel Phantoms and Monte Carlo Methods

S.A. Natouh

Renewable Energies and Water Desalination Research Center, Department of Medical application of Radioisotopes, Tripoli, Libya

Abstract— **VMC-dc is a computer program that simulates the irradiation of the human body by external sources. It uses a voxel phantom produced at Yale University and the Monte Carlo technique to simulate the emission of photons by a point, ground, cloud source or X-ray source. It then transports the photons through the human body phantom and calculates the dose to each body region**.

This paper shows firstly the validation of VMC-dc by comparison with Federal Guidance Report No. 12. The source for the submersion dose calculations is a semi-infinite cloud containing a uniformly-distributed amount of activity of ^{131}I emitter photons of unit strength (1 Bq m^{-3}) surrounding a human phantom standing on the soil at the air-ground interface. The effective dose was calculated using VMC-dc program and compared with the value given in the Federal Guidance Report No.12. Secondly the program VMC-dc was then applied to the calculation of the effective dose and the total dose received by each organ / tissue due to a quantity of ^{131}I released into the environment at 45 GBq (Fleurus nuclear accident).

For the validation of VMC-dc code, results show a good agreement for the effective dose due to cloud immersion obtained using VMC-dc and Federal Guidance Report No. 12. The accumulated effective dose received by hypothetical person living in the exposure area for 3 months due to a quantity of ^{131}I released into the environment at 45 GBq is 3.4 nano Sv.

Keywords— **VMC-dc code, Monte Carlo Simulation, External exposure**

I. Introduction

Radioactive releases from various nuclear facilities may contribute to radiation exposure through an external exposures by direct radiation from plumes or deposited radionuclides and internal exposures due to inhalation and ingestion of radioactive material. Exposure to I-131, especially in childhood, increases the risk for hypothyroidism, thyroid nodules, and cancer [1].

The radiation dose depends strongly on the temporal and spatial distribution of the radionuclide to which a human is exposed. Estimation of the dose to tissues of the body from radiations emitted by an arbitrary distribution of a radionuclide in an environmental medium is an extremely difficult computational task [2].

VMC is a computer program that simulates the irradiation of the human body by external sources. It uses a voxel phantom produced at Yale University and the Monte Carlo technique to simulate the emission of photons by a point, ground, cloud source or X-ray source. It then transports the photons through the human body phantom and calculates the dose to each body region [3].

The mode considered in this work for external exposure is a semi-infinite cloud containing a uniformly-distributed amount of radioactive ^{131}I emitter photons surrounding a human phantom standing on the soil at the air-ground interface. Calculations of the effective dose and the dose received by each organ / tissue, as performed for this work, involve the validation of VMC-dc by comparison with the Federal Guidance Report No. 12 and the situation - Fleurus nuclear accident - of a gaseous leak of a quantity 45 GBq of ^{131}I radioisotope [4].

II. Method and Material

The work performed for this paper, involve tow steps:

1. The validation of VMC-dc, was made for a semi-infinite cloud of activity concentration (1 Bq m^{-3}). The effective dose was calculated and compared with the value given in the Federal Guidance Report No. 12 [2].
2. The situation of a gaseous leak of a radioisotope of iodine, ^{131}I, that was detected at a large medical radioisotope laboratory (August 23-24, 2008 Fleurus, Belgium) was considered. The quantity of radioactivity released into the environment was estimated at 45 GBq ^{131}I [4]. The radionuclide concentration is assumed to remain constant for every exposure period of 8 days ($t_{1/2}$ of ^{131}I). The gamma-ray dose received by an individual on the ground at the center of a semi- infinite hemisphere cloud of radius 5 Km was calculated by running VMC-dc code for exposure period of three months. For a hypothetical person remaining three months at the exposure area, the total dose received by each organ / tissue is shown in Table 1 whereas the accumulated effective dose as function of time is shown in Fig 1.

O. Dössel and W.C. Schlegel (Eds.): WC 2009, IFMBE Proceedings 25/III, pp. 573–575, 2009.
www.springerlink.com

Table 1 Total organ/tissue doses for three months of exposure

Organ/Tissue	Organ doses in nanoGy
Gonads	3.444
Bone marrow	2.719
Colon	2.549
Lung	2.997
Stomach	2.375
Bladder	3.661
Liver	2.819
Oesophagus	2.997
Thyroid	9.965
Skin	4.183
Bone surface	4.341
Adrenals	10.737
Brain	3.999
Upper large int.	2.336
Small intestine	2.359
Kidney	3.219
Muscle	3.520
Pancreas	4.90
Spleen	3.060
Eye lens	9.522

III. Result and Discussion

The effective dose values obtained by using VMC-dc program and that published in Federal Guidance Report No. 12 are 14.3 and 18.2 femto Sv per Bq s m^{-3} respectively. The differences are due to the two types of simulators used – FGR: geometric, VMC: voxel – are quite different**.** More over the difference in the results is due to air conditions and gender-specific phantoms considered in the calculation.

VMC-dc program was running for 1.5E09 histories because for the small tissues such as eye lens, adrenals and the thyroid, the lower the number o f photon interactions in that tissue, the large number of "histories" required before the calculated dose becomes more representative. Other wise the tissue doses are reported as average doses.

The total organ/tissue doses for a period of three months of exposure, is shown in Table 1for submersion in a semi-infinite cloud source of 45 GBq ^{131}I, as calculated for this work.

Eye lens, adrenals and the thyroid doses have largest values. However they have small tissue weighting factor comparing to the other organs, thus it has a little contribution to the effective dose.

Fig. 1 shows a total dose accumulated over the time period of three months. This paper dealt only with external exposure; the problem of internal contamination was not considered.

External exposure due to immersion in contaminated air or water or to radiation from an overhead plume usually makes only small contribution to the total dose received by members of the public [5].

Fall-out of radioiodine was one of the most important factors in human irradiation in the contaminated areas. Radioiodine from food and inhalation accumulates in the thyroid gland, where it may produce large doses. Almost all of the dose is due to β-particles. ^{131}I was the predominant source of exposure during the first weeks after the accident, but its contribution was negligible thereafter when compared with long-lived nuclides like 137Cs and 90Sr, owing to its half-life of eight days [5]. This is what has been illustrated in Fig. 1.

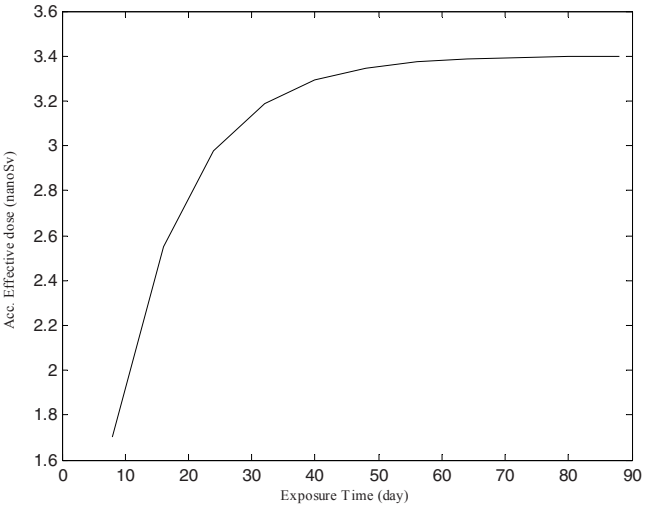

Fig. 1 Accumulated doses as a function of time

IV. Conclusions

- The results show that the Monte Carlo program and voxel phantoms can provide adequate photon transport results.
- The validation of the code to existing standards provides confidence that the results are consistent and confident.

- VMC-dc is a computer code that can be confidently used to evaluate radiological releases to the environment. Moreover VMC-dc makes dose calculations simpler.
- Although ^{131}I is a short-lived radionuclide, it may contribute significantly to the dose in the first weeks after a release.

V. References

1. Scientific information for health professionals at http//www.iodine131.org/2rad-dose.htm.
2. Keith F. Eckerman and Jeffrey C. Ryman September 1993, EPA-402-R-93-081, Federal guidance report no. 12, External exposure to radionuclides in air, water, and soil.
3. VMC-cd program at www.doseinfo-radar.com.
4. List of civilian radiation accidents at http://en.wikipedia.org.
5. IARC Monographs on the evaluation of carcinogenic risks to humans at http://monographs.iarc.fr/ENG/Monographs/vol75/mono75-5.pdf.

Towards higher level of patient safety and control of medical exposure in Bulgaria

J. Vassileva

National Centre of Radiobiology and Radiation Protection, Sofia, Bulgaria

Abstract— Medical uses of ionizing radiation are the major man-made source of exposure of the Bulgarian population. The requirements of the International Basic Safety Standards for protection against ionizing radiation and the EURATOM Directive 97/43 were fully harmonized in the Bulgarian legislation and many actions have been undertaken for their practical implementations. In October 2005 new regulation has been enforced for radiation protection at medical exposure. A department for Radiation Protection at Medical Exposure was established at the National centre of Radiobiology and Radiation Protection in order to lead the practical implementation of the Ordinance. New objective requirements to radiological equipment were set and licensees were obliged to put into operation Quality control program. First Diagnostic Reference doses were given in 2005 based on the limited own experience from the First national survey in conventional performed in 2002-2003 within the Bulgarian-German twinning project. Further enlargement of dose surveys and improvement of RP practice at medical use of radiation were realized within the Bulgarian-Finnish Twining project "Strengthening of administrative structures for radiation protection and safety use of ionizing radiation in diagnostics and therapy".

New radiation protection training programs for medical specialist were elaborated including recent knowledge on patient protection. Several national training courses with international lecturers were performed

Keywords— Medical exposure, patient safety

I. Introduction

Bulgaria is a small European country with about 7.5 million inhabitants. According to the classification used by the UNCEAR in the purposes of comparison of medical exposure, Bulgaria is a country of first level of health care with about 26 000 physicians, that means 1 physicians per less than 1000 population [1]. The use of ionizing radiation for medical diagnostic examinations contributes to over 83% of man-made radiation sources in the country and is only exceeded by the natural background of a source of exposure. The main source is diagnostic radiology contributing to about 24 % of the average total radiation exposure for the Bulgarian population.

In order to put into strict control the medical exposure many actions were undertaken by the international organizations in recent years. The ICRP stated in its Publication 60 from 1990: "*Because most procedures causing medical exposures are clearly justified and because the procedures are usually for the direct benefit of the exposed individuals, less attention had been given to the optimization of protection in medical exposure than in most other applications of radiation sources. As a result there is considerable scope for dose reduction*" [2]. These facts have focused attention to the need to improve the radiological protection of patients in diagnostic radiology, nuclear medicine and radiotherapy. The International Basic Safety Standards for Protection against Ionizing Radiation and for the Safety of Radiation Sources (BSS) published in 1996 [3], as well as the Safety Guide for Radiological protection for Medical Exposure to Ionizing Radiation give the scope of the principles and practical measures for radiation protection. For European Member states the Council Directive 97/43/EURATOM for health protection of individuals against the dangers of ionizing radiation in relation to medical exposures [4] is mandatory and it was transposed into Bulgarian legislation by the Ordinance of the Ministry of Health No30 from 31 October 2005 for Protection of Individuals at Medical Exposure, promulgated in State Gazette № 91 of November 15, 2005. This regulation fully adopts the international standards in the field of medical exposure in regard to justification and optimization of radiological procedures and also put new demands to the equipment use for medical exposure.

II. National activities

A Department for Radiation Protection at Medical Exposure was established at the National centre of Radiobiology and Radiation Protection in order to lead the practical implementation of the Medical Exposure Ordinance.

In the period 2002-2004 in the framework of a Bulgarian-German twinning project BG/2000/IB/EN 01-05 "Radiation Protection and Safety at the Medical Use of Ionizing Radiation" successfully completed by the National Centre of Radiobiology and Radiation Protection (NCRRP). Under the institutional part of the project activities have been started to transpose and implement the international requirements as well as to set up a Quality assurance (QA)

O. Dössel and W.C. Schlegel (Eds.): WC 2009, IFMBE Proceedings 25/III, pp. 576–577, 2009.
www.springerlink.com

system for Radiology in the country. During the project a large scale national patient dose survey in Diagnostic Radiology has been conducted by the NCRRP with measurement of patient doses during common radiography examinations. As a result national reference patient dose levels were elaborated and included in the Ordinance. Patient dose surveys explored the real status of the clinical practice and existing potential for dose reduction in Bulgarian hospitals. For many decades all X-ray sources in the country have been under strict surveillance in respect to occupational and public safety but quality assurance as a means for optimization of patient radiation protection needs to be further expanded. The Ordinance No30 stated new demands to radiological practices and set higher requirements to radiological equipment, which have not been previously included in the Bulgarian legislation. It obliges the licensee to put into operation a Quality control program for the radiological equipment comprising three types of tests: acceptance test - to ensure correct operation of safety features; commissioning tests - to ensure that the equipment is ready for clinical use and meet the national requirements and routine constancy (periodical) tests – to detect changes in performance during use and to guarantee the performance efficacy and safety. To the end of 2008 commissioning tests were performed for all radiological equipment in use but many efforts are still needed for full understanding and implementation of quality control system.

Further enlargement of dose surveys and improvement of radiation practice at medical use of radiation were realized within the Bulgarian-Finnish Twining project BG 2006/IB/SO 01 “Strengthening of administrative structures for radiation protection and safety use of ionizing radiation in diagnostics and therapy”. Within the project national surveys in conventional radiography and fluoroscopy, interventional radiology and CT were performed and new Diagnostic reference levels were elaborated. Many meetings, workshops and trainings were performed on different topics – quality audit in radiotherapy and radiology; preventing accidents and incidents in radiotherapy, dosimetry, etc

According to the national regulations, the activities with sources of ionizing radiation (SIR), which affect the safety, shall be performed only by individuals with the necessary professional qualification, who have obtained an individual license following a special procedure. The National Centre of Radiobiology and Radiation Protection at the Ministry of Health is the main training provider for the professionals working with medical SIR (about 4000 persons). Specialized training programs were elaborated for each qualification level of staff in nuclear medicine (NM), diagnostic radiology (DR) and radiotherapy (RT).

National Centre of Radiobiology and Radiation Protection has organised a number of national training courses with invited lecturers abroad, most of them supported by the International Atomic Energy Agency.

For medical exposure BSS and EURATOM Directive 97/43 requires involvement of medical physics expert. The practical approach to combine both functions in one expert is adopted in Regulation for radiation protection at medical exposure, which was enforced by the Ministry of Health in 2005. Training programs for medical physicists and qualification requirements for medical physics experts were generally revised.

CONCLUSIONS

Because the medical uses of ionizing radiation represent the largest source of exposure, special attention must be paid to minimizing the risk. Radiological protection programs in medicine must allow the exposure to be sufficient to obtain adequate diagnostic information and to provide effective treatment. The new Bulgarian legislation in the field accounts for this principle but the practical implementation requires furthers activities to assure justification and optimization of radiological procedures. The final aim is to assure high quality and safe medical use of radiation

REFERENCES

1. National Statistical Institute of Republic of Bulgaria at http://www.nsi.bg/
2. International Commission on Radiological Protection. 1990 Recommendations of the ICRP 60. Ann ICRP, 21 Nos 1-3, Pergamon Press, Oxford, 1991.
3. International Atomic Energy Agency. International basic safety standards for protection against ionizing radiation and for the safety of radiation sources, Safety Series, IAEA, Vienna, 1995.
4. European Commission. Council Directive 97/43/EURATOM of 30 June 1997 on health protection of individuals against the dangers of ionizing radiation in relation to medical exposure, Official Journal of the EC, L180, V22, 1997.

Author: Jenia Vassileva
Institute: National Centre of Radiobiology and Radiation Protection
Street: 132 Kliment Ohridsky
City: Sofia
Country: Bulgaria
Email: j.vassileva@ncrrp.org

Establishment of *In-vitro* ^{60}Co Dose Calibration Curve for Dicentrics in National Biodosimetry Laboratory of Malaysia

N. Jamal, A. R. Rahimah, N. Yusof, N. N. L. Bo, Y. Talib, J. M. Napiah and R. Dahalan

Malaysian Nuclear Agency, 43000 Kajang, Malaysia

Abstract— **The purpose of this study was to establish an *in-vitro* ^{60}Co dose calibration curve for dicentric assay technique. Sample from six volunteers were irradiated using ^{60}Co at doses of 0, 0.25, 0.5, 1.0, 2.0 and 4 Gy. The blood samples were surrounded by 4 mm Polyvinyl chloride (PVC). These were irradiated at a dose rate of 0.98 Gy min^{-1}. Blood specimens were then cultured and processed using dicentric assay technique. The observed dose calibration data were fitted to a linear quadratic model using Dose Estimate Ver 2.0, established by Health Protection Agency, UK. The calibration curve parameters were compared with results from other studies. The dose calibration curve for dicentrics yield is: Yield = (0.0010 ± 0.0000) + (0.0899 ± 0.0002)D + (0.0185±0.0001)D^2, (Weighted χ^2 = 7.4510, on 3 df, P=0.05). The value of α was higher, while β value was lower than the other reported studies. We have established a dose calibration curve for the induction of chromosome aberrations in human lymphocytes from blood irradiated with ^{60}Co γ-ray in a dose range of 0.0-4.0 Gy. This curve may be useful for *in- vitro* dose reconstruction.**

Keywords— **Dicentric Assay , ^{60}Co, Dose Calibration Curve.**

I. Introduction

Ionizing radiation is a strong clastogen, causing chromosome breakage, and resulting in cytogenetic aberrations in exposed cells. Accurate estimation of the level of absorbed dose is important immediately after exposure as a guide for medical treatment and at longer times after exposure to assess possible health consequences. Cytogenetic analysis of peripheral blood lymphocytes can provide a biological estimation of the dose received in exposure to ionizing radiation [1]. A number of cytogenetic techniques have been developed to measure radiation exposure and generally produce dose estimation, including dicentric, Fluorescence In Situ Hybridization (FISH), micronuclei and Premature Chromosome Condensation (PCC) assay [2,3].

The dicentric assay technique remains the gold standard for early-response in accident-biodosimetry and defining dose assessment [2,3]. Dicentric is the aberration type that is most frequently used in biological dosimetry. This is because it clearly involves an interaction (or exchange) between two chromosomes. In this assay technique, activated lymphocytes are arrested in metaphase and fixed for slide preparations. The metaphase spreads are then analyzed for the presence of dicentric and ring chromosomes.

This assay technique is generally accepted as the most specific, sensitive and currently available method for determining doses from recent (i.e. within days to about 6 months) exposure to ionizing radiation [4]. It could be especially useful in providing evidence of non-uniform exposure and conformation of individuals in a high dose exposure triage category, and the most sensitive method of quantifying the radiation dose in the absence of physical measurements due to its ability to estimate the average whole-body dose [2]. It is a reliable and useful tool in medical management of radiation accident victims [4].

Establishing a competent biodosimetry laboratory that is capable of performing cytogenetic analysis for dose estimation is vital in a country like ours, where recently a large use of ionizing radiation are in place. It has been recommended that each laboratory intended to carry out biological dosimetry should have its own *in-vitro* dose calibration curve for dose reconstruction [2].

The purpose of this study was to establish the *in-vitro* dose calibration curve for ^{60}Co with dicentric assay technique. This curve is a useful tool for dose reconstruction in medical management of radiation accident victim in the country.

O. Dössel and W.C. Schlegel (Eds.): WC 2009, IFMBE Proceedings 25/III, pp. 578–581, 2009.
www.springerlink.com

II. Materials and Method

A. Irradiation

6 ml of freshly taken blood specimens were collected from six healthy volunteers; Malay (n=2), Chinese (n= 2) and Indian (n=2) respectively. Those volunteers are aged between 24 to 51 years old. Blood was collected in lithium heparin tube. Blood samples from all volunteers were divided into 1ml aliquots, in lithium heparin tube.

ىray from a ^{60}Co teletherapy unit ELDORADO 8 # 104 located at the Secondary Standard Dosimetry Laboratory (SSDL), Malaysian Nuclear Agency is used to irradiate the sample. Sample from each volunteer was irradiated at 0, 0.25, 0.5, 1.0 and 4.0 Gy respectively. These were irradiated at a dose rate of 0.98 Gy min^{-1}. 4mm Polyvinyl chloride (PVC) is used as an absorbing material surrounding the lithium heparin tube. The experimental set-up is shown in Fig 1. After irradiation, blood samples were kept at 37ฺC for one hour to allow for any chromosomal repair to take place [3].

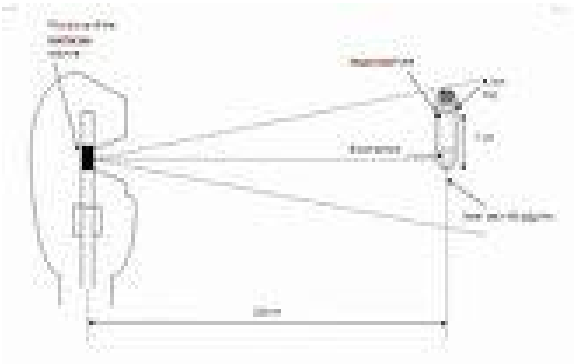

Fig. 1: Experimental set-up

B. Scoring

Blood samples were cultured into the 10 ml of complete culture media in the 25 cm^2 flask. Lymphocytes in blood were stimulated to divide by addition of 300 µl of 2.5 mg/ml stock phytohemaglutinin (PHA), and incubated at 37°C with 5% CO_2 for 48 hours. After 45 hours of incubation, 100 µl of 10 µg/ml stock colcemid was added to the culture and incubated for an additional 3 hours to arrest cells in metaphase. Following the full incubation period, the cultured blood cell was harvested and fixed. In harvesting lymphocytes, the hypotonic 0.075M potassium chloride solution was applied to break red blood cells and fixative mixture of 1:3 acetic acid/methanol was added to fix the lymphocytes. The fixative process was repeated 3 times while the first fixer was added extremely slowly to prevent cells clumping. The fixed lymphocytes were then kept in 4°C fixative in fridge for future slide preparation. Slide was prepared by dropping 2-3 drops of cells in fixative on grease-free slide and Giemsa stained for observation [1-3].

Slides from each culture were scored by a single scorer. At least 400 first division metaphase cells or 50 dicentrics were scored per sample. In addition, number of centric rings and excess acentric fragments were also recorded. Conventional microscope, Olympus BH2-BHT (Olympus, Japan) was used in this study.

C. Curve Fitting

The pooled observed dose calibration data were fitted to a linear quadratic model using Cytogenetics Dose Estimation software program Ver 2.0, Health Protection Agency, UK [5]. The method is based on weighted least square fitting. The standard *u*-test was used to test the yield of chromosome aberrations with dose for poisson probabilities. If the value of *u* is greater than ± 1.96, the under or over dispersion of chromosome aberration yield is significant at 5% [1,5]. The method is also based on the concept that for poisson distribution, the ratio of variance (ط^2) to mean (y) is equal to 1. The calibration curve parameters were compared with results from other studies.

III. Result and Discussion

Establishing *in-vitro* dose calibration curves is important for the reconstruction of radiation dose in an exposed radiation worker in any standard biodosimetry laboratory. The *in-vitro* dose calibration curve is comparable to the effect of *in-vivo* irradiation [6].

The yield of chromosome aberration with dose was fitted to a linear quadratic model [1-3]:

$$Y = C + \text{ىD} + \text{ىD}^2 \quad (1)$$

Where Y is the yield of aberration for dose D, C is the baseline aberration frequency in the control population, سand س are linear and quadratic coefficient respectively.

Fig. 2 shows a dose calibration curve for dicentrics in human lymphocytes exposed to incremental radiation doses

from ^{60}Co ـray. The 95% confidence intervals are also shown on the curves. The dose calibration curve for dicentrics yield is: Yield = (0.0010 ± 0.0000) + (0.0899 ± 0.0002)D + (0.0185±0.0001)D^2, (Weighted ظ^2 = 7.4510, on 3 df,, P=0.05).

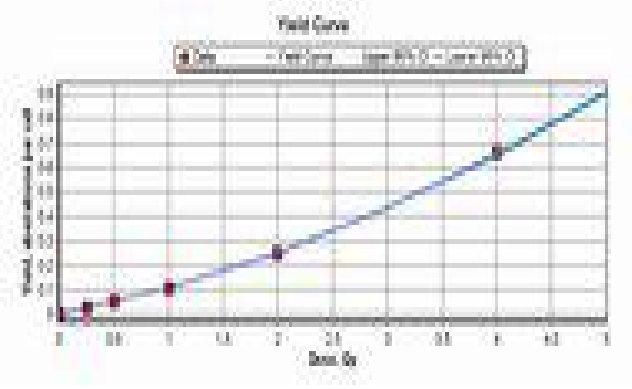

Fig. 2 Dose calibration curve for dicentrics in human lymphocytes exposed to incremental radiation doses from ^{60}Co ـray

Table 1 shows pooled data of dicentrics frequency in lymphocytes of blood samples exposed *in-vitro* to ^{60}Co ـray. It shows that the distribution of dicentrics follows a poisson distribution except at 0.5 to 4.0 Gy where u >± 1.96. This over dispersion at those dose points may be explained by a small irradiated sample volume used in this study that may results in nonuniformity of irradiation at high dose [1].

Table 1 Pooled data of dicentrics frequency in lymphocytes of blood samples exposed in-vitro to ^{60}Co ـray

Dose (Gy)	No. of cell scored	Dicentric per cell ± SE	Total dicentric	Dicentric distribution per cell			u	ظ^2/y
				0	1	2		
0	3000	0.003 ±0.001	10	2990	10	0	-0.122	1.570
0.25	2874	0.024 ±0.003	70	2804	70	0	-0.917	1.540
0.5	2958	0.055 ±0.004	163	2795	163	0	-2.110	1.490
1.0	2540	0.103 ±0.006	262	2278	262	0	-3.670	1.410
2.0	2569	0.249 ±0.010	639	1948	603	18	-6.890	1.270
4.0	1508	0.663 ±0.021	1000	617	782	109	-12.200	0.875

The (ظ^2/y) value of dicentric yield was close to 1, ranging form 0.875 to 1.570. This indicates that the calibration curve is following poisson distribution.

Table 2 shows results of comparison of the calibration curve parameters for dicentric yield, using ^{60}Co with results from other studies. It shows that س which is a linear coefficient is larger than the values reported by Edwards, 1997 [7] Voisin *et.al*., 2004 [8] Lloyd *et. al*.,1986 [9] Bauchinger *et. al*., 1983[10]. While س which is a quadratic coefficient is lower than the values reported by Edwards, 1997 [7] Voisin *et.al*., 2004 [8] Lloyd *et. al*.,1986 [9] Bauchinger *et. al*., 1983[10]. The difference can be explained by the fact that a small irradiated sample volume used in this study that may results in nonuniformity of irradiation at high dose [1]. Furthermore, our study sample are those from three major ethnic groups in Malaysia, namely Malay, Chinese and Indian. The difference in genetic factors and lifestyle may also contribute to the differences [11]. However, further investigation is needed as to study the effect of genetic on chromosome aberration among three different major ethnic groups in Malaysia.

Table 1 Comparison of calibration curve parameters for dicentric yield using ^{60}Co with results from other studies

Source	س± SE (Gy^{-1})	س± SE (Gy^{-2})
Edwards [7]	0.018 ± 0.003	0.060 ± 0.006
Voisin et.al, [8]:		
Laboratory A	0.0187 ± 0.0056	0.0527± 0.0046
Laboratory B	0.0371 ± 0.0085	0.0547± 0.0039
Laboratory C	0.0128 ± 0.0031	0.0640± 0.0022
Lloyd et al, [9]	0.016 0±.005	0.065 ± 0.003
Bauchinger et al. [10]	0.011 ± 0.004	0.056 ± 0.003
Present study	0.0899± 0.0002	0.0185 ±0.0001

IV. CONCLUSIONS

We have established a dose calibration curve for the induction of chromosome aberrations in human lymphocytes from blood irradiated with ^{60}Co ـray in a dose range of 0.0-4.0 Gy. This curve may be useful for *in-vitro* dose reconstruction.

ACKNOWLEDGMENT

This work was undertaken as part of e-science project under grants of the MOSTI: 03-03-01-SF0029. We acknowledge the co-operation of the respective blood donors for their participation in the project. We thank the SSDL of Malaysia for allowing us to use ^{60}Co teletherapy unit ELDARADO 8 # 104.

REFERENCES

1. Senthamizhchelvan S, Pant G S, Rath G K, et al (2007) Biodosimetry Using Chromosome Aberrations in Human Lymphocytes. Radiat Prot Dosim 123: 241-45.
2. International Atomic Energy Agency. (2001) Cytogenetic Analysis for Radiation Dose Assessment A Manual. Vienna, IAEA. STI/DOC/10/405.
3. International Atomic Energy Agency (1986) Biological Dosimetry: Chromosome Aberration Analyses for Dose Assessment. Vienna, IAEA. STI/PUB/10/260.
4. Bender M A, Awa A, Brooks A L et al. (1988) Current status of cytogenetic procedures to detect and quantify previous exposure to radiation. Mutat. Res 196: 103-159.
5. Ainsbury L. Dose Estimate: Cytogenetics Dose Estimation Software. Health Protection Agency, U K. 15 May 2008.
6. Koksal G, Pala F S, Dalci D O. *In vitro* dose-response curve for chromosome aberrations induced in human lymphocytes by 60Co gamma-radiation. Mutat Res 329:57-61
7. Edwards A A. (1997) The Use of Chromosomal Aberrations in Human Lympocytes for Biological Dosimetry. Radiat Res 148:S39-S44.
8. Viosin P, Roy L, Hone P A et al. (2004) Criticality Accident Dosimetry by Chromosomal Analysis. Radiat Prot Dosim 110:443-447.
9. Lloyd D C, Edwards A A, Prosser J S (1986) Chromosome aberrations induced in human lymphocytes by in vitro acute x and gamma radiations. Radiat Prot Dosim 15:83-88.
10. Bauchinger M, Schmid E, Streng S et al. (1983) Quantitative analysis of the chromosome damage at first division of human lymphocytes after ^{60}Co ـirradiation. Radiat Environ Biophys 22:225-229.
11. Hall E J (2000) Radiobiology for the Radiologist. 5th edn. Lippincott, Williams and Wilkins, Philadelphia, USA.

Use macro [author address] to enter the address of the corresponding author:

Author: Noriah Jamal
Institute: Malaysian Nuclear Agency
Street: 43000 Kajang
City: Selangor
Country: Malaysia
Email: noriahj@nuclearmalaysia.gov.my

A Simple Temperature Measuring Device for a Calorimeter System for Adsorbed Dose Measurements

B. Blad

Department of Radiation Physics, University Hospital, Lund, Sweden

Abstract— **A calorimeter can be used for absolute absorbed dose measurements. This paper describes a temperature measuring device for a calorimeter system. The measurement system consists of a measurement bridge with two precision thermistors and two resistors connected to a chopper amplifier. The bridge is driven with a square wave. This makes it possible to subtract error signals from real signals. The filtered signal is sample and hold before subtracted in an operational amplifier. A test unit is build and temperature curves are generated from radiation from a linear accelerator. Present system can measure doserates higher than 1.5 Gy/min.**

Keywords— **Temperature measuring device, calorimeter and radiation dosimetry.**

I. Introduction

A calorimeter is a fundamental instrument for measuring absorbed dose in a radiation beam. It measures the temperature increase caused by the radiation. The advantage of this method is that the expected temperature difference can be calculated from the absorbed dose. However, the change in temperature is very small, in the order of 0.001 °C /Gy. The measurement system has to be stable and sensitive and the measurement result is affected by how well the ambient temperature can be isolated from the measurement chamber.

Two main types of calorimeter system are obtainable, where the measurement chambers are water or graphite. For ionization radiation water behaves similar as living tissue and radiation generating devices are often calibrated using water. However, the specific heat for water is low compare to graphite; about 1.0 and 2.2 kJ/kg ·K respectively.

Calorimeter system often uses one temperature sensor formed one arm of a Wheatstone bridge circuit connected to an amplifier and to a registration device [1]. McEwen et al also used the Whetstone bridges constructed from precision resistors with very low temperature coefficient (<1 ppm/°C) and thermistors [2]. The reason for two bridges was to increase sensitivity and reliability. In order to reduce the uncertainty Williams and Rosser replaced their d.c. temperature measurement system by an a.c. system. Their main components were the bridge, a lock-in-amplifier, thermistors and resistance networks [3].

The aim of this work is to design a simple but reliable temperature measuring device for a graphite calorimeter.

II. Method and results

Our system contains a Wheatstone bridge with two precision resistors and two thermistors. The tolerance of the resistors is ±0.1 % and temperature coefficient is less than ±5 ppm/°C, with a value of 90 Ωk and 0.33 W from General Resistance. The used resistors in the bridge were selected to be better than the specification. The thermistors are temperature matched of NTC-type from Rhopoint, type ACC/ACW. A block diagram of the temperature measuring device is presented in figure 1.

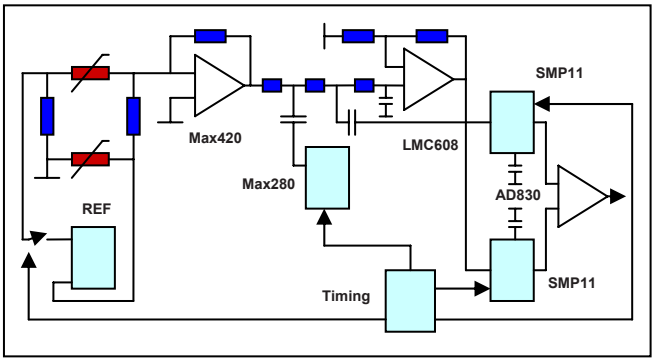

Fig. 1

The bridge is driven by a square wave generated by a floating reference voltage MAX 6250 and a fast relay. The frequency of the square wave was set to 2 Hz. The bridge is connected to a CMOS chopper-stabilized amplifier MAX 420 designed for high accuracy amplification. The maximum offset is 5 μV, while the guaranteed drift limit is 0.05 μV/°C. Amplification factor can be varied by using different values of the precision resister in the loop.

The amplified square wave is filtered in a 5th-order all-pole instrumentation lowpass filter, MAX 280, with a very low DC error (a DC offset of 50 μV). Further noise reduction and amplification is accomplished in a LMC 6081. The noise level is 600 μV_{RMS}.

The amplified and lowpass filtered square wave is connected to two sample and hold circuits SMP-11. The first circuit holds when voltage is applied on the bridge and the

O. Dössel and W.C. Schlegel (Eds.): WC 2009, IFMBE Proceedings 25/III, pp. 582–584, 2009.
www.springerlink.com

second circuit holds when no voltage is applied on the bridge. The outputs from the sample and hold circuits are subtracted in an instrumentation amplifier, AD 830. The reason for this procedure is to subtract any present DC errors in the whole system. The output signal is used for data analysis.

The temperature measuring device operates at about 27 °C. The temperature measurement range is determined by the used amplification factor of the system. The temperature of the graphite detector has to match that temperature. A heating unit and the temperature measuring device are used to maintain a constant temperature in the detector compensating for any variation in the ambient room temperature. During irradiation the same amount of heat is transferred to the detector and additional heat from the irradiation is registered as increase in output of the temperature measuring device.

The detector, the heating devise, the Wheatstone bridge and measuring electronics is mounted in a metallic box. A picture of the device is presented in figure 2.

Fig. 2

In figure 3 the result of an initial test of the system is presented. A digital oscilloscope (a Tekscope from Tektronix) was used to visualize the temperature change during radiation. 10^{-3} °C corresponds to an output voltage of 0.2 V of the measuring system.

A 6 MV linear accelerator from Philips, a SL75/5 was used for the experiment. By changing the pulse repetition frequency (400 Hz, 200 Hz and 100 Hz) of the accelerator, three doserates were exposed to the detector (6 Gy/min, 3 Gy/min and 1.5 Gy/min). The temperature measuring device was positioned at a distance of 80 cm from the target of the accelerator.

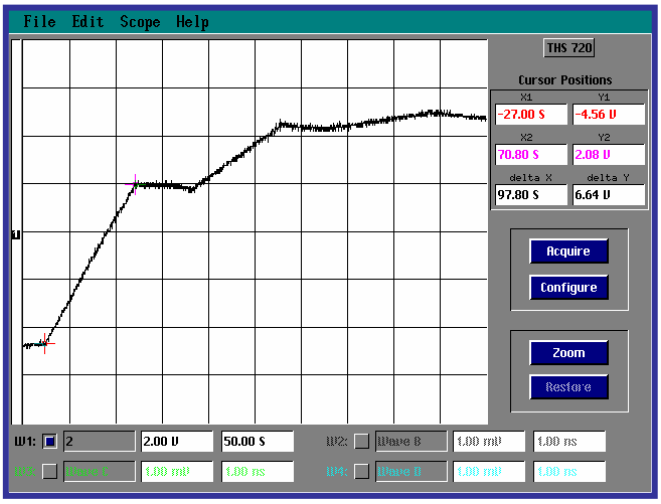

Fig. 3

The accuracy of the temperature measuring device is further visualized in figure 4, which shows the output voltage as a function of resistance change from 90 kΩ. The thermistors in the bridge were replaced by resistors with known values. God agreement was observed between the output voltage and the change in resistance.

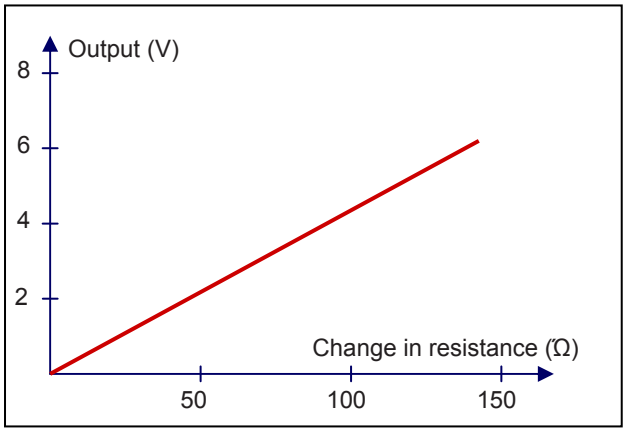

Fig. 4

III. Conclusions

This simple temperature measuring device was able to follow the temperature variation caused by radiation from a linear accelerator. To be able to use this system in the clinic for absolute dose measurement further work has to be done to isolate the detector from the ambient room temperature.

References

1. Domen Steve R (1980) Thermal diffusivity, specific heat and thermal conductivity of A-150 plastic. Phys Med Biol Vol 25 No 1 93-102.
2. McEwen M R and Duane S (2000) A portable calorimeter for measuring absorbed dose in the radiotherapy clinic. Phys Med Biol 45 3675-3691.
3. Williams A J and Roosser K E (2000) Development of the NPL Water Calorimeter. Proceedings of NPL Workshop of recent advancees in calorimetric absorbed dose standards ISSN 1369-6793 CIRM 42 130-137.

Author: Börje Blad
Institute:Department of Radiation Physics, University Hospital
Street: Klinikgatan 7
City: Lund
Country: Sweden
Email: borje.blad@skane.se

Effect of Modulated Microwave Radiation on Brain Electrical Oscillations

H. Hinrikus, M. Bachmann, J. Lass, A. Suhhova, V. Tuulik

Department of Biomedical Engineering, Technomedicum of Tallinn University of Technology, Tallinn, Estonia

***Abstract*— The aim of this study was evaluation of the effect of modulated microwave exposure on human electroencephalographic (EEG) rhythms. The experiments were carried out on four different groups of healthy volunteers. The 450 MHz microwave radiation modulated at 7 Hz (first group, 19 subjects), 14 and 21 Hz (second group, 13 subjects), 40 and 70 Hz (third group, 15 subjects), 217 and 1000 Hz (fourth group, 19 subjects) frequencies was applied. The field power density at the scalp was 0.16 mW/cm^2. The calculated spatial peak SAR averaged over 1 g was 0.303 W/kg. Ten cycles of the exposure (1 min off and 1 min on) at fixed modulation frequencies were applied. Our results showed that microwave exposure increased the EEG energy at EEG frequencies lower or close to the modulation frequency. No effect was detected at EEG frequency bands higher than the modulation frequency. Statistically significant changes were caused by exposure in the EEG alpha and beta frequency bands; no significant effect was detected in the theta band. Rate of subjects with significant changes in the EEG was 16-33% in different groups.**

Keywords— **EMF effect, microwave exposure, EEG rhythm, non-thermal effect, modulated radiation.**

I. Introduction

Effects of microwave radiation on human brain physiology have become of major interest with increasing applications of telecommunication devices [1, 2]. During recent decades, the reports of possible non-thermal microwave effects are often contradictory and effect of low-level electromagnetic field (EMF) on human nervous system has become a subject of discussions.

Alterations induced by EMF in the electroencephalographic (EEG) signals can be an efficient measure of the EMF effect on brain bioelectrical activity and therefore frequently used for evaluation. Several investigators have reported that exposure to a low-level microwave produces alterations in the EEG signal and/or brain behaviour [3, 4, 5, 6, 7, 8]. However, some authors were unable to confirm their previous findings in their later studies [9]. The conclusion reported in other studies is that the exposure to microwave does not alter the resting EEG [10].

Telecommunication devices use modulated microwave radiation. Modulation has been shown to play crucial role in microwave effects on EEG and cerebral blood flow: only modulated microwave radiation produced changes in human EEG and cerebral blood flow intensity [11]. Pulse-modulated EMF exposure enhanced EEG power in the alpha frequency range [7, 11]. Exposure to EMF without pulse modulation did not enhance power in the waking or sleep EEG [12]. However, the observed effects of pulse-modulated microwave were subtle and the underlying mechanisms remain unknown.

Most of experiments have been performed at one modulation frequency or using mobile phone with complex spectrum of modulation frequencies. Diversity in experimental conditions causes difficulties in comparison of the experimental results at different modulation frequencies.

The aim of this study was evaluation of the effect of modulated microwave exposure on the EEG at different modulation frequencies in identical experimental conditions. To accomplish this purpose, experiments at modulation frequencies 7, 14, 21, 40, 70, 217 and 1000 Hz were performed using the same exposure conditions and methods for EEG analysis. Relative changes caused by modulated microwaves in power of the EEG theta, alpha and beta rhythms were selected as a measure.

II. Methods and equipment

A. Subjects

The experiments were carried out on four different groups of healthy young volunteers. The first group consisted of 19 persons (aged 19-23), 10 male and 9 female; the second group of 13 persons (aged 21-30), 4 male and 9 female; the third group of 15 persons (aged 21-24), 8 male and 7 female and the fourth group of 19 persons (aged 21-24), 8 male and 11 female

All the subjects selected were without any medical or psychiatric disorders. The persons who declared tiredness or sleepiness before the experiment were excluded. After the recordings, they were asked how they were feeling during the experiment. The subjects reported neither alertness nor any strain experienced during the recordings. The experiments were conducted with understanding and written consent of each participant.

O. Dössel and W.C. Schlegel (Eds.): WC 2009, IFMBE Proceedings 25/III, pp. 585–588, 2009.
www.springerlink.com

During the experiments the subjects were in dark laboratory room, lying in a relaxed position, eyes closed and ears blocked.

All subjects passed the experimental protocols with exposure and sham. The subjects were not informed of their exposure during the experiment; however, they were aware of the possibility of being exposed. During each double-blind test session, the exposed and sham-exposed subjects were randomly assigned by computer. A computer also randomly assigned the succession of modulation frequencies.

The study was conducted in accordance with the Declaration of Helsinki and was formally approved by the local Medical Research Ethics Committee.

B. Microwave exposure

Microwave exposure was provided identical for all recordings; the only exception was difference in modulation frequencies. Modulation at 7 Hz was applied: for the first, at 14 and 21 Hz for the second, at 40 and 70 Hz for the third and at 217 and 1000 Hz for the fourth group of subjects. Exposure conditions were the same for all subjects in the group.

The 450 MHz electromagnetic radiation was generated by the Rhode & Swartz signal generator model SML02. The microwave signal was 100% pulse-modulated by the pulse modulator SML-B3 duty cycle 50% and amplified by the Dage Corporation power amplifier model MSD-2597601. The 1W electromagnetic radiation output power was guided by a coaxial lead to the 13cm rod quarter-wave antenna, located 10 cm from the skin on the left side of the head. The spatial distribution of the electromagnetic radiation power density was measured by the Chauvin Arnoux Fieldmeter C.A 43 field strength meter. The measurements were performed by the Central Physical Laboratory of the Estonian Health Protection Inspection. During the experiments, the stability of the electromagnetic radiation level was monitored by the IC Engineering Digi Field C field strength meter. Estimated from the measured calibration curves, the average field power density of the modulated microwave at the skin from the left side of the head was 0.16 mW/cm^2. The specific absorption rate (SAR) was calculated using SEMCAD software. The calculated spatial peak SAR averaged over 1 g was 0.303 W/kg.

C. Recording protocol and equipment

All subjects completed the session with microwave exposure and sham.

The protocol with exposure lasted 40 minutes (20 minutes for the first group), during which the resting eyes closed EEG was continuously recorded. Twenty exposure cycles were applied during the recording: in every even minute the radiation modulated at fixed modulation frequency was switched on and during every odd minute switched off. The first ten exposure cycles were performed at one and the last ten at second modulation frequency. Selection of 14 or 21 Hz, 40 or 70 Hz and 217 or 1000 Hz as first or second modulation frequency was randomly assigned. Ten exposure cycles were applied for the first group where only modulation only at 7 Hz frequency was applied.

Sham recording session used the same protocol, except that the microwave power was switched off.

For each recording session, the exposure conditions (exposed or sham) were randomly assigned between subjects.

The Cadwell Easy II EEG measurement equipment was used for the EEG recordings. The EEG was recorded using 9 electrodes, which were placed on the subject's head according to the international 10-20-electrode position classification system. The channels for analysis were chosen to cover the entire head: frontal- FP1, FP2; temporal- T3, T4; parietal- P3, P4; occipital- O1, O2; and the reference electrode Cz. The EEG recordings were stored on a computer with a 400 Hz sampling frequency.

The artifacts at the modulation frequencies were removed from the EEG signals by off-line filtering during the pre-processing of the signals in the LabVIEW programming and signal-processing environment.

D. EEG analysis

Relative changes in the recorded EEG signal between the cycle segments with and without exposure were selected as a measure for detection of the microwave effect on the EEG rhythms.

The powers of four basic EEG frequency bands: theta (4 – 6,8 Hz), alpha (8 – 13 Hz), beta1 (15 – 20 Hz) and beta2 (22 – 38 Hz) were extracted from the total EEG band 0.5 – 48 Hz by filtering. Such a selection excluded the modulation frequencies 7, 14, 21, 70, 217 and 1000 Hz and their harmonics as well as related artifacts from the further analysis. Elliptic band-stop filters with an attenuation of 50 dB in the stop-band were used. The energies of the different EEG frequency bands (theta, alpha, beta1 and beta2) were analyzed separately.

Next, the average energies for segments with and without microwave were compared. Comparison intervals were selected as the first 30 seconds from the beginning of reference segment and microwave exposed segment of the each exposure cycle. The relative change in the energy of the recording segments with and without microwave was selected for further analysis. Parameter S_c for a cycle was calculated as follows:

$$S_c = \left(\frac{s_2}{s_1} - 1 \right) \times 100\% \quad (1)$$

where s_1 and s_2 were the average energies inside the comparison segments without and with microwave exposure respectively. For sham recordings the same parameter was calculated for comparison segments as first 30 seconds of even and first 30 seconds of odd minutes of the recordings.

The effect of microwave exposure on a subject was calculated by averaging the values of parameter S_c over ten cycles of exposure at the fixed modulation frequency. The parameter S_n characterizing the relative change for a subject was calculated as

$$S_n = \frac{1}{10} \sum_{c=1}^{10} S_c \quad (2)$$

where S_c is the value of elative changes calculated according to (1) for a cycle.

The Student t-test was used for statistical evaluation. The Bonferroni correction for multiple-comparisons was applied with a 0.05 confidence level.

III. Results and discussion

Graphs of relative changes caused by microwave exposure in the power of different EEG rhythms at different modulation frequencies in P3-P4 channels for all groups are presented in Fig. 1a, b, c, d. Results for sham recordings of all four groups are presented for comparison. Obvious is increase in the EEG power in all frequency bands (except EEG theta band) at all modulation frequencies (except 1000 Hz) compared to sham exposure. Statistically significant changes were detected not for all modulation frequencies and not for all subjects. The rate of affected subjects varies from 16 to 33% in different groups.

Relative changes caused by microwave in the EEG theta power are close to these in sham recordings and no significant changes detected at any modulation frequency (Fig. 1a). The highest values have microwave produced changes in the EEG alpha power (Fig. 1b). However, statistical evaluation revealed significant changes only at 14 and 21 Hz modulation frequencies. The values of relative changes are less for the EEG beta1 frequency band, but statistically significant changes are revealed at four modulation frequencies: 14, 21, 40 and 70 Hz (Fig, 1c). Microwave exposure causes statistically significant changes at four modulation frequencies also in the EEG beta2 frequency band (Fig, 1d). However, the modulation frequencies are different: 21, 40, 70 and 217 Hz.

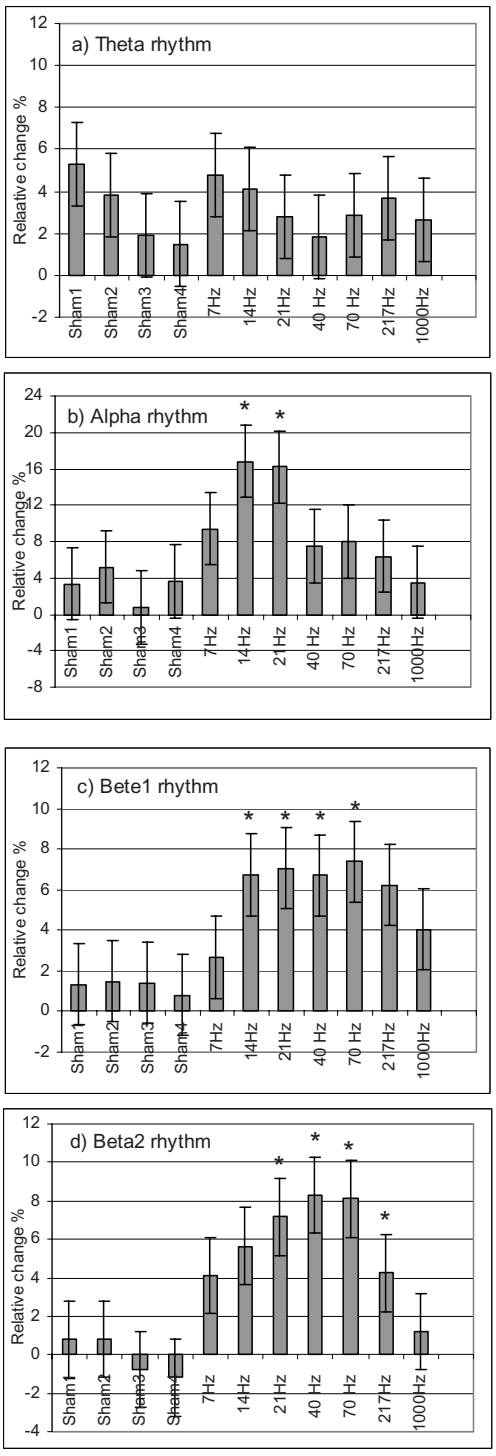

Fig. 1. Calculated value of relative changes in the EEG power caused by microwave exposure in different EEG frequency bands at different modulation frequencies averaged over each group of subjects. Statistically significant after Bonferroni correction ($p<0.05$) marked *.

It seems characteristic that the frequency of the affected EEG band increases with increase of the modulation frequency. Statistically significant changes occurred at modulation frequencies close or higher that the EEG rhythm frequency. No significant changes were revealed at 7 and 1000 Hz modulation frequencies. The EEG theta rhythm was not affected by microwave exposure. These results are in good agreement with our previous findings [13].

The experimental data showed that changes in the EEG rhythms caused by pulse-modulated low-level microwave exposure are different at different modulation frequencies. Frequency dependence of the effect confirms that the influence of microwave radiation on EEG can not be thermal, because our experimental conditions (100% pulse modulation, 50% duty cycle) provide constant microwave energy and consequently heating at all modulation frequencies.

The level of applied microwave exposure was much lower than recommended 1999/519/EC limitations of exposure of the general public based on thermal effect

Our results support the idea that the physiological influence of the microwave exposure on the cortical activation depends on the modulation frequency. This conclusion is in good agreement with the results reported by other authors who have demonstrated that the exposure to a pulse-modulated microwave alters brain physiology, as reflected in the regional changes of cerebral blood flow. Furthermore, the modulation paradigm was shown to be critical for microwave-induced increases of cerebral blood flow [11].

IV. CONCLUSIONS

Our experimental results show, that exposure to pulse modulated 450 MHz microwave radiation alters brain electrical oscillations. Furthermore, the frequencies of excited EEG bands are related to the modulation frequency of radiation.

ACKNOWLEDGMENT

This study was supported by the Estonian Science Foundation Grant No 6632, by the Estonian targeted financing project SF0140027s07, and by the European Union through the European Regional Development Fund.

REFERENCES

1. Cook CM, Saucier DM, Thomas AW, Prato FS (2006) Exposure to ELF magnetic and ELF-modulated radiofrequency fields: the time course of physiological and cognitive effects observed in recent studies (2001-2005). Bioelectromagnetics 27: 613-627.
2. Valentini E, Curcio G, Moroni F, Ferrara M, De Gennaro L, Bertini M. (2007) Neurophysiological Effects of Mobile Phone Electromagnetic Fields on Humans: A Comprehensive Review. Bioelectromagnetics 28: 415-432
3. Huber R, Graf T, Cote KA, Wittmann L, Gallmann E, Matter D, Schuderer J, Kuster N, Borbely AA, Achermann P (2000) Exposure to pulsed high-frequency electromagnetic field during waking affects human sleep EEG. NeuroReport 11: 3321-3325
4. Krause CM, Sillanmäki L, Koivisto M, Häggqvist A, Saarela C, Revonsuo A, Laine M, Hämäläinen H (2000) Effects of electromagnetic field emitted by cellular phones on the EEG during a memory task. NeuroReport 11: 761-764
5. Lass J, Tuulik V, Ferenets R, Riisalo R, Hinrikus H (2002) Effects of 7 Hz-modulated 450 MHz electromagnetic radiation on human performance in visual memory tasks. International Journal of Radiation Biology. 78: 937-944
6. Hinrikus H, Parts M, Lass J, Tuulik V (2004) Changes in human EEG caused by low-level modulated microwave stimulation. Bioelectromagnetics 25: 431-440
7. Curcio G, Ferrara M, Moroni F, D'Inzeo G, Bertini M, De Gennaro L (2005) Is the brain influenced by a phone call? An EEG study of resting wakefulness. Neuroscience Resesrch. 53: 265–270
8. Bachmann, M, Kalda, J, Lass, J, Tuulik, V, Säkki, M, Hinrikus, H (2005) Non-linear analysis of the electroencephalogram for detecting effects of low-level electromagnetic fields. Med Biol Eng Comput 43: 142–149
9. Krause CM, Haarala C, Sillanmaki L, Koivisto M, Alanko K, Revonsuo A, Laine M, Hamalainen H (2004) Effects of electromagnetic field emitted by cellular phones on the EEG during an auditory memory task: a double blind replication study. Bioelectromagnetics 25: 33-40
10. Krause CM, Sillanmäki L, Koivisto M, Häggqvist A, Saarela C Revonsuo A, Laine M, Hämäläinen H (2000) Effects of electromagnetic fields emitted by cellular phones on the electroencephalogram during a visual working memory task. International Journal of Radiation Biology. 76: 1659-1667
11. Huber R, Treyer V, Schuderer J, Berthold T, Buck A, Kuster N, Landolt H P, Achermann P (2005) Exposure to pulse-modulated radio frequency electromagnetic fields affects regional cerebral blood flow. European Journal of Neuroscience. 21: 1000–1006
12. Huber R, Treyer V, Borbely AA, Schuderer J, Gottselig JM, Landolt HP, Werth E, Berthold T, Kuster N, Buck A, Achermann P (2002) Electromagnetic fields, such as those from mobile phones, alter regional cerebral blood flow and sleep and waking EEG. Journal of Sleep Research. 11: 289–295
13. Hinrikus H, Bachmann M, Lass J, Tomson R, Tuulik V (2008) Effect of 7, 14 and 21 Hz modulated 450 MHz microwave radiation on human electroencephalographic rhythms. International Journal of Radiation Biology 84: 69-79

Use macro [author address] to enter the address of the corresponding author:

Author: Hiie Hinrikus
Institute: Tallinn University of Technology
Street: Ehitajate Rd 5
City: Tallinn
Country: Estonia
Email: hiie@cb.ttu.ee

Dosimetric impact of accidental irradiations on radiotherapy facility workers and considerations on personal monitoring

D. Fondevila[1], S. Rivera[1], R. Sansogne[1], V. Suarez[1], R. Barrientos[2], J. Vita[3], S. Pereira Duarte[3], M. L. Filomia[1], L. Rafailovici[1]

[1] Vidt Centro Médico, Buenos Aires, Argentina
[2]Instituto de Radiaciones Salta. Salta, Argentina
[3] Centro de Oncología y Radioterapia de Mar del Plata, Mar del Plata, Argentina

Abstract— **The possibility of an accidental irradiation of a linac-based radiotherapy facility worker always exists if an operator remains in avertedly within the treatment room when the radiation beam is turned on.**

Two distinct irradiation situations can be identified: (1) the operator passes partially within the primary radiation beam, (2) the operator only receives secondary radiation (mainly head leakage and patient scatter radiation).

This work estimates, by theoretical calculation and experimental verification, the resulting effective doses derived in these situations for different conservative irradiation scenarios and discusses the resulting implications for occupational dose monitoring.

A number of relevant conclusions can be mentioned:

These accidental irradiations can never pose a deterministic radiation effect on the worker due to the fractionated nature of the radiotherapy treatment scheme. It can be seen that for case (1) situations, being this the worst irradiation condition, the effective dose will most likely be below the ICRP annual dose limit for normal working conditions (20mSv). In these situations the whole body personal dosimetry monitoring device will give extremely inexact results due to the highly inhomogeneous nature of the volume irradiation. Careful consideration must be given to these cases in order avoid misinterpretations of the personal dosimeter readings. A reconstruction of the specific irradiation conditions will most likely be needed in order to arrive at a good theoretical estimate of the effective dose.

For case (2) situations, calculated values range from 4mSv to 0.1mSv under conservative working hypothesis. Nevertheless, experimental measurements have showed a number of factors that lower these estimates, causing a large number of the irradiation situations to go dosimetrically unnoticed by the personal dosimetry monitoring system due to their low magnitude (<0.1mSv). This may lead the uninformed radiation protection officer or operator to unjustifiably distrust the results of the personal dosimetry system.

Keywords— **Accidental irradiations, radioprotection, personal dose monitering.**

I. Introduction

The radioprotection of workers of linac-based radiotherapy facilities rests mainly on the adequate design of the treatment vault shielding and the correct operation of the door safety interlock for beam interruption when an intrusion occurs. Nevertheless, the possibility of an accidental irradiation always exists if an operator remains in avertedly within the bunker when the beam is turned on.

Two distinct situations can be identified for accidental irradiations within the treatment vault:

Case (1): The operator passes partially within the primary radiation beam.
Case (2): The operator only receives secondary radiation (mainly head leakage and patient scatter radiation)

This work estimates, by theoretical calculation and experimental verification, the resulting effective doses derived in these situations for different conservative irradiation scenarios and discusses the resulting implications for occupational dose monitoring.

II. Materials and Methods

Case (1): Primary radiation beam irradiation

It is assumed that the worker places his body partially within the primary radiation beam at 1m from the isocenter past the patient plane for a total of 1Gy patient dose for that specific beam. Patient attenuation is considered and the ICRP N°103 [1] tissue weighting factors are used for assessing the resulting effective dose.

Case (2): Secondary radiation situations

Secondary radiation within the treatment vault has two main components: Head leakage radiation (A) and patient scattered radiation (B)
(10MV or higher energy accelerators are excluded form this analysis. Neutron production was not considered.)

O. Dössel and W.C. Schlegel (Eds.): WC 2009, IFMBE Proceedings 25/III, pp. 589–592, 2009.
www.springerlink.com

A. Head leakage radiation component

The NCRP 151 document [2] formulation for head leakage radiation evaluation can be adapted for in-treatment room worker effective dose (Dl) due to an accidental irradiation as

$$D_l = \frac{D_{patient} x\, 10^{-3}}{d_l^2}$$

Where,

$D_{patient}$ = patient absorbed dose for one irradiation beam [Gy]

d_l = distance to the accelerator head [m]

D_l = effective dose [Sv] (The equivalent and effective doses are taken as equal just as a conservative working assumption.)

B. Patient scatter radiation component

The NCRP 151 document [2] formulation for patient scatter radiation evaluation can be adapted for in- treatment room worker effective dose (D_{ps}) due to an accidental irradiation as

$$D_{ps} = \frac{D_{patient}\, a}{d_{sca}^2\, d_{\sec}^2}\left(\frac{F}{400}\right)$$

Where,

$D_{patient}$ = patient absorbed dose for one irradiation beam [Gy]

d_{sca} = distance from the x-ray target to the scattering object (patient) [m]

d_{sec} = distance from the scattering object (patient) to the calculation point [m]

a = scatter fraction of the primary–beam absorbed dose that scatters from the patient at a particular angle [adim]

F = field area at mid-depth of the patient at 1m [cm^2]

III. IRRADIATION SCENARIOS

It was assumed that the worker involved in the accidental irradiation remains within the treatment room at a specified point during the whole treatment time for that beam. We propose a patient dose of 1Gy for the hypothetical irradiation, considering that 2Gy is a typical treatment dose and that the total daily dose will most likely be administered with a two or more field composition. A 15cm x 15cm field size was assumed as a typical treatment field (F = 225 cm2).

Two different geometric irradiation scenarios were assumed:

Scenario I: Downward oriented beam (Gantry on top). In this case the scatter angle is 90°, and different distances to the isocenter were evaluated.

Scenario II: Laterally oriented beam.(Gantry at 90° or 270° depending on the treatment machine gantry angle convention). Calculation point rotates around the isocenter at a fixed distance (for example, 1, 2 and 3 meters) and at a height of the isocenter from the floor.

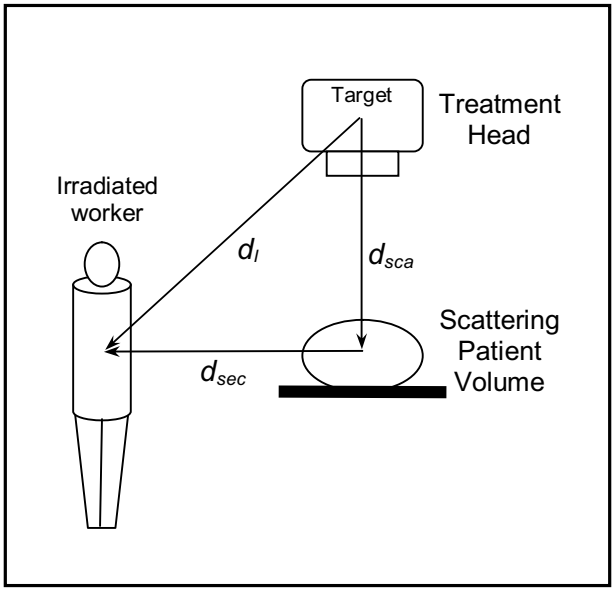

Figure 1: Diagram with the calculation geometries for *Scenario I* situations showing a cross sectional view of the treatment room containing the radiation target, the scattering patient volume and the facility worker involved in the accidental irradiation. A downward oriented beam is assumed with a 90° scatter angle. Distances from the x-ray target to the scattering patient volume (d_{sca}), from the scattering object to the calculation point (d_{sec}) and from the x-ray target (leakage source) to the calculation point (dl) are shown.

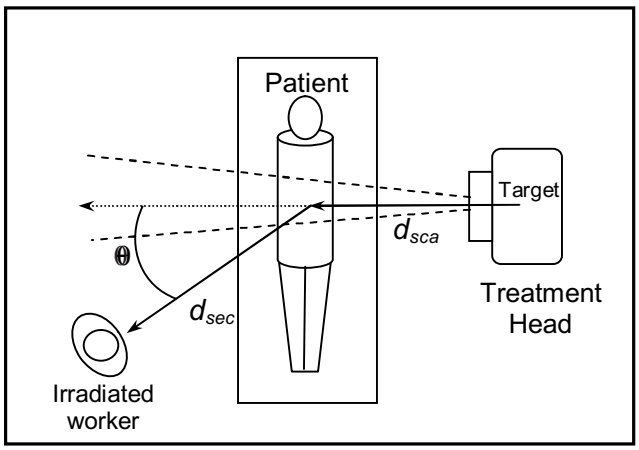

Figure 2: Diagram with the calculation geometries for *Scenario II* showing a floor plant view of the treatment room containing the radiation target, the scattering patient volume and the facility worker involved in the

accidental irradiation. Laterally oriented beam and a fixed distance to the isocenter is assumed with a varying scatter angle (θ). Distances from the x-ray target to the scattering patient volume (d_{sca}), from the scattering object to the calculation point (d_{sec}) are shown.

IV. RESULTS

Case (1): Conservative estimates of the effective dose for these situations show values below the 20mSv level.

Case (2): The head leakage and patient scatter dose calculations are shown in Tables 1, 2, 3 and 4, along with the corresponding calculation parameters for scenarios I and II.

Table 1: Values for calculated leakage radiation component (Dl), patient scatter component (Dps) and total dose (Dtotal) are shown for *Scenario I* with different geometric conditions, and the following parameter values: d_{sca}=1m; a = 4.26x10^{-4} (90° scatter angle for 6MVmost conservative assumption); F=225cm^2 and $D_{patient}$=1Gy. (See *Scenario I* layout in Fig. 1.)

Dtotal (mSv)	Dl (mSv)	Dps (mSv)	d sec (m)	dl (m)
1.76	0.8	0.96	0.5	1.1
0.74	0.50	0.24	1	1.4
0.41	0.31	0.11	1.5	1.8
0.26	0.20	0.06	2	2.2
0.18	0.14	0.04	2.5	2.7
0.13	0.10	0.03	3	3.2
0.10	0.08	0.02	3.5	3.6

Table 2: Values for calculated leakage radiation component (Dl), patient scatter component (Dps) and total dose (Dtotal) are shown for *Scenario II* with different geometric conditions, and the following parameter values: d_{sca}=1m; d_{sec}=1m; F=225cm^2 and $D_{patient}$=1Gy. Values of the scattering fraction (a) were taken from [3] for 6MV as a conservative working assumption. (See *Scenario II* layout in Fig. 2.)

Dtotal (mSv)	Dl (mSv)	Dps (mSv)	θ (°)	a (adim)	dl (m)
1.83	0.27	1.56	30	2.77E-03	1.9
1.07	0.29	0.78	45	1.39E-03	1.8
0.79	0.33	0.46	60	8.24E-04	1.7
0.74	0.5	0.24	90	4.26E-04	1.4
1.88	1.71	0.17	135	3.00E-04	0.8
3.89	3.73	0.16	150	2.87E-04	0.5

Table 3: Values for calculated leakage radiation component (Dl), patient scatter component (Dps) and total dose (Dtotal) are shown for *Scenario II* with different geometric conditions, and the following parameter values: d_{sca}=1m; d_{sec}=2m; F=225cm^2 and $D_{patient}$=1Gy. Values of the scattering fraction (a) were taken from [3] for 6MV as a conservative working assumption. (See *Scenario II* layout in Fig. 2.)

Dtotal (mSv)	Dl (mSv)	Dps (mSv)	Angle (°)	a (adim)	dl (m)
0.51	0.12	0.39	30	2.77E-03	2.9
0.33	0.13	0.2	45	1.39E-03	2.8
0.26	0.14	0.12	60	8.24E-04	2.6
0.26	0.2	0.06	90	4.26E-04	2.2
0.50	0.46	0.04	135	3.00E-04	1.5
0.69	0.65	0.04	150	2.87E-04	1.2

Table 4: Values for calculated leakage radiation component (Dl), patient scatter component (Dps) and total dose (Dtotal) are shown for *Scenario II* with different geometric conditions, and the following parameter values: d_{sca}=1m; d_{sec}=3m; F=225cm^2 and $D_{patient}$=1Gy. Values of the scattering fraction (a) were taken from [3] for 6MV as a conservative working assumption. (See *Scenario II* layout in Fig. 2.)

Dtotal (mSv)	Dl (mSv)	Dps (mSv)	Angle (°)	a (adim)	dl (m)
0.24	0.07	0.17	30	2.77E-03	3.9
0.16	0.07	0.09	45	1.39E-03	3.8
0.13	0.08	0.05	60	8.24E-04	3.6
0.13	0.10	0.03	90	4.26E-04	3.2
0.19	0.17	0.02	135	3.00E-04	2.4
0.23	0.21	0.02	150	2.87E-04	2.2

V. DISCUSSION

Experimental verification was carried out using an ionizing chamber ambient dose detector in integrating mode during actual patient irradiations in various accelerator facilities as to check the overall validity of these results. It was seen from these measurements that a number of factors come in to play during real patient irradiations that lower the dose values with respect to these theoretical estimates.

International accelerator design standards require leakage radiation to be below 0.1% of the useful beam radiation [4]. Nonetheless it is a well known fact [5] that equipment manufactures oftentimes protect their machines to higher standards than legally required (0.05% or less of the useful beam). Values as low as 0.02% of the useful beam were measured in this work, therefore reducing by a factor of 5 the head leakage component of these theoretical estimates.

Attenuation of patient scatter radiation within the same patient lowers this radiation component, as for example with 90° scatter. It is noted that an excess of 10cm to 15cm of attenuating tissue in the exit of the scattered

radiation will reduce this component to roughly 75% of the estimated value for a 6MV beam.

Objects in the line of the irradiated worker to the x-ray target (as for example, patient, treatment couch, etc.) will lower the estimated head leakage component by a factor proportional to the attenuation of the radiation in that object. It is noted that roughly every 3cm in steel will lower this component by a factor of 2 (TVL=10cm of steel for 6MV primary beam [2]).

Other factors lowering the theoretical estimates are:

It is highly unlikely that an operator will remain unaware of the BEAM ON condition when the irradiation begins therefore remaining within the bunker during the whole treatment time for that application. Note that once the operator enters the maze of the accelerator room on his way out, attenuation on the maze walls will make the exit transit dose negligible.

In the postulated hypothetical scenarios it was assumed that the worker remains within the bunker at the specified point for a total of 1Gy of patient dose. In modern radiotherapy with its multiple field composition this hypothesis is clearly overestimating.

VI. CONCLUSIONS

1. These accidental irradiations can never pose a deterministic radiation effect on the worker due to the fractionated nature of the radiotherapy treatment scheme.
2. For irradiations occurring partially within the primary radiation beam (worst irradiation scenario) the effective doses will most likely be below the ICRP annual dose limit for normal working conditions (20mSv).
3. In these primary beam irradiations the whole body personal dosimetry monitoring device will give extremely inexact results due to the highly inhomogeneous nature of the volume irradiation. Careful consideration must be given to these cases in order avoid misinterpretations of the real situation. A reconstruction of the specific irradiation conditions will most likely be needed in order to arrive at a good theoretical estimate of the effective dose.
4. A large number of the irradiation situations will go dosimetrically unnoticed by the personal dosimetry monitoring system due to their low magnitude (<0.1mSv). This may lead the uninformed radiation protection officer or operator to unjustifiably distrust the results of the personal dosimetry system, as was the case with the initial motivation of this investigation.

REFERENCES

[1] ICRP 2007. The 2007 Recommendations of the International Commission on Radiological Protection. ICRP Publication 103, Elsevier Ltd.

[2] National Council on Radiation Protection and Measurement, *Structural Shielding Design and Evaluation for Megavoltage X- and Gamma-Ray Radiotherapy Facilities, NCRP Report 151* (National Council on Radiation Protection and Measurements, Bethesda, Maryland, 2005).

[3] Taylor, P.L., Rodgers, JE. and Shobe, J. (1999) Scatter fractions from linear accelerators with x-ray energies from 6 to 24 MV. Med. Phyis, **26** (8)**,** 1442-1446.

[4] IEC (1981) Safety of Medical Electrical Equipment Part 2: Particular Requirements for Medical Electron Accelerators in the range 1MeV to 50MeV Publication 601-2-1 (International Electro-Technical Commission)

[5] IPEM (1997) The Design of Radiotherapy Treatment Room Facilities. The Institute of Physics and Engineering in Medicine. Report N°75

What Are the Radiation Risks to Communicate?

J.H. Hendry

Meadowside, Adlington, Macclesfield, UK

Abstract— **The types and levels of risk associated with certain ranges of radiation dose are summarised from recommendations of the International Commission on Radiological Protection in 2007. There are estimates of threshold doses for various lethal radiation-induced syndromes, and for reactions in various tissues and organs including the lens (concerning cataracts) and heart (cardiovascular disease) which are still being re-evaluated. Doses in diagnostic procedures are summarised and related to risk estimates for such doses. Fluoroscopy, cardiology and multiple-CT are the areas of diagnostic radiology where the level of dose may cause some concern. These concerns need to be placed in context with the benefits of the procedures, and with risks in other aspects of life.**

Keywords— **Risk estimates, threshold doses, diagnostic radiology.**

I. Categories of Radiation Risk: Stochastic Effects

In order to discuss radiation risks in the context of radiology it is necessary to summarise the types and levels of risk associated with certain ranges of doses.

Most adverse health effects of radiation exposure may be grouped in two general categories. The first category comprises 'stochastic' effects. These are cancer and heritable effects in individuals exposed to low doses, owing to mutation of single somatic cells, or heritable disease in their offspring due to mutation of single reproductive (germ) cells. Based upon cancer incidence data, from atomic bomb survivors and other sources, the risk of radiation-induced cancer is 5.5 % per sievert (Sv) for the whole population and 4.1 % for adult workers. The sievert is the special name for the unit of equivalent dose, which allows for the greater effectiveness of different radiation types compared to Cobalt-60 gamma rays (dose in gray, Gy); the unit of both sievert and gray is joule per kilogram. For radiation-induced heritable disease up to the second generation the risk is very much smaller at 0.2 % per Sv for the whole population and 0.1 % per Sv for adult workers. For doses of 1 to a few Sv, these risk values are known fairly accurately. For lower doses, a direct proportionality is assumed between risk and dose. This is widely debated, but the ICRP in 2007 judged that there were no good scientific reasons to include the possibilities of supra-linear dose responses or of a low dose threshold in cancer risk calculations for the purposes of radiological protection. On this basis it was recommended that the linear-no-threshold model, should remain as a prudent basis for the practical purposes of radiological protection at low doses and low dose rates. Also there is a judged factor of 2 that generalises the usually lower biological effectiveness (per unit of dose) of radiation exposures at low doses and low dose rates, as compared to exposures at high doses and high dose rates. Below around 100 mSv there are no robust data available to substantiate the extrapolation, and at such low doses the risk estimates should be considered as projections.

There are some clear sex differences in risk, and also some age-related differences. The risk of radiation-induced cancer is higher in children than in adults. This is partly because children are more sensitive. Also, cancer is a multistage process that takes many years, often decades, to develop and children have a longer postirradiation life for that development than older adults. Genetic susceptibility to radiation-induced cancer involving strongly expressed genes was judged to be too rare to appreciably distort estimates of population risk; the potential impact of common but weakly expressing genes remained uncertain. Cancer risk following in-utero exposure was judged to be no greater than that following exposure in early childhood. Weighting factors are also available for individual tissues and organs.

II. Categories of Radiation Risk: Tissue Reactions (Deterministic Effects).

The second category of adverse health effects of radiation exposure comprises harmful tissue reactions (so-called 'deterministic' effects), which are those due in large part to the killing/ malfunction of populations of cells following high doses. Because the effects are cell-population based, rather than single-cell based, a threshold dose would be expected. This is the dose at which sufficient cells in the tissue or organ have been injured in order to damage its function. The more cells are injured, the severer is the functional injury, and hence the severity of injury, not just its frequency, increases with increasing dose. Estimates of threshold doses are now available for various lethal radiation-induced syndromes, and for various tissues and organs (Tables 1,2). Substantially less than 1% of a general population is very radiosensitive because of inherited mutations in

O. Dössel and W.C. Schlegel (Eds.): WC 2009, IFMBE Proceedings 25/III, pp. 593–595, 2009.
www.springerlink.com

important DNA damage-sensing or repair genes. Dose responses for in-utero radiation-induced tissue reactions, malformations and neurological effects were judged to show dose thresholds above around 100 mGy; uncertainty remained on the induction of IQ deficits but at low doses the risk was judged to be of no practical significance. It was also concluded that risks of non-cancer disease at low doses remained most uncertain and no specific judgement was possible.

Table 1. Estimates of the thresholds for deterministic effects in the adult human testes, ovaries, lens and bone marrow [1]

	Threshold		
Tissue and effect	Total dose received in a single brief exposure (Gy)	Total dose received in highly fractionated or protracted exposures (Gy)	Annual dose rate if received yearly in highly fractionated or protracted exposures for many years (Gy y^{-1})
Testes			
Temporary sterility	0.15	NA	0.4
Permanent sterility	3.5-6.0	NA	2.0
Ovaries			
Sterility	2.5-6.0	6.0	>0.2
Lens			
Detectable opacities	0.5-2.0	5	>0.1
Visual impairment (Cataract)[1]	5.0	>8	>0.15
Bone marrow			
Depression of hematopoiesis	0.5	NA	>0.4

[1]Under revision.

Two tissue reactions where the risk values are being re-evaluated, are cataracts and cardiovascular disease. The data for the Chernobyl clean-up workers, supported by other recent clinical data, argue against the current guidelines for a putative radiation dose–effect threshold for cataract development of 5 Gy for protracted doses. Instead, the data indicate that any threshold for cataracts is several times lower than that upon which current permissible exposure limits are based; the upper-limit threshold dose is about 0.7 Gy. For cardiovascular disease, recently analysed data for the atomic bomb survivors and various groups of patients receiving scattered doses to the heart from radiotherapy, could indicate a threshold dose of only a few Gy.

Table 2. Projected threshold estimates of the acute absorbed doses for 1% incidences of morbidity and mortality involving adult human organs and tissues after whole body gamma ray exposures [1]

Effect	Organ/tissue	Time to develop effect	Absorbed dose (Gy)[a]
Morbidity:			*1% Incidence*
Temporary sterility	Testes	3-9 weeks	~0.1
Permanent sterility	Testes	3 weeks	~6
Permanent sterility	Ovaries	< 1week	~3
Depression of blood-forming process	Bone marrow	3-7 days	~0.5
Main phase of skin reddening	Skin (large areas)	1-4 weeks	<3-6
Skin burns	Skin (large areas)	2-3 weeks	5-10
Temporary hair loss	Skin	2-3 weeks	~4
Cataract (visual impairment)	Eye	Several years	~1.5[b]
Mortality:			
Bone marrow syndrome:			
- without medical care	Bone marrow	30-60 days	~1
- with good medical care	Bone marrow	30-60 days	2-3
Gastro-intestinal syndrome:			
- without medical care	Small intestine	6-9 days	~6
- with conventional medical care	Small intestine	6-9 days	>6
Pneumonitis	Lung	1-7 months	6

(i) [a]Most values rounded to nearest Gy; ranges indicate area dependence for skin and differing medical support for bone marrow.
[b]Preliminary new value suggested, still under re-evaluation.

III. DOSES IN DIAGNOSTIC PROCEDURES

Doses in diagnostic procedures (Table 3) are usually kept as low as possible. Fluoroscopy can deliver high doses when used repeatedly, and there have been severe cases of skin lesions reported. Accumulated doses in repeated nuclear cardiology procedures can be around 60 mSv or higher, and when used for arrhythmia ablation, doses can be 1 Gy with a few percentage of patients getting more than 3 Gy. CT has become much more widespread, often with multiple scans on patients. A recent large study estimated cumulative radiation exposure and lifetime attributable risk (LAR) of radiation-induced cancer from CT scanning of adult patients [3]. The cohort comprised 31,462 patients who underwent diagnostic CT in 2007 and had undergone

190,712 CT examinations over the prior 22 years. Each patient's cumulative CT radiation exposure was estimated by summing typical CT effective doses. Thirty-three percent of patients underwent five or more lifetime CT examinations, and 5% underwent between 22 and 132 examinations. Fifteen percent received estimated cumulative effective doses of more than 100 mSv, and 4% received between 250 and 1375 mSv. Associated LAR had mean and maximum values of 0.3% and 12% for cancer incidence and 0.2% and 6.8% for cancer mortality, respectively. CT exposures were estimated to produce 0.7% of total expected baseline cancer incidence and 1% of total cancer mortality. Seven percent of the cohort had estimated LAR greater than 1%, of which 40% had either no malignancy history or a cancer history without evidence of residual disease.

Table 3. Doses in some diagnostic procedures (summarised from [2])

	Dose
Mammography	2 mGy to breast
Diagnostic PET imaging	Up to 7 mGy to uterus
Cerebral angiography	10 mGy
Nuclear medicine diagnosis	Up to 13 mGy to body, up to 20 mGy to gonads
Fluoroscopy	22-45 mGy per minute, up to 20 minutes
Multiple head scan CT	40-60 mGy average
Multiple body scan CT	10-40 mGy average
CT fluoroscopy	0.2-0.5 Gy to skin
Diagnostic catheterization	0.7-2.2 Gy to skin, multiplied by number of procedures

IV. RADIATION RISKS IN CONTEXT

Radiation risks in radiological procedures need to be considered regarding the benefits of the procedures, and in context with other risks. A 2% risk of a fatality in workers in mines or agriculture over a lifetime (Table 4), is a similar projected lifetime risk of a radiation-induced cancer for a young adult receiving around 400 mSv. This dose would be received by a few percentage of patients receiving multiple CT body scans. The particular patients in this percentage cannot be identified, because of the probabilistic/stochastic nature of radiation-induced cancer. This is different from the tissue reactions after higher doses like in fluoroscopy, where all patients given a certain high dose will have some sort of reaction although it may vary in severity between individuals. These aspects need to be communicated to patients in need of radiological procedures.

Table 4. Fatal accident rates for workers in the USA [2]

	Mean rate/ million/ year[1]	Converted to % Risk/ 50 years
All groups	90	0.45
Trade	40	0.20
Manufacture	60	0.30
Service	40	0.20
Government	90	0.45
Transport/ public utilities	240	1.20
Construction	320	1.60
Mines and quarries	430	2.15
Agriculture (1973-1980)	400	2.00

[1]Based on National Safety Council Accident Facts 1989

REFERENCES

1. International Commission of Radiation Protection Publication 103 (2008) 2007 recommendations of the ICRP, including Annexes on Quantities used in radiation protection, Biological effects of radiation, and Bases for judging the significance of the effects of radiation. Ann ICRP 37: issues 2-4, 1-332
2. Hall EJ and Giaccia AJ. (2006) Radiobiology for the radiologist. Lippincott, Williams and Wilkins, Philadelphia
3. Sodickson A, Baeyens PF, Andriole KP et al (2009) Recurrent CT, cumulative radiation exposure, and associated radiation-induced cancer risks from CT of adults. Radiology 251:175-184

Initiatives of IRPA in Risk Communication

Kenneth R. Kase, Ph.D

International Radiation Protection Association
c/o CEPN, 28 rue de la Redoute, F92260, Fontenay-aux-Roses, France

***Abstract*— The International Radiation Protection Association (IRPA) is engaged in efforts to provide guidance to its member societies for engaging stakeholders and for improving the radiation safety culture. Both of these activities involve aspects of risk communication. This paper describes the portions of these efforts that are relevant to risk communication and the approach taken by IRPA.**

Keywords— risk, communication, radiation protection, safety culture

I. Introduction

The International Radiation Protection Association (IRPA) is an association of 48 member societies representing 61 countries, with approximately 17,000 individual members. IRPA's role is described by the following:

- To provide a medium for communication and advancement of radiation protection throughout the world
- To encourage the establishment of radiation protection societies
- To support international meetings
- To encourage international publications dedicated to radiation protection
- To encourage the establishment and continous review of universally acceptable radiation protection standards and recommendations
- To encourage professional enhancement

Relative to risk communication, the first and the last points are the most important. To assist in advancing radiation protection IRPA has produced a document, "Guiding Principles for Radiation Protection Professionals on Stakeholder Engagement" [1] for use by its member societies. This document was adopted at the 2008 International Congress and societies have been asked to report on experience in implementation at 4 regional congresses in 2010. To encourage professional enhancement IRPA has initiated the development of a document on the subject of, "Improving Radiation Protection Culture". Both of these areas speak to risk communication.

II. Stakeholder Engagement

The guidance document on stakeholder engagement aims to aid members of IRPA Associate Societies in promoting the participation of all relevant parties in the process of reaching decisions involving radiological protection which may impact on the well being and quality of life of workers and members of the public, and on the environment. It provides guidance on developing trust and credibility throughout the decision making process in order to improve the sustainability of any final decisions. To accomplish these goals ten principles are enumerated:

1. Identify opportunities for engagement and ensure the level of engagement is proportionate to the nature of the radiation protection issues and their context.
2. Initiate the process as early as possible, and develop a sustainable implementation plan.
3. Enable an open, inclusive and transparent stakeholder engagement process.
4. Seek out and involve relevant stakeholders and experts.
5. Ensure that the roles and responsibilities of all participants, and the rules for cooperation are clearly defined
6. Collectively develop objectives for the stakeholder engagement process, based on a shared understanding of issues and boundaries.
7. Develop a culture which values a shared language and understanding, and favours collective learning.
8. Respect and value the expression of different perspectives.
9. Ensure a regular feedback mechanism is in place to inform and improve current and future stakeholder engagement processes.
10. Apply the IRPA Code of Ethics in their actions within these processes to the best of their ability.

Of these principles numbers 1, 3, 7 and 8 seem to be the most relevant to risk communication.

O. Dössel and W.C. Schlegel (Eds.): WC 2009, IFMBE Proceedings 25/III, pp. 596–598, 2009.
www.springerlink.com

To ensure the level of engagement is proportionate to the nature of the radiation protection issues and their context the complexity of the problem and its risk must be considered. The more complex the radiological protection problem and the more serious the risk, or the perception of the risk, the greater is the justifiable investment in engagement. Increasing awareness about the risks associated with some activities, concerns over environmental deterioration or loss of public confidence in some organisations are all likely to broaden or shift the range of stakeholders that need to be engaged.

Enabling an open, inclusive and transparent stakeholder engagement process requires including all the issues, sharing information and identifying trusted parties. All the issues entering into the decision should be considered, with openness, to identify, select and discuss any associated uncertainties. Information that is needed to build a collective understanding of the problem must be shared openly, starting in particular with risk communication. A responsible 'gatekeeper' or custodian' who is trusted and respected by all parties must be identified for the knowledge pool.

A culture that values a shared language and understanding is necessary to resolve questions about risk. Understanding can be seriously compromised by the use of jargon and technical language, acronyms and abbreviations. Consequently this must be avoided or the jargon explained and understood by all participants. A "common language" should be developed that is sufficiently precise scientifically not to offend the various experts but also sufficiently rooted in common, every-day experience to be meaningful to all those involved. Training of stakeholders leading to the creation of a shared knowledge base essential to a full understanding of the issues may be necessary.

Respecting and valuing the expression of different perspectives is extremely important when engaging various stakeholders, especially when discussing risk. Each participant in the process should recognise the uniqueness, different backgrounds, sensibilities and different perspectives of all participants. Evaluation of uncertainties in the assessments where expert opinion is divided should be undertaken in an open, accessible and clear manner. Finally, a climate of mutual respect and cooperation should be maintained.

III. Radiation protection Culture

Improving the radiation protection culture also includes some aspects of risk communication. A working group within the IRPA associated societies has been formed to develop a guidance document on this topic.

The purpose of a radiation protection culture involves vigilance and responsibility. We are currently faced with two major challenges both of which also impact the medical physics community. The first is to maintain a high degree of competence and to continue making progress in radiation protection. Second is to recognise that the use of radiation sources in new sectors, new companies or new countries may lead to some risk to the continued application of the ALARA principle in radiation protection. One way of preventing or at least mitigating this risk is to root radiation protection in the general culture and to develop a radiation protection culture.

Two questions arise, "What is a radiation protection culture?" and "How can it be developed?" A radiation protection culture includes training courses founded on a strong set of working knowledge to be transmitted; "reflex" attitude and transparency; and clear responsibilities assigned to regulators, operators and employees. A radiation protection culture is an integral part of a general safety culture. It must be developed throughout the community using ionising radiation including the medical, nuclear and conventional industry.

The development of such a culture requires sharing values and handing them down to new generations. There should be an effort to standardise quality teaching for knowledge of radiation science, risks, practices, and to encourage optimisation throughout the professions using ionising radiation. Basic tools are needed to support knowledge (e.g., guidelines, e-tools, etc) and attitude, including the appropriate communication of risks. Professionals in the field must act daily to assure appropriate behaviour and the involvement of all relevant individuals. Finally, professional associations, such as IRPA and IOMP should include in their meetings discussions and promotion of such a culture.

IV. Conclusions

Needless risks and loss of credibility are the consequences of every uncontrolled or unnecessary

exposure to radiation. The above mentioned challenges require involvement from all the international radiation protection community.

References

1. International Radiation Protection Association (2009) Guiding Principles for Radiation Protection Professionals on Stakeholder Engagement. www.irpa.net

Investigation of Image Quality and Patient Doses in X-Ray Diagnostic Radiology in Zimbabwe

Godfrey Mukwada[1], Walter Nyakodzwe[1], Virginia Tsapaki[2], and Madan Rehani[3]

[1] Parirenyatwa Group of Hospitals, Harare, Zimbabwe
[2] Konstantopoulio Hospital, Athens, Greece
[3] International Atomic Energy Agency, Vienna, Austria

Abstract- **The main objective of this study was to estimate patient doses in conventional radiography and corresponding image quality in Zimbabwe, as part of an International Atomic energy Agency (IAEA) project (RAF/9/033). Three government hospitals and 5 private centers were selected with a total of 20 X-ray machines. Films were graded for a week at the radiographer and radiologist level. A radiologist was asked to assign A, B, C grade to films (A- clearly accepted without any remarks, B- accepted with some remarks and C- rejected). Quality Control (QC) was done including film processing and viewing areas. The QC included: 1) kVp consistency, 2) output linearity, 3) beam quality, 4) viewing box illumination and 5) darkroom tests. After QC and possible corrective actions, film grading was repeated. Results before QC and after QC were analyzed. Patient doses were determined in terms of Entrance Surface Air-Kerma (ESAK) for the following X-ray examinations: 1) Lumbar spine (L/S) AP and LAT, 2) Abdomen, 3) Pelvis, 4) Chest PA, 5) Skull AP and LAT. Patient doses were reevaluated after QC and corrective actions. There was image quality improvement from category B and C to category A after QC (1-12%). ESAKs in this study were much lower than IAEA GL for all examinations investigated.**

Keywords— Radiography, patient dose, optimization

I. Introduction

During the recent years, patient dose has become a major issue [1]. Due to the increasing awareness and greater realization of the effects of ionizing radiation, X-ray users are now more demanding of dose information and dose reduction [2]. Zimbabwe is a developing country with a population of 12 million people living in 10 provinces each of which having facilities to carry out X-ray diagnostic examinations. There are approximately 200 conventional X-rays systems and about 8 CT scanners in the country. About 70% of this equipment is functional at any given time. Most of the equipment is in Harare, the capital city of Zimbabwe. In 1995, an act of parliament was established to monitor the use of radiation in the country. This was followed, by the establishment of the Radiation Authority of Zimbabwe in 2005, the purpose of which was to regulate the use of ionizing radiation.

The latest UNSCEAR report in 2000 showed that considerable radiation doses are received by patients undergoing X-ray examinations in some countries [3]. Zimbabwe could not be an exception. This study, therefore, seeks to investigate the doses received by patients undergoing common X-ray diagnostic procedures and find ways of optimizing radiation protection. The study was performed under the International Atomic energy Agency (IAEA) project RAF/9/033 and results are presented here.

II. Materials and Methods

Because of economic challenges and feasibility of the study, it was carried out only in Harare. Three government hospitals and 5 private centers were selected. A total of 20 conventional radiography generators were selected. The availability of radiologists and permission by the owners of the facilities were the determining factors in selection. Films were graded for a week at two levels: a) at the radiographer and b) at the radiologist level. The European Commission (EC) guidelines on quality criteria for diagnostic radiography were distributed to the participating facilities [4]. This was done to reduce inter-observer variability. Radiographers were asked to keep daily record of films used and films repeated, to get the repeat rate in every radiography room. At radiologist's level, a radiologist was asked to assign A, B, C grade to films (A-clearly accepted without any remark or reservation, B-accepted with some remark/reservations and C-should be rejected). The number of films in each category was summarized on daily basis for one week. Causes for B & C grade film were indicated on the data sheet. Quality Control (QC) was done including film processing and viewing conditions. The QC included: 1) kVp consistency, 2) output linearity, 3) beam quality, 4) viewing box illumination and 5) darkroom tests. After QC and possible corrective actions, film grading was repeated. Results before QC and after QC were analyzed.

Patient doses were determined in terms of Entrance Surface Air-Kerma (ESAK) for the following X-ray

O. Dössel and W.C. Schlegel (Eds.): WC 2009, IFMBE Proceedings 25/III, pp. 599–601, 2009.
www.springerlink.com

examinations: 1) Lumbar spine (L/S) AP and LAT, 2) Abdomen, 3) Pelvis, 4) Chest PA, 5) Skull AP and LAT. Patient doses were reevaluated after QC and corrective actions. The results were compared with those before QC and with the recent literature.

III. Results

Of the proposed 20 X-ray machines, air kerma measurements could only be performed only on 14 systems due to local problems. Table 1 shows participating hospitals, types of X-ray machines as well as their age (A) in years.

Table 1. Participating hospitals, hospital rooms count (R), X-ray machine and processor manufacturers, as well as their age (A) in years .

Hospital	R	Generator		Processor	
		Type	A	Type	A
PGH	1	Siemens	7	Konica	7
	2	Siemens	7	Konica	7
CGH	1	Siemens	7	Konica	7
	2	Siemens	12	Konica	7
Baines (MC)	1	Bennett	16	Kodak	8
	2	GEC	-	Kodak	8
HCH	1	Philips	15	Art technik	7
Sidar	1	Shimadzu	6	Agfa	6
DIC	1	Siemens	13	Konica	6
	2	Siemens	7	Konica	12
Westend	1	GEC	12	Med photo	8
	2	GEC	12	Med photo	8
Baines (Ave)	1	Philips	21	Konica	1 ½
	2	Shimadzu	29	Konica	1 ½

The age (A) of X-ray machines ranged from 7 years to 29 years, with an average of 11 years. The processors were basically of 4 types, with the Konica Company dominating. The average A of the processors was 7 years and it was common to have one processor for more than one X-ray machine.

Table 2 shows the change in Image Quality (IQ) before and after QC. There was image quality improvement from category B and C to category A after QC. The improvement ranged from 1% to 12%. It should be noted that a reduction of IQ (increase of B and C films of 3% and 4%) was also observed in the 2 rooms of one particular hospital. Variation of this kind in subjective scoring with change of person can be anticipated. Eleven centers achieved a reduction in rejected films up to a maximum of 12.7%. The reduction in reject rate after QC was on average 3.75%.

Table 2 shows A, B and C percentage before and after QC and corrective actions in all hospitals. Last column is the % of change in image quality from category B and C to category A after QC (BC to A).

H	R	IQ % before QC			IQ % after QC			% change B and C to A
		A	B	C	A	B	C	
PGH	1	65	30	5	69	29	2	4
	2	61	22	17	69	20	11	8
CGH	1	81	14	5	84	11	5	3
	2	84	11	5	85	9	6	1
HCH	1	62	25	13	68	30	2	6
DIC	1	79	16	5	80	14	6	2
	2	77	17	6	79	16	5	2
Westend	1	70	14	16	77	15	8	7
	2	65	13	22	77	13	10	12
Baines (MC)	1	87	4	9	83	13	4	-4
	2	85	6	9	82	13	5	-3
Baines (Aves)	1	71	29	0	73	21	6	2
	2	83	17	0	86	14	0	3
Sidar	1	81	19	0	87	11	2	6

Table 3 shows ESAK values before (ESAKb) and after (ESAKa) QC as well as the percentage change (% C) in ESAK. The results are presented in mean values for all participating hospitals or centers in the selected examinations. The highest dose reduction was 12.5%. This was on chest PA examination which is the most common conventional radiography examination in Zimbabwe. A slight dose increase was found, however, for skull lateral examination (1.9%).

Table 3. Mean ESAK values before (ESAKb) and after (ESAKa) QC as well as the percentage change (% C) in ESAK are shown in this table for all hospitals.

	Chest PA	Lumbar AP	Lumbar LAT	Pelvis	Abdomen	Skull AP	Skull LAT
ESAKb	0.16	2.05	4.74	1.71	1.87	1.53	1.04
ESAKa	0.14	2.01	4.45	-	1.64	1.45	1.06
% C	**12.5**	**2.0**	**6.1**	**-**	**12.3**	**5.2**	**1.9**

IV. Discusssion

The specific study is the first in Zimbabwe regarding image quality assessment and patient dose. The study revealed that a number of factors that affected image quality had to be identified and corrected. These factors included the condition of viewing boxes and dark rooms, as well as the imaging parameters set on the X-rays machines by the technologists. It is common to underestimate the influence of illumination of the viewing box to image quality. In this study, it was found that some of the viewing boxes had poor illumination. Furthermore, many centres were replenishing the chemicals of the processors once or twice a week. Some centres that were not very busy could replenish their chemicals once in three weeks. Simple corrective actions were applied and the results indicated image quality improvement after these actions.

Comparison of ESAKa with the latest literature is found in Table 4 [5]. Mean ESAK in chest examination is comparable to other countries. In general, mean ESAK values found in this study are lower compared with other countries. The last row of the table presents also the IAEA guidance levels (GL) [6]. Zimbabwe ESAKs are much lower than IAEA GL for all examinations investigated.

Table 4. Mean ESAK of this study (last row) is compared with corresponding values of various countries as reported by Muhogora et al [5].

Country	Chest PA	LS AP	LS LAT	Pelvis	Abdomen	Skull AP
UK	0.15	5	11.7	4.7	3.8	2.3
Australia	0.12	6.1	15.1	4.2	3.9	1.9
Canada	0.11	3.34	-	2.35	-	-
Finland	0.24	8.8	18.2	7.1	6.2	3.4
Taiwan	0.52	5.91	18.9	4.77	5.13	2.6
Korea	0.21	2.8	6.17	2.33	2.44	2.04
Zimbabwe	**0.14**	**2.01**	**4.45**	**-**	**1.64**	1.45
IAEA GL	0.4	10	30		10	5

.

V. Conclusions

Image quality can be improved without sophisticated and expensive quality control equipment. Mean radiation doses, in terms of ESAK, for patients undergoing standard conventional radiographic examinations in selected hospitals were below the published GL.

Acknowledgment

The work was supported by the IAEA through the TC project number RAF/9/033 “Strengthening on Radiation Protection of patients and Medical Exposure Control”. The authors are grateful to the IAEA, the administrators, radiologists and radiographers of participating centres.

References

1. Rehani M. the IAEA’s activities in radiological protection in digital imaging (2008). Radiat Prot Dosim129 (1-3): 22-28.
2. Tsapaki V, Tsalafoutas I.A, Chinofoti I et al (2007). Radiation doses to patients undergoing standard radiographic examinations: a comparison between two methods. Br J Radiol 80: 107-112.
3. United Nations Scientific Committee on the Effects of Atomic Radiation (UNSCEAR 2000). Sources and Effects of Ionising Radiation. Report to the General Assembly, with Scientific Annexes. New York: United Nations.
4. European guidelines on quality criteria for radiographic images. EUR 16260 (European Commission) (1996).
5. Muhogora et al (2008). Patient Doses in Radiographic Examinations in 12 Countries in Asia, Africa and Eastern Europe: Initial Results from IAEA projects. AJR 190(6):1453-61.
6. International Atomic Energy Agency. Dosimetry in diagnostic radiology: an international code of practice. Technical reports series no. 457 (Vienna: IAEA) (2007).

Author: Virginia Tsapaki
Institute: Konstantopoulio Hospital
Street: 1 Ifaistou, 14569 Anixi,
City: Athens
Country: Greece
Email: virginia@otenet.gr

Convenient Method of Thermal Neutron Measurement Using Imaging Plates in Proton Therapy

T. Fujibuchi[1,2], Y. Tanabe[1], T. Isobe[1], H. Kawamura[1,2], T. Terunuma[1,3], K. Yasuoka[1,3], T. Matsumoto[4], J. Nishiyama[4], H. Harano[4], and T. Sakae[1,3]

[1]Graduate School of Comprehensive Human Sciences, University of Tsukuba, Tsukuba, Japan
[2]Department of Radiological Sciences, Ibaraki Prefectural University of Health Sciences, Ami, Japan
[3]Proton Medical Research Center, University of Tsukuba, Tsukuba, Japan
[4]National Metrology Institute of Japan, National Institute of Advanced Industrial Science and Technology, Tsukuba, Japan

Abstract— **In proton therapy, measurement of secondary neutron emission is important, because such radiation can influence the occurrence of secondary cancers and the radioactivity of the treatment room. In this study, we investigated the possibility of neutron detection using a neutron imaging plate (IP) and a general IP.**

The upper limit of measurable neutron fluence by an IP system is primarily controlled by the readout range of the scanner that is used. Within this limit, a reasonable linear response of the IP to a neutron fluence was maintained. To separate thermal neutron from other radiation, we covered a part of the IPs with 1.5 mm thick cadmium plates and 1.0 mm thick lead plates. The neutron IP was shielded from thermal neutrons by the cadmium cover and the measured intensity was reduced. However, in the general IP, the intensity increased slightly in the region covered with cadmium because of prompt gamma-ray production. A further increase in intensity occurred in the lead-covered region due to interaction with photons. Moreover, the neutron field was calculated by PHITS Monte Carlo simulations, and the elements of secondary radiation which were produced in the neutron IP and metal plates were confirmed.

From the results of this study, thermal neutrons and other radiation could be detected by using IPs and cadmium plates, suggesting the potential of such devices as practical neutron detectors.

Keywords— **Thermal Neutron fluence, Imaging plate (IP) dosimetry, Fading characteristics, Prompt gamma-ray, Monte Carlo simulation**

I. Introduction

In proton therapy, the evaluation of secondary neutron generation is important, because such secondary radiation may lead to tumor formation in patients, increase radiation levels in the treatment room, and so on [1, 2]. In this study, we investigate the use of an imaging plate (IP) for convenient evaluation of neutron dose. An IP is a radiation detector, which utilizes a photostimulable phosphor of $BaFBr:Eu^{2+}$. Latent images on the IP created by ionizing radiation are scanned by a stimulating laser beam and are read by a photomultiplier as photo-stimulated luminescence. Such devices have been widely used for the quantitative measurement of two-dimensional intensity distributions of various types of ionizing radiation.

In this study, the application of IPs for neutron detection has been investigated with the aim of realizing a practical dosimetry system for therapy. The linearity between intensity and thermal neutron fluence has been measured to identify the practical upper limit of measurable dose. Fading characteristics have also been studied for quantitative dose evaluation. It was found that thermal neutrons and other forms of radiation could be detected using IPs and metal plates.

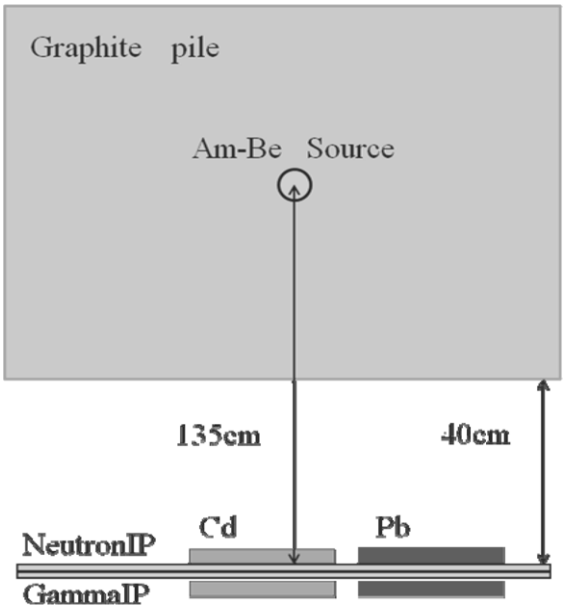

Fig. 1 Arrangement for the measurement of linearity characteristics of the IPs

O. Dössel and W.C. Schlegel (Eds.): WC 2009, IFMBE Proceedings 25/III, pp. 602–605, 2009.
www.springerlink.com

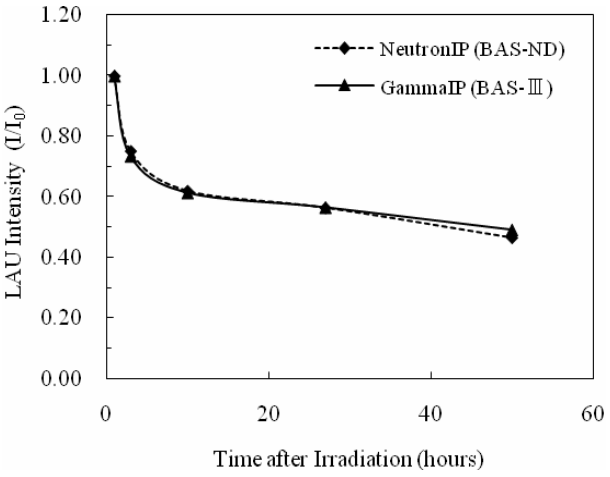

Fig. 2 Normalized fading curves of LAU intensity

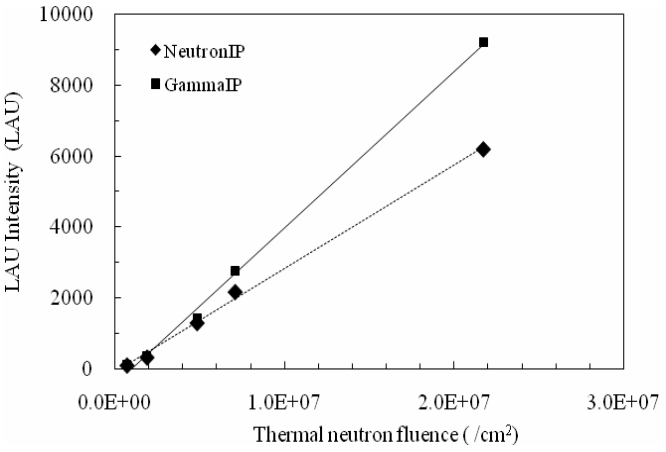

Fig. 3 Linearity of LAU intensity with neutron fluence

II. Materials and Methods

A. Apparatus and experimental setup

To detect incident neutrons and photons, we used a neutron IP (BAS-ND: Fuji Photo Film Co., Ltd.) and a general IP (BAS-III: Fuji Photo Film Co., Ltd.) (referred to as the gamma IP) [3]. Sections of the IPs were shielded from thermal neutrons and photons by masking one area with a cadmium plate (20 mm × 40 mm × 1.5 mm) and another with a lead plate (20 mm × 40 mm × 1 mm) on the upper and lower surfaces. Neutron and photon irradiation was carried out on individual neutron and gamma IPs, and also on the stacked structure shown in Fig. 1. We used a thermal neutron standard field in a graphite pile (rectangular size: 190 cm × 190 cm × 230 cm) with a neutron source of Am-Be (148 GBq), which was calibrated at the National Institute of Advanced Industrial Science and Technology. The IPs were placed at a distance of 40 cm from the surface of the graphite pile, and were removed after several hours of exposure. The experimental setup is shown in Fig. 1. To measure the degree of fading resulting from the radiation exposure, we scanned the IPs using a laser reader (FLA-7000: Fuji Photo Film Co., Ltd.) 24 hours later. The thermal neutron fluence rate at the position where the IPs were exposed was measured by a ^{3}He proportional counter (SP9: CENTRONIC). In addition, to compensate for the difference in gamma ray sensitivity of the IPs and the influence of the plates, tests were carried with ^{137}Cs as a radiation source.

B. Fading characteristics

It is known that the latent image caused by radiation exposure in an IP fades as time goes by: the so-called "fading" effect. Fading curves have been reported for α-rays [4, 5], β-rays [5], γ-rays [6-8], X-rays [9, 10] and electron beams [11]. This fading effect is an important aspect of dosimetry using IPs.

Fading characteristics up to 50 hours after irradiation were measured for a 10 MV X-ray beam (0.025 Gy) at 25 °C. The normalized fading curves of the linear arbitrary unit (LAU) intensity are shown in Fig. 2.

C. Linearity of LAU intensity during neutron exposure

The LAU intensity was measured for various neutron fluences from 7.0×10^{5} cm^{-2} (3 hours irradiation) to 2.2×10^{7} cm^{-2} (90 hours irradiation). The neutron fluence rate measured by the proportional counter was 6.565×10^{1} cm^{-2} s^{-1} under the conditions shown in Fig. 1. Figure 3 shows the linearity of IPs as a function of neutron fluence, and it can be seen that a reasonably linear response exists over a wide range of fluences.

D. Effects of metal plates

Figure 4 shows the LAU profile for the stacked structure shown in Fig. 1 following 30 hours of neutron exposure. In the neutron IP, the region covered by Cd is shielded from neutrons and the LAU value decreases. On the other hand, in the gamma IP, the LAU value is slightly higher in the Cd-covered region and higher again in the Pb-covered region.

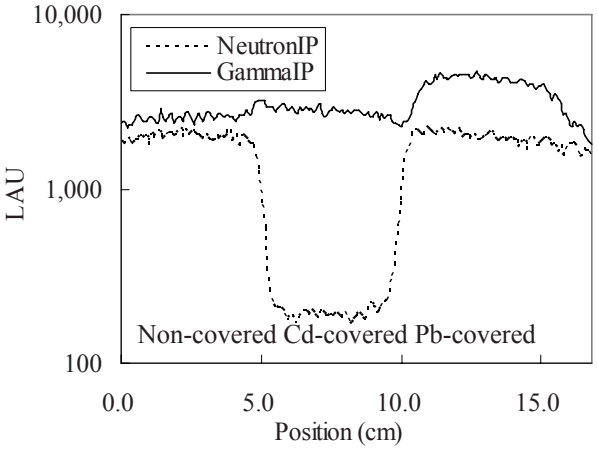

Fig. 4 Profile of LAU in stacked IPs following 30 hours of neutron exposure.

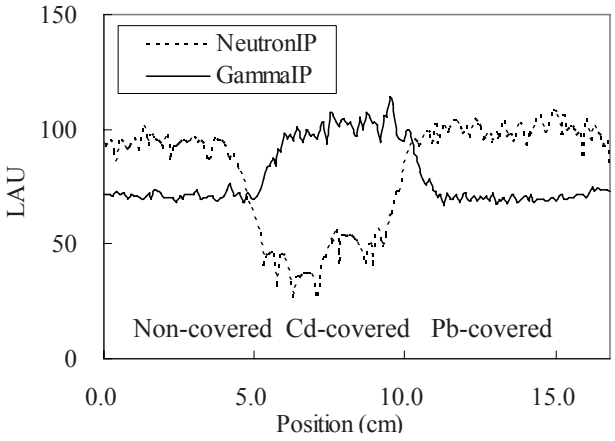

Fig. 5 Profile of LAU in isolated IPs following 3 hours of neutron exposure.

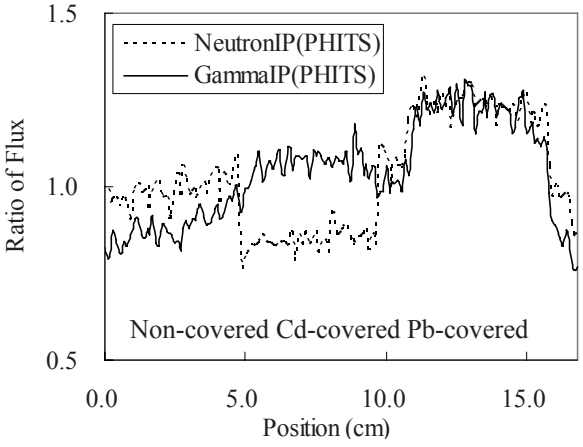

Fig. 6 Calculated photon flux in irradiated IPs.

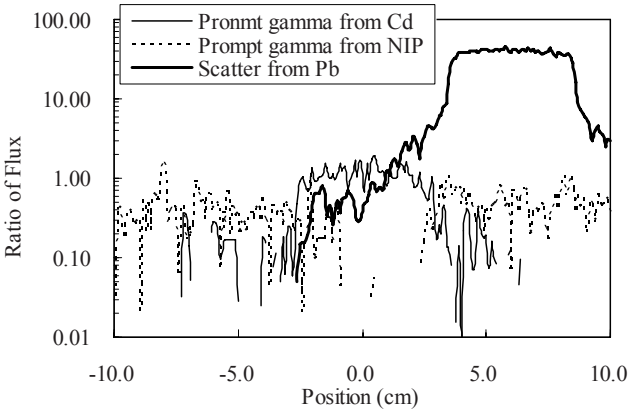

Fig. 7 Profile of prompt gamma production and scattering calculated by PHITS.

Figure 5 shows the results of similar measurements for isolated IPs (non-stacked) following 3 hours of neutron exposure. In this case the exposure time was three hours. As before, for the neutron IP, the LAU value decreases in the Cd-covered region. However, for the gamma IP, the LAU value is higher only in the Cd-covered region and not in the Pb-covered region.

Following exposure of the gamma IP to gamma rays from ^{137}Cs, the LAU value decreases in the Cd-covered region but increases in the Pb-covered region. From these results, the LAU increase in the Pb-covered region of the gamma IP stacked （Fig.4） is likely to be related to the interaction of neutrons with gadolinium, leading to prompt gamma ray emission followed by Compton scattering in the Pb. Also, the LAU increase in the Cd-covered region during neutron irradiation of the gamma IP alone (Fig.5) is thought to be due to prompt gamma ray emission from Cd.

E. Monte Carlo simulation

Subsequently, the experimental setup shown if Fig. 1 was simulated using the particle and heavy ion transport calculation code (PHITS: JAEA) [12], and the fluence rates and energy spectra of photons, electrons, and neutrons irradiating the IPs and the metal plates were calculated

The calculated photon flux at the IP position is shown in Fig. 6. The value in the Cd-covered region is seen to decrease in the neutron IP, and the value in all covered parts of the gamma IP is seen to increase, similar to Fig. 4. Figure 7 shows the profile of prompt gamma rays from the neutron IP and cadmium, and scattering from Pb.

Fig. 8 Regions of IPs with different radiation conditions

F. Conversion from LAU intensity to thermal neutron fluence

To convert from LAU intensity to thermal neutron fluence, we devised the following method:

The neutron IP and gamma IP stacked, and two different thicknesses of covering cadmium plates are used. Radiation components can be divided into categories A to F below.

- A = Thermal neutron fluence from source
- B = Epithermal and fast neutrons from source
- C = Gamma-rays from source
- $f(A)$, $f'(A)$ = Prompt gammas from Cd, Cd_2
- D, D^2 = Attenuation in Cd, Cd_2 = $exp^{-\mu t}$, $exp^{-\mu 2t}$
- $g(A)$ = Prompt gammas from neutron IP
- E = Attenuation in neutron IP
- $h(A)$, $h'(A)$ = Attenuation of prompt gammas
- F = Relative response between neutron IP and gamma IP

In these formulae, $f(A)$, $g(A)$, and $h(A)$ are functions of thermal neutron fluence.

The IPs are divided into six regions, as shown in Fig. 8. Each region is subject to the following radiation conditions:

$$1 = A + B + C$$
$$2 = B + C \times D + f(A)$$
$$3 = B + C \times D^2 + f'(A)$$
$$4 = [C \times E + g(A)] \times F$$
$$5 = [C \times E \times D + h(A)] \times F$$
$$6 = [C \times E \times D^2 + h'(A)] \times F$$

From these relationships, it is possible to derive the thermal neutron fluence.

III. Conclusions

In this study, thermal neutrons and other forms of radiation were detected using metal plates in combination with IPs. The results indicated that such a system can act as an effective thermal neutron detector.

References

[1] Moyers M. F., Benton E. R., Ghebremedhin A. et al.: Leakage and scatter radiation from a double scattering based proton beamline. Med. Phys. 35, 2008, 128-144.

[2] Hall E. J., Intensity-modulated radiation therapy, protons, and the risk of second cancers. Int. J. Radiat. Oncol. Biol. Phys. 65, 2006, 1–7.

[3] Karasawa Y., Kumazawa S., Niimura N.: The character and application of a neutron imaging plate. Physica B, 1998, 241-243, 139-141.

[4] C. Mori, A. Matsumura, Nucl. Instr. and Meth. A 312, 1992, 39.

[5] T. Suzuki et al., J. Nucl. Sci. Technol. 34 (5), 1997, 461.

[6] R. Yamadera et al., Radioisotopes 42, 1993, 676.

[7] M. Takebe et al., Jpn. J. Appl. Phys. 34, 1995, 4197.

[8] C. Mori et al., Nucl. Instr. and Meth. A 339, 1994, 278.

[9] T. Buecherl, C. Rausch, H. Seggern, Nucl. Instr. and Meth. A 333 (1993) 502.

[10] S. Nakamura, K. Inabe, Ionizing Radiation 23 (2), 1997, 53 (in Japanese).

[11] T. Oikawa, D. Shindo, K. Hiraga, J. Electron Microsc. 43, 1994, 402.

[12] Iwase H., Niita K. and Nakamura T.: Development of a general-purpose particle and heavy ion transport Monte Carlo code J. Nuc. Sci. Technol. 39, 2002, 1142-1151.

Author: Toshioh Fujibuchi
Institute: Graduated School of Comprehensive Human Sciences, University of Tsukuba
Street: Ten-nohdai 1-1-1
City: Tsukuba
Country: Japan
Email: fujibuchi@ipu.ac.jp

Dosimetric Evaluation of Movement of Tumor Target Using Intensity Modulation Radiation Therapy (IMRT) for Lung Cancer Patients

Sung Kyu Kim[*], Myung Se Kim[*], Min Kyu Kang[*], Ji Hoon Choi[*], Byoung Yong Kim[†], Sang Ryul Lee[†‡], and Sung Joon Kim[†]

[*]Department of Radiation Oncology, School of Medicine, [†]Department of Physics, College of Science, Yeungnam University, Daegu, Korea, [‡]Department of Neurosuergery, Ajou University Medical Center, Suwon, Korea

Purpose: To evaluate radiation dose delivered to tumor target due to the movement of cancer in the treatment of intensity modulation radiation Therapy (IMRT) for lung cancer patients.

Keywords: Intensity modulation radiation therapy, Movement of tumor position, Dose verification.

Material and Methods: Center position in radiation therapy should be accurately confirmed, patent position must also be accurate without movement, and therefore accurate dose be irradiated in the absence of movement of tumor target, because IMRT performs a radiation therapy by modulating the intensity of radiation according to the area divided to the irradiated area of 0.5 x 0.5 cm^2.

Radiation therapy equipments used in this IMRT experiment were Varian 21EX linear accelerator (Varian Medical Systems, Palo Alto, CA, USA) with photon energies of 10 MV**,** and radiation therapy treatment planning system (Eclipse version 6.5**,** Varian, Palo Alto, CA). The dose verification of the IMRT was performed by using IMRT QA phantom which was self-developed in our institution for the measurement of dose for the movement.

Radiation dose was evaluated for the patients' berating rate of 8, 14, and 18 bpm (breaths per minute) in the cases of tumor target moving up and down with 1 cm and 1.5 cm. The dose of moving PTV was measured by using TLD, the measurement points were 1 cm away from the top**,** bottom**,** left**,** and right sides of PTV center, respectively.

Fig. 1.The photography of self-developed phantom used for quality assurance in intensity modulated radiation therapy.

O. Dössel and W.C. Schlegel (Eds.): WC 2009, IFMBE Proceedings 25/III, pp. 606–608, 2009.
www.springerlink.com

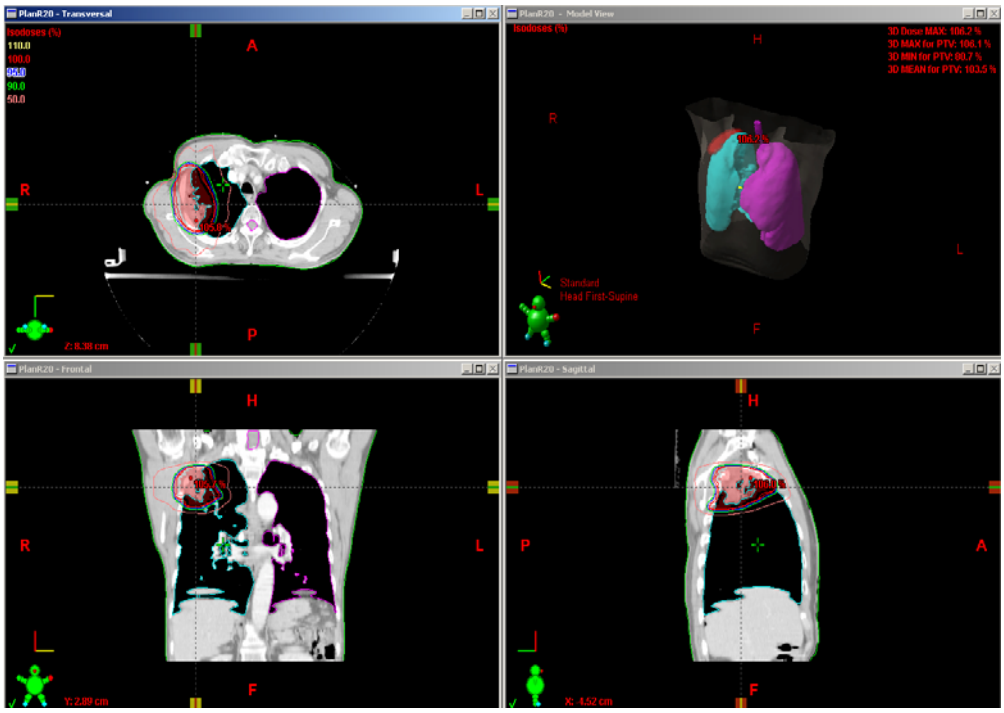

Fig. 2. Results of radiation treatment planning in intensity modulated radiation therapy for a lung cancer

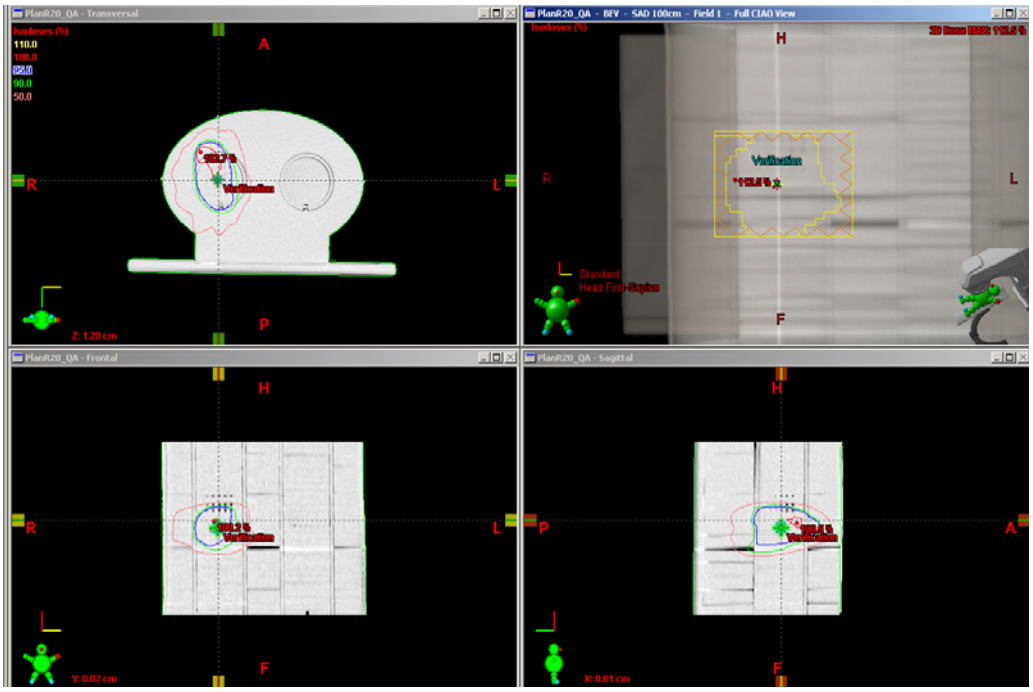

Fig. 3. Results of quality assurance of intensity modulated radiation therapy for a lung cancer using the self-developed phantom.

Results: The IMRT for lung cancer patients was successfully performed. Radiation therapy treatment planning was composed of 7 portals, i. e., 0, 330, 300, 270, 240, 210, and 180 degree angles, Dose for the PTV was allowed to maximum of 103% and minimum of 97% to be below 30% and above 0% 20 for lung and spinal dose volume constraint of V20 (20 Gy), respectively.

Dose differences were evaluated from -5.8% to 3.8% for the 8 bpm, from -5.6% to 5.4% for the 14 bpm, and from -9.3% to 8.5% for the 18 bpm at the moving condition of 1 cm of tumor position, respectively.

Meanwhile, dose differences were evaluated from -6.4% to 5.8% for the 8 bpm, from -4.1% to 11.5% for the 14 bpm, and from -3.8% to 11.7% for the 18 bpm at the moving condition of 1.5 cm of tumor position, respectively.

Conclusions: The dose delivery was more accurate in the state of less movement from the result of comparison between 1 cm and 1.5 cm movement of tumor position, and also the difference of dose distribution was less in the case of lower bpm than higher bpm for breaths per minute.

Indoor Radon Concentration in the City of Sharjah, United Arab Emirates

Hussein M. Elmehdi and Bassam Rashed

Department of Applied Physics, College of Sciences, University of Sharjah
P.O. Box: 27272 Sharjah, United Arab Emirates. Email: hmelmehdi@sharjah.ac.ae

Abstract— **We report the first indoor radon concentration measurements in the coastal city of Sharjah, United Arab Emirates (UAE). The measurements were carried out using an active radon detector in the living rooms in 61 houses in various parts of the city following the EPA protocol. Radon concentrations were found to range between 7 and 71 Bq/m^3 in the winter months, with little variations from the summer months. These concentrations were lower than the world average radon concentrations and comparable to measurements performed in other cities of the region.**

Keywords— **Radon Concentration, Sharjah, UAE, active measurements, EPA protocol.**

I. Introduction

Radon is a naturally occurring radioactive noble gas that is colorless, odorless, and tasteless, that is formed from the decay of radium. It is seven times heavier than air, which means that its concentration is greatest near floors of houses and dwellings. In addition, and because of its low boiling point, i.e. -61.8 ^{o}C, radon has the ability to seep through the earth curst into the atmosphere we live in, making its way through the different soil and rocky constituents of the earth's layers. Radon is considered a health hazard and it represents the highest percentage of naturally found ionizing radiation, where the inhalation of radon and its decay products is responsible for half of the annual effective dose received by the human due to natural radiation sources. Radon concentrations vary from one place to another depending on the geological characteristics of the soil and the underlying geological structure of the area [1]. It has been reported that the indoor concentration of radon reaches 10 times higher than its outdoor concentration [2]. In general, the concentration of radon in houses depends on the geological environment of the house, geography, soil water content, permeability of the soil surrounding the house and the engineering and structural designs of houses, especially those related to ventilation [3]. In addition, indoor radon concentrations can accumulate in closed rooms, which accordingly increase the heath risks. Radon concentrations are seasonal, dropping in the summer months when the temperature is generally higher [4].

The main isotope of radon is ^{222}Rn, which is produced in the alpha decay of ^{226}Ra, in the radioactive chain of ^{238}U. It has an average life time of 3.8 days. Its concentration in dwellings varies widely from room to room, depending on the above mentioned factors, including personal behavior. Exposure to high radon concentrations have been linked to lung cancer [5].

In the UAE, no studies have been carried out to assess radon concentrations up to date, which makes this study the first assessment of radon concentrations in the country. As a start, we will be reporting radon concentrations in houses in the city of Sharjah, UAE, which is part of a comprehensive study that will include measuring radon concentrations in other UAE cities as well as radon concentrations in water, soil and dwellings, including schools hospitals and tourist attractions, such as museums and historical sites.

The coastal city of Sharjah is the capital city of the Emirate of Sharjah. It is located in the northern part of the United Arab Emirates (UAE) on the coast of the Arabian Gulf (also known as the Persian Gulf). It is located at the eastern side of the Arabian Peninsula, see Fig 1. The population of the city is approximately 800,000 according to the 2008 statistics [6]. The geology of the city of Sharjah is similar to that of neighboring emirates where it is divided into two distinct parts; the desert floor, the coastal plains, the aeolian sands and gravel plains makes first part while the second part comprises Oman Mountains [7].

Fig 1: The location of the coastal city of Sharjah, UAE.

O. Dössel and W.C. Schlegel (Eds.): WC 2009, IFMBE Proceedings 25/III, pp. 609–611, 2009.
www.springerlink.com

II. Materials and Methods

Because of the natural characteristics of radon gas (colorless, odorless, etc.), it is impossible to detect directly, even at high concentrations. One needs special "radon detectors" to accurately measure its concentrations. There are special methods that are commonly used, the first of which is the so-called "passive" technique. It means that there are no active elements in the system to detect radon gas, only components that can register the alpha particles, an example of which are the thin alpha tracks, which usually are mounted in places of interest, and then taken for further analysis to count the tracks and calculate radon concentrations. The second method, which is employed in this study, is the active approach, which uses highly accurate and calibrated radon detectors to measure radon concentrations directly.

In our continuous active radon concentration measurements we used the solid state alpha detector called Radd7, made by Durridge Company Inc, USA. It contains a solid state detector made of a semiconductor material (silicon) that converts alpha radiation directly to an electrical signal.

The tests were conducted in the "lowest area in the house that is used, or could be adapted for use, as a living area". The detector was placed near the center of the room, about 3 - 4 feet above the floor, avoiding walls, vents, fireplaces, windows, draft, and direct sunlight. The air intake was at least 30 inches (75 cm) above the floor, and away from the walls. Because of diurnal variation of radon levels, the test period was set to take two days (48 hours). As required by the EPA protocols, which requires an average taken over at least two days. Radon concentration was recorded every hour and an average of 24 measurements is taken.

III. Results and Discussion

Fifty two measurements where made in houses across the city sharjah. These include first floor rooms, second floor rooms and reception rooms, the later of which is a room designated for guests, which makes it used very little. For each single measurement, radon concentration was measured using two cycles. In each cycle, radon concentration was measured every hour over a 24 hour period, following the United States Environmental Protection Agency (EPA) protocol [8]. For each site, the measurement was repeated three times and average was calculated. An example of a typical measurement over a twenty four period in one of the sites is shown in Figure 2. The measurements were performed in the winter months (December – February) where the temperature average is about 23 ^{o}C. In addition, and for comparison purposes, radon concentrations were measured again in the summer months (June – August) for approximately 1/3 of the sites. The results of these measurements are shown in Fig 3. It should be noted that in the summer months the average temperature reaches as high 49 ^{o}C.

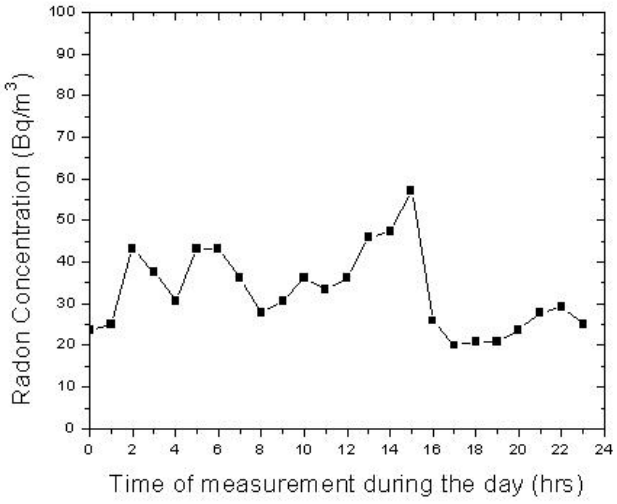

Figure 2: a typical radon concentration measurement which runs for twenty four hours.

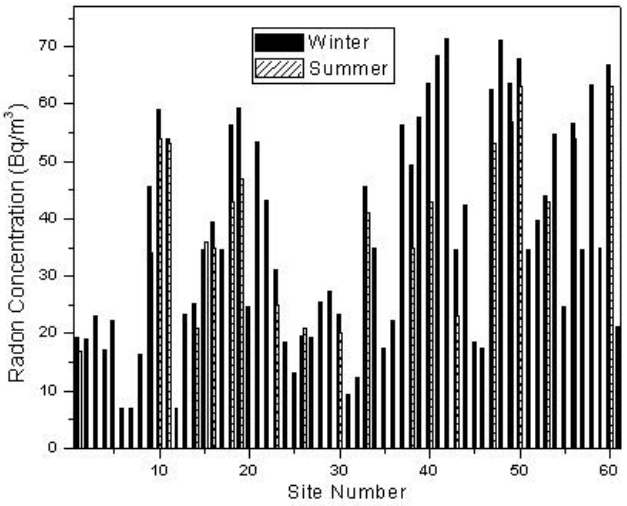

Fig. 3: Radon concentrations in 61 sites in the city of Sharjah, UAE in winter and summer.

For the winter months radon concentrations in houses in the city of Sharjah ranged from 7 Bq/m^3 to 71 Bq/m^3, with an overall arithmetic average of 35.5 Bq/m^3, see figure 3. In comparison, radon concentration in the summer months drop slightly, which may be attributed to the fact that the

climate of the UAE is moderately warm even the in the winter months with an average temperature of 23 ^{0}C. The frequency of radon concentrations in sharjah houses were also calculated and shown in Figure 4.

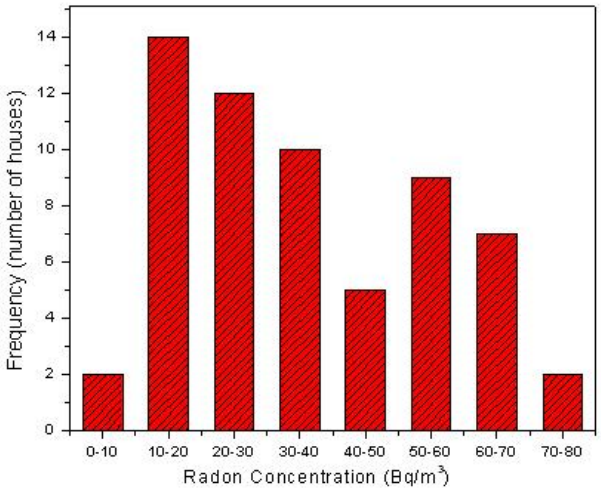

Fig. 4: The frequency of radon concentrations in city of Sharjah houses.

Approximately 1/3 of the houses have radon concentrations less than 20 Bq/m^3, while 19 houses reported radon concentration of 50 Bq/m^3 or higher. It should be noted that the calculated radon concentration average for the city of Sharjah is below the mean world wide radon concentration of 46 Bq/m^3. In comparison to neighboring countries of similar climate and geography, such as Kingdom of Saudi Arabia (KSA), our measured radon concentration average agrees with the measured average concentration of of 35 Bq/m^3 [9], however, the variation of radon concentration in KSA is bigger ranging for 7 Bq/m^3 to values above 150 Bq/m^3.

IV. Conclusions

In this paper, we reported the first radon concentrations measurements in coastal city of sharjah, UAE. Sixty one houses distributed through out the city were investigated using an active radon monitor. Radon concentrations in the winter months were found to vary from 7 Bq/m^3 to 71 Bq/m^3, with an arithmetic average of 35 Bq/m^3. This value is below the world radon concentration average of 46 Bq/m^3. In the summer months, the concentration was found to drop slightly.

Acknowledgment

The authors wish to thank the College of Graduate Studies and Research for providing funding for this research.

References

1. Nason, R and Cohen, B. L. (1980). Correlation between ^{226}Ra in soil, ^{222}Rnin soil and gas and Rn in adjacent houses. Health Physics. 52, 73-74.
2. Narayana, Y., et al. (1998). Seasonal variations of indoor radon levels in costal Karnataka on the south cost of India. Radiation Meas. **29**, 19-25.
3. Levesque, B. et. Al. (1997). Radon in residences: influence of geological and housing characteristics. Health Physics, **72**(86), 907-914.
4. Sainz, C. et al. (2007). Analysis of the main factors affecting the evaluation of the radon dose in the workplace: the case of tourist caves.
5. Zunic, Z. S.. et. Al. (2007). Radon survey in the high natural radiation region of Niska Banja, Sebia. Environ. Radioact. **92**,165-174.
6. http://en.wikipedia.org/wiki/Sharjah_(city)
7. http://www.mapsofworld.com/united-arab-emirates/geography/geology.html
8. "Indoor Radon and Radon Decay Product Measurement Device Protocols", Protocol for Using Continuous Radon Monitors (CR) to Measure Indoor Radon Concentrations. Available at: http://www.epa.gov/iedweb00/radon/pubs/devprot3.html#2.1
9. M. I. Al-Jarallah_ and Fazal-ur-Rehman (2006). Indoor radon concentration measurements in the dwellings of the Al-Jouf region of Saudi Arabia. Radiation Protection Dosimetry (2006), Vol. 121, No. 3, pp. 293–296

Author: Hussein M Elmehdi
Institute: Department of Applied Physics, University of sharjah
Street: PO Box 27272
City: Sharjah
Country: United Arab Emirates
Email: hmelmehdi@sharjah.ac.ae

A Placebo-Controlled Study of Far Infrared Ray Applied to 'Phantom Limb'

Chi-Yu Huang[1], Rong-Sen Yang[2], Te-Son Kuo[1,3], and Kai-Hsiung Hsu[4]

[1] Department of Electrical Engineering, Biomedical Group, National Taiwan University, Taipei, Taiwan
[2] Department of Orthopaedics, College of Medicine, National Taiwan University, Taipei, Taiwan
[3] Institute of Biomedical Engineering, National Taiwan University, Taipei, Taiwan
[4] Department of Biomechatronic Engineering, National Ilan University, I-Lan, Taiwan

Abstract—**This report describes a placebo-controlled study of far infrared ray (FIR) applied to a below-knee amputee. We discovered that the phantom limb sensation could be induced with the phantom limb site exposed to FIR. Following an appropriate period of FIR on the absent limb, the amputee was able to perceive warm sensation for his phantom limb, a sensation much weaker than that with his normal leg exposed to FIR. This finding has been tested by a series of placebo-controlled experiments, indicating that the absent limb play an important role in perceiving the warm sensation and is in close connection with the phantom limb sensation. Although the underlying mechanism of this connection remains to be elucidated, the treatment based on our findings for the phantom limb pain relief has showed significant success.**

Keywords—**Phantom limb sensation, Far infrared ray**

I. Introduction

Phantom limb sensations, common in amputees, refer to the sensations of perceiving the absent limb for amputees while painful sensations are referred to as phantom limb pains [1]. The occurrence of the phantom limb pain is up to 60~80% among all amputees and usually more than 80% of the amputees experienced phantom limb sensations [1-4].

The mechanisms of the phantom limb pain and phantom limb sensation are still unclear, although three main categories of theories have been proposed, including peripheral-factors theories, central-factors theories and psychological-factors theories, respectively [2,3,5-7]. The peripheral-factors theories hold that the phantom limb perception is due to the generation of the stump impulses while the central-factors theories maintain that the phantom limb perception is a result of the sensitization of the central nervous system [2,5,7,8]. The neuromatrix and cortical reorganization are two major theories of the central-factors theories associated with the phenomena of the phantom limb [9-14]. Both peripheral and central factors have been regarded as determinants of phantom limb pain [1,2,7]. Psychological factors do not seem to contribute to the cause but may affect the severity of the phantom limb pain [7,15,16].

These theories, nonetheless, are not able to give explanation to all the phantom limb phenomena, and are not immediately associated with the treatments for phantom limb pain [2,3,5,6,17]. Further investigations in phantom limb perception are still wanted [2,3,6].

In this study, we propose a hypothesis that the phantom sensation can be induced by appropriate stimulation on the phantom limb site. This hypothesis was tested by examining the phantom limb sensation induced by applying far infrared ray (FIR) to the phantom limb site, and placebo-controlled design was adopted for all trials.

II. Materials and Methods

The subject for this study is a 60-year-old male with his left leg amputated below the knee due to a car accident 8 years ago (Fig. 1). The amputee did not report phantom limb pain while clear phantom limb sensation was claimed for his left shank, left instep, left sole and left toes.

Fig. 1 The subject and the setup of the placebo trials using an opaque curtain.

O. Dössel and W.C. Schlegel (Eds.): WC 2009, IFMBE Proceedings 25/III, pp. 612–615, 2009.
www.springerlink.com

A far-infrared emitter (TY-101N, WS Far IR Medical Tech. Co. Ltd.) with the peak energy at the wavelength 8 μm was used as the FIR source. The power density of the FIR is 20 mW/cm^2 at 20 cm away. In order to differentiate the effect of FIR on the phantom limb from that on the stump or the rest of the amputee's body, insulator plates were used to separate the emitter from the subject. Thermometers and FIR power meters were placed next to the subject to monitor the temperature and far infrared radiation during the FIR exposure.

Placebo-controlled experiments were conducted by applying FIR to the subject's normal leg (denoted by *R*) and the phantom leg (denoted by *L*) while FIR emitter with power off was randomly present as the placebo trial (denoted by *X*). In addition, an opaque curtain was set between the upper half of the subject's body and the FIR emitter and a beep sound was rung at the end of each trial. Each radiation lasted for 20 minutes with at least 15 minutes between trials. For each trial, the subject was asked about the site of the warm sensation perceived following 20-minute FIR.

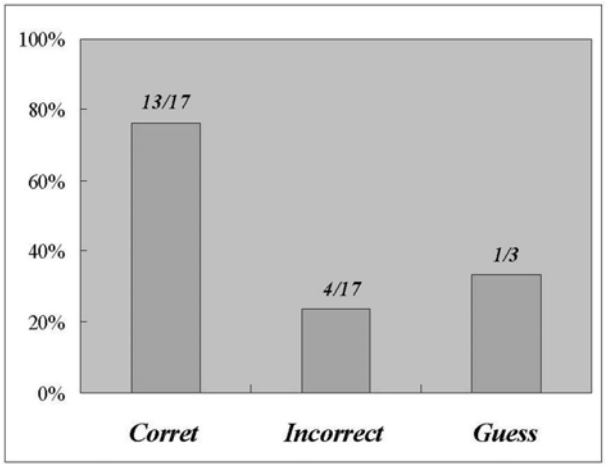

Fig. 2 The assessment of the subject's perceptive responses to far infrared ray and the probability by guess.

III. Results

The subject reported that he could sense a little warmth on his phantom instep or toes for most trials after a series of radiation on the phantom limb. Although unaware of what applied on his legs, the subject was able to identify his phantom limb sensation resembled that warmed up by a tungsten lamp on his absent limb. The warm sensation for his right leg (intact limb) as well as left leg (absent limb) was similar although the intensity for the absent limb was much lower.

Thermometers and electromagnetic power meters next to the subject showed no temperature or electromagnetic power variation during FIR exposure, indicating that the warm sensation was not originated from the stump or the rest of the body.

Out of 17 trials of the placebo-controlled experiments, 13 answers were given correctly by the subject while the subject described the perceptions for the other four trials as indistinguishable initially and gave incorrect answers when asked to give definite responses (Table 1). Fig. 2 shows the assessment of the subject's perception following FIR exposure and the probability by guess. The ratio for correct answers is 76.5% (13/17), much higher than the guess probability at 33.3% (1/3), suggesting that the perception of the phantom sensation was in agreement with the FIR stimulation.

Table 1 Results of the subject's perception

No.	FIR Location	Subject's perception	True/False
1	*R*	R	***T***
2	*L*	L	***T***
3	*X*	L	***F***
4	*L*	L	***T***
5	*R*	R	***T***
6	*X*	N	***T***
7	*L*	N	***F***
8	*R*	R	***T***
9	*X*	N	***T***
10	*L*	N	***F***
11	*R*	R	***T***
12	*L*	L	***T***
13	*X*	L	***F***
14	*R*	R	***T***
15	*X*	N	***T***
16	*R*	R	***T***
17	*L*	L	***T***

The subject's left leg exposed to FIR was denoted by L, right leg by R and sham radiation by X. The subject's warm perception on left leg was denoted by L, right leg by R and no perception by N.

IV. Disscusion

In 1522, Ambrose Pare first reported an amputee's description about the pain in the absent amputated leg [18,19]. Since then, the perceptions of an amputee's absent limb have been regarded as "phantom" phenomena. Various theories have been proposed to elucidate this mystery, and

the nervous system has become the target responsible for these "phantom" issues [9,10,12-14,20,21]. Despite the development of these theories, the treatments for phantom limb pain are usually unsuccessful [22-24].

In this study, we considered the phantom limb site that amputees specified hundreds of years ago as the origin of phantom sensation, and hypothesized that the phantom sensation can be induced by appropriate stimulation on the phantom limb site.

The results of placebo-controlled experiments were positive about our hypothesis that the subject could perceive the warm sensation induced by applied FIR at the phantom limb site. As the readings of thermometers and electromagnetic power meters confirmed that the FIR was not applied to the stump or other regions, we concluded that the warm sensations were not originated from the stump or the rest of the body. These results are in good agreement with our hypothesis, implying that the absent limb is connected with the amputee in an unidentified form of communication. Based on this idea, we designed a novel treatment modality for phantom limb pain by applying FIR to phantom limb site. The preliminary results of such treatments show significant effect on phantom pain relief.

In this study, 13 correct answers were obtained out of 17 placebo-controlled trials while the other four trials were considered as indistinguishable initially by the subject. This indistinguishable assessment was attributed to the subject's frequent and weak warm sensation of his own phantom limb since its amputation, as well as to the insufficient FIR for these trials. In this study, 20-minute FIR was adopted due to the subject's irritation with a single trial longer than 20 minutes whereas 40-minute exposure was recommended by the manufacture. For some trials, as a result, he could not differentiate the FIR responses from his proprietary warm sensations of his phantom limb. Nonetheless, the ratio for correct answers (76.5%) is still significantly higher than the guess probability at 33.3%, indicating that the perception of the phantom sensation was in agreement with the stimulation.

No current neurophysiologic theories can explain how the absent limb can affect the neural signals and phantom sensations can be perceived by the amputee. Although unclear about the mechanism of the connection between the absent limb and phantom limb sensation, we believe that a hidden human biological system may exist and be in connection with the "phantom limb." Further investigations are needed to verify our hypothesis as well as to elucidate this "phantom" connection.

V. Conclusions

We discovered that the phantom limb sensation could be induced with the phantom limb site exposed to FIR. Following an appropriate period of FIR on the absent limb, the amputee was able to perceive warm sensation for his phantom limb. The results of this study suggest that the absent limb is connected with the amputee in an unidentified form of communication.

References

1. Nikolajsen L, Jensen TS. In: Koltzenburg M, McMahon SB, editors. (2005) Wall and Melzack's Textbook of Pain. Amsterdam: Elsevier, pp. 961-71.
2. Flor H. (2002) Phantom-limb pain: characteristics, causes, and treatment. Lancet Neurol 1(3):182-9.
3. Giummarra MJ, Gibson SJ, Georgiou-Karistianis N, Bradshaw JL. (2007) Central mechanisms in phantom limb perception: the past, present and future. Brain Res Rev 54(1):219-32.
4. Jensen TS, Krebs B, Nielsen J, Rasmussen P. (1983) Phantom limb, phantom pain and stump pain in amputees during the first 6 months following limb amputation. Pain 17:243-56.
5. Davis RW. (1993) Phantom sensation, phantom pain, and stump pain. Arch Phys med Rehablil 74:79-91.
6. Flor H, Nikolajsen L, Jensen TS. (2006) Phantom limb pain: a case of maladaptive CNS plasticity? Nat Rev Neurosci. 7(11):873-81.
7. Hill A. (1999) Phantom limb pain: a review of the literature on attributes and potential mechanisms. J Pain Symptom manage 17:125-42.
8. Canavero, S. (1994) Dynamic reverberation: A unified mechanism for central and phantom pain. Med Hypotheses 42:203-207.
9. Flor H, Elbert T, Knecht S, Wienbruch C, Pantev C, Birbaumer N, Larbig W, Taub E. (1995) Phantom-limb pain as a perceptual correlate of cortical reorganization following arm amputation. Nature 375(6531):482-4.
10. Grüsser SM, Winter C, Mühlnickel W, Denke C, Karl A, Villringer K, Flor H. (2001) The relationship of perceptual phenomena and cortical reorganization in upper extremity amputees. Neuroscience 102:263-72.
11. Melzack R. (1990) Phantom limbs and the concept of a neuromatrix. Trends Neurosc 13:88-92.
12. Merzenich MM, Nelson RJ, Stryker MP, Cynader MS, Schoppmann A, Zook JM. (1984) Somatosensory cortical map changes following digi amputation in adult monkeys. J Comp Neurol 224:591-605.
13. Pons TP, Garraghty PE, Ommaya AK, Kaas JH, Taub E, Mishkin M, (1991) Massive Cortical Reorganization After Sensory Deafferentation in Adult Macaques. Science 252(5014):1857-60.
14. Ramachandran VS, Rogers-Ramachandran D, Stewart M. (1992) Perceptual correlates of massive cortical reorganization. Science 258(5085):1159-60.
15. Katz J. (1992) Psychophysiological contributions to phantom limbs. Can. J. Psychiatry 37:282-98.
16. Sherman RA, Sherman CJ, Bruno GM. (1987) Psychological factors influencing chronic phantom limb pain: an analysis of the literature. Pain 28:285-95.
17. Sherman RA, Sherman CJ, Gall NG. (1980) A survey of current phantom limb pain treatment in the United States. Pain 8:85-99.
18. Keil G. (1990) So-called initial description of phantom pain by Ambroise Pare.'Chose digne d'admiration et quasi incredible':the douleur es parties mortes et amputees'. Fortschr Med 108:62-66.

19. Paré A. (1634) Workes of that Famous Chirurgion Ambrose Parey. Translated out of Lattine and compared with the French, by Tho. Johnson. Thomas Cotes and R Young, London.
20. Davis KD, Kiss ZH, Luo L, Tasker RR, Lozano AM, Dostrovsky JO. (1998) Phantom sensations generated by thalamic microstimulation. Nature 391(6665):385-7.
21. Yamamoto T, Katayama Y, Obuchi T, Kano T, Kobayashi K, Oshima H, Fukaya C. (2006) Thalamic Sensory Relay Nucleus Stimulation for the Treatment of Peripheral Deafferentation Pain. Stereotact Funct Neurosurg 84:180-3.
22. Flor H. (2008) Maladaptive plasticity, memory for pain and phantom limb pain: review and suggestions for new therapies. Expert Rev Neurother 8(5): 809–18.
23. Finnerup NB, Sindrup SH, Jensen TS. (2007) Chronic neuropathic pain: mechanisms, drug targets and measurement, Fundam. Clin. Pharmacol. 21, 129-136.
24. Moulin DE, Clark AJ, Gilron I et al. (2007) Pharmacological management of chronic neuropathic pain - consensus statement and guidelines from the Canadian Pain Society. Pain Res Manag. 12(1):13-21.

The address of the corresponding author:

Author: K.S. Hsu
Institute: Department of Biomechatronic Engineering, National Ilan University
Street: No.1 Shen-Nung Rd, Sec. 1
City: I-Lan
Country: Taiwan
Email: khhsu@niu.edu.tw

Identification of Neutron-Induced Isotopes in Varian LINAC System

Keun Yeong Kim[1], Jungwon Kwak[1], Sung Ho Park[2], Eun Kyung Choi[2],
Jong Hoon Kim[2], Sang-wook Lee[2], Si Yeol Song[2], Sang Min Yoon[2], and Seung Do Ahn[2]

[1] Department of Radiation Oncology, Asan Medical Center, Seoul, South Korea
[2] Department of Radiation Oncology, Asan Medical Center, College of Medicine, University of Ulsan, Seoul, South Korea

Abstract— **To investigate the neutron-induced radioactivity, we have measured and analyzed the energy spectrum of decay gammas in external radiotherapy system. The measurements has performed with two of Clinac 21EX and Clinac 21EX platinum (Varian Medical System, USA) using a NaI crystal detector placed inside LINAC heads. After the spectrum had taken for 1 hour of data acquisition (DAQ) time, sequentially we took another spectrum under the same condition for 58 ~ 59 hours of the DAQ time. The ratios of full peak areas in the two gamma spectrums was compared with the ratio calculated with the lifetimes of isotopes corresponding to the decay gamma energy. The comparison method provides the identification of the induced isotopes using not only the decay energy of secondary gammas but also the lifetime of isotopes. The ratios of full peak areas for candidates was calculated as 40.6 (^{203}Pb), 27.7 (^{187}W), 34.6 (^{82}Br), 58.8 (^{54}Mn) and 34.7 (^{57}Ni). The area ratios of full peaks tagged by gamma energy spectrum were measured to be 39.5, 25.3~28.0, 29.3, 25.2 and 35.9~38.8 respectively, which are consistent within errors.**

Keywords— **Neutron-induced radioactivity, Varian LINAC, Gamma spectroscopy**

I. Introduction

In medical linear accelerators (LINAC), neutrons are generated when LINACs are operated with a high energy (more than 10MVp) x-ray beam [1-8]. The secondary neutrons are unnecessary in x-ray radiation treatments for cancer patients. On the contrary, these neutrons can cause the radiation complication for patients and the safety problem for radiation workers and therapists. Several studies of induced isotopes after radiation treatments already have reported. Especially, the issue of the neutron-induced radioactivity in the components of LINACs has been focused by radiotherapy centers and manufacturers [1-6].

The photonuclear interactions and neutron capture processes are involved in the production of neutron-induced radioactivity. These reactions can be formalized as

$$\text{Photonuclear interaction:} \quad X + {}^{A}_{Z}T = n + {}^{A-1}_{Z}D \qquad (1)$$

$$\text{Neutron capture process:} \quad n + {}^{A}_{Z}T = {}^{A+1}_{Z}D \qquad (2)$$

where the ${}^{A}_{Z}T$ is the target nuclide of atomic number Z and atomic mass number A; D is the daughter nuclide of the same atomic number Z to the target. The atomic mass numbers of secondary nuclides equal to A-1 after photonuclear interaction and to A+1 after neutron capture process.; X is a x-ray photon which has energy high enough to interact with nucleus via the photonuclear interaction; n is the neutron produced by the photonuclear reaction. The resulting nucleus in both interactions may be radioactive and may subsequently undergo β^+ and γ decay [3].

According to previous studies, the highest radioactivity due to secondary neutrons was measured in the gantry head of LINAC, since it had been exposed by the highest photon fluence. This radioactivity can significantly contribute to the radiation hazard for therapists and radiation workers [1, 2]. However, the investigation was not sufficiently established for some Varian LINACs. So, we have measured and analyzed the gamma spectrum from the neutron-induced radioactivity in the LINAC systems.

II. Material and Method

The gamma spectrum from the decay process of induced isotopes have been measured for two of Clinac 21EX, and Clinac 21EX platinum which have been operated in high energy mode of 15 MV x-ray (Varian Medical System, USA).

The data acquisition (DAQ) system consisted of a Thallium-doped Sodium Iodide (NaI) detector (802, Canberra, USA) coupled with a Photo-Multiplier Tube (PMT), a preamplifier (276, Ortec, USA), an amplifier (590A, Ortec, USA), and a Multi-Channel Analyzer (MCA) (Trump-Pci, Ortec., USA). The energy scale of the spectrums was calibrated using a ^{137}Cs source.

In order to obtain the gamma spectrum as long as possible, the experiments were started on a Friday afternoon after clinical treatments had been completed. The NaI crystal detector was placed inside the LINAC head with the open collimators as shown in Fig. 1.

O. Dössel and W.C. Schlegel (Eds.): WC 2009, IFMBE Proceedings 25/III, pp. 616–619, 2009.
www.springerlink.com

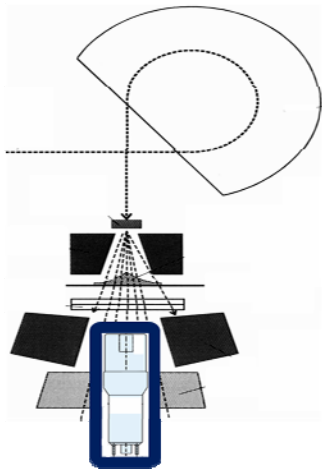

Fig. 1 Schematic view of experimental setup

After measuring a gamma spectrum for 1 hour of DAQ time, sequentially we took another spectrum in the same geometric condition for 58~59 hours.

The spectrums were analyzed using a purpose-made software program Gammavision-32 (Ortec, USA) and ROOT(version 5, CERN, Switzerland). The calibrated spectrum was readjusted to correct the nonlinearity of energy scale with the well known gamma peaks. The number of events of which the secondary gamma deposited its full energy inside the NaI detector could be extracted by fitting the area of Gaussian peaks assuming the 2nd polynomial background within the 3 sigma window of the peaks. For overlapped peaks, the multi-Gaussian and 2nd polynomial equation have been used as the fitting function with an enlarged fitting region. The event ratio of full peaks taken in the different DAQ time was compared with the value calculated using a formalized decay function (Eq. 3).

$$I(t) = I(0) \cdot e^{-(\frac{\ln 2}{T_{1/2}})\cdot t} \tag{3}$$

, where $T_{1/2}$ is the half-life time and I(t) is a radioactivity of the isotope at time t. The event ratio for a different DAQ time was calculated as following Eq. 4.

$$\frac{\int_{1}^{60} I(t)\,dt}{\int_{0}^{1} I(t)\,dt} = \frac{e^{-\frac{\ln 2}{T_{1/2}}} - e^{-\frac{60\cdot \ln 2}{T_{1/2}}}}{1 - e^{-\frac{\ln 2}{T_{1/2}}}} \tag{4}$$

The isotopes were tagged by the characteristic energy of secondary gammas in the decay processes and also the ratio of the fitted areas for full peaks corresponding to the decay energy. The decay energy and the lifetime of isotopes were used to identify the isotopes.

In a general case, the energy resolution dependence for scintillation detector σ/E as a function of the incoming radiation energy E can be expressed by the Eq. 5:

$$\frac{\sigma}{E} = \frac{a}{\sqrt{E}} \oplus \frac{b}{E} \oplus c \tag{5}$$

where $\oplus$ represents quadratic addition, *a* is the stochastic term determined by the fluctuation of the deposited energy; *b* is the "noise" term determined by the noise of the photoreceiver; and *c* is a constant term determined by the light output non-uniformity of the scintillation material [10]. The fitting parameter *b* and *c* are much smaller than *a,* so that they are negligible. Then the energy resolution formula can be rewritten as Eq. 6.

$$\sigma = a\sqrt{E} \tag{6}$$

Since the widths of each peak have a dependence on their peak energy, the energy resolution information is also helpful to examine the peak identification.

III. Result and Discussion

The target, primary collimator and jaws of LINACs are mainly made of tungsten (W). The flattening filters are consisted of steel alloy. Copper (Cu), nickel (Ni) and lead (Pb) are the main components of shielding materials placed inside accelerators. Based on these atomic components, the candidates of neutron-induced isotopes could be selected as listed in Table 1.

Table 1. Candidates of the isotopes in the medical linear accelerator head

Radionuclide	Half-life	Gamma energy (keV)	Produced by
W-187	23.7 h	480, 686	^{186}W(n,r)^{187}W
Cu-62	9.74 m	511	Annihilation
Ni-57	35.6 h	1378, 1920	^{58}Ni(r,n)^{57}Ni
Al-28	2.24 m	1778	^{27}Al(n,r)^{28}Al
Fe-59	44.5 d	1099, 1292	^{58}Fe(n,r)^{59}Fe
Mn-54	312 d	835	^{55}Mn(r,n)^{54}Mn
Cr-51	28 d	320	^{50}Cr(n,r)^{51}Cr
Co-57	272 d	122	^{58}Ni(r,n)^{57}Co

The gamma energy spectrums have been measured for the three VARIAN LINACs as shown in Fig 2. Total 7

peaks have been resolved in each spectrum as listed in Table 2. Each peak has been identified to the decay gammas from isotopes by fitting a Gaussian function and 2nd polynomial background. The area of the Gaussian function represents the number of events in which a decay gamma deposits its total energy to the effective volume of NaI crystal detector. In the same DAQ condition, the detection efficiency of mono-energetic gammas would be same. The area ratio of peaks for different DAQ times is dependent on the DAQ time and the half-life time of isotopes as shown in Eq. 4.

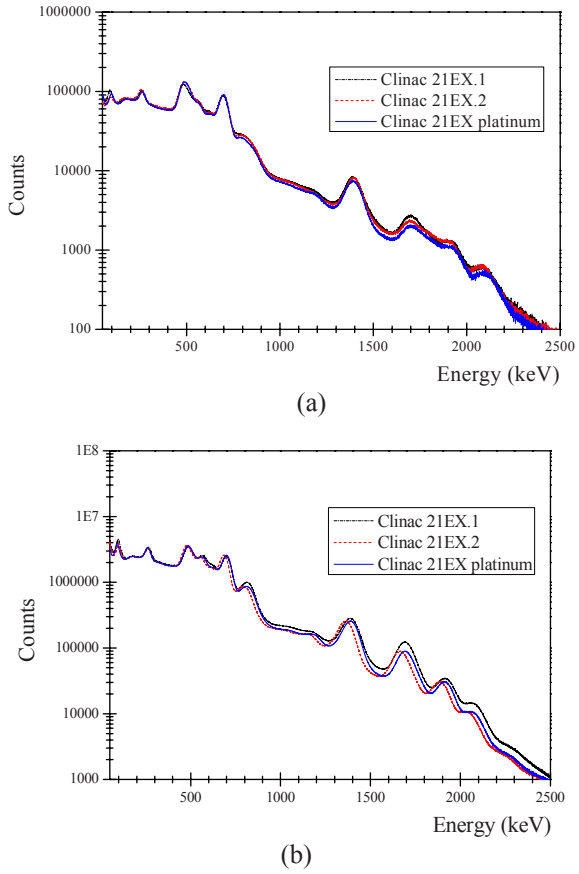

Figure 2. Decay gamma spectrums obtained at three LINAC heads: (a) 1 hour DAQ time (b) 58 (Clinac 21EX.1) and 59 hours DAQ time

The ratios of full peak area of two spectra which are under the same experimental condition except DAQ time were shown in table 2. The comparison with the calculated ratios from candidate half-life was made in table 3.

Table 2. Full peak area ratio of the obtained spectra

Peak	E (keV)	Clinac 21EX.1		Clinac 21EX.2		Clinac 21EX.p		Avg.	
		59/1 ratio	σ	58/1 ratio	σ	59/1 ratio	σ	Ratio	σ
1	261	35.8	0.1	39.4	0.1	43.4	0.1	39.5	0.1
2	482	25.3	0.1	27.3	0.1	23.3	0.1	25.3	0.1
3	562	33.6	0.1	25.7	0.1	28.5	0.1	29.3	0.1
4	693	31.1	0.1	25.6	0.1	27.3	0.1	28.0	0.1
5	806	43.9	0.3	20.2	0.2	11.6	0.1	25.2	0.1
6	1382	35.5	0.1	36.1	0.1	36.1	0.1	35.9	0.1
7	1900	23.1	0.5	43.9	1.7	49.3	1.4	38.8	0.8

Table 3. Candidates of neutron-induced isotopes and calculated peak ratio for their half-life times

Peak	E (keV)	Candidates				Full peak area ratio
		Isotope	E (keV)	Half-life	Lifetime ratio	
1	261	^{203}Pb	297	51.9 h	40.6	39.5±0.1
2	482	^{187}W	480	23.7 h	27.7	25.3±0.1
3	562	^{82}Br	554	35.3 h	34.6	29.3±0.1
4	693	^{187}W	686	23.7 h	27.7	28.0±0.1
5	806	^{54}Mn	835	312 d	58.8	25.2±0.1
6	1382	^{57}Ni	1378	35.6 h	34.7	35.9±0.1
7	1900	^{57}Ni	1920	35.6 h	34.7	38.8±0.8

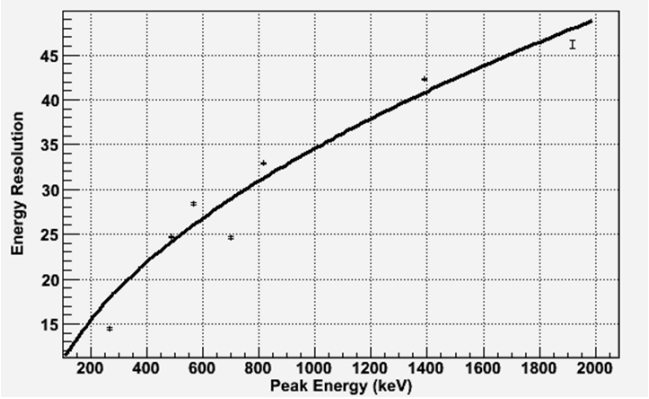

Fig. 3 Fitting parameter of peak width values (points) and fitting energy resolution curve (solid curve)

Figure 3 show the fitting results of the peak widths corresponding to their peak energy. The fitting curve was used the energy resolution relation as listed in Eq. 6. Some of peak values disagree with fitting curve. These differences result from the contamination of gamma-rays of other isotopes or the background unstability. Though the resolution

analysis, the systematic error of the peak area ratio was examined.

IV. Conclusions

In this study, we could identify the neutron-induced isotopes in Varian linear accelerators operated in high-energy mode, using decay energy spectrum and decay lifetime. The activation predominated in the tungsten which is the main components of LINAC head. Successive study will be continued for quantitative results. That would be expected to be necessary for radiation safety issue.

Acknowledgment

This work was supported by nuclear technology development program (M20806000066-08B0600-06610) of Korea Science and Engineering Foundation (KOSEF) and Ministry of Education, Science, and Technology (MEST), Korea government. .

References

L Ahlgren and L E Olsson. (1988) Induced activity in a high-energy linear accelerator. Phys. Med. Biol., vol. 33, 3:351-354

A Almen, L Ahlgren and S Mattsson. (1991) Absorbed dose to technicians due to induced activity in linear accelerators for radiation therapy. Phys. Med. Biol., vol. 36, 6:815-822

Yi Zhen Wang, Michael D. C. Evans, and Ervin B. Podgorsak (2005) Characteristics of induced activity from medical linear accelerators. Phys. Med., vol. 32, 9:2899-2910

Helmut W Fischer, Ben E Tabot, and Bjorn Poppe (2006) Activation process in a medical linear accelerator and spatial distribution of activation products. Phys. Med. Biol., vol. 51, N461-N466

M Roig, V Panettieri, M Ginjaume, and A Sanchez-Reyes (2004) Photonuclear isotope characterization of a Siemens KDS 18 MV linac head. Phys. Med. Biol., vol. 49, N243-246

E. Stranden (1977) Activity induced in patients by high energy X-ray therapy. Phys. Med. Biol., vol. 22, 2:348-352

A. Ma, J. Awotwi-Pratt, A. Alfuraih, N. M. Spyrou (2008) Monte Carlo study of photoneutron production in the Varian Clinac 2100C linac. J. Radioanalytical and Nuclear Chemistry, vol. 276, 1:119-123

N L Powell, A Newing, M A Bullen, C Sims, and S F Leaton (1987) A radiation safety survey on a Clinac-20 linear accelerator. Phys. Med. Biol., vol. 32, 6:707-718

Ortec, Maestro-32 A65-B32 software user's manual, software Version 6.0

G.I. Britvich, I.G. Britvich, V.G. Vasil'chenko, V.A. Lishin, V.F. Obraztsov, V.A. Polyakov, and A.S. Solovjev (1999) Search for new scintillators for high-energy resolution electromagnetic calorimeters. Nuclear Instruments and Methods in Physics Research A, vol. 426, 453-463

Author: Sung Ho Park
Institute: Asan Medical Center/ Dept. of Radiation Oncology
Street: 388-1 Pung Nap Dong, Song Pa Gu,
City: Seoul
Country: South Korea
Email: michael@amc.seoul.kr

Estimation of Core Temperature Elevation in Humans and Animals for Radio-Frequency Exposures

A. Hirata[1] and O. Fujiwara[1]

[1] Department of Computer Science and Engineering, Nagoya Institute of Technology, Nagoya, Japan

Abstract—**According to the international safety guidelines/standards for human protection, the whole-body averaged specific absorption rate (WBA-SAR) is used as a metric. In order to understand the relationship between WBA-SAR and core temperature elevation, a theoretical solution or a closed formula for estimating core temperature elevation is highly desirable. In this study, we derive a formula for simply estimating core temperature elevation in humans and animals for whole-body radio-frequency exposure. This formula is based on a well-known bioheat equation. The core temperature elevation estimated with this formula is found to be in reasonable agreement with the computational results of finite-difference time-domain computation incorporated in anatomically-based models. Based on the formula, the main factors influencing the core temperature elevation are specified as the perspiration rate and the body surface area-to-weight ratio. For the same WBA-SAR, the temperature rise in the child is found to be smaller than that of the adult due to the body-surface area-to-weight ratio.**

Keywords— **radio-frequency exposure, core temperature elevation, whole-body averaged specific absorption rate, radiation protection**

I. Introduction

There has been increasing public concern about the adverse health effects of human exposure to electromagnetic waves. In radio-frequency (RF) regions, elevated temperature (1-2^{o}C) resulting from energy absorption is known to be a dominant factor inducing adverse health effects such as heat exhaustion and heat stroke [1]. In the international safety guidelines/standards [2, 3], the whole-body averaged specific absorption rate (WBA-SAR) is used as a metric of human protection for RF whole-body exposure. The threshold of the WBA-SAR is noted as 4-8 W/kg. This threshold is based on the fact that RF exposure of laboratory animals in excess of approximately 4 W/kg has revealed a characteristic pattern of thermoregulatory response [4]. In addition, decreased task performance by rats and monkeys has been observed at WBA-SAR in the range of 1–3 W/kg [5]. According to [6], the physiological heat loss mechanisms are different for different species. In particular, small animals would be poor models for human beings. However, the relationship between WBA-SAR and core temperature elevation in humans for RF whole-body exposures has not been discussed sufficiently, nor has the difference due to species.

We have developed an electromagnetic-thermal simulation code based on a finite-difference time-domain (FDTD) scheme with anatomically-based body phantoms for humans [7] and rabbits [8]. The unique aspect of our computational code is that it can take into account the time evolution of core or blood temperatures. A theoretical solution or a closed-form expression for estimating core temperature elevation is highly desirable for a greater understanding of the relationship between WBA-SAR and core temperature elevation, since such computational schemes take a long time to analyze the time course of core temperature elevation. Semi-analytical expressions of the thermoregulatory response in humans have been proposed in several studies (e.g., [9, 10]), and its applicability for RF exposures has been discussed by comparative measurements [11]. In these models, the human body is divided into several parts and their corresponding parameters are required. Although these models can be extensively applied, a simpler formula can be derived by focusing on the estimation of core temperature elevation from RF energy absorption.

In the present study, we derive a formula for simply estimating the core temperature elevation in humans by RF whole-body exposure. The validity of the formula is confirmed by comparing to the results with the FDTD scheme.

II. Models and Methods

A. Numeric Phantoms

The computational phantoms used in the present study are illustrated in Fig. 1. Whole-body voxel phantoms for a Japanese adult male and a Japanese adult female were developed by Nagaoka et al. [12]. Volunteers were selected whose dimensions were close to the average values of Japanese. The male volunteer was 22 years old, 1.73 m tall and weighed 65.0 kg; the female volunteer was 22 years old, 1.6 m tall and weighed 53.0 kg. The numeric phantoms were developed based on the magnetic resonance images of these volunteers. The resolution of the phantoms was 2 mm segmented into 51 anatomical regions. A phantom for children

O. Dössel and W.C. Schlegel (Eds.): WC 2009, IFMBE Proceedings 25/III, pp. 620–623, 2009.
www.springerlink.com

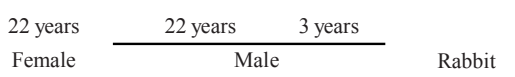

Fig. 1. Human and rabbit numeric phantoms

threes year of age was developed by applying a freeform deformation algorithm to the male phantom [13]. In this model, a total of 66 body dimensions was taken into account, and then shrunk with different scaling factors. Manual editing was applied in order to maintain their anatomical validity. The resolution of these phantoms was kept to 2 mm. The height and weight of the child phantom are 0.9 m and 13 kg. A voxel phantom for a rabbit has been developed in [14]. The resolution of the phantom was 1 mm segmented into 12 anatomical regions. This was constructed on the basis of X-ray CT images taken at Kanazawa Medical University, Japan. The width, depth, and height of this model were 123 mm, 260 mm, and 152 mm, respectively. The weight of the rabbit phantom was 2.0 kg.

B. Electromagnetic Dosimetry

The FDTD method is used for investigating the RF power absorbed in the numeric phantoms. For a truncation of the computational region, we adopted perfectly matched layers as the absorbing boundary. To incorporate the numeric phantoms into the FDTD scheme, the dielectric properties of tissues were required. These properties were determined by 4-Cole-Cole extrapolation [15]. For harmonically varying fields, the SAR is defined as

$$\mathrm{SAR} = \frac{\sigma}{2\rho}|\hat{E}|^2 = \frac{\sigma}{2\rho}(|\hat{E}_x|^2 + |\hat{E}_y|^2 + |\hat{E}_z|^2) \tag{1}$$

where $\hat{E}_x$, $\hat{E}_y$, and $\hat{E}_z$ are the peak values of the electric field components, σ and ρ, which denote the conductivity and the mass density of the tissue, respectively.

C. Thermal Dosimetry

Our computational code for the temperature calculation was given in our previous studies for humans [7] and rabbits [8], in which validate our code by comparison with measurements. The computational method of our thermal dosimetry is given briefly, since it is based on our formula. The air temperature is 28 ^{o}C as a thermoneutral condition. Note that computational thermal dosimetry in humans has been conducted extensively for whole-body exposures in different scenarios.

For calculating temperature elevations in the numeric phantoms, a bioheat equation was used [16]:

$$C(\mathbf{r})\rho(\mathbf{r})\frac{\partial T(\mathbf{r},t)}{\partial t} = \nabla\cdot(K(\mathbf{r})\nabla T(\mathbf{r},t)) + \rho(\mathbf{r})SAR(\mathbf{r}) + A(\mathbf{r}) - B(\mathbf{r},t)(T(\mathbf{r},t) - T_B(t)) \tag{2}$$

where $T(\mathrm{r},t)$ and $T_B(t)$ denote the respective temperatures of tissue and blood, C represents the specific heat of tissue, K represents the thermal conductivity of tissue, A represents the basal metabolism per unit volume, and B represents the term associated with blood perfusion. In rabbits, it takes far less time due to their smaller dimensions and higher blood perfusion rate than those of humans. The boundary condition between air and tissue for (2) is given by the following equation:

$$-K(r)\frac{\partial T(\mathbf{r},t)}{\partial n} = h(\mathbf{r})\cdot(T_s(\mathbf{r},t) - T_e) + SW(t) \tag{3}$$

where h, T_s, and T_e denote, respectively, the heat transfer coefficient, surface temperature, and air temperature. The heat transfer coefficient h is given by the summation of radiative heat loss h_{rad} and convective heat loss h_{conv}. SW represents the perspiration rate, which will be discussed in the next subsection. The thermal constants of tissue used in the present study have also been summarized [8], [9]. Different heat transfer coefficient between tissue and air are used dependent on body part. Specifically, the heat transfer coefficient between skin and air and that between tissue and internal air for human models are 4.0 W/m^2/^{o}C and 13 W/m^2/^{o}C. For the rabbit model, the respective values of the heat transfer coefficient between the skin and air, that between internal air and tissue, and that between ear lobe and air is 0.65 W/m^2/^{o}C, 13 W/m^2/^{o}C, and 2.5 W/m^2/^{o}C.

The blood temperature is changed with time according to the following equation in order to satisfy thermodynamic laws [17]:

$$T_B(t) = T_{B0} + \int_t \frac{Q_{BTOT}(t)}{C_B\rho_B V_B}dt \tag{4}$$

$$Q_{BTOT}(t) = \int_V B(t)(T_B(t) - T(\mathbf{r},t))dV \tag{5}$$

where Q_{BTOT} is the rate of heat acquisition of blood from body tissues. C_B (=4000 J/kg·^{o}C), ρ_B (=1050 kg/m^3), and V_B denote the specific heat, mass density, and total volume of blood.

For a temperature elevation above a certain level, blood perfusion was activated in order to carry away the excess

heat produced [18, 19]. As to the blood perfusion for all tissues except the skin, the regulation mechanism was governed by the local tissue temperature. Blood perfusion was equal to its basal value when that temperature remained below a certain level. Once the local temperature exceeded a given threshold, blood perfusion increased almost linearly with the temperature in order to carry away the heat produced. The main difference between humans and rabbits in the thermoregulatory response is that the sweat glands in rabbits are virtually nonfunctional, allowing us to neglect this mechanism. Then, the perspiration rate was simplified to be zero in the rabbit. The perspiration coefficients in the humans are assumed to depend on the temperature elevation in the skin and/or hypothalamus.

III. FORMULA DERIVATION

In this section, we derive a formula for simply estimating the core temperature elevation with WBA-SAR. Let us consider the heat balance of a biological body, given by [6]:

$$M + P_{RF} - P_t = P_s \tag{6}$$

where M is the rate at which thermal energy is produced through metabolic processes, P_{RF} is the RF power absorbed in the body, P_t is the rate of heat transfer at the body surface, and P_S is the rate of heat storage in the body. From (6), the total heat balance between the body and air is essential to characterize core temperature elevation. More specific expression for (6) is given in the following equation based on (2) and (3).

$$\begin{aligned}&\int_0^t \int_V \big(A(\mathbf{r},\tau) - A_0(\mathbf{r})\big) dV d\tau + \int_0^t \int_V SAR(\mathbf{r}) \cdot \rho(\mathbf{r}) dV d\tau \\ &- \left\{ \int_0^t \int_S h(\mathbf{r}) \big(T(\mathbf{r},\tau) - T_0(\mathbf{r})\big) dS d\tau + \int_0^t \int_S SW(\tau) dS d\tau \right\} \\ &= \int_V \big(T(\mathbf{r},\tau) - T_0(\mathbf{r})\big) \cdot \rho(\mathbf{r}) \cdot C(\mathbf{r}) dV\end{aligned} \tag{7}$$

where T_o and A_o are the thermal steady temperature and basal metabolic rate without RF exposures. The first term of (8) represents the energy due to the metabolic increment caused by the temperature elevation. In the present study, this term is ignored for simplicity, since that energy evolves secondarily via the temperature elevation due to RF energy absorption [11].

Then, we obtained the following equation, as (7) suggests that the SAR and temperature distributions can be assumed to be uniform over the body:

$$\begin{aligned}\big(T(t) - T_0\big) \cdot W \cdot C_{WBave} &= SAR_{WBave} \cdot W \cdot t \\ &- \int_0^t \big(T(\tau) - T_0\big) d\tau \cdot \int_S (h(\mathbf{r}) + sw(t)) dS\end{aligned} \tag{8}$$

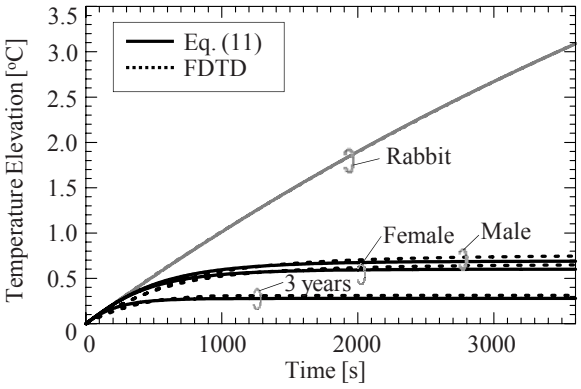

Fig. 2. Time course of core temperature elevation in human and rabbit models at 0.4 W/kg.

where $W = \rho_{WBave} \cdot V$ is the weight of the model [kg], SAR_{WBave} is the WBA-SAR[W/kg], and C_{WBave} is the mean value of the specific heat [J/kg °C]. $sw(t)$ is a coefficient identical to $SW(t)$ except that the temperature is assumed to be uniform. Then, by differentiating (9), the temperature elevation is obtained as

$$T(t) \simeq T_0 + \frac{W \cdot SAR_{WBave}}{S(H_{eff} + sw(t))} \cdot \left(1 - \exp\left(- \frac{S(H_{eff} + sw(t))}{W \cdot C_{WBave}} t \right) \right) \tag{9}$$

IV. RESUTLS AND DISCUSSION

Fig. 2 shows the time course of core temperature elevation for WBA-SAR at 0.4 W/kg in adult male and female models, and 3-year-old child model. The RF frequency is 2 GHz. From Fig. 2, the FDTD-derived and estimated core temperature elevation in less than a few minutes are in good agreement for different models and/or WBA-SAR values. On the other hand, some difference can be observed from a few minutes until reaching the thermally-steady state. The main reason for this difference can be attributed to our assumption that the temperature elevation in the body is spatially constant over the whole body. For different WBA-SAR, the difference between FDTD and (9) was less than 30%.

From (9), the steady-state core temperature elevation is largely influenced by the body surface area-to-weight ratio S/W [m^2/kg]. Note that the body surface area-to weight ratio was 0.041 m^2/kg for the adult male, 0.043 m^2/kg for the adult female, and 0.060 m^2/kg for the three-year-old child. The dominant factor influencing the thermal time constant is also the same as that of the steady-state core temperature elevation, since the specific heat marginally depends on the human models of different genders and/or ages. These can be confirmed in Fig. 2, in which the steady-state tempera-

ture elevation and thermal time constant in the three-year-old child model are smaller than those of the adult models. The FDTD-computed results given in these figures also support the conclusion based on the proposed formula.

V. SUMMARY

We proposed a formula which estimates the core temperature elevation in the human models with the WBA-SAR. As a result, the core temperature elevations estimated with the formula are in reasonable agreement with the results obtained with the FDTD computation (less than 30% difference), which takes much longer. We clarified the main factors influencing the core temperature elevation as the body surface area-to-weight ratio and perspiration rate. Then, the temperature elevation in the child is smaller than that of the adult for the same WBA-SAR mainly due to the body area-to-weight ratio. This is close related to RF research agenda by World Health Organization [20], which pays attention to temperature rise in children. The temperature elevation in the human is smaller than that in rabbits due to perspiration rate in addition to the difference in area-to-weight ratio, suggesting that guidelines based on animals yield conservative estimation.

ACKNOWLEDGMENT

This work was supported in part by Strategic Information and Communications R&D Promotion Programme (SCOPE)

REFERENCES

1. ACGIH, Threshold limit values for chemical substances and physical agents and biological exposure indices (Cincinnati OH) , 1996.
2. ICNIRP, "International Commission on Non-Ionizing Radiation Protection Guidelines for limiting exposure to time-varying electric, magnetic, and electromagnetic fields (up to 300 GHz)", *Health Phys.*vol.74, no.4, pp.494-522, Apr. 1998.
3. IEEE, "IEEE standard for safety levels with respect to human exposure to radio frequency electromagnetic fields, 3 kHz to 300 GHz," C95-1, 2005.
4. S. M. Michaelson, "Biological effects and health hazard of RF and MW energy; fundamentals and overall phenomenology. In: Biological effects and dosimetry of nonionizing radiation, New York, Plenum Press 337-357, 1983.
5. J. A. D'Andrea et al, "Behavioral and physiological effects of chronic 2450-MHz microwave irradiation of the rat at 0.5 mW/cm^2," *Bioelectromagnetics*, vol.7, pp.45-56, 1986.
6. E. R. Adair and D. R. Black, "Thermoregulatory responses to RF energy absorption," *Bioelectromagnetics Suppl*., vol.6, S17-S38, 2003.
7. A. Hirata, T. Asano, and O. Fujiwara, "FDTD Analysis of body-core temperature elevation in children and adults for whole-body exposure," *Phys. Med. Biol.*, vol.53, pp.5223-5238, 2008.
8. A. Hirata et al, "Computational model for calculating body-core temperature elevation in rabbits due to whole-body exposure at 2.45 GHz", *Phys. Med. Biol.*, vol.53, pp.3391-3404, 2008.
9. D. Fiala, K. J. Lomas, and M. Stohrer, "Computer prediction of human thermoregulation and temperature responses to a wide range of environmental conditions," *Int J Biometeorol*, vol.45, no.3, pp.143-159, 2001.
10. J. A. J. Stolwijk and J. D. Hardy, "Control of body temperature," In *Handbook of Physiology, Section 9, Reactions to environmental agents* Edited by: Douglas HK. Bethesda, MD: American Physiological Society, pp.45-69, 1977.
11. K. R. Foster and E. R. Adair, "Modeling thermal responses in human subjects following extended exposure to radiofrequency energy," Biomed. Online, vol.3, 4, 2004.
12. T. Nagaoka, et al, "Development of realistic high-resolution whole-body voxel models of Japanese adult male and female of average height and weight, and application of models to radio-frequency electromagnetic-field dosimetry," *Phys. Med. Biol.*, vol.49, pp.1-15, 2004.
13. T. Nagaoka, E. Kunieda, and S. Watanabe, "Proportion-corrected scaled voxel models for Japanese children and their application to the numerical dosimetry of specific absorption rate for frequencies from 30 MHz to 3 GHz," *Phys. Med. Biol.*, vol.53, pp.6695-6711, 2008.
14. K. Wake et al, "Development of a 2.45-GHz local exposure system for in vivo study on ocular effects," *IEEE Trans Microwave Theory & Tech.* vol.55, pp.588-596, 2007.
15. S. Gabriel, R. W. Lau, and C. Gabriel, "The dielectric properties of biological tissues: III. Parametric models for the dielectric spectrum of tissues," *Phys. Med. Biol.* vol.41, pp. 2271-293, 1996.
16. H. H. Pennes, "Analysis of tissue and arterial blood temperatures in resting forearm," *J. Appl. Physiol.*, vol.1, pp.93-122, 1948.
17. A. Hirata et al, "Computational verification of anesthesia effect on temperature variations in rabbit eyes exposed to 2.45-GHz microwave energy," *Bioelectromagnet*, vol.27 , pp.602-612, 2006.
18. K. R. Foster and R. Glaser, "Thermal mechanisms of interaction of radiofrequency energy with biological systems with relevance to exposure guidelines," *Health Phys*., vol.92, pp.609-620, 2007.
19. M. Hoque and O. P. Gandhi, "Temperature distribution in the human leg for VLF-VHF exposure at the ANSI recommended safety levels," *IEEE Trans Biomed Eng*, vol.35, pp.442-449, 1988.
20. http://www.who.int/peh-emf/research/rf_research_agenda_2006.pdf

Mammography Services in Malaysia: Review of Patient Dose Surveys in Mammography

Muthuvelu P. et al.

drpirunthavany@moh.gov.my, mpvany@gmail.com

Introduction

Malaysia is a participant in the IAEA Project RAS 9047 and a survey of mammography practice was carried out from the point of optimization of radiation protection in mammography.

Mammography is a reliable method for detecting lesions in the breast. It requires high standards of image quality and equipment performance because of the extremely low contrast between normal and pathological areas in the breast. Mammography is considered as the single most important diagnostic tool in the early detection of breast cancer. The aim is to produce reliable high-contrast, high-resolution images at the lowest radiation dose consistent with high image quality. In order to obtain high quality mammograms at an acceptable breast dose, it is essential to use the correct equipment and perform regular quality control tests on the mammography equipment.

The initial stages of the study (2007-2008) involved measurement of the average glandular dose to the standard ACR phantom. The study is ongoing and at present (2009) has progressed to measuring the clinical average glandular dose using the EUREF protocol. The results from the latter part of the ongoing study will be presented at the conference. The performance of the imaging system was checked by using a high-contrast resolution tool. The image quality was assessed and evaluated using the RMI 156 phantom.

Background

In Malaysia, the Quality Assurance Program (QAP) for mammography was initiated in 1995 by the Ministry of Health (MOH). It was based on the American College of Radiology Model. The QAP was launched as a strategy to evaluate the quality of services provided in a planned and systematic manner. The components of the QAP comprise acceptance testing, quality control (QC), calibration, maintenance of equipment, performance indicator analysis, audit, continuous professional education including training and refresher courses, documentation and sufficient qualified, trained and experienced staff and other resources.

Regular QC is done to ensure that the equipment and associated facilities function and continue to function optimally. The performance indicator is used to monitor the program performance, initiate investigation, take corrective action and institute improvement measures. The audit is done to determine conformance and to take corrective action for improvement. Training is necessary to gain and update the knowledge of the staff and documentation is required for the purpose of reference and records. There should be enough staff and other resources to carry out the program effectively. Film reject rate analysis is an indicator used to monitor the efficiency of the staff and equipment. A high percentage may be an indicator for the breakdown in efficiency. Statistical analysis is also needed for process control.

O. Dössel and W.C. Schlegel (Eds.): WC 2009, IFMBE Proceedings 25/III, pp. 624–627, 2009.
www.springerlink.com

A low dose level indicator and good image quality indicates the effectiveness of the QAP. The QC of mammography equipment and associated facilities is necessary to achieve consistently high quality mammograms, to limit radiation dose to the patient, to minimize the number of women undergoing repeat examinations, to minimize the number of women for further views, and to minimize the number of unnecessary invasive procedures. The subtle attenuation difference between normal and diseased tissues in the breast requires a very high degree of resolution.

Factors affecting performance of the dedicated mammography unit include the x-ray tube voltage, alignment, image viewing conditions, AEC calibration and radiation output. The basic tests that need to be done are the mammography unit assembly evaluation, collimation assembly test, kVp accuracy and reproducibility, beam quality assessment, AEC system performance, breast entrance exposure and average glandular dose and image quality evaluation.

Methodology

The performance of the imaging system was checked by using the American College of Radiology (ACR) high-contrast resolution tool. The image quality was assessed using the ACR accredited RM156 phantom. Image quality was scored by 2 qualified medical physicists according to ACR protocols and viewed on the same viewbox. The same cassette and x-ray films from the same box were used and the films were processed according to the normal and standard practice of each facility.

Dose measurements were done using the Unfors and the PTW Diados dosemeters. The average glandular dose (AGD) is the special dose quantity used in mammography. AGD is the reference term (ICRP 1987) for radiation dose estimation for mammography i.e. the average absorbed dose in the glandular tissue in a uniformly compressed breast. AGD value depends on the X-ray beam quality (HVL), breast thickness and composition. It is defined as the mean or average dose to the glandular tissue within the breast. The exposure dose in mammography from 1995 till 2008 was routinely evaluated according to the ACR guidelines. As direct estimation of the AGD is not feasible, it is often estimated from the measurements of the breast entrance skin exposure and converted to AGD by applying conversion factors (ACR, 1999; Wu, 1991). The ACR specifies that the AGD should not exceed 3 mGy per view for screen-film image receptors (ACR, 1994; Frank, 2005; Suleiman et al., 1999). This method for estimating the MGD to the breast of a patient consisted of collecting the data on compressed breast tissue (CBT). The application of a compression force to the breast during image acquisition is to immobilise the breast to limit motion artefacts, and to reduce breast thickness, which limits scatter effects and makes breast thickness approximately uniform. The tube voltage, and mAs and target/filter combination for each patient was also noted. The breast entrance skin exposure was measured by using the ionization chamber placed in the x-ray field. The exposure measured (mR) was converted to the AGD according to ACR recommendations (American College of Radiology, 1999).

Starting in late 2008 and presently in 2009, the AGD is calculated according to the method provided in Appendix 1 of EUREF European guidelines for quality assurance in mammography screening (Third or Forth Edition; www.euref.org). The formula D=Ke*g*c*s is used where, Ke is the entrance surface air kerma and the factors g, c, s are conversion and correction coefficients. The g-factor corresponds to a glandularity of 50% and is a function of

PMMA/Breast thickness and half value layer (HVL). The c-factor takes into account breast composition for different patient age groups (50-64 and 40-49 y). The s-factor corrects for differences in x-ray spectra (anode/filter combination).

The AGD can be determined by first getting the incident air kerma measurements on the standard phantom and standard breast. Incident air kerma is the air kerma from the incident beam on the central x-ray beam axis at the focal-spot-to surface distance at the skin entrance plane. Only primary radiation incident on the patient or phantom is measured. Backscattered radiation is not included. Individual AGD can be determined by the incident air kerma (AK) measurements and the use of the conversion factors for breast thickness.

If Incident AK is represented by K_i, then:

ESAK (mGy) = Y (mGy/mAs) x mAs x [FDD/(FRD-phantom thickness)]^2 x BSF

The output, $Y = K_i$ /mAs $_{output}$, This is measured in manual mode at known kVp & anode/filter combination. This factor Y is pre-determined and is then used to measure ESAK in clinical situations where the mAs will vary according to the thickness of the individual patient. The FDD is the focus to detector distance, measured during determination of output, FID is the focus to receptor distance, t_p is the breast thickness and BSF is the backscatter factor. Backscatter factor is a function of HVL (Jansen et al. 1994) and if the information on the HVL is lacking, a backscatter factor of 1.09 can be applied.

The AGD **cannot be measured directly**, but it is derived from measurements of the HVL and of the ESAK (with a standard phantom) making use of tabulated conversion factors which have been derived from Monte Carlo calculations and verified experimentally. **AGD= ESAK x g x c x s.**

Results and Discussion

The results of the resolution test show a mean of 11 lp/mm.

kVp Setting	No. of Mammography Units	Mean Optical Density	Spatial Resolution (lp/mm) Values			
			Range	Mean	1st Quartile	3rd Quartile
26	19	1.38	9 - 14	11.9	11.0	12.5
28	20	1.44	8 - 13	11.7	11.0	12.0
30	20	1.46	8 - 14	11.7	11.0	12.0

The results of the image quality using the RMI 156 phantom showed an average score of **4 fibres, 3 specks and 3 masses** which are acceptable under the ACR protocols.

No. of Mammography Units	AGD (mGy)
10	0 – 0.5
3	0.6 – 1.0
3	1.1 – 1.5
3	1.6 – 2.0
0	2.1 – 2.5
1	2.6 – 3.0

Both the dosimeters gave comparable readings in mGy with maximum deviation of 5%. In an earlier study in Malaysia the mean AGD was found to be 1.05 [Jamal et al.,The British Journal of Radiology, 76 (2003), 238–245). In this study the mean AGD for 20 mammography units surveyed was found to be 1.04 mGy.

Conclusions

The mammograms were within the acceptable image quality criteria and average glandular dose limits in this survey. The result shows that the mean phantom MGD values obtained is consistent with studies from other countries and is well below the standard of 3 mGy (ACR).

Surveys of image quality and patients doses in simple radiographic examinations in Armenia

K.Stepanyan[1], R.Mkrtchyan[2], A.Gabrielyan[3]

[1] Research Center of Radiation Medicine and Burns, Department of Radiation Safety Ministry of Health, Yerevan, ARMENIA, k.stepanyan@web.am
[2] "Santa Nerses Great" Hospital, Yerevan, ARMENIA
[3] Polyclinic No 20, X-ray Department , Yerevan, ARMENIA

This study was conducted in the frameworks of IAEA TC Regional Project RER 9/093 in order to develop national program of Quality Assurance (QA). There were considered entrance surface air kerma (ESAK), image quality and films reject analysis for average-sized patients in 6 Hospitals (6 X-ray rooms). The examinations were conducted during 2007-2009 in 2 stages. The dosimetry of patients was performed using ESAK and then taking into account the exposure and backscatter factors for selected examinations. The image quality was assessed in accordance with EC image quality criteria. There were studied X-ray examinations of chest-PA, Spine-Lat, Skull, Pelvic for 10 patients for each projection. The following corrective actions were used for each of X-ray room: increase of kV, decrease of mAs, increase of FFD, correction of additional filtration, optimization of film processing quality and darkroom fog.

The median value of ESAK for chest-PA examinations reduced from 0.86 - 3.78 mGy to 0.13 – 0.30 mGy (max. 96% reduction), Lumbar spine PA reduced from 9.56 – 17.58 mGy to 5.95 – 11.76 mGy (max. 38% reduction), Lumbar spine Lat reduced from 16.6 – 40.96 mGy to 11.9 – 21.2 mGy (max. 48 % reduction), Skull PA reduced from 12.3- 13.3 to 3.7 – 5.2 mGy (max. 70% reduction) and Pelvic AP reduced from 8.8 – 19.1 mGy to 6.5 – 10.4 mGy (max. 46% reduction). The image quality ameliorated up to 40%. A number of rejected films reduced from 12.6% to 5.6%. Reduction of culling from over/under exposure was 37%, and from processing - 26.7%. The conducted examinations allowed the Armenian radiologists to demonstrate that by means of simple and low-cost methods the image quality can be significantly ameliorated and patients' doses reduced.

Keywords - **Quality Assurance, patient doses, image quality, films reject, X-ray examinations**

O. Dössel and W.C. Schlegel (Eds.): WC 2009, IFMBE Proceedings 25/III, p. 628, 2009.
www.springerlink.com

Evaluation of Average Glandular Doses in UAE Hospitals

N.K. ALmazrouei[1], F. Alkaabi[2], J. Janaczek[2], S.A .Gilani[1], A. Zitouni[1], J. AlSuwaidi[1], and S. Alkalbani[1]

[1]Dubai Health Authority/Dubai Hospital/Medical Physics department, Dubai, UAE
[2] Tawam Hospital/Medical Physics department, AlAin, UAE

A national survey of patient exposure in mammography started recently in the United Arab Emirates, within the framework of the IAEA regional project on patient exposure in radiology. In this respect, the survey began with seven participating hospitals, all users of digital mammography and it will be extended gradually to other groups of hospitals. The insufficiency of available qualified Medical Physicist teams and also of equipment, combined with the vast workload of all hospitals in the country do not allow a large scale survey at the moment. The main purpose of this work is to determine the Average Glandular Dose in mammography facilities using tissue-mimicking phantoms to ensure that exposed patients are not submitted to high X-ray doses. The AGD values determined by the Physicists were checked against the relevant international standards and compared to the AGD values generated by the mammography system. Prior to the dosimetry work, image quality and X-ray beam parameters were checked for compliance with the applicable standards.

Patient dosimetry, Average Glandular Dose, Radiation Protection, Entrance Surface Air Kerma

I. Introduction

In the United Arab Emirates (UAE), the number of mammography examinations has been rising steadily the past few years due to the rapid economic growth of the country and the increasing use of computed & digital radiography systems (CR and DR), as film-based mammography systems are being abandoned progressively.

At present, there is a growing concern about the radiation doses incurred by patients when undergoing breast examinations. For this reason, the UAE has decided to join the IAEA Task4 project to undertake a survey of patient exposure in digital mammography in several Hospitals. As a first step, 7 Hospitals were selected to participate to this survey. Seven stationary and 01 mobile mammography machines have been included in the measurements.

The objective of this work was to evaluate the Average Glandular Dose (D_G) resulting from exposure to mammographic X-rays while the ultimate aim of the project remains the establishment of Dose Reference Levels (DRL) in the UAE.

In this study, the 45 mm thick ACR accreditation phantom was used to simulate breast tissue. The methodology adopted follows the guidance provided by the International Atomic Energy Agency for the measurement of the Entrance Surface Air Kerma ($K_{a,e}$) and EUREF European guidelines for the calculation of Average Glandular Dose D_G.

It is worth noting that the quantities and symbols used in this paper are those suggested by the International Commission on radiation Units and Measurements (ICRU) in its publication 74 [Ref. 1].

II. Methods and Procedures

A. Quality Control of the Mammography Machines

Prior to the Dosimetry work, image quality tests were performed at clinical settings to ensure that the X-ray machines were functioning properly, in accordance to the manufacturer's specifications. All parameters relevant to X-ray beam (mainly kVp, HVL) and image (specs, fibers, and masses) were found within acceptable standards.

B. Contrast-to-Noise Ratio (CNR)

The Contrast-to-Noise Ratio (CNR) was determined [Ref.2] by placing a square-shaped 2 cm x 2 cm piece of aluminum of thickness 0.2 mm on the PMMA phantom, 6 cm from the edge of the phantom and table, in the centre of the phantom. An image was obtained by making an exposure with the automatic exposure control. Two ROIs of 4 cm^2 were selected in the saved image to calculate the mean (S) and the standard deviation (σ). The Contrast-to-Noise Ratio (CNR) is obtained using the equation:

$$CNR = \frac{S_{AL} - S}{\sqrt{(\sigma_{AL}^{\ 2} + \sigma^{\ 2})}}$$

Where S_{AL} is the mean for the area covered by aluminum, S the mean for the phantom, σ_{AL} standard deviation for aluminum, σ standard deviation for the phantom.

C. Average Glandular Dose, D_G

The measurements of the Entrance Surface Air Kerma $K_{a,e}$ were performed in two steps. First, the ACR phantom

O. Dössel and W.C. Schlegel (Eds.): WC 2009, IFMBE Proceedings 25/III, pp. 629–631, 2009.
www.springerlink.com

was exposed to X-ray beams using automatic mode to get the kVp, mAs, and target/filter combination used in each facility. Then, the phantom was removed and a similar exposure was performed in manual mode with no phantom.

Dedicated ionization chambers fitted to suitable Multimeters were utilized to measure the Incident Air Kerma. The value of $K_{a,e}$, the Entrance Surface Air Kerma (ESAK) is deduced after correction for backscattering.

In Hospitals #1, 2, and 3, a PTW 6 cc ion chamber was used with a PTW UNIDOSE meter.

In Hospital #4, a 3.3 cc Victoreen 6000-529 chamber was used with a NeroMax 8000 Multimeter.

The Average Glandular Dose D_G is calculated as:

$$D_G = K_{a,e}.\ g.\ c.\ s$$

Where: g= factor corresponds to granularity of 50%

c= factor corrects for any difference in breast composition from 50% granularity

s= factor corrects for differences due to the choice of X-ray spectrum

III. Experimental Results:

The Table below summarizes the results obtained in this study

Table – experimental results

		Hosp 1 (2 Machines)		Hosp 2	Hosp3	Hosp 4		Hosp 5		Hosp 6		Hosp 7
Machine Brand		Hologic Selenia	Hologic Selenia	GE	Hologic Selenia	Hologic Lorad		GE		Plan Med-Sophie classic		Siemens - Balance
A/F comb.		Mo/Mo	Mo/Mo	Mo/Rh	Mo/Mo	Mo/Mo	Mo/Rh	Mo/Mo	Mo/Rh	Mo/Mo	Mo/Rh	Mo/Mo
kVp		28	29	28	29	31	30	27	27	26	26	26.5
mAs		84.2	73.1	65	96.0	57.4	59.5	70	70	160	100	100
Contrast-to-Noise Ratio (CNR)	Phantom Thickness	4.5 cm	4.5 cm	4.5 cm	4.5 cm	2 cm	2 cm	4.5	4.5	4.5	4.5	4.5
	CNR value	4.62	5.06	6.66	4.5	6.66	5.75	5.5	4.93	-	-	-
	Min. CNR Required [Ref.1]	4.91	4.91	4.91	4.91	5.49	5.49	4.91	4.91	4.91	4.91	4.91
$K_{a,e}$ [mGy]		9.92	9.87	5.66	15.48	11.95	7.5	6.55	4.94	7.82	5.32	8.78
Determined AGD [mGy]		1.94	1.69	1.13	3.03	2.33	1.66	1.28	1.21	1.7	1.3	1.9
AGD [mGy] Generated by the mammography system		2.08	1.59	1.42	2.66	2.24	1.85	NA	NA	NA	NA	NA
% Difference between determined and generated AGD		7.2 %	5.9 %	25.6 %	12.2 %	3.8 %	12.0 %	NA	NA	NA	NA	NA

IV. Discussion:

The determination of the Average Glandular Dose using a breast-mimicking phantom such as the ACR accreditation phantom is useful for assessing the output of the mammography machines under study. With the exception of one machine (Hospital 3), the Average Glandular Doses obtained were below the recommended value of 2.5 mGy [Ref. 3].The difference between the AGD values determined by the Physicist and those generated by the system is not important, thus justifying a survey of patient doses on the basis of the AGD recorded by the system.Regarding the Contrast-to-Noise Ratio, the shaded values on the above Table are inferior to the minimum CNR required. Remedial action in the 2 facilities is needed to increase the CNR above the required value.

V. Conclusions:

This pilot study on radiation exposure in mammography concerned 7Hospitals in the UAE and will be extended to a larger number of facilities in the near future. The results obtained show that quality control and patient Dosimetry are crucially needed in order to ensure a safer and efficient use of mammographic X-rays on patients whether for routine diagnosis or cancer screening.

VI. References:

[1] Journal of the ICRU Vol. 5 No 2 (2005) Report 74- Oxford University Press
[2] Chapter 3 – Quantities and Units for Measurement and Calculation in Medical X-Ray Imaging.
[3] IAEA Group Training on Radiation Protection in Diagnostic and Interventional Radiology, 7-18 May 2008, Udine (Italy)
[4] 4th edition of the European Guidelines for Quality Assurance in Breast Cancer Screening and Diagnosis (EUREF) – Office for Official Publications of the European Communities, 2006

Author: Najlaa Khalfan ALmazrouei
Institution: Dubai Hospital
City: Dubai
Country: UAE
Email: nkalmazrouei@dha.gov.ae

Patient Individual Equivalent Dose Calculations for CT Examinations

R. Schmidt[1], J. Wullf[1], B. Kästner[2], D. Jany[1], J.T. Heverhagen[2], M. Fiebich[1], and K. Zink[1]

[1] Institut für Medizinische Physik und Strahlenschutz, University of Applied Sciences, Gießen, Germany
[2] Medizinisches Zentrum für Radiologie, Klinik für Strahlendiagnostik, University of Marburg, Marburg, Germany

Abstract— **The aim of this study is the comparison of patient specific dose-estimation in computed tomography (CT) of a dedicated Monte Carlo simulation tool with precalculated data of anthropromorphic phantoms.**

The developed tool *GMctdospp*, which allows the calculation of dose to defined structures, was employed to determine equivalent dose to lungs of six randomly chosen CT thorax-scans. The results for the estimation of lung dose were compared with the CTExpo program. To allow a better comparability the Monte Carlo data was calibrated to the $CTDI_{air}$ values of CTExpo for a Siemens VolumeZoom scanner with 4x2.5 mm collimation and 15 mm table shift at 90mAs. The Monte Carlo simulations included filter geometries and energy spectra provided by the vendor.

Equivalent doses to the lung of the single CT-scans varied between 5.2 mSv and 7.9 mSv. The simulation times needed for a statistical uncertainty of less than 1% was approximately 10 minutes. The value obtained from the CTExpo tool and thus from an generalized anthropromorphic phantom was 6.4 mSv for this type of scan. Hence, the lung dose is influenced by the individuality of the patient by ~20%.

Keywords— **CT, effective dose, monte carlo**

I. Introduction

Computed tomography (CT) is the main contributor to the collective dose in radiology, although used only in a fraction of all x-ray examination procedures [1]. Further, the utilization of multi-detector CT is increasing [2]. One central aim of radiation protection is to minimize the organ dose and the resulting effective dose in medical x-ray applications [3,4]. In order to compare and optimize different scanner-protocols, dose to the patient should be known accurately.

Aim of this study was the determination of organ doses of individual patient geometries with the use of a Monte Carlo (MC) based tool *GMctdospp* [5]. In contrast to precalculated data [6,7] based on simulation and measurement with phantoms, the individual calculations allow a higher precision for estimated of individual doses in principle.

In the present study lung dose for six individual CT-thorax scans with identical parameters were calculated with the *GMctdospp* tool and compared with each other. A principle verification of the results was carried out with the CTExpo tool [8], which is based on precalculated data.

II. Material and Methods

A. Description of the *GMctdospp* tool

GMctdospp allows to read in any DICOM based CT-data including organ structure contouring in DICOM-RT format [9]. Scan parameters can be adjusted and the simulation is steered and analyzed with the graphical front end of *GMctdospp*. For Monte Carlo simulation the general purpose code system EGSnrc is used, extended by a user-code, which allows the rotation of the source, including of form-filter geometries and fast kerma-based calculations. A further description of the *GMctdospp* tool can be found in Ref 5.

B. Organ dose calculation

In order to calculate dose to an organ, a calibration factor (CF) must be established, following the definition of DeMarco et al. [12]. This CF is specific to the chosen x-ray energy E and the beam collimation BC. It is determined as the ratio of a measured and a simulated dose:

$$CF_{E,BC} = \frac{\left(D_{air,measured\ per\ mAs}\right)_{E,BC}}{\left(D_{air,simulated\ per\ particle}\right)_{E,BC}} \quad (1)$$

The simulated dose to a voxel is hence calculated with

$$D_{i\,absolut,E,BC} = D_{i\,simulated,E,BC} \cdot CF_{E,BC} \cdot TotalmAs \quad (2)$$

The *TotalmAs* is the tube-current multiplied with the number of rotations and time per rotation.

The equivalent dose H_T can be determined according to ICRP 60 and ICRP 103 respectively, by multiplying the radiation weighting factor w_r with the mean absorbed dose of the organ [13, 14].

$$H_T = w_r \cdot \frac{\sum_{i \in Organ} D_{i\,absolute,E,BC} \cdot \rho_i \cdot v_i}{\sum_{i \in Organ} \rho_i \cdot v_i} \quad (3)$$

O. Dössel and W.C. Schlegel (Eds.): WC 2009, IFMBE Proceedings 25/III, pp. 632–634, 2009.
www.springerlink.com

In the above ρ_i is the density of a voxel with volume v_i. For a photon beam w_r is set to unity.

The statistical uncertainty of the MC calculated organ dose can be estimated by the error propagation of each voxel uncertainty ΔD_i determined in the simulation. Neglecting uncertainties in density, volume and weighting factors yields:

$$\left|\frac{\Delta H_T}{H_T}\right| \approx \frac{\sqrt{\sum_{i \in Organ} (\Delta D_i)^2}}{D_{mean\ Organ}} \qquad (4)$$

C. Calibration

The factor CF in this study was connected to the CTExpo tool allowing for a better comparison in subsequent organ dose calculations.

The scan protocol of a given set of thorax scans (Siemens Volume Zoom 4, helical thorax protocol, 120 kV, 4x2.5 mm collimation, 15 mm table shift, 90 mAs), the CF was determined with

$$CF_{120kV,4x2,5mm} = \frac{CTDI_{air,CTExpo\ per\ mAs} * BC_{4x2,5mm}}{L_{10\,cm} * D_{air,simulated\ per\ particle}} \qquad (5)$$

where $CTDI_{air}$ (CTDI: computed tomography dose index [15]) corresponds to the given value of CTExpo for this scanner and L is the intergration interval of the CTDI-chamber. The simulation yielding the $D_{air,\ simulated\ per\ particle}$ value was determined in a simulation of a corresponding CTDI-chamber model.

D. CT-thorax series

The equivalent dose to the lungs was calculated for six, randomly chosen male CT thorax-scans. The lung was contoured on a threshold-basis semiautomatic segmentation toll with the Eclipse treatment planning system (Varian) and exported in the DICOM-RT format. The original CT resolution was used in the simulations as dosegrid. The simulations were performed on the complete scan varying between 24 cm and 36 cm length.

The energy spectrum and the form-filter geometry of the used scanner were provided by the manufacturer. For the MC simulations the image information represented in CT numbers (or Hounsfield units [HU]) was converted to a density and a material for each voxel, using the same ramp as described in [5].

III. Results And Diskussion

Table 1 summarizes the resulting equivalent doses to the lungs for the six CT-series in comparison to the value of CTExpo. A variation of 20 % can be observed, mainly caused by the different patient geometries (also see Fig. 1). Figure 2 shows two of the six calculated dose distributions.

One must keep in mind, that the simulation can only be performed with the available reconstructed image data of the patient.

Calculation times for each patient was in the order of 10 minutes on a desktop PC (Intel XEON E5420 2,5 GHz) with the achieved statistical uncertainties given in table 1.

Table 1 Comparison of the equivalent doses to the lung for the CT-series and CTExpo according to ICRP 60 [12]. In second column the structure volume and in the fourth the statistical uncertainty of the simulation is shown

CT-series index	Volume[dm³]	H_T [mSV]	Uncert. [%]
1	10,00	6,4	0,81
2	5,34	7,9	0,70
3	4,71	6,6	0,83
4	6,89	7,6	0,79
5	5,56	7,0	0,83
6	4,88	5,2	0,84
CTExpo	-	6,4	-

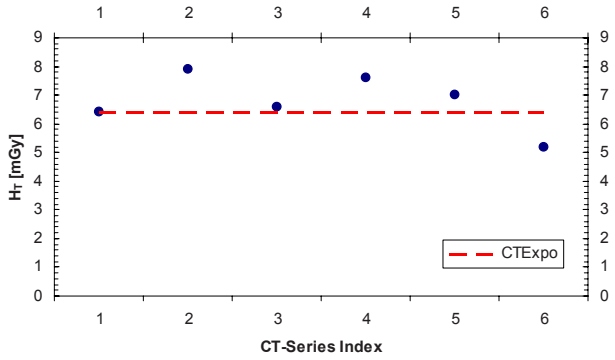

Fig. 1 Variations in equivalent doses to the lung of CT-series 1-6

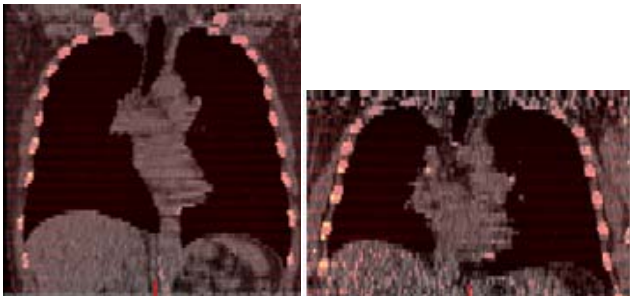

Fig. 2 Virtual frontal slices of CT-series 4 (left) and 6 (right). The dose distribution is visualized as colour-coded overlay.

IV. Conclusion

The presented results demonstrate the capability of the *GMctdospp* tool to calculate individual dose distributions based on patients image data. An individual estimation of equivalent dose to the lungs shows deviation from generalized phantoms of up to 20%. The efficient and easy to use program *GMctdospp* is qualified for this type of calculations.

References

1. Shrimpton PC, Wall BF (1995) The increasing importance of x-ray computed tomography as a source of medical exposure. Radiat Prot Dosim 57(1/4): 413-415
2. Brix G, Nagel HD, Stamm G et al. (2003) Radiation exposure in multi-slice versus single-slice spiral CT: results of a nationwide survey. Eur Radiol 13:1979-1991
3. Rat der Europäischen Union (1997) Richtlinie 97/43/Euratom über den Gesundheitsschutz von Personen gegen die Gefahren ionisierender Strahlung bei der medizinischen Exposition. Amtsblatt der Europäischen Gemeinschaften L 180
4. Bundesumweltministerium (2003) Verordnung über den Schutz vor Schäden durch Röntgenstrahlen (1987/2003). Bundesumweltministerium, Berlin, http://www.bmu.de
5. Schmidt R, Wulff J, Kästner B et al. (2009) Monte Carlo based calculation of patient exposure in X-ray CT-examinations. IFMBE Proc. Vol. 4, 4th European Conf. of the Int. Fed. for Med. and Biol. Eng., Antwerp, Belgium, 2008, pp 2487-2490
6. Schrimpton PC, Jones DG, Hillier MC et al. (1991) Survey of CT practice in the UK; Part 2: dosimetric aspects. NRPB-249, HMSO, London: 48
7. Zankl M, Panzer W, Drexler G (1991) The calculation of dose from external photon exposures using reference human phantoms and monte carlo methods part VI: organ doses from computed tomographic examinations. GSF-Bericht30/91, GSF-Forschungszentrum, Oberschleißheim
8. Stamm G, Nagel HD (2002) CT-Expo – A novel program for dose evaluation in CT. Fortschr Röntgenstr 174: 1570–1576
9. Dicom at http://medical.nema.org/
10. Kawrakow I, Rogers DWO (2006) The EGSnrc Code System: Monte Carlo Simulation of Electron and Photon Transport. NRCC Report No. PIRS-701, National Research Council of Canada
11. Wulff J, Keil B, Auvanis D et al. (2007) Dosimetrische Evaluation von Augenlinsen-Protektoren in der Computertomographie – Messungen und Monte-Carlo-Simulationen. Z Med Phys 18:9–26
12. DeMarco JJ, Cagnon CH, Cody DD, et al. (2005) A Monte Carlo based method to estimate radiation dose from multidetector CT (MDCT): cylindrical and anthropomorphic phantoms. Phys Med Biol 50:3989–4004
13. ICRP 103 (2007) The 2007 recommendations of the international commission on radiological protection. ICRP Publication 103, Annals of the ICRP 37(2-4), Amsterdam, Boston, Yena, Elsevier, 2008
14. ICRP 60 (1990) 1990 recommendations of the international commission on radiological protection. ICRP Publication 60, Annals of the ICRP 21(1-3), Oxford, New York, Frankfurt, Pergamon Press, 1991
15. IEC 60601-2-44 (2001) Medical electrical equipment - Part 2-44: Particular requirements for the safety of X-ray equipment for computed tomography

Author: Ralph Schmidt
Institute: Institut für Medizinische Physik und Strahlenschutz, Fachhochschule Gießen-Friedberg
Street: Wiesenstr. 14
City: Gießen
Country: Germany
Email: ralph.schmidt.123@gmail.com

Monitoring Patient Peak Skin Doses in Interventional Cardiology by Means of XR-RV2 Gafchromic Films

A.M. Habra[1], S. Jimmy[2], S. Dorairaj[2], R. Sasidhran[2], A. Gilani[1], H. Habibi[2], T. Majwal[2], A. Zitouni[1], and J. AlSuwaidi[1]

[1]Dubai Health Authority/Dubai Hospital, Medical Physics Section, Dubai, U.A.E.
[2]Dubai Health Authority/Dubai Hospital, Cardiology Section, Dubai, U.A.E.

***Abstract*- A survey of patient exposure in interventional cardiology is being conducted in Dubai Hospital, as part of the IAEA regional project on patient exposure in radiology. Because of the limited number of Gafchromic films available, the survey was conducted only in Dubai Hospital, a major medical institution in the City of Dubai. This Hospital receives a large number of patients annually for diagnosis and therapy purposes. The aim of the survey is to assess the Peak Skin Doses (PSD) incurred by cardiac patients undergoing angioplasty procedures. The technique adopted for this work uses a special Gafchromic film type XR-RV2 and is very practical for localizing the irradiated areas and determining the relevant PSD. Using a comparison tablet provided by the manufacturer with the films, the dose range resulting from the procedure can be rapidly estimated. A more refined method using a film digitizer (dedicated scanner) and appropriate software such as ImageJ allows the determination of the PSD.**

Prior to the dosimetry work, image quality and X-ray beam output were checked for compliance with the applicable standards.

Keywords- **Coronary Angioplasty, Peak Skin Dose (PSD), ImageJ**

I. Introduction

X-ray Interventional cardiology procedures on patients may induce serious skin injuries such as cataract, permanent epilation, telangiectasia, dry desquamation, and dermal necrosis, for which the thresholds [ICRP 85] are 5, 7, 10, 14, and 18 Gray, respectively. In Dubai Hospital, the Cath Lab receives over 2,000 patients per year for diagnostic and interventional procedures, out of which a significant number undergo interventional procedures like Coronary angioplasty, peripherals such as Carotid, Aorta & Renal angioplasties along with permanent pacemaker, ICD, and CRT insertions. In order to assess the radiological impact on patients, the Hospital decided to join the IAEA project relevant to patient exposure in interventional cardiology.

The first phase of the program that started in June 2007 concerned a survey of Kerma-Area-Product results for about 1000 patients and was completed in late 2008.

The second phase, which is the subject of this paper, is related to the determination of Peak Skin Doses (PSD) for angioplasty patients only and was launched back in February 2009. The self-developing Gafchromic film XR-RV2 was used for this purpose.

II. Material & Methods

A. Performance Tests and Beam Output

Prior to the dosimetry work, performance tests and dose rate measurements were conducted on the X-ray Biplane machine to check the functioning status of the system, using Leeds Test Tools and appropriate radiation-measuring devices.

The imaging parameters Gray Scale, Low Contrast Sensitivity, Overall Image Performance, Image Geometry, Spatial Resolution, and Image Uniformity were found in agreement with the relevant standards.

Dose Rates for normal mode, boost mode, and maximum output were checked and found within acceptable standards.

B. Dosimetry

In this work, XR-RV2 Gafchromic films were used to determine the peak skin doses received by patients undergoing angioplasty procedures. This type of film change color after exposure to high X-ray doses. The optical density of the film is correlated to X-ray dose to determine the Peak skin Dose.

For each box of Gafchromic films, one unexposed film was used to record the Background level.

The calibration of Gafchromic films was performed using 2x2 cm film pieces placed at the exit of the X-ray tube and a calibrated flat 30 cc ionization chamber over the pack of films.

After that, the monitoring of Peak Skin Dose (PSD) was started for angioplasty patients, starting in March 2009. The procedure followed is quite simple; a Gafchromic film is placed beneath the patient pad during the interventional procedure and collected after the procedure is completed.

The exposed film is stored for 24 hours before analysis. For a quick estimation of the peak skin doses incurred by

O. Dössel and W.C. Schlegel (Eds.): WC 2009, IFMBE Proceedings 25/III, pp. 635–636, 2009.
www.springerlink.com

angioplasty patients, a comparator strip provided by the film manufacturer was used.

A more elaborate method involving the use of a flatbed scanner Epson 10000XL for digitizing the films and a software ImageJ for image analysis has been implemented with the aim of generalizing its use in the future.

III. Results

The Table below shows the range of Peak Skin Doses incurred by 50 Angioplasty patients in Dubai Hospital. The results are presented in accordance to the levels included in the Gafchromic comparison strip.

Table 1: Patient Skin Dose Results

PSD ranges	<0.5Gy	0.5-1Gy	1–2Gy	2–4Gy	>4Gy
No. of patients	32	10	5	3	None
Percentage	64%	20%	10%	6%	0%

Many films have been discarded from this study because of improper manipulation.

IV. Discussion

The range of Peak Skin Doses incurred by angioplasty patients in Dubai Hospital were estimated using mainly the Gafchromic comparison tablet because of the rapidity of the technique. The scanner method is a time-consuming method requiring repeated calibration, extensive precautions and numerous tests; for this reason it was only used for qualitative purposes on few films. For the purpose of this work, only the magnitude of the Peak Skin Doses was of interest for verifying the levels of exposure in interventional cardiology at Dubai Hospital.

V. Conclusion

The Gafchromic XR-RV2 film is a very practical tool for the assessment of the peak skin doses received by patients in interventional cardiology. The first survey conducted in Dubai Hospital for a limited number of patients allowed Medical physicists and cardiologists to get some useful information on the exposure levels involved in their practice.

The values recorded in the Cath Lab facility show that for the large majority of patients in Dubai Hospital, the peak skin doses were less than 2 Gy. A few have received between 2 and 4 Gy. At these levels, the probability of skin injuries is relatively low. The survey will continue for further investigations.

Future work will include more refined studies using the scanner method and linking PSD to other dose parameters such as KAP, exposure time, angulations, frame rate, etc…

References

1. IAEA Guidance on Radiation Protection in Diagnostic and Interventional Radiology
2. GAFCHROMIC®XR-RV2, An ideal tool to measure surface peak skin dose in Interventional radiation guided by fluoroscopy, ISP, NY, Oct 2007.
3. ImageJ at http://rsb.info.nih.gov/ij/docs/menus/file.html

Author: Azza Mustafa Habra
Institute: Dubai Health Authority, Dubai Hospital
Street: Al-Khaleej Street
City: Dubai
Country: United Arab Emirates
Email: amHabra@dha.gov.ae

Survey and Reduction of Patient Doses in Computed Tomography

L. AlBalooshi[1], A. Rahanjam[2], M. AlHallag[2], S.A. Gilani[1], S. Buhumaid[1], A. Zitouni[1], and J. AlSuwaidi[1]

[1]Dubai Health Authority/Dubai Hospital, Medical Physics Section, Dubai, U.A.E.
[2]Dubai Health Authority/Dubai Hospital, Radiology Section, Dubai, U.A.E.

***Abstract*- A survey of patient exposure in Computed Tomography was taken up by a team of Physicists from Dubai hospital in 2008 after the UAE joined the IAEA regional project on patient exposure in radiology, RAS/9/047. Nine major Hospitals from both public and private sectors in Dubai area were selected to participate to the survey. Phase 1 of the program consisted on checking the image quality of the CT machines in each Hospital and measuring the values of the $CTDI_w$ by means of the head (16 cm of diameter) and body (32 cm of diameter) cylindrical PMMA phantoms. After the conclusion of the first phase, Phase 2 was launched at Dubai Hospital, a major Governmental Hospital in Dubai, as a pilot study consisting of collecting dose-Length-Product (DLP) values generated by the CT system after CT examinations are completed. The examinations included in the study were brain, chest, and the combination Abdomen & Pelvis CT procedures, which are the most common in the Hospital. Furthermore, the recorded DLP values were compared to and found much higher than the Dose Reference Levels (DRL) established in the UK [Ref. 1]. The situation called for a remedial effort to reduce rapidly patient doses in Computed Tomography. The corrective actions undertaken jointly by Medical Physicists and radiology staff (the users) reached its objectives as the technical measures taken allowed a drastic reduction of the DLP values, bringing down patient exposure to acceptable levels, closer to the standards prevailing in international practice. The experience gained at Dubai Hospital is being implanted in the rest of the participating hospitals**

Keywords- **Computed Tomography, CTDI, DLP,**

I. Introduction

Computed Tomography (CT) is an essential diagnostic tool in diagnostic and interventional radiology. However, it accounts for the largest collective dose due to medical exposure, exceeding 60% in some countries where CT machines are largely available. The relatively higher radiation risk due to this modality requires a strong control of doses incurred by patients during CT procedures. In the United Arab Emirates, the number of CT facilities has been increasing quite fast during the past few years, owing to the constant expansion of the health sector in a fast developing country. By the same token, the increasing awareness of the radiological risks involved with CT among radiation users incited some hospitals to engage in dose-reducing programs, notably those relevant to governmental institutions. In this respect, the UAE joined the IAEA Regional Project on patient exposure in diagnostic and interventional radiology.

II. Material & Methods

A. Performance Tests on the CT machines

Prior to the dosimetry work, the CT machines were submitted to a series of quality control tests using the ACR accreditation phantom to ensure that the CT image parameters were within the applicable standards. In this respect, the following parameters were checked: high contrast resolution, low contrast resolution, image uniformity, noise, artifacts, alignment light accuracy, table incrementation, slice thickness, and CT Number. Overall, with the exception of some minor deficiencies which were corrected, all machines passed the QC tests successfully.

B. Dosimetry: $CTDI_w$ Measurements

The first part of the dosimetry study concerned the determination of $CTDI_w$ for each machine using head & body phantoms, a 10 cm pencil ion chamber fitted to the NeroMax8000 Multimeter. IAEA guidance [Ref.2] was used to execute the experimental work.

The machines involved in this task were quite different from one hospital to another, ranging from single slice to 64-slice CT.

The following equation was used to determine the weighted CTDI for the head and body phantoms:

$$CTDI_w = 1/3\ CTDIcenter + 2/3\ [Ave.\ CTDIperipherals]$$

Where CTDIcenter is the value of the CTDI at the center hole of the phantom and Ave. CTDIperipherals is the average value of the CTDI for the peripheral holes.

Further, the normalized values ${}_nCTDI_w$ were deduced and compared to IMPACT-UK reference values.

O. Dössel and W.C. Schlegel (Eds.): WC 2009, IFMBE Proceedings 25/III, pp. 637–639, 2009.
www.springerlink.com

The second part of the dosimetry work consisted of collecting DLP values for brain, chest abdomen & pelvis CT examinations directly from the system, after the examination of each patient is completed. The patients selected for this study weighted between 65 and 85 Kilograms. This work was conducted only in Dubai Hospital as a pilot study with the aim of extending it to other hospitals once it is completed with conclusive results. The preliminary DLP survey lasted from January 2008 to June 2008 and corrective actions were taken afterwards. A second survey, with corrective actions, was started in July 2008 and lasted until January 2009.

III. Results

Table 1 below shows the values of nCTDIw for the 9 participating hospitals

Table 1: $_{n}CTDI_{w}$ values measured in 9 hospitals in Dubai

HOSPITAL	CT MACHINE	nCTDIw/mAs 16 cm head	nCTDIw/mAs 32 cm body
HOSPITAL 1	4-SLICE	**0.17**	**0.09**
HOSPITAL 2 (2 machines)	4-SLICE	**0.18**	**0.08**
	64-SLICE	**0.30**	**0.18**
HOSPITAL 3	4 -SLICE	**0.09**	**0.04**
HOSPITAL 4	16 -SLICE	**0.20**	**0.03**
HOSPITAL 5	SINGLE SLICE	**0.14**	**0.59**
HOSPITAL 6	64 - SLICE	**0.08**	**0.02**
HOSPITAL 7	64 - SLICE	**0.23**	**0.04**
HOSPITAL 8	(64 Slice) Dual sources	**0.057**	**0.10**
HOSPITAL 9	64 - SLICE	**0.38**	**0.17**

The preliminary DLP survey was conducted from January to June 2008 for brain, chest, and abdomen & pelvis examinations. The data collected revealed DLP values much higher than expected, quite far from the guidance levels suggested by the IAEA or the dose Reference Levels established in several countries, as in UK for example. These findings prompted the Medical physics team to take action jointly with the users to find the cause of that situation and work towards the reduction of the DLP.

Therefore, all dose parameters used in the CT protocols which used manual settings were verified and changes were suggested, on the basis of the findings. For instance, kVp, mAs, slice thickness, and scanned volume were adapted more proficiently to the type of patient and examination involved, while for the previous practice the parameters used were strictly standard. In a further stage, the Automatic Exposure Control was systematically used whenever possible. By January 2009, the patient doses were reduced considerably, as shown on table 2, thanks to the joint effort of Physicists and the radiology staff. It is worth noting that the reduction of DLP values was achieved with practically no deterioration of image quality.

Table 2: Comparison of Average and maximum DLP values before and after corrective actions

CT examination	DOSE-LENGTH-PRODUCT (DLP), mGy			
	Monthly Average DLP		Monthly Maximum DLP	
	Previous Practice	**After Reduction**	Previous Practice	**After Reduction**
Chest CT	500 to 600	**Around 400**	Over 700	**Less than 500**
Brain CT	900 to 1000	**Less than 800**	900 to 1300	**800 to 900**
Abdomen & Pelvis	800 to 1000	**500 to 600**	2000 to 3000	**Less than 700**

IV. Discussion

The work undertaken in hospitals to evaluate patient exposure in Computed Tomography has been very effective and beneficial to CT users. In all hospitals, the measurement of CTDI values provided useful information about the output of the machines and their potential impact on image quality and patient exposure. The values of normalized CTDI obtained in 9 hospitals were found lower than the reference values suggested by the UK group impact.

The pilot study conducted in one major hospital showed that it is possible to reduce patient doses by applying safer and more efficient techniques. For instance, it was possible to reduce the patient DLP for abdomen & pelvis examinations by mor than 50 %. Appreciable DLP reductions were also obtained for brain and chest examinations. Further reductions are expected to be achieved in the course of the project.

V. Conclusion

The project on patient exposure in Computed Tomography is of high importance due to the large contribution of CT to the global collective dose from radiation medicine.

The results achieved so far show the effectiveness of the program in reducing patient doses. It is expected that the

results achieved by the team of Physicists in the participating hospitals, notably in Dubai Hospital will translate into wider gains in patient safety once the experienced acquired is transferred to a much larger number of hospitals.

References

1. National survey of doses from CT in the UK: 2003 - The British Journal of Radiology, 79 (2006), 968–980.
2. IAEA Guidance on patient dosimetry in Computed Tomography (Project material provided by the Agency)

Evaluation of Patient Doses from Verification Techniques in Image-Guided Radiotherapy (IGRT)

V. Dufek[1], I. Horakova[1], L. Novak[1], O. Koncek[2], V. Richter[3], and L. Janeckova[3]

[1] National Radiation Protection Institute, Prague, Czech Republic
[2] Faculty Hospital Motol, Prague, Czech Republic
[3] Regional Hospital Liberec, Liberec, Czech Republic

Abstract— **The purpose of this work was an evaluation of organ doses and effective doses from kilovoltage (kV) Cone-beam CT (CBCT) scans and from pairs of orthogonal kV image projections for two different treatment sites (a head and a pelvis). Measurements of organ doses were performed in an anthropomorphic Rando phantom by means of thermoluminescent dosimeters (TLDs). Irradiations were performed using On-Board Imager (OBI) and X-ray Volume Imaging (XVI) systems.**

Keywords— **Patient dose, Cone-beam CT (CBCT), pair of orthogonal kV image projections, IGRT.**

I. Introduction

In radiotherapy, patient doses can be divided into two groups: planned and concomitant doses. Planned doses represent therapeutic doses prescribed into target volume. In contrast to planned doses, concomitant doses are unwanted and are caused by escaped and scattered therapeutic radiation and by imaging procedures during radiotherapy process.

Image-guided radiotherapy (IGRT) uses particularly kilovoltage CBCT scans and pairs of orthogonal kV image projections to improve patient setup procedure and to increase the tumor control probability.

On the other hand, using these verification techniques also causes delivering higher doses to healthy organs or tissues. These doses are small compared with the therapy dose but not negligible, because they can lead to a higher risk of developing secondary malignancies. Therefore these concomitant doses should be evaluated and minimized.

The purpose of this work was to carry out a measurement of organ doses from kilovoltage CBCT scans and from pairs of orthogonal kV image projections for two different treatment sites (the head and the pelvis ones) and an evaluation of effective doses.

II. Materials and Methods

A. Imaging systems

The measurements were performed at two hospitals. At hospital No. 1, scans or image projections were acquired using On-board Imager (OBI). OBI is manufactured by Varian Medical Systems (Palo Alto, CA). At hospital No. 2, scans or image projections were acquired using X-ray Volume Imaging (XVI). XVI is manufactured by Elekta (Crawley, UK). Both devices are mounted at the gantry of the linear accelerator. The X-ray source and the flat panel detector are placed on robotic arms attached to the gantry.

B. Calibration of thermoluminescent dosimeters

Thermoluminescent dosimeters LiF: Mg, Cu, P (MCP-N, TLD Poland) were used for organ dose measurements. These chips have dimensions 4.5 x 4.5 x 0.9 mm^3. A calibration was performed in kilovoltage (125 kV) beam of OBI.

TLDs were irradiated in water phantom at the depth of 2 cm by various absorbed doses (0,1 – 66 mGy). The response of TLDs was than compared with absorbed dose to water assessed by ionization chamber TW30001 (0.6 cm^3) placed in the same position. The ionization chamber has an air kerma calibration traceable to the national standard (Czech Metrology Institute). Calculation of an absorbed dose was based on protocol TRS 277 [1].

C. Placement of thermoluminescent dosimeters

All measurements were performed in a male Rando phantom (The Phantom Laboratory, Salem, NY). Distribution of TLDs and organs in the Rando phantom is shown in Table 1. For localization of the organs in the Rando phantom, an anatomical CT atlas [2] and data published in literature [3, 4, 5] were used.

Table 1 Distribution of TLDs and organs in the Rando phantom

Organ or tissue	No. of TLDs	Slices of Rando phantom
Testes	2	34
Bladder	4	29-32
Small intestine	6	24-29
Colon	4	24-27
Gall bladder	3	23-27
Kidney	4	21-24
Stomach	4	20-23
Pancreas	2	22-23
Liver	6	19-23
Spleen	3	20-22
Adrenals	2	21-22
Lung	11	10-20
Esophagus	3	12,14,16

O. Dössel and W.C. Schlegel (Eds.): WC 2009, IFMBE Proceedings 25/III, pp. 640–643, 2009.
www.springerlink.com

Heart	3	16-18
Breast	2	16-17
Thyroid	2	8-9
Lens	2	3
Skin (pelvis)	6	25-35
Skin (chest)	6	14-24
Skin (head and neck)	6	1-12
Prostate	2	34
Thymus	2	12
Salivary gland	4	6-7
Oral mucosa	4	6-7
Brain	4	2-4
Bone marrow (pelvis)	5	30-34
Bone marrow (outside pelvis)	4	8-15

D. Irradiation of Rando phantom using CBCT scans

At hospital No. 1, the phantom was irradiated using OBI system. For a head scan and a pelvis scan, the parameters of CBCT scan were almost the same. Used 368° CBCT scan was characterized by 125 kV and 264 mAs. The pelvis scan length was 13.7 cm in half fan mode with a half bow tie filter. The head scan length was 14.0 cm in full fan mode with a full bow tie filter.

At hospital No. 2, the phantom was irradiated using XVI system. For a head scan and a pelvis scan, the parameters differed considerably. The 360° CBCT scan of a pelvis was characterized by 120 kV and 1040 mAs (prostate preset). The use of M10 collimator defined the scan length of 13.5 cm. The CBCT scan of the head was made by a 200° arc rotation (with the gantry angle of 320° to 160° in clockwise direction) of the X-ray source around the isocentre. The scan was characterized by 100 kV and 36.1 mAs. For the head scan, the use of S20 collimator defined the scan length of 27.7 cm.

E. Irradiation of Rando phantom using a pair of orthogonal kV image projections

Rando phantom was irradiated at hospital No. 1 by means of two orthogonal kV image projections using an OBI system. One projection was acquired in anterior-posterior (AP) direction, another one in lateral direction. All kV image projections at hospital No. 1 had a size of 18 cm x 18 cm at isocentre. Orthogonal kV image projections of a pelvis were done with 75 kV, 4 mAs (the AP projection) and with 120 kV, 20 mAs (the lateral projection). Orthogonal kV image projections of a head were done with 85 kV, 3.6 mAs (the AP projection) and with 65 kV and 2.4 mAs (the lateral projection).

At hospital No. 2, the parameters of the pelvis image projections were 120 kV, 5 mAs (the AP projection) and 120 kV, 6.4 mAs (the lateral projection). Parameters of the head image projections were 100 kV and 0,5 mAs for both the AP projection and the lateral projection. The size of image projection was 27.7 cm x 27.7 cm at isocentre. Orthogonal projections were acquired using a XVI system.

F. Calculation of absorbed dose D

The absorbed dose D was calculated from measured thermoluminescent (TL) response M of TLDs as follows:

$$D = (M - M_0) \cdot N_D \cdot k_s \cdot k_Q \cdot k_{lin} \cdot k_f \qquad (1)$$

where M_0 is TL response of background dosimeters, N_D is absorbed dose calibration factor, k_S is correction factor for the individual sensitivity of TLDs, k_Q is energy correction factor of TLDs, k_{lin} is non-linearity correction factor and k_f is fading correction factor.

G. Calculation of organ dose D_T

The formula for calculation of organ dose D_T was following:

$$D_T = \sum_i f_i \cdot D_i \qquad (2)$$

where f_i is the fraction of the total mass of the specified organ in the slice i of the Rando phantom, D_i is the average dose in part of the specified organ within the slice i. For most organs, the values of f_i are published in literature [3, 4]. Alternatively, the organ dose D was calculated simply using average value.

H. Calculation of effective dose E

The effective dose E was calculated from organ doses D_T as follows:

$$E = \sum_T w_T H_T = \sum_{T,R} w_T w_R D_{T,R} \qquad (3)$$

where w_T is the tissue weighting factor and w_R is the radiation weighting factor.

Two different sets of tissue weighting factors were used for calculation of an effective dose, ICRP 60 [6] and ICRP 103 [7].

III. Results

I. Organ doses from CBCT scans

The organ doses from CBCT scans measured at hospital No. 1 and No. 2 are shown in Table 2.

Table 2 Organ doses (in mGy) from CBCT scans

	Hospital No. 1		Hospital No. 2	
Organ or tissue	Pelvis scan	Head scan	Pelvis scan	Head scan
Testes	10.3	<0.1	6.5 °	<0.1
Bladder	16.6	<0.1	38.3 °	<0.1
Small intestine	7.8	<0.1	9.6 °	<0.1
Colon	5.8	<0.1	4.4 °	<0.1
Gall bladder	1.3	<0.1	1.4 °	<0.1
Kidney	1.2	<0.1	1.2 °	<0.1
Stomach	0.7	<0.1	0.6 °	<0.1

Pancreas	0.9	<0.1	0.9 º	<0.1
Liver	0.5	0.1	0.5 º	<0.1
Spleen	0.7	0.1	0.6 º	<0.1
Adrenals	0.4	<0.1	0.7 º	<0.1
Lung	0.1	0.4	0.2 º	<0.1
Esophagus	0.1	0.7	0.1 º	0.2
Heart	0.2	0.2	0.1 º	<0.1
Breast	0.1	0.3	0.2 º	<0.1
Thyroid	<0.1	13.0	<0.1 º	1.1
Lens	<0.1	15.5	<0.1 º	1.6
Skin (pelvis)	9.4	<0.1	24.4 º	<0.1
Skin (chest)	0.7	0.5	0.7 º	<0.1
Skin (head and neck)	<0.1	11.3	<0.1 º	1.3
Prostate			10.3	
Thymus			<0.1	
Salivary gland			<0.1	
Oral mucosa			<0.1	
Brain			<0.1	
Bone marrow (pelvis)			25.6	
Bone marrow (outside pelvis)			<0.1	

º Averaged organ doses from two measurements

J. *Effective doses from CBCT scans*

The effective doses from CBCT scans calculated from the measured organ doses are shown in Table 3.

Table 3 Effective doses (in mSv) from CBCT scans

According to	ICRP 60	ICRP 103
		Pelvis CBCT scan
Hospital No. 1	4.15 *	2.69 *
Hospital No. 2	4.25 *	3.05 *
Hospital No. 2	5.85	4.77
		Head CBCT scan
Hospital No. 1	0.85 *	0.74 *
Hospital No. 2	0.08 *	0.07 *

* Underestimated effective doses

K. *Organ doses from orthogonal kV image projections*

The organ doses from two kV image projections measured at hospital No. 1 and No. 2 are shown in Table 4.

Table 4 Organ doses (in mGy) from a pair of orthogonal kV image projections

	Hospital No. 1		Hospital No. 2	
Organ or tissue	Pelvis images	Head images	Pelvis images	Head images
Testes	0.3 º	<0.1	1.0	<0.01
Bladder	0.7 º	<0.1	0.8	<0.01
Small intestine	0.4 º	<0.1	0.4	<0.01
Colon	0.2 º	<0.1	0.4	<0.01
Gall bladder	0.1 º	<0.1	0.1	<0.01
Kidney	0.1 º	<0.1	<0.1	<0.01
Thyroid	<0.1 º	0.2	<0.1	0.04
Lens	<0.1 º	0.6	<0.1	0.07
Skin (pelvis)	0.8 º	<0.1	0.6	<0.01
Skin (head and neck)	<0.1 º	0.2	<0.1	0.06
Prostate	0.4 º	<0.1	0.5	<0.01
Salivary gland	<0.1 º	0.1	<0.1	0.04
Oral mucosa	<0.1 º	0.1	<0.1	0.04
Brain	<0.1 º	0.1	<0.1	0.02
Bone marrow (pelvis)	0.9 º	<0.1	0.5	<0.01
Other organs [+]	<0.1 º	<0.1	<0.1	<0.01

º Averaged organ doses from two measurements

[+] Other organs include stomach, pancreas, liver, spleen, adrenals, lung, esophagus, heart, breast, skin (chest), thymus and bone marrow (outside pelvis)

L. *Effective doses from two kV image projections*

The effective doses from pairs of orthogonal kV image projections calculated from the measured organ doses are shown in Table 5.

Table 5 Effective doses (in mSv) from two orthogonal kV image projections

According to	ICRP 60	ICRP 103
		Pelvis images
Hospital No. 1	0.18 º	0.15 º
Hospital No. 2	0.42	0.27
		Head images
Hospital No. 1	0.01	0.01
Hospital No. 2	<0.01	<0.01

º Averaged effective doses from two measurements

IV. DISCUSSION

The expanded uncertainty in the absorbed dose measurement using TLDs was lower than 20 % (k=2) for doses higher than approximately 0,5 mGy. The expanded uncertainty included the uncertainty of absolute dose calculation based on protocol TRS 277 [1], the uncertainty of TL readings, the uncertainty of dose response nonlinearity and the uncertainty connected with energy dependence of MCP-N chips. The measurement of absorbed doses lower than 0,5 mGy was characterized by higher uncertainty considering nonlinear dependence of TL response on an absorbed dose. To measure higher TL signals, CBCT scans were performed three times and kV image projections were performed thirty times.

Only some measurements were repeated due to limited access to the hospitals (organ doses from a CBCT scan of pelvis at hospital No. 2 and from kV image projections of pelvis at the hospital No. 1). Differences in organ doses (from two measurements) were within 10 %. The highest differences were in organs situated on the surface of the Rando phantom.

Comparison of measured doses from CBCT scans was performed between two hospitals and between measured

data and published data (TL measurements, Monte Carlo simulations).

Comparison of measured doses from two kV image projections was performed also between two hospitals and between measured data and reported data (TL measurements). In addiction, measured organ doses from kV image projections were compared with organ doses estimated by PCXMC. Calculated effective dose was compared with effective dose estimated from measured incident air kerma.

As seen from Table 3 and Table 5, the organ doses from CBCT scans and from kV image projections measured at both hospitals differ (for the reason of different kV, mAs, etc.).

The organ doses from CBCT scans measured at hospital No. 1 were compared with organ doses (also measured using TL chips in Random phatom) reported by Kan et al. [8]. The measured and the reported doses are comparable in irradiated sites. The measured organ doses outside irradiated sites are approximately 2 - 4 times lower than the reported ones. Different organ doses can be caused by different placing of CBCT scans in longitudinal axis, by different organ localization in both Rando phantoms and by different number (and also diverse distribution) of TLDs in the same organs.

The measured organ doses from CBCT scans were also compared with the organ doses calculated using Monte Carlo method [9, 10]. For comparison, doses were normalized to the same mAs. The measured organ doses are comparable or slightly higher.

For comparison of effective doses from CBCT scans, it is necessary to consider that values marked with star in Table 3 are underestimated (organ doses were not measured in bone marrow, brain). The underestimated effective doses at hospital No. 1 are lower than effective doses reported by Kan et al. [8]. The effective dose from the pelvis CBCT scan at hospital No. 2 is comparable to the effective dose reported by Gu et al. [9].

To this date, there are not enough data for doses from pairs of kV image projections in the literature. The absorbed doses from the pair of kV image projections measured on skin in the irradiated site of a pelvis are similar to the doses reported by Osei et al. [11]. The measured organ doses from the pair of kV image projections in the irradiated sites were found to be comparable to the doses calculated using PCXMC computer code. The measured organ doses in peripheral sites are considerably higher (in some cases even ten times higher) than doses calculated by PCXMC. These differences in peripheral sites can be caused by large uncertainties of organ dose estimate using PCXMC, by comparing very low doses and by the dose response nonlinearity of TL chips in low dose area.

The effective doses from the pair of kV image projections at hospital No. 1 (calculated from TLD measurement) are similar to the effective dose estimated from measured incident air kerma using semi-empirical conversion coefficient published in [12].

V. Conclusions

The organ doses in 27 organs from CBCT scans and from the pair of orthogonal kV image projections were measured for pelvis and head treatment. Effective doses were also calculated. The maximum dose from CBCT scans was 38.4 mGy and the maximum dose from kV image projections was 0.9 mGy. Organ doses depend mostly on distance from the irradiated sites and also on parameters such as mAs and kV.

For CBCT scans, effective doses range from 0.07 to 5.85 mSv and for two kV image projections, from 0.01 to 0.42 mSv. Presented effective doses refer to one CBCT scan or one pair of kV image projections. Effective dose to patient depends also on the number of scans or image projections during the whole radiotherapy process.

This study was supported by the grant of State office for nuclear safety n. 4/2009.

VI. Reference

1. INTERNATIONAL ATOMIC ENERGY AGENCY, Absorbed Dose Determination in Photon and Electron Beams: An International Code of Practice, Technical Reports Series No. 277 (2nd edn in 1997), IAEA, Vienna
2. Fleckenstein P, Tranum-Jensen J (2001) Anatomy in Diagnostic Imaging. Saunders
3. Perisinakis K et al. (2002) Radiation dose and associated risk from transmission scans using 153Gd line sources in cardiac SPECT studies. Health Physics 83(1):66-74
4. Golikov V Y, Nikitin V V (1989) Estimation of the mean organ doses and the effective dose equivalent from Rando phantom measurements. Health Physics 56(1):111-115.
5. Scalzetti E M et al. (2008) A method to obtain organ doses in a Rando phantom. Health physics 95(2):241-244
6. International Commission on Radiological Protection. 1990 recommendations of the International Commission on Radiological Protection. In: ICRP Publication 60. Ann. ICRP (1991) Oxford, UK: Pergamon Press.
7. International Commission on Radiological Protection (ICRP). 2007 recommendations of the international commission on radiological protection. ICRP Publication 103. Ann. ICRP (2007).
8. Kan M W et al. (2008) Radiation dose from cone beam computed tomography for image-guided radiation therapy. Int J Radiat Oncol Biol Phys 70(1):272-279
9. Gu J et al. (2008) Assessment of patient organ doses and effective doses using the VIP-Man adult male phantom for selected cone-beam CT imaging procedures during image guided radiation therapy. Rad. Prot. Dos. 131(4):431-443
10. Ding G X et al. (2008) Accurate patient dosimetry of kilovoltage cone-beam CT in radiation therapy. Med Phys. 35(3):1135-1144
11. Osei E K et al. (2009) Dose assessment from an online kilovoltage imaging system in radiation therapy. J Radiol Prot. 29(1):37-50
12. Murphy M J et al. (2007) The management of imaging dose during image-guided radiotherapy: report of the AAPM Task Group 75. Med Phys. 34(10): 4041-63

Author: Vladimir Dufek

- Institute: National Radiation Protection Institute
- Street: Bartoskova 28
- City: Prague
- Country: Czech Republic
- Email: la.dufek@seznam.cz

Biological Effects of Ionising Radiation-with Special Emphasis on Low Level Doses

C. Streffer

University Clinics Essen, Essen, Germany

Abstract- **Cancer induction is assumed to be dominating for radiation risk in the low dose range (<100 mSv). Generally it cannot be determined by epidemiology after such low doses for a normal population. The risk is extrapolated from medium and high dose ranges therefore. For prospective radiological protection a linear dose response without a threshold (LNT) is proposed although this has not been definitely proven until now. It is therefore assumed that biological studies can contribute in order to solve the question whether health effects are caused by small radiation doses. In this respect many studies have been focussed on DNA damage, chromosomal aberrations, and more recently on epigenwetic (non-targeted) effects, gene expression and proteomics.**

It is necessary to evaluate the mechanisms which lead to radiation-induced health effects. Biological phenomena are modulating these effects. Such phenomena are adaptive response, apoptosis, bystander effects, DNA repair, genetic disposition, genomic instability and immunological phenomena. Many data have been published with respect to these effects after radiation during recent years. However, it is usually unknown with which steps these processes interfere in the development of health effects. Further quite often the dose response of these biological effects is also unclear in the low dose range.

It has to be recognized that the radiation effects are dependent on the age of the exposed person, on sex and on genetic disposition. With respect to exposures of patients the pathological features of the disease may also have relevant implications on radiosensitivity. Under such conditions and uncertainties for the evaluation of radiation risk in the low dose range it is not justified to calculate risk values like deaths after doses in the range of several mSv for a general population of patients. However, this can be done in individual cases.

Keywords- **Adaptive Response, Carcinogenesis, genomic instability, genetic disposition**

I. Introduction

The diagnostic procedures in X-ray diagnostic and nuclear medicine cause exposures to ionising radiation in dose ranges of 1 and several 10 mSv per single investigation. However, the medical use of technologies with exposures to ionising radiation causes the highest man-made exposures to the population (averaged doses per caput) in industrialized countries, it increases during last years due to procedures like CT and interventional radiology. The average doses reach the range of radiation doses caused by exposures from natural sources [1]. Therefore the knowledge about the possible risk which may be connected to such radiation doses is of great interest and may be of concern for the individual patient as well as for radiohygienic aspects to the total population.

II. Epidemiological Data

The epidemiological studies of radiation-induced cancer incidence and mortality of the survivors of the atomic bombing in Hiroshima and Nagasaki are still the basis for risk estimates. The main conclusions are [2,3]:

- Up to radiation doses of 2 Sv the data can be described BEST by a linear dose response curve without a threshold.
- A statistically significant increase of cancer (all solid cancers) is observed after radiation doses >120 mSv.
- The excess relative risk per Gy (Sv) is about 0.47 for persons at the age of 70 years and exposure at age of 30 years averaged over both sexes.
- Women are more radiosensitive than men by a factor of about 1.7.
- Children and adolescents are generally more radiosensitive than adults.
- Strong differences exist with respect to the radiosensitivity between the different organs and tissues.

ICRP derived a risk factor of 5×10^{-2} per Sv for stochastic effects after exposure to low LET radiation in the low dose range with low dose rates and of 10^{-1} per Sv for high LET radiation from these studies. These factors are used for prospective radiological protection in the low dose range [4]. Quite a number of other epidemiological studies about the induction of cancer in humans after exposure to ionising radiation are more or less compatible with the data from Hiroshima and Nagasaki [5,6]. In all studies no significant increase of cancer induction has been found in the low dose range (<100 mSv). The data which have been obtained with the studies on the atomic bomb survivors show strong fluctuations around the linear dose response

O. Dössel and W.C. Schlegel (Eds.): WC 2009, IFMBE Proceedings 25/III, pp. 644–647, 2009.
www.springerlink.com

below doses of 100 mSv. This can be explained by two possibilities:

1. No cancers are induced after exposures to such low radiation doses.
2. Cancers are induced after these low doses but the effect is so small that it is hidden by the fluctuations of the "spontaneous" cancer.

The fluctuations of the annual cancer rate is even with the population of the U.S.A. so large that the expected cancer mortality after radiation doses (low LET, low dose rate) of 100 mSv can hardly be discovered [7]. An individual cancer which may have been caused by ionising radiation can by no means be distinguished from cancers which originate from endogenous or other unknown causes (e.g. "spontaneous" cancer). There does not exist a specific signature for radiation which would make such a distinction possible [7]. The evaluation of the mechanism of carcinogenesis may clarify whether cancers can be induced by low radiation doses and how the dose response curve looks like in the low dose ranges for diagnostic procedures. It is a great challenge for radiobiological research to contribute to the solution of these questions.

III. Mechanism of Carcinogenesis

The present concept for the mechanism of cancer development is roughly the following: The initial events are changes/damage of DNA e.g. by ionising radiation which may be repaired completely or the damaged cell starts to proliferate with either unrepaired or misrepaired DNA. The prominent DNA changes after exposure to ionising radiation are: Breaks of the polynucleotide strands, (single strand breaks (SSB) or double strand breaks (DSB)), Base damage, either a DNA base is completely lost or a base is radio-chemically altered [7]. Analyses of the track structure and of the distribution of ionisation events in the DNA helices revealed that clusters of damage frequently occur after exposure to ionising radiation. When damaging events occur in the direct neighbourhood to an SSB or DSB "complex SSBs" or "complex DSBs" are formed. These DNA damages can be repaired by different, very sophisticated enzymatic pathways. The complex regulation and the efficiency of these processes are dependent on the type of the DNA damage. In general the DNA repair of DSB and especially of complex DSB is slower and more difficult than that of other damage types. With DSB also misrepair can occur. Misrepaired DSB may be involved in the initial steps for the development of cancer.

These mechanisms are not fully understood until now. The occurrence of clustered DNA damage is unique for ionising radiation [1,7,8]. Chemical toxic agents generally cannot generate such clustered complex DNA damage in the low dose range. The damaging events of such agents are usually isolated events in the low dose range. Further the quantitative distribution of the various damage types is dependent on the radiation quality. Low LET radiation induces less DSB and especially less complex DSB than high LET radiation [1,7]. This is apparently the reason for the general observation that DNA damage of high LET radiation is repaired slower and less efficient than DNA damage of low LET radiation and therefore high LET radiation leads to higher radiation effects than low LET radiation when equal absorbed doses are compared.

In all living mammalian cells DNA is associated with proteins mainly histones in order to form chromatin. After radiation exposure several DNA damage associated histone modifications have been described. Thus the histone H2AX becomes phosphorylated locally to the DNA damage and appears as γ-H2AX which is recognized by antibodies so that the spots with the DNA damage can be made visible with immunofluorescence microscopy. By this technique DSB can be recognized and counted in a very sensitive manner. Thus it has been shown that DSB can be observed after low LET radiation doses of several mSv [9]. Further it has been shown that the efficiency of DNA repair is dependent on the genetic disposition. The radiosensitivity of individuals can differ widely due to the genetic disposition. In some extreme cases with genetic syndromes a repair deficiency exists [1,7].

In the case of no repair or misrepair the following daughter cells will carry a radiation-induced mutation, further proliferation can then lead to cell transformation, malignant cells are formed. These processes are often called the initiation of cancer. The malignant transformed cells may stay silent in tissues for many years, during which they can be removed by apoptosis or immune defence. However, also further mutations by radiation or facilitated by genomic instability (see later) may alter the regulation of cell proliferation which stimulate the whole process to result in pre-cancer stages. After further cell proliferation and mutations a carcinoma in situ is formed which then can develop to cancer with metastases. These processes are usually called promotion and progression of cancer. Thus in summary the development of cancer is mainly accomplished by several successive mutations and extensive cell proliferation. It is assumed that a cancer develops from one single malignant cell. A cancer diagnosed in the clinic has around one or even several billion cells [7]. The latency period (time for the development of a cancer) for most leukaemia is in the range of 5 to 10 years and for most solid cancers in the range of decades. Thus the development lasts very long and the regulation of cell proliferation is a key issue in the whole very complex process which is a

sequence of a number of biological phenomena which have partly lost the regulatory – often feedback, haemostatic mechanisms - control [7]. The open questions are: Where does ionising radiation interfere with the developmental chain (during initiation or promotion?)? What is the dose response and the shape of the dose response curve?

IV. Dose Modifying Phenomena

Extensive biological studies have demonstrated during recent years that several biological phenomena can modulate the dose response in the low dose range. The dose response curve may be modified in various ways in the dose ranges where no significant epidemiological data on cancer induction are available (linear, curvilinear, threshold?) [1,7]. Very important phenomena are DNA-repair processes which have already been discussed. Further adaptive response, apoptosis, bystander effects, genetic disposition, genomic instability, hyperradiosensitivity and immune response have to be mentioned. Some of these phenomena will be discussed in the following.

Adaptive response has been frequently observed during the last 20 years with many organisms starting with bacteria up to mammalian organisms including humans [10]. In general biological objects, usually cells like bacteria or human lymphocytes, are irradiated with a low radiation dose (adapting dose in the range of 5 to 200 mGy), about 4 to 24 hours later a higher dose (challenging dose in the range of 1 to several Gy) is given and then the biological effects (with lymphocytes usually chromosome aberrations) are measured. In parallel the effect of the challenging dose only is measured. Quite often the radiation effect is reduced with the combination of adapting dose plus challenging dose in comparison to the effect of the challenging dose alone. The cells have become more resistant against ionising radiation within the interval, they are adapted. Apparently the DNA repair has become more efficient by adaptation [10,11]. Such effects have been shown in many cases throughout the whole animated nature with prokaryotic as well as eukaryotic organisms.

However, the effects can be very different between individuals. The adaptive response is apparently dependent on the genetic disposition. No adaptive response was observed in cells from individuals with hyperradiosensitive syndromes like Ataxia telangiectesia (AT). Several studies have shown that no or very little adaptive response developed with high LET radiation. During prenatal development no or little adaptive response could be observed and further it has been found that adaptive response decreases apparently with age. It has also to be considered that very distinctive conditions with respect to the seize of the adapting dose and its dose rate, the time interval between adapting and challenging dose and other parameters have to be kept within certain limits in order to observe adaptive response [11]. Thus it can be concluded that adaptive response is a very important biological phenomenon of high scientific interest. However, it has a number of limitations, it is not an universal phenomenon, it does not operate in generality under all conditions.

Apoptosis is a very powerful cellular mechanism to eliminate damaged or no longer needed cells e.g. during prenatal development. It can be increased after radiation exposure and it is assumed that apoptosis may also eliminate malignant cells so that the cancer risk is reduced. It has further been shown that small radiation doses can induce an adaptation to increased apoptotic activities but again this differs very much between individuals [11]. Apoptotic cell death is induced by complex intracellular signal transduction mechanisms which is triggered and regulated by a number of molecular factors (e.g. the tumour suppressor p53). These factors are also connected sometimes to the cycle of cell proliferation. Therefore apoptosis can certainly be a mechanism to reduce the development of cancer after radiation but there are a number of situations were this mechanism does not operate.

For a long time it was accepted that the radiation-induced chromosomal damage is expressed at the first mitosis taking place after a radiation exposure. Nowadays it is well-known, that new chromosomal aberrations also appear at much later mitotic cell divisions. For such experiments female mice were irradiated after conception when the conceptus was still in the zygote(1-cell) stage. An increased number of chromosomal aberrations was found not only in the first cell division of the embryo but also in fibroblasts which were obtained from foetuses just before birth. This means that a normal foetus had developed from the irradiated zygote but some further radiation damage had developed and was expressed in the foetal cells many cell generations later around birth. The cells had developed an increased “instability of the genome” [12]. Surprisingly the patterns of the chromosomal aberrations in the foetal fibroblasts (exposed as the zygote) are the same as in foetal cells from non-irradiated zygotes while the patterns are different in the first mitosis after radiation exposure. Such effects have been found in many cell systems and organisms (in vivo and in vitro) during the last 20 years [4-8].

Besides cytogenetic effects genomic instability has also been observed for a number of other biological endpoints e.g. cell survival, cell transformation. It can also be transmitted to the next generation of mice. Not quite clear is the dose response, the lowest radiation doses are usually in the range of several hundredmGy X-rays after which significant effects for the increase of genomic instability could be measured. However, an increase of DSB was

observed 25 cell generations after a radiation exposure with 1 mGy carbon ions [13]. This radiation dose is averaged over all cells, however, only one in 18 cells is exposed under these conditions. Thus the dose in the exposed cell is around a factor of twenty higher. Nevertheless these data show that possibly small doses can induce genomic instability. Under the conditions of radiation-induced genomic instability the damage is not expressed in the irradiated cell but in cells many cell generationslater which have not been exposed to radiation. These effect are epigenetic in nature and the term "non-targeted" effect is used quite frequently.

Experimental studies have shown during last years a so-called bystander effects. Thus it has been observed in cell cultures with single cell irradiation that not only the exposed cells show a response but also unexposed neighbour cells [14]. These bystander effects have been mainly studied with cells in vitro. They may lead to an enhancement of the radiation effects in vivo. However, also protective effects have been discussed in this connection.

All these phenomena may have the ability to modify the dose response in the low dose range. In which way and at which stage this could happen is unclear. The mechanisms for bystander effects and for the increase of genomic instability are not clear at all. Genomic instability is apparently associated with cancer in general and this is not limited to the cancer itself but involves the whole individual [7]. In a similar way the radiation response is modulated by physiological modalities like age and sex. The influence of the genetic disposition has been mentioned before. Some individuals with an extreme radiosensitivity exist of whom the genetic disposition has been described [4,7].

V. Conclusions

Epidemiological cancer studies are needed in order to estimate risk factors, however, they will not solve the open question about the risk in the low dose range (<100 mSv). Biological studies show effects (e.g. DSB; chromosome aberrations) down to dose ranges of several to 50 mSv. These studies often support the view that no threshold exists for certain radiation effects like mutations. How much such effects contribute to the development of health effects has to be solved. Studies of „new biology"-processes modulate and interact with the development of late radiation health effects. They may lead to a modification of the LNT model but the impact and in which way this occurs cannot be foreseen in the moment [4,6,7].

Radiation-induced cancer is dependent on many factors. It differs from organ to organ according to organ-specific, regulatory biological processes. Therefore the dose response is different for various cancer entities etc. The LNT model is appropriate for prospective radiological protection and may be valid for certain very radiosensitive situations e.g. the induction of thyroid carcinomas in children. However, for individual risk evaluation individual factors (e.g. sex, age, exposure conditions, cancer entity, possible genetic predisposition) have to be used. The LNT model in connection with effective dose should not be used for such purposes. In the low dose range the uncertainties of dose estimates and risk evaluation are high and should be considered. The radiation exposures from natural sources and other background risks e.g. of cancer interfere with the risk evaluation in the very low dose range. Collective dose usually based on low individual doses is useful for the comparison of radiation exposures e.g. of technologies, of countries, it is not useful for risk evaluation [4,7]. Risks in the dose range of medical diagnostics can in most cases only be estimated by calculation and not by definite measurements.

References

1. UNSCEAR (2000). Sources and Effects of Ionizing Radiation. United Nations, New York.
2. 2…. Preston, D.L., Shimizu, Y., Pierce, D.A., Suyama, A. und Mabuchi, K. (2003). Studies of mortality of Atomic Bomb Survivors. Report 13: Solid cancer and noncancer disease mortality: 1950-1997. Radiat. Res. 160, 381-407.
3. Preston, D.L., Ron, E., Tokuoka, S. et al. (2007). Solid cancer incidence atomic bomb survivors: 1958-1998. Radiat. Res. 168, 1-64.
4. ICRP (2007). The 2007 Recommendations of the International Commission on Radiological Protection. ICRP Publications 103. Pergamon Press, Oxford, New York, Frankfurt, Seoul, Sydney, Tokyo.
5. BEIR (2005). Health Effects from Exposure to Low Levels of Ioniz., BEIR VII, Radiation. National Academy Press, Washington, D.C.
6. Streffer, C., Bolt, H., Follesdal, D. et al. (2004). Low Dose Exposures in the Environment, Springer, Berlin Heidelberg-New York.
7. Streffer, C. (2009) Radiological protection: Challenges and fascination of biological research. Strahlenschutzpraxis 15, 35-45.
8. BMU (2008) Umweltradioaktivität und Strahlenbelastung im Jahre 2007
9. Löbrich, M. and Kiefer, J. (2006). Assessing the likelihood of severe side effects in radiotherapy. Int. J. Cancer 118, 2652-2656.
10. UNSCEAR (1994). Sources and Effects of Ionizing Radiation.United Nations, New York, S. 215.
11. Streffer, C. (2004). Adaptive response – a universal phenomenon for radiological protection? In: Proceedings of the IRPA 11, Madrid, Full Paper 1a24.
12. Pampfer, S. and Streffer, C. (1989). Increased chromosome aberration levels in cells from mouse fetuses after zygote X-irradiation. Int. J. Radiat. Biol. 55, 85-92.
13. Okada, M, Okabe A, Uchihori Y, Kitamura H, Sekine E, Ebisawa S, Suzuki M, Okayasu R. (2007) Single extreme low dose/low dose rate irradiation causes alteration in lifespan and genome instability in primary human cells. Brit. J. Cancer 96,:1707-1710.
14. Lorimore, S.A., Coates, Ph.J. and Wright, G.. (2003). Radiation-induced genomic instability and bystander effects: inter-related nontargeted effects of exposure to ionizing radiation. Oncogene 22, 1068-1069.

Quality and Radiation Doses in Mammograms: Brazil Sampling Data

R.B.Medeiros[1], H. Schelin [2], S. Dias[3], F. Mecca[4], M.S. Nogueira[5], T.Silvata[5], P.Costa[6], T.Furquim[7], [8]E. Vieira, [9]I.Brasileiro, [9]H.J.Khoury

[1] Universidade Federal de São Paulo - UNIFESP, São Paulo, Brazil
[2] Universidade Federal do Paraná – UFPR, Paraná, Brazil
[3] Instituto de Radioproteçao e Dosimeria-IRD, Rio de Janeiro, Brazil
[4] Instituto Nacional de Câncer-INCA, Rio de Janeiro, Brazil
[5] Universidade Federal doTriângulo Mineiro - UFTM, Minas Gerais, Brazil
[6]Universidade de São Paulo–Instituto de Física, São Paulo, Brazil
[7]Universidade de São Paulo–Instituto de Eletrotécnica e Energia, São Paulo, Brazil
[8]Centro Federal de Educação Tecnológica- CEFET– Piauí, Brazil
[9]Universidade Federal de Pernambuco – UFPE, Pernambuco, Brazil

Abstract— **The Brazilian Ministry of Health at 453/98 directive requires the implementation of the QAP and settles doses reference values (10 mGy for a 4.5 cm breast) and requirements for the radiological exams practices. The Brazilian College of Radiology (Colegio Brasileiro de Radiologia – CBR) coordinates a quality program certification issuing a quality accreditation certificate to services that fulfill the quality requirements established in the current legislation . The purpose of this work is to verify the image quality criteria observance and compare the skin entrance dose and glandular doses with the national and international requirements. The data related to mammograms quality and doses evaluations were collected in 11 institutions of five States during 2007 and 2008. The skin entrance doses and the glandular average doses were estimated. The image quality was verified based on the criteria established by European Community Guide. The results showed a large dispersion for the glandular doses values. The reference values were 3.27mGy (CC incidence) and 3.36 mGy (MLO incidence).The skin entrance dose values were bellow the reference value established by the Brazilian Ministry of Health for all the institutions, although not all the quality criteria have been fulfilled. Besides the regions difficulties the quality program of CBR associated to AQP requirements of 453/98 directive have been accomplished and good results have been collected in Brazil.**

Keywords— **mammogram, image quality, glandular average dose, skin entrance dose, reference dose.**

I. Introduction

The Cancer National Institute (Instituto Nacional de Cancer -INCA), an organization from Health Ministry of Brazil states that cancer profile in Brazil follows developed countries, in the sense that it is related to population aging. According to this institute, in 2008, was estimated a higher number of breast cancer cases in the south and southeast of the country probably due to the majority of the equipments distribution on those regions (1). The Brazilian Institute of Geography and Statistics (IBGE – Instituto Brasileiro de Geografia e Estatistica) confirms this unequal distribution (2).

A good quality of image is mandatory for the early cancer diagnostic, and for such it is necessary periodic performance tests on the mammographic equipment as part of quality assurance program (QAP) to avoid repetitions or recalls, resulting in unnecessary exposures responsible for increasing risk-benefit rate(3).

The Brazilian Ministry of Health at 453/98 directive requires the implementation of the QAP and settles doses reference values and requirements for the radiological exams practices, aiming to protect patients and employees (3). It establishes a skin entrance dose of 10 mGy for a 4.5 cm breast.

The Brazilian College of Radiology (Colegio Brasileiro de Radiologia – CBR) coordinates a quality program certification issuing a quality accreditation certificate to services that fulfill the quality requirements established in the current legislation (4). The certification process is volunteer and the number of applicants is small (~ 370 clinics) comparing to the existing services. At this point, surveys like this can contribute with data that help to reach better results of quality with acceptable risks.

O. Dössel and W.C. Schlegel (Eds.): WC 2009, IFMBE Proceedings 25/III, pp. 648–651, 2009.
www.springerlink.com

The data at this work are part a pilot study supported by Atomic Energy International Organization (OIEA) promoted during 2007 and 2008 in order to evaluate the protection conditions of patients at medical exposures through sampling data of three regions of Brazil. It purposed to verify the image quality criteria observance and compare the skin entrance dose and glandular doses with the national and international requirements (5). The results might contribute to optimize the doses and to reach higher early breast cancer detection.

II. Methodology

The data related to mammograms quality and doses evaluation were collected in private and public institutions from three Brazilian regions: south, southeast and northeast of five States, during 2007 (11 institutions) and 2008 (7 of the 11 institutions). For this, medical physicists collaborated in order to measure the skin entrance doses and estimate the glandular average doses meanwhile the physicians verified the image quality based on the criteria established by European Community Guide (CE)(5).

The cranial-caudal (CC) and medium lateral oblique (MLO) images were gotten from 4 and 6 cm breast thicknesses (compressed) with 50% glandular tissue.

$$D_G = c_{D_G,K_i} \cdot s \cdot K_i \qquad (1)$$

The air kerma incident values (Ki) and average glandular doses (DG) were gotten using the American College of Radiology (ACR) phantom. The average glandular dose was estimate from incident kerma and half-value-layer (HVL) using the equation 1, were C DG,Ki is the conversion coefficient from kerma to glandular dose and s is a factor which depends on target material and filter.

III. Results

The Figure 1 presents the compliance percentages with the CE image quality criteria for the projections CC and MLO, considering the sum of images from the 11 centers evaluated. The data show that the images percentages that fulfilled the CE criteria are higher in the MLO projection, comparing to the CC projection.

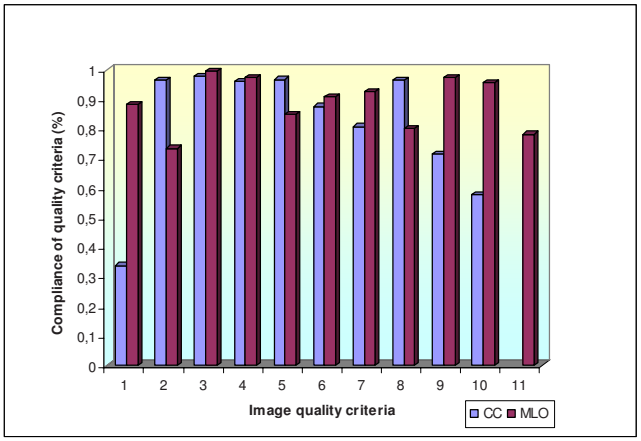

Fig. 1 - Compliance percentages with the CE image quality criteria for CC and MLO incidences.

The Figures 2 and 3 present the "box & whiskers" glandular average dose distribution for CC and MLO incidences.

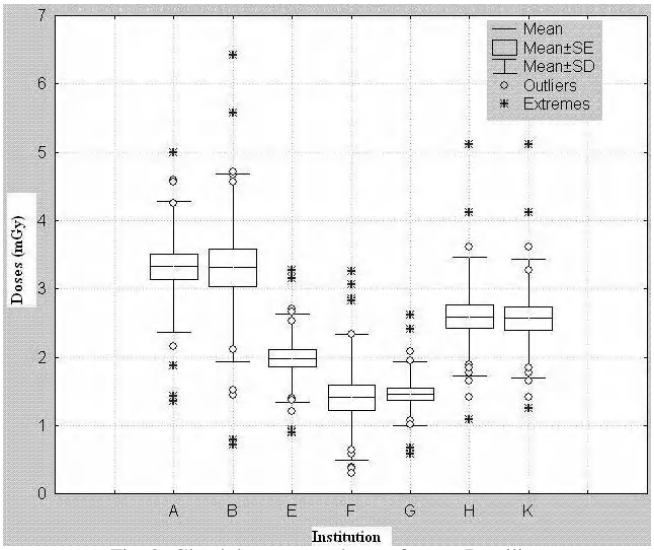

Fig. 2- Glandular average doses of seven Brazilian Institutions gotten of breast image CC incidence.

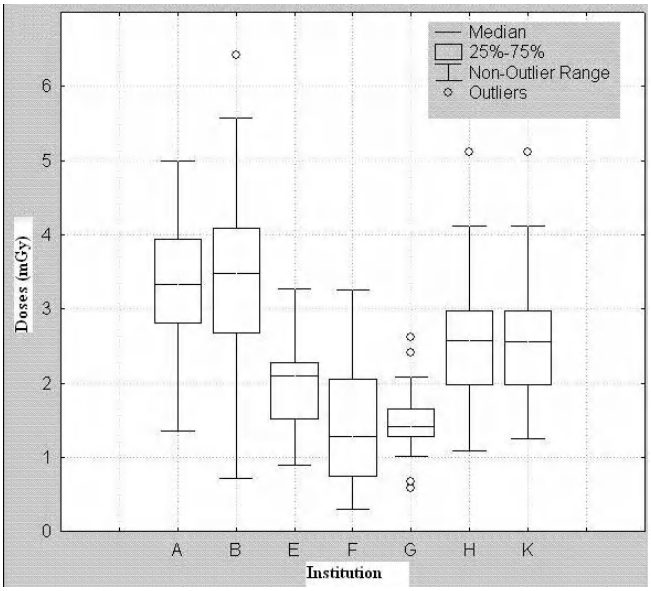

Fig. 3- Glandular average doses of seven Brazilian institutions gotten of breast image MLO incidence.

The Figures 4 and 5 present the glandular average doses histograms related to the images (CC and MLO incidences) that fulfilled more than 70% of the European Community criteria.

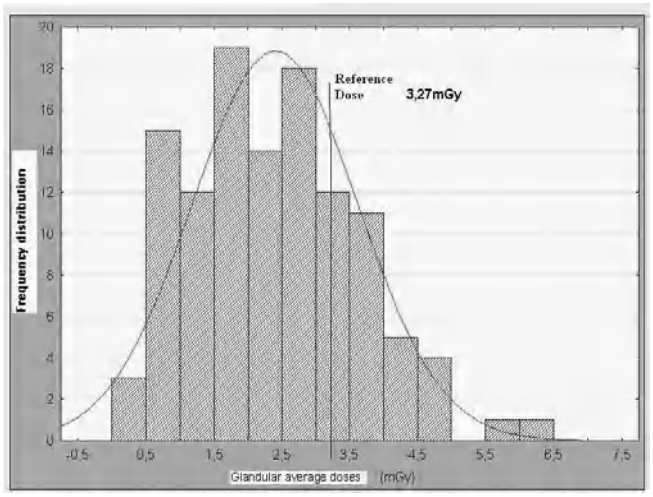

Fig. 4- Glandular average doses histogram of Brazilian institutions gotten from breast image CC incidence.

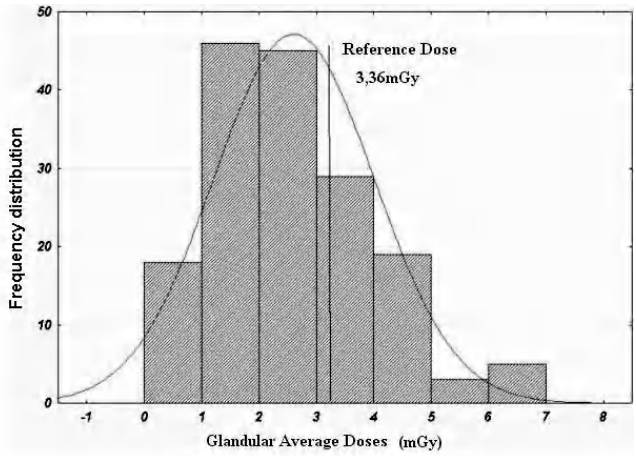

Fig. 5- Glandular average doses histogram of Brazilian institutions gotten from breast image MLO incidence.

The glandular average doses (DG) and air kerma values (Ki) are presented in the Table 1.

Table 1 kerma values (Ka,i) and glandular average doses gotten with the ACR phantom

Institution	**A**	**B**	**E**	**F**	**G**	**H**	**K**
K_i (mGy)	6.50	9.73	13.45	9.33	8.47	5.39	10.03
D_G (mGy)	1.40	2.18	2.55	1.85	1.61	1.20	2.11

IV. Discussion

The screening is an adopted strategy for the early cancer detection and the good quality of images is essential to get maximum benefit of this process. It is also relevant to know the associated doses in order to guarantee proper conditions of population protection. This study permitted to verify the quality associated with radiation doses thanks to the collaboration of physicists and physicians of diverse regions of Brazil. Although the QAP be required in the country since 1998 until know the national results is not fully known. Several countries have implemented the QAP and have made the inspection before and after the program. The results have pointed out for a significant percentage of increased quality through the control of some technical factors, as follow: glandular average dose, skin entrance dose, image quality evaluated using phantom images, film processing and dark room evaluation (6).

The results of the sampling from different regions showed a large dispersion of glandular dose values, although just in a few cases were higher than the European Community reference value (3mGy). Some of the institutions are medical school hospitals what can partially explain the dispersion range. In Brazil is only established a reference value for skin entrance dose and this value was fulfilled by all the institutions, although not all the quality criteria have been fulfilled.

In the different regions of country it was observed that the pectoral muscle has not been visualized in some of the CC images suggesting that this criterion, although essential, is not always required by the specialist. The criterion that requires the skin visualization was the least attended indicating unsuitable exposure conditions. In the MLO incidence the angle below the breast was not visualized indicating breast positioning inadequacy. These results are also explained by the difficulties to implement the exam suggesting the necessity of training. Besides the regions difficulties the quality program of CBR associated to AQP requirements of 453/98 directive have been accomplished and good results have been collected.

V. Conclusion

Although have been detected a large dispersion of glandular dose among the institutions the values are acceptable considering the different characteristics of the involved institutions.

The positioning and exposure conditions were the main parameters responsible for image quality losses contributing the non fulfilled of all the quality criteria.

Acknowledgment

The authors are thankful to International Atomic Energy Agency by technical and financial support.

References

1. INCA - Instituto Nacional de Câncer. http://www.inca.gov.br/conteudo_view.asp?id=1793 (accessed in April, 2009)
2. IBGE – Instituto Brasileiro de Geografia e Estatistica- www.ibge.gov.br (accessed in March, 2009)
3. Brazilian Health Ministry. Portaria da Secretaria de Vigilância Sanitária n°453. Diretrizes de Proteção Radiológica em Radiodiagnóstico Médico e Odontológico. Diário Oficial da União, Brasília, 02 de janeiro de 1998.
4. Colégio Brasileiro de Radiologia. http://www.cbr.org.br/programasdequalidade/PQ_MAMA.htm (accessed in April, 2009)
5. European Commission- European Guidelines on Quality Criteria for Diagnostic Radiographic Images in Paediatrics, Eur 16261,1996.
6. Suleiman, O.H., Spelic, D.C., McCrohan JL, Symonds GR, Houn F. Mammography in the 1990s: The United States and Canada. Radiology 210 (1999) 345 a 351.

Use macro [author address] to enter the address of the corresponding author:

Author: Regina Bitelli Medeiros
Institute: Universidade Federal de São Paulo
Street: R.Mirasol, 313
City: São Paulo
Country: Brazil
Email: rbitelli@cfhr.epm.br

Patient Dose Versus Image Quality in Digital Mammography at Instituto Português de Oncologia de Coimbra (IPOC) – Portugal

A.M.F. Fausto[1,2], A. Roda[3], M.C. Lopes[3], S. Neves[4], S. Pereira[4], M.C. de Sousa[3], and H.J. Khoury[5]

[1] Universidade Estadual de Santa Cruz/DCET, Ilhéus, Brasil
[2] Universidade de Aveiro/Departamento de Física, Aveiro, Portugal
[3] IPOCFG, E.P.E., Serviço de Física Médica, Coimbra, Portugal
[4] IPOCFG, E.P.E., Serviço de Radiologia, Coimbra, Portugal
[5] Universidade Federal de Pernambuco/DEN, Recife, Brasil

Abstract— **In the scope of the optimization of patient protection process (ALARA concept), the assessment of the patient radiation dose is not enough; image quality must be taken into consideration. The aim of this work is double: 1- to assess the image quality in clinical practice using the subjective rating scales of the European Guidelines on Quality Criteria for Diagnostic Radiographic Images, and 2- to estimate patient doses for the digital mammography exams carried out in the Instituto Português de Oncologia de Coimbra (IPOC) for auditing compliance with the European Diagnostic Reference Levels (DRL). The study sample was constituted by 81 patients randomly chosen, providing a total of 264 images, i.e. 134 images for the cranio-caudal (CC) projection and 130 images for the medium lateral oblique (MLO) projection. 25 images have been selected of each projection with compressed breast thickness between 4 and 6 cm and with four images per case (CC and MLO), for which the image quality was assessed by two radiologists. 8 exposures in the CC incidence and 11 exposures in the MLO incidence, representing respectively 32% and 44% of the evaluated images for each projection presented a good diagnostic image, i.e. accomplished at least 70% of all the analyzed criteria. The local patient doses were determined for 69 CC and 55 MLO incidences with compressed breast thicknesses between 4 and 6 cm. The mean entrance surface dose values are below the European DRL of 10 mGy and the mean average glandular dose values are below the suggested European limit dose value of 2.5 mGy.**

Keywords— **Digital mammography, entrance surface dose, average glandular dose, image quality assessment.**

I. Introduction

Optimization means keeping the dose "as low as reasonably achievable, economic and social factors being taken into account" (ICRP 60). For diagnostic medical exposures this implies patient doses which are consistent with the required image quality and necessary for obtaining the desired diagnostic information.

In that scope and to comply with the Council Directive 97/43/Euratom, all X-ray units should be the subject of measurements at regular intervals to enable the assessment of representative doses to patients and check the compliance with the diagnostic reference levels (DRLs) for diagnostic examinations. Additionally, according to the Portuguese legislation (Decree Law nº 180/2002), in the scope of the medical radiological exposures, the head of the installation has to assure the establishment of recommendations in what concerns the patient radiation dose and he should also assure that the radiological exposures are in agreement with the European DRL where available.

At IPOC, mammography is one of the most common examinations practiced in the radiology department (~7943 exams/year). The aim of this work is to investigate the image quality and the patient dose for the local mammography examinations according to the European Guidelines on Quality Criteria for Diagnostic Radiographic Images [1] [2].

II. Materials and Methods

In this study, mammographic examinations were performed using the digital system from General Electric - Senographe DS (GE Medical Systems) installed at the Radiology Department of IPOC. The system is a flat-panel based FFDM.

81 women exams were randomly included in the study, providing a total of 264 images, i.e. 134 images for cranio-caudal (CC) projection and 130 images for medio-lateral oblique (MLO) projection. Mean values for the age of patients and the compressed breast thickness were (60±12) years and (52±14) mm, respectively.

In the population considered in our study, a sub-group of 17 patient cases was selected for evaluation of the clinical image quality (25 images for each protocol, CC and MLO). The thickness of the breast was measured by the compression device. The conditions for selection of the patients were: the thickness of the compressed breast between 40-60 mm and with four images per exam (CC and MLO). Mean values for the age of patients and the compressed

O. Dössel and W.C. Schlegel (Eds.): WC 2009, IFMBE Proceedings 25/III, pp. 652–655, 2009.
www.springerlink.com

breast thickness were (55±12) years and (52±5) mm, respectively.

For patient dose determination, three groups of exams have been established: Group I - those exams that have fulfilled at least 70% of all image quality criteria; Group II - all patients that presented breast thickness compressed (E) among $40 < E \leq 60$ mm; the mean value for these compressed breast thicknesses was (50±6) mm; Group III - all exams of our sample. Entrance surface air-kerma (ESAK) and average glandular dose (AGD) were estimated for all patients following the methodology proposed in the European Protocol on Dosimetry in Mammography [3].

A. Evaluation of the Clinical Image Quality

Evaluation of image quality is an essential component in the optimization of patient protection process, since the final dose data is irrelevant if a good diagnostic image from the mammograms has not been reached. So the images were evaluated on the basis of the image quality criteria published in the European Guidelines on Quality Criteria for Diagnostic Radiographic Images [1]. In order to reduce radiologist's subjectivity each criterion was evaluated in absolute terms. Each radiologist chose "1" (positive evaluation) if the criterion was fulfilled and "0" if not, for independent images.

The image criteria in most cases specify important anatomical structures that should be visible on a radiograph to make possible accurate diagnosis. Some of these criteria depend fundamentally on correct positioning and cooperation of the patient, whereas others reflect technical performance of the imaging system. In Table 1 the quality criteria for CC projection are presented (similar are defined for MLO).

B. Determination of the entrance surface air kerma (ESAK)

Entrance surface air-kerma (ESAK) is the air kerma at a point on a plane corresponding to the entrance surface of the breast, without backscatter.

It was calculated from the radiation output at the specific kVp and mAs settings used for each patient, and corrected by the source-skin distance. The exposure parameters were extracted from the images.

Table 1 Image Criteria for Cranio-Caudal Projection

	Image criteria related to position
1.	Visually sharp reproduction of pectoral muscle at image margin
2.	Visually sharp reproduction of retroglandular fat tissue
3.	Visually sharp reproduction of medial breast tissue
4.	Visually sharp reproduction of lateral glandular tissue
5.	No skinfolds seen
6.	Symmetrical images of left and right breast
	Image criteria related to exposure parameters
7.	Visualization of skin outline with bright light (but barely without it)
8.	Reproduction of vascular structures seen through most dense parenchyma
9.	Visually sharp reproduction of all vessels and fibrous strands and pectoral muscle margin (absence of movement)
10.	Visually sharp reproduction of skin structure (rosettes from pores) along the pectoralis muscle

Radiation output measurements of the X-ray machine were performed with an ionisation chamber from Radcal (Mod. 10x9-6M) with a radiation monitor controller Radcal (Mod. 9095). Before and during the period of data collection the quality control tests of the X-ray system were periodically carried out. All the parameters verified were within the equipment tolerance limits.

C. Determination of the entrance surface dose (ESD)

In the European Commission documents [1] [3 [4], the currently available European DRLs for diagnostic radiology in mammography are expressed in terms of entrance surface dose (ESD) per image, for single views. The DRL value for breast CC radiograph and breast MLO radiograph is 10 mGy for a standard-sized patient with 5 cm compressed breast. In this study the ESD (mGy) was calculated from the ESAK including backscatter radiation.

$$ESD = ESAK \times B \qquad \text{(mGy)} \qquad (2)$$

where B is the backscatter factor. It is typically 1.09 for breast examinations [1].

D. Determination of the average glandular dose (AGD)

AGD was calculated from the ESAK and from the conversion coefficients calculated by Dance [5] [6] according to the following expression:

$$AGD = c_{D_G,K}\, s\, ESAK$$

Where:

- $c_{D_G,K}$ is the conversion coefficient from the ESAK to AGD; it depends on the HVL [5]. The procedure to obtain the HVL at different kVps was the standard [3].
- s is a correction factor depending on the anode/filter combination [6].

III. Results and Discussion

If we consider the total score of approval of each item for all images of each individual protocol, the total percentage of positive evaluation is 61.6% for CC and 60.7% for MLO incidence.

The fulfillment of criteria for image quality is presented in Figure 1 for CC, and in Figure 2 for MLO. The results are summarized in Table 2.

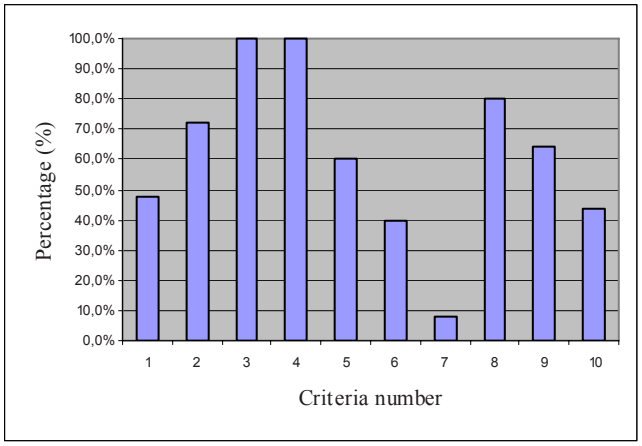

Fig. 1 Image quality evaluation for CC projection expressed as percentage of average scoring for each criterion

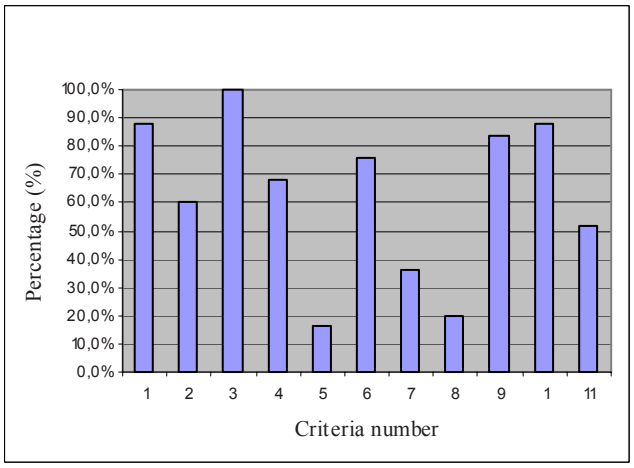

Fig. 2 Image quality evaluation for MLO projection expressed as percentage of average positive scoring for each criterion

Table 2 Summary of results of the approval criteria of image quality

Criteria	Projection.	Results
3, 4	CC	100%
3	MLO	100%
2, 8	CC	≥ 70%
1, 6, 9 e 10	MLO	≥ 70%
1, 5, 6, 9 e 10	CC	≥ 30 and < 70%
2, 4, 7 e 11	MLO	≥ 30 and < 70%
7	CC	< 30
5 e 8	MLO	< 30

Considering a good diagnostic image the one which accomplish at least 70% of all the analyzed criteria, 8 exposures in the CC incidence and 11 exposures in the MLO exposures have reached this result, representing respectively 32% and 44% of the evaluated images for each projection (Group I).

The mean entrance surface dose values were calculated for the Group I and for the Group II (69 exposures in the CC incidence and 55 exposures in the MLO incidence). The results are summarized in Table 3 with the respective mean, minimum and maximum values.

Table 3 Mean, minimum and maximum values of local ESD for Group I (rating score of image quality ≥70%) and Group II

Breast Projection	ESD (mGy)					
	Group I			Group II		
	Mean	Min.	Max.	Mean	Min.	Max.
CC	(5.0±0.7)	4.0	6.1	(4.8±0.8)	2.8	6.5
MLO	(5.0±0.6)	4.2	5.9	(4.9±0.7)	3.4	6.7

Comparing these results with the European DRL of 10 mGy, we can see that the local dose levels are significantly below the recommended values. This could be an indication of problems with image quality. But as we observed that the patient doses for Group I and Group II are similar, we can conclude that the lack of compliance with the image quality criteria is not related with dose.

In Table 4 the mean, minimum and maximum values of AGD for Groups I, II and III of CC and MLO projections are presented.

Table 4 Calculated local values of AGD

AGD (mGy)	CC Projection			MLO Projection		
	Mean	Min	Max	Mean	Min.	Max
Group I (19 exams)	(1.2±0.2)	0.98	1.51	(1.2±0.2)	0.99	1.43
Group II (124 exams)	(1.1±0.2)	0.69	1.58	(1.2±0.2)	0.67	1.66
Group III (264 exams)	(1.3±1.0)	0.46	11.24	(1.4±0.9)	0.56	9.62

If we compare the results with the European suggested limit dose value for digital mammography of 2.5 mGy [2], the local mean AGD are below for all the three groups.

IV. Conclusions

The evaluation of image quality is a key component in the determination of patient doses in mammography. However, for a usual hospital workload the assessment of image quality in terms of international standards is often considered too time-consuming. Nevertheless, in this study we have succeeded in having the contribution of two radiologists for the image quality evaluation of 50 mammography exams. This was the first approach of a more complete quality assurance program for digital mammography to be developed at our institution, in the near future. Important actions have already been initiated in the hospital to optimize the procedures for patient radiation protection with the aim of achieving high-quality mammograms. Nevertheless, the image quality survey carried out has identified a low scoring in image quality that should be re-evaluated. Digital mammography quality criteria are not yet internationally standardized. On the other end a full quality control of the radiological installation, integrating all system components, has to be implemented.

The patient dose assessment for the local mammography examinations revealed doses well below the dose limits established in the European guidelines. However the low doses are not related with the lack of compliance with the image quality criteria.

This study aims at contributing to the required discussion and review of the relevant concepts and parameters which need to be appropriated to digital mammography.

Acknowledgment

The authors wish to thank Dr. Idílio Gomes, head of the Radiology Department, for providing the opportunity to perform this study and to the whole staff at the mammography sector especially to Ana Lopes, Paula Santos, Isabel Cruz and Silvina Simões for their help.

References

1. European Commission. European Guidelines on Quality Criteria for Diagnostic radiographic images. (Luxembourg: CEC), 1996, EUR 16260 EN
2. European guidelines for quality assurance in breast cancer screening and diagnosis. (Luxembourg: CEC) Fourth Edition (2006).
3. European Commission. European protocol on dosimetry in mammography. Zoetelief, J, Fitzgerald, M, Leitz, W and Säbel, M, (Luxembourg: CEC), 1996, EUR 1623 EN
4. European Commission. Radiation Protection 109 – Guidance on diagnostic reference levels (DRLs) for medical exposure. 1999
5. Dance, R. D (1990) Monte Carlo calculation of conversion factors for the estimation of mean glandular breast dose. Phys. Med. Biol 35:1211-1219
6. Dance, R. D., Skinner, C. L., Young, K. C., Beckett, J. R. and Kotre, C. J. (2000) Additional factors for the estimation of mean glandular dose using UK mammography protocol. Phys. Med. Biol. 45: 3225–3240.

Author: Agnes M F Fausto
Institution: Universidade de Aveiro / Departamento de Física
Adress: Campus Universitário de S. Tiago
Postal Code: 3810-193
City: Aveiro
Country: Portugal
Email: amffausto@uesc.br

Image Gently: An International Education and Communication Campaign in Radiology to Promote Radiation Protection for Children

Keith J. Strauss MSc[1], Priscilla F. Butler, MS[2], Marilyn J. Goske MD[3], Thomas L. Toth[4], Kimberly E. Applegate MD, MS[5], Gregory Morrison, CAE, MA, RTR, and CNMT[6]

[1]Children's Hospital Boston, Department of Radiology, Harvard Medical School, Boston, Massachusetts, USA
[2]American College of Radiology, Reston, Virginia, USA
[3]Department of Radiology, Cincinnati Children's Hospital Medical Center, University of Cincinnati, College of Medicine, Cincinnati, Ohio, USA
[4]GE Medical Systems, Milwaukee, Wisconsin, USA
[5]Department of Radiology, Riley Hospital for Children, Indianapolis, Indiana, USA
[6]American Society of Radiologic Technologists, Albuquerque, New Mexico, USA.

Abstract– The Alliance for Radiation Safety in Pediatric Imaging represents over 600,000 health care professionals in 37 professional organizations. This alliance is an international coalition that raises awareness and promotes opportunities to decrease radiation dose to children during diagnostic imaging. The *Image Gently* campaign, the Alliance's first operation, focuses on managing radiation dose while maintaining good image quality during pediatric CT imaging.

The success of *Image Gently* results from a broad scope of health care professionals working effectively together to achieve its common goal. Working effectively with all the professional organizations that represent all stakeholders is a key to achieving broad scope of participation. This diversification leads to the development of a wide variety of clinical and technical educational materials about CT imaging. Each presentation is targeted to specific/multiple stakeholders; each is widely disseminated using multi media.

In 2008, *Image Gently* posted universal guidance that allows facilities to develop pediatric CT protocols. This guidance is designed to maintain the same pediatric patient radiation dose regardless of the patient's size. Although the *Image Gently* guidance provides less aggressive dose reduction than 'cutting edge' techniques used in some pediatric institutions, it provides a reasonable starting point to explore further dose reduction. These protocols are targeted to the adult hospital or clinic that occasionally images children and is not aware that its pediatric CT doses may exceed its adult doses.

The *Image Gently* campaign is dynamic. It is currently collecting scientific data that will lead to reduction of systematic errors currently present in the displayed dose values on CT scanners when performing pediatric imaging. The Alliance is also working on the development of other modules to address effective use of pediatric radiation dose in the imaging modalities of general fluoroscopy, interventional fluoroscopy, and nuclear medicine.

Keywords– **CT, Pediatrics, Radiation Dosage, Radiation Protection**

I. Introduction

The *Image Gently* campaign is an international education and awareness campaign designed to raise awareness and promote opportunities to decrease radiation dose to children in diagnostic imaging[1; 2]. Mass medial communication campaigns are an accepted method for eliciting change in societal attitudes, increasing knowledge and achieving social and behavioral change that will improve the health of the population[3]. This methodology has demonstrated that practical, straightforward safety messages on radiation protection targeted to medical professionals throughout the international radiology community, utilizing multiple media, can affect awareness and likely lead to change in practice on a local level. This paper discusses steps to use partnerships, timely educational materials, and development of scientific data necessary to change imaging equipment development. The goal of the campaign is to effectively manage radiation dose to children during imaging procedures that use ionizing radiation while maintaining high quality imaging.

II. Partnerships

Part of the strategy of social marketing is creating partnerships to increase the likelihood of success. The Alliance for Radiation Safety in Pediatric Imaging, the sponsor of the *Image Gently* campaign, was founded in 2007 by four professional organizations—the Society for Pediatric Radiology, the American Association of Physicists in Medicine, the American College of Radiology, and the American Society of Radiologic Technologists. These organizations have been joined by 33 affiliate organizations (both within the US and internationally) representing radiologists, medical physicists, and technologists. Through these Alliance organizations, health messages reach over

O. Dössel and W.C. Schlegel (Eds.): WC 2009, IFMBE Proceedings 25/III, pp. 656–659, 2009.
www.springerlink.com

600,000 health care professionals at relatively little cost by utilizing the infrastructure and communications of each Alliance organization.

While the initial alliance was a good first step, it was too limited to achieve all of the goals of *Image Gently* in computed tomography (CT). CT manufacturing companies engineer and design the equipment. Federal regulatory agencies regulate the manufacturing process while local governments regulate the end user. Medical physicists measure the radiation output of the CT scanner and work with the vendor to improve image quality. Radiologic technologists acquire and process the scan data while pediatric radiologists provide oversight and interpret the acquired images.

To engage the CT manufacturers and regulatory agencies, *Image Gently* held a CT Vendor Summit Meeting in August, 2008, to enable communication among all stakeholders. This summit meeting established a commitment on the part of CT manufacturers to address systematic errors in the display of pediatric radiation doses on their scanners and to work with Alliance members to create educational materials to improve pediatric applications and the operation of each manufacturer's CT scanner. In addition, the summit fostered the creation of a Pediatric CT Physics Work Group within the Medical Imaging & Technology Alliance (MITA) within the United States to develop scientific data on the attenuation characteristics of the pediatric body during CT imaging. The Summit also established a working relationship between the Alliance and International Electro-Technical Commission.

III. Educational Materials

The *Image Gently* campaign has employed a range of media, including print (scientific journals, trade publications), the internet (through e-mail, list serves, websites), and posters. The website, imagegently.org, is the cornerstone of the campaign's educational resources. It has a distinctive logo and simple message that is repeated in its communication. The campaign website allows for individuals and medical practices to "sign on" to the campaign and pledge to "image gently" to promote radiation protection in their practice setting. Recently the campaign has created an *Image Gently* Imaging Record card for parents to record information on the date, place, and type of imaging exam for their child. A two and an eight page parent brochure is available on the website for medical practices to use to inform parents about medical imaging. This brochure is currently being translated into 8 languages and will soon be posted on the website. A Practice Quality Improvement module, slides on radiation protection, and scientific references are also included on the site.

One of the unique features of the website is the guidance for developing pediatric CT protocols. Following this simple guidance results in CT technique factors designed to maintain the same pediatric patient radiation dose regardless of the patient's size. If adult radiological technique factors are used for children, the radiation dose to the newborn will be more than doubled relative to the adult. This occurs due the loss of attenuation of the radiation by over lying tissues of the adult patient that are not present in the pediatric body. Figure 1 illustrates that an anthropomorphic phantom in the Posterior Anterior (PA) dimension of a newborn is approximately 10 cm while the adult is represented by a 25 cm PA projection[4]. Although the *Image Gently* guidance provides less aggressive dose reduction than those 'cutting edge' techniques used in some pediatric institutions, it provides a reasonable starting point to explore further dose reduction. These protocols are targeted to the adult hospital or clinic that occasionally images children and is not aware that its pediatric CT doses may exceed its adult doses.

While considerable work has been published in the literature on protocols to reduce dose to children undergoing CT examinations for specific CT Scanners[5-15], these published protocols cannot be used universally; the influence of CT scanner design on patient dose must be removed. This is achieved by having the facility contact their qualified medical physicist to perform radiation output measurements on the site's scanner and estimate the

Fig. 1 Three CT dosimetry phantoms. Phantom on the left is a nested 32 cm CTDI phantom, 16 cm CTDI phantom, and 10 cm diameter cylindrical phantom. The two phantoms to the right are anthropomorphic phantoms of the thorax of a newborn infant (9 cm PA) and medium sized adult (25 cm PA). Both anthropomorphic phantoms contain different plastics that simulate the attenuation of lung tissue and age appropriate spine. A 12-inch ruler lies on the table in front of the three phantoms.

$CTDI_{vol}$ using standard 16 and 32 cm CTDI PMMA phantoms[16]. This allows the qualified medical physicist to compare the dose of the facility to appropriate reference values[17] and adjust the site's adult techniques if necessary to provide reasonable adult patient doses. Once reasonable adult doses for the abdomen and head are established or verified, the radiologic technique factors of these two exams are inserted into the *Image Gently* worksheet which automatically scales the mAs values relative to the adult baseline as a function of their PA thickness. The *Image Gently* protocols assume that the kVp and pitch of the scans remain fixed as patient size varies.

By the fall of 2009, seven modules for CT technologists will be posted that provide dose saving strategies for children undergoing indicated CT scans on different manufacture's CT units. These educational materials would not be possible without the commitment by the CT manufacturers to provide necessary technical information about their CT product lines—a commitment established as a result of the CT Vendor Summit discussed above.

IV. Display of Pediatric Patient CT Dose

Dose information reported currently on CT scanners is a dose index based on CTDI adult head or body size reference phantoms[16] as required by international standards (IEC). The CTDI dose index does not represent the dose for the various sizes of pediatric patients encountered in clinical practice. Size-adjusted dose that better represents the dose received by small patients would facilitate improved dose management and more appropriate use of CT for pediatric imaging.

The Alliance in conjunction with MITA is investigating the use of a patient attenuation value (PAV) that can be derived from the patient scan projection radiograph or an axial CT image to model a phantom with a similar attenuation values from which patient dose as a function of patient size can be reported. The image pixel values for an axial image can be converted from HU values to their water normalized values. The square root of the sum of the water-normalized pixel values defines the PAV, assuming the patient is substantially within the image region.

Early results show that the ratio of $CTDI_{vol}$ dose values for different diameter CTDI phantoms is remarkably similar for different conditions of operation and is reasonably independent of scanner make and model. This could lead to a universal function of reasonable accuracy that could be used to scale the reported dose for a give CTDI phantom to a value the better represents the patient's dose. It is likely that this method could also be used in a similar fashion to scale anthropomorphic phantom dose values or organ dose values determined from Monte Carlo simulations as a function of size based on PAV and normalized to a reported reference phantom dose.

V. Conclusions

The success of *Image Gently* in managing pediatric CT radiation dose while maintaining high quality imaging is the result of a broad scope of health care professionals working effectively together to achieve a common goal. The broad scope of participation is the result of the campaign working effectively with all the professional organizations that represent all the stakeholders in successful CT scanning. This diversification has lead to the development of a wide variety of educational materials addressing both clinical and technical aspects of CT imaging. Each presentation is targeted to specific/multiple stakeholders and each one is widely disseminated using multi media.

The *Image Gently* campaign is dynamic. In addition to posted educational materials, it is currently collecting scientific data that will hopefully lead to the reduction of systematic errors currently present in the displayed dose values on state-of-the-art CT scanners. The Alliance is also currently working on the development of other modules to address effective use of pediatric radiation dose in the imaging modalities of general fluoroscopy, interventional fluoroscopy, and nuclear medicine.

References

1. Goske MJ, Applegate KE, Boylan J et al. (2008) Image Gently(SM): a national education and communication campaign in radiology using the science of social marketing. J Am Coll Radiol 5:1200-1205.
2. Goske MJ, Applegate KE, Boylan J et al. (2008) The Image Gently campaign: working together to change practice. AJR Am J Roentgenol 190:273-274.
3. Buchbinder R, Gross DP, Werner EL et al. (2008) Understanding the characteristics of effective mass media campaigns for back pain and methodological challenges in evaluating their effects. Spine 33:74-80.
4. Strauss KJ, Goske MJ, Frush DP et al. (2009) Image gently vendor summit: working together for better estimates of pediatric radiation dose from CT. AJR Am J Roentgenol [In Press]
5. Paterson A, Frush DP (2007) Dose reduction in paediatric MDCT: general principles. Clin Radiol 62:507-517.
6. Verdun FR, Schnyder P, Gutierrez D et al. (2006) Patient dose optimization in pediatric computerized tomography. Rev Med Suisse 2:1752-1757.
7. Fefferman NR, Bomsztyk E, Yim AM et al. (2005) Appendicitis in children: low-dose CT with a phantom-based simulation technique--initial observations. Radiology 237:641-646.
8. Shah R, Gupta AK, Rehani MM et al. (2005) Effect of reduction in tube current on reader confidence in paediatric computed tomography. Clin Radiol 60:224-231.

9. Mayo JR, Kim KI, MacDonald SL et al. (2004) Reduced radiation dose helical chest CT: effect on reader evaluation of structures and lung findings. Radiology 232:749-756.
10. Greess H, Lutze J, Nomayr A et al. (2004) Dose reduction in subsecond multislice spiral CT examination of children by online tube current modulation. Eur Radiol 14:995-999.
11. Ratcliffe J, Swanson CE, Hafiz N et al. (2003) Assessment of image quality of a standard and two dose-reducing protocols in paediatric pelvic CT. Pediatr Radiol 33:177-182.
12. Frush DP, Slack CC, Hollingsworth CL et al. (2002) Computer-simulated radiation dose reduction for abdominal multidetector CT of pediatric patients. AJR Am J Roentgenol 179:1107-1113.
13. Morgan HT (2002) Dose reduction for CT pediatric imaging. Pediatr Radiol 32:724-728; discussion 751-724.
14. Westerman BR (2002) Radiation dose from Toshiba CT scanners. Pediatr Radiol 32:735-737; discussion 751-734.
15. Fox SH, Toth T (2002) Dose reduction on GE CT scanners. Pediatr Radiol 32:718-723; discussion 751-714.
16. Shope TB, Gagne RM, Johnson GC (1981) A method for describing the doses delivered by transmission x-ray computed tomography. Med Phys 8:488-495.
17. New CT Accreditation Dose Requirements Effective January 1, 2008 at http://www.acr.org/accreditation/FeaturedCategories/ArticlesAnnouncements/NewDoseReq.aspx

Digital image quality indexes for CIRS SP01 and CDMAM 3.4 mammographic phantoms.

P.Mayo[1], F.Rodenas[2] , G.Verdú[3] and J.M.Campayo[4]

[1] Research and Development Department, TITANIA Technological Services S.L., Valencia, Spain
[2]Mathematical Department, Polytechnic University of Valencia, Valencia, Spain
[3]Nuclear and Chemicall Department, Polytechnic University of Valencia, Valencia, Spain
[4]Radiation Protection Service, Hospital Clinico Universitario de Valencia, Spain

***Abstract*— In Mammographic phantom images are usually used to study the quality of images obtained by determined mammographic equipment. The digital image treatment techniques allow carrying out an automatic analysis of the phantom image. Nowadays, the digital radiographic equipments are replacing the traditional film-screen equipments and it is necessary to update the parameters to guarantee the quality of the process. In this work we apply some techniques of digital image processing to compute a specific image quality indexes for mammographic phantoms, namely CIRS SP01 and CDMAM 3.4. to study the evolution of this parameter with different varying conditions of the mammographic equipment. The indexes are calculated from a scoring system based on a designed algorithm which analyses the phantom image by means of an automatic detection of the test objects in each phantom.**

Keywords— **Mammographic phantom, image processing, quality index**

I. Introduction

The mammography is an effective radiographic technique to detect breast cancer because can detect small changes of density in breast tissue. The methods and tools developed in the work let the assessment of the image quality obtained at different mammographic units studying the digitized images [1]. The advantages of using digitized images are many, as that they let the objective analyses of the mammographic image, so the image evaluation is independent of availableness of the human expert assessors [2,3].

About the technology, film-screen equipments are well-proven systems for projection radiography. In conventional mammography, the exposure setting need to be chosen such that the important x-ray information is in the sensitive region of the film. Film-screen equipments have limited dynamic range and difficulties in post processing. The main differences of the digital systems, the main differences between them are in the detector technology and in the signal processing. In digital detectors, the information of the x-ray beam is converted into an electrical signal, and then in digital values. Digital systems have a wide dynamic range of detector wide, so there is no saturation in dark or white regions, and there is no variability in image quality due to chemistry and temperature fluctuations associated with film processing

II. Materials and methodology

A. CIRS SP01 and CDMAM 3.4 mammographic phantoms

The mammographic phantoms that we have used are CIRS SP01 and CDMAM 3.4. The CIRS SP01 phantom has some test objects to simulate typical pathologies of the breast as microcalcifications, masses or fibers with different thickness and diameters, and has other test objects for the calibration of the image like the reference 50%-50% optical density, 100% gland, 100% fat and the horizontal and vertical resolution measured as line pair per millimetre. The phantom sketch is reflected in Figure 1, showing the number of test objects, shape and distribution.

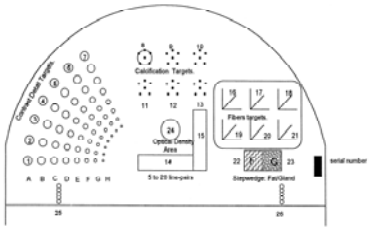

Fig. 1 Sketch of the mammographic phantom CIRS SP01

The *CDMAM* 3.4 phantom is made of an aluminium base with gold disks of varying thickness and diameters, which is attached to a plexiglas cover. The gold disks diameter range from 0.06 to 2.0 mm and thickness from 0.03 to 2.0 μm, resulting in a radiation contrast range of 0.5-30% at standard mammography exposure conditions. The phantom is used with 4 plexiglass plates, each one with a thickness of 10 mm. The disks are located in a matrix of 16 rows and 16 columns, rotated forty-five degrees to minimize influences

O. Dössel and W.C. Schlegel (Eds.): WC 2009, IFMBE Proceedings 25/III, pp. 660–663, 2009.
www.springerlink.com

of the heel effect that causes optical density variations. Figure 2 shows a sketch of CDMAM 3.4 phantom.

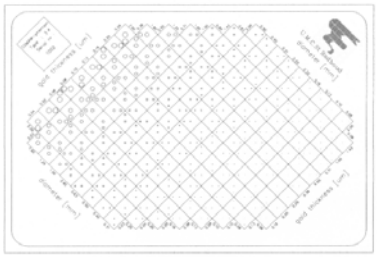

Fig. 2 Sketch of the mammographic phantom CDMAM 3.4

B. Image Processing Methods

The digital mammographic equipment used is GE Senographe DMR with reader and printer system Profet CS by Fuji and the photostimulable phosphor screens FUJI FCR 5000 MA. It is a storage phosphor system with dual sided imaging reader. The material of the anode is Mo and the material of the filter is Mo-Rh. The images have been obtained with a resolution of 508 dpi, that is 50 μm per pixel in dicom format without preprocessing.

We have developed the analysis of the mammographic phantom image quality by means of automatical processing techniques for the CIRS SP01 phantom. All the algorithms have been implemented in Matlab 7.0. Specific details about how we developed this processing algorithms could be seen in a previous work [4]. The digital image analysis provides information about the phantom test objects as the size, the exact position, the shape, the contrast.. that is useful to characterize the phantom image obtained. We have considered subimages of each phantom test area of the initial mammographic image to carry out the analysis of the microcalcification area, the resolution area, the low contrast area, the reference density area…etc.

We have analysed the CDMAM 3.4 phantom by the *CDCOM* software [5] in which the algorithm determines the border of the phantom, resolve its position and the centre of its contrast-detail combinations by the Hough transform. After that, the programme tests with a statistical method if the average contrast-detail is greater than the average background, to consider the combination as detected.

III. IMAGE QUALITY INDEXES

It is important the definition of a parameter that can characterize in an objective way the mammographic phantom image quality. In this sense we have defined an image quality index (*IQI*) for the CIRS SP01 phantom based on a scoring scheme that uses the number of microcalcifications detected in each group and the resolution limit measured as line pairs per millimetre detected at horizontal and vertical resolution area. So for the microcalcifications area the IQI is obtained multiplying the factor corresponding to the number of microcalcifications detected in each group with a factor that depends on the group of microcalcifications. For the resolution zone, the scoring scheme is based on the resolution threshold obtained at the horizontal and vertical resolution. Finally, IQI is the sum of both scores. In the following tables are the scoring factors for the calculation of the IQI.

Table 1: Scoring scheme for the microcalcification groups and resolution zone for the Image Quality Index (IQI) for the CIRS SP01 mammographic phantom.

Nº of group of microcalc.	10	9	8	13	12	11
Factor	1.0	1.5	2.0	2.5	3.0	3.5

Nº micros detected in each group	6	5	4	3	2	1	0
Factor	3.0	2.5	2.0	1.5	1.0	0.5	0.0

Line pairs millimetre (lp/mm)		5	6	7	8	9	10
Score	***Horizontal resolution***	0.5	1	2	4	8	12
	Vertical resolution	1	2	4	8	12	16

The Image Quality Figure (*IQF*) is the image index for the evaluation of the image quality of the CDMAM 3.4 mammographic phantom:

$$IQF_{inv} = \frac{1}{\sum_{i=1}^{n^{o}cols} C_i \cdot D_{i,th}} \cdot 100$$

where $D_{i,th}$ is the threshold diameter in the contrast column i and C_i is the value of the thickness of the gold disks of the column. Another way to study the image quality of the CDMAM 3.4 phantom is the contrast detail curve that is a graphical representation in which the gold disk

thickness and diameter are plotted for each contrast-detail combination detected in the image of the phantom

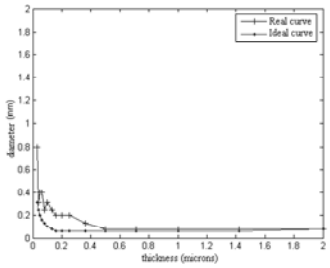

Fig. 3 Contrast detail curve for an image of the CDMAM 3.4 mammographic phantom.

IV. Results

In this work we have analysed different mammographic images acquired from a digital equipment in dicom 3.0 format and study the manner in which the functioning conditions (kV and mAs) of the mammographic equipment affect the contrast and the results for the image quality index of the digital images for both phantoms.

In table 2 are shown the results for the IQI for the CIRS SP01 mammographic phantom. The microcalcification groups and pl/mm that are not detected, are not in the table.

Table 2: Results for the image quality index (IQI) for the CIRS SP01 phantom

		23kv 136mAs	*26kv 65mAs*	*28kv 42mAs*	*30kv 30mAs*	*33kv 20mAs*
Group 10	***Micro. detected***	6	6	6	6	6
Group 9	***Micro. detected***	6	6	5	6	6
Group 8	***Micro. detected***	6	6	6	6	4
Group 13	***Micro. detected***	6	5	6	4	3
Resol	***Horizontal (pl/mm)***	7	8	8	8	8
	Vertical (pl/mm)	7	7	7	7	7
IQI		27.00	27.75	28.25	26.50	23.25

The image quality index is sensitive to the working conditions of the digital mammographic equipment, because the values of the index are different for each image. From the results in Table 2, we see that the best image quality is for medium voltage and load, because the value for IQI is bigger.

In tables 3 is shown the values for the image quality index *IQF* for the CDMAM 3.4 phantom at different radiographic techniques, varying kV and mAs, with handle mode (AEC: +0) and on other hand, with kV fixed at 28kV varying mAs in an automatic mode (AEC:+2, AEC:-2).

Table 3: Results for the image quality index (IQF) for the CDMAM 3.4 phantom

kV	*AEC*	*mAs*	*IQI*
26	+0	101	126.10
28	+0	55	127.70
30	+0	32	116.14
28	-2	40	105.28
28	+2	75	138.22

From the results above we can see that when the radiographic equipment is working in handle mode, as the kilovoltage is growing the value of *IQF* decreases, so the image quality is lower because the detail detected is minor at bigger kV (for example at 30 kV, some little objects are not detected). In automatic mode for the same kV at 28 kV, as the mAs is growing for AEC: +2, the *IQF* grows so the image quality is better because the quantum noise decreases as the mAs increases.

V. Conclusions

The analysis carried out in this work indicates that both indexes IQI and IQF can be used to determine the image quality of CIRS SP01 and CDMAM 3.4 mammographic phantoms because they are sensitive to the working conditions of the mammographic equipments. The method let the comparison of different images between themselves and with a reference image obtained by determined functioning conditions of the equipment. The phantom used CIRS 11A, SP01 brings information that can simulate anatomical changes that are searched in clinical images due its complete test-objects design. The CDMAM 3.4 mammographic phantom is specially designed for digital mammographic equipments and the IQF is an adequate parameter to detect abnormal functioning of the equipment so it could be used as a quantitative parameter of image quality in the quality control of the mammographic equipment.

As future works, we want to have more practical application of both image quality indexes in mammographic facilities to obtain more clinical experience.

ACKNOWLEDGMENT

The authors wish to thank Clinical Hospital of Valencia their collaboration in testing these phantoms in their facilities.

REFERENCES

1. Working Party of Radiologists, Quality Assurance Coordinating Group, Computer aided detection in mammography, NHSBSP Publication nº 48, (2001).
2. K.W. Brooks, J.H. Trueblood, K.J. Kearfott and D.T. Lawton, Automated analysis of the American Collegue of Radiology mammographic accreditation phantom images, Medical Physics, 24, 709-723, (1997).
3. D.P. Chakraborty, Computer analysis of mammography phantom images (CAMPI): An application to the measurement of microcalcification image quality of directly acquired digital images, Medical Physics 24, 1269-1277, (1997).
4. Mayo P. et al, (2004) Automatic evaluation of the image quality of a mammographic phantom, Computer Methods and Programs in Biomedicine, 73/2, 115-128.
5. Nijmegen University Medical Centre, Department of Radiology, CDCOM Manual: software for automated readout of CDMAM 3.4 image (2004)

Corresponding author:
- Patricia Mayo Nogueira
- Research and Development Department, TITANIA Technological Services S.L.
- Sorolla Center, local 10, Avda. de las Cortes Valencianas, nº 58, 46015
- Valencia
- Spain
- p.mayo@titaniast.com

Residual Radiation of Medical Linear Accelerators: Special Radiation Protection Aspects

J. Kóbor

Radiation Protection Service , Dept. of Oncotherapy, University Pécs, Hungary
joseph.kobor@aok.pte.hu

Abstract: **Medical linear accelerators (LINAC-s) are the most common teletherapy radiation treatment units today. They contain no radioactive isotopes, but their high-energy (Xhigh,E>10 MeV) photon radiation and neutron capture can produce short-living radioactive isotopes in the unit and in the air outside.We investigated this residual radiation which means a not forgettable radiation safety problem in the medical practice.**

Keywords – **residual, radiation, medical,accelerator**

I. INTRODUCTION

Medical linear accelerators (LINAC-s) are the most common radiation teletherapy treatment units today. They contain no radioactive isotopes, but their high-energy (Xhigh,E> 10 MeV) photon radiation and neutron capture can produce short-living radioactive isotopes in the unit, head, beam track, and in the air outside. There is an increased background radiation level which dependent on time about units after terminating patient treatment radiation. Technicians and other workers who enter the treatment room and work on patient positioning or manipulate on unit will be exposed to gamma and beta radiation, the residual radiation has radiation protection significance on them.

Creation of residual radiation in LINAC and in air environment is explained on Tables 1/a and, 1/b. where we show the most important activating reactions going in the LINAC during therapeutic radiation on :

Table 1/a

Creation of isotopes in medical linear accelerators with high energy (Emax > 10 MeV) "Bremsstrahlung"

Reactions:

Neutron capture: (n, γ)
Product radiation: ß, γ

Photoeffect in nucleus: (γ, n)
(γ, p)

Product radiation: ß, ß+, γ
(E>10 MeV, "giant resonances")

Table 1/b

Creation of gaseous radioactive component from most important nuclides in the air:

^{14}N (γ, n) ^{13}N
Radiation: ß+ Halftime: 10 min.

^{16}O (γ, n) ^{15}O
Radiation: ß+ Halftime: 2.06 min.

Isotopes created in head after (*Orton et al.*) on Table 2:

O. Dössel and W.C. Schlegel (Eds.): WC 2009, IFMBE Proceedings 25/III, pp. 664–666, 2009.
www.springerlink.com

Table 2.

4 Radionuclides produced in medical accelerators

Reaction	Mode of decay	Half-life	Photon energy (MeV)
$^{27}Al(n,\gamma)^{28}Al$	β-	2.3 min	1.780
$^{63}Cu(\gamma,n)^{62}Cu$	β+	9.7 min	0.511
$^{55}Mn(n,\gamma)^{56}Mn$	β-	2.6 hr	0.847
$^{63}Cu(n,\gamma)^{64}Cu$	β+/β-	12.7 hr	1.346
$^{65}Cu(\gamma,n)^{64}Cu$	β+/β-	12.7 hr	1.346
$^{186}W(n,\gamma)^{187}W$	β-	23.9 hr	0.479/0.686
$^{58}Ni(\gamma,n)^{57}Ni$	β+	36.0 hr	1.378/1.920

II.MEASUREMENTS

- Residual dose output and cumulative dose mesurements were done in the isocentre of LINAC Type Philips (Elekta) SLI Plus after it was in use. (After running of 1000, 1500, 2500 Monitor Units) The measurements were made with mobile Geiger-Mueller counters and ionic chamber detectors.

Dose-dependence on treatment dose (Monitor Units) and time were measured. Residual dose output dependence on time were measured after terminating treatment radiation. Dose and dose output of residual radiation are figured on Fig.1.

Fig. 1.

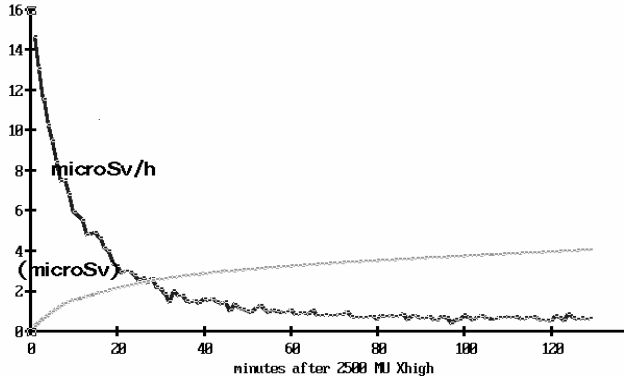

Low-resolution (50 channels in O-3 MeV range) gamma-spectrometry were made to identify some isotopes created by activation in the LINAC . Measuring unit was simple mobile solid state scintillation detector with crystal of NaJ(Tl) . (Resolution on ^{137}Cs 667 KeV photopeak is about 10%) On Fig.2, time is going from upper spectrum on to downstairs. Normal background spectrum below.

Fig.2

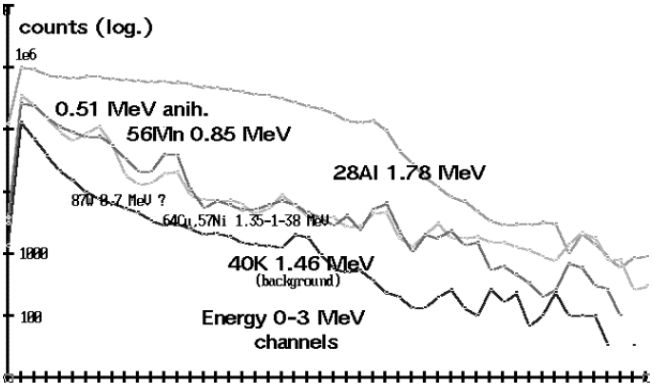

Special measurements were done to identify gaseous components. Air in plastic bag was irradiated and removed from the treatment room and measured with inplugged detector. Anihilation peak was found (Fig.3) the time dependence of which was measured

Fig.3

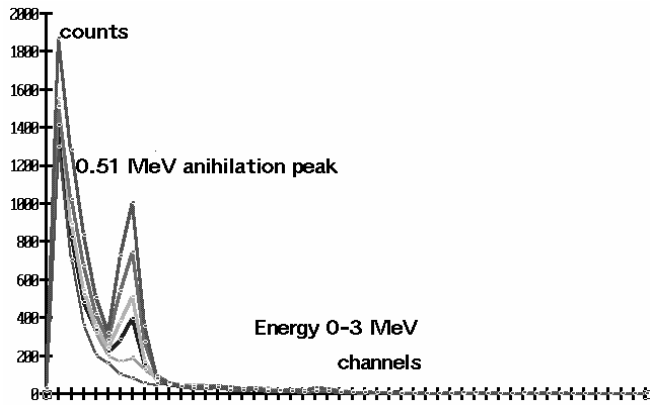

The peak areas depending on time are shown on Fig. 4.

Fig. 4

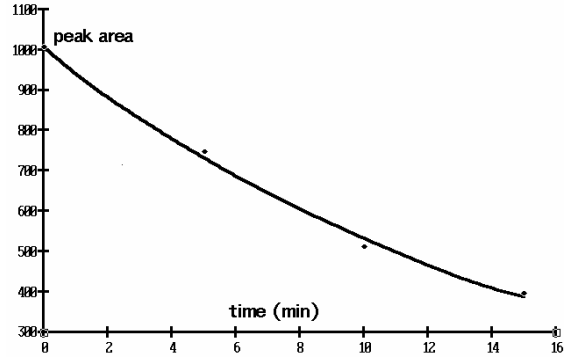

- Basic dose assessment were made for technical and medical staff.

III. RESULTS

The decay curve of residual radiation is very difficult :first half-time of residual radiation is about 7 minutes, second half-time is about 18.5 minutes and third half-time is about 50 minutes. Cumulative dose of the residual radiation in the isocentre is about 3.95 microGray after 2500 Monitor Units beam when we measured to 2 hours continuosly. 5 nuclides identified in spectra, and ^{13}N in the air with decay time. Health care people do their job near to the isocentre, so assuming a linear function between Monitor Units and residual radiation dose the cumulative added dose for health care staff should be appr. 2-5 mSv/year from extemal gamma component calculating with normal patient care. Physicists and servicemen who has to reach into unit should be exposed much more.and locally. .Investigation on personal dose from gaseous component is not ready yet. The radiation safety problem on LINAC residual radiation has to be followed with attention.

REFERENCE

Orton,C. :Photoneutrons AAPM/IOMP Course Book „The Physics of Radiation Therapy" June 10-14, 1999, Romania

Measurement of Orthovoltage X-Ray Intensity with a Lithium Niobate Transducer

Wesley Pontes[1], Aparecido Augusto de Carvalho[1], Marcelo Augusto Assunção Sanches[1], Ricardo Luiz Barros de Freitas[1], Mauro Henrique de Paula[2], and Walter Katsumi Sakamoto[3]

[1] Department of Electrical Engineering, São Paulo State University - UNESP, Ilha Solteira, SP 15385-000, Brazil.
[2] Physics Department of Federal University of Mato Grosso do Sul, Campo Grande, MS 79070-900, Brazil.
[3] Depto. Physics and Chemistry, São Paulo State University – UNESP, Ilha Solteira, SP 15385-000, Brazil.

Abstract — **A microcontrolled instrument for measuring the energy fluence rate (or intensity) of X-ray pulses in the orthovoltage range of 120 to 300 kV is described. The prototype instrument consists of a pyroelectric sensor, a low-noise high-sensitivity current-to-voltage converter, a microcontroller and a digital display. The response of the instrument is nonlinear with the intensity of the radiation. The precision is better than 3%. The equipment is inexpensive, rugged, simple to construct and has good long-term stability.**

Keywords — **pyroelectric sensor, x-ray intensity, orthovoltage range, energy fluence rate, microcontrolled instrument.**

I. Introduction

Kilovoltage (40-300 kV) X-ray beams have been used in radiation therapy and radiobiology. This energy range is normally divided into two regions of clinical and radiobiological interest: a) low energy (or superficial) X-rays, generated at tube potentials lower than or equal to 100 kV; b) medium energy (or orthovoltage) X-rays, generated at tube potentials higher than 100 kV.

The orthovoltage X-rays equipment is used in cancer treatment radiotherapy when the lesion of interest is at a depth not exceeding 3 cm. The effectiveness of radiation on tissues depends on the delivery of an adequate dose to the entire volume of the tumor without causing severe damage to surrounding normal tissues. The most important method for dosimetry of low and medium energy X-rays for radiotherapy and radiobiology is based on ionization chambers calibrated in air in terms of air kerma [1]. Although regulations and requirements have enabled the use of radiation relatively safe, there are some risks for patients. An alternative measure of risk is energy imparted which is expressed in joule and is independent of spectrum. However, to calculate energy imparted, it is necessary to measure the energy fluence (Jm^{-2}) of the X-ray beam. Except for the calorimetry, which is not practical in the clinical setting, all current methods for measuring X-ray depend on ionization or physiochemical reaction, which have a spectral dependence. De Paula *et al.* described a dosimeter made of pyroelectric material that can measure the intensity of X-ray in the medical diagnostic range [2]. In a pyroelectric material the polarization P depends on the temperature T. The pyroelectric coefficient p is dP/dT at a particular temperature T. Basically, a pyroelectric sensor consists of a pyroelectric thin wafer with metal electrodes on opposite faces. Often, the material is oriented such that its polar axis is perpendicular to the electrode faces. When the sensor is heated by incident radiation the polarization change depends on both the temperature change and the pyroelectric coefficient of the material. The change in polarization appears as a charge on the capacitor formed by the pyroelectric material and the two electrodes. Pyroelectric sensors have been used for measuring nonionizing radiation as infrared [3] and microwave [4], and various forms of ionizing radiation [5,6].

Results have suggested that pyroelectric sensors may be useful for measuring X-ray intensity in the medical diagnostic range [7] and in mammography [8,9].

In this paper we demonstrate a novel and simple instrument can be used to measure energy fluence rate or intensity of X-rays in the orthovoltage range of 120 to 300 kV. The key element of the instrument is a pyroelectric sensor.

II. Materials and Methods

The prototype instrument consists of a pyroelectric sensor, a low-noise, high-sensitivity current-to-voltage converter, a microcontroller, and a digital display. Figure 1 shows the block diagram of the instrument.

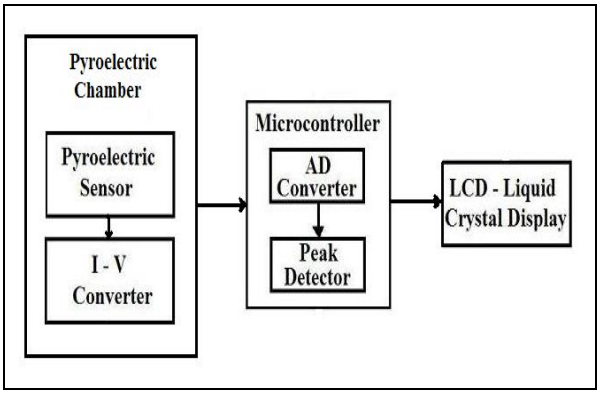

Fig. 1 Block diagram of the instrument

O. Dössel and W.C. Schlegel (Eds.): WC 2009, IFMBE Proceedings 25/III, pp. 667–670, 2009.
www.springerlink.com

The pyroelectric sensor is a Lithium Niobate ($LiNbO_3$), ceramic (10 mm x 10 mm and 1 mm thick). The sensor was placed inside an aluminum enclosure (pyroelectric chamber). In order to minimize noise from external sources the current-to-voltage converter was placed inside the aluminum enclosure. The operational amplifier OPA 111 (Burr-Brown) is the main component of the high-sensitivity converter. For this kind of application it has good characteristics, such as very high input impedance (10^{14} Ω// 3 pF), very low input bias (0.8 pA) and offset currents (0.5 pA). To protect the electronic circuit against the radiation, it was placed inside a compartment in the piroelectric chamber that was shielded with an alloy (cerobend 70), composed of 50% of bismuth, 27% of lead, 13% of tin, and 10 % of calcium, 7 mm thick. Photographs of the pyroelectric chamber are shown in Figures 2a and 2b.

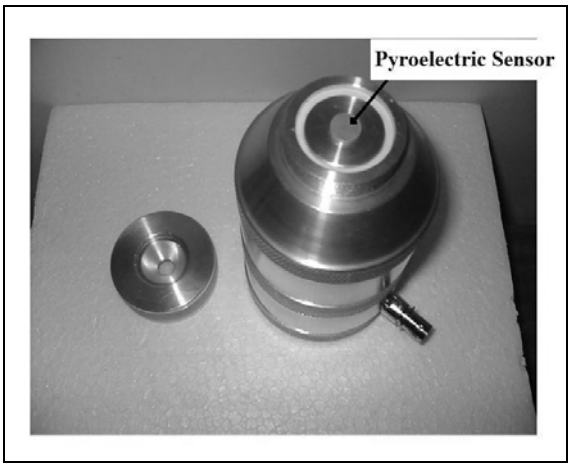

Fig. 2a Pyroelectric chamber

Fig. 2b Pyroelectric chamber shielded with an alloy

The signals in the output of the converter are noise filtered and then fed into the microcontroller acquisition section. The microcontroller (PIC 16F777, Microship) was used to execute measurement software and send results to a digital display by its digital output port. A photograph of the instrument is shown in Figure 3.

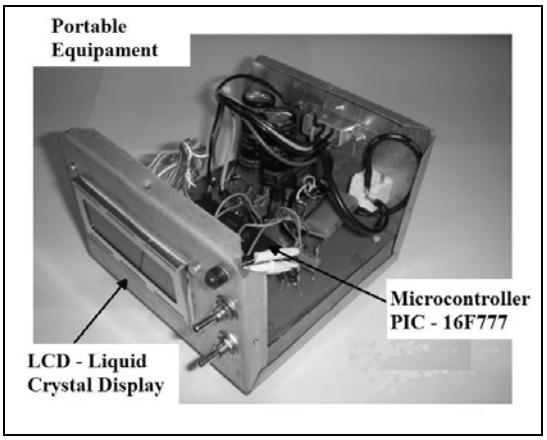

Fig. 3 Pyroelectric equipment

The irradiations were carried out using an orthovoltage X-ray equipment (Siemens Stabilipan II) at the Federal University of Mato Grosso do Sul, in Campo Grande-MS. The peak tube potential varied from 120 to 300 kV. For each tube potential there is a fixed current that ranges from 20 to 12 mA. Aluminum and copper filters were used, resulting in equivalent photon energies of the beam between 34.7 and 178.2 keV. Equivalent photon energy of the beam was determined from its measured half-value layer. The distance from the tube target (X-ray source) to the pyroelectric sensor was 50 cm, which is used in patients during the treatment. The exposure rate of radiation was measured with a calibrated 0.6 cm^3 cylindrical ionization chamber, connected to a FARMER electrometer, model 2570, designed for clinical use in the orthovoltage range. Intensity of the beam was calculated from the measured X-ray exposure rate and equivalent photon energy of the beam [10]. We measured with an ionization chamber the percentage of the incident radiation absorbed by the pyroelectric sensor for each energy produced by the orthovoltage equipment. The beam was collimated and the ionization chamber was placed behind the sensor.

Some tests were carried out to investigate radiation-induced degradation of the sensor. The piezoelectric constant d_{33} was measured with a piezo tester (Model 8000, Pennebaker, American Piezo Ceramics, USA) interfaced with a digital multimeter (Micronta) before and after the sensor had been subjected to about 0.2 C/kg (760 Roentgens) of radiation in the orthovoltage energy range.

III. Results

Table 1 shows the percentage of the incident radiation absorbed by the pyroelectric sensor at different tube potentials (kV). The pulses at the current-to-voltage converter output were recorded with an oscilloscope (Tektronix, model 3012). The precision was better than 2% when the measurements of the amplitude of the pyroelectric signal were made with the oscilloscope and better than 3% when made with the circuit microcontroller-display.

Table 1 Percentage of incident radiation absorbed by the pyroelectric sensor

Tube Potential (kV)	Tube Current (mA)	Percentage of absorption (%)
120	20	95.8
180	20	91.7
200	20	86.7
250	15	75.8
300	12	60.3

The response of the instrument with the radiation energy fluence rate is shown in Figure 4.

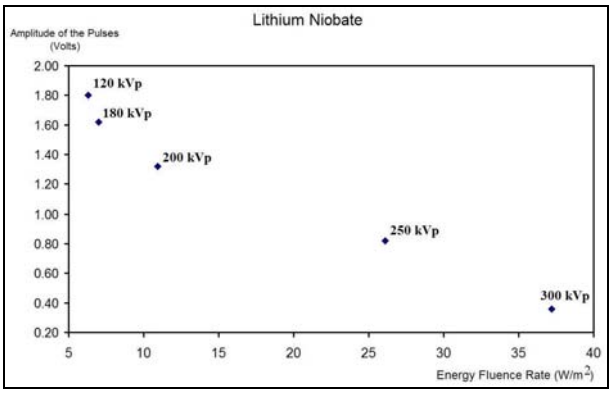

Fig. 4 Amplitude of the pulses versus radiation energy fluence rate

The relationship between the amplitude of the pulses (S in volt), at the current-to-voltage converter output, and the energy fluence rate (ψ in W/m^2) of the X-ray pulse is nonlinear. The equation

$$S = 1.8e^{-0.037\psi} \text{ (volts)} \quad (1)$$

provides a good fit to the data.

The maximum noise measured at the instrument's output was 90 mV. Assuming that a signal-to-noise ratio of at least five is necessary to make the measurements, the minimum intensity the instrument can measure is 0.77 W/m^2 at 120 kVp.

The value of the piezoelectric constant d_{33} (63 pC/N) remained the same before and after the sensor received a high dose (0.2 C/kg) of irradiation.

The long-term stability of the instrument is good. The difference between measurements performed with the interval of one month was lower than 3%.

IV. Discussion

Although the relationship between the sensor response and the energy fluency rate is nonlinear, there is no double value of voltage for different energy fluence rates, indicating that the instrument can be used for measuring intensity in the orthovoltage range.

V. Conclusion

A pyroelectric instrument was implemented for measuring x-ray intensity in the orthovoltage range of 120 to 300 kV. Its response is nonlinear with the energy fluence rate. This is not a problem because the instrument calibration curve can be stored in the microcontroller memory. The precision of the instrument is better than 3%. When an oscilloscope was used for measuring the pyroelectric signal amplitude the precision was better than 2%. Considering a signal noise ratio of five, the minimum energy fluency rate the instrument can measure is 0.77 W/m^2 at 120 kV. The piezoelectric coefficient d_{33} remained the same after the sensor received a high exposure (0.2 c/kg of radiation, indicating that the piezoelectric properties of the sensor did not change. The instrument can be useful in monitoring the radiation output of orthovoltage X-ray units.

Acknowledgment

To FAPESP, CNPq, and CAPES which gave financial support to accomplish this project. The authors would like to thank professors Thomaz Ghiladi Netto (University of São Paulo, Ribeirão Preto), Walter Katsumi Sakamoto, and José Antonio Malmonge (São Paulo State University, Ilha Solteira) for many helpful suggestions.

References

1. Ma, C.M., Coffey, C.W., DeWerd, L.A., LIU, C., Nath, R., Setzer, S.M., and Seuntjens, J. P.: *'AAPM protocol for 40-300 kV x-ray beam dosimetry in radiotherapy and radiobiology'*, Med. Phys., 2001, 28, (6), pp. 868-893.
2. De Paula, M.H., Carvalho, A.A., Mascarenhas, S., and Zimmerman, R.L.: *'A new radiation dosimeter using a pyroelectric detector'*, Med. Phys., 1984, 11, (6), pp. 866-868.
3. Shaulov, A., and Simhony, M.: *'Pyroelectric voltage response to rectangular infrared signals in triglycine sulphate and strontium-barium niobate'*, J. Appl. Phys., 1972, 43, (4), pp. 1440-1444.
4. White, D.J., and Wieder, H.H.: *'Microwave-induced pyroelectric response in ferroelectric TGS'*, J . Appl. Phys., 1963, 34, (8), pp. 2487-2488.
5. Cruvinel, P.E., Mascarenhas, S., Miranda, J., and Flocchini, R.G.: *'The use of a perovskite crystal as a detector for proton beam current'*, IEEE Trans. Nucl. Sci., 1992, 39, (1), pp. 25-2.
6. Crestana, S.B., Mascarenhas, S., Geraldo, L.P., and Carvalho, A.A.: *'A new technique for thermal neutron detection using pyroelectric ceramics'*, Nucl. Instrum. Methods Physics Res., 1992, A311, pp. 558-562.
7. De Carvalho, A.A., and Alter, A.J.: *'Measurement of X-ray Intensity in Medical Diagnostic Range by a Ferroelectric Detector'*, IEEE Trans. Ultrason., Ferroelect., Freq. Contr., 1997, 44, (6), pp. 1198-1203.
8. De Carvalho, A.A., Brassalotti, A.L., De Paula, M.H., and Alter, A.J.: *'Use of a lithium niobate detector for measuring X-ray intensity in mammographic range'*, Electron. Lett., 2004, 40, (18), pp. 1097-1098.
9. De Paula, M.H., De Carvalho, A.A., Brassalotti, A.L., Alter, A.J., Sakamoto, W.K., Malmonge, J.A., and Almeida, A.: *'Microcontrolled pyro-electric instrument for measuring X-ray intensity in mammography'*, Med. Biol. Eng. Comp., 2005, 43, (6), pp. 751-755.
10. Johns, H.E., and Cunningham, J.R.: *'The Physics of Radiology'* (Charles C. Thomas, Springfield, IL, 1983).

Address of the corresponding author:

Author: Aparecido Augusto de Carvalho
Institute: Department of Electrical Engineering - São Paulo State University – UNESP.
Street: Avenida Brasil, 56.
City: Ilha Solteira.
Country: Brazil.
Email: carvalho.aparecido@gmail.com

SURVEY OF IMAGE QUALITY AND RADIOGRAPHIC TECHNIQUE OF PEDIATRIC CHEST EXAMINATIONS PERFORMED IN BRAZIL

Helen J. Khoury[1], Vinícios Saito de Barros[1],Hugo R. Schelin[2], Lorena E. Porto[2], Simone Kodlulovich[3], Ana Cecília Azevedo[4], Regina Bitelli Medeiros[5]

[1] Laboratório de Metrologia e Radiações Ionizantes – DEN/UFPE – Recife, Brazil
[2] Programa de Pós-Graduação em Engenharia Biomédica e Informática Industrial – CPGEI/UTFPR - Curitiba, Brazil
[3] Instituto de Radioproteção e Dosimetria – IRD/CNEN – Rio de Janeiro, Brazil
[4] Escola Nacional de Saúde Pública – CESTEH/FIOCRUZ – Rio de Janeiro, Brazil
[5] Departamento de Diagnóstico por Imagem – UNIFESP – São Paulo, Brazil

Abstract – **This work presents the results of a survey of Entrance Surface Air Kerma (Ke) values, image quality and radiographic exposure parameters used in pediatric chest examinations performed in Brazil. The study is part of the activities of the IAEA Regional Project RLA/9/057 whose objective is to optimize the radiological protection of patients in diagnostic and interventional radiology, nuclear medicine and radiotherapy. The survey was performed in four hospitals in Brazil. The study group consisted of 420 pediatric patients from two age groups (Group I- from two days to one year, Group II- from four to six years of age) undergoing chest PA/AP examinations. At the time of the examination the exposure parameters (kVp, mAs, focal-spot-to-film distance, etc.) and patient information (gender, height, weight and age) were recorded. The radiographic image quality was evaluated by the local radiologist based on the European Guidelines on Quality Criteria for Diagnostic Radiographic Images in Pediatrics. The results showed that the exposure parameters used on newborn patients were in the majority outside the 60-65kV range recommended by the European Guidelines for a good radiographic practice. In the case of examinations of patients with age between 4 and 6 years, 80% were performed with a peak tube voltage within the 60-80 kV range, as recommended by the European Guidelines. The K_e values, for both patient groups showed a wide dispersion, ranging from 30.7 µGy to 163.8 µGy for the newborn patients and from 34.5 µGy to 236.6 µGy for infant patients. It is possible to conclude that, in the Brazilian hospitals participating in this project, the radiographic techniques of pediatric chest images and the radiation protection need to be optimized.**

Keywords **– pediatric radiology, quality image, radiation protection**

I. INTRODUCTION

There is a growing concern about the amount of absorbed dose by patients submitted to radiographic examinations[1-3]. This concern is greater in the case of children who have a longer life expectancy than adults and are more sensitive to ionizing radiation[4]. For radiodiagnostic purposes, the image obtained must have the largest amount of information and should be obtained with the lowest possible dose. In general the number of pediatric patients in the radiology department is lesser than of adults, and therefore the x-ray equipment is not dedicated just to pediatrics. Consequently the equipment is not optimized for this purpose. The monitoring and control of the received doses using dosimeters[5] or other techniques are a form to detect possible failures in the radiographic procedure. The purpose of the present work is to estimate the Entrance Surface Air Kerma (K_e) of chest x-ray pediatric examinations performed in AP/PA projections in four hospitals in Brazil (two in Rio de Janeiro, one in Curitiba and one in Recife).

II. METHODOLOGY

This study restricted the age of the patients to newborn (up to 30 days old) and children with age groups between 4 and 6 years old. The morphologic-medical data of the patients and the radiological techniques were collected in the occasion of each exam. For each patient a table was elaborated, in which we wrote down the patient´s data (identification code, gender, PA thickness, weight and height), the exposure parameters used (kV, mAs, focal-film distance and total filtration) and characteristics of the radiographic equipment and of the image receiving system.

The Entrance Surface Air Kerma (K_e) was estimated using the following equation 1:

$$K_e(kV) = Y_{exam}.Q_{exam}.\left(\frac{1}{FSD}\right)^2.BSF \quad (1)$$

where:

Y_{exam} is the output of the x-ray tube in $mGy.mAs^{-1}$, at 1 m distance from the focal-spot, for the kVp value used in examination. This value was obtained by the interpolation from the curve of the output of the x-ray tube versus the voltage. The output was previously measured with a calibrated ionization chamber, placed at 100 cm from the x-ray focus and at 25 cm from the table top, in order to prevent inaccurate readings caused by backscattering.

Q_{exam} is the product of the current, in mA, and the exposure time, in *s*, used in the examination.

FFD is the focal-spot to film distance, in *m*.

BSF is the backscatter factor. The value 1.35 was adopted for all patients.

Quality assurance tests were performed in all x-ray equipments. The tests included kVp, exposure time accuracy and reproducibility, HVL and exposure current-rime product (mAs) linearity. The image quality was also verified and the K_e values corresponding to the images that fulfilled at least 80%

O. Dössel and W.C. Schlegel (Eds.): WC 2009, IFMBE Proceedings 25/III, pp. 671–674, 2009.
www.springerlink.com

of the ECC (European Community Commission) were used to estimate the value of the reference dose. The image quality was evaluated based on the European Guidelines Criteria for Diagnostic Radiographic Images in Pediatrics[6]. Tables 1 and 2 present a list with the image Quality Criteria for diagnostic examinations of chest PA/AP projection for pediatric patients.

Table 1- Quality Criteria for diagnostic images in chest PA/AP projection for newborn patients[7].

Item	Image Criteria
1	Performed at peak of inspiration
2	Reproduction of the thorax without rotation and tilting
3	Reproduction of the chest must extend from cervical trachea to T12/L1
4	Reproduction of vascular pattern in central half of lungs
5	Visually sharp reproduction of the trachea and proximal bronchi
6	Visually sharp reproduction of the diaphragm and costo-phrenic angles
7	Reproduction of the spine and paraspinal structures
8	Visualization of the retrocardiac lung and the mediastinum

Table 2- Quality Criteria for diagnostic images in chest PA/AP projection for pediatric patients, beyond the newborn period[7].

Item	Image Criteria
1	Performed at peak of inspiration, except for suspected foreign body aspiration
2	Reproduction of the thorax without rotation and tilting
3	Reproduction of the chest must extend from cervical trachea to T12/L1
4	Reproduction of vascular pattern in central 2/3 of the lungs
5	Visually sharp reproduction of the trachea and proximal bronchi
6	Visually sharp reproduction of the diaphragm and costo-phrenic angles
7	Reproduction of the spine and paraspinal structures
8	Visualization of the retrocardiac lung and the mediastinum

III. RESULTS AND DISCUSSION

For the age range studied, the K_e was calculated through the exposition parameters. Height, weight, thickness, kVp, mAs, focal-table and focal film distance were used. The exposure parameters used for chest examinations in AP/PA projections and their average values are shown in Table 3. This table shows the large variation in the exposure parameters in the same intervals.

Table 3- Average, minimum and maximum values of the exposure parameters used by the institutions in Brazil for chest x-ray examination in PA/AP projection for newborn and 4-6 years old patients.

Hospital	Patient Group I Newborn			Patient Group II 4-6 years old		
	Tube potential (kV)	Current time product (mAs)	FFD (cm)	Tube potential (kV)	Current time product (mAs)	FFD* (cm)
A	46.9 (40-55)	1.86 (1.6-2.5)	83,6 (50-110)	60 (40-72)	2.1 (1.5-6.4)	153.5 (95-192)
B	72.3 (66-77)	1.9 (1.6-2.5)	111 (110-115)	77.9 (70-85)	2.1 (1.5-6.4)	140 (110-200)
C	57 (53,5-63)	1.3 (1.25-1.6)	118.0 (110-120)	61 (53-81)	1.63 (1.25-1.8)	150.0 (110-190)
D	69.7 (56-77)	2.5 (1.6-2.5)	110.0 (107-116)	76 (73-81)	2.2 (1.6-3.2)	138.0 (110-180)

Figure 1 shows the Entrance Surface Air Kerma (K_e) obtained in each institution for the chest AP/PA radiographic examinations of patients in the age group 0-1 year. The data shows that the K_e values of the in institution C show less variation when compared with the other institutions. This possibly occurs because of the small fluctuation in the value of the high voltage (kV) used by this institution. Table 2 shows the percentages that fulfill the criteria of quality of image from the European Community[7]. It is observed that criterion 2 (reproduction of the thorax without rotation or tilting) is the one that presents less fulfillment. This is probably due to errors in the positioning of the patient and also because patient immobilization devices were not used.

Figure 2 shows the Entrance Surface Air Kerma (K_e) obtained in each institution for the chest AP/PA radiographic examinations of patients in the

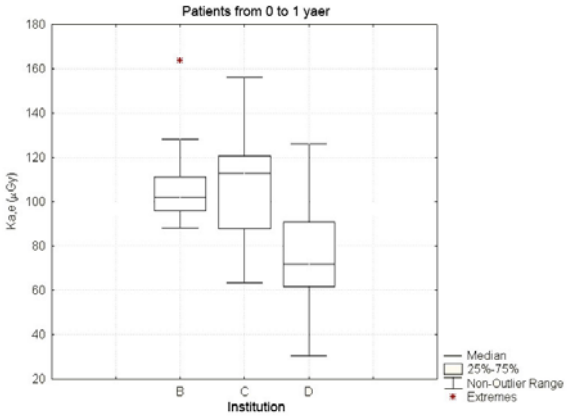

Figure 1 – Distribution of the Entrance Surface Air Kerma (K_e) for chest examinations for each institution for chest examinations in AP projections with age group from 0 to 1 year old.

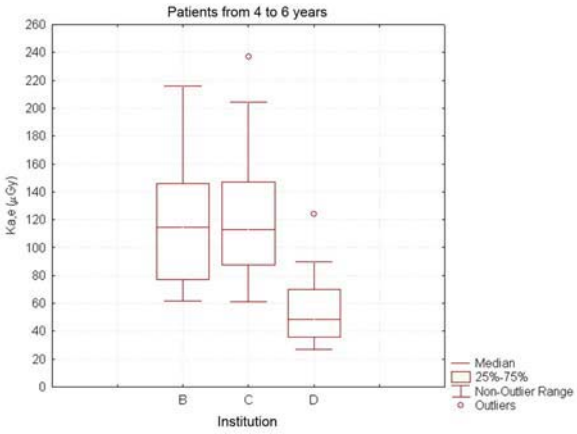

Figure 2 – Distribution of the Entrance Surface Air Kerma (K_e) for chest examinations for each institution for chest examinations in AP projections with age group from 4 to 6 years old.

age group 4-6 years. The data show that the K_e values of the in institution D are lower than the one obtained by the other institutions.

Table 4 shows the result in percentage of the image quality established by the CEC Guidelines for chest AP/PA radiographs. The number presented reflects the percentage of criteria attended in each radiographic image. It was not possible to evaluate the image quality in all the institutions due to the poor involvement of the radiologists working in each radiology department.

Table 4 – Percentage of images in each institution that attend each of the criteria of the CEC for chest examinations.

	Quality Criteria	Institution		
		B	C	D
Group I newborn	1	96%	76%	80%
	2	64%	88%	48%
	3	88%	96%	72%
	4	80%	100%	84%
	5	96%	100%	88%
	6	96%	100%	88%
	7	100%	100%	84%
	8	100%	100%	84%
Group II 4-6 years	1	80%	56%	76%
	2	88%	84%	60%
	3	72%	88%	63%
	4	88%	100%	88%
	5	92%	92%	88%
	6	96%	100%	96%
	7	88%	92%	88%
	8	100%	88%	84%

The Entrance Surface Air Kerma is closely connected to the image quality. Even if the value of the K_e is low, it is essential to observed that the image quality is in accordance with the standards established by the CEC. The ideal is that the K_e is inside the limits with the best image quality possible in order that the information for the ideal diagnosis will not be lost. Tables 5 and 6 show the relations between the percentages found in each institution for the quality criteria and the K_e given in µGy. Their values are given in the maximum, minimum and average value.

Table 5 – Percentage of the images that reached the quality criteria in relation to the K_e for patients with age group of 0 to 1 year.

Institution	Percentage of images with ≥ 80% of the quality criteria fulfilled	Entrance Surface Air Kerma (µGy)		
		Min	Average	Max
B	84%	88.3	107.8	163.8
C	92%	63.3	109.6	154.0
D	48%	30.7	71.1	126.0

The data shows that institution D has the lowest percentage of images that fulfill the CEC criteria and also presented low dose values, indicating that the procedure was not optimized. Considering the values of K_e of the three institutions, an average value

of 101.0 μGy is obtained, and a corresponding value of 75% of the distribution that is 92.9 μGy, that is larger than the established value of 80 μGy for AP chest image for newborn patients.

Table 6 – Percentage of the images that reached the quality criteria in relation to the K_e for patients with age group of 4 to 6 years.

Institution	Percentage of images with ≥ 80% of the quality criteria fulfilled	Entrance Surface Air Kerma (μGy)		
		Min	Average	Max
B	76%	79.5	115.5	236.6
C	72%	61.0	116.6	216.0
D	52%	34.5	55.5	123.9

The data shows that institution D has the lowest percentage of images that fulfill the CEC criteria and also presented low dose values, indicating that the procedure was not optimized. Considering the values of K_e of the three institutions an average value of 100.3 μGy is obtained, and a corresponding value of 75% of the distribution that is 123.9 μGy, that is larger than the established value of 100.3 μGy. This value is larger than the reference value from the CEC for age groups between 4 and 6 years that is 100 μGy.

IV. CONCLUSION

This study has demonstrated the large variation of the exposure parameters used in hospitals in Brazil, indicating that there are no protocols to perform pediatric x-ray examinations. The use of anti-scattering grids contribute for the high value of the Entrance Surface Air Kerma observed, indicating that the procedures are not optimized and that there is an urgent necessity to reduce the dose in pediatric patients. For newborn patients a revision of the examination procedures is necessary in order to reduce the high values of Entrance Surface Air Kerma, without affecting the quality of the image.

V. ACKNOWLEGEMENTS

The authors would like to thank the staff of all hospitals participating in this study and the IAEA for the financial support.

VI. REFERENCES

1. Azevedo, A C P, Mohammedan, K E M, Rosa, L, A R, Grebe, M R N, Bobcat, M C B. *Dose measurements Using Thermoluminescent Dosimeters and Dose Cal Software at Two Pediatric Hospitals in Rio de Janeiro*. Applied Radiation and Isotopes 59, April 2003.
2. Mohamadain, K E M, Rosa, L, A R, Azevedo, A C P, Guebel, M R N, Boechat, M C B, Habani, F. *Dose Evaluation for Paediatric Chest X-Ray Examinations in Brazil and Sudan: Low Doses and Reliable Examinations Can Be Achieved in Developing Countries*. Physics in Medicine and Biology, 49 March 2004 – UK.
3. Montgomery, A, Martin, C, J. *A Study of the Application of Paediatric Reference Levels.* The British Journal of Radiology 73 (2000) 1083-1090.
4. NRPB – National Radiological Protection Board Occupational Public and Medical Exposure. Documents of NRPB, vol 4, N° 2 - 1993 UK National Radiological Protection Board, Chilton.
5. NRPB 1992, Institute of Physical Science in Medicine and Dosimetry. *Working Party National Protocol for Dose Measurements in Diagnostic Radiology*. IPS, New York.
6. European Commission. *European Guidelines on Quality Criteria for Diagnostic Radiographic Images in Paediatrics*. Brussels, Luxemburg. 1996
7. Sociedad Española de Física Médica – *Protocol Español de control de cualidad em radioagnóstico* – SEFM-SEPR, 1993.
8. NRPB 1999 *Guidelines on Patient Dose to Promote the Optimization of Protection for Diagnostic Medical Exposures* vol 10 (UK) p 1.
9. Oliveira, ALR; Lunelli, N; Schelin, HR; Tilly, J; Rogacheski, E; Khoury, HJ; Paschuk, S; Soboll, D; Azevedo, AC. *Avaliação de dose de entrada na pele em pacientes pediátricos através de medidas dosimétricas*. XII Congresso Brasileiro de Física Médica. Junho 2007.

Effect of Different Ultrasonic Duty cycle and Exposure Duration on the Amyloid-β 25-35 Induced PC-12 Apoptosis

Chun-Yi Chiu, Show-Huie Chen, and Shyh-Hau Wang

Department of Biomedical Engineering, Chung Yuan Christian University, Chung Li, Taiwan

Abstract—**Amyloid-β (Aβ) was showed to be able to induce the apoptosis of neuronal cells leading to the occurrence of Alzheimer's disease (AD). As those cells were stimulated by optical energy, the Aβ induced apoptosis was greatly inhibited. Hence, current study aims to further explore the effect of ultrasonic insonification on the neuronal cells. Experiments on PC-12 cells added with a 20 μM Aβ 25-35 to induce cellular apoptosis were performed. These cells were stimulated by 1MHz ultrasound of a fixed 150 mW/cm^2 $_{(SATA)}$ intensity associated respectively with different exposure durations from 1 to 10 minutes and duty cycles from 10 to 100%. The response of cells after acoustic stimulation for 24 and 48 hours was assessed via microscopic morphology and cell death measured by typical MTT assay. Results showed that the cell death was not significantly different corresponding to those cells with or without adding Aβ under ultrasonic stimulation. In accordance with 150mW/cm^2 ultrasound exposure of 20% duty cycle for 3 minutes, Aβ induced neuronal cells apoptosis was decreased. This study demonstrated that the effect of diminishing neuronal cells from apoptosis could be regulated by the insonation of appropriate ultrasonic doses.**

Keyword: **Ultrasound, PC-12, Amyloid-β, Duration, Duty cycle**

I. Introduction

Alzheimer's disease is a syndrome originated from the loss of neurons in a certain brain regions corresponding to the presence of such fibrillar deposits as the amyloid plaque and neurofibrillar tangle [1]. Amyloid-β is neurotoxic and was found able to induce the apoptosis of neuronal cells for the progress of AD [2-5]. It therefore is crucial to develop means to inhibit the Aβ induced apoptosis of neuronal cells for the treatment of AD. Presently, many studies to diminish the progress of the neurodegenerative disorder by either chemical [6-9] or physical treatments [10] have performed, in which most of these studies were carried out *in vitro*. Several chemicals, including protein kinase C [6], Zinc [7], Estrogen [8], and Lithium [9], have found experimentally capable of protecting neuronal cells from Aβ-induced apoptotic cell death. In addition to chemical treatments, the optical stimulation by light-emitting diode (LED) irradiation [10] was also verified able to decrease the Aβ 25-35 induced apoptosis of PC12 cells. Results demonstrated that a 0.9 W/m^2 intensity of LED irradiating on PC12 cells for 60 minutes was able to significantly diminish Aβ-induced apoptosis.

Ultrasound is a mechanical wave that has been applied to stimulate biological tissues and cultured cells [11-14]. Specifically, those ultrasonic stimulations with low intensities were found capable of regenerating neural tissues in a wound region [12]. On the other hand, those high intensity ultrasounds tend to suppress the proliferation of cancer cells [13] leading the effect of therapeutic low intensity ultrasound on cells and tissues to be owing to the non-thermal effect of ultrasound [15].

Recently, the effect of various low intensity ultrasounds on the Aβ-induced apoptosis of neuronal cells has explored [16]. The possibility that non-thermal effect of ultrasound might protect neurons against or slow down the pathogenesis of neurodegenerative disorders has not examined clearly. In this study, the addition of toxic protein Aβ 25-35 into PC-12 cells, a well characterized cellular model system commonly used for the study of neuronal apoptosis [17], adding Aβ before and after ultrasound exposure and two parameters ultrasound of low intensities 150 mW/cm^2 were employed to stimulate cells. The response of cells was measured with typical MTT assay to determine the percentile of neuron cell death for further evaluation.

II. Materials and methods

A. Cells Culture

The rat adrenal gland pheochromocytoma cell line (PC-12) was obtained from Bioresearch Collection and Research Center at Food Industry Research and Development Institute, Hsin Chu, Taiwan. The cells were cultured in a RPMI 1640 (GIBCO, BRL) culture medium supplemented with 5% heat-inactivated horse serum (GIBCO, BRL) and 10% fetal bovine serum (Biological Industries) at 37^{o}C in a humidified incubator containing 95% air and 5% CO_2. The medium was replaced regularly for every two days. For each experiment, PC-12 cells were rinsed with medium from the culture flasks and then were centrifuged. Subsequently, they were seeded in a 24-well culture plate (Corning, NY, USA) with the concentration of 5×10^4 cells/ml for all experiments.

B. Amyloid β-peptide 25-35

The powder of Amyloid β-peptide fragment 25-35 (AnaSpec, CA, USA) was dissolved in 1mL distilled water to prepare for a concentration of 1 mg/mL.

O. Dössel and W.C. Schlegel (Eds.): WC 2009, IFMBE Proceedings 25/III, pp. 675–678, 2009.
www.springerlink.com

C. Ultrasound Exposure

The PC-12 before or after adding with Aβ 25-35 for inducing cell death were exposed to low intensity ultrasound. The insonification condition includes the use of a 1MHz ultrasound of fixed 20% duty cycle and 150 mW/cm^2 in a period of 3minutes. Subsequently, PC-12 cells were sampled at 24 and 48 hours after that the ultrasound was exposed.

Further experiments were arranged to investigate the exposure duration and duty cycle effects on the Aβ 25-35 treated cells. After that Aβ 25-35 was added into the culture medium, the cells were brought onto the holder for ultrasound insonification. A 1 MHz nonfocused transducer was driven at 1 kHz pulse repetition frequency to generate a fixed ultrasound intensities of 150 mW/cm^2 (SATA). Different exposure durations and duty cycles were adjusted respectively to allow ranging from 1 to 10 minutes and 10 to 100%. The subsequent experiments were designated into four groups: cells without ultrasound exposure as the control group, cells only under ultrasound exposure, cells only added with Aβ 25-35, and cells with both Aβ 25-35 and ultrasound exposure. For each experiment, the control group of cells was also brought to the holder at the same time as those of PC-12 cells being stimulated acoustically to assure that the same experimental factors may be applied onto all experimental cells. The experimental arrangement for the exposure of ultrasound on the cultured cells is shown in Fig. 1, which includes a temperature controller to regulate the temperature of the distilled water in the distilled water tank and that an oscilloscope was used to monitor the output voltage of the ultrasonic generator simultaneously.

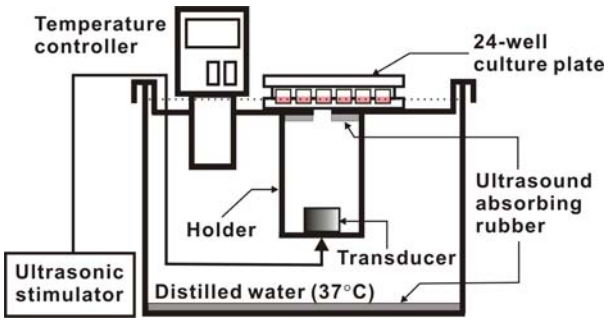

Fig.1. The experiments arrangement of stimulating cells by ultrasound.

Table 1, Parameters for ultrasound insonation with various exposure durations

Frequency, MHz	1
Duty cycle, %	20
Pulse repetition frequency, kHz	1
Aβ concentration, μM	20
Ultrasound intensity, mW/cm^2	150
Exposure duration, minute	1, 3, 5, and 10

TABLE 2, Parameters for ultrasound insonation with various duty cycles

Frequency, MHz	1
Duty cycle, %	10, 20, 50, and 100
Pulse repetition frequency, kHz	1
Aβ concentration, μM	20
Intensity mW/cm^2	150
Exposure duration, minute	1

The parameters for ultrasound exposure were summarized in Table 1 and 2. The cells of various groups were sampled at 24 and 48 hours after the ultrasound exposure.

D. Assessments of Cell Viability

MTT assay was used to evaluate the viability of PC-12 cells. It is based on the cleavage of the yellow tetrazolium salt MTT into purple formazan by metabolically active cells. The formazan crystals were soluble in DMSO (Sigma, St. Louis, MO, USA) solution. Each plate of sampled cells was added with a 100 μl of MTT of a 5 mg/ml concentration to incubate for four hours following the solubilization of the crystals. All procedures were isolated from light source. A total of four experiments was carried out with that each experiment contained three cell samples from different culture plates. The optical absorption of extracellular fluids was measured by the ELISA reader.

E. Data Analysis

Results were quantitatively assessed by the rate of cell death using the formula given as,

$$\text{Percentile of cell death (\%)} = \left(\frac{OD_0 - OD_n}{OD_0} \right) \times 100\%$$

where OD_0 and OD_n indicate respectively the optical densities of cells sampled at the beginning and a certain time of each experiment.

III. RESULTS

Results of different time point for adding Aβ 25-35 before or after ultrasound exposure on the Aβ-induced apoptosis were shown in Fig.2 (a). The percentile of neuron cells death was measured at 24 and 48 hours by MTT assay. Apoptotic cells were also evidenced by cell shrinkage, plasma membrane blebbing, chromatin condensation, and nuclear fragmentation. Before or after a 20 μM Aβ were added into PC-12 cells without ultrasound accordingly the significant increase of cell death, higher than about 55%, was found at both 24 and 48 hours in two different ultrasound treatments. On the other hand, the cell death remains almost unchanged corresponding to cells in the control group and only under ultrasound exposure.

Interestingly, there are no significant differences between adding Aβ before and after ultrasound exposure. But through longer incubated, the percentage of cell death at 48 hours is higher than those at 24 hours. As a result of these data, ultrasound exposure on cells after adding Aβ is ma de the criterion for following experiments.

The Aβ-induced apoptosis of PC-12 exposed to different ultrasound durations were sampled at 24 and 48 hours after ultrasound treatment using MTT assay. The frequency was fixed at 1MHz with 20% duty cycle, 150mW/cm^2 for 1, 3, 5 and 10 minutes. After only ultrasound exposure to PC-12 cells without any Aβ, the significant increase of cell viability, higher than about 25%, was found at 24 hours in the 3 min experiments. It is suggested that PC-12 exposed in this situation could induce cell proliferation. On the other hand, the percentage of cell death was reduced about 50% corresponding to cells in the Aβ group at 1 min groups after 24 hours. After 48 hours, cells treated by ultrasound for 3 and 5 min can be decreased about 60%, shown in Fig.2(b).

Results of different duty cycle on PC-12 after ultrasound exposure on the Aβ-induced apoptosis were shown in Fig.2(c). The frequency was fixed at 1MHz with 150mW/cm^2 intensity for 1 minutes using various duty cycle 10, 20, 50 and 100%, respectively. The percentile of neuron cells death was measured at 24 and 48 hours by MTT assay. After only ultrasound exposure to PC-12 cells without any Aβ, the cell death increase slightly, about 5-10%, found at both 24 and 48 hours in all experiments. It purpose that ultrasound might induce cell death or cell differentiation to result in diminish cell viability. PC-12 incubated with 20 μM Aβ were expose to different duty cycles ultrasound, the significant decrease of cell death, about 60%, compare with Aβ groups at 20% group at 24 hours after exposure.

In comparison with results, as cells were insonated by the 150 mW/cm^2 ultrasound at 1 MHz, the percentile of cell death tended to decrease at 1 minute with 20% duty cycle after 24 hours. In addition, only 1 MHz ultrasound exposed to PC-12 could enhance the cell proliferation.

Due to the time of ultrasound exposure is much shorter than that of a study with optical stimulation [9], those ambient factors affecting on the cultured cells were diminished. The temperature variation was within 1^{o}C in culture plate before and after ultrasound exposure indicating that viability changes of cells could be associated with the non-thermal effect of low intensity ultrasound [13]. The effect of ultrasound on cells could be due to the instantaneous variation of mechanical wave that varies the permeability of cell membrane for ions transportation.

IV. Discussion

A 1 MHz ultrasound of different exposure doses was applied to simulate PC-12 cells with and without cells are so predominant with the addition of Aβ similarly to previous reports [1,2]. The effect of low intensity ultrasound on PC-12 tends to be beneficial to diminish cell death. Specifically, results showed that stimulations by 1 minute and 20% duty cycle ultrasound may respectively diminish Aβ induced apoptosis compared with those of only Aβ treatment groups. Cell repair was slightly increased and cell viability was raised found by the MTT assay. This study suggested that the Aβ induced PC-12 cells apoptosis could be diminished with the insonation of an appropriate ultrasonic dose.

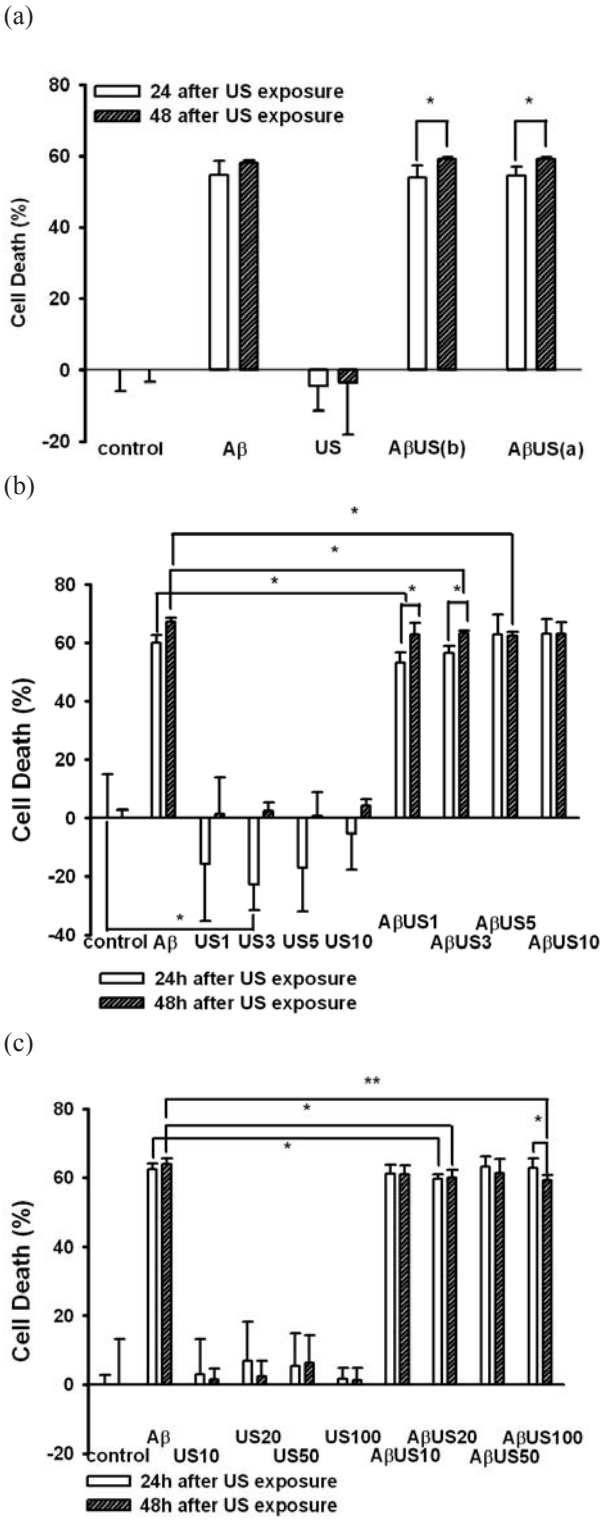

Fig. 2 Experiments on PC-12 cells exposed to Aβ and/or ultrasonic exposure. Cell death percentages were measured by MTT assay. Values represent the mean ± SD of three experiments. This study was performed 24 and 48 hours after exposure to 20 μM of Aβ. (a) cells with ultrasound exposure before and after adding Aβ;. (b) cells with ultrasound exposures of different ultrasound durations at 24 and 48 hours. (c) with ultrasound exposures of different ultrasound duty cycles at 24 and 48 hours. *: p<0.05; **: p<0.005; ***: p<0.001.

V. Conclusion

In this study, a 1 MHz ultrasound with different duty cycles and durations were applied to simulate PC-12 cells with and without adding with amyloid-β protein. The death of neuron cells are so predominant with the addition of Aβ similarly to previous reports [1,2]. The effect of low intensity ultrasound on PC-12 tends to be beneficial to diminish cell death. Specifically, results showed that stimulations by ultrasound with 20% duty cycle for 3 minutes insonation tend to diminish Aβ induced apoptosis compared with those of Aβ groups at 24 hours. This study suggested that the Aβ induced PC-12 cells apoptosis may be diminished with ultrasound insonifiation of different parameters.

Acknowledgements

This work was supported by the NSC of Taiwan of the grants: NSC 95-2221-E-033-003-MY3 and NSC 97-2627-M-033-003.

References

[1] Alzheimer A (1907) A characteristic disease of the cerebral cortex. Allgemeine Zeitschrift fur Psychiatria und Psychisch-Gerichtliche Medizin 44:146-148.
[2] Glenner G G, Wong C W (1984) Alzheimer's disease: initial report of the purification of a novel cerebrovasular amyloid protein. Biochem Biophys Res Commun 120:885-890.
[3] Cotman C W, Anderson A J (1995) A potential role for apoptosis in neurodegeneration and Alzheimer's disease. Mol Neurobiol 10:19-45
[4] Loo D T, A. Copani G, Pike C J et al. (1993) Apoptosis is induced by beta-amyloid in cultured central nervous system neurons. Proc Natl Acad Sci USA 90:7951-7955.
[5] Watt J A, Pike C J, Walencewicz-Wasserman A J et al. (1994) Ultrastructural analysis of β-amyloid-induced apoptosis in cultured hippocampal neurons. Brain Res 66:147-156.
[6] Ueda K, Yagami T, Kagayama H et al. (1996) Protein kinase inhibitor attenuates apoptotic cell death induced by amyloid β protein in culture of the rat cerebral cortex. Neurosci Lett 203:175-178.
[7] Lovell M A, Xie C, Markesbery W R (1999) Protection against amyloid beta peptide toxicity by zinc. Brain Res 823:88-95.
[8] Hosoda T, Nakajima H, Honjo H (2001) Estrogen protects neuronal cells from amyloid β-induced apoptotic cell death. Neuroreport 12: 1965-1970.
[9] Alvarez G, Munoz-Montano J R, Satrustegui J et al. (1999) Lithium protests cultured neurons against-amyloid-induced neurodegeneration. FEBS Lett 453:260-264.
[10] Duan R, Zhu L, Liu T C-Y et al. (2003) Light emitting diode irradiation protect against the amyloid beta 25-35 induced apoptosis of PC12 cell in vitro. Lasers Surg Med 33:199-203.
[11] Dyson M, Pond J B, Josep J h et al. (1968) The stimulation of tissue regeneration by means of ultrasound. Clin Sci 35:273-285.
[12] Crisci A R, Ferreira A L (2002) Low-intensity pulsed ultrasound accelerates the regeneration of the sciatic nerve after neurotomy in Rats. Ultrasound Med Biol 28:1335-1341.
[13] Takeuchi S, Watanabe T, Sato T et al. (2001) Basic study on the effect of ultrasound exposure upon suppression of cancer cell proliferation. IEEE Ultrasonics Symposium 1319-1322.
[14] Chiu C Y, Chen S H, Wang S H (2003) Effect of low intensity pulsed ultrasounds on the proliferation of fibroblast. 12th ICBME conf, Singapore, 2003.
[15] (1998) Other non-thermal bio-effects: Organs, Cells and Tissues. Ultrasound Med Biol 24:S35-S39.
[16] Chiu C Y, Chen S H, Wang S H et al. (2005) Effect of ultrasonic intensity on the Amyloid-beta induced apotosis of PC-12 cells. 2005 IEEE Int. Ultrasonics symposium, Rotterdam Netherlands, 2005.
[17] Pittman R N, Wang S W, Dibenedetto A J et al. (1993) A system for characterizing cellular and molecular events in programmed neuronal cell death. J Neurosci 13:3669-3680.

Author: Chun-Yi Chiu, Show-Huie Chen and Shyh-Hau Wang
Institute: Department of Biomedical Engineering, Chung Yuan Christian University
Street: 200 Chung Pei Rd.
City: Chung Li
Country: Taiwan
Email: shyhhau@cycu.edu.tw

Study of Entrance Surface Skin Dose in Veterinary Radiology

G.R. Veneziani[1], L.C. Matsushima[2], R.M. Fernandez[1], and L.L. Campos[2]

[1]Instituto de Biociências (IBB-UNESP), Botucatu, Brazil.
[2]Instituto de Pesquisas Energéticas e Nucleares (IPEN-CNEN), São Paulo, Brazil.

Abstract — **This study aims the evaluation of the radiation dose levels involved in veterinary radiology and to contribute to review the procedures for performing radiographic exams in animals in the Department of Veterinary Radiology of Faculdade de Medicina Veterinária e Zootecnia of Universidade Estadual Paulista (FMVZ-UNESP/Brazil). The obtained results has shown to be extremely important the assessment of doses involved in veterinary diagnostic radiology procedures both to protect the occupationally exposed workers and to optimize the delivered doses to the animals.**

Keywords— **absorbed dose, thermoluminescence dosimetry, veterinary radiology.**

I. INTRODUCTION

The human radioprotection is a very recent issue, which came almost with the discovery of X-rays by Roentgen in 1885. This concern relates a series of measures to protect the human being and their descendants against possible unwanted effects caused by ionizing radiation [(1)].

The International Commission on Radiological Protection (ICRP)'s current position regarding protection of the environment is set out in its Publication 60 (ICRP 1991) [(2)]. "*The Commission believes that the standards of environmental control needed to protect man to the degree currently thought desirable will ensure that other species are not put at risk*" [(2)]. This concept of deriving such data sets for reference fauna and flora is therefore similar to that of the reference individual (Reference Man) used for human radiological protection, in that it is intended to act as a basis for many calculations and decisions [(3)].

The basic guidelines for radiological protection in Brazil are regulated by Secretaria de Vigilância Sanitária - SVS by the Decree 453 of June 1st, 1998 [(4)] and for Comissão Nacional de Energia Nuclear - CNEN Norm NN-3.01 [(1)] in view the risks of use of ionizing radiation and the need to establish a national policy for radiological protection in the field of radiology. The basic principles governing the rules above are three: the justification of the practice, the optimization of radiological protection and the limitation of individual doses.

The principle of justification is the basic principle of Radiological Protection which states that any practice or source should be permitted unless it produces sufficient benefit to the exposed individuals or to society in order to offset the hazard that may be caused [(1,4)]. The principle of optimization requires that the facilities and practices involving the use of ionizing radiation should be planned, implemented and enforced so that the magnitude of individual doses, the number of people exposed and the likelihood of accidental exposures are as low as reasonably achievable ALARA ("*as low as reasonable achievable"*) [(1,4)]. Finally the principle of limitation provides that the limits for individual doses are values of effective dose or dose equivalent, set for occupational exposure and exposure from the public practice audited, whose magnitude should not be exceeded [(1,4)].

The majority of our information on the exposure and effects of radiation relates to, and has been obtained to serve the needs of, the radiological protection of human beings. Similarly, much of our information on the behavior, effects, and distribution of man-made radionuclides in the environment has also been derived to meet the needs of human radiological protection [(3)].

It is necessary that a system for radiological protection of non-human organisms be harmonized with the principles for the radiological protection for humans [(3)]. This work used the rules and regulations involved with the concepts of radiological protection specified for the man together the techniques of termoluminescence dosimetry to evaluate the risks incurred by the animals subjected to X-rays exams to check for pulmonary metastasis.

II - MATERIALS AND METHODS

The procedures were divided into three steps:

TL dosimeters irradiation: All the radiographic investigations were performed in the Faculdade de Medicina Veterinária e Zootecnia da Universidade Estadual Paulista (FMVZ-UNESP) in the city of Botucatu/Sao Paulo state. Each procedure was carried out by the acquisition of three chest radiographic images, two latero-lateral and one ventro-dorsal of dogs with suspect of pulmonary metastasis. Figure 1 illustrates the correct positioning of the animals in the two projections mentioned above.

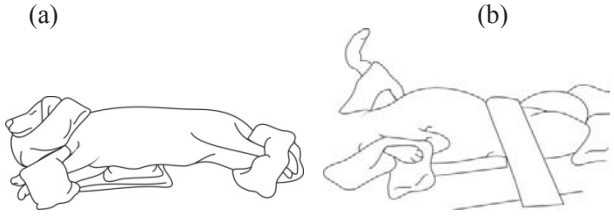

Figure 1- Latero-lateral (a) and ventro-dorsal positioning (b) used to obtain the radiographic image.

O. Dössel and W.C. Schlegel (Eds.): WC 2009, IFMBE Proceedings 25/III, pp. 679–681, 2009.
www.springerlink.com

Twenty seven chest images of different dogs' breeds were monitored. During the procedures the values of the thicknesses of the two projections (latero-lateral and ventro-dorsal) were measured and was possible to measure the source-skin surface distance of the animal. According to the animal size different irradiation field sizes were necessary to acquire the chest image. Values of the kV and mAs were also taken for each image, which were used for the simulation of the dogs' irradiation of each investigation procedure. It is important to point out that the dosimeters were stored into a lead shield before and after the radiation exposure (two plastic badges were used as control group), thus providing more accurate measurements.

After all data acquisition, the simulations of dogs' irradiations were performed with the same X-rays device (SHIMADZU model EZY-RAD 125 kV of FMVZ-UNESP) and a cubic water phantom filled with distilled water, assuring the reproducibility of all parameters mentioned before. The water phantom was positioned in the center of the table allowing the correct adjustment of the light field with the area of the plastic badges. Afterwards, the dosimeters were sent to the Instituto de Pesquisas Energéticas e Nucleares (IPEN/CNEN-SP) in order to evaluate the doses and further analysis of the results.

Dosimeters calibration: The irradiation of the dosimeters for the calibration curve obtaining was performed in the Instruments Calibration Laboratory of IPEN (LCI – IPEN) with the X-rays device used for radiodiagnostic and a water phantom filled with distilled water. In order to obtain the dose-response curves it was used 9 dosimeters of $CaSO_4$:Dy (positioned in their plastic badges containing three filters: lead filter- 1 mm tick, lead 0.8 mm with a central hole 2 mm and plastic- 3 mm tick) for each of the following dose values: 1.5; 2.0; 2.5; 3.5 e 4.0 mGy. The irradiation control, beam energy (kV), as well as the irradiation time to obtain the desired doses was done by the program "*Lab VIEW 7.0"*. As the energy value of the beam energy used to chest examinations varied between 50 and 70 kV, these kV values were used to obtain the dose-response curves of the dosimeters. The water phantom was correctly positioned and the field size was adjusted with the $CaSO_4$:Dy dosimeters in a way to guarantee the reproducibility of the radiographic images acquisition.

TL Reading: After the X ray exposure the thermoluminescent response was evaluated using a thermoluminescent reader *Harshaw* model 3500. All measures were carried out 24 h after irradiation.

III - RESULTS AND DISCUSSION

The dose-response curves obtained to the plastic filter, with beam energies of 50 kV and 70 kV are shown in Figure 2. Using the dose-response curve and its linear fitting equation shown in Figure 2, it was possible to estimate the entrance surface skin doses of the animals for each radiographic investigation performed. The results show the skin dogs entrance doses using the simulation discussed in item II.

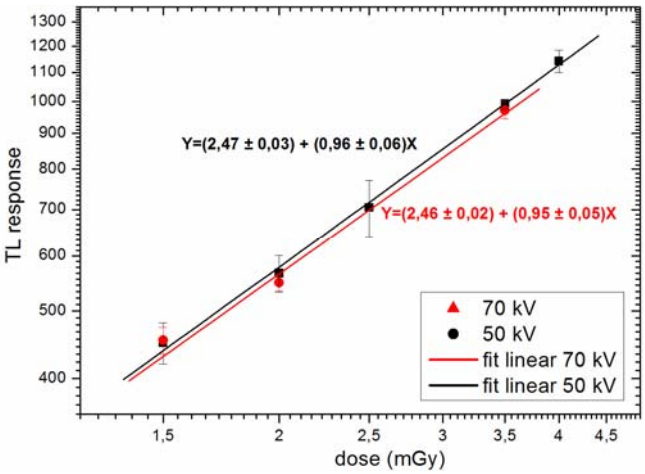

Figure 2- Dose-response curves of plastic filter for X rays beam with energies of 50 kV and 70 kV.

To evaluate the results the animals were divided into three groups: small, medium and big size dogs. The number of monitored exams was 5, 9 and 13 with average field size of 20 x 25 cm, 25 x 30 cm and 30 x 40 cm, respectively.

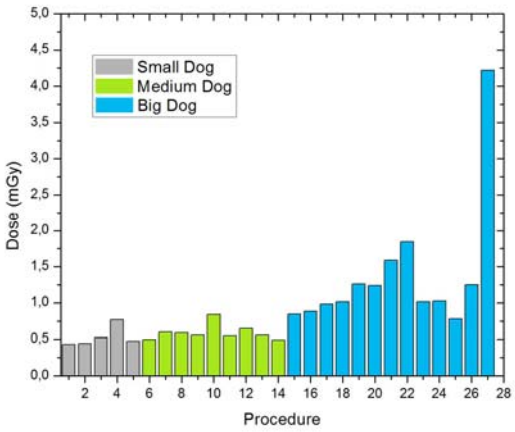

Figure 3- Entrance surface skin doses received for small, medium and big size dogs submitted to chest X-rays to check pulmonary metastasis.

Figure 3 presents the entrance surface skin doses of the animals according to each procedure monitored. The 5 first procedures (grey bars) referring to the small size dogs, the

following 9 procedures (green bars) referring to the medium size dogs and the 13 remaining procedures (blue bars) referencing to the big size dogs.

The average dose received by the small size dogs was 0.53 mGy, where the minimum dose was 0.43 mGy and the maximum dose was 0.77 mGy. This difference comes from the necessity of repetition of the imaging procedure since it is difficult to control the animals' movements.

The average dose for the medium size dogs was 0.59 mGy, where the minimum dose was 0.49 mGy and the maximum dose was 0.84 mGy. It can be noticed an increase in the dose values compared to the small size animals. The analysis of the results shows that the average dose value for the big size dogs was 1.45 mGy, which is a value higher than to the smaller-sized animals. It is important to point out that the average was calculated only for the first 12 investigations because the procedure 13th corresponds to an isolated case where the animal was extremely obese and for which many repetitions of the imaging procedures were performed. The dose received by this dog was 4.22 mGy, in other words, a relatively high dose in the veterinary radiology routine. The minimum dose registered was 0.84 mGy and the maximum was 1.85 mGy.

It is important to mention that there are no reference dose values in the literature showing the dose limit in animals, however for a standard human in a similar procedure the reference dose is 2.3 mGy (summing the three projections), described in Decree 453 of SVS [(4)].

The biggest problem of the veterinary radiology is the immobilization of the animal, which cannot be anesthetized due to the high costs and simplicity of the procedures which is fast and painless. Therefore, most of the time it is necessary to repeat the imaging procedures, increasing the dose received by the animals.

The obtained results indicate that the doses received by occupationally exposed workers and the animal owners that participate of the procedures helping in the immobilization and positioning can exceed the regulatory limits and it is necessary to optimize the delivered doses to the animals.

IV – Conclusions

The obtained results has shown to be extremely important the assessment of the doses involved in veterinary diagnostic radiology procedures both to protect the occupationally exposed workers and animals´ owners and to optimize the delivered doses to the animals. New procedures can be developed aiming to reach a good exam image and safe radiological protection conditions.

Acknowledgments

The authors are thankful to CNPq, FAPESP and CNEN by the financial support.

References

1-Nacional Commission of Nuclear Energy, (*Norm CNEN NN-3.01)*. *Diretrizes Básicas de Proteção Radiológica*. Rio de Janeiro, (2006).

2- International Commission on Radiological Protection, *Recommendations ICRP,* ICRP Publication 60 (1991).

3-International Commission on Radiological Protection, *A Framework for Assessing the Impact of Ionizing Radiation on Non-human Species*, ICRP Publication 91 (2002).

4-Ministry of Health (Decree 453). *Diretrizes de Proteção Radiológica em Radiodiagnóstico Médico e Odontológico*. Regulamento Técnico do Ministério da Saúde, Brazil (1998). http://www.anvisa.gov.br/legis/portarias/453_98.htm

Author:Glauco Rogério Veneziani
Institute: Instituto de Biociências
Street: Distrito de Rubião Jr., s/n° Postcode: 18618-000
City: Botucatu-SP
Country: Brazil
Email: venezianigr@gmail.com

Uranium and radon in the Italian Western Alps

Luca Gentile[1]; Walter Sartor[2] Giuseppe Rachino & Paulo Rachino [3];
1Hekth local agency ASL CN1 Cuneo , Italy
2 Environmental Protection Agency Arpa Cuneo , Italy
3 National Hospital ASO S. Croce e Carle Cuneo

***Abstract*—** Italian uranium mineralizations in the western Alps crop out between Maira Valley and the village of Pietra Ligure on the coast. Since the 1950's, various research has been performed around Besimauda Mount, near the village of Peveragno close the city of Cuneo Piedmont. This brought jobs and better living conditions to the area, since miners could earn three times more than farmers. Consequently, uranium was renamed "peuranium", the gold of Peveragno. Nevertheless, during the second half of the 1950's, the first deaths of local miners occurred and, in 1982, any further research was halted.
Beginning in the 1980's, uranium formations and radioactive waters became a point of interest for radioprotection studies in addition to a social problem. Measures show indoor radon concentration exceeding the regional mean value and scientific papers, classifying radon a carcinogenis agent, have alarmed the population and public administrators. Thus Uranium in now referred to as "the monster of the mount".

Epidemiologic data, however, do not reveal significant increases in the death rate for lung cancer

***Keywords*—**western alp, discovery of uranium, miners, epidemiology

THE DISCOVERY

Autunite from the Lurisia mine was first described in 1912 by Pia Bassi, a student of the ˝Mineralogy Institute of Turin University˝, as a yellow mineral encrusting a flagstone known as "Pietra di Lurisia".

In 1918, the Office of Study and Research within the Ministry of the Army and Ammunitions, invited Marie Curie to evaluate the consistency of the Italian uranium field. M.me Curie arrived in Lurisia on August 15th, 1918 with Lt. Camillo Porlezza, former director of the General Chemistry Institute at Pisa University. They asked about Pietro Percivalle, a miner working at the local uranium mine. As Percivalle remembers: "I was in Mondovì, ready to go back to the battlefront, when my commandant told me 'leave and go home. Tomorrow, in Lurisia, M.me Curie will arrive. She wants to visit your mine. Nobody better than you can guide her."

M.me Curie stayed in Lurisia on the 15th and 16th of August. Percivalle saw the scientist perform several tests using strange devices taken out of a bag. But he never understood what M.me Curie told her companions since they spoke in French.

Beatrice Percivalle, Pietro's daughter, explains that "at that time Lurisia was a small village, used by cattle farmers, coming from nearby neighborhoods to cure their animals with local spring water. There was a rumour that this water was miraculous".

Thanks to M.me Curie too, the discover of radioactive properties in some of Lurisia's waters gave life to therapeutic activities on human beings.

MINERS & THE URANIUM FEVER

On November 14th 1918 , the Garbarino-Sciaccaluga Company from Genoa, obtained a research and utilization permit on radioactive springs, and built a great spa in the Lurisia area.

After 1918, newspapers reported strange news about radium as an energy source related to inhalation treatments and radioactive mud baths.

Lurisia uranium minerals are part of a system dated at permo-trias, which formations emerge bemintween Maira Valley and Pietra Ligure. In this area, since 1950, a lot of research has been performed on mineral deposits located around the Besimauda Mount, in the Peveragno municipality.

In 1947-1948 , Professor Sergio Venzo, of Milan University, carried out a survey on behalf of "Società Mineraria e Chimica per l'uranio" (The Mineral and Chemical Society for Uranium). In 1949, the Montecatini Society started to mine in the Rio Freddo site, in the municipality of Peveragno. In 1953, "Ente Ricerche Nucleari" (Nuclear Research Authorities) performed an aerial topography of the Besimauda Mount area, investigating also bordering areas. This research brought work and better living conditions to the area since miners could earn three times more than a farmer. Newspapers referred to uranium as "peuranium", the gold of Peveragno. Cuneo and Mondovì became uranium capitals, and miners, coming from other regions, brought new celebrations, such as Santa Barbara, and the Miss Uranium contest

O. Dössel and W.C. Schlegel (Eds.): WC 2009, IFMBE Proceedings 25/III, pp. 682–684, 2009.
www.springerlink.com

Fig 1: newspaper of the period. The title "Piedmont uranium fever" remind the golden fever in Klondike

Fig 2: photos taken from beauty contests of the period 1950-60. On the left: the "Atomic Queen". On the right "Miss Uranium" handling an acetylene torch.

In 1956, the first death occurred. Local miners were the most affected, registering one death per year. The reason seemed to be the use of dry drilling, while expert miners, from other regions, employed wet drilling. These facts are reported in "Quelli dell'uranio". Data show that 50% of the deaths were caused by silicosis, and there was not a cancer rate which exceeded a normal population. Thus, the most important risk factor seemed to be the dust rising from mining operations. This effect could have been increased by exposure to radon and other radioactive dust, to nitrous vapours deriving from mines, to air debit, or the increase of inspired air due to working conditions. The influence of tobacco, instead, seems to be moderate.

The ICRP paper, "Lung cancer risk from radon indoor exposure" states that the interaction between radon inhalation and smoke depends upon the degree of exposure to radon and the exposure sequence between the two factors. For example, some dogs, exposed at the same time to radon and smoke, showed a lower lung cancer frequency. This was supposed to have been caused by mucus production induced by smoke. Other studies point out, for chronic exposure, an additive risk factor.

Last, we have to underline that the geological research was performed in 1982, and real mining activity never developed. Studies showed, in fact, high uranium concentrations, but poor power of the minerals.

RADIOPROTECTION & EPIDEMIOLOGY

Several tests on radon indoor exposure have been performed around Besimauda Mount, in Boves, Chiusa Pesio and Peveragno municipalities. In 1990, 48 LR115 dosimeters were positioned, for a period of 6-7 months. From February to September, measured values were in the range of 20 Bq/m3 -340 Bq/m3, with a mean value of 64 Bq/m3.

In 1993, 22 dosimeters were left in Peveragno, 312 in Boves and Chiusa Pesio, obtaining mean values of 222 Bq/m3for Boves, 136 Bq/m3 for Chiusa Pesio and 222 Bq/m3 for Peveragno. 12% of buildings presented values above 400 Bq/m3.

At the end of the 90's, the Environmental Protection Agency (ARPA) performed several tests, showing less than 10% of total results above 500 Bq/m3. A successive survey operated by ARPA and the Agency for Public Health (ASL) showed the limit of 500 Bq/m3 was not exceeded in any of the work places investigated.

The study assumes that radon indoor concentration around Besimauda Mount is correlated to the distance from uranium minerals, according to a log-normal distribution. This is explained with the action of remobilization on uranium salts operated by water courses.

Measurements of dissolved radon in spring water, and total alfa and beta activity in mineral waters pointed out higher values in Besimauda Mount area. The concentration of radon in water shows a variation of 20% and 30% during the year resulting from values approximate zero in the hydric supplying and because of turbulences in the pipes.

Water	Sample	Bq/l	2σ [Bq/l]
1	Bottle	63	13
2	Bottle	20	4

Water	Sample	Bq/l	2σ [Bq/l]
1	Buvette	18000	3600
2	Buvette	600	120

Table 1: concentration of radon in spring waters. Measures 9 and 10 show the reduction due to turbulences in pipes

Surveys showing values exceeding the mean value of 69 Bq/m3 registered in the rest of Piedmont, and scientific papers classifying radon as a carcinogen agent have alarmed administrators and inhabitants. Nevertheless,

epidemiologic data do not point out a significant excess in death rate for lung cancer.

To this end, we refer to ICRP 22, performed between 1972 and 1986 on a population of one million in Yanjiang, China, exposed to high background radiation of 2.1 mGy/y. Data showed little decrease in death rate for lung cancer compared to a control population exposed to 0.77 mGy/y.

Sex	SMR	Lcl SMR	Ucl SMR
Men	77,76	65,97	91,04
Women	65,32	42,22	96,49

Table 2: overall data relating to Boves, Peveragno Chiusa Pesio (1980-2002)

Areas / sex	1984 -2002 SMR	Lcl SMR	Ucl SMR
PEVERAGNO m	61,73	43,19	85,51
PEVERAGNO w	56,05	20,42	122,16
CHIUSA PESIO m	95,02	68,99	127,63
CHIUSA PESIO w	77,13	30,84	159,11
BOVES m	79,19	62,25	99,31
BOVES w	64,88	33,44	113,45

Table 3: specific data for each village

$$SMR = \frac{n}{\sum_i (Tr_i * p_i)} * 100 \qquad (1)$$

Where
n = observed events
Tr_i = death rate for standard population for age class i
p_i = observed population for age class i .

SMR represents increase or decrease in death rate between geographic area under analysis and the whole population.

CONCLUSIONS

Currently, minerals do not seem to be useful for mining purposes. And least of all they seem to be a risk factor, even if new methods for further epidemiologic analysis are desirable.

REFERENCES

- Giuseppe e Paolo Rachino "Quelli dell'uranio" ed Primalpe Cuneo Italy 2007
- Giuseppe e Paolo Rachino " Miniere e Minerali " ed Gribaudo Cuneo 1999
- Luca Gentile, Patriza Mondino Giuseppe Rachino "Le rosette di uranio della Besimauda" la Ciapera 1999 magazine CAI BSD– Cuneo
- Luca Gentile Uranio e Radon nelle alpi cuneesi Tesi Scuola specializzazione in fisica sanitaria Pisa University 1998
- AAVV Banca Dati Mortalità a livello comunale in Piemonte 2004 Do.R.S. - Centro Regionale di Documentazione per la Promozione della Salute - Grugliasco e "Servizio di Epidemiologia - ASL 5 – Grugliasco
- ICRP paper Vol.22 n.1 1991

Use macro [author address] to enter the address of the corresponding author:

Author: Luca Gentile
Institute: *"Hekth local agency"* ASL CN1
Street: Via Boggio 12
City: Cuneo
Country: Italy
Email: lgentile@asl15.it

Tube Housing Leakiness Radiation and Patient Related Radiation Protective Measures – Gonads Radiation Exposure from Panoramic Radiography

M. Burwinkel[1], A. Baumeister[1], M. Sänger[2], and B. d´Hoedt[1]

[1] Department of Oral Surgery (and Oral Radiology), University Medical Center of the Johannes Gutenberg University Mainz, Germany
[2] Department of Radiooncology and Radiotherapy, University Medical Center of the Johannes Gutenberg University Mainz, Germany

Abstract— **The purpose of this study was to compare patient- and apparatus related radiation protective measures considering gonad radiation exposure at panoramic radiography. The local dose (yGv) in the region of the gonads of a male Alderson-Rando-Phantom was measured by the dosimeter Tol-F (Berthold Technology, Germany) during panoramic radiography (PR) by the digital Orthophos XG plus®(Sirona / Bensheim, Germany). Different radiation protective measures was investigated during constant exposure parameters. In the second part of the survey the same ionisation chamber recorded the scattered radiation at the gonads level of the none protected phantom at various case shielding. Without protection apron the dose near to gonads amounted to 0,36 µGy in the mean (initial value), with ventrally applied X-ray apron 0,05 µGy (86% dosage reduction) and with ventral semi apron 0,025 µGy (93 % dosage reduction). At the investigation of tube housing leakiness radiation on the gonads level of the phantom 0,38 µGy was measured, at closed collimator (5mm lead) 0,36 µGy, at shielding the bottom of the apparatus 0,01 µGy. During a PR with opened Collimator (normal collimation) and additional basal shielding an equivalent dose of 0,03 µGy could be ascertained. The reinforced shielding at the bottom of the apparatus reduced the gonads radiation exposure to 92%. Concerning the gonadal protection the optimized patient related and the reinforced apparatus related radiation protection did not differ significantly. At Orthophos XG plus® the tube housing leakiness radiation is an significant factor of the nevertheless relative small radiation exposure of the gonads. The obvious reduction of the gonads exposure by ventral applying of apron or semi apron justifies this simple radiation protective precaution. An additional basal shielding on the apparatus fits the same way. At panoramic radiography the scattered radiation from the primary radiation beam is not significant determining the gonad dose.**

Keywords— **radiation protection, gonads radiation exposure, panoramic radiography, leakiness radiation, lead apron.**

I. Introduction

The International Commission on Radiation Protection (ICRP) published general recommendations based on the following general principles: Justification with a patient benefit, optimisation by keeping exposure as low as reasonably practicable (ALARP) and limitation with patient or occupational limits of exposure dose. Their recommendations are incorporated into national legislation and guidelines which may vary from one country to another. The Guidance notes for dental practitioners on the safe use of X-ray equipment 2001 concluded that there is no justification for routine use of lead apron for patient in dental radiology [1]. In Germany the x-ray Ordinance prescribe that every part of the patient which is not in the primary beam is to protect as well as possible (RöV § 25) [2]. The confusion and controversy which surrounded the use of lead apron is the main instigating factor of this study.

Many recent survey yield on dosimetry in dental radiography [3] but only a few study refer to the radiation exposure beyond the primary beam especially aimed at the gonad exposure [4,5,6]. Generally the gonad exposure is not included in calculation of the actual dose at dental radiography, because the organ dose of the gonads are considered as not measurable respective as very small [7]. Therefore the justification for routine use of lead apron at the panoramic radiography is frequently disbelieved. The lead apron can produce an artefact shade [8] or impede the rotation of the apparatus. Both statements are the main position against the lead apron.

So up to now an hardly academically noted field becomes visual focus in the dentistry, that is the protection of the patient against scattered radiation [9]. The apparatus-inherent radiation protection controlled by the CE- certification has to be differed from the radiation protection close to patient taking responsibility by the user. The following examination compares these two categories analytically in order to contribute to clarification of the following questions:

- Are the local dosages in the near of the gonads significantly influenced by applying a lead apron?
- Is the protection optimized by modification of the lead apron geometry?
- Which part plays the apparatus leakiness radiation?

O. Dössel and W.C. Schlegel (Eds.): WC 2009, IFMBE Proceedings 25/III, pp. 685–688, 2009.
www.springerlink.com

II. Material and Methods

The dosages were measured quite close to male gonads of an X-ray phantom (Alderson-Rando-Phantom) compared different options of radiation protection and lead aprons positions. The effects of reinforced case shielding were put in proportion to it.

Table 1 Test parameters

Patient near radiation protection
• None (neither semi apron nor apron)
• Apron with ventral full protection
• Apron with dorsal full protection
• Semi apron ventrally worn
• Semi apron dorsally worn
• Shield ventrally worn on the neck
Apparatus related protection
• Closed collimator (lead 5 mm thick)
• normal apparatus shielding
• additional apparatus shielding with ventilation slots
• Additional basal apparatus shielding without ventilation slots
• Open collimator
• normal apparatus shielding
• Additional basal apparatus shielding without ventilation slots

X-ray technique: The Orthophos XG plus (Fa. Sirona, Bensheim, Germany) was used as digital panoramic radiography apparatus. All measurements were ascertained at a standard panoramic radiography at 73 kV tension, 8 mA amperage and a radiation time of 14, 1 seconds per rotation.

Dosimetry: The original size of measurement displayed at the dosimeter in the present experimental examination is the photon-equivalent dose (H_X) in Sievert (Sv) Because of its low local resolution we term it the local dose close to gonads in Gray (Gy). The dosimeter Tol-F (Berthold Technology GmbH & Co. KG, Bad Wildbad, Germany) is particularly developed for radiation protection works at dose rates from 0,01 µGy/h to 10 mGy/h in the proportional field with gas enhancement by secondary ionisation. The ionisation dosimeter is calibrated by the beta radiation apparatus strontium 90 (25 kBq) before each measuring cycle.

The dosimeter tube can be easily placed close to gonads of the X-ray phantom. For the measurement of the scattered radiation respective leak radiation two values were accumulated for the validation of the measuring system and the average values were calculated. As under the present experimental assembly, the measuring probe only records the dose in immediate closeness to the male gonads, so reflects no surface-dose per se, the measuring adjustment can only have model character and register the accruing effects more approximately than quantitatively.

Phantom: A male Alderson-Rando-Phantom (Alderson Reaseach Lab., Stanford, Connecticut, USA) was used as an anthropomorphic absorption- and scattered medium. This whole-body phantom consists of a human skeleton which is embedded in isocyanate. With a density of 0,985g/cm³ the material transformed in a human shape shows an approximately tissue equivalent X-ray absorption. The X-ray phantom easily dismanteled in 35 horizontal layers is designed in height and weight for the reference human being (175 cm, 73,5 kg) (ICRP 1976).

Radiation protection: The *patient related* radiation protection was effected by an lead apron, semi apron and an dental x-ray shield, each used with an lead equivalent value of 0,5 mm (Mavic GmbH, Munich, Germany). The panoramic lead apron covers the shoulders and one side of the trunk of the body completely and the other side only partially (Fig.1).

Fig. 1 Experiment setup: Rando-Phantom in the panoramic unit Orthophos XG plus with the Tol-F –probe on the level of the gonads, Mavic –panoramic lead apron in the ventral position – semi apron and the lead shield in the background.

For the determination of the *case leakiness* radiation and for the additional apparatus shielding served lead lamellas of a thickness of 1,25mm at the bottom of the apparatus (Fig. 2). For sealing of the radiation exit window four layers were conglutinated (~equivalent value of lead of 5mm).

Fig. 2 Additional shielding with ventilation crevices at the bottom of the X-ray apparatus (1,2 mm lead)

III. Results

A. Patient related measurements

Without radiation protective apron the dose averaged 0,36 µGy (initial value), with ventrally applied apron 0,05 µGy (14 % of the initial value), at dorsal position 0,125 µGy (35 %). Under the ventrally worn loincloth 0,025 µGy (7 %) were measured as well as at dorsal position of loincloth 0,35 µGy (3%). By using a radio protective shield ventrally worn on the neck the dose quite close to gonads increased to 0,37 µGy (+3%). (Table 2)

Table 2 Influence of the patient related radiation protective measurements

	without protection	Shield ventral	Semi apron dorsal	Apron dorsal	Apron ventral	Semi apron ventral
Dose in µGy	0,36	0,37	0,35	0,125	0,05	0,025
Dose in % of the initial value	100%	103 %	97 %	35 %	14 %	7 %

B. protective measures related to the X-ray apparatus

The influence of case leakiness radiation was measured in the gonadal region of the Phantom. In this experimental constellation the local dose amounted to 0,38 µGy without patient related radiation protection, at closing of the radiation exit window 0,36 µGy, at basal sealing of the radiation apparatus case 0,01 µGy and during panoramic radiography with opened radiation exit window and additional basal shielding 0,03 µGy.

Table 3 Influence of radiation protective measures related to the apparatus

	Dose in µGy	Dose in % of the initial
Without additional shielding	0,38	100 %
only collimator field shielded with 5 mm lead	0,36	95 %
Collimator field closed with lead, case shielded with lead basal with ventilation slots	0,13	34 %
Collimator field closed with lead, case shielded basal without ventilation slots	0,01	3 %
Collimator field open, case shielded with lead basal without ventilation slots	0,03	8 %

At closing of the radiation exit window the dose in region of the gonads still amounted to 95% of the initial value. The basal shielding of the case could reduce the dose quite close to gonads to 34% at leaving of the ventilation slots and at complete basal covering to 8% of the initial value.

IV. Discussion

In most surveys referring to dosimetry by X-ray, thermoluminescence-detectors (TLD) are used, which needs 10 or more X-ray applications until they have absorbed enough energy to get actually in an effective measurable range. The estate of the small sized TLD's mainly founds on their great local resolution. So, those are especially proper to measurements in the primary used radiation field. Requesting radiation outside the primary radiation beam on the one hand there is expected dose rate in range round about 0,1 µGy by dental radiographic diagnostics, on the other hand the local resolution specially plays a tangential part at dose coverage on the body surface. Thence measurements were made by means of ionisation dosimetry.

In opposite to all the other protective measurements in or study (apron dorsal or radio-protective shield ventral) the

ventral worn semi-apron reflected in the most effective dose reduction (93%) followed by the ventral applied apron (dose reduction of 86%). The shield performed worst as additive strewing object. The more nearer the gonads were blanketed, the more effective its protection. Following our measurements, thyself the semi-apron implicated a highly significant reduction of the gonadal dose. In an comparable setting Rother detected with TLDs in the region of the Gonads of an Alderson-Rando Phantom 0,143 µGy without and 0,047 µGy with a lead apron [6]. Regarding the strew- and weakening coefficients of water, you cannot expect, that the gonads receive a measurable dose with the origin within the torso. The absolute values in the present survey 0,36 µGy in about 73cm distance to the primary used radiation beam have to astonish respectively have an another origin. The test results suggest, that about 95% of the local dose in the gonadal region result from the apparatus leakiness radiation.

The basal shielding of the casing could reduce the dose near the gonads to 8% of the initial value. Therefore the comparison between the apron and the basal case shielding had no significant difference concerning its radiation protection potential in result.

In case of patients with shorts necks shades of the apron may be resulted. Therefore to avoid this on patients with short necks, there should be applied a ventral semi apron.

If other fabricator of panoramic-X-ray units offers a better apparatus shielding (more than the CE-certification requires) is to prove in further studies. Never the less we should point out that the justification with a patient benefit, the right technique with an exact limitation of the x-ray field, and the optimisation of the exposure parameters and not at last the careful investigation and documentation (and archiving) are still the most important aspects of radiation protection.

V. Conclusion

In the panoramic unit Orthophos XG (Sirona, Bensheim/ Germany) the leakage radiation is the main part of the scattered radiation on the level of the male gonads. Wearing an lead apron, or in case of short necks, wearing an semi apron is a high efficient radiation protection of the mail gonads. Because of the rotation of the x-ray beam of panoramic units the lead apron should cover the whole trunk of the patient as an armless jacket with a backward plunging neckline.

The alternative sanction to the lead apron is a shielding of the apparatus above the CE-norm which questioning the leakiness radiation. If other dental units for panoramic or cone beam computer tomography (CBCT) shows the similar scattered radiation profile or provided with more efficient apparatus shielding is still to investigate. The real reduction of the effective radiation dosage by using the lead apron is not comparable with the potential which lies in the general principles of radiation protections concerning the handling of the primary x-ray beam [1,10]. Never the less, the lead apron should be routinely used in panoramic radiography and only in exceptional cases we could abandon these simple and efficient option of radiation protection.

Acknowledgment

Special thanks applies to Prof. Dr. H. Schmidberger, director of the Department of Radiooncology of University Medical Center of the University Mainz, for benignant hire of the Rando-Phantom and the measuring instrument.

References

1. NRPB 1994 Guidelines on radiology standards in primary dental care. National Radiological Protection Board, Vol. 5 Nr. 3 1994 in Guidance notes for dental practitioners on safe use of X-ray equipment 2001, NRPB/DoH, London
2. Peinsipp N, Roos G, Weimer G (2003) Röntgenverordnung RöV, Forkel, S 177
3. Gijbels F, Jacobs R, Bogaerts R, Debaveye D, Verlinden S, Sanderink G (2005) Dosimetry of digital panoramic imaging. Part I: patient exposure. Dentomaxillofac Radiol;34: 145-149
4. Bean LR, Devore WD (1969) The effect of protective aprons in dental roentgenography. Oral Surg Oral Med Oral Pathol. 28:505-8.
5. Wood ER, Harris AM, van der Merwe EJ, Nortje CJ (1991) The lead apron revisited: Does it reduce gonadal radiation dose in dental radiology? Oral Surg Oral Med Oral Pathol. 71:642-6
6. Rother UJ (2006) Moderne bildgebende Verfahren in der Zahn-, Mund- und Kieferheilkunde, Urban & Fischer 67
7. White SC (1992) Assessment of radiation risk from dental radiography. Dentomaxillofac Radiol 21:118-126
8. Chomenko AG (1977) Leaded apron artifact on panoramic radiograph. Oral Surg Oral Med Oral Pathol. 44(3):489-90
9. Gibbs SJ, Pujol A, McDavid WD, Welander U, Tronje G. (1988) Patient risks from panoramic x-rays. ZWR 97 (9):782-6
10. Kaeppler G, Dietz K, Reinert S (2006) The effect of dosisreduction on the detection of anatomical structures on panoramic radiographs. Dentomaxillofac Radiol 35,271-277

Dr. Matthias Burwinkel
Department of Oral Surgery,
University Medical Center of the Johannes Gutenberg University
Augustusplatz 2
D-55131 Mainz
Germany
burwinkel@oralchir.klink.uni-mainz.de

Author Index